This document is the intellectual property of the fib – International Federation for Structural Concrete. All rights reserved.
This PDF of fib Bulletin 95 is intended for use and/or distribution solely within fib National Member Groups.

fib CEB-FIP

aci

Bulletin 95



Fibre Reinforced Concrete: From Design to Structural Applications

Proceedings of the ACI-*fib*-RILEM International Workshop - FRC2018

ACI SP-343
Technical report

This document is the intellectual property of the fib – International Federation for Structural Concrete. All rights reserved.
This PDF of fib Bulletin 95 is intended for use and/or distribution solely within fib National Member Groups.

Bulletin 95

fib CEB-FIP

aci

Fibre Reinforced Concrete: From Design to Structural Applications

Technical Report

Proceedings of the ACI-*fib*-RILEM
International Workshop - FRC2018

August 2020

This document is the intellectual property of the fib – International Federation for Structural Concrete. All rights reserved.
This PDF of fib Bulletin 95 is intended for use and/or distribution solely within fib National Member Groups.

Approval for this bulletin

Subject to priorities defined by the Technical Council and the Presidium, the results of the *fib*'s work in commissions and task groups are published in a continuously numbered series of technical publications called *bulletins*. The following categories are used:

Category:	**Approval by**:
Technical report	Task group and chairpersons of the commission
State-of-the-art report	Commission
Manual / Guide to good practice / Recommendation	Technical Council
Model code	General Assembly

Any publication not having met the above requirements will be clearly identified as a preliminary draft.

fib Bulletin 95 is published as a technical report and is a collection of contributions to a workshop that was co-sponsored by the *fib* and the American Concrete Institute (ACI). The authors have presented their individual views. Although these contributions have not been discussed in any of the *fib*'s working bodies, the subject matter is highly topical and believed to be of general interest to members of the *fib*.

This bulletin is also published as an ACI special publication, ACI SP-343.

Cover image: Marseille - MuCEM museum / J4, photograph courtesy of Fred Romero.
Architects: Rudy Ricciotti and Roland Carta - Lighting by Yann Kersalé - 2009-13.
Flickr source on Creative commons licence: https://creativecommons.org/licenses/by/2.0/

© Fédération internationale du béton (*fib*), 2020.

Although the International Federation for Structural Concrete / Fédération internationale du béton (*fib*) and the the American Concrete Institute (ACI) do their best to ensure that all the information presented in this publication is accurate, no liability or responsibility of any kind, including liability for negligence, is accepted in this respect by these organizations, their members, employees or agents.

All rights reserved. No part of this publication may be reproduced, modified, translated, stored in a retrieval system or transmitted in any form or by any means – electronically, mechanically, through photocopying, recording or otherwise – without prior written permission from the *fib*.

ISSN 1562-3610
ISBN 978-2-88394-142-7
https://doi.org/10.35789/fib.BULL.0095
Layout by Corinne Bottollier Dépois (*fib*).
Printed by DCC Document Competence Center Siegmar Kästl e.K., Germany

This document is the intellectual property of the fib – International Federation for Structural Concrete. All rights reserved.
This PDF of fib Bulletin 95 is intended for use and/or distribution solely within fib National Member Groups.

Acknowledgements

Editors:

Bruno Massicotte
Ecole Polytechnique de Montréal, Canada

Fausto Minelli
University of Brescia, Italy

Barzin Mobasher
Arizona State University, USA

Giovanni Plizzari
University of Brescia, Italy

Authors by chapter

Chapters	Main Authors	DOI
1	Plückelmann, S. ; Breitenbücher, R.	https://doi.org/10.35789/fib.BULL.0095.Ch01
2	Li, L.; Cao, M.	https://doi.org/10.35789/fib.BULL.0095.Ch02
3	Vrijdaghs, R.; di Prisco, M.; Vandewalle, L.	https://doi.org/10.35789/fib.BULL.0095.Ch03
4	Galeote, E.; Blanco, A.; Cavalaro, S.H.P.; de la Fuente, A.	https://doi.org/10.35789/fib.BULL.0095.Ch04
5	Galeote, E.; Blanco, A.; Cavalaro, S.H.P.; de la Fuente, A.	https://doi.org/10.35789/fib.BULL.0095.Ch05
6	Juhasz, K.P.; Schaul, P.; Winterberg, R.	https://doi.org/10.35789/fib.BULL.0095.Ch06
7	Javadian, A.; Mahdavi, A.; Benamrane, O.; Majeed, M.; Aoude, H.	https://doi.org/10.35789/fib.BULL.0095.Ch07
8	Chelha, F.; Alam, S. Y.; Bendimerad, A.Z.; Loukili, A.	https://doi.org/10.35789/fib.BULL.0095.Ch08
9	Ferrara, L.; Asensio, E.C.; Lo Monte, F.; Snoeck, D.; De Belie, N.	https://doi.org/10.35789/fib.BULL.0095.Ch09
10	Ortiz-Navas, F.; Scaroni, L.; Navarro-Gregori, J.; Serna-Ros, P.	https://doi.org/10.35789/fib.BULL.0095.Ch10
11	Ortiz-Navas, F.; Navarro-Gregori, J.; Serna Ros, P.; Leiva Herdocia, G.	https://doi.org/10.35789/fib.BULL.0095.Ch11
12	Barros, J.A.O.; Foster, S.J.	https://doi.org/10.35789/fib.BULL.0095.Ch12
13	De Smedt, M.; De Wilder, K.; Anastasopoulos, D.; Reynders, E. ; De Roeck, G.; Vandewalle, L.	https://doi.org/10.35789/fib.BULL.0095.Ch13
14	Winterberg, R.; Rodrìguez, L.M.; Cámara, R.J.; Abad, D.S	https://doi.org/10.35789/fib.BULL.0095.Ch14
15	Galeote, E.; Blanco, A.; de la Fuente, A.	https://doi.org/10.35789/fib.BULL.0095.Ch15
16	Meda, A.; Rinaldi, Z.; Spagnuolo, S.; De Rivaz, B.; Giamundo, N.	https://doi.org/10.35789/fib.BULL.0095.Ch16
17	Juhasz, K.P.; Schaul, P.	https://doi.org/10.35789/fib.BULL.0095.Ch17
18	Yao, Y.; Bakhshi, M.; Nasri, V.; Mobasher, B	https://doi.org/10.35789/fib.BULL.0095.Ch18
19	Conforti, A.; Trabucchi, I.; Tiberti, G.; Plizzari, G.A.; Caratelli, A; Meda, A.; Moro, S.; Hunger, M.	https://doi.org/10.35789/fib.BULL.0095.Ch19
20	Massicotte, B.; Cordoni, N.	https://doi.org/10.35789/fib.BULL.0095.Ch20
21	Pourzarabi, A.; Colombo, M.; Martinelli, P.; di Prisco, M.	https://doi.org/10.35789/fib.BULL.0095.Ch21
22	Zani, G.; Colombo, M.; Failla, C.; di Prisco, M.	https://doi.org/10.35789/fib.BULL.0095.Ch22
23	Trabucchi, I.; Conforti, A.; Tiberti, G.; Plizzari, G.A.; Winterberg, R.	https://doi.org/10.35789/fib.BULL.0095.Ch23
24	Bernard, E. S.	https://doi.org/10.35789/fib.BULL.0095.Ch24
25	Dancygier, A.N.; Karinski, Y.S..	https://doi.org/10.35789/fib.BULL.0095.Ch25

This document is the intellectual property of the fib – International Federation for Structural Concrete. All rights reserved.
This PDF of fib Bulletin 95 is intended for use and/or distribution solely within fib National Member Groups.

26	Fantilli, A.P.; Tondolo, F.	https://doi.org/10.35789/fib.BULL.0095.Ch26
27	Frazão, C.; Barros, J.; Bogas, A.; Pilakoutas, K.; de Sousa, C.M.	https://doi.org/10.35789/fib.BULL.0095.Ch27
28	Kitazawa, K.; Sato, Y.; Naganuma, K.; Kaneko, Y.	https://doi.org/10.35789/fib.BULL.0095.Ch28
29	Monte, R.; de la Fuente Antequera, A.; Dominigues de Figueiredo, A.	https://doi.org/10.35789/fib.BULL.0095.Ch29
30	Aoude, H.; Li, Y.; Bastami, R.; Ibrahim, F.M.	https://doi.org/10.35789/fib.BULL.0095.Ch30
31	Poveda, E.; Ruiz, G.; Cifuentes, H.; Yu, R.C.; Zhang, X.X.	https://doi.org/10.35789/fib.BULL.0095.Ch31
32	Antroula, G.; Stavroula, P.	https://doi.org/10.35789/fib.BULL.0095.Ch32
33	Ranjbarian, M.; Mechtcherine, V.	https://doi.org/10.35789/fib.BULL.0095.Ch33
34	Bernard, E. S.	https://doi.org/10.35789/fib.BULL.0095.Ch34
35	Vieira, M.M.; Cavalaro, S.H.P.; Aguado, A.	https://doi.org/10.35789/fib.BULL.0095.Ch35
36	Amin, A.; Gilbert, R.I.	https://doi.org/10.35789/fib.BULL.0095.Ch36
37	Berrocal, C.G.; Lundgren, K.; Löfgren, I.	https://doi.org/10.35789/fib.BULL.0095.Ch37
38	de la Fuente, A.; Cavalaro, S.H.; Bairán, J.M.	https://doi.org/10.35789/fib.BULL.0095.Ch38
39	Zanotti, C.; Randl, N.; Gar, P.S.; Far, B.K.; Steiner, M.	https://doi.org/10.35789/fib.BULL.0095.Ch39
40	Turgeon-Mallette, V.; Sorelli, L.; Conciatori, D.; Réthore, J.	https://doi.org/10.35789/fib.BULL.0095.Ch40
41	Ding, Y.;Li, D.; Zeng, W.	https://doi.org/10.35789/fib.BULL.0095.Ch41
42	Fargier-Gabaldon, L.B.; Al-Tameemi, M.; Parra-Montesinos, G.J.	https://doi.org/10.35789/fib.BULL.0095.Ch42
43	Plückelmann, S.; Breitenbücher, R.	https://doi.org/10.35789/fib.BULL.0095.Ch43
44	Fantilli, A.P.; Nishiwaki, T.; Lisi, V.; Longo, M.	https://doi.org/10.35789/fib.BULL.0095.Ch44
45	Look, K.; Mark, P.	https://doi.org/10.35789/fib.BULL.0095.Ch45
46	Valente, T.; Barros, J.; Lourenço, L.	https://doi.org/10.35789/fib.BULL.0095.Ch46
47	Lucchini, S.S.; Facconi, L.; Minelli, F.; Plizzari, G.A.	https://doi.org/10.35789/fib.BULL.0095.Ch47
48	Redaelli, D.; Nseir, J.Y.	https://doi.org/10.35789/fib.BULL.0095.Ch48
49	Rossi, P.; Davian-Desnoyers, D.; Tailhan, J.L.	https://doi.org/10.35789/fib.BULL.0095.Ch49
50	Charron, J.P.; Desmettre, C.; Cantin Bellemare, E.	https://doi.org/10.35789/fib.BULL.0095.Ch50
51	Loser, R.; Justs, J.; Lura, P.	https://doi.org/10.35789/fib.BULL.0095.Ch51
52	Bastami, R.; Li, Y.; Algassem, O.; Aoude, H.	https://doi.org/10.35789/fib.BULL.0095.Ch52
53	Randl, N.; Mészöly, T.	https://doi.org/10.35789/fib.BULL.0095.Ch53

This document is the intellectual property of the fib – International Federation for Structural Concrete. All rights reserved.
This PDF of fib Bulletin 95 is intended for use and/or distribution solely within fib National Member Groups.

Foreword

This bulletin presents a compilation of the papers presented at the 3rd International workshop on Fibre-Reinforced Concrete, "FRC2018, from Design to Structural Applications". The workshop was a joint ACI - Rilem - *fib* event, which expresses inter-federation collaboration and broad expertise.

The aim of the workshop was to provide state-of-the-art information on recent progress in term of specifications development, actual applications, and to expose users and researchers to tomorrow's challenges in the design and construction of a wide variety of structural applications. The topic is thus fitting and is a clear supplement to the work of *fib* TG4.1 "Fibre-reinforced concrete". The aim of TG4.1 is to make theoretical and practical developments in the field of fibre-reinforced concrete materials technology, rheology and materials characterisation and modelling and to present these developments in code-type formulations.

Recently, it was decided to merge the work of TG4.1 and TG4.2 "Ultrahigh performance fibre reinforced concrete" to prepare one joint bulletin. At the time of writing, this bulletin is being finalised. Also, a framework bulletin for the *fib* Model Code MC2020 will be prepared.

I'm very grateful to Fausto Minelli (University of Brescia, Italy), for making the colossal effort to convert this collection of papers into an *fib* bulletin. And many thanks to Corinne Bottollier-Dépois for formatting this bulletin.

Tor Arne Martius-Hammer
Deputy chair of Commission 4: *Concrete and Concrete Technology*

This document is the intellectual property of the fib – International Federation for Structural Concrete. All rights reserved.
This PDF of fib Bulletin 95 is intended for use and/or distribution solely within fib National Member Groups.

Preface

The first international FRC workshop supported by RILEM and ACI was held in Bergamo (Italy) in 2004. At that time, a lack of specific building codes and standards was identified as the main inhibitor to the application of this technology in engineering practice. The workshop aim was placed on the identification of applications, guidelines, and research needs in order for this advanced technology to be transferred to professional practice.

The second international FRC workshop, held in Montreal (Canada) in 2014, was the first ACI-*fib* joint technical event. Many of the objectives identified in 2004 had been achieved by various groups of researchers who shared a common interest in extending the application of FRC materials into the realm of structural engineering and design. The aim of the workshop was to provide the State-of-the-Art on the recent progress that had been made in term of specifications and actual applications for buildings, underground structures, and bridge projects worldwide.

The rapid development of codes, the introduction of new materials and the growing interest of the construction industry suggested presenting this forum at closer intervals. In this context, the third international FRC workshop was held in Desenzano (Italy), four years after Montreal. In this first ACI-*fib*-RILEM joint technical event, the maturity gained through the recent technological developments and large-scale applications were used to show the acceptability of the concrete design using various fibre compositions.

The growing interests of civil infrastructure owners in ultra-high-performance fibre-reinforced concrete (UHPFRC) and synthetic fibres in structural applications bring new challenges in terms of concrete technology and design recommendations. In such a short period of time, we have witnessed the proliferation of the use of fibres as structural reinforcement in various applications such as industrial floors, elevated slabs, precast tunnel lining sections, foundations, as well as bridge decks. We are now moving towards addressing many durability-based design requirements by the use of fibres, as well as the general serviceability-based design. However, the possibility of having a residual tensile strength after cracking of the concrete matrix requires a new conceptual approach for a proper design of FRC structural elements.

With such a perspective in mind, the aim of FRC2018 workshop was to provide the State-of-the-Art on the recent progress in terms of specifications development, actual applications, and to expose users and researchers to the challenges in the design and construction of a wide variety of structural applications.

Considering that at the time of the first workshop, in 2004, no structural codes were available on FRC, we have to recognize the enormous work done by researchers all over the world, who have presented at many FRC events, and convinced code bodies to include FRC among the reliable alternatives for structural applications. This will allow engineers to increasingly utilize FRC with confidence for designing safe and durable structures.

This document is the intellectual property of the fib – International Federation for Structural Concrete. All rights reserved.
This PDF of fib Bulletin 95 is intended for use and/or distribution solely within fib National Member Groups.

Many presentations also clearly showed that FRC is a promising material for efficient rehabilitation of existing infrastructure in a broad spectrum of repair applications. These cases range from sustained gravity loads to harsh environmental conditions and seismic applications, which are some of the broadest ranges of applications in Civil Engineering.

The workshop was attended by researchers, designers, owner and government representatives as well as participants from the construction and fibre industries. The presence of people with different expertise provided a unique opportunity to share knowledge and promote collaborative efforts. These interactions are essential for the common goal of making better and sustainable constructions in the near future.

The workshop was attended by about 150 participants coming from 30 countries. Researchers from all the continents participated in the workshop, including 24 Ph.D. students, who brought their enthusiasm in FRC structural applications.

For this reason, the workshop Co-chairs sincerely thank all the enterprises that sponsored this event. They also extend their appreciation for the support provided by the industry over the last 30 years which allowed research centers to study FRC materials and their properties, and develop applications to making its use more routine and accepted throughout the world. Their important contribution has been essential for moving the knowledge base forward.

Finally, we appreciate the enormous support received from all three sponsoring organizations of ACI, *fib* and Rilem and look forward to paving the path for future collaborations in various areas of common interest so that the developmental work and implementation of new specifications and design procedures can be expedited internationally.

June 2018

Bruno Massicotte, Fausto Minelli, Barzin Mobasher, Giovanni Plizzari

This document is the intellectual property of the fib – International Federation for Structural Concrete. All rights reserved.
This PDF of fib Bulletin 95 is intended for use and/or distribution solely within fib National Member Groups.

Contents

Foreword i

Preface ii

1. Mechanical characterization 1

Round-Robin Test on Various Test-Methods for Flexural Behavior of Steel Fiber Reinforced Sprayed Concretes 2
Plückelmann, S. ;Breitenbücher, R.
https://doi.org/10.35789/fib.BULL.0095.Ch01

A new multi-scale hybrid fiber reinforced cement-based composites 12
Li, L.; Cao, M.
https://doi.org/10.35789/fib.BULL.0095.Ch02

A sectional approach for the bending creep of FRC based on uniaxial tension creep tests 20
Vrijdaghs, R.; Di Prisco, M.; Vandewalle, L.
https://doi.org/10.35789/fib.BULL.0095.Ch03

Optimized quality control procedure with the Barcelona test and the inductive method for FRC 30
Galeote, E.; Blanco, A.; Cavalaro, S.H.P.; de la Fuente, A.
https://doi.org/10.35789/fib.BULL.0095.Ch04

Influence of the beam size on the residual strength of high performance fibre reinforced concrete 40
Galeote, E.; Blanco, A.; Cavalaro, S.H.P.; de la Fuente, A.
https://doi.org/10.35789/fib.BULL.0095.Ch05

Influence of test methodology on the applicability of test results of fibre reinforced concrete for design 50
Juhasz, K.P.; Schaul, P.; Winterberg, R.
https://doi.org/10.35789/fib.BULL.0095.Ch06

Parameters affecting the properties of plain and fiber reinforced self-sonsolidating concrete. 60
Javadian, A.; Mahdavi, A.; Benamrane, O. ;Majeed, M.; Aoude, H.
https://doi.org/10.35789/fib.BULL.0095.Ch07

This document is the intellectual property of the fib – International Federation for Structural Concrete. All rights reserved.
This PDF of fib Bulletin 95 is intended for use and/or distribution solely within fib National Member Groups.

Mechanical characterization of fiber reinforced floor screeds: Influence of glass fibers on shrinkage and cracking mechanisms 70
Chelha, F.; Alam, S. Y.; Bendimerad, A.Z.; Loukili, A.
https://doi.org/10.35789/fib.BULL.0095.Ch08

An application oriented state-of-art and research-need perspective on self-healing fibre-reinforced cementitious composites 80
Ferrara, L.; Asensio, E.C.; Lo Monte, F.; Snoeck, D.; De Belie, N.
https://doi.org/10.35789/fib.BULL.0095.Ch09

2. Shear 90

Experimental study of shear transfer in polypropylene fibre-reinforced concrete using pre-cracked push-off specimens 91
Ortiz-Navas, F.; Scaroni, L.; Navarro-Gregori, J.; Serna-Ros, P.
https://doi.org/10.35789/fib.BULL.0095.Ch10

Shear crack behaviour and shear deformation of polypropylene fibre-reinforced concrete slender beams 101
Ortiz-Navas, F.; Navarro-Gregori, J.; Serna Ros, P.; Leiva Herdocia, G.
https://doi.org/10.35789/fib.BULL.0095.Ch11

Fibres as shear reinforcement in RC beams: an overview on assessment of material properties and design approaches 111
Barros, J.A.O.; Foster, S.J.
https://doi.org/10.35789/fib.BULL.0095.Ch12

Experimental investigation of shear-critical prestressed steel fibre reinforced concrete beams 121
De Smedt, M.; De Wilder, K.; Anastasopoulos, D.; Reynders, E. ; De Roeck, G.; Vandewalle, L.
https://doi.org/10.35789/fib.BULL.0095.Ch13

3. Bridges/Elevated Slabs/Precast Elements/Tunnel Linings 132

Segmental Lining Design using Macro Synthetic Fibre Reinforcement 133
Winterberg, R.; Rodrìguez, L.M.; Cámara, R.J.; Abad, D.S
https://doi.org/10.35789/fib.BULL.0095.Ch14

Effect of reinforcement configuration on the ductility requirements of real-scale slabs 143
Galeote, E.; Blanco, A.; de la Fuente, A.
https://doi.org/10.35789/fib.BULL.0095.Ch15

This document is the intellectual property of the fib – International Federation for Structural Concrete. All rights reserved.
This PDF of fib Bulletin 95 is intended for use and/or distribution solely within fib National Member Groups.

Experimental Behaviour of Precast Tunnel Segments in Steel Fiber Reinforcement with GFRP Rebars 153
Meda, A.; Rinaldi, Z.; Spagnuolo, S.; De Rivaz, B.; Giamundo, N.
https://doi.org/10.35789/fib.BULL.0095.Ch16

Opportunities for synthetic fibre reinforcement in concrete tramlines 163
Juhasz, K.P.; Schaul, P.
https://doi.org/10.35789/fib.BULL.0095.Ch17

Closed-form Solutions for Interaction Diagrams of Hybrid Fiber-Reinforced Tunnel Segments 173
Yao, Y.; Bakhshi, M.; Nasri, V.; Mobasher, B.
https://doi.org/10.35789/fib.BULL.0095.Ch18

An experimental study on the use of polypropylene macrofibers in precast segments for hydraulic and metro tunnel lining 185
Conforti, A.; Trabucchi, I.; Tiberti, G.; Plizzari, G.A.; Caratelli, A;
Meda, A.; Moro, S.; Hunger, M.
https://doi.org/10.35789/fib.BULL.0095.Ch19

Design of precast prestressed SFRC T-girders for accelerated sustainable bridge construction 195
Massicotte, B.; Cordoni, N.
https://doi.org/10.35789/fib.BULL.0095.Ch20

FRC Hybrid slabs: reliability of Model Code approaches 205
Pourzarabi, A.; Colombo, M.; Martinelli, P.; di Prisco, M.
https://doi.org/10.35789/fib.BULL.0095.Ch21

Optimization of partially prefabricated HyFRC slabs 215
Zani, G.; Colombo, M.; Failla, C.; di Prisco, M.
https://doi.org/10.35789/fib.BULL.0095.Ch22

Structural behavior of precast tunnel segments with macro-synthetic fibers during TBM operations: a numerical study 225
Trabucchi, I.; Conforti, A.; Tiberti, G.; Plizzari, G.A.; Winterberg, R.
https://doi.org/10.35789/fib.BULL.0095.Ch23

This document is the intellectual property of the fib – International Federation for Structural Concrete. All rights reserved.
This PDF of fib Bulletin 95 is intended for use and/or distribution solely within fib National Member Groups.

4. Seismic and Special Loading Conditions 235

Seismic Performance of Fibre Reinforced Concrete in the Absence of Bars 236
Bernard, E. S.
https://doi.org/10.35789/fib.BULL.0095.Ch24

RC Beams with Steel Fibers - Towards Better Determination of their Minimum Conventional Reinforcement Ratio 246
Dancygier, A.N.; Karinski, Y.S..
https://doi.org/10.35789/fib.BULL.0095.Ch25

Residual crack width in RC and R/FRC ties subjected to repeated loads 254
Fantilli, A.P.; Tondolo, F.
https://doi.org/10.35789/fib.BULL.0095.Ch26

An experimental investigation on the post-cracking behaviour of Recycled Steel Fibre Reinforced Concrete 262
Frazão, C.; Barros, J.; Bogas, A.; Pilakoutas, K.; de Sousa, C.M.
https://doi.org/10.35789/fib.BULL.0095.Ch27

Finite Element Analyses of Seismic Response of a 22-story RC Wall Building subjected to Drying Shrinkage Cracking and Application of SCRPCC 272
Kitazawa, K.; Sato, Y.; Naganuma, K.; Kaneko, Y.
https://doi.org/10.35789/fib.BULL.0095.Ch28

Closed loop control in crushing test for fibre reinforced concrete pipes 282
Monte, R.; de la Fuente Antequera, A.; Dominigues de Figueiredo, A.
https://doi.org/10.35789/fib.BULL.0095.Ch29

Effect of synthetic fibers on the quasi-static and blast behaviour of reinforced concrete beams 292
Aoude, H.; Li, Y.; Bastami, R.; Ibrahim, F.M.
https://doi.org/10.35789/fib.BULL.0095.Ch30

This document is the intellectual property of the fib – International Federation for Structural Concrete. All rights reserved.
This PDF of fib Bulletin 95 is intended for use and/or distribution solely within fib National Member Groups.

Strain-based fatigue failure criterion for steel-fiber reinforced concrete 302
Poveda, E.; Ruiz, G.; Cifuentes, H.; Yu, R.C.; Zhang, X.X.
https://doi.org/10.35789/fib.BULL.0095.Ch31

Performance of Ductile FRCC under Cyclic Loads and Non-Linear FE Simulation 310
Antroula, G.; Stavroula, P.
https://doi.org/10.35789/fib.BULL.0095.Ch32

Cyclic Damage on PVA Microfibre Embedded in Cementitious Matrix in Alternating Tension-Compression Regime 321
Ranjbarian, M.; Mechtcherine, V.
https://doi.org/10.35789/fib.BULL.0095.Ch33

5. Service Conditions and Durability 330

Reduction of Flexural Crack Widths Using Synthetic Fibres in Reinforced Concrete 331
Bernard, E. S.
https://doi.org/10.35789/fib.BULL.0095.Ch34

Influence of chloride-initiated corrosion on the surface aspect of steel fibre reinforced cementitious composites 341
Vieira, M.M.; Cavalaro, S.H.P.; Aguado, A.
https://doi.org/10.35789/fib.BULL.0095.Ch35

Serviceability Limit State Design of SFRC Members 351
Amin, A.; Gilbert, R.I.
https://doi.org/10.35789/fib.BULL.0095.Ch36

The effect of fibres on corrosion of reinforced concrete 361
Berrocal, C.G.; Lundgren, K.; Löfgren, I.
https://doi.org/10.35789/fib.BULL.0095.Ch37

Influence of the Post-Cracking Residual Strength Variability on the Partial Safety Factor 371
de la Fuente, A.; Cavalaro, S.H.; Bairán, J.M.
https://doi.org/10.35789/fib.BULL.0095.Ch38

This document is the intellectual property of the fib – International Federation for Structural Concrete. All rights reserved.
This PDF of fib Bulletin 95 is intended for use and/or distribution solely within fib National Member Groups.

Comparability of bond tests for repair and retrofit of concrete structures with Fiber Reinforced Concrete 381
Zanotti, C.; Randl, N.; Gar, P.S.; Far, B.K.; Steiner, M.
https://doi.org/10.35789/fib.BULL.0095.Ch39

Characterization and Prediction of Microcracking in Reinforced UHPFRC Beams under Bending 391
Turgeon-Mallette, V.; Sorelli, L.; Conciatori, D.; Réthore, J.
https://doi.org/10.35789/fib.BULL.0095.Ch40

Investigation of fiber effect on the geometrical property of crack and water permeability of cracked concrete 401
Ding, Y.;Li, D.; Zeng, W.
https://doi.org/10.35789/fib.BULL.0095.Ch41

Evaluation of Effective Moment of Inertia for Calculation of Short-Term Deflections of Steel Fiber Reinforced Concrete Flexural Members 411
Fargier-Gabaldon, L.B.; Al-Tameemi, M.; Parra-Montesinos, G.J.
https://doi.org/10.35789/fib.BULL.0095.Ch42

6. Structural Applications and Rehabilitation 421

Experimental Investigation of Hybrid Concrete Elements with Varying Fiber Reinforcement under Concentrated Load 422
Plückelmann, S.; Breitenbücher, R.
https://doi.org/10.35789/fib.BULL.0095.Ch43

The behaviour of concrete columns confined by UHP-FRCC jacketing 432
Fantilli, A.P.; Nishiwaki, T.; Lisi, V.; Longo, M.
https://doi.org/10.35789/fib.BULL.0095.Ch44

A holistic calculation and design tool for structural SFRC members 442
Look, K.; Mark, P.
Longo, M.
https://doi.org/10.35789/fib.BULL.0095.Ch45

FRCcalc - Software for design of fiber reinforced concrete elements according to MC2010 recommendations 452
Valente, T.; Barros, J.; Lourenço, L.
https://doi.org/10.35789/fib.BULL.0095.Ch46

This document is the intellectual property of the fib – International Federation for Structural Concrete. All rights reserved.
This PDF of fib Bulletin 95 is intended for use and/or distribution solely within fib National Member Groups.

Retrofitting a full-scale two-story hollow clay block masonry building by Steel Fiber Reinforced Mortar coating 462
Lucchini, S.S.; Facconi, L.; Minelli, F.; Plizzari, G.A.
https://doi.org/10.35789/fib.BULL.0095.Ch47

7. HPFRC 473

Structural behavior of prestressed Ultra-High Performance Fibre-Reinforced Concrete beams with and without openings: comparison between experimental results and finite element modelling techniques. 474
Redaelli, D.; Nseir, J.Y.
https://doi.org/10.35789/fib.BULL.0095.Ch48

Use of a Probabilistic Explicit Cracking Model for Analysing the mechanical behaviour of an Ultra-High Performance Fibre Reinforced Concrete (UHPFRC) Beam Subjected to Shear Loading 484
Rossi, P.; Davian-Desnoyers, D.; Tailhan, J.L.
https://doi.org/10.35789/fib.BULL.0095.Ch49

UHPFRC Precast slabs and field-cast joints of the Isabey-Darnley pedestrian bridge 494
Charron, J.P.; Desmettre, C.; Cantin Bellemare, E.
https://doi.org/10.35789/fib.BULL.0095.Ch50

Practical considerations on the application of the recent SIA 2052 guidelines on testing of Ultra-high-performance fiber-reinforced concrete 504
Loser, R.; Justs, J.; Lura, P.
https://doi.org/10.35789/fib.BULL.0095.Ch51

Effect of Fibers on the Flexural Behaviour of Beams Built with High-Strength Concrete and High-Strength reinforcement 514
Bastami, R.; Li, Y.; Algassem, O.; Aoude, H.
https://doi.org/10.35789/fib.BULL.0095.Ch52

Fiber effect on shear behavior of UHPC beams 524
Randl, N.; Mészöly, T.
https://doi.org/10.35789/fib.BULL.0095.Ch53

This document is the intellectual property of the fib – International Federation for Structural Concrete. All rights reserved.
This PDF of fib Bulletin 95 is intended for use and/or distribution solely within fib National Member Groups.

1) MECHANICAL CHARACTERIZATION

This document is the intellectual property of the fib – International Federation for Structural Concrete. All rights reserved.
This PDF of fib Bulletin 95 is intended for use and/or distribution solely within fib National Member Groups.
FRC2018: Fibre Reinforced Concrete: from Design to Structural Applications
Joint ACI-*fib*-RILEM International Workshop

Round-Robin Test on Various Test-Methods for Flexural Behavior of Steel Fiber Reinforced Sprayed Concretes

Sven Plückelmann[1], Rolf Breitenbücher[1]

[1] : Ruhr University Bochum, Institute of Building Materials, Bochum, Germany.

Abstract

According to the actual European standard EN 14487-1 the potential of steel fiber reinforced sprayed concrete is characterized by flexural strength tests (first peak, ultimate and residual). In most cases, this is performed by a four-point bending test on beam specimens, specified in EN 14488-3. As an alternative test method, a three-point bending test on square panels with notch is recommended by EFNARC. It is argued as main benefit of the latter test method, that the geometry and dimensions of the panels are equal to those of specimens used for measuring the energy absorption capacity according to EN 14488-5. Hence, the specification of the ductility of fiber reinforced concretes according to EN 14487-1 in terms of residual strength and energy absorption capacity can be achieved preparing only one type of specimen. Furthermore, the EFNARC guideline points out a smaller scatter of test results, compared to the beam tests according to EN 14488-3.

Before the EFNARC method will be considered in EN 14487-1, the relevant CEN TC 104/WG10 requests for adequate proofs. These were performed within a round-robin test (RRT) on testing the flexural behavior of steel fiber reinforced sprayed concrete by the standardized EN 14488-3 method as well as by the proposed EFNARC method. The aim of this RRT was to investigate the comparability and correlation between the two test methods. Furthermore, the scatter of both methods was assessed. The RRT has been organized by Ruhr University Bochum, in whose labs the steel fiber reinforced sprayed concrete specimens (beams according to EN 14488-3 and square panels according to EFNARC guideline) were produced using a robotic spraying machine. The specimens were then tested in five independent laboratories Europe-wide. The results of this RRT are presented in detail. With regard to the residual strength, the relevant material parameter for steel fiber reinforced sprayed concrete, a tendency towards a slightly lower scatter was detected for the EFNARC test method.

Keywords

Sprayed concrete, steel fibers, round-robin test, flexural behavior

This document is the intellectual property of the fib – International Federation for Structural Concrete. All rights reserved.
This PDF of fib Bulletin 95 is intended for use and/or distribution solely within fib National Member Groups.

1 Introduction

The specification of the ductility of fiber reinforced sprayed concrete according to EN 14487-1 is ascertained by the classification of its residual strengths and/or energy absorptions capacity. In most cases, the residual strengths will be determined if the concrete characteristics are used in a structural design model. According to EN 14487-1, the determination of flexural strengths has to be performed by a four-point bending test on beam specimens specified in EN 14488-3. The residual strengths are classified by a minimum strength level defined for specific intervals of deflection according to EN 14487-1.

With regard to the main field of application of fiber reinforced concrete (i.e. rock stabilization in tunneling) further information concerning the concrete's energy absorption capacity can be essential. The energy absorption capacity has to be determined by performing a bending test on square panels, which are supported on their four edges and loaded centrically with a point load. This test method is specified in EN 14488-5 and was developed by the "National Rail-way Company (SNCF)" in order to simulate the typical loading scenario in terms of biaxial bending. By analogy to the classification of residual strengths, the energy absorption classes are also defined in EN 14487-1.

In EN 14487-1 it is explicitly pointed out that a direct comparison between the two different methods for the specification of ductility by means of residual strengths and energy absorption capacity is not feasible. Depending on project-specific requirements related to the quality of the concrete it could be necessary to perform both test methods. Consequently, in this case, two different types of specimens have to be prepared and tested under different testing conditions.

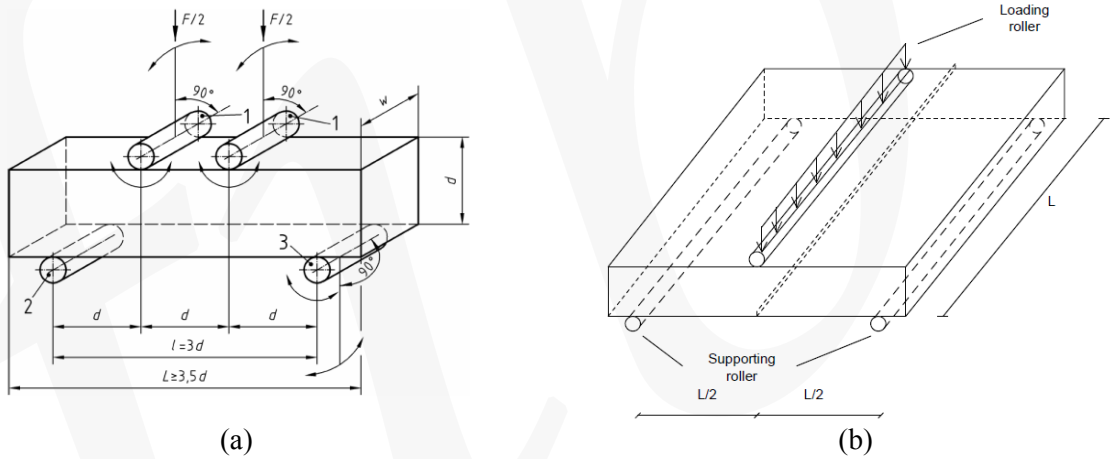
As an alternative test method to the four-point bending test on beams according to EN 14488-3, a three-point bending test on square panels with notch is recommended by EFNARC. The respective guideline was published in 2011. In this guideline, a series of arguments for performing the EFNARC method instead of the EN 14488-3 method are indicated. As an example, it is argued as main benefit of the EFNARC test method, that the geometry and dimensions of the panels are equal to those of specimens used for measuring the energy absorption capacity according to EN 14488-5. Hence, only one type of specimen has to be prepared for the determination of both material characteristics. Moreover, the EFNARC guideline points out a smaller scatter of test results compared to the beam tests according to EN 14488-3. However, if the scatter of results within the EFNARC test method is lower compared to the EN 14488-3 method remains to be examined, particular as in both guidelines it is noted that there is a lack of information in terms of precision. Even though it is a matter of fact, before the EFNARC test method will be considered in EN 14487-1, the relevant CEN TC 104/WG10 requests for adequate proofs. These were performed within a round-robin test (RRT) on testing the flexural behavior of steel fiber reinforced sprayed concrete by the standardized EN 14488-3 method as well as by the proposed EFNARC method. The aim of this RRT, that was organized and coordinated by the Institute for Building Materials of the Ruhr University Bochum, was to investigate the comparability and correlation between the two test methods. Furthermore, the scatter of both methods was assessed.

This document is the intellectual property of the fib – International Federation for Structural Concrete. All rights reserved.
This PDF of fib Bulletin 95 is intended for use and/or distribution solely within fib National Member Groups.

2 Test methods

The flexural strengths (first peak, ultimate and residual) according to EN 14488-3 are determined by testing beam specimens with dimensions of 75 (height) × 125 (width) × 500 (min. length) mm³, cut from sprayed panels. The beams are tested in a four-point bending test setup (Figure 1a), whereby the total span length (distance between supporting rollers) is 450 mm and the distance between the loading rollers is 150 mm. The applied load is measured as a function of deflection.

According to EFNARC, the flexural strengths (limit of proportionality, ultimate and residual) are determined by performing a three-point bending test on notched panel specimens with dimensions of 600 (width) × 600 (length) × 100 (height) mm³. The span length is 500 mm (Figure 1b). The notch depth is 10 mm and correspondingly, the effective cross section in the mid-span (h_{sp}) is 90 mm. The panels should be prepared by levelling its surface at a panel thickness of 100 mm immediately after spraying. By analogy to EN 14651, the test method for metallic fiber concrete, the load-crack mouth displacement (CMOD) curve is recorded.



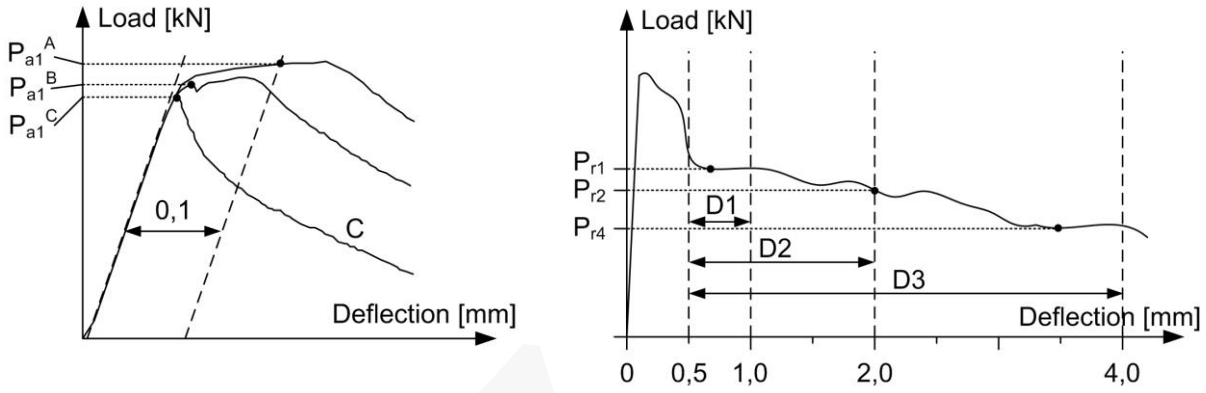
(a) (b)

Figure 1: Test setup according to EN 14488-3 (a) and according to EFNARC (b)

For both test methods, the ultimate flexural strength f_{ult} is calculated from the maximum load P_{ult}/F_{ult}. According to EN 14488-3, the first peak strength f_{fp} is calculated from the first peak load P_{a1}, corresponding to first crack formation, as shown in Figure 2a. In consistency with the residual strength classes defined in EN 14487-1, the residual strengths (f_{r1}, f_{r2}, f_{r4}) are calculated from the minimum loads (P_{r1}, P_{r2}, P_{r4}) of the load-deflection curves that lie within the intervals D1 (0,5 mm – 1 mm), D2 (0,5 mm – 2 mm) and D3 (0,5 mm – 4 mm) (Figure 2b).

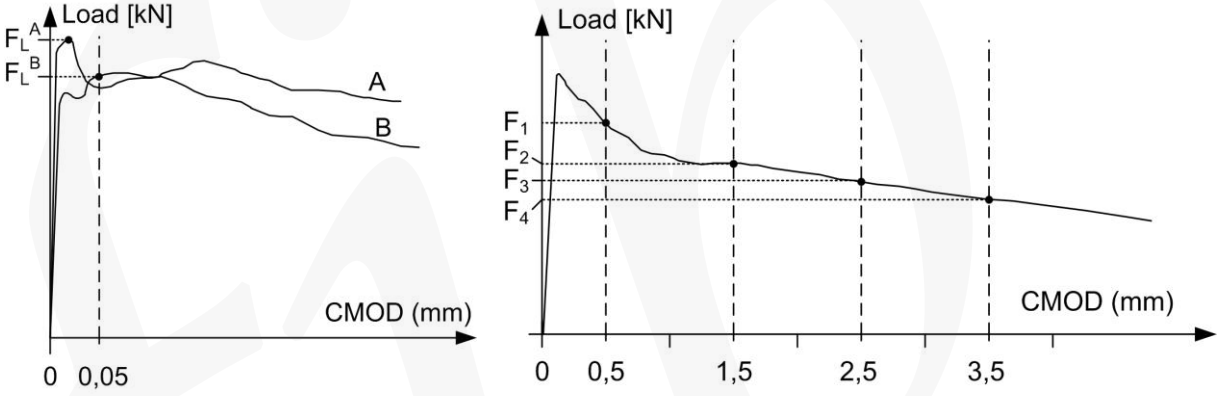
In case of the EFNARC test method, the LOP $f_{ct,L}$ is calculated from the maximum load F_L recorded in the CMOD interval between 0 mm and 0.05 mm (Figure 3a). As illustrated in Figure 3b, the residual strengths (f_{R1}, f_{R2}, f_{R3}, f_{R4}) are calculated from the loads F_j (j=1, 2, 3, 4) corresponding with $CMOD_j$ (j=1, 2, 3, 4). Note that the classification of the residual strengths according to EN 14487-1 is not feasible, because the residual strengths classes are not conform to the definition of the residual strengths according to EFNARC.

This document is the intellectual property of the fib – International Federation for Structural Concrete. All rights reserved.
This PDF of fib Bulletin 95 is intended for use and/or distribution solely within fib National Member Groups.



(a) (b)

Figure 2: First peak load P_{fp} (a) and loads P_{ri} for the determination of residual strength (b) according to EN 14488-3



(a) (b)

Figure 3: Load F_L for the determination of the LOP (a) and load F_j for the determination of residual strengths according to EFNARC

3 Round-Robin Test (RRT)

3.1 General

In order to investigate the comparability and correlation between the two test methods and to determine the scatter, a round-robin test (RRT) was conducted within the scope of TC 104/WG10. The RRT has been organized by the Institute for Building Materials, Ruhr University Bochum. In whose labs the steel fiber reinforced sprayed concrete specimens were produced using a robotic spraying machine. The specimens were then tested in five independent laboratories Europe-wide.

3.2 Materials

The test specimens (beams according to EN 14488-3 and panels according to EFNARC) were produced by spraying a wet-mix concrete. The base-mix design of the sprayed concrete aimed at strength class C30/37 is listed in Table 1. An ordinary Portland cement (450 kg/m³ CEM I 42.5 R) was used at a water-cement-ratio of 0.45. The base-mix contained 1600 kg/m³ of aggregates with a maximum grain size of 8 mm. The fiber content was 50 kg/m³ and the

This document is the intellectual property of the fib – International Federation for Structural Concrete. All rights reserved.
This PDF of fib Bulletin 95 is intended for use and/or distribution solely within fib National Member Groups.

characteristics of the steel fibers used are listed in Table 2. The dosage of accelerator was set to 5.5 % relative to the content of cement, in order to enable the surface leveling immediately after spraying execution, in case of preparing panels (cf. chapter 3.3).

Table 1: Base-mix design of sprayed concrete

Constituents	**Unit**	**Content**
Cement (CEM I 42.5 R)	[kg/m³]	450
Aggregates (sand, gravel) (grading curve ~ B8)	[kg/m³]	1600
Steel fiber (DRAMIX 3D 65/35 BG)	[kg/m³]	50
Water	[kg/m³]	202.5
w/c-ratio	[-]	0.45
Superplasticizer (PCE)	[%]	0.56
Retarder	[%]	0.4
Injection at the nozzle: Accelerator (alkali-free)	[%]	5.5

Table 2: Characteristic of steel fibers

Characteristics	**Unit**	**DRAMIX 3D 65/35 BG**
Shape	[-]	end-hooked
Length	[mm]	35
Diameter	[mm]	0.55
Slenderness (l/d)	[-]	65
Tensile strength f_t	[MPa]	1345

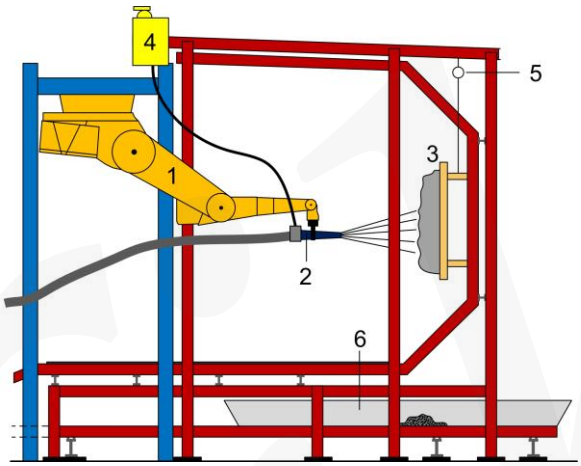
3.3 Production and preparation of test specimens

The wet-mix concrete was sprayed by using the robotic spraying machine available at Ruhr-University Bochum in order to simulate practical and realistic conditions, similar to a real tunnel construction site. This robotic spraying machine allows for a minimization of manual influences on the quality of sprayed concrete, which could have a negative influence on the reproducibility of results. Figure 4 illustrates a schematic description of the sprayed concrete testing rig in the laboratory of Ruhr University Bochum.

Ready-mixed concrete (base-mix, see Table 1) was transported from a local concrete plant to the laboratory (RUB). The concrete was pumped to the robot and sprayed through the nozzle (Ø42 mm) onto the wooden baseplate. During spraying execution, the robot followed a programmed pattern of vertical and horizontal movements including nozzle oscillations. The spraying distance was approximately 1.0 m, similar to typical field scenarios. In the case of preparing panels according to EFNARC, the sprayed concrete on the baseplate was leveled to the required thickness of 100 mm by screeding its surface with a steel profile immediately after the spraying execution. According to ENFARC, any subsequent surface treatment (e.g. grinding, saw cutting etc.) of the hardened sprayed concrete is not permitted. For this reason, the dosage of accelerator had to be adjusted to ensure that on the one hand, the solidification process of the concrete has progressed so far that the concrete was stable enough to stuck on the vertical baseplate, and on the other hand, that the screeding of the surface after spraying execution was still possible. In the case of preparing the EN 14488-3 beams, a surface

This document is the intellectual property of the fib – International Federation for Structural Concrete. All rights reserved.
This PDF of fib Bulletin 95 is intended for use and/or distribution solely within fib National Member Groups.

leveling was not necessary. After spraying (and leveling), the sprayed concrete was covered with wet jute and plastic membrane and cured for 24 hours. Afterwards, the specimens were cut from shotcrete baseplate. The panels were notched by using a saw with a diamond blade. The prepared specimens were then stored in a fog room (relative air humidity: ≥95 %, temperature of 20±2 °C) and cured for 7 days. Afterwards, the specimens were stored at a temperature of 20±2 °C and a relative air humidity of 65±5 % until shipping to the participating laboratories.

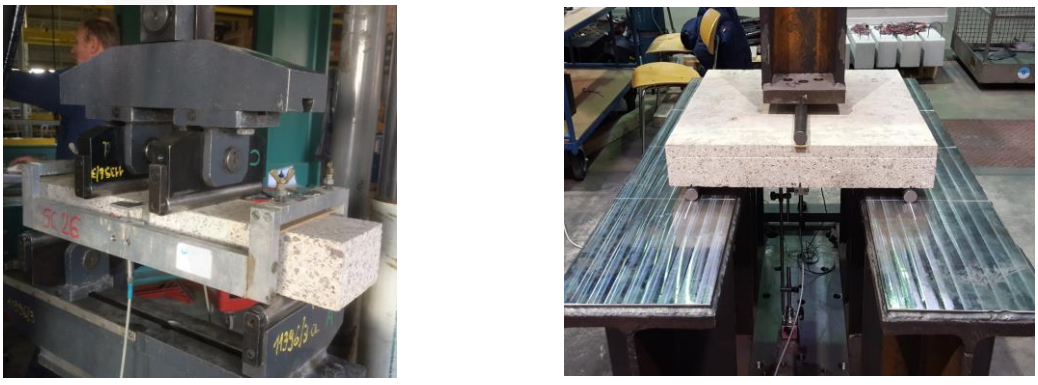


LEGEND
1 Robot
2 Nozzle
3 Palette with sprayed concrete
4 Accelerator reservoir
5 Weighing scale
6 Rebound collection

Figure 4: Schematic description of the sprayed concrete testing rig (RUB)

3.4 Flexural tests

Until performing the flexural tests, the specimens were stored under water for one week within the respective laboratories, in order to avoid residual stresses due to shrinkage. In each laboratory 3 beams and 4 panels were tested (In total: 15 beams/20 panels). The allocation of specimens to the respective laboratories was random. The age of the sprayed concrete at the time of testing was 60 ± 2 days. The participating laboratories were obliged to follow the normative specifications as strict as possible. Figure 5 shows the test setup of the 4-point bending test on beams according to EN 14488-3 (a) and the 3-point bending test according to EFNARC (b).



(a) (b)

Figure 5: Test setup of 4-point bending test on beams according to EN 14488-3 (a) and 3-point bending test on square panels with notch according to EFNARC (b)

This document is the intellectual property of the fib – International Federation for Structural Concrete. All rights reserved.
This PDF of fib Bulletin 95 is intended for use and/or distribution solely within fib National Member Groups.

4 Results

4.1 General characteristics of fresh and hardened concrete

In order to ensure a good pumpability, a flowable consistency of the ready-mixed concrete was required. This requirement was achieved by adding PCE-superplasticizer in the concrete plant (see Table 1). Depending on the actual transport time of the concrete truck and its discharge time, the consistency, immediately before spraying execution, was between 620 mm and 540 mm (flow table test according to EN 12350-5). The general characteristics of the fresh concrete (i.e. base-mix) are listed in Table 3. The fiber content of the base-mix was measured in a non-destructive way by means of a special test device based on the principle of electromagnetic induction (Breitenbücher and Rahm, 2009). It was between 46 kg/m³ and 53 kg/m³. The targeted strength class C30/37 was proved by conformity check on cube specimens casted with the base-mix according to EN 206 ($f_{cm,cube}$=46 MPa). The mean value of the compressive strength of the sprayed concrete determined on drilling cores taken from the spayed concrete base plates at the time of testing the flexural strengths was 55 MPa.

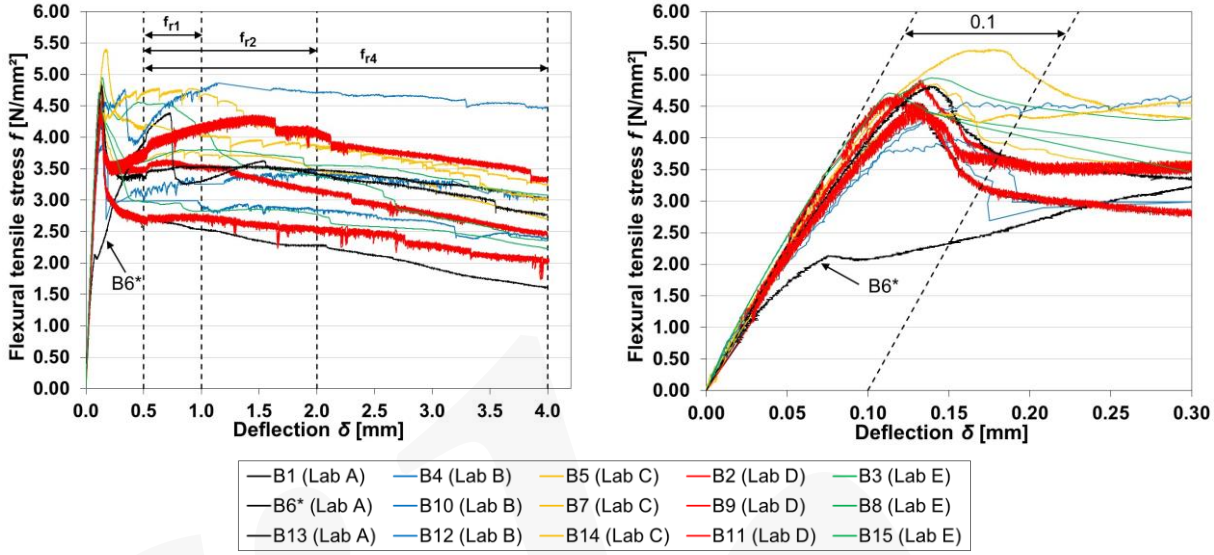
Table 3: General characteristics of the fresh concrete (base-mix)

Characteristic	**Unit**	**Test-Method**	**Mean value**
Consistency	[mm]	EN 12350-5	580
Bulk density	[kg/dm³]	EN 12350-6	2.301
Air void content	[vol.-%]	EN 12350-7	2.1

4.2 Flexural strengths according to EN 14488-3 and EFNARC

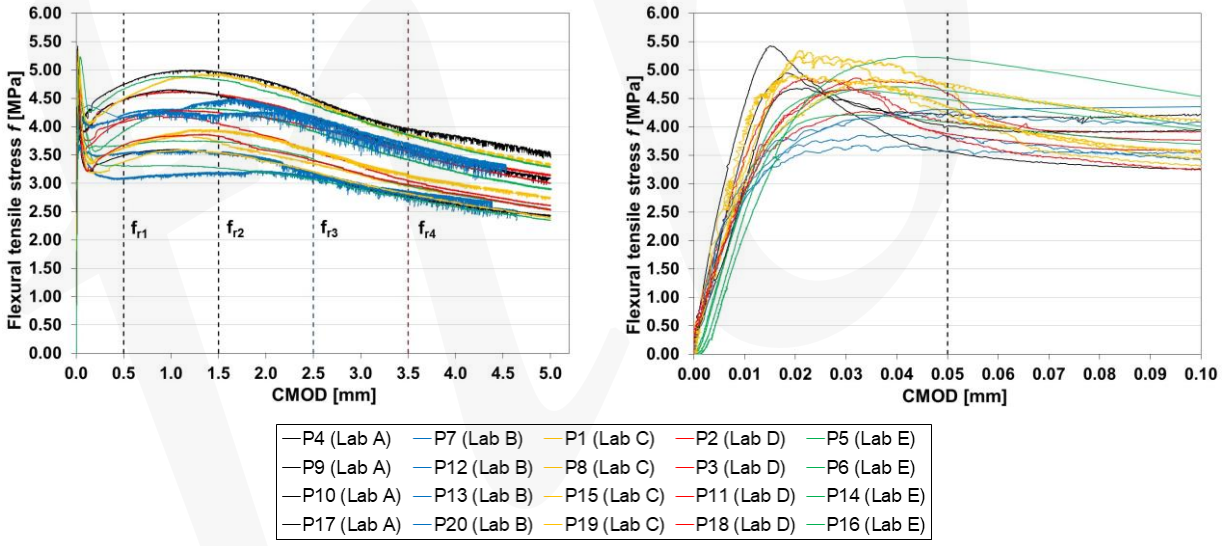
In Figure 6 and Figure 7 the stress-deflection and stress-CMOD curves of all specimens (beams according to EN 14488-3: B1-15; panels according to EFNARC: P1-20) tested within the RRT and the respective laboratories (Lab A-E) are illustrated. These stress-displacement curves feature the characteristic shape for steel fiber reinforced concrete under bending load. The specimens are characterized by a linear stress-displacement behavior in the pre-peak branch. It can be seen, that the initial structural behavior of the beams and panels is very similar, respectively. After reaching the first stress peak (first peak strength f_{fp}/LOP $f_{ct,L}$), accompanied by first crack formation, a sudden drop of the curves can be observed. With increasing deformation, the load-bearing capacity persists due to the load transfer of the crack bridging fibers. This ductile post-cracking behavior is characterized by the more or less horizontal shape of the curves in the post-cracking zone. The stress-CMOD curves of the panels clearly show a further stress increase in the post-cracking zone. This increase leads to a second stress maximum in the range between 0.5 mm ≤ CMOD ≤ 2.0 mm followed by a gradual slope with increasing deformation. The stress-deflection curves of the beams partially also exhibit a stress increase in the post-cracking zone. Compared to the stress-CMOD curves of the panels, most of the stress-deflection curves of the beams are characterized by an unsteady and jagged development in the post-cracking zone. Hence, an exact range of deformation for the stress maximum in the post-cracking zone cannot be located considering all curves. However, from a global point of view, a gradual slop in the post-cracking zone can be observed, too. The smoother and even more regular development of the stress-CMOD curves compared to the stress-deflection curves is mainly attributed to the fact that more fibers were intersecting the crack area in the case of the panels due to their larger cross-sections.

This document is the intellectual property of the fib – International Federation for Structural Concrete. All rights reserved.
This PDF of fib Bulletin 95 is intended for use and/or distribution solely within fib National Member Groups.



(a) (b)

Figure 6: Stress-deflection curves of beam specimens according to EN 14488-3 in the interval of [0 mm – 4.0 mm] (a) and [0 mm – 0.30 mm] (b)



(a) (b)

Figure 7: Stress-CMOD curves of panel specimens according to EFNARC in the interval of [0 mm – 5.0 mm] (a) und [0 mm – 0.10 mm] (b)

The flexural tensile strengths (first peak/LOP, ultimate and residual) were calculated from the presented stress-displacement curves of the beams and panels (cf. chapter 2). The total mean values MV, standard deviations s and variation coefficients v were determined and are listed in Table 4 and Table 5. It should be noted, that beam specimen B6* showed an unrepresentative characteristic in the pre-peak branch of the stress-deflection curve (see Figure 6b). It appears that this beam has been pre-damaged, possibly during transport delivery. Hence, beam specimen B6* was excluded from the calculation.

This document is the intellectual property of the fib – International Federation for Structural Concrete. All rights reserved.
This PDF of fib Bulletin 95 is intended for use and/or distribution solely within fib National Member Groups.

Table 4: Flexural strengths of beam specimens according to EN 14488-3

Flexural strength	**Mean value *MV* [N/mm²]**	**Standard deviation *s* [N/mm²]**	**Variation coefficient *v* [%]**
Ultimate strength f_{ult}	4.68	0.33	7.1
First peak strength f_{fp}	4.65	0.34	7.4
Residual strength f_{R1}	3.45	0.62	17.8
Residual strength f_{R2}	3.26	0.52	16.0
Residual strength f_{R4}	2.75	0.61	22.2

Table 5: Flexural strengths of panel specimens according to EFNARC

Flexural strength	**Mean value *MV* [N/mm²]**	**Standard deviation *s* [N/mm²]**	**Variation coefficient *v* [%]**
Ultimate strength f_{ult}	4.70	0.48	10.2
LOP $f_{ct,L}$	4.68	0.49	10.4
Residual strength f_{R1}	3.93	0.49	12.5
Residual strength f_{R2}	4.07	0.55	13.4
Residual strength f_{R3}	3.73	0.49	13.2
Residual strength f_{R4}	3.26	0.43	13.0

Interestingly, despite different specimen geometrics and test conditions, the total mean values of the ultimate flexural strengths of the beams ($f_{ult,beams,MV}$=4.68 MPa) and panels ($f_{ult,panels,MV}$=4.70 MPa) are almost identical (cf. Table 4 and Table 5). However, the total scatter of the ultimate flexural strengths it slightly larger for the panels ($s_{panels}(f_{ult})$=0.48 MPa, $v_{panels}(f_{ult})$=10.8 %) compared to the beams ($s_{panels}(f_{ult})$=0.33 MPa, $v_{panels}(f_{ult})$=7.1 %). This could be attributed to the predefined crack location caused by the notch in the case of panel specimens. The absolute as well as statistical mean values of the first peak strengths f_{fp} and LOPs $f_{ct,L}$ differ only marginally from those of the ultimate flexural strengths f_{ult} (cf. Table 4 and Table 5). This is mainly attributed to the subcritical fiber content of 50 kg/m³. As a result, the post-cracking stresses do not exceed the first peak stresses. In some exceptional cases of both test methods, the post-cracking stresses exceed the first peak stresses. However, in these cases, they were only very slightly lager ($\Delta_{max,beams}=f_{ult} - f_{fp}$=0.4 MPa, $\Delta_{max,panels}=f_{ult} - f_{ct,L}$=0.22 MPa). For these cases, it could be expected that the distribution and orientation of steel fibers in the cracked area of the specimens was comparatively favorable.

In Table 4 and Table 5 it can be seen, that the residual strengths determined for the beams ($f_{R1,MV}$=3.45 MPa, $f_{R2,MV}$=3.26 MPa, $f_{r4,MV}$=2.75 MPa) are slightly lower than the residual strengths of the panels ($f_{R1,MV}$=3.93 MPa, $f_{R2,MV}$=4.07 MPa, $f_{r3,MV}$=3.73 MPa, $f_{r4,MV}$=3.26 MPa). The total scatter of the residual strengths is larger compared to the scatter of the ultimate strengths as well as first peak strengths and LOPs, respectively. Comparing the total standard deviations or variation coefficients of residual strengths it can be seen, that the scatter of results for the beams tested according to EN 14488-3 (0.52 MPa $\leq s(f_{Ri,beams,MV}) \leq$ 0.62 MPa, 16.0 % $\leq v(f_{Ri,beams,MV}) \leq$ 22,2 %) were somewhat larger than for panels tested according to EFNARC (0.43 MPa $\leq s(f_{Ri,panels,MV}) \leq$ 0.55 MPa, 12.5 % $\leq v(f_{Ri,panels,MV}) \leq$ 13.4 %). However, it should be noted that a direct comparison between the absolute as well as the statistical values of the residual strengths of the beams and panels is unfeasible due to their different definitions (cf. chapter 2).

This document is the intellectual property of the fib – International Federation for Structural Concrete. All rights reserved.
This PDF of fib Bulletin 95 is intended for use and/or distribution solely within fib National Member Groups.

5 Concluding remarks

The results of the RRT presented in the present paper allow to draw the main concluding remarks listed in the following.

1. With regard to the total mean values of ultimate strengths as well as first peak strengths and LOPs, the test results showed an almost exact correlation between the test methods. The total scatter of ultimate strengths as well as first peak strengths and LOPs was slightly larger for the EFNARC test method compared to the EN 14488-3 method.
2. The total mean values of residual strengths determined according to EN 144883-3 were slightly lower than these determined according to EFNARC. The total scatter of residual strengths was somewhat larger for the EN 14488-3 method compared to the EFNARC method. However, a direct comparison between the absolute as well as the statistical values of the residual strengths of the beams and panels is unfeasible due to their different definitions.
3. All in all, it can be stated that there are no significant differences concerning the scatter of results. Hence, it is quite conceivable that the EFNARC method would be considered in EN 14487-1. However, the classification of residual strengths according to EN 14487-1 needs to be adapted.
4. For a final evaluation of both test methods, further comparative studies (i.e. larger numbers of test specimens, variation of fiber content and fiber types etc.) are necessary.

6 Acknowledgements

The Authors would like to give their appreciation to the laboratories participating in the Round-Robin Test (Belgian Building Research Institute, Sigma béton, Global Product Innovation Italcementi S.p.A – Heidelberg Cement Group, Technical University of Munich) and to Bekaert-Maccaferri Underground Solutions BVBA for financial support.

7 References

Breitenbücher, R., Rahm, H. (2009). *Zerstörungsfreie Bestimmung des Stahlfasergehalts und der Stahlfaserorientierung im Frisch- und Festbeton: Neues Prüfverfahren – Messgenauigkeit und Reproduzierbarkeit.* Beton, Issue 58, No. 3 (2009), pp. 88-93.

EFNARC (2011). *Testing sprayed concrete – EFNARC three point bending test on square panel with notch – Flexural tensile strength of fibre reinforced concrete on sprayed test specimen*, June 2011

EN 206 (2016). *Concrete - Specification, performance, production and conformity.*

EN 12350-5 (2009). *Testing fresh concrete – Part 5: Flow table test.*

EN 12350-6 (2009). *Testing fresh concrete – Part 6: Density.*

EN 12350-7 (2009). *Testing fresh concrete – Part 7: Air content – Pressure methods.*

EN 14487-1 (2005). *Sprayed concrete – Part 1: Definitions, specifications and conformity.*

EN 14488-3 (2006). *Testing sprayed concrete – Part 3: Flexural strengths (first peak, ultimate and residual) of fibre reinforced beam specimens.*

EN 14488-5 (2006). *Testing sprayed concrete – Part 5: Determination of energy absorption capacity of fibre rein-forced slab specimens.*

EN 14651 (2005). *Test method for metallic fibre concrete – Measuring the flexural tensile strength (limit of proportionality (LOP), residual).*

This document is the intellectual property of the fib – International Federation for Structural Concrete. All rights reserved.
This PDF of fib Bulletin 95 is intended for use and/or distribution solely within fib National Member Groups.
FRC2018: Fibre Reinforced Concrete: from Design to Structural Applications
Joint ACI-*fib*-RILEM International Workshop

A new multi-scale hybrid fibre reinforced cement-based composites

Li Li[1,2], Mingli Cao[2]

[1] : Northwest A&F University, Yangling, China.

[2] : Dalian University of Technology, Dalian, China.

Abstract

Nowadays polyvinyl alcohol (PVA) and steel hybrid fibre reinforced cement-based composites (HFRCC) are studied to resist static, seismic and impact loading. In this research, calcium carbonate (CaCO3) whisker is introduced to develop a multi-scale HFRCC, with 35mm hooked end steel fibre, 6mm PVA fibre and CaCO3 whisker. The compressive and flexural behaviors of the new HyFRCC are explored. Compared to the conventional hybrid fibers (steel fibre and PVA fibre), the addition of multi-scale fibres (steel fibre, PVA fibre and CaCO3 whisker) can improve the compressive strength and toughness of cement-based composite. Multi-scale fibre usage leads to notable increase to both the flexural strength and flexural toughness values of cement-based composite. Based on these test results, we can conclude that there is a remarkable fiber synergy in multi-scale hybrid fibre reinforced cement-based composites with 35mm hooked end steel fibre, 6mm PVA fibre and CaCO3 whisker. Moreover, it seems possible that the steel fibres and PVA fibres can be partly replaced by CaCO3 whiskers, which is very beneficial in decreasing the production cost of HFRCC for potential structural applications.

Keywords

Multi-scale hybrid fibre, $CaCO_3$ whiskers, compressive behavior, flexural behavior

This document is the intellectual property of the fib – International Federation for Structural Concrete. All rights reserved.
This PDF of fib Bulletin 95 is intended for use and/or distribution solely within fib National Member Groups.

1 Introduction

Conventional cement-based composites are very brittle materials and the failure of cement-based composites is a progressive and multilevel process, pre-existing or newborn micron-cracks grow to meso-cracks and macro-cracks. Eventually, the macro-cracks lead to the fracture (Banthia & Soleimani, 2005; Nguyen et al., 2012; Bentz, 2000). In this sense, combination of fibres with different sizes and constitutions is generally drawn into cement-based composites to restrict the growth of cracks at different stages in the failure process and improve its mechanical properties. Unfortunately, traditional hybrid fibres can hardly delay micro crack initiation and propagation because of the relatively large length and diameter (Li et al., 2015; Parveen et al., 2013).

For a few years, the authors have worked on the development of a new hybrid fibre reinforced cement-based composites (HFRCC), including steel, polyvinyl alcohol (PVA) fibre and calcium carbonate ($CaCO_3$) whisker. Compared with conventional HyFRCC (only including steel and PVA fibres) (Soe et al., 2013), the steel and PVA fibres were partly replaced by cheaper $CaCO_3$ whiskers (approximately $236 per ton) mainly to improve the mechanical performance as well as reduce the production cost. These researches reveal that the introduction of $CaCO_3$ whisker can improve mechanical properties of HFRCC effectively by micro-reinforcement and positive fibre synergy with the meso-fibre (PVA fibre) and macro-fibre (steel fibre) (Cao, Zhang, Lv, & Xu, 2014; Cao, Zhang & Lv, 2014; Cao, Zhang & Wei, 2013). The new HFRCC could be used to strengthen and retrofit the bridge and hydraulic structures. Although previous studies presented the optimal steel, PVA fibre and whisker content for mechanical properties and economical efficiency including short steel fibre (13mm length), no information is available about the mechanical properties of this new HFRCC including long steel fibre (35mm length).

It is clearly that the shape and size of fibre have significant impact on the mechanical properties of fibre reinforced cement-based composites. Hence, the objective of this research is studying mechanical properties of this new HFRCC including long hooked end steel fibre (35mm length) in laboratory to evaluate if the excellent static behaviour of this material can be stretched to the HFRCC with longer steel fibre.

2 Experimental program

P.O 42.5R ordinary portland cement (Specific surface area: 356m^2/kg, 45μm sieve residue: 14.60%, Dalian Onoda Cement Co. Ltd.), and quartz sand (Fineness modulus: 2.51, media sand, Dalian) were used as the major ingredients in the matrix. A high performance water-reducer (Polycarboxylic acid based, water reducing ratio: 32%, Sika Co. Ltd.) was used to modify the fluid properties of mortars in 0.24–0.53% proportions of cement mass. Chemical constituents of $CaCO_3$whisker (Fengzhu Co. Ltd.) are shown in Table 1. Physical properties of steel fibre (Bekaert Co. Ltd.), PVA fibre (Wanwei Co. Ltd.) and whisker are tabulated in Table 2 and their morphologies are shown in Fig.1.

Table 1: Chemical constituents of whisker (wt.%)

CaO	**SiO_2**	**Al_2O_3**	**Fe_2O_3**	**CO_2**	**MgO**	**SO_3**
54.93	0.29	0.11	0.07	42.07	2.14	0.31

This document is the intellectual property of the fib – International Federation for Structural Concrete. All rights reserved.
This PDF of fib Bulletin 95 is intended for use and/or distribution solely within fib National Member Groups.

Table 2: Physical properties of fibres and whisker

Fibre type	**Length(mm)**	**Aspect ratio(*l*/*d*)**	**Tensile strength (MPa)**	**E-modulus (GPa)**	**Density (kg/m^3)**
Steel fibre	35	63.6	≥2 000	210	7800
PVA fibre	6	151.1	1529.5	36.7	1300
Whisker	0.02-0.03	10-60	3 000-6 000	410-710	2860

Note: Long steel fibre is hooked end steel fibre.



(a) 35mm hooked end steel fibre (b) 6mm PVA fibre (c) $CaCO_3$ whisker

Figure 1: Morphologies of fibres and whisker

Control specimens, without any fibre and whisker addition, were prepared in the light of the mixture proportioning presented in Table 3. Control specimens were used to assess the influence of fibres and whisker additions. Based on the control specimen proportioning, 5 other mix groups with different type and dosage of steel fibre, PVA fibre and whisker were made as illustrated in Table 4.

Table 3: Mix proportioning of the control specimens (kg/m^3)

Cement	**Water**	**Quartz sand**
1220	366	610

This document is the intellectual property of the fib – International Federation for Structural Concrete. All rights reserved.
This PDF of fib Bulletin 95 is intended for use and/or distribution solely within fib National Member Groups.

Table 4: Content of different fibre in HFRCC.

Group	Fibre type	Volume fraction（%）		
		Steel fibre	PVA fibre	Whisker
Pure	Plain	0	0	0
S2	35mm hooked end steel fibre and 6mm PVA fibre	2	0	0
S1.5P0.5		1.5	0.5	0
S1.5P0.4W1		1.5	0.4	1
S1.25P0.75		1.25	0.75	0
S1.25P0.55W2		1.25	0.55	2

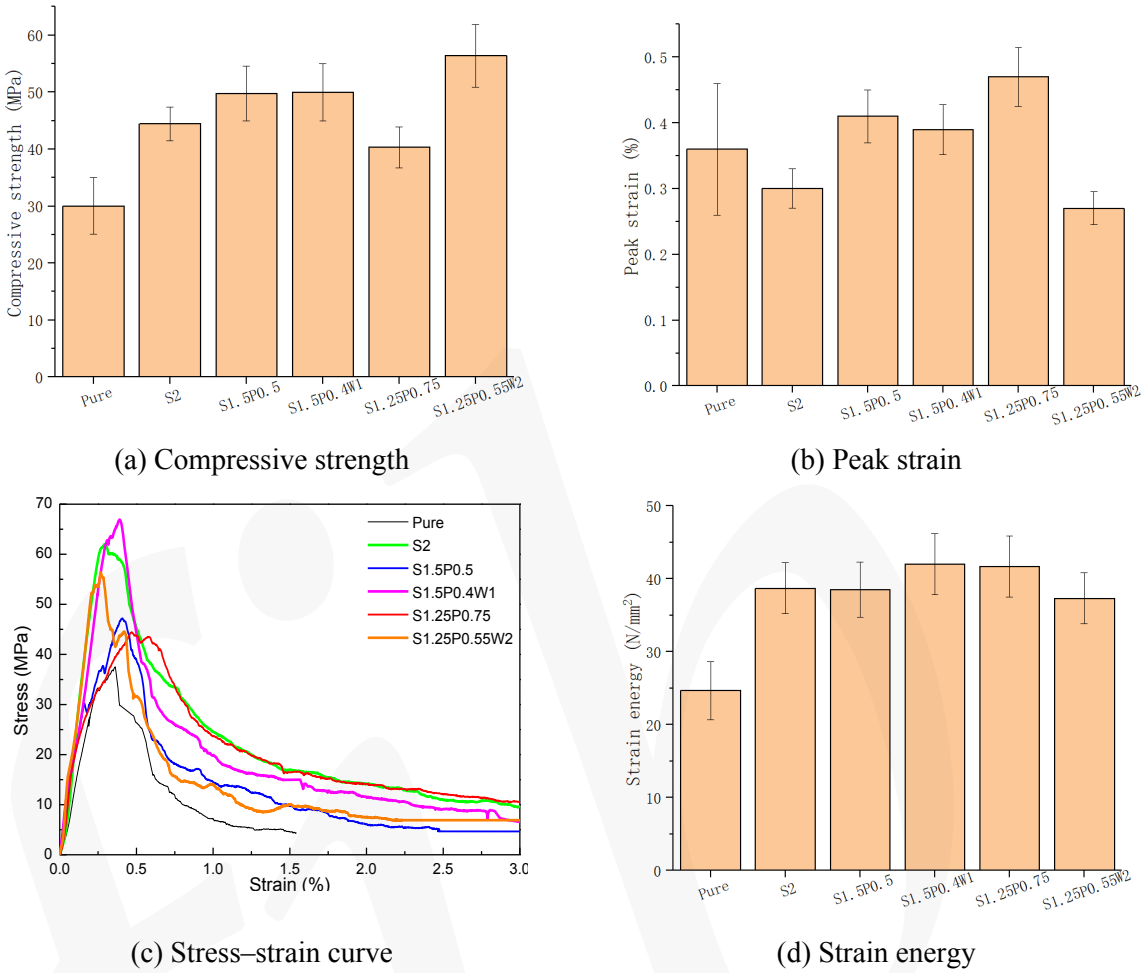
Three prismatic and three cube specimens of each group were casted, all of the results discussed in this research were the average value of the three specimens. Prismatic specimens with dimensions of 100 (width) × 100(thickness) ×400(length) mm^3 were employed to test flexural behaviour. The cylinder specimens with dimensions of Φ100 (diameter) × 200(height) mm^3 were employed to test compressive behaviours. For the flexural testing, a computer-controlled electro-hydraulic servo universal equipment of 300kN capacity was employed according to ASTM C1609/C1609M. For the compressive strength testing, a computer-controlled electro-hydraulic servo universal equipment of 2000kN capacity at a displacement rate of 1 mm/min was used according to ASTM C469/C469M.

3 Results and analysis

3.1 Compressive behaviors

The compressive strengths of all mixtures are shown as Figure 2(a). The fibre-reinforced mortars presented a higher compressive strength than that of the pure mortar. The employ of a 2% volume of steel fibre (S2) led an appreciable improvement in compressive strength. The compressive strength value of cement-based composites with steel and PVA hybrid fibres (S1.5P0.5 and S1.25P0.75) were reduced gradually as the PVA fibre amount increased. The introduction of whiskers (S1.5P0.4W1 and S1.25P0.55W2) enhanced the compressive strength of mortar with steel and PVA hybrid fibres and compressive strength of S1.5P0.4W1 was higher than S2, which was caused by the filler effect of whiskers (Cao, Zhang & Wei, 2013).

This document is the intellectual property of the fib – International Federation for Structural Concrete. All rights reserved.
This PDF of fib Bulletin 95 is intended for use and/or distribution solely within fib National Member Groups.



(a) Compressive strength (b) Peak strain

(c) Stress–strain curve (d) Strain energy

Figure 2: Compressive behaviors of various mixtures

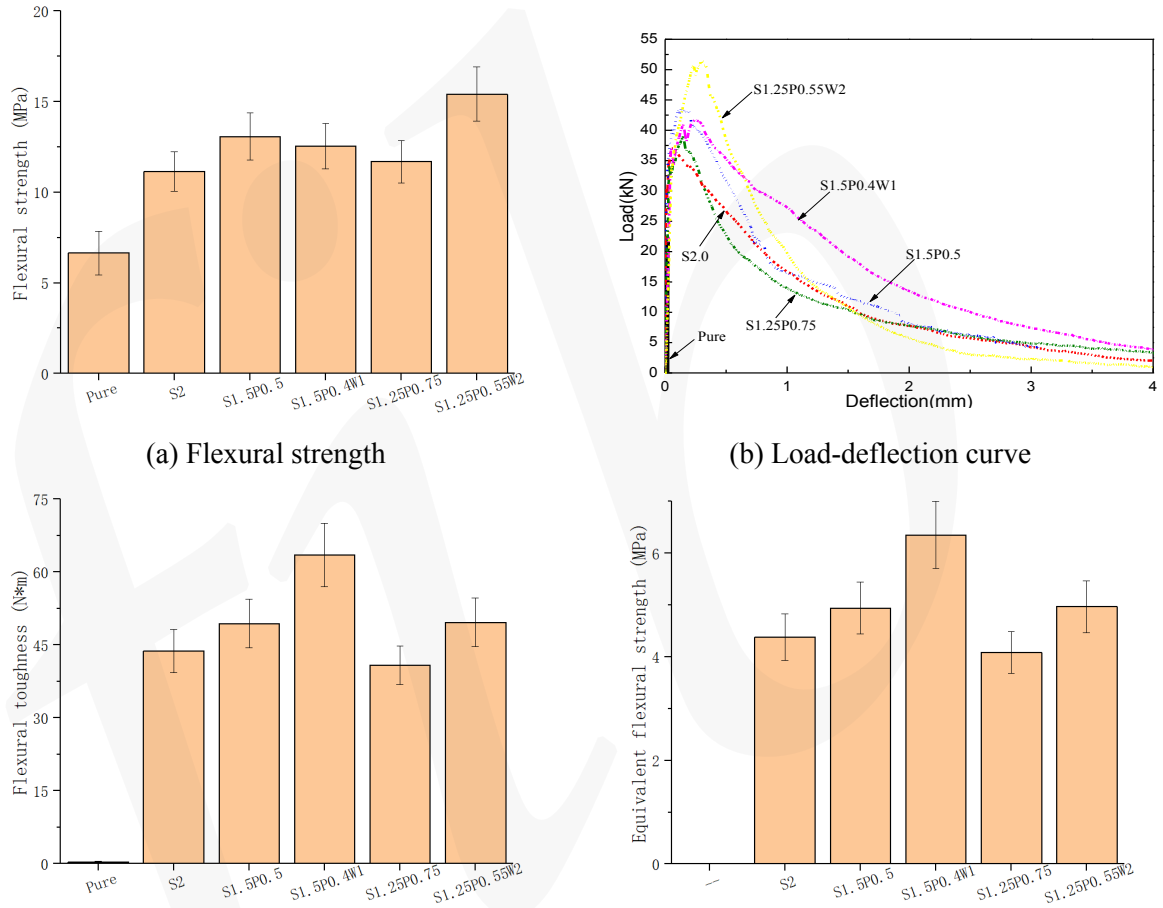
The peak strains of all mixtures are presented in Figure 2(b). Compared to pure mortar, the introduction of steel, PVA hybrid fibre and $CaCO_3$ whiskers can enhance the peak strain. The maximum value of peak strain reached 0.47% for S1.25P0.75. The stress–strain curves of various composites in uniaxial compression are presented in Figure 2(c). Compared to the control group Pure, the descending or softening branch of the stress–strain curve can be improved by hybrid fibres. Strain energy, which is calculated by the area under the stress–strain curve, is employed to assess the compressive toughness of various mixtures, as shown in Figure 2(d). S2 presented the greatest strain energy, followed by S1.5P0.4W1. The error bars indicate that fibres decrease the data scatters of compressive behaviours of mortar, as shown in Figure 2.

3.2 Flexural behaviors

The flexural strengths for all composites are shown as Figure 3(a). Compared to the control group Pure, all fibre-reinforced mortar presented a significant improvement in flexural strength. Mixture S1.25P0.55W2 presented the greatest flexural strength with an increase more than 130%. Compared to S2, S1.25P0.55W2 still reached nearly 40% of increase in flexural strength. The conventional hybrid fibre-reinforced mortar attained a 5–17% increase in flexural strength, while the multi-scale hybrid fibre-reinforced mortar attained a 13–38%

This document is the intellectual property of the fib – International Federation for Structural Concrete. All rights reserved.
This PDF of fib Bulletin 95 is intended for use and/or distribution solely within fib National Member Groups.

increase in flexural strength. These reinforcing effects may result from the smaller size and greater length-diameter ratio of PVA fibre and whisker. The multi-scale hybrid fibre system can restrict micro- and meso-cracks in mortar before peak load, hence increase the ultimate flexural tensile stress capacity more efficiently than conventional hybrid fibre system. The compressive and compressive strength in this research are lower than those in previous studies due to bigger specimens and longer steel fiber. (Cao, Zhang, Lv, & Xu, 2014; Cao, Zhang & Lv, 2014; Cao, Zhang & Wei, 2013)



(a) Flexural strength (b) Load-deflection curve

(c) Flexural toughness (d) Equivalent flexural strength

Figure 3: Flexural behaviors of various mixtures

The flexural behaviours of composites are also evaluated by the load-deflection curves shown as Figure 3(b). All fibre reinforced mortars presented an appreciable increase in the softening branch of the load-deflection curve. Generally, the steel and PVA hybrid fibre reinforced mortars presented more extended softening branch than that of S2 resulting from the positive hybrid effect of steel and PVA fibres. And the multi-scale hybrid fibre-reinforced mortars (S1.5P0.4W1) reached the most extended softening branch in all mixtures. The introduction of $CaCO_3$ whisker in the steel and PVA hybrid fibre reinforced mortars attained further increase in flexural response. This may result from the multi-scale design of the hybrid fibres and whisker.

This document is the intellectual property of the fib – International Federation for Structural Concrete. All rights reserved.
This PDF of fib Bulletin 95 is intended for use and/or distribution solely within fib National Member Groups.

The flexural toughness was employed to assess energy absorption capacity of specimens. The flexural toughness (T_b) is examined by measuring the area under the load-deflection curve up to a deflection of 3mm as presented in Figure 3(c). The addition of fibres and whisker led to notable enhancement to the flexural toughness of various mixes. Compared to mono-steel fibre reinforced mortar (S2), the steel and PVA hybrid fibre mortars (S1.5P0.5) could reach higher flexural toughness. The multi-scale HFRCC (S1.5P0.4W1 and S1.25P0.55W2) could improve flexural toughness of beams more efficiently than the conventional HFRCC (S1.5P0.5 and S1.25P0.75). This is likely result from the fibre synergy of the multi-scale system. The error bars indicate that fibres decrease the data scatters of flexural behaviours of mortar, as shown in Figure 3.

The equivalent flexural strength was employed to assess residual load-carrying ability of beams. The equivalent flexural strength is calculated by $\sigma_b = T_b L / (\delta_{tb} b h^2)$, where σ_b is the equivalent flexural strength (MPa); T_b is flexural toughness (N·m); δ_{tb} is a specific deflection value (mm, and set to 3mm here); b, h, L are width, depth and span of beam, respectively. The multi-scale HFRCC (S1.5P0.4W1 and S1.25P0.55W2) reached a greater equivalent flexural strength than the conventional HFRCC (S1.5P0.5 and S1.25P0.75), which is similar to the results of flexural toughness. This presents that the multi-scale HFRCC have a greater residual load-carrying ability than that of the conventional HFRCC.

4 Concluding remarks

A new kind of multi-scale fiber-reinforced cement-based composite, which contains 35mm hooked end steel fibre, 6mm PVA fibre and $CaCO_3$ whisker, was designed and tested for compressive and flexural behavior. The experimental findings, being presented in the present paper, allow to draw the main concluding remarks listed as follows.

1. From test results it turns out that, compared to the conventional hybrid fibers (steel fibre and PVA fibre), the addition of multi-scale fibres (steel fibre, PVA fibre and $CaCO_3$ whisker) can improve the compressive strength and toughness of cement-based composite.
2. Multi-scale fibre usage leads to notable increase to both the flexural strength and flexural toughness values of cement-based composite.
3. Based on these test results, we can conclude that there is a remarkable fiber synergy in multi-scale hybrid fibre reinforced cement-based composites with 35mm hooked end steel fibre, 6mm PVA fibre and $CaCO_3$ whisker.
4. It seems possible that the steel fibres and PVA fibres can be partly replaced by $CaCO_3$ whiskers, which is very beneficial in decreasing the production cost of fiber reinforced concrete for potential structural applications.
5. As the new HFRCC could be used to strengthen and retrofit the bridge and hydraulic structures, the durability of this new HFRCC should be carefully studied in the future.

5 Acknowledgements

The Authors would like to give their appreciation to the support of the Natural Science Foundation of China under Grant No. 51678111 and No.51478082.

This document is the intellectual property of the fib – International Federation for Structural Concrete. All rights reserved.
This PDF of fib Bulletin 95 is intended for use and/or distribution solely within fib National Member Groups.

6 References

Banthia N. & Soleimani SM (2005), *Flexural response of hybrid fibre-reinforced cementitious composites*. ACI Material Journal, 6, 382-389.

Bentz DP (2000), *Influence of silica fume on diffusivity in cement-based materials: II. Multi-scale modeling of concrete diffusivity*. Cement and Concrete Research, 30(7):1121-1129.

Cao M., Zhang C., Lv H., & Xu L. (2014), *Characterization of mechanical behavior and mechanism of calcium carbonate whisker-reinforced cement mortar*, Construction and Building Materials, 66, 89-97.

Cao M., Zhang C., & Lv H. (2014), *Mechanical response and shrinkage performance of cementitious composites with a new fiber hybridization*, Construction and Building Materials,57, 45-52.

Cao M., Zhang C., & Wei J. (2013), *Microscopic reinforcement for cement based composite materials*. Construction and Building Materials, 40, 14-25.

Li Q, Liu J, Xu S (2015), *Progress in Research on Carbon Nanotubes Reinforced Cementitious Composites*. Advances in Materials Science and Engineering, 307435, 1-16.

Nguyen VP, Stroeven M & Sluys LJ (2012), *Multiscale failure modeling of concrete: Micromechanical modeling, discontinuous homogenization and parallel computations*. Computer Methods in Applied Mechanics and Engineering, 201-204, 139-156.

Parveen S, Rana S, Fangueiro R (2013), *A Review on Nanomaterial Dispersion, Microstructure, and Mechanical Properties of Carbon Nanotube and Nanofiber Reinforced Cementitious Composites*. Journal of Nanomaterials. 710175, 1-19.

This document is the intellectual property of the fib – International Federation for Structural Concrete. All rights reserved.
This PDF of fib Bulletin 95 is intended for use and/or distribution solely within fib National Member Groups.
FRC2018: Fibre Reinforced Concrete: from Design to Structural Applications
Joint ACI-*fib*-RILEM International Workshop

A sectional approach for the bending creep of FRC based on uniaxial tension creep tests

Rutger Vrijdaghs[1], Marco di Prisco[2], Lucie Vandewalle[1]

[1] : Department of civil engineering, KU Leuven, Leuven, Belgium.

[2] : Department of structural engineering, Politecnico di Milano, Milan, Italy.

Abstract

The creep behavior of FRC elements remains an important obstacle to use FRC in structural applications. Owing to the residual post-cracking strength properties of FRC, creep deformations play an important role in the cracked sections and influence durability and SLS requirements of structural elements. Therefore, it is of high importance to take creep deformations into account in the design phase.

In this paper, the results of an experimental campaign involving both bending tests and uniaxial tensile creep tests on polymeric FRC are presented. In the bending tests, a notched FRC beam is subjected to loading-unloading cycles while the deformations over the cracked section were recorded. The uniaxial tensile creep tests were performed on precracked FRC samples to quantify time-dependent crack growth.

The bending behavior of FRC can be accurately predicted by the uniaxial constitutive model of Model Code 2010 in the loading phase assuming a plane section approach. For the unloading phases, a bilinear deformation distribution is assumed and a scalar damage evolution function is fitted by an inverse analysis algorithm. The results of the sectional analysis compared favorably with the experimentally observed data.

Finally, a sectional analysis approach is developed and presented in which bending creep deformations are calculated using the uniaxial creep compliances. The initial stress and deformation distribution in the cracked section is predicted by the inverse analysis. The results show that the bending creep deformations of FRC can be quite large, and creep coefficients as high at 7 are observed within 120 days. However, it should be noted that the creep algorithm does not (yet) take into account additional cracking in time, and as such, the predicted creep deformations are a lower limit of what can be expected in reality. More research is needed to upgrade the algorithm to allow predictions including the time-dependent cracking behavior.

Keywords

Sectional analysis, creep of FRC, polymeric FRC, tensile and bending creep

This document is the intellectual property of the fib – International Federation for Structural Concrete. All rights reserved.
This PDF of fib Bulletin 95 is intended for use and/or distribution solely within fib National Member Groups.

1 Introduction

Fiber reinforced concrete (FRC) is a composite material in which fibers are added to the fresh concrete mix [1, 2]. These fibers are mainly used to improve the properties of the concrete in the hardened state. In structural applications, fibers can partially or totally replace the traditional reinforcement. For these purposes, the fibers provide an enhanced post-cracking tensile strength in the hardened state by bridging crack faces [3]. Commercially available fibers can be made from a number of different materials: steel, glass, synthetic and natural being the most common types [4].

Until recently, the research effort has been focusing on the properties of FRC in the fresh and hardened state [5, 6]. It has been found that the inclusion of fibers decreases plastic shrinkage cracking [7] and flowability [8] in the fresh state. In the hardened state, fibers provide a post-cracking strength to the matrix [9-11]. However, investigations on the long-term structural properties of FRC have only recently become a research focal point. The recently published Model Code 2010 [12] acknowledges that time-dependent effects may significantly alter the behavior of structural elements, both in the serviceability limit state and in the ultimate limit state. In the former, creep may cause unwanted and unacceptable deflections of FRC beams [13, 14], whilst in the latter, the residual load-bearing capacity of elements may be significantly lower than the design value based on the short-term strength assessment. However, the Model Code (MC10) does not provide design rules to take long-term behavior into account. It is clear that further research on the long-term structural properties of FRC is required.

One of these time-dependent phenomena is creep. In this paper, two topics are discussed. Firstly, the results of an experimental campaign into the creep behavior of cracked polypropylene FRC under sustained uniaxial tension loading is presented. Furthermore, the results of the creep tests were modelled in the dedicated finite-element program DIANA. Secondly, a sectional approach is presented in which the results of the uniaxial tensile creep tests can be incorporated. By using inverse analysis to determine stresses and crack widths in the cracked section of the beam, creep functions are assigned to the discretized beam section. In this way, the results of the uniaxial tensile tests can be input for a sectional approach for the bending creep of cracked FRC.

2 Experimental program

The experimental program focusses on a normal strength concrete (f_{cm} = 43 MPa) with 1 percentage of volume of polypropylene fibers and consists of a series of short-term characterization and long-term creep tests on three different levels: (1) single fiber [15], (2) pull-out behavior [16] and (3) FRC performance [17]. In this paper, the results of the FRC scale will be shortly presented and discussed, the details can be found in literature [17, 18].

On the FRC level, the material is firstly characterized in short-term tests, both in bending (n = 12) according to the European Standard EN 14651 as well as in uniaxial tension (n = 4) in a specifically designed tensile frame, which allows uniform crack width opening by manual eccentric load application. Furthermore, 6 beams were tested in a EN14651 three-point bending configuration with loading-unloading cycles at CMOD = 0.1, 0.2, 0.3, 0.4 and 0.5 mm to determine the unloading behavior. Five additional LVDTs were placed over the cracked section to measure crack opening and closing upon un- and reloading in bending. The test specimen, setup and loading speed were identical to the EN 14651 test specimen and 5 un- and reloading

This document is the intellectual property of the fib – International Federation for Structural Concrete. All rights reserved.
This PDF of fib Bulletin 95 is intended for use and/or distribution solely within fib National Member Groups.

cycles were considered at 0.1, 0.2, 0.3, 0.4 and 0.5 mm. A photo of the cyclic setup is shown in Figure 1, clearly showing the 5 LVDTs.

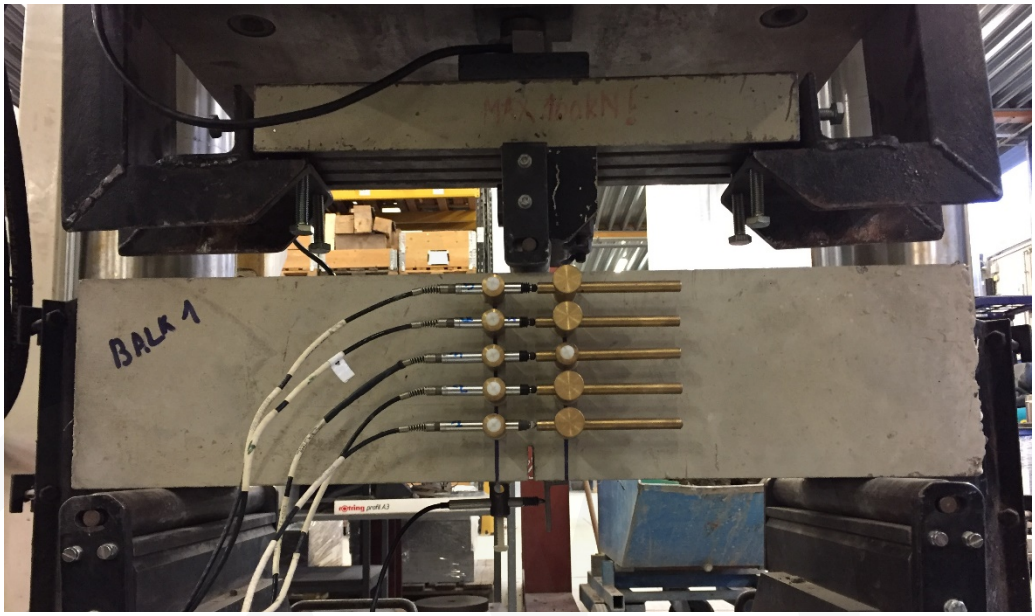


Figure 1: Photo of the cyclic bending setup with 5 additional LVDTs over the cracked section

Secondly, 14 specimens were cored from the two halves of FRC beams after flexural testing and subjected to uniaxial tensile creep loading. The cores were precracked to an initial crack width of 0.2 mm. Two different load ratios were considered, i.e. 30 % and 45 % of the residual strength at the precracking level. Of the 14 creep specimens, 7 have already been subjected to at least 6 months of sustained loading; the 7 other specimens are still running. All tensile tests are performed in a climate controlled room at a constant temperature and relative humidity of 20 °C and 60 %, respectively. In Table 1 an overview of the different tests is given.

Table 1: Number of tests specimens in the experimental program

Loading configuration	**Uniaxial tension[†] (Eccentric load application)**	**Bending (EN 14651)**
Short-term characterization	n = 4	n = 12
Cyclic loading		n = 6
Creep tests	n = 14 (7 finished, 7 running)	
- 30 %	n = 7 (4 finished, 3 running)	
- 45 %	n = 7 (3 finished, 4 running)	

[†] tests performed in a climate controlled room (20 °C, 60 %)

This document is the intellectual property of the fib – International Federation for Structural Concrete. All rights reserved.
This PDF of fib Bulletin 95 is intended for use and/or distribution solely within fib National Member Groups.

2.1 Bending results

The results of the EN 14651 bending tests are shown in Figure 2(a), and assuming a lognormal distribution for the determination of the characteristic values, the FRC is classified according to the Model Code 2010 [12] as a ***2d*** concrete.

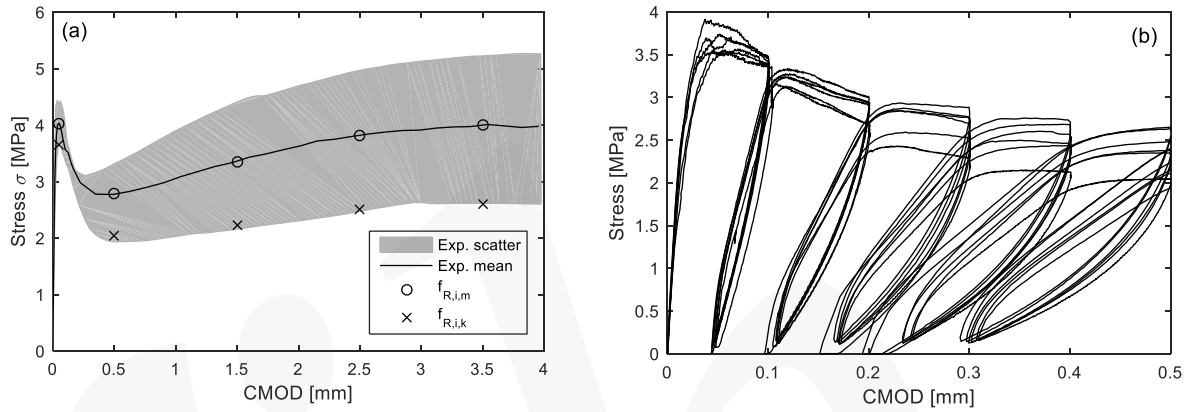


Figure 2: (a) EN 14651 bending results (b) Cyclic bending results for CMODs = 0.1 – 0.5 mm.

The results of the 6 cyclic tests on FRC are shown in Figure 2(b), only showing the CMOD until 0.5 mm as this is the area of interest. Note that the results of the cyclic tests are not included in the full bending tests and have not been taken into account in the post-cracking strength classification.

2.2 From bending to uniaxial results

The results of the 12 full EN 14651 bending test can also be used to predict the uniaxial behavior, i.e. the stress-crack width (σ-w) behavior based on equation found in the Model Code and as proposed by di Prisco et al. [19].

In the pre-peak region, equation 5.1-29 and 5.1-30 of MC10 are used with a structural characteristic length l_{cs} = 125 mm, as proposed in section §5.6-8 of MC10, to transform the σ-ε relation into a σ-w curve. The adopted tensile strength of the concrete is assumed to be the mean value of the tensile strength determined from the compressive strength and from the bending tensile strength, equation 5.1-3a and 5.1-8a respectively in MC10, refer to Equation 1.

$$f_t = 0.5 \times \left(0.3 \cdot f_{ck}^{\frac{2}{3}} + \frac{0.06 \cdot h^{0.7}}{1+0.06 \cdot h^{0.7}} \cdot f_L \right) \quad (1)$$

For the post-peak behavior, an immediate drop in strength is observed in accordance with the MC10 equation 5.6-10, based on the fracture energy of the concrete matrix. Following this drop in strength, the approach proposed in [19] is adopted, relating the residual strength parameters f_{R1} and f_{R3} to the uniaxial tensile behavior at crack width w = 0.5 and 2.5 mm.

In this way, a multi-linear constitutive σ-w relationship is calculated based on the EN 14651 bending results and the compressive strength of concrete. The results of this approach are shown in the following section, in comparison with the experimentally obtained results.

This document is the intellectual property of the fib – International Federation for Structural Concrete. All rights reserved.
This PDF of fib Bulletin 95 is intended for use and/or distribution solely within fib National Member Groups.

2.3 Uniaxial results

In uniaxial tension, 4 specimens are tested until a crack width of 4 mm was recorded and 14 specimens have been precracked to an initial crack width of 0.2 mm. The results of all 18 uniaxial tension tests are shown in Figure 3(a), and highlighted to a crack width of 0.3 mm in Figure 3(b). Note the unloading branch for the 14 creep specimens at w = 0.2 mm.

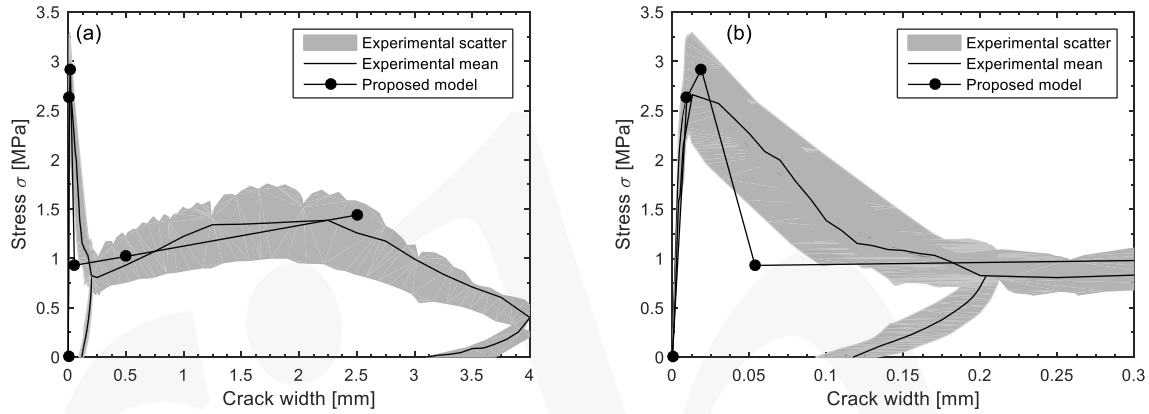


Figure 3: Uniaxial results together with the proposed model for (a) the whole test (b) until w = 0.3 mm

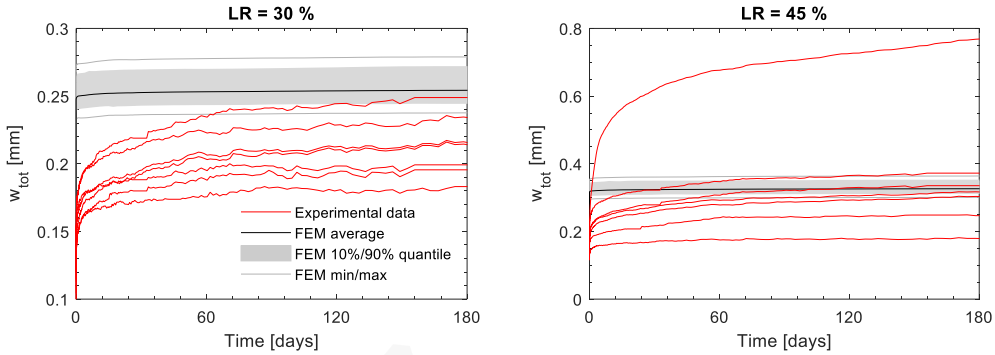
From Figure 3, it is clear that the combined MC10-[19] model is able to accurately describe the uniaxial behavior based on bending results. The model however predicts a larger strength loss in the immediate post-peak region, but this can be attributed to the relatively low stiffness of the tensile frame which cannot absorb the energy release associated with matrix cracking.

Following the precracking, the samples are subjected to creep tensile loading at two different load ratios, i.e. 30 % and 45 %. In this paper, the results for the 7 completed creep tests are shown in the next section together with the numerically obtained creep deformations.

3 Numerical analysis

The finite element analysis aims to describe and predict the creep behavior in uniaxial tension based on the results of the single fiber and pull-out behavior, using a discrete treatment of the fibers. The details of the model characteristics and calibration are given elsewhere [20]. In Figure 4 the results of the numerical analysis are shown together with the experimentally observed creep deformations. Note that the general trend is quite accurately captured, but the initial deformations upon loading are overestimated by the numerical model. This is attributed to low fiber stiffness in the numerical model which is calibrated on the secant modulus defined in EN 14889-2. However, since the load application in the FEM is instantaneous, the tangent modulus is better suited to capture the initial deformation at the instantaneous load application. Nevertheless, the creep deformations as obtained from the FEA are retained.

This document is the intellectual property of the fib – International Federation for Structural Concrete. All rights reserved.
This PDF of fib Bulletin 95 is intended for use and/or distribution solely within fib National Member Groups.



(a) (b)

Figure 4: Comparison of the creep deformations of the experiments and the numerical model for (a) 30 % and (b) 45 %

4 Sectional analysis

Even though FEA is a very powerful tool, in most real design problems, it is quite often prohibitively expensive to construct, run and analyze the results. Therefore, most design approaches consider a sectional approach which can be easily understood and adopted. In this section, a proposal for such a sectional approach is given to take creep deformation into account. The basis of this approach is a discretized cracked section subjected to bending moments. Uniaxial creep deformations are then assigned to the discretized elements in the cracked section.

4.1 Loading path – plane section

Before creep deformations can be taken into account, the first step is to calculate the stresses in the cracked section, both upon loading (i.e. following the EN 14651 test) and unloading (i.e. at the beginning of the creep test). Since the σ-w constitutive relation is known, it is possible to calculate the stresses upon loading, assuming a plane cracked section, ensuring horizontal equilibrium is fulfilled. The resulting bending moment can then be compared against the experimentally observed. The results of the calculation are shown in Figure 5(a) until CMOD = 4 mm and in Figure 5(b) until CMOD = 0.5 mm. The approach is able to quite accurately capture the test results, albeit it overestimates the tensile strength of the concrete somewhat. Except near the bending tensile strength, the sectional predictions remains within the experimental bounds for the entire test.

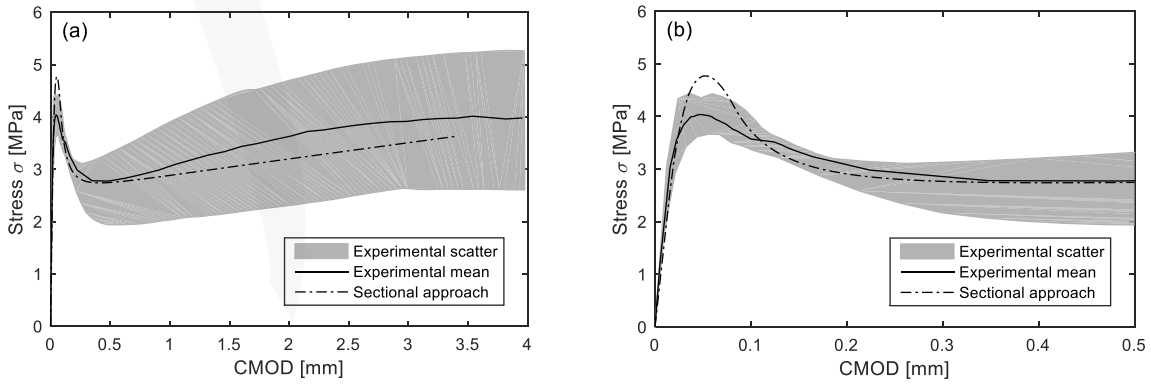


Figure 5: Comparison of the sectional approach and the experimental results for (a) complete test and (b) until 0.5 mm

This document is the intellectual property of the fib – International Federation for Structural Concrete. All rights reserved.
This PDF of fib Bulletin 95 is intended for use and/or distribution solely within fib National Member Groups.

4.2 Unloading path – bilinear

Upon unloading, the plane section approach cannot be assumed correct anymore, as unloading under such an assumption would entail complete recovery of crack widths, which is not observed experimentally. Therefore, a bilinear deformation distribution over the section height is proposed with the inflexion point at the height of the undamaged zone. The bilinear distribution is calibrated on the unloading paths of the FRC bending tests, refer to Figure 2(b). The inputs for the inverse analysis are the CMOD values and the applied force, and the algorithm finds the scalar damage evolution $D(w)$ as a function of the total deformation w. The optimized parameter is the sum of the squared force ΔH and moment error ΔM. The inverse analysis algorithm for the unloading is summarized below:

Given $F_{ext,i}$ and $CMOD_i$ for all unloading points i,

Find $D(w)$ in a bilinear deformation distribution,

Such that $\Delta E = \sqrt{\Delta H^2 + \Delta M^2}$ is minimized,

With $\begin{cases} \Delta H = b \cdot \Sigma \sigma_j \\ \Delta M = \left(b \cdot \Sigma\left(y_j \cdot \sigma_j\right) - M_{ext}\right)/M_{ext} \end{cases}$

for all elements j over the height of the section

The results of the model are quite accurate as 99 % of all unloading points i have an error ΔH and ΔM between ±5 N and ±1.5 %, respectively. Note that the experimentally observed deformations upon unloading over the height of the section are not used (refer to Figure 1), and as such, these experimental data points can be used to validate the model. The comparison between the model and experimental data is shown in Figure 6, for the full load (100 %) and at a load ratio of 50 % at unloading from different CMOD values (0.1 – 0.5 mm).

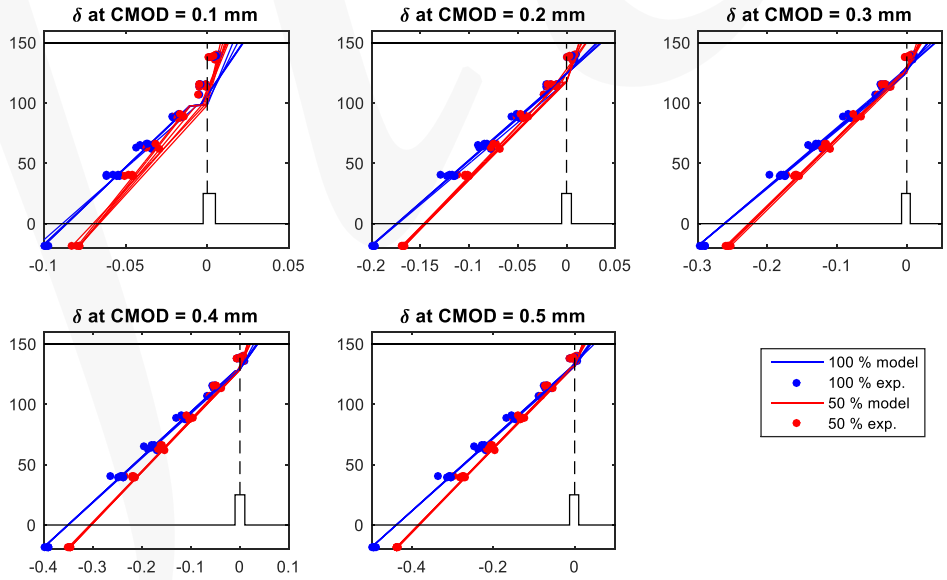


Figure 6: Deformation profiles predicted by the model in comparison with experimental data

The lines show the deformation predicted by the model, while the dots indicate experimental data. Note that at full load, the bilinear model predicts a linear deformation profile, which is

This document is the intellectual property of the fib – International Federation for Structural Concrete. All rights reserved.
This PDF of fib Bulletin 95 is intended for use and/or distribution solely within fib National Member Groups.

expected as shown in section 4.1. At lower loads, the linear profile quickly becomes bilinear in order to achieve residual deformations. As stated, the experimental deformations (dots in the figure) are not used in the inverse analysis but show a good agreement with the predicted model deformations. The scalar damage evolution is shown in Figure 7(a), indicating that damage accumulates very quickly. The damage evolution is calculated independently for every unloading step, but the results show that all curves are in relatively close agreement with each other. As an example, the stress distribution over the sectional height is shown in Figure 7(b) upon unloading from 0.5 mm for the full load (100 %) and at 50 %.

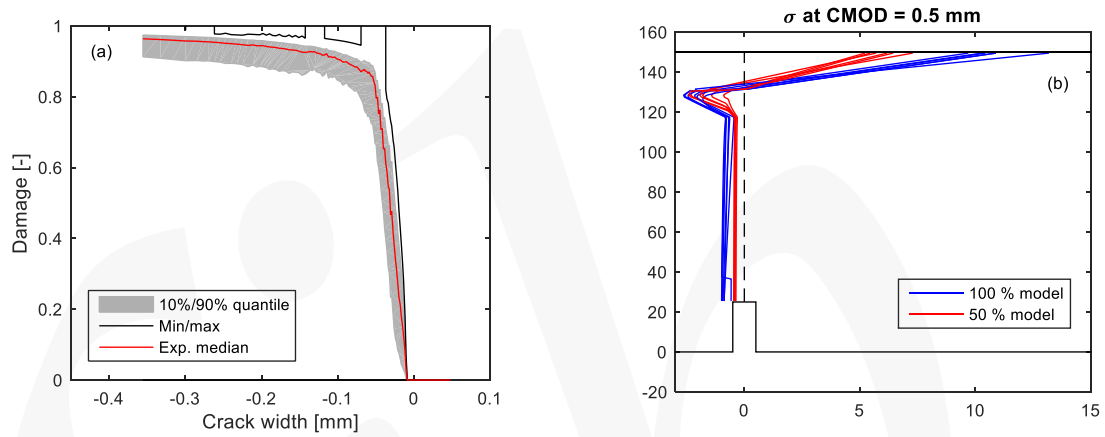


Figure 7: (a) scalar damage evolution for all specimens (b) stress profiles for 100 % and 50 %

4.3 Creep implementation

The deformation and stress profile shown in Figure 6 and Figure 7(b) at 50 % load after unloading from CMOD = 0.5 mm can be used as a starting point to predict bending creep based on the uniaxial creep compliance functions. It is assumed that the undamaged tensile creep behavior is identical to the undamaged compressive creep, and that the damaged tensile creep compliance is independent of the initial crack width. Under these assumptions, the creep deformation of an FRC beam under bending can be calculated, and it is shown in Figure 8(a) and (b) in terms of an increase in CMOD and the creep coefficient φ (defined as $CMOD(t)/CMOD_0$) respectively.

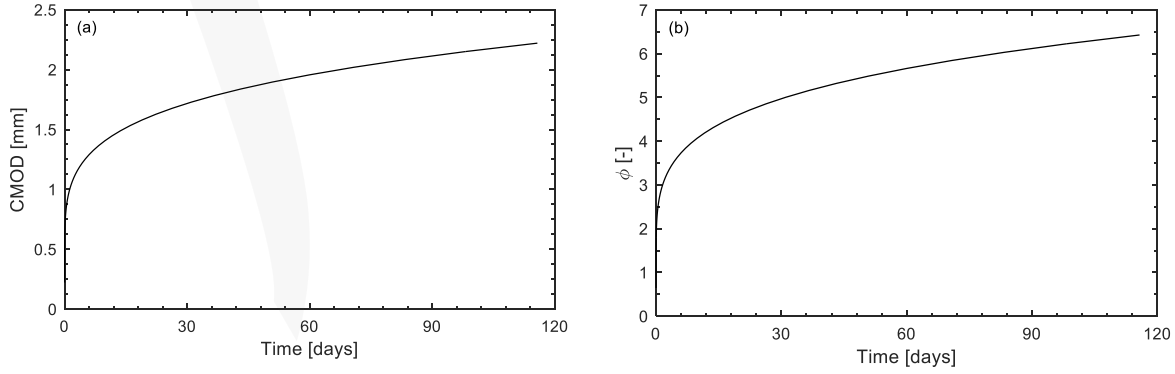


Figure 8: Increase in (a) CMOD and (b) creep coefficient for the bending test at 50 %

This document is the intellectual property of the fib – International Federation for Structural Concrete. All rights reserved.
This PDF of fib Bulletin 95 is intended for use and/or distribution solely within fib National Member Groups.

While these results provide an indication of the expected increase in deformations, it should be noted that in the real beam, a stress redistribution will take place owing to the increase of the crack height, a smaller compressed zone and higher associated compressive stresses, further increasing the creep deformations. This needs further investigation, both on an experimental level as well as in the sectional approach. Nevertheless, the results presented here can serve as a first indication and, as such, are a lower limit of the real deformations that can be expected. As has been shown, these CMOD increases are significant and should be taken into account where SLS requirements are of importance.

5 Conclusion

In this paper, the results of an experimental campaign involving bending tests and uniaxial tensile creep tests are presented. In the bending tests, a cyclic behavior of loading – unloading cycles is imposed to investigate residual crack widths and the unloading performance.

Furthermore, a sectional approach is presented that is able to accurately predict and describe the deformations and stresses in the cracked section at the loading and unloading cycles. In the former case, a linear deformation distribution is sufficient to describe the behavior. For the latter cycles, a bilinear distribution is needed to predict the residual crack widths upon unloading. A scalar damage function is fitted in an inverse analysis to come to the results, which compare favorably with the experimental data.

Lastly, the results of the stress and deformation profiles is used to predict bending creep based on the uniaxial creep behavior of undamaged and cracked FRC. While the approach presented here predicts reasonable results, it should be noted that the creep prediction does not take time-dependent cracking into account. As such, the predicted creep deformations with creep coefficients exceeding 7 after 120 days should be regarded as the lower limit of the real deformations. More research is needed to update the creep calculations to include all effects. Nevertheless, the approach presented here provides interesting insights into the stress distribution in cracked sections of FRC.

6 Acknowledgements

The first author gratefully acknowledges the financial support of the Agency for Innovation by Science and Technology in Flanders (IWT).

7 References

[1] Balaguru, P. and S.P. Shah, *Fiber-Reinforced Cement Composites*. 1992, Texas, USA: Mcgraw-Hill.
[2] Bentur, A. and S. Mindess, *Fibre Reinforced Cementitious Composites*. 1990, England: Elsevier Science Publishers LTD. 449.
[3] di Prisco, M., G. Plizzari, and L. Vandewalle, *Fibre reinforced concrete: new design perspectives.* Materials and Structures, 2009. 42(9): p. 1261-1281.
[4] ACI Committee 544, *State-of-the-Art Report on Fiber Reinforced Concrete*, J.I. Daniel, Editor 2002, American Concrete Institute.

This document is the intellectual property of the fib – International Federation for Structural Concrete. All rights reserved.
This PDF of fib Bulletin 95 is intended for use and/or distribution solely within fib National Member Groups.

[5] *Fibre-Reinforced Concrete*. RILEM Proceedings of the 6th RILEM Symposium (BEFIB 2004), PRO39, BEFIB 2004, ed. M. di Prisco, R. Felicetti, and G.A. Plizzari. Bagneux, France: RILEM Publications S.A.R.L.

[6] *Fibre Reinforced Concrete*. RILEM Proceedings of the 5th RILEM Symposium (BEFIB 2000), PRO15, BEFIB 2000, ed. P. Rossi and G. Chanvillard. Bagneux, France: RILEM Publications S.A.R.L.

[7] Grzybowski, M. and S.P. Shah, *Shrinkage Cracking of Fiber Reinforced Concrete.* ACI Materials Journal, 1990. 87(2): p. 138-148.

[8] Pasini, F., et al., *Experimental study of the properties of flowable fiber reinforced concretes*, in *6th International RILEM Symposium on Fibre Reinforced Concretes*, M. di Prisco, R. Felicetti, and G.A. Plizzari, Editors. 2004, RILEM Publications SARL. p. 279 - 288.

[9] Barros, J., et al., *Post-cracking behaviour of steel fibre reinforced concrete.* Materials and Structures, 2005. 38(1): p. 47-56.

[10] di Prisco, M., L. Ferrara, and M.G.L. Lamperti, *Double edge wedge splitting (DEWS): an indirect tension test to identify post-cracking behaviour of fibre reinforced cementitious composites.* Materials and Structures, 2013. 46(11): p. 1893-1918.

[11] Buratti, N., C. Mazzotti, and M. Savoia, *Post-cracking behaviour of steel and macro-synthetic fibre-reinforced concretes.* Construction and Building Materials, 2011. 25(5): p. 2713-2722.

[12] fédération internationale du béton (fib), *Model Code 2010 First complete draft*, 2010.

[13] Kurtz, S. and P. Balaguru, *Postcrack creep of polymeric fiber-reinforced concrete in flexure.* Cement and Concrete Research, 2000. 30(2): p. 183-190.

[14] MacKay, J. and J.F. Trottier, *Post-crack creep behavior of steel and synthetic FRC under flexural loading*, in *Shotcrete: More Engineering Developments*. 2004, Taylor & Francis. p. 183-192.

[15] Vrijdaghs, R., M. di Prisco, and L. Vandewalle, *Creep Deformations of Structural Polymeric Macrofibers*, in *Creep Behaviour in Cracked Sections of Fibre Reinforced Concrete: Proceedings of the International RILEM Workshop FRC-CREEP 2016*, P. Serna, A. Llano-Torre, and S.H.P. Cavalaro, Editors. 2017, Springer Netherlands: Dordrecht. p. 53-61.

[16] Vrijdaghs, R., M. di Prisco, and L. Vandewalle, *Short-term and creep pull-out behavior of polypropylene macrofibers at varying embedded lengths and angles from a concrete matrix.* Construction and Building Materials, 2017. 147: p. 858-864.

[17] Vrijdaghs, R., M. di Prisco, and L. Vandewalle, *Uniaxial tensile creep of a cracked polypropylene fiber reinforced concrete.* Materials and Structures, 2018. 51(1): p. 5.

[18] Vrijdaghs, R., M. di Prisco, and L. Vandewalle, *Creep of cracked polypropylene fiber reinforced concrete*, in *9th RILEM International Symposium on Fiber Reinforced Concrete - BEFIB2016*, N. Banthia, M. di Prisco, and S. Soleimani-Dashtaki, Editors. 2016, RILEM Publications: Vancouver, BC, Canada. p. 199-208.

[19] di Prisco, M., M. Colombo, and D. Dozio, *Fibre-reinforced concrete in fib Model Code 2010: principles, models and test validation.* Structural Concrete, 2013. 14(4): p. 342-361.

[20] Vrijdaghs, R., M. di Prisco, and L. Vandewalle, *A Numerical Model for the Creep of Fiber Reinforced Concrete*, in *fib Symposium 2017: High Tech Concrete*, D.A. Hordijk and M. Luković, Editors. 2017, Springer International Publishing: Maastricht, The Netherlands. p. 366-373.

This document is the intellectual property of the fib – International Federation for Structural Concrete. All rights reserved.
This PDF of fib Bulletin 95 is intended for use and/or distribution solely within fib National Member Groups.
FRC2018: Fibre Reinforced Concrete: from Design to Structural Applications
Joint ACI-*fib*-RILEM International Workshop

Optimized quality control procedure with the Barcelona test and the inductive method for FRC

Eduardo Galeote[1], Ana Blanco[2], Sergio H.P. Cavalaro[2], Albert de la Fuente[1]

[1] : Universitat Politècnica de Catalunya, Barcelona, Spain.

[2] : Loughborough University, Loughborough, United Kingdom.

Abstract

The optimization of resources and materials with the objective of cutting costs has a great relevance at all stages of the design of a structure, including the quality control. In fibre-reinforced concrete (FRC), the three-point bending tests are performed routinely as means of quality control to determine the residual strength. Nevertheless, the high scatter of its results and its complex setup requiring special equipment encourages the use of alternative tests to determine the post-peak strength of FRC. In this respect, the Barcelona test arises as an alternative method to characterize FRC due to a more reduced variability of the results, a lower concrete consumption and the simplicity of its execution. Moreover, the inherent heterogeneity of FRC directly affects the content of fibers within the concrete, which is one of the main factors governing the post-cracking strength of FRC. In this regard, the inductive method is proposed as a complementary test to assess the content of fibres during quality control using the same specimens to be tested under the Barcelona test. Therefore, the main aim of this study is to present a methodology to correlate the three-point bending test with the Barcelona test and show the feasibility of using the latter as an alternative method. Furthermore, the combination of the Barcelona test with the inductive method leads to a more complete characterisation of FRC.

Keywords

FRC, quality control, bending test, Barcelona test, inductive method, content of fibres

This document is the intellectual property of the fib – International Federation for Structural Concrete. All rights reserved.
This PDF of fib Bulletin 95 is intended for use and/or distribution solely within fib National Member Groups.

1 Introduction

The three-point bending test is one of the most extended methods to determine the post-cracking strength of FRC. This test is extensively used for design given that the geometry of the specimens and the Mode I fracture crack propagation are representative of the real behaviour of an element subjected to flexural stresses. However, as suggested by the Belgian standard NBN B 15-238, the three-point bending test is not a suitable method for the systematic quality control of FRC. This is mainly due to the high coefficient of variation, which can reach values above 20% [1,2]. Additionally, the complex setup of the test requiring big-sized samples, high precision equipments and a closed-loop configuration hinder the execution of the test and increase the costs.

Alternative methods can therefore be used in an attempt to overcome the drawbacks of the three-point bending test. In this context, and according to the *fib* Model Code 2010 [3], the use of alternative tests can be accepted if correlation factors are proven. In this regard, the Barcelona test [2] arises as an alternative to streamline the quality control given its simpler setup and lower scatter [4]. In order to meet project requirements, a minimum strength of the material is usually specified in quality control. If the test results do not reach this minimum value, the material must be discarded and a new batch of concrete must be manufactured. In this sense, the mere fact of changing the test methodology would reduce the scatter as well as the amount of material rejected and, hence, the costs while meeting the acceptability criteria.

Given the influence of the content of fibres on the post-cracking strength of FRC, the standard EN 14721 describes the procedure to perform the control of the content of steel fibres in FRC. According to this, fresh concrete needs to be washed and hardened concrete samples need to be crushed to separate the fibres. This results in a highly time-consuming procedure to determine the content of fibres thus limiting the number of samples that can be tested. For this, an alternative test such as the inductive method [5] is here presented. It consists of a non-destructive test that may be conducted within less than a minute providing the content of fibres through a calibrated relation between the inductance and the content of fibres.

Even in the case of different cracking mechanisms, the use of correlations between concrete properties measured through different test methods is a common and widely accepted procedure. For example, there are several equations available to transform the indirect tensile strength measured in the Brazilian test into the indirect flexural strength measured with bending tests [6]. In the case of FRC, Minelli et al. [7] already proposed a correlation between the Round Panel Test and the UNI flexural test based on the energy released and the residual strength.

The main objective of this document is to describe the methodology to correlate the results of the Barcelona test and the bending test for quality control given a concrete mix and type of fibre. Moreover, the procedure to determine the content of fibres using the inductive test and the method for its calibration is also presented. The correlation proposed represents a tool towards a simpler, faster and less expensive quality control of FRC based on the Barcelona test (BCN). This approach is in line with the *fib* Model Code 2010 and may also serve as an example for future correlations with other tests applied to FRC.

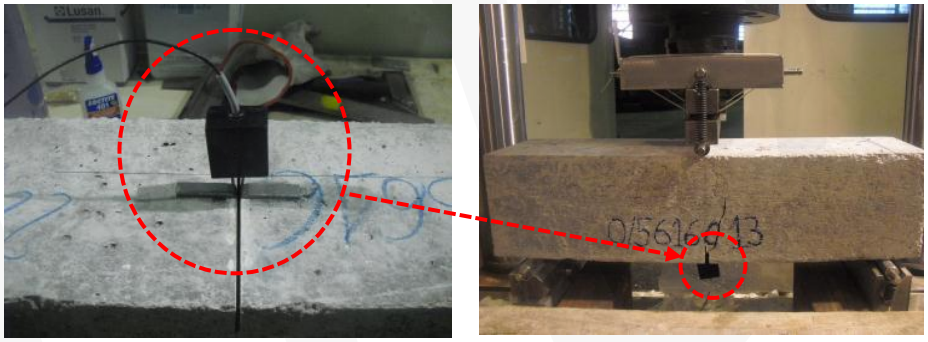
This document is the intellectual property of the fib – International Federation for Structural Concrete. All rights reserved.
This PDF of fib Bulletin 95 is intended for use and/or distribution solely within fib National Member Groups.

2 Experimental program

2.1 Specimens and tests

Three batches of the same FRC mix with a reinforcement of 30 kg/m^3 of steel fibres were produced to be tested under the three-point bending test and the Barcelona test. For this, prismatic beams with dimensions of 150x150x600mm and cubic specimens of 150x150 mm were casted for the flexural test and the Barcelona test, respectively. For batch 1 (B1), 10 prismatic and 20 cubic specimens were casted. For batches 2 and 3 (B2 and B3), 5 prismatic beams and 10 cubic samples were produced per each batch.

The bending test was conducted according with EN 14651 with a notch at the mid-span of each beam, thus weakening the central section of the specimen where the load was applied. A CMOD (Crack Mouth Opening Displacement) transducer was placed at the notch between two steel sheets (see Figure 1) to simultaneously record the crack opening and the load with a closed-loop configuration. The test is controlled through the CMOD at a rate of 0.05 mm/min until the crack opening reached 0.10 mm. Afterwards, the speed was increased to 0.20 mm/min until a crack opening of 4 mm was achieved, point at which the test was considered to be totally performed.



(a) (b)

Figure 1: CMOD (a) and general overview of the three-point bending test (b)

The inductive method may be used to determine both the orientation and the content of fibres in either cubic or cylindrical samples. The inductive test is a recently developed method to characterize steel fibre reinforced concrete [5,8]. For such a test, the specimens must be placed within a plastic container with an established cylindrical geometry as shown in Figure 2. Copper or aluminum wire coils rolled around the container constitute the sensor element of the system. A small electrical current goes through the coil and produces a magnetic field around the device, interacting with the steel fibres inside the concrete and providing the inductance as data output. Based on the equations developed in previous research [8,9], the orientation number and the contribution of the fibres in each direction may be assessed.

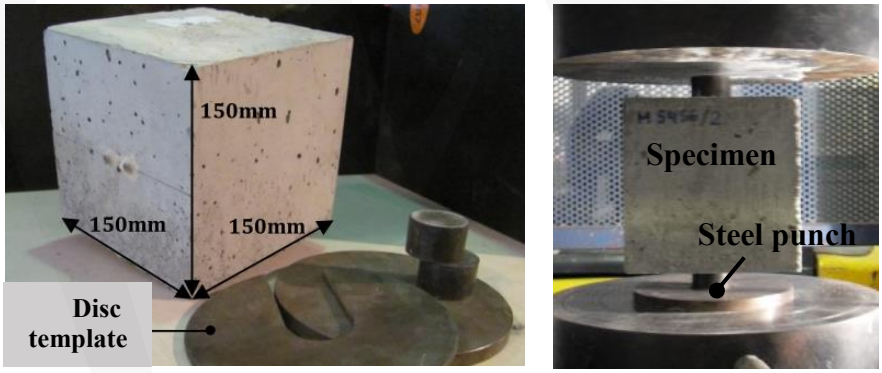
This document is the intellectual property of the fib – International Federation for Structural Concrete. All rights reserved.
This PDF of fib Bulletin 95 is intended for use and/or distribution solely within fib National Member Groups.



Figure 2: Inductive method equipment

After conducting the inductive test in the cubic samples of the three batches, the Barcelona test was performed according to the procedure described in UNE 83515 and as depicted in Figure 3. Two steel cylindrical punches are placed concentrically above and below the cubic specimen. These punches have a diameter of ¼ of the diameter of the inscribed cylinder in the cubic sample and a height of 25 mm. The hydraulic press transmits a load through the punches to the sample at a constant rate of 0.5 mm per minute. The compression load applied onto the punches produces a conical triaxial stress state from the centre to the edges of the specimen. This results in an increase of the diameter of the sample and, thus, in concrete cracking when the peak tensile strength is reached leading to the activation of the fibres.

Based on the standard UNE 83515, the crack opening is measured through the Total Circumferential Opening Displacement (TCOD). However, previous research [10] describes an analytical correlation between the TCOD and the vertical displacement, this leading to avoid the necessity of using the TCOD transducer while replacing cylindrical specimens for cubic ones. In this paper, the approach based on the vertical displacement is used for determining the residual strength with the Barcelona test.



(a) (b)

Figure 3: Cubic specimen and punches (a); test setup (b)

The content of fibres inside the specimen can be estimated based on a correlation between the real content of fibres of the sample and the inductance measurements obtained through the inductive test. To calibrate such correlation according with the type of fibre used in this experimental program, 6 cubic specimens were crushed after having performed the Barcelona test. The fibres of these specimens were separated from concrete and weighted to determine the content. This content was subsequently correlated with the inductance measurements of the inductive test at the three perpendicular directions of the specimen.

This document is the intellectual property of the fib – International Federation for Structural Concrete. All rights reserved.
This PDF of fib Bulletin 95 is intended for use and/or distribution solely within fib National Member Groups.

3 Results

3.1 Post-cracking strength

The average results of the three-point bending tests conducted on the three batches are presented in Table 1. The residual strengths at crack openings of 0.5, 1.5, 2.5 and 3.5 mm (f_{R1}, f_{R2}, f_{R3} and f_{R4}, respectively) are shown, along with the coefficient of variation (CV) of each parameter. The results of the residual strength of cubic specimens tested under the Barcelona test and determined as described in the standard UNE 83515 are shown in

Table 2. The results show the average residual strength for vertical displacements of 0.5, 1.5, 2.5 and 3.5 mm ($f_{R0.5}$, $f_{R1.5}$, $f_{R2.5}$ and $f_{R3.5}$, respectively), as well as the scatter associated to each strength.

Table 1: Bending test results of B1, B2 and B3

Parameter	B1		B2		B3		B1-B2-B3	
	Average	CV %	Average	CV %	Average	CV %	Average	CV %
f_{R1} [MPa]	2.36	22.2%	3.10	23.6%	3.02	23.9%	2.83	14.4 %
f_{R2} [MPa]	2.49	26.1%	3.06	24.8%	3.17	25.6%	2.91	12.7 %
f_{R3} [MPa]	2.39	26.9%	2.83	22.1%	3.03	23.8%	2.75	11.8 %
f_{R4} [MPa]	2.27	27.5%	2.60	23.5%	2.80	23.2%	2.56	10.4 %

Table 2: Barcelona test result of B1, B2 and B3

Parameter	B1		B2		B3		B1-B2-B3	
	Average	CV %	Average	CV %	Average	CV %	Average	CV %
$f_{R0.5}$ [MPa]	1.48	14.0%	1.54	9.1%	1.47	23.3%	1.50	2.5 %
$f_{R1.5}$ [MPa]	1.05	17.7%	1.02	12.0%	0.98	22.6%	1.02	3.5 %
$f_{R2.5}$ [MPa]	0.86	19.0%	0.75	19.0%	0.80	20.8%	0.80	6.9 %
$f_{R3.5}$ [MPa]	0.74	21.2%	0.60	24.6%	0.68	21.3%	0.67	10.4 %

The results show that Batch 1 presented the lowest residual strengths when conducting the three-point bending test. With the exception of f_{R1}, B1 also presented the highest scatter among the three batches, even though the dispersion was also similarly high in B2 and B3 with CV around 23% and 25%. Conversely, the results of the Barcelona test present the highest residual strengths in B1, with the exception of $f_{R0.5}$. Notice that lower residual strengths when compared to the three-point bending test are achieved, which is mainly attributed to the different cracking mechanism and the higher cracking area.

Regardless of the different results among batches, the average strengths (B1-B2-B3) in both the bending and the Barcelona test present a more reduced scatter. Considering the three batches together, for the bending test the CV is reduced to a value around 12%, whereas in the Barcelona test the average scatter is 5.8%. The similarity between the mechanical strength of the different batches reflects the homogeneity of the material, thus revealing a properly manufacturing procedure.

This document is the intellectual property of the fib – International Federation for Structural Concrete. All rights reserved.
This PDF of fib Bulletin 95 is intended for use and/or distribution solely within fib National Member Groups.

3.2 Correlation between tests

In order to achieve a correlation between the mechanical parameters of both tests, it is necessary to determine an equation using the experimental results obtained through the three-point bending test and the Barcelona test. A parametric analysis yielded that if using the load and the energy of the Barcelona test at displacements of 0.5, 1.5, 2.5 and 3.5 mm it is possible to obtain a correlated value of the load of the bending test at crack openings of 0.5, 1.5, 2.5 and 3.5 mm. Each crack opening of the bending test is correlated with the displacement counterpart of the Barcelona test in Equation 1. In other words, to obtain the flexural load at a CMOD of 0.5 mm ($F_{3PBT,0.5}$), the load and the energy of the Barcelona test at displacements 0.5 mm ($F_{BCN,0.5}$ and $E_{BCN,0.5}$) needs to be used.

$$F_{3PBT,i} = a \cdot F_{BCN,i} + b \cdot E_{BCN,i}^2 \quad (1)$$

At a first stage, it is necessary to count with results of both the bending and the Barcelona test so the parameters *a* and *b* of Eq. 1 can be calibrated given that both values depend on the properties of the concrete and the fibres and need to be recalibrated under any mixture of fibre modification. In this regard, the experimental results of B1 and B2 were used for the calibration, while B3 was used to verify the results. For this, instead of using only the average values of B1 and B2, the results of all the specimens tested were used in order to have a higher amount of data and increase the reliability of the correlation with more accurate results of *a* and *b*.

Notice that B1 presented 10 specimens for the three-point bending test and 20 for the Barcelona test. The results of the Barcelona test were therefore averaged by pairs, thus obtaining 10 results to be correlated with the 10 results of the bending test. The same procedure was followed for B2, which presented 6 specimens for bending and 12 for the Barcelona test. The parameters *a* and *b* after the calibration are shown in Table 3 for each crack opening.

Table 3: Calibrated parameters of correlation

CMOD [mm]	***a***	***b***
0.5	$1.19 \cdot 10^{-1}$	$7.11 \cdot 10^{-4}$
1.5	$1.76 \cdot 10^{-1}$	$1.80 \cdot 10^{-4}$
2.5	$1.76 \cdot 10^{-1}$	$1.53 \cdot 10^{-4}$
3.5	$1.95 \cdot 10^{-1}$	$8.94 \cdot 10^{-5}$

A schematic representation of how to obtain the load and the energy parameters of the bending and the Barcelona test is shown in Figure 4. The energy of the Barcelona test is calculated as the area under the Load-displacement curve up to the selected displacement. The example represents the parameters for a CMOD or a vertical displacement of 0.5 mm, even though the rest of parameters are calculated similarly.

This document is the intellectual property of the fib – International Federation for Structural Concrete. All rights reserved.
This PDF of fib Bulletin 95 is intended for use and/or distribution solely within fib National Member Groups.

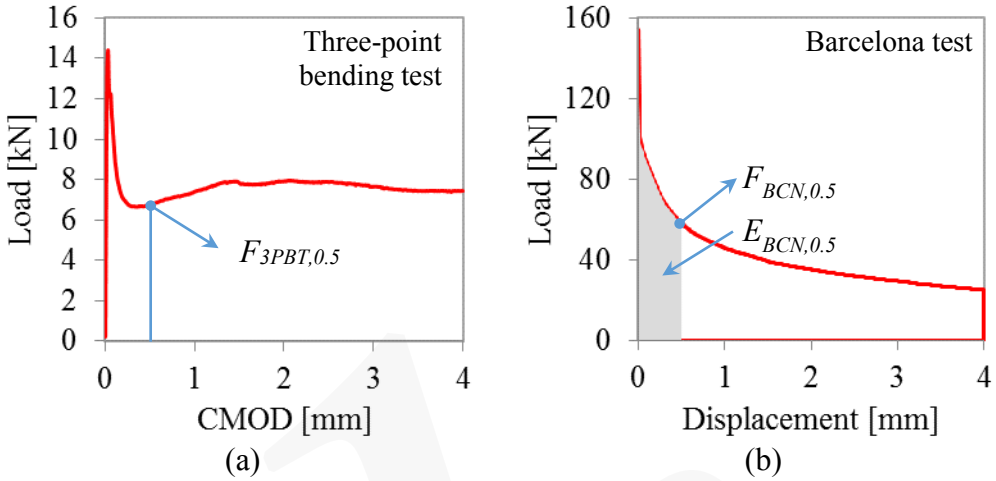
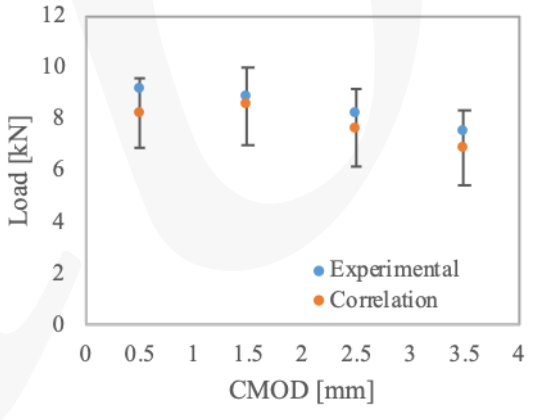


Figure 4: Three-point bending test (a) and Barcelona test curve (b)

The values in Table 4 show the experimental results of the bending test compared to the results of the correlation calculated with the parameters in Table 3 and the experimental results of the Barcelona test for B3. A confidence interval of 99% for each load and crack opening is also presented according to the results of the calibration.

Table 4: Experimental and correlated results

CMOD [mm]	F_{3PBT}^{exp} [kN]	F_{3PBT}^{corr} [kN]	$CI_{99\%}$ [kN]
0.5	9.14	8.24	1.33
1.5	8.85	8.53	1.51
2.5	8.26	7.64	1.54
3.5	7.55	6.84	1.45



A general overview of the results shows similar trends of both the experimental results and the correlated values. It is noteworthy that the average experimental results of the three-point bending test are slightly higher than the average results obtained by the correlation. The lowest value of the confidence interval corresponds to a safety margin that reduces the value of the experimental result to remain on the conservative side.

3.3 Assessment of the fibre content

Taking advantage of the interaction between the magnetic field and the fibres, it is possible to estimate a relation between the inductance and the content of fibres. For this, the inductance results on three perpendicular directions of the cubic specimen were determined (I_1, I_2 and I_z). Additionally, the real content of fibres in the specimen needs to be assessed. For this, 6 specimens of B1 were crushed and the fibres separated manually from the concrete.

This document is the intellectual property of the fib – International Federation for Structural Concrete. All rights reserved.
This PDF of fib Bulletin 95 is intended for use and/or distribution solely within fib National Member Groups.

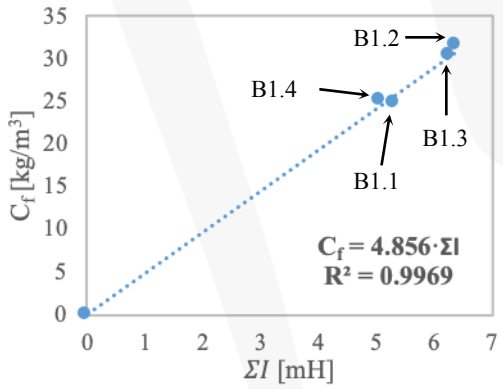
Table 5 shows the results of the inductance along with the content of fibres in each specimen determined after crushing.

Table 5: Inductive method results and content of fibres

Specimen designation	**Dimensions [mm]**	**I_1 [mH]**	**I_2 [mH]**	**I_Z [mH]**	**ΣI_i [mH]**	**Real fibre content [kg/m³]**
B1.1	150x150	2.30	2.27	0.76	5.33	24.7
B1.2	150x150	2.62	2.59	1.18	6.39	31.6
B1.3	150x150	2.47	2.40	1.42	6.29	30.5
B1.4	150x150	2.11	2.09	0.87	5.07	25.2
B1.5	150x150	2.48	2.44	0.85	5.77	29.4
B1.6	150x150	2.49	2.21	0.81	5.51	26.3

These results show an average content of fibres of 27.95 kg/m³ with a variability of 10.5%. This scatter is mainly attributed to the heterogeneity of the material and the random distribution of fibres within the concrete, as well as the reduced volume of the samples if compared to other test methods. In this regard, the production of the specimens is also affected by this heterogeneity thus resulting in different measured contents of fibres in specimens manufactured out of the same batch.

Based on previous research [8], the relation between the inductance and the content of fibres is shown in Figure 5. The X-axis represents the sum of the inductances measured in the three perpendicular directions ($\Sigma I = I_1 + I_2 + I_Z$) and the Y-axis states for the content of fibres (C_f). To determine this relation, only the results of B1.1, B1.2, B1.3 and B1.4 were used in order to verify the goodness of fit with B1.5 and B1.6. The relation between ΣI-C_f can be subsequently used to estimate the content of fibres of the rest of the specimens after conducting the inductive test.



Specimen	**Real fibre content [kg/m³]**	**Estimated fibre content [kg/m³]**	**Difference**
B1.5	29.4	28.0	4.7%
B1.6	26.3	26.8	1.7%

Figure 5: ΣI-C_f relation and real-estimated fibre content comparison in B1.5 and B1.6

The relation between the inductance and the content of fibres present an adjustment of R^2=0.99. Hence, a comparison between the real and the estimated content of fibres in B1.5 and B1.6 results in a maximum difference of 4.7%. Accordingly, the estimation of the fibre content in the specimens of B2 and B3 is shown in Figure 6 with the average real content of 27.95 kg/m³ obtained for the specimens of B1 as reference. In B2, the estimated content of

This document is the intellectual property of the fib – International Federation for Structural Concrete. All rights reserved.
This PDF of fib Bulletin 95 is intended for use and/or distribution solely within fib National Member Groups.

fibres was generally lower than the average real content, while in B3 fibres presented a closer content to the average content measured in B1.

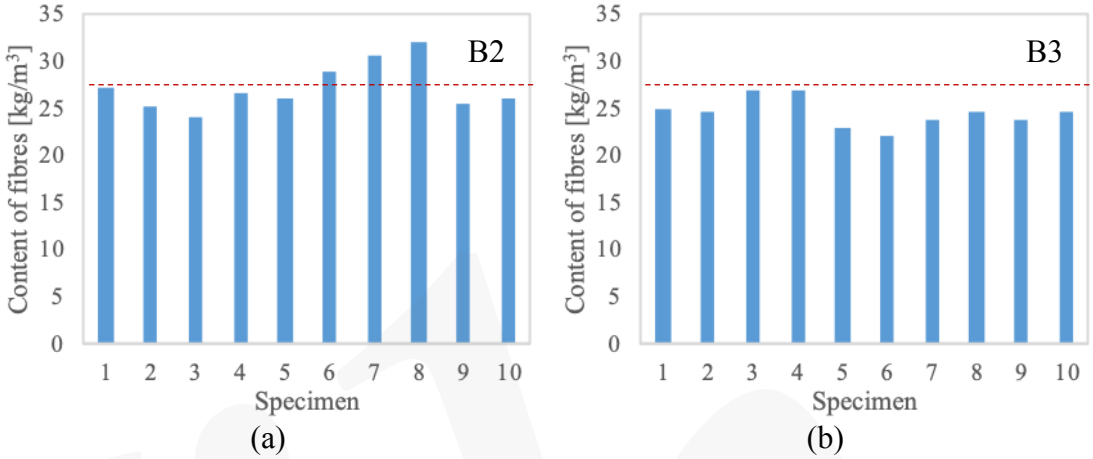


Figure 6: Content of fibres in specimens of B2 (a) and B3 (b)

The results show an average content of fibres of 27.32 and 24.63 kg/m^3 for B2 and B3, respectively. The associated scatter of these results are 9.3% and 6.2% considering the 10 specimens analyzed in each batch. The variability in the estimated contents should not be attributed only to the inductive method but also to the intrinsic variability of the content of fibres in FRC, as shown for the real contents determined in B1.

4 Concluding remarks

The simplicity of the Barcelona test represents a clear asset with respect to the three-point bending test. The smaller dimensions of the specimens compared to those required for the bending test or the lack of complex initial preparation such as the cut of the notch allows reducing the time of testing and simplifies the testing procedure. Another important advantage of the Barcelona test is that it does not require additional devices and the test can be performed in a conventional compressive equipment, thus reducing the costs.

According to the results of the correlation and the estimation of the content of fibres using the inductive test, several conclusions may be drawn from this study:

- The differences between the average experimental-correlated results range from a minimum 3.6% to a maximum of 9.8%. In this case of study, these differences were even lower than the scatter between batches when conducting the three-point bending test.
- The confidence intervals reveal maximum differences of 1.5 kN with respect to the average result of the correlation. These CI may be used to reduce the correlated value to remain on the conservative side with a 99% of probability that the experimental result of conducting a bending test would present a higher result than the correlation.
- The parameters *a* and *b* of the correlation equation determined for the concrete mixes of this study reach more accurate values when increasing the number of experimental results for the calibration. In this regard, it is important to count with

This document is the intellectual property of the fib – International Federation for Structural Concrete. All rights reserved.
This PDF of fib Bulletin 95 is intended for use and/or distribution solely within fib National Member Groups.

enough data to calibrate the results and minimize the differences with respect to the expected experimental results.

- The content of fibres was estimated using the inductive method with a relation presenting a goodness of fit of R^2=0.99. The correlation between the inductive measurements and the content of fibres needs, however, to be calibrated for each type of fibre. The scatter of the content of fibres in different specimens may be attributed to the inherent heterogeneity of FRC.

5 Acknowledgements

The authors wish to express their gratitude to the Spanish Ministry of Economy, Industry and Competitiveness for the economic support in the scope of the project SAES (BIA2016-78742-C2-1-R). The first author also acknowledges the Spanish Ministry of Education, Culture and Sport for providing support through the FPU grant.

6 References

[1] B. Parmentier, E. De Grove, Dispersion of the mechanical properties of FRC investigated by different bending tests, Tailor Made Concr. Struct. (2008).
[2] C. Molins, A. Aguado, S. Saludes, Double Punch Test to control the energy dissipation in tension of FRC (Barcelona test), Mater. Struct. 42 (2009) 415–425.
[3] International Federation for Structural Concrete, fib Model Code for Concrete Structures 2010, 2010.
[4] P. Pujadas, A. Blanco, S.H.P. Cavalaro, A. de la Fuente, A. Aguado, Multidirectional double punch test to assess the post-cracking behaviour and fibre orientation of FRC, Constr. Build. Mater. 58 (2014) 214–224.
[5] J.M. Torrents, A. Blanco, P. Pujadas, A. Aguado, P. Juan-García, M.Á. Sánchez-Moragues, Inductive method for assessing the amount and orientation of steel fibers in concrete, Mater. Struct. 45 (2012) 1577–1592.
[6] R. Perumal, Correlation of Compressive Strength and Other Engineering Properties of High-Performance Steel Fiber–Reinforced Concrete, J. Mater. Civ. Eng. 27 (2015) 04014114.
[7] Minelli, F. and Plizzari, G.A. (2011). A new round panel test for the characterization of fiber reinforced concrete: a broad experimental study. Journal of Testing and Evaluation, 39(5), 889-897.
[8] S.H.P. Cavalaro, R. López, J.M. Torrents, A. Aguado, Improved assessment of fibre content and orientation with inductive method in SFRC, Mater. Struct. 48 (2015) 1859–1873.
[9] S.H.P. Cavalaro, R. López-Carreño, J.M. Torrents, A. Aguado, P. Juan-García, Assessment of fibre content and 3D profile in cylindrical SFRC specimens, Mater. Struct. 49 (2016) 577–595.
[10] P. Pujadas, A. Blanco, S. Cavalaro, A. de la Fuente, A. Aguado, New analytical model to generalize the barcelona test using axial displacement, J. Civ. Eng. Manag. 19 (2013) 259–271.

This document is the intellectual property of the fib – International Federation for Structural Concrete. All rights reserved.
This PDF of fib Bulletin 95 is intended for use and/or distribution solely within fib National Member Groups.

Influence of the beam size on the residual strength of high performance fibre reinforced concrete

Eduardo Galeote[1], Ana Blanco[2], Sergio H.P. Cavalaro[2], Albert de la Fuente[1]

[1] : Universitat Politècnica de Catalunya, Barcelona, Spain.

[2] : Loughborough University, Loughborough, United Kingdom.

Abstract

The influence of size effect becomes an issue particularly relevant during the characterization stage of concrete at laboratory scale. The dimensions of the specimens have a direct influence on the strength measured and, therefore, selecting an appropriate specimen size is of utmost importance in order to obtain representative results to be used in the design of a structure. The notched beam test to characterize FRC is among the most extended methods to determine the design parameters of the residual strength, mainly associated to crack openings of 0.5 mm and 2.5 mm (f_{R1} and f_{R3}, respectively). The main objective of this study was to determine the influence of the beam dimensions on these two parameters. For this, an analytical model able to reproduce the flexural behavior of FRC was developed. Additionally, an experimental program involving high performance fibre reinforced concrete (HPFRC) beams of dimensions 40x40x160, 100x100x400 and 150x150x600 mm was conducted. The parameters of the analytical model were calibrated for each specimen dimension using the results of the experimental program. The results show a clear influence of the size of the specimen, mainly attributed to the area of fracture and the crack cross-section.

Keywords

FRC, size effect, constitutive law, back-calculation, specimen dimension

https://doi.org/10.35789/fib.BULL.0095.Ch05

This document is the intellectual property of the fib – International Federation for Structural Concrete. All rights reserved.
This PDF of fib Bulletin 95 is intended for use and/or distribution solely within fib National Member Groups.

1 Introduction

High performance fibre reinforced concrete (HPFRC) is a well-suited material to design slender elements and reduce concrete sections while keeping a high bearing capacity. However, the use of HPFRC is still limited mainly due to the high costs of production and a general reluctance in using non-conventional materials. It is for this reason important to delve into the behaviour of HPFRC in order to encourage its use in those situations in which it can arise as the most optimal solution.

The fib Model Code 2010 (MC2010) includes design recommendations for fibre reinforced concrete (FRC). In this regard, the constitutive law for FRC defines the post-cracking behaviour in terms of a Strength-Strain diagram with parameters obtained from standardised beams under three-point bending tests. Nevertheless, the response of concrete elements is affected by the so called size-effect. Even though this issue has already been addressed in the literature, the MC2010 does not specify clearly how to take into account the influence of the dimensions of the elements.

Previous studies have reported the advantages of using small beams to characterize FRC [1] since they are easier to handle and can be more representative of slender structural elements. In this line, the influence of using small beams to conduct bending tests and determine the parameters of the constitutive law for FRC should be assessed. For this, an experimental program involving four mixes of HPFRC with contents of fibres of 90 and 190 kg/m^3 was designed. For each mix, beams of three different dimensions were casted and tested under a three-point bending configuration to determine the post-cracking parameters. These parameters were used to calculate the constitutive law for FRC and subsequently compute a Strength-CMOD curve by means of a back-analysis.

The experimental results exhibit a clear influence of the dimensions of the beams on the residual strength of FRC. Additionally, the results of the back-analysis where compared to the experimental curves revealing that the parameters of the constitutive law of FRC should be calculated considering proportional crack openings and constant rotations. These are reasonable results given that strains remain constant and equal in the different beam dimensions.

2 Experimental program

2.1 Materials and specimens

Four high performance fibre reinforced concrete (HPFRC) mixes with fibre contents of 90 and 190 kg/m^3 and water to cement ratios (w/c) of 0.16 and 0.23 were produced. The content of fibres was increased by replacing an equivalent volume of silica sand in order to keep the content of cement constant. Nanosilica was introduced in a content of 5% over the cement weight (o.c.w.). The lower water content in mixes M90A and M190A was compensated with a greater content of superplasticizer. Further details of the mix proportioning are shown in Table 1.

Given the dimensions of the smallest specimens, microfibers were used in this experimental program. The use of microfibers leads to a higher number of fibres per volume

This document is the intellectual property of the fib – International Federation for Structural Concrete. All rights reserved.
This PDF of fib Bulletin 95 is intended for use and/or distribution solely within fib National Member Groups.

unit, which has several advantages such as scatter reduction [2]. The properties of the microfibers used in this experimental program are presented in Table 2.

Table 1: Concrete mixes

Materials	**M90A**	**M190A**	**M90B**	**M190B**
CEM I 52.5R [kg/m^3]	800	800	800	800
Silica sand 3 – 4 mm [kg/m^3]	1131	1098	1129	1098
Filler ($CaCO_3$) [kg/m^3]	200	200	200	200
Water [kg/m^3]	129	129	185	185
Nanosilica [l/m^3]	40	40	40	40
Superplasticizer [l/m^3]	32	32	16	16
Steel fibres [kg/m^3]	90	190	90	190

Table 2: Characteristics of the fibres

Characteristic	**Steel microfibres**	
Fibre shape	Straight	
Length [mm]	13	
Diameter [mm]	0.20	
Tensile strength [MPa]	2750	
Elastic modulus [GPa]	200	

The average results of the mechanical characterization of the four concrete mixes, along with their coefficient of variation (CV), is shown in Table 3. For each concrete mix, 3 cubic specimens of 150x150 mm and 3 cylindrical φ150x300 mm samples per mix were produced. Moreover, 3 prismatic samples with dimensions of 150x150x600 mm, 6 samples of 100x100x400 mm and 9 samples of 40x40x160 mm were casted, thus resulting in a total amount of 108 prismatic beams of three different dimensions. The cubic specimens were used to perform the compressive test according with EN 12390-3, the cylindrical samples to assess the modulus of elasticity following the indications of EN 12390-13 and the prismatic specimens to determine the flexural and residual strength through the three-point bending test with EN 14651. Bending tests were conducted keeping depth-span ratios constant, leading to spans of 133, 333 and 500 mm for specimens of 40x40x160, 100x100x400 and 150x150x600 mm, respectively.

3 Results

3.1 Post-cracking strength

The three-point bending test was conducted on beams of three different sizes to determine the influence of the dimensions on the flexural strength. To compare the average flexural strength between the different sized beams, the results are addressed in terms of Strength-Rotation (θ). The idea of using the rotation as an alternative parameter to CMOD in different sized

This document is the intellectual property of the fib – International Federation for Structural Concrete. All rights reserved.
This PDF of fib Bulletin 95 is intended for use and/or distribution solely within fib National Member Groups.

specimens for comparison purposes has been also supported by other authors [1]. The curves Strength-Rotation (θ) in Figure 1 exhibit the average rotation-hardening behaviour and a clear influence of the specimen size on the residual strength.

Table 3: Mechanical characterization of the concrete mixes

Parameter/ Size [mm]		**M90A**		**M190A**		**M90B**		**M190B**	
		Average [MPa]	**CV [%]**	**Average [MPa]**	**CV [%]**	**Average [MPa]**	**CV [%]**	**Average [MPa]**	**CV [%]**
f_{cm}		115.9	0.7	117.2	0.5	108.8	2.4	100.3	6.8
E_{cm}		36337	0.5	37674	0.5	32807	0.3	34095	9.3
f_{LOP}	40	10.38	4.4	9.80	15.6	8.67	10.9	8.06	7.3
	100	9.08	8.4	8.83	4.2	8.61	3.8	10.09	3.4
	150	8.02	6.5	9.54	6.8	7.86	2.3	8.16	-
f_{R1}	40	16.00	5.7	21.17	21.7	14.54	9.7	23.78	14.9
	100	13.98	2.1	23.01	8.9	13.72	12.9	19.07	10.4
	150	14.58	5.8	17.83	7.6	12.06	6.9	16.35	-
f_{R2}	40	14.09	6.2	17.46	22.8	12.71	10.2	20.17	19.2
	100	13.97	2.1	21.85	10.7	13.07	11.7	17.32	13.2
	150	14.63	4.0	16.96	2.7	11.99	4.0	15.75	-
f_{R3}	40	11.92	7.6	13.44	20.7	10.31	13.1	15.91	23.3
	100	12.53	3.9	18.00	13.8	11.54	11.4	13.88	15.2
	150	13.03	3.8	14.73	4.6	10.36	3.9	13.00	-
f_{R4}	40	10.00	8.7	10.61	19.1	8.30	16.7	12.64	23.7
	100	10.89	4.7	14.18	14.4	9.80	12.3	10.77	15.7
	150	11.18	3.7	11.99	4.3	8.69	3.6	10.37	-

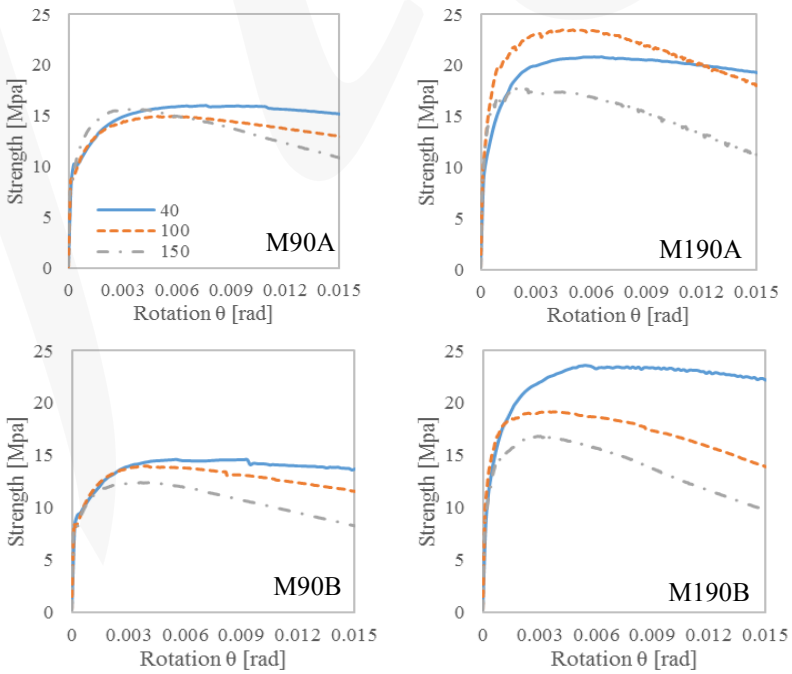


Figure 1: Residual strength of M90A, M190A, M90B and M190B for different dimensions

This document is the intellectual property of the fib – International Federation for Structural Concrete. All rights reserved.
This PDF of fib Bulletin 95 is intended for use and/or distribution solely within fib National Member Groups.

In line with the results of previous researches [3,4], the strength in mixes M90B and M190B decreased as the specimen size increased. However, such a clear trend between the strength and the size of the specimen could not be identified in mixes M90A and M190A. In M90A, the residual strength of large specimens was lower than in small samples even though up to a rotation of 0.006 rad the results of the three dimensions were similar. In M190A, 100 mm specimens exhibit the highest strength, whereas the lowest is obtained in specimens of 150 mm depth. Unlike in M90A, M90B or M190B, the smallest specimen (40 mm) of M190A did not display the greatest performance, but lower than 100 mm and higher than 150 mm.

The average f_{LOP} and the average maximum strength of the four HPFRC mixes are shown in Figure 2. Even though some cases exhibit greater performances while increasing the specimen size, the general trend indicates a reduction of both strengths with greater dimensions of the samples.

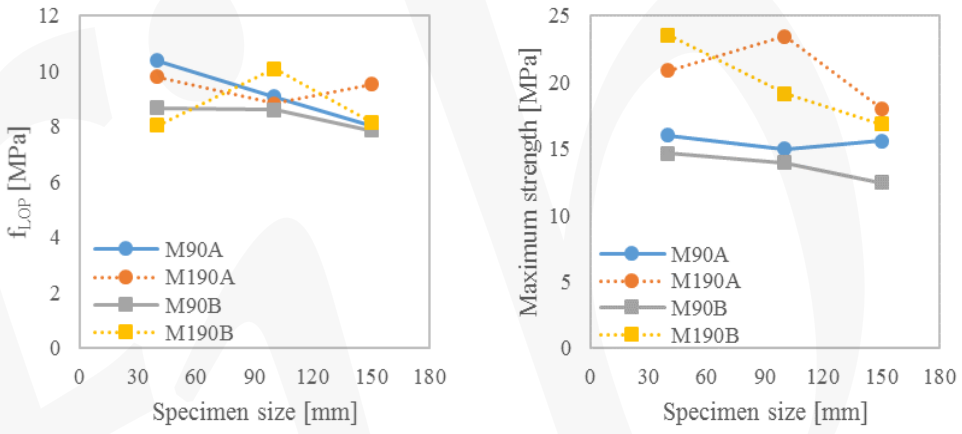


Figure 2: Size effect on (a) f_{LOP} and (b) maximum strength

The addition of different contents of fibres marginally influences the results of f_{LOP} given that this parameter is mainly dependent on the matrix properties. Notice that in the smallest specimens, mixes M90A and M190A presented higher values of f_{LOP} than mixes M90B and M190B, a behaviour that is a direct consequence of the w/c ratio. Moreover, the lower strength of mixes with 190 kg/m^3 with regard to their counterpart with 90 kg/m^3 confirms that increasing the content of fibres does not entail a greater cracking strength. Indeed, the lower results of mixes M190A and M190B with regard to M90A and M90B, respectively, may be a consequence of a higher induced porosity in the matrix as a result of the higher content of fibres [5,6].

The results in Figure 2b clearly show how increasing the content of fibres enhances the maximum residual strength. This effect is a direct consequence of increasing the amount of fibres in the cracked section [7,8]. The results also indicate the influence of the w/c ratio on the residual strength attributed to an improved bond strength at the fibre-matrix interface for lower w/c ratios [9].

The rotation at the maximum residual strength was assessed for the four mixes and three sizes of specimens. Figure 3 displays the rotation vs. specimen size relation with a generalised trend showing a decrease of the rotation while increasing the dimension of the specimen.

This document is the intellectual property of the fib – International Federation for Structural Concrete. All rights reserved.
This PDF of fib Bulletin 95 is intended for use and/or distribution solely within fib National Member Groups.

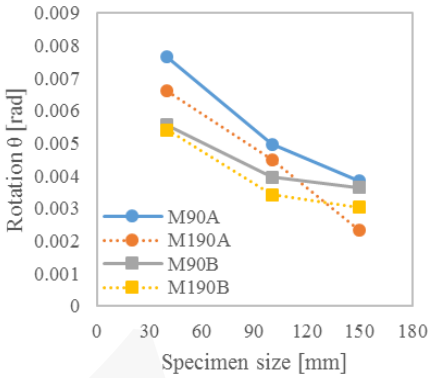


Figure 3: Size effect on rotation capacity at maximum residual strength

As the size of the specimen decreases, so does the rotation at the maximum residual strength. This decreasing trend with larger specimen dimensions is mainly attributed to the mutual dependency of the rotation and the maximum residual strength: the apparition of cracks activates the pull-out mechanism of the fibres and, for a same rotation, the crack opening in larger specimens is wider than in smaller samples. Therefore, the necessary external load to produce the pull out of the fibres should be higher in smaller than in larger specimens. Accordingly, the rotation in smaller elements should be higher than in larger to achieve an equivalent pull out and thus the maximum cracking strength.

It is worth mentioning that each mix involved the production of approximately 320 specimens, many of them for additional studies not related to the research described herein. The long time required for casting such a large number of specimens could have initiated the setting of concrete even before of having finished the casting of the specimens. This may have had a negative impact on the hardened behaviour of the samples, which could explain certain trends of the results.

3.2 Back-calculation

A back-calculation based on an analysis of evolutionary sections (AES) [10] with a multi-layer approach was used to determine analytically the flexural behaviour of FRC. In order to conduct the AES, several assumptions were adopted:

(i) Sections remain plane after loading or imposed strains.
(ii) Strain compatibility: perfect bond between concrete and fibres is assumed.
(iii) Shear stress strains are negligible and not considered.

The constitutive model of the MC2010 describing the behaviour of FRC at the post-cracking stage was implemented in the AES using the experimental data of the three-point bending tests of the four mixes. Different dimensions of specimens were analysed while the parameters of the constitutive law of the MC2010 are based on the results of the standardised beams with dimensions 150x150x600 mm. In this regard, the MC2010 suggests considering the characteristic length (l_{cs}) to be equal to the depth of the structural element to be designed.

The post-peak parameters of the constitutive model (f_{Fts}, f_{Ftu}) are obtained out of the residual strengths f_{R1} and f_{R3}, for which two approaches (Figure 4) may be considered when calculating these parameters. The first approach (Figure 4a) consists of considering the full

This document is the intellectual property of the fib – International Federation for Structural Concrete. All rights reserved.
This PDF of fib Bulletin 95 is intended for use and/or distribution solely within fib National Member Groups.

crack openings (FCO) of 0.5 and 2.5 mm regardless of the dimension of the specimen. The second approach (Figure 4b) suggests using an equivalent crack opening (ECO) depending on the depth of the specimen.

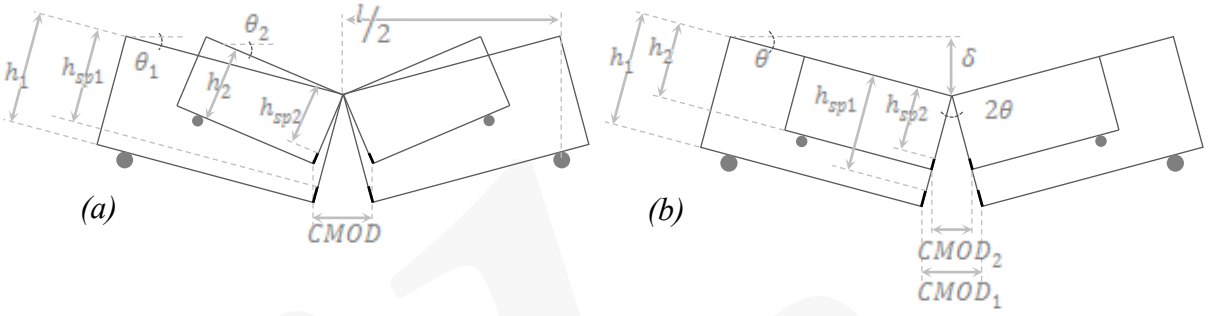


Figure 4: FCO approach (a) and ECO approach (b)

The approach affects both strains ε_{SLS} and ε_{ULS} since these parameters are calculated through the value of the crack opening. The mechanism of the FCO exhibits a CMOD in smaller specimens comparatively higher than in bigger samples. In this case, a constant CMOD entails greater deflections and larger strains ε_{SLS} and ε_{ULS} when reducing the specimen dimension (Figure 5a). Conversely, the ECO leads to identical deflections and strains for different sized beams with varying values of $CMOD_1$ and $CMOD_3$ with the beam size (Figure 5b).

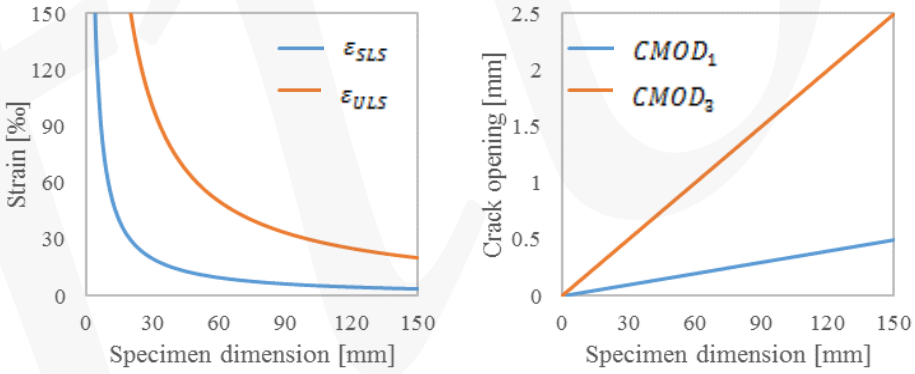


Figure 5: Strain variation for FCO (a) and CMOD variation for ECO (b)

3.3 Comparison of approaches

The parameters of the constitutive law present different values depending on the approach and have a direct influence on the results of the AES. Figure 6 shows the experimental curves of the four mixes compared to the analytical curves of the AES using the FCO and the ECO approaches with the constitutive law for FRC. The results are shown in terms of Strength-Rotation up to θ=0.02 rad, which corresponds to a strain at the notch ε=40‰. Notice that in specimens of 150 mm only one analytical curve is presented given that for this dimension the parameters of both approaches coincide.

This document is the intellectual property of the fib – International Federation for Structural Concrete. All rights reserved.
This PDF of fib Bulletin 95 is intended for use and/or distribution solely within fib National Member Groups.

A comparison between the analytical curves obtained using the FCO and the ECO approach reveals that calculating the constitutive law using the ECO approach, the analytical Strength-Rotation curves present a more accurate fitting with regard to the experimental results. These differences lay both on the strains and on the strengths associated to each approach. In addition, the content of fibres seems to affect the data fitting.

Up to the cracking point, there are no differences between approaches and the experimental result. This is attributed to the fact that up to this point, both approaches are defined according to the tensile strength branch of plain concrete as described in the MC2010, with both approaches sharing the same parameters. From this point onwards, and at the cracked stage, the differences on the constitutive law arise entailing the variations between the experimental and the analytical results.

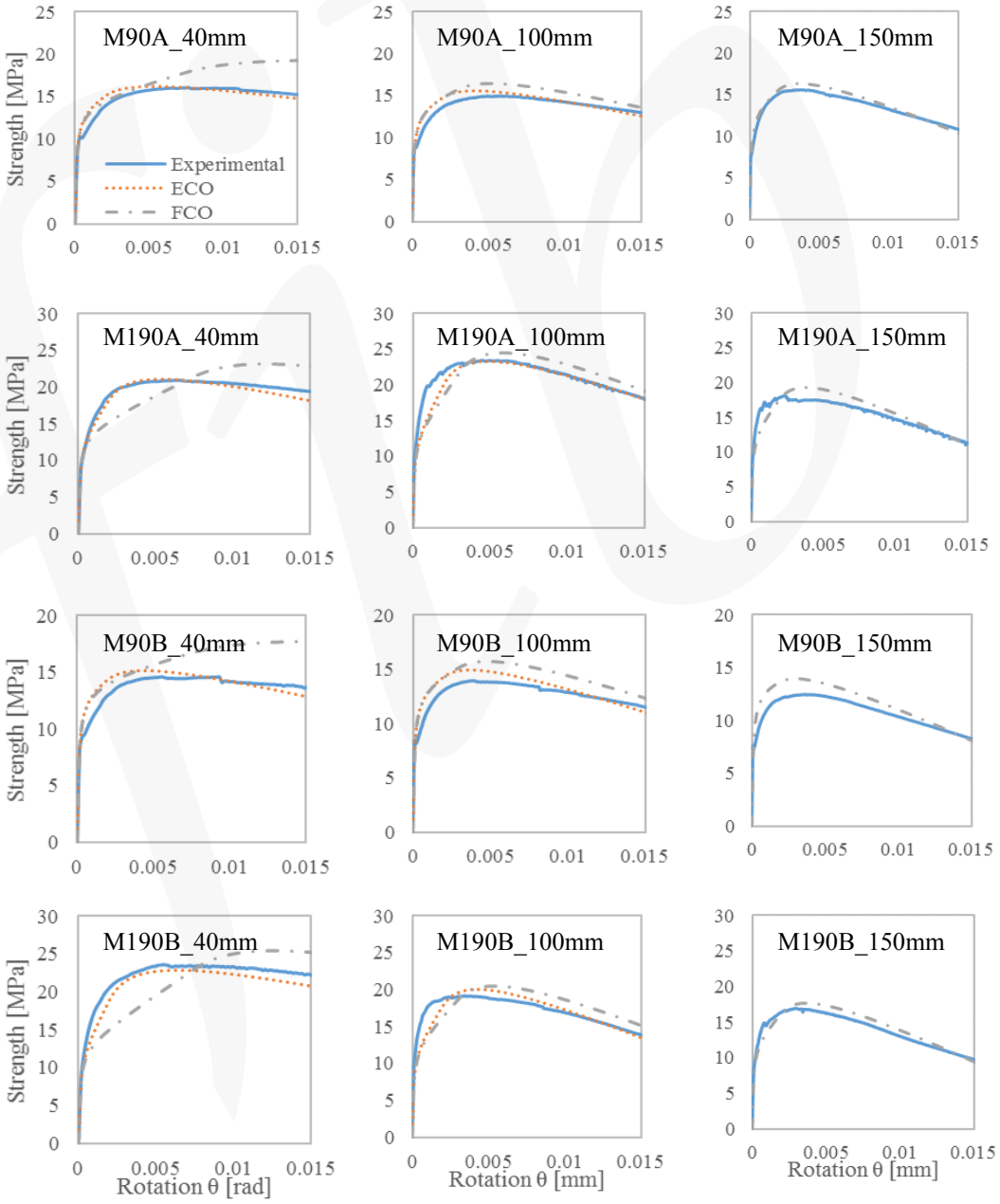


Figure 6: Comparison of experimental and analytical results

This document is the intellectual property of the fib – International Federation for Structural Concrete. All rights reserved.
This PDF of fib Bulletin 95 is intended for use and/or distribution solely within fib National Member Groups.

The differences between these two approaches become more pronounced while decreasing the size of the specimens. Notice the great variation between approaches at the specimens of 40mm. These variations also depend on the content of fibres of the mixes. In contents of 90 kg/m^3, the results of both the FCO and ECO present the same values up to a rotation θ=0.005 rad. From this point on, the FCO exhibits a higher strength than the ECO and the experimental results, the latter two presenting minimal differences. For contents of 190 kg/m^3, the FCO underestimates the strength up to a rotation of approximately θ=0.007 rad while overestimating it from this rotation on. Conversely, the ECO fits the experimental results along the entire curve.

4 Concluding remarks

Based on the results of the experimental program, the influence of the size effect on the flexural behaviour of HPFRC was assessed. Additionally, the constitutive law of the MC2010 was calculated using different sized specimens through a back-analysis and compared to the experimental data. According to the results presented, the following conclusions may be drawn:

- A clear influence of the dimensions of the specimens was observed on the residual strength of HPFRC. The post-cracking strength generally decreased while increasing the size of the element. Such a trend was more evident for the highest w/c ratio.
- The content of fibres has a strong influence on the maximum residual strength. The rotation at which the maximum strength is achieved decreases while the element size increases. This is attributed to the higher rotation required in smaller specimens to achieve an equivalent pull out of the fibres to larger samples.
- The analytical results of the AES fit more accurately the experimental curve when using the ECO to calculate the parameters of the constitutive law especially for reduced elements. In the largest specimens, the results of the ECO and the FCO coincide.

5 Acknowledgements

This research has been possible due to the economic funds provided by the SAES project (BIA2016-78742-C2-1-R) of the Spanish Ministry of Economy, Industry and Competitiveness. The first author acknowledges the Spanish Ministry of Education, Culture and Sport for providing support through the FPU fellowship. The authors also want to express their gratitude to Escofet S.A. for the collaboration during the experimental program.

6 References

[1] Giaccio G, Tobes JM, Zerbino R. Use of small beams to obtain design parameters of fibre reinforced concrete. Cem Concr Compos 2008;30:297–306.
[2] Vandewalle L. Hybrid fiber reinforced concrete. In: KONSTA-GDOUTOS MS, editor. Meas. Monit. Model. Concr. Prop., Dordrecht: Springer Netherlands; 2006, p. 77–82.

This document is the intellectual property of the fib – International Federation for Structural Concrete. All rights reserved.
This PDF of fib Bulletin 95 is intended for use and/or distribution solely within fib National Member Groups.

[3] Nguyen DL, Kim DJ, Ryu GS, Koh KT. Size effect on flexural behavior of ultra-high-performance hybrid fiber-reinforced concrete. Compos Part B Eng 2013;45:1104–16.
[4] Yoo D-Y, Banthia N, Yang J-M, Yoon Y-S. Size effect in normal- and high-strength amorphous metallic and steel fiber reinforced concrete beams. Constr Build Mater 2016;121:676–85.
[5] Yu R, Spiesz P, Brouwers HJH. Mix design and properties assessment of Ultra-High Performance Fibre Reinforced Concrete (UHPFRC). Cem Concr Res 2014;56:29–39.
[6] Söylev TA, Özturan T. Durability, physical and mechanical properties of fiber-reinforced concretes at low-volume fraction. Constr Build Mater 2014;73:67–75.
[7] Zerbino R, Tobes JM, Bossio ME, Giaccio G. On the orientation of fibres in structural members fabricated with self compacting fibre reinforced concrete. Cem Concr Compos 2012;34:191–200.
[8] Zhou B, Uchida Y. Influence of flowability, casting time and formwork geometry on fiber orientation and mechanical properties of UHPFRC. Cem Concr Res 2017;95:164–77.
[9] Lawler JS, Zampini D, Shah SP. Microfiber and Macrofiber Hybrid Fiber-Reinforced Concrete. J Mater Civ Eng 2005;17:595–604.
[10] De La Fuente A, Aguado A, Molins C, Armengou J. Numerical model for the analysis up to failure of precast concrete sections. Comput Struct 2012;106–107:105–14.

This document is the intellectual property of the fib – International Federation for Structural Concrete. All rights reserved.
This PDF of fib Bulletin 95 is intended for use and/or distribution solely within fib National Member Groups.
FRC2018: Fibre Reinforced Concrete: from Design to Structural Applications
Joint ACI-*fib*-RILEM International Workshop

Influence of test methodology on the applicability of test results of fibre reinforced concrete for design

Karoly Peter Juhasz[1], Peter Schaul[2], Ralf Winterberg[3]

[1] : Budapest University of Technology and Economics, Department of Mechanics, Materials & Structures, Műegyetem rakpart 1-3, Budapest, Hungary

[2] : Budapest University of Technology and Economics, Department of Construction Materials and Technologies, Műegyetem rakpart 1-3, Budapest, Hungary

[3] : BarChip Inc., Okayama, Japan

Abstract

The design of fibre reinforced shotcrete (FRS) hard rock linings is commonly based on the Q-System or Barton charts. This performance based design approach assess the results of experimental tests, carried out on panel specimens according to existing standards or guidelines. This is different to the general methodology to assess and determine the performance of fibre reinforced concrete (FRC) using standardized beam tests.

Panel and beam test results yield significantly different information on the performance of FRC and it is problematic to correlate them. The beam test yields a stress-strain relationship for a small displacement range only. Based on the significantly different working and failure mechanisms, structural tests to evaluate the post-crack performance and the ductility of FRS linings are typically conducted on different types of panels rather than on traditional beams. As a consequence, test results based on beam tests may lead to an overestimation of FRC performance in panels and vice versa. In order to avoid uneconomic designs the most appropriate material must be found using the most appropriate test methodology.

This paper discusses the difficulty in correlating test results obtained from beams and panels as well as the discrepancy in performance of different FRC using different test methodologies and aims to provide guidance on materials, testing and design.

Keywords

Synthetic fibre, FEA, panel test, testing methods

This document is the intellectual property of the fib – International Federation for Structural Concrete. All rights reserved.
This PDF of fib Bulletin 95 is intended for use and/or distribution solely within fib National Member Groups.

1 Introduction

The basis of the design for fibre reinforced shotcrete tunnel linings was stated in the middle of the 20th century. From these years the design procedure changed more from empirical to scientific, however the traditional and well-established recommendations will not be out of the daily practice. The basis of the shotcrete lining design in hard rock tunneling was quantitative tables, like the Q-Chart. Nowadays, with advanced finite element software, the rock separation and layering can be modelled, and from the calculated stresses the necessary fibre reinforcement for the shotcrete can be determined.

The Q-system was developed for classification of rock masses and ground and for evaluating the requirements for support in tunnels or rock caverns. It was developed by the Norwegian Geotechnical Institute (NGI) in the middle of the '70-s, originally included a little more than 200 tunnel case histories, mainly from Scandinavia (Barton et al., 1974). The system was updated to include more than 1000 cases (Grimstad and Barton, 1993). It is a classification system for estimates of tunnel support, based on a numerical assessment of the rock mass quality using several parameters. To get the overall rock mass quality a formula with three different quotients can be used, where the first parameters represent the relative measure of the rock size, the second quotient is described as an indicator of the inter-block shear strength, and the third quotient is described as the active stresses. The formula can be seen below:

$$Q = \frac{RQD}{J_n} \times \frac{J_r}{J_a} \times \frac{J_w}{SRF} \tag{1}$$

where:

- RQD: Rock quality designation (degree of jointing)
- J_n: Number of joint sets
- J_r: Roughness of the most unfavourable joint or discontinuity
- J_a: Joint alteration number
- J_w: Joint water reduction factor
- SRF: Stress reduction factor

From the Q value groups can be made to categorize the ground according to the rock mass quality. If the capacity of the rock is not sufficient, a common strengthening is to use fibre reinforced shotcrete and bolting. To define the necessary fibre reinforcement the energy absorption of the fibre reinforced shotcrete must be determined. This parameter can be obtained by means of panel tests (square or round), i.e. by measuring the middle point deflection and the reaction force. A further detailed overview on the design of fibre reinforced shotcrete linings is given in Nitschke and Winterberg (2016).

There are several recommendations for panel tests based on the geometry of the panel, the loading supports and the method of the loading. In Europe the basis of the panel tests were the recommendations of EFNARC (1996). Nowadays we use the harmonized European panel testing standard EN 14488-5:2006, which also employs a 600×600×100 mm centrally loaded square panel, but is supported by a continuous 20 mm wide steel frame (Bjoentegaard 2018).

This document is the intellectual property of the fib – International Federation for Structural Concrete. All rights reserved.
This PDF of fib Bulletin 95 is intended for use and/or distribution solely within fib National Member Groups.

In North America and in Australia round determinate panel (RDP) tests according to ASTM C 1550 (2012) are carried out, using a 75 mm thick panel with a diameter of 800 mm on three-point pivoted supports. To obtain a better fibre distribution and to reduce variability it is also possible to do super-size round panels with a diameter of 1200 mm and a thickness of 150 mm. These different panel tests all have in common that the specimens should be sprayed at the site and are not externally or internally compacted. For comparison, cast specimens that are compacted by vibration can also be used.

To design tunnels with Finite Element Analysis (FEA) software the measured energy absorption values are not sufficient; it is required to determine different concrete-specific and fibre reinforced concrete-specific parameters as well. One of the key parameters is the residual flexural strength, which describes and quantifies the fibre effect in the concrete. This parameter can be determined by using the harmonized European beam test EN 14651:2005, measuring the load vs. the crack mouth opening displacement (CMOD). This is a three-point bending test with a notch in the centre of the beam span. Material parameters can be gained from the residual flexural strength values according to different guidelines (Model Code 2010, 2012; RILEM, 2003; OVBB, 2008; ACI 544, 1999) which can be used in calculations. The parameters can be gained also form four point bending tests like ASTM C1609.

The process of a panel test is relatively quicker compared to a beam test, with a lower variability of results. The beam tests need more preparation and the results could be misleading because of limited crack propagation and the variability is usually high with COV's up to over 30%. There are methods to reduce the variability, but this makes the tests even more complex (Juhasz, 2015). Similar research has been done by Bernard (Bernard, 2002) comparing beam and panel tests (square and round panels).

Laboratory research is presented in this paper, where panels and beams were tested. Results were compared and a numerical FEA model was made to estimate the results of both types of test with the same material model parameters. The possibility of estimating the material parameters from panel tests was then examined.

2 Laboratory test

2.1 Test matrix

Sprayed panels and cast beams were produced to complete the previously presented test matrix (Juhasz et al., 2017). With this the results of plain concrete and FRC using three dosages of macro synthetic fibres (BarChip 48) were completed using one typical shotcrete fibre (BarChip 54). For the new series, three square panels and three beams were made. The specimens were produced in a tunnel jobsite in Poland and the test was carried out at the Adolf Czako Laboratory of the Department of Mechanics, Materials & Structures, Budapest University of Technology and Economics. The tests were conducted using a Zwick Z150 universal testing machine. The test matrix can be seen in Table 1, with the new series in the right-most shaded column.

For the tests a sprayed concrete mixture was designed according to Table 2.The panels were sprayed and the beams were cast at the field. The model was a simplified model, it did not take into consideration some effect, like the fibre orientation, which can has a significant role in the fibre work (Juhász, 2019). The macro synthetic fibre was BarChip 54 with

This document is the intellectual property of the fib – International Federation for Structural Concrete. All rights reserved.
This PDF of fib Bulletin 95 is intended for use and/or distribution solely within fib National Member Groups.

3.0 kg/m^3 dosage. The fibre length is 54 mm, it is continuously embossed and has a minimum tensile strength of 640 MPa.

Table 1: Test matrix

Fibre dosage	Plain concrete	2.5 kg/m^3 BC48	5.0 kg/m^3 BC48	7.5 kg/m^3 BC48	3.0 kg/m^3 BC54
Square panels	SQ PC 1-3	SQ 2.5 1-3	SQ 5.0 1-3	SQ 7.5 1-3	SQ 3.0 1-3
	cast	cast	cast	cast	sprayed
Beams	B PC 1-4	B 2.5 1-4	B 5.0 1-4	B 7.5 1-4	B 3.0 1-3
	cast	cast	cast	cast	cast

Table 2: Concrete mix design

Component	Type	[kg/m^3]
Cement	Holcim	400
Silica fume	Mapeplast SF	40
Sand d_{max}= 8mm		1320
Superplasticizer	Mapei Nrg 1012	3.0
Fibres	BarChip 48 and 54	2.5; 3.0; 5.0; 7.5
w/c	0.5	

The beam and the panel test specimens were all stored under water according to EN 12390-3 and EN 14488-5. The specimens' testing date was at the age of 28 days.

2.2 Testing methods

The panel tests were carried out according to the EN 14488-5 standard. The geometry of the specimen was 600×600 mm with 100 mm thickness. The panels were tested on a steel support frame according to the standard mentioned above (see Figure 1).

A levelling mortar layer was applied between the sample and both the loading block and the square support frame. The test was displacement controlled with a speed of 1 mm per minute. The load-deflection curve was recorded and the test was continued until a deflection of at least 30 mm was reached at the centre point of the slab. This also allows to investigate the fibre effects in larger crack widths.



Figure 1: Setup of panel test according to EN 14488-5:2006

This document is the intellectual property of the fib – International Federation for Structural Concrete. All rights reserved.
This PDF of fib Bulletin 95 is intended for use and/or distribution solely within fib National Member Groups.

Beam testing was similar to the specification of ASTM C1609. The test was a four point bending test of the macro synthetic FRC specimens with a length of 700 mm, cross-section of 150×150 mm on 450 mm span). The loading of the beam was in the third points of the beam. The testing machine used was the same deflection controlled universal testing machine used for the panel tests. The testing speed was 0.25 mm/min up to 0.5 mm centre point deflection, and 1.0 mm/min thereafter. The test was continued out to 4 mm deflection. The load and the centre point displacement were recorded during the test.

3 Test results

The square panel test results can be seen in Figure 2 and the beam test results in Figure 3. Compared to the previous research (see Figures 4 and 5) the sprayed panel results had a larger dispersion, and also the tests with the four point beams led to a higher variability. It can be also seen that the dispersion of the post-crack beam results are significantly higher than in case of the panels. The resulting crack patterns of the panels were absolutely different, depending on the fibre dose rate (see Figure 6). The general post-crack behaviour of the panels and the beams is similar: after the peak load a small drop can be seen and after this the fibres engage and provide a stable performance.

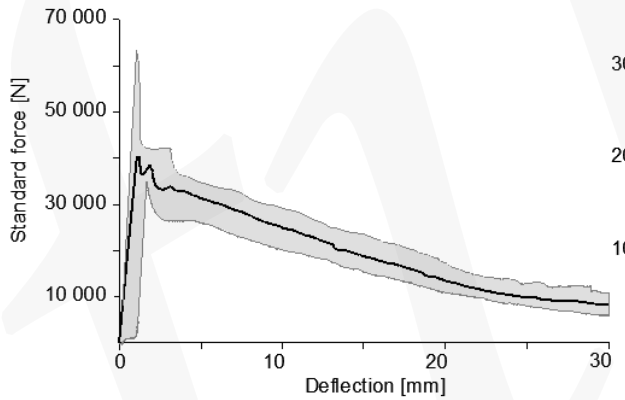


Figure 2: Sprayed square panel test results

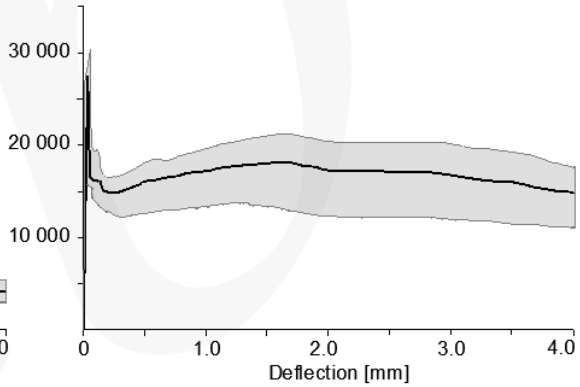


Figure 3: Cast beam test results

Due to the high variability the mean values of the beam results are not normative and the results had to be modified. To calculate a modified mean value, after the test the number of the fibres on the cracked cross section was counted in five different layers. With this method developed by Juhász (Juhasz, 2013) the effect of fibre orientation and the improper location are eliminated from the results. This modified mean value better represents the real capacity of the fibres.

By raising the dosage of fibres in the concrete more and more cracks appear. To compare the effect of the fibres with different dosages the area under the load-deflection curve in the case of panels, and the area under the load-CMOD diagram, can be calculated.

This document is the intellectual property of the fib – International Federation for Structural Concrete. All rights reserved.
This PDF of fib Bulletin 95 is intended for use and/or distribution solely within fib National Member Groups.

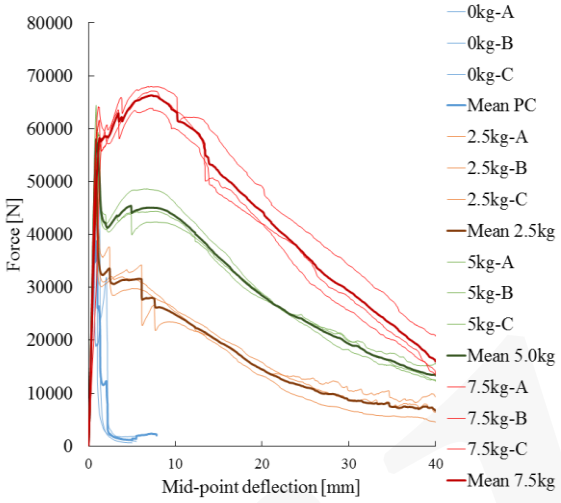


Figure 4: Cast square panel test results

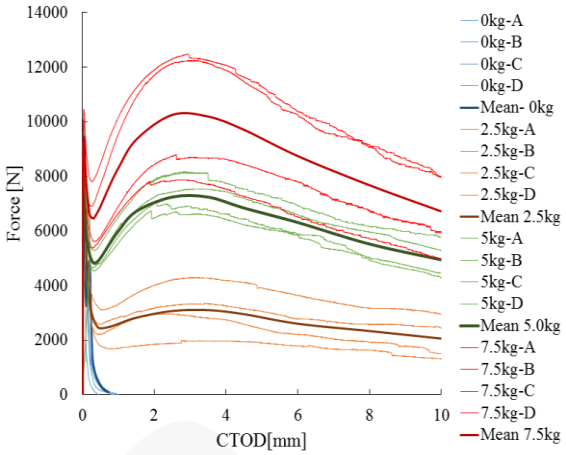
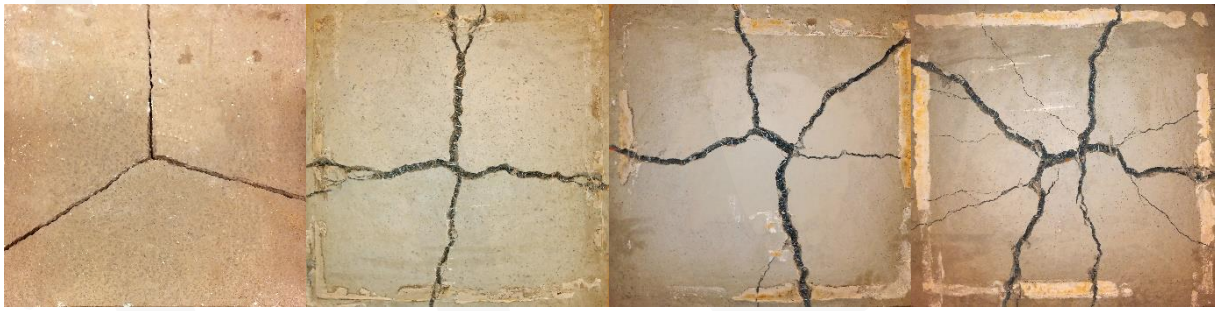


Figure 5: Cast beam test results

Due to their different working mechanism, the correlation between panel and beam tests can't be formulated directly, but the test could be modelled using advanced Finite Element Analysis (FEA).



Plain concrete 2.5 kg 5.0 kg 7.5 kg

Figure 6: Ultimate crack patterns of the panels

4 Numerical modelling

4.1 Material model of concrete and FRC

The behaviour of FRC material is analysed using ATENA (Cervenka et al., 2016) for non-linear analysis of concrete structures. ATENA is capable of a realistic simulation of concrete behaviour in the entire loading range with ductile as well as brittle failure modes as shown for instance in Cervenka (2002). It is based on the finite element method and non-linear material models for concrete, reinforcement and their interaction. The tensile behaviour of concrete is described by smeared cracks, crack band and fracture energy and the compressive behaviour of concrete by a plasticity model with hardening and softening. The constitutive model is described in detail in Cervenka & Papanikolaou (2008). The non-linear solution is performed incrementally with equilibrium iterations in each load step. Numerous other models can be used to approximate the post-cracking capacity of FRC. The model presented in the ITAtech guideline (ITAtech Activity Group Support, 2016) was used here.

This document is the intellectual property of the fib – International Federation for Structural Concrete. All rights reserved.
This PDF of fib Bulletin 95 is intended for use and/or distribution solely within fib National Member Groups.

A thin band with micro-cracks will appear due to the tensile stress in the concrete – which is called the crack process zone. By increasing the stress the concrete reaches its tensile strength when the micro cracks are touching each other. After this point the tensile capacity of the concrete will decrease, the cracks will bypass or cross the aggregates and then the entire section will be crossed by a macro crack. The area under the "tensile stress – crack width" diagram is the fracture energy.

The fracture energy of the concrete is influenced by a number of factors which are clearly not related to the concrete's strength class. Most of the existing design methods neglect the fracture energy of the concrete and do not pay much attention to the tensile strength. However, when designing FRC structures these parameters cannot be ignored.

The main goal in this method is to separate the fracture energy of the concrete (G_F) and added fracture energy by the fibres (G_{Ff}). According to previous research (Juhász, 2015) the added fracture energy depends on the fibre type, dosage and cement mortar (cement, water and sand). By knowing these values the added fracture energy can be defined and used as a parameter partly independent from the concrete.

The most sophisticated model of FRC material represents an extension to the fracture-plastic constitutive law (Cervenka & Papanikolaou, 2008). It describes the tensile behaviour according to the material response measured in tests point-wise in terms of the stress-strain relationship. The first part of the diagram is the usual stress-strain constitutive law. After exceeding the localization strain ε_{loc} the material law assumed for the characteristic crack band width L_{ch} is adjusted to the actual crack band width L_t. The characteristic crack band width (characteristic length) is the size (length) for which the defined material law is valid. The same procedure (with eventually different characteristic length) is used for the compression part of the material law. The softening law in compression is linearly descending and the end point of the softening curve is defined by the plastic displacement w_d. By increasing the material parameter w_d the contribution of the fibres to the compressive behaviour of concrete is considered. Another important parameter for FRC modelling is the reduction of the compressive strength due to developing cracks that determine how the strength is reduced while the material is subjected to lateral tension.

The numerical verification was made using ATENA. To get a proper result the full experimental setup had to be modelled, including the loading device, the supports and the levelling mortar layer. To be able to model the curling rise of the panel's corners from the steel formwork, a non-linear interface material was applied between the concrete panel and the centrally located steel loading plate.

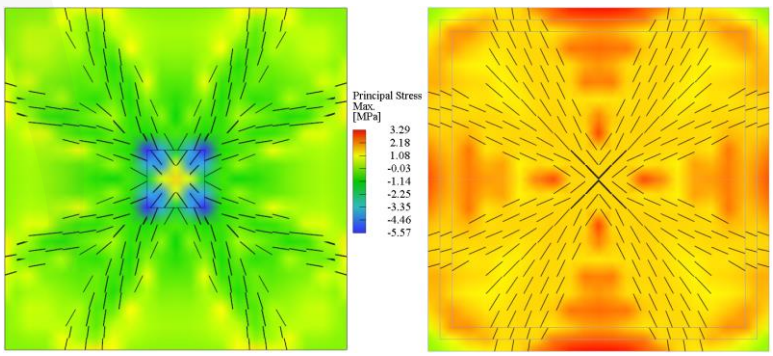


Figure 7: Numerical model of the panel with upper surface (left) and bottom surface (right)

This document is the intellectual property of the fib – International Federation for Structural Concrete. All rights reserved.
This PDF of fib Bulletin 95 is intended for use and/or distribution solely within fib National Member Groups.

The material parameter of this layer was adjusted as for the parameters of the mortar layer to simulate friction as well. The compressive strength of the interface layer was 10-times higher than the shear and tension capacity. The virtual test was displacement controlled to be able to model the post-crack behaviour of the panel. During the analysis the mid-point deflection and the reaction force was measured.

Structural hexahedra mesh was used in the model to obtain the proper crack propagation. The size of the brick elements was 25 mm in every case. Figure 7 shows the principal stress and cracks of the panel when modelled by FEA (upper surface of the panel on the left and lower surface on the right). The material parameters used were determined by inverse analysis.

5 Results of the numerical model

The mean values of the tests and the numerical results of the panels can be seen in Figure 8a. The behaviour and value of the numerical model closely matches the test results for each dosage of fibre. The peak load is almost the same, and the slope of the curve from FEA is close to the test curve for each fibre dosage. Note that the maximum difference in the areas under the curves was only 7%.

Using the same material parameters the beam tests were modelled with ATENA and the results can be seen in Figure 8b. The differences in the areas under the curves range from 4% to 18% using modified mean values, and 4% to 10% using mean values.

Material parameters can be derived from panel tests, where there is much lower variability of the results than for beam tests. The residual strength parameter is a function of the fibre dosage, which produced a nearly linear function in the test series. Using FEA a correlation can be made between the dosage of fibres and their performance. Even using a linear residual strength model the correlation is acceptable, leading to a proper material model.

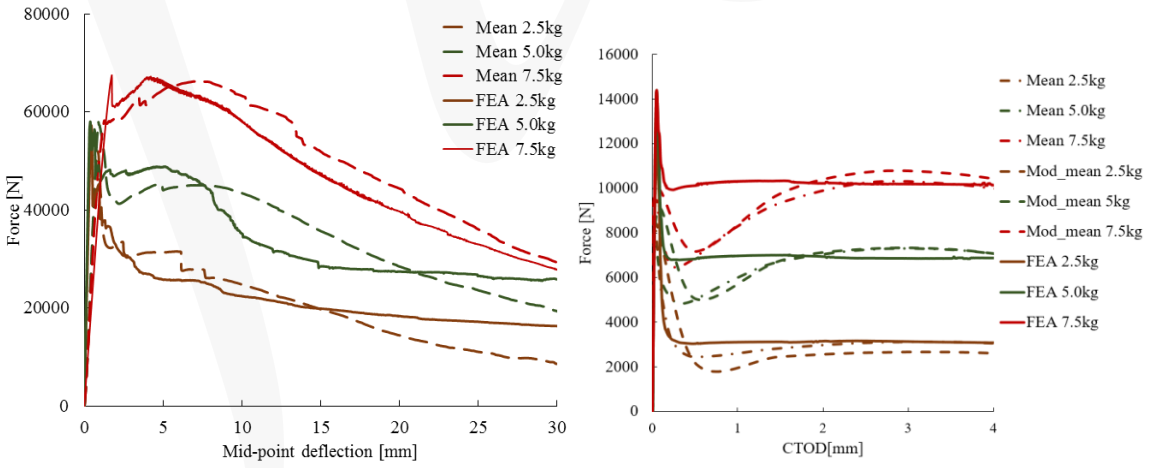


Figure 8: Results of the panel (a) and beam tests (b) with their modelling by FEA

This document is the intellectual property of the fib – International Federation for Structural Concrete. All rights reserved.
This PDF of fib Bulletin 95 is intended for use and/or distribution solely within fib National Member Groups.

6 Conclusion

Macro synthetic fibre reinforced concrete structures are becoming more common in the tunnelling industry, especially in shotcrete tunnel linings. Both for the design and for their calculation the performance of the fibres in the concrete has to be determined. The current tests used in Europe are the square panel test and the three point bending beam test which define the fibre reinforced concrete's post crack performance. Beam tests are more common to designers, although they have an inherent high variability. Square panel tests provide a more favourable variability, but the material parameters cannot be directly obtained from their results so far. However, the square panel test results can be used to determine the fibre reinforced concrete energy absorption which can be applied in the design with the Q-Chart.

To try to find a correlation between fibre reinforced concrete panel and beam tests, a laboratory test series was carried out using a typically used sprayed concrete mixture and both beams and panels were cast with different dosages of macro synthetic fibres. According to the results a direct correlation cannot be found between the two different testing methods because of the different working and failure mechanisms: while in the case of square panels the number of cracks increases with an increase in the amount of fibres added, opposed to the beam tests where there is only one crack located in the centre of the beam due to strain localization in a static determinate setup.

A numerical model was developed to be able to do further calculations from the panel results. A finite element material model was defined for all square panel tests with an inverse analysis calculation undertaken which well corresponds to the area under the individual load-deflection curves. This defined material model is capable of calculating the beam performance using the same material properties and thus, the further calculation and design became possible. It could be useful for design engineers to verify a material model using only panel tests. Further research is planned to determine the performance of different fibres in panels and beams and to compile a database for design engineers with the test results.

7 References

ACI Committee 544.4R-88. (1999), *Design Considerations for Steel Fibre Reinforced Concrete*, ACI Committee 544, Farmington Hills: American Concrete Institute. 18 p.

ASTM C 1550 (2012), *Standard Test Method for Flexural Toughness of Fiber Reinforced Concrete (Using Centrally Loaded Round Panel)*

Bernard, E.S. (2002), *Correlations in the behavior of fibre reinforced shotcrete beam and panel specimens,* Materials and Structures 35. pp 156-164.

Bjoentegaard, O., Myren, S., (2018), *Fibre Reinforced Sprayed Concrete Panel tests - test procedures and Influencing Factors*. In: Kusterle, W. (Ed.), Proc. Spritzbeton-Tagung 2018, Alpbach, Austria, January 11 and 12.

Cervenka, J., Papanikolaou V.K. (2008), *Three dimensional combined fracture-plastic material model for concrete*, International Journal of Plasticity (24). pp 2192-2220.

Cervenka, V., Jendele, L., Cervenka, J. (2013), *ATENA Program Documentation: Part 1 Theory,* Prague: Cervenka Consulting s.r.o. 318 p.

EFNARC. (1996), *European Specification for Sprayed Concrete. European Federation for Specialist Construction Chemicals and Concrete Systems*, www.efnarc.org

EN 14487-1, (2005), *Sprayed concrete - Part 1: Definitions, specifications and conformity* Brussels: European Committee for Standardization (CEN). 41 p.

This document is the intellectual property of the fib – International Federation for Structural Concrete. All rights reserved.
This PDF of fib Bulletin 95 is intended for use and/or distribution solely within fib National Member Groups.

EN 14488-3, (2006), *Testing sprayed concrete, part 3: Flexural strengths of fibre reinforced beam specimens*, Brussels: European Committee for Standardization (CEN). 12 p.

EN 14488-5, (2006), *Testing sprayed concrete - Part 5: Determination of energy absorption capacity of fibre reinforced slab specimens,* Brussels: European Committee for Standardization (CEN). 8 p.

EN 14651, (2005), *Test method for metallic fibered concrete - Measuring the flexural tensile strength (limit of proportionality (LOP), residual)*

EUROCODE EN 1992. (2004), *European Code for design of concrete structures,* Brussels: European Committee for Standardization)

fib Model Code 2010, (2012), *Bulletin 65 and 66*, Fédération Internationale du Béton, Lausanne.

Grimstad, E., Barton, N. (1993), *Updating of the Q system for NMT,* Proceedings of the International Symposium on Sprayed Concrete. Modern Use of Wet Mix Sprayed Concrete for Underground Support, Fagernes. Oslo: Norwegian Concrete Association. 18 p.

ITAtech Activity Group Support (2016), *ITAtech Guidance for Precast Fibre Reinforced Concrete Segments – Vol. 1: Design aspects,* ITAtech Report N°7. Avignon: Longrine. 48 p.

Juhász, K.P. (2013), *Modified fracture energy method for fibre reinforced concrete*, in Fibre Concrete 2013: Technology, Design, Application (ed. Kohoutkova A, et al). Prague: Faculty of Civil Engineering Department of Concrete and Masonry Structures. pp. 89-90

Juhász, K.P. (2015), *Evaluation of fibre reinforced concrete beam test results based on the examination of the real fibre distribution*, In: 8th International Conference Fiber Concrete 2015, Prague. 9 p.

Juhász, K.P., Nagy, L., Schaul, P., (2017), *Correlation of the results of the standard beam and EFNARC panel test,* Proceedings of the World Tunnel Congress 2017, Bergen, Norway, 09–15 June 2017

Juhász, K.P (2019), *Analytical model for rigid (steel) and flexible (synthetic) fibre mixing in concrete* In: IOP Conf. Series: Materials Science and Engineering 596

Kolmar, W. (1986), *Beschreibung der Kraftuebertragung über Risse in nichtlinearen Finite-Element-Berechnungen von Stahlbetontragwerken*, Dissertation, T.H. Darmstadt.

Menétrey, P., William K.J. (1995), *Triaxial Failure Criterion for Concrete and Its Generalization,* ACI Structural Journal 92(3). pp 311-318.

Nitschke, A., Winterberg, R., (2016), *Performance of Macro Synthetic Fiber Reinforced Tunnel Linings,* Proceedings of the World Tunnel Congress 2016, San Francisco, USA, 22–28 April 2016

Österreichische Vereinigung für Beton- und Bautechnik, (2008*), Richtlinie Faserbeton.* Wien: Österreichische Vereinigung für Beton- und Bautechnik, 109 p.

RILEM TC 162-TDF. (2003), *Final recommendation of RILEM TC 162-TDF: Test and design methods for steel fibre reinforced concrete,* Materials and Structures 36 (262). pp 560–567.

This document is the intellectual property of the fib – International Federation for Structural Concrete. All rights reserved.
This PDF of fib Bulletin 95 is intended for use and/or distribution solely within fib National Member Groups.
FRC2018: Fibre Reinforced Concrete: from Design to Structural Applications
Joint ACI-*fib*-RILEM International Workshop

Parameters affecting the properties of plain and fiber reinforced self-consolidating concrete

Armin Javadian[1], Amir Mahdavi[1], Othman Benamrane[2], Muslim Majeed[3] and Hassan Aoude[4]

[1] : Master's graduate, University of Ottawa

[2] : Undergraduate student, University of Ottawa

[3] : Technical officer and Researcher, University of Ottawa

[4] : Associate Professor, University of Ottawa

Abstract

This study examines the effect of fiber properties, single fiber type and hybrid fibers on the fresh-state and hardened-state properties of self-consolidating fiber-reinforced concrete (SCFRC). As part of the study, 16 mixtures are examined with variables including the effect of fiber type, length, aspect ratio, and hybrid use of fibers (short and long fibers). Properties in the fresh state are studied using standard SCC tests including: slump flow, V-funnel and visual stability index (VSI) tests. Mechanical properties are studied by testing prisms under four-point flexural loading in accordance with the ASTM C1609 standard. The results demonstrate that self-consolidating FRC mixtures are possible at moderate fiber contents, however, once the limiting fiber contents are exceeded workability and mix uniformity are lost. The results also show the effects of fiber content, fiber type, fiber properties and hybrid fibers on the flexural toughness of SCFRC.

Keywords

FRC, steel fibers, Hybrid fibers, SCC, SCFRC, Workability, Toughness

This document is the intellectual property of the fib – International Federation for Structural Concrete. All rights reserved.
This PDF of fib Bulletin 95 is intended for use and/or distribution solely within fib National Member Groups.

1 Introduction

The addition of fibers to concrete improves its tensile capacity, post-cracking resistance, and toughness. In structural load-bearing members, the use of fiber reinforced concrete (FRC) also improves shear resistance, flexural ductility and confinement, and reduced rebar congestion in reinforced concrete structural components is possible (Minelli and Plizzari, 2013; Campione et al. 2010). However, the use of fibers in traditional concrete reduces workability and can result in difficulties during concrete placement, particularly at the higher fiber contents required for structural applications. The combined use of self-consolidating concrete (SCC) and steel fibers has been proposed as a solution to this problem (Khayat and Roussel, 2000).

When compared to conventional fiber-reinforced concrete (FRC), self-consolidating fiber-reinforced concrete (SCFRC) can eliminate or reduce the need for vibration, which can allow a uniform dispersion of fibers (Ferrara and Meda, 2006; Ferrara et al. 2007). Research has shown that fresh-state and hardened-state characteristics of SCFRC can be affected by the volume fraction, length and aspect ratio of fibers. Grünewald (2004) showed that there is a direct relationship between the aspect ratio of fibers and flowability of SCC reinforced with fibers. According to his research, mixes containing fibers with higher aspect ratio showed lower workability in comparison to mixes containing fibers with lower aspect ratio. Similarly, Grünewald (2004) showed that using longer fibers leads to reduction of the workability and an increase of segregation probability of SCFRC. In addition, this study reported that the steel fiber volumetric ratio should be limited to less than 2%, to maintain adequate workability in SCFRC. Researchers have also shown that the hybrid use of fibers having different lengths can positively affect the fresh-state properties of fiber-reinforced SCC (Sahmaran and Yaman, 2005 and 2007). While important research exists on SCFRC there is a need for further studies to examine how fiber properties (content, type) affect both the fresh and hardened state properties of SCFRC. The effect of hybrid fibers on the properties of SCFRC also deserves further study.

This paper presents the results of a study examining the effect of fiber properties and hybrid fibers on the fresh-state and hardened-state properties of self-consolidating fiber-reinforced concrete (SCFRC). As part of the study, 16 mixtures were examined with variables including the effect of fiber type, length, aspect ratio, and hybrid use of fibers. Properties in the fresh state are studied using standard SCC tests including: slump flow, V-funnel and visual stability index (VSI) tests. Mechanical properties are studied by testing standard cylinders in compression and prisms under four-point flexural loading in accordance with the ASTM C1609 standard.

2 Experimental program

2.1 Reference SCC mixture

Table 1 lists the composition of the reference SCC mix in this study. It is noted that the granular skeleton of the base SCC mix was not optimized for each fiber. Rather, the same reference SCC mixture was used for all fibers. The mix was selected based on a series of 19 trial batches that aimed at producing a stable SCC mix having a slump flow ≥ 700 mm and 28-day compressive strength ≥ 40MPa, before adding the fibers (Javadian, 2012). As shown in Table 1, the mix contained general use blended cement with 8 percent silica fume (GUB-8SF) and Type S ground granulated blast furnace slag (GGBFS). The examined water-cement ratio was 0.44. The aggregates were well-graded crushed limestone granulate having a maximum size of 12.5 mm and natural sand (80μm-5mm) with an apparent density of 2723 kg/m^3 and

This document is the intellectual property of the fib – International Federation for Structural Concrete. All rights reserved.
This PDF of fib Bulletin 95 is intended for use and/or distribution solely within fib National Member Groups.

absorption of 0.3 %. The coarse aggregate was selected taking into consideration the fiber lengths (i.e. fiber length ≥ 2 × aggregate size). A polycarboxylate-based super plasticizer (ADVA Cast 575), complying with ASTM C494 Type F, was used to increase workability and segregation resistance. An air-entraining admixture was also used in this mix (Sika Air 260). Using this base mix, a total of 16 SCFRC mixtures were studied, each with a different combination of fiber type and content as described in the next section.

Table 1: SCC mix design (base mix)

GUB-8SF (kg/m^3)	Slag (kg/m^3)	Crushed limestone (kg/m^3)	Natural sand (kg/m^3)	W/C ratio	Air entrainment (ml/m^3)	Super plasticizer (L/100kg/cm)
400	100	810	780	0.44	590	0.48

2.2 Fibers and SCFRC mixtures

Four types of steel fibers and one type of macro-synthetic fiber were considered in this study. The properties of the ZP, BP, 5D, ML and Tuff fibers are summarized in Table 2 and sample photos of the fibers are shown in Figure 1f. The ZP and BP fibers have length of 30 mm and come with a hooked-end geometry. The BP fibers have a relatively higher-strength (f_{fy} = 2300 MPa vs. 1100 MPa) and a larger aspect-ratio (l_f/d_f= 80 vs. 55). The 5D fibers have a length of 60 mm with an optimized hook-geometry to improve anchorage. The brass-coated ML micro-fibers were 13 mm in length, with a tensile strength of 3100 MPa and aspect-ratio of 43. The macro-synthetic TUF fiber has a length of 51 mm (cross-section of 0.37 x 1.1 mm, aspect-ratio = 74), a tensile strength of 625 MPa, and partially fibrillates when mixed in concrete.

As shown in Table 3, a total of 16 SCFRC mixes were investigated in this study. The same base mix was used for all concrete batches. Parameters studied include; the effect of fiber type, length, aspect-ratio, content and hybrid fibers. The mix nomenclature reflects the fiber type (ZP, BP, 5D, ML, TUF) and fiber content (0%, 0.4%, 0.8%, 1.2% or 1.6% by volume of concrete) in each SCFRC mix. For example, SCC0% represents the control mix, SCC0.8%ZP indicates a mix with 0.8% of ZP steel fibers, while mix SCC0.8%ZPML indicates the combined use of 0.4% ZP and 0.4% ML hybrid fibers. Grünewald (2004) notes fiber length should be at least 2 times relative to the maximum aggregate. Four of the fibers (ZP, BP, 5D and TUF) meet this criterion, however this limit is not met for the shorter ML fibers (13 mm). This was deemed acceptable since fiber clustering is more serious for longer fibers (Grünewald, 2004).

Table 2: Fiber type and dimensions

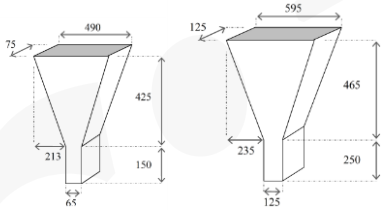
Fiber ID	Type	Shape	Diameter (mm)	Length (mm)	Aspect ratio	Tensile strength (MPa)
ZP	Steel	Hooked	0.55	30	55	1100
BP	Steel	Hooked	0.3	30	80	2300
5D	Steel	Hooked	0.9	60	65	2300
ML	Steel	Straight	0.3	13	43	2500
TUF	Synthetic	Fibrillating	0.37 x 1.1	51	74	625

2.3 Fresh-State and Hardened-state tests

The fresh-state properties of the mixtures were studied using the slump flow test and V-funnel test. A modified fiber funnel, which had larger dimensions when compared to the standard V-funnel (Grünewald 2004), was also used (see Figure 1a). The consistency and segregation resistance of the mixes was also assessed qualitatively using the visual stability index (VSI) test, where VSI ratings of 0, 1, 2 and 3 correspond to mixtures which are "highly stable" (no evidence of segregation/bleeding), "stable" (no evidence of segregation/slight

This document is the intellectual property of the fib – International Federation for Structural Concrete. All rights reserved.
This PDF of fib Bulletin 95 is intended for use and/or distribution solely within fib National Member Groups.

bleeding), "unstable" (slight mortar halo and/or aggregate pile in centre of concrete mass) and "highly unstable" (clear segregation with large mortar halo and/or aggregate pile in centre of concrete mass), respectively. Results from the workability tests are summarized in Table 3, Figure 2 and Table 4. In addition to examining the fresh-state behaviour, the mechanical properties of the SCFRC mixtures were also studied. For each mix, standard cylinders and prisms were tested in compression and flexure at an age of 28 days (see Figure 1d). Table 3 and Figure 2e report the average compressive strength values (f_c') of the concrete produced and obtained from the testing of three 100 mm diameter by 200 mm long cylinders in accordance with the ASTM C39 standard. Figure 4 shows samples of flexural load-deflection responses obtained from testing 100 x 100 x 400 mm prisms in accordance with the ASTM C1609 standard. Results in terms of maximum flexural stress (f_r) and toughness (T_{150}) corresponding to the area under the curves up to deflection = L/150, are reported in Figures 2 and 3.



(a) Dimensions: standard and modified (fiber) V-funnels


(b) Slump flow test

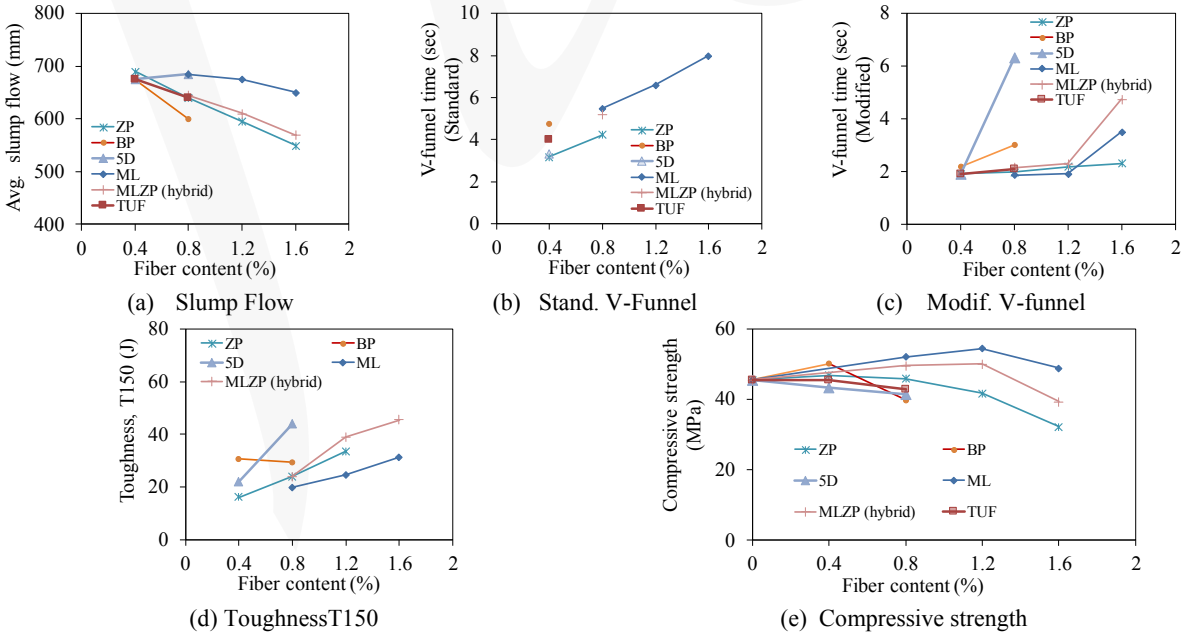

(c) Modified V-funnel test


(d) Cylinder (compression) test


(e) Prism test


(f) Steel fiber properties (from left to right): ML, ZP, BP, 5D fibers

Figure 1: Fresh-state tests, hardened-state tests, and fiber properties



(a) Slump Flow (b) Stand. V-Funnel (c) Modif. V-funnel

(d) ToughnessT150 (e) Compressive strength

Figure 2: Test results as a function of fiber content/type

This document is the intellectual property of the fib – International Federation for Structural Concrete. All rights reserved.
This PDF of fib Bulletin 95 is intended for use and/or distribution solely within fib National Member Groups.

Table 3: SCFRC mixes characteristics and summary of results

Mix ID	Average slump flow (mm)	Visual stability index	Standard V-funnel flow-out time (s)	Modified V-funnel flow-out time (s)	Compressive strength f_c (MPa)	f_r (MPa)	T_{150} (J)
SCC0%	755	0	2.9	1.85	45.5	4.7	-
SCC0.4%ZP	690	0	3.2	1.91	46.8	4.0	16.1
SCC0.8%ZP	640	1	4.3	1.98	45.9	5.1	24.0
SCC1.2%ZP	595	1	blocked	2.18	41.7	5.7	33.5
SCC1.6%ZP	550	2	blocked	2.30	32.2	-	-
SCC0.4%BP	675	1	4.8	2.18	50.2	5.2	30.6
SCC0.8%BP	600	3	blocked	3.00	39.8	4.9	29.3
SCC0.4%5D	675	1	3.3	1.91	43.4	4.9	22.0
SCC0.8%5D	685	3	blocked	6.30	41.3	7.1	44.0
SCC0.4%TUF	675	1	4.0	1.90	45.5	-	-
SCC0.8%TUF	640	3	blocked	2.10	42.8	-	-
SCC0.8%ML	685	0	5.5	1.86	52.1	6.2	19.8
SCC1.2%ML	675	1	6.6	1.91	54.4	5.8	24.6
SCC1.6%ML	650	3	8.0	3.50	48.8	6.7	31.3
SCC0.8%ZPML	645	0	5.2	2.14	49.5	6.7	24.0
SCC1.2%ZPML	610	1	blocked	2.29	50.0	6.5	39.0
SCC1.6%ZPML	570	3	blocked	4.74	39.3	8.3	45.5

3 Discussion of the Results

3.1 Effect of Fiber content

As expected, the addition of fibers leads to reduction in SCC workability with reduction in mean slump flow and increase in V-funnel time. For the ZP series, the slump flow decreased from 755 mm for the base SCC mix to 690 mm, 640 mm, 595 mm and 550 mm after addition of 0.4%, 0.8%, 1.2% and 1.6% ZP fibers, respectively. For the ML series, mean slump flows of 685, 675 and 650 mm were recorded for fiber contents of 0.8%, 1.2% and 1.6% (see Figure 3). The addition of fibers also increased the viscosity of the mixtures. The V-funnel flow time increased from 1.9 seconds for the base mix, to 3.2 seconds and 4.3 seconds at fiber contents 0.4% and 0.8% of ZP fibers, with blockage at 1.2% and 1.6% ZP fibers. The tendency for segregation also increased at higher fiber contents, with VSI being increased from 1 at fiber content of 1.2%ZP and 1.2%ML fibers, to VSI = 2 & 3 at 1.6% ZP & 1.6ML fibers, respectively. When compared to the ZP fibers, the use of 0.4% BP fibers resulted in a moderate reduction of the slump flow (675 mm vs. 690 mm) and an increase in V-funnel flow time (4.8 seconds vs. 3.2 seconds) with VSI changing from 0 to 1. The slump flow of the BP mix reduces further to 600 mm at 0.8% fibers, with blocking in the standard V-funnel. VSI also increases from 1 to 3 when going from 0.4% to 0.8% fibers. Similar trends are observed for the longer 5D fibers and macro-synthetic fibers, where the slump flow reduced and viscosity and segregation increase as the fiber content increases.

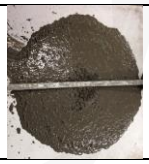
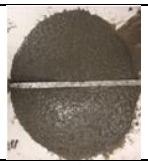
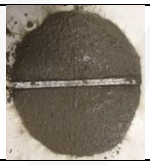
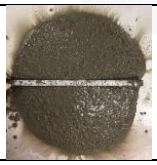
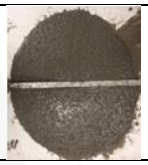
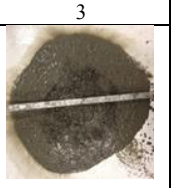
In general, adding fibers in plain SCC slightly increased the compressive strength for the case of the mixtures with moderate contents of steel and synthetic fibers. As shown in Figure 3, with the exception of the mix with 5D fibers, all other mixes with 0.4% fibers attain higher compressive strengths when compared to the control plain SCC mix. Among the series with a fiber content of 0.4%, the mix with high-strength and high aspect ratio BP fibers shows the best performance with 50.28 MPa, which is 10% higher than the strength of plain SCC. However,

This document is the intellectual property of the fib – International Federation for Structural Concrete. All rights reserved.
This PDF of fib Bulletin 95 is intended for use and/or distribution solely within fib National Member Groups.

the opposite trend is observed when the higher fiber contents are used or in the case of mixtures which showed poor segregation resistance. For example, for the ZP series, an increase of the fiber content beyond 0.8% to 1.6% reduces the cylinder strength noticeably from 45.9 MPa to 32.2 MPa owing to the observed loss in uniform fiber distribution and increased segregation at this higher fiber content. A similar observation is made in the case of the BP fibers when going from the 0.4% to 0.8% fibers. Comparison of the results for the TUF synthetic fiber type shows that this fiber does not have any considerable impact on the compressive properties of mixes. In this series increasing fiber content from 0.4% to 0.8% led to strengths of 45.5 MPa and 42.8 MPa, respectively, which are comparable to the strength of the plain SCC mix.

Figure 4 shows the flexural load versus deflection responses obtained from the testing of 100 x 100 x 400 mm beams in accordance with the ASTM C1609 standard. Results in terms of maximum flexural strength (f_r) and toughness (T_{150}) corresponding to the area under the curves up to a deflection = L/150, are reported in Table 3. Figure 3 compares the T_{150}values in a bar-chart diagram while Figure 2d plots the T_{150} toughness results as a function of fiber content and type. As expected, the results show that the SCC without fibers shows a brittle and sudden failure after the appearance of the first crack. When fibers are added, concrete can carry significant load after cracking. In general, toughness improves as fiber content increases. For example, in the ZP series, increasing the fiber content to 1.2% causes toughness to reach 33.5J, which is a relative increase of 108% and 40% when compared to the case of the mixes with 0.4% and 0.8% ZP fibers, respectively. The results also show that flexural-hardening behaviour becomes possible at some of the higher fiber contents (e.g. at 1.2% ZP and 0.8% 5D fibers).

Table 4: Summary of visual stability index (VSI) test results

					
ML series	Control (0%)	0.8%ML	1.2%ML	1.6%ML	
VSI	0	0	1	3	
					
ZP series	Control (0%)	0.4%ZP	0.8%ZP	1.2%ZP	1.6%ZP
VSI	0	0	1	1	2
					
BP & 5D series	Control (0%)	0.4% BP	0.8% BP	0.4%5D	0.8%5D
VSI	0	1	3	1	3
					
HYB & TUF series	0.8%MLZP	1.2%MLZP	1.6%MLZP	0.4%TUF	0.8%TUF
VSI	0	1	3	1	3

This document is the intellectual property of the fib – International Federation for Structural Concrete. All rights reserved.
This PDF of fib Bulletin 95 is intended for use and/or distribution solely within fib National Member Groups.

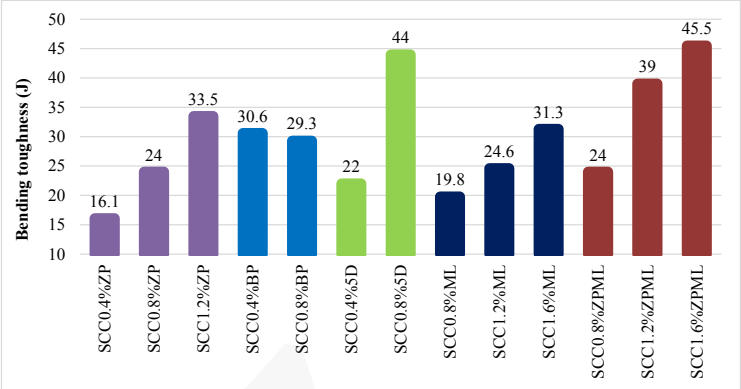


Figure 3: Comparison of bending toughness for the different mixes

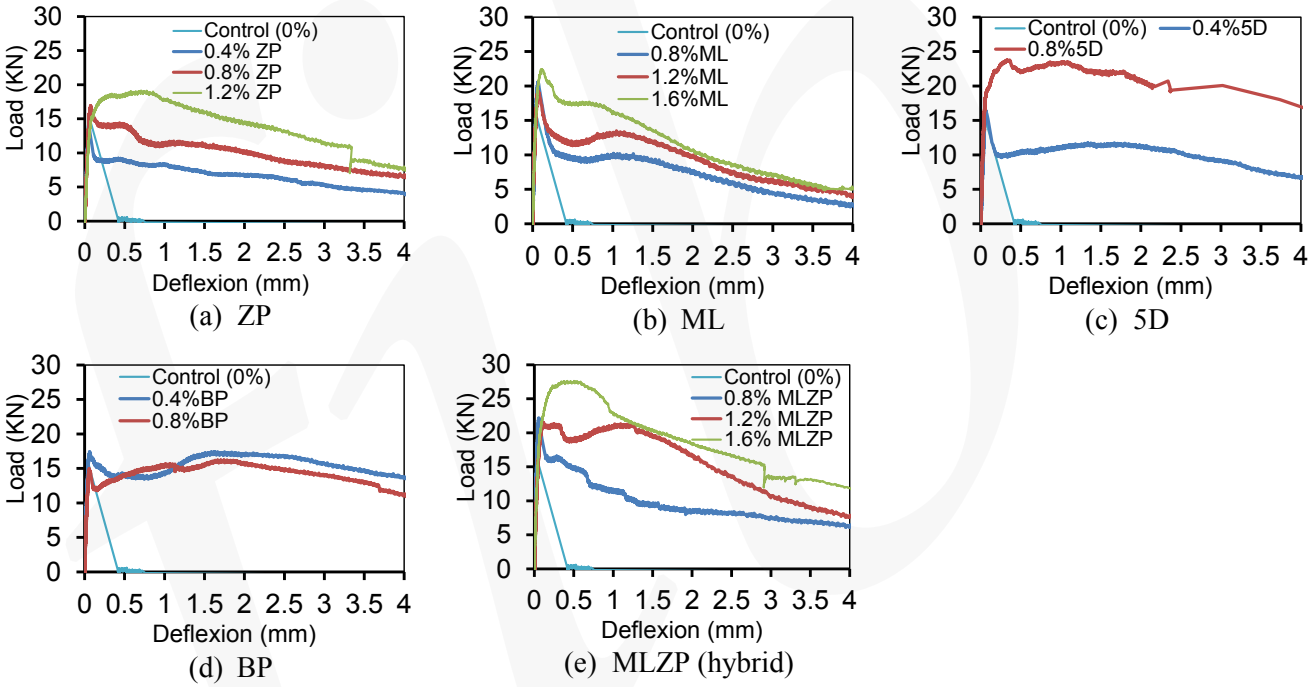


Figure 4: Flexural Load versus deflexion for the beams in each series

3.2 Effect of Aspect ratio

In addition to the fiber content, workability of SCFRC can also be affected by the aspect ratio. The effect of this parameter can be investigated by comparing the results from the ZP and BP fibers, which had the same length of 30 mm but different aspect ratios (l/d) of 55 and 80. The use of BP fibers in the plain SCC mix significantly reduced the slump flow of SCC, while adding ZP fibers caused a more modest decrease in slump flow with increasing fiber content (see Figure 2a). As an example, the mix with 0.8%ZP had a 640 mm slump flow while the same mix with BP fibers had a slump flow of 600 mm. The effect of increasing aspect ratio can also be observed from the V-funnel test results. For the standard V-funnel test, the mix with 0.8% BP blocked, while the flow out time was 3 seconds in the modified V-funnel. In comparison flow-out times of 4.3 and 2.0 seconds were recorded for the 0.8% ZP mix (see Figure 2b). The results confirm that fibers with a higher aspect ratio have greater impact on workability of SCFRC.

This document is the intellectual property of the fib – International Federation for Structural Concrete. All rights reserved.
This PDF of fib Bulletin 95 is intended for use and/or distribution solely within fib National Member Groups.

The effect of fiber aspect ratio on toughness is shown in Figure 5a. In general, the results show that the BP fibers relatively increase in the bending toughness when compared to the mixes with ZP fibers. As can be seen in Figure 3, the bending toughness of the mix with 0.4% of ZP was 16.1 J while this value is 30.6 J for the mix with 0.4%BP fibers. Moreover, it is noted that use of 0.4%BP results in flexural-hardening behaviour, whereas a larger amount of fibers was required in order to initiate this behaviour for the ZP series (1.2% fibers). Increasing fiber content from 0.4% to 0.8% caused bending toughness of mixes with ZP fiber to increase from 16J to 24J, on the other hand the same fiber content in the mixes with BP fibers increased the toughness of the beams to 30.6J and 29.3J, respectively. The results demonstrate that the use of fibers with increased aspect-ratio can improve toughness, the use of higher fiber contents can results in a loss of mix uniformity due to workability-related issues, which can in turn affect mechanical properties, in addition to causing placement problems during construction. This problem can be solved by developing SCFRC mix designs which are tailored for the specific type of fiber and fiber content used in the mix (e.g. as proposed by Ferrara et al. 2007).

3.3 Effect of Fiber length

Another parameter that affects the characteristics of SCFRC is the fiber length. The effect of this parameter can be studied by comparing the results from mixes with ML (13 mm length), ZP (30 mm length) and 5D fibers (60 mm length). A survey of the results for the mixes with low fiber content (0.4%) show that the SCFRC with 5D fibers shows the greatest reduction in workability among the group, while the best results are observed for the shorter ML fibers (see Figure 2). At a 0.8% content segregation occurs for the 5D fibers, while the ML fibers show a higher slump flow when compared to the ZP fibers. Similar trends can be seen in the results of the modified V-funnel test. When considering the mixtures with 0.8% fibers, the highest flow-out time of 6.3 seconds is recorded for the 5D mix, while the flow-out times of the ZP and ML mixtures were 2.0 and 1.9 seconds, respectively. The results demonstrate the high segregation and blocking probability of the mix with 0.8%5D.

It is interesting to note that a significant increase in compressive strength was obtained in the case of the shorter ML micro-fibers (13 mm long) when compared to the macro-fibers (30 and 60 mm). For instance, the use of 0.8% of ML increased the cylinder strength to 52.1 MPa while the compressive strength of the mix with 0.8% of 5D fibers was 41.3 MPa. Shorter fibers have a greater ability to arrest micro-cracks, which initiate in the pre-peak stage of the compressive stress-strain response. This effect is most significant in the mix with 1.2% of ML as this mix achieved the highest strength among all SCFRC batches (54.4 MPa).

The impact of fiber length on the performance of SCFRC in bending is investigated by comparing the flexural toughness results for specimens contains 0.8% of ML (13mm), ZP (30mm) and 5D (60mm) fibers (see Figures 3 and 5b). It can be observed that the mix with ML micro fibers shows the lowest toughness among the different fiber groups. As a comparison, the use of 0.8 %ZP fibers results in a toughness T_{150}^{D} of 24J while this value for the mix with ML was 19.8J. The best overall toughness is observed for the mix with 5D fibers, which shows a significantly higher toughness of 44J, a relative increase of 122% when compared to the companion mix with ML fibers. However, the results show that the use of micro-fibers results in a greater effect on initial cracking strength as observed when comparing the first peak loads for the different mixes. Thus, it can be concluded that fibers with longer length and improved anchorage properties (i.e. hooked ends) have a greater effect on improving the overall toughness of SCFRC, while micro-fibers have a more pronounced effect on the initial cracking strength.

This document is the intellectual property of the fib – International Federation for Structural Concrete. All rights reserved.
This PDF of fib Bulletin 95 is intended for use and/or distribution solely within fib National Member Groups.

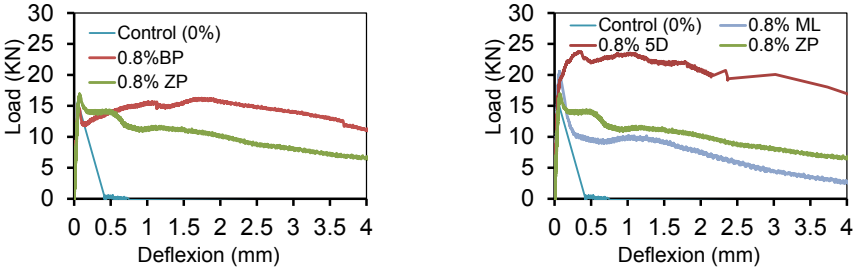


Figure 5: Comparison of Toughness results: effect of (a) aspect ratio, (b) fiber length

3.4 Effect of Hybrid Fibers (Combined use of ZP and ML)

This section reviews the results for the hybrid SCFRC mixes (ZP + ML fibers). As shown in Figure 2, the slump flow results of the hybrid mixes follow the same trend observed in the ZP series. At fiber contents of 0.8% and 1.2%, the effect of hybrid fibers on the v-funnel flow-out times is considered negligible compared to the companion non-hybrid mixes. The same was observed for the visual stability test. Slight changes were observed in the homogeneity and stability of the mixtures with 0.8% and 1.2% fibers. However, increasing the fiber content beyond 1.2% to 1.6% led to a more noticeable increase of about two times in the modified V-funnel test reading, while this increased, also fiber dosage caused a high level of segregation with a recorded visual index value of 3 (see Table 3).

The study of the load-deflection curves in Figure 4e shows that the responses of the hybrid specimens show a synergy effect with the shorter fibers allowing for an increase in peak strength and longer fibers allowing for an improvement in toughness. In particular (despite the observed VSI), the performance of the 1.6% hybrid mix is impressive and shows significant peak strength combined with high toughness (T_{150}^{D} = 45.5 J, which is the largest among all studied mixes). Examination of the response curves also shows that an increase in hybrid fiber content from 0.8% to 1.2% led to an enhanced post-cracking response, with initiation of flexural-hardening behaviour. Increasing the hybrid fiber content further from 1.2% to 1.6% increased the overall toughness from 39J to 45.5J (see Figure 3).

4 Concluding remarks

This paper examined the effect of steel fibers (content, aspect-ratio, length, type) and hybrid fibers on the fresh and hardened-state properties of self-consolidating fiber-reinforced concrete (SCFRC). The following conclusions can be drawn from this study:

1. The addition of fibers decreases the workability of SCC. In addition, an increasing fiber content of SCC beyond certain limits (which are mainly function of fiber length and aspect ratio) can lead to high levels of segregation and loss of mix uniformity;
2. Using fibers with higher aspect-ratio (as in the case of the BP fibers) and longer length (as in the case of the 60 mm 5D fibers) reduces workability and increases the potential for segregation. In contrast, the use of micro-fibers (e.g. ML fibers) has little effect on fresh-state characteristics of SCFRC as long as the limiting fiber content is not exceeded;
3. The addition of a low amount of fibers can increase the compressive strength of SCC, although this effect is more significant in mixes with micro fibers (e.g. 20% strength gain when using 1.2% ML fibers). At higher fiber contents slight strength reduction was

This document is the intellectual property of the fib – International Federation for Structural Concrete. All rights reserved.
This PDF of fib Bulletin 95 is intended for use and/or distribution solely within fib National Member Groups.

observed, with a considerable loss in strength when the limiting fiber content of each fiber type is exceeded;

4. The addition of fibers significantly improves the flexural behaviour of SCC and the enhancement becomes more prominent as the fiber content is increased. Furthermore, SCFRC with higher fiber contents can show flexural-hardening behaviour (with peak load being higher than the first cracking load), leading to further improvements in SCFRC toughness. SCFRC mixes with macro-fibers show higher bending toughness in comparison with mixes with micro fibers (with the latter having greater effect on the first-cracking strength). Use of fibers with longer length or increased aspect ratio can result in further improvement of toughness of SCFRC. The use of hybrid fibers was also shown to improve overall toughness of SCFRC.

In this study the granular skeleton of the base SCC mix was not optimized for each fiber, and therefore this point should be considered when interpreting the results. Ferrara et al. (2007) proposed a mix design method where fibers are included in the granular skeleton using a fictitious aggregate fraction and the concept of the "equivalent fiber diameter", with $d_{eq,fiber} = \frac{3l_f}{1+2(l_f/d_f)} \frac{\gamma_{fiber}}{\gamma_{aggregate}}$, and where: l_f, d_f = fiber length, fiber dimeter; and γ_{fiber}, $\gamma_{aggregate}$ = specific gravity of the fiber and aggregate, respectively. Using this approach, the coarse aggregate fraction can be modified to compensate ("make space") for the addition of fibers while accounting for the fiber properties. This approach is recommended for SCFRC.

5 References

Campione, G., Fossetti, M. & Papia, M. (2010), *Behavior of fiber-reinforced concrete columns under axially and eccentrically compressive loads*. ACI Structural Journal, 107 (3), 272-281.

Ferrara L. and Meda, A. (2006). *Relationship between Fiber distribution, workability and the mechanical properties of SFRC applied to precast roof elements*. Materials and Structures, 39 (4), 411-420.

Ferrara, L., Park, Y. D., & Shah, S. P. (2007). *A method for mix-design of fiber-reinforced self-compacting concrete*. Cement and Concrete Research, 37(6), 957-971.

Grünewald, S. (2004). *Performance-based design of self-compacting fiber reinforced concrete*. Department of Structural and Building Engineering, Ph.D. Thesis, Delft University of Technology.

Javadian, A. (2012). *Properties of plain and fiber reinforced self-consolidating concrete*. Department of Civil Engineering, M.Eng. Report, University of Ottawa.

Khayat, K.H. and Roussel,Y. (2000). *Testing and performance of fiber-reinforced, self-consolidating concrete*. Materials and Structures, 33 (6), 391-397.

Minelli, F. and Plizzari, G.A. (2013). *On the Effectiveness of Steel Fibers as Shear Reinforcement.* ACI Structural Journal, 110(3), 379-389.

Sahmaran, M. Yurtseven, A. and Yaman, I. O. (2005). *Workability of hybrid fiber reinforced self-compacting concrete*. Building and Environment, 40 (12), 672-1677.

Sahmaran, M. and Yaman, I. O. (2007). *Hybrid fiber reinforced self-compacting concrete with a high-volume coarse fly ash*. Construction and Building Materials, 21(1), 150-156.

This document is the intellectual property of the fib – International Federation for Structural Concrete. All rights reserved.
This PDF of fib Bulletin 95 is intended for use and/or distribution solely within fib National Member Groups.
FRC2018: Fibre Reinforced Concrete: from Design to Structural Applications
Joint ACI-*fib*-RILEM International Workshop

Mechanical characterization of fiber reinforced floor screeds: Influence of glass fibers on shrinkage and cracking mechanisms

Fella Chelha[1]; Syed Yasir Alam[1]; Ahmed Zakarya Bendimerad[1]; Ahmed Loukili[1]

[1] : Institut de Recherche en Génie Civil et Mécanique (GeM), UMR-CNRS 6183, Ecole Centrale de Nantes, France.

Abstract

Self-compacting mortars and concretes for horizontal structures are cementitious mixtures that are both fluid and homogeneous, with the particularity of flowing under the effect of their own weight. Thanks to their homogeneous texture they offer the possibility of achieving good quality of finishing and many such advantages become the reason for their applications especially in slabs and floors.

However, self-compacting mortars or concretes show considerable shrinkage and cracking problems when used in floors and slabs (Weiss et al., 1998). Because of their large moisture exchange surfaces, the floor screeds are subjected to significant drying effects and in particular plastic shrinkage. If the movements are restrained, the risk of cracking is high. In this respect the use of fibers is a good alternative to using reinforcement bars and welded wire mesh. Indeed on site a clear decrease in cracking caused mainly by the shrinkage can be observed as soon as the fibers are incorporated in the screed.

This study is conducted to demonstrate the effectiveness and the effects of glass fibers on the control of cracking phenomena due to shrinkage by determining their mechanisms of action at young age. The study is carried out in two parts: Firstly, free shrinkage behavior is analyzed in the fiber reinforced floor screed. Secondly, the restrained behavior at young ages using recently developed uni-axial tensile testing machine is investigated.

Keywords

Shrinkage; glass fibers; self-compacting mortar; floor screed; cracking

This document is the intellectual property of the fib – International Federation for Structural Concrete. All rights reserved.
This PDF of fib Bulletin 95 is intended for use and/or distribution solely within fib National Member Groups.

1 Introduction

Concrete is the most used material in the world with about 1m^3 per person per year, due to the availability of its constituents and its perpetual application in the construction industry. Several researchers have been interested in improving its properties, especially in terms of compressive strength, which gave birth to high performance concrete (HPC) or even ultra-high performance concrete (UHPC). However, its low tensile strength and cracking is a real shortcoming, the addition of steel reinforcement in this respect generally increases the tensile strength and limits the crack opening at the scale of the structure but the concrete remains fragile at the microscopic scale. When concrete is subjected to cracking, it can affect the durability and safety of the structure; moreover the increase in the quantity of steel considerably increases the cost of the project.

Self-leveling concrete or self-compacting concrete (SCC) for horizontal structures, are concretes that are both fluid and homogeneous, with the particularity to flow under the effect of their own weight (Loukili, 2011), perfectly matching the most complex forms of formwork and avoiding any contribution of vibration energy. Indeed, thanks to their fluid and homogeneous texture they offer the possibility of achieving high density of reinforcement and a good quality of finishing and facing, their rapid concreting consequently allows the reduction of the time of implementation. These advantages make these concretes the reason for many applications, especially in slabs and floors.

However, self-compacting mortars or concretes show considerable shrinkage and cracking problems thus compromising the visual and durable appearance of the structure (Weiss et al., 1998). Because of their large air exchange surfaces, the fluid screeds are subjected to significant drying effects, and in particular plastic shrinkage. If further movements are hindered the risk of cracking is high. In this respect the fibers are a good alternative to reinforcement bars and welded mesh, indeed they can limit the opening of cracks.

The aim of this research is to study the influence of small dosage microfibers on the early age behavior of fiber reinforced cementitious floor screeds. The purpose of the experimental program is to show the mechanism by which the glass fibers reduce the microcrack and their effect before the initiation of the macrocrack. To do this, the tests were based on the measurement of free plastic shrinkage and tensile strength at young age. In fact, considering the decoupled approach of cracking at young age, these two tests make it possible to highlight the effect of the fibers on the mechanical action (free plastic shrinkage) and the strength (tensile strength and strain capacity before rupture). These tests are then correlated with other measurements. A variation of the fiber dosage was made to determine the optimum fiber dosage.

2 Experimental program

2.1 Material properties

Four mixes of self-compacting mortars were tested in the present research with and without fibers as shown in Table 1. The mortar mix composition (water to cement ratio equal to 0.6) remains the same however; the fiber dosage was varied in order to determine the optimal dosage which allows the reduction of the microcracking and thus the elimination of cracking at an early age.

This document is the intellectual property of the fib – International Federation for Structural Concrete. All rights reserved.
This PDF of fib Bulletin 95 is intended for use and/or distribution solely within fib National Member Groups.

Table 1: Mix properties

Mix designation	Fiber type	Fiber dosage [kg/m^3]
Ref-0-F	-	-
M-06-F	Alkali Resistant Microfiber Diameter = 200 µm Length = 12 mm	0.6
M-18-F		1.8
M-30-F		3.0

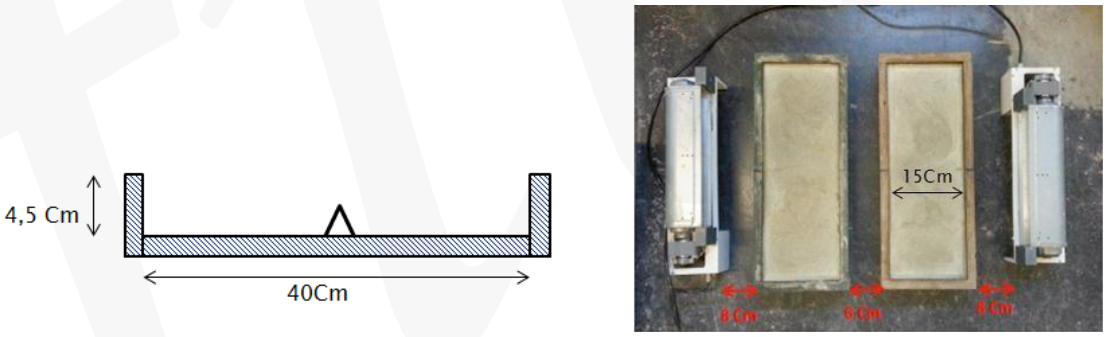
Fibers used in this study had an aspect ratio of 60 and were composed of drawn glass filaments with 72 GPa elastic modulus and a tensile strength of 1700 MPa. The filaments were bonded using a chemical agent. For a better resistance to basic media of mortar, the fibers are chemically treated with zirconium oxide, these fibers are designated AR (Alkali-Resistant).

2.2 Experimental Procedure

The experimental procedure of each test is explained below. At least two specimens were tested for each type of test and for each fiber dosage:

1- <u>Cracking in the fresh state:</u>

Early age cracking was performed on a mold 4.5 cm deep. In order to initiate the cracking, a notch was placed in the middle of the mold.



(a) (b)

Figure 1: (a) Cracking mold at young age (b) Cracking assembly with ventilation

In order to ensure the repeatability of the tests, two tests were performed on each mix. To accelerate cracking, the material was subjected to intense drying using two fans placed at equal distance from the edge of each mold as shown in the Figure 1. At 24 hours of casting, the surface of the mold is photographed and processed using the Image software in order to measure the cracking area.

2- <u>Plastic shrinkage, Mass loss and Setting:</u>

The device for measuring the plastic shrinkage allows a linear horizontal measurement of the strain (Figure 2). The two molds were made of steel 7 × 7 × 28 cm^3 the inner walls were covered with a Teflon sheet to avoid friction. The two lateral walls of 7 × 7 cm^2 are pierced with a circular hole allowing the passage of the laser beams. When the sample shrinks, it

This document is the intellectual property of the fib – International Federation for Structural Concrete. All rights reserved.
This PDF of fib Bulletin 95 is intended for use and/or distribution solely within fib National Member Groups.

drives the two PVC plates positioned at each extremity, so the laser sensor measures the displacement of the two plates. The shrinkage strain then represents the ratio between the measured displacement of the two plates and the initial length of the sample. The tests were conducted in a room where the atmosphere is conditioned at 20±1°C and 50±5% relative humidity.

The follow-up of the mass loss is carried out in parallel with the plastic shrinkage, the measurement is carried out on an electronic balance, and the mortar is poured in a plastic mold and placed on the balance. Measurement acquisition was done every 5 minutes.

The setting time test was carried out according to EN 196-3. The measurement of the setting time was carried out automatically using the apparatus consisting of 6 specimens and equipped with a standard needle of 1.13 mm diameter. The needle automatically sinks into the sample at a random position every 10 minutes under the effect of a load of 700 g, thus allow following the evolution of the consistency of the mortar.

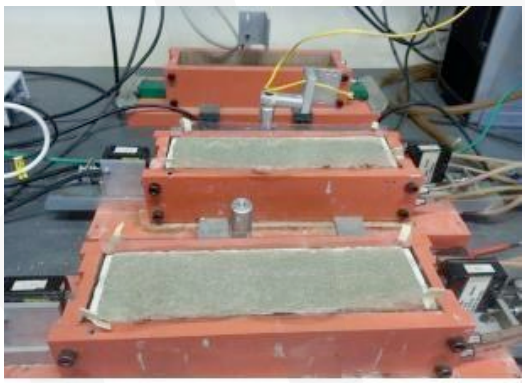


Figure 2: Plastic shrinkage measurement device

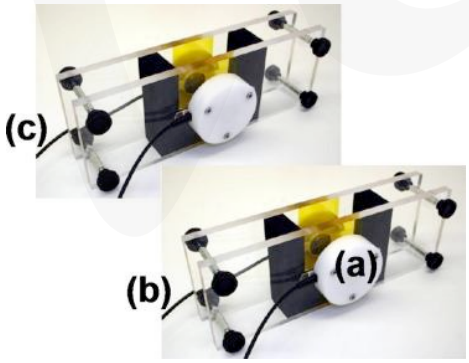


Figure 3: FreshCon system for measuring the velocity of ultrasonic waves: (a) piezoelectric sensor (b) mold for P waves (c) mold for S waves

3- Evolution of elastic modulus by ultrasonic wave:

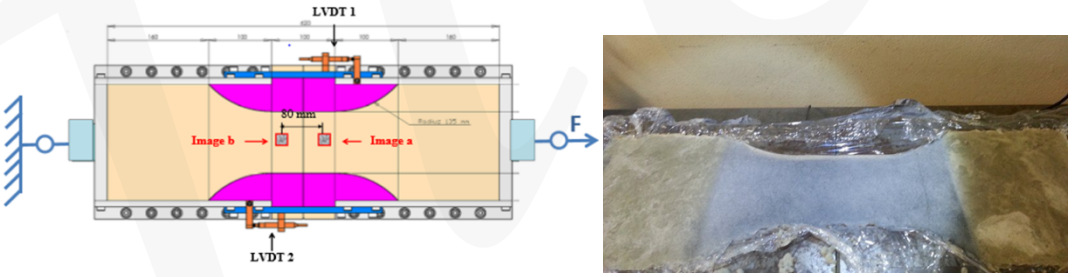
The evolution of the elastic properties of concrete at a young age was followed by the FreshCon system, which measures the velocity of P and S ultrasonic waves (Figure 3). This device was originally developed at the University of Stuttgart to analyze the setting and curing of any type of material (concrete and fresh mortar). The device consists of a mold consisting of two polymethacrylate (PMMA) walls secured by four screws. It is equipped

This document is the intellectual property of the fib – International Federation for Structural Concrete. All rights reserved.
This PDF of fib Bulletin 95 is intended for use and/or distribution solely within fib National Member Groups.

with an ultrasonic transmitter and a transducer (transmitter and receiver). The U-shaped mold is made of foam with high damping properties to absorb the waves through the mold around the concrete sample (450 cm^3 volume). A pulse whose amplitude was amplified is generated (800 V with 2.5 µsec pulse width) at regular intervals selected during this test. Longitudinal compressional ultrasonic waves are then transmitted through the concrete sample, and the signal is received by an ultrasound receiver after scanning the sample and returned to the data acquisition card (DAQ card). The software automatically calculates the time required for the wave to go from the transmitter to the receiver and deduces the speed. The test is carried out in an air conditioned room at 20°C and 50% RH. The evolution of the dynamic properties (Poisson's ratio and modulus of elasticity Edyn) was obtained as a function of the velocity of the compressional waves (P) and the shear waves (S).

4- Direct tensile test at young age:

The tensile test was carried out on the direct draft machine which was designed and developed in the GeM laboratory (Figure 4). The fresh mortar was poured into a bone-shaped steel mold. The narrow part in the center of the mold (105 mm wide, 100 mm long and 100 mm deep) makes it possible to concentrate the stresses and consequently to locate the cracking in this zone. The mold consists of two parts, one fixed part connected to a frame by means of a ball joint, and one moving part connected by another ball joint to the electric loading machine of 40 KN capacity controlled by computer, with displacement or load control. A force sensor is located between the moving part of the mold and the electric actuator. Two LVDT sensors fixed on either side of the mold make it possible to measure the relative displacement between the two parts of the mold. The friction between the mold and the frame is reduced by the application of oil between the bottom of the mold and its support. The support is free to move horizontally since it is placed on rails.



(a) (b)

Figure 4: Direct tensile strength testing (a) schematic diagram (b) mortar specimen placed in mold with center part for DIC application.

The test was performed at ambient temperature of 20°C and a humidity of 50%. The test was carried out at 24 hours (approximately 12 hours after start of setting) with displacement control at the speed of 8 x 10^{-3} mm/s. We measured the displacement of concrete by the technique of digital image correlation (DIC). DIC is a non-destructive method that measures the movement of a material between two consecutive images. According to the experimental procedure developed, a camera, placed above the mold, makes it possible to take a picture of the cracking zone (the narrowed area of the mold). The acquisition of the images takes place every second simultaneously with the acquisition of force data and LVDT displacement of the

This document is the intellectual property of the fib – International Federation for Structural Concrete. All rights reserved.
This PDF of fib Bulletin 95 is intended for use and/or distribution solely within fib National Member Groups.

machine. By applying a speckle pattern in the cracking zone, the displacement of a point between two instants is calculated. The displacement of this point corresponds to the average value of the displacement of a sub frame defined by a pixel value and a gray intensity, the principle of the image correlation consists in finding in the deformed image a maximum of likelihood with the sub-image considered in the reference image. Image processing was done using the 2D VIC software which gives displacement field. Thanks to the scaling image captured before the start of the test, the images were calibrated, so that the software gives the equivalent of one pixel in micrometer. The displacements can then be translated into micrometers.

Subsequently, the displacement of two points was determined. The actual deformation of the concrete was deduced from the relative difference of the displacements of these two points divided by the distance which separates them.

3 Results and Discussion

3.1 Effect of fibers on cracking at young age

The young cracking test was conducted with wind on cracking benches. At 24 hours casting time, we photographed the cracking benches. Image processing by Image J software allows us to determine crack area and crack length at the top surface of specimen. The results are collated in the following histograms (Figure 5). Ref-0-F cracks throughout the length of the specimen along the notch. The opening of the crack, which represents the ratio between the surface and the crack length, is of the order of 0.2 mm. The addition of fibers in the mix shows their ability to close the cracks at young age. M-06-F shows a reduction of the surface and the crack length by about 80%. For this mix, the crack opening was very small and could not be measured using the image analysis. No crack was observed on the cracking benches for the other mixes.

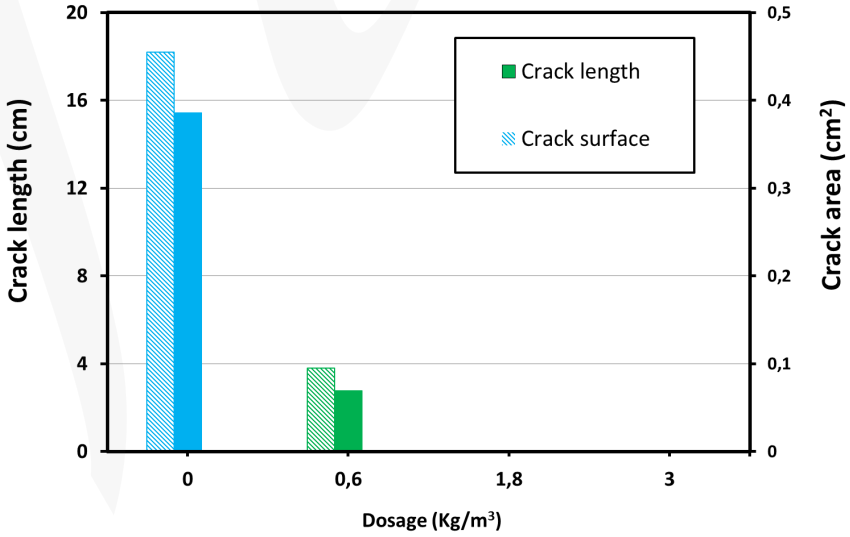


Figure 5: Effect of fiber dosage on crack length and crack surface

This document is the intellectual property of the fib – International Federation for Structural Concrete. All rights reserved.
This PDF of fib Bulletin 95 is intended for use and/or distribution solely within fib National Member Groups.

3.2 Fiber role in the diminution of Plastic Shrinkage

Plastic shrinkage is the consequence of several physio-chemical phenomena encountered in concrete or mortar at a young age. These phenomena are examined in this study by plastic shrinkage measurement to understand its origin and its development. At the same time, mass loss measurements, the setting time test and the evolution of elastic properties at young age were also carried out.

Figure 6 shows the results of plastic shrinkage with the variation of fiber dosage. It is to remember that non shrinkage reducing admixture was used in this study. The Ref-0-F has a greater shrinkage (of the order of 2300 µm/m) compared to mixes with different fiber dosages. Indeed we note that the addition of fibers decreases shrinkage, these results are compatible results found in the literature (Messan et al., 2011). They studied the influence on the shrinkage at a young age of glass fibers and ethylene-vinyl acetate EVA based cement mortar and found that the glass fibers reduce the free shrinkage. The reduction was greater in fiber based mortar as compared to EVA polymer based mortar. In our study, the extent of shrinkage was reduced by about 46% with a dosage of 0.6 kg/m^3, however a dosage of 1.8 kg/m^3 leads to a decrease of about 60%, then a stability with a dosage of 3 kg/m^3 was noted. These results show that the decrease in shrinkage contributes to the decrease in cracking at young age observed on cracking benches, an optimal dosage of 1.8 kg/m^3 was noted.

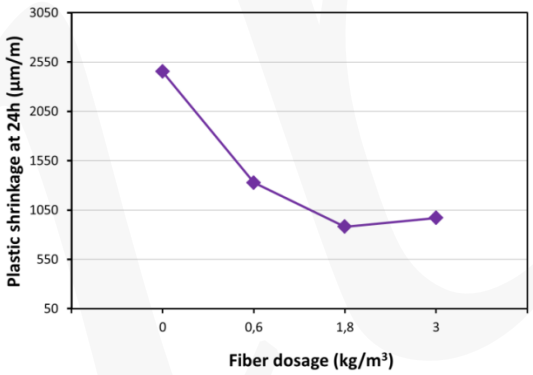


Figure 6: Influence of fiber dosage on plastic shrinkage at 24h

The measurement of the mass loss is an indicator of the evaporation of water and it allows elucidating the drying phenomenon. The derivative determines the rate by which evaporation occurs, or in other words the kinetics of drying. It is noted for all mixes that the rate of evaporation increases rapidly from the initial hours (about 3 hours of the water-cement contact), this corresponds to the drying of the surface water after settling of the solid particles. A decrease in the evaporation rate is subsequently observed, this decrease corresponds to the dormant period where the hydration reaction is slowed down. After 10h, a stabilization of the evaporation rate is observed before a slight increase of slope, this correlates with the start of setting, in fact the hydration of the cement causes a release of heat, the excess of water which has not been consumed in hydration will evaporate.

The setting test makes it possible to take into account the influence of the fibers on the hydration of the mortar. It is noted that the addition of the fibers has very little influence on the setting time. Thus it can be deduced that the fibers do not influence the hydration of the mortar. It is also noticed that there is a decrease in the mass loss compared to the reference in particular after the first hours. A dosage of 3 kg/m^3 (M-30-F) causes 34% decrease in mass

This document is the intellectual property of the fib – International Federation for Structural Concrete. All rights reserved.
This PDF of fib Bulletin 95 is intended for use and/or distribution solely within fib National Member Groups.

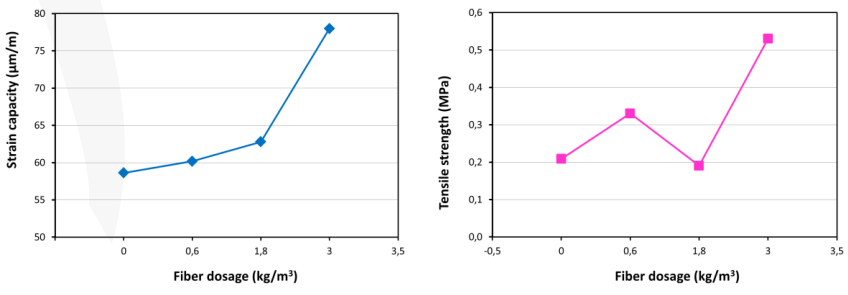
loss, and therefore drying, compared to the reference followed by the dosage of 0.6 kg/m^3 (M-06-F) with approximately 17.45% reduction and finally a reduction of 13.75% for a dosage of 1.8 kg/m^3 (M-18-F). This reduction in mass loss, even if minimal, contributes to the reduction of the plastic shrinkage, indeed, the influence of the fibers on the evaporation was observed from the first hours and which correspond to the compaction of the particles, this puts us assuming that the fibers can trap the flow of water by hindering the consolidation of the solid particles.

3.3 Fiber role in the evolution of mechanical properties at young age

The Young's modulus increases after the beginning of setting and characterizes the rigidity of the material. No difference was observed on the evolution of the modulus by the addition of fibers for the dosages 0.6 and 1.8 kg/m^3. However with the dosage of 3 kg/m^3 an acceleration of the kinetics is observed in particular during the first 40 hours. Subsequently, the curve of mix M-30-F joins the other curves and the values of the modulus after 48h are almost same (22.5 GPa in average).

At young age, crack opening can be related to the strain capacity of the material before failure. A high strain capacity indicates a reduced risk of cracking. In this study, the strain capacity corresponds to the tensile strain before failure and was determined from the direct tensile test at 24 hours. The material quickly fails (Young's modulus being very small) at this age (at around 4 GPa) as it has not yet attained a considerable tensile strength. The duration of the test is on average 100 seconds, compared to the concrete which can reach 2000 seconds (Cortas, 2012). Relative displacement is measured between these two points on the concrete surface at each side of the final crack. This displacement divided by the distance between the two points allows us to determine the strain capacity of the material.

Figure 7 shows the results of the strain capacity and the maximum tensile strength before failure at 24 hours as a function of the fiber dosage respectively. It is found that the strain capacity increases according to the fiber dosage. At a dosage of 3 kg/m^3 the strain capacity reached 78µm/m, an increase of about 34%, compared to an increase of 8% and 5% for dosages 1.8 and 0.6 kg/m^3 respectively. A quite similar observation is made for the tensile strength, little variation compared to the reference was observed for the dosage 0.6 kg/m^3 and a slight decrease for a dosage of 1.8 kg/m^3. An increase of 0.3 MPa was noted for the dosage of 3 kg/m^3 compared to the reference. Thus, the effect of fibers on tensile strength is more noticeable at high dosages. The cementitious matrix used in this study is a self-compacting mortar with a high W/C ratio (0.6) and therefore withstands little in tension. The contribution of the fibers at low dosage is therefore minimal, however at high dosages the fibers make it possible to take up some part of the stress.



(a) (b)

Figure 7: (a) Strain capacity at 24 hours (b) Tensile strength at 24 hours

This document is the intellectual property of the fib – International Federation for Structural Concrete. All rights reserved.
This PDF of fib Bulletin 95 is intended for use and/or distribution solely within fib National Member Groups.

The determination of the strain rate before the failure which corresponds to the slope of the deformation curve allows us to see a decrease in the deformation rate as soon as the fibers are incorporated in the matrix. Figure 8 presents the average results for each mix. Indeed, the failure in the case of the reference has been reached quickly compared to other mixtures, this indicates that the fibers, by closing the microcracks, decelerate the propagation of the crack; the redistribution of the stresses from one fiber to the other prolongs the deformation and consequently the failure time. The strain rate does not further decrease by increasing the fiber dosage may be due to the reason that the failure is now occurring at the interface between fiber and matrix (not inside the matrix).

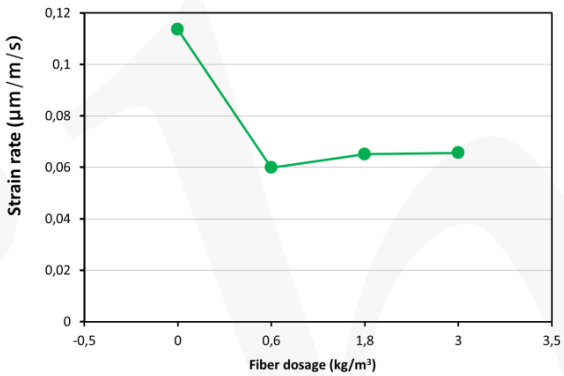
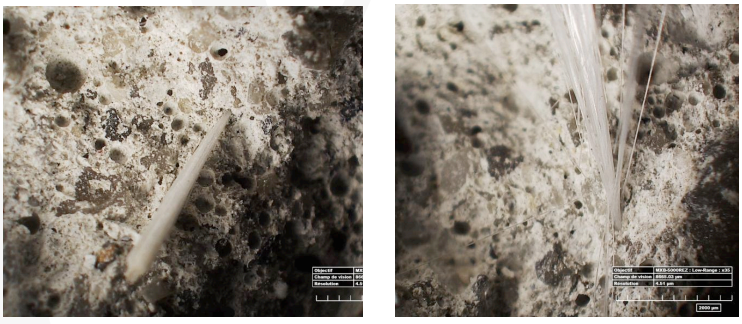


Figure 8: Effect of fiber dosage on strain rate at failure

The fracture is produced essentially by sliding of the fibers in the matrix. Figure 9 shows a microscopic view of a magnification × 35 of the failure plane after the tensile test, it is observed that after the tensile fracture, the fiber has remained in one half of the material without breaking, this indicates the sliding of fibers with respect to matrix. The fibers used are multi filaments bonded with the aid of the sizing; after failure it is seen on some fibers a detachment of the filaments due to an arrangement of fibers that is not in the same plane as the loading.



(a) (b)

Figure 9: Microscopic view of fiber at the fracture surface

4 Concluding remarks

The effect of chopped glass fibers at early age was highlighted in this study by a decoupled approach to cracking. The reduction of the cracking was confirmed by the crack bench as soon as fibers were incorporated. This reduction is due to both the decrease of the plastic

This document is the intellectual property of the fib – International Federation for Structural Concrete. All rights reserved.
This PDF of fib Bulletin 95 is intended for use and/or distribution solely within fib National Member Groups.

shrinkage and the increase of the deformation capacity, in other words a reduction of the stress and an improvement of the resistance.

Several phenomena have contributed to the reduction of plastic shrinkage; the parallel tests have led to a reduction in drying which can be caused by hindrance of consolidation of solid particles or entrapment of water by the fibers. It can be concluded that the action of microfibers is in this case is physical.

The mechanical action of the fibers on the deformation capacity has been advantageous. Based on these results an optimal dosage of 1.8 kg/m^3 in chopped glass microfibers can be considered. This choice is justified by the best fiber yield in reducing plastic shrinkage (up to 60% at the optimum 1.8 kg/m^3) compared to their mechanical efficiency (34% for a dosage of 3 kg/m^3).

5 References

Cortas, R. (2012). *Nouvelle approche expérimentale pour la maitrise de la fissuration du béton jeune : Influence de la nature et de la saturation des granulats*. PhD thesis Ecole Centrale de Nantes and Université libre de Bruxelles.

Loukili, A. (2011). *Les Bétons Auto-Plaçants* (Hermes Sci).

Mangat, P. ., & AZARI, M. . (1990). *Plastic shrinkage of steel fibre reinforced concrete*. Materials and Structures, 23(3), 186–195.

Messan, A., Ienny, P., & Nectoux, D. (2011). *Free and restrained early-age shrinkage of mortar: Influence of glass fiber, cellulose ether and EVA (ethylene-vinyl acetate)*. Cement and Concrete Composites, 33(3), 402–410.

Naaman, A. E., Thanasak, W., & Hauser, G. (2005). *Influence of different fibers on plastic shrinkage cracking of concrete*. Aci Materials Journal, 102(1), 49–58.

Rozière, E., Granger, S., Turcry, P., & Loukili, A. (2007). *Influence of paste volume on shrinkage cracking and fracture properties of self-compacting concrete*. Cement and Concrete Composites, 29(8), 626–636.

Turcry, P. (2004). *Retrait et Fissuration des Betons Autoplaçants Influence de la Formulation*. PhD thesis, Ecole Centrale de Nantes.

Stefan, L., Benboudjema, F.,Torrenti, J,M., Bissonnette, B. (2010). *Prediction of elastic properties of cement pastes at early ages*. Computational Materials Science, 47, 775-784

Weiss J. W., Yang W., Shah S. P. (1998). *Shrinkage Cracking of Restrained Concrete Slabs*. Journal of Engineering Mechanics, 124, 765.

This document is the intellectual property of the fib – International Federation for Structural Concrete. All rights reserved.
This PDF of fib Bulletin 95 is intended for use and/or distribution solely within fib National Member Groups.

FRC2018: Fibre Reinforced Concrete: from Design to Structural Applications
Joint ACI-*fib*-RILEM International Workshop

An application oriented state-of-art and research-need perspective on self-healing fibre-reinforced cementitious composites

Liberato Ferrara[1], Estefania Cuenca Asensio[1], Francesco Lo Monte[1], Didier Snoeck[2] and Nele De Belie[2]

[1] : Department of Civil and Environmental Engineering, Politecnico di Milano, Italy.

[2] : Magnel-Vandepitte Laboratory for Structural Engineering and Building Materials, Faculty of Engineering and Architecture, Ghent University, Belgium.

Abstract

The design of building structures and infrastructures is mainly based on four concepts: safety, serviceability, durability and sustainability. The latter is becoming increasingly relevant in the field of civil engineering. Reinforced concrete structures are subjected to conditions that produce cracks which, if not repaired, can lead to a rapid deterioration and would result in increasing maintenance costs to guarantee the anticipated level of performance. Therefore, self-healing concrete can be very useful in any type of structure, as it allows to control and repair cracks as soon as they to occur.

As a matter of fact, the synergy between fibre-reinforced cementitious composites and self-healing techniques may result in promising solutions. Fibres improve the self-healing process due to their capacity to restrict crack widths and enable multiple crack formation. In particular, cracks smaller than 30-50 μm are able to heal completely. Moreover, in the case of High Performance Fibre Reinforced Cementitious Composites (HPFRCC), high content of cementitious/pozzolanic materials and low water-binder ratios are likely to make the composites naturally conducive to self-healing.

In this framework the main goal of this paper is twofold.

On the one hand, a state-of-the-art survey on self-healing of fibre-reinforced cementitious composites will be provided. This will be analysed with the goal of providing a "healable crack opening based" design concept which could pave the way for the incorporation of healing concepts into design approaches for FRC and also conventional R/C structures.

On the other hand, the same state-of-the-art will be instrumental in identifying research needs, which still have to be addressed for the proper use of self-healing fibre-reinforced cementitious composites in the construction field.

Keywords

Self-healing; fibre-reinforced cementitious composites; test methods; healable crack width.

This document is the intellectual property of the fib – International Federation for Structural Concrete. All rights reserved.
This PDF of fib Bulletin 95 is intended for use and/or distribution solely within fib National Member Groups.

1 Introduction

The durability of reinforced concrete structures is, as of today the most serious concern of the construction industry. Reinforced concrete structures more and more frequently exhibit earlier and faster and more and more severe decay of their level of performance in the service scenarios and conditions they have been supposedly designed for. In current design codes, it is appropriately recognized that the achievement of the required durability is the complex outcome of the suitable choice of structural concept and shape, material selection and production, as well as of the enforcement of "operational" design criteria, which limit the crack width under the anticipated actions to suitable scenario-based threshold values [1,2].

In order to provide effective control of the crack width, Fibre-Reinforced Concrete (FRC) has been developed over the past fifty years. Thanks to the dispersed fibre reinforcement, an effective control of crack width can be achieved throughout the entire structure and starting from the very early ages. In fact, because of their wire-like shape, fibres are able to interact with cracks much finer than what is obtainable with the smallest commercially available bar diameters [3]. The boundaries of this concept have been pushed forward up to the formulation of the so-called High Performance Fibre Reinforced Cementitious Composites (HPFRCCs), whose composition is designed through micro-mechanical concepts based on fibre pull-out and crack tip toughness balance. Thanks to this, after the formation of a first crack, fibres effectively provide a through crack stress redistribution, which enables new multiple cracks to be formed while controlling the opening of the previously formed ones, which are basically stopped from further widening, up to the unstable localization of a single major crack. This makes the material able to "spread" the entity of a single damage (crack) into a series of tightly spaces and narrowly opened multiple cracks, whose single width is hence possibly much less detrimental to the structural durability [4].

The composition of this category of advanced cementitious composites features high contents of cement and supplementary binders, with either pozzolanic (*e.g.* fly ash, silica fume) or delayed cementitious activity (slag) and low water content. The resulting high amount of reactive material remains un-hydrated inside the bulk volume of a structural element. Upon cracking this material may become exposed to outdoor environment and can further react in the presence of liquid or vapour water. Delayed hydration reactions as well as carbonation ones can be activated, and the reaction products precipitate onto the crack surfaces sealing it. The reconstruction of the through-crack matrix continuity and, in case, matrix densification at the interface with the fibres, which also yields improved fibre-matrix bond, may also result in the "proprie dictum" material healing, i.e. a recovery of the post-cracking mechanical performance, including load bearing capacity, stiffness, toughness [5-7].

The presence of a homogenously dispersed fibre reinforcement, effectively controlling and limiting the crack width, is helpful to self-healing, since narrower cracks are definitely much easier to be healed. Different techniques have been proposed and validated to stimulate and enhance the aforementioned autogenous healing capacity, making its effectiveness less scattered and more reliable. The most consolidated ones consist in the use of crystalline admixtures [8, 9] and superabsorbent polymers (SAPs) [10].

The latter are characterized by a high water absorption capacity, as high as several hundred times their initial weight. Such a characteristic being reversible, the water initially absorbed by SAPs when added into concrete can constitute a long term reservoir able to feed the self-

This document is the intellectual property of the fib – International Federation for Structural Concrete. All rights reserved.
This PDF of fib Bulletin 95 is intended for use and/or distribution solely within fib National Member Groups.

healing reactions over time. Moreover, if being exposed to water at a cracked surface, the swelling of SAPs can contribute to an initial physical blocking effect in the cracks, while the chemical healing starts developing. The technique has been validated in [11-15], the obvious negative effects of SAP addition on the concrete strength remaining the major hindrance to its wider use, mainly in load-bearing structural applications. However, in a strain-hardening mixture, there is a positive effect of autogenous shrinkage mitigation and internal curing [16,17] increasing its strength next to the reduction in strength due to macro-pore formation [18,19]. Overall, the strength was not statistically significantly different [20].

Crystalline admixtures generally consist of a proprietary mix of active chemicals, included in a carrier of cement and sand. Because of their highly hydrophyllic nature, they are able to react with water, cement particles and with the soluble phase of cement hydration products, and form CSH and other pore blocking precipitates. These products increase the density of the CSH phase and deposit in the existing capillaries and micro-cracks, activating the self-repairing process. The mechanism is analogous to the formation of CSH and the resulting crystalline deposits become integrally bound with the hydrated cement paste, thus contributing to a significantly increased resistance to water penetration under pressure. Research on crystalline admixtures as stimulators of the autogenous healing capacity has been conducted in [8, 9], confirming the effectiveness of the healing products not only in sealing the cracks, even under aggressive environmental conditions, such as chloride exposure [21] but also in restoring the through-crack stress transfer capacity, both in the case of plain and fibre reinforced concrete [22-24] and under repeated cracking/healing actions [35]. In the case of HPFRCCs an interesting synergy has been highlighted at the fibre-matrix bond level between the dispersed fibre reinforcement and the healing products in the crack, most likely resulting in a sort of distributed “chemical self-prestressing” from which the recovery of the material performance can greatly benefit [25].

Natural vegetable fibres, also employed in the formulation of HPFRCCs, can provide a twofold action. While contributing to an effective control of the crack propagation phenomena, they can also act as reservoirs and transport medium of water throughout the cementitious matrix, absorbing water during the wet stages of wet/and dry cycles and releasing it during the dry periods. This contributes to the activation of delayed hydration and carbonation reactions responsible of crack healing [26]. They have been also shown effective, also through improved fibre-matrix bond promoted by healing, in triggering, after healing, the formation of cracks at new locations instead of the reopening of the healed ones.

Coherently with what is already well known with reference to other engineering materials, including, among others, polymers, metals, asphalts and paintings, [27], the possibility of engineering or stimulating the self-repairing functionalities in cement-based construction materials would enhance the material and structural durability also resulting into reduced maintenance needs over an extended service life [28]. This paper aims at providing a comprehensive and application-oriented review of the current knowledge on the healing capacity of FRCCs. Though state of the art reports on the topic have already been published [5,6], the authors in this paper will analyse the so far garnered knowledge highlighting the most relevant experimental variables through which the phenomenon can be described, governed and predicted, aiming at the formulation of durability assessment based design criteria. In the same framework, the concept for the experimental identification of the aforesaid variables will also be discussed. Finally, with the same design-wise application-oriented purpose, the most urgent research needs will be identified and discussed, which need

This document is the intellectual property of the fib – International Federation for Structural Concrete. All rights reserved.
This PDF of fib Bulletin 95 is intended for use and/or distribution solely within fib National Member Groups.

to be tackled to remove those hindrances which still limit a widespread market penetration of the self-healing technologies in a promising synergy with FRCs.

2 A design-wise interpretation of what we know: defining the "healable crack" concept

As from recently published literature surveys [29-31] on the self-healing capacity of cement based materials, the two main characters on stage are the crack which has to be healed and the water. This, being present in multiple ways in the environment where a cracked structure is in service, is essential to activate the delayed hydration and carbonation reactions responsible of the stimulated autogenous crack sealing and healing phenomena.

In fact, the crack governs the healing process as a whole primarily through its width and depth, since a narrower and less deep crack will be healed more easily than a wider and deeper one. In a real structural design framework, the "crack width" is the calculated output of a structure service scenario, which encompasses the anticipated type and level of actions, the exposure conditions, the dimensions of the structure and reinforcement details as well as the material characteristics and performance. All the aforementioned variables contribute to the definition of an "accepted" serviceability and/or durability scenario, including the deformation state of the structural element, one of whose distinctive parameters is the crack width itself.

More than fifty years of scientific research and technological development in the field of Fibre-Reinforced Concrete (FRC) and Cementitious Composites (FRCCs) have clearly demonstrated that one of the benefits achievable through the implementation of the FRC technology is the possibility of achieving, all the other variables held constant, a deformation state characterized by thinner, in case more tightly spaced, cracks, as compared to conventional reinforced concrete. This is beneficial, as above said, for the sealability/healability of the cracks, and leads to rethink the same concept of serviceability crack opening-based design through the formulation of a "healable crack width" concept.

The definition of the threshold values for the healable crack width has to take into account the following multiple variables:

- the material composition, which governs the quantity of available reactive material, through the water/binder ratio, the presence of supplementary cementitious materials, featuring either pozzolanic or delayed cementitious activity, and of tailored healing stimulating additions, such as crystalline admixtures and super-absorbent polymers. The unreacted material, when in contact with water, can activate the healing reactions. Other factors included in the mix composition may also affect the healing, such as the type and grading of aggregates, which, on the one hand, affect the tortuosity of the crack path and hence the ease with which the water can penetrate into it, starting the healing reactions. On the other hand, grading and roughness of aggregates, which also affects the "cohesive" nature of the cracks in concrete because of aggregate bridging, plays a role in the ease of through crack matrix reconstruction as well as on the effectiveness of the durability and mechanical performance recovery. The same applies to the type and geometry of fibres, since some fibre types, such as PVA ones, through their chemical affinity with cement hydration products, are able to act as deposition sites for the healing products, providing a

This document is the intellectual property of the fib – International Federation for Structural Concrete. All rights reserved.
This PDF of fib Bulletin 95 is intended for use and/or distribution solely within fib National Member Groups.

further stimulus to healing. Functionalisation of the fibre surface, together with their deformed geometrical shape, may also contribute to an enhancement of the fibre matrix bond through the healing product deposition and thus have a multiplying effect on the healing-related recovery of the mechanical performance of the composite [26].

- The age of cracking, which affects the effectiveness of the healing and hence the healable crack width: the older the age of concrete at the formation of a crack, the lower the available quantity of unreacted material and hence the slower and less probable the healing and the smaller the maximum healable width of the crack. In this respect, HPFRCCs, featuring a higher binder content and water/binder ratios as low as well below the stoichiometric values, may preserve higher amounts of unreacted material even at later ages, thus guaranteeing an appreciable healing potential in the long term [32,33].
- The exposure conditions, with main reference to the (dis)continuous presence of water and/or moisture, its temperature, pressure and presence of other substances diluted in it.
- The structural service scenario in the cracked state, with reference to the presence and nature of actions which have caused cracking and which the structure may fully or partially continue to sustain during its service life. In reinforced concrete structures the intrinsic cohesive nature of concrete cracks as well as the presence of reinforcement results in the constant presence of a through-crack sustained tensile stress, due to permanent and variable actions. The same holds as well for structures made of FRC and HPFRCC, whose enhanced tensile and flexural fracture toughness enables the material to resist not-negligible residual stresses up to quite large crack opening values. The effects of these stress states, and their interaction with the long-term behaviour of the composite, including post-cracking tensile and flexural creep, have to be taken into account in assessing the healing potential of the cracks and hence in quantifying the threshold values of healable crack widths.

  On the other hand, there are structural applications, which typically benefit from the implementation of the FRC technology, where a crack formed at earlier ages, *e.g.* during transient situations, may later experience, in the persistent service design scenario, through crack compressive stresses whose effect on the healing is likely to be favourable. This is the case, for example, of precast tunnel segments, which, behaving like simply supported beams during transport and handling, may experience flexural cracks, whereas, once the tunnel annulus is completed, experience mild circumferential compressive stresses. “Healability” of the aforementioned cracks all along the tunnel service life can substantially enhance the durability of the structure, also contributing to optimizing, if not reducing, conventional waterproofing and maintenance operations.

  The type and nature of actions which have caused the cracks and which may also be present during the service life of a structure, while the healing occurs, is also of importance in determining the healable crack width, cyclic and repeated actions interacting with the kinetics of healing also through the severity of the cracking and damage state. Structural applications with FRC and HPFRCC may feature interesting peculiar potentials. A balance between the crack width and spacing and the frequency of the repeated actions could be sought. In this way, thanks to the through crack stress redistribution capacity and the ongoing healing, repeated actions may result in the formation of new, freshly healable, cracks (Figure 1) in the “non-crack saturated” free space between the existing ones, rather than in the progressive reopening of the same

This document is the intellectual property of the fib – International Federation for Structural Concrete. All rights reserved.
This PDF of fib Bulletin 95 is intended for use and/or distribution solely within fib National Member Groups.

existing ones, which will obviously feature a lower and lower healing potential. When self-healing FRCCs, because of their high damage tolerance, are employed as a strengthening/retrofitting material against accidental actions such as earthquake, the self-healing functionality may provide a longer service life of the retrofitting, making it able to survive a higher number of events and thus increasing the resilience of the application.

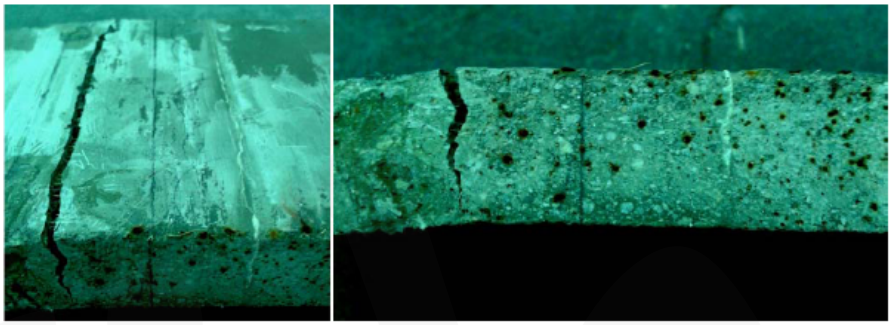


Figure 1: healed crack and newly formed crack in sisal + steel HPFRCC specimen.

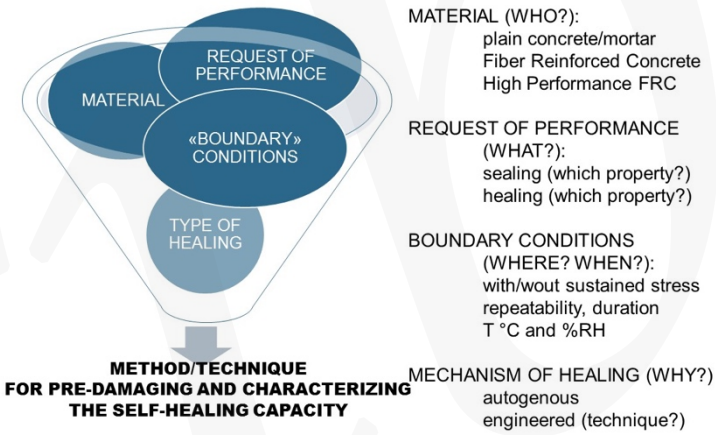


Figure 2: Experimental identification of "healable crack width": the 5W concept

3 How to experimentally identify the healable crack width?

In the previous section, the concept of healable crack width has been introduced and analysed in its essence and with reference to the main variables it depends on, as a corner stone for the definition of a design approach able to incorporate the self-healing concepts and exploit their benefits through related design choices. From a design-wise perspective, the definition of the healable crack concepts needs to be substantiated also through the definition of one or more experimental methods which have to allow not only its experimental quantification but also what the "healability" of the crack does imply in terms of recovery of durability.related and mechanical performance.

A survey on the topic has been recently published [29], highlighting how the definition and choice of the test method have to obey to a 5W concept (Figure 2). The methodology chosen to identify the application-related healable crack width threshold consists of a pre-cracking stage and a healing-assessment one and it is the outcome of a decision process encompassing:

- The material *(who?)* and its cracking toughness, ranging from weaker and more brittle

This document is the intellectual property of the fib – International Federation for Structural Concrete. All rights reserved.
This PDF of fib Bulletin 95 is intended for use and/or distribution solely within fib National Member Groups.

ones, such as lime mortars and plain concrete (which may favour the choice of inducing the damage through compression tests and measuring the healing through the recovery of compressive load bearing capacity and resonance frequency), to progressively tougher ones, such as FRC (for which the existing 3-point bending standard tests on notched prismatic beams may hold for pre-cracking and assessment of the healing-related recovery of post-cracking residual load bearing capacity) to HPFRCCs, whose one-of-a-kind tensile behaviour requires the adoption for both pre-cracking and healing of direct tension tests, 4-point bending tests or newly conceived Double Edge Wedge Splitting test.

- The requested performance *(what?)* in terms of crack closure, recovery of durability or mechanical performance. Healing assessment based on durability recovery may rely upon durability standard tests, which also dictate the choice of the specimen geometry and pre-cracking methodology. Healing assessment based on the recovery of mechanical performance is based on comparative evaluation of the response of the same specimen during pre-cracking and as retested in the post-healing stage.
- The boundary conditions *(where? when?)*, which encompass exposure conditions and structural service scenario, as described in the previous section.
- The mechanisms of healing *(why?)*, which dictates the need of not only relying upon a single test method but rather on a thorough methodology combining visual crack sealing evaluation, measurement of durability related and/or mechanical recovery and establishment of mutual correlation between the garnered measurements, all completed by the micro- (and nano-)scale characterization of the healed cracks and healing products.

4 Envisioning the future: designing the healable crack width!

The definition and experimental quantification of the healable crack width are governed by a complex set of variables which have to take into account and replicate as realistically close as possible the intended structural service scenario. The level of confidence required for the formulation of a design criterion and prescription is actually hardly achievable through experiments only, though based on multinational round-robin type cooperation. In this respect it is of the utmost importance to use a multi-physics modelling approach, able to describe and predict material aging, deterioration, healing and related evolution of the material properties, which can allow a time- and cost-effective holistic evaluation of the healing scenario [30].

It is also worth remarking that in a design oriented perspective this has to be coupled with a likewise sound model for the uncertainty, aiming at “an appropriate balance between accuracy and user-friendliness in the light of the limited availability of information and intended use of the design concept” [34]. In this respect, the approach proposed by Altmann and Mechtcherine [34] is the pathway to be followed.

Moreover, the benefits of using a self-healing fibre-reinforced concrete technology cannot be fully appreciated unless the design outcomes and predictions are consistently incorporated into a Life Cycle Analysis (LCA) framework, to assess the obtained benefits in terms of the whole Life Cycle Cost (LCC) and environmental footprint, through the achievement of a more efficient structural use of the material and an extended durability, which results in less frequent and intensive and expensive maintenance. All these benefits have also to be quantified in a social acceptance framework, through Social Life Cycle Assessment (SLCA), resulting in an added-value synergy between FRCCs and self-healing materials [35,36].

This document is the intellectual property of the fib – International Federation for Structural Concrete. All rights reserved.
This PDF of fib Bulletin 95 is intended for use and/or distribution solely within fib National Member Groups.

5 Concluding remarks

The potentials inborn in the synergy between FRC/FRCCs and self-healing concrete technologies have been revised proposing the definition of a ***healable crack width*** concept which may represent the first step for the incorporation of self-healing concepts into a codified design approach. To substantiate this concept from a design-wise operational point of view, the following needs hold:

- To provide a sound experimental methodology aimed at the quantification of the healable crack as a function of the material, the anticipated service scenario and the required performance as a function of the intended structural use. This has to rely upon a "holistic" characterization of the healing, encompassing crack sealing, recovery of durability and mechanical performance and characterization of healed cracks and healing products.

- To develop a multi-physics based model of the evolution of the material performance, including degradation, aging and healing, coupled with a model of the uncertainty which enables predicting with sufficient confidence the time evolution of the structural performance and provide output for LCA/LCC/SLCA evaluation of the benefits of using self-healing fibre reinforced cementitious composites in building new and/or retrofitting existing structures.

6 Acknowledgements

The cooperation between the two groups of authors is taking place in the framework of the COST Action CA15202 "SARCOS" (http://www.sarcos.enq.cam.ac.uk). E. Cuenca and L. Ferrara acknowledge the financial support of the PoliMi International Fellowships 2015.

7 References

[1] *fib*, International Federation for Structural Concrete (2012). Model code 2010.
[2] di Prisco, M., Plizzari, G. and Vandewalle, L. (2009). Fiber reinforced concrete. New design perspectives. Materials and Structures, 42 (9), 1261-1281.
[3] Naaman, A.E. and Reinhardt, H.W. (2006). Proposed classification of HPFRC composites based on their tensile response. Materials and Structures, 39 (5), 547-555.
[4] Li, V., Lim, Y. and Chan, Y. (1998). Feasibility of a passive smart self-healing cementitious composite. Composites Part B: Engineering, 29, 819-827.
[5] Cuenca, E. and Ferrara, L. (2017). Self-healing capability of FRC. State of the art and perspectives. Journal of the Korean Society of Civil Engineers, 21(7), 2777-2789.
[6] Snoeck, D. and De Belie, N. (2015). From straw in bricks to modern use of microfibers in cementitious composites for improved autogenous healing. A review. Construction and Building Materials, 95, 774-787.
[7] Gosh, S.K. (ed.) (2009). Self-Healing Materials: Fundamentals, Design Strategies, and Applications. Wiley. ISBN 9783527318292.
[8] Mihashi, H. and Nishiwaki, T. (2012). Development of engineered self-healing and self-repairing concrete – State-of-the-art report. Journal of Advanced Concrete Technology, 10, 170-184.
[9] Snoeck, D. and De Belie, N. (2016). Repeated autogenous healing in strain-hardening cementitious composites by using superabsorbent polymers. ASCE Journal of Materials

This document is the intellectual property of the fib – International Federation for Structural Concrete. All rights reserved.
This PDF of fib Bulletin 95 is intended for use and/or distribution solely within fib National Member Groups.

in Civil Engineering, 28(1), 1-11.

[10] Snoeck, D., Steuperaert, S., Van Tittelboom, K., Dubruel, P. and De Belie, N. (2012). Visualization of water penetration in cementitious materials with superabsorbent polymers by means of neutron radiography. Cement and Concrete Research, 42(8), 1113-1121.

[11] Snoeck, D., Van Tittelboom, K., Steuperaert, S., Dubruel, P. and De Belie, N. (2014). Self-healing cementitious materials by the combination of microfibers and superabsorbent polymers. Journal of Intelligent Material Systems and Structures, 25(1), 13-24.

[12] Gruyaert, E., Debbaut, D., Snoeck, D., Díaz, P., Arizo, A., Tziviloglou, E., Schlangen, E., De Belie, N. (2016). Self-healing mortar with pH-sensitive superabsorbent polymers: testing of the sealing efficiency by water flow tests. Smart Materials and Structures, 25 (084007), 11 p. DOI: 10.1088/0964-1726/25/8/084007.

[13] Snoeck, D., Dewanckele, J., Cnudde, V., and De Belie, N. (2016). X-ray computed microtomography to study autogenous healing of cementitious materials promoted by superabsorbent polymers. Cement and Concrete Composites, 65, 83-93.

[14] Lee, H.X.D., Wong, H.S., and Buenfeld, N.R. (2016). Self-sealing of cracks in concrete using superabsorbent polymers. Cement and Concrete Research, 79, 194-208.

[15] Borg, R.P., Cuenca, E., Gastaldo Brac, E.M. and Ferrara, L. (2018). Crack sealing capacity in chloride rich environments of mortars containing different cement substitutes and crystalline admixtures. Journal of Sustainable Cement Based Materials, 7(3), 141-159.

[16] Snoeck D., Pel L. and De Belie N. (2017). The water kinetics of superabsorbent polymers during cement hydration and internal curing visualized and studied by NMR. Science Repository , 7(9514), 1-14.

[17] Snoeck D., Jensen O.M. and De Belie N. (2015). The influence of superabsorbent polymers on the autogenous shrinkage properties of cement pastes with supplementary cementitious materials. Cement and Concrete Research,74, 59-67.

[18] Snoeck D., Schaubroeck D., Dubruel P. and De Belie N. (2014). Effect of high amounts of superabsorbent polymers and additional water on the workability, microstructure and strength of mortars with a water-to-cement ratio of 0.50. Construction and Building Materials, 72, 148-57.

[19] Snoeck D., Dewanckele J., Cnudde V. and De Belie N. (2016). X-ray computed microtomography to study autogenous healing of cementitious materials promoted by superabsorbent polymers. Cement and Concrete Composites, 65, 83-93.

[20] Snoeck D, Van Tittelboom K, Steuperaert S, Dubruel P and De Belie N. (2014). Self-healing cementitious materials by the combination of microfibres and superabsorbent polymers. Journal of Intelligent Materials Systems and Structures, 25(1):13-24

[21] Roig-Flores, M., Moscato, S., Serna. P. and Ferrara, L. (2015). Self-healing capability of concrete with crystalline admixtures in different environments. Construction and Building Materials, 86, 1-11.

[22] Roig Flores, M., Pirritano, F., Serna Ros, P. and Ferrara, L. (2016). Effect of crystalline admixtures on the self-healing capability of early-age concrete studied by means of permeability and crack closing tests. Construction and Building Materials, 114, 447-457.

[23] Ferrara, L., Krelani, V. and Moretti, F. (2016). On the use of crystalline admixtures in cement based construction materials: from porosity reducers to promoters of self-healing. Smart Materials and Structures, 25 084002 (17pp) DOI:10.1088/0964-1726/25/8/084002.

This document is the intellectual property of the fib – International Federation for Structural Concrete. All rights reserved.
This PDF of fib Bulletin 95 is intended for use and/or distribution solely within fib National Member Groups.

[24] Cuenca, E., Tejedor, A. and Ferrara, L. (2018). A methodology to assess crack sealing effectiveness of crystalline admixtures under repeated cracking-healing cycles. Submitted to Construction and Building Materials.
[25] Qian, S., Zhou, J., De Rooij, M., Schlangen, E., Ye, G., and Van Breugel, K. (2009). Self-healing behavior of strain hardening cementitious composites incorporating local waste materials. Cement and Concrete Composites, 31, 613-621.
[26] Ferrara L., Ferreira, S.R., Krelani, V., Della Torre, M., Silva, F. and Toledo Filho, R.D. (2015). "Natural fibres as promoters of autogenous healing in HPFRCCs: results from an on-going Italy-Brasil cooperation", in M.A. Chiorino et al., eds., ACI SP305.
[27] De Rooij, M.R., Van Tittelboom, K., De Belie, N. and Schlangen, E. (eds.) (2013). Self-Healing phenomena in Cement-based materials. State-of-the-Art Report of RILEM Technical Committee 221-SHC. Springer, 266 pp. ISBN: 978-94-007-6623-5.
[28] Ferrara, L., Krelani, V. and Carsana, M. (2014). A fracture testing based approach to assess crack healing of concrete with and without crystalline admixtures. Construction and Building Materials, 68, 515-531.
[29] Ferrara, L., Van Mullem, T., Alonso, M.C., Antonaci, P., Borg, R.P., Cuenca, E., Jefferson, A., Ng, P.L., Peled, A., Roig, M., Sanchez, M., Schroefl, C., Serna, P., Snoeck D., Tulliani, J.M. and De Belie, N. (2018). Experimental characterization of the self-healing capacity of cement based materials and its effects on the material performance: a state of the art report by COST Action SARCOS WG2. Construction and Building Materials, 167, 115-142.
[30] Jefferson, T., Javierre, E., Lee Freeman, B., Zaoui, A., Koenders, E. and Ferrara, L. (2018). Research progress on numerical models for self-healing cementitious materials. Advanced Materials and Interfaces, 5(17), 1-19 DOI: 10.1002/admi.201701378.
[31] De Belie, N., Gruyaert, E., Al-Tabbaa, A., Antonaci, P., Baera, C., Bajare, D., Darquennes, A., Davies, R., Ferrara, L., Jefferson, T., Litina, C., Miljevic, B., Otlewska, A., Ranogajec, J., Roig-Flores, M., Pain, K., Lukowski, P., Serna, P. Tulliani, J.M., Vucetic, S., Wang, J., Jonkers, H.M. (2018). A review of self-healing concrete for damage management of structures. Advanced Materials and Interfaces, 5(19), 1-28 DOI: 10.1002/admi.201800074.
[32] Ferrara, L., Krelani, V., Moretti, F., Roig Flores, M. and Serna Ros, P. (2017). Effects of autogenous healing on the recovery of mechanical performance of HPFRCCs: part 1. Cement and Concrete Composites, 83, 76-100.
[33] Ferrara, L., Krelani, V. and Moretti, F. (2016). Autogenous healing on the recovery of mechanical performance of HPFRCCs: part 2. Cement and Concrete Composites, 73, 299-315
[34] Altmann, F. and Mechtcherine. V. (2013). Durability design strategies for new cementitious materials. Cement and Concrete Research, 54, 114-125.
[35] Van Belleghem B., Van den Heede P., Van Tittelboom K. and De Belie N. (2017). Quantification of the Service Life Ex-tension and Environmental Benefit of Chloride Exposed Self-Healing Concrete. Materials, 10(5), 1-22.
[36] Rigamonti, S., Cuenca, E., Arrigoni,-A., Dotelli, G. and-Ferrara, L. (2019). Self-healing concrete vs. conventional waterproofing systems in underground structures: a cradle to gate LCA comparison with reference to a case study. In: Life-Cycle Analysis and Assessment in Civil Engineering: Towards an Integrated Vision – Caspeele et al. (eds.), 2019 Taylor & Francis Group, London, ISBN 978-1-138-62633-1, 2277-2284.

This document is the intellectual property of the fib – International Federation for Structural Concrete. All rights reserved.
This PDF of fib Bulletin 95 is intended for use and/or distribution solely within fib National Member Groups.

2) SHEAR

This document is the intellectual property of the fib – International Federation for Structural Concrete. All rights reserved.
This PDF of fib Bulletin 95 is intended for use and/or distribution solely within fib National Member Groups.
FRC2018: Fibre Reinforced Concrete: from Design to Structural Applications
Joint ACI-*fib*-RILEM International Workshop

Experimental study of shear transfer in polypropylene fibre-reinforced concrete using pre-cracked push-off specimens

Francisco Ortiz-Navas[1], Luca Scaroni[2], Juan Navarro-Gregori[1], Pedro Serna-Ros[1]

[1] : Polytechnic University of Valencia, Valencia, Spain.

[2] : University of Brescia, Brescia, Italy.

Abstract

Shear transfer mechanisms in fibre-reinforced concrete (FRC) have been studied by many authors based on push-off specimens. However, only few studies have used pre-cracked push-off specimens to examine the real shear and normal stresses transferred through the crack. In this paper it is presented the experimental results of twenty-one pre-cracked push-off specimens tested under direct shear. Specimens were manufactured using plain concrete (PC), polypropylene fibre-reinforced concrete (PFRC), and steel fibre reinforced concrete (SFRC). In PFRC and SFRC specimens, fibre was dosed in 10kg/m^3 and 30kg/m^3 respectively. Nevertheless, both types of dosages were selected in order to provide similar post-cracking behaviour to the specimens. Five types of pre-crack openings were set up (W = 0, 0.25, 0.50, 0.75 and 1.0 mm) by an external steel frame system that confined the specimens during the tests. Afterwards, pre-cracked specimens were tested under direct shear where the crack kinematic (opening and slip displacements) as well as stresses (shear and normal) were recording during the tests. Finally, a comparison of behaviour between PC, SFRC and PFRC is done. Experimental results show the ability of both fibres to increase shear stress as well as shear stiffness in FRC specimens compared to PC ones. Moreover, it is evidenced that both type of fibres provided similar shear improvements despite of being different in material and shape.

Keywords

Push-off, shear crack, PFRC, SFRC, Shear behaviour.

This document is the intellectual property of the fib – International Federation for Structural Concrete. All rights reserved.
This PDF of fib Bulletin 95 is intended for use and/or distribution solely within fib National Member Groups.

1 Introduction and objectives.

Shear failure of concrete elements is brittle and potentially dangerous. To understand this, several studies have been performed in the last century, some of them focusing on studying the shear transfer mechanisms in concrete elements. However, this mechanism are still a topic of discussion among researchers since many factors that act simultaneously have to be considered.

According to experimental results, it is well-known that steel fibres enhance concrete shear capacity, improve ductility and provide good crack control(Choi et al. 2007; Minelli et al. 2014; Parra-Montesinos 2006). This improvement in concrete behaviour is due mainly to the bridging effect provided by fibres. In recent years, the use of polypropylene fibres with larger dimensions and surface treatment has extended to structural applications, including shear reinforcement. Studies have demonstrated the efficiency of polypropylene fibres to enhance the shear behaviour of concrete elements (Conforti et al. 2017; Navarro-Gregori et al. 2016). However, information in the literature about the real mechanisms of shear transfer in PFRC elements and the role that polypropylene fibres play in cracks is lacking.

Different kinds of testing methods and specimens have been proposed in the literature to determine shear strength and to study shear transfer mechanisms. The push-off specimen, first developed by Mattock and Hawkins (Mattock and Hawkins 1972) to investigate interfaces in reinforced concrete, have become one of the principal test methods to study the direct shear transfer mechanisms. In fact these small specimens provide an accurate understanding of the load transfer mechanism and allow a bigger experimental campaign compared to full-scale specimens (Randl 2013).

The shear behaviour of a push-off specimen depends on whether the specimen has been pre-cracked or not. Behaviour in pre-cracked specimens depends on the shear transfer mechanisms that take place at the single crack location (aggregate interlock, dowel action, or the axial restraint of the reinforcement that crosses the shear plane). Thus pre-cracked specimens reduce ultimate shear stress and increase slip displacements compared to uncracked specimens (Mattock and Hawkins 1972). Nowadays, a new test methodology of the push-off test in pre-cracked specimens has been developed to better study the shear transfer in PC and FRC cracks (Echegaray-Oviedo et al. 2017). Nevertheless, most studies using push-off have been performed using steel fibre in normal-strength and self-consolidating concrete (Cuenca and Serna 2010; Echegaray-Oviedo et al. 2013; Lee 2007). However, no studies have been done using macro-synthetic fibres.

The objective of the present study was to determine the contribution of polypropylene fibres to shear transfer, as well as to determine if this contribution results similar that the contribution provided by steel fibres with similar post-cracking behaviour tan polypropylene ones. For this purpose, pre-cracked push-off specimens were tested under direct shear. Five pre-crack opening were used (W = 0, 0.25, 0.50, 0.75 and 1.0 mm) which were controlled by an external steel frame system that confines specimens. Finally, results are compared between the three types of concretes (PC, PFRC and SFRC) used.

2 Experimental programme

Twenty-one specimens (seven PC, six SFRC and eight PFRC) were manufactured and tested. The studied parameters were: concrete type and pre-crack opening. Figure 1 shows the

This document is the intellectual property of the fib – International Federation for Structural Concrete. All rights reserved.
This PDF of fib Bulletin 95 is intended for use and/or distribution solely within fib National Member Groups.

geometry of specimens which are characterized to have a "Z"-shape constituted two L-blocks: ACTIVE and PASSIVE blocks. Specimens were horizontally cast onto a steel formwork and cured at room temperature. Two metal plates (260x10x6 mm) incorporated into the formwork were used to create a trapezoidal notch, as seen in the cross- sectional detail in Figure 1. Four connector links of threaded rods (10 mm diameter) were embedded in specimens before casting. These connector links were used to fix the specimen to the external frame during the pre-cracking process and the push-off test. Finally, in order to better control de crack opening during the pre-cracking process, in five specimens (1PC, 2SFRC and 2PFRC) a stirrup of 8mm was placed at middle depth of the specimen as Figure 1shows.

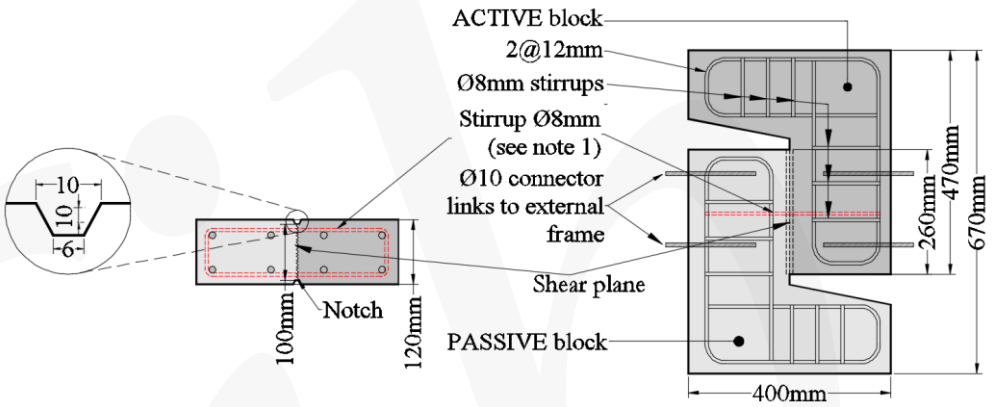


Figure 1: Geometry and reinforcement details of the push-off specimen

(Note1: Stirrup only placed in specimens Z6-PC, Z12-SFRC, Z20-SFRC, Z16-PFRC and Z24-PFRC)

2.1 Material properties

A high-workability normal-strength concrete was used in all the specimens. Six batches of concrete mixtures were prepared to cast specimens. The mixture proportions by the weight of all the specimens were 1:3.2:1.7:0.3:0.5 for 350 kg/m^3 of CEM I 42.5N cement: sand (0/4), coarse aggregate (6/12), coarse aggregate (12/20): water. To obtain the desired high workability, superplasticiser was dosed in the order of 1-1.1% (percentage of cement weight) in the PC and SFRC mixtures, and in the order of 1.4-1.5% in the PFRC mixture. According to EN 12350-8:2011, the slump flow test was 612 mm on average. The mix design was carried out for a characteristic concrete compressive strength of 35 MPa. Specimens were cured at room temperature (see Figure 2a).

In PFRC specimens, polypropylene fibres of 48mm length and 0.85mm diameter were dosed in a rate of 10 kg/m^3. The synthetic fibre was 100% monofilament polyolefin with 400MPa of tensile strength and 4700 MPa of modulus of elasticity. In the other hand, in SFRC specimens, hooked-end steel cold-drawn fibres were dosed with a rate of 30 kg/m^3. Fibres were 0.9 mm in diameter with 60 mm long (aspect ratio of 65), with tensile strengths of 2,300 MPa and 2,100,000 MPa of modulus of elasticity (see Figure 2b).

This document is the intellectual property of the fib – International Federation for Structural Concrete. All rights reserved.
This PDF of fib Bulletin 95 is intended for use and/or distribution solely within fib National Member Groups.

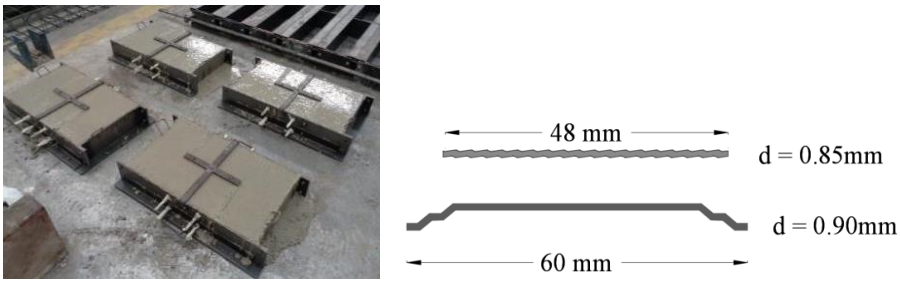


Figure 2: (a) Cast of specimens and (b) fibre geometry

Concrete compression strength (f_c) was determined according to EN 12390-3 on 24 cylindrical specimens (4 specimens per batch) of 150x300 mm. According to EN 14651, 14 notched prismatic specimens of 150x150x600 mm were employed to determine the residual flexural tensile strength (f_{Rj}) of PFRC and SFRC (see Figure 3). The mean values of f_c and f_{Rj} (coefficient of variation in brackets) are summarised in Table1.

Table 1: Mechanical proprieties of the push-off specimens.

Property	RC	SFRC	PFRC
f_c [MPa]	41.6 (0.04)	39.9 (0.04)	42.4(0.03)
E_c[MPa]	29420 (0.04)	28901 (0.02)	29621 (0.05)
f_L [MPa]	4.51 (0.06)	4.86 (0.08)	4.42 (0.08)
$f_{R,1}$ [MPa]	-	3.00 (0.30)	2.97 (0.17)
$f_{R,2}$ [MPa]	-	3.73 (0.23)	4.29 (0.19)
$f_{R,3}$ [MPa]	-	3.83 (0.21)	4.74 (0.17)
$f_{R,4}$ [MPa]	-	3.60 (0.28)	4.83 (0.18)

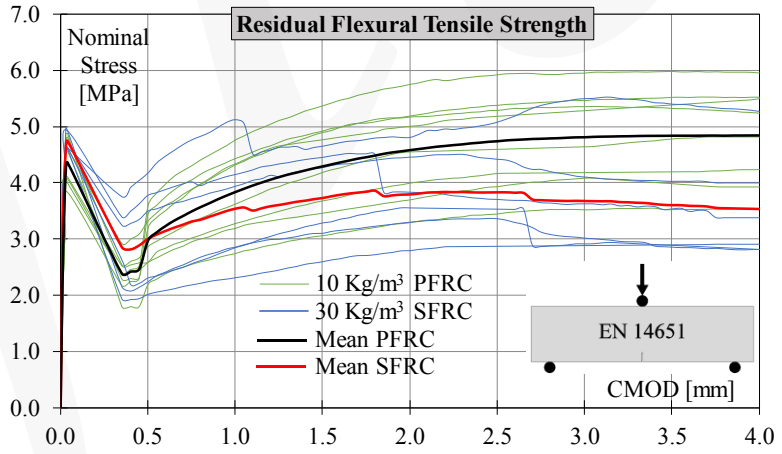


Figure 3: Nominal stress-CMOD responses according to EN 14651

2.2 Test Setup

The entire test was divided into two phases: the pre-cracking process and the push-off test. During the pre-cracking process, all the specimens were intentionally pre-cracked along the shear plane. By placing the specimen horizontally, two steel knifes (one placed over the

This document is the intellectual property of the fib – International Federation for Structural Concrete. All rights reserved.
This PDF of fib Bulletin 95 is intended for use and/or distribution solely within fib National Member Groups.

baseplate and other in the hydraulic jack) cracked the specimen (Load was step-wisely applied by a hydraulic jack of 500 kN at a rate of 200 N/seg) by splitting of the concrete as indicated in Figure 4, In order to control the crack, the specimen was confined by a rigid external steel restrain frame. Moreover, four steel springs placed on the baseplate prevented any undesired rotation of the active and passive blocks during the pre-cracking process. Crack opening was measured during this stage by PTs and DEMECs placed on the specimen surface. Before the push-off test, to the crack opening obtained during the pre-cracking process, is added a desired initial crack looseness (W = 0, 0.25, 0.50, 0.75 and 1.0 mm) in order to study the effect of initial crack openings in the shear transferring.

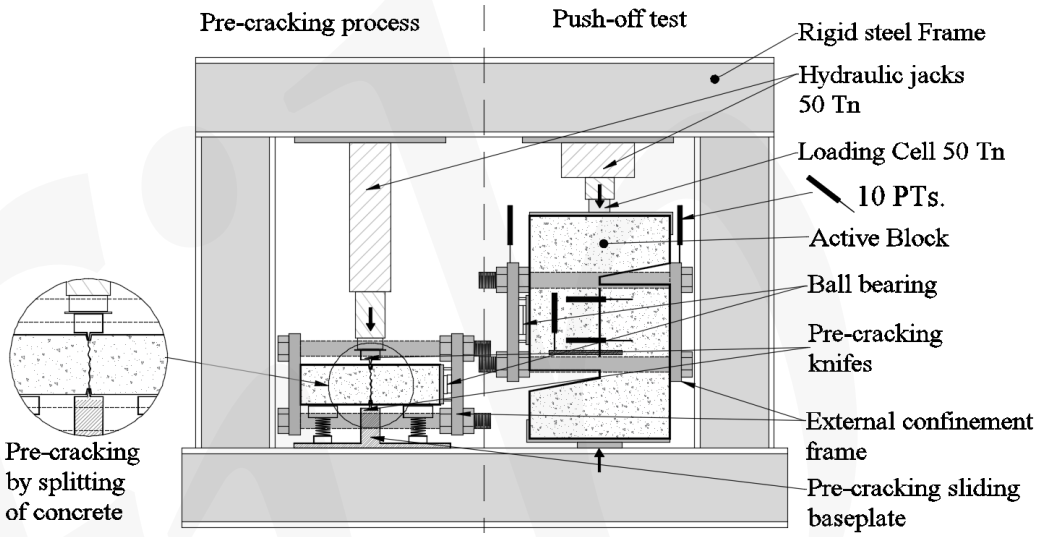


Figure 4: Setup for pre-cracking and the push-off test.

During the push-off stage (see Figure 4), the load was applied to the active block by a hydraulic jack of 500 kN at a rate of 50 N/seg. The specimen was loaded until a slip displacement of 10 mm was reached. During the test, both the crack opening and slip displacements along the shear plane were measured by LVDTs, while electrical gauges placed on the external reinforced bars of the restrain frame were used to measure indirectly the normal stresses in the crack. To reduce the frictional forces between the specimen and the external restraint frame as much as possible, a ball bearing device was placed between the active block and the external restrain frame. Further details about the test setup and test components can be seen in (Echegaray-Oviedo et al. 2017).

3 Test results and analysis.

The shear behaviour of PFRC was analysed by means of crack opening or crack slip, *versus* shear and normal stresses. Table 2 summarises the test results of the tested specimens. The values of crack opening w, and of the shear τ and normal σ stresses corresponding to a 2-mm crack slip, are reported. Shear stress resulted from the load acting along the shear plane and the shear force transmitted by the restraint frame, while normal stress was calculated based on the strain of the external steel bars placed on the restraint frame. In order to better compare the test results shown in Table 2, shear stresses were normalised. It is worth mentioned that specimens that content a stirrup are those with a letter "S" at the end of the specimen's name.

This document is the intellectual property of the fib – International Federation for Structural Concrete. All rights reserved.
This PDF of fib Bulletin 95 is intended for use and/or distribution solely within fib National Member Groups.

Table 2: Push-off test results at 1 mm and 5mm of slip displacement

ID	V_f [Kg/m^3]	w_0 [mm]	Slip = 1mm			Slip = 5mm		
			τ_{1mm} [MPa]	w_{1mm} [mm]	σ_{1mm} [MPa]	τ_{5mm} [MPa]	w_{5mm} [mm]	σ_{5mm} [MPa]
Z6-PC-S	0	0.15	5.98	0.47	0.89	6.13	1.24	2.91
Z2-PC		0.41	4.29	0.77	0.74	5.68	2.15	5.13
Z3-PC		0.73	2.36	1.22	0.66	4.57	2.65	3.09
Z4-PC		0.80	1.70	1.71	0.72	3.94	3.07	3.81
Z8-PC		0.84	1.43	1.38	0.71	3.50	2.82	3.33
Z1-PC		1.12	0.88	1.68	0.37	2.91	2.95	1.73
Z7-PC		1.13	1.90	1.83	1.06	5.36	3.69	4.63
Z12-SFRC-S	30	0.08	6.43	0.51	1.47	6.20	1.23	2.81
Z20-SFRC-S		0.09	6.99	0.52	1.09	7.16	1.22	2.08
Z19-SFRC		0.10	5.61	0.94	1.02	6.97	2.38	3.51
Z17-SFRC		0.25	4.50	0.79	0.55	5.04	2.59	3.60
Z10-SFRC		0.35	3.89	1.48	1.18	5.82	3.08	3.95
Z11-SFRC		1.32	2.82	1.95	0.42	3.75	3.56	3.30
Z24-PFRC-S	10	0.11	6.93	0.46	1.35	7.14	1.03	2.84
Z16-PFRC-S		0.17	6.74	0.57	1.17	7.74	1.31	3.30
Z21-PFRC		0.18	3.48	0.91	0.93	3.41	1.81	2.09
Z23-PFRC		0.18	5.10	1.02	1.28	4.74	2.44	3.66
Z15-PFRC		0.35	4.42	0.92	1.01	4.58	2.48	2.89
Z13-PFRC		0.58	3.48	1.25	0.87	4.69	2.48	3.22
Z14-PFRC		0.87	2.66	1.51	0.66	4.42	2.97	2.97
Z22-PFRC		1.12	3.85	2.05	0.46	4.66	4.35	3.71

As we can see in Table 2, the highest values of the shear stresses were obtained when the initial crack opening w_0 was the lowest in the PC, PFRC and SFRC specimens. This effect also can be seen in Figure 5, where the crack kinematic, crack opening vs. shear stresses, slip displacement vs. shear stresses and crack opening vs. normal stresses recorded during the tests of PFRC specimens is presented.

Figure 5c and d show the influence of initial crack opening on the shear stress in PFRC specimens. If specimens with low and large w_0 are compared between them, for example specimens Z23-PFRC (w_0=0.18mm) and Z14-PFRC (w_0=0.87mm), it can be observed that the shear transmitted at s =1mm, resulted greater in that specimen with the lowest w_0 (5.09 MPa for Z23-PFRC and 2.75 MPa for Z14-PFRC). This influence of w_0 is also observed in the normal stresses (σ) transmitted through the crack (see Figure 5d). Thus, at larger the initial crack opening is, less σ is transferred through crack.

Figure 5b additionally shows a comparison (hatched area) of the shear stresses between Z22-PFRC and Z7-PC, both with similar w_0 (over 1mm). As it could be seen, fibres can transmit high shear stress despite the large w_0. In fact, it could also be seen that polypropyelne fibres improved the shear stiffness in Z22-PFRC up to 1.4mm of crack opening was reached. This significant differences is due to the ability of fibres of bridging the crack faces, which provide post-cracking resistance to concrete matrix, and an improvement of stresses transmitted by aggregate interlock.

This document is the intellectual property of the fib – International Federation for Structural Concrete. All rights reserved.
This PDF of fib Bulletin 95 is intended for use and/or distribution solely within fib National Member Groups.

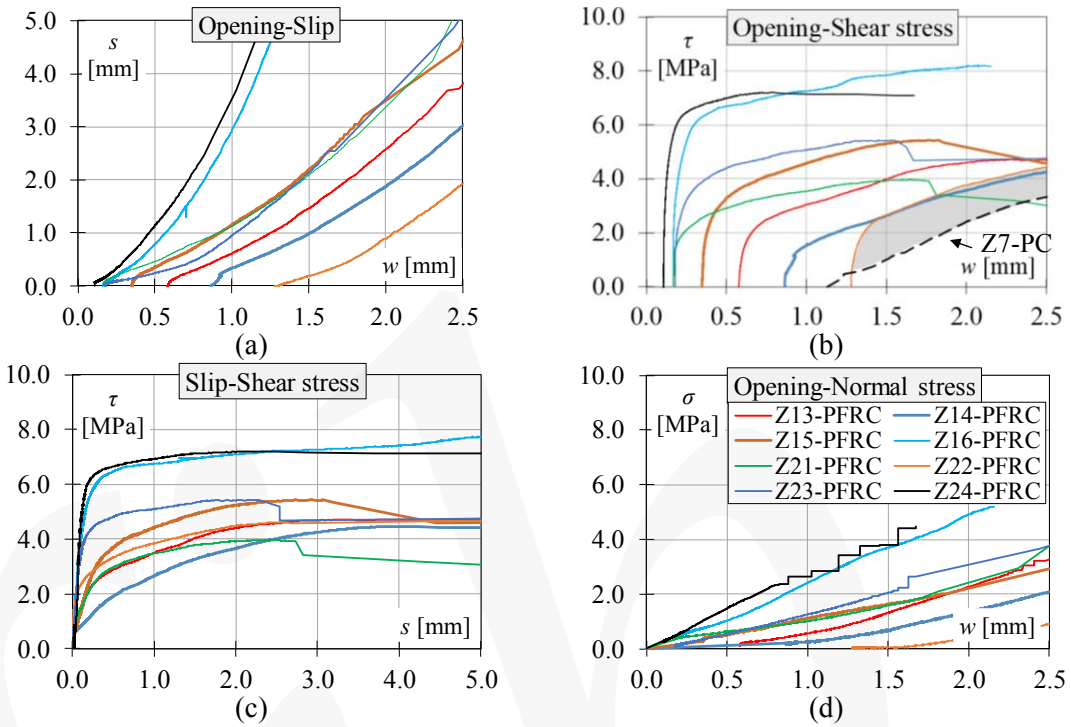


Figure 5: Influence of initial crack opening on shear behaviour in PFRC

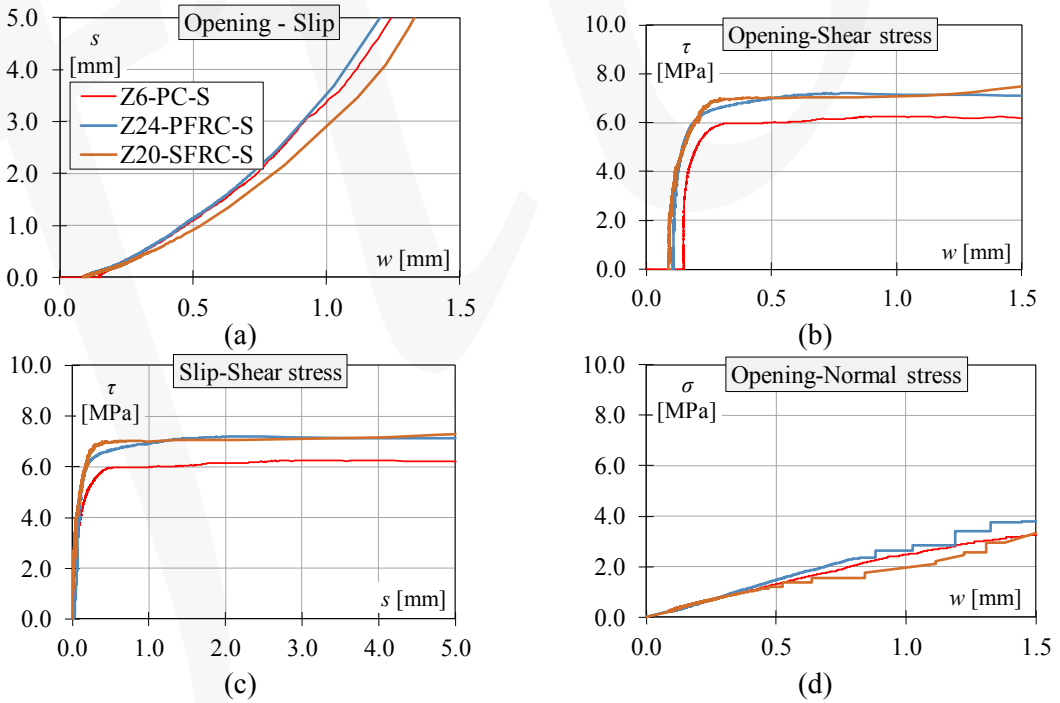


Figure 6: Push-off experimental results for PC, SFRC and PFRC with w_0=0 mm

This document is the intellectual property of the fib – International Federation for Structural Concrete. All rights reserved.
This PDF of fib Bulletin 95 is intended for use and/or distribution solely within fib National Member Groups.

In order to compare the shear performance between the three concrete types used (PC, SFRC and PFRC), Figure 6 displays a direct comparison between some specimens that contain a stirrup and similar initial crack openings. It can be seen that PFRC and SFRC specimens reached similar shear behaviour between them (see Figure 6b and c). Moreover, it also could be seen that greater shear stresses were transferred in both FRC specimens in comparison to control specimen (Z6-PC-S). In fact when slip s = 1mm and 5mm, the polypropylene and steel fibres improved the shear stress by approximately 17%, which is around of 1 MPa. This improvement in behaviour also could be observe in Figure 6b where crack opening vs. shear stresses are plotted. Concerning to normal stresses, as it could be seen in Figure 6d, the three specimens compared presented quite similar normal stress behaviour.

With the aim of observing the evolution of shear and normal stresses at different crack openings and slip displacements, the experimental results of PC and PFRC have been arranged and plotted in Figure 7a and b to plot tendency lines. To build the tendency lines, the points at the same crack opening (0.5, 1.0, 1.5, 2.0 and 2.5 mm) were identified from the different test results obtained with the specimens. Having identifying the point, their corresponding values of shear stress τ, normal stress σ and slip δ were positioned on a coordinate plane, as Figure 7a and b indicate. When all the points were placed on the plane, it was possible to trace a tendency line that showed the average trend of the points according to crack opening w. It is important to outline that the graphs in Figure 6 are arranged similarly to the Walraven experimental tests on the aggregate interlock.

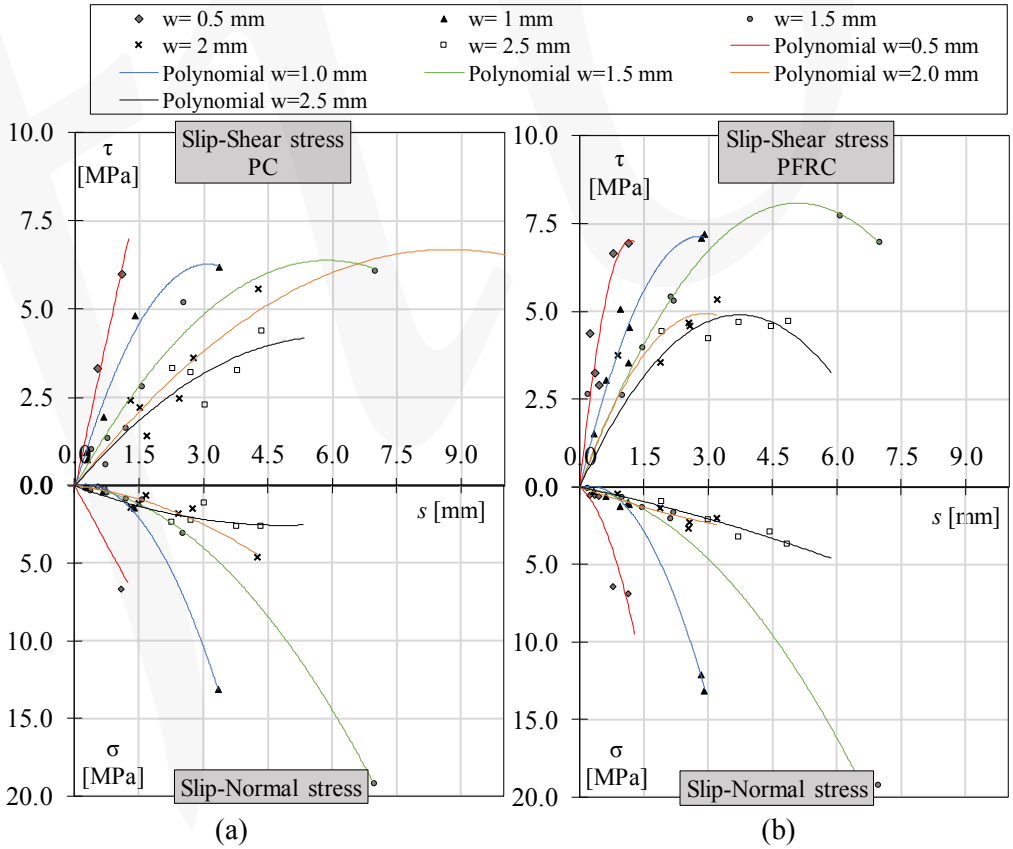


Figure 7: Shear interaction diagram for the (a) PC, (b) PFRC

This document is the intellectual property of the fib – International Federation for Structural Concrete. All rights reserved.
This PDF of fib Bulletin 95 is intended for use and/or distribution solely within fib National Member Groups.

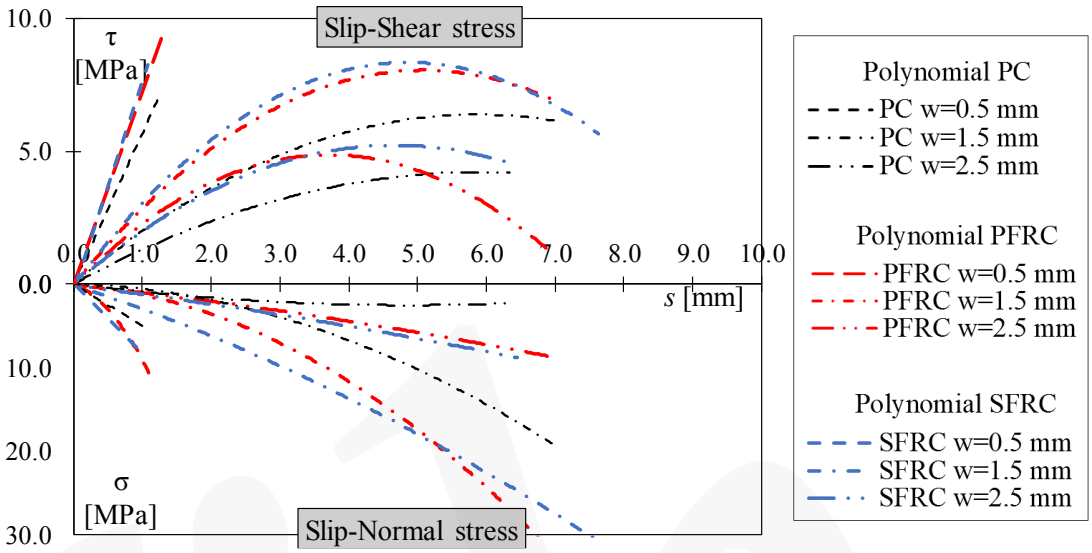


Figure 8: Comparison of shear interaction among PC, SFRC and PFRC.

Figure 7a and b clearly shows that shear and normal stresses resulted great when less slip, as well as, crack opening were obtained. In fact, although cracks presented great opening in PC, the crack could transfer considerable shear and normal stresses due to aggregate interlock. Moreover, it could also be observes that when crack slips s = 3mm and w = 1.5mm, the shear stress in PC was 5.0MPa, and was 5.0MPa in PFRC. This result proves the effectiveness of polypropylene fibres to transfer stresses through a shear crack.

Finally Figure 8 shows a comparison among the three types of concretes at three different crack openings (0.5, 1.5 and 2.5mm). It could be seen clearly the contribution of fibres to increase the shear and normal stresses transferred in the crack. This contribution resulted greater at large crack openings than small ones. In fact, both types of FRC presented quite similar shear and normal behaviour between them. This clearly demonstrate that, although polypropylene and steel fibres differ in material , geometry and amount of fibres in the matrix (10kg/m^3 in PFRC and 30Kg/m^3 in SFRC), since both type of fibres provided similar residual flexural strength, comparable shear behaviour is obtained.

4 Concluding remarks

In this study, push-off tests were performed on 21 "Z"-shaped push-off specimens. Based on the obtained results, the following conclusions can be drawn:

1. It has been evidence the effectiveness of aggregate interlock to transfer tangential and normal stresses in plain concrete shear cracks. In fact, it is observed that despite of great crack opening (over 1mm), the aggregate interlock results an effective mechanism to transfer stresses.

2. It is observed that polypropylene fibres dosed in 10kgm^3, incremented the shear and normal stresses transmitted in the crack from 0.5 to 2.0MPa approximately. In fact, this increment is more evident at large opening and slip displacement of the crack.

This document is the intellectual property of the fib – International Federation for Structural Concrete. All rights reserved.
This PDF of fib Bulletin 95 is intended for use and/or distribution solely within fib National Member Groups.

3. It was observed that PFRC and SFRC specimens presented very similar shear behaviour. This is attributed to both fibres provided similar residual flexural tensile strength to the concrete. These results confirms that regardless of fibre type (volume, material, shape, length, and diameter), if fibres provided similar residual flexural strengths, similar shear performance will take place. Thus, evaluating the shear performance of FRC element as a function of residual flexural tensile strengths results convenient.

5 Acknowledgement

This work forms part of Project "BIA2016-78460-C3-1-R" supported by the State Research Agency of Spain

6 References

Choi, K. K., Wight, J. K., and Park, H. G. (2007). "Shear strength of steel fiber-reinforced concrete beams without web reinforcement." *ACI Structural Journal*, 104(1), 12–21.

Conforti, A., Minelli, F., and Plizzari, G. A. (2017). "Shear behaviour of prestressed double tees in self-compacting polypropylene fibre reinforced concrete." *Engineering Structures*, Elsevier Ltd, 146, 93–104.

Cuenca, E., and Serna, P. (2010). "Shear behavior of Self-Compacting concrete and Fiber-Reinforced concrete Push-Off specimens." *RILEM Bookseries*, 429–438.

Echegaray-Oviedo, J., Navarro-Gregori, J., Cuenca, E., and Serna, P. (2013). "Upgrading the push-off test to study the mechanisms of shear transfer in FRC elements." *Proceedings of the 8th International Conference on Fracture Mechanics of Concrete and Concrete Structures, FraMCoS 2013*, (August 2015), 1012–1021.

Echegaray-Oviedo, J., Navarro-Gregori, J., Cuenca, E., and Serna, P. (2017). "Modified push-off test for analysing the shear behaviour of concrete cracks." *Strain*, 53(6), 1–17.

Lee, G. (2007). "Direct shear behaviour of steel fibres in a cementitious matrix." *School of Civil and Environmental Engineering*, The University of New South Wales.

Mattock, A., and Hawkins, N. (1972). "Shear Transfer in Reinforced Concrete—Recent Research." *Journal of the Prestressed Concrete*, 11(44).

Minelli, F., Conforti, A., Cuenca, E., and Plizzari, G. (2014). "Are steel fibres able to mitigate or eliminate size effect in shear?" *Materials and Structures*, 47(3), 459–473.

Navarro-Gregori, J., Mezquida-Alcaraz, E. J., Serna-Ros, P., and Echegaray-Oviedo, J. (2016). "Experimental study on the steel-fibre contribution to concrete shear behaviour." *Construction and Building Materials*, Elsevier Ltd, 112, 100–111.

Parra-Montesinos, G. J. (2006). "Shear strength of beams with deformed steel fibers." *Concrete International*, 28(11), 57–66.

Randl, N. (2013). "Design recommendations for interface shear transfer in fib Model Code 2010." *Structural Concrete*, 14(3), 230–241.

This document is the intellectual property of the fib – International Federation for Structural Concrete. All rights reserved.
This PDF of fib Bulletin 95 is intended for use and/or distribution solely within fib National Member Groups.
FRC2018: Fibre Reinforced Concrete: from Design to Structural Applications
Joint ACI-*fib*-RILEM International Workshop

Shear crack behaviour and shear deformation of polypropylene fibre-reinforced concrete slender beams

Francisco Ortiz Navas[1], Juan Navarro-Gregori[1], Pedro Serna Ros[1], Gabriel Leiva Herdocia[1]

[1]: Institute of Science and Concrete Technology, ICITECH, Universitat Politècnica de València, Valencia, 46022, Spain.

Abstract

In recent years, much research has shown improvements in shear behaviour and deformation capability when an adequate amount of macro fibres is provided in concrete. However, very few experiments have used macro synthetic fibres. In this paper, the shear capability of deformation in slender beams was studied by analysing the shear crack path, the crack opening-slip relationship and shear deformation of polypropylene fibre-reinforced concrete (PFRC) beams. Shear cracks and deformations were measured by non-contact image measurement techniques. The results are compared with those of plain concrete (PC), steel fibre-reinforced concrete (SFRC) and reinforced concrete (RC) beams. Both types of fibres were dosed so that similar average residual tensile strengths would remain similar to one another. The crack path analysis results showed that synthetic fibres delayed the formation of shear cracks and their propagation into compression zone, and improved the behaviour of secondary cracks due to loss of bond with longitudinal reinforcement. Finally, the crack opening-slip relationship varied widely along the crack and location in beams.

Keywords

Polypropylene fibre, shear strength, shear deformation, image-measurement.

This document is the intellectual property of the fib – International Federation for Structural Concrete. All rights reserved.
This PDF of fib Bulletin 95 is intended for use and/or distribution solely within fib National Member Groups.

1 Introduction

For decades, numerous studies have been performed to improve the mechanical properties of concrete by introducing fibres into the matrix (ACI 1996). Part of this research has focused on how to enhance the shear behaviour of concrete elements. Actually, many research works have evidenced the effectiveness of steel fibres as shear reinforcement when an adequate amount of fibres is provided to ensure toughness and ductility (Choi et al. 2007; Minelli et al. 2014) However, macro-synthetic fibres, with larger dimensions and surface treatment, have been developed to transmit significant toughness to concrete, and their use has extended to structural applications, including shear reinforcement. In the last few years, studies have demonstrated the efficiency of polypropylene to enhance the shear behaviour of concrete elements (Conforti et al. 2017; Navarro-Gregori et al. 2016).

Even though these studies can certainly be considered to represent the good progress made in knowledge about the shear behaviour of elements reinforced by macro-synthetic fibres, a limited number of experimental results, and only a few factors that affect shear strength, have been studied to date in the presence of macro-synthetic fibres.

In RC beams without stirrups, the aggregate interlock is considered one of the primary factors of shear resistance. This mechanism dissipates as crack opening increases. Experimental tests have shown that in RC beams without stirrups, the maximum crack opening along the main diagonal shear crack reaches 0.5 mm before collapse. The crack bridging provided by steel fibres can alter the aggregate interlock by restricting slip along the crack and increasing shear strength. This post cracking behaviour allows cracks to continue resisting stresses despite increasing shear crack opening. Apart from the bridging effect, studies have shown that steel fibres delay diagonal crack propagation, which allows the compressed zone to remain higher and deeper, and lets the beam remain stable even at higher loads (Zarrinpour and Chao 2017). Moreover, it has been seen that the presence of fibres increase the stiffness of the dowel zone since fibres are capable of containing the dowel crack growth (Bahia 1979).

Non-contact image measurement is a computer technique used to track displacements of the targets located on the surface of an element. To take measurements, the technique requires images from a specific surface before deformation (image of reference) and during tests (deformed image). The computer software adjusts intrinsic and extrinsic distortions, and compares the relative displacement between targets in different load stages. This technique is a reliable way to study crack behaviour in concrete elements (Dias-da-Costa et al. 2011).

The main objective of this paper is to study the cracked behaviour of shear-critical PFRC beams. It particularly intends to study (a) the crack pattern evolution, (a) shear deformation on beams, and (c) the kinematic behaviour of critical diagonal cracks. For this propose, an experimental programme that considered eight PFRC beams was carried out and is presented below.

This document is the intellectual property of the fib – International Federation for Structural Concrete. All rights reserved.
This PDF of fib Bulletin 95 is intended for use and/or distribution solely within fib National Member Groups.

2 Experimental programme

Eight full scale beams were analysed to better understand the shear behaviour of PFRC, and their similarities with SFRC and RC beams. The beams, with a shear span to effective depth ratios of 3.80 and 4.80, and fibre contents of 10 kg/m^3 (PFRC) and 30 kg/m^3 (SFRC) were tested under a concentrated load at mid-span.

2.1 Specimen geometry and material properties

To meet the research objectives, an experimental programme was carried out on two series of four full beam specimens, namely series A1 and A2. Figure 1 and Table 1 show the geometric dimensions and reinforcement details of all the tested beams: designation, span L, depth h, width b, slenderness a/d, area of longitudinal reinforcement A_s, area of transverse reinforcement A_{st}, type, and fibres content.

The geometric and reinforcement details of the two series of beams were inspired in the classic series of concrete beams by Bresler and Scordelis in 1963, and reproduced in 2004 by Vecchio and Shim (Bresler and Scordelis 1963; Vecchio and Shim 2004). Each series consists in beams with the same dimensions and longitudinal reinforcement ratio, and contains one specimen of PFRC, SFRC, PC and RC with stirrups.

Table 1: Geometry and reinforcement of specimens

Specimen	Concrete Type	L [mm]	h [mm]	d [mm]	b [mm]	a/d	A_s	A_{st}	Fibre Type	Fibre Content [kg/m^3]
0A1	PC	3660	552	472	305	3.9	3D20+ 3D25 (1.68%)			
0AP1	PFRC								PP[1]	10
0AS1	SFRC								S[2]	30
A1	RC							D8at330mm (0.10%)		
0A2	PC	4570				4.8	4D20+ 4D25 (2.23%)			
0AP2	PFRC								PP	10
0AS2	SFRC								S	30
A2	RC							D8at330mm (0.10%)		

[1] PP = Polypropylene, [2] S = Steel, [3] D = Diameter in millimetres.

A high workability normal strength concrete was used for all the beams. Several batches of concrete mixtures were prepared in a concrete batching plant to cast beams. The mixture proportions/weight of all the beams were 1:3.2:1.7:0.3:0.5 for 350 kg/m^3 of CEM I 42.5N cement: sand (0/4), coarse aggregate (6/12), coarse aggregate (12/20): water. To obtain the desired high workability, superplasticiser was dosed in the order of 1-1.1% (the percentage of cement weight) in the PC, RC and SFRC mix, and in the order of 1.4-1.5% in PFRC. According to EN 12350-8:2011, the slump flow test was 612 mm on average. The mix design was carried out for a characteristic concrete compressive strength that equalled 35 MPa.

For the PFRC beams, polypropylene macro-synthetic fibres were used at a dose of 10 kg/m^3. The synthetic fibres were 100% monofilament polyolefin with an equivalent diameter of .85mm

This document is the intellectual property of the fib – International Federation for Structural Concrete. All rights reserved.
This PDF of fib Bulletin 95 is intended for use and/or distribution solely within fib National Member Groups.

and a length of 48 mm (see Figure 2b). The tensile strength and modulus of elasticity, as reported by the manufacturer on the data sheet, were 400 MPa and 4,700 MPa, respectively. For the SFRC beams, hooked ends steel cold-drawn fibres were used at a dose of 30 kg/m^3. Fibres were 0.9 mm in diameter and 60 mm long (aspect ratio of 65), with a tensile strength of 2,300 MPa and 2,100,000 MPa of modulus of elasticity (see Figure 2c).

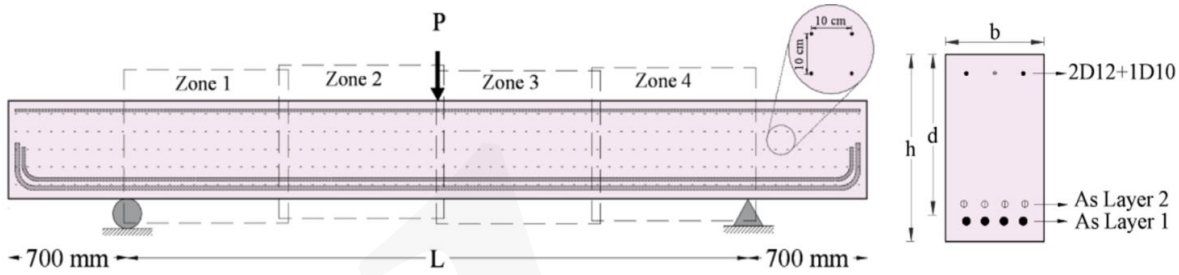


Figure 1: Geometry details of the beams

Concrete compression strength was determined according to EN 12390-3 with 32 cylindrical specimens (4 specimens per batch) of 150x300mm. The mean concrete compressive strength (coefficient of variation in brackets) value was: 41.3 MPa (3.7%), 41.0 MPa (4.3%) and 43.1 MPa (4.6%) for PC, SFRC and PFRC, respectively.

Additionally, 14 notched prismatic specimens of 150x150x600mm were employed to determine the residual flexure strength of PFRC and SFRC according to EN 14651. Figure 2a represents the Stress *vs*. the Crack Mouth Opening Displacement (CMOD) of both fibre-reinforced concretes. The limit of proportionally f_{Lm} and the average values of residual flexure strengths $f_{R,1m}$, $f_{R,3m}$, for SFRC were 5.07 MPa (C.V.=0.08), 3.96 MPa (C.V.=0.33), 4.89 MPa (C.V.=0.30), whereas for PFRC were 5.53 MPa (C.V.=0.08), 2.85 MPa (C.V.=0.17) and 4.45 MPa (C.V.=0.20). It could be observed that SFRC residual strengths presented more coefficient of variability (C.V) than PFRC ones. This is due to the number of steel fibres in the matrix resulted less than in PFRC, thus, there is more probability of fibre dispersion in SFRC than PFRC. The obtained properties fulfilled the MC2010 requirements for use in structural applications: $f_{R,1m}/ f_{Lm} = 0.78 > 0.40$, $f_{R,3m} / f_{R,1m} = 1.24 > 0.50$ for SFRC; $f_{R,1m}/ f_{Lm} = 0.52 > 0.40$, $f_{R,3m} / f_{R,1m} = 1.56 > 0.50$ for PFRC. As one objective was to compare the SFRC and PFRC elements, both doses of fibres were selected to obtain a similar residual strength between one another.

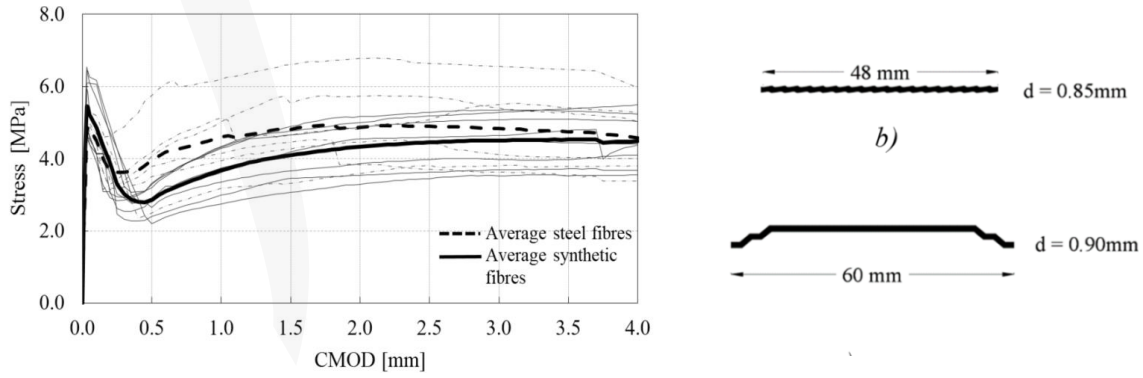


Figure 2: a) Average Residual Flexural Strength, b) Synthetic fibre and c) Steel fibre details

This document is the intellectual property of the fib – International Federation for Structural Concrete. All rights reserved.
This PDF of fib Bulletin 95 is intended for use and/or distribution solely within fib National Member Groups.

For the test setup, beams were simply supported and loaded at mid-span. Load was applied at an average constant deflection rate of 0.30±0.10 mm/min under the displacement control conditions of deflection at mid-span. Potentiometric transducers were employed to measure deflection at mid-span. Moreover, to analyse crack openings and shear deformation, targets were painted on the beam surface at 100-mm intervals in the vertical and horizontal directions (see Figure 1). Four high-resolution digital cameras were used to capture images every 10 seconds during the test. Each image covered one zone, as indicated in Figure 1. By a non-contact image-based displacement technique, the relative displacements between the selected targets were measured, hence deformations and strains could be calculated. Lens distortion, and the extrinsic parameters of the camera, were calibrated before measurements were taken.

2.2 Test results.

Table 2 summarises the test results of both series. We can see that by using 10 kg/m^3 of polypropylene fibres in the PFRC beams, the shear stress resisted by the section rose by 70% compared to the PC beams. Additionally, the deflection of the PFRC beams was similar to their corresponding RC beams with stirrups. Despite these results, the PFRC beams did not reach the same mode of failure as the RC beams with stirrups (shear compression), and failed by diagonal tension. Similar results to the PFRC beams were obtained with the SFRC beams in both series. It is worth mentioned that Diagonal tension resulted a brittle and abrupt failure whereas shear compression failure was characterized by the presence of many inclined cracks, which grow and reduce the compression zone, with the beam failing at the end by splitting in the compression zone

Table 2: Summary of the test results

Specimen	Concrete	P_{peak}	V_{peak}	v_u	$v_u / \sqrt{fc}$	$\delta_{peak\ load}$	Mode of Failure
OA1	PC	312.1	156.06	1.12	0.17	5.74	Diagonal Tension
OAP1	PFRC	446.7	223.34	1.58	0.24	15.81	Diagonal Tension
0AS1	SFRC	466.5	233.24	1.62	0.25	15.62	Diagonal Tension
A1	RC	472.7	236.35	1.67	0.27	16.31	Shear Compression
OA2	PC	339.0	169.52	1.22	0.19	12.06	Diagonal Tension
OAP2	PFRC	486.3	243.13	1.73	0.26	28.02	Diagonal Tension
0AS2	SFRC	455.6	227.80	1.58	0.25	30.94	Diagonal Tension
A2	RC	478.4	239.19	1.71	0.27	25.96	Shear Compression

3 Analysis of the test results

3.1 Shear crack pattern evolution

For the purpose of understanding the global effect of fibres on the crack behaviour of beams, a crack pattern of series A1 was represented for each 100 kN load until the instant prior to failure. PC beams, 0A1, were taken as a control to compare the effects of fibres on crack patterns.

On all the beams, the inclined shear cracks progressed from a bending crack and propagated initially to the loading point. The main inclined crack was located at an approximately similar distance from the depth of the beams from the mid-span. As we can see in Figure 3, the crack patterns of all the beams are similar to one another until 300 kN. The magenta dashed line in

This document is the intellectual property of the fib – International Federation for Structural Concrete. All rights reserved.
This PDF of fib Bulletin 95 is intended for use and/or distribution solely within fib National Member Groups.

Figure 3 represents the load level when shear cracks started to appear on all the beams. The first shear crack on the 0A1 beam appeared at 175 kN, while shear cracks appeared at 221, 235 and 225 kN on the 0AP1, 0AS1 and A1 beams, respectively.

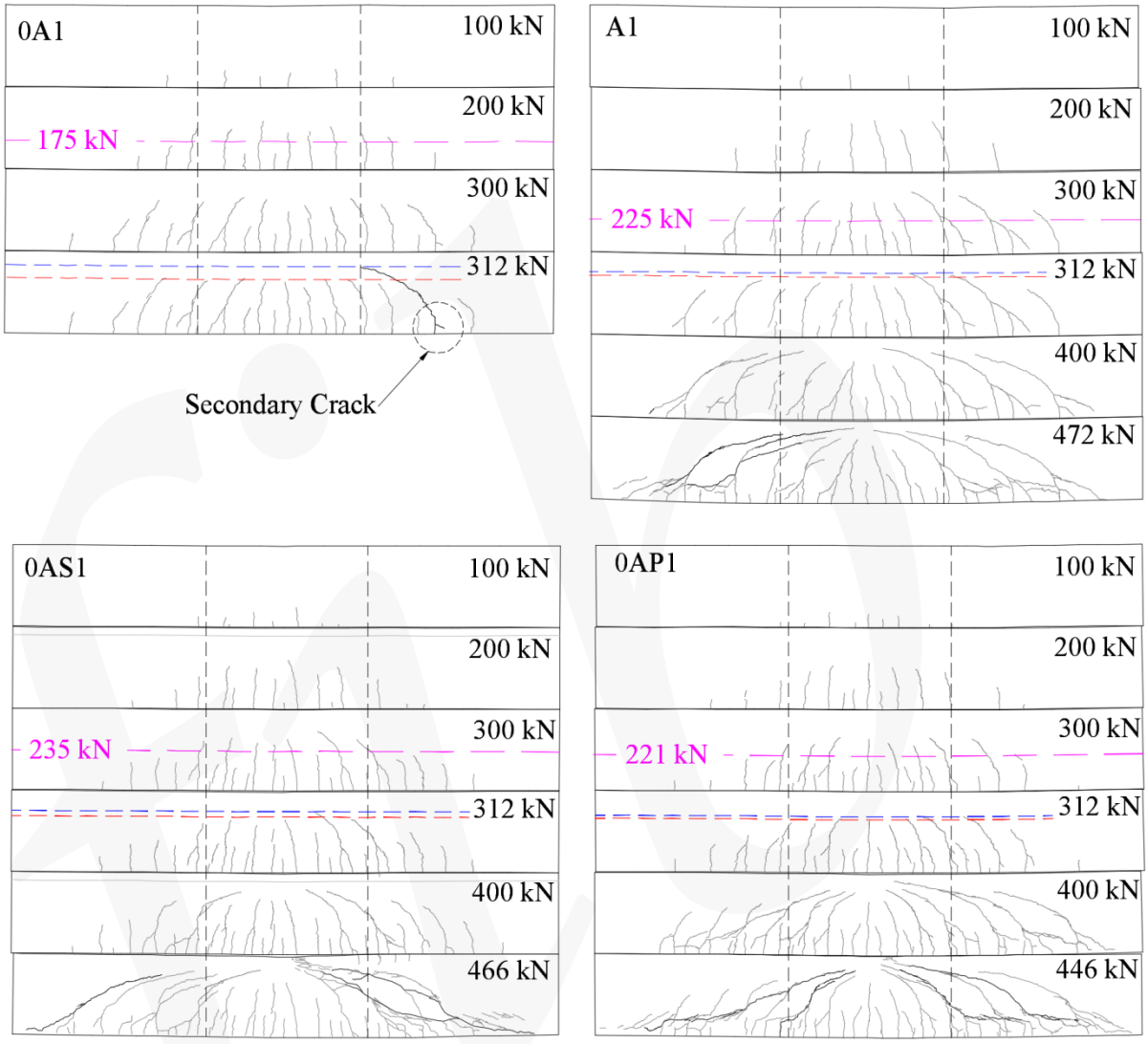


Figure 3: Crack path for series A1 and A2

With increasing load, shear cracks continued propagating to the loading and bearing plates. The 0A1 beam failure was produced by abrupt shear crack opening when a secondary crack, due to longitudinal reinforcement bond loss, started to appear (see Figure 3). This secondary crack was probably a result of an uncontrolled dowel action crack. When comparing PFRC and SFRC to RC with stirrups, we found that the beams which contained fibres developed more cracks due to the concrete splitting along the tensile longitudinal rebar than the RC beams without stirrups, and were almost similar to the RC with stirrups. The postcracking stress transfer due to the polypropylene fibres controlled the secondary crack propagation, as stirrups do, and allowed the dowel action to continue acting as a shear transfer mechanism by providing the beam with a greater shear load capacity.

This document is the intellectual property of the fib – International Federation for Structural Concrete. All rights reserved.
This PDF of fib Bulletin 95 is intended for use and/or distribution solely within fib National Member Groups.

Moreover before 0A1 beam failure, a main diagonal crack propagated quickly towards the loading point. In Figure 3, a graphic comparison of crack propagation among beams is represented by red and blue dashed lines. A red dashed line shows the main diagonal crack depth at 300kN, while a blue one denotes the diagonal crack depth at 312kN. As shown, at a similar shear force increment nearly no crack propagation existed on the PFRC, SFRC and RC beams. This delay in crack propagation allowed the compression zone to continue resisting shear stress and provided beams with a greater shear load capacity.

3.2 Shear Deformation

In the present section, the shear ductile provided by fibres was analysed in the A2 series. With non-contact image displacement techniques, two average shear strains were calculated from the relative displacement of four selected targets. In the first case, the four selected targets arranged a square panel of 400x400mm. In all the beams, the square area was located on the side of the beam where the main diagonal crack appeared at a similar distance from the effective depth of the beams from the mid-span. This area was selected because, theoretically, it is the location where the maximum shear stress took place.

Figure 4 shows the shear stress–strain response of the square panel. We can see that, initially, the shear stiffness for SFRC and PFRC was greater than in the PC beams, and was similar to the RC beams. This stiffening improvement provided by the fibres resulted in the delayed formation of shear cracks, as mentioned in Section 3.1 and shown in Figure 3. Furthermore, the shear stress–strain response showed shear stiffness decreases at a stress of approximately 1.25 MPa, and the shear strain significantly increased.

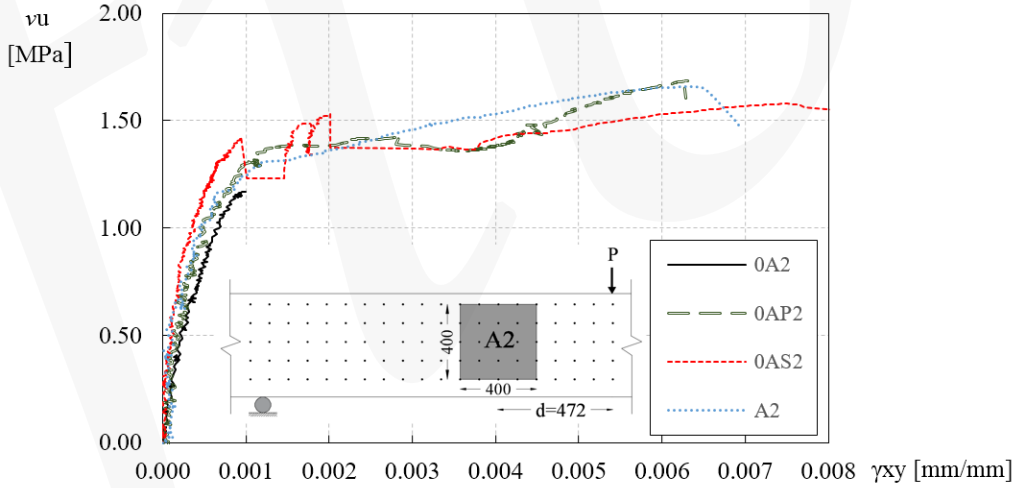


Figure 4: Shear stress - strain response

When comparing the shear strains between beams PC and PFRC (Figure 4), we found that the shear strain at peak stress on the PC beam was in the order of 0.8 mm/m, while the strain was approximately 6.5 mm/m for the PFRC beams. This increase in shear strain represented around 8-fold the shear strain provided by the PC beams, and was almost the same shear stress-strain provided by the A2 beam, including transverse reinforcement.

The increment in ductility provided by the polypropylene fibres is observed in Figure 5, where the contribution of shear deformation to vertical deflection is represented and compared with flexural deflection.

This document is the intellectual property of the fib – International Federation for Structural Concrete. All rights reserved.
This PDF of fib Bulletin 95 is intended for use and/or distribution solely within fib National Member Groups.

In order to experimentally determine the shear contribution to beam deflection, the relative displacements of eight targets, which represented two rectangular panels, were measured. Finally, the average shear strain of each panel was determined. Shear deflection was calculated by multiplying the shear span length L/2 (see Table 1) by the average shear strain determined from both rectangular panels. Total deflection was also measured during the test with one potentiometric displacement transducer located at the mid-span of the beams.

The load deflection response presented in Figure 5 shows that the main contribution to total deflection was due to the flexure in the early load stages, which increased linearly up to 400kN. Afterwards, the dominant deflection was due to shear. This shear contribution, as shown in Figure 4, was due to the significant reduction in shear stiffness because of beam degradation (increment in shear cracks and crack opening, as shown in Figure 3).

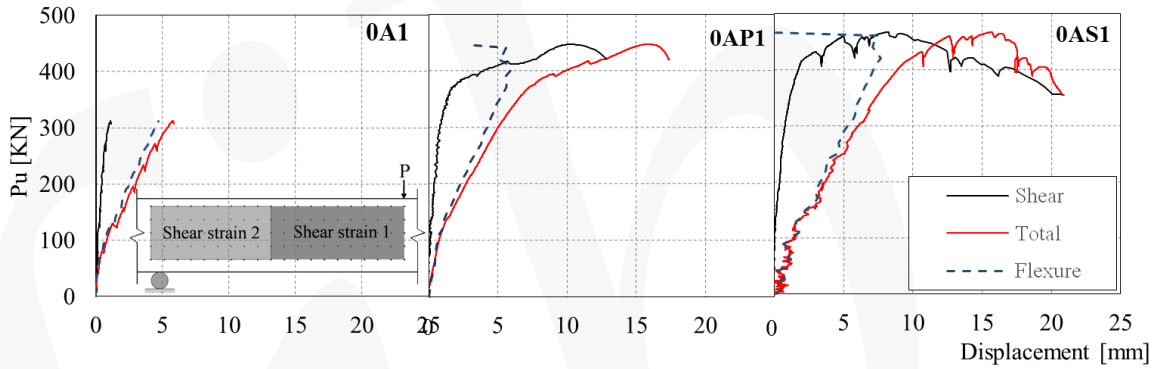


Figure 5: Contribution of shear deformation to deflexion in the A1 series.

3.3 Crack opening – slip relationship

In order to study the relationship between the crack opening and slip of the critical diagonal shear crack, the critical shear crack was gauged at different beam depths (L1 – L4) by non-contact image measurement techniques (see Figure 6). In order to analyse the interaction between the adjacent diagonal shear cracks, four cracks (C1-C4) were selected and gauged (see Figure 6).

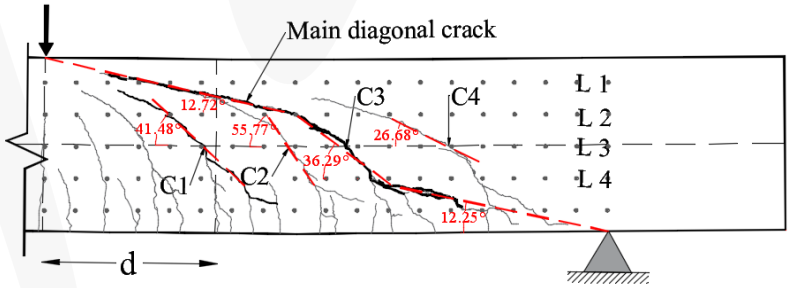


Figure 6: Crack pattern in beam 0AP1at 400kN

Figure 7a-c shows the evolution of the main diagonal crack (C3) during the test. The largest crack opening took place at approximately the mid-depth of the beam (L2) and was around 6 mm. Crack opening and slip vary along crack depth, and their relationship is variable and depends mainly on its inclination. When inclination is around 45 degrees, as in layers L2-L4, the relationship comes close to 1. If cracks are less than 45 degrees, a dominant crack opening prevails over crack slip. Another factor that influences this relationship is the location of the

This document is the intellectual property of the fib – International Federation for Structural Concrete. All rights reserved.
This PDF of fib Bulletin 95 is intended for use and/or distribution solely within fib National Member Groups.

crack on the beam. According to Figure 7d-f, the cracks placed approximately at the mid-shear span have a crack opening-slip relationship that comes close to 1.

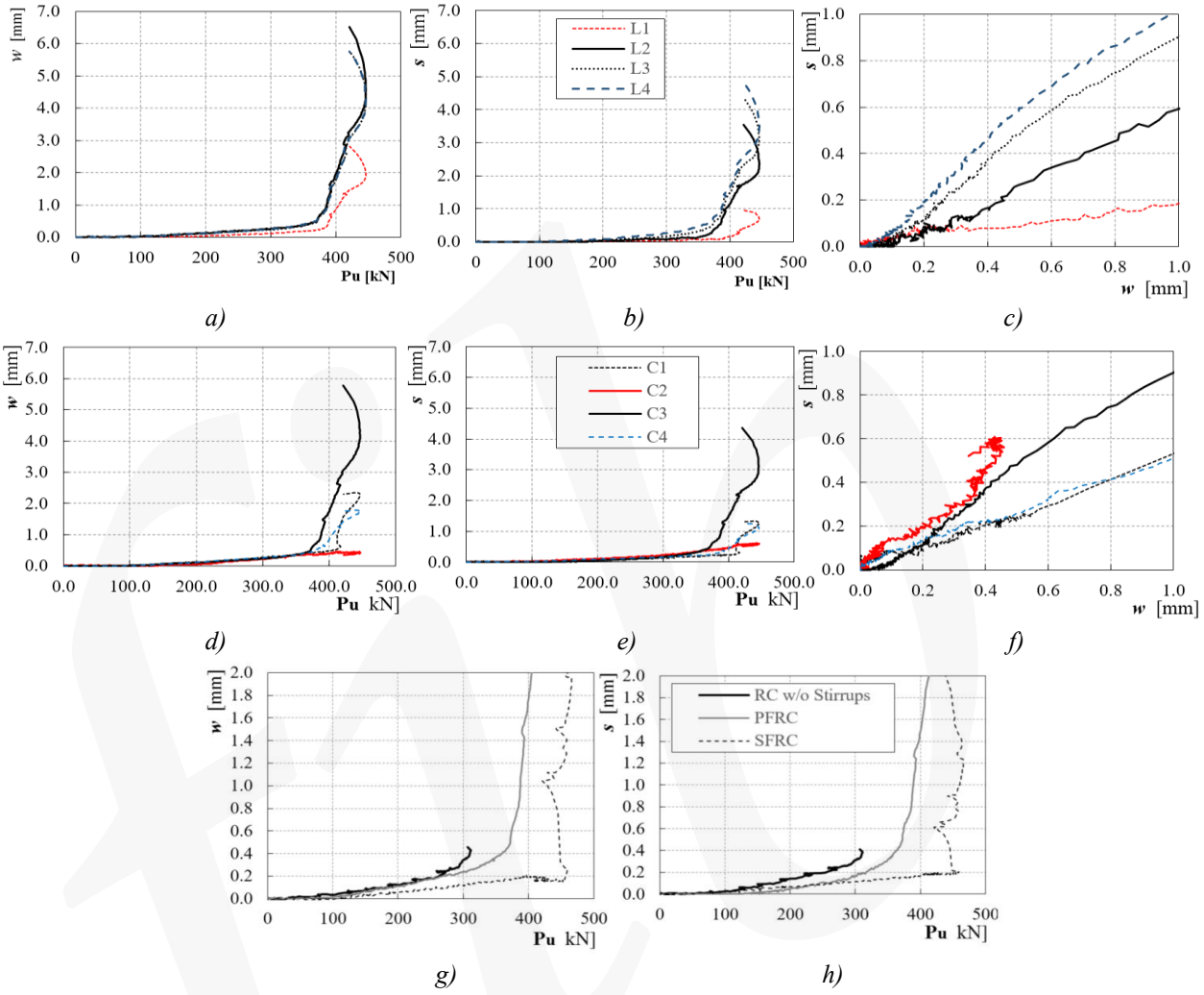


Figure 7: Crack opening and slip relationships

Finally, a comparison of the shear crack behaviour among PFRC, SFRC and PC was studied. To measure the equivalent cracks (similar crack inclination) in all the beam cases, the measured diagonal crack was located at a distance of two effective depths from the loading point on the same side of the beam and at the same depth (L3). As seen in Figure 7g, the crack openings of PFRC and PC behave similarly until 300kN, while the SFRC crack remains more closed. Moreover, similar slip trends between steel and polypropylene fibres are seen in Figure 7h, where the recorded slip for PFRC and SFRC is less at 300 kN compared to the PC cracks. This slip restriction clearly shows that fibres improve the shear transfer between crack faces and allows the aggregate interlock to act longer compared with PC beams.

This document is the intellectual property of the fib – International Federation for Structural Concrete. All rights reserved.
This PDF of fib Bulletin 95 is intended for use and/or distribution solely within fib National Member Groups.

4 Concluding remarks

In this study, shear tests were performed on PC, PFRC, SFRC and RC with stirrups. Based on the obtained results, the following conclusions can be drawn:

1. Macro-synthetic fibres added to beams with no transverse reinforcement achieved a similar response to reinforced concrete beams with transverse reinforcement, but did not change the mode of failure to a ductile one.
2. PFRC and SFRC beams presented more secondary cracks due to splitting along the flexural rebar than PC beams and were similar to RC beams. The bridging effect provided by fibres controlled secondary crack propagation, as stirrup does, and allowed the dowel action to continue acting as a shear transfer mechanism.
3. Macro-synthetic fibres improved shear deformation and provided nearly 8-fold more shear ductility than plain concrete.
4. Macro-synthetic fibres reduced the slip between crack faces, improved shear transfer, and allowed aggregate interlock to act longer compared to PC cracks.

5 Acknowledgements

Project “BIA2016-78460-C3-1-R” supported by the State Research Agency of Spain

6 References

ACI. (1996). *ACI 544.1R-96 State-of-the-Art Report on Fiber Reinforced Concrete*. Farmington Hills.

Bahia, R. N. S. and H. M. (1979). “Influence of Fiber Reinforcement on the Dowel Resistance to Shear.” *ACI Journal*, 76(2).

Bresler, B., and Scordelis, A. C. (1963). “Shear strength of reinforced concrete beams.” *Journal of the American Concrete Institute*, 60(1), 51–72.

Choi, K. K., Wight, J. K., and Park, H. G. (2007). “Shear strength of steel fiber-reinforced concrete beams without web reinforcement.” *ACI Structural Journal*, 104(1), 12–21.

Conforti, A., Minelli, F., and Plizzari, G. A. (2017). “Shear behaviour of prestressed double tees in self-compacting polypropylene fibre reinforced concrete.” *Engineering Structures*, Elsevier Ltd, 146, 93–104.

Dias-da-Costa, D., Valença, J., and Júlio, E. N. B. S. (2011). “Laboratorial test monitoring applying photogrammetric post-processing procedures to surface displacements.” *Measurement*, 44(3), 527–538.

Minelli, F., Conforti, A., Cuenca, E., and Plizzari, G. (2014). “Are steel fibres able to mitigate or eliminate size effect in shear?” *Materials and Structures*, 47(3), 459–473.

Navarro-Gregori, J., Mezquida-Alcaraz, E. J., Serna-Ros, P., and Echegaray-Oviedo, J. (2016). “Experimental study on the steel-fibre contribution to concrete shear behaviour.” *Construction and Building Materials*, Elsevier Ltd, 112, 100–111.

Vecchio, F. J., and Shim, W. (2004). “Experimental and Analytical Reexamination of Classic Concrete Beam Tests.” *Journal of Structural Engineering*, 130(3), 460–469.

Zarrinpour, M. R., and Chao, S.-H. (2017). “Shear Strength Enhancement Mechanisms of Steel Fiber-Reinforced Concrete Slender Beams.” *ACI Structural Journal*, 114(3), 729–742.

This document is the intellectual property of the fib – International Federation for Structural Concrete. All rights reserved.
This PDF of fib Bulletin 95 is intended for use and/or distribution solely within fib National Member Groups.
FRC2018: Fibre Reinforced Concrete: from Design to Structural Applications
Joint ACI-*fib*-RILEM International Workshop

Fibres as shear reinforcement in RC beams: an overview on assessment of material properties and design approaches

Joaquim A.O. Barros[1], Stephen J. Foster[2]

[1] : Full Prof., ISISE, University of Minho, Guimarães, Portugal.

[2] : Professor and Head, School of Civil and Environmental Engineering, UNSW Sydney.

Abstract

For the development of reliable physical-mechanical models for predicting the behaviour of fibre reinforced concrete structures at service and strength limit conditions, constitutive models simulating comprehensibly the governing phenomena must be used. In this context, simulating the post-cracking mechanisms of the fibres, and their symbiotic relationship with the cementitious matrix that surrounds them, is required for the development of realistic modelling approaches that accurately represent empirical observations. Several experimental test setups and inverse analysis procedures have been proposed to derive the fundamental stress-crack width (σ–w) law, but a consensus still does not exists on the best strategy for its determination. In structures governed by shear, fibre reinforcement increases the stiffness and shear stress transfer across a crack, but a methodology to capture the contribution of fibres in this regards is challenging. To overcome this, a clear strategy is needed in deriving relationships that simulate fibre reinforcement mechanisms in the mobilized fracture modes and, also, develop design approaches capable of capturing the relevant contributions of the fibres. This study firstly reviews current inverse analysis models used to describe the tensile (Model I fracture) relationship for FRC and, secondly, discusses a newly proposed model, referred to as the integrated shear model (ISM). The ISM is developed from mesoscale observations from gamma- and X-ray imaging on FRC elements under Modes I and II fracture conditions. The resulting model is compared to test data reported in the literature and a good correlation is observed.

Keywords

Shear capacity, Mode I fracture parameters, Inverse analysis, Analytical models.

This document is the intellectual property of the fib – International Federation for Structural Concrete. All rights reserved.
This PDF of fib Bulletin 95 is intended for use and/or distribution solely within fib National Member Groups.

1 Introduction

One of the most promising applications of fibre reinforcement for concrete structures is in one-way and punching shear. It is recognized that the post-cracking tensile capacity provided by fibre reinforcement in cement based materials (represented by the post-cracking stress versus crack opening relationship, σ-w) is the most relevant in terms of describing the behaviour at serviceability and strength limit states, as well as for durability and other design limit conditions. Several experimental test setups and inverse analysis procedures have been proposed to define the σ-w relationship; however, a consensus still does not exist on the best strategy for determining it. As current design models concentrate solely on specifying the post-cracking direct tensile strength, defined as Mode I fracture, inverse analysis procedures for the determination of the tensile response dominate the literature.

A methodology to capture the contribution of fibre reinforcement is challenging, and the lack of a good physical understanding may contribute to the reasons why fibre reinforcement is not being routinely specified by designers, despite the high potential evidenced by the available research. To overcome this, a clear strategy is needed in deriving the fundamental relationships that simulate fibre reinforcement mechanisms in the mobilized fracture modes and, also, in developing design approaches capable of capturing all relevant contributions of fibre reinforcement. As outlined above, current design model approaches concentrate on Mode I fracture in their determination of ultimate limit state conditions; however, slip along a crack dictates that Mode II mechanisms are relevant.

In this paper the concept of a physical-mechanical model, referred to as the integrated shear model (ISM), is described for determining the shear strength of beams where Mode II fracture is considered. By using the experimental results of steel fibre reinforced concrete (SFRC) beams failing in shear, collected in a database, the predictive performance of the ISM is assessed. The results are compared to *fib* Model Code 2010 (MC2010) model results for determining one-way shear capacity of beams.

2 Strategies for evaluating the post-cracking tensile capacity for design at the strength limit state

2.1 Experimentally-based approaches

2.1.1 Three-point notched prims bending test (3PNBT)

According to MC2010, the σ-w relationship to be used for simulating the post-cracking tensile capacity of FRC is determined from the residual flexural strength parameters, f_{Rj}, obtained by performing three point notched prism bending tests (3PNBT), where a force versus crack mouth opening displacement (CMOD) is registered. For an ultimate limit state (ULS) analysis, one of two models may be used: the rigid-plastic model of constant value of f_{Ftu} up to w_u; and the (ii) linear model defined by the following two pair of values: $w = 0$, $\sigma = f_{Fts}$; $w = w_u$,$\sigma = f_{Ftu}$, where w_u is the ultimate crack opening corresponding to the ULS criterion (for shear it is recommended that $w_u =$ 1.5 mm). For the rigid-plastic model, the ultimate residual tensile strength is determined from $f_{Ftu} = f_{R3}/3$, while for the linear model, the serviceability and ultimate residual tensile strengths are obtained from:

This document is the intellectual property of the fib – International Federation for Structural Concrete. All rights reserved.
This PDF of fib Bulletin 95 is intended for use and/or distribution solely within fib National Member Groups.

$$f_{Fts} = 0.45 \cdot f_{R1} \tag{1}$$

$$f_{Ftu} = f_{Fts} - \frac{w_u}{CMOD_3\,(=2.5mm)} \cdot \left(f_{Fts} - 0.5 \cdot f_{R3} + 0.2 \cdot f_{R1}\right) \geq 0 \tag{2}$$

According to several authors, this methodology to derive the σ–w relationship for a FRC (Salehian and Barros 2017, Lameiras *et al.* 2015, Amin *et al.* 2015) leads to unsafe predictions when compared to the results determined in direct tensile test (DTT). By cutting a notch in the specimen, the crack propagation is promoted through a section that may not be the one if this notch was not there. For the case where the notched plane is not aligned with the weakest one, for instance being crossed by a higher number of fibres (or more effectively arranged in terms of distribution and orientation) than of other weakest planes, the rotation process associated to the fracture propagation in a 3PNBT can promote the favourable snubbing fibre reinforcement mechanism (Lee and Foster 2007, Voo and Foster 2009), which contributes for the overestimation of the fracture performance of a FRC when evaluated from this test.

2.1.2 Direct tensile test (DTT)

The evaluation of the fracture parameters in strain softening FRC is performed in specimens where a notch is executed in an attempt of forcing just one surface where the fracture energy is consumed. The drawbacks pointed out to the 3PNBT are, therefore, also applicable to the DTT, although the detrimental effect of the curvature in the 3PNBT is not so significant in DTT. In an attempt to escape the detrimental effect of notches, some authors use dog-bone type specimen, since this configuration has a high probability of capturing the weakest fracture zone, despite the smallest width in the central transversal section of the specimen that favours the propagation of the fracture through this plane. To avoid this weakness, a dog-bone type configuration with a constant cross section in the central part of the specimen has also been used (Susetyo 2009, Deluce and Vecchio 2013, Pereira *et al.* 2012, Carnovale and Vecchio 2014), but fracture in the transition zone at the extremities of the central part of the specimen can occur. For determining the influence of fibre distribution and orientation some authors evaluate the fracture parameters in specimens extracted from relatively large elements, with cast conditions and volumetric parameters being as representative as possible of that in the real structure (Lameiras *et al.* 2015, Abrishambaf *et al.* 2013, Abrishambaf *et al.* 2016).

2.1.3 Double edge wedge splitting test (DEWST)

The double edge wedge splitting test (DEWST) was proposed by di Prisco *et al.* (2013) for the evaluation of the Mode I fracture properties of FRC. A pair of triangular grooves with a right angle, designated by "V-notch", is introduced transversally on the upper and lower faces of the specimen in its contact zones with the loading and supporting systems. The compressive force is applied through two steel bars laid into the V-notches.

2.1.4 Modified splitting tensile test (MSTT)

The prismatic geometric configuration of the DEWST is not the most appropriate for extracting specimens from bulk FRC when the effect of fibre distribution and orientation on the post-cracking tensile capacity of FRC is intended to be assessed. To address this, the modified splitting tensile test (MSTT) was proposed by Lameiras *et al.* (2015). The MSTT specimen has a circumferential geometric configuration and can be prepared by slicing

This document is the intellectual property of the fib – International Federation for Structural Concrete. All rights reserved.
This PDF of fib Bulletin 95 is intended for use and/or distribution solely within fib National Member Groups.

cylinder cores extracted from the bulk FRC (Alves *et al.* 2012, Barros *et al.* 2015). Besides the difference on the geometric configuration of the specimen, in the MSTT is introduced a pair of notches (one in each face of the specimen) in the loading plane in order to avoid the formation of cracks other than the one coinciding with the notched plane. However, the already reported detrimental effects in consequence of promoting the localization of the fracture surface are also applicable to the MSTT.

2.1.5 Round panel test (RPT)

The round panel test (RPT) described in ASTM C-1550 has a diameter (d_{RP}) of 800 mm, a thickness (h_{RP}) of 75 mm and a radius to the supports (S_{RP}) of 375mm. Since normally three cracks are formed in the panel test, at an approximate relative angle of 120 degrees between them, fibres of almost all possible orientations bridge the cracks. Thus, the influence of fibre orientation on the fibre reinforcement mechanisms is potentially well captured. Therefore, this type of test is suitable for FRC slabs and shells. For being easier of handling, round panels of smaller dimensions (d_{RP}=600 mm, h_{RP}=60 mm, S_{RP}=275mm) have been also proposed (Minelli and Plizzari 2011). From round RPT it is obtained the force versus central deflection (F-u_v), as well as the energy versus deflection (U-u_v), where U is the area behind the F-u_v.

2.2 Inverse analysis

The results from the 3PNBT are currently used to derive, by inverse analysis (IA), the Mode I fracture parameters of FRC, namely the stress at crack initiation, the Mode I fracture energy and the shape of the σ-w. The most common IA strategy is based on FEM, where 2D line interface finite elements (IFE) are located on the specimen's symmetry axis for modelling the fracture propagation. In the remaining parts of the specimen serendipity plane-stress finite elements (SPSFE) are generally used (Sena-Cruz *et al.* 2004). Instead of using IFE for modelling the fracture initiation and propagation, the column of material above the notch can be simulated by SPSFE with a smeared crack model by adopting a Gauss-Legendre integration scheme of 1×2 IP in order to force the propagation of the crack along the specimen symmetry axis, over the aligned integration points (Pereira *et al.* 2008). By adopting these IA strategies a tendency for overestimation the post-cracking tensile capacity is reported by several authors (Salehian and Barros 2017, Lameiras *et al.* 2015, Amin *et al.* 2015). In fact, in the IA it is assumed that the fracture propagation occurs along the notched plane, while in real tests the cracks are tortuous (higher fracture surface), and even micro- and meso-cracks generally form during the propagation of the macro-crack. Improved versions of the IA are being proposed by several researchers (Oliveira e Souza and Gettu 2006, Amin *et al.* 2015, Foster *et al.* 2017). In the strategy proposed by Foster *et al.* (2017), a σ–w relationship is derived, dependent of the f_{Rj}, but capable of reproducing the σ-w response in direct tensile tests:

$$\sigma(w) = k_G \min\left(0.4 f_{R2} + 1.2\left(f_{R4} - f_{R2}\right)\xi(w),\ f_{ctk,\min}\right) \tag{3}$$

$$\xi(w) = \alpha w - 0.25 \tag{4}$$

where for the prism bending test configuration of EN 14651 and RILEM TC 162-TDF $\alpha = 5/12$, for the configuration of ASTM C1609 $\alpha = 1/3$, and for the Italian Guideline $\alpha = 43/84$, $f_{ctk,\min}$ is the minimum characteristic tensile strength of the matrix (and may be taken as $f_{ctk,\min} = 0.7\left(0.3 f_{ck}^{2/3}\right)$) and k_G is a factor that takes into account fibre alignment due to

This document is the intellectual property of the fib – International Federation for Structural Concrete. All rights reserved.
This PDF of fib Bulletin 95 is intended for use and/or distribution solely within fib National Member Groups.

casting bias and wall influences that occur in the prism bending test, being equal to 0.7 for the ASTM 1609 test and 0.6 for the EN 14651, RILEM TC 162-TDF and UNI 11039 tests.

For slab and shell type FRC structures, the σ–w relationship can also be derived by using the results (F-u_v) of RPT described in section 2.1.5. By coupling a moment-rotation model described elsewhere (Barros *et al.* 2015), with an approach for predicting the F-u_v registered in these type of tests that takes into consideration the kinematic conditions of the parts of the panels rotating in turn of the formed cracks, Salehian *et al.* (2014) developed a strategy for deriving, by inverse analysis, the σ–w relationship that characterizes the post-cracking tensile capacity of the panel's FRC.

3 Approaches for modelling the shear capacity of RC beams

By performing push-off tests (Figure 1), Lee and Foster (2006a,b) demonstrated that the orientation of fibres crossing the faces of a crack has a decisive influence on the fibre pull-out constitutive law (FPCL), mainly when shear sliding is the main relative movement of the crack's faces. This influence is represented schematically in Figure 2, showing that fibres at more obtuse angle are first activated and fibres at more acute angles are the last to be activated.

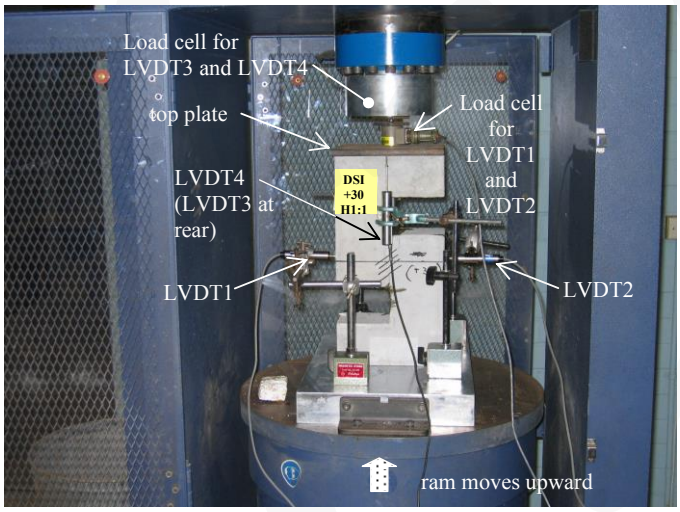


Figure 1: Push-off tests (Lee and Foster 2006a,b)

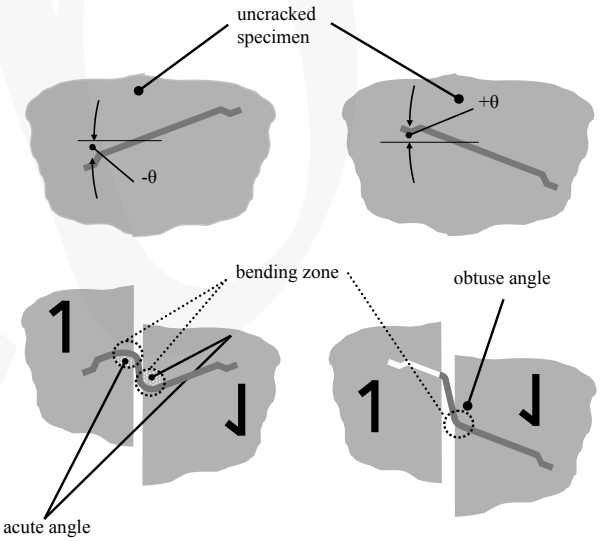


Figure 2: Schematic representation of fibre engagement (Lee and Foster 2006a)

From experimental tests, and supported by gamma-ray and X-ray imaging, Htut (2010) proposed that the crack opening displacement in the vertical direction (subscript "v") at the point where a fibre becomes engaged (i.e. carries significant force) is:

$$w_{ev} = \frac{1}{3.5} d_f \tan^3\left(\frac{\gamma_{u,i}}{\gamma_u^{\max}} \frac{\pi}{2}\right) \tag{5}$$

$$\gamma_{u,i} = \left|\bar{\varphi}_i - \phi_u\right| \quad \text{for} \quad 0 \le \gamma_{u,i} \le \pi \tag{6}$$

This document is the intellectual property of the fib – International Federation for Structural Concrete. All rights reserved.
This PDF of fib Bulletin 95 is intended for use and/or distribution solely within fib National Member Groups.

$$\gamma_u^{\max} = |\phi_u| + \pi/2 \quad \text{for} \quad \pi/2 \le \gamma_u^{\max} \le \pi \tag{7}$$

where d_f if the fibre diameter, $\gamma_{u,i}$ is the angle between fibre orientation representative of the interval "i" and the loading direction, $\bar{\varphi}_i$ represents the fibre orientation of the ith interval (towards the normal to the critical diagonal crack, CDC, plane, taken as positive in the clockwise direction), and ϕ_u is the orientation of loading towards the orthogonal to the crack (Figure 3). In the formulation the subscripts u and i indicate the evaluation is performed at shear failure stage and for the fibres of the ith interval in the fibre orientation profile (FOP). The fibres of a generic i^{th} interval are only activated if the vertical crack opening of the CDC, determined by the modified compression field theory (MCFT), w_{uv}, is higher than w_{ev}.

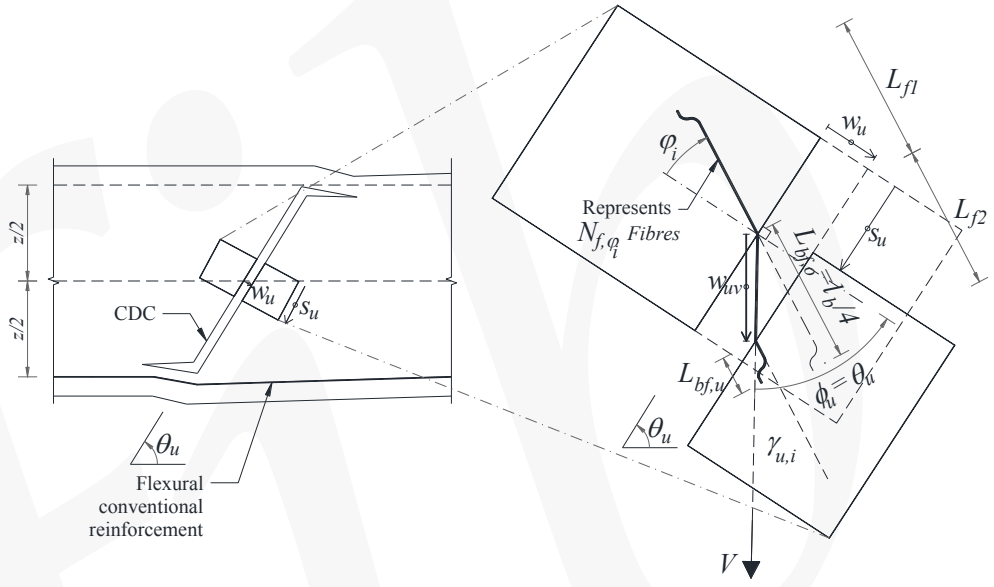


Figure 3: Kinematics of fibre pull-out according to the UVEM

By integrating and coupling in the same approach: i) a FOP for determining the number of fibres crossing the shear crack in discrete intervals of fibre orientation (following the approach proposed by Oliveira, 2010); ii) the fibre pull-out constitutive law (FPCL) determined according to the unified variable engagement model (UVEM); iii) and the MCFT for the evaluation of the crack width at the shear failure stage (w_u) (Bentz *et al.* 2006), Barros and Foster (2018) proposed an Integrated Shear Model (ISM) for predicting the shear capacity of reinforced concrete SFRC beams (R/SFRC). According to the UVEM, the FPCL at crack displacement corresponding to shear failure stage ($w = w_u$) is obtained from:

$$P_{\bar{\varphi}_i}^{FPCL}\left[w_{uv}(w_u)\right] = k_{u,i}\pi d_f \tau_{bu,i} L_{bf,o} \tag{8a}$$

$$k_{u,i} = \begin{cases} 0 & \text{... for } \begin{cases} w_{uv} < w_{ev,i} \\ w_{uv} \ge L_{bf,o} \\ L_{bf,o} - w_{uv} \ge L_{cru,i} \end{cases} \\ \dfrac{2\left(L_{bf,o} - w_{uv}\right)}{l_f} & \text{... for } w_{ev,i} \le w_{uv} < L_{bf,o} \end{cases} \tag{8b}$$

This document is the intellectual property of the fib – International Federation for Structural Concrete. All rights reserved.
This PDF of fib Bulletin 95 is intended for use and/or distribution solely within fib National Member Groups.

In this equation l_f is the fibre length, $L_{bf,o}$ is the average bonded length of fibres crossing the failure plane on the short embedment side (Figure 3), considered equal to $l_f/4$ according to Wang (1989), and the critical fibre embedment length, above which fibre fails in tensile rupture is:

$$L_{cru,i} = \frac{d_f}{2}\frac{\bar{\sigma}_{fu}}{\tau_{bu,i}} \tag{9}$$

$$\bar{\sigma}_{fu} = \sigma_{fu}\frac{\pi}{2\gamma_u^{\max}} \tag{10}$$

where $\bar{\sigma}_{fu}$ is the fibre's effective tensile strength and σ_{fu} is its uniaxial tensile strength. The average fibre bond strength is given by:

$$\tau_{bu,i} = k_b\sqrt{f_{cm}} + f\left[1-\cos\left(\frac{\gamma_{u,i}}{2}\right)\right] \tag{11}$$

where $f = 4.5$ MPa is the maximum frictional resistance of the fibre due to the snubbing effect, and k_b is a bond coefficient dependent on type of steel fibre, with values available elsewhere (Ng. *et al.* 2012).

The concrete and fibre reinforcement contribution for the shear capacity of an R/SFRC beam is determined from:

$$V_{Rd,F} = k_f\left(V_{Rd,c} + V_{Rd,f}\right) \tag{12}$$

where:

$$V_{Rd,c} = \frac{k_p k_v}{\gamma_F}\sqrt{f_{ck}}\,z b_w \text{ with } \sqrt{f_{ck}} \le 8MPa \tag{13}$$

$$V_{Rd,f} = \frac{F_{fuk}\left[w_{uv}\left(w_u\right)\right]}{\gamma_F} \tag{14}$$

where $F_{fuk}\left[w_{uv}\left(w_u\right)\right]$ is evaluated considering the FOP, the FPCL representative of each domain adopted for the FOP, and the corresponding number of fibres crossing the CDC:

$$F_{fuk}\left[w_{uv}\left(w_u\right)\right] = \sum_{i=1}^{n\Delta\varphi} P_{fuk,\varphi_i}\left[w_{uv}\left(w_u\right)\right] \tag{15}$$

where $n\Delta\varphi$ is the number of intervals in the fibre orientation range [0-90°] adopted for the evaluation of the FOP, and $P_{fuk,\varphi_i}\left[w_{uv}\left(w_u\right)\right] = P_{\varphi_i}^{FPCL}\left[w_{uv}\left(w_u\right)\right]N_{f,\varphi_i}$ is the force supported by the number fibres with an inclination φ_i (N_{f,φ_i}), obtained for a crack opening representative of the shear failure condition, w_u, where φ_i is the angle between the direction of the fibres representative of the ith fibre orientation interval and the orthogonal to the crack plane.

In Eq. (12) k_f is a parameter that simulates the contribution of the flanges of T- and I-section beams to the shear capacity of R/SFRC beams (Barros and Foster 2018). In Eq. (13), z=0.9d is

This document is the intellectual property of the fib – International Federation for Structural Concrete. All rights reserved.
This PDF of fib Bulletin 95 is intended for use and/or distribution solely within fib National Member Groups.

the effective shear depth (d is the internal arm of the flexural reinforcement), k_p is a parameter that simulates the favourable effect of prestress in terms of extra shear capacity (Barros and Foster 2018), k_v is a size effect parameter determined according to the recommendations of the MCFT (Bentz *et al.* 2006), and γ_F is a safety factor. Testing the ISM using a database of 122 reinforced SFRC beams, a predictive performance better than the MC2010 approaches was obtained (Figure 4). In all analyses unit values were used for the safety factors, and average values were used for the material properties.

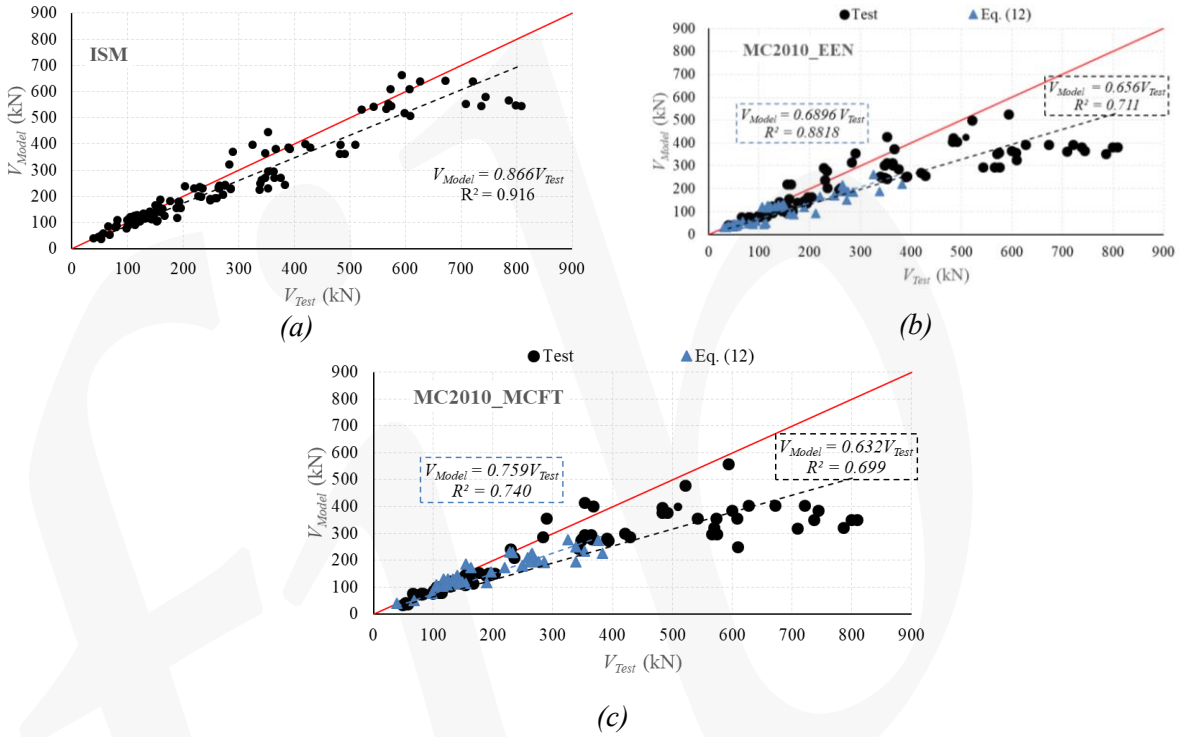


Figure 4: Models performance: (a) ISM; (b) MC2010_EEN; (c) MC2010_MCFT

The MC2010_EEN model indicated in Fig. 6b is based on:

$$V_{Rd,F} = \left\{ \frac{0.18}{\gamma_c} k \left[100\rho_{eq} \left(1 + 7.5 \frac{f_{Ftuk}}{f_{ctk}} \right) f_{ck} \right]^{1/3} + 0.15\sigma_{cp} \right\} b_w d_{eq} \tag{16}$$

The MC2010_MCFT approach indicated in Fig. 6c represents the MC2010 model based on the MCFT:

$$V_{Rd,F} = \frac{1}{\gamma_F} \left(k_v \sqrt{f_{ck}} + k_f f_{Ftuk}(w_u) \cot\theta \right) z b_w \qquad \text{with } \sqrt{f_{ck}} \le 8MPa \tag{17}$$

where $f_{Ftuk}(w_u)$ is obtained from Eq. (3). The details of these two MC2010 formulations are available elsewhere (MC2010, 2013).

The one-way shear models are evaluated and their performance compared. The average and test-to-model prediction ratio (λ) and coefficient of variation (CoV) for the ISM approach was 1.12 and 16.6%, respectively, whereas for the MC2010_EEN and MC2010_MCFT models the averages and CoV were 1.32 and 23.4% and 1.32 and 24.2%, respectively.

This document is the intellectual property of the fib – International Federation for Structural Concrete. All rights reserved.
This PDF of fib Bulletin 95 is intended for use and/or distribution solely within fib National Member Groups.

4 Concluding remarks

This paper reports on the different tests used for determining Mode I fracture properties of FRC, and in their application to design models for the determination of shear strength of beams. Shear in reinforced concrete beams, however, involves both sliding and opening displacements and consideration of Mode I fracture alone does not allow for all relevant contributions to behaviour in shear to be considered. A new model for shear is outlined, the integrated shear model (ISM), that has its basis in experimental observations on Model II fracture, including observations from gamma- and X-ray imaging that allow for fibre behaviour during pull-out to be fully observed and considered. The results show that the analytical model performs well when compared with the test data and better than existing approaches.

5 Acknowledgements

The authors wish to acknowledge the grant SFRH/BSAB/114302/2016 provided by FCT and the Australian Research Council grant DP150104107, as well as the support provided by the UNSW for the research activities carried out under the status of Visiting Professorial Fellow for the first author. The support of the FCT through the project PTDC/ECM-EST/2635/2014 is also acknowledged.

6 References

Abrishambaf, A.; Cunha, V.; Barros, J.A.O., "The influence of fibre orientation on the post-cracking tensile behaviour of steel fibre reinforced self-compacting concrete", Fracture and Structural Integrity Journal, Volume 31, 1, 38-53, January 2016.

Abrishambaf, A.; Barros, J.A.O.; Cunha, V.M.C.F, "Relation between fibre distribution and post-cracking behaviour in steel fibre reinforced self-compacting concrete panels", Cement & Concrete Research, 51, 57-66, 2013.

Alves, N.; Barros, J.A.O.; Nunes, Â; Lourenço, L.A.P., "Steel fibre reinforced self-compacting concrete for grid foundations of single-family houses", 8th RILEM International Symposium on Fibre Reinforced Concrete: challenges and opportunities, Eds: Joaquim Barros et al., 12pp., 19-21 September 2012.

Amin, A.; Foster, S.J.; Muttoni, A., "Derivation of the σ-w relationship for SFRC from prism bending tests", Structural Concrete, 16(1), 93-105, 2015.

ASTM C1550-05, Standard Test method for Flexural Toughness of Fiber Reinforced Concrete (Using Centrally Loaded Round Panel). West Conshohocken, PA, USA: ASTM International; 2005.

ASTM 1609/C1609-12, "Standard test method for flexural performance of fiber-reinforced concrete (using beam with third-point loading)", ASTM, 9 pages, 2012

Barros, J.A.O.; Foster, S., "An integrated approach for predicting the shear capacity of fibre reinforced concrete beams", in appreciation for eventual publication in an ISI Journal, January 2018.

Barros, J.A.O.; Taheri, M.; Salehian, H., "A model to simulate the moment-rotation and crack width of FRC members reinforced with longitudinal bars", Engineering Structures, 100, 43-56, October 2015.

Bentz EC, Vecchio FJ, Collins MP. Simplified modified compression field theory for calculating shear strength of reinforced concrete elements. ACI Structural Journal, 103:614–624, 2006.

Carnovale, D.; Vecchio, F.J., "Effect of fiber material and loading history on shear behavior of fiber-reinforced concrete", ACI Structural Journal, 111(5), 1235-1244, 2014.

Deluce, J.R.; Vecchio, F.J., "Cracking behaviour of steel fibre reinforced concrete members containing conventional reinforcement", ACI Structural Journal, 110(3), 481-490, 2013.

This document is the intellectual property of the fib – International Federation for Structural Concrete. All rights reserved.
This PDF of fib Bulletin 95 is intended for use and/or distribution solely within fib National Member Groups.

di Prisco M., Ferrara L., Lamperti M.L., "Double edge wedge splitting (DEWS): an indirect tension test to identify post-cracking behaviour of fibre reinforced cementitious composites", Materials and Structures 46 (11):1893-1918, 2013.

EN 14651. Test method for metallic fibre concrete-measuring the flexural tensile strength (limit of proportionality (LOP), residual). European Committee for Standardization; 2007: p. 17.

Foster, S.J.; Agarwal, A; Amin, A., "Design of SFRC Beams for Shear using Inverse Analysis for Determination of Residual Tensile Strength", Structural Concrete [DOI: 10.1002/suco.201700100], 2017.

Htut TNS. Fracture processes in steel fibre reinforced concrete. PhD dissertation. School of Civil and Environmental Engineering, The University of New South Wales, UNSW Sydney, Australia; 2010.

Lameiras, R.M.; Barros, J.A.O., Azenha, M.A.D., "Influence of casting condition on the anisotropy of the fracture properties of Steel Fibre Reinforced Self-Compacting Concrete (SFRSCC)", Cement and Concrete Composites, 59, 60-76, May 2015.

Lee GG, Foster SJ. Behaviour of steel fibre reinforced mortar in shear II: Gamma ray imaging. UNICIV Report No. R-445. The University of New South Wales, UNSW Sydney, Australia; 2006b.

Lee GG, Foster SJ. Behaviour of steel fibre reinforced mortar in shear I: Direct shear testing. UNICIV Report No. R-444. The University of New South Wales, UNSW Sydney, Australia; 2006a.

Minelli F, Plizzari GA. A new round panel test for the characterization of fiber reinforced concrete: a broad experimental study. ASTM J Test Eval 2011; 39(5):889–97 [ISSN:1945-7553].

Model Code 2010. fib Model Code for Concrete Structures 2010. International Federation for Structural Concrete (fib). Ernst & Sohn, Berlin, Germany; 2013.

Oliveira FL. Design-oriented constitutive model for steel fiber reinforced concrete. PhD dissertation. Department of Project and Construction Engineering, UPC, Catalonia, Spain; 2010.

Pereira, E.N.B.; Fischer, G.; Barros, J.A.O., "Direct assessment of tensile stress-crack opening behavior of Strain Hardening Cementitious Composites (SHCC)", Cement and concrete Research, 42, 834-846, 2012.

Pereira, E.B.; Barros, J.A.O., Camões, A.F.F.L., "Steel fiber reinforced self-compacting concrete – experimental research and numerical simulation", ASCE Struct. Eng. Journal, 134(8), 1310-1321, August 2008.

Salehian, H.; Barros, J.A.O., "Prediction of the load carrying capacity of elevated steel fibre reinforced concrete slabs", Composite Structures Journal, 170, 169-191, 2017.

Salehian, H.; Barros, J.A.O.; Taheri, M., "Evaluation of the Influence of Post-Cracking Response of Steel Fibre Reinforced Concrete (SFRC) on Load Carrying Capacity of SFRC Panels", Construction and Building Materials Journal, 73, 289-304, December 2014.

Sena-Cruz, J.M.; Barros, J.A.O.; Ribeiro, A.F.; Azevedo, A.F.M.; Camões, A.F.F.L., "Stress-crack opening relationship of enhanced performance concrete", 9th Portuguese Conference on Fracture, ESTSetúbal, Portugal, p. 395-403, 18-20 February 2004.

Susetyo, J., "Fibre reinforcement for shrinkage crack control in prestressed, precast segmental bridges", PhD thesis, University of Toronto, Canada, 2009.

UNI 11039. Steel Fiber Reinforced Concrete—Part I: Definitions, Classification Specification and Conformity—Part II: Test Method for Measuring First Crack Strength and Ductility Indexes. Italian Board for Standardization: Rome, Italy; 2003.

Voo, Y.L.; Foster, S., "Reactive powder concrete analysis and design of RPC girders", Lambert Academic Publishing, 2009.

Wang, Y., "Mechanics of fiber reinforced cementitious composites", Ph.D. Thesis, MIT, May 1989.

This document is the intellectual property of the fib – International Federation for Structural Concrete. All rights reserved.
This PDF of fib Bulletin 95 is intended for use and/or distribution solely within fib National Member Groups.
FRC2018: Fibre Reinforced Concrete: from Design to Structural Applications
Joint ACI-*fib*-RILEM International Workshop

Experimental investigation of shear-critical prestressed steel fibre reinforced concrete beams

Maure De Smedt[1], Kristof De Wilder[1], Dimitrios Anastasopoulos[2], Edwin Reynders[2], Guido De Roeck[2], Lucie Vandewalle[1]

[1] : Building Materials and Building Technology Section, Department of Civil Engineering, KU Leuven, Belgium

[2] : Structural Mechanics Section, Department of Civil Engineering, KU Leuven, Belgium

Abstract

This paper presents the experimental results of prestressed steel fibre reinforced concrete (SFRC) beams and it compares analytical model predictions with these results. Six beams were subjected to a force-controlled four-point bending test until failure. The three investigated parameters were the fibre dosage, the amount of prestressing force and the presence of shear reinforcement. During the test, failure mode and load, as well as deformations, displacements and cracking pattern properties were observed by means of conventional measurement devices and advanced optical techniques, including Bragg grated optical fibres and digital image correlation technique. Additionally, material properties were determined according to standardized European tests. The experimental results were compared to analytical predictions according to shear design equations in Model Code 2010. For the six beams, an average experimental-to-predicted failure load ratio of 1.43 was found with a coefficient of variation of 7.2%. Furthermore, four other analytical models for shear design of SFRC are investigated, namely DRAMIX Guideline, RILEM TC 162-TDF sigma-epsilon method, CNR-DT 204/2006 model and a model proposed by Soetens. All models underestimate the shear capacity of prestressed SFRC beams. The underestimation increases for a higher prestress level, whereas the correlation with the fibre dosage varies within the models.

Keywords

Shear, prestressed steel fibre reinforced concrete, experimental mechanics, analytical models, advanced optical measurement techniques

This document is the intellectual property of the fib – International Federation for Structural Concrete. All rights reserved.
This PDF of fib Bulletin 95 is intended for use and/or distribution solely within fib National Member Groups.

1 Introduction

Since the first studies of reinforcing concrete with fibres in the 1960s [1,2], steel fibre reinforced concrete (SFRC) has been optimized and numerous experiments have been performed to describe and investigate the material's behavior. The advantages such as an improved ductility, a higher energy absorption capacity and an increased flexural strength are generally accepted nowadays [3-5]. It is currently established that adding steel fibres to the concrete mixture can have a beneficial effect on the overall structural response in both the ultimate limit state (ULS) and the serviceability limit state (SLS). However, determining the actual contribution of the steel fibres to the overall structural capacity still remains open for discussion.

Previous research has mainly been focused on the flexural behavior of SFRC [6-10], although the very brittle shear failure mode could specifically benefit from the enhanced post-cracking behavior provided by the steel fibres. An overview of 52 experimental investigations of the shear behavior and capacity in the last 50 years can be found in [12]. Most of them confirm the effectiveness of steel fibres as shear reinforcement and the improvement of the overall ductility and a better crack growth control. Moreover, the shear behavior of SFRC beams without additional shear reinforcement is reported to be similar to or even better than beams with solely shear reinforcement. However, a drawback of most experiments is that the size of the specimens is relatively small with respect to structural concrete elements in building industry.

Another benefit of the application of SFRC is the possible economic interest because of its cost- and time-effectiveness, especially in precast industry. SFRC can be cost- and time-effective by (partially) replacing the conventional (shear) reinforcement, which requires a lot of time and manual labor. Since most of the precast structural elements are pretensioned, it is profitable to investigate prestressed SFRC elements. Moreover, a prestressing force has a positive influence on the overall shear capacity [11]. From the 52 experimental investigations [12], only 10 of them are performed with (partially) prestressed SFRC beams.

Due to the complex behavior of both shear and SFRC, and the many interrelated parameters, analytical and numerical modelling of shear in SFRC beams remains unclear [13]. This is the main reason for the lack of international building codes for the shear behavior of SFRC. As a consequence, the use of SFRC is still limited with respect to its potentials. Some considerable steps forward in the utilization of SFRC are taken by developing Model Code 2010 [14] and other analytical models [23-26], although each of them have their advantages and disadvantages in correctly estimating the shear capacity of prestressed SFRC elements.

This paper reports an experimental research of the shear behavior and capacity of prestressed SFRC beams with a length of 7 m. It aims to contribute to the overall understanding of shear in structural SFRC elements and to investigate existing analytical design models. In the first section, the experimental program is elaborated, with specific attention to the experimental setup and the use of advanced optical measurement methods (i.e. stereo-vision digital image correlation and Bragg grated optical fibres). Secondly, the results are presented and the influence of the parameters is discussed. The experimental results are compared to analytical predictions according to existing design codes and some results of the advanced optical techniques are presented.

This document is the intellectual property of the fib – International Federation for Structural Concrete. All rights reserved.
This PDF of fib Bulletin 95 is intended for use and/or distribution solely within fib National Member Groups.

2 Experimental program

2.1 Specimen geometry and material properties

The experimental program contains six I-shaped beams with a constant height, made by the local precast manufacturer Ergon nv, Belgium. Table 1 gives an overview of the main characteristics and the denotation of the beams (numbered from B401 to B406). Each beam has a length of 7000 mm, a height of 630 mm, an effective depth of 557 mm, a flange width of 240 mm and a web width of 70 mm. Figure 1 shows the cross section of the specimens. All specimens are prestressed with 7-wire low-relaxation strands (nominal diameter of 12.5 mm): seven at the bottom and one at the top of the beams. The stress value in the strands σ_{p0} is equal to 1488 MPa for B401, B402 and B403 (initial prestrain of $7.5 \cdot 10^{-3}$ mm/mm), and equal to 750 MPa for B404, B405 and B406 (initial prestrain of $3.8 \cdot 10^{-3}$ mm/mm). Although reducing stress levels below the allowable is unconventional in industry, it is applied to investigate the influence of the prestressing force on the shear capacity with a constant longitudinal reinforcement ratio (ρ_l equals 0.0167). In four of the six beams, the conventional shear reinforcement is replaced by steel fibres (Dramix RC-80/30-CP, length 30 mm, diameter 0.38 mm, and tensile strength 3070 MPa). These fibres are added to the fresh concrete mixture in different dosages, namely 20 kg/m³ (B402 and B405) or 40 kg/m³ (B403 and B406). Two beams without steel fibres (B401 and B404) have conventional shear reinforcement (single-legged stirrups with nominal diameter 6 mm, centre-to-centre distance 150 mm and ρ_w equal to $2.693 \cdot 10^{-3}$). Both ends of the beams are provided with splitting reinforcement over 200 mm (nominal diameter 8 mm and centre-to-centre distance 50 mm) in order to withstand the gradual growth of the prestressing force over the height and the length.

Table 1: Overview of experimental program and investigated parameters.

	$\rho_w = 2.693 \cdot 10^{-3}$ $V_f = 0$ kg/m³	$\rho_w = 0$ $V_f = 20$ kg/m³	$\rho_w = 0$ $V_f = 40$ kg/m³
$\sigma_{p0} = 1488$ MPa	B401	B402	B403
$\sigma_{p0} = 750$ MPa	B404	B405	B406

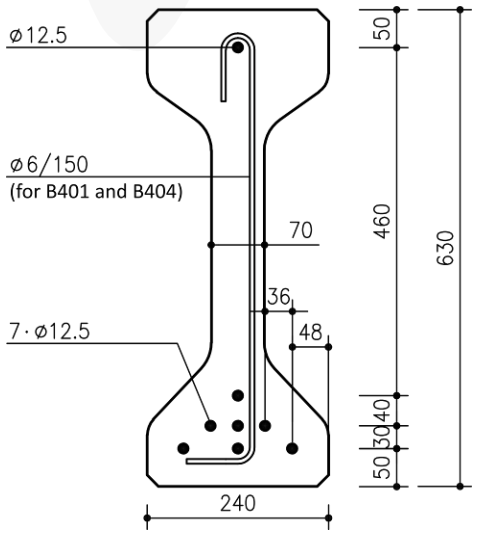


Figure 1: Cross section (and shear reinforcement layout for B401, B404), with units in mm.

This document is the intellectual property of the fib – International Federation for Structural Concrete. All rights reserved.
This PDF of fib Bulletin 95 is intended for use and/or distribution solely within fib National Member Groups.

Depending on the amount of steel fibres, three different concrete mixtures are used [12]. All mixtures are designed to have a characteristic cylindrical compressive strength f_{ck} of 50 MPa (concrete class C50/60). The mean cylindrical compressive strength was measured on 17 cylinders according to the European Standard EN 12390-3 [15] and equaled 74.3 MPa with a standard deviation of 6.7 MPa. Other hardened material properties are determined as well, the results can be found in [12]. Furthermore, the CMOD (crack mouth opening displacement) – stress curves of the SFRC mixtures are measured [16] (presented in Figure 2). The concrete mixture with 20 kg/m³ steel fibres shows a softening behavior and the mixture with 40 kg/m³ a hardening behavior, under bending loads. According to the classification system for the post-cracking strength of SFRC in the Model Code 2010 [14], the first mixture is classified as 1e (B402) and 2c (B405), and the second mixture as 7b (both B403 and B406).

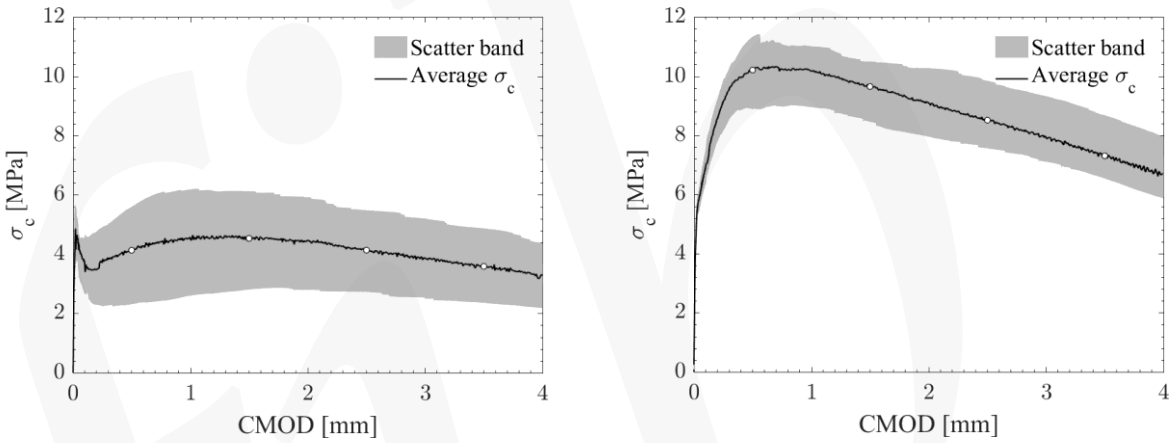


Figure 2: CMOD - σ curves for the beams with steel fibres: (a) 20 kg/m³ of steel fibres (B402, B405); (b) 40 kg/m³ of steel fibres (B403, B406).

2.2 Test setup and adopted measurement techniques

The six beams are subjected to a force-controlled four-point bending test, performed by a hydraulic press (Instron, maximum capacity 2.5 MN). Figure 3 and Figure 4 present the experimental setup. The distance between the supporting points equals 5000 mm, resulting in a shear span of 2200 mm and a shear span-to-effective depth ratio of 3.95, designed to obtain shear failure. A progressive damage loading scheme is followed, with a loading rate of 0.25 kN/s and an unloading rate of 0.25 kN/s (first cycle) or 1.0 kN/s (second cycle).

During testing, several techniques are used to measure the deformations, displacements, cracking pattern, failure load and failure mode. The load and displacement of the press are recorded and the displacements at the supports and at midspan are continuously measured by LVDTs and an optical photoelectric sensor (OPT) respectively. Furthermore, the advanced optical measurement techniques of stereo-vision Digital Image Correlation (DIC) and Bragg grated optical fibres (OPTFIB, FBG) are used as well. Two DIC systems are applied to all beams to analyse the full-field displacement and deformation field of two indicated areas of interest (refer to Figure 3). This contactless measurement method takes images of the undeformed and deformed state of the defined area (covered with a black and white speckle pattern as shown in Figure 4(a,b)), and it calculates the displacement by correlating these

This document is the intellectual property of the fib – International Federation for Structural Concrete. All rights reserved.
This PDF of fib Bulletin 95 is intended for use and/or distribution solely within fib National Member Groups.

images. More details can be found in literature [12,17-19]. The optical fibres engraved with 14 FBG sensors are used on beam B403 (top flange) and B404 (top and bottom flange) to accurately monitor the horizontal strains in the flanges. It relies on the analysis of the wavelength spectrum which is reflected by the Bragg gratings. If a change in length of the fibre occurs, a shift in the reflected wavelength is induced (positive shift is an elongation). The fibres are mechanically fixed into brass anchoring blocks glued on the concrete surface, refer to Figure 4(c). More details can be found in literature [12,19-22].

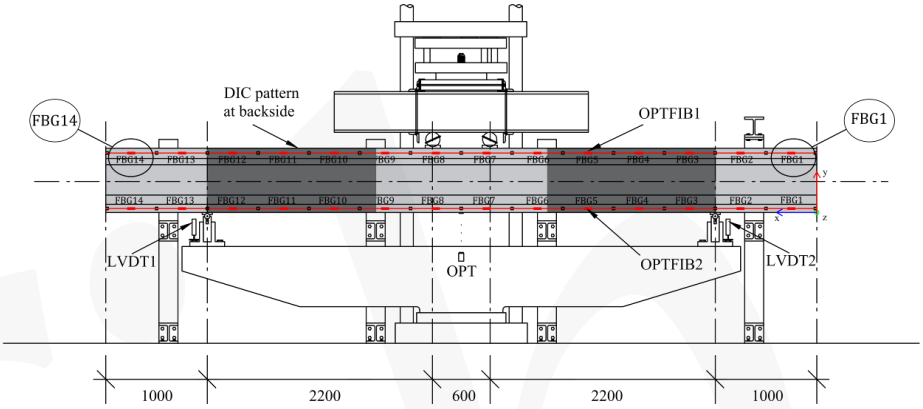


Figure 3: Schematic representation of the experimental setup with indication of measurement methods LVDT, OPT, DIC (at backside), OPTFIB and Bragg gratings FBG.



(a) (b) (c)

Figure 4: Details of the experimental setup: (a) Setup with DIC pattern; (b) Camera setup for DIC; (c) Optical fibre.

3 Results and discussion

3.1 Structural behavior and influence of parameters

Table 2 and Figure 5 present the experimentally observed failure modes and loads. All six beams failed in a shear failure mode due to diagonal tension (S-DT), as designed. Inclined web cracking causes yielding and rupture of the shear reinforcement for B401 and B404, and the steel fibres are pulled out of the concrete matrix in case of B402, B403, B405 and B406. No fibre rupture was observed. Figure 6(a) shows the corresponding load-displacement curves at the location of the loading point. It clearly shows the post-cracking behavior of all specimens, even for B402 which is highly prestressed with a relatively low fibre dosage. During the progressive damage scheme, the stiffness of each beam decreases due to the developing web shear cracks.

This document is the intellectual property of the fib – International Federation for Structural Concrete. All rights reserved.
This PDF of fib Bulletin 95 is intended for use and/or distribution solely within fib National Member Groups.

Furthermore, the influence of the main parameters can be distinguished. An increased fibre dosage for beams with a constant prestressing force and without shear reinforcement (comparing B402 to B405 and B403 to B406) leads to a larger post-cracking behavior and multiple cracks at failure; a less brittle failure due to a redistribution of the internal forces and a gradual energy dissipation; and an increased shear capacity. Furthermore, beams without steel fibres but with shear reinforcement (B401 and B404) have the largest post-cracking behavior but the shortest elastic region and crack load; and one major crack and very brittle failure occurs. Replacing the used amount of shear reinforcement by 40 kg/m³ of steel fibres results in a similar shear capacity for the tested specimens.

A decreased prestressing force while remaining the longitudinal reinforcement ratio constant (comparing B404 to B401, B405 to B402 and B406 to B403) leads to a limited elastic region and a decreased first crack load; the occurrence of bending cracks at first (refer to Section 3.3 and Figure 8); an increased inclination of the shear cracks from 20° to 30° with the horizontal axis; a lower amount of released energy and a less brittle failure; and a decreased shear capacity but an unchanged deflection at midspan. Furthermore, smaller crack widths at the moment of failure are observed due to the decreased failure load (refer to section 3.3 and Figure 7).

Table 2: Experimental failure modes and loads, compared to analytical predictions using EC2 and MC2010. S-DT denotes shear crack mode due to diagonal tension.

Specimen	σ_{p0} [MPa]	V_f [kg/m³]	Failure mode	$V_{u,exp}$ [kN]	$V_{u,pred}$ [kN]	$V_{u,exp}$ / $V_{u,pred}$
B401	1488	0	S-DT	256.4	174.3	1.47
B402	1488	20	S-DT	218.5	148.2	1.47
B403	1488	40	S-DT	254.4	161.3	1.58
B404	750	0	S-DT	202.5	146.8	1.38
B405	750	20	S-DT	164.1	129.0	1.27
B406	750	40	S-DT	197.4	137.6	1.43

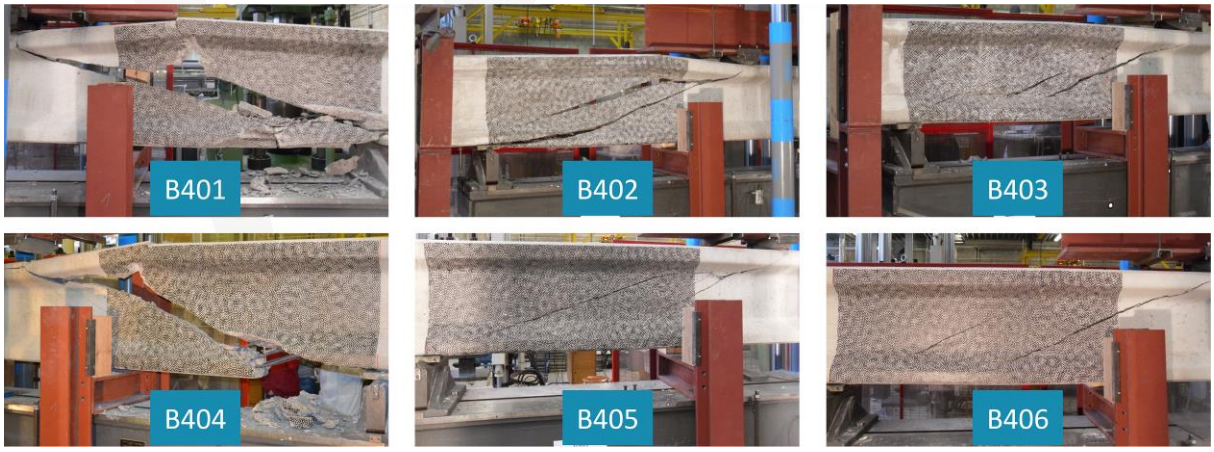
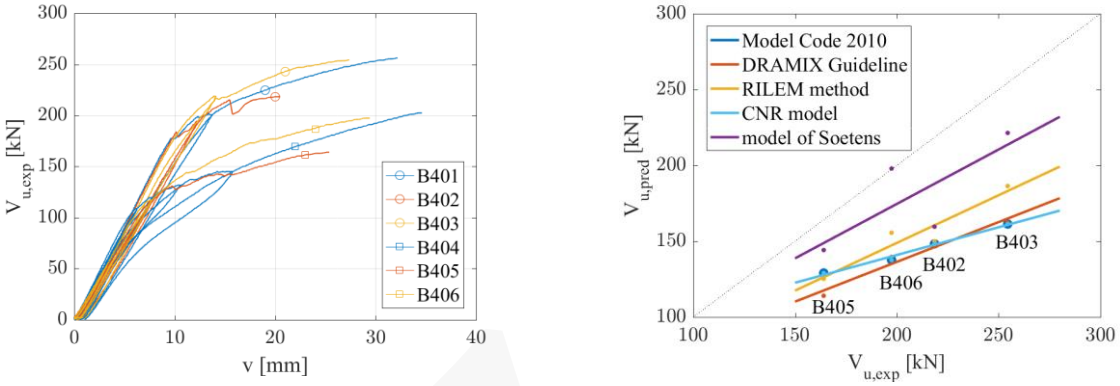


Figure 5: Experimentally observed shear failure modes of the six beams.

This document is the intellectual property of the fib – International Federation for Structural Concrete. All rights reserved.
This PDF of fib Bulletin 95 is intended for use and/or distribution solely within fib National Member Groups.



(a) (b)

Figure 6: Results of the four-point bending tests of the six beams: (a) Load-displacement curves as experimentally observed at location of the loading point; (b) Comparison of failure loads and analytical predictions of the shear capacity of SFRC beams.

3.2 Analytical models of the shear capacity

The experimentally observed failure loads of the beams ($V_{u,exp}$) are compared to analytical predictions ($V_{u,pred}$), based on different models and by omitting safety factors and using the measured average material properties. Eurocode 2 (EC2, [23]) is used for B401 and B404, and Model Code 2010 (MC2010, [14]) for B402, B403, B405 and B406 since EC2 does not provide design rules for SFRC beams. The predictions and the ratio $V_{u,exp}$ / $V_{u,pred}$ are shown in Table 2. The predicted failure loads are an underestimation of the experimentally observed ones, for all the beams. The mean experimental-to-predicted failure ratio equals 1.43 with a coefficient of variation of 7.2%. Therefore, the design procedures of EC2 and MC2010 result in safer failure loads, even if safety factors are omitted and average material properties instead of design values are used. Additionally, EC2 calculations only account for the shear capacity of the reinforcement and neglect the concrete contribution to the shear capacity. However, the concrete contribution will increase by an increasing prestressing force [11]. This influence is solely taken into account in the determination of the angle between the concrete compression strut and the horizontal axis (cot θ), although cot θ is limited to 3, leading to the higher experimental-to-predicted ratio of B401 compared to B404.

Furthermore, the shear capacity of the prestressed SFRC beams is also predicted using other analytical models for SFRC, i.e. the DRAMIX Guideline [24], the RILEM Method [25], the CNR model [26], and the model proposed by Soetens [27]. The results in Figure 6(b) show an underestimation of the predicted shear capacities for all the SFRC beams in all the models, similarly to EC2 and MC2010. The experimental-to-predicted ratio varies between 1.00 (model of Soetens for B406) and 1.58 (MC2010 for B403). Therefore, the design values of the shear capacity will be even safer and could be too conservative, leading to expensive designs. Besides, the CNR model is identical to MC2010, since both are based on the research of Minelli [28-29]. The model of Soetens is the most divergent by its lowest $V_{u,exp}$ / $V_{u,pred}$ ratio (1.16), but the highest coefficient of variation (13.2%) leading to a higher model uncertainty. The DRAMIX Guideline is a rather outdated method as it includes the fibre properties instead of the post-cracking behavior (by the mean ultimate residual tensile strength for SFRC based on the residual flexural tensile strengths as shown in Figure 2).

This document is the intellectual property of the fib – International Federation for Structural Concrete. All rights reserved.
This PDF of fib Bulletin 95 is intended for use and/or distribution solely within fib National Member Groups.

Lastly, the experimental-to-predicted ratio of all models increases for a higher prestressing force (comparing B401 to B404, B402 to B405, and B403 to B406). Therefore, the influence of the prestressing force is not completely correctly estimated in the different models, especially for higher prestressing values. The contribution of the steel fibres in the different models remains more discordant. For MC2010, the experimental-to-predicted ratio increases for an increased fibre dosage. However, the effect is reversed for the RILEM method and the model of Soetens. Depending on the model, the influence of a higher steel fibre dosage is better estimated and vice versa for other models. As a final point, not only the experimentally observed failure loads, but also the different analytical predictions show that the shear capacities of beams with shear reinforcement and beams with 40 kg/m³ steel fibres are comparable (B401 to B403, B404 to B406). It can be concluded that replacing the amount of shear reinforcement $\rho_w = 2.693 \cdot 10^{-3}$ by 40 kg/m³ of steel fibres results in a similar shear capacity for the specimens tested in this research.

3.3 Results of DIC and FBG measurements

In this section, two examples of possible results obtained by DIC and FBG measurements are presented. Firstly, smaller crack widths at the moment of failure are observed for a decreased prestressing force, since the failure load is decreased as well. The crack widths can be measured during the loading procedure using the DIC results. Figure 7 shows the location of virtual extensometers over the length of the main crack and the obtained dimensionless load-crack width relation. For B402 (high prestressing force), the crack width increases rapidly right before failure and opens 5 to 6 mm. For B405 (low prestressing force), the crack width enlarges more gradually and opens 3 to 4 mm.

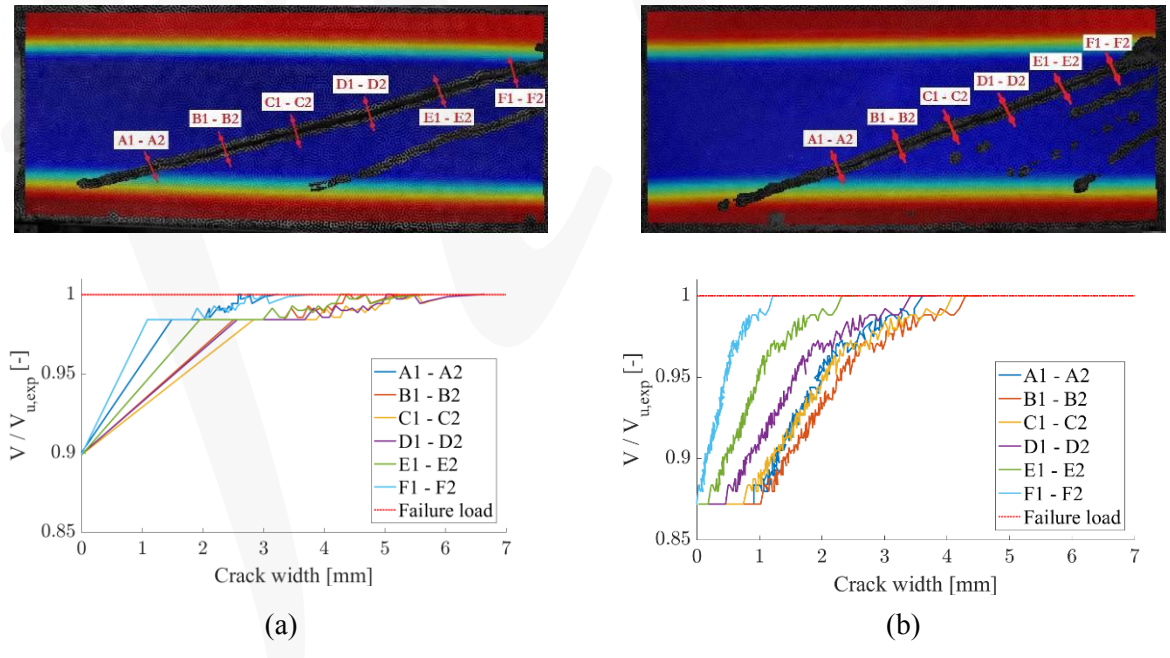
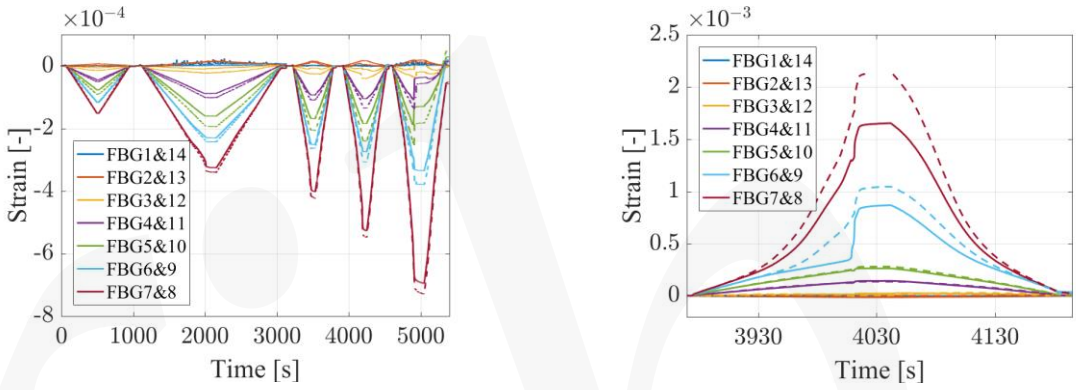


Figure 7: Crack widths (bottom) measured by virtual extensometers (top) in DIC method: (a) B402, $V_{u,exp}$ = 218.5 kN; (b) B405, $V_{u,exp}$ = 164.1 kN.

Secondly, a decreased prestressing force leads to the occurrence of bending cracks before shear cracks. For B404, these vertical cracks at the bottom of the beam's midspan are

This document is the intellectual property of the fib – International Federation for Structural Concrete. All rights reserved.
This PDF of fib Bulletin 95 is intended for use and/or distribution solely within fib National Member Groups.

measured by the FBGs. Figure 8 shows the symmetrical horizontal strain data along the 14 FBGs (FBG numbering according to Figure 3): (a) negative strains (shortening) of the top flange due to compression during five cycles of the progressive damage loading scheme; and (b) positive strains (elongation) of the bottom flange due to tension during the fourth loading cycle. The first cracks appear in the beam's midspan at FBG7&8 and FBG6&9 (Figure 8(b)). The lower compression force of the non-fully prestressed strands causes the tensile stresses to exceed the tensile strength sooner, leading to the bending cracks. The largest cracks develop in the shear-critical area right before failure (FBG5&10 and FBG4&11, Figure 8(a)).



(a) (b).

Figure 8: Horizontal strain data from FBGs on beam B404. FBGs are placed symmetrical with FBG1&14 at the beam's ends and FBG7&8 at the middle: (a) Top flange during progressive loading; (b) Bottom flange during fourth loading cycle.

4 Conclusions

This paper presented the results of six I-shaped prestressed steel fibre reinforced concrete beams subjected to a four-point bending test until failure. The three investigated parameters were the amount of prestressing, the amount of shear reinforcement and the fibre dosage. Besides traditional mechanical measurement systems, stereo-vision digital image correlation and Bragg grated optical fibres were used, leading to more detailed results on crack widths and horizontal strains respectively. The experimental failure loads were compared to analytical predictions according to shear design equations in Eurocode 2 and Model Code 2010. For the six beams, an average experimental-to-predicted failure load ratio of 1.43 was found with a coefficient of variation of 7.2%. Furthermore, four other analytical models for shear design of SFRC are investigated, namely DRAMIX Guideline, RILEM TC 162-TDF sigma-epsilon method, CNR-DT 204/2006 model and a model proposed by Soetens. It is concluded that all models underestimate the shear capacity of prestressed SFRC beams. The underestimation increases for a higher prestress level, whereas the correlation with the fibre dosage varies within the models.

5 Acknowledgements

The Authors would like to give their appreciation to Ergon nv for supplying the precast pretensioned SFRC beams. They also wish to express their gratitude to the Research Foundation Flanders (FWO) under Research Project G099014N.

This document is the intellectual property of the fib – International Federation for Structural Concrete. All rights reserved.
This PDF of fib Bulletin 95 is intended for use and/or distribution solely within fib National Member Groups.

6 References

[1] Romualdi, J.P. and Batson, G.B. (1963). *Mechanics of crack arrest in concrete*. ASCE Engineering Mechanics Journal, 89(3):147-168.
[2] Romualdi, J.P. and Mandel, J.A. (1964). *Tensile strength of concrete affected by uniformily distributed closely spaced short lengths of wire reinforcement*. ACI journal, 61(6):657-671.
[3] di Prisco, M., Plizarri, G. and Vandewalle, L. (2009). *Fibre reinforced concrete: new design perspectives*. Materials and Structures, 42(9):1261-1281.
[4] Lee, M.K. and Barr, B.I.G. (2004). *An overview of the fatigue behaviour of plain and fibre reinforced concrete*. Cement and Concrete Composites, 26(4):299-305.
[5] Parvez, A. and Foster, S.J. (2015). *Fatigue behaviour of steel-fiber-reinforced concrete beams*. ASCE Structural Engineering Journal 141(4).
[6] Lim, T.Y., Paramasivam, P. and Lee, S.L. (1987). *Bending Behavior of Steel-Fiber Concrete Beams*. ACI Structural Journal, 84(6):524-536.
[7] Qian, C.X. and Patnaikuni, I. (1999). *Properties of high-strength steel fiber-reinforced concrete beams in bending*. Cement & Concrete Composites, 21(1):73-81.
[8] Lappa, E.S., et al. (2006). *Bending performance of high strength steel fibre reinforced concrete - Static and fatigue loading conditions*. Measuring, Monitoring and Modeling Concrete Properties, 133-138.
[9] Bywalski, C. and Kaminski, M. (2011). *Estimation of the bending stiffness of rectangular reinforced concrete beams made of steel fibre reinforced concrete*. Archives of Civil and Mechanical Engineering, 11(3):553-571.
[10] van Zijl, G.P.A.G. and Mbewe, P.B.K. (2012). *Towards a Design Model for Steel Fiber Reinforced Concrete in Bending*. High Performance Fiber Reinforced Cement Composites 6(2):221-229.
[11] De Wilder, K., et al. (2015). *Experimental investigation on the shear capacity of prestressed concrete beams using digital image correlation*. Engineering Structures, 82(1):89-92.
[12] De Smedt, M. (2016). *Experimental and analytical analysis of the shear capacity of prestressed steel fibre reinforced concrete beams*. Master thesis, KU Leuven, Belgium.
[13] Hwang, J.H., et al. (2013). *Shear Behavior Models of Steel Fiber Reinforced Concrete Beams Modifying Softened Truss Model Approaches*. Materials, 6(10):4847-4867.
[14] Fédération International du Béton *fib* (2012). *Model Code for Concrete Structures 2010*.
[15] CEN (2009). *NBN EN 12390-3: Testing hardened concrete part 3: Compressive strength of test specimens*.
[16] CEN (2014). *EN 14651: Test method for metallic fiber concrete – measuring the flexural tensile strength (limit of proportionality (LOP), residual)*.
[17] Lava, P., et al. (2009). *Assessment of measuring errors in DIC using deformation fields generated by plastic FEA*. Optics and Lasers in Engineering, 47(7-8):747-753.
[18] Lava, P., et al. (2010). *Study of systematic errors in strain fields obtained via DIC using heterogeneous deformation generated by plastic FEA*. Optics and Lasers in Engineering, 48(4):457-468.
[19] De Wilder, K., et al. (2016). *Experimental analysis of the mechanical behaviour of shear-deficient pretensioned steel-fibre reinforced concrete beams*. In BEFIB 2016 – 9th RILEM International Symposium in Fiber Reinforced concrete, Vancouver, Canada.

This document is the intellectual property of the fib – International Federation for Structural Concrete. All rights reserved.
This PDF of fib Bulletin 95 is intended for use and/or distribution solely within fib National Member Groups.

[20] Othonos, A. and Kalli, K. (1999). *Fiber Bragg Gratings: Fundamentals and Applications in Telecommunications and Sensing*. Norwood, MA, USA: Artec House.
[21] Luyckx, G., et al. (2011). *Strain Measurements of Composite Laminates with Embedded Fibre Bragg Gratings: Criticism and Opportunities for Research*. Sensors, 11(1):384-408.
[22] Anastasopoulos, D., et al. (2018). *Damage identification using modal strains identified from operational fiber-optic Bragg grating data*. Structural Health Monitoring, 17(6):1441-1459.
[23] CEN (2005). *EN 1992-1-1: Eurocode 2: Design of Concrete Structures – Part 1-1.*
[24] Technical Committee of Bekaert nv (1995). *DRAMIX Guideline: Design of concrete structures – steel wire fibre reinforced concrete structures with or without ordinary reinforcement.*
[25] Vandewalle, L., et al. (2000). *RILEM TC162-TDF: Test and design methods for steel fibre reinforced concrete – Design of steel fibre reinforced concrete using the σ-ε-method*. Materials and Structures, 33(226):75-81.
[26] CNR (2007). *Guide for the design and construction of fiber-reinforced concrete structures.*
[27] Soetens, T. (2015). *Design models for the shear strength of prestressed precast steel fiber reinforced concrete girders*. PhD thesis, UGent, Belgium.
[28] Minelli, F. and Plizzari, G.A. (2013). *On the effectiveness of steel fibers as shear reinforcement.* ACI Structural Journal, 110(3):379-389.
[29] Conforti, A. and Minelli, F. (2016). *Compression field modelling of fibre reinforced concrete shear critical deep beams: a numerical study.* Materials and Structures, 49(8):3369-3383.

This document is the intellectual property of the fib – International Federation for Structural Concrete. All rights reserved.
This PDF of fib Bulletin 95 is intended for use and/or distribution solely within fib National Member Groups.

3) BRIDGES/ELEVATED SLABS/PRECAST ELEMENTS/TUNNEL LININGS

This document is the intellectual property of the fib – International Federation for Structural Concrete. All rights reserved.
This PDF of fib Bulletin 95 is intended for use and/or distribution solely within fib National Member Groups.
FRC2018: Fibre Reinforced Concrete: from Design to Structural Applications
Joint ACI-*fib*-RILEM International Workshop

Segmental Lining Design using Macro Synthetic Fibre Reinforcement

Ralf Winterberg[1], Luis Mey Rodríguez[2], Rolando Justa Cámara[3], David Sualdea Abad[4]

[1] BarChip Inc., Japan (formerly: Elasto Plastic Concrete, Singapore)

[2] Ingemey Consultores, Madrid, Spain.

[3] Acciona Infraestructuras SA, Madrid, Spain.

[4] Keller Cimentaciones, S.L.U., Madrid, Spain (formerly: Acciona Infraestructuras SA)

Abstract

Fibre reinforced concrete (FRC) is becoming widely utilized in segmental linings due to the improved mechanical performance, robustness and durability of the segments. Further, significant cost savings can be achieved in segment production and by reduced repair rates during temporary loading conditions. The replacement of traditional rebar cages with fibres further allows changing a crack control governed design to a purely structural design with more freedom in detailing.

Macro synthetic fibres (MSF) are non-corrosive and thus ideal for segmental linings in critical environments. Although fibre reinforcement for segments is relatively new, recent publications such as the ITAtech "Guidance for precast FRC segments – Volume 1: Design aspects" or the British PAS 8810 "Tunnel design – Design of concrete segmental tunnel linings – Code of practice" have now given more credibility to this reinforcement type and the basis for design.

This paper presents and discusses the design methodology for precast tunnel segments and in particular the tasks associated with the use of MSF reinforcement. Temporary loadings as well as long term load behaviour will be addressed. A case history from the Santoña–Laredo General Interceptor Collector, currently under construction in northern Spain, will illustrate the specific benefits of MSF reinforcement for segmental linings.

Keywords

Macro synthetic fibre, fibre reinforced concrete, segmental lining, TBM, segment design

This document is the intellectual property of the fib – International Federation for Structural Concrete. All rights reserved.
This PDF of fib Bulletin 95 is intended for use and/or distribution solely within fib National Member Groups.

1 Introduction

Wide use of structural fibres in initial (temporary) and final (permanent) linings worldwide has shown the importance of fibres in underground construction, with growing interest among the designers, engineers and the referring authorities. Over the last 20 years, fibre reinforced concrete (FRC) segmental tunnel linings have been adopted in numerous projects around the world. A comprehensive overview of these projects is given in the ITA WG2 report (2016).

Structural fibres can replace or reduce ordinary rebar cages, acting as the primary structural reinforcement. Significant cost savings are often achieved by the use of fibres; mainly by the partial or entire replacement of ordinary reinforcement in the production, but also by improving the robustness, serviceability and durability and hence, reducing maintenance costs.

Macro synthetic fibre reinforced shotcrete (MSFRS) has reached maturity as an engineered material and is widely used in all forms of sprayed tunnel linings, for temporary as well as permanent ground support in both, mining and civil tunnel applications (Nitschke and Winterberg, 2016).

The application in precast tunnel segments is relatively new. However, MSF has distinct advantages over steel reinforcements, e.g. non-corrosive and doesn't suffer from matrix embrittlement and the inherent performance loss with age (Bernard, 2014). Further, continuous research and development yields high performing fibres that meet the particular specifications of the tunnel projects. Executed references can be found in ITAtech report no. 7 (2016).

Replacing the steel rebar cages of tunnel segments with non-corrosive fibre reinforcement not only yields an excellent durability. Moreover, the fibres near the surface reinforce the otherwise vulnerable concrete cover and provide crack control and impact resistance, minimising repair and reject rates and in turn the project costs.

The replacement of traditional rebar cages with macro synthetic fibres further allows changing a crack control governed design for durability (SLS) to a purely structural ULS design with more freedom in detailing and potential cost savings.

Although the use of MSF reinforcement for tunnel segments is relatively new, recent publications such as the ITAtech report no. 7 (2016) or the British PAS 8810 (2016) have now given more credibility to this reinforcement type and the basis for the design.

2 Segmental lining design

2.1 Introduction

There are currently no particular design standards or guidelines for macro synthetic fibre reinforced concrete (MSFRC). The regular design methodologies for steel fibre reinforced concrete (SFRC) apply. Macro synthetic fibre can be used when the project specifications and performance criteria are met: "if concrete reinforced with this fibrous synthetic reinforcement exhibits adequate post-cracking residual strengths then it can be considered suitable for structural purposes as well as SFRC" (ITA WG2, 2015).

This document is the intellectual property of the fib – International Federation for Structural Concrete. All rights reserved.
This PDF of fib Bulletin 95 is intended for use and/or distribution solely within fib National Member Groups.

In the past, the absence of global standards for steel fibres hasn't come in the way of their acceptance and use in various applications. Continuous developments and successfully completed projects show that the same currently applies to high performance synthetic fibres.

2.2 Fibre reinforced concrete segments

The design of FRC is based on its tensile performance, i.e. the crack-bridging capacity provided by the fibres. Experimental tests are carried out to determine the tensile characteristics. The post-cracking behaviour of fibre reinforced concrete can be determined indirectly on bending beams with displacement-controlled machines. The Model Code 2010 (2012) is today the internationally most recognized standard for the design of FRC. The post-crack performance characterisation follows the European harmonized standard EN 14651 (2005).

The segment designs typically aim at largely compressed sections with little to moderate bending moments. Additional reinforcement may be only required for temporary load cases, typically for TBM propulsion, in the form of bursting ladders at joints.

Large tunnels or tunnels in soft grounds might still require traditional steel reinforcement due to high bending moments in temporary or permanent condition. In these cases hybrid reinforcement, i.e. a combination of fibre and cage, is often the most durable and cost-efficient solution due to the partial replacement of rebar by fibres (Plizzari and Cominoli, 2005).

2.3 Ring segmentation

To better accomplish a fibre only solution, smaller segments should be adopted in order to limit the segments' aspect ratio, i.e. the ratio of developed length over thickness (see Figure 1). A larger number of smaller segments reduces the stiffness of the ring and in turn the acting bending moments on the segments. Further, the risk of damage during handling and temporary load conditions is minimized.

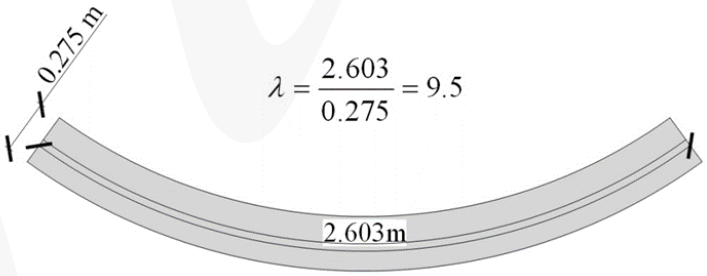


Figure 1: Definition of the segment aspect ratio

The experience of several executed FRC tunnels suggests that an aspect ratio not exceeding a value of 10 safely permits the use of FRC only (ITAtech 2016). However, other parameters such as the tunnel diameter, overburden and the ground conditions also must likewise allow replacing rebars with fibres, verified by the structural design.

2.4 SLS design

Segments reinforced with traditional steel rebar cages require tight serviceability limits in order to protect the steel reinforcement from corrosion. Crack width control in SLS is often

This document is the intellectual property of the fib – International Federation for Structural Concrete. All rights reserved.
This PDF of fib Bulletin 95 is intended for use and/or distribution solely within fib National Member Groups.

provided by heavy conventional reinforcement, which has no or little structural function. Fibre reinforcement has proven to be very effective in crack control and at the same time providing higher durability than traditional rebar reinforcement. Thus, the replacement of steel rebar by fibre, where structurally possible, not only yields economic benefits but also creates significant freedom in design and detailing. FRC without conventional reinforcement is able to limit the developing crack width where load-redistribution is possible as given in statically indeterminate elements (rotation capacity), such as tunnel segments under axial thrust (DBV 2001).

Recent research has shown that the addition of high performance macro synthetic fibres to steel rebar reinforced concrete reduces crack width and crack spacing by 30% in bending of simply supported beams (Bernard, 2018). Thus, MSF can add a significant gain of design life to steel reinforced concrete structures, such as hybrid reinforced segments.

2.5 ULS design

A typical design approach for FRC segmental linings is the use of Moment-Normal Force interaction diagrams or Moment-Thrust Capacity Limit Curves (Nitschke and Winterberg, 2016). The factored design load couples acting on the section must remain within the N–M envelope.

The FRC material properties are herein derived from the beam tests, which are eventually used as the basis to determine the stress-strain relationship of the concrete on the tension side. The idealized stress-strain diagram enables setting up the capacity limit curves, which are obtained by equilibrium iterations on a given cross-section.

3 The Santoña–Laredo Project

3.1 Project introduction

The Santoña–Laredo General Interceptor Collector is a 1.5 km subsea tunnel currently under construction in northern Spain. The tunnel is part of the Santoña Marshlands Sanitation Project. It is constructed with a 4.30 m Mixshield TBM across the Santoña bay using macro synthetic fibre reinforced concrete segments. The review of the manufacturing process and especially of the design of the tunnel segments led to the decision to replace conventional rebar cages with macro synthetic fibre (see Winterberg et al., 2018 for a detailed overview on this project).

3.2 Segmental lining design

Apart from the potential cost savings in the production, the review of the design of the tunnel segments to meet the aggressive marine environment led to the decision to replace the conventional rebar cage with BarChip macro synthetic fibre.

To better accommodate the fibre reinforced concrete solution, smaller segments were adopted in order to limit the segments' aspect ratio. The tunnel has an internal diameter of 3.50 m with a segment thickness of 250 mm. The segmentation was selected to be "5+1", with three rectangular segments, two counter keys and a half size key stone (Figure 2). This yields a segment aspect ratio of 8.6 which is below the before mentioned limit of 10.

This document is the intellectual property of the fib – International Federation for Structural Concrete. All rights reserved.
This PDF of fib Bulletin 95 is intended for use and/or distribution solely within fib National Member Groups.

The structural design of the FRC segments, employing a concrete class C45/55, is based on the Spanish EHE-08 (2008) and the fib Model Code 2010 (fib 2012). The FRC has to comply with two ductility criteria, following Annex 18 of EHE-08:

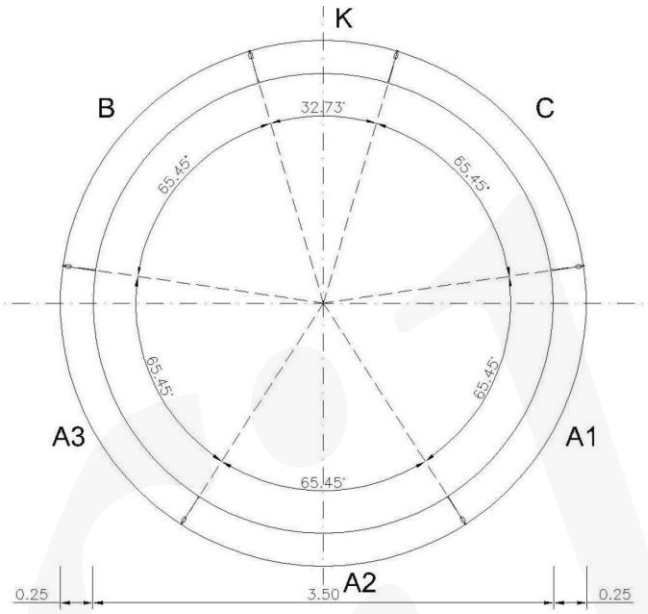


Figure 2: Ring segmentation

- $f_{R1k} \geq 0.4\, f_{ctk,fl}$ and
- $f_{R3k} \geq 0.2\, f_{ctk,fl}$

where the flexural performance is determined according to the European harmonised testing standard EN 14651. This means minimum ductility requirements at different displacements, retaining min. 40% of the flexural strength (cracking stress) as a residual performance in SLS (0.5 mm Crack Mouth Opening Displacement) and minimum 20% in ULS (2.5 mm CMOD).

The following characteristic flexural values have been adopted for the design of the segments using the N–M interaction diagram:

$$f_{ctk,fl} = 3.60 \text{ MPa},\ f_{R1k} = 1.50 \text{ MPa} \text{ and } f_{R3k} = 1.50 \text{ MPa}$$

Testing trials were conducted at the laboratory of the Polytechnic University of Catalunya (UPC) in Barcelona, Spain, in order to corroborate these values. The chosen dose rate of 5.0 kg/m^3 of BarChip48 exceeded the specified residual design values. Apart from the standard beam tests within the frame of these trials, parallel testing was executed employing the Double Punching Test or "Barcelona Test" (UNE 83515, 2010). This test methodology uses smaller specimens and reduces the efforts related to quality control as compared to beam testing. A correlation of $R^2 = 0.9$ was attained between the two test methods so that the frequency of the complex beam tests could be reduced.

3.2.1 Design for permanent conditions

The structural analysis for permanent conditions due to geostatic loading was carried out for seven critical chainages, where the particular ground conditions were expected to yield the critical load combinations. The conditions comprise *min./max. overburden*, *max. water pressure* and *combinations thereof*.

In a slurry shield drive, assuming normal operating conditions of the machine, deformations of the terrain, which determine the loads on the ring, depend on several factors that can be summarized in:

(a) Deformation ahead of the front;

(b) Radial deformation around the shield;

(c) Radial deformation in the tail of the shield;

This document is the intellectual property of the fib – International Federation for Structural Concrete. All rights reserved.
This PDF of fib Bulletin 95 is intended for use and/or distribution solely within fib National Member Groups.

(d) Pressure adjustment of pore and drainage in the long run.

These analyses have been carried out using FLAC3D finite element analysis (FEA).

Using the Muir-Wood formula to determine the ring stiffness and an experimentally based model to determine the strength development of the injection mortar for an assumed advance rate of eight rings per day, the ruling load combinations as N–M couples acting on the segmental lining have been found. The structural design for ULS uses N–M capacity envelopes. These axial force–bending moment interaction diagrams are a common tool for the design of final linings (Nitschke and Winterberg 2016).

The FRC material properties are given as the earlier mentioned characteristic flexural values, which have been corroborated by the experimental test results. These flexural values are the basis for the stress-strain relationship of the concrete on the tension side using a simplified stress block, which was determined to $f_{Ftuk} = f_{R3k}/3 = 0.50$ MPa according to MC2010 (fib 2012). Further, a partial material safety factor of 1.5 was applied to determine the final tensile design value of $f_{tud} = 0.33$ MPa out to a maximum strain of 2% (CMOD3). The idealized stress-strain diagram enables setting up the capacity limit curves, which are obtained by equilibrium iterations on a given cross-section.

Figure 3 shows the factored design load couples plotted into the N–M capacity envelope. The design is adequate for the chosen C45/55 concrete class and 5.0 kg/m^3 of BarChip48 fibre as the primary reinforcement. The ring is well under axial compression due to the governing normal forces. Very moderate bending moment is acting on the ring so that tensile stresses are minimised. This shows that the ring detailing has been well designed to accommodate a fibre only solution for the given permanent load conditions. The N–M interaction diagram further shows remarkable provisions in load bearing capacity given by the fibre reinforced concrete section.

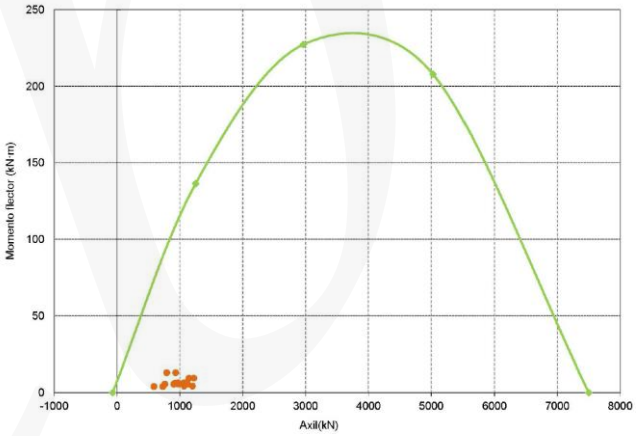


Figure 3: N–M capacity envelope for the FRC section and factored design load couples

The radial joints, i.e. the joints between the segments of a ring, have been checked against maximum compressive stress and bursting. Ground settlement was found to be minimal so that birdsmouthing due to ring ovalisation has not been considered here. Further, guiding rods in the radial joints ensure that the segments are connected with minimal offset, which in turn could produce additional eccentricity and stresses. The compressive design capacity of 5.37 MN/m of the section exceeds by far the maximum acting load, which is 1.22 MN/m. The bursting stresses were checked with FLAC3D and remained with 0.89 MPa well below the design tensile capacity of the plain concrete which is 1.77 MPa. Thus, no additional reinforcement was required.

This document is the intellectual property of the fib – International Federation for Structural Concrete. All rights reserved.
This PDF of fib Bulletin 95 is intended for use and/or distribution solely within fib National Member Groups.

3.2.2 Design for temporary conditions

Loads resulting from handling of the segments, i.e. demoulding, turning and stacking have also been checked against the design tensile strength of plain concrete at the referring ages. The post crack performance given by the fibre reinforcement has not been taken into account here and linear analysis was carried out. This is to avoid any cracking of the segments at the temporary loading stages. To simplify the FEA model, the ring joint was modelled as the developed segment length (Figure 4).

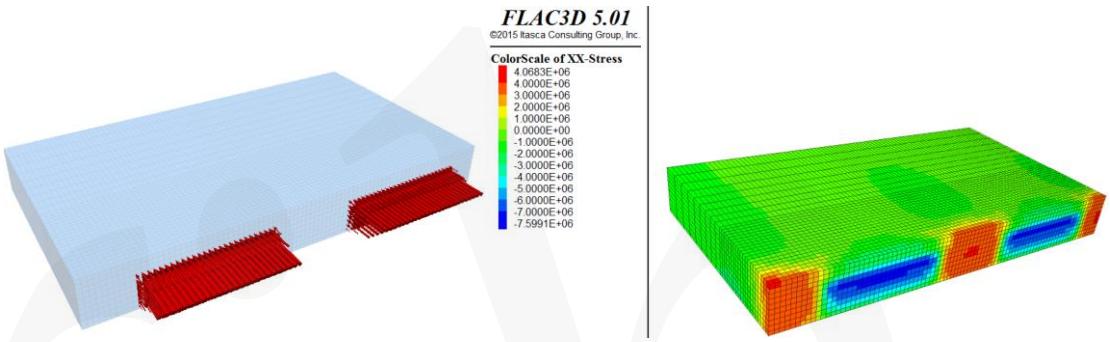


Figure 4: Model of ring joint loading during thrust (left) and resulting spalling stresses (right).

The ring joints have been checked against the loads from jacking forces during TBM propulsion. Maximum thrust force of the Mixshield TBM is 16,275 kN, distributed over 11 jacks, i.e. two jacks per segment and one on the keystone. The compressive stress under the jacking pads remains well below the admissible stress. However, bursting stresses required special attention and were modelled and analysed with FLAC3D. Two cases need to be distinguished: tangential stresses along the ring joint face, which can lead to spalling, and stresses into the depth of the segment, which can lead to splitting. Figure 4 shows the model adopted in the FEA and the resulting tangential spalling stresses under jacking thrust.

The maximum spalling stresses were determined to be 4.07 MPa, exceeding the tensile capacity of the concrete as well as the post-crack residual tensile strength provided by the fibres. Integration of the stresses yielded a tensile force of 50.8 kN, which required 1.17 cm^2 additional reinforcement at the ring joints. This is provided as bursting ladders, consisting of 3 nos. dia. 8 mm that are connected with a dia. 6 mm continuous stagger bar.



Figure 5: Segment mould with bursting ladder in place (left) and a cast segment with BarChip macro synthetic fibre as primary reinforcement and (provisional) bursting ladder as secondary reinforcement (right)

This document is the intellectual property of the fib – International Federation for Structural Concrete. All rights reserved.
This PDF of fib Bulletin 95 is intended for use and/or distribution solely within fib National Member Groups.

Figure 5 shows the bursting ladder placed in the mould. For reasons of stiffness of the ladders and related ease of placing them in the moulds, they have been continued along the radial joints and just connected at the trailing segment edge. Note that the radial joints did not require additional reinforcement. This is a measure to ease and reduce manual handling with regards to production cycle times.

The gradient of stress distribution on the jacking face is shallow in perpendicular direction. Hence, the splitting stresses did not exceed the design tensile strength of plain concrete and thus, no additional reinforcement was required.

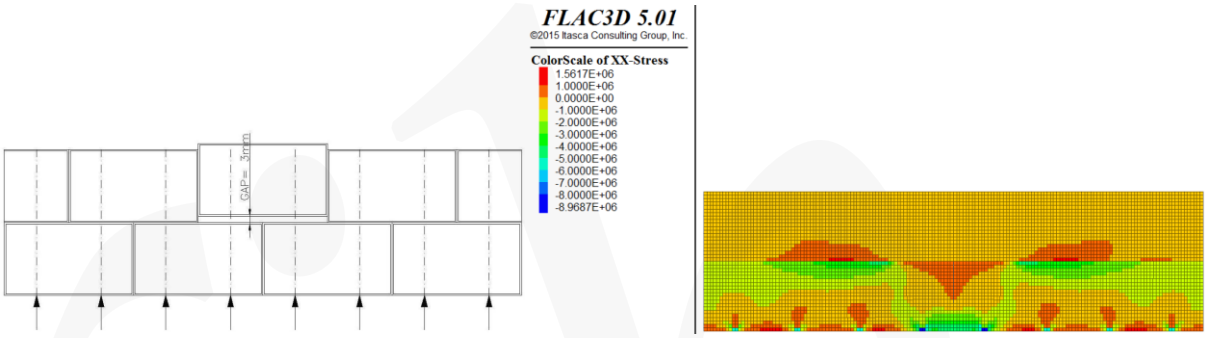


Figure 6: Adopted gapping model during thrust (left) and resulting stresses in the segments (right)

The effect of segment gapping during TBM propulsion, due to imperfect ring build, was also verified with FLAC3D. A gap of 3 mm width between an offset segment and the lastly installed ring was analysed (Figure 6). Also, in this load case the resulting stresses remained below the design tensile strength of plain concrete and no additional reinforcement was required.

3.3 Economic aspects

The initial segment design yielded a conventional steel reinforcement cage of 95 kg/m^3. Regarding improvements in the precast operations and the related cost savings the main contractor Acciona Infraestructuras reviewed this design with Ingemey Consultores, the final design consultant. Switching to BarChip fibre reinforcement eliminated more than 80% of the steel reinforcement. The remaining bursting ladders (16 kg/m^3) are solely for the temporary jacking forces where the synthetic fibre is the primary segment reinforcement.

Aside from the direct cost advantages, the switch to macro synthetic fibre eliminated the rebar cage and its inherent labour and reduced production cycle times by nearly 50%. A cost assessment including segment manufacture and reduced repair or reject rate, due to significantly improved robustness of the FRC segments, revealed a total cost saving of nearly 40% for the rings, compared to the traditional rebar cage design (see Table 1 in Annexure).

4 Conclusions

Ongoing research and continuous developments on macro synthetic fibre and macro synthetic fibre reinforced concrete have made it today being a modern and cost-efficient construction material.

Eliminating durability issues with regard to corrosion of the primary reinforcement yields significant advantages for the design, since it is no longer governed by serviceability limits.

This document is the intellectual property of the fib – International Federation for Structural Concrete. All rights reserved.
This PDF of fib Bulletin 95 is intended for use and/or distribution solely within fib National Member Groups.

Substantial time and cost savings can be attained using fibres by reducing the cost-intensive labour to prepare, place and control standard rebar reinforcement. This applies especially to the complex reinforcement cages of precast tunnel segments. Furthermore, costs related to maintenance by replacing rejected or by repairing damaged segments can be significantly reduced.

The experience gained in the Santoña-Laredo project shows that macro synthetic fibre reinforced segments perform very robust and satisfactory even under difficult conditions (Winterberg et al. 2018).

These types of utility tunnelling projects (sewage, power, irrigation or hydropower underground pipelines) are widely present in the world market and they can raise a huge opportunity for macro synthetic fibre reinforced concrete segmental linings, profiting from the given advantages.

The successful completion of this project will build further confidence in macro synthetic fibre reinforced segmental linings. The success and gained experience of this project will lead to the implementation of this technology in other tunnel projects.

5 References

Bernard, E.S. 2014. Age-dependent changes in post-cracking performance of fibre reinforced concrete for tunnel segments. Proceedings of the 15th Australian Tunnelling Conference 2014, Sydney, 17-19 September

Bernard, E.S. 2018. Reduction of Flexural Crack Widths Using Synthetic Fibres in Reinforced Concrete. Proceedings FRC 2018, Fibre Reinforced Concrete: from Design to Structural Applications, Desenzano, Italy, 28–30 June 2018

DBV 2001. Merkblatt Stahlfaserbeton, Ausgabe Oktober 2001 (Guide to good practice Steel fiber reinforced concrete, German Concrete Association, final edition October 2001)

EHE-08 2008. Instrucción de Hormigón Estructural. Anejo 14 “Hormigón con fibras”, Spanish Concrete Design Code

EN 14651 2005. Test method for metallic fibered concrete - Measuring the flexural tensile strength (limit of proportionality (LOP), residual)

fib 2012. fib Model Code 2010 for Concrete Structures. International Federation for Structural Concrete, Lausanne, Switzerland

ITA WG2 2016. Twenty years of FRC tunnel segments practice: lessons learnt and proposed design procedure. Report from ITA/AITES Working Group 2 Research, www.ita-aites.org

ITAtech 2016. ITAtech Guidance for Precast Fibre Reinforced Concrete Segments – Vol. 1 Design Aspects. ITAtech Activity Group Support, ITAtech Report No. 7, April 2016, www.ita-aites.org

Nitschke, A. and Winterberg, R. 2016. Performance of Macro Synthetic Fiber Reinforced Tunnel Linings. Proceedings of the World Tunnel Congress 2016, San Francisco, USA, 22–28 April 2016

PAS 8810 2016. Tunnel design – Design of concrete segmental tunnel linings – Code of practice. The British Standards Institution, BSI Standards Ltd

This document is the intellectual property of the fib – International Federation for Structural Concrete. All rights reserved.
This PDF of fib Bulletin 95 is intended for use and/or distribution solely within fib National Member Groups.

Plizzari G.A. and Cominoli L. 2005. Numerical Simulations of SFRC Precast Tunnel Segments. In Proceedings of ITA-AITES 2005, Underground space use: Analysis of the past and lessons for the future, Erdem Y. and Solak T. Eds., Istanbul (Turkey), May 7-12, pp. 1105-1111.

UNE 83515 2010. Fibre reinforced concrete. Determination of cracking strength, ductility and residual tensile strength. Barcelona test. Spanish Standard

Winterberg, R., Justa Cámara, R. and Sualdea Abad, D. 2018. Santoña–Laredo General Interceptor Collector – Challenges and Solutions. Proceedings FRC 2018, Fibre Reinforced Concrete: from Design to Structural Applications, Desenzano, Italy, 28–30 June 2018

6 Appendix

Table 1: Comparative cost assessment of the segment Production – FRC vs. conventional rebar cage

Number of Rings in Project	Segments / Ring	m3 of Concrete / Ring		Segmentation
1218	**6**	**3.534**		**5 + 1**

1) BarChip Fibre Reinforced Segments				
	Unit Cost / m3	m3 / Ring	**Cost / Ring**	
C45/55 Fibre Reinforced Concrete	115.00 €	3.534	€ 406.41	Pouring, vibrating, etc. not considered
Fibre dispenser				not used, bag emptied on the sand in the skip
		KG / m3		
Rebar: Bursting ladders	1.10 €	16.0	€ 62.20	including manufacture, storage, etc.
	Man-hours / Ring	Cost / Hour		
Labour to place bursting ladders	0.25	25.00 €	€ 6.25	
	Percentage	Segments for repair		
% of segments requiring major repairs	0.5%	37		estimated from experience
	Man-Hours / Segment	Cost / Hour		
Labour for repair	3	25.00 €	€ 2.28	
Cost of craneage in/out repair areas	1	25.00 €	€ 0.76	not carried in/out for repairing
Administration/QC costs	1	50.00 €	€ 1.52	
	Cost / Segment	Total Cost		
Cost of repair materials	4.20 €	155.40 €	€ 0.13	
Total Cost/Ring			**€ 479.54**	

2) Rebar Cage Reinforced Segments				
	Unit Cost / m3	m3 / Ring	**Cost / Ring**	
C45/55 Concrete with 95 kg/m3 cages	156.00 €	3.534	€ 551.30	
Cage Fabrication	Man-Hours / Ring	Cost / Hour		
Labour for fabrication	3	25.00 €	€ 75.00	fabrication of the cage
Administration/QC Costs	0.5	50.00 €	€ 25.00	
Jigs / Spacers	0.5	25.00 €	€ 12.50	preparing spacers
Rebar fabrication shed area				
Welding / tie wire	0.25	25.00 €	€ 6.25	
Placing of Cages Into Moulds	Man-hours / Ring	Cost / Hour		
Labour to place cages	0.5	25.00 €	€ 12.50	
Cost of craneage	0.5	25.00 €	€ 12.50	
QC costs (checking cover)	0.5	50.00 €	€ 25.00	
Repair of Damaged Segments	Percentage	Segments For Repair		
% of segments requiring major repairs	2.0%	147		estimated from experience
	Man-hours / Segment	Cost / Hour		
Labour for repair	3	25.00 €	€ 9.05	
Cost of craneage in/out repair areas	1	25.00 €	€ 3.02	
Administration / QC Costs	1	50.00 €	€ 6.03	
	Cost / Segment	Total Cost		
Cost of repair materials	4.20 €	617.40 €	€ 0.51	
Total Cost / Ring			**€ 738.66**	

This document is the intellectual property of the fib – International Federation for Structural Concrete. All rights reserved.
This PDF of fib Bulletin 95 is intended for use and/or distribution solely within fib National Member Groups.
FRC2018: Fibre Reinforced Concrete: from Design to Structural Applications
Joint ACI-*fib*-RILEM International Workshop

Effect of reinforcement configuration on the ductility requirements of real-scale slabs

Eduardo Galeote[1], Ana Blanco[2], Albert de la Fuente[1]

[1] : Universitat Politècnica de Catalunya, Barcelona, Spain.

[2] : Loughborough University, Loughborough, United Kingdom.

Abstract

The use of fibres has proved to be a competitive solution since they might replace partially or totally the rebar reinforcement. Nevertheless, the main drawback that faces the use of fibres is the lack of experimental evidence concerning the performance of elements under flexural stress in the presence of different reinforcement configurations. Given that flexural tests are conducted in standardized specimens with fibres as the only reinforcement, it is important to determine the response of larger elements, whose test configuration and behaviour may be more representative of real structures. In this regard, this research focuses on the characterization of full-scale elements and analyse their response following the ductility design philosophy of the *fib* Model Code 2010. For this, five slabs that are 400 mm deep, 1000 mm wide and 3000 mm long were manufactured with different contents of fibres and rebar configurations. These elements were tested under flexural conditions and analysed in terms of strength and ductility. The influence of the reinforcement configuration on the number of cracks appearing and their average width was also assessed. The results indicate that the content and type of fibres proposed did not meet the minimum ductility requirements when only fibres were used as reinforcement. Conversely, the slabs with hybrid and only traditional reinforcement verified the ductility criteria in varying degrees.

Keywords

FRC, real-scale tests, ductility, design optimization, crack width

This document is the intellectual property of the fib – International Federation for Structural Concrete. All rights reserved.
This PDF of fib Bulletin 95 is intended for use and/or distribution solely within fib National Member Groups.

1 Introduction

Segments for tunnel linings are mainly subjected to compressive stresses and low bending moments during service life and, therefore, no cracks are expected to appear under such loading situation. Conversely, during transitory stages as demoulding, stocking, transport or manipulation, the segments behave as isostatic slabs subjected to flexural stresses and higher bending moments. Consequently, these transient stages present more restrictive conditions and the reinforcement must be calculated accordingly.

Following the design specifications, structural elements require a certain degree of ductility in failure regime. This ductility is provided by a minimum amount of reinforcement that guarantees that the ultimate failure moment M_u of the structure can resist the cracking moment M_{cr}. The relation between M_u and M_{cr} displays three possible scenarios depending on the ductility degree achieved by the structure as shown in Figure 1. In case that the design moment M_d is lower than M_{cr}, a critical behaviour would be required to assure the ductility of the structure. In the event that M_d was higher than M_{cr}, a supracritical behaviour would be necessary.

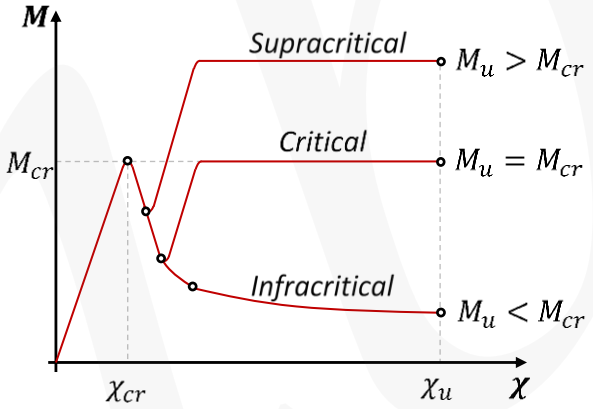


Figure 1: Ductility criteria of a structure

During transient stages segments are subjected to their self-weight and the weight of additional segments stacked on top. These loads, even though being more restrictive, produce low bending moments that are not high enough to achieve M_{cr}. In that situation, a critical reinforcement would suffice to provide enough ductility to the structure. Even though this reinforcement has traditionally consisted of rebars, the increasing use of fibres with structural purposes has proved to replace partially or totally a rebar reinforcement [1–3]. Numerous examples in previous studies [4] support the feasibility of using fibres as an alternative reinforcement.

The main focus of this document is to provide evidence on how a partial substitution of traditional reinforcement by fibres may be used to fulfill the minimum ductility requirements according to the *fib* Model Code 2010 [5]. For this, an experimental program involving five slabs with rebar reinforcement, fibres and a combination of bars and fibres are presented. The results show that when reducing the rebar reinforcement, the contribution of fibres is able to compensate this rebar reduction to achieve the ductility requirements.

This document is the intellectual property of the fib – International Federation for Structural Concrete. All rights reserved.
This PDF of fib Bulletin 95 is intended for use and/or distribution solely within fib National Member Groups.

2 Experimental program

2.1 Concrete mix and specimens

To optimize the manufacture of tunnel segments and meet their design requirements, it is necessary to reach high strengths at early ages for demoulding and stacking purposes. This is achieved by using a high content of cement and microsilica, whose pozzolanic contribution increases the strength of concrete at early ages. The reduction of workability due to the use of fibres may be compensated by adding superplasticizer. Moreover, adding an air entraining agent improves the workability in the fresh state and enhances the durability. Additionally, short polypropylene fibres reduce the likelihood of spalling on the segments in the event of fire.

Three batches were produced: one mix of plain concrete (PC) and two mixes of fibre reinforced concrete (FRC) with contents of 25 and 30 kg/m^3 of steel hooked-end fibres (FRC-25 and FRC-30, respectively) with a length of 35 mm, diameter of 0.55 mm and tensile strength of 1325 MPa. The concrete proportioning (Table 1) remained constant for the three batches, except for the fibres added in the FRC dosages.

Table 1: Concrete mix

Material	**Content [kg/m^3]**
Cement II B-M 42.5R	400
Microsilica	16
Water	143
Natural sand 0/8	387
Sand 0/8	461
Coarse aggregate 8/16	352
Coarse aggregate 16/22	652
Superplasticizer	1.5% o.c.w.
Air Entraining Agent	0.03 – 0.10% o.c.w.
Polypropylene fibre - Φ0.18 mm / L=6 mm	1.5

The characterization of the material involved compressive tests on cubic samples of 150x150 mm. The modulus of elasticity was determined by testing cylindrical specimens of dimensions Φ150x300 mm. Three-point bending test on small beams (150x150x600 mm) were additionally performed in the case of the FRC mixes to assess the cracking and residual strength. Table 2 presents the average results of these tests along with the coefficient of variation (CV).

This document is the intellectual property of the fib – International Federation for Structural Concrete. All rights reserved.
This PDF of fib Bulletin 95 is intended for use and/or distribution solely within fib National Member Groups.

Table 2: Characterization results of the three mixes

Parameter [MPa]	**PC**		**FRC-25**		**FRC-30**	
	Average	**CV %**	**Average**	**CV %**	**Average**	**CV %**
f_{cm}	65.8	3.9	81.5	4.3	96.8	2.3
E_{cm}	37442	3.6	35510	1.4	39760	1.2
f_{LOP}	-	-	5.48	4.5	6.03	16.2
f_{R1}	-	-	3.33	20.5	3.87	33.8
f_{R2}	-	-	1.84	27.0	2.14	30.7
f_{R3}	-	-	0.91	23.1	1.39	21.0
f_{R4}	-	-	0.65	24.5	1.02	14.7

2.2 Slabs and test setup

Five slabs with a length of 3.0 m, a width of 1.0 m and a height of 0.4 m were produced with the three concrete mixes of Table 2. The reinforcement combinations consisted of one slab reinforced with steel deformed bars (RCS), two slabs with fibre contents of 25 and 30 kg/m^3 (FRCS-25 and FRCS-30) and two additional slabs with a hybrid combination of traditional reinforcement and fibres in contents of 25 and 30 kg/m^3 (HRCS-25 and HRCS-30). The reinforcement at the bottom surface in RCS consisted of 8φ10, which was subsequently reduced in both HRCS to 8φ8. According with tensile experimental tests, steel rebars presented an average tensile strength of 652.8 MPa. A schematic representation of the reinforcement configuration is shown in Figure 2.

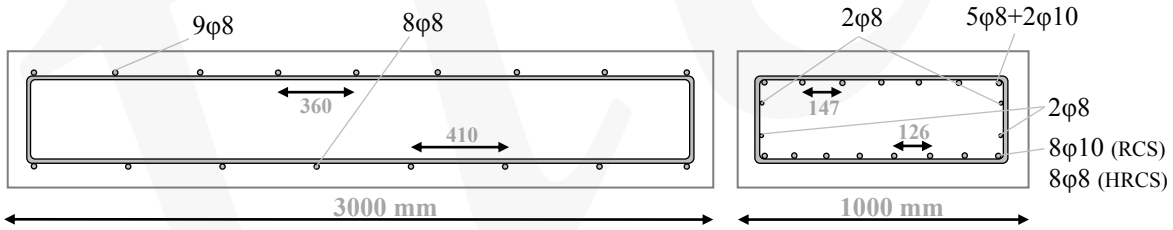


Figure 2: Reinforcement configuration

The tests were based on a four-point isostatic configuration with a span of 2.7 m and a distance between loading points of 0.9 m. The piston connected to the frame applied the load through a stiffened steel beam which transmitted the load to two HEB 140 placed crosswise along the width of the slab (Figure 3). Between the HEB 140 beam and the slab, a neoprene sheet 10 mm thick and 100 mm wide was placed to ensure full contact. The supports at the edges of the slabs consisted of two neoprene sheets 20 mm thick and 200 mm wide.

This document is the intellectual property of the fib – International Federation for Structural Concrete. All rights reserved.
This PDF of fib Bulletin 95 is intended for use and/or distribution solely within fib National Member Groups.

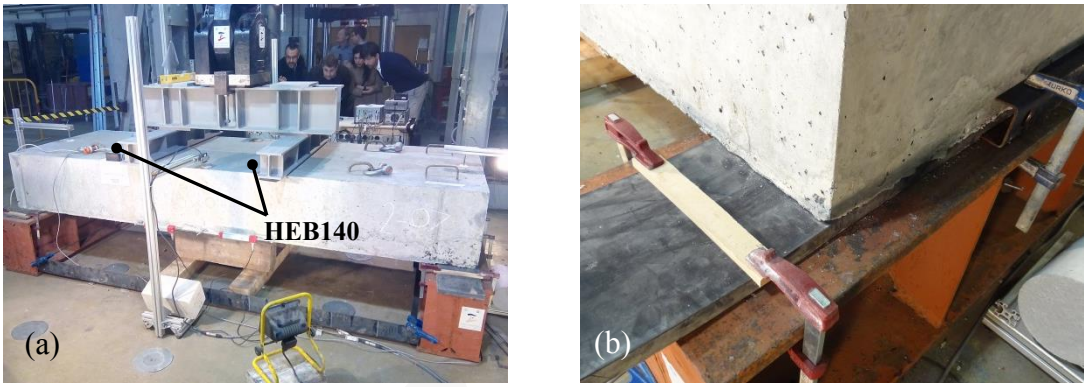


Figure 3: Test setup (a) and neoprene support (b)

The test was performed with displacement control and divided in two stages with different loading rates. In the first stage, the displacement rate was set to 0.4 mm/min and lasted until the element cracked. Subsequently, the rate increased to 1.0 mm/min during the post cracking stage. A laser to measure the deflection at the mid-span was placed over the surface of the slab at both sides of the element and at 50 mm from the lateral edge. The crack opening was also measured at both sides of the slab through two displacement transducers encompassing the distance between the two HEB beams. Additionally, one LVDT with gauge capacity of ±5 mm measured the vertical displacement of each support at the edges. Figure 4 shows further details of the measuring instrumentation.

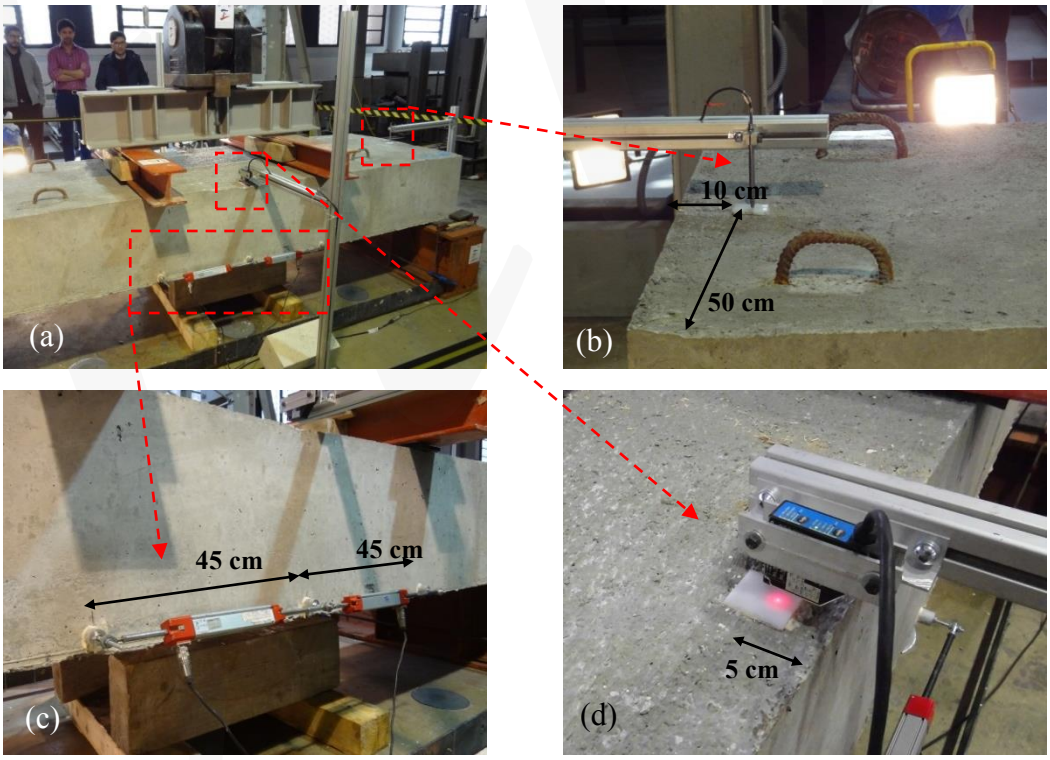


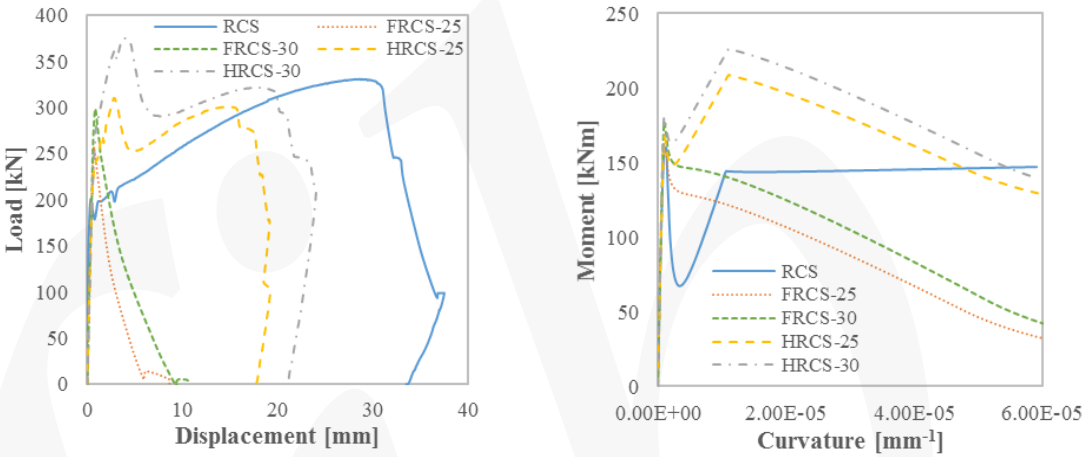
Figure 4: Overview of the instrumentation (a); LVDT transducer (b); displacement transducer (c) and laser (d)

This document is the intellectual property of the fib – International Federation for Structural Concrete. All rights reserved.
This PDF of fib Bulletin 95 is intended for use and/or distribution solely within fib National Member Groups.

3 Results

3.1 Midspan deflection and ductility assessment

The ductility of the slabs is represented in terms of Load-Displacement and Moment-Curvature in Figure 5. The Load-Displacement curve is directly obtained from the data recorded during the test, whereas the Moment-Curvature diagrams (M-χ) are determined through a sectional analysis [6] using the material characterization results as data input. The results display the influence of the reinforcement configuration on the behavior of the slabs.



(a) (b)

Figure 5: Curves for Load-Displacement (a) and Moment-Curvature (b)

The cracking load (P_{cr}) of the slabs ranges from a minimum of 201 kN (RCS) to a maximum of 297 kN (FRCS-30), with an average P_{cr} of 245 kN and a coefficient of variation of 14.4%. The scatter of these results is mainly associated to the variability of the flexural tensile strength of concrete. Moreover, these differences may also be appreciated in the critical bending moment M_{cr}, given that both P_{cr} and M_{cr} depend on the flexural tensile strength of concrete.

After cracking, the load bearing capacity of the bars in RCS is activated and the bars begin to absorb the tensile stresses increasing the strength and the deformations up to an ultimate load of 330 kN and deflection of 29.33 mm. Conversely, the slabs FRCS-25 and FRCS-30 presented a brittle behaviour exhibiting a strength drop after cracking. Notice that regardless of the brittle behaviour, the deflection of FRCS-30 is higher than in FRCS-25, effect that is mainly attributed to the higher amount of fibres in FRCS-30.

Hybrid reinforced slabs present a hardening behavior after cracking exhibiting the maximum loads P_{max} at low deflections, reaching results of 308 kN and 375 kN in HRCS-25 and HRCS-30, respectively. After such hardening behavior, there is a subsequent load drop after P_{max} at deflections of 5.0 mm (HRCS-25) and 7.6 mm (HRCS-30). This load drop is mainly attributed to the debonding of the hooks, producing an energy release that transfers the main load bearing capacity to the rebars. From this point onwards, and as a result of the fibre debonding process, the contribution of the fibres is smaller and the rebars assume the main load carrying capacity showing a deflection-hardening behaviour up to the ultimate load. Notice that after the load drop, the slope of the curve is parallel to the slope exhibited by RCS,

This document is the intellectual property of the fib – International Federation for Structural Concrete. All rights reserved.
This PDF of fib Bulletin 95 is intended for use and/or distribution solely within fib National Member Groups.

which means that rebars are the main resisting elements against loads. The ultimate loads in HRCS-25 and HRCS-30 are 301 kN and 322 kN, respectively, show that increasing the fibre content from 25 to 30 kg/m^3 did not enhance significantly the ultimate load.

However, the higher amount of fibres in HRCS-30 entailed a greater deflection with respect to HRCS-25, which is a result of the contribution of the fibres against the deflection of the slabs. It is noteworthy that the ultimate deflection of RCS reaches 29.33 mm, whereas for slabs HRCS-25 and HRCS-30 the ultimate deflections are 14.88 mm and 18.73 mm, respectively. The main reason for these differences is reduction of the rebars in hybrid reinforced slabs.

The M-χ diagram for RCS presents a critical ductile behaviour. Notice that after M_{cr} a brittle failure occurs until rebars activate the load bearing capacity. The ultimate bending moment for RCS according to the M-χ diagram is 147 kNm, while the experimental results yields a M_u of 149 kNm. The brittle behaviour of FRCS-25 and FRCS-30 in the Load-Displacement curve turns into an infracritical response in the M-χ diagram. In this regard, the use of a higher content of fibres results in higher bending moments.

Hybrid reinforced slabs present a M_u of the same magnitude as M_{cr}, even though for small curvatures, the bending moment in HRCS-25 and HRCS-30 is significantly higher than M_{cr}. After this point, the bending moment decreases up to M_u due to the progressive reduction of the contribution of the fibres, revealing the behavior already exhibited in the Load-Displacement curves of the experimental tests. The failure curvature of HRCS-25 and HRCS-30 is controlled by the rebars, which fail at the same curvature than in RCS. At this point, the M_u of HRCS-25 and HRCS-30 according to the M-χ model is 129 kNm and 139 kNm whereas the experimental M_u are 135 kNm and 145 kNm, respectively.

3.2 Crack patterns and crack width

The position and the shape of the cracks were sketched after each test and are shown in Figure 6. Both sides of each slab are represented taking the bottom surface of the slab as the symmetry axis showing both the main and the secondary cracks. Two pictures of the main cracks in RCS and HRCS-30 are also presented.

The only elements with crack localization were slabs FRCS-25 and FRCS-30 due to the brittle failure. The rest of the slabs presented two cracks in at least one of the faces. In line with previous studies [7], ramifications appeared especially at the main cracks. These ramifications branch off at the half top of the slab and tend to follow the direction of the longitudinal reinforcement placed at the top surface. As reported in previous studies [8], increasing the amount of fibres also produced a greater number of cracks. Notice that fibres increase the post-cracking strength of the elements and reduce the bond transfer length [9].

To analyse the crack width, the central 90 cm of the slabs were studied given that in a four-point configuration there is no shear contribution at the section between loading points and only cracks due to flexural stresses appear. The total crack width at this section was measured using the displacement transducers placed at each side of the slab and the number of cracks provided by the sketches of the crack patterns. Therefore, the average crack width was calculated dividing the total distance measured with the displacement transducers by the number of cracks. The results Load-Crack width are presented in Figure 7 for slabs RCS, HRCS-25 and HRCS-30. Given the brittle failure of FRCS-25 and FRCS-30 no results of crack width are presented for these slabs.

This document is the intellectual property of the fib – International Federation for Structural Concrete. All rights reserved.
This PDF of fib Bulletin 95 is intended for use and/or distribution solely within fib National Member Groups.

The results reveal how the fibres and their content clearly increase the load capacity of the slabs, especially at small crack widths. The hybrid reinforced slabs present a peak load at crack widths of approximately 0.5 mm, with a subsequent drop of the load followed by a deflection-hardening behaviour up to the ultimate load. After the load drop, slabs HRCS-25 and HRCS-30 follow a parallel behaviour to RCS, thus indicating that are the rebars in hybrid reinforced slabs which carry the main load capacity until failure.

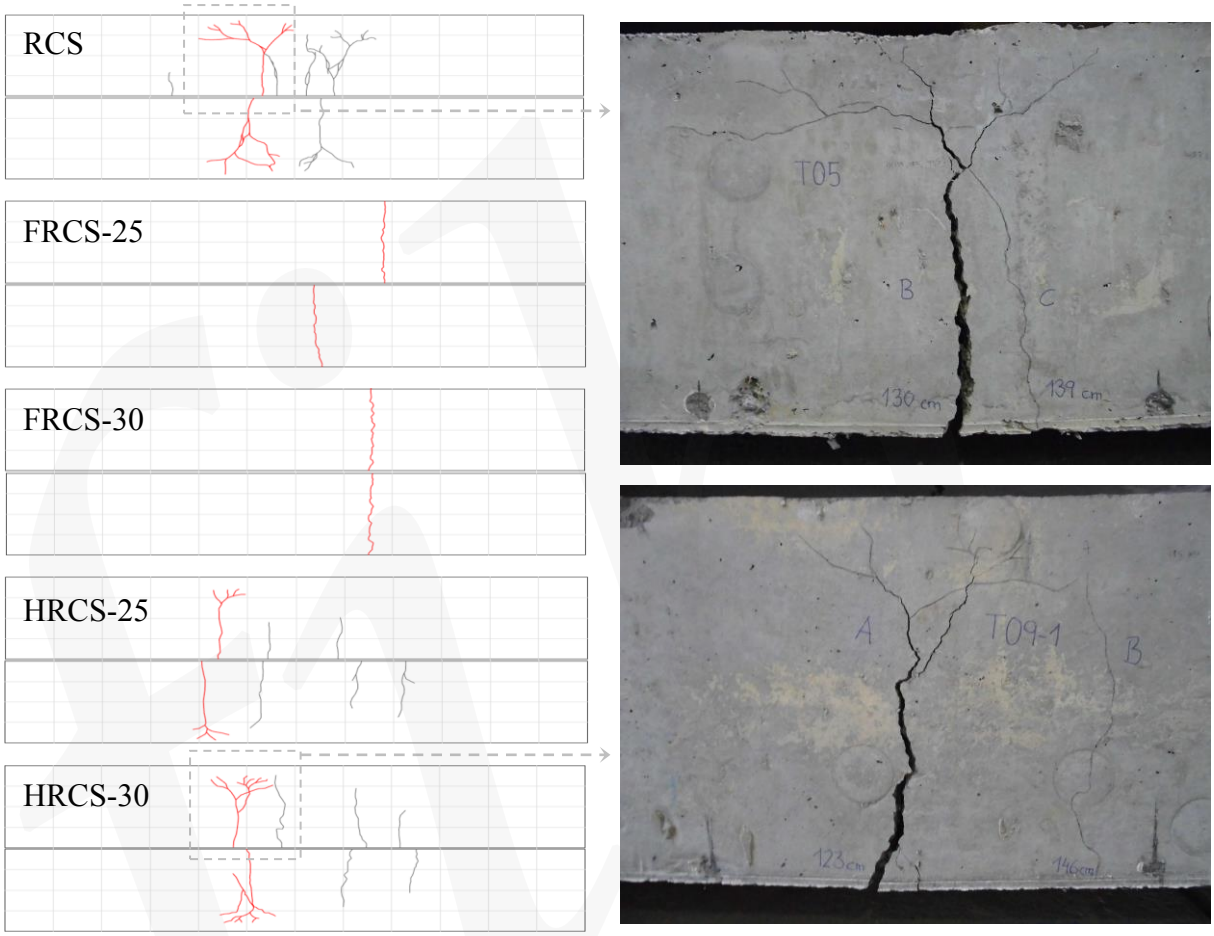


Figure 6: Crack patterns of the slabs

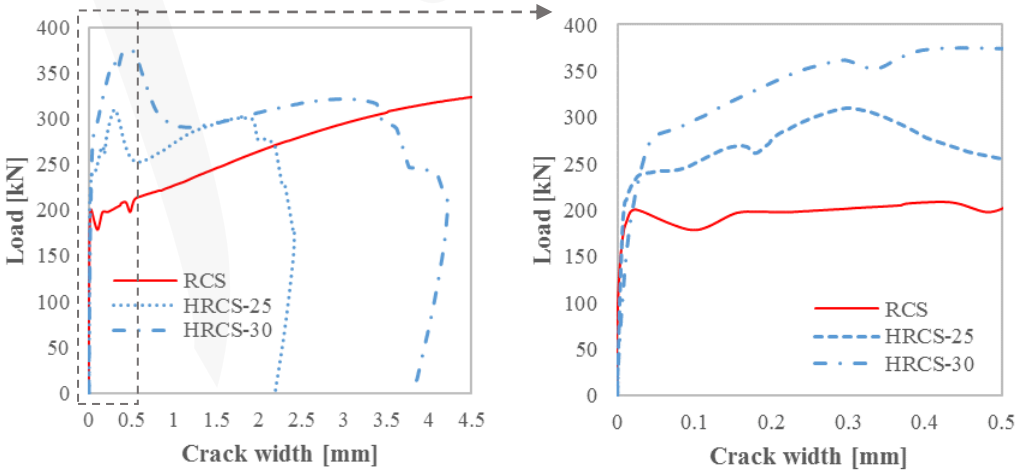


Figure 7: Curves Load-Crack width for RCS, HRCS-25 and HRCS-30

This document is the intellectual property of the fib – International Federation for Structural Concrete. All rights reserved.
This PDF of fib Bulletin 95 is intended for use and/or distribution solely within fib National Member Groups.

4 Concluding remarks

According to the results obtained in the experimental program and the analysis of the M-χ diagrams, there are different solutions and reinforcement combinations that verify the ductility requirements. In this regard, several specific conclusions may be drawn:

- The slab reinforced only with traditional reinforcement (RCS) presented a critical behaviour with an ultimate moment M_u of the same magnitude as M_{cr}. A reduction of the number of rebars would lead to a M_u smaller than M_{cr}, thus not verifying the minimum ductility criteria. The addition of fibres in HRCS-25 and HRCS-30 compensates the rebar reinforcement reduction yielding a M_u comparable to M_{cr}.
- The highest deflection was reached by the slab RCS. The deflection decreased in both HRCS-25 and HRCS-30 with respect to RCS mainly due to the reduction of rebar reinforcement. Slabs FRCS-25 and FRCS-30 presented a brittle failure with the lowest deflection. However, the higher content of fibres in FRCS-30 led to a greater deflection with regards to FRCS-25. The effect of fibres in reaching higher values of deflection was also observed in HRCS-25 and HRCS-30.
- Crack localization was observed in FRCS-25 and FRCS-30. The rest of the slabs presented at least two cracks and, in the case of the hybrid reinforced slabs, additional cracks were also detected. The fibres reduced the average crack width and enhanced the performance at small crack widths.

5 Acknowledgements

The authors want to express their gratitude to Acciona-Ghella Joint Venture for the support during the experimental program. The development of this research has also been possible owe to the economic funds provided by the SAES project (BIA2016-78742-C2-1-R) of the Spanish Ministry of Economy, Industry and Competitiveness. The first author also acknowledges the Spanish Ministry of Education, Culture and Sport for providing the FPU fellowship.

6 References

[1] A. Caratelli, A. Meda, Z. Rinaldi, P. Romualdi, Structural behaviour of precast tunnel segments in fiber reinforced concrete, Tunn. Undergr. Sp. Technol. 26 (2011) 284–291.
[2] A. de la Fuente, A. Blanco, P. Pujadas, A. Aguado, Diseño óptimo de dovelas de hormigón reforzado con fibras para el revestimiento de túneles, Hormigón Y Acero. 65 (2014) 267–279.
[3] L. Liao, A. de la Fuente, S. Cavalaro, A. Aguado, Design of FRC tunnel segments considering the ductility requirements of the Model Code 2010, Tunn. Undergr. Sp. Technol. 47 (2015) 200–210.
[4] G. Tiberti, F. Minelli, G. Plizzari, Reinforcement optimization of fiber reinforced concrete linings for conventional tunnels, Compos. Part B Eng. 58 (2014) 199–207.
[5] International Federation for Structural Concrete, fib Model Code for Concrete Structures 2010, 2010. www.fib-international.org.
[6] A. De La Fuente, A. Aguado, C. Molins, J. Armengou, Numerical model for the

This document is the intellectual property of the fib – International Federation for Structural Concrete. All rights reserved.
This PDF of fib Bulletin 95 is intended for use and/or distribution solely within fib National Member Groups.

analysis up to failure of precast concrete sections, Comput. Struct. 106–107 (2012) 105–114.

[7] P. Pujadas, A. Blanco, A. Fuente, A. Aguado, Cracking behavior of FRC slabs with traditional reinforcement, Mater. Struct. 45 (2011) 707–725.

[8] P. Bernardi, E. Michelini, F. Minelli, G. Tiberti, Experimental and numerical study on cracking process in RC and R/FRC ties, Mater. Struct. Constr. 49 (2016) 261–277.

[9] P.H. Bischoff, Tension Stiffening and Cracking of Steel Fiber-Reinforced Concrete, J. Mater. Civ. Eng. 15 (2003) 174–182.

This document is the intellectual property of the fib – International Federation for Structural Concrete. All rights reserved.
This PDF of fib Bulletin 95 is intended for use and/or distribution solely within fib National Member Groups.
FRC2018: Fibre Reinforced Concrete: from Design to Structural Applications
Joint ACI-*fib*-RILEM International Workshop

Experimental Behaviour of Precast Tunnel Segments in Steel Fiber Reinforcement with GFRP Rebars

Alberto Meda[1], Zila Rinaldi[1], Simone Spagnuolo[1], Benoit De Rivaz[2], Nello Giamundo[3]

[1] : University of Rome Tor Vergata, Rome, Italy.

[2] : BMUS, Aalst, Belgium.

[3] : ATP, Angri, Italy.

Abstract

The interest in using fiber reinforced concrete (FRC) for the production of precast segments in tunnel lining, installed with Tunnel Boring Machines (TBMs), is continuously growing, as witnessed by the studies available in literature and by the actual applications. The possibility of adopting a hybrid solution of FRC tunnel segments with Glass Fiber Reinforced Polymer (GFRP) reinforcement is investigated herein. Full-scale tests were carried out on FRC segments with and without GFRP cage, with a typical geometry of metro tunnels. In particular, both flexural and point load full-scale tests were carried out, for the evaluation of the structural performances (both in terms of structural capacity and crack pattern evolution) under bending, and under the TBM thrust. Finally, the obtained results are compared, in order to judge the effectiveness of the proposed technical solution.

Keywords

Tunnel segments, hybrid solution, Fiber reinforced concrete, GFRP reinforcement, full scale tests.

This document is the intellectual property of the fib – International Federation for Structural Concrete. All rights reserved.
This PDF of fib Bulletin 95 is intended for use and/or distribution solely within fib National Member Groups.

1 Introduction

In the last few years the adoption of fiber reinforced concrete (FRC) in precast tunnel segments, has encountered a great interest, as witnessed by theoretical and experimental studies (Plizzari and Tiberti, 2008; Caratelli et al., 2011; Liao et al., 2015), and actual applications (Kasper et al. 2008, De La Fuente et al., 2012, Caratelli et al., 2012). The solution of adopting FRC elements, without any reinforcement, provides the great advantages, in terms of cost and precast production. Nevertheless, in some part of the tunnel, for particular loading condition (typically under prevalent bending actions, as in cross-passage or shallow tunnel), the FRC solution could not satisfy the design requirement. In this the adoption of a hybrid system, with the addition of rebars, could be a realistic solution.

The possibility of adopting glass fiber reinforced polymers (GFRP) reinforcement in precast tunnel segments in ordinary concrete was investigated (Caratelli et al., 2016; Caratelli et al., 2017; Spagnuolo et al., 2017). GFRP rebars in concrete structures can be proposed as an alternative to the traditional steel rebars, mainly when a high resistance to the environmental attack is required. Indeed, GFRP reinforcement does not suffer corrosion problems and its durability performance is a function of its constituent parts (Micelli and Nanni 2004; Chen et al. 2007). From the mechanical point of view, the GFRP rebars are characterised by an elastic behaviour in tension up to the failure, and, with respect to the steel ones, present higher tensile capacity, lower elastic modulus, and lower weight (Nanni 1993; Benmokrane et al. 1995; Alsayed et al. 2000). The compression strength is often neglected, due to its low value. GFRP is also electrically and magnetically non-conductive, but sensitive to fatigue and creep rupture (Almussalam et al. 2006). Furthermore, the structural effects of the low elastic modulus and poor bond behavior (Cosenza et al. 1997; Yoo et al. 2015, Coccia et al., 2017) have to be considered. Due to all these aspects, this type of reinforcement is not suitable for all applications, but it appears appropriate for tunnel segments, both for provisional and permanent elements (Caratelli et al., 2016; Caratelli et al., 2017).

In order to evaluate the synergic effect of the above mentioned composite materials, tunnel segments, with a typical metro tunnel geometry, made in FRC with and without GFRP bars were cast and experimentally tested. Both bending and point load tests are carried out, in order to evaluate the structural performances, both in terms of strength and crack width. The obtained results are finally compared and discussed.

2 Segment geometry and materials

Four full-scale fiber reinforced concrete segments were cast in moulds available at the Laboratory of the University of Rome Tor Vergata. The specimens have an external diameter of 6400 mm, thickness of 300 mm, and width of about 1400 mm (Fig. 1). Two of the four segments were further reinforced with a perimetric GFRP cage.

This document is the intellectual property of the fib – International Federation for Structural Concrete. All rights reserved.
This PDF of fib Bulletin 95 is intended for use and/or distribution solely within fib National Member Groups.

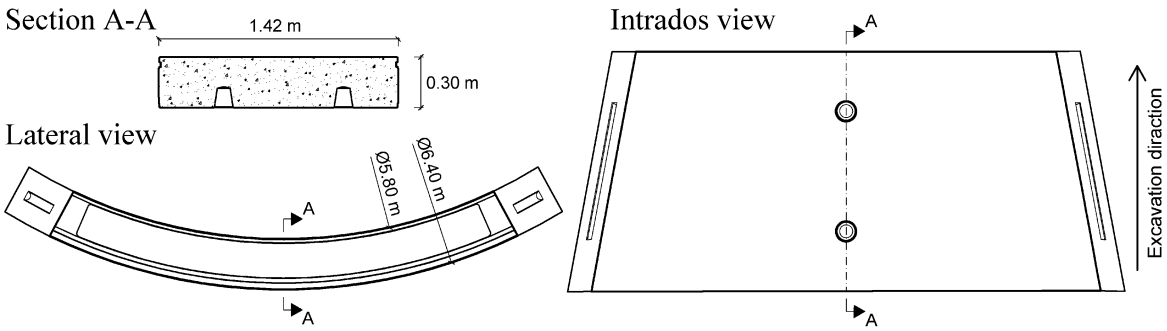


Figure 1: Segment geometry

Steel fibers Bekaert Dramix 4D 80/60BG were added to the concrete matrix with a content of 40 Kg/m^3. The average compressive strength, measured on 6 cubes having 150 mm side, was equal to 62.35 MPa.

The tensile behavior was characterized through three-point bending tests on eight 150x150x600 mm notched specimens according to the EN 14651. The diagrams of the nominal stress versus the crack mouth opening displacements (CMOD) are plotted in Figure 2.

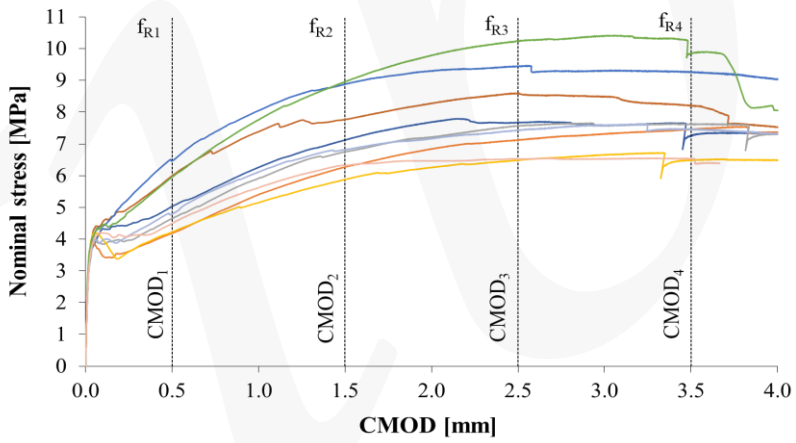
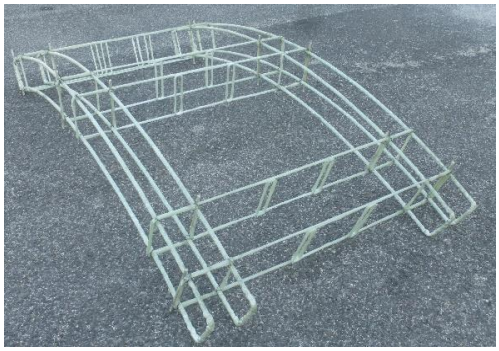


Figure 2: Results of the beam bending tests

Two fiber reinforced segment, named SFRC-GFRP, were further reinforced with a perimetric Glass Fiber Reinforced Polymeric (GFRP) cage, as shown in Figure 3. The GFRP bars have a nominal diameter of 18 mm, and are characterized by Young's Modulus of about 40 GPa, and ultimate tensile strength equal to 1000 MPa.

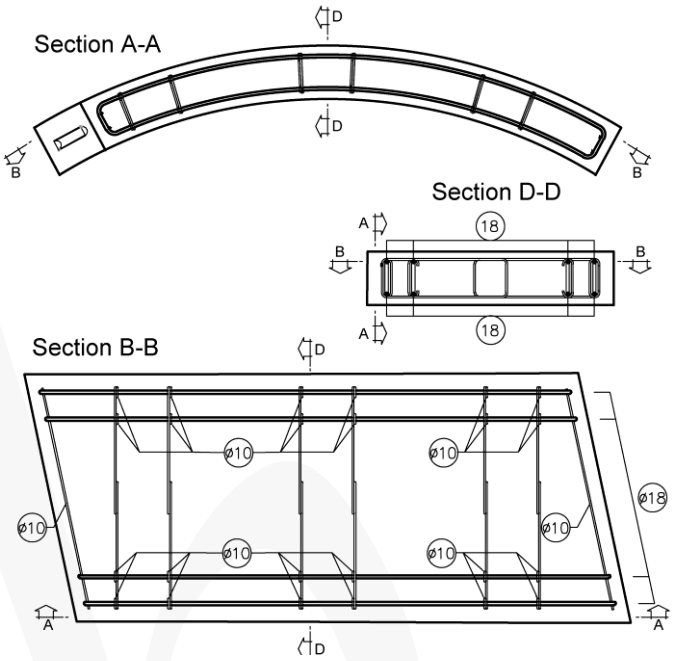
This document is the intellectual property of the fib – International Federation for Structural Concrete. All rights reserved.
This PDF of fib Bulletin 95 is intended for use and/or distribution solely within fib National Member Groups.



a)



b)



c)

Figure 3: a) GFRP cage; b) Casting phase; and c) Reinforcement details.

For both the segment typologies (SFRC-steel fiber reinforced segments without any reinforcement and SFRC-GFRP), both flexural and point load full-scale tests were carried out, for the evaluation of the structural performances (both in terms of structural capacity and crack pattern evolution) under bending, and under the TBM thrust.

3 Bending tests

The bending tests were performed with the loading set-up illustrated in Figure 4, in displacement control, by adopting a 1000kN electromechanical jacket, with a PID control and by imposing a stroke speed of 10 µm/sec.

The segments were placed on cylindrical support with a span of 2000 mm and the load, applied at the midspan, was transversally distributed be adopting a steel beam as shown in Figure 4. The measure devices, consisting in three potentiometer wires and two LVDTs, are shown in Figure 4.

This document is the intellectual property of the fib – International Federation for Structural Concrete. All rights reserved.
This PDF of fib Bulletin 95 is intended for use and/or distribution solely within fib National Member Groups.



Figure 4: Bending test set-up and instrumentation

3.1 Bending test results

The behaviour of the segments SFRC and SFRC-GFRP are compared in Figure 5, where the average value of the displacement, measured by the three potentiometer wires, is plotted versus the load. The first cracks appeared for a load value of about 125 kN and 120 kN, for the SFRC and SFRC-GFRP segment, respectively. In both the cases the first cracks were opened on the lateral surfaces close to the midspan and propagates on the intrados.

After a first comparable almost elastic response, the SFRC-GFRP segment presented a peak load about 63% higher than the SFRC one (367 kN against 225 kN of the SFRC segment). The maximum crack widths, measured at different load steps, are compared in Table 1. The obtained results clearly show the synergic effects of the two materials in reducing the crack widths, with respect to SFRC solution, of about 60%. Finally, the evolution of the crack patterns, at the intrados surface, are compared in Figure 6.

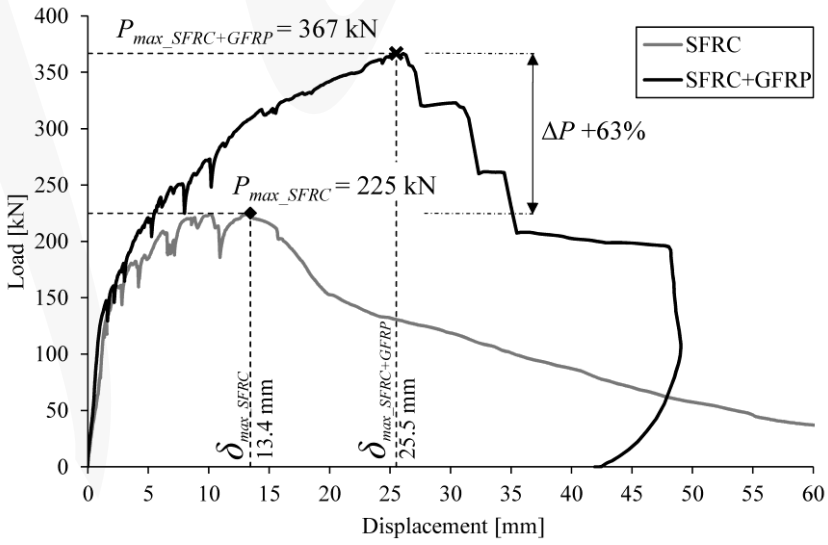


Figure 5: Bending test. Load- average displacement: comparison between SFRC and SFRC-GFRP segments.

This document is the intellectual property of the fib – International Federation for Structural Concrete. All rights reserved.
This PDF of fib Bulletin 95 is intended for use and/or distribution solely within fib National Member Groups.

Table 1: Maximum crack widths: comparison

Loading							
Load [kN]	125	160	180	210	222	250	270
Crack width							
SFRC	<0.05	0.25	0.35	0.60	1.00	n/a**	n/a**
SFRC-GFRP	<0.05	0.10	0.15	n/a*	0.35	0.45	0.70

n/a*= measure not available since the crack width was not recorded at this load step
n/a**= measure not available since the segment did not reach this load value

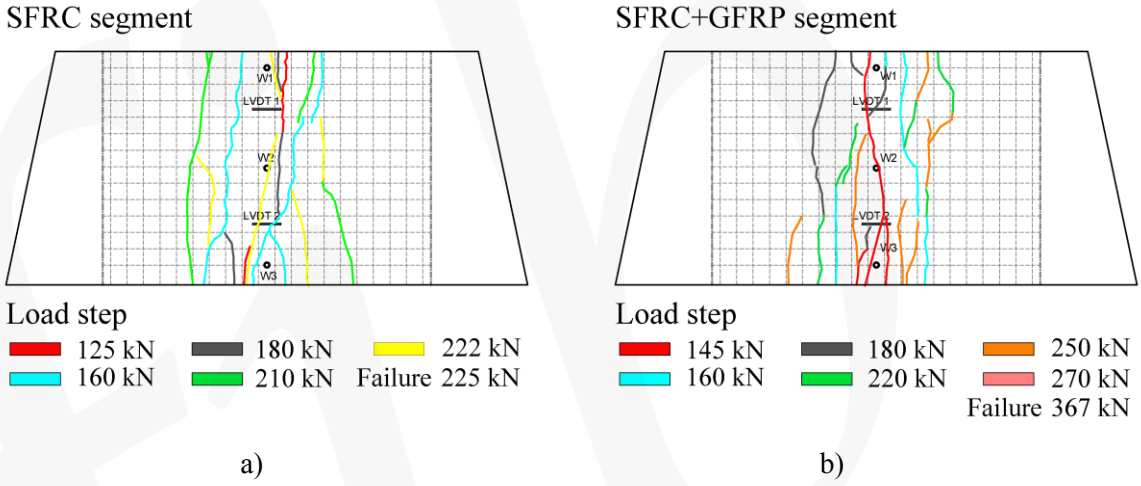


Figure 6: Bending test: crack pattern: a) SFRC segment; b) SFRC-GFRP segment

4 Point load tests

The point load test was performed by applying three-point loads at the segment, and adopting the same steel plates used by the TBM machine (Fig. 7). A uniform support is considered, as the segment is placed on a stiff beam suitably designed (Meda et al., 2016). The case of non-uniform support is highlighted in (Spagnuolo, 2020). Every jack, having a loading capacity of 2000 kN, is inserted in a close ring frame made with HEM 360 steel beams and 50 mm diameter Dywidag bars (Fig. 7). The load was continuously measured by pressure transducers. Six potentiometer transducers (three located at the intrados and three at the extrados) measure the vertical displacements, while two LVDTs transducers are applied between the load pads, to measure the crack openings. (Fig. 7).

This document is the intellectual property of the fib – International Federation for Structural Concrete. All rights reserved.
This PDF of fib Bulletin 95 is intended for use and/or distribution solely within fib National Member Groups.

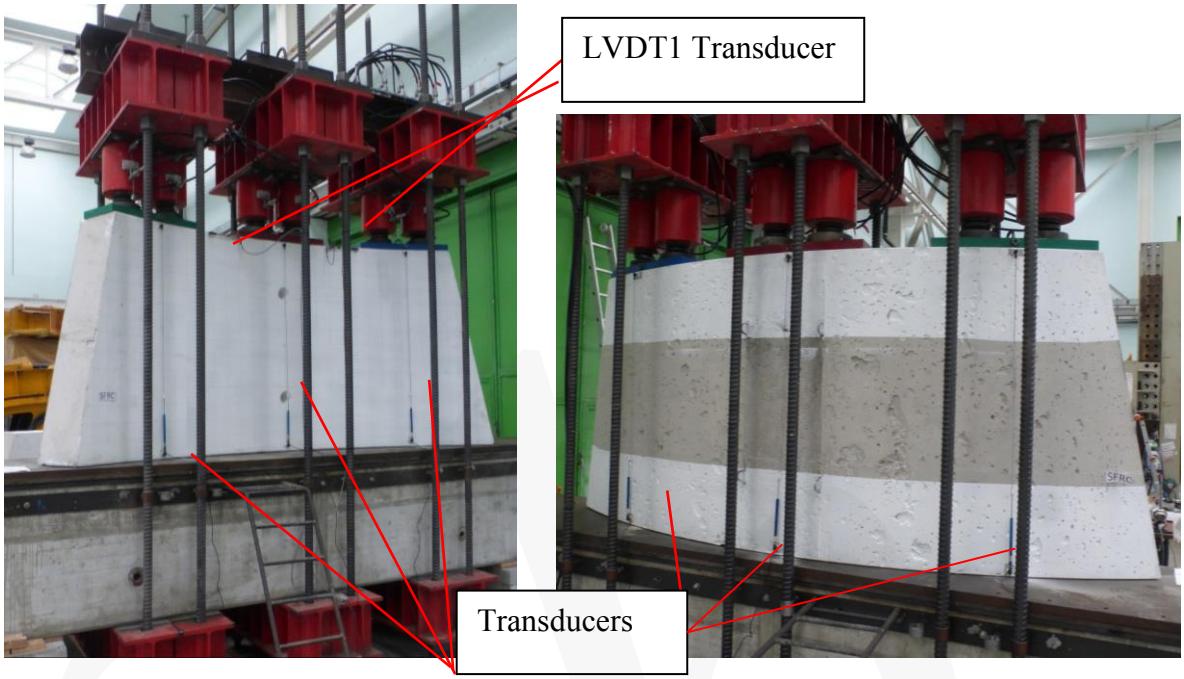


Figure 7: Point load test and instrumentation

Two cycles were performed, as shown in Figure 8. The chosen reference load levels equal to 1580 kN and 2670 kN (for each pad) refer to the service load and unblocking thrust of the TBM machine.

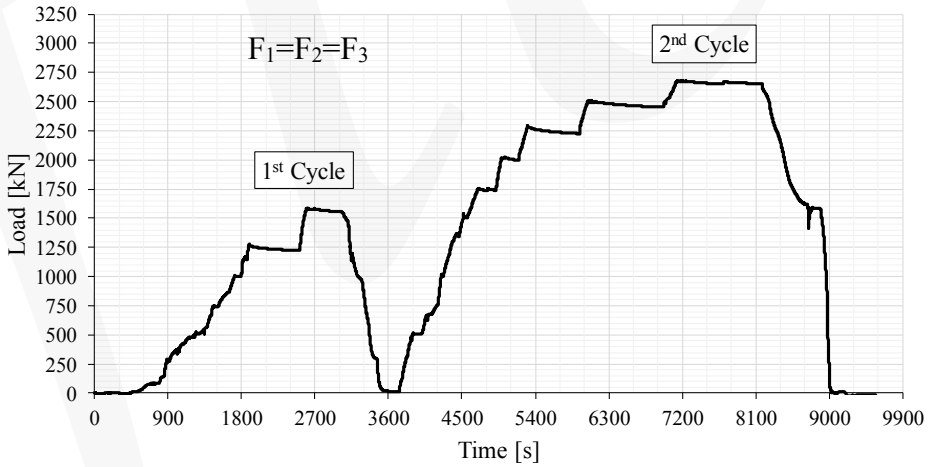


Figure 8: Point load test: Load (single pad) vs Time; a) SFRC; b) SFRC-GFRP segment

The final crack pattern after the point load test is shown in Figure 9, for both the segments SFRC and SFRC-GFRP. Similar patterns were registered. The first cracks appeared for a load level of 1250 kN (for each steel pad) between two pads at the top and lateral surfaces (Figs. 9a and 9b), in both the cases. Besides the splitting cracks (between the pads), a bursting crack (under the point load), formed in both the cases.

This document is the intellectual property of the fib – International Federation for Structural Concrete. All rights reserved.
This PDF of fib Bulletin 95 is intended for use and/or distribution solely within fib National Member Groups.

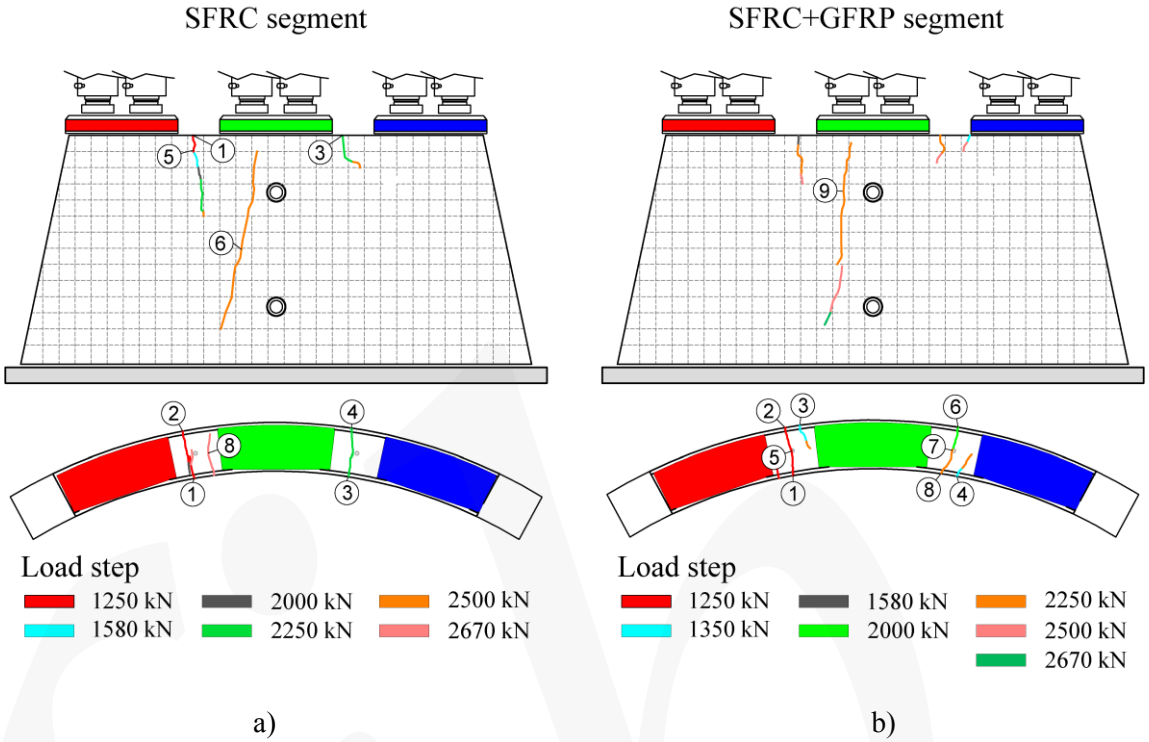


Figure 9: Point load test; Crack pattern: a) SFRC segment; b) SFRC-GFRP segment

Finally, the crack widths measured for the segments SFRC and SFRC-GFRP, at three significant load steps (related to the first cracking, service load and maximum TBM thrust load), are compared in Table 2.

The addition of the perimetric cage led to halve the crack width under the service load, and to reduce it of about 37.5%, under the unblocking thrust force. Furthermore, a reduction of the crack width of about 33% was measured after the complete unloading.

Table 2: Maximum crack widths: comparison

Load		**Maximum crack width [mm]**	
		SFRC	**SFRC -GFRP**
1st crack [kN]	1250	0.05	<0.05
Service load [kN]	1580	0.10	0.05
Unblocking thrust*[kN]	2670	0.40	0.25
Unload [kN]	0	0.15	0.10

Note: * For metro tunnel, TBM pushing capacity coincides with unblocking thrust

5 Concluding remarks

The experimental results of full-scale tunnel segments, subjected to flexural tests and TBM thrust actions, presented in the paper, allows to draw the main concluding remarks listed in the following.

This document is the intellectual property of the fib – International Federation for Structural Concrete. All rights reserved.
This PDF of fib Bulletin 95 is intended for use and/or distribution solely within fib National Member Groups.

1. The results of bending tests, clearly show the synergic effects of the two materials (fibers and GFRP reinforcement) by increasing the peak load and reducing the crack width.
2. The results of the point load test confirm the effectiveness of the solution, since the addition of the perimetric cage led to halve the crack width under the service load, and to reduce it under the unblocking thrust force, and at the complete unloading, respectively.

6 References

Almusallam, T., H., Al-Salloum, Y., A. (2006). "Durability of GFRP Rebars in Concrete Beams under Sustained Loads at Severe Environments." Journal of Composite Materials, Vol. 40, No 7, pp. 623-637.

Alsayed, S.H., Al-Salloum, Y.A., Almusallam, T.H. (2000). "Performance of glass fiber reinforced plastic bars as a reinforcing material for concrete structures." Composite Part B: Engineering, Vol. 31, No 6-7, pp. 555-567.

Benmokrane, B., Chaallal, O., Masmoudi, R. (1995). "Glass fibre reinforced plastic (GFRP) rebars for concrete structure." Construction and Building Materials, Vol. 9(6). 353-364.

Caratelli A., Meda A., Rinaldi Z., Romualdi P. (2011) "Structural behaviour of precast tunnel segments in fiber reinforced concrete". Tunnelling and Underground Space Technology 26, Elsevier,.pp. 284-291.

Caratelli, A., Meda, A., Rinaldi, Z. (2012). "Design according to MC2010 of a fibre-reinforced concrete tunnel in Monte Lirio, Panama". Structural Concrete, Vol. 13, Issue 3;. pp. 166-173.

Caratelli, A., Meda, A., Rinaldi, Z., Spagnuolo S. (2016). "Precast tunnel segments with GFRP reinforcement". Tunnelling and Underground Space Technology vol. 60 (Nov. 2016) pp. 10–20.

Caratelli, A., Meda, A, Rinaldi, Z., Spagnuolo, S., Giona Maddaluno. (2017). Optimization of GFRP reinforcement in precast segments for metro tunnel lining. Composite Structures 181, pp. 336–346.

Chen, Y., Davalos, J. F., Kim, H-Y. (2007). "Accelerated aging tests for evaluations of durability performance of FRP reinforcing bars for concrete structures." Composite Structures, Vol. 78, March, pp. 101–111.

Coccia, S., Meda, A., Rinaldi, Z. (2015). "On shear verification according to the fib Model Code 2010 in FRC elements without traditional reinforcement". Structural Concrete. Volume 16. Issue 4. Dec. 2015. Pp. 518-523.

Coccia S., Meda, A., Rinaldi, Z. Spagnuolo, S. (2017). Influence of GFRP skin reinforcement on the crack evolution in RC ties. Composites Part B. Vol. 119, pp. 90-100.

Cosenza, E., Manfredi, G., and Realfonzo, R. (1997). "Behavior and Modeling of Bond of FRP Rebars to Concrete." Journal of Composites for Construction, Vol. 1(2), pp. 40-51.

De la Fuente A, Pujadas P, Blanco A, Aguado A. (2012) Experiences in Barcelona with the use of fibres in segmental linings. Tunnelling and Underground Space Technology 2012; 27(1):60-71.

Di Carlo, F., Meda, A., Rinaldi, Z. (2016). "Design procedure of precast fiber reinforced segments for tunnel lining construction". Structural Concrete. Volume 17 (5), 747-759.

Ding, Y., Ning, X., Zhang, Y., Pacheco-Torgal, F., Aguiar J.B. (2014). Fibres for enhancing of the bond capacity between GFRP rebar and concrete. Construction and Building Materials 51; pp. 303–312.

This document is the intellectual property of the fib – International Federation for Structural Concrete. All rights reserved.
This PDF of fib Bulletin 95 is intended for use and/or distribution solely within fib National Member Groups.

fib Model Code for Concrete Structures 2010. (2013). Ernst &Sohn.

Issa, M., S., Metwally, I., M., Elzeiny, S., M. 2011 Influence of fibers on flexural behavior and ductility of concrete beams reinforced with GFRP rebars. Engineering Structures 33 (2011) 1754–1763

Kasper, T, Edvardsen C, Wittneben G, Neumann D. (2008) Lining design for the district heating tunnel in Copenhagen with steel fibre reinforced concrete segments. Tunnelling and Underground Space Technology; 23(5):574-587.

Kim, B. Doh, J-H., Yi, C.-K, Lee, J.-Y. (2013). Effects of structural fibers on bonding mechanism changes in interface between GFRP bar and concrete, Composites: Part B 45; pp 768–779.

Liao, L., De La Fuente A, Cavalaro S, Aguado A. (2010). "Design of FRC tunnel segments considering the ductility requirements of the Model Code 2010". Tunnelling and Underground Space Technology 2015; 47:200-210.

Meda, A., Rinaldi, Z., Caratelli, A., Cignitti, F. (2016). "Experimental investigation on precast tunnel segments under TBM thrust action" Engineering Structures, Volume 119, 15 July 2016, Pages 174-185.

Micelli, F., Nanni, A. (2004). "Durability of FRP rods for concrete structures." Construction and Building Materials Vol. 18, No 7, September, pp. 491–503.

Nanni, A. (ed.). (1993). "Fiber-Reinforced-Plastic (GFRP) Reinforcement for Concrete Structures: Properties and applications." Elsevier Science. Developments in Civil Engineering, 42, p.450.

Plizzari, GA, Tiberti G. (2008). "Steel fibers as reinforcement for precast tunnel segments. Tunnelling and Underground Space Technology; 21(3-4).

Qin, R., Zhou, A., Lau, D. (2017).Effect of reinforcement ratio on the flexural performance of hybrid FRP reinforced concrete beams. Composites Part B 108; pp. 200-209.

Spagnuolo, S., Meda, A., Rinaldi, Z., Nanni, A. (2017). Precast Concrete Tunnel Segments with GFRP Reinforcement. Journal of Composites for Construction. ASCE.

Spagnuolo, S., Meda, A., Rinaldi, Z., Nanni, A. (2018). Curvilinear GFRP bars for tunnel segments applications. Composites Part B, 141, pp. 137–147.

Spagnuolo, S. (2020 – In Press). "Influence of non-uniform support on FRC and hybrid precast tunnel segments with glass fiber reinforced polymer bars under TBM thrust". 1° fib Symposium on Concrete and Concrete Structures. October 15th, 2019. University of Parma, Italy.

Wang, H., Belarbi, A. (2011). "Ductility characteristics of fiber-reinforced-concrete beams reinforced with FRP rebars, Construction and Building Materials 25, pp. 2391–2401.

Wang, H., Belarbi, A. (2013). Flexural durability of FRP bars embedded in fiber-reinforced-concrete. Construction and Building Materials 44; pp. 541–550.

Wona, J. P., Park, C. G, Kim, H.H, Lee, S.W, Jang, C.I. (2008). Effect of fibers on the bonds between FRP reinforcing bars and high-strength concrete. Composites: Part B 39, pp. 747–755.

Yang, J.M., Min, K. H., Shih, H. O. Yoon, Y. S. (2012). Effect of steel and synthetic fibers on flexural behavior of high-strength concrete beams reinforced with FRP bars. Composites: Part B 43; pp. 1077–1086.

Yoo, D-Y., Kwon K-Y., Park J-J., Yoon Y-S. (2015). "Local bond-slip response of GFRP rebar in ultra-high-performance fiber-reinforced concrete." Composite Structures Vol. 120, pp. 53–64.

This document is the intellectual property of the fib – International Federation for Structural Concrete. All rights reserved.
This PDF of fib Bulletin 95 is intended for use and/or distribution solely within fib National Member Groups.
FRC2018: Fibre Reinforced Concrete: from Design to Structural Applications
Joint ACI-*fib*-RILEM International Workshop

Opportunities for synthetic fibre reinforcement in concrete tramlines

Karoly Peter Juhasz[1], Peter Schaul[2],

[1] : Budapest University of Technology and Economics, Department of Mechanics, Materials & Structures, Műegyetem rakpart 1-3, Budapest, Hungary

[2] : Budapest University of Technology and Economics, Department of Construction Materials and Technologies, Műegyetem rakpart 1-3, Budapest, Hungary

Abstract

In the past decade macro synthetic fibre reinforcement has become widely used for concrete track slabs including tramlines. By using macro synthetic fibres as a reinforcement in concrete slabs both the casting time and manual work will decrease, while the concrete's ductility will increase. In addition the durability will be higher with using synthetic fibres, and the carbon footprint will be lower compared to steel mesh or fibre reinforcement. In most cases the steel reinforcement can be omitted entirely from the structures using macro synthetic fibres. The uniformly distributed fibres in the concrete can increase the residual flexural strength of the concrete independently from the location. This makes it possible to use the fibres in both cast in situ and precast elements used for tramlines. The calculation process for these structures always has to comprise of both the static load, the dynamic load and the effect of cyclic loading, i.e. fatigue. These load calculations can be handled using advanced finite element analysis software, which is specialized for concrete and fibre reinforced concrete structures. The paper will present the opportunities for using macro synthetic fibres together with the process of designing fibre reinforced concrete tramlines.

Keywords

Macro synthetic fibre reinforced concrete, finite element analysis, tramline design, concrete track slab.

This document is the intellectual property of the fib – International Federation for Structural Concrete. All rights reserved.
This PDF of fib Bulletin 95 is intended for use and/or distribution solely within fib National Member Groups.

1 Introduction

Today the rail construction of modern concrete slab track plays a prominent role in the construction industry. Besides keeping in mind having an economic solution, more emphasis is placed on its durability and its resistance to environmental factors such as moisture, de-icing salts etc. The economic solution can be achieved primarily by decreasing the thickness of the slab and shortening the construction time. Durability can be significantly increased by designing for fatigue and by using materials that are resistant to these environmental factors. Because of this macro synthetic fibres are being used more often for the reinforcement of the concrete for both cast in place or precast structures.

Corrosion resistance is the greatest benefit of macro synthetic fibre where durability can be assured but also synthetic fibres behave better with dynamic loads than steel fibres, therefore their use for tramline or railway track slab is very favourable. Added to this are the economic advantages such as a reduction in labour who would traditionally set and tie the steel reinforcement into place.

The first macro synthetic fibre reinforced track slab was constructed in Japan in 2002: Elasto Ballast track railway (Ridout, 2009). The goal of using macro synthetic fibre was, beside the reduction of the vibration and noise, to increase the speed of the construction process. The track slab was made using a traditional slab structure with a pre-stressed concrete sleepers on it supporting the rails (Figure 1). The reinforcement was a hybrid of traditional steel bar reinforcement together with macro synthetic.



Figure 1: Elasto Ballast track railway (Ridout, 2009)

The first synthetic fibre reinforced track slab in Europe was the Docklands Light Railway near London in 2004. The slab was reinforced with 6 kg/m^3 macro synthetic fibre reinforcement (BarChip48 high quality macro syntethic fibre) which made the construction process considerably faster (Ridout, 2009).

This document is the intellectual property of the fib – International Federation for Structural Concrete. All rights reserved.
This PDF of fib Bulletin 95 is intended for use and/or distribution solely within fib National Member Groups.

The first only macro synthetic fibre concrete cast in place tramline in Europe was built in Szeged, Hungary. Macro synthetic fibre was considered over steel reinforcement as at a certain point in the track it was not possible to use any steel reinforcement due to the operation of a special switch that collected stray current and so this part of the track was reinforced with macro synthetic fibre reinforced concrete. Because of the positive experiences and cost saving in this part of the track the contractor changed to this solution for the entire track and thus replaced all the steel reinforcement with macro synthetic fibres (Nagy et.al. 2014; Nagy et.al. 2015a; Nagy et.al. 2015b).

Beside the cast in place solution the use of precast concrete tramline elements started to spread, mainly because of the same benefits of shortening construction time. These elements also needed to be designed for temporary situations, such as demoulding, lifting, transporting and placing on site. The first and only macro synthetic fibre reinforced precast concrete track to date is the PreCast Advanced Truck (PCAT) system (Hammond, 2016). This precast element is highly optimised both by the dosage of the fibre and its geometrical shape.

In this paper both the cast in place and precast macro synthetic fibre reinforced concrete tramline structures and their design processes will be presented.

2 Cast in place tramlines

One of the most common structures for tramlines is the cast in place track slab. There are several proprietary track slab configurations commonly using either the poured in place form worked track slab or the track slab extruded machine. In the first case after installing the formwork the slab is filled with macro synthetic fibre reinforced concrete, and the joints are installed after each section of the track slab is poured. Each pour is then mostly connected with steel dowels. In the second case the machine continuously pours the macro synthetic fibre reinforced concrete between the moving formwork. In this case the joints are made by saw cutting the slab, which reduces the likelihood of any crack formation.

2.1 Szeged tramline

In 2010 and 2011, during the extension and reconstruction process of the A and C sections of tramline Nr. 1 in Szeged in an areas of the so-called loops which was a major tram intersection, it was necessary to have concrete track slabs that contained no steel reinforcement. Therefore, it was an idea to use macro synthetic fibre-reinforced concrete in these sections. At that time, only synthetic microfibers had been used for concrete reinforcement in Hungary, the effects of which are mostly seen in the case of fresh concrete: through reducing the rate of plastic shrinkage cracking. However, in hardened concrete only macro synthetic fibres have any structural impact. While exploring foreign technologies, it was found a suitable building material for this purpose was a Japanese-developed macro synthetic fibre. During the design process it turned out that traditional reinforcement could be replaced entirely by the use of this macro synthetic fibre in this application. After a technical and financial analysis it also became clear to the general contractor that the desired structure could be built more economically and faster, furthermore: not only could it be applied in the critical sections where no steel reinforcement was allowed, but also it could be used in the other sections of the tram tracks. Based on the above, a unanimous consensus was reached by the Client, the General Contractor and the Designer to try out the new technology. The new technology was designed for and initially tested on non-critical track areas (RAFS-CDM)

This document is the intellectual property of the fib – International Federation for Structural Concrete. All rights reserved.
This PDF of fib Bulletin 95 is intended for use and/or distribution solely within fib National Member Groups.

such as at road junctions, turn-outs, current tracks, bus bays and vibration damping tram tracks.



Figure 2: Tram line in Szeged, Hungary

During the design process the dynamic loads of trams and buses were taken into account, then the load-bearing capacity, serviceability and fatigue limits were checked in accordance with Eurocode (EUROCODE, 2004). Finite element analysis was made on the basis of the recorded material model recommended by RILEM TC 162-TDF (Vandewalle, et.al., 2002). According to the calculations the tramway met the standard loads and load combinations.

2.2 Tramlines around the world

The Szeged tramway project was a huge success. After the system proved to be fully functional several other tram tracks were constructed using very similar solutions and using macro synthetic fibres. These tram tracks were constructed in St. Petersburg, Russia, and in Tallinn, Estonia. In Hungary the success also continued and led to the partial reconstruction of Budapest tramlines Nr. 18 and Nr. 1, as well as the complete track reconstruction of the Nr. 3 tramline using this solution.

2.3 Finite element analysis of the tramlines

Initially the finite element analysis of the tramlines was made by using Ansys finite element software. This software can handle the Rankine and Von-Misses combined failure criteria, which is a good approach for a fibre reinforced concrete material as the effect of the fibres is taken into consideration as a plastic model after the cracking (after yield point). Although because of the plastic material model both the crack propagation and the crack width of the concrete cannot be properly determined.

Due to this only a concrete specific finite element software should be use for the design and optimisation of fibre reinforced concrete tramlines. The two most well-known software are the ATENA and the DiANA. In our design ATENA software was used. ATENA uses Menétrey-William and Rankine combined fracture-plastic failure surface (Rankine cube is at the tension side) (Cervenka and Papanikolaou, 2008). Tension is handled by a fracture model,

This document is the intellectual property of the fib – International Federation for Structural Concrete. All rights reserved.
This PDF of fib Bulletin 95 is intended for use and/or distribution solely within fib National Member Groups.

based on the classic orthotropic smeared crack formulation and the crack band approach. It uses the Rankine cube failure criterion and it can be used as a rotated or a fixed crack model. The plasticity model for concrete in compression uses the William-Menétrey failure surface (Menétrey and William, 1995). Changing aggregate interlock is taken into account by a reduction of the shear modulus with growing strain, along the crack plane, according to the law derived by Kolmar (Kolmar, 1986). The model showed that the concrete met the stress-strain diagram criteria according to Eurocode 2 (Eurocode, 2004). The crack width was calculated from the stress-crack width diagram determined by means of inverse analysis with the help of the characteristic length which is a function of the size of the element and the angle of the crack within the element. This method is the only method that could realistically represent the cracks in a quasi-brittle material which is the main advantage of this advanced material model.

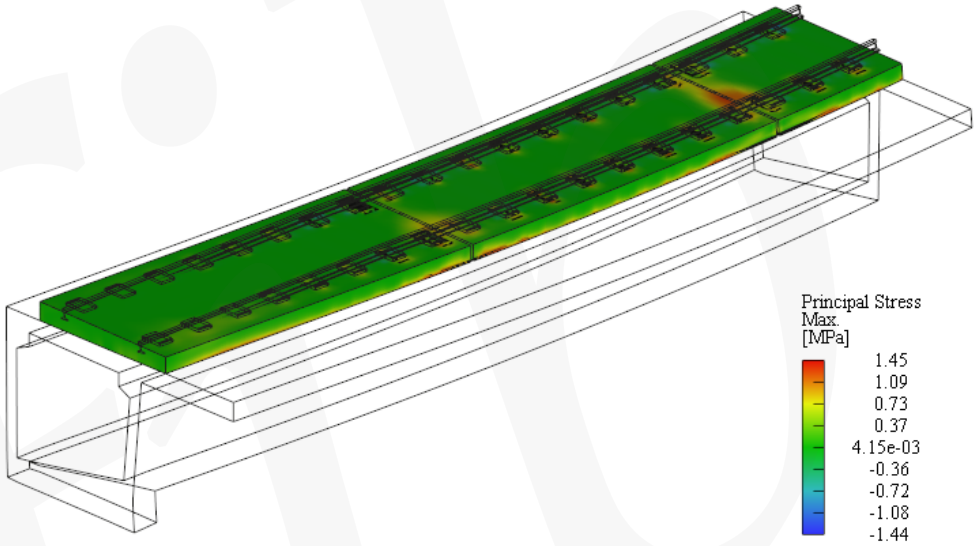


Figure 3: Tramline on a viaduct calculation with ATENA

However, it is important to note that these models only define the peak strength of the material and not the post-cracking response. Numerous other models can be used to approximate the post-cracking capacity of FRC such as the Modified Fracture Energy Method (Juhász, 2013) presented in the ITAtech guideline (ITAtech Activity Group Support, 2015) which was used here.

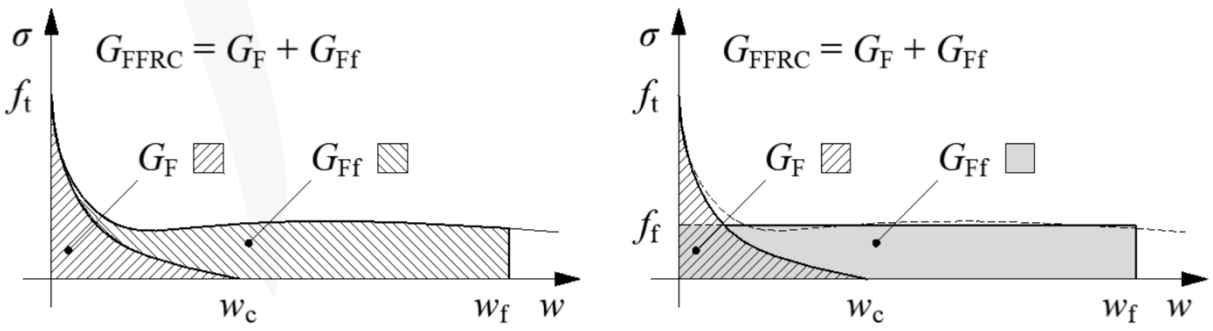


Figure 4: (a) Fracture energy of FRC (b) Tensile function used in the calculations

This document is the intellectual property of the fib – International Federation for Structural Concrete. All rights reserved.
This PDF of fib Bulletin 95 is intended for use and/or distribution solely within fib National Member Groups.

When stresses exceed the tensile strength of the concrete it will crack. There will be residual stress at the crack surface that is dependent on the crack width opening distance. This stress is associated with an energy, called fracture energy (G_F). Fibres increase this fracture energy (G_{Ff}), thereby making the concrete a more ductile material. The most important criterion for the selection of the FRC material model is to be able to model this increased fracture energy ($G_{F,FRC}$) and select a value that is appropriate to the FRC used for a design (see Figure 4).

3 Precast concrete tramlines

Another important trend in tramline structures is the precast concrete track slabs. These elements are made in precast concrete factories and transported to site. These elements will be subjected to other loads beside above their final load cases such as early age demoulding, rotation, lifting, stacking, transporting and installation on site. Usually these elements are made from concrete with higher strengths i.e. from C40/50 than the cast in place slabs i.e. from C25/30. Generally the precast elements have a higher dosage of macro synthetic fibre to the track slabs that are cast in place.

3.1 The PCAT system

PreCast Advanced Track (PCAT) is a precast concrete slab structure (Hammond, 2016). PCAT is a lightweight slab structure manufactured entirely from macro synthetic fibre reinforced concrete without steel reinforcement being required. This ensures that if the concrete cracks there is no steel to corrode providing a long life structure, as fibres continue right to the edge of the structure and so enhances durability and resistance to accidental damage. The use of fibre reinforcement in precast slab structures can also reduce maintenance, material costs and the fibre reinforcement is safer to handle than steel during manufacture. The PCAT slab design is based on a channel beam upper profile which provides a high modulus slab structure which maximising the slab's strength and minimises the stiffness needed for the track foundation.

The slabs connect to each other with a dry male female joint for initial alignment and then with curved bolt connections. This is designed to permit the rapid laying and joining process to form the monolithic structure. Curved steel connectors between adjacent units are easily inserted and tensioned from the slab surface as erection proceeds. This allows rapid installation to take place from the newly laid track even in tunnels with restricted space. Uniquely, if needed, PCAT slabs can be simply decoupled, levels adjusted or slabs removed and replaced without affecting the rest of the track structure.

Two types of slabs were developed to serve all potential installation requirements. One is aforementioned standard slab (off-street slab) with the side beams which is highly optimised and can easily installed. The other one is a more robust structure but with a straight upper surface and with hidden rails (on-street slab). This type of the slab can be used in streets and thanks to the sunk rails the traffic can easily cross the slab. The maximum length of both types is 5000 mm, the minimum thickness of the off-street slab is 150 mm and the thickness under the rails in case of on-street slab is 200 mm. The slabs were designed for 120 year lifetime.

This document is the intellectual property of the fib – International Federation for Structural Concrete. All rights reserved.
This PDF of fib Bulletin 95 is intended for use and/or distribution solely within fib National Member Groups.

3.2 Finite element model of the structure

The numerical modelling of the PCAT slabs were done with ATENA finite element software. The finite element models of the structures can be seen in Figure 5. The goal of using FEA was to design the slab and see the deformation and crack propagation in different loading scenarios.

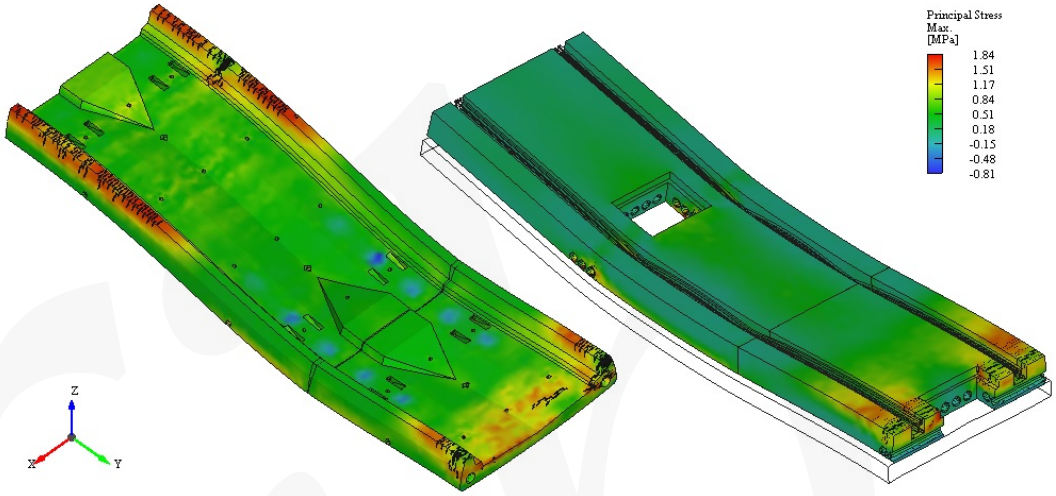


Figure 5: Principal stresses and cracks in deformed ATENA model

To ensure that the design model reflected the real structure's behaviour, all the details were modelled including the connection ducts, the injection holes, the rail sleepers and the rails with their exact geometry. A one and a one half slab was modelled to be able to investigate the behaviour of the joints. For the connecting surface an interface material was determined, which could only support compression stresses. During the loading process it was found that the slabs could open along the connection surface and the ducts bear the tension stresses. Under the slabs a bedding layer and a HBM (Hydraulically Bound Mixture) layer was modelled. For the subgrade non-linear springs were used. To investigate the effect of the soil parameters all the models were checked for a higher stiffness (350 MPa) and a lower stiffness (175 MPa) HBM layer.

In the model various material model configurations were used for the different structural elements. For the concrete slab the previously presented concrete material was used. For modelling the subbase and the subgrade linear elastic materials were used with different elastic moduli. The same material model was used for the sleepers as well. For the steel elements, such as the rails and connection cables a Von Misses material model was used which could handle the yield of the steel elements. Two different interface elements were used, one to model the friction between the concrete slab and the steel duct, and one to model the transfer of the compression forces between the two slabs. The parameters were determined in both case to be as close to the real behaviour as possible.

To check all the possible effects on the slabs, different loading scenarios were carried out in the finite element software as its lifecycle the track slab will be subjected to various conditions. Because the slab is pre-cast the first loading will come from demoulding of the element. In this case a time dependent material model was used, which means the material

This document is the intellectual property of the fib – International Federation for Structural Concrete. All rights reserved.
This PDF of fib Bulletin 95 is intended for use and/or distribution solely within fib National Member Groups.

parameters changed during the analysis following the hardening of the concrete. With this analysis the optimum demoulding time can be estimated as well. To the demoulding load a lifting and tearing force was added to the early age concrete slab. After this, but also in early ages, a rotation effect occurs: the demoulding was made upside down, but the racking of the precast slabs were in the other direction. In this two load case the lifting and rotating of the elements were also checked. The next situation was the storing load case. In this case the weight of three elements were added to the slab, simulating the effect of the stacking. The highlighted design target was to check the ultimate and serviceability limit states under the train's load and thus the geometry of the trains were added. To examine the worst loading case, and to model the passage of the train, seven different loading scenarios were carried out in different positions. In the Ultimate Limit State (ULS) the principal stresses were checked and in the Serviceability Limit State (SLS) the crack widths and the vertical displacements were checked. During the calculation the unequal rail loading was also taken into consideration. To be able to calculate the effect of the cyclic loading fatigue analysis was done also for all the loading positions. The number of the cycles were calculated back from the estimated lifetime of the structure and the average daily traffic, and it leads to 20 000 000 cycles. The finite element software calculated two additional fatigue strains for the maximum fracturing strain (Pryl et al. 2010), one handled the tensile strength reduction during the cyclic load (according to the Wöhler curve), and the other takes into consideration the crack opening effect during the cyclic load.

The structure complied with all the design requirements both in ULS and in SLS. In ULS the target was that the structure resists the loads with the appropriate safety factors and with design material parameter values without the failure of the structure. In SLS the aim was that the crack widths should be less than the value according to Eurocode 2 (0.2 mm). Both design cases met the requirements in every loading position and design situation. The slabs deformation followed the expectation under the different loads. The connection between the two slabs worked well. It also can be seen that the structure is highly optimized. In ULS several cracks appeared in the surface of the structure, but without failure, and in SLS almost no visible cracks appeared in the structure.

3.3 Real scale test

The PCAT slab was installed within their test pit to measure the actual deflection of the slab along the structure using an applied load at various locations. The position of the load was replicated the arrangement used in the FEM simulation. The PCAT off-street slab was designed for 12 tonne axle loads. For the testing it was proposed, after the first suite of loading at 8 tonne that the load be increased in 4 tonne increments up to 24 tonne, subject to slab performance during the test. It was a static test, no cyclic loading was applied to the structure in this phase of testing. Table 1 shows the concrete mix design used for the slabs.

1. Table: Concrete mix design

Materials	**Batch Weight [kg/m^3]**
Aggregate 1: 4/10mm limestone	802
Aggregate 2: 0/4mm Sand	842
Limestone Powder	130
Cement: Cem I Class 52.5N	400
Fibres: synthetic fibres	5.0
Admixture: Superplasticizer	3.0

This document is the intellectual property of the fib – International Federation for Structural Concrete. All rights reserved.
This PDF of fib Bulletin 95 is intended for use and/or distribution solely within fib National Member Groups.

The loading of the slab was carried out using the Rail Trackform Stiffness Tester (RTST) (Figure 6) which was been developed by AECOM to replicate the loading requirements of high-speed or heavy-haul lines through the use of an increased range of pulse-loading conditions. The RTST apparatus is mounted on a transport frame that can be moved along on rubber-caterpillar tracks whilst off track and then switched to rail wheels. On ballasted track geophones measure the deflection response of the ballast, sub-ballast, formation and subgrade enabling assessment of layer stiffness. During testing of the PCAT slab an array of 9 geophones were positioned above the concrete slab surface to record the deflection in microns.

To ensure the previously presented numerical model's property, a finite element analysis was calculated for the RTST test. The model contained the whole test setup including: the concrete pit, the compacted soil, and the two slabs with the previously mentioned detail. The effect of the RTST was added to the slab with using a steel plate which corresponds to the loading beam's foot. The measured value in the finite element model was the vertical deflection. It was measured at 9 different points replicating where the geophones were positioned for the actual test. The position of the loading plate in the finite element model followed the RTST machines position in the test. The measuring points were according to Figure 6.

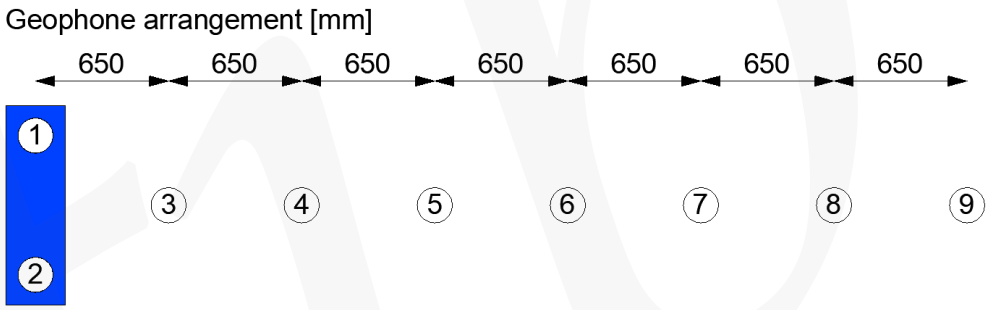


Figure 6: The measuring points of RTST testing (AECOM PCAT Test report)

The results in every loading case were close to each other. The finite element analysis closely mirrored what happened in reality and the differences between the measured deflections in the model and in the test was less than 0.1 mm. Only one loading scenario was where the difference was higher than modelled and this was where the load was positioned over the female joint. This was outlined in the AECOM report which determined a very poor subgrade stiffness in this area. The results of the test and the FEA can be seen in Figure 7.

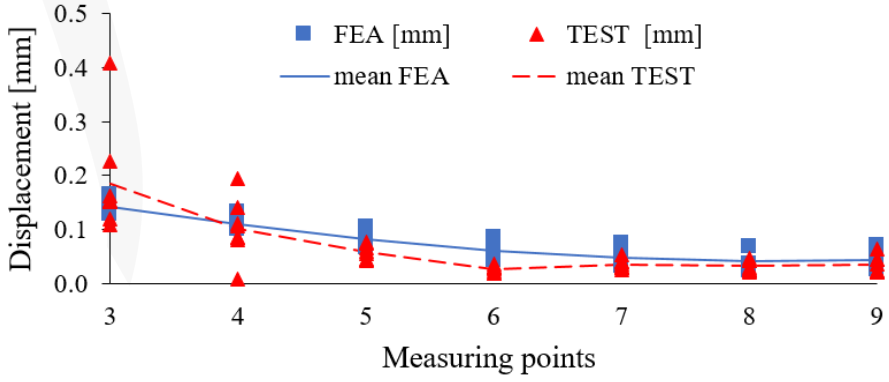


Figure 7: Results of RTST and FEA

This document is the intellectual property of the fib – International Federation for Structural Concrete. All rights reserved.
This PDF of fib Bulletin 95 is intended for use and/or distribution solely within fib National Member Groups.

4 Summary

The use of macro synthetic fibre reinforced concrete has become more and more popular in the building industry and thus also in the concrete track slab constructions. Track slab structures are typically heavily exposed to weather and mechanical loads, and because of this must have sufficient ductility and durability. At the same time the repair or replacement of these elements is difficult as generally the traffic must be stopped for a long periods during this process. Based on these criteria the use of macro synthetic fibre is a good alternative reinforcement to mesh and steel bars. The concrete reinforced with the already mixed in corrosion-free fibres is easy to handle and the track slab can be constructed faster, thus by using FRC, labour can be decreased and the ductility increased. Further macro synthetic fibres are better for dynamic loads also, which is a significant advantage of this type of construction.

Design and optimizing of the track slab means the determining of the required thickness of the track slab and the macro synthetic fibre dosage for the varying load cases, such as ultimate and serviceability limit state, and fatigue. For these special tasks advanced finite element software is needed. The influence of the fibres could be taken into account by the modification of the fracture energy of the plain concrete. These design models have been validated by full scale laboratory tests.

5 References

Cervenka, J., Papanikolaou, V. K. (2008), *Three dimensional combined fracture-plastic material model for concrete*, International Journal of Plasticity (24) pp. 2192-2220.

EUROCODE EN 1992 (2004), *European Code for design of concrete structures: European Committee for Standardization*, Brussels.

Hammond, J. (2016), *Construction and Reinforcement*, Railing Professional October 2016 Issue, pp. 162-163.

ITAtech Activity Group Support 2015, (2015), *ITAtech Design Guidance For Precast Fibre Reinforced Concrete Segments*, ITAtech Report n7, draft.

Juhász K. P. (2013), *Modified fracture energy method for fibre reinforced concrete*, Fibre Concrete 2013: Technology, Design, Application, pp. 89-90.

Kolmar, W. (1986), *Beschreibung der Kraftuebertragung über Risse in nichtlinearen Finite-Element-Berechnungen von Stahlbetontragwerken*, Dissertation, T.H. Darmstadt.

Menétrey, P., William, K. J. (1995), *Triaxial Failure Criterion for Concrete and Its Generalization*, ACI Structural Journal, 92(3), pp. 311-318.

Nagy J., Juhász K. P., Mészáros A. (2014), *The beginning: the tramway in Szeged*, Innoteka, 2014 September, pp. 24-25.

Nagy J., Juhász K. P., Herman S., Herman K. (2015a), *Az első magyar, műanyag szállal erősített és füvesített villamospálya 1. rész (The first Hungarian synthetic fibre reinforced and grassed tramline 1st part)*, Sínek világa, 2015/2, pp. 18-21.

Nagy J., Juhász K. P., Herman S., Herman K. (2015b), *Az első magyar, műanyag szállal erősített és füvesített villamospálya 2. rész (The first Hungarian synthetic fibre reinforced and grassed tramline 2nd part)*, Sínek világa, 2015/3, pp. 10-14.

Ridout, A. (2009), *Macro-fibre-reinforced concrete slab track*, Concrete, September 2009, pp. 16-18.

Vandewalle, L., et al. (2002), *RILEM TC 162-TDF : Test and design methods for steel fibre reinforced concrete,* Materials and Structures, Vol. 33, January-February 2000, pp 3-5.

This document is the intellectual property of the fib – International Federation for Structural Concrete. All rights reserved.
This PDF of fib Bulletin 95 is intended for use and/or distribution solely within fib National Member Groups.
FRC2018: Fibre Reinforced Concrete: from Design to Structural Applications
Joint ACI-*fib*-RILEM International Workshop

Closed-form Solutions for Interaction Diagrams of Hybrid Fiber-Reinforced Tunnel Segments

Yiming Yao[1], Mehdi Bakhshi[2], Verya Nasri[2], Barzin Mobasher[3]

[1] : Key Laboratory of Concrete and Prestressed Concrete Structures of Ministry of Education, School of Civil Engineering, Southeast University, Nanjing, China.

[2] : AECOM, New York, United States.

[3] : Arizona State University, Tempe, United States.

Abstract

Precast concrete segments are the predominant support method used in tunnels dug by Tunnel Boring Machines (TBM) in soft ground and weak fractured rock, providing the initial and final ground support. Conventionally, steel bars are used in concrete segments to resist tensile stresses due to all loading cases from the time of casting through service condition. With traditional reinforcement, a significant amount of time and labor are needed to assemble the cages and place the reinforcing bars. Fiber reinforced concrete (FRC) has become more attractive for its use in tunnel lining construction as a result of improved post-cracking performance, crack control characteristics and capability of partial replacement of steel bars. Due to the strength requirements in large-diameter tunnels, which are subjected to embedment loads and TBM thrust jack forces, the use of FRC is not adequate as the sole reinforcing mechanism. Therefore, the hybrid fiber-reinforced concrete (HRC) combining both rebars and steel fibers is frequently used in practice. Tunnel segmental linings are designed for load cases that occur during manufacturing, transportation, installation, and service conditions. With the exception of two load cases of TBM thrust jack forces and longitudinal joint bursting load, segments are subjected to combined axial force and bending moment. Therefore, P-M interaction diagrams have been used as the main design tool for tunnel engineers.

Standard FRC constitutive laws recently allow for a significant residual strength in tension zone below the neutral axis. However, design capacity of HRC segment is significantly underestimated using conventional Whitney's rectangular stress block method, especially for tension-controlled failure, since the contribution of fibers in tension zone is ignored. Methods that currently incorporate contribution of fibers on P-M diagrams are based on numerical and finite-element analyses, which are normally more complicated and not readily to be implemented for practical design tools. Closed-form solutions of full-range P-M interaction diagram considering both rebar and fiber contributions are presented in this paper for HRC segments. The proposed model is verified with experimental data of compression tests with eccentricity as well as other numerical models for various cases of HRC sections. Results show that using appropriate material models for fiber and reinforcing bar, engineers can use the proposed methodology to obtain P-M interaction diagrams for HRC tunnel segments.

Keywords

Analytical method; fiber; hybrid fiber-reinforced concrete; interaction diagram; tunnel, lining; residual strength; segment; TBM

This document is the intellectual property of the fib – International Federation for Structural Concrete. All rights reserved.
This PDF of fib Bulletin 95 is intended for use and/or distribution solely within fib National Member Groups.

1 Introduction

Precast concrete segments reinforced with steel bars are the predominant support method used in tunnels dug by Tunnel Boring Machines (TBM), where a significant amount of time and labor are needed to assemble the cages and place the reinforcing bars (Bakhshi and Nasri 2014a; b). Alternatively, fibers may considerably improve the concrete post-cracking behavior, and allow for better crack control and shrinkage, fatigue and impact resistance (Bakhshi and Nasri 2015; Briffaut et al. 2016). In addition, fibers may enhance handling and placement of precast concrete segments by reducing job-site labor requirements. Furthermore, uniform dispersion of fibers throughout the segment guarantees the presence of the reinforcement action in areas around the segment face, where bursting and spalling stresses develop during the TBM jacking process (Bakhshi and Nasri 2014c; d). The use of FRC is sometimes not adequate as the sole reinforcing material, especially for large diameter tunnels. Therefore, a hybrid solution of combined rebar and fiber reinforcement has been adopted (Plizzari 2009; Tiberti et al. 2015). In shallow large-diameter tunnel segments, low internal axial forces and high bending moments as well as high TBM thrust forces are present. Such loading conditions impose high localized flexural, bursting and spalling stresses that can be better resisted by reinforcing bars than fibers (Tiberti 2009). Also, in large-diameter tunnels with an increased ratio between the tunnel diameter and lining thickness, segments are more likely to withstand the high flexural stresses due to imperfections and irregular construction (Tiberti 2009).

Tunnel segmental linings are mainly subjected to combined axial force and bending moment due to multiple loading cases that occur during manufacturing, transportation, installation, and service conditions (ACI 544 2016). Axial force-bending moment interaction (P-M) diagram is therefore an important tool that tunnel engineers use for the structural design. This diagram, originally presented by Whitney and Cohen (1956), continues to be widely used today (Hernandez-Montes et al. 2005) and has been investigated extensively by numerous researchers (Bresler 1960; Parme et al. 1966; Rotter 1985). However, most of the work carried out using the Whitney's rectangular stress block only considers concrete strength in compression zone, which significantly underestimated the design capacity of FRC or hybrid fiber-reinforced concrete (HRC) tunnel segments. ACI 544.7R (ACI 544 2016) presents a simplified method for derivation of the P-M interaction diagram for precast concrete segments reinforced solely by fibers. However, the method cannot be extended to HRC segments using a superposition approach as steel material model was not considered. Methods that incorporate contribution of fibers and steel rebar in the tensile zone of cross section are based on numerical and finite-element analyses to construct the P-M interaction diagrams of HRC sections (Chiaia et al. 2007, 2009; de la Fuente et al. 2012; Tiberti 2009). Despite of popularity and abundance of numerical methods, closed-form solutions offer important advantages for engineering problems including computational efficiency, readily parametric studies, and easy to be implemented into a simple and user-friendly spreadsheet program. Mobasher et al. (2015) derived closed-form solutions for analysis of flexural load-deflection of HRC beams subjected to pure bending. Although, this methodology has been proved robust in design of HRC elements subjected to pure bending, the model needs to be significantly modified so that the effects of axial forces on flexural capacity can be fully captured.

This paper presents material models, derivations and for the first time, closed-form solutions to construct a full range P–M interaction diagram of HRC segments considering the

This document is the intellectual property of the fib – International Federation for Structural Concrete. All rights reserved.
This PDF of fib Bulletin 95 is intended for use and/or distribution solely within fib National Member Groups.

contributions of fibers in the post-cracking strength in addition to reinforcing bars. The proposed methodology covers all the failure modes in the tunnel precast segments subjected to the combined axial forces and bending moments. Parametric studies for key design parameters are presented. The model is verified by simulating experimental results from published data for HRC columns and several other model-predicted and numerical results for HRC precast segmental and cast-in place concrete tunnel linings. A spreadsheet based program has also been developed and available for general users to readily construct the interaction diagram with the present method. The proposed P–M diagram based on the associated program can be used as a tool for design of HRC tunnel segments especially in large diameter tunnels.

2 Model Derivations

2.1 Multi-linear stress-strain models

The objective of this study is to develop the analytical closed-form solutions of the P-M interaction diagram of the HRC section. Fig. 1 presents three distinct material models used in the derivation of parametric response of HRC beams addressing concrete and steel's tensile and compressive piecewise linear constitutive laws. Note that material variables are normalized with respect to tensile modulus E and the first cracking tensile strain ε_{cr}. Fig. 1(a) shows the tension model with an elastic tensile stress with modulus E increasing up to the first cracking tensile strength of coordinates (ε_{cr}, σ_{cr}). In the post-crack region, the tensile stress is constant at $\sigma_p = \mu\sigma_{cr} = \mu\varepsilon_{cr}E$ and terminates at the ultimate tensile strain $\varepsilon_{tu} = \beta_{tu}\varepsilon_{cr}$. The simplified bilinear tension model is capable of covering a wide range of tension softening behavior exhibiting both deflection-hardening and deflection-softening responses in flexure (Soranakom and Mobasher 2007). Strain hardening behavior, which normally requires high steel fiber dosages (1-2% by volumetric fraction or a dosage of 77-154 kg/m^3), can be also captured by extending the proposed tension model and including a hardening branch (Yao 2016). Fig. 1(b) shows the elastic-perfectly plastic compression response with a modulus $E_c = \gamma E$. The plastic range initiates at strain $\varepsilon_{cy} = \omega\varepsilon_{cr}$ corresponding to yield stress $\sigma_{cy} = \omega\gamma\varepsilon_{cr}E$ and terminated at $\varepsilon_{cu} = \lambda_{cu}\varepsilon_{cr}$. The effect of lateral ties on the compressive behavior is characterized by an improved compressive strength $\sigma_{cy,c} = \omega_c\gamma\varepsilon_{cr}E$ and ultimate strain $\varepsilon_{cu,c} = \lambda_{cu,c}\varepsilon_{cr}$. Fig. 1(c) is the elastic-perfectly plastic steel model using yield strain and stress of $\varepsilon_{sy} = \kappa\varepsilon_{cr}$ and $f_{sy} = \kappa n\varepsilon_{cr}E$. Stress-strain curve of steel is terminated at the specified strain limits defined by the design codes discussed in the following sections. Fig. 1(d) shows the steel parameters defined as area $A_s = \rho_g bh$ at the reinforced depth αh for both compression and tension rebar. The compression reinforcement ratio, ρ_g', is assumed equal to the tension reinforcement ratio, ρ_g, throughout this study.

The material models for tension and compression of FRC and steel rebar are presented as:

$$\sigma_t(\varepsilon_t) = \begin{cases} E\varepsilon_t & 0 \le \varepsilon_t \le \varepsilon_{cr} \\ \mu E\varepsilon_{cr} & \varepsilon_{cr} < \varepsilon_t \le \varepsilon_{tu} \\ 0 & \varepsilon_t > \varepsilon_{tu} \end{cases} ; \quad \frac{\sigma_t(\beta)}{E\varepsilon_{cr}} = \begin{cases} \beta & 0 \le \beta \le 1 \\ \mu & 1 < \beta \le \beta_{tu} \\ 0 & \beta > \beta_{tu} \end{cases} \tag{1}$$

This document is the intellectual property of the fib – International Federation for Structural Concrete. All rights reserved.
This PDF of fib Bulletin 95 is intended for use and/or distribution solely within fib National Member Groups.

unconfied :

$$\sigma_c(\varepsilon_c)=\begin{cases}E_c\varepsilon_c & 0\le\varepsilon_c\le\varepsilon_{cy}\\ E_c\varepsilon_{cy} & \varepsilon_{cy}<\varepsilon_c\le\varepsilon_{cu};\\ 0 & \varepsilon_c>\varepsilon_{cu}\end{cases}\qquad \frac{\sigma_c(\lambda)}{E\varepsilon_{cr}}=\begin{cases}\gamma\lambda & 0\le\lambda\le\omega\\ \gamma\omega & \omega<\lambda\le\lambda_{cu}\\ 0 & \lambda>\lambda_{cu}\end{cases}$$

confined :

$$\sigma_{c,c}(\varepsilon_c)=\begin{cases}E_c\varepsilon_c & 0\le\varepsilon_c\le\varepsilon_{cy,c}\\ E_c\varepsilon_{cy,c} & \varepsilon_{cy,c}<\varepsilon_c\le\varepsilon_{cu,c};\\ 0 & \varepsilon_c>\varepsilon_{cu,c}\end{cases}\qquad \frac{\sigma_{c,c}(\lambda)}{E\varepsilon_{cr}}=\begin{cases}\gamma\lambda & 0\le\lambda\le\omega_c\\ \gamma\omega_c & \omega_c<\lambda\le\lambda_{cu,c}\\ 0 & \lambda>\lambda_{cu,c}\end{cases}\qquad (2)$$

$$f_s(\varepsilon_s)=\begin{cases}E_s\varepsilon_s & 0\le\varepsilon_s\le\varepsilon_{sy}\\ E_s\varepsilon_{sy} & \varepsilon_s>\varepsilon_{sy}\end{cases};\qquad \frac{f_s(\chi)}{E\varepsilon_{cr}}=\begin{cases}n\chi & 0\le\chi\le\kappa\\ n\kappa & \chi>\kappa\end{cases}\qquad (3)$$

where normalized independent variables for strains are defined as $\beta=\varepsilon_t/\varepsilon_{cr}$, $\lambda=\varepsilon_c/\varepsilon_{cr}$ and $\chi=\varepsilon_s/\varepsilon_{cr}$.

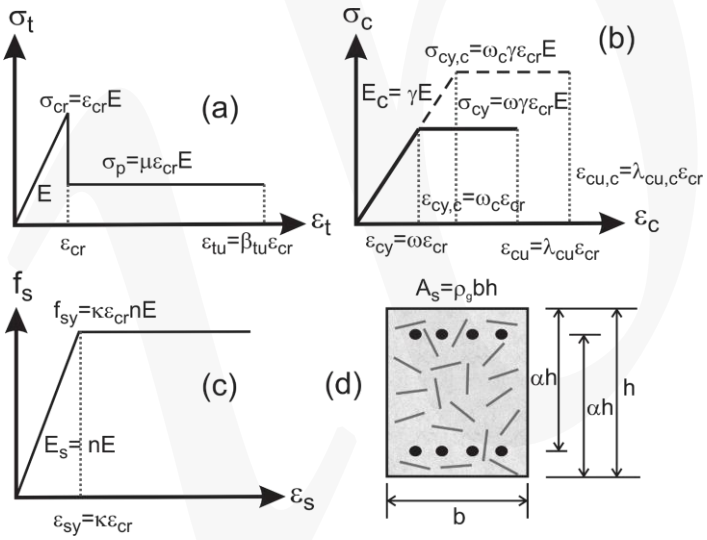


Fig. 1: *Material models including (a) FRC tensile model, (b) FRC compressive model, (c) steel model, (d) cross section.*

Demands of sufficient ductility of members under compression and bending actions require the use of lateral confinement, which results in a modification of the effective stress-strain relationship in compression. Since the present model is developed based on normalized parameters, the improved strength and strain limits due to confinement can be directly assigned according to the specific design considerations and available experimental data. A numerical example was given by authors (Yao et al. 2018) to incorporate fib Model Code equations into lateral confinement effects on compressive strength and ultimate strain.

2.2 Derivation of axial force and bending moment

In derivation of axial force (P) and bending moment (M) for a rectangular cross section, the assumption of plane section remaining plane is used. Axial and flexural deformations are incrementally imposed by taking the normalized strain at the bottom extreme fiber β as the

This document is the intellectual property of the fib – International Federation for Structural Concrete. All rights reserved.
This PDF of fib Bulletin 95 is intended for use and/or distribution solely within fib National Member Groups.

independent variable (λ represents the strain at the top extreme fiber). In this study, the compressive strain is defined as positive, and the stress and force terms follow the same sign convention. The stress distributions are obtained by applying linear strain distribution across the depth using the material models mentioned in section 2.1. Different modes of failure including all compression, compression-controlled and tension-controlled are determined depending on the strain at bottom extreme fiber and strain of steel.

The stress distributions of different modes of failure are shown in Fig. 2. The Mode 1 corresponds to range where the entire cross section is under compression, with two sub-modes: 1.1 extreme compression fiber exceeds yield strain in compression ($\lambda \geq \omega$), 1.2 extreme compression fiber does not exceed yield strain in compression ($0 < \lambda < \omega$); Mode 2 corresponds to compression controlled failure where the steel in tensile region has not yielded ($-\kappa \leq \chi \leq 0$), which also includes two sub-modes: 2.1 no tension crack ($-1 \leq \beta \leq 0$) and 2.2 tension crack ($\beta<-1$). Finally, Mode 3 corresponds to the tension controlled failure ($-0.005/\varepsilon_{cr} < \chi \leq -\kappa$) with two scenarios existing in each sub-stage: 3.1 when the compression steel is elastic or 3.2 when the compression steel is yielding. Under modes 2 and 3, where the bottom extreme fiber is in tension ($\beta < 0$), a parameter k is introduced to represent the normalized height of natural axis:

$$kh = h_{c1} + h_{c2}$$
$$\frac{\lambda_{cu}\varepsilon_{cr}}{kh} = \frac{-\beta\varepsilon_{cr}}{h-kh} \quad or \quad \beta = -\frac{1-k}{k}\lambda_{cu} \tag{4}$$

The stresses are then integrated over the area in each zone to obtain the parametric solutions of force terms, and the solution for the depth of neutral axis can be obtained analytically. Internal moment is obtained by integrating the force components using the distance to the center line as the moment arm. Normalized force and moment in different modes are presented in Table 1, where the force (P_i) and moment (M_i) are normalized with respect to the values P_{cr} and M_{cr} at tensile cracking:

$$P_i = P_i' P_{cr}; \qquad P_{cr} = bhE\varepsilon_{cr} \tag{5}$$

$$M_i = M_i' M_{cr}; \qquad M_{cr} = \frac{1}{6}bh^2 E\varepsilon_{cr} \tag{6}$$

Strain limits of the materials are required by design codes to ensure sufficient ductility of structural members. Ultimate compressive strain of concrete and ultimate tensile elongation of reinforcing steel are normally specified as the ductility limits of RC sections. For example, ACI 318-14 (2014) and CSA 23.3-14 (CSA 2014) specify a maximum concrete compressive strain of 0.003 for normal strength concrete (NSC) and at least 14% elongation for ductile steel. fib Model Code 2010 (2013) uses a maximum strain of 0.0035 for NSC with characteristic strength up to 50 MPa which reduces to 0.0028 for high strength concrete (HSC) up to 90 MPa. Four ductility classes were defined for reinforcing steel with characteristic elongation at maximum force up to 8%. The present model is derived based on two ultimate variables for ultimate strain in the extreme compression fiber of ε_{cu}, and ultimate tensile strain of β_{tu}. The desired strain limits can be assigned to the model parameters to accommodate the design codes of different countries as well as materials strength, classes and confinement conditions.

This document is the intellectual property of the fib – International Federation for Structural Concrete. All rights reserved.
This PDF of fib Bulletin 95 is intended for use and/or distribution solely within fib National Member Groups.

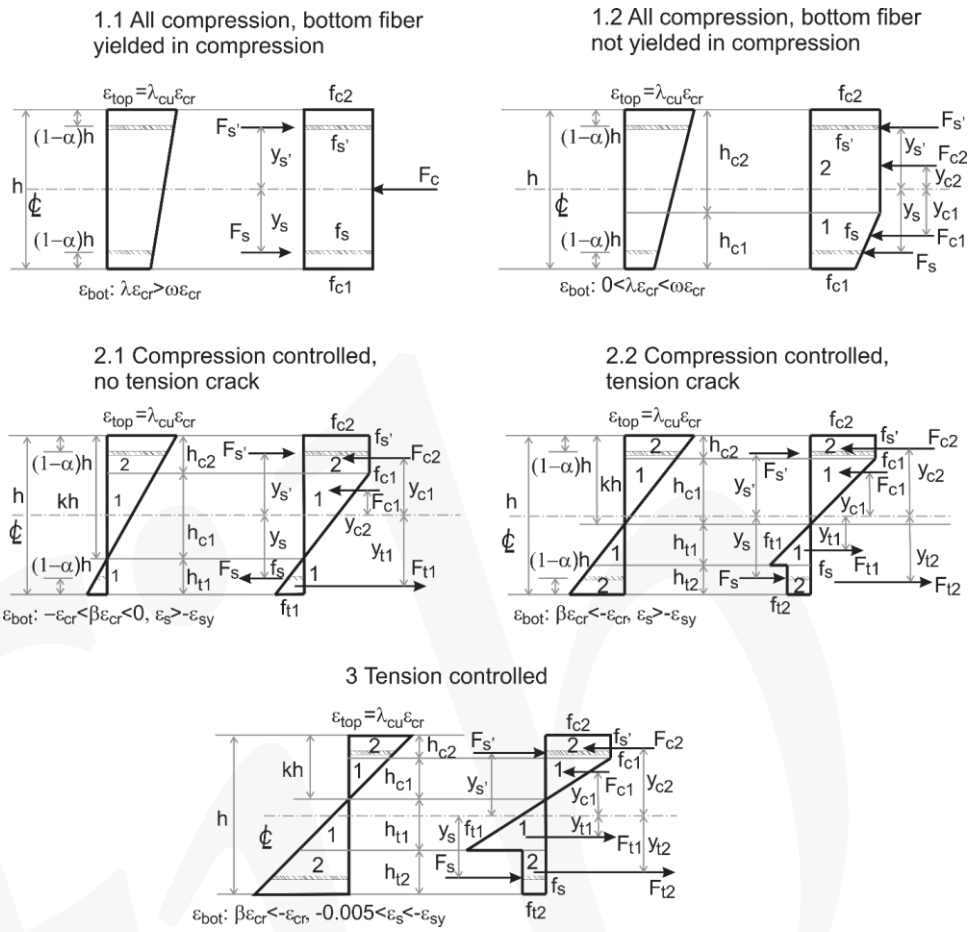


Fig. 2: *Strain and stress diagrams at different failure modes including 1.1 all compression with bottom fiber yielded in compression, 1.2 all compression while bottom fiber is not yielded, 2.1 compression controlled, no tension crack, 2.2 compression controlled with crack in tension, 3 tension controlled.*

Using the derivations for axial force and bending moment under different cases, one can generate P-M interaction diagram based on intersections of two competing modes and the shorter length of the P-M Vector. A MATLAB code and an interactive spreadsheet were developed to implement the analytical expressions. A base numerical model for normal strength HRC is used to illustrate the modelling procedure with material properties: σ_{cy} = 40 MPa, E = 30 GPa, ε_{cr} =110(10)$^{-6}$, ε_{cu} = 0.0035, σ_p = 1.1 MPa, E_s = 210 GPa, f_{sy} = 500 MPa, ρ_g = 0.25%, steel elongation to failure of 12%, and reinforcement depth ratio 0.9. The normalization of parameters results in : μ =*0.33,* β_{tu} = 2000, γ = 1.0, ω = 12, λ_{cu} = 32, n = 7, κ = 19, and α = 0.9. Note that the full range interaction diagram can be obtained at much lower steel strain values compared to the elongation to failure, so the maximum β attained in this case was 776. The normalized interaction diagram is shown in Fig. 3, with all the modes of potential failure identified.

This document is the intellectual property of the fib – International Federation for Structural Concrete. All rights reserved.
This PDF of fib Bulletin 95 is intended for use and/or distribution solely within fib National Member Groups.

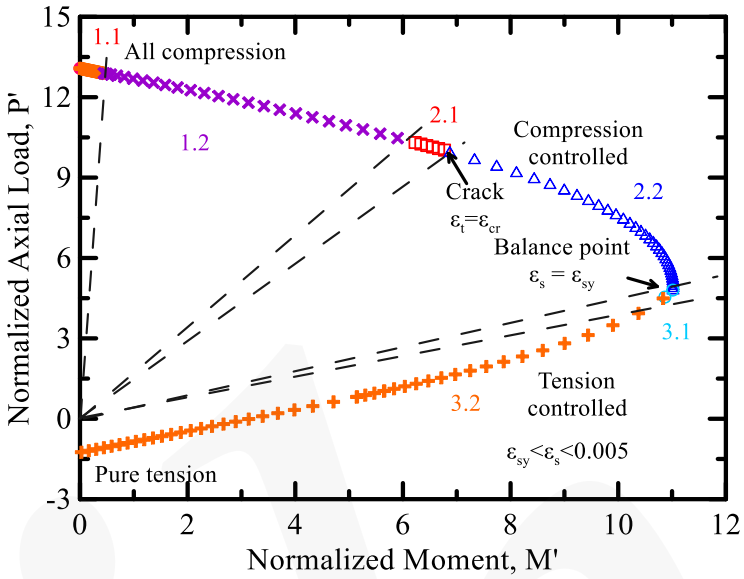


Fig. 3: Normalized P-M diagram showing different failure modes.

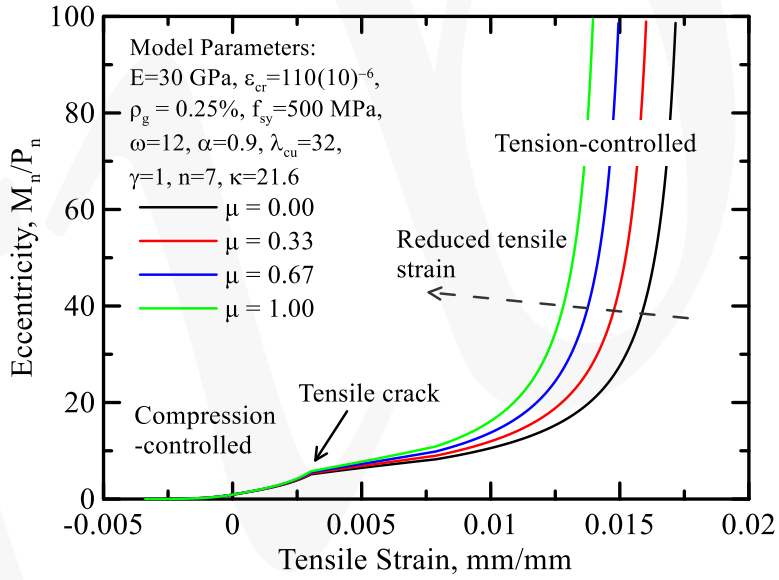


Fig. 4: Normalized P-M diagram showing different failure modes including 1.1 all compression

Besides the interaction diagram, the force and/or moment responses at limit states can also be correlated with the ductility parameters such as the strain and curvature. Serviceability based design limits can be readily identified and the effects of main parameters can also be revealed. Fig. 4 illustrates the variations of tensile strain at the extreme fiber with the eccentricity e (M_n/P_n), where the effects of μ are investigated. Two stages of low and high eccentricities are identified in the curves. The behavior in the first stage is dominated by compressive action when steel fibers have not played a role yet. As bending moment increases and the first tensile crack occurs, the behavior gradually turns into flexural action and the mode of failure is dominated by tension. In this stage, the effects of fiber bridging are more pronounced in improving the moment capacity and reducing the deformation at same loading level. As Fig. 4 shows, considerable reduction in tensile strain is observed with

This document is the intellectual property of the fib – International Federation for Structural Concrete. All rights reserved.
This PDF of fib Bulletin 95 is intended for use and/or distribution solely within fib National Member Groups.

increasing μ value. Since stress-strain (σ-ε) relation based on continuous mechanics is used in this model, the tensile strain actually represents the average strain distribution over a region limited by a length parameter called characteristic length l_{cs}. The characteristic length connects the strain to crack opening within this region, which can be expressed by $w = l_{cs}\varepsilon$ (di Prisco et al. 2013). Therefore, the reduction in tensile strain essentially corresponds to the reduced crack opening with addition of steel fibers.

Table 2: Normalized force and moment for each mode

Parameter	Mode	Normalized expression
Force	1.1	$P_{11}^{'} = 2\kappa n\rho_g + \omega\gamma$
	1.2	$P_{12}^{'} = \dfrac{(\lambda^2 + \omega^2 - 2\omega\lambda_{cu})\gamma + 2n\rho_g(\chi+\kappa)(\lambda-\lambda_{cu})}{2(\lambda-\lambda_{cu})}$
	2.1	$P_{21}^{'} = -\dfrac{(\omega^2\gamma - 2\omega\gamma\lambda_{cu} + \beta\lambda_{cu})k}{2\lambda_{cu}} + n\rho_g(\chi+\kappa) + \dfrac{\beta}{2}$
	2.2	$P_{22}^{'} = (-\dfrac{\omega^2\gamma}{2\lambda_{cu}} + \omega\gamma)k + \dfrac{2\beta\mu + 2\mu - 1}{2\beta}(k-1) + n\rho_g(\chi+\kappa)$
	3.1	$P_{31}^{'} = (-\dfrac{\omega^2\gamma}{2\lambda_{cu}} + \omega\gamma)k + \dfrac{2\beta\mu + 2\mu - 1}{2\beta}(k-1)$
	3.2	$P_{32}^{'} = (-\dfrac{\omega^2\gamma}{2\lambda_{cu}} + \omega\gamma)k + \dfrac{2\beta\mu + 2\mu - 1}{2\beta}(k-1) - n\rho_g(\lambda_{cu}-\kappa) + \dfrac{n\rho_g(\alpha-1)}{k}\lambda_{cu}$
Moment	1.1	$M_{11}^{'} = 0$
	1.2	$M_{12}^{'} = \dfrac{C_1\lambda_{cu}^{\,2} + C_2\lambda_{cu} + C_3\beta^2 + 2\omega^3\gamma}{2(\beta-\lambda_{cu})^2}$
	2.1	$M_{21}^{'} = C_4k^2 + C_5k + C_6$
	2.2	$M_{22}^{'} = C_7k^2 + C_8k + C_9(\chi-\kappa) + C_{10}$
	3.1	$M_{31}^{'} = C_7k^2 + C_8k - 2C_9 + C_{10}$
	3.2	$M_{32}^{'} = C_7k^2 + C_8k + C_{11} + \dfrac{C_{12}}{k}$

where $k = \dfrac{\lambda_{cu}}{\beta+\lambda_{cu}}$, $C_1 = 6n\rho_g(2\alpha-1)(\chi-\kappa)$, $C_2 = 12\beta^2 n\rho_g(2\alpha+1)(\kappa-\chi) - 3\beta\gamma\omega(\omega-2\lambda_{cu})$,

$C_3 = \beta^2 C_1 - \gamma\omega^2(2\omega-3\lambda_{cu})$, $C_4 = -\dfrac{\omega^3\gamma}{\lambda_{cu}^{\,2}} + \dfrac{3\omega^2\gamma}{\lambda_{cu}} - 3\omega\gamma + \beta$, $C_5 = -\dfrac{1}{2}(\dfrac{3\omega^2\gamma}{\lambda_{cu}} - 6\omega\gamma + \beta)$,

$C_6 = 3n\rho_g(2\alpha-1)(\chi-\kappa) - \dfrac{\beta}{2}$, $C_7 = -\dfrac{\omega-3\lambda_{cu}}{\lambda_{cu}^{\,2}}\gamma\omega^2 - 3(\gamma\omega+\mu) - \dfrac{6\mu-3}{\beta} + \dfrac{3\mu-2}{\beta^2}$,

$C_8 = -\dfrac{3\gamma\omega^2}{2\lambda_{cu}} + 3(\gamma\omega+\mu) + \dfrac{18\mu-9}{2\beta} + \dfrac{6\mu-4}{\beta^2}$, $C_9 = -3n\rho_g(2\alpha-1)$, $C_{10} = -\dfrac{6\mu-3}{2\beta} - \dfrac{3\mu-2}{\beta^2}$,

$C_{11} = C_{10} - C_9(\kappa+\lambda_{cu})$, $C_{12} = C_9(1-\alpha)\lambda_{cu}$

This document is the intellectual property of the fib – International Federation for Structural Concrete. All rights reserved.
This PDF of fib Bulletin 95 is intended for use and/or distribution solely within fib National Member Groups.

3 Model verification

The proposed model is verified using a case study of precast tunnel lining segments reinforced by rebars and steel fibers. Tiberti (2009) performed numerical analysis on different case studies of the tunneling segments with internal diameters ranging from 7.25 m to 14.9 m. The effect of steel fibers was considered in the study by using a similar concept of residual tensile strength "χ" that ranges from 0 to 0.75. Each case was performed in two configurations: plain SFRC and HRC sections with ρ=0.4%. Other assumptions include the design compressive strength of the concrete f_{cd} = 22.7 MPa, tensile strength f_{cld} = 1.6 MPa, concrete modulus E = 35 GPa, design yielding strength of steel f_{yd} = 391 MPa and steel modulus E_s = 200 GPa. The case study of "Barcelona" lining with a tunnel diameter of 10.9 m is presented in this work by comparing the original analysis with the proposed model.

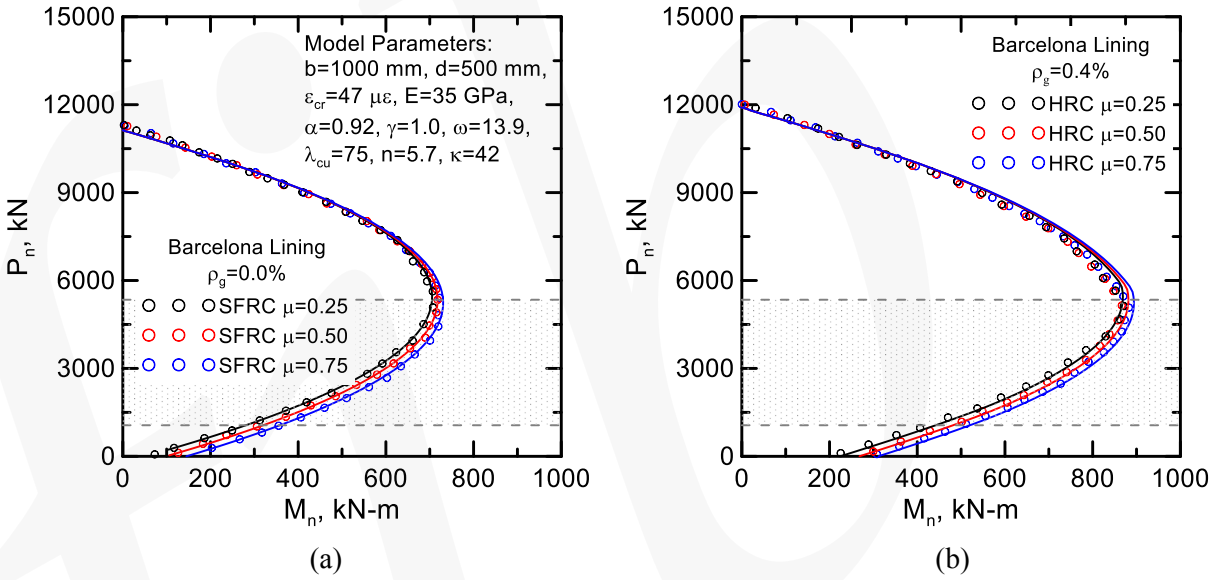


Fig. 5: P-M diagram for the Barcelona lining configuration: (a) SFRC section, and (b) HRC section (Tiberti 2009).

Fig. 5 compares the interaction diagrams for the sections made of SFRC and HRC for the Barcelona lining configuration. The geometries and model parameters are indicated in the figures. Same values of residual strength in original study are assigned to μ, which are 0.25, 0.50 and 0.75. Similarly, increments in the ultimate moment capacity are observed with increasing μ value. The shaded area represents the region of axial force under investigation which is referred to as "normal ring force" defined in the original study (range of tunnel overburden height considered from 1 to 4 times of the tunnel external diameter). It is shown that the range of normal ring force investigated is located in a favorable region of the domains where the fiber resistance is considerable.

Steven and Empelmann (2014) tested a series of UHPFRC columns reinforced high strength steel rebars (560 MPa) and 1.25% of steel fibers. Eccentric loads were applied to the set of columns with a cross section of 250 mm by 250 mm (concrete cover is 20 mm) and reinforcement ratio of 1.8%. The ultimate loads and bending moments obtained from the experiments are compared in Fig. 6 with the P-M diagram constructed by the proposed model. Due to the difficulty in testing actual size cross sections with large eccentricity, the experimental data points mainly fall in compression-controlled mode.

This document is the intellectual property of the fib – International Federation for Structural Concrete. All rights reserved.
This PDF of fib Bulletin 95 is intended for use and/or distribution solely within fib National Member Groups.

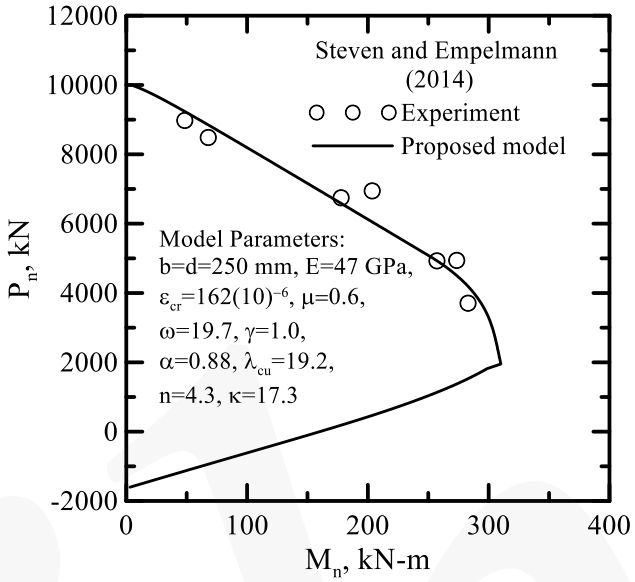


Fig. 6: Comparison of proposed P-M diagram and experimental results for UHPFRC columns tested by Steven and Empelmann.

4 Concluding remarks

This paper presents, for the first time, analytical solutions to construct full range P-M interaction diagram for HRC segments based on parametric multi-linear material models for tension and compression of FRC matrix and steel model for rebar. All failure modes including all compression, compression controlled and tension controlled were covered and the closed-form equations for each case were explicitly derived. The accuracy of the model was verified by simulating experimental results from the literature for cases of structural columns, and comparison with model-predicted results of other established numerical and finite-element analyses on precast concrete segments and cast-in-place concrete tunnel linings. Results show that using appropriate material models for fiber and reinforcing bar, engineers can use the proposed methodology to obtain P-M interaction diagrams for HRC tunnel segments. The proposed methodology can be used by tunnel engineers as one of their main tools for design of HRC segments that are subjected to combined axial force and bending moment.

5 References

ACI 544. (2016). *544.7R-16 Report on Design and Construction of Fiber-Reinforced Precast Concrete Tunnel Segments*. ACI Committee 544.

ACI Committee 318, and American Concrete Institute. (2014). *Building code requirements for structural concrete (ACI 318-14): an ACI standard : commentary on building code requirements for structural concrete (ACI 318R-14), an ACI report*.

Bakhshi, M., and Nasri, V. (2014a). "Review of international practice on critical aspects of segmental tunnel lining design." Los Angeles, United States.

Bakhshi, M., and Nasri, V. (2014b). "Guidelines and methods on segmental tunnel lining analysis and design-Review and best practice recommendation." Iguassu Falls, Brazil.

Bakhshi, M., and Nasri, V. (2014c). "Developments in design for fiber reinforced concrete segmental tunnel Lining." Montreal, Canada.

This document is the intellectual property of the fib – International Federation for Structural Concrete. All rights reserved.
This PDF of fib Bulletin 95 is intended for use and/or distribution solely within fib National Member Groups.

Bakhshi, M., and Nasri, V. (2014d). "Design considerations for precast tunnel segments according to international recommendations, guidelines and standards." Vancouver, Canada.

Bakhshi, M., and Nasri, V. (2015). "Design of segmental tunnel linings for serviceability limit state." Dubrovnik, Croatia.

Bresler, B. (1960). "Design Criteria for Reinforced Columns under Axial Load and Biaxial Bending." *Journal Proceedings*, 57(11), 481–490.

Briffaut, M., Benboudjema, F., and D'Aloia, L. (2016). "Effect of fibres on early age cracking of concrete tunnel lining. Part II: Numerical simulations." *Tunnelling and Underground Space Technology*, 59, 221–229.

Chiaia, B., Fantilli, A. P., and Vallini, P. (2007). "Evaluation of minimum reinforcement ratio in FRC members and application to tunnel linings." *Materials and Structures*, 40(6), 593–604.

Chiaia, B., Fantilli, A. P., and Vallini, P. (2009). "Combining fiber-reinforced concrete with traditional reinforcement in tunnel linings." *Engineering Structures*, 31(7), 1600–1606.

CSA. (2014). *A23.3-14 - Design of concrete structures*. CSA.

fib - federation internatioale du beton. (2013). *fib Model Code for Concrete Structures 2010*. Ernst & Sohn, Lausanne, Switzerland.

de la Fuente, A., Pujadas, P., Blanco, A., and Aguado, A. (2012). "Experiences in Barcelona with the use of fibres in segmental linings." *Tunnelling and Underground Space Technology*, 27(1), 60–71.

Hernandez-Montes, E., Gil-Martin, L. M., and Aschheim, M. (2005). "Design of Concrete Members Subjected to Uniaxial Bending and Compression Using Reinforcement Sizing Diagrams." *Structural Journal*, 102(1), 150–158.

Mobasher, B., Yao, Y., and Soranakom, C. (2015). "Analytical solutions for flexural design of hybrid steel fiber reinforced concrete beams." *Engineering Structures*, 100, 164–177.

Parme, A. L., Nieves, J. M., and Gouwens, A. (1966). "Capacity of Reinorced Rectangular Columns Subject to Biaxial Bending." *Journal Proceedings*, 63(9), 911–924.

Plizzari, G. (2009). *Construction methodologies and structural performance of tunnel linings: optimisation of the structural, technological and functional performance, of construction methodologies and materials, in tunnel linings*. Starrylink Editrice, Brescia, Italy.

di Prisco, M., Colombo, M., and Dozio, D. (2013). "Fibre-reinforced concrete in fib Model Code 2010: principles, models and test validation." *Structural Concrete*, 14(4), 342–361.

Rotter, J. M. (1985). "Rapid Exact Inelastic Biaxial Bending Analysis." *Journal of Structural Engineering*, 111(12), 2659–2674.

Soranakom, C., and Mobasher, B. (2007). "Closed-Form Solutions for Flexural Response of Fiber-Reinforced Concrete Beams." *Journal of Engineering Mechanics*, 133(8), 933–941.

Steven, G., and Empelmann, M. (2014). "UHPFRC-Columns with high-strength longitudinal reinforcement." *Beton- und Stahlbetonbau*, 109(5), 344–354.

Tiberti, G. (2009). "Concrete tunnel segments with combined traditional and fiber reinforcement: optimization of the structural behaviour and design aspects." Ph.D. Dissertation, University of Brescia, Brescia, Italy.

This document is the intellectual property of the fib – International Federation for Structural Concrete. All rights reserved.
This PDF of fib Bulletin 95 is intended for use and/or distribution solely within fib National Member Groups.

Tiberti, G., Conforti, A., and Plizzari, G. A. (2015). "Precast segments under TBM hydraulic jacks: Experimental investigation on the local splitting behavior." *Tunnelling and Underground Space Technology*, 50, 438–450.

Whitney, C. S., and Cohen, E. (1956). "Guide for Ultimate Strength Design of Reinforced Concrete." *Journal Proceedings*, 53(11), 455–490.

Yao, Y. (2016). "Characteristics of Distributed Cracking for Analysis and Design of Strain Hardening Cement Based Composites." Ph.D. Dissertation, Arizona State University, Tempe, AZ.

Yao, Y., Bakhshi, M., Nasri, V., and Mobasher, B. (2018). "Interaction diagrams for design of hybrid fiber-reinforced tunnel segments." *Materials and Structures*, 51(1), 35.

This document is the intellectual property of the fib – International Federation for Structural Concrete. All rights reserved.
This PDF of fib Bulletin 95 is intended for use and/or distribution solely within fib National Member Groups.
FRC2018: Fibre Reinforced Concrete: from Design to Structural Applications
Joint ACI-*fib*-RILEM International Workshop

An experimental study on the use of polypropylene macrofibers in precast segments for hydraulic and metro tunnel lining

Antonio Conforti[1], Ivan Trabucchi[1], Giuseppe Tiberti[1], Giovanni A. Plizzari[1], Angelo Caratelli[2], Alberto Meda[2], Sandro Moro[3], Martin Hunger[4]

[1] : University of Brescia, Brescia, Italy.

[2] : University of Rome "Tor Vergata", Rome, Italy.

[3] : BASF Construction Chemicals Italia, Treviso, Italy.

[4] : BASF Construction Solutions GmbH, Trostberg, Germany.

Abstract

There is a growing interest in the scientific community on the structural applicability of polypropylene macrofibers without or in combination with conventional reinforcement as spread reinforcement for precast tunnel segmental linings. Polypropylene macrofibers could be used in precast tunnel segments as shear reinforcement and for withstanding splitting and spalling tensile stresses which occur under and between Tunnel Boring Machine (TBM) rams, respectively. Fibers could also simplify and speed up the tunnel element production process. In this context, the present study investigates the possibility of using polypropylene macrofiber reinforcement in precast tunnel segments for both hydraulic and metro tunnel linings. Four full-scale segments (two counter-key segments of a hydraulic tunnel and two trapezoidal shaped segments of a metro tunnel) were experimentally evaluated under point load test. The latter simulate the TBM actions on segments during the excavation process (TBM thrust jack phase), which is generally the most critical temporary loading condition for segments. Two reinforcement solutions were studied: a typical conventional reinforcement (reference samples) and a combination of polypropylene macrofibers and conventional reinforcement (hybrid solution). Polypropylene macrofibers were observed to be very effective in combination with conventional reinforcement, underlining the fibers ability in controlling both splitting and spalling phenomena.

Keywords

Fiber reinforced concrete; Polypropylene macrofibers; Point load test; Precast tunnel segments; TBM thrust jack phase.

This document is the intellectual property of the fib – International Federation for Structural Concrete. All rights reserved.
This PDF of fib Bulletin 95 is intended for use and/or distribution solely within fib National Member Groups.

1 Introduction

The application of the Tunnel Boring Machine (TBM) thrust jack forces is a crucial temporary loading condition during tunnel lining construction, which may govern the design procedure (Blom, 2002; Bakhshi et al., 2014) and the amount of reinforcement (fibers or conventional rebars) used in these elements. In fact, after assembling a complete ring, the TBM moves forward by pushing the thrust jacks on the latest assembled ring (TBM thrust jack phase). High concentrated forces are introduced in the back lining which generate high stresses in the concrete under the thrust shoes. In addition, since each tunnel segment, depending on the segment configuration adopted, are loaded by two or more thrust shoes, the combined effect of the TBM loads determine (between the corresponding loading areas) tensile stresses in the local tangential direction. The latter are generally the results of the local demand of compatibility and they generally lead to cracks defined in the literature as spalling cracks (Fenwick et al., 1986; De Waal, 1999). The use of Fiber Reinforced Concrete (FRC) in precast tunnel lining has been continuously rising (ITA report n.16, 2016; ACI 544.7R-16, 2016; *fib* bulletin No. 83, 2017). FRC without or in combination with conventional reinforcement is an adequate solution in order to fulfill the need of improving the design requirements of segmental linings in terms of bearing capacity, crack control and water-tightness. The enhancement of the general structural behavior together with the simplification of the industrialized production of precast tunnel segments are probably the two main key-factors among designers, practitioners and contractors for the growing interest on fiber reinforcement. Steel fiber reinforced concrete has been generally used in precast tunnel elements. However, in the last decade, important research efforts have been devoted to the development of new types of structural macro-synthetic fibers. The latter are now able to impart significant toughness and ductility to concrete (Ortiz-Navas et al., 2018), guaranteeing also a high resistance to the environmental attack. Therefore, polypropylene macrofibers for use in underground structures are raising interest in the scientific community.

Within this framework, the structural applicability of polypropylene macrofibers in precast tunnel segments was evaluated in the present research study by testing full-scale segments under point load test. The latter reproduces the actions on segments during TBM thrust jack phase. Two different tunnel linings were considered: a hydraulic tunnel with an internal diameter of 320 cm (125.98 in.) and a metro tunnel with an internal diameter of 580 cm (228.35 in.). By varying rebar amount and material toughness, both conventional reinforcement (considered also as reference) and hybrid reinforcement (combination of polypropylene macrofibers and a low amount of longitudinal reinforcement) solutions were studied and compared.

2 Experimental program

The hydraulic tunnel considered herein (Figure 1a) is characterized by an internal diameter of 320 cm (125.98 in.) and a thickness of 25 cm (9.84 in.) (internal diameter-to-thickness ratio equal to 12.8). As shown in Figure 1a, each lining ring is composed by six segments; the precast tunnel segment considered is the counter-key one, which is characterized by an inclined side, an average length of 181 cm (71.26 in.) and a width of 120 cm (47.24 in). According to the original tunnel project, the design thrust load during TBM thrust jack phase (in terms of single shoe load) was 785 kN (176 kip), while the maximum thrust load was 1130 kN (254 kip).

This document is the intellectual property of the fib – International Federation for Structural Concrete. All rights reserved.
This PDF of fib Bulletin 95 is intended for use and/or distribution solely within fib National Member Groups.

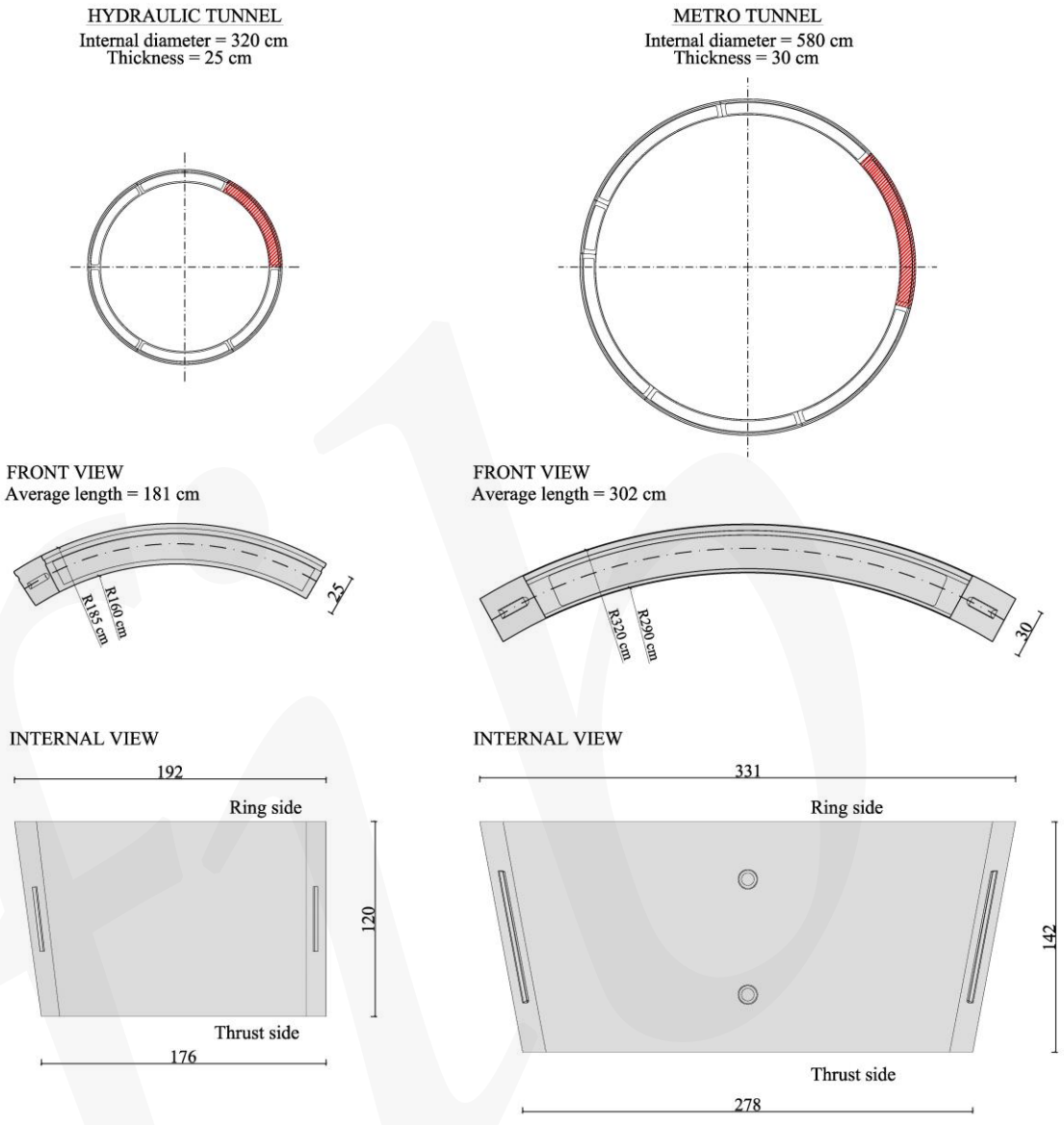


Figure 1: Hydraulic (a) and metro (b) tunnel linings with the indication of the precast tunnel segments studied (Notes: 1 cm = 0.394 in.)

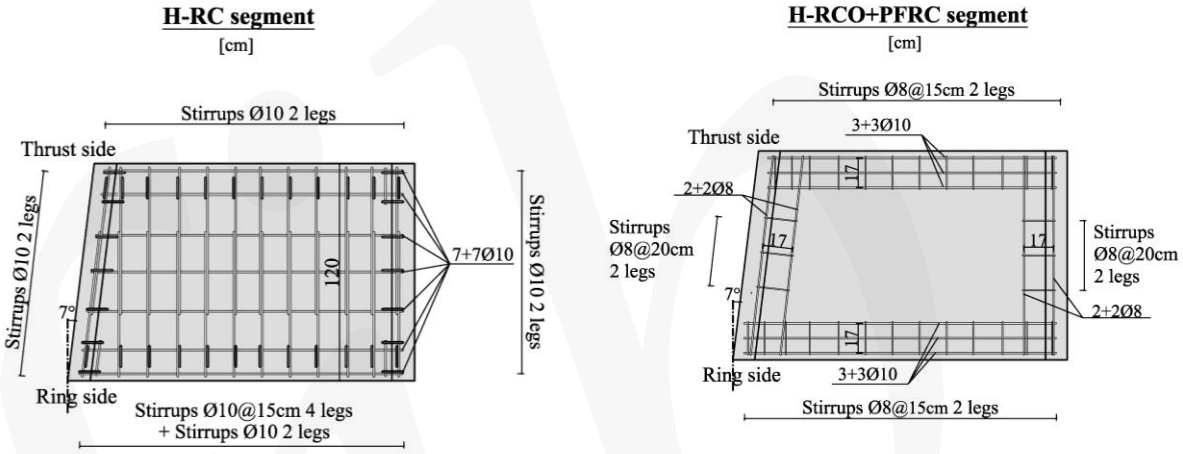
Concerning the metro tunnel (Figure 1b), the trapezoidal shaped precast tunnel segment studied is characterized by a thickness of 30 cm (11.81 in.) with an average length of 302 cm (118.90 in.) and a width of 142 cm (55.90 in.). This segment is part of a metro tunnel characterized by an internal diameter of 580 cm (228.35 in.) (internal diameter-to-thickness ratio equal to 19.3) excavated by a TBM, in which the lining ring is composed by six segments (Figure 1b). According to the original tunnel project, the design thrust load and the maximum thrust load for each pad was 1160 kN (261 kip) and 2160 kN (485 kip), respectively.

For both Hydraulic (specimen designation: H) and Metro (specimen designation: M) tunnel segments, the following two reinforcement solutions were considered:

This document is the intellectual property of the fib – International Federation for Structural Concrete. All rights reserved.
This PDF of fib Bulletin 95 is intended for use and/or distribution solely within fib National Member Groups.

1. conventional reinforcement solution (hydraulic tunnel segment H-RC and metro tunnel segment M-RC), in which the typical amount of conventional reinforcement for practice was adopted. These segments (H-RC and M-RC) are also considered as reference samples;
2. hybrid solution (hydraulic tunnel segment H-RCO+PFRC and metro tunnel segment M-RCO+PFRC), in which a combination of reinforcing bars and polypropylene macrofibers was properly designed to obtain an optimized reinforcement solution.

Figure 2 shows the reinforcement details of hydraulic tunnel segments, while Figure 3 reports the reinforcement adopted in the metro tunnel segments.



Clear concrete cover on curved rebars = 3.5 cm
Effective depth *(d)* = 21.0 cm
$\rho_s = A_s/(b \cdot d) = 0.22\%$
Steel content = 114 kg/m^3

(a)

Clear concrete cover on curved rebars = 3.5 cm
Effective depth (*d*) = 21.0 cm
$\rho_s = A_s/(b \cdot d) = 0.18\%$
Steel content = 52 kg/m^3
Polypropylene macrofibres: 10 kg/m^3

(b)

Figure 2: Reinforcement details of hydraulic tunnel segments in conventional reinforcement (a) and hybrid solution (b) (Notes: 1 cm = 0.394 in.; 1 kg/m^3 = 0.0624 lb/ft^3)

The conventional reinforcement solution is characterized by a double reinforced section with 7Ø10 and 10Ø10 curved rebars both as compression and tension reinforcement for H-RC and M-RC segments, respectively. The clear concrete cover on curved rebars was 3.5 cm (1.37 in.) in H-RC segment and 4.0 cm (1.57 in.) in M-RC sample, leading to a longitudinal reinforcement ratio ($\rho_s=A_s/(b \cdot d)$ where A_s is the total area of longitudinal tension reinforcement, b is the segment width and d is the effective depth) around 0.22% in both segment typologies. In addition, a minimum amount of transverse reinforcement was adopted (stirrups Ø10@15 cm (5.90 in.) 4 legs in H-RC; stirrups Ø8@15 cm (5.90 in.) 6 legs in M-RC). Stirrups Ø10 with 2 legs were placed along segment sides to withstand radial splitting forces. The steel content of this reinforcement solution results equal to 114 kg/m^3 (7.11 lb/ft^3) and 100 kg/m^3 (6.24 lb/ft^3) in H-RC and M-RC segments, respectively.

The hybrid solution corresponds to a combination of fibers and rebars, as proposed by Plizzari et al. (2007), whose design principles are reported in details in Tiberti (2014). In this reinforcement solution, both rebars and fibers withstand flexural stresses and control spalling cracks, whereas fibers hold up to splitting and shear stresses (Tiberti (2014)). In this research,

This document is the intellectual property of the fib – International Federation for Structural Concrete. All rights reserved.
This PDF of fib Bulletin 95 is intended for use and/or distribution solely within fib National Member Groups.

two connected chords (3+3Ø10) and 10 kg/m^3 (0.62 lb/ft^3) of synthetic macrofibers made of polypropylene (Table 1) were adopted. Considering the same clear concrete cover of RC segments, the longitudinal reinforcement ratio was equal to 0.18% in H-RCO+PFRC and 0.13% in M-RCO+PFRC segment. It is worth underlining that this ratio is smaller in metro segments; this reduction was possible due to the very good results given by the hybridization of rebars and fibers in the hydraulic tunnel segments. In fact, the experimental program on metro tunnel segments (M-RC and M-RCO+PFRC) was carried out after the one on hydraulic tunnel segments (H-RC and H-RCO+PFRC). The overall steel content of the hybrid solution was in both cases 60% smaller than the one of RC segments, which can be seen in Figure 3 for the example of the metro tunnel segment. This significantly simplifies steel cage construction and positioning.

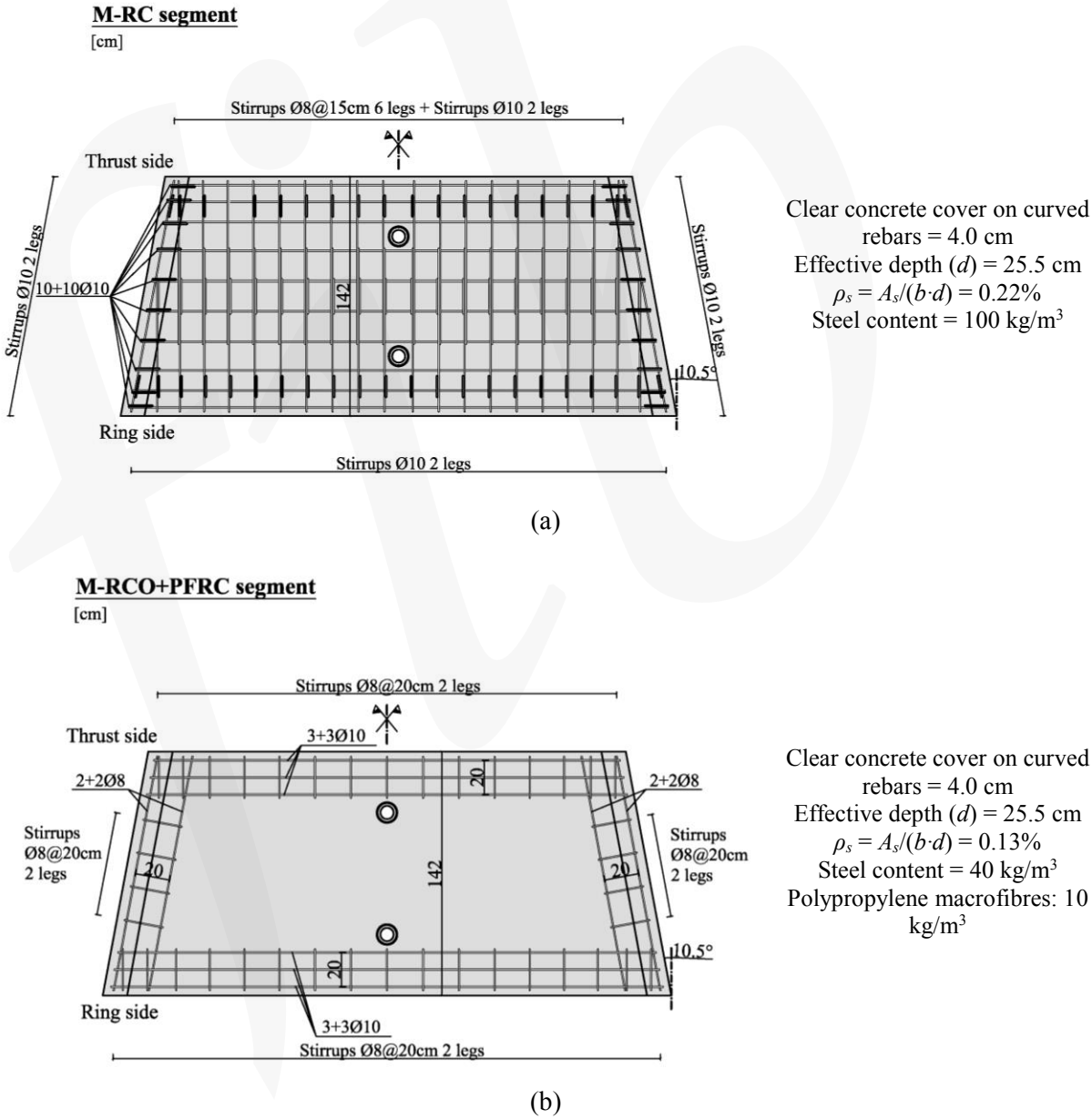


Figure 3: Reinforcement details of metro tunnel segments in conventional reinforcement (a) and hybrid solution (b). (Notes: 1 cm = 0.394 in.; 1 kg/m^3 = 0.0624 lb/ft^3)

This document is the intellectual property of the fib – International Federation for Structural Concrete. All rights reserved.
This PDF of fib Bulletin 95 is intended for use and/or distribution solely within fib National Member Groups.

Table 1: Properties of synthetic macrofibers made of polypropylene

Type	Polypropylene
Shape	Embossed
Length [mm]	54
Diameter [mm]	0.81
Aspect ratio [-]	67
Tensile strength [MPa]	> 552
Elastic modulus [MPa]	6000
Density [kg/m^3]	910
Notes: 1 mm = 0.0394 in.; 1 MPa = 145 psi; 1 kg/m^3 = 0.0624 lb/ft^3	

Table 2 summarizes, for any segment type, the cubic ($f_{c,cube}$) and cylindrical (f_c) compressive strength, where f_c was estimated as 83% of $f_{c,cube}$. The compressive strength was observed to be very similar between the segments of any tunnel typologies (i.e. around 59 MPa (8.55 ksi) and 52 MPa (7.54 ksi) for hydraulic and metro tunnel, respectively). Concerning the post-cracking behavior of polypropylene fiber reinforced concretes adopted in H-RCO+PFRC and M-RCO+PFRC segments, mean values and experimental scatter (coefficient of variation, CV are provided in brackets) are also reported for the limit of proportionality (f_L) and the residual strengths at CMOD of 0.5 and 2.5 mm (0.02 to 0.10 in.) ($f_{R,1}$ and $f_{R,3}$ according to EN 14651 (2005)). It can be observed that macro-synthetic fibers provide significant post-cracking resistance to concrete at different crack widths, leading to have a material for possible structural use and able to substitute the minimum amount of shear reinforcement according to *fib* Model Code 2010 (2012).

Table 2: Mean values of concrete compressive strength and residual flexural tensile strengths (evaluated according to EN 14651, 2005) of hydraulic and metro tunnel segments

Tunnel	Hydraulic (H)		Metro (M)	
Segment	H-RC	H-RCO+PFRC	M-RC	M-RCO+PFRC
$f_{c,cube}$ [MPa]	58.1 (0.05)	60.1 (0.03)	51.3 (0.04)	52.4 (0.05)
f_c [MPa]	48.2	49.8	42.5	43.5
f_L [MPa]	-	4.47 (0.11)	-	4.38 (0.07)
$f_{R,1}$ [MPa]	-	3.05 (0.26)	-	3.42 (0.11)
$f_{R,3}$ [MPa]	-	4.66 (0.29)	-	5.17 (0.14)
Notes: 1 MPa = 145 psi.				

3 Precast tunnel segments for hydraulic tunnel lining

Figure 4a summarizes the loading system adopted for hydraulic tunnel segments. The load was applied by two loading shoes (#1 and #2) using hydraulic jackets able to apply 3000 kN (674 kip) per pad. Concerning the instrumentation, potentiometric transducers (V#1 and V#2) were placed to evaluate the vertical shortening under the loading shoes. An LVDT was arranged to capture the spalling crack width between loading shoes.

This document is the intellectual property of the fib – International Federation for Structural Concrete. All rights reserved.
This PDF of fib Bulletin 95 is intended for use and/or distribution solely within fib National Member Groups.

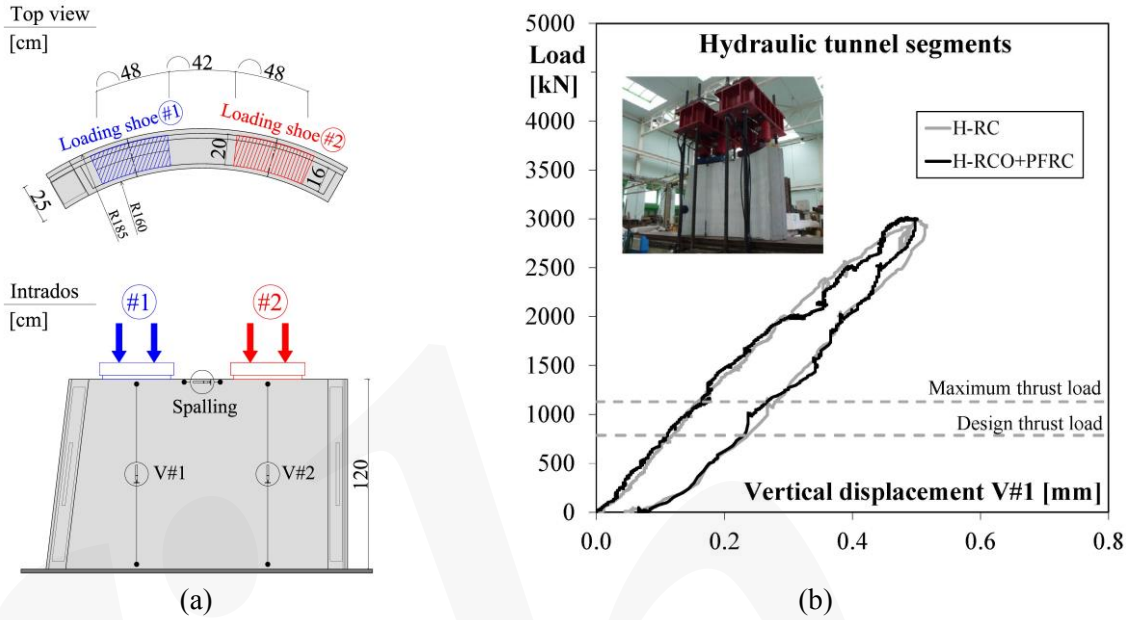


Figure 4: Point load tests on hydraulic tunnel segments: test set-up (a) and experimental response in terms of single shoe load vs. V#1 displacement curves (b) (Notes: 1 mm = 0.0394 in.; 1 kN = 0.2248 kip)

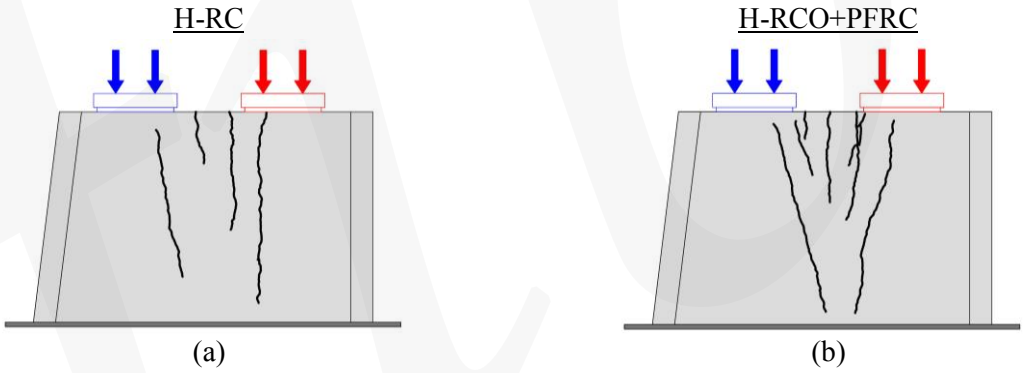


Figure 5: Final crack patterns of H-RC (a) and H-RCO+PFRC (b) segments

Figure 4b shows the experimental results of point load tests in terms of single shoe load vs. vertical displacement V#1 for H-RC and H-RCO+PFRC segments. In addition, Figure 5 reports the final crack pattern of segments. It can be observed that both segments were able to reach the maximum applied load of 3000 kN (674 kip) (much higher than both design and maximum thrust loads) showing a very similar stiffness and final crack pattern. The latter was characterized by spalling cracks between loading shoes (the first spalling crack appeared at 750 kN (169 kip)) and splitting cracks under both loading shoes (cracking for splitting was observed at a load of about 1500 kN (337 kip) and 2500 kN (562 kip) under loading shoe #2 and #1, respectively). At both design and maximum thrust loads only a spalling crack were observed and the maximum crack opening was similar for H-RC and H-RCO+PFRC segments, i.e. 0.05 mm (0.002 in.). Therefore, H-RCO+PFRC segment showed a global structural response similar to the H-RC one with a good control of spalling cracks. In fact, in the hybrid segment smaller and more closely spaced spalling cracks were observed as compared to H-RC segment (Figure 5). The spalling crack depth along segment resulted

This document is the intellectual property of the fib – International Federation for Structural Concrete. All rights reserved.
This PDF of fib Bulletin 95 is intended for use and/or distribution solely within fib National Member Groups.

smaller as well. Noteworthy is also that polypropylene macrofibers in the hybrid solution were the only reinforcement used to withstand tangential splitting cracks and they were able to control them in a similar way of rebars in the RC sample. This underlines the efficiency of polypropylene macrofibers as splitting reinforcement. This confirms the previous results obtained by Tiberti et al. (2015) on prismatic samples in polypropylene fiber reinforced concrete subjected to a high-concentrated load.

4 Precast tunnel segments for metro tunnel lining

Segments were subjected on the thrust side to the actions of two loading shoes (#1 and #2) according to the scheme shown in Figure 6a. Both shoe dimensions (77 cm (30.32 in.) long and 30 cm (11.81 in.) wide) and their relative distance (145 cm (57.08 in.) from center to center) were the same to the ones adopted in the construction of the real metro tunnel. Figure 6a also shows the instrumentation adopted, which was similar to the one adopted for hydraulic tunnel segments (vertical shortening V#1-V#2 measured by potentiometric transducers and spalling crack width captured by a LVDT).

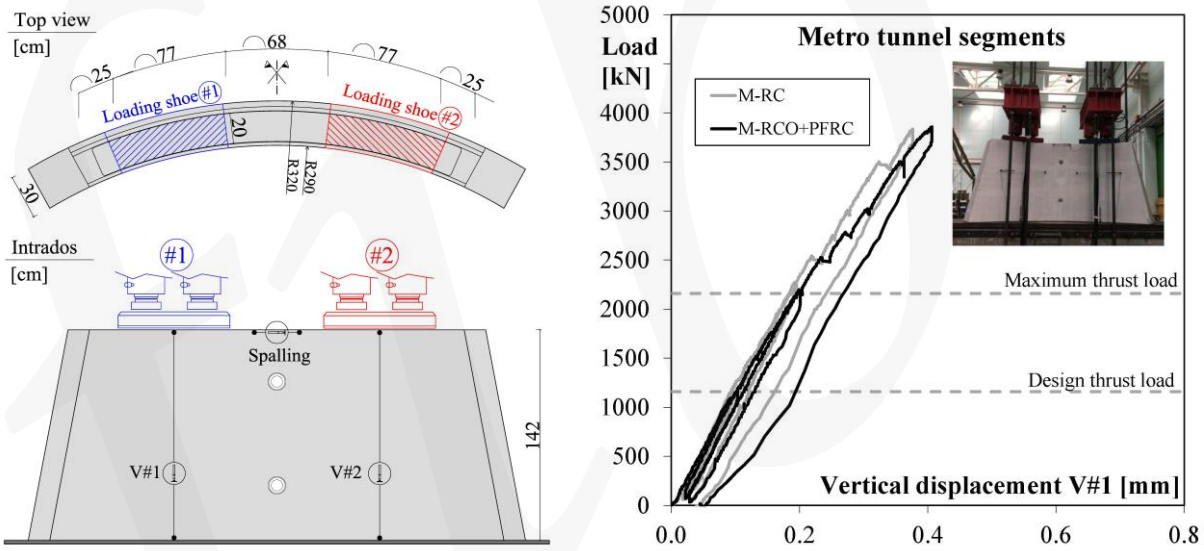


Figure 6: Point load tests on metro tunnel segments: test set-up (a) and experimental response in terms of single shoe load vs. V#1 displacement curves (b) (Notes: 1 mm = 0.0394 in.; 1 kN = 0.2248 kip)

Figure 6b shows the load vs. vertical displacement under the loading shoes #1 for M-RC and M-RCO+PFRC segments. It can be observed that both reinforcement solutions allowed the segments to reach the maximum capacity of the loading system, i.e. 4000 kN (899 kips) per shoe. The latter is significantly higher than the design and the maximum thrust loads and it was reached by both segments showing a similar stiffness. In fact, the vertical shortening V#1 was about 0.38 mm (0.0149 in) and 0.40 mm (0.0157 in.) at the maximum applied load for M-RC and M-RCO+PFRC segment, respectively. Figure 7 shows the final crack pattern of both segments. It should be noticed that both reinforcement solutions showed a similar crack pattern evolution, characterized by an uncracked stage up to the spalling crack load (which was 1210 kN (272 kip) for M-RC and 1095 kN (246 kip) for M-RCO+PFRC

This document is the intellectual property of the fib – International Federation for Structural Concrete. All rights reserved.
This PDF of fib Bulletin 95 is intended for use and/or distribution solely within fib National Member Groups.

segments) and a cracked stage in which spalling cracks developed and splitting cracks appeared. Splitting cracks under both loading shoes #1 and #2 occurred at a load of about 2500 kN (562 kip) in both reinforcement solutions. After the cracking load for spalling, multiple cracks developed in both segments in the area between loads.

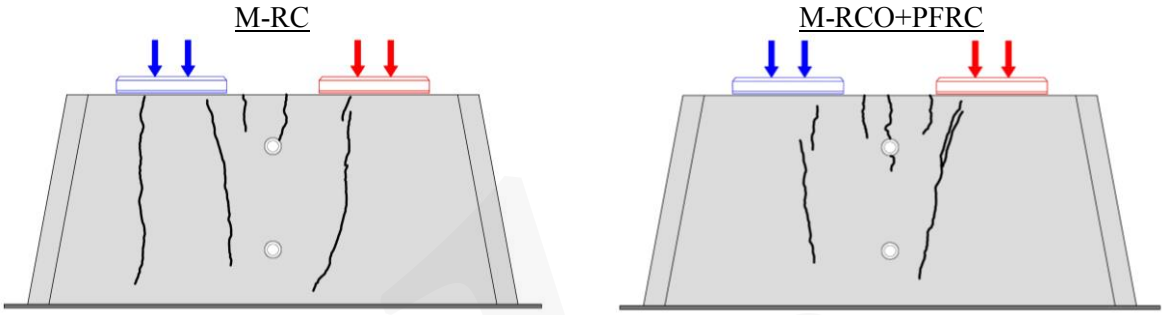


Figure 7: Final crack patterns of M-RC (a) and M-RCO+PFRC (b) segments

The spalling crack width was comparable in M-RC and M-RCO+PFRC segments, even if it resulted slightly higher in the hybrid reinforcement solution (e.g. +15% at the load of 4000 kN (899 kip), which is 3.5 times greater than the design thrust load). At the design load, this crack was not present in RC segment, while it was very small in M-RCO+PFRC one. Concerning the spalling crack propagation along segment, in Figure 7 it can be underlined that, according to the values of crack width, a slightly higher crack depth was observed in M-RCO+PFRC segment (49.8 cm (19.60 in.)) as compared to RC one (40 cm (15.75 in.)). A more diffused multiple cracking was observed in the hybrid segment. This confirms that both reinforcement solutions were able to control the cracking phenomena arising in the spalling area, even if a slightly better performance was provided by the traditional reinforcement solution. The splitting cracks, as already underlined, arose in both segments under point loads at a load of about 2500 kN (562 kip). Consequently, these cracks are not present at design thrust load, but they could appear before the maximum one is reached. These cracks were well controlled at any load levels by polypropylene macrofibers in the M-RCO+PFRC segment by a transverse stress redistribution that continuously provide equilibrium with the external applied load. Therefore, both reinforcement solutions guaranteed the force equilibrium and a good control of splitting cracks up to maximum capacity of the loading system (which is of about two times greater than the maximum thrust load). These results on metro tunnel segments extend and confirm the previous outcomes obtained on hydraulic samples (Section 3), underlining, once again, the positive effects given by the hybridization of polypropylene macrofibers and conventional reinforcement in precast tunnel segments.

5 Concluding remarks

The structural applicability of polypropylene macrofibers in precast tunnel segments for both hydraulic and metro tunnel linings has been experimentally evaluated under point load test. The latter simulate the TBM actions on segments during the excavation process, i.e TBM thrust jack phase. Based on this experimental study on full-scale samples, the following conclusions can be drawn:

1. The combination of the polypropylene fiber reinforced concrete under investigation

This document is the intellectual property of the fib – International Federation for Structural Concrete. All rights reserved.
This PDF of fib Bulletin 95 is intended for use and/or distribution solely within fib National Member Groups.

and a low amount of rebars (longitudinal reinforcement ratio ρ_s around 0.15%) is an attractive reinforcement solution for both hydraulic and metro tunnel segments.

2. During thrust jack phase, segments reinforced by either conventional or hybrid reinforcement are expected to show a very similar structural response both in terms of bearing capacity, stiffness and crack width control. In fact, under point load tests, RC and RCO+PFRC segments showed a comparable experimental behavior (both in case of hydraulic and metro tunnel segments).

3. The adopted polypropylene fiber reinforced concrete can be used in precast tunnel segments to withstand tensile forces in the splitting zones under TBM loading shoes. Spalling crack control and flexural resistance is guaranteed by an optimized combination of fibers and a low amount of curved rebars.

Further tests should carried out by considering other polypropylene macrofibres, reinforcement combinations and segment geometries.

6 References

ACI Committee 544 (2016). *Report on Design and Construction of Fiber Reinforced Precast Concrete Tunnel Segments.* ACI 544.7R-16, American Concrete Institute, p. 36.

Bakhshi, M., and Nasri, V. (2014). *Review of international practice on critical aspects of segmental tunnel lining design*. Proceedings of North American Tunneling, p. 274-282.

Blom, C.B.M. (2002). *Design philosophy of concrete linings for tunnels in soft soils.* Ph.D Thesis, Delft University of Technology, The Netherlands.

EN 14651 (2005). *Precast concrete products – test method for metallic fibre concrete – Measuring the flexural tensile strength*, European Standard.

Fenwick, R.C., and Lee, S.C. (1986). *Anchorage zones in prestressed concrete members.* Magazine of concrete research, Vol. 38, No. 135, 77-89.

fib bulletin No. 83 (2017). *Precast tunnel segments in fibre-reinforced concrete*. *fib* WP 1.4.1, p. 168, ISBN: 978-2-88394-123-6.

fib Model code 2010, (2012). International Federation for Structural Concrete, Bulletins 65 and 66, ISBN 978-2-88394-105-2 and ISBN 978-2-88394-106-9.

ITA report n. 16 (2016). *Twenty years of FRC tunnel segments practice: lessons learnt and proposed design principles*. p. 71, ISBN 978-2-970-1013-5-2.

Ortiz-Navas, F., Navarro-Gregori, J., Leiva-Herdocia, G.E., Serna, P., and Cuenca, E. (2018). *An experimental study on the shear behaviour of reinforced concrete beams including macro-synthetic fibres*. Construction and Building Material, Vol. 169, 888-899.

Plizzari, G.A., and Tiberti, G. (2007). *Structural behaviour of SFRC tunnel segments*, Proceedings of the 6th FraMCos, Vol. 3, pp. 1577-1584, ISBN 978-0-415-44066-0.

Tiberti, G. (2014). *Concrete tunnel segments with combined traditional and fiber reinforcement: optimization of the structural behavior and design aspects*, Ph.D. Thesis, University of Brescia, , Aracne editrice s.r.l., pp. 396, ISBN 978–88–548–7005–5.

Tiberti, G., Conforti, A., and Plizzari, G.A. (2015). *Precast segments under TBM hydraulic jacks: experimental investigation on the local splitting behavior*, Tunnelling and Underground Space Technology, Vol. 50, 438-450.

Waal, R.G.A. de (1999). *Steel fiber reinforced tunnel segments.* Ph.D Thesis, Delft University of Technology, The Netherlands.

This document is the intellectual property of the fib – International Federation for Structural Concrete. All rights reserved.
This PDF of fib Bulletin 95 is intended for use and/or distribution solely within fib National Member Groups.
FRC2018: Fibre Reinforced Concrete: from Design to Structural Applications
Joint ACI-*fib*-RILEM International Workshop

Design of precast prestressed SFRC T-girders for accelerated sustainable bridge construction

Bruno Massicotte[1], Nicola Cordoni[2]

[1] : Polytechnique Montreal, Montreal, Canada.

[2] : WSP, Vancouver, Canada.

Abstract

Accelerated bridge construction is becoming a subject of major importance and, combined use of steel fibre reinforced concrete (SFRC) and prestressing, this construction technique offers a unique opportunity to fulfill the demand of more sustainable infrastructure with enhanced durability and life-cycle cost reduction. Research projects carried out at Polytechnique Montreal in the past 20 years have demonstrated that the combined use of prestressing, SFRC, prefabrication and ultra-high performance fibre reinforced concrete (UHPFRC) allows developing more economical and durable bridges. A project on precast T-girders was initiated with the aim of developing a new set of prestressed girders for new bridges in the 10 to 30 m span range using conventional prestressing and shear reinforcement, reduced top flange transverse reinforcement and field-cast UHPFC longitudinal joints between girders. It is anticipated that bridge built with this concept will only require minimum maintenance over a 75-year service life in harsh environmental conditions.

Keywords

Precast; Prestressing; SFRC; Bridges; Accelerated Bridge Construction; Sustainability

This document is the intellectual property of the fib – International Federation for Structural Concrete. All rights reserved.
This PDF of fib Bulletin 95 is intended for use and/or distribution solely within fib National Member Groups.

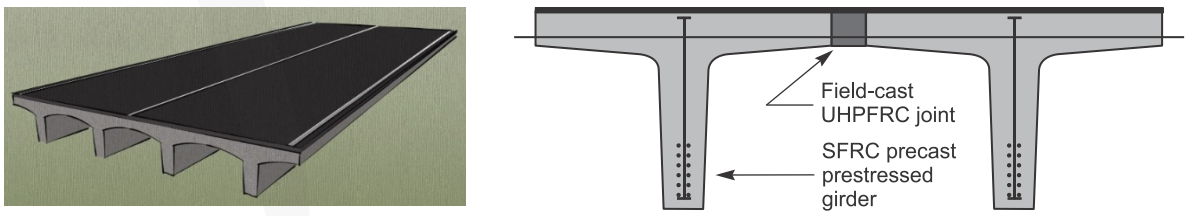
1 Introduction

1.1 Context

Accelerated bridge construction is a subject of major importance in North-America and is needed in many regions for the replacement of existing concrete infrastructure that have experienced durability issues. In many cases bridge replacement is a cause of major traffic disruption and solutions that combine accelerated construction, enhanced durability and low life-cycle costs are favorably considered. The use of steel fibre reinforced concrete (SFRC) in new structural elements offers a unique opportunity to fulfill all these requirements and several innovative solutions have been proposed in the past two decades. However the lack of design codes has impaired a broad implementation of these innovations for structural applications. Recent introduction of design codes and guidelines worldwide (fib 2010; AFGC, 2012; Australia, 2014; CSA, 2019), enables now to develop and implement new structural applications involving SFRC with the objective of building structures that meet sustainable development principles at a competitive initial cost. Research carried out at Polytechnique Montreal since the mid 1990's (Massicotte et al., 2016) demonstrated that the combined use of prestressing, SFRC, prefabrication and ultra-high performance fibre reinforced concrete (UHPFRC) allows developing more economical and durable bridges. In that perspective, a major research program that includes several projects and topics has been carried out at Polytechnique Montreal since 2007 for developing entirely precast bridge components that incorporate SFRC and UHPFRC with the objective of improving structural performances in service conditions (SLS) while keeping or improving safety at ultimate limit states (ULS).

1.2 Innovative precast SFRC bridge concept

A project on precast T-girders was initiated with the aim of developing a new set of prestressed girders for new bridges in the 10 to 30 m span range, typically covering 25% of bridge network. The proposed concept (Massicotte et al. 2012), illustrated in Figure 1, combines SFRC, bounded and unbonded prestressing, conventional longitudinal reinforcement, optimised conventional shear reinforcement, reduced top flange transverse reinforcement (Massicotte et al. 2016) and field-cast UHPFRC longitudinal joints between adjacent girders. The concept also uses precast barrier walls developed in previous studies (Namy et al., 2015). With this concept, it is anticipated that the bridge will only require minimum maintenance over a 75-year service life in harsh environment, essentially to replace the asphalt layer.



(a) Bridge superstructure (b) T-beam cross-section and reinforcement

Figure 1: Proposed bridge concept with SFRC and reduced reinforcement

This document is the intellectual property of the fib – International Federation for Structural Concrete. All rights reserved.
This PDF of fib Bulletin 95 is intended for use and/or distribution solely within fib National Member Groups.

1.3 Scope of the research project

The research project was aimed at fully designing this new bridge concept based on existing knowledge and using available design analytical tools following the philosophy of existing bridge codes. The paper presents the main design parameters, the final concept and some results of the validation process.

2 Design criteria

2.1 Innovative concept

The proposed concept main innovation consists in the combination of steel fibres, optimised prestressing layout and reduced conventional reinforcement, for flexure and shear, for both longitudinal and transverse load effects. The use prestressing remains the most efficient solution for the design main structural elements such as bridge girders whereas adopting a SFRC mix allows improving serviceability, strength and durability performances. Moreover, the proper use of fibre concrete allows reducing the member cross-section dimensions, eliminating secondary reinforcements, simplifying stirrup and prestressing tendon configuration. The concept requires using field-cast UHPFRC longitudinal joints between adjacent girders, a technology that is becoming common practice in North-America (Graybeal, 2014; Marleau and Massicotte, 2019).

2.2 Project background

Two research projects provided the background knowledge for the T-girder development. De Brouker (2013) tested 8 large rectangular precast and prestressed girders made with SFRC. The specimens, tested in flexure and shear, contained a combination of prestressing strands, conventional flexural reinforcement and reduced shear reinforcement. In these tests, conventional reinforcement, and bonded or unbonded prestressing strands were used for the bottom reinforcement layer. All other longitudinal reinforcements consisted of bonded prestressed strands. Observed crack spacing with SFRC was not significantly affected by the type reinforcement used. However, un-expected shear failure observed during a bending test related with the principal tensile stress orientation in prestressed girders for a specimen without stirrup strongly support the use of a minimum amount of stirrups. Faggio (2014) optimised the shape of the T-girder flange such that local truck wheel effects would mostly induce arching action, thereby minimising positive and negative transverse bending moments in the T-flange. With this concept, only one layer of transverse conventional reinforcement located at the bottom third of the flange is need when used with SFRC, as concept developed and used previous bridge construction (Massicotte et al. 2016).

2.3 Design criteria

The proposed T-girders bring new design challenges. Firstly, these girders are relatively light, an advantage in precast construction. However this implies that traffic load effects are dominant: the bending moment due to the girder self-weight represents only 25% of the design bending moment in service. This raises concerns related to creep deflection due to high prestressing forces. Secondly, although using fibres allows accepting cracking under service loads, high-cycle fatigue may become an issue for the lowermost reinforcement. Therefore,

This document is the intellectual property of the fib – International Federation for Structural Concrete. All rights reserved.
This PDF of fib Bulletin 95 is intended for use and/or distribution solely within fib National Member Groups.

based on previous research studies (Massicotte et al., 2012) findings, the following design criteria and construction procedure were selected:

- horizontal prestressed bonded strands are used as the primary longitudinal reinforcement for all sections studied avoiding using parabolic or inclined strands for simplicity and for minimising fabrication costs;
- T15 strands with an average final tension stress of 1300 MPa are considered;
- the longitudinal prestressing are installed in two stages, a first-one balancing girder self-weight during storage, and a second one activated just before construction to meet the desired required performance according to the expected remaining creep deflection;
- the lower reinforcement layer may consists of bonded or un-bonded prestressed strands, or conventional reinforcing bars depending on the desired performance;
- a minimum amount of stirrups must be used to avoid the incertitude associated with the fibre orientation and cold joints, CSA-S6 (2014) minimum limit of $\rho_v = 0.06\sqrt{f'_c}/f_y$ is recommended, with a maximum stirrup spacing of $h/2$;
- the stress range limitation in longitudinal reinforcement associated with fatigue limit states is limited to 125 MPa as specified in CSA-S6 (2014);
- a target fibre volume ratio equal to 1% per volume (±80 kg/m^3) is suggested to ensure a uniform fibre distribution over the entire cross-section, and consequently a reasonable scatter of the tensile properties;
- a girder depth equal to $L/25$ is chosen to ensure a proper stiffness for limiting traffic load induced deflection below the common limit of $L/800$ in the preliminary design stage.

2.4 SFRC mix design and characteristic tensile properties

The selected SFRC mechanical characteristics are based on the self-compacting mix successfully used past projects for fabricating large scale prestressed precast girders (De Brouker, 2013). Hooked-end 35 mm long and 0.55 mm in diameter fibers with at 1300 MPa tensile strength were selected for their efficiency in service conditions for controlling flexural crack opening both longitudinally in the girder web and transversely in the girder flange, and for their efficiency at ultimate in shear. The use of longer fibres would create concrete placement issues in the congested web whereas shorter fibres would present limited efficiency for limiting crack spacing in service. A specified compressive of 70 MPa was chosen based on the prestressing requirements at the various construction stages but also to be consistent with the fibre selection. Higher compressive strength would necessitate fibres with enhanced ductility whereas lower strength would require fibres with enhanced anchorage.

The 1% fibre volume indicated above is only indicative. The selected characteristic design properties indicated in Figure 2 can be obtained with various SFRC mixes. The average tensile properties obtained with the suggested mix are shown for illustration. The maximum crack width was established at 0.2 mm in service conditions and 1.5 mm at ultimate in shear as justified below.

This document is the intellectual property of the fib – International Federation for Structural Concrete. All rights reserved.
This PDF of fib Bulletin 95 is intended for use and/or distribution solely within fib National Member Groups.

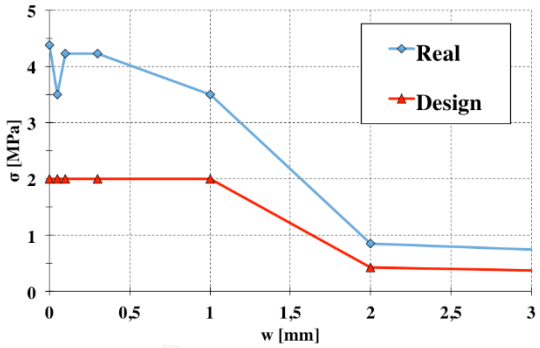


Figure 2: Selected characteristic SFRC tensile properties

2.5 Material resistance factors

The material resistance factors for reinforcement and conventional concrete indicated in Table 1 are those of the Canadian Bridge Code (CSA, 2014). The factor for SFRC in tension was selected equal to that of normal concrete which is less than the value determined by Bélanger (2000) for SFRC bridge decks.

Table 1: Material resistance factors (CSA-S6)

Material	Resistance factor
Concrete	$\phi_c = 0.75$
SFRC – post-cracking	$\phi_F = 0.75$
Reinforcing bars	$\phi_s = 0.90$
Prestressing strands	$\phi_p = 0.95$

3 Precast section design

3.1 Cross-section geometry

The cross-section dimensions are shown on Figure 3 for the 20 m span girders. The geometrical characteristics were chosen to standardise the cross-section profile for reducing the costs related with the production process, mainly associated to the formworks. The cable configuration and the geometrical limitations for the beam web were chosen to minimise any issues related with the fibre flow and optimise fibre orientation. The lateral profile of the web is inclined with the top flange and bottom dimensions kept constant for all beam size. The use of a minimum transverse reinforcement is envisaged: single 15 mm in diameter stirrups at the center of the web between the two rows of strands, as indicated on Figure 2. Live load deflection limitation governed the depth of the girders which is slightly more than the target $L/25$ limit. With the deeper girders the issue related cracking and the associated fatigue concern under live load disappeared.

The number of strands and their associated eccentricity with respect to the girder center of gravity are given in Table 2 for the two-stage prestressing application procedure. A first group of strands with an eccentricity e_1 are tensioned to balance the girder self-weight. A second level of prestressing force (e_2) would be applied at the construction time. The total prestressing force allows the beams to reach the required capacity to meet serviceability and ultimate design

This document is the intellectual property of the fib – International Federation for Structural Concrete. All rights reserved.
This PDF of fib Bulletin 95 is intended for use and/or distribution solely within fib National Member Groups.

criteria. For spans longer than 25 m, T sections become less effective and a larger bottom flange is necessary. This was not explored in this project.

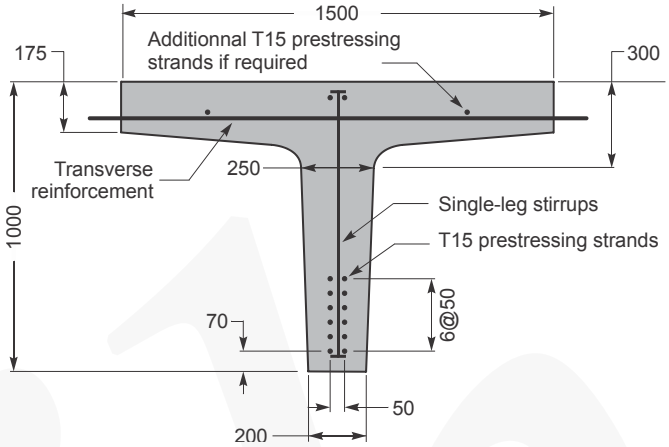
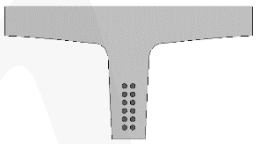
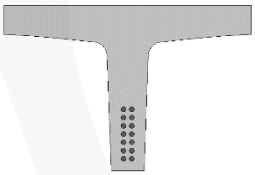
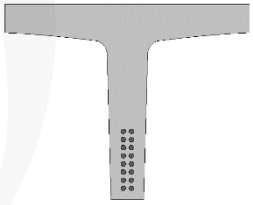


Figure 3: Transverse cross-section for the 20 m span SFRC girders

Table 2: Main geometric characteristics of the three designed sections

Span	15 m	20 m	25 m
Geometry and prestressing			
Height [mm]	800	1000	1200
y_{cg} from top [mm]	222	312	420
# strands	12	14	16
e_1 [mm] (# strands)	310 (6)	425 (8)	540 (10)
e_2 [mm] (# strands)	460 (6)	600 (6)	740 (6)

3.2 Preliminary design in flexure

A preliminary validation of the section design was done using AIS (Massicotte et al, 2014), a sectional analysis software, which performs a stress integration over a section, allowing for the calculation of the nonlinear flexural strength at all loading stages. The use of three types of longitudinal reinforcement for the lowermost layer was investigated: bonded T15 tendons, un-bonded T15 tendons and 30 mm diameter reinforcing bars. The case of normal concrete without fibres with bonded prestressing strands was also analysed. The moment-crack width response for two cases is presented in Figure 4 whereas the numerical values are given in Table 3. The design moment strength for service and ultimate conditions are also illustrated.

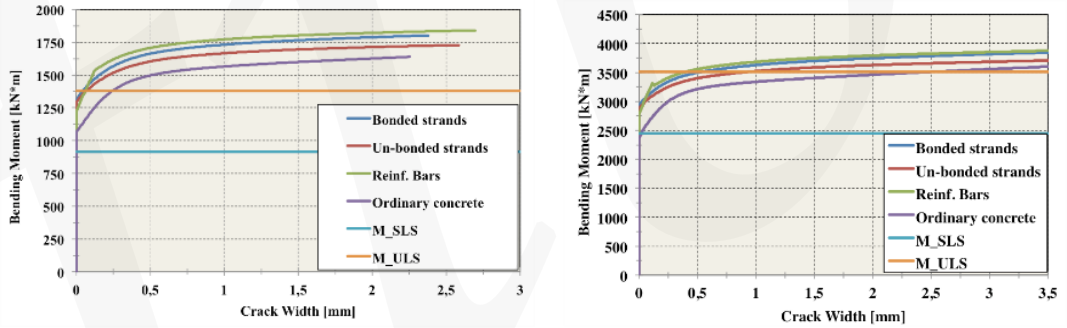
The maximum capacity is attained for all reinforcement configurations. The use of reinforcing bars or bonded tendons provides, as expected, a larger ultimate bending capacity than using unbonded tendons because the stress increase for unbonded tendons remains zero during the loading phases. Stress ranges in the longitudinal reinforcement are calculated

This document is the intellectual property of the fib – International Federation for Structural Concrete. All rights reserved.
This PDF of fib Bulletin 95 is intended for use and/or distribution solely within fib National Member Groups.

between the application of dead and live loads. This preliminary study tends to confirm that there are no substantial advantages in terms of carrying capacity, cracking pattern and stress range to privilege one type of longitudinal reinforcement for the bottom layer, as also found experimentally. The choice of unbonded strands for the lower layer could be recommended to limit the stress range associated with fatigue if cracking was allowed, which is not the case here.

Table 3: Design parameters for different bottom longitudinal reinforcements

15 m span	Bonded strands	Un-bonded strands	Reinforcing bars	Normal concrete
M_{cr} [kN-m]	1318	1299	1222	1072
M_r [kN-m]	1802	1729	1841	1639
$\Delta\sigma_{reinf.}$ [MPa]	63	0	64	63
20 m span	Bonded strands	Un-bonded strands	Reinforcing bars	Normal concrete
M_{cr} [kN-m]	2040	2016	1931	1582
M_r [kN-m]	2757	2649	2789	2579
$\Delta\sigma_{reinf.}$ [MPa]	65	0	74	54
25 m span	Bonded strands	Un-bonded strands	Reinforcing bars	Normal concrete
M_{cr} [kN-m]	2924	2874	2779	2384
M_r [kN-m]	3853	3721	3889	3615
$\Delta\sigma_{reinf.}$ [MPa]	57	0	94	98



(a) L =15 m (b) L = 25 m

Figure 4: Moment–crack width relations using different longitudinal reinforcements

3.3 Preliminary design for shear

The adopted transverse reinforcement consists of 15 mm diameter single-leg stirrups spaced s=h/2 (see Fig. 2). The shear resistance is calculated following the Canadian Bridge Code for the concrete (V_c) and reinforcement (V_s) contributions. The fibre contribution (V_F) was determined using Casanova and Rossi (1996) proposal such that:

$$V_r = V_c + V_s + V_F \quad (1)$$

$$V_c = \phi_c b_v d_v \beta \sqrt{f'_c} \quad (2)$$

$$V_s = \phi_s A_v f_y \left(d_v / s \tan\theta\right) \quad (3)$$

This document is the intellectual property of the fib – International Federation for Structural Concrete. All rights reserved.
This PDF of fib Bulletin 95 is intended for use and/or distribution solely within fib National Member Groups.

$$V_F = \phi_F b_v d_s f_F \quad (4)$$

For prestressed concrete girders, the contribution of the horizontal prestressing force is included in V_c through parameter β, equal to 0.4 in this case according to CSA-S6 (2014). The fibre contribution was taken as the post-cracking strength corresponding to a crack width of 1.5 mm as suggested in the Australian Code (Foster, 2016), equal to 1.25 MPa for the material properties used in this design (see Fig. 2). The validity of this assumption will be verified below. Table 4 presents the details of the calculated load effects and strength for the 3 selected spans.

Table 4: Preliminary design for shear

Span	V_c [kN]	V_F [kN]	V_s [kN]	V_r [kN]	V_f [kN]	V_f / V_r
15 m	325	122	187	634	490	0.77
20 m	407	152	187	746	590	0.79
25 m	488	182	187	857	680	0.79

3.4 Design validation

Design validation was carried out using nonlinear finite element analysis. SFRC behaviour was modelled by a concrete constitutive model EPM3D (Massicotte and Ben Ftima 2015) used as user's subroutine in Abaqus/Explicit (Hibbitt et al. 2014). EPM3D is a general model for the nonlinear analysis by finite elements of plain, reinforced, and fibre-reinforced concrete structures. The postcracking behaviour is considered as an intrinsic material property defined by a softening stress-crack opening σ-w response. The performance of the concrete constitutive model for SFRC was demonstrated by de Montaignac et al. (2013) for SFRC girders with flexural reinforcement, and by Cordoni (2015) for the behaviour of SFRC prestressed girders.

The primary goal of the nonlinear analyses is to validate the results obtained by the simplified approaches and to investigate more in detail the behaviour of the structure according to the load evolution up to the failure. Refined 3D models using typically 50 mm brick elements were developed for each girder type. Bending and shear behaviour were validated. For bending, a uniform load was applied on the model whereas for shear, a point load was applied at different distance from supports to obtain the most critical location.

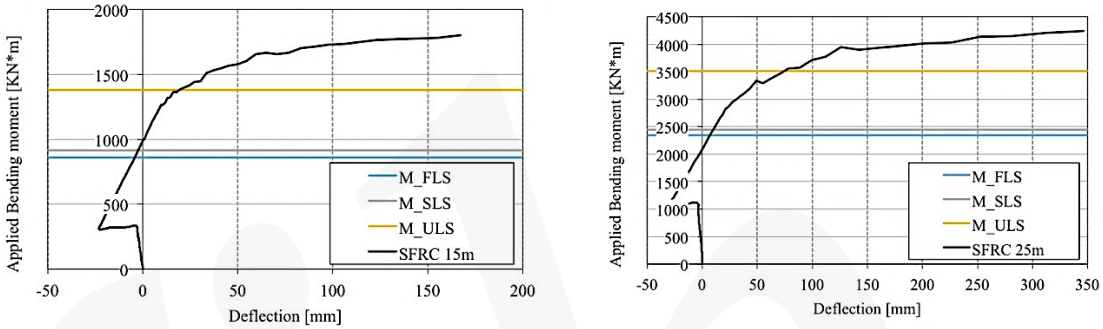
Figure 5 presents the moment deflection response of the 15 m and 25 m girders whereas Table 5 gives the main results for the three different spans analysed. These values can be compared to the preliminary responses presented in Figure 4 and in Table 3. NLFEA and simple sectional analysis provided very comparable results. In all cases NLFEA showed closely spaced cracks in service whereas a few cracks governed the behaviour at failure which was attributed to the rupture of presetressing strands.

The shear strength was validated in two ways: for the girder cross-section as designed, and also for the cross-section without stirrups in order to obtained the contribution to the shear strength of concrete and fibres. In all cases, the least shear resistance was obtained for a point load located at a distance equal twice the member depth from support. In this case the combined contribution of the fibres was determined equal to 1.45 MPa, which is slightly larger than the value of 1.25 MPa selected in the preliminary design.

This document is the intellectual property of the fib – International Federation for Structural Concrete. All rights reserved.
This PDF of fib Bulletin 95 is intended for use and/or distribution solely within fib National Member Groups.

Table 5: Nonlinear finite element analysis results

	M_r [kN-m]	Δ_{ULS} [mm]	$M_{1st\ crack}$ [kN-m]	$\Delta\sigma_{FLS}$ [MPa]	Δ_{SLS} [mm]
15 m	1833	209	1155	62	13
20 m	2880	291	1831	62	19
25 m	4242	347	2559	64	24



(a) L =15 m (b) L = 25 m

Figure 5: Moment–deflection behaviour obtained using NLFEA

4 Concluding remarks

The paper presented the predesign of three different T-cross-sections combining the contribution of SFRC and prestressing for bridges spanning 15, 20 and 25 m. The preliminary design carried out by simplified methods was verified using nonlinear finite element analysis. The final sections respect the design criteria chosen for SLS, FLS and ULS. The most restrictive design criterion was the deflection calculated at the serviceability limit state. This criterion forced to increase the height of the sections with respect to the initial idea in the previous research project. In doing so, no cracking was obtained in service conditions in the girders. The study highlighted a pronounced ductility offered by the addition of the fibres both for bending failure and shear failure.

At ULS, even if the fibre contribution to bending capacity is marginal, steel fibres offer an important gain in terms of shear capacity. A simple formula, which considers an average tensile strength offered by fibres along the diagonal shear crack, seems to be an efficient and quick way to determine the fibre contribution to the shear resistance. Selecting the tensile strength from the post-cracking tensile relation at a crack width of 1.5 mm yielded sensible results. However, this method still requires further investigation for considering the influences of governing parameters such as cross-section geometry, aggregate size, prestressing level, and fibre characteristics.

5 Acknowledgements

The authors gratefully acknowledge the financial support which was provided by the Natural Sciences and Engineering Research Council of Canada, the Quebec Granting Agency (FRQNT) and the Quebec Ministry of Transportation.

This document is the intellectual property of the fib – International Federation for Structural Concrete. All rights reserved.
This PDF of fib Bulletin 95 is intended for use and/or distribution solely within fib National Member Groups.

6 References

AFGC, 2013. Ultra-high performance fibre-reinforced concretes – French recommendations. Association Française du Génie Civil, Paris, France.

DR AS 5100.5 (2014), *Draft for Public Comment Australian Standard, Bridge Design Part 5:Concrete*, Standards Australia, Sydney, Australia.

Bélanger, A. (2000), *Design of SFRC bridge decks with reduced reinforcement*. M.A.Sc. Thesis, Polytechnique Montreal, Montreal, Canada. (In French).

Casanova, P., Rossi, P. (1996), *Analysis of metallic-fibre reinforced concrete beams submitted to bending*. Materials and Structures, 29, 354-361.

CSA (2014), *Canadian Highway Bridge Design Code - CSA-S6-14*. Canadian Standard Association, Toronto, Ontario, Canada.

CSA (2019), *Canadian Highway Bridge Design Code - CSA-S6-19 Draft*. Canadian Standard Association, Toronto, Ontario, Canada.

De Broucker, W. (2013). *Flexural and shear behaviour of prestressed SFRC girders*. M.A.Sc. Thesis, Polytechnique de Montréal, Montreal, Canada. (In French).

de Montaignac, R.; Massicotte, B.; Charron, J.-P. (2013), Finite element modelling of SFRC members in bending. Magazine of Concrete Research, 65(10), 1122-1146.

Faggio, L. (2014). Design of SFRC T-girder flanges with UHPFRC fiel-cast joints. Polytechnique Montréal. (In French).

Graybeal, B. A. 2014. Design and Construction of Field-Cast UHPC connections. Rapport FHWA-HRT-14-084, Federal Highway Administration, Virginia, USA.

fib, International Federation for Structural Concrete (2012). Model code 2010, Final Complete Draft, Bulletins 65 and 66, March 2012-ISBN 978-2-88394-105-2 and April 2012-ISBN 978-2-88394-106-9

Foster, S. 2016. FRC design according to the draft Australian bridge code. Fibre Reinforced Concrete: from Design to Structural Applications - FRC 2014: ACI-*fib* International Workshop, Editors: B. Massicotte, J.-P. Charron, G. Plizzari, B. Mobasher, FIB Bulletin 79 – ACI SP-310, 29-40.

Hibbitt, H.D.; Karlson, B.I.; Sorensen, E.P. (2014), ABAQUS version 6.14, finite element program. Hibbitt, Karlson and Sorensen, Providence, R.I., USA.

Marleau, B. and Massicotte, B. 2019. Fatigue performance on field-cast connections in UHPFRC. Research report SR18-02, GRS, Polytechnique Montreal, Montréal, Canada (in French).

Massicotte, B., Forget, M., Conciatori, D. 2012. Development of entirely precast bridges – Design of a new girder type. Research report. Polytechnique Montréal, Montreal, Canada. (In French).

Massicotte, B.; Ben Ftima, M. (2015), EPM3D-v3.4- A user-supplied constitutive model for the nonlinear finite element analysis of concrete structures. Research report SR15-01, Polytechnique Montreal, Canada.

Massicotte, B., Faggio, L., Cordoni, N., Nour, A. and Conciatori, D. 2016. Design and construction of SFRC bridge decks: Building on past experiences and recent developments. Fibre Reinforced Concrete: from Design to Structural Applications - FRC 2014: ACI-*fib* International Workshop, Editors: B. Massicotte, J.-P. Charron, G. Plizzari, B. Mobasher, FIB Bulletin 79 – ACI SP-310, 419-434.

Namy M., Charron, J.-P., Massicotte, B. 2015. Structural behavior of cast-in-place and precast concrete barriers subjected to transverse static loading and anchored to bridge deck overhangs. Can. Journal of Civil Eng. 42 (2), 120-129.

This document is the intellectual property of the fib – International Federation for Structural Concrete. All rights reserved.
This PDF of fib Bulletin 95 is intended for use and/or distribution solely within fib National Member Groups.
FRC2018: Fibre Reinforced Concrete: from Design to Structural Applications
Joint ACI-*fib*-RILEM International Workshop

FRC Hybrid slabs: reliability of Model Code approaches

Ali Pourzarabi[1], Matteo Colombo[1], Paolo Martinelli[1], Marco di Prisco[1]

[1] : Politecnico di Milano, Department of Civil and Environmental Engineering, Milan, Italy.

Abstract

Fibre reinforced concrete (FRC) material is characterized by a high intrinsic scatter in the results when tested according to standard notched beams. However, it is observed that structures affected by a high stress redistribution show a significantly reduced scatter in their structural behaviour. Therefore, the use of the characteristic material constitutive parameters from a standard test leads to overly conservative design. The Model Code 2010 has introduced a coefficient, named structural redistribution factor, that is able to take into account a reduced variability of the structural response, when compared to that identified from a standard material test.

The paper investigates the behaviour of FRC slabs to highlight the difference in structural response of FRC elements with respect to the expected response computed according to the standard specimens used for material characterization. To this aim, FRC slabs of 2×2 m, 15 cm thick, supported on four points at the mid-span of each side, are tested under a point load. Different slab solutions (R/C, FRC only and a Hybrid solution with FRC and steel rebars) are compared and discussed. The material considered can be classified as 5b according to Model Code 2010. A yield line approach is also adopted to validate the formulation proposed by Model Code 2010 for the structural redistribution factor in the cases investigated.

Keywords

Fibre reinforced concrete, redistribution factor, redundancy, heterogeneity, yield line, slab.

This document is the intellectual property of the fib – International Federation for Structural Concrete. All rights reserved.
This PDF of fib Bulletin 95 is intended for use and/or distribution solely within fib National Member Groups.

1 Introduction

The advent of design guidelines and codes for structural applications of fibre reinforced concrete is opening the door for engineers and designers to exploit the enhanced properties of fibre reinforced concrete (FRC), both in serviceability and ultimate limit state. The Model Code 2010 (MC 2010, 2012) has proposed two stress-crack opening laws in uniaxial tension defined for the post-cracking behavior of FRC. The development of these tensile post-cracking relationships is derived from a standard three-point bending test (3PB) on notched specimens which results are expressed in stress-Crack Mouth Opening Displacement (CMOD). The residual stress values at a CMOD of 0.5 mm (corresponding to SLS condition) and 2.5 mm (corresponding to ULS condition), named respectively f_{R1} and $f_{R3,}$ are related to uniaxial post-cracking tensile behavior through a simplified inverse analysis based on equilibrium (di Prisco et al. 2016).

While a 3PB test according to EN 14651 (EN 14651, 2005) is an accepted method for the characterization of FRC, the results obtained from such a test, suffer from a high scatter, which is mainly due to the small fracture plane, the low number of fibres in the ligament area (Bernard and Xu, 2017; Minelli and Plizzari, 2011), and the fibre distribution (Colombo et al., 2017). The high dispersion of the post-peak tensile properties obtained from bending tests leads to smaller characteristic values of residual strength parameter, directly affecting the design strength parameters. Nevertheless, it has been observed that for structures capable of redistributing stresses, and in which large crack surfaces dominate the failure process, even if the material topological variability in the structure remains high (di Prisco et al., 2016b), the structural behavior shows a very low dispersion (Sorelli et al., 2006). Accordingly, design of a FRC structure with characteristic values of parameters obtained from a highly scattered testing modality leads to over-conservative design solutions and may downplay the cost-competitiveness of FRC as a structural material.

There are some references in the literature (CNR-DT 204, 2006; di Prisco et al. 2009; DaftSb, 2014) which propose methods for taking into account the redistribution capacity of the structure and the volume involved in the fracture process, to compensate for the low characteristic values of the material properties. MC 2010 (MC 2010, 2012) proposes the application of a redistribution factor, $K_{RD,}$ which is explained in the following section.

2 Redistribution factor definition

According to the MC 2010, if a FRC structure is able to redistribute stresses, the design resistant load, $P(f_{Fd})$ could be increased through the introduction of the K_{Rd} factor to obtain the ultimate design resistant load, P_{Rd}:

$$P_{Rd} = K_{Rd} P(f_{Fd}) \tag{1}$$

The MC 2010 (MC 2010, 2012) proposes a structural analysis considering a heterogenous material that is randomly assigned to different cells in the structure as the basis for K_{Rd} computation. The constitutive material parameters, f_{R1} and $f_{R3,}$ defining the post peak residual resistance of FRC, are assumed to have a normal distribution starting from the statistical parameters obtained from characterisation test, based on which a probability distribution is obtained for the load carrying capacity of the structure, P^{max}. MC 2010 suggests the following relationship for the K_{Rd} estimation:

This document is the intellectual property of the fib – International Federation for Structural Concrete. All rights reserved.
This PDF of fib Bulletin 95 is intended for use and/or distribution solely within fib National Member Groups.

$$K_{Rd}^{MC} = \frac{P_{rand,k}^{\max}}{P_{rand,m}^{\max}} \frac{f_{Ftu,m}}{f_{Ftu,k}} \leq 1.4 \tag{2}$$

In eq. 2 subscripts "k" and "m" refer to the characteristic and mean value of the variables and the "rand" subscript, indicates that the variables are derived considering a random distribution of the material constitutive properties. $f_{Ftu,m}$ and $f_{Ftu,k}$ are the mean and characteristic value of the ultimate residual tensile FRC strength . Other definitions have been recently introduced for the redistribution factor (di Prisco et al., 2016a), specifically suited for ductile structure that are able to sustain large CODs. These expressions are as follows:

$$K_{Rd3} = \frac{P_{rand,k}^{u}}{P_{rand,m}^{u}} \frac{f_{Ftu,m}}{f_{Ftu,k}} \tag{3}$$

$$K_{Rd4} = \frac{P_{rand,k}^{u}}{P_{\hom,k}^{u}} \tag{4}$$

The P^u term in both expressions refer to the ultimate load. In K_{Rd3}, P^u is substituted by the P^{max} in the original expression proposed by MC 2010 (MC 2010, 2012). Clearly, for structure that exhibit a global ductile behaviour, K_{Rd3} and K_{Rd}^{MC} will be equal. The $P_{\hom}^{u}$ term in K_{Rd4} is derived from a single analysis considering the homogenous distribution of material properties.

The definition of redistribution factor presented in the new revision of the Eurocode 2, κ_G, is equal to K_{Rd4} with the difference that it will be only applied to the design value of FRC constitutive tensile strength, $f_{Ftu,k}/\gamma_F$, instead of multiplying directly the ultimate design load.

2.1 Computation of the K_{Rd}

Computation of the K_{Rd} factor is possible through a nonlinear finite element model (NLFEM) (di Prisco et al., 2016), a yield line approach (Colombo et al., 2017), or through empirical formulas that take into account fracture volume and/or the redistribution capacity (CNR-DT 204, 2006; DaftSb, 2014). While a NLFEM is capable of taking into account both the redistribution capacity and the fracture volume, a yield line approach accounts only for the fracture volume. However, results reported in (di Prisco et al., 2018) show comparable results obtained from both methods for K_{Rd} estimation, with the yield line approach being easier to implement. Hence, in the present work the yield line approach is implemented for the K_{Rd} computation.

In a yield line approach, the material heterogeneity is introduced by a discretization of the yield line and by assigning to each segment of this discretization a random value of the material properties. To do so, a normal distribution is considered for the post-peak material parameters, f_{R1} and f_{R3}, with the estimates of the mean value and its standard deviation taken from the characterization tests. A linear elastic-linear softening material model is assigned to each yield line segments by assuming a random value of the percentile (assumed to be equal for f_{R1} and f_{R3}) and thus computing the corresponding value of f_{R1} and f_{R3} and therefore of f_{Fts} and f_{Ftu}. In this way, by using these stochastic material parameters, the ultimate bending moment per unit width, m_u, can be also derived by means of a plane section approach. The ultimate moment per unit width, m_u, is a function of the stochastic variables; therefore, P^u results to be a random quantity. The mean and characteristic values of the ultimate load, P^u, and the ultimate limit state residual tensile strength of the FRC, f_{ftu}, are used to derive the K_{Rd} factor.

This document is the intellectual property of the fib – International Federation for Structural Concrete. All rights reserved.
This PDF of fib Bulletin 95 is intended for use and/or distribution solely within fib National Member Groups.

3 Experimental program

The experimental program reported in this work consists of the results obtained from 9 standard notched specimens tested in a three-point bending setup, and 6 concrete slabs with dimensions of 2×2×0.15 m tested under a concentrated central load and supported on four supports at midspan of each side. Two nominally identical tests were performed for each case under study.

Three different slab solutions were studied: SFRC without any reinforcement (SFRC: SF1 and SF2), plain concrete with steel rebars in two directions (R/C: R1 and R2) and a Hybrid solution in which fibre reinforcement was used together with traditional steel rebars (Hybrid: Hyb1 and Hyb2). Figure 1a shows a picture with the general set-up of the slab tests.

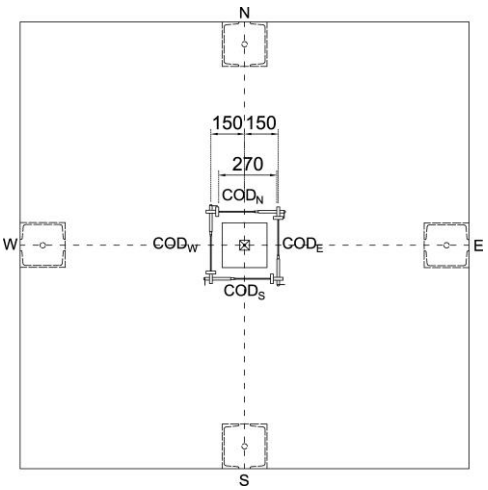
3.1 Material and specimen preparation

The mix design of the SFRC used in the study is given in Table 1. The plain concrete used resembles the SFRC with the exclusion of the fibres. A self-consolidating concrete with a mean compressive strength of 58 MPa, containing 35 kg/m^3 of Dramix® 4D fibre by Bekaert with a length of 60 mm and diameter of 0.9 mm was utilized.

The tests here presented are part of a larger experimental campaign in which a global number of 29 prismatic beams and 32 slabs were cast. The prismatic beams, used for the mechanical characterization were cast with the same SFRC used for the slabs (Table 1). For both Hybrid and R/C slabs two orders of reinforcement were adopted at the bottom of the slabs with a minimum cover of 30 mm. In both the cases (Hybrid and R/C), the two orders of reinforcement are parallel to the slab sides and are made of 12ϕ12 mm steel rebars. All the specimens were cast in a job site where the plain and fibre reinforced concrete were delivered by a truck and the molds were filled by pumping the concrete directly from the truck. Vibration was not applied, and the slabs were cast from the centre of the molds. After casting, the specimens were covered with wet burlaps for some days and afterwards, they were left in atmospheric condition until the testing days.



(a)



(b)

Figure 1: (a) slab test setup (b) configuration of the LVDTs at the bottom of the slab shown from the top view

This document is the intellectual property of the fib – International Federation for Structural Concrete. All rights reserved.
This PDF of fib Bulletin 95 is intended for use and/or distribution solely within fib National Member Groups.

Table 1: material mix design

Cement (Cem IV 42.5R) (kg/m^3)	380
Sand 0/4 (kg/m^3)	425
Sand 0/8 (kg/m^3)	850
Gravel 8/14 (kg/m^3)	425
Slag (kg/m^3)	100
w/b	0.36
Fibre (kg/m^3)	35
Superplasticizer (% of cement weight)	1.2

3.2 Testing and instrumentation

The three-point bending tests were carried out according to EN 14651 (2005) on notched prismatic beams of 600×150×150 mm with a clear span of 500 mm and a three-point bending scheme. The CMOD is measured by a clip gauge and nominal stress vs. CMOD curves are obtained for each specimen.

The slabs were tested under a central concentrated load and they were supported at the mid-length of each side on square steel plates of 20×20×2.5 cm. An electro-mechanical jack with a capacity of 1000 kN was used and a constant displacement rate of 20 µm/sec was imposed to the loading head. A piece of neoprene sheet was placed between the slab and supports and beneath the loading point to prevent the direct contact of steel on concrete. An anchorage device was adopted to connect the slab to the supports by screwing a 20 mm bolt. Among the measurements carried out on each slab, 5 are chosen to be discussed in this paper which are, the vertical deflection under the loading point measured by a potentiometer and 4 Crack Opening Displacement (COD) measurements taken in a square configuration in the central region beneath the slab by as many Linear Variable Displacement Transducers (LVDT). The gauge length is about 27 cm and the position of the instruments used are shown in Figure 1b.

4 Discussion of experimental results

Figure 2 shows the nominal stress - CMOD results obtained from the standard notched specimens and Table 2 reports the mean value, standard deviation (SD), coefficient of variation (CV), and the characteristic strength values according to a log-normal distribution for flexural tensile strength ($f_{ct,Fl}$), and post peak residual strength values (f_{R1}, f_{R2}, f_{R3}, and f_{R4}) according to MC 2010. Based on the provisions of the MC 2010, the SFRC material could be classified as a "5b" material. It is evident that there is a significant scatter in the results obtained from the characterization test with a CV varying between 14% to 26% for the residual strength parameters remaining in a common range for dispersion of residual strength properties.

Figures 3a and 3b illustrate the load-deflection and load-COD results obtained for the 6 slabs tested. COD value represented in this figure is the average between the different COD measurements (COD_N, COD_S, COD_W, COD_E). In Figure 3a the load-deflection curve for R1 specimen is not shown due to problems in recording the deflection of this slab.

This document is the intellectual property of the fib – International Federation for Structural Concrete. All rights reserved.
This PDF of fib Bulletin 95 is intended for use and/or distribution solely within fib National Member Groups.

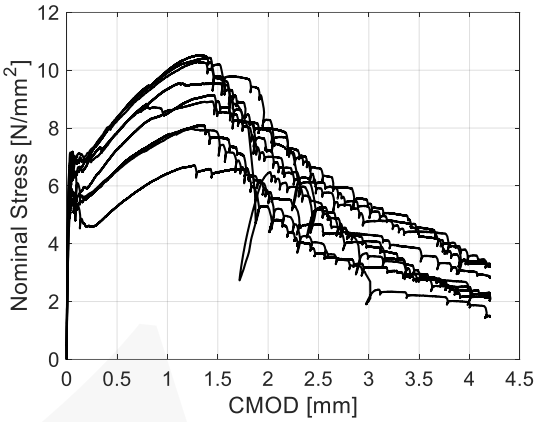


Figure 2: Stress-CMOD results obtained from the three-point bending test

Table 2: Three-point bending test results according to provisions of MC 2010

	f_{ct-fl}	f_{R1}	f_{R2}	f_{R3}	f_{R4}
Mean (MPa)	6.32	7.36	8.73	5.2	3.39
SD (MPa)	0.53	1.05	1.22	0.96	0.88
CV	0.08	0.14	0.14	0.18	0.26
Characteristic (MPa)	5.34	5.39	6.48	3.5	1.97

It is worth to note that while there is a significant scatter in the results obtained for the SFRC notched specimen, the overall structural behavior of the two slabs made of SFRC (SFi) is very repeatable both in terms of deflection and cracking up to the deflection corresponding to the first crack localization, that occurs at different deflections for the two slabs. This indicates the need for the introduction of a coefficient which can take into account the effect of both the structural redundancy and the fractured volume involved in the collapsing mechanism to predict the load bearing capacity of FRC structures.

The predefined failure plane on a notched specimen having a small surface area that is largely influenced by the orientation and number of fibres, causes the high variability of the material behavior. At a structural level, due to the stress distribution capacity and the larger volume involved in the failure process, the behavior becomes closer to the mean behavior identified in the standard characterization tests. Next section focuses specifically on this issue.

Looking at load vs. deflection curves, R1 and R2 slabs abandon the linear behavior before than SFRC and Hybrid ones. The divergence occurs at approximately 120 kN in the load-deflection behavior and at roughly 50 kN in the load-COD measurement. At these load levels, while the R/C slabs undergo a significant reduction in the slope, whether considering deflection or cracking behavior, the slabs incorporating steel fibres go through a smooth nonlinear response, up to about 200 kN. At this load level, both deflection and COD for the R/C slabs are almost twice of those of the SFRC and Hybrid slabs.

The deflection for SFRC and Hybrid slabs at 200 kN is in the range of 3 to 3.6 mm, while the R2 slab sustains a deflection of 6.5 mm. Considering the COD, the SF1 and SF2 slabs experience a crack opening of 0.55 mm, and Hyb1 and Hyb2 slabs sustain a COD of 0.38 and 0.5 mm, however the COD for R1 and R2 slabs is 1 and 1.25 mm. After 200 kN, the SFRC

This document is the intellectual property of the fib – International Federation for Structural Concrete. All rights reserved.
This PDF of fib Bulletin 95 is intended for use and/or distribution solely within fib National Member Groups.

slabs go through a new phase which seems to be dominated by the pull-out mechanism of the fibres.

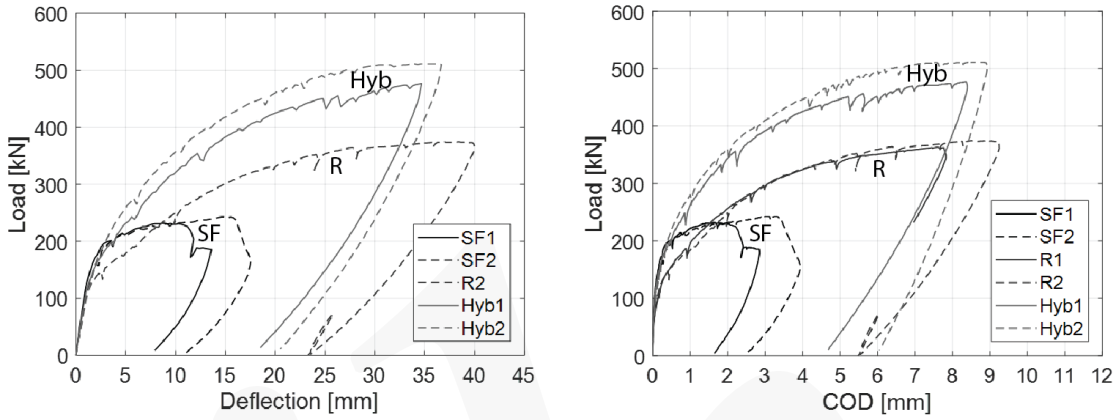


Figure 3: Results obtained for 6 slab tests (a) load-deflection and (b) load-COD

During this phase, there is an increase of 5% and 10% in the load for SF1 and SF2 slabs reaching the maximum load of 232 and 243 kN at a deflection of 10.3 and 15.4 mm respectively.

Clearly, slabs with reinforcing rebars, provide a much higher deflection capacity compared to the SFRC slabs. Both R/C and Hybrid series continue to attain higher loads until there is the yielding of the reinforcements, at which the response goes towards a plateau. The maximum load reached for R1, R2, Hyb1 and Hyb2 slabs before stopping the tests are 363, 374, 478, and 511 kN respectively corresponding to a deflection of 39.3 mm for R2 and 34.7 and 36.4 mm for Hyb1 and Hyb2, and a COD of 7.7, 9.1, 8.3, and 8.8 the four specimens respectively.

5 Yield line approach for K_{Rd} estimation

In the present work, the yield line approach is adopted for the SFRC and Hybrid series in order to find the redistribution factor by introducing the material heterogeneity. It is also used for the R/C slab with both the characteristic and mean values of homogenous material. The yield line pattern is chosen to form a circular fan, which is liable to occur for slabs under a concentrated load (Park and Gamble, 2000) and is in accordance with the experimental failure mechanism as shown in Figure 4a for a general case of Hybrid slab. The failure mechanism adopted is shown in Figure 4b. To introduce material heterogeneity, the yield line is discretised into 50 slices on the perimeter of the circular fan, and each positive yield line is divided into 10 segments. A total number of 200 simulations are carried out to take into account material heterogeneity. The internal and external works taking into account the effect of self-weight can be defined as follow:

$$W_I = \left[\sum_{i=1}^{50}\left(m_{xi}^{-}cos^2\phi_i + m_{yi}^{-}sin^2\phi_i\right)\Delta\phi + \frac{1}{R}\sum_{i=1}^{50}\sum_{j=1}^{10}\left(m_{xij}^{+}sin^2\phi_i + m_{yij}^{+}cos^2\phi_i\right)\Delta r\,\Delta\phi\right]\delta$$

$$W_I = \left[\sum_{i=1}^{50} m_{ri}^{-}\,\Delta\phi + \frac{1}{R}\sum_{i=1}^{50}\sum_{j=1}^{10} m_{ri}^{+}\Delta r\,\Delta\phi\right]\delta \qquad (5)$$

This document is the intellectual property of the fib – International Federation for Structural Concrete. All rights reserved.
This PDF of fib Bulletin 95 is intended for use and/or distribution solely within fib National Member Groups.

$$W_E = P\delta + \frac{q\pi R^2 \delta}{3} \tag{6}$$

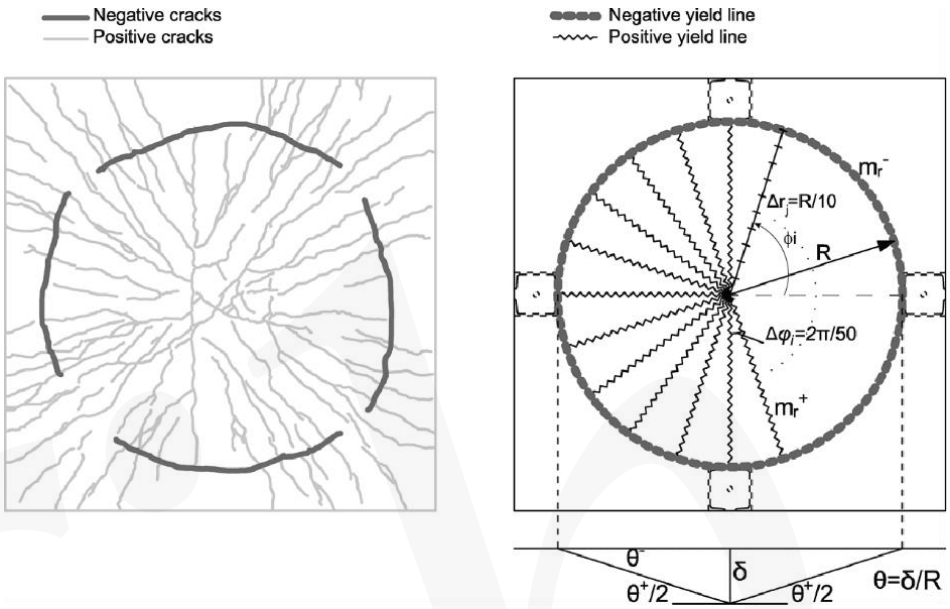


Figure 4: (a) crack pattern of a Hybrid specimen (b) the yield line pattern and the parameters used in the discretization

In Eqs. (5) and (6) P is the concentrated load, δ is the vertical displacement of the centre of the slab, R is the radius of the circular fan, m_r^+ and m_r^- are the positive and negative ultimate bending moments on the yield lines, m_x^+ and m_y^- are the ultimate positive and negative bending moments in the direction of the reinforcements, and $\Delta\varphi_i$ and Δr_j are the discretisation intervals on the angle and the radius segment length of the circular fan. The heterogeneity has been introduced assigning to each segment a random value of the resistant bending moment per unit width as described in par. 2.1.

The ultimate loads obtained for the slabs in different circumstances are given in Table 3. Also the value of the safety factor is given in the same table for each solution. $P^u_{exp,m}$ is the mean value of the ultimate load obtained in the experiments. $P^u_{rand,m}$ values are obtained considering the average response taking into account material heterogeneity, by introducing a random assignment of the material parameters, f_{R1} and f_{R3} into the segments of the yield lines (Colombo et al., 2017). $P^u_{hom,m}$ and $P^u_{hom,k}$ are obtained respectively by carrying out a single simulation with the mean and characteristic values of post-peak residual strength assumed as homogenous. $P(f_{Fd})$ is the design load for the slabs worked out from the yield line method considering characteristic material properties and a safety factor of 1.5 at the material level. It is evident that considering heterogeneity of the material in the yield line analysis leads to very low dispersion for the ultimate load with a standard deviation of 1.77 and 1.51 kN for the SFRC and the Hybrid slabs respectively. It is also interesting to notice that the chosen failure mechanism is a very close approximation of the ultimate experimental load.

Table 4 gives the values for the redistribution factors K_{Rd}^{MC}, K_{Rd3}, K_{Rd4}, κ_G, the corresponding ultimate design loads computed based on these coefficients, and the safety factor obtained as the ratio of the ultimate experimental load to the obtained ultimate resistant design load. Examining K_{Rd3}, given that the $P^u_{rand,m}$, and $P^u_{rand,k}$ are very close, the redistribution factor is

This document is the intellectual property of the fib – International Federation for Structural Concrete. All rights reserved.
This PDF of fib Bulletin 95 is intended for use and/or distribution solely within fib National Member Groups.

mainly influenced by the material ratio, $f_{Ftu,m}/f_{Ftu,k}$, which gives close values of 1.66 and 1.67 for the SFRC and Hybrid slabs respectively. Looking at K_{Rd4} a value of 1.48 is obtained for the SFRC slab. However, as the behaviour of the Hybrid slab is mainly controlled by the reinforcements, the introduction of the heterogeneity derived from the SFRC material has less influence on the ultimate load estimation. Therefore, a smaller redistribution factor of 1.17 is computed for this case. Given the global deflection capacity of the slabs, the value of K_{Rd}^{MC} coincides with K_{Rd3}, consequently, the upper bound of 1.4 is chosen.

Concerning the safety factors, and referring to Table 3 for the R/C slab, a safety factor of 1.88 is obtained, while following the method proposed in the MC 2010, a safety factor of 1.64 and 1.25 is obtained for the SFRC and Hybrid slabs, and following the method proposed in the new revision of Eurocode 2 a safety factor of 1.99 and 1.80 is obtained for the SFRC and Hybrid specimens. It should be considered that the higher value of safety factor after introduction of the κ_G for the Hybrid case, 1.80, compared to the original one obtained based on design values of material properties, 1.75, is due to the fact that in the definition of tensile constitute law for FRC in the new revision of Eurocode 2, the characteristic values of residual strength values, $f_{R,1k}$ and $f_{R,3k}$, are limited to 0.6× $f_{R,1m}$ and 0.6× $f_{R,3m}$ which are adopted for the current computation. It is noticed that if the designer applies the K_{RD} factor to the whole resistant load, no distinction is made between the fibre contribution and the contribution of the conventional reinforcement.

Table 3: Results obtained for the ultimate load from the yield line approach

Load	**Slab type**		
	SFRC	**R/C**	**Hybrid**
$P^u_{exp,m}$ [kN]	237.5	368.6	494.5
$P^u_{rand,m}$ [kN]	233.45	-	467.29
$P^u_{rand,k}$ [kN]	230.52	-	464.78
P^u_{std} [kN]	1.77	-	1.51
$P^u_{hom,m}$ [kN]	233.9	259.7	467.43
$P^u_{hom,k}$ [kN]	155.3	198.9	397.16
$P(f_{Fd})$ [kN]	103.6	195.9	282.4
$\gamma = P^u_{exp,m} / P(f_{Fd})$	2.29	1.88	1.75

Table 4: The redistribution factor obtained for the SFRC and Hybrid series.

K_{Rd} **definition**	**SFRC**			**Hybrid**		
	K_{Rd}	P_{Rd}	$\gamma = P^u_{exp,m} / P_{Rd}$	K_{Rd}	P_{Rd}	$\gamma = P^u_{exp,m} / P_{Rd}$
K_{Rd3}	1.66	172	1.38	1.67	471.6	1.04
K_{Rd4}	1.48	153.3	1.55	1.17	330.4	1.50
K_{Rd}^{MC}	1.4	145	1.64	1.4	395.4	1.25
κ_G	1.48	119.5	1.99	1.17	275.5	1.80

This document is the intellectual property of the fib – International Federation for Structural Concrete. All rights reserved.
This PDF of fib Bulletin 95 is intended for use and/or distribution solely within fib National Member Groups.

6 Concluding remarks

The present work investigates the effect of stress redistribution and fracture volume on structural behavior of FRC structural slabs. To this aim, nine standard notched specimens and six concrete slabs reinforced with steel fibres, reinforcing bars and their hybrid combination were tested and the redistribution factor, K_{Rd} was obtained for different cases based on a yield line approach.

The results clearly showed the need for a coefficient to compensate for the high variability of characterization test results. The yield line method adopted for computation of the K_{Rd} for the SFRC slab, shows that the value of 1.4 chosen as the upper bound in the MC 2010 for the redistribution factor, is a safe limit. The κ_G approach suggested in the Eurocode Annex by TC250/ SC2/ WG1/TG2 committee is able to guarantee a safety coefficient γ for SFRC only and Hybrid slabs comparable with that of R/C slab.

7 References

Bernard, E.S. and Xu, G.G., (2017). *Influence of fibre count on variability in post-crack performance of fibre reinforced concrete*, Materials and Structures, 50(3):169.

CNR-DT 204 (2006). Guidelines for design, construction and production control of fibre reinforced concrete structures, National Research Council of Italy.

Colombo, M., Martinelli, P. and di Prisco, M., (2017). *On the evaluation of the structural redistribution factor in FRC design: a yield line approach*. Materials and Structures, 50(1):100.

DafStb Guideline (2014). Steel fibre reinforced concrete, German Committee for reinforced concrete

di Prisco, M., Plizzari, G.A., Vandewalle, L., (2009). *Fiber reinforced concrete: new design perspectives*, Material & Structures, 42 (9) 1261-1281.

di Prisco, M., Martinelli, P. and Dozio, D., (2016a). *The structural redistribution coefficient K_{Rd}: a numerical approach to its evaluation*. Structural Concrete, 17(3), 390-407.

di Prisco M, Martinelli P, Parmentier B (2016b). *On the reliability of design approach for FRC structures according to MC2010: the case of elevated slabs*, Structural Concrete, (4), 588-602.

di Prisco, M., Martinelli, P and Colombo, M. (2018). *On the Design Response of a FRC Statically Undetermined Structure*. In: High Tech Concrete: Where Technology and Engineering Meet, 422

EN 14651 (2005). CEN, *Test method for metallic fibre concrete. Measuring the flexural tensile strength (limit of proportionality (LOP), residual,* CEN, p. 20.

fib, International Federation for Structural Concrete (2012). Model code 2010, Final Complete Draft, Bulletins 65 and 66, March 2012-ISBN 978-2-88394-105-2 and April 2012-ISBN 978-2-88394-106-9.

Minelli, F. and Plizzari, G., (2011). *A new round panel test for the characterization of fiber reinforced concrete: a broad experimental study*. Journal of testing and evaluation, 39(5), 889-897.

Park, R. and Gamble, W.L., (2000). Reinforced concrete slabs. John Wiley & Sons.

Sorelli, L.G., Meda, A. and Plizzari, G.A., (2006). *Steel fiber concrete slabs on ground: a structural matter*. ACI Structural Journal, 103(4), 551.

This document is the intellectual property of the fib – International Federation for Structural Concrete. All rights reserved.
This PDF of fib Bulletin 95 is intended for use and/or distribution solely within fib National Member Groups.
FRC2018: Fibre Reinforced Concrete: from Design to Structural Applications
Joint ACI-*fib*-RILEM International Workshop

Optimization of partially prefabricated HyFRC slabs

Giulio Zani[1], Matteo Colombo[1], Claudio Failla[2], Marco di Prisco[1]

[1] : Politecnico di Milano, Dept. of Civil and Environmental Eng., Milano, Italy.

[2] : Magnetti Building, Carvico (BG), Italy.

Abstract

A new partially prefabricated elevated slab has been recently introduced in two different industrial buildings, to propose a viable alternative to the classical double tee deck with the addition of an in-situ RC topping. The solution is characterized by an adjustable spacing in the orthogonal direction, 40 mm thick FRC plates used as *predalles* and a cast-in-place FRC finishing, designed according to a continuous slab resting on the simply-supported beams. The proposed deck is a structural solution that tries to fit different issues like construction speed, transport and cost reduction, structural optimization, high fire resistance (R120) and quality performance. All elements are made of SFRC, characterized by different mix designs. This paper presents a design investigation on this kind of floor element, aimed at optimizing the global structural solution by minimizing the whole floor weight. Longitudinal and transverse bending, as well as vibration limit state, were considered in the design. The optimization strategy will be here presented, through the discussion of the parameters considered in the design, the variables taken into account and the constraints adopted within the procedure. A Model Code 2010 design approach was followed.

Keywords

Elevated slab; HyFRC; SFRC; fiber-reinforced concrete; precast concrete; prestressed concrete; structural optimization

This document is the intellectual property of the fib – International Federation for Structural Concrete. All rights reserved.
This PDF of fib Bulletin 95 is intended for use and/or distribution solely within fib National Member Groups.

1 Introduction

Steel Fiber Reinforced Concrete elevated slabs are an interesting design solution, because they can simultaneously guarantee robustness, high construction speed, flexibility and economy, especially if combined with conventional reinforcement disposed only in limited zones (di Prisco et al. 2014). This last concept allows the designer to use both a diffused reinforcement (fibers), valid at the same time for bending, shear and punching, and a concentrated reinforcement optimized in its alignment only in critical areas, where crack propagations followed by localizations require an increased bending or shear resistance to face the effective loads at serviceability and ultimate limit states. The possibility to calibrate the structural reinforcement is one of the main advantages of RC structures, because it allows to better use the material resources and reduces the ductility requirements called to reach the maximum bearing capacity of the whole structure. In the paper, an industrial deck solution (di Prisco et al., 2016) aimed at combining both the advantages of prefabrication and cast-in-place solutions is investigated. Classical TT elements are substituted by pre-stressed prefabricated beams, designed to reach a high fire resistance, and thin prefabricated slabs with integrated lattice girders (*predalles*), resting on the top chords of the beams. These latter elements allow to increase and adjust the spacing of the beams, reducing the transport costs without penalizing the construction speed. The final cast-in-place layer guarantees a two-way stiffness, not only in its own plane, but also in bending, thus profiting of the slab redundancy. Starting from two existing case studies, the paper describes a design optimization aimed at minimizing the global weight of the structural solution. This investigation follows the Model Code provisions (di Prisco et al 2009, di Prisco et al. 2013, EN 14651 2005, *fib* 2013) and represents a preliminary approach, since further developments are needed to guarantee a comprehensive structural design.

2 Structural solution

The structural solution investigated in this paper is a composite slab consisting of longitudinal precast and prestressed FRC beams simply supporting thin prefabricated components (*predalles*) integrated with steel lattice girders embedded in a cast-in-place SFRC aimed at guaranteeing longitudinal and transverse continuity of the floor.

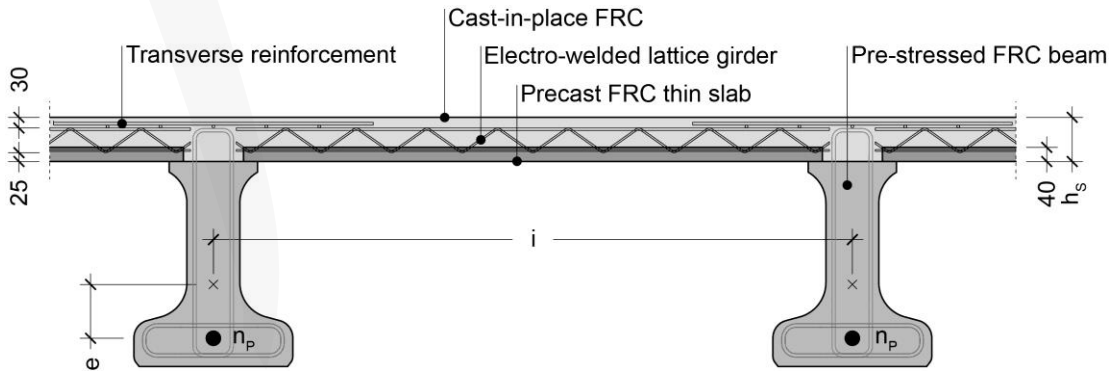


Figure 1: General scheme of the proposed structural solution

This document is the intellectual property of the fib – International Federation for Structural Concrete. All rights reserved.
This PDF of fib Bulletin 95 is intended for use and/or distribution solely within fib National Member Groups.

A scheme of the structural solution is presented in Figure 1, where the different parts of the system are highlighted. In the present study, all the components are supposed to be made by an FRC material classified as 3c, according to the Model Code 2010.

This structural solution has already been designed and applied by an Italian company (DSC Erba) in two different industrial buildings in Italy. The first case, placed in the city of Como, is characterized by a span of 14 m and a characteristic live load of 15 kN/m^2, while, in the second one, a 9.5 m span and a characteristic live load equal to 6 kN/m^2 represent the design conditions of a new internal story that had to be added to an existing structure located in Bobbio Piacentino, close to Piacenza.

In the case of the building placed in Como, the spacing *i* between the beams is equal to 1.7 m, the thickness of the top FRC layer is 100 mm, while the depth of the prestressed beam is 580 mm. In the case of the building in Bobbio Piacentino, the spacing *i* between the beams is equal to 2 m, the thickness of the top layer is - also in this case - equal to 100 mm, while the depth of the beam is 420 mm.

The purpose of this paper is to move from the traditional design approach employed in these two applications to an automatic optimization procedure of the whole composite floor, aimed at maximizing the beam spacing, generally minimizing the permanent structural load.

3 Optimization procedure

An optimization procedure was implemented to define the optimal solution for a given longitudinal span and for a given characteristic live load (q) acting over the floor. In particular, 3 different spans (L=10, 15 and 20 m) and as many live load conditions (q=10, 20 and 30 kN/m^2) were considered in this study. Due to the fact that the cost of the considered structural solution increases with the number of beams adopted, in the first place the maximum possible distance between beams was defined, referring to the transverse bending behaviour. Secondly, the beams characterized by the smallest weight and able to satisfy Serviceability and Ultimate Limit state conditions were obtained by means of a constrained minimization procedure. In this preliminary approach, the material properties were not considered as variables, but were supposed to be *a priori* fixed. In particular, a FRC class 3c according to the Model Code 2010 was assumed for the tensile behaviour of all the materials, while compressive class C45 was selected for both the precast elements (beams and *predalles*) and the cast-on-site topping layer.

3.1 Transverse bending

The transverse bending of the floor was studied considering both transient and final conditions. In particular, previous experimental activities carried out on the proposed structural solution (di Prisco et al. 2016) allowed to investigate the behaviour of the *predalle* slab in the transient phase and allowed to identify as critical mechanism the buckling of the lattice girder top rebar, in a situation in which the top layer is not hardened, i.e. is unable to provide a lateral restraint. This phenomenon was observed to arise with an experimental buckling length equal to $l_0 = 0.62l$, being l the distance between two welding points (200 mm). On the contrary, when the top layer is hardened, the ULS bending condition becomes the governing mechanism. In this situation, both positive and negative bending moments, respectively at the transverse slab mid-span and over the beam head, govern the ultimate response.

This document is the intellectual property of the fib – International Federation for Structural Concrete. All rights reserved.
This PDF of fib Bulletin 95 is intended for use and/or distribution solely within fib National Member Groups.

Taking advantage of these considerations, if the type of electro-welded lattice girder is selected, the maximum beam spacing can be defined according to the following criteria:

- ULS criterion in the transient condition, when the top concrete layer is still in its fresh-state; in this case, the maximum span of the *predalles* slab is limited by the compressive buckling of the girder upper rebar.
- ULS criterion in the final phase, according to which the maximum span of the slab can be defined assuming the bending failure of the composite slab. In this case, the beam spacing was computed assuming the failure as governed by positive bending moment and assuming to introduce a proper amount of additional reinforcing rebars just over the head of the beams, so as to avoid the transverse bending failure mechanism to be governed by negative bending (Figure 1).
- SLS vibration criterion, that allows to evaluate the span of the slab that corresponds to a natural frequency of the first mode of vibration equal to at least 5 Hz.
- SLS deflection criterion, in order to define the maximum span able to guarantee a transverse deflection smaller than $i/250$, being i the beam spacing.

Among all the spans computed according to the introduced criteria, the minimum value was adopted as the maximum beam spacing corresponding to the selected electro-welded lattice girder.

Several lattice girder solutions available on the market were taken into account. The considered set is characterized by the same triangular shape, but with different geometry (bar diameters and girder depths). A scheme of the selected electro-welded lattice girder is given in Figure 2, while all the geometrical properties are available in Table 1.

For all the electro-welded lattice girders considered, the thickness of the precast *predalle* was supposed to be constant and equal to 40 mm, while the height of the top layer of FRC, cast on site to guarantee the floor continuity, was defined assuming a constant 30 mm cover of the upper rebar of the girder.

The procedure for the definition of the maximum beam spacing here described was adopted for all the electro-welded lattice girders considered and for all the live loads taken into account. It is worth to note that, due to the criteria adopted in the definition of the beam spacing, this parameter does not depend upon the longitudinal span of the floor.

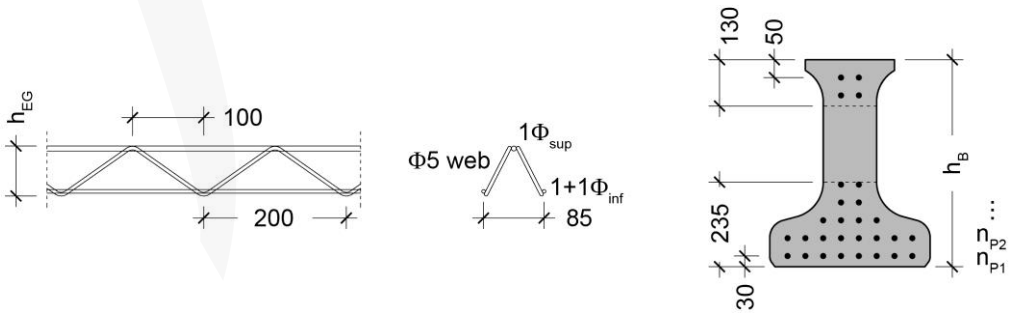


Figure 2: Geometrical properties of the electro-welded lattice girder and of the secondary beam cross section, together with the position of tendons (measures in mm)

This document is the intellectual property of the fib – International Federation for Structural Concrete. All rights reserved.
This PDF of fib Bulletin 95 is intended for use and/or distribution solely within fib National Member Groups.

Table 1: Electro-welded lattice girder properties

Designation	EG1	EG2	EG3	EG4	EG5	EG6
h_{EG} [mm]	70	95	125	125	165	205
Φ_{inf} [mm]	5	5	5	6	5	5
Φ_{sup} [mm]	7	7	7	7	7	8

3.2 Longitudinal bending

Following the selection of the electro-welded lattice girder, therefore the definition of the maximum distance between the beams related to each span and load case, the depth of the beam and the tendons distribution within the beam central cross-section were defined focusing on the longitudinal bending behaviour. To this aim, an optimization procedure able to minimize the weight of the structural element was implemented.

In this optimization procedure, the width of the cross-section web was not considered as a variable, but was supposed to be fixed and equal to 150 mm, since preliminary considerations showed that a further reduction of the web thickness causes a decrease of the beam fire safety that does not allow the structural solution to reach the R120 requirement. Moreover, the possible distribution scheme of the tendons was also kept as constant, because of production requirements, and changes in the arrangement of the reinforcement or deliberately prevented bond along the beam length were ignored in this preliminary analysis. All the tendons were supposed to be pre-stressed with an initial stress σ_{p0} equal to 1300 MPa and a *forfait* value of pre-stress losses was taken into account, by considering a final pre-stress σ_p=1000 MPa. The shape of the cross-section was also considered as a constant and, in particular, the upper and the lower bulbs do not change with the beam height; in this sense, only the depth of the central web, characterized by a constant width, was assumed variable (Figure 2).

The general constrained minimization procedure can be defined as the problem of finding a vector $\boldsymbol{x}$ that is a local minimum to a scalar function $f(\boldsymbol{x})$ subjected to constraints on the possible values of $\boldsymbol{x}$. In a general form it can be written as:

$$\min_{\boldsymbol{x}} f(\boldsymbol{x}) \text{ such that } \begin{cases} \boldsymbol{c}(\boldsymbol{x}) \leq \boldsymbol{0} \\ \boldsymbol{A} \cdot \boldsymbol{x} \leq \boldsymbol{b} \\ \boldsymbol{l} \leq \boldsymbol{x} \leq \boldsymbol{u} \end{cases} \quad (1)$$

In the case under study, the considered scalar function $f(\boldsymbol{x})$ is the weight of the beam, while the unknown vector $\boldsymbol{x}$ consists of the depth of the beam cross section and other 7 variables respectively representing the number of 7W-0.5" tendons n_i at the *i-th* reinforcement row, as shown in Figure 2.

Table 2: Variables adopted in the minimization procedure, together with their lower and upper bounds

Variable	h_B [mm]	n_{P1}	n_{P2}	n_{P3}	n_{P4}	n_{P5}	n_{P6}	n_{P7}
Lower bound	380	0	0	0	0	0	0	0
Upper bound	1200	8	8	4	2	2	2	2

This document is the intellectual property of the fib – International Federation for Structural Concrete. All rights reserved.
This PDF of fib Bulletin 95 is intended for use and/or distribution solely within fib National Member Groups.

The function ***c(x)*** represents the non-linear constraints, while matrix ***A*** and vector ***b*** describe additional linear constraints. Finally, ***l*** and ***u*** represent respectively the lower and upper bounds of the unknown vector ***x***, listed in Table 2.

The optimization problem was solved adopting a Sequential Quadratic Programming (SQP) algorithm. The SQP method (Fletcher 1987, Gill et al. 1981, Powell 1983 and Hock et al. 1983) allows to closely simulate the Newton's method for constrained optimization, just as it is done for unconstrained optimization. At each major iteration, an approximation of the Hessian of the Lagrangian function is made, using a quasi-Newton updating method. This is then used to generate a Quadratic Programming sub-problem, whose solution is used to form a search direction for a line search procedure.

The linear constraints adopted in this algorithm are such to take into account that the number of tendons distributed on a row should never decrease moving from the beam centroid to both the upper and lower cross-section chords.

The non-linear function ***c(x)*** takes into account all the design checks related to the bending behaviour of the beam, both at the serviceability (SLS) and ultimate (ULS) limit state of the structural solution, in transient as well as in permanent phases.

In particular, the following conditions were imposed:

- SLS stress control at both the upper and the lower chords of the beam mid-span cross-section, when the tendons are released (time t = 0), and therefore just the beam self-weight is applied.
- SLS stress control at both the upper and the lower chords of the beam mid-span cross-section, when the topping concrete is in a fresh state (time $t = 0^{+}$), therefore additional permanent loads are taken into account, but just the beam cross-section is considered in the calculation.
- SLS stress control at both the upper and the lower chords of the beam mid-span cross-section, in the case of a minimum distributed load applied when the topping layer has hardened ($t = 0^{++}$); in this case, only permanent loads are taken into account, but the whole composite cross-section is considered in the calculation.
- SLS stress control at both the upper and the lower chords of the beam mid-span cross-section, in the case of maximum load consisting of both permanent and live loads ($t=\infty$); also in this case, the whole composite cross-section is considered in the calculation.
- Ultimate limit state bending capacity, in terms of resisting bending moment M_{Rd} at the mid-span of the composite solution, at time $t = \infty$.
- SLS deflection of the composite solution, both considering live load only and live load in combination with permanent loads.
- SLS vibration control by imposing a first natural frequency of the composite solution larger than 5Hz.

This document is the intellectual property of the fib – International Federation for Structural Concrete. All rights reserved.
This PDF of fib Bulletin 95 is intended for use and/or distribution solely within fib National Member Groups.

4 Results

The results of the optimization procedure introduced in the previous paragraph are discussed in this section.

First of all, the results related to the transverse bending behavior of the floor and the resulting maximum beam spacing obtained with the previously described procedure are summarized in Table 3. In the same table, for each girder considered, the maximum beam spacing corresponding to the different adopted criteria is listed. The minimum value for each girder is highlighted by using bold characters, and finally rounded to a 0.25m-stepped practical value. It is worth to note that, among all the criteria selected, the buckling failure of the upper bar of the girder always represents the most critical situation, thus indicating that, since this situation is not a permanent one, temporary shoring might be considered if a larger beam distance is desired. Nevertheless, in this case this alternative solution is not taken into account and the beam spacing related to this buckling failure is considered as the limit one.

Figure 3 shows the trend of the maximum beam spacing with respect to the thickness of the composites floor slab (*predalles* + FRC topping layer).

Table 3: Maximum beam spacing [m] for the different electro-welded lattice girders, for the different live loads considered.

Live load q [kN/m^2]	Girder Designation	ULS Buckling	ULS Bending	SLS Deflection	SLS Vibration	Rounded spacing
10	EG1	**1.86**	3.03	5.17	3.70	1.75
	EG2	**1.98**	3.42	6.11	4.05	1.75
	EG3	**2.07**	3.86	7.20	4.43	2.00
	EG4	**2.07**	4.21	7.20	4.43	2.00
	EG5	**2.16**	4.40	8.61	4.90	2.00
	EG6	**2.70**	4.90	9.96	5.33	2.50
20	EG1	**1.86**	2.27	4.28	3.70	1.75
	EG2	**1.98**	2.59	5.09	4.05	1.75
	EG3	**2.07**	2.95	6.05	4.43	2.00
	EG4	**2.07**	3.22	6.05	4.43	2.00
	EG5	**2.16**	3.40	7.29	4.90	2.00
	EG6	**2.70**	3.84	8.51	5.33	2.50
30	EG1	**1.86**	1.89	3.80	3.70	1.75
	EG2	**1.98**	2.16	4.53	4.05	1.75
	EG3	**2.07**	2.48	5.39	4.43	2.00
	EG4	**2.07**	2.71	5.39	4.43	2.00
	EG5	**2.16**	2.88	6.53	4.90	2.00
	EG6	**2.70**	3.26	7.65	5.33	2.50

This document is the intellectual property of the fib – International Federation for Structural Concrete. All rights reserved.
This PDF of fib Bulletin 95 is intended for use and/or distribution solely within fib National Member Groups.

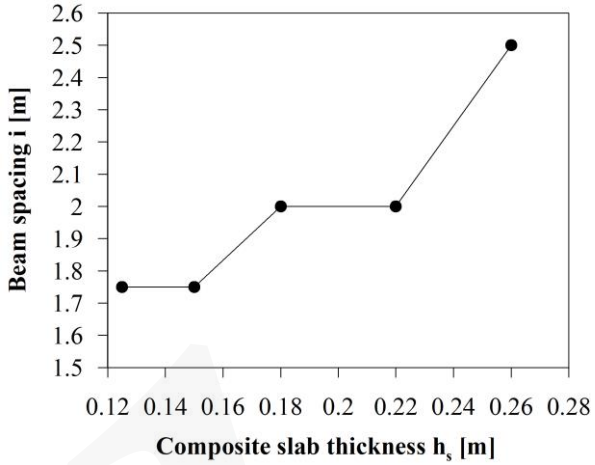


Figure 3: Beam spacing vs. thickness of composite top slab

The global results of the optimization procedure are presented in Figure 4, where the global permanent loads g_0 of the considered structural solution are represented as a function of the beam spacing, respectively for longitudinal beam spans equal to 10, 15 and 20 m. The solution highlighted with a dashed circle corresponds to that selected as an optimum solution, since it is the one that, among all the solutions detected, guarantees the smallest permanent load.

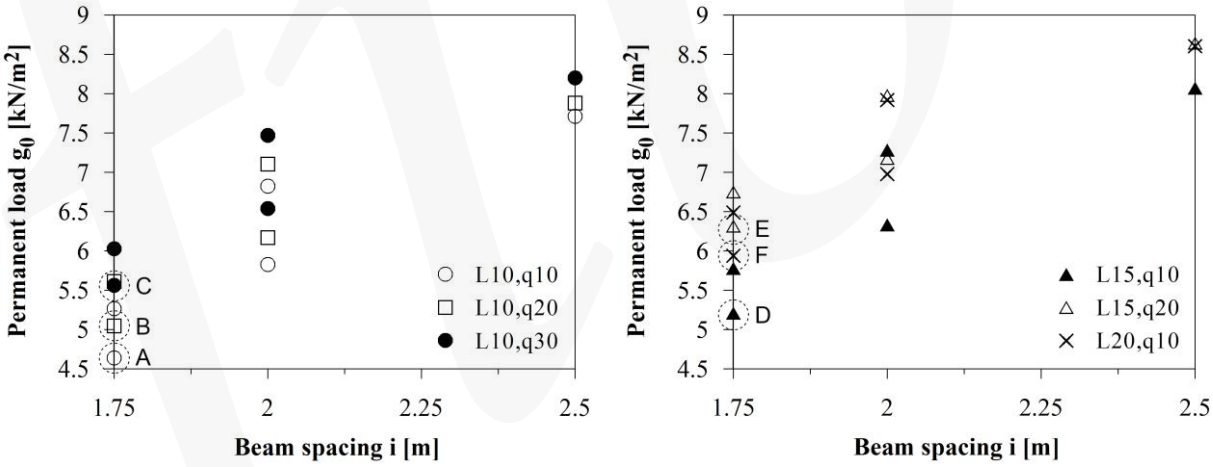


Figure 4: Permanent load g_0 vs. beam spacing

Looking at the results, it is worth nothing that only in the case of a 10 m span a solution was found for all the live loads considered. In the case of a 15 m span, no solution was found within the selected range for a live load equal to 30 kN/m^2, while in the case of a span equal to 20 m, just a live load of 10 kN/m^2 leads to a solution able to satisfy all the constraints within the imposed limits and considering the maximum beam spacing selected. It is important to point out that, to allow the solution to bear larger loads even when high spans are required, the beam spacing could be reduced.

Figure 5 displays the optimum solutions selected for all the considered spans and loads, together with the equivalent tendon force N_P and the associated permanent load g_0.

This document is the intellectual property of the fib – International Federation for Structural Concrete. All rights reserved.
This PDF of fib Bulletin 95 is intended for use and/or distribution solely within fib National Member Groups.

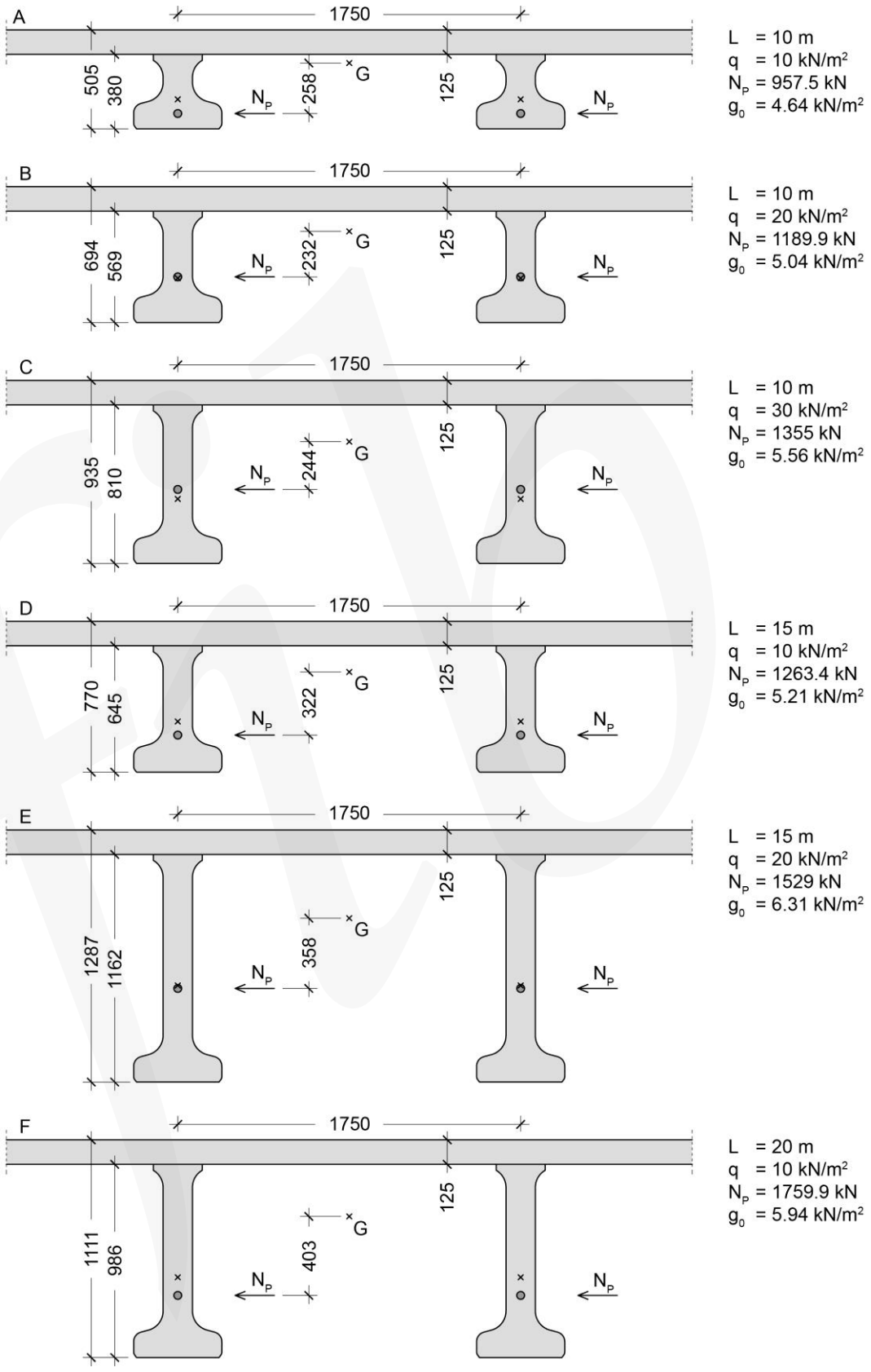


Figure 5: Optimum solutions provided by the optimization algorithm

This document is the intellectual property of the fib – International Federation for Structural Concrete. All rights reserved.
This PDF of fib Bulletin 95 is intended for use and/or distribution solely within fib National Member Groups.

5 Conclusions

The paper presents a preliminary optimization procedure applied to a new FRC solution for partially prefabricated slabs. The main goal is to maximize the beam spacing and to reduce the global permanent load of the structure. The preliminary procedure here presented simply focus on longitudinal and transverse bending behaviours. All the other checks, such as shear and fire resistance, need to be carried out in the aftermath of the solution choice. Further investigation will also comprise these parameters in the optimization procedure and will include alternative cross-sections, such as the beam ends.

Looking at the results of the optimization algorithm, it is interesting to compare the beam height obtained with the presented approach with those proposed in the two real cases recently designed and built in Italy. Assuming the live loads and the beam spacing available in Como (beam depth 580 mm) and in Bobbio Piacentino (beam depth 420 mm), the automatic procedure leads to satisfactory beam depths, respectively equal to 560 and 380 mm.

6 References

di Prisco Marco, Colombo Matteo, De Wilder Kristof, Vandewalle Lucie, 2016. *A new FRC solution for a partially prefabricated industrial deck*. In: FRC: The Modern Landscape. BEFIB 2016. Proceedings of the 9th RILEM International Symposium on Fibre Reinforced Concrete. p. 1407-1421, RILEM Publications S.A.R.L., ISBN: 978-2-35158-187-2, Vancouver

di Prisco, M., Plizzari, G., Vandewalle, L., 2014. *Structural design according to fib MC 2010: comparison between RC and FRC elements*. In FRC 2014 Joint ACI-fib International Workshop - Fibre Reinforced Concrete: from Design to Structural Applications, Editors: Charron J.P., Massicotte B., Mobasher B., Plizzari G., Montreal, Canada.

di Prisco, M., Colombo, M., Dozio, D., 2013. *Fibre-reinforced concrete in fib Model Code 2010: Principles, models and test validation*, Structural Concrete, 14 (4), 342-361.

di Prisco, M., Plizzari, G., Vandewalle, L., 2009. *Fibre reinforced concrete: New design perspectives*, Materials and Structures/Materiaux et Constructions, 42 (9), 1261-1281.

European Committee for Standardization, EN 14651, 2005. *Test method for metallic fibered concrete - Measuring the flexural tensile strength (limit of proportionality - LOP, residual)*, 17.

Fédération Internationale du Béton (fib), 2013. f*ib Model Code for Concrete Structures 2010*, Berlin (Germany): Wilhelm Ernst und Sohn Verlag für Architektur, p. 402.

Fletcher, R., 1987. *Practical Methods of Optimization*, John Wiley and Sons.

Gill, P.E., W. Murray and M.H.Wright, 1981. *Practical Optimization*, London, Academic Press.

Hock, W. and K. Schittkowski, 1983. A *Comparative Performance Evaluation of 27 Nonlinear Programming Codes*, Computing, Vol. 30, p. 335.

Powell, M.J.D., 1983. *Variable Metric Methods for Constrained Optimization*, Mathematical Programming: The State of the Art, A. Bachem, M. Grotschel and B. Korte, eds.) Springer Verlag, 288–311.

This document is the intellectual property of the fib – International Federation for Structural Concrete. All rights reserved.
This PDF of fib Bulletin 95 is intended for use and/or distribution solely within fib National Member Groups.
FRC2018: Fibre Reinforced Concrete: from Design to Structural Applications
Joint ACI-*fib*-RILEM International Workshop

Structural behavior of precast tunnel segments with macro-synthetic fibers during TBM operations: a numerical study

Ivan Trabucchi[1], Antonio Conforti[1], Giuseppe Tiberti[1], Giovanni Plizzari[1] and Ralf Winterberg[2]

[1] : University of Brescia, Brescia, Italy.

[2] : Elasto Plastic Concrete, Singapore.

Abstract

The use of fiber reinforced concrete in tunnel linings, with or without conventional rebars, has increased in the two last decades, especially in segmental linings. In the meanwhile, in the scientific community there was a growing interest on macro-synthetic fibers for use in underground structures. Within this framework, the present study investigates the possibility of using macro-synthetic fiber reinforcement in precast tunnel segments by means of a numerical study.

Firstly, an experimental program based on three point bending tests was carried out on polypropylene fiber reinforced concretes (PFRCs) characterized by different fiber contents in order to assess their post-cracking residual strength. Secondly, the corresponding stress vs. crack opening laws, representative of the PFRCs investigated, were calculated through inverse analysis procedure. Then, a segment of a typical tunnel lining having small diameter was adopted as reference to optimize the reinforcement solution (macro-synthetic fibers and conventional rebars, i.e. hybrid solution) and to study its structural behavior by numerical analyses. Particular attention was devoted to the Tunnel Boring Machine (TBM) thrust jack phase, in which the TBM moves forward by pushing the thrust jacks on the bearing pads of the latest assembled ring, introducing high-concentrated forces in the lining.

Keywords

Fiber reinforced concrete; Macro-synthetic fibers, Numerical analyses; Splitting phenomena; Thrust jack.

This document is the intellectual property of the fib – International Federation for Structural Concrete. All rights reserved.
This PDF of fib Bulletin 95 is intended for use and/or distribution solely within fib National Member Groups.

1 Introduction

In the last two decades, Fiber Reinforced Concrete (FRC), with or without conventional rebars, was progressively adopted in several precast tunnel lining projects (ITA report n.16, 2016; ACI 544.7R-16, 2016, *fib* bulletin 83, 2017). Steel Fiber Reinforced Concrete (SFRC) have been generally used for tunnel linings even though there is a general growing interest in the scientific community on macro-synthetic fibers for use in structural applications (Nitschke A.G. et al., 2016; Conforti et al., 2017).

The design process of segmental concrete linings in ground conditions is principally governed by the load cases that can be implemented in the so-called ring models (Blom, 2002), which correspond to the standard load case (embedded ground condition) and the uplift load case (grouting process). Furthermore, other possible mechanisms, occurring during the lining construction process, can result in crack patterns in tunnel segments that are frequently observed in practice. Under this point of view, the application of Tunnel Boring Machine (TBM) thrust jack forces is a crucial phase (Tiberti et al., 2015; Liao et al., 2015). Although this phenomenon occurs in the temporary lining building stage, it tends to govern the amount of reinforcement. Likewise, the final state when the lining is loaded by the ground pressure which interests the entire lining lifetime (Blom, 2002; Groeneweg, 2007). During TBM operations the distribution of stresses in tunnel elements is complicated; therefore, the crack patterns developing in this stage should be carefully evaluated in order to capture the effectiveness of fiber reinforcement. Non-linear finite models are necessary for better studying this temporary phase. The numerical modelling of tunnel segments during this phase requires special attention to boundary conditions and possible unfavorable conditions that may occur during the lining construction.

Within this framework, the present research work aims to evaluate the possibility of using macro-synthetic fiber reinforcement in precast tunnel segments in combination or not with traditional rebars by studying a tunnel lining having small diameter. Firstly, fracture properties of two Polypropylene Fiber Reinforced Concretes (PFRCs) were determined. Secondly, non-linear numerical analyses were developed to study the TBM thrust jack phase, which strongly affects the optimized reinforcement (fibers + rebars) in precast tunnel segments. Special attention was devoted to possible irregularities (e.g.: eccentric placement of TBM thrust shoes), since they remarkably influence local and global behavior of segments.

2 Material properties

An experimental program was developed for the characterization of PFRCs adequate for tunnel elements. Continuous embossed polypropylene (PP) fibers 48 mm long with a diameter of 0.70 mm (aspect ratio of 68), tensile strength of 640 MPa, an elastic modulus of 12 GPa and a density of about 900 kg/m^3 were adopted. Fibers were added to a base concrete with a target mean cube compressive strength of about 60-65 MPa (typical of precast applications) in two different amounts: 6 kg/m^3 (PFRC6 series) and 10 kg/m^3 (PFRC10 series); which was proven to be upper and lower PP fibers dosages in order to obtain PFRCs adequate for structural purposes according to MC2010 (Trabucchi et al., 2019). Both PFRCs were produced by a planetary concrete mixer.

The mixture proportion (by weight) of both PFRC6 and PFRC10 was 1:1.83:0.75:1.3:0.37 for 460 kg/m^3 of CEM II/A-LL 42.5R cement: sand (0-4): gravel (4-12): gravel (12-20):

This document is the intellectual property of the fib – International Federation for Structural Concrete. All rights reserved.
This PDF of fib Bulletin 95 is intended for use and/or distribution solely within fib National Member Groups.

water. Super-plasticizer was 0.7% and 1.4% of cement content, for PFRC6 and PFRC10, respectively. Both mixtures exhibited a good and comparable workability (slump of 160 mm and 120 mm for PFRC6 and PFRC10, respectively). For each matrix, twelve small beams 150x150x550 mm according to EN 14651 (2005) for determining post-cracking behavior and twelve cubes 150x150x150 mm for evaluating concrete compressive strength were produced.

Figure 1 represents the nominal stress vs. CMOD (Crack Mouth Opening Displacement) curves of notched small beams of concrete PFRC6 (a) and PFRC10 (b). In addition, Figure 1 summarizes the mean mechanical properties of the two types of concrete (CV provided in parenthesis), in terms of cube ($f_{c,cube}$) and cylinder compressive strength (f_c=0.83·$f_{c,cube}$). The limit of proportionality f_L and the mean values of residual flexure strengths $f_{R,1}$, $f_{R,2}$, $f_{R,3}$, $f_{R,4}$ (corresponding to CMOD values of 0.5, 1.5, 2.5 and 3.5 mm, respectively) are listed in Figure 1 as well. A comparable result dispersion in terms of post-cracking mechanical properties can be observed between concretes, i.e. CV ranging from 0.10 to 0.17. Both mixtures showed a stable post-cracking response. PFRC matrixes were characterized by a softening behavior with a load drop after the peak load, followed by an increment of the residual flexural tensile strength. For larger values of crack width, a soft and progressive decrease of the residual flexural tensile strength was observed. By using higher fiber contents, the load drop (after the peak) decreases and the increment of the residual flexural tensile strength becomes more pronounced. These good post-cracking performances given by the adopted PP fibers are mainly due to their embossed shape, which significantly increases the bond between fibers and matrix and, to their elastic modulus and tensile strength. The obtained fracture properties of PFRC6 and PFRC10 fulfill the requirements of *fib* Model Code 2010 ($f_{R,1k}/f_{L,k}$ > 0.4 and $f_{R,3k}/f_{R,1k}$ > 0.5) for use in structural elements. Moreover, the toughness of both PFRCs allow to satisfy the requirement of Equation 7.7-14 of Model Code 2010 ($f_{Ftuk} \geq 0.08 \cdot f_{ck}^{1/2}$) in order to use fibers as minimum shear reinforcement. Considering $f_{R,jk} = f_{R,j}$ (1-1.64·CV) according to *fib* Model Code 2010 (2012) the following ratios and characteristic values are obtained: $f_{R,1k}/f_{L,k}$=0.44, $f_{R,3k}/f_{R,1k}$=1.33 and f_{Ftuk}=1.01 MPa for PFRC6; $f_{R,1k}/f_{L,k}$=0.60, $f_{R,3k}/f_{R,1k}$=1.44 and f_{Ftuk}=1.53 MPa for PFRC10.

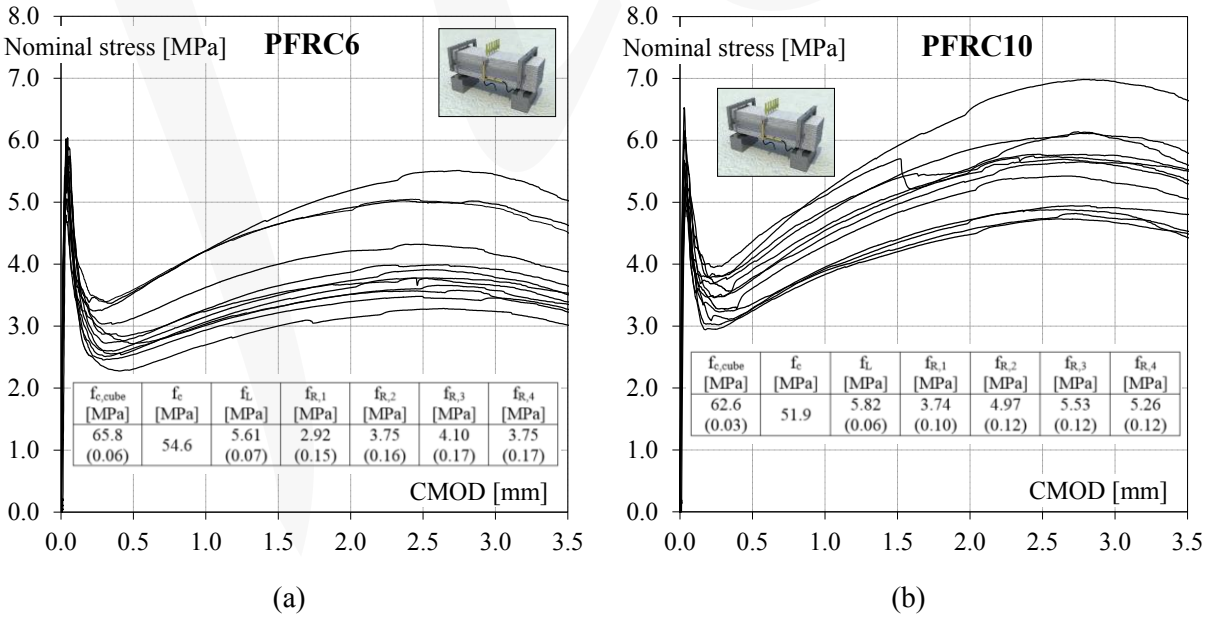


Figure 1: Mechanical properties and nominal stress vs. CMOD curves for concrete PFRC6 (a) and PFRC10 (b)

This document is the intellectual property of the fib – International Federation for Structural Concrete. All rights reserved.
This PDF of fib Bulletin 95 is intended for use and/or distribution solely within fib National Member Groups.

3 Precast tunnel lining geometries

A typical precast tunnel lining characterized by a small diameter was studied, internal diameter of 3200 mm, a thickness of 200 mm (external diameter of 3600 mm) and lining aspect ratio equal to 16, were assumed. The lining is representative of typical water supply, gas pipeline, waste water or electrical supply tunnels (ITA report n.16, 2016). Each lining ring is composed by six universal tapered tunnel segments as shown in Figure 2. Hence, the tunnel segment presents an average length of 1780 mm. Two pairs of thrust jacks act on each tunnel segment and two bearing pads are positioned on its rear face (ring joint, Figure 2). It was assumed a so-called French thrust jack configuration, where the bearing pads are perfectly aligned with TBM thrust shoes (Groeneweg, 2007). The average service thrust load was assumed equal to 1 MN for each TBM shoe. This service load corresponds to an equivalent tunnel overburden ranging from 4-5 tunnel diameters, according to the simplified model proposed by Rijke (2006) for evaluating the TBM thrust jack forces in ground condition. The maximum thrust load was assumed equal to 1.5 MN per shoe.

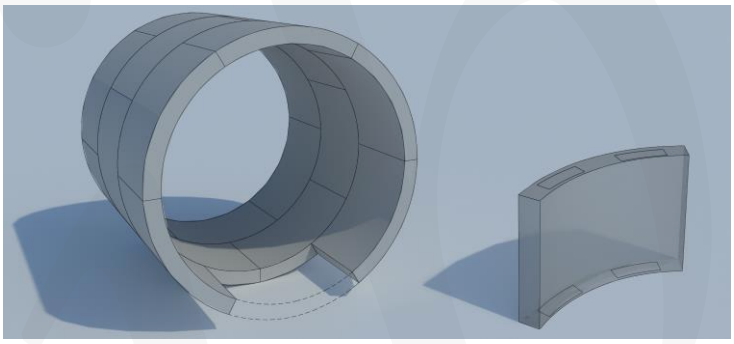


Figure 2: Precast tunnel lining geometry

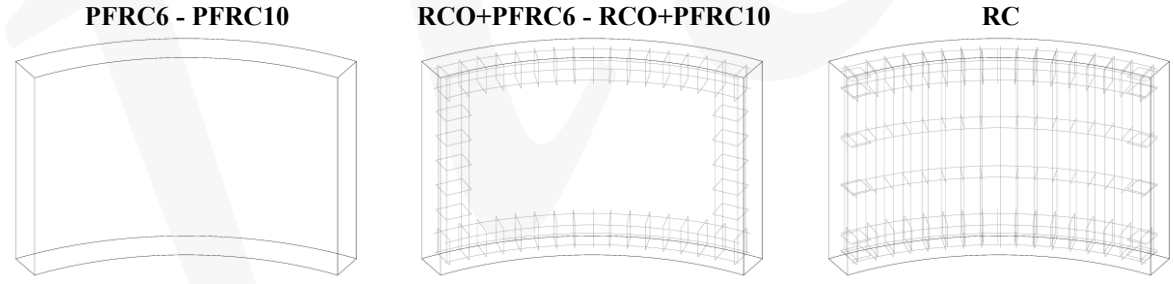


Figure 3: Adopted reinforcement configurations

The following three reinforcement solutions were studied (Figure 3):

1. PFRC6 and PFRC10 segments: PP fiber reinforcement only. Flexural, shear, spalling and splitting stresses are withstood by fibers only;
2. RCO+PFRC6 and RCO+PFRC10 segments: hybrid solution based on a combination of PP fibers and conventional reinforcement; (4+4)Ø10 curved bars were used in two connected chords and PP fibers were adopted for withstanding

This document is the intellectual property of the fib – International Federation for Structural Concrete. All rights reserved.
This PDF of fib Bulletin 95 is intended for use and/or distribution solely within fib National Member Groups.

splitting, shear stresses and to control spalling phenomenon in combination with rebars. Stirrups Ø6 with 2 legs@100 mm were used for each chord;

3. RC segment: typical conventional reinforcement generally adopted in practice corresponding to (6+6)Ø10 curved rebars, stirrups Ø8 with 4 legs@100 mm (shear reinforcement) and local stirrups Ø8 with 2 legs@100 mm for splitting stresses.

4 Numerical modelling

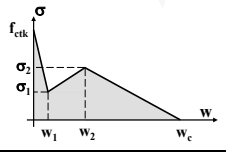
The numerical analyses were performed by means of the finite element code DIANA 10.1 (2016) by considering different loads and boundary conditions. The numerical analyses were carried out by increasing progressively the applied load in order to evaluate the development of the crack pattern in the segments: the characteristic mechanical properties of materials were used, as suggested by *fib* bulletin 83 (2017).

Different reinforcement configurations were considered and special attention was devoted to the influence of possible irregularities that could occur during the TBM thrust jack phase. The following loading configurations were considered: 1) normal loading condition: perfect placement of TBM thrust shoes and perfect positioning of the segments on the previous assembled ring; 2) eccentric placement of TBM shoes: an outward eccentricity of about 20 mm was considered; 3) un-even supports: the partial loss of the contact (due to a possible gap) in one support was considered; 4) un-even supports combined with outward eccentricity as a combination of previous mentioned irregularities.

4.1 Material modelling

Stress vs. crack opening law was calculated by means of inverse analyses. A discrete concrete crack model was used and tri-linear post-cracking law was adopted. In particular, the characteristic experimental curves of three point bending tests were calculated for PFRC6 and PFRC10 in order to retrieve the corresponding uni-axial post-cracking laws, whose parameters are reported in Table 1. Based on the mean values of cylindrical compressive strengths, the corresponding characteristic values were estimated (f_{ck}= f_c – 8 MPa according to *fib* Model Code 2010 (2012), see Table 1). The elastic modulus (E_c) and characteristic tensile strength, f_{ctk} are reported as well; the latter were estimated according to *fib* Model Code 2010 (2012). The uniaxial compressive behavior of concrete was described by means of the model proposed by Thorenfeldt (1987). Moreover, the increase of compressive strength due to lateral confinement was considered by means of the model of Selby and Vecchio (1993). Steel B450C (Eurocode 2, 2004) was adopted for both transverse and longitudinal reinforcement. In numerical analyses a yielding and ultimate tensile strength equal to 475 MPa and 572 MPa were considered; a Von-Mises yielding criterion with strain-hardening was assumed.

Table 1: Main parameters adopted in the numerical analyses

ID	Tri-linear post-cracking law	E_c [GPa]	f_{ck} [MPa]	f_{ctk} [MPa]	w_1 [mm]	σ_1 [MPa]	w_2 [mm]	σ_2 [MPa]	w_c [mm]
PFRC6		37.9	46.6	2.72	0.05	0.58	1.20	1.10	7.00
PFRC10		37.2	43.9	2.62	0.05	0.80	1.50	1.55	6.50

This document is the intellectual property of the fib – International Federation for Structural Concrete. All rights reserved.
This PDF of fib Bulletin 95 is intended for use and/or distribution solely within fib National Member Groups.

4.2 Precast tunnel segment modelling

A three dimensional numerical model of one single tunnel segment with two pairs of actuators was adopted (Figure 2). Twenty-nodes iso-parametric solid brick elements were used in combination with interface elements. The latter were used to simulate the support through radial joints provided by the adjacent rings and to consider the interaction between adjacent segments belonging to the same ring. The supports provided by previous assembled ring were localized on the bearing pads surfaces (Figure 2). The in-plane and out-of-plane stiffness of interface elements were calibrated by means of imposed displacement analyses previously carried out with the aim of simulating the interaction between segments through radial and longitudinal joints (Trabucchi, 2015). A total strain rotating smeared crack model was used for concrete behavior after cracking. Hence, the stress vs. crack opening laws of PFRCs investigated (Table 1) must be transformed in stress vs. strain relationships by referring to a crack bandwidth (h), which was assumed as the average size of the element (about 52 mm) as suggested by Rots (1988). Steel reinforcing rebars were simulated with embedded reinforcement; the total amount of fiber and traditional rebars were previously listed in Figure 3.

4.3 Numerical results

The main aim of the numerical study presented herein was to evaluate the bearing capacity and crack development of precast tunnel elements during the TBM thrust phase. In Figure 4 the maximum loads obtained in the numerical analyses are reported as a function of tunnel reinforcement solution and loading condition. In absence of irregularities (normal loading condition), all the reinforcement arrangements were able to withstand a bearing capacity higher than the maximum TBM thrust load (i.e. 1500 kN per each shoe), since the maximum load ranges from 2100 kN per shoe (PFRC6 and PFRC10 segment) to about 2800 kN per shoe (RC segment). Figure 4 shows the effect of possible irregularities in reducing the bearing capacity on each reinforcement configuration, with respect to the normal loading condition. In presence of an outward eccentricity the reduction varies from 10 to 20%, depending on the reinforcement configuration considered. The most severe condition seems the loss of a support (uneven support) combined with an outward eccentricity, which leads to an average reduction of the maximum load around 40% with respect to the normal loading condition.

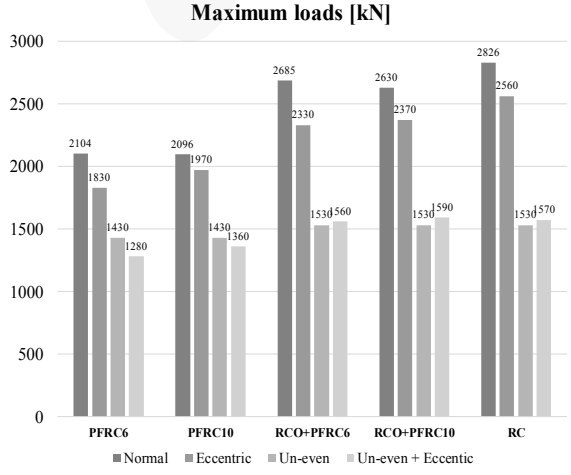
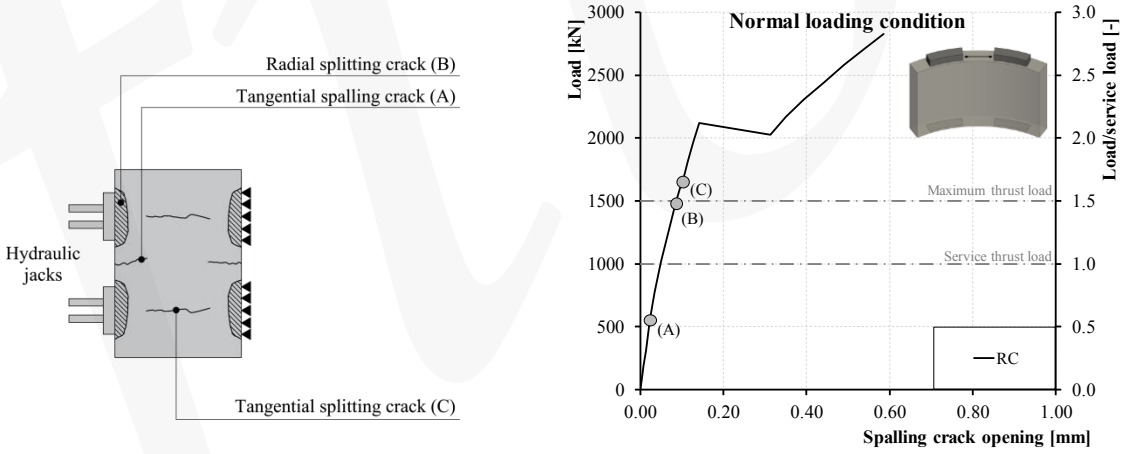


Figure 4: Maximum loads evidenced in the non-linear numerical analyses

This document is the intellectual property of the fib – International Federation for Structural Concrete. All rights reserved.
This PDF of fib Bulletin 95 is intended for use and/or distribution solely within fib National Member Groups.

It is particularly important to study the local crack development, since it affects the global behavior. Figure 5a reports the crack pattern for RC segment under normal loading condition. The first crack appears between the loading surfaces at a load of about 0.54 times the service load (hereafter s.l.). The spalling crack development was evaluated by considering the relative displacement between two points astride the crack. The corresponding base of measurement is about 315 mm, and the resulting diagram is shown in Figure 5b for the RC configuration. It should be noted that the diagram plotted in Figure 5b could be considered a conservative estimation of the crack width, since the elastic deformation was included in the diagram and a single crack was basically assumed. Even if spalling cracks generally do not compromise the segment equilibrium, they represent an important issue with respect to the lining behaviour. Splitting cracks due to local radial tensile stresses occurred under the TBM shoes at about 1.48 s.l.; afterwards, when reaching 1.65 times the service load, tangential splitting cracks appeared in the segment. Figure 5b clearly evidences that spalling crack occur earlier with respect to splitting ones, resulting in larger crack widths. This tendency can be further emphasized in presence of irregularities. In Figure 6 the spalling crack development between the TBM thrust shoes for all the investigated segments is shown for the normal and eccentric loading conditions. By referring to the normal loading condition, the segments reinforced by fibers only (PFRC6 and PFRC10) were able to guarantee a maximum load approximately two times the service one due to an inadequate control of local spalling phenomena for high load levels. On the contrary, hybrid reinforcement and RC solutions were able to control local splitting phenomena enabling a further increase of the global bearing capacity up to 2.8 times s.l. However, a sudden increase of the estimated spalling crack width was observed at a load of about 2 times the service load (when a PFRC only solution fail).



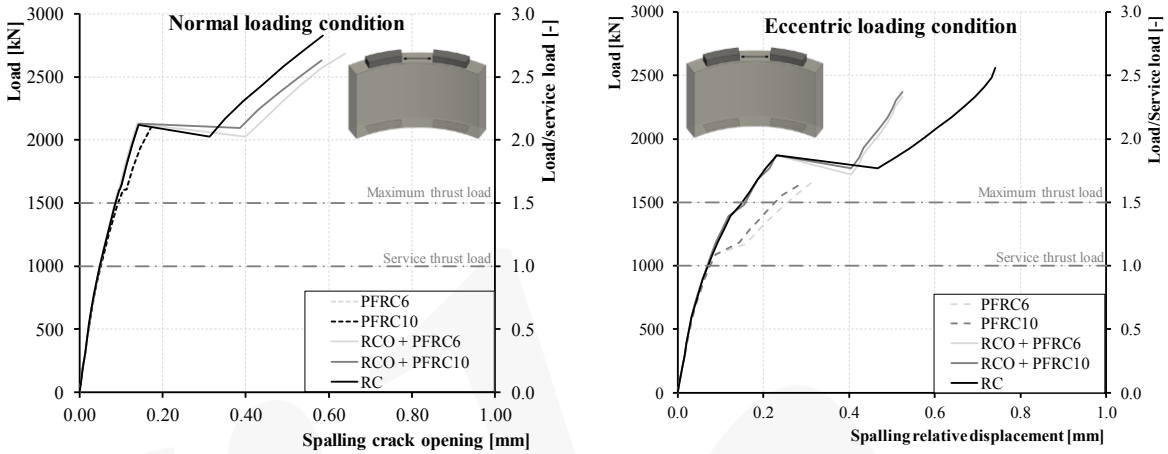
(a) (b)

Figure 5: Typical final crack pattern occurring in the investigated tunnel segments (a); load vs. spalling crack opening curve of RC segment (b)

In case of eccentric placement of the TBM thrust shoes (Figure 6b), the aforementioned tendencies can be more clearly pointed out, since larger spalling crack widths were observed in all the numerical analyses due to the detrimental effect of this irregularity. In fact, PFRC6 and PFRC10 segments present much larger crack widths with respect to RC one, and they were not able to control cracking propagation for loads higher than 1.65 times the service load. At service load both PFRCs configurations present an estimated spalling crack width of about 2.5 times greater the one exhibited in the normal loading condition. The hybrid and RC

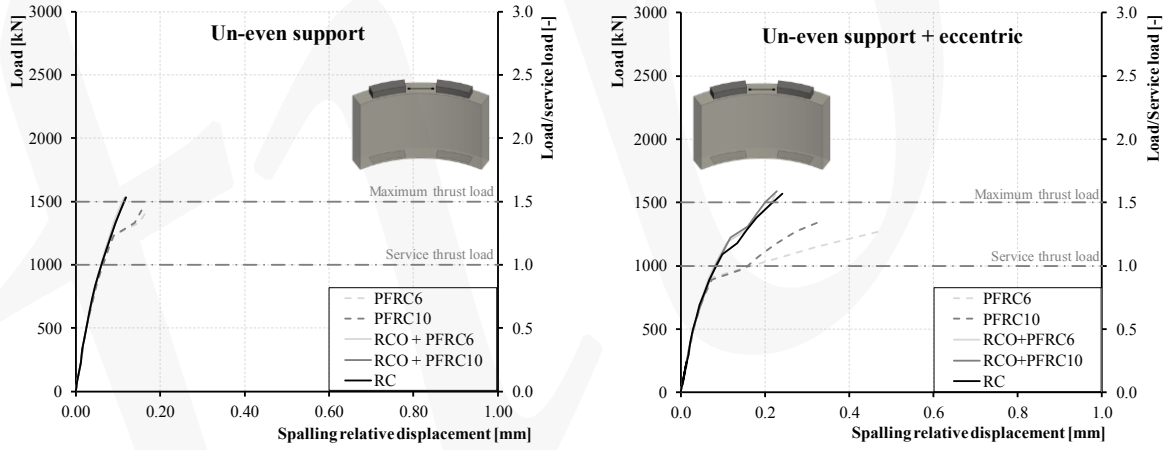
This document is the intellectual property of the fib – International Federation for Structural Concrete. All rights reserved.
This PDF of fib Bulletin 95 is intended for use and/or distribution solely within fib National Member Groups.

configurations exhibit a rather high bearing capacity (around 2.5 s.l) for the eccentric loading condition, as result of a good control of spalling crack phenomenon.



(a) (b)

Figure 6: Spalling crack development between TBM thrust shoes for the investigated tunnel segments: normal (a) and eccentric (b) loading condition



(a) (b)

Figure 7: Spalling crack development between TBM thrust shoes for the investigated tunnel segments: un-even support (a) and un-even support with eccentric (b) loading condition

In Figure 7 the local behavior between the TBM rams is plotted for the un-even support loading condition without eccentricity and with. In the latter case, it was assumed that half of the contact area of one support is not active in carrying the loads due to a possible local gap with the previous assembled ring. In other words, one and half supports were considered instead of having two supports. It is worthwhile noticing that in this case the segment tends to tilt and to locally deflect, especially in the region where the support was partially missing. Consequently, during the numerical analyses the longitudinal displacements (parallel to the longitudinal axis of the tunnel) were also carefully monitored. Similarly, special attention was devoted to the behavior of interface elements used for simulating the interaction of the segment under investigation with adjacent elements. Figure 7b shows the results concerning the combination of un-even support loading condition and possible eccentric placement of the

This document is the intellectual property of the fib – International Federation for Structural Concrete. All rights reserved.
This PDF of fib Bulletin 95 is intended for use and/or distribution solely within fib National Member Groups.

hydraulic jacks, in order to emphasize the effects of irregularities. It can be observed that all segment configurations investigated present a noticeable reduction of the bearing capacity in presence of the un-even support condition (Figure 7) due to local concrete crushing in the segment region under the smallest rear support.

5 Conclusions

The main purpose of this research was the evaluation of macro-synthetic fibers as possible reinforcement solution of precast tunnel segments characterized by a small diameter (3200 mm). Based on the present numerical study, the following conclusions can be drawn:

1. In case of normal loading condition, PFRC and RCO+PFRC segments demonstrated adequate structural performance at both service and maximum TBM thrust loads.
2. In case of unfavorable conditions, which may occur during the construction of the lining, all reinforcing configurations showed reduced bearing capacity. For example, the partial loss of the supports behind the segment (un-even support) can lead to an average reduction of the maximum applied load of about 40% with respect to the normal loading condition.
3. The segment with fiber reinforcement only (PFRC6 and PFRC10) tends to be more vulnerable in terms of expected spalling crack widths in case of unfavorable conditions, especially for loads higher than 1.5 times the service load. It is recommended to avoid as much as possible the occurrence of these irregularities when using this type of reinforcement solution.
4. The combination of a low amount of conventional rebars and macro-synthetic fibers reinforcement demonstrated a local and global behavior of segments similar to the one observed in the RC solution, even when a critical loading condition occurs, (i.e. occurrence of un-even supports combined with the outward eccentricity).

6 Acknowledgement

The Authors would like to thank Engineers Daniele Rivetta and Andrea Piardi, as well as the technicians Luca Martinelli, Augusto Botturi, Domenico Caravaggi and Andrea Delbarba, for the assistance in performing the experimental program. A special acknowledgement goes to Engineer Antonio Mudadu for the assistance in performing the numerical analyses.

7 References

ACI Committee 544 R16 (2016), *Report on Design and Construction of Fiber Reinforced Precast Concrete Tunnel Segments*, ACI 544.7R-16, American Concrete Institute, pp. 36.

Blom C.B.M. (2002), *Design philosophy of concrete linings for tunnels in soft soils*, Ph.D Thesis, Delft University of Technology, The Netherlands, pp. 184.

Conforti, A., Minelli, F., Plizzari, G.A., and Tiberti, G. (2017), *Comparing test methods for the mechanical characterization of fiber reinforced concrete,* Structural Concrete, 1-14, https://doi.org/10.1002/suco.201700057.

This document is the intellectual property of the fib – International Federation for Structural Concrete. All rights reserved.
This PDF of fib Bulletin 95 is intended for use and/or distribution solely within fib National Member Groups.

Conforti, A., Tiberti, G., Plizzari, G.A., Caratelli, A., and Meda A. (2017), *Precast tunnel segments reinforced by macro-synthetic fibers,* Tunnelling and Underground Space Technology, Vol. 63, pp. 1-11.

DIANA – Finite Element Analysis (2016), *User's Manual release 10.1. TNO DIANA BV*, Delft, The Netherlands. Edited by Jonna Manie and Wijtze Pieter Kikstra.

EN 14651 (2005), *Precast concrete products – test method for metallic fibre concrete – Measuring the flexural tensile strength.* European Standard.

Eurocode 2 (2004), *Design of concrete structures.* European Standard.

fib Bulletin 83 (2017), *Precast tunnel segments in fibre-reinforced concrete, W.P. 1.4.1 Tunnels in fiber reinforced concrete,* ISSN 1562-3610, ISBN 978-2-88394-123-6.

Groeneweg T.W. (2007), *Shield driven tunnels in ultra high strength concrete, reduction of the tunnel lining thickness,* Graduate Thesis, Delft University of Technology, The Netherlands, January, 2007.

ITA report n. 16 (2016), *Twenty years of FRC tunnel segments practice: lessons learnt and proposed design principles,* April 2016, pp. 71, ISBN 978-2-970-1013-5-2.

Liao L., De la Fuente A., Cavalaro S. and Aguado, A. (2015), *Design of FRC tunnel segments considering the ductility requirements of the Model Code 2010,* Tunnelling and Underground Space Technology, Vol. 47, pp. 200-210.

Model Code 2010 - Final draft (2012), *fib Bulletin 65. Volume 1,* pp. 350, ISBN 978-2-88394-105-2; *fib Bulletin 66. Volume 2,* pp. 370, ISBN 978-2-88394-106-9.

Nitschke A. G. and Winterberg R. (2016), *Performance of macro-synthetic fiber reinforced tunnel linings.* In: Proceedings of the World Tunnel Congress 2016, San Francisco (U.S.A.), 22-28 April, 2016, full-paper available on usb-stick, 10 p.

Rijke, Q.C. de (2006), *Innovation of stress and damage reduction in bored tunnels during construction based on a shield equilibrium model,* Graduate Thesis, Utrecht, Delft University of Technology and Holland Railconsult.

Rots J.G. (1988), *Computational modeling of concrete fracture,* Ph. D Thesis, Delft University of Technology, The Netherlands, pp. 132.

Selby R.G. and Vecchio F.J. (1993), *Three dimensional constitutive relations for reinforced concrete,* Univ. Toronto, Civil. Eng., Toronto, Canada.

Thorenfeldt E., Tomaszewicz A. and Jensen J. J. (1987), *Mechanical properties of high-strength concrete and applications in design.* In Proc. Symp. Utilization of High-Strength Concrete, Stavanger, Norway.

Tiberti G., Conforti A. and Plizzari G.A. (2015), *Precast segments under TBM hydraulic jacks: Experimental investigation on the local splitting behavior,* Tunnelling and Underground Space Technology, Vol. 50, August 2015, pp. 438-450, doi: http://dx.doi.org/10.1016/j.tust.2015.08.013.

Trabucchi I. (2015), *Studio numerico di rivestimenti per gallerie realizzati in conci prefabbricati,* Master Thesis, University of Brescia, pp. 250.

Trabucchi I., Conforti A., Tiberti G., Mudadu A and Plizzari G.A. (2019), *Flexural behavior of precast tunnel segments reinforced by macro-synthetic fibers*. In: Proceedings of the World Tunnel Congress 2019, Naples (Italy), 03-09 May, p. 9

This document is the intellectual property of the fib – International Federation for Structural Concrete. All rights reserved.
This PDF of fib Bulletin 95 is intended for use and/or distribution solely within fib National Member Groups.

4) SEISMIC AND SPECIAL LOADING CONDITIONS

This document is the intellectual property of the fib – International Federation for Structural Concrete. All rights reserved.
This PDF of fib Bulletin 95 is intended for use and/or distribution solely within fib National Member Groups.
FRC2018: Fibre Reinforced Concrete: from Design to Structural Applications
Joint ACI-*fib*-RILEM International Workshop

Seismic Performance of Fibre Reinforced Concrete in the Absence of Bars

Erik Stefan Bernard[1]

[1] : Technologies in Structural Engineering Pty Ltd, Sydney, Australia.

Abstract

Numerous investigations of the effect of fibre addition on the seismic performance of conventionally reinforced concrete members have been published. These generally show that fibres can improve robustness and survivability during reverse-cycle loading, but the dosage rate of fibre required to achieve significant improvements in performance is substantial. Recently, pure FRC members have increasingly been used in structures such as tunnel linings, including both fibre reinforced shotcrete and pre-cast FRC segments. Concerns have been raised about the absence of data on the seismic resistance of such members given that all previous research on seismic performance has essentially involved hybrid members incorporating both steel reinforcing bars and fibres.

The present investigation has focused on the reverse-cycle flexural performance of FRC members in the absence of conventional steel reinforcing bars. Laboratory testing was performed on plain, bar-reinforced, and steel fibre reinforced concrete members, and their performance was compared. The tests indicate that steel fibres provide a small improvement in flexural capacity under reverse-cycle loading compared to plain concrete, but that the robustness of pure FRC members is relatively poor compared to steel bar-reinforced members incorporating steel stirrups. The data suggest that, when used at practical dosage rates, large hooked-end steel fibres cannot be relied upon to provide seismic performance in flexure comparable to steel bar reinforced concrete members.

Keywords

Reverse-cycle loading, Fibre reinforced concrete, post-crack performance, seismic loading, robustness, conventional reinforcement

This document is the intellectual property of the fib – International Federation for Structural Concrete. All rights reserved.
This PDF of fib Bulletin 95 is intended for use and/or distribution solely within fib National Member Groups.

1 Introduction

The potential benefit of including fibres within Reinforced Concrete (RC) members to improve performance in response to seismic loading has been investigated in many previous studies (eg. Filiatrault et al, 1995; Gefken and Ramey, 1989; Bayasi and Gebman, 2002). The majority of previous research has focused on using steel fibres in addition to conventional steel stirrups to provide enhanced confinement to concrete within a member. This research (Jiuru et al, 1992; Filiatrault et al, 1994; Bayasi and Gebman, 2002; Billington and Yoon, 2004) has demonstrated that steel fibres are relatively effective in this application, but suffer the problem that their stiffness can make them difficult to consolidate within an already tight reinforcement cage, especially if they are relatively long (>40 mm). Moreover, the minimum dosage of steel fibre required to provide a significant enhancement in capacity is so high that the economics of replacing stirrups with steel fibres is questionable.

Many early studies demonstrated that steel fibres can increase seismic resistance through their capacity to enhance confinement (Craig et al, 1984; Lakshmipathy and Shanthakumar, 1986; Jindal and Sharma, 1987), but later studies addressed the issue of potentially reducing the amount of confining steel (by increasing the spacing between stirrups) through the inclusion of steel fibres (Bayasi and Gebman, 2002; Tavallali et al, 2014). In general, these studies showed that stirrup spacing could be increased while at the same time maintaining seismic resistance, but very high levels of steel fibre reinforcement (typically 1-2% by volume) were required to achieve this.

An alternative to steel fibres for enhancement of seismic resistance is the use of macro-synthetic fibres. This type of fibre usually offers the advantage of being flexible so that consolidation is easier between reinforcing bars, and generally offer superior ductility at wide crack widths compared to steel fibres. Several recent small-scale investigations (Ma et al, 2012; Ma et al, 2012; Carnovale, 2012; Osorio et al, 2014; Bernard, 2016) have indicated that macro-synthetic fibres can produce meaningful improvements in seismic resistance if used in combination with conventional steel reinforcing bars and stirrups.

Ductility in reinforced concrete members is an important property to satisfy strength requirements in response to many forms of structural loading. However, there is some concern over how fibres perform across cracks that repeatedly open and close. Moreover, cracks arise in many orientations during reverse-cycle loading, so loss of lateral confinement may potentially degrade fibre performance. Reverse-cycle loading appears to produce different responses in FRC compared to monotonic flexural loading, so good performance in pure bending tests such as ASTM C1609/C1609M and EN14651 does not necessarily predict good performance in a seismic event. A combination of fibres and conventional reinforcement results in well distributed strain under reverse-cycle loading leading to a multitude of small cracks. When fibres are used in the absence of conventional steel bars, flexural cracks are more widely spaced and strain localisation is likely to be more concentrated, especially if the axial compressive stress is low. The result is a limited number of wide cracks.

Some recent applications for FRC have involved the complete replacement of conventional steel bars with fibres. Examples include FRC tunnel segments, Fibre Reinforced Shotcrete tunnel linings, and cast-in-place FRC tunnel linings. While evidence exist that tunnel linings are not particularly sensitive to seismic loading (Hashash et al, 2001; Hashash et al, 2005), damage can still occur so the capacity of an FRC lining to satisfactorily support load during an earthquake needs to be quantified in the design process. Little published information exists

This document is the intellectual property of the fib – International Federation for Structural Concrete. All rights reserved.
This PDF of fib Bulletin 95 is intended for use and/or distribution solely within fib National Member Groups.

regarding the seismic performance of FRC in the absence of steel bars, so designers of FRC tunnel linings in seismically active areas have tended to rely instead on the post-crack performance of FRC measured in standard beam tests. The present experimental investigation has sought to expand upon available information regarding the seismic performance of flexural members comprised of FRC in the absence of steel bars.

2 Experimental program

The experimental program consisted of a series of reverse-cycle tests on beam-columns made of plain concrete and steel FRC, with some specimens also reinforced with conventional steel bars and stirrups. Each set of nominally identical beam-columns was cast using a 32 MPa concrete mix conforming to the design listed in Table 1. The steel FRC mixtures included either 20 or 40 kg/m^3 Dramix RC65/60 3D fibres both with and without conventional reinforcing bars (Table 2). The specimens were cast and consolidated in a horizontal position, stripped after two days, and cured in lime-saturated water for four months before testing. Compressive strength results are listed in Table 2.

Moment was induced in each specimen through the application of two lateral point loads located 250 mm on each side of the midpoint to induce a region of uniform bending moment at the centre (Figure 1a). Reverse-cycle loading was applied laterally in accordance with ACI-374 to induce bending moments that ultimately caused failure of the section. An axial compressive stress of 4 MPa was imposed on each specimen throughout testing. Lateral displacement was measured at the centre and used to calculate the drift. Moments were corrected for the P-Δ effect to arrive at the total moment imposed at the central region of each specimen.

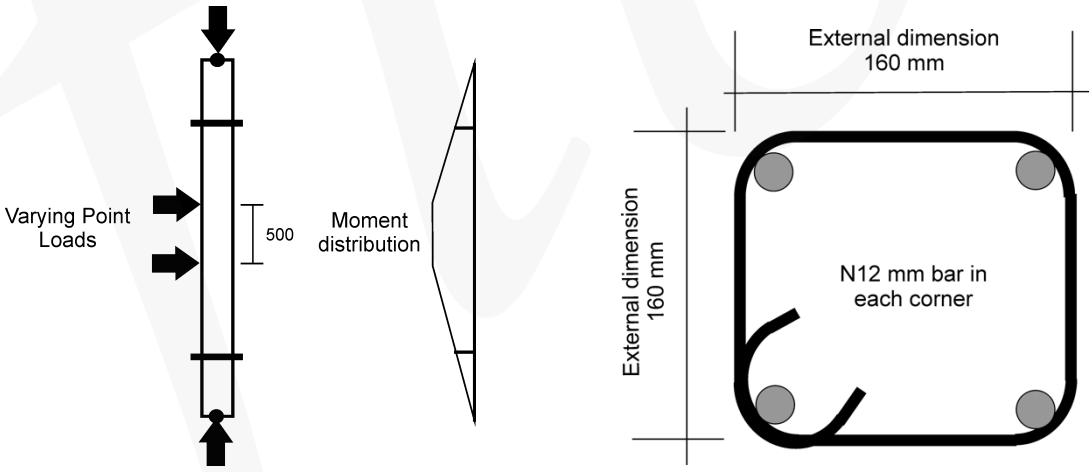


Figure 1: (a) Two-point lateral loading on each beam-column specimen, and (b) stirrup configuration

The experimental apparatus developed for this investigation incorporated two servo-hydraulic actuators placed at right angles (Figure 2). Axial load was applied using a 250 kN MTS servo-controlled actuator operating in load-control. The lateral load was imposed using a 100 kN MTS servo-controlled actuator operating in stroke-control. All the equipment was mounted on a 5500 × 2650 mm slotted steel work plate measuring 150 mm thick on a 600 mm deep steel waffle-plate. The concrete beam-columns were bolted into place between two large

This document is the intellectual property of the fib – International Federation for Structural Concrete. All rights reserved.
This PDF of fib Bulletin 95 is intended for use and/or distribution solely within fib National Member Groups.

end pivots in the longitudinal direction while axial tension rods spanned the distance between the pivots in order to prevent slip between the mounting blocks and the slotted steel base.

The beams-columns all measured 2000 mm in length and 200 × 200 mm in cross-section. The conventionally reinforced specimens had one 12 mm longitudinal reinforcing bar in each corner (Figure 1b). The RC beam-columns included stirrups consisting of 6 mm plain round bar bent into a fully enclosed square with 40 mm long end hooks. These stirrups were spaced 250 mm apart along the length of each member. With the pivots included, the column measured 2524 mm total length. The 12 mm N-grade deformed longitudinal steel bars had a nominal tensile yield strength of 500 MPa and exhibited normal levels of post-yield ductility. These bars did not meet code requirements for ductility in response to seismic loading (AS/NZS 4671) but are the most common bars used in the Australian market. The cover to the bars was nominally 20 mm from each face. Four replicates were produced and tested for each reinforcement configuration.

3 Test Results

Each series of four beam-columns was tested at the same age, using the same ACI 374-based testing procedure, leading to destructive failures of the type shown in Figures 3 and 4, and moment-drift curves of the type shown in Figures 5 and 6. The plain concrete specimens survived remarkably well, with the cracks initially opening and closing in a rocking manner without much damage accumulating in the adjoining concrete up to 5% drift. However, beyond about 8-10% drift, longitudinal cracks started to appear perpendicular to the flexural cracks and finally most of the specimens suffered a shearing failure. The central part of each specimen generally broke into large pieces of concrete and collapsed by the end of the test.

Table 1:. Mix design for 32 MPa concrete mix used in all trials.

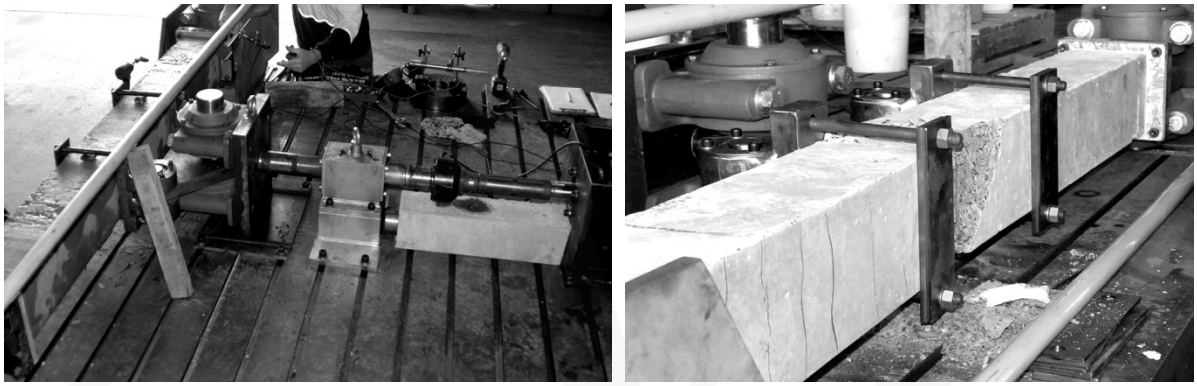
Ingredient	**Quantity (kg/m^3)**
10 mm CRG	1000
Coarse sand	460
Fine sand	250
GP cement	280
Fly ash	100
LR Water reducer	1330 mL/m^3

Table 2: Test series and reinforcement characteristics for the five sets of specimens tested.

Reinforcement	**Number of Beam-columns**	**Compressive strength (MPa)**
Plain Concrete	4	47.0
Plain Concrete with bars	4	43.5
SFRC, 20 kg/m^3	4	50.0
SFRC, 40 kg/m^3	4	47.3
Hybrid, 20 kg/m^3	4	50.0
Hybrid, 40 kg/m^3	4	47.3

This document is the intellectual property of the fib – International Federation for Structural Concrete. All rights reserved.
This PDF of fib Bulletin 95 is intended for use and/or distribution solely within fib National Member Groups.

The steel FRC specimens behaved in a similar manner to the plain concrete beam-columns but the peak moment sustained was slightly greater (Figures 7-9). The fibres helped the concrete hold together better than the plain concrete, but the final mode of failure was dominated by shear (Figure 3a) and resembled the plain concrete specimen failures. After failure, many fibres protruded from the broken concrete and appeared to be undamaged in the reverse-cycle loading process (Figure 4b). The concrete appeared to break-up around the fibres such that the fibres apparently did little work during the failure process.



(a) (b)

Figure 2: (a) Lateral reverse-cycle loading mechanism, and (b) initial loading and damage to beam-column

The bar-reinforced plain concrete specimens and hybrid SFRC-RC members exhibited a substantially different mode of behaviour during the reverse-cycle tests. Initially, a multitude of small flexural cracks arose in the central uniform-moment region up to about 5% drift, but one crack steadily became larger than the others leading to yielding and rupture of the bars at this point. For the plain concrete specimens with bars, break-up of the concrete was quite rapid and flexural performance deteriorated quickly beyond about 10% drift. For the SFRC-RC hybrid specimens, concrete broke up around the dominant central crack leading to an apparent swelling of the beam at around 12+% drift, but the fibres continued to hold the concrete together. Inevitably, the concrete became so degraded that it crushed in compression (Figure 4a). The hybrid beam-columns generally shortened by about 50-70 mm by the time each test was completed.

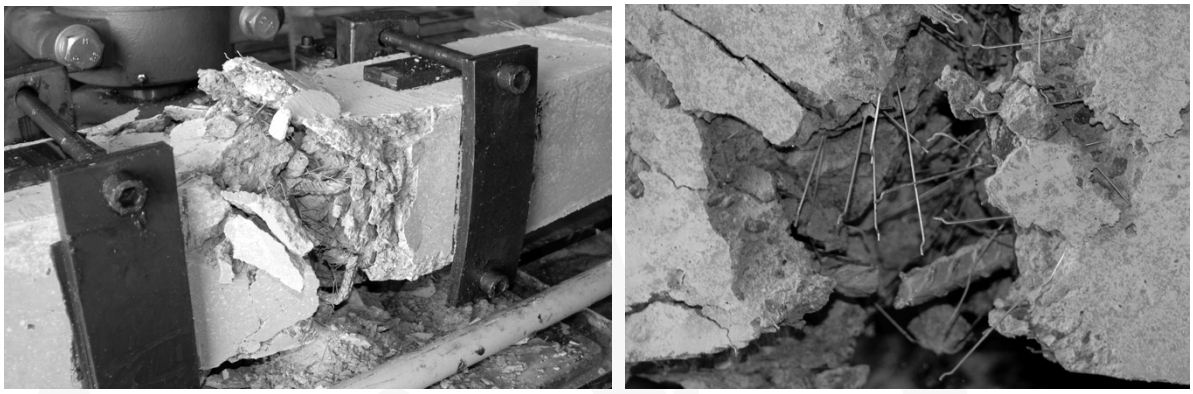


(a) (b)

Figure 3: (a) Shearing failure, and (b) crushing, for SFRC and hybrid beam with 20 kg/m3 steel fibre.

This document is the intellectual property of the fib – International Federation for Structural Concrete. All rights reserved.
This PDF of fib Bulletin 95 is intended for use and/or distribution solely within fib National Member Groups.

Inspection of the moment-drift curves in Figures 5 and 6 reveals that the peak moment capacity for the bar-reinforced beam-columns was far greater than that exhibited by the plain concrete or pure SFRC specimens. The maximum drift supported by the hybrid specimens prior to collapse was also somewhat greater. These aspects of performance will depend on the amount of steel present as conventional reinforcement, and the ductility characteristics of the steel. In the present tests, normal (N-grade) bars of modest ductility were used (AS/NZS 4671). Given that final failure appeared to be governed by rupture of the bars, substantially greater robustness is likely if E-grade high ductility bars are used in the place of N-grade bars.



(a) (b)

Figure 4: (a) Failure for hybrid reinforced with 40 kg/m^3, (b) largely undamaged fibres after testing

Performance of the beam-columns was expressed in two ways: moment capacity in each cycle of loading normalised relative to the maximum moment sustained (Figure 7), and peak moment sustained in each load cycle (Figure 8 and 9). The former reveals the relative robustness of the three forms of reinforcement (plain, SFRC, and conventional bars) while the latter reveals the absolute magnitude of moment capacity. Both Figures 7 and 8 show some differences in capacity in the initial ascending part of the curve for the plain and SFRC specimens. This was caused by slight differences in the geometry of the specimens and loading (which led to a slight difference in initial stiffness), but disappeared once cracking commenced. At small deformations (2-3% drift) all the specimens essentially behaved the same. Beyond this, the type of reinforcement present began to influence behavior. At large deformations, some specimens within each set failed earlier than others, so there are numerous 'zero magnitude' points along the horizontal axis of each graph from about 9% drift upwards. These have been included in the curve-fits, which is why the curve-fits to mean performance for each set of specimens trends downward toward 17-18% drift. No plain concrete or SFRC specimen survived beyond 17% drift.

The results for the conventionally-reinforced beam-columns tested in reverse-cycle loading are shown in Figure 9. This figure indicates that the bar reinforcement contributed to a dramatic increase in peak moment capacity and ductility compared to SFRC. It also reveals that an increase in steel fibre dosage rate led to a steady increase in robustness at large drifts (12+%) illustrating the value of adding fibres to a conventionally reinforced section. However, it is surprising that the bar-reinforced plain concrete specimens deteriorated in performance more rapidly than the plain concrete specimens that lacked reinforcement entirely. This was possibly caused by the fact that the plain unreinforced concrete specimens displayed a 'rocking' behaviour at the primary hinge with each cycle of reverse-cycle loading

This document is the intellectual property of the fib – International Federation for Structural Concrete. All rights reserved.
This PDF of fib Bulletin 95 is intended for use and/or distribution solely within fib National Member Groups.

that led to a relatively slow rate of performance deterioration. In contrast, the bar-reinforced beam-columns made with plain concrete suffered numerous cracks that linked up to cause general crushing of the concrete at the higher moments sustained in the presence of the conventional reinforcement.

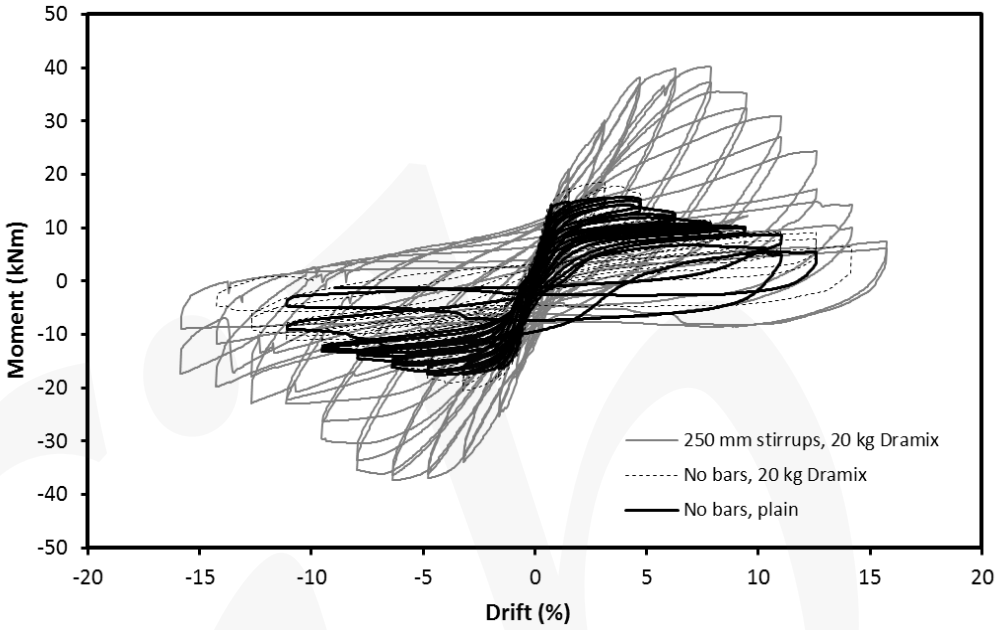


Figure 5: Typical moment-drift curves for plain concrete beams compared to beams reinforced with 20 kg/m^3 Dramix RC65/60 3D fibres, with and without 12 mm longitudinal bars and 6 mm stirrups at 250 mm centres.

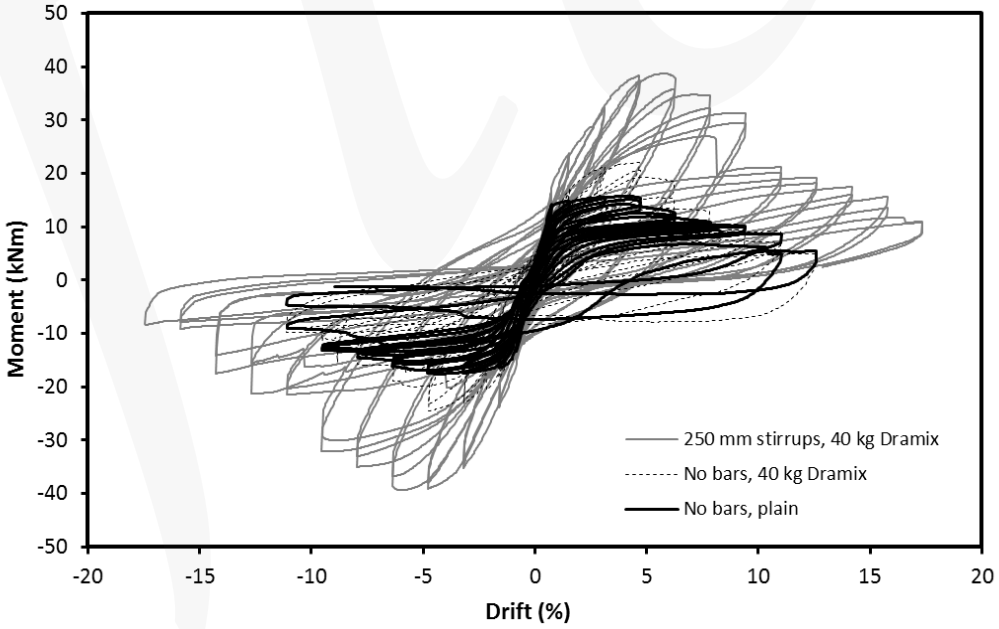


Figure 6: Typical moment-drift curves for plain concrete beams compared to beams reinforced with 40 kg/m^3 Dramix RC65/60 3D fibres, with and without 12 mm longitudinal bars and 6 mm stirrups at 250 mm centres.

This document is the intellectual property of the fib – International Federation for Structural Concrete. All rights reserved.
This PDF of fib Bulletin 95 is intended for use and/or distribution solely within fib National Member Groups.

While the data in Figure 9 indicates that adding steel fibres to an RC section improves robustness, it also shows that the reverse-cycle moment capacity of the hybrid specimens was substantially greater than the performance of the SFRC and plain concrete specimens that lacked conventional reinforcement. The lower set of curves, peaking at between 15-22 kNm moment, are the same curve-fits shown in Figure 8. The magnitude of the difference in performance will depend on the dosage rate of fibre and percentage of conventional steel bar reinforcement, but the stark difference in performance revealed in Figure 9 illustrates the fact that steel fibres are *not* an effective substitute for conventional bar reinforcement in seismic applications.

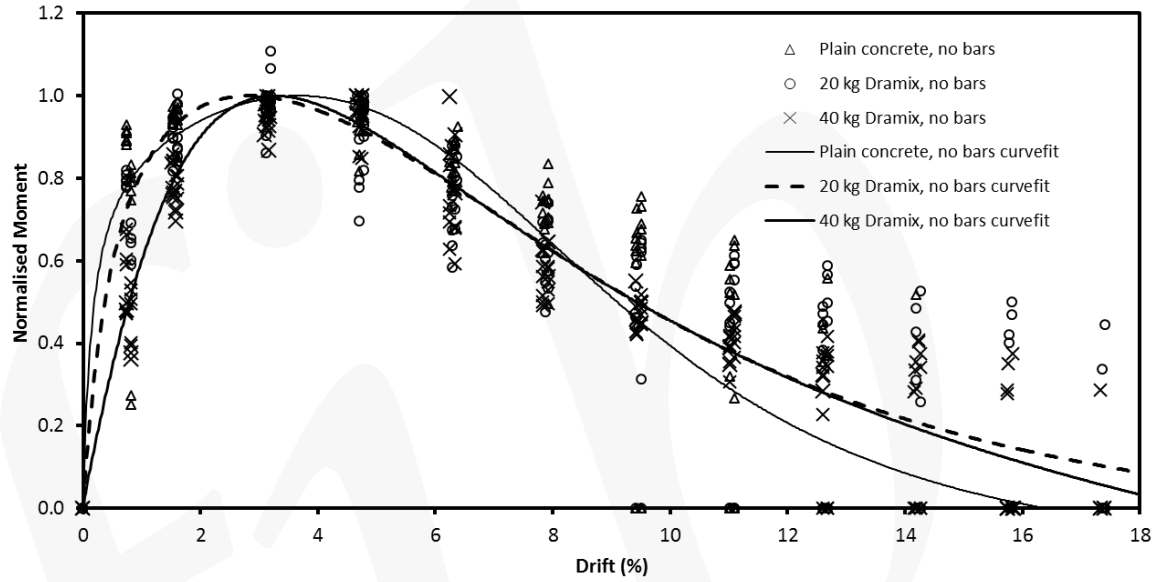


Figure 7: Relationship between drift and normalised moment for plain concrete beams compared to beams reinforced with 20 and 40 kg/m^3 Dramix RC65/60 3D fibres, with no reinforcing steel.

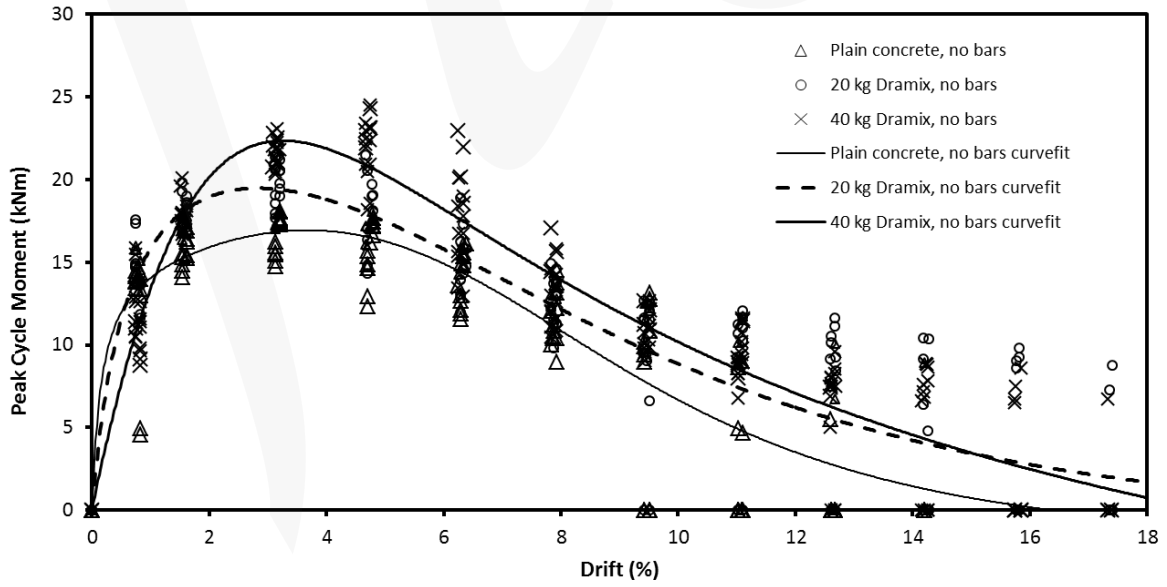


Figure 8: Relationship between drift and peak cycle moment for plain concrete beams compared to beams reinforced with 20 and 40 kg/m^3 Dramix RC65/60 3D fibres, with no reinforcing steel.

This document is the intellectual property of the fib – International Federation for Structural Concrete. All rights reserved.
This PDF of fib Bulletin 95 is intended for use and/or distribution solely within fib National Member Groups.

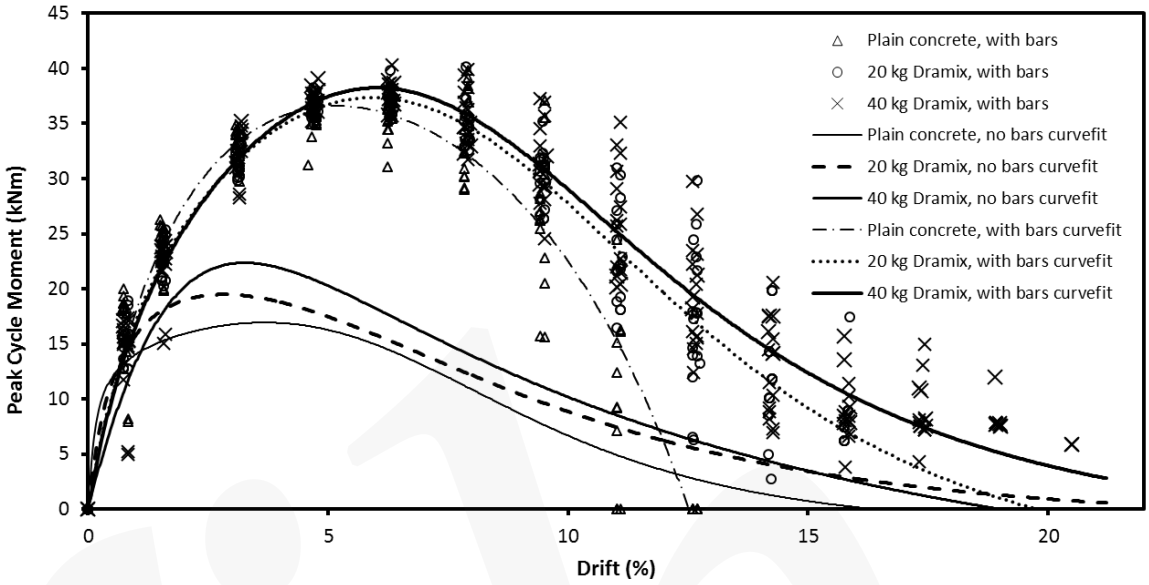


Figure 9: Relationship between drift and peak cycle moment for plain concrete and SFRC beams compared to hybrid beams reinforced with 20 and 40 kg/m^3 Dramix RC65/60 3D fibres.

4 Concluding remarks

Reverse-cycle load tests have been performed on beam-columns comprised of either plain concrete, steel FRC, or reinforced with conventional steel bars, to assess the relative resistance of each configuration to potential seismic loading. The tests demonstrated that steel FRC performs similarly to plain concrete, but with a small improvement in peak load and drift capacity that is proportional to the dosage rate of steel fibre added. However, inclusion of conventional steel reinforcing bars results in a level of reverse-cycle load resistance that is substantially greater than that provided by steel fibres on their own. Inclusion of steel fibres within a hybrid beam-column that is also reinforced with conventional steel bars results in a steady improvement in reverse-cycle load resistance that is sensitive to the dosage rate of fibres added.

5 Acknowledgements

The Author acknowledges the support provided by Joshua Tolhurst and Keith Clarke in conducting the majority of the tests described in this paper.

6 References

ACI 374 .2R13, 2013. "Guide for Testing Reinforced Concrete Structural Elements under Slowly Applied Simulated Seismic Loads", *American Concrete Institute*, Farmington Hills, MI.

AS/NZS 4671: 2001 *Steel Reinforcing Materials*, Standards Australia, Sydney.

Bayasi, Z. and Gebman, M., 2002. "Reduction of Lateral Reinforcement in Seismic Beam-Column Connection via Application of Steel Fibers", *ACI Structural Journal*, Vol. 99, No. 6, pp 772-780.

This document is the intellectual property of the fib – International Federation for Structural Concrete. All rights reserved.
This PDF of fib Bulletin 95 is intended for use and/or distribution solely within fib National Member Groups.

Bernard, E.S. 2016. "Enhancement of Seismic Resistance of Reinforced Concrete Members Using Embossed Macro-Synthetic Fibers", *WTC 2016*, San Francisco, April 22-28.

Billington, S. and Yoon, J. 2004. "Cyclic Response of Unbonded Posttensioned Precast Columns with Ductile Fiber-Reinforced Concrete." *J. Bridge Eng*., 9(4) pp353–363.

Carnovale, D.J. 2012. "Behaviour and Analysis of Steel and Macro-Synthetic Fiber Reinforced Concrete Subjected to Reversed Cyclic Loading: A Pilot Investigation", *Master of Applied Science thesis*, Department of Civil Engineering, University of Toronto.

Craig, R., Mahadev, S., Patel, C., Viteri, M., and Kertesz, C., 1984. "Behavior of joints using reinforced fibrous concrete", *Fiber Reinforced Concrete*, Proceedings of the International Symposium, SP-81, (ed. G. Hoff), American Concrete Institute, Farmington Hills, MI, pp125-167.

Filiatrault, A., Ladicani, K. and Massicote, B., 1994. "Seismic Performance of Code-Designed Fiber-Reinforced Concrete Joints", *ACI Structural Journal*, 91(5), pp564-571.

Filiatrault, A., Pineau, S., and Houde, J., 1995. "Seismic Behavior of Steel Fiber-Reinforced Concrete Interior Beam-Column Connection", *ACI Structural Journal*, 92(5), pp543-552.

Gefken, P. and Ramey, M., 1989. "Increased Hoop Spacing in Type 2 Seismic Joints Using Fiber Reinforced Concrete", *ACI Structural Journal*, 86(2), pp168-172.

Hashash, Y.M.A., Hook, J.J., Schmidt, B., and Yao. J.I.C., 2001. "Seismic design and analysis of underground structures", *Tunnelling and Underground Space Technology* 16, pp247–293

Hashash, Y.M.A., Park, D., and Yao, J.I.C., 2005. "Ovaling deformations of circular tunnels under seismic loading, an update on seismic design and analysis of underground structures", *Tunnelling and Underground Space Technology* 20, pp435–441

Jindal, R., and Sharma, V., 1987. "Behavior of Steel Fiber Reinforced Concrete Knee-type Beam-Column Connections", *Fiber Reinforced Concrete Properties and Applications*, SP-105, (ed. SP Shah and GB Batson), American Concrete Institute, Farmington Hills, MI, pp475-491.

Jiuru, T., Chaobin, H., Kaijian, Y., and Yongcheng, Y., 1992. "Seismic Behavior and Shear Strength of Framed Joints Using Steel Fiber Reinforced Concrete", ASCE *Journal of Structural Engineering*, 118(2), pp341-358.

Lakshmipathy, M., and Shanthakumar, A., 1986. "Experimental Verification of the Behavior of Reinforced Fibrous Concrete Frames Subjected to Seismic Loading", Paper 8.15, RILEM Symposium: *Developments in Fiber-Reinforced Cement and Concrete*, Vol. 2, Sheffield, 14pp.

Ma, H., Wang, H., Li, Z., Sun, K. and Zhang, X., 2012. "Experimental Study on the Seismic Performance of Macro-Synthetic Fiber- Reinforced Concrete Ductile Columns", *Advanced Materials Research*, Vols. 446-449, pp 2345-2350.

Ma, H., Zhou, L.,Li, Z., Wang, H., Hao, X, Sun, X., and Zhang, X., 2012. "The Effect of Macro-Synthetic Fiber on the Seismic Performance of Reinforced Concrete Columns Carried out by Experiment Study", *Advanced Materials Research* Vols. 479-481, pp 1220-1224.

Osorio, L.I., Paultre, P., Eid, R., and Proulx, J., 2014. "Seismic Behavior of Synthetic Fiber-Reinforced Circular Columns", *ACI Structural Journal*, 111(1), pp189-200.

Tavallali, H., Lepage, A., Rautenberg, J.M., and Pujol, S., 2014. "Concrete Beams Reinforced with High Strength Steel Subjected to Displacement Reversals", *ACI Structural Journal*, 111(5), pp1037-1048.

This document is the intellectual property of the fib – International Federation for Structural Concrete. All rights reserved.
This PDF of fib Bulletin 95 is intended for use and/or distribution solely within fib National Member Groups.
FRC2018: Fibre Reinforced Concrete: from Design to Structural Applications
Joint ACI-*fib*-RILEM International Workshop

RC Beams with Steel Fibres - Towards Better Determination of their Minimum Conventional Reinforcement Ratio

Avraham N. Dancygier[1], Yuri S. Karinski[1]

[1] : Technion – Israel Institute of Technology, Haifa, Israel

Abstract

Minimum longitudinal reinforcement ratio in reinforced concrete (RC) beams is determined by criteria that refer to flexural capacity. However, relatively recent experiments have shown that RC beams with steel fibres (RFRC beams) with the above-determined minimum reinforcement, exhibit a pronounced reduction in their flexural ductility, compared with similar plain RC beams. This phenomenon was characterized by cracking localization, when only one or two cracks widened significantly more than the other cracks did. This led to increase of the steel plastic strains, even up to its rupture, in the rebars that crossed these cracks. The ductility reduction in this case impairs the structural response of RFRC beams compared with RC beams without fibres. Therefore, this effect of the fibres must also be considered when determining the minimum longitudinal reinforcement ratio in RFRC beams.

The paper presents analysis of test results that pertain to flexural ductility in RFRC beams and its relation with the cracking localization phenomenon. This phenomenon may be quantified by the ratio between the number of the significantly wide cracks and the total number of flexural cracks. It is shown that RFRC beams with smaller reinforcement ratios had higher cracking localization. It is also shown that as the reinforcement ratio decreases below a certain value, which is considerably larger than the minimum required by the codes, the flexural ductility decreases as well. Within this range of small reinforcement ratio, these two trends are related, whereas for larger reinforcement ratios, there is no effect of cracking localization on the flexural ductility.

Keywords

Cracking localization; Fibre-reinforced concrete; Flexural ductility; Minimum reinforcement ratio

This document is the intellectual property of the fib – International Federation for Structural Concrete. All rights reserved.
This PDF of fib Bulletin 95 is intended for use and/or distribution solely within fib National Member Groups.

1 Introduction

Addition of fibers to a concrete mix is expected to improve cracking control, i.e., to reduce crack width and spacing at service loads (e.g., Vandewalle, 2000, Redaelli and Muttoni, 2007). Fibers are also expected to increase the material's ultimate strain and its toughness (e.g., Bentur and Mindess, 2007), exhibited in the material post-peak tensile behaviour (*fib* 2013, di Prisco et al. 2013). Therefore, RC flexural elements that include steel fibres (RFRC elements) are expected to have enhanced flexural ductility (see definition in Chapter 2). However, relatively recent experiments have shown that both normal strength (Schumacher et al. 2009, Dancygier and Berkover 2016) and high strength (Dancygier and Savir 2006, Yoo and Yoon 2015) RFRC beams with low longitudinal reinforcement, exhibited a pronounced reduction in their flexural ductility, compared with similar plain RC beams.

This ductility reduction is associated with cracking localization phenomenon. This phenomenon is characterized by significant widening of one or only few cracks, compared with the other cracks, at loads that are larger than the steel yielding load (Dancygier and Savir 2006, Yoo and Yoon 2015, Dancygier and Berkover 2016). This widening leads to significant local elongation of the rebars, which are bridging the wide crack (and hence, to large local steel strains), and cause the beam plastic hinge length to be relatively short. The phenomenon of cracking localization was also observed in tensile tests of prismatic RFRC bars (Redaelli and Muttoni 2007, Deluce and Vecchio 2013, Dancygier et al 2017).

Yet, design codes require fore RC beams and slabs minimum longitudinal reinforcement ratio. This ratio is determined by criteria that refer to flexural capacity, but not to the flexural ductility. This is because in plain RC flexural elements, low reinforcement ratios are associated with relatively high ductility (e.g., Park and Paulay, 1975). However, as mentioned above, this is not the case for RFRC elements. Therefore, there is a need to derive another criterion for the minimum reinforcement ratio in RFRC flexural elements, which accounts for both capacity and ductility of the structure.

The paper deals with this ductility reduction and presents overview, analysis and discussion of our test results that pertain to flexural ductility in RFRC beams and its relation with the cracking localization phenomenon. These experimental data can be used for a further, better determination of the minimum conventional reinforcement ratio is RFRC beams. Note that data and analysis that are presented in this paper refer to concrete mixes with relatively long (>30 mm) steel fibers that exhibit a softening behaviour in tension.

2 Reduction of flexural ductility

A common definition of flexural ductility is the ratio between the ultimate and yield deflections. The latter is the deflection of a flexural element (beam or slab) when its tension reinforcement starts to yield. Because most flexural elements have some post-peak capacity without a significant reduction in strength, Park (1989) suggested that it is reasonable to consider part of this capacity. Therefore, in this study the ultimate deflection was defined as the deflection at 0.99 of the maximum bending moment at the post-peak range (following Dancygier and Berkover, 2016).

Results from two experimental programs of high and normal strength RFRC beams (HSC and NSC, respectively) are presented. The programs included four-point bending tests (Figure 1) of plain (control) and fibre-reinforced beam specimens.

This document is the intellectual property of the fib – International Federation for Structural Concrete. All rights reserved.
This PDF of fib Bulletin 95 is intended for use and/or distribution solely within fib National Member Groups.

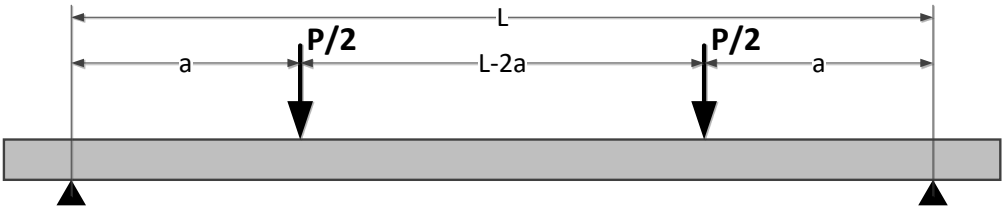


Figure 1: Four-point bending scheme of the RFRC beams

The first program (Dancygier and Savir, 2006) was of HSC, 200x300-mm (width x height) cross-section specimens with a total span, L=3.5 m and three shear spans (a) of 1.0, 1.25 and 1.5 m (refer to Figure 1). Concrete compressive strength at 28 days was 115~130 MPa (measured in 100-mm, 7-days wet cured cubes). Two different types of 35 and 60 mm long, hooked-end steel fibres, with aspect ratios of 64 and 67, were given at 60 kg/m^3 (ρ_f=0.76% in volume). In addition, control, plain RC specimens were also tested. The conventional reinforcement ratios, ρ, were 0.28, 0.56 and 3.5%.

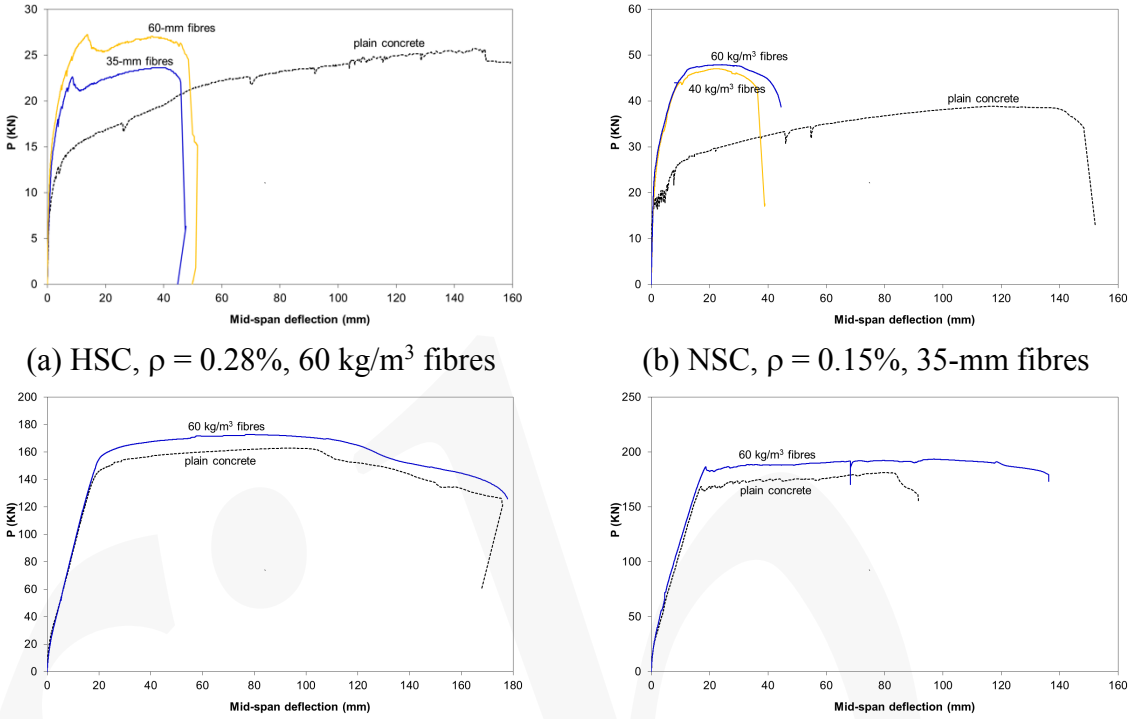
The second program (Dancygier and Berkover, 2016) was of NSC, 240x300-mm (width x height) cross-section specimens with a total span, L=3.2 m and a shear span a=0.85 m. Concrete compressive strength at 28 days was 27~38 MPa (measured in 100-mm, 7-days wet cured cubes) with 35-mm, hooked-end steel fibres (aspect ratio of 64) that were given at 40 and 60 kg/m^3 (0.5 and 0.76% in volume). Similar to the first program, control, plain RC specimens were tested as well. The conventional reinforcement ratios ranged from 0.15 to 3.3%.

During the above experimental works, no tests were conducted to measure the post-peak properties of the concrete mixes with steel fibers. Such tests of notched beams (according to EN 14651, 2007) were conducted in following studies of similar NSC mixtures and they yielded the following parameters (for 60 kg/m^3 of 35-mm fibers): f_{R1}=6.9 MPa, f_{R2}=7.4 MPa, f_{R3}=6.6 MPa, f_{R4}=5.9 MPa.

Figure 2 shows examples of load-mid-span deflection curves obtained in both programs. It is clear from Figures 2a and 2b that the moment capacities of the RFRC beams with relatively low reinforcement ratios were evidently larger than those of the control RC beams. This result presumably indicates that the required minimum reinforcement ratio for RFRC beams may be reduced (compared with the plain RC specimens). Yet, it is also evident from these figures that there is a significant decrease of flexural ductility of the specimens with fibres. This reduction occurred for all tested types and amounts of fibres. Hence, to guarantee sufficient ductility of RFRC beams their minimum reinforcement ratio should be increased.

When the reinforcement ratio increased, the flexural ductility of the RFRC beams increased as well (Figure 2c) and for a larger reinforcement ratio, the ductility of the RFRC beam was higher than that of the control RC specimen (Figure 2d). It can be seen that for ρ=0.15 and 0.28% there was a reduction of ~67% in terms of the ultimate deflection; for ρ=0.94%, the ultimate deflections were about the same and for ρ=1.26% the increase of this deflection was ~33%.

This document is the intellectual property of the fib – International Federation for Structural Concrete. All rights reserved.
This PDF of fib Bulletin 95 is intended for use and/or distribution solely within fib National Member Groups.

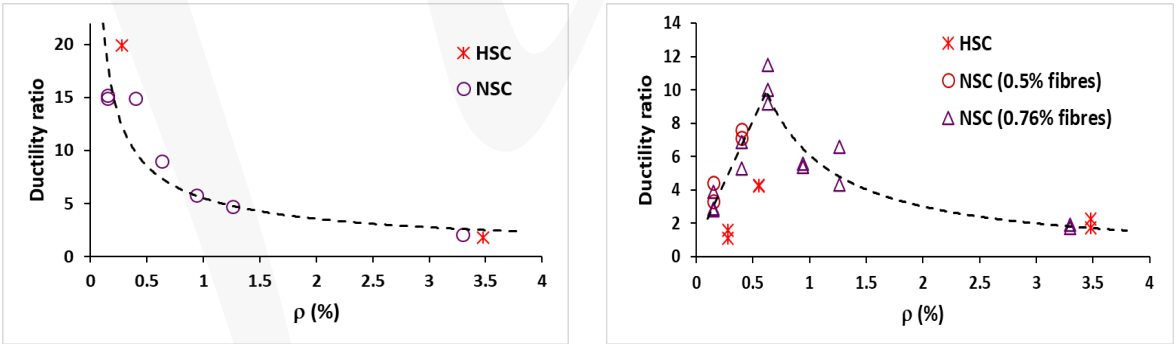


(a) HSC, ρ = 0.28%, 60 kg/m^3 fibres (b) NSC, ρ = 0.15%, 35-mm fibres

(c) NSC, ρ = 0.94%, 35-mm fibres (d) NSC, ρ = 1.26%, 35-mm fibres

Figure 2: Examples of load-deflection curves of NSC and HSC specimens, with and without fibres

The effect of the conventional reinforcement ratio on the flexural ductility for both NSC and HSC beam specimens is shown in Figure 3 (The ductility ratios in the figure were obtained as explained at the beginning of this chapter). The dashed lines in the figure are trend-lines that have been plotted according to the NSC experimental points.



(a) Plain RC specimens (b) RFRC specimens

Figure 3: Flexural ductility vs. conventional reinforcement ratio

The results in Figure 3a conform to the classical monotonic increase of ductility with decreasing ρ. This is not the case for the results obtained with the RFRC specimens (Figure 3b). The ductility monotonic increase is observed for decreasing reinforcement ratios that are larger than a certain value (~0.6% in the presented test results) while for the lower ratios the ductility decreases with decreasing ρ. Note that the value of ~0.6% is considerably larger than the minimum required by the codes. Hence for RFRC beams there exists some optimal value

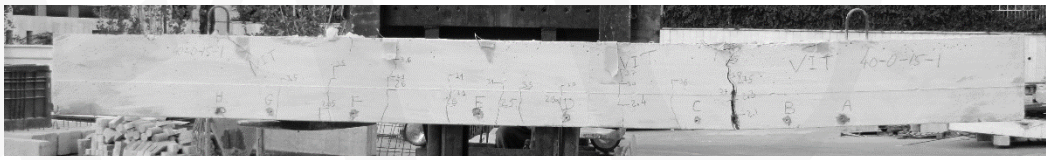
This document is the intellectual property of the fib – International Federation for Structural Concrete. All rights reserved.
This PDF of fib Bulletin 95 is intended for use and/or distribution solely within fib National Member Groups.

of reinforcement ratio for which the flexural ductility reaches its maximum value. Following the above discussion regarding ensuring sufficient ductility of RFRC beams, their minimum reinforcement ratio should be increased according to this optimal point.

3 Cracking localization

As stated above, the flexural ductility reduction is caused by cracking localization, which is characterized by significant widening of one or only few cracks, compared with the other ones. According to Dancygier and Karinski (2014) the level of cracking localization is quantified by the ratio m/n, where m is the number of significantly wide cracks and n is the total number of cracks. Here, a crack was considered significantly wide if its width was at least an order of magnitude larger than the average crack width, observed under service load (i.e., prior to rebars yielding). Smaller m/n ratios indicate higher localization levels and vice versa. This chapter deals with study of this phenomenon in flexural NSC RFRC elements ("second program" in the above chapter). The total number of cracks, n, was counted within the constant moment zone of these specimens, up to yielding of the conventional reinforcement and the number of wide cracks, m, was counted at the end of the test.

In specimens with $\rho = 0.15\%$ only a single wide crack was observed (for both 40 and 60 kg/m^3 of fibres), as shown in Figure 4a. When the reinforcement ratio increased, the number of wide cracks increased as well, where for $\rho = 3.3\%$ all cracks widened almost uniformly (which is typical of plain RC beams), Figure 4b.



(a) $\rho = 0.15\%$



(b) $\rho = 3.3\%$

Figure 4: Examples of different levels of cracking localization

Figure 5 shows m/n ratios vs. ρ for both fibres contents. The ratios plotted in the figure are averages for each specimen type, which is defined by the conventional reinforcement ratio.

The monotonic increase of cracking localization level with ρ, from $m/n \approx 0.17$ (at $\rho=0.15\%$) to 1.0 (at $\rho=3.3\%$) is evident from the figure. It is also evident that m/n is more affected by ρ at its lower range.

This document is the intellectual property of the fib – International Federation for Structural Concrete. All rights reserved.
This PDF of fib Bulletin 95 is intended for use and/or distribution solely within fib National Member Groups.

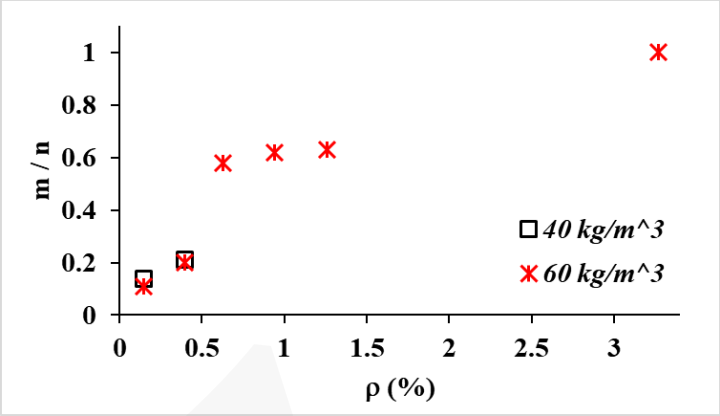


Figure 5: Levels of cracking localization vs. ρ

4 Relation between flexural ductility and cracking localization

The dependences of the ductility ratio and of cracking localization level m/n on ρ (Figures 3b and 5, respectively) are combined in Figure 6 to show the relation between these two parameters. It can be seen that qualitatively, this relation is similar to the one shown in Figure 3b and that there is a transition point at the vicinity of ρ = 0.63%. This means that up to this point (m/n ≈ 0.55) there is an influence of the cracking localization on the flexural ductility ratio, according to which, decrease of m/n (i.e., increase of cracking localization) leads to a decrease of the ductility. This effect is more pronounced for lower m/n ratios, corresponding to lower amounts of reinforcement. For m/n larger than ~0.55 cracking localization diminishes and it no longer affects the flexural ductility, which varies with reinforcement ratio as in plain RC beams.

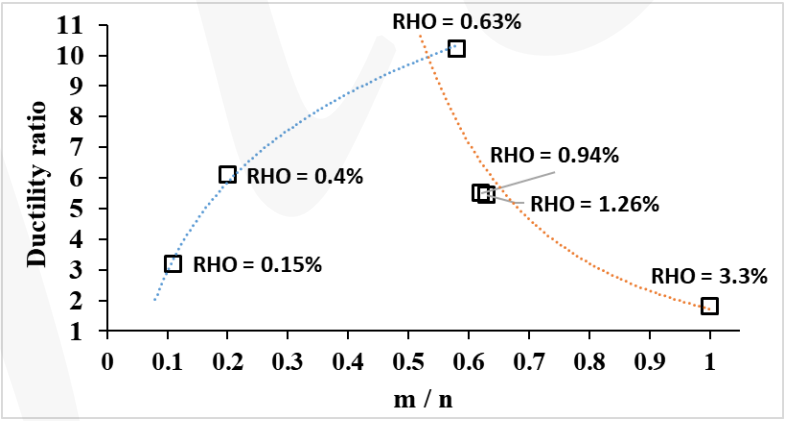


Figure 6: Relation between flexural ductility and m/n ('RHO' indicates the conventional reinforcement ratio)

This finding indicates that the minimum reinforcement ratio in RFRC beams, discussed at the end of section 2, may be obtained in terms of cracking localization level. For the given concrete strength, and fibre type and content, this level (m/n) is equal to ~0.55. For other cases this level may be obtained theoretically, based on the fibres non-uniform distribution along the beam (such model for tensile RFRC elements is presented in Dancygier and Karinski, 2014).

This document is the intellectual property of the fib – International Federation for Structural Concrete. All rights reserved.
This PDF of fib Bulletin 95 is intended for use and/or distribution solely within fib National Member Groups.

5 Concluding remarks

The paper presents test results that pertain to flexural ductility in RFRC beams and its relation with the cracking localization phenomenon. The results were obtained from two series of four-point-bending tests of NSC and HSC RFRC beams. These results show that the ductility ratios of all specimens in these experiments with low reinforcement ratios are significantly smaller than those of similar plain RC beams. When the reinforcement ratio increased, the flexural ductility of the RFRC beams increased as well and for a larger reinforcement ratio, the ductility ratios of the RFRC beams were higher than those of the control RC specimens. Hence, to guarantee sufficient ductility of RFRC beams, their minimum reinforcement ratio should be increased. In addition, processing of the experimental data shows that as the reinforcement ratio decreases below a certain value (~0.6% for NSC), which is considerably larger than the minimum required by the codes, the flexural ductility also decreases. For larger amounts of conventional reinforcement the dependence of ductility on the reinforcement ratio in RFRC and plain RC beams is similar.

The reduction of flexural ductility is caused by cracking localization, which is characterized by significant widening of one or only few cracks, compared with the other ones. This phenomenon may be quantified by the ratio between the number of the significantly wide cracks and the total number of flexural cracks. It is shown that RFRC beams with smaller reinforcement ratios had higher cracking localization. Within a range of small reinforcement ratio under ~0.6%, the dependences of ductility and cracking localization on ρ are similar, which means that there is an influence of the cracking localization on the flexural ductility ratio. For larger reinforcement ratios, the localization level diminishes and its influence on ductility no longer exists.

Following the above discussion regarding ensuring sufficient ductility of RFRC beams, their minimum reinforcement ratio should be increased according to a transition point up to which ductility decreases with ρ. This point may be obtained in terms of cracking localization level (m/n, refer to Figure 6).

6 Acknowledgements

This work is partly supported by the Israeli Ministry of Immigrant Absorption (through a joint grant from the Centre for Absorption in Science and the Committee for Planning and Budgeting of the Council for Higher Education under the framework of the KAMEA Program). The research grant is greatly appreciated.

7 References

Bentur A, Mindess S (2007). *Fibre reinforced cementitious composites, 2nd edition*. New York: Taylor & Francis.

CEN (2007). *EN 14651:2005+A1:2007. Test method for metallic fibre concrete – Measuring the flexural tensile strength (limit of proportionality (LOP), residual)*.

Dancygier AN, Savir Z (2006). *Flexural behavior of HSFRC with low reinforcement ratios*. Eng Str; 28(11): 1503-1512.

Dancygier AN, Karinski YS (2014). *Probabilistic model of the cracking localization in axially loaded fibrous reinforced concrete bars*. Eng Str; 79: 417-426.

This document is the intellectual property of the fib – International Federation for Structural Concrete. All rights reserved.
This PDF of fib Bulletin 95 is intended for use and/or distribution solely within fib National Member Groups.

Dancygier AN, Berkover E (2016). *Cracking localization and reduced ductility of fiber-reinforced concrete beams with low reinforcement ratios*. Eng Str; 111: 411-424.

Dancygier AN, Karinski YS, Navon Z (2017). *Cracking localization in tensile conventionally reinforced fibrous concrete bars*. Const Build Mat, 149: 53-6

Deluce JR, Vecchio FJ (2013). *Cracking behavior of steel fiber-reinforced concrete members containing conventional reinforcement*. ACI Struct J; 110(3): 481-490.

di Prisco M, Colombo M, Dozio D (2013). *Fibre-reinforced concrete in fib model code 2010: Principles, Models and Test Validation*. Struct Concr; 14(4): 342–361.

fib, International Federation for Structural Concrete, SAG 5 (2013). *Model Code for concrete structures 2010*. Wilhelm Ernst & Shon.

Park R (1989). *Evaluation of ductility of structures and structural assemblages from laboratory testing.* Bulletin of The New Zealand National Society for Earthquake Engineering; 22: 155-166.

Park A, Paulay T (1975). *Reinforced concrete structures.* John Wailey & Sons.

Redaelli D, Muttoni A (2007). *Tensile behaviour of reinforced ultra-high performance fiber reinforced concrete element*. Proc fib Symposium: Concrete structures: stimulators of development. Dubrovnik, Croatia.

Schumacher P, Walraven JC, den Uijl JA, Bigaj-van Vliet A (2009). *Rotation capacity of self-compacting steel fibre reinforced concrete beams*. HERON; 54: 127-161.

Vandewalle L (2000). *Cracking behaviour of concrete beams reinforced with a combination of ordinary reinforcement and steel fibers*. Mat and Struct; 33: 164-70.

Yoo DY, Yoon YS (2015). *Structural performance of ultra-high-performance concrete beams with different steel fibers*. Eng Str; 102: 409–423.

This document is the intellectual property of the fib – International Federation for Structural Concrete. All rights reserved.
This PDF of fib Bulletin 95 is intended for use and/or distribution solely within fib National Member Groups.
FRC2018: Fibre Reinforced Concrete: from Design to Structural Applications
Joint ACI-*fib*-RILEM International Workshop

Residual crack width in RC and R/FRC ties subjected to repeated loads

Alessandro P. Fantilli[1], Francesco Tondolo[1]

[1] : Politecnico di Torino, DISEG – Department of Structural, Building and Geotechnical Engineering.

Abstract

Durability of reinforced concrete (RC) structure is mostly related to the ability of concrete cover to protect the embedded rebar from corrosion initiation and propagation. As cracks due to loads or rheological phenomena are almost inevitable, the geometry of crack pattern in service is a key parameter that needs to be evaluated in plain and fiber-reinforced R/FRC members. In fact, not only the direct ingress of aggressive agents, such as oxygen and water, is a function of crack width, but also concrete carbonation and the chloride ion ingress are accelerated by the presence of wide cracks. Furthermore, the use of fiber reinforced concrete requires detailed investigations, in order to define the relationship between durability and crack width even in presence of cyclic loads. Accordingly, in this research project, crack width is measured by using traditional mechanical strain gauges and a new device based on the optical conoscopic holography. The latter allows the non-contact measure of crack profile, at the end of each loading cycle, both in plain and fiber-reinforced ties subjected to sets of repeated loads. As a result, contrarily to crack width at the peak of load, the width of residual cracks is not always reduced by the presence of fiber, and this could affect the durability of RC and R/FRC structures.

Keywords

Durability, non-contact measure, reinforcement percentage, cyclic loading.

This document is the intellectual property of the fib – International Federation for Structural Concrete. All rights reserved.
This PDF of fib Bulletin 95 is intended for use and/or distribution solely within fib National Member Groups.

1 Introduction

In reinforced concrete (RC) structures the limitation of crack width is generally required to guarantee the durability of construction. Crack is a direct connection between the inner part of the RC element and the atmosphere, and allows the aggressive agents to reach the reinforcement. In other words, wide cracks can be responsible of the corrosion of steel rebar.

Cracking is unavoidable for RC elements both during service and at ultimate limit state. Nevertheless, corrosion takes place when the protective layer of oxide becomes unstable. The forming oxides could seal the cracks around the steel bar, especially in the case of narrow cracks, even if the sealing effect depends on the evolution of crack pattern during the service life. For instance, due to the presence of repeated actions, crack width can increase with the number of cycles (Giordano at al. 2011). In this case, the effects of corrosion have to be added to the residual slip between steel and concrete at the end of each loading cycle (Bresler and Bertero 1968). As these residual crack widths can impair the durability of concrete structures, in the present paper the effect of cyclic actions on the cracking phenomenon of RC ties is investigated.

Under monotonic loads, the presence of fibers, randomly distributed within the cement matrix, gives a valuable contribution to the reduction of crack width and crack depth (Chiaia et al. 2009). Nevertheless, in the current literature, the crack patter generated in fiber-reinforced concrete (FRC) members subjected to repeated tensile loads is scarcely investigated. Accordingly, by using a laser scanner technology, in addition with a traditional mechanical strain gauge measurement, residual crack widths are herein measured both in RC and R/FRC ties. The specimens are similar to those used by Bresler and Bertero (1968) to analyze the residual stresses both in concrete and rebar at the end of three sets of cyclic loads. In what follows, the preliminary results of a wider experimental campaign, also including the natural corrosion stage of the samples, is presented.

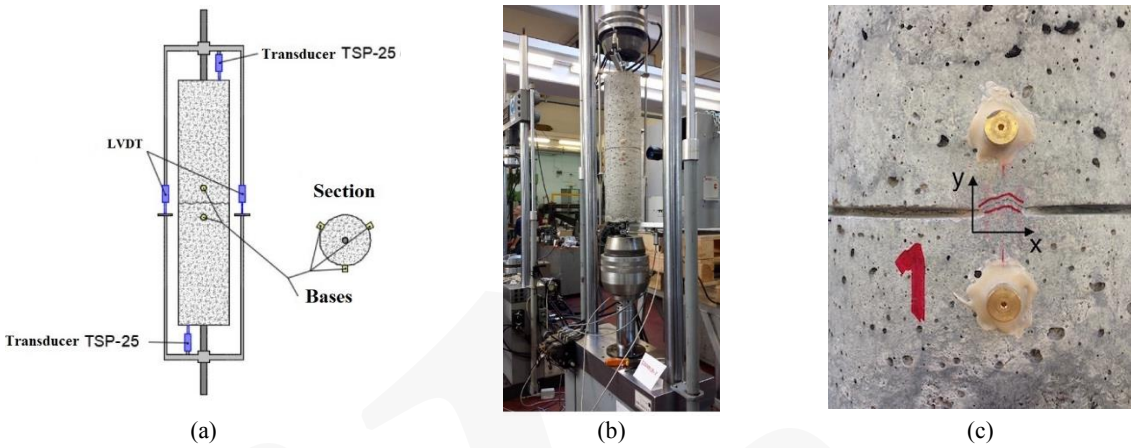
2 Experimental program

The specimens consist of RC and R/FRC ties with circular cross section shown in Fig.1, where a scheme of the test setup is illustrated. On each specimen, three couples of supports for the mechanical extensometer (positioned at 120 degrees around the specimens in Fig.1a) were installed. Two potentiometer transducers were positioned on the ends of the specimens to measure the relative slip between the reinforcing bar and the concrete, whereas two LVDTs were used to obtain the whole elongation of the reinforcing bar (see Fig.1a).

The whole experimental campaign included 20 RC and 20 R/FRC specimens grouped in the 8 series reported in Table 1, which differ only by the presence of fibers and of geometrical properties.

FRC specimens contain 0.5% in volume of steel fibers with hooked ends, which have a length of 30 mm and an aspect ratio equal to 45. As shown in Table 1, a single set of RC and R/FRC samples are composed by specimens with:

This document is the intellectual property of the fib – International Federation for Structural Concrete. All rights reserved.
This PDF of fib Bulletin 95 is intended for use and/or distribution solely within fib National Member Groups.



(a) (b) (c)

Figure 1: The specimens investigated in this research project: (a) the arrangement of the instrumentation, (b) picture of a specimen during the test, (c) the couple of supports # 1 used to measure the crack width through a mechanical strain gauge and laser acquisition area.

Table 1: The specimens tested in uniaxial tension

Series	Number of specimens	Bar diameter	Concrete diameter	$\rho=A_s/A_c$	Specimen length	Fiber volume
		[mm]	[mm]	[%]	[mm]	[%]
D10-LP	5	10	87	1.34	420	-
D10-HP	5	10	60.4	2.82	250	-
D20-LP	5	20	174	1.34	680	-
D20-HP	5	20	121	2.81	400	-
D10-LF	5	10	87	1.34	420	0.5
D10-HF	5	10	60.4	2.82	250	0.5
D20-LF	5	20	174	1.34	680	0.5
D20-HF	5	20	121	2.81	400	0.5

- two types of rebar, whose diameters are 10 and 20 mm and yielding strength is equal to f_y=510 MPa;

- four different diameters of the concrete cross-section (i.e., 60.4, 87, 121, and 174 mm for low and high percentage of reinforcement). By combining the two rebar with the four concrete cross-sections, the RC and R/FRC specimens show high reinforcement ratio ρ = 2.81% (named H in Table 1) and low reinforcement ratio ρ = 1.34% (named L in Table 1). All the specimens were cast vertically;

- four lengths of the ties (i.e., 250, 400, 420, and 680 mm) in order to obtain a single crack in the middle of the element. The length were defined in accordance with tension-stiffening model used by Fantilli and Chiaia 2013.

This document is the intellectual property of the fib – International Federation for Structural Concrete. All rights reserved.
This PDF of fib Bulletin 95 is intended for use and/or distribution solely within fib National Member Groups.

In Table 1, a single specimen has the label DXX-LP-Z, in which XX indicates the diameter of the rebar, L or H stand for low or high reinforcement ratio, P is used for plain concrete, and F for fiber reinforced concrete. Finally, Z is the number of the specimen tested for each series.

Before the tensile test, a notch was created in the middle of the tie, in order to trigger the crack and monitor the crack opening in the three un-notched parts of the same cross-section (one of them is shown in Fig. 1c). In this way, it is possible to compare the values of the residual crack width measured by both mechanical strain gauges and a laser scanner.

A universal testing machine with a maximum loading capacity of 100 kN was used to tests the samples D10, whereas for the specimens D20 the loading capacity was 250 kN. In all the cases, the driving parameter of the uniaxial tensile test was the maximum stress of the reinforcing bar, which remained lower than the nominal yielding strength (i.e., 510 MPa). In this way, the conditions in service were reproduced along with the three sets of the cycles reported in Table 2. Before applying the cyclic load of the three sets, cracks were completely created in each specimen by applying a static tensile load. As the specimen was completely unloaded at the end of each cycle, a mechanical strain gauge measured the width of the crack in the three un-notched parts shown in Fig.1c, then a ConoProbe laser machine was used to scan the same zones (Critelli et al. 2016).

Table 2: Sets of cycles for the mechanical test setup

Set of cycles	**Number of cycles**	**Maximum steel stress**	**Minimum steel stress**
[-]	[-]	[MPa]	[MPa]
1	10	300	0
2	30	350	0
3	20	420	0

3 Results of the tests

Uniaxial compression tests, performed on cylinder (height = 300 mm and diameter =150 mm), revealed an average compressive strength of 28.5 MPa for plain concrete, and 41.5 MPa for FRC. In addition, the average tensile strengths, measured through Brazilian tests, were 3.45 MPa and 4.70 MPa for plain and FRC, respectively. For each series (see Table 1), 5 specimens were tested, and the average value of crack width was calculated. When more than one crack appeared on the external surface of the specimens (see Table 3), the value of crack width, referred to the notched cross-section, was calculated using the average on the specimens revealing 1 crack for specimens with 20 mm rebar diameter and 3 cracks for specimens with 10 mm rebar diameter.

Table 3: Cracks in the tested specimens

Series	**Number of specimens with 1 crack**	**Number of specimens with 2 cracks**	**Number of specimens with 3 cracks**
D10-LP	0	1	4
D10-HP	0	0	3
D20-LP	5	0	0
D20-HP	5	0	0

This document is the intellectual property of the fib – International Federation for Structural Concrete. All rights reserved.
This PDF of fib Bulletin 95 is intended for use and/or distribution solely within fib National Member Groups.

D10-LF	0	3	2
D10-HF	0	0	3
D20-LF	5	0	0
D20-HF	5	0	0

Figure 2 shows the evolution of crack depth in one of the scanned zones of the specimen D20-LPC-4, measured with the ConoProbe device. The same area (of 2×2 mm and aligned to the basis of the mechanical strain gauge) around the crack is scanned just after the formation of the crack (Fig.2a), and at the end of three sets of cycles (Fig.2b-d). The same procedure was also applied on the other two un-notched parts of the specimen. In this way, it is possible to have three measurements of the same crack, on which the missing alignment of reinforcing bar and concrete can produce a bending moment. Therefore, the residual crack width of a single specimen was considered as the average value of these measurements.

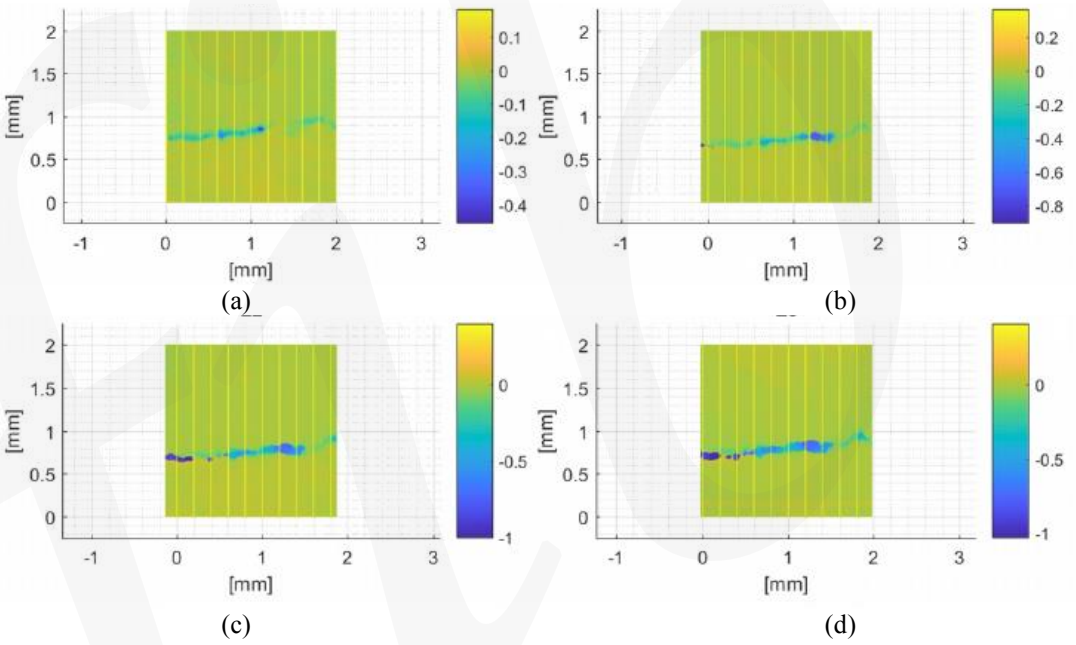


Figure 2: Color mapping of crack depth in the specimen D20-LPC-4 at the unloading subsequent to: (a) the formation of the crack; (b) the first cycle; (c) the second cycle; (d) the third cycle.

It is important to state that the laser measurements were possible only at the end of unloading stage, as the vibration of the testing machine during loading can alter the quality of the mapping. Therefore, crack widths at the peak of loads were only measured through mechanical strain gauges.

For each series (see Table 1), 5 specimens were tested, and the average value of crack width was calculated. When more than one crack appeared on the external surface of the specimens (e.g., D10-LP and D10-LF series), the value of crack width, referred to the notched cross-section, was calculated using the average on the specimens revealing 1 crack for specimens with 20 mm rebar diameter and 3 cracks for specimens with 10 mm rebar diameter.

This document is the intellectual property of the fib – International Federation for Structural Concrete. All rights reserved.
This PDF of fib Bulletin 95 is intended for use and/or distribution solely within fib National Member Groups.

The results of the tests in terms of crack width *vs.* number of cumulative cycles are illustrated in Fig.3. In particular, in each diagram the crack width of two similar series (with and without fibers) are compared both at the peak of load and at the end of each cycle. As the stabilized crack pattern is not reached at same level of the steel stress, the initial crack width is different in all the four couples of series reported in Fig.3.

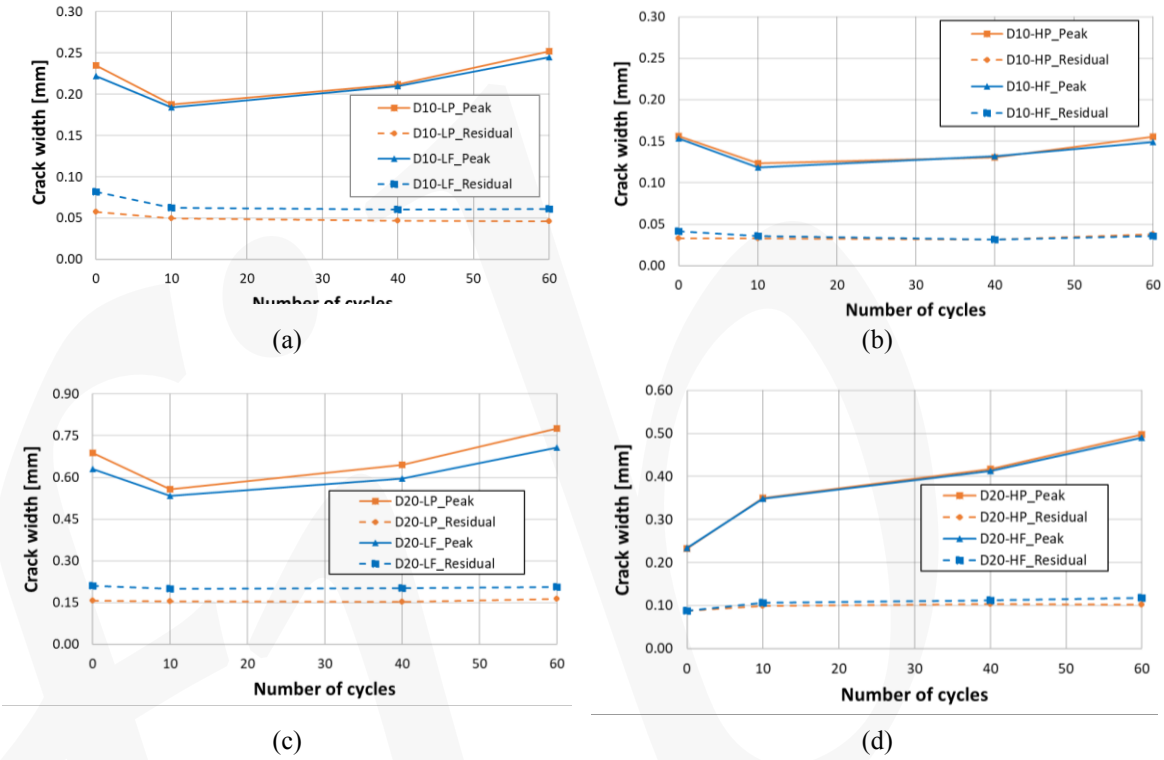


Figure 3: Average values of crack width (peak – continuous lines, and residual – dashed lines) for the same type of specimens (RC – orange lines, and R/FRC – blue lines): (a) D10-LP and D10-LF, (b) D10-HP and D10-HF, (c) D20-LP and D20-LF, (d) D20-HP and D20-HF.

In the case of low reinforcement ratio (Fig.3a and Fig.3c), at the peak of load, crack width in RC specimens (continuous orange lines) are always larger than that of FRC specimens (continuous blue lines). Whereas, there is not a great difference between plain concrete and fiber-reinforced ties when the reinforcement ratio is higher (Fig.3b and Fig.3d). Accordingly, the fiber capability of bridging the crack surfaces is more evident when the resultant of bond stresses at the interface between rebar and concrete is low, as happens herein in the specimens with ρ =1.34. As the load increases with the number of cycles, crack width increases as well, also denoting a progressive reduction of the bond between steel and concrete during the cycles. In addition, larger crack widths were also measured in the larger specimens, according to the size-effect phenomena evidenced by Fantilli and Chiaia (2015) and by Tiberti et al. (2015).

Moreover, residual cracks show different widths depending on the presence of fibers, especially in the case of low reinforcement ratio (Fig.4a and Fig.4c). Nevertheless, residual

This document is the intellectual property of the fib – International Federation for Structural Concrete. All rights reserved.
This PDF of fib Bulletin 95 is intended for use and/or distribution solely within fib National Member Groups.

crack width in R/FRC samples (dashed blue lines) is generally larger than that of the corresponding RC ties crack width in RC specimens (dashed orange lines). In particular for specimens type D10L the differences at end of the four loading stages (cracking, end of each set of cycles) reported in the Figure 4 are: 42%, 26%,29% and 32% respectively, for type D10H the differences are: 26%, 8%, 0% and 6% respectively; for type D20L the differences are: 34%, 29%, 32% and 25% respectively; for type D20H the differences are: 1%, 7%, 9% and 15% respectively. This result can be ascribed to the well-known mismatch of the crack surfaces that occurs at unloading (Hordijk 1991), which seems furtherly amplified by the presence of fibers that crosses the crack with an arbitrary angle. In all the cases, residual crack widths are more or less constant regardless of the number of cycles, and, similarly to the crack width at peak, they are wider at larger scale.

The values of residual crack width taken with the Conoprobe laser are also reported in Fig.4, where a comparison with those measured through a mechanical strain gauge is made. The latter generally provides narrower crack with respect to that detected by the laser scanner. Indeed, the laser perform a direct measure of the crack width (see the measurement procedure reported in Critelli et al., 2017), which is unaffected by the state of strain of the compressed concrete surrounding the crack at unloading (Bresler and Bertero 1968). This is particularly true for the ties with high reinforcement ratio, even if for larger scale (Fig.4d) the difference between the two types of measurements reduces with respect to the lower scale (Fig.4b).

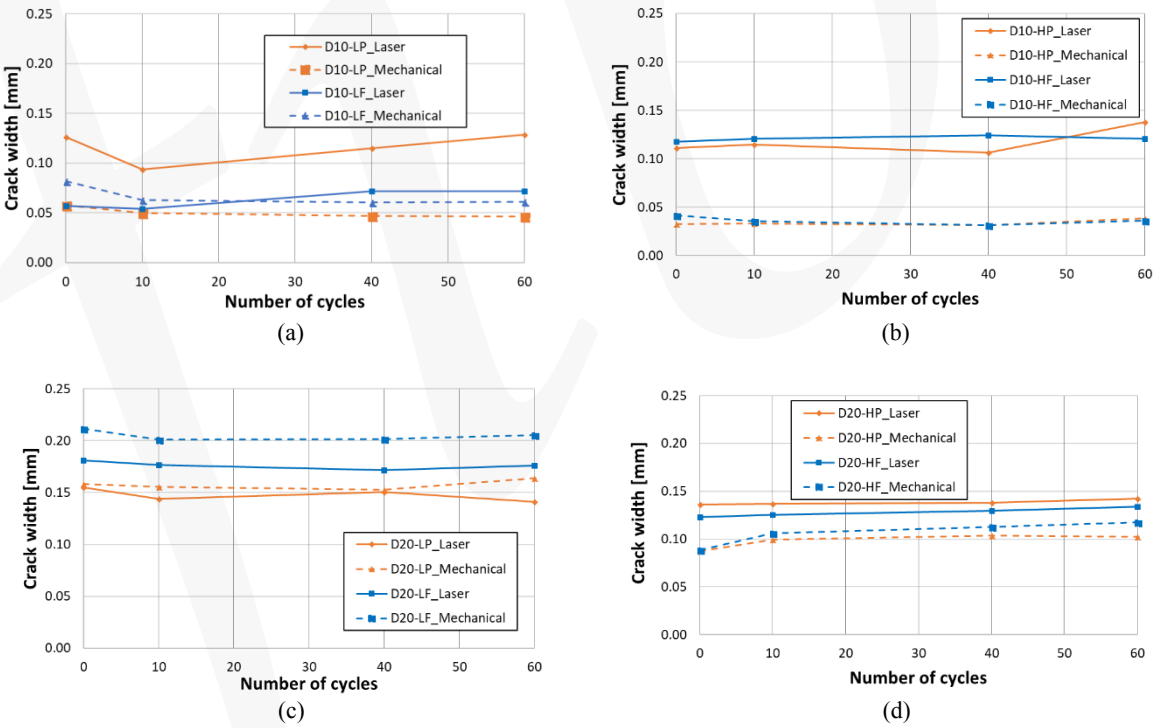


Figure 4: Average values of residual crack width measured with Conoprobe laser (continuous lines) and mechanical strain gauges (dashed lines) for the same type of specimens (RC – orange lines, and R/FRC – blue lines): (a) D10-LP and D10-LF, (b) D10-HP and D10-HF, (c) D20-LP and D20-LF, (d) D20-HP and D20-HF.

On the contrary, in the case of low reinforcement ratio (Fig.4a and Fig.4c), the crack width measured with the laser Conoprobe is more or less similar to that taken with the strain gauge.

This document is the intellectual property of the fib – International Federation for Structural Concrete. All rights reserved.
This PDF of fib Bulletin 95 is intended for use and/or distribution solely within fib National Member Groups.

In other words, if the durability of reinforced concrete structures is the aim of the structural analysis, the measure of crack width performed with the use of mechanical strain gauges could not be always conservative.

4 Conclusions

According to the results of the experimental analysis previously described, the following conclusion can be drawn:

- in reinforced concrete ties subjected to repeated loads, the presence of fibers reduces crack width at the peak of loads, especially in the case of low reinforcement ratio;
- conversely, at complete unloading, residual cracks tend to be larger in the ties made with fiber-reinforced concrete;
- the use of Conoprobe laser provides larger values of crack widths than the traditional measurements performed with mechanical strain gauges, especially in the case of high reinforcement ratio.

As large residual crack width can induce steel corrosion, future works will be devoted to study the durability of the cracked ties. More precisely, other tests will be performed, after a period of accelerated corrosion, on all the RC and R/FRC specimens investigated herein.

5 Acknowledgements

This work was supported by the Italian Ministry of Education (PRIN 2015). The Authors would like to thank Nicola Critelli and Simone Scuteri for their valuable work.

6 References

Bresler, B., Bertero, V., *Behavior of Reinforced Concrete Under Repeated Load*. Journal of the Structural Division, 94(6), 1567-1592, 1968.

Chiaia, B., Fantilli, A.P., Vallini P. *Evaluation of crack width in FRC structures and application to tunnel linings*. Materials and Structures, 42 (3), 339–351, 2009

Critelli, N., Cesetti, A., Fantilli, A.P., Tondolo, F., *Measuring crack width in RC and R/FRC ties through laser scanner*. In Ninth International Structural Engineering and Construction Conference - Resilient Structures and Sustainable Construction. Valencia (Spain), 2017.

Fantilli, A.P., Chiaia, B., *The golden ratio in the crack pattern of reinforced concrete structures*. ASCE Journal of Engineering Mechanics, vol. 139(9), 1178–1184, 2013

Giordano, L., Mancini, G., Tondolo, F., *Reinforced concrete members subjected to cyclic loading and corrosion*. Journal of Advanced Concrete Technology, 9(3), 277-285, 2011.

Hordijk, D.A., *Local approach to fatigue of concrete*. Dissertation, Delft University of Technology, 1991.

Tiberti, G., Minelli, F., Plizzari, G., *Cracking behavior in reinforced concrete members with steel fibers: A comprehensive experimental study*. Cement and Concrete Research, 68(2), 24-34, 2015.

This document is the intellectual property of the fib – International Federation for Structural Concrete. All rights reserved.
This PDF of fib Bulletin 95 is intended for use and/or distribution solely within fib National Member Groups.

An experimental investigation on the post-cracking behaviour of Recycled Steel Fibre Reinforced Concrete

Cristina Frazão[1], Joaquim Barros[1], J. Alexandre Bogas[2], Kypros Pilakoutas[3], Christoph de Sousa[1]

[1] : ISISE, University of Minho, Guimarães, Portugal.

[2] : CERIS-ICIST, Instituto Superior Técnico, Technical University of Lisbon, Portugal.

[3] : The University of Sheffield, United Kingdom.

Abstract

Steel fibres resulting from the industry of tyre recycling can be efficiently employed for the reinforcement of concrete structures. Recycled Steel Fibre Reinforced Concrete (RSFRC) is a promising candidate with technical, environmental and economic benefits for the development of ductile, high strength and durable structural elements.

The heterogeneity of the geometry of each Recycled Steel Fibre (RSF) due to the recycling process of the tires, can provide a plurality of strengthening mechanisms to concrete that promote efficiency and durability, as long as the RSFRC composition is carefully adjusted to the presence of RSF.

For assessing the potentialities of recycled steel fibres (RSF) as concrete reinforcement, an experimental program was performed in the present study by comparing the following properties of concrete reinforced with industrial steel fibres (ISF) and with RSF: compressive strength, modulus of elasticity, flexural strength, flexural toughness and indirect tensile strength.

The obtained results suggest that RSF reinforcement can significantly reduce the brittle behaviour of concrete by improving its toughness and post-cracking resistance. For the adopted industrial and recycled fibres, the last ones have not presented inferior post-cracking strengthening performance than the first ones.

Keywords

Recycled steel fibres, industrial steel fibres, RSFRC, ISFRC, post-cracking behaviour.

This document is the intellectual property of the fib – International Federation for Structural Concrete. All rights reserved.
This PDF of fib Bulletin 95 is intended for use and/or distribution solely within fib National Member Groups.

1 Introduction

In a world that is becoming increasingly sensitive to the need of protecting the environment, the ability to build concrete structures using sustainable resources is an exciting and attractive proposition with environmental and economic benefits.

Nowadays, pneumatic tyres are among the most widespread industrial products and, giving the best use to tyres that have reached their end-of-life is still a societal challenge. In recent years, several efforts have been done for using different by-products obtained from the recycling of waste tyres, such is the case of deriving constituents for the concrete industry (Pilakoutas *et al.* 2004, Micelli *et al.* 2014, Zamanzadeh *et al.* 2015, Martinelli *et al*. 2015).

Steel Fibre Reinforced Concrete (SFRC) is increasingly adopted to produce in-situ and prefabricated concrete structures, as partial or total replacement of conventional reinforcement, reducing their construction time and labor costs necessary for the placement of the conventional rebars in reinforced concrete structural elements. SFRC can also be an auxiliary reinforcement for shrinkage reduction and crack control that contribute for the enhancement of the durability of concrete structures.

Cracking is a common pathology in the concrete structures that can cause a significant (or complete) loss of their effectiveness. In this case, discrete fibres are considered ideal candidates for the reinforcement of concrete elements, since the random nature of their distribution provides an almost isotropic reinforcement. The crack opening restraint provided by the reinforcement mechanisms of steel fibres bridging the cracks leads to a significant increase of post-cracking load bearing capacity and energy absorption performance, since the stress redistribution provided by fibre reinforcement allows an ultimate load much higher than the cracking load (Salehian *et al.* 2014).

Steel fibres resulting from the industry of tyre recycling have high potential as an effective reinforcement of concrete, especially in terms of improving its post-cracking tensile behaviour, and increase its flexural, shear and impact strength (Pilakoutas *et al.* 2004, Micelli *et al.* 2014, Zamanzadeh *et al.* 2015, Martinelli *et al*. 2015). The heterogeneity of this fibre system (with regard to the geometry, composition and microstructure of each fibre) provides a plurality of strengthening mechanisms that can be an advantage, as long as these mechanisms are effectively activated, which requires scientific methodologies on the production of Recycled Steel Fibre Reinforced Concrete (RSFRC) and its application.

In this context, this study reports the results of an experimental research carried out at the University of Minho (Portugal) that aims to investigate the post-cracking behaviour of RSFRC and perform its comparison to the one registered in Industrial Steel Fibre Reinforced Concrete (ISFRC), by performing 3-point notched beam bending tests, round panel tests and double edge wedge splitting tests (DEWST). The methodologies adopted and the experimental results are presented and discussed.

2 Experimental program

2.1 Recycled Steel Fibres

The recycled steel fibres (RSF) used in this research were recovered by a shredding process of post-consumed truck tires, being the steel separated from the rubber by an

This document is the intellectual property of the fib – International Federation for Structural Concrete. All rights reserved.
This PDF of fib Bulletin 95 is intended for use and/or distribution solely within fib National Member Groups.

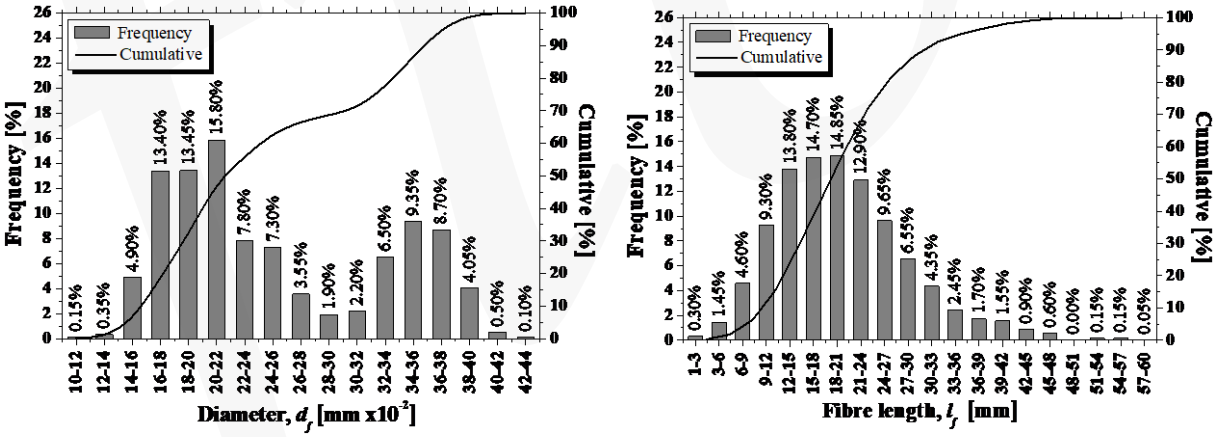
electromagnetic separator. These RSF have irregular geometry with various lengths and diameters (Fig. 1a). For comparison purposes, hooked ends steel fibres of l_f =33 mm, d_f =0.55 mm, l_f / d_f =60, and yield stress of 1230 MPa were also used (Fig. 1b).



(a) (b)

Figure 1: General view of multi fibres and the geometry of a single fibre: Recycled Steel Fibres (a); Industrial Steel Fibres (b)

A detailed characterization of the RSF employed in this experimental work was performed on a sample of 2000 fibres in order to evaluate by a statistical analysis, the variability of the geometric properties after the shredding process of tires recycling. Figures 2a and 2b report respectively, the frequency distribution of the measured fibre diameter , d_f (using a micrometer) and fibre length, l_f (distance between the outer ends of the fibre).



(a) (b)

Figure 2: Frequency distribution of: Fibre diameter measurements (a); Fibre length measurements (b)

According to Fig. 2a, the diameters of RSF are characterized by a multimodal (two) distribution, in agreement with the literature (Martinelli *et al*. 2015). Figure 2b highlight unimodal distribution of fibre length, which can be attributed to the shredding and cutting procedures performed within the recycling plant (Martinelli *et al*. 2015).

Table 1 presents some relevant statistical data obtained from Fig. 2a and 2b, including the minimum (Min), the maximum (Max), the average, the median, the modal value and range, the standard deviation (StD) and the coefficient of variation (CoV).

This document is the intellectual property of the fib – International Federation for Structural Concrete. All rights reserved.
This PDF of fib Bulletin 95 is intended for use and/or distribution solely within fib National Member Groups.

Table 1: Geometric characterization of used RSF

Parameters	Min	Max	Average	Median	Mode (value)	Mode (range)	StD	CoV (%)
Diameter, d_f (mm)	0.11	0.43	0.25	0.22	0.20	0.20-0.22	0.08	30.2
Length, l_f (mm)	1	60	20	19	21	18-21	8	41.6
Aspect ratio, λ	28	347	110	104	130	80-90	44	39.9

Comparing the obtained results with those already reported in the literature for the geometric properties of other RSF, the obtained average values of d_f, l_f and λ were quite similar to those reported by other authors who used the same procedure for its measurement (Aiello *et al*. 2009, Centonze *et al*. 2012, Martinelli *et al*. 2015). However, other authors observed lower average values of l_f and λ for RSF.

2.2 Mix composition

RSFRC and ISFRC of equal composition (Table 2) were produced with 1% of fibres (by volume of concrete, V_f), CEM I 42.5 R Portland cement (C), fly ash (FA), fine river sand (FS) (maximum aggregate size of 1.19 mm and fineness modulus of 1.91), coarse river sand (CS) (maximum aggregate size of 4.76 mm and fineness modulus of 3.84) and crushed granite (CA) (maximum aggregate size of 19.10 mm and fineness modulus of 6.64), water (W) and a polycarboxylate based superplasticizer (SP) with the commercial designation MasterGlenium SKY 617. The mix design was based on the packing density optimization method suggested in Barros *et al.* (2007). For comparison purposes, specimens of plain concrete (PC) were also produced before the addition of V_f=1% of RSF.

Table 2: Composition for 1 m^3 of concrete (C_f=content of fibres in kg/m^3)

Concrete	C(kg)	FA(kg)	LF(kg)	FS(kg)	CS(kg)	CA(kg)	W(L)	SP(L)	C_f (kg)	W/C
RSFRC1% **ISFRC1%**	400	200	-	147	735	597	173	7.2	75.8 78.6	0.31

The workability of fresh plain concrete, RSFRC1% and ISFRC1% was determined by the Abrams slump-flow test according to the recommendation of EN 12350-8 (2010). The average slump was 250 mm for plain concrete, 100 mm for RSFRC1% and 130 mm for ISFRC1%, which is within the consistency Class S5 for plain concrete and Class S3 for RSFRC and ISFRC, according to the EN 206-1 (2007). As expected, adding fibres to fresh concrete results in a loss of workability, but the alterations on the mix composition for the production of RSFRC1%, according to the adopted method, have assured the same consistency class of ISFRC1%.

The compressive strength of these concretes were determined at 28 days in cylinders of 150 mm diameter and 300 mm height according to the EN 12390-3 (2009) and EN 12390-13 (2012), respectively. The average values of compressive strength (f_{cm}) and Young's modulus (E_{cm}) are presented in Table 3.

This document is the intellectual property of the fib – International Federation for Structural Concrete. All rights reserved.
This PDF of fib Bulletin 95 is intended for use and/or distribution solely within fib National Member Groups.

Table 3: Relevant results of compressive tests

	PC	RSFRC	ISFRC
E_{cm} (GPa) (CoV%)	25.76 (*3.49*)	24.31 (*10.04*)	26.80 (*3.11*)
f_{cm} (MPa) (CoV%)	43.45 (*4.12*)	39.42 (*3.72*)	48.87 (*2.43*)

A slight decrease of compressive strength and modulus of elasticity was observed in RSFRC comparing with the control mix (PC). This may have been caused by the relatively high number of fibres and their heterogeneous geometry in the RSFRC that increase the volume of the interfacial transition zone (ITZ) between fibre and matrix, and may also have increased the void percentage in the matrix. In addition, RSFRC was produced with significantly lower slump, which affects the homogeneity and air content of concrete. However, in the case of ISFRC of similar slump, the opposite occurred, and a slight increase of the compressive strength and the modulus of elasticity was observed.

2.3 Post-cracking behaviour of RSFRC

The post-cracking behaviour of RSFRC1% and ISFRC1% was analysed using different test methods, namely, 3-point bending tests, round panel tests and splitting tensile tests.

2.3.1 Three-point notched beam bending tests (3PNBBT)

The flexural behaviour of PC, RSFRC1% and ISFRC1% was characterized by executing three point notched beam bending tests (3PNBBT) according to the CEB-FIP Model Code recommendations (2013) in terms of curing procedures, position and dimensions of the notch sawn into the specimen, load and specimen support conditions, main characteristics of the equipment and measuring devices, and test procedure (Fig. 3). The notched beam bending test favors a stable propagation of the crack, initiated at the notch located at the mid-span of the beam, that may not be the weakest cross section. In these circumstances, the post-cracking flexural tensile capacity can be overestimated.



Figure 3: Test setup of the bending test

Figure 4 represents the average force-deflection (*F-u*) and force-CMOD responses registered in the PC (3 beams), RSFRC (2 beams) and ISFRC (5 beams) at 28 days.

This document is the intellectual property of the fib – International Federation for Structural Concrete. All rights reserved.
This PDF of fib Bulletin 95 is intended for use and/or distribution solely within fib National Member Groups.

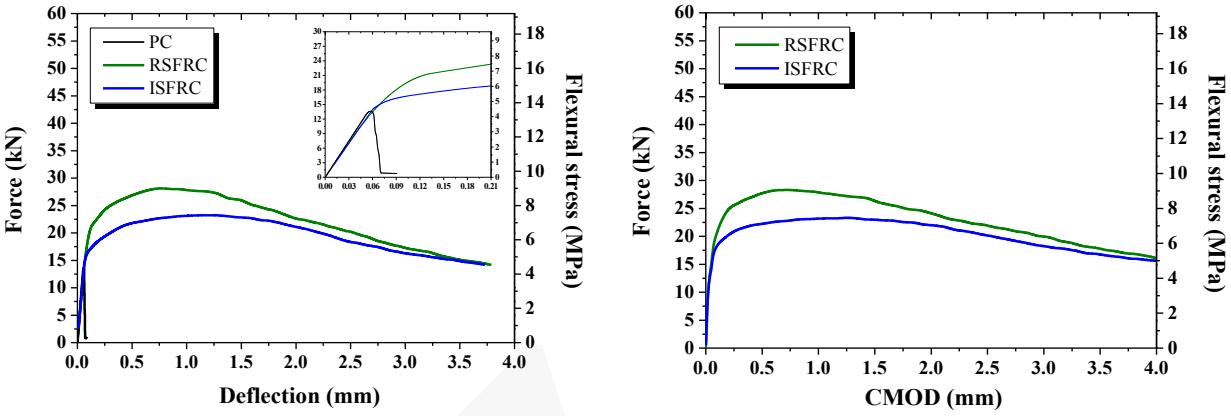


Figure 4: Average force/flexural stress versus deflection (a) and Average force/flexural stress versus crack width (b) for specimens of PC, RSFRC and ISFRC

The average values and corresponding CoV of the flexural tensile strength, $f_{ctm,fl}$, and the energy absorbed up to a deflection of 3.5 mm, G_{fm}, which represents the area under the *F-u* curves (Fig. 4a) up to this deflection, were 4.43 MPa (6.27%) and 0.07 N/mm (0.77%) for PC, 9.11 MPa (8.87%) and 4.25 N/mm (11.67%) for RSFRC1% and 7.66 MPa (8.17%) and 3.13 N/mm (10.87%) for ISFRC1%. Up to a deflection of about 3.5 mm, the RSFRC1% has presented higher flexural capacity and energy absorption performance than ISFRC, contrary to what has been reported in the literature (Zamanzadeh *et al*. 2015). The highest difference has occurred for crack width levels corresponding to serviceability limit state (SLS) conditions. The reinforcement performance of both FRCs has become closer with the increase of the crack width, which indicates that they will have similar performance for ultimate limit state (ULS) conditions. From the obtained force-CMOD relationship (Fig. 4b), the residual flexural tensile strength parameters ($f_{R,1}$, $f_{R,2}$, $f_{R,3}$ and $f_{R,4}$) were calculated according to CEB-FIP Model Code recommendations (2013). The obtained results are presented in Table 4 and confirmed the higher effectiveness of RSF comparing with ISF in terms of bending behaviour.

Table 4: Relevant results of flexural tests

		$f_{R,1}$ **(MPa)**	$f_{R,2}$ **(MPa)**	$f_{R,3}$ **(MPa)**	$f_{R,4}$ **(MPa)**
RSFRC1%	AVG	8.87	8.41	7.02	5.72
	CoV (%)	*6.78*	*11.87*	*13.74*	*14.27*
ISFRC1%	AVG	7.12	7.39	6.58	5.42
	CoV (%)	*6.51*	*10.36*	*13.99*	*13.86*

2.3.2 Round Panel tests

To characterize the flexural toughness of RSFRC1% and ISFRC1%, round panel tests with three-point supports (RPT-3ps) were carried out according to the recommendations of ASTM C1550 (2005). In order to facilitate handling and placing the specimens, the RPT-3ps were conducted on smaller round panels with 600 mm diameter and 60 mm thickness, simply supported on three pivots with the symmetrical arrangement at 120 degrees, and subjected to a central load (Fig. 5). According to Minelli and Plizzari (2010), such a

This document is the intellectual property of the fib – International Federation for Structural Concrete. All rights reserved.
This PDF of fib Bulletin 95 is intended for use and/or distribution solely within fib National Member Groups.

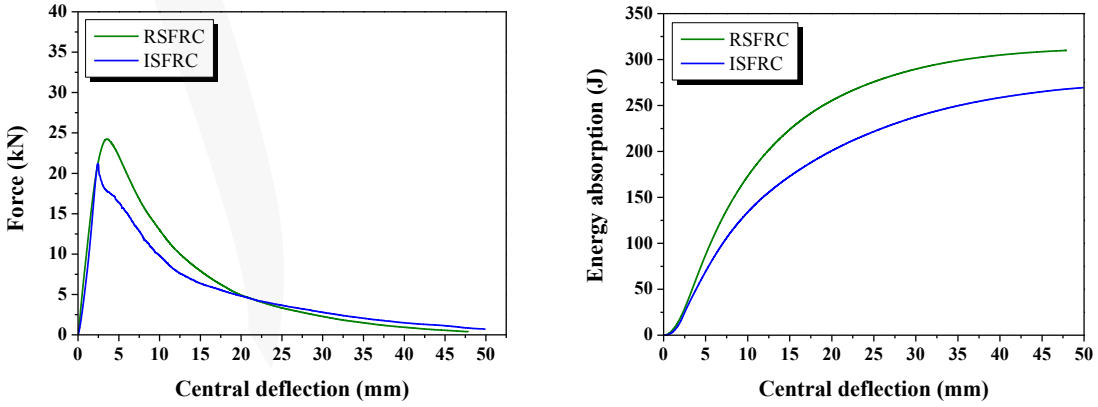
reduction of the panel's diameter and thickness does not affect the scatter and repeatability of the test results when compared to the standard specimens of ASTM C1550 (2005). The RPT-3ps tests were performed in displacement control by imposing a deflection rate of 4 mm/min at the center of the panel up to a central displacement of at least 45.0 mm. This test is appropriate to evaluate the fibre reinforcement efficiency for slab and shell type FRC structures, since the formation of cracks with different orientation that occurred in the round panels mobilizes more representatively the fibre reinforcement mechanisms that really occur in this type of structures (Salehian *et al.* 2014).



(a) (b)

Figure 5: Round panel test: Test setup (a); One of the three pivots of the supporting system for RPT (b)

The average force-central deflection and energy absorption-central deflection relationships of 3 round panels of RSFRC1% and ISFRC1% are depicted in Figure 6. The average values and corresponding CoV of the energy absorbed up to the central deflection of 40 mm, W_{fm}, which represents the area under the *F-u* curves (Fig. 6a) up to this deflection, were 307.4 J (11.16%) for RSFRC1% and 258.5 J (11.36%) for ISFRC1%. The crack failure pattern of each round panel was formed by three cracks at angles of about 120º, with the panel breaking into 3 pie-shaped wedges at large deflections, which caused low variability of the results (Bernand and Xu 2008). Like in the 3PNBBT, the RSFRC1% has also provided higher flexural capacity and energy absorption performance than ISFRC1% in the RPT. The higher aspect ratio and number of RSF can justify this better performance of RSFRC1% (Micelli *et al.*, 2014).



(a) (b)

Figure 6: Average force versus central deflection (a), and Average energy absorption versus central deflection (b) of RSFRC1% and ISFRC1% panels

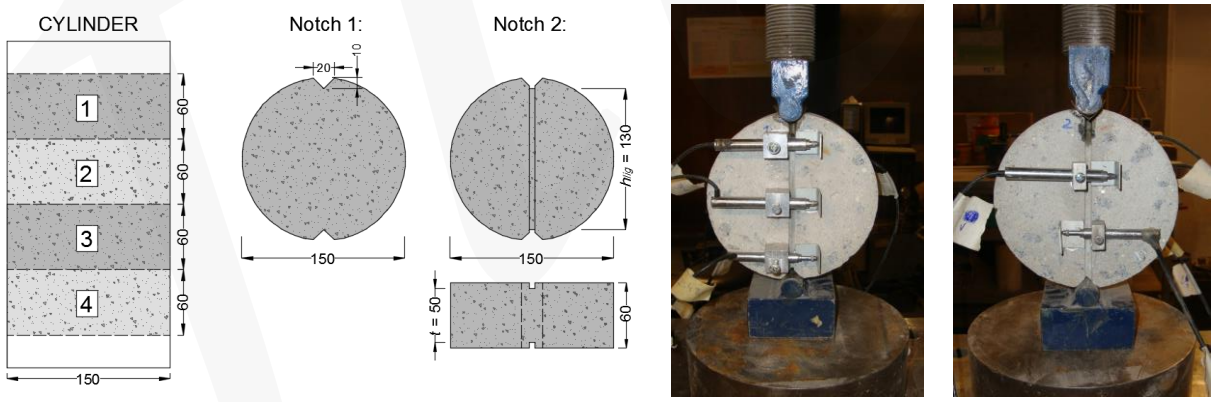
This document is the intellectual property of the fib – International Federation for Structural Concrete. All rights reserved.
This PDF of fib Bulletin 95 is intended for use and/or distribution solely within fib National Member Groups.

2.3.3 Splitting tensile tests

Double edge wedge splitting tests (DEWST) were performed on four cylindrical specimens of each concrete mix with ϕ150x60 mm obtained by cutting from moulded ϕ150x300 mm specimens, as shown in Fig. 6.

In each specimen, 5 mm deep notches were executed parallel to the loading direction, in order to set the specimen's fracture surface along the notched plane (notch 2 in Fig. 7a). Following the procedure adopted by di Prisco *et al.* (2013), a V-shaped groove with 45º inclination was also executed at the ends of the notched plane, as illustrated in Fig. 7a (notch 1). The objective of this V-shaped groove was to induce a stress field corresponding to an almost pure mode I fracture in the notched plane.

The splitting tests were conducted under displacement control using an external LVDT that was positioned on the actuator to control the vertical deformation of the specimen. The following displacement rates were adopted: 1.0 µm/s up to the displacement of 2.0 mm; 2.0 µm/s from 2.0 mm up to 3.0 mm; 4.0 µm/s until the end of the test. For an accurate detection and tracking of the crack propagation, five LVDTs were used to measure the crack opening displacement along the fracture surface (Fig. 7b), three on the front face and two on the rear face of the specimen. The DEWST were carried out according with a new test method (Lameiras *et al.*, 2015) that results from the combination of the methodology proposed by di Prisco *et al.* (2013) for indirect evaluation of the mode I fracture properties of fibre reinforced concrete (FRC) and the Modified Splitting Tensile Test (MSTT) introduced by a group of researchers from the University of Minho (Abrishambaf *et al.* 2015), which tried to overcome the limitations of each test method, deviating the crosswise compressive stresses from the fractured section while a unique fracture plane is likely to be obtained.



(a) (b) (c)

Figure 7: (a) Cutting of cylinders in ϕ150x60 mm specimens and implementation of the respective specimen's notches (units in millimeters);(b) Test setup for splitting tensile tests - Specimen front view; (c) Specimen back view

Figure 8 shows the average splitting tensile stress ($\sigma_{t,split}$) versus crack width curves for RSFRC1% and ISFRC1%, where $\sigma_{t,split}$ was determined from the following equation, as proposed by di Prisco *et al.* (2013):

$$\sigma_{t,split} = \frac{0.89 \cdot P}{t \cdot h_{lig}} \quad (1)$$

This document is the intellectual property of the fib – International Federation for Structural Concrete. All rights reserved.
This PDF of fib Bulletin 95 is intended for use and/or distribution solely within fib National Member Groups.

where P is the compressive load, and t and h_{lig} are the thickness and the effective length of the notched region that defines the plan of failure, respectively. The crack width in X-axes corresponds to the average values measured by the five LVDTs during the loading stage of the specimens (Fig. 7b and 7c).

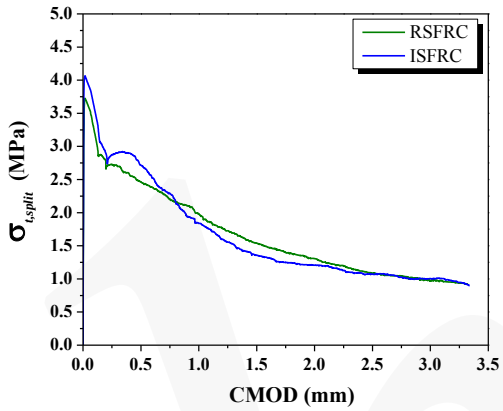


Figure 8: Average splitting tensile stress versus crack width for RSFRC1% and ISFRC1%

According to Fig. 8, RSFRC1% showed similar values of indirect tensile strength and post-cracking behaviour to the ones registered in ISFRC1%. The average values and corresponding CoV of the energy due to fracture propagation at a crack width of 3 mm, G_{Fm}, which corresponds to the area under the softening curve (Fig. 8) up to this crack width, were 5.21 N/mm (13.97%) for RSFRC1% and 5.14 N/mm (23.93%) for ISFRC1%. These results do not corroborate the results obtained in 2.3.1 and 2.3.2, which may be attributed to the differences between the test setups, particularly with regard to the crack opening process, which is more constant in DWEST than in 3PNBBT and RPT-3ps, being different the activated reinforcement mechanisms.

3 Concluding remarks

The experimental findings presented in the present paper allows to point out the following observations:

1. The geometric characterization of RSF pointed to a multimodal distribution of the fibre diameter and a unimodal distribution of the fibre length and aspect ratio, in agreement with the literature.
2. RSF caused a slight reduction of the compressive strength of concrete.
3. From 3-point notched beam bending tests and round panel tests, RSFRC exhibited higher flexural strength and energy absorption capacity than ISFRC of equal composition.
4. No significant differences were observed between the post-cracking tensile behaviour of RSFRC and ISFRC in double edge wedge splitting tests.

4 Acknowledgements

The authors wish to acknowledge the support from FCT through PTDC/ECM-EST/2635/2014 project, as well as the collaboration of CiviTest Company in the production of concretes. The 1st and 5th author would like to thank the FCT for the financial support through the Research Grants PD/BD/113638/2015 and PD/BD/52657/2014, respectively. The supplying of RSF and ISF from Twincon and Maccaferri Companies, respectively, is also acknowledged.

This document is the intellectual property of the fib – International Federation for Structural Concrete. All rights reserved.
This PDF of fib Bulletin 95 is intended for use and/or distribution solely within fib National Member Groups.

5 References

Abrishambaf A., Barros J.A.O., Cunha V.M.C.F. (2015). *Tensile stress–crack width law for steel fibre reinforced self-compacting concrete obtained from indirect (splitting) tensile tests*. Cement & Concrete Composites, 57, 153-165.

Aiello, M.A.; Leuzzi F.; Centonze, G.; Maffezzoli, A. (2009). *Use of steel fibers recovered from waste tyres as reinforcement in concrete: Pull-out behaviour, compressive and flexural strength*. Waste Management, 29, 1960-1970.

ASTM C1550-05 (2005*). Standard test method for flexural toughness of fiber reinforced concrete (using centrally loaded round panel). ASTM International.*

Barros J., Pereira E., Santos S. (2007). *Lightweight panels of steel fibre reinforced self-compacting concrete*. Journal of Materials in Civil Engineering, 19(4), 295-304.

CEB *fib Model Code 2010 – Volume 1*. Tomas Telford, Lausanne, Switzerland, 2013.

Centonze, G.; Leone, M.; Aiello, M.A. (2012). *Steel fibers from waste tires as reinforcement in concrete: A mechanical characterization*. Construction and Building Materials, 36, 46-57.

di Prisco M., Ferrara L., Lamperti M.L. (2013). Double edge wedge splitting (DEWS): an indirect tension test to identify post-cracking behaviour of fibre reinforced cementitious composites. Materials and Structures, 46 (11), 1893–1918.

EN 206-1 (2007). *Concrete – Part 1: Specification, performance, production and conformity*. IPQ, Lisbon, pp. 21.

EN 12350-8 (2010). *Testing fresh concrete – Part 8*: *Self-Compacting Concrete - Slump-flow test*.

EN 12390-3 (2009). *Testing hardened concrete – Part 3: Compressive strength of specimens*.

EN 12390-13 (2012). *Testing hardened concrete – Part 13: Determination of secant modulus of elasticity in compression*.

Lameiras R., Barros J., Azenha M. (2015). *Influence of casting condition on the anisotropy of the fracture properties of Steel Fibre Reinforced Self-Compacting Concrete* (SFRSCC). Cement & Concrete Composites, 59, 60-76.

Martinelli, E.; Caggiano, A.; Xargay, H. (2015). *An experimental study on the post-cracking behaviour of Hybrid Industrial/Recycled Steel Fibre-Reinforced Concrete*. Construction and Building Materials, 94, 290-298.

Micelli F., Leone M., Centonze G., Aiello M. (2014). *Chapter: Go Green: Using Waste and Recycling Materials, Infrastructure Corrosion and Durability Sustainability Study*, Edited by Yang Lu, OMICS Group eBooks, USA.

Minelli, F. and Plizzari, G.A. (2011). *A new round panel test for the characterization of fiber reinforced concrete: a broad experimental study*. Journal of Testing and Evaluation, 39(5), 889-897.

Pilakoutas K., Neocleous K., Tlemat H. (2004). *Reuse of tyre steel fibres as concrete reinforcement*. Proceedings of the ICE: Engineering Sustainability, 157(3), 131-138.

Salehian, H.; Barros, J.A.O.; Taheri, M. (2014). *Evaluation of the influence of post-cracking response of steel fibre reinforced concrete (SFRC) on load carrying capacity of SFRC panels*. Construction and Building Materials, 73, 289-304.

Zamanzadeh Z., Lourenço L.A.P., Barros J.A.O. (2015). *Recycled Steel Fibre Reinforced Concrete failing in bending and in shear*. Construction and Building Materials, 85, 195-207.

This document is the intellectual property of the fib – International Federation for Structural Concrete. All rights reserved.
This PDF of fib Bulletin 95 is intended for use and/or distribution solely within fib National Member Groups.
FRC2018: Fibre Reinforced Concrete: from Design to Structural Applications
Joint ACI-*fib*-RILEM International Workshop

Finite Element Analyses of Seismic Response of a 22-story RC Wall Building subjected to Drying Shrinkage Cracking and Application of SCRPCC

Keisuke Kitazawa[1], Yuichi Sato[1], Kazuhiro Naganuma[2], Yoshio Kaneko[1]

[1] : Kyoto University, Kyoto, Japan.

[2] : Nihon University, Tokyo, Japan.

Abstract

This paper attempts to investigate the effectiveness of Steel Chip Reinforced Polymer Cementitious Composite (SCRPCC) to reduce the seismic drift of high rise building by employing finite element method. Steel chips are produced when a steel plate is precisely machined on a numerically controlled lathe. To verify the influence of drying shrinkage on the structural performance of entire buildings, seismic response analyses of a 22-story RC wall building subject to drying shrinkage cracking are conducted.

The analyzed building was damaged in 1985 Mexico Earthquake. In the analyses, drying shrinkage is considered by conducting the drying shrinkage cracking analyses before dynamic seismic vibration analyses to examine the influence of drying shrinkage. For each case of the analyses, two kinds of materials are used; ordinary concrete and SCRPCC.

The shrinkage of 8,400-day drying period induces cracks in the walls of top floor as well as the first floor. The maximum drift of the building is increased in the NS direction by the shrinkage cracking while reduced in the EW direction. The maximum total drift of the building during the seismic vibration is reduced by 3.5% in the NS direction and 8.9% in the EW direction by using the SCRPCC instead of the ordinary concrete. The average crack width of the building is reduced by 11.1% by the SCRPCC.

Keywords

Drying shrinkage crack, Steel chip reinforced polymer cementitious composite, 3D FEM

This document is the intellectual property of the fib – International Federation for Structural Concrete. All rights reserved.
This PDF of fib Bulletin 95 is intended for use and/or distribution solely within fib National Member Groups.

1 Introduction

Reducing of CO_2 emission became important tasks in the entire industry. Among others, construction industry represents one of the major constituents of industrial waste (ex. Keoleian et al. 2005). The reuse of steel materials contributes to a reduction in the environmental load. Numerous attempts have been made to reuse the waste produced by the iron and steel industry. For example, there is an idea of using steel chips as a replacement material for fine aggregate in concrete (ex. Alwaeli and Nadziakiewicz 2012). The use of steel chips, which are waste products of the iron and steel industry, is economically efficient and environmentally sound because it reduces the total amount of industrial waste.

The authors attempted to develop and implement steel chip reinforced cementitious composite (SCRCC), which is reinforced with steel chips instead of conventional steel fibers. The steel chips are produced when steel plates are precisely machined on numerically controlled lathes. In a previous study (Kanada et al. 2011), fundamental material tests clarified that SCRCC has properties that are similar to FRCC. To enhance strength, adhesion, bond, waterproofness and durability of building structures, the polymer cement composite (PCC) is one of the promising solutions (Ohama 1987).

An experiment was conducted to predict the shrinkage cracking behavior of SCRCC (Hong et al. 2015). Then a simplified method was proposed to predict the drying shrinkage cracks of Hong's four restrained wall specimens made of SCRPCC incorporated with 2D finite element analyses (Ida et al. 2016). In this method, the effective drying shrinkage strain is evaluated by multiplying a coefficient to consider the influence of the tensile creep strain. This method has been justified by means of the tensile creep tests and the comprehensive parametric study.

This paper analytically investigates the influence of the drying shrinkage cracks on the seismic vibration of a 22-story RC wall building. It has been thought that the shrinkage cracks may reduce the stiffness of the RC building and affect the vibration characteristics, but few attempt of quantitative estimation has been conducted. The analyses in this paper employ the Ida's method to estimate the long period (8400 days, or approximately 23 years) drying shrinkage behavior of 3D finite element model of the entire building. The building model is then subjected to the dynamic time history analyses by applying 3D acceleration record. It is supposed that the shrinkage crack increase the response drift of the building during the vibration while the response of a building made of the SCRPCC will be reduced because the SCRPCC reduce the opening of shrinkage cracks. These phenomena are quantitatively discussed in the following sections.

2 Analysis method of drying shrinkage crack

2.1 Steel Chip Reinforced Polymer Cementitious Composite (SCRPCC)

Steel chips are produced when a steel plate is precisely machined on a numerically controlled lathe (*Fig. 1*). Now, all these steel chips occurred during machining are being buried as wastes. Ordinary steel chips are lubricated with oil during precise machining. And the shape of steel chip is not uniform as shown in left picture. But the steel chips used in this study (right) are almost equal in shape, and are not lubricated with oil during precise machining work. And the steel grade is only 235 N/mm^2-class (density: 7.86 g/cm^3). Thus, they have the effect of stable reinforcement in the cementitious composites.

This document is the intellectual property of the fib – International Federation for Structural Concrete. All rights reserved.
This PDF of fib Bulletin 95 is intended for use and/or distribution solely within fib National Member Groups.

The mix proportions of cementitious composites assumed in this study are given in *Table 1*. Polymer cement composite is used as binder. Ordinary Portland cement is used as a cement. Polymeric admixture used is ethylene vinyl acetate (EVA) emulsion which is a fluid milk-white solution with a solid content of 45% and the density 1.07 g/cm^3. An antifoaming agent is used to control the entrained air with 1% by mass on polymer. River sand is used as a fine aggregate. Steel chip contents of 2% by volume are used in this study.

The compressive and splitting tensile strengths of cementitious composites are listed in *Table 2*. The compressive strengths of PCC and SCRPCC are slightly higher than 40 N/mm^2. In contrast to the tensile strength of PCC at 3.6 N/mm^2, that of SCRPCC is 4.9 N/mm^2. *Figure 2* shows the relationship between compressive stress and strain and the relationship between tensile stress and crack width. Comparing to PCC, SCRPCC presents higher strength and ductility both in the compression and the tension side because of the bridge effect of the steel chips.



Figure 1: Ordinary steel chips (left) vs steel chips (right)

Table 1: Mix proportion of PCC/SCRPCC

	PCC	SCRPCC
W/B (%)	30	30
Water (kg)	24	24
Cement (kg)	80	80
Fine aggregate (kg)	160	142.2
Polymer (kg)	8	8
Steel chip (Vol. %)	0	2
Antifoaming Agent (kg)	0.08	0.08

Table 2: Mechanical properties of materials

	PCC	SCRPCC
Compressive strength f_{c28} (N/mm^2)	41.8	44.8
Strain corresponding to f_{c28}: ε_c (×10^{-3})	3.33	3.25
Splitting tensile strength f_{t28} (N/mm^2)	3.62	4.89

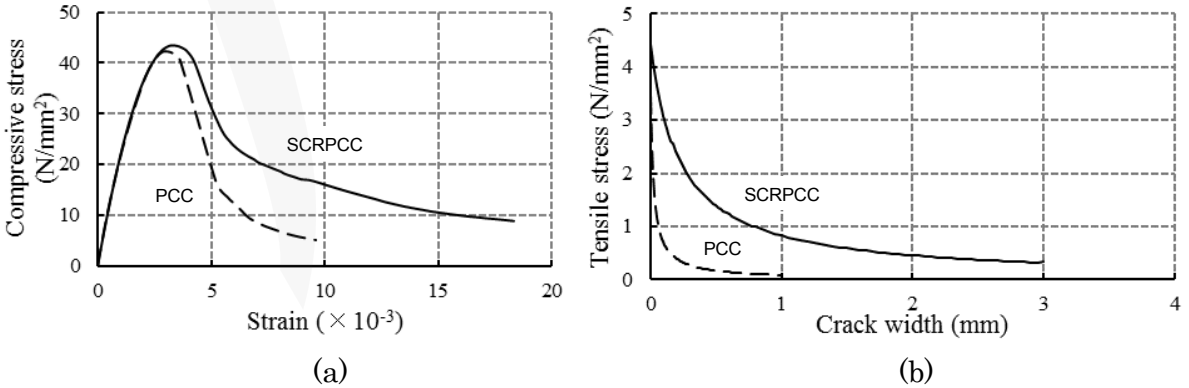


Figure 2: Mechanical properties of PCC and SCRPCC: Compressive stress – strain relationships (a); tensile stress – crack width relationships (b)

This document is the intellectual property of the fib – International Federation for Structural Concrete. All rights reserved.
This PDF of fib Bulletin 95 is intended for use and/or distribution solely within fib National Member Groups.

2.2 Ida's Method (Ida 2016)

The analysis method proposed by Ida (Ida et al 2016) adopts the bond model based on fib Model Code 2012 (fib 2012), models of shrinkage strain and creep based on CEB-FIP Model Code 1990 (CEB-FIP 1990), and a finite element program developed by Naganuma et al. (Naganuma et al. 2004). The finite element program is incorporated with the discrete-like crack simulation method developed by one of the authors (Sato and Naganuma 2012). The discrete-like crack simulation method was developed by aiming at an explicit computation of crack widths, which used to be impossible by using the conventional smeared crack-based finite element method. The summed strain ε_{sc_e} of the shrinkage strain and the creep strain is evaluated by Eq. (1) in this paper.

$$\varepsilon_{sc\_e} = K\varepsilon_{sc} \quad (1)$$

where

K = coefficient considering the influence of creep; ordinary concrete 0.6, SCRPCC: 0.54; and

ε_{sc} = drying shrinkage strain based on CEB-FIP Model Code 1990.

Before proceeding to the analysis of building, outlines of two examples are presented in the following sections. These examples will verify the feasibility of this method although the coefficient K maybe varied by the stress conditions as well as the weather conditions and further studies will be required to extend its applicability.

2.3 Example 1: Ordinary concrete wall

The RC walls in Kheder's study (Kheder 1997) are subjected to 60-day drying shrinkage at the average temperature of 35°C and the average relative humidity from 10% to 20%. The predicted shrinkage strain based on the temperature and humidity was $1{,}100\times10^{-6}$. Four walls had been analysed by a different method in the authors' previous study (Sato and Naganuma 2012). Only a typical wall is selected here and analysed by the proposed method. This wall (1E2) is 2,000 mm high, 4,000 mm long, and 150 mm thick and contains orthogonally arranged steel bars 10 mm in diameter. The reinforcement ratio is 0.2%. The compressive and tensile concrete strength, the elastic modulus of concrete, the yield stress and elastic modulus of steel bar, which are not given in the literature, are assumed as 30 N/mm^2, 2.7 N/mm^2, 25,300 N/mm^2, 525 N/mm^2, and 200,000 N/mm^2, respectively.

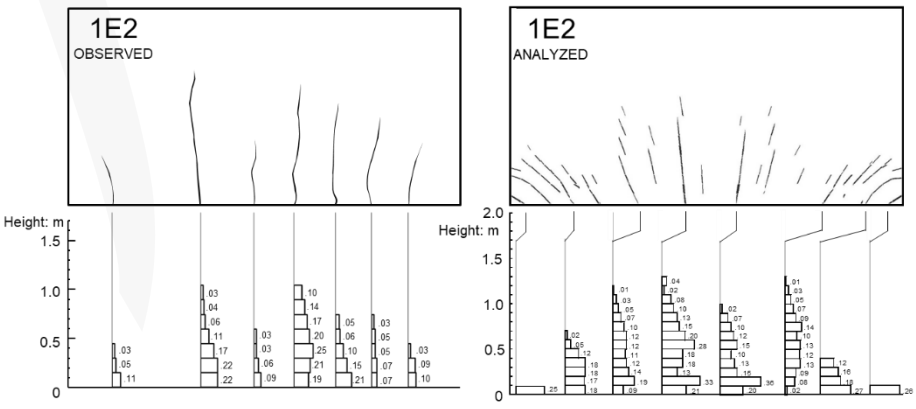


Figure 3: Drying shrinkage crack pattern of Wall 1E2 (Kheder 1997)

This document is the intellectual property of the fib – International Federation for Structural Concrete. All rights reserved.
This PDF of fib Bulletin 95 is intended for use and/or distribution solely within fib National Member Groups.

The water/binder ratio is assumed to be 50% while the weight of coarse aggregate per unit volume 1200 kg/m^3. The wall is modelled by four-node plane stress elements each 100 mm square. The bottom of the wall is fixed. One analysis step corresponds to one material day and the analysis is conducted for 60 material days. *Figure 3* compares the cracks of Wall 1E2 between observed and analysed patterns. The lower half of the figure indicates the crack widths. The analysed distributions and widths roughly agree the observed data.

2.4 Example 2: SCRPCC wall

In Hong's study (Hong et al. 2015), four wall specimens of size 150×300×2500 mm were prepared for restrained drying shrinkage tests as shown in *Fig.4*. In this section, one of the four specimens is selected (Specimen SCRPCC10) as typical example. The specimen was made of SCRPCC described in Section 2.1 and contains ten steel bars 6.4 mm in diameter (reinforcement ratio ρ = 0.72%). The yield stress and elastic modulus are 426 N/mm^2, and 189,000 N/mm^2, respectively. The drying test was continued for 24 weeks, the average temperature and the relative humidity were approximately 15°C and 62%, respectively. *Figure 5* shows relationship between drying shrinkage and drying period. The shrinkage strain at 24 weeks was around 700×10^{-6}. The specimen is modelled by four-node plane stress elements each 25 mm square. In the analyses, the observed relationships were replaced by smoothly fitted curves as shown in *Fig. 5*.

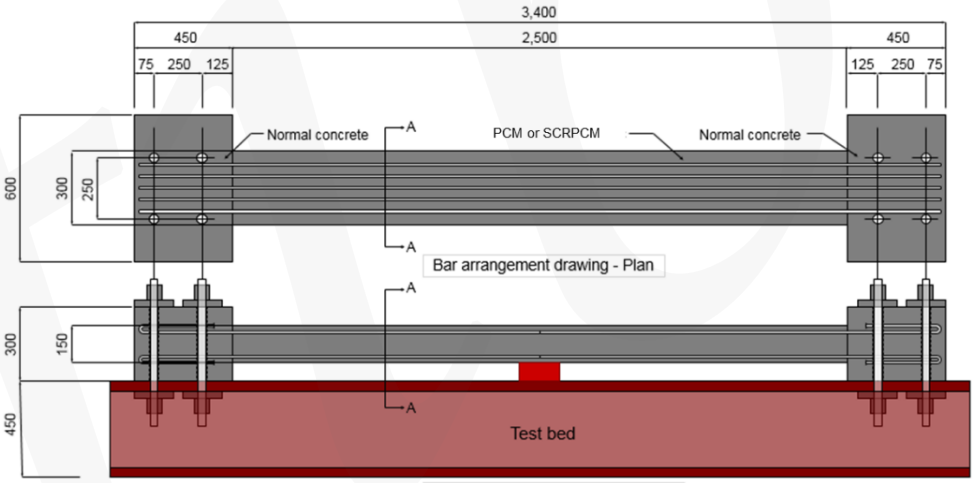


Figure 4: Restrained wall specimens of drying shrinkage test

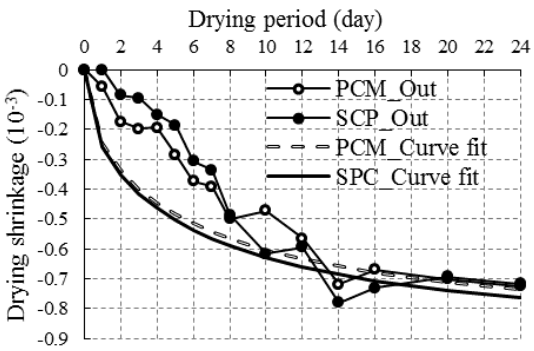


Figure 5: Relationships between drying shrinkage strain and drying period

This document is the intellectual property of the fib – International Federation for Structural Concrete. All rights reserved.
This PDF of fib Bulletin 95 is intended for use and/or distribution solely within fib National Member Groups.

Figure 6 compares the drying shrinkage crack patterns of each specimen and the distributions of the crack widths along the longitudinal direction of the specimens between the test and the analyses. The crack widths are the maximum values attained during the drying period. The analyses simulate well these tendencies.

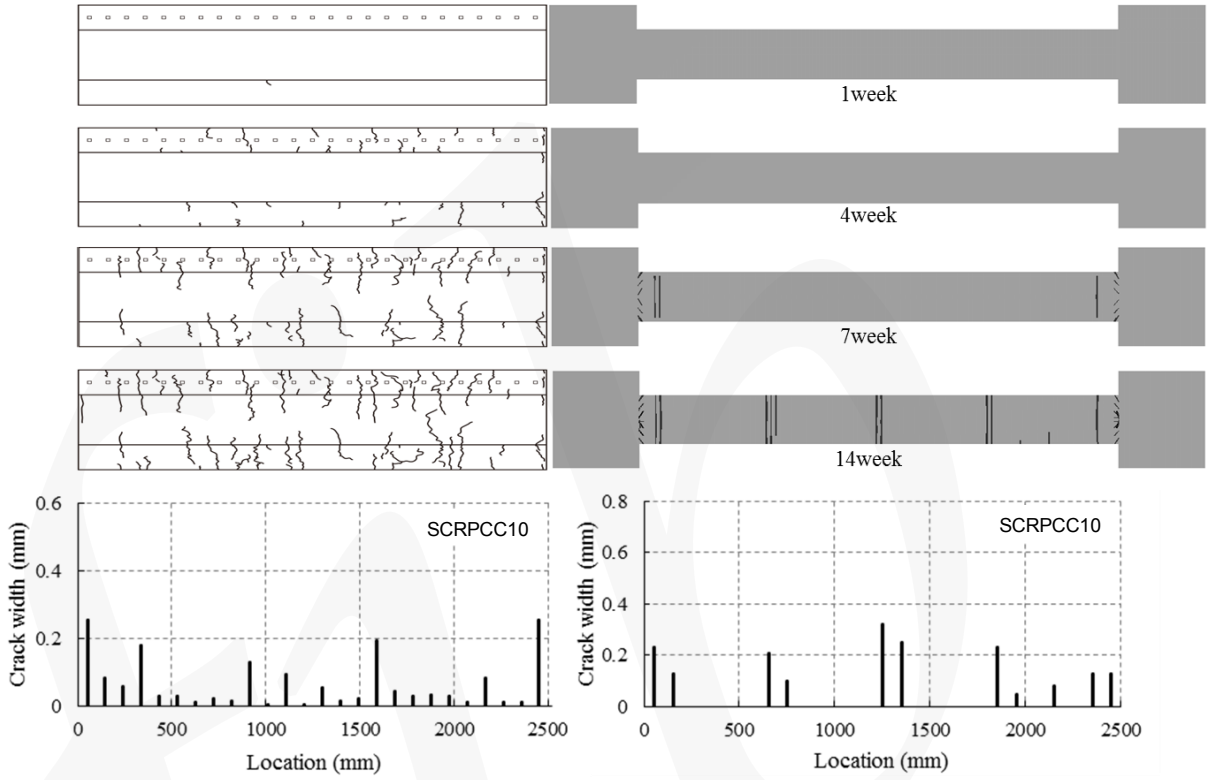


Figure 6: Drying shrinkage crack patterns and widths of SCRPCC10 by test (left) and FEM (right)

3 Analyses of 22-story RC wall building

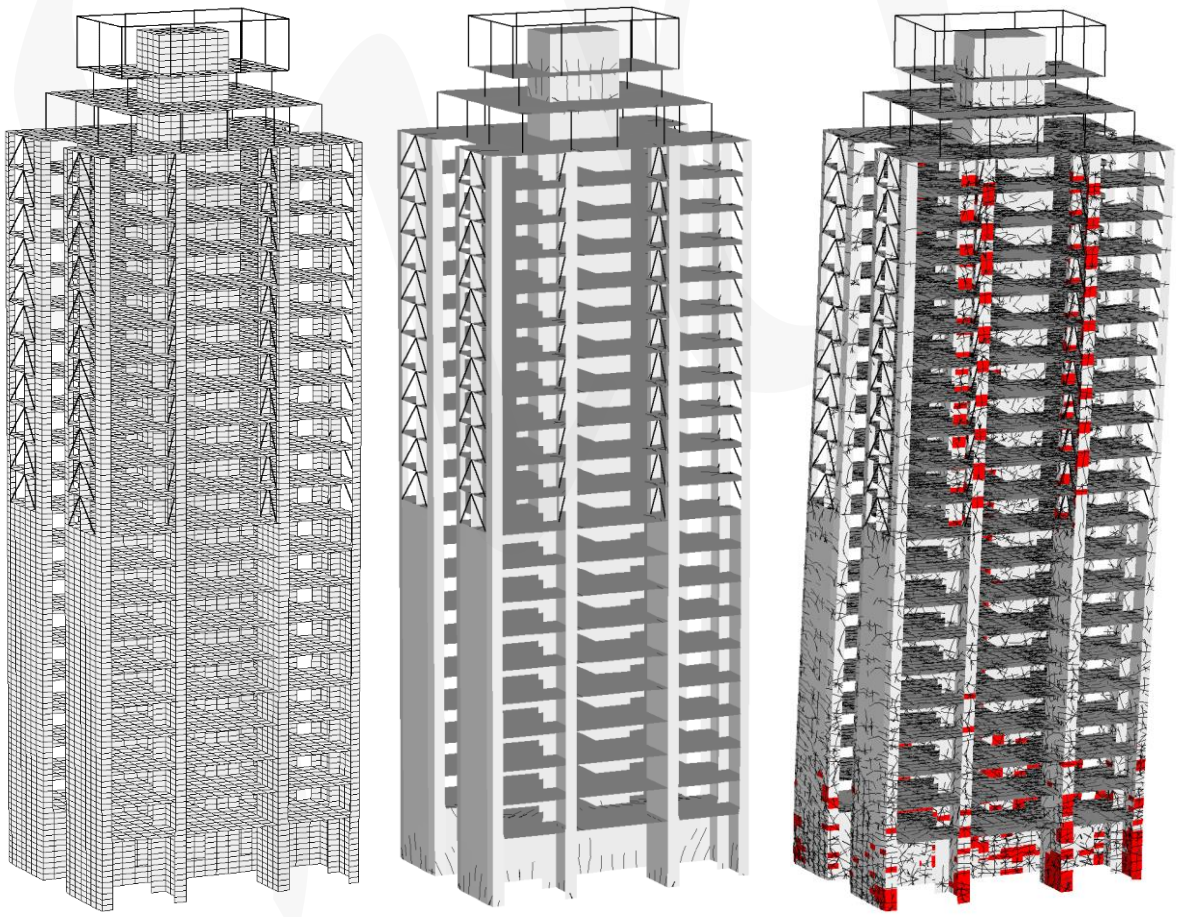
3.1 Finite element modeling

The analyzed building is 22-story-high RC wall building (***Fig. 7a***) located in Nonoalco Tlatelolco housing complex in Mexico City and severely damaged in the 1985 Mexico Earthquake (AIJ 1986, Petrovski et al. 1988). The structure is 68.81 m-high, composed of 200 mm-thick walls and 280 mm-thick waffle slabs. The reinforcement ratios of the walls range from 0.23% up to 1.13%, and the bar diameter from 9.4 mm up to 31.8 mm. The building was designed based on old guidelines in 1950's and it is not probable that a new kind of FRC like the SCRPCC is used for such an old structure. However, the building was supposed to attain large drifts by relatively long-period vibration so as the concrete material was subjected to critical stresses and strains. This may be one of ideal conditions to examine the performance of the SCRPCC.

The analyses conduct the drying shrinkage cracking computations before the time history analyses. The analysis parameters are the material (ordinary concrete and the SCRPCC) and

This document is the intellectual property of the fib – International Federation for Structural Concrete. All rights reserved.
This PDF of fib Bulletin 95 is intended for use and/or distribution solely within fib National Member Groups.

consideration of drying shrinkage (with/without shrinkage crack analyses). Therefore, four cases are analyzed; (1) ordinary concrete without shrinkage, (2) SCRPCC without shrinkage, (3) ordinary concrete with shrinkage, and (4) SCRPCC with shrinkage. The same constitutive models are adopted for the ordinary concrete and SCRPCC except the tensile softening characteristic (*Fig. 2b*). The drying shrinkage strain is calculated based on the CEB-FIP Model Code 1990 and impose the strain corresponding to 8400 days to the building by the initial 250 steps. For the time history seismic response analyses, an acceleration data SCT1 (AIJ 1986) recorded is input to the north-south, east-west and up-down direction. The building model is made of 18,228 four-node quadrilateral shell elements and 226 two-node truss elements. The former are used for the wall while the latter for the braces. Each quadrilateral shell element is divided into ten layers along the thickness direction so that the element can consider the out-of-plane bending. The total degrees of freedom of the model are 111,865. The gravity acceleration is input at the initial two steps. Then the time history analyses are conducted by 0.01-second time increment up to 6000 steps (i.e., 60 seconds). The coefficients β=0.25 and γ=0.5 of time increment are adopted for Newmark β method. Damping is primary stiffness proportional type, and we add 1% damping in a rate of primary natural period 1.22 seconds, which is evaluated by the eigenvalue analyses using the Subspace iteration method.



(a) (b) (c)

Figure 7: Finite element modelling and analysed crack patterns and crushing distributions: (a) Mesh division; (b) Cracks pattern of SCRPCC model after 8400-day drying period; (c) Cracks and crushing of SCRPCC model at maximum drift during SCT1 vibration

This document is the intellectual property of the fib – International Federation for Structural Concrete. All rights reserved.
This PDF of fib Bulletin 95 is intended for use and/or distribution solely within fib National Member Groups.

3.2 Analyses results

Figure 7b shows crack pattern of the SCRPCC model after the 8,400-day drying period. The shrinkage cracks are found in the walls of the first floor and the elevator shaft of the top floor. *Figure 7c* shows the distributions of cracks and crushing parts (red colored) at the maximum drift (40.90 sec.) of the same building. The cracks and crushing parts are densely distributed in the lower floors. *Figure 8* compares the relationships between total drift and time in NS and EW directions. The ordinary concrete models are indicated by the black lines while the SCRPCC model by the red lines. Each model attained the maximum drift around 1%. The vibration patterns look similar, but considerable differences are found with respect to the maximum drift.

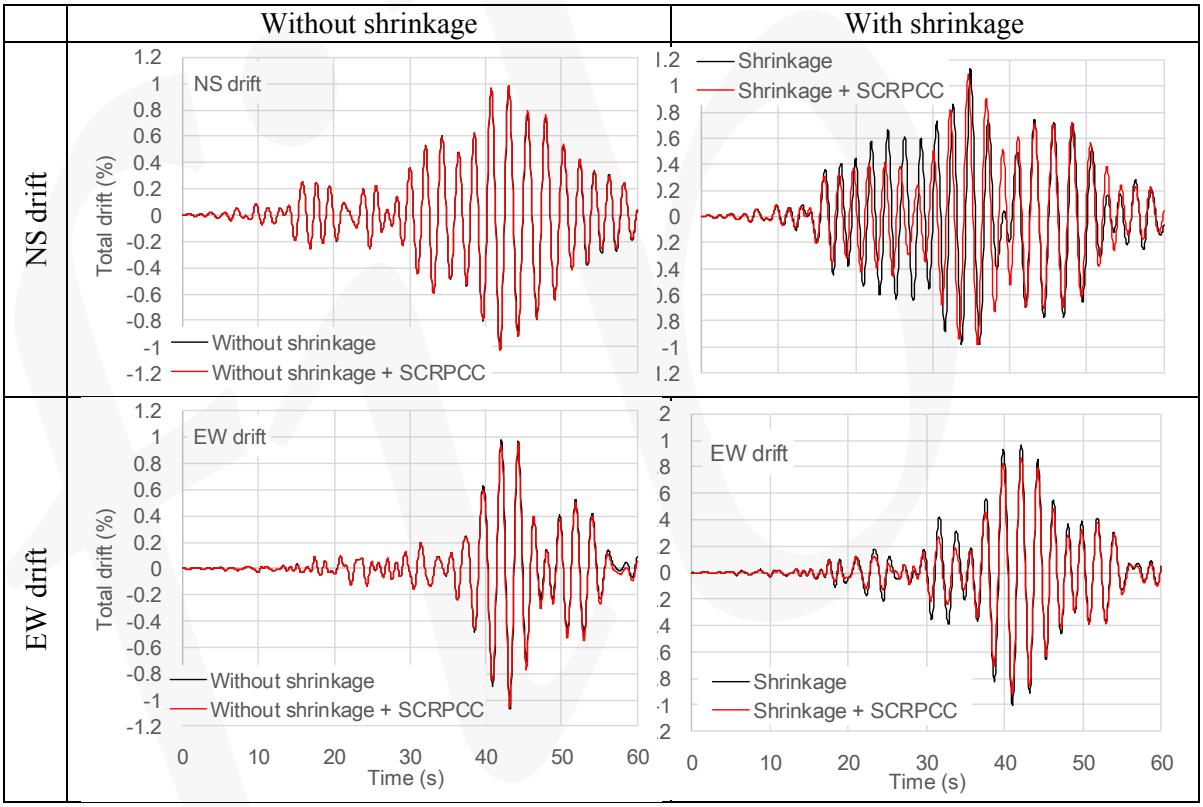


Figure 8: Relationships between total drift and time in NS and EW directions

Table 3 summarizes the analyses results. For the north-south (NS) direction, the maximum drift of the ordinary concrete model is increased by 10.8% (i.e. from 1.02% to 1.13%) by considering the shrinkage. The increasing rate is reduced to 6.9% (i.e. from 1.02% to 1.09%) by the SCRPCC. For the east-west (EW) direction, the maximum drift of the ordinary concrete model is decreased by 5.6% (i.e. from 1.07% to 1.01%). It is supposed that the shrinkage cracks and the cracks induced during the vibration excessively elongate the natural period of the building and reduce the resonance effect with the ground motion. The maximum drift of the SCRPCC model is reduced by 13.2% (i.e. from 1.06% to 0.92%), which is considerably smaller than the ordinary concrete model. *Figure 9* compares the relationship between the average crack width and time. The average crack widths of the models without the shrinkage are 0.35 mm for

This document is the intellectual property of the fib – International Federation for Structural Concrete. All rights reserved.
This PDF of fib Bulletin 95 is intended for use and/or distribution solely within fib National Member Groups.

the both model. If the shrinkage is considered, the width is increased up to 0.45 mm for the ordinary concrete model. The width is reduced to 0.40 mm for the SCRPCC model.

Table 3: Results of drying shrinkage crack analyses and dynamic time history analyses

		Without shrinkage		With shrinkage	
		Ordinary concrete (1)	**SCRPCC (2)**	**Ordinary concrete (3)**	**SCRPCC (4)**
Maximum drift (%)	**NS direction**	1.02	1.02	1.13	1.09
	EW direction	1.07	1.06	1.01	0.92
Average crack width (mm)	**After 8400 days**	--	--	0.21	0.18
	After dynamic analysis	0.35	0.35	0.45	0.40

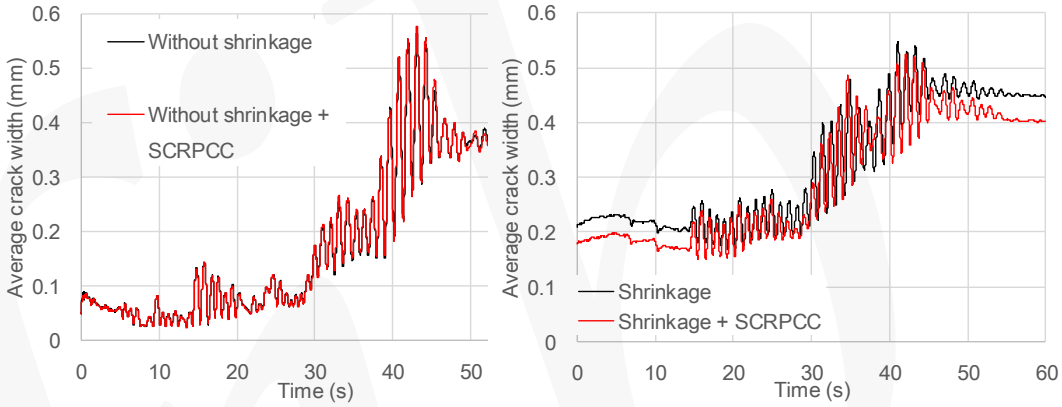


Figure 9: Relationships between average crack width and time

4 Conclusion

The seismic response and cracking characteristics of a 22-story RC wall building damaged in the 1985 Mexico Earthquake are investigated by employing finite element method. The drying shrinkage crack is considered and the usage of SCRPCC is attempted to reduce the influence of the crack. The following remarks can be made based on the study of this paper.

1. The shrinkage of 8,400-day drying period induces cracks in the walls of top floor as well as the first floor. The maximum drift of the building is increased in the NS direction by the shrinkage cracking while reduced in the EW direction.
2. The maximum total drift of the building during the seismic vibration is reduced by 3.5% in the NS direction (i.e. from 1.13% to 1.09%) and 8.9% in the EW direction (i.e. from 1.01% to 0.92%) by using the SCRPCC instead of the ordinary concrete.
3. The average crack width of the building is reduced by 11.1% (i.e. from 0.45 mm to 0.40 mm) by the SCRPCC.

In future research, the sensitivity of analyses under varying degrees of applicable design shrinkage strains will be examined as well as making comparisons with the conventional steel fibers and polypropylene fibers. This research was carried out by Mr. Kenta Ueda, a former undergraduate student of Faculty of Engineering, Kyoto University with great effort. We express our gratitude here.

This document is the intellectual property of the fib – International Federation for Structural Concrete. All rights reserved.
This PDF of fib Bulletin 95 is intended for use and/or distribution solely within fib National Member Groups.

5 References

AIJ, Architectural Institute of Japan (1986) Report on disaster investigation of 1985 Mexico Earthquake (in Japanese)

AIJ, Architectural Institute of Japan (2008) Recommendations for Environmentally Conscious Practice of Reinforced Concrete Buildings (in Japanese)

Alwaeli, M. and Nadziakiewicz, J. (2012) Recycling of Scale and Steel Chips Waste as a Partial Replacement of Sand in Concrete. Construction and Building Materials, 28(1), 157-163.

CEB-FIP (1990) Model Code for Concrete Structures, Comite´ Euro-International du Beton-Fe´de´ration International de la Precontrainte.

fib, International Federation for Structural Concrete (2012). Model code 2010, Final Complete Draft, Bulletins 65 and 66, March 2012-ISBN 978-2-88394-105-2 and April 2012-ISBN 978-2-88394-106-9, 233–239.

Hong, S., Sato, Y., Kaneko, Y., and Kimura, S. (2015) Prediction of Drying Shrinkage Cracking of Eco-efficient Steel Chip Reinforced Cementitious Composite Considering Tensile Creep, Journal of Advanced Concrete Technology, 13, 393-402. DOI: 10.3151/jact.13.393.

Kanada, M., Sato, Y., and Kaneko, Y. (2011) Seismic Retrofit of Exposed Column Basement Using Steel Chip Reinforced Cementitious Composite. Proceedings of Constructional Steel, 19, 155-162. (in Japanese)

Keoleian, G. A., Kendall, A., Dettling, J. E., Smith, V. M., Chandler, R., Lepech, M. D., and Li, V. C. (2005) Life Cycle Modeling of Concrete Bridge Design: Comparison of Engineered Cementitious Composite Link Slabs and Conventional Steel Expansion Joints. Journal of Infrastructure Systems, 11(1), 51-60.

Kheder, G. F. (1997) A New Look at the Control of Volume Change Cracking of Base-Restrained Concrete Walls. ACI Structural Journal, 94(3), 262-270.

Ida, Y., Hong, S., Kimura ,S., Sato, Y. and Kaneko, Y. (2016) Prediction of Drying Shrinkage Cracks of Steel Chip Reinforced Polymer Cement Mortar. Advanced Concrete Technology 14, 739-752, DOI: 10.3151/jact.14.739.

Naganuma, K., Yonezawa, K., kurimoto, O. & Eto, H. (2004) Simulation of nonlinear dynamic response of reinforced concrete scaled model using three-dimensional finite element method. Proceedings of the 13th World Conference on Earthquake Engineering (WCEE13), Vancouver, BC, Canada, 586.

Ohama, Y. (1987) Principle of Latex Modification and Some Typical Properties of Latex-Modified Mortars and Concretes. ACI Materials Journal, 84, 511-518.

Petrovski, J., Jordanovski, L., Zelenovic, V. and Kladek, I (1988) Influence of soil-structure interaction on dynamic response of high-rise building in Mexico City due to September 19, 1985 Earthquake, Proceedings of Ninth World Conference on Earthquake Engineering, Tokyo-Kyoto, Japan, VII, 309-314

Sato, Y. and Naganuma, K. (2012) Discrete-like Crack Simulation by Smeared Crack-based FEM --Reinforced Concrete Wall Subjected to Shrinkage, Proceedings of Bond in Concrete 2012, Vol. 1, Brescia, Italy, 193-200.

This document is the intellectual property of the fib – International Federation for Structural Concrete. All rights reserved.
This PDF of fib Bulletin 95 is intended for use and/or distribution solely within fib National Member Groups.
FRC2018: Fibre Reinforced Concrete: from Design to Structural Applications
Joint ACI-*fib*-RILEM International Workshop

Closed loop control in crushing test for fibre reinforced concrete pipes

Renata Monte[1], Albert de la Fuente Antequera[2], Antonio Domingues de Figueiredo[1]

[1] : University of São Paulo. São Paulo, Brazil.

[2] : Barcelona Tech (UPC). Barcelona, Spain

Abstract

The mechanical behaviour of fibre reinforced concrete pipes (FRCP) is usually verified through three-edge bearing test (TEBT). More recent studies propose a design approach according to the *fib* Model Code 2010, involving the evaluation of mechanical behaviour in both service (SLS) and ultimate (ULS) limit states. The challenge consists in assessing with the proper accuracy and reliability the mechanical parameters by means of the TEBT method. This is generally performed using a hydraulic equipment with load control and without using devices to measure the diametric displacement. In this research program, TEBT was carried out using three different control systems. Two closed-loop controls, using pipe diametric displacement or actuator displacement, and an open-loop control by loading rate. The crack width development was also measured simultaneously with the diametric displacement, only for closed-loop control. An increase in the post-crack strength of the FRCP were observed when the closed-loop system was used. The results show significant differences between the mechanical performances of pipes tested in open or closed-loop control. Conversely, closed-loop tests performed with actuator displacement control or pipe diametric displacement control show no significant differences. Crack opening measurement allows establishing a linear correlation with diametric displacement, this permitting to establish the values corresponding to the SLS and ULS deformation and respective loads. Consequently, the connection with the Model Code approach becomes possible as well as the design optimization of the FRCP.

Keywords

Fibre reinforced concrete. Concrete pipes. Crushing test. Closed-loop control.

This document is the intellectual property of the fib – International Federation for Structural Concrete. All rights reserved.
This PDF of fib Bulletin 95 is intended for use and/or distribution solely within fib National Member Groups.

1 Introduction

Concrete pipes (CPs) are widely used in infrastructure construction, especially sewage and drainage systems. Fibre reinforced concrete pipes (FRCPs) have been studied for total or partially substitution of the steel-bars with technical and economic advantages (Haktanir *et al*., 2007; de la Fuente et al., 2012; Abolmaali et al., 2012; de la Fuente *et al*., 2013; Park *et al*., 2015). Despite of the advantages, their use has not been consolidated yet. This could be associated with: (1) the inertia involved in changes among CP manufacturers; (2) engineering community lacking knowledge of the properties of FRC and design processes; (3) FRCPs must be designed iteratively using the three-edge bearing test (TEBT); and (4) the lack of systematic and representative characterization tests of the FRC post–cracking strength, which could be performed in the facilities of the same precast plant.

A systematic method for the design of FRCPs was proposed for steel fibres (de la Fuente et al., 2012) and synthetic fibres (de la Fuente et al., 2013) based on the use of the Model for the Analysis of Pipes (MAP) (de la Fuente et al., 2011). This method simulates numerically the TEBT and the non-linearities resulting from the cracking and the subsequent bending moment redistribution; the parameters related to the post-cracking behaviour of the fibre reinforced concrete (FRC) being an input of the model. More recently, BCN tests were implemented as the characterization procedure to obtain the tensile performance of the FRCs and the suitability of the constitutive equation to simulate the behavior of FRCPs was assessed (Monte et al., 2016).

The mechanical behaviour of CPs is commonly evaluated through the TEBT, detailed in several standards (EN 1916, 2002; NBR 8890, 2018; ASTM C497, 2018). The European and Brazilian standards stipulate two different test procedures for pipes reinforced with steel bar or fibres. According to these, the TEBT for FRCPs requires a cyclic loading procedure. Another relevant aspect is the fact that these standards only prescribe the load control without any concern to the displacement control during the test. In previous experimental programs involving FRCPs (Figueiredo, 2008), it was proved that the post-failure behaviour of pipes obtained by continuous or cyclical tests do not show significant differences. The use of LVDTs in the test leads to a better identification of the force-displacement relationships, consequently the structural verification could be easier and accurately carried out (Figueiredo et al., 2012).

Historically, it is known that the main limitation of tests performed with open loop systems lead to uncertainties in the residual strength determination for low crack opening levels (Golaparatnam and Gettu, 1995). Previous studies (Gettu et al., 1996; Banthia and Dubey, 1999; Gupta and Banthia, 2007) showed that the open system flexural test performed with prismatic specimens may provide a reduction of the residual strength measured in comparing with the values obtained with closed loop systems, especially when a softening behavior occurs. The same limitations could be associate to the TEBT with the same conditions (Figueiredo, 2008). Therefore, there is both lower reliability and accuracy of open-loop tests, which induced the adoption of closed loop systems for flexural standard tests for FRC basic characterization and should be analyzed for TEBT.

The main objective of this research is to present an experimental program focusing the three-edge bearing test of SFRCPs (steel fibre reinforced concrete pipes) performed with different control systems, establishing correlations between pipes diametric displacement and crack width. Also, the constitutive equation derived from BCN tests is used to simulate the TEBT behaviour to compare with closed loop control results.

This document is the intellectual property of the fib – International Federation for Structural Concrete. All rights reserved.
This PDF of fib Bulletin 95 is intended for use and/or distribution solely within fib National Member Groups.

2 Research program

2.1 Experimental program

The experimental program involved the real scale production of SFRCPs pipes with internal diameter D_i = 1000 mm, thickness h = 90 mm and length l = 1190 mm. The materials consumption, in kg/m³, was 320:720:1200:110 (cement:sand:coarse:water). The SFRCPs were manufactured with steel fibres of the type DRAMIX® RC80/60BN (length l_f = 60 mm, diameter d_f = 0.75, Young modulus E_f = 210,000 N/mm² and a tensile strength f_{fu} = 1100 N/mm²). The fibre dosages were 10 kg/m³, 20 kg/m³ and 30 kg/m³. The pipes were produced by using vibro-compression system and these were demoulded after production as regularly occurs in the industry.

Five cylindrical specimens with a diameter of 150 mm and a height of 300 mm were moulded simultaneously with pipe production. Due to the dry consistency of this concrete, the moulding was carried out on a vibrating table in three layers, with intense densification by the application of 50 strokes with a steel socket in each layer. Two specimens were used for compressive tests. The other three specimens were cut in half height for the Barcelona tests.

The Barcelona (BCN) test was standardized by UNE 83515:2010. The test configuration involved the measuring the circumferential displacement with an extensometer, but an alternative setup controlling the axial displacement without the need of the extensometer was proposed by Pujadas et. al. (2013). In this new test configuration, the load is applied by the plates of the machine at a constant rate of displacement of 0.5 mm/min. The cracking load (F_{cr}) is obtained when the stresses reach the indirect tensile strength of the concrete matrix and, after that, the fibres bridge the crack resulting residual loads for different axial displacement levels i ($F_{R,i}$). The inductive method (Cavalaro et al., 2015) was used to assess the steel fibre content of each specimen destinated to the BCN tests. This is an important verification due to the difficulties associate to the exact fibre content control during the pipes production in the factory.

The pipes were tested after the age of 28 days in the TEBT by following the continuous procedure proposed by Figueiredo et al., (2012). The vertical displacements were measured with LVDTs positioned at the crown and haunches of the pipe (Fig. 1a). Simultaneously the major crack opened at the crown was measured with two LVDTs, as illustrated in Fig. 1b.



(a)



(b)

Figure 1: Instrumented pipe during the TEBT (a); Crack width measurement in the crown (b)

This document is the intellectual property of the fib – International Federation for Structural Concrete. All rights reserved.
This PDF of fib Bulletin 95 is intended for use and/or distribution solely within fib National Member Groups.

The TEBTs were performed using a 200 kN hydraulic servo-actuator with a stroke length of 200 mm. A servo-controller model ODIN 1400 was used to control the test setup, operating digital loop at a frequency of 4 kHz. Two types of closed loop control were tested. The first is the actuator displacement control (ADC) used an internal LVDT to provide the displacement signal for position feedback. The second type is the diametric displacement control (DDC), where the feedback control is provided through a LVDT positioned at the crown to measure the diametric displacement. The European standard indicates a continuous load application at a rate between 20 kN/m and 25 kN/m per minute. The Brazilian standard is less restrictive, this specifying at a rate between 5 kN/m and 35 kN/m per minute. The closed loop test implies using a displacement rate. The controller was set with the displacement rate of 0.7 mm/min for ADC or 0.5 mm/min for DDC. The closed loop control results were compared to open loop control results (load control - LC) presented in de la Fuente et al., (2012). These pipes were produced at the same industry facilities with fibre contents of 20 and 35 kg/m³, with the same internal diameter and thickness, and designed for reaching equivalent resistant class.

2.2 Numerical analysis

The Model for the Analysis of Pipes (MAP) was used to simulate the global response of the pipe during the TEBT. This model was already presented in other scientific publications (de la Fuente et al., 2012; de la Fuente et al., 2013; Monte et al., 2016). The simulations were carried out taking into account the nominal dimensions of the pipe (thickness - h and length - l).

The tensile behaviour of FRC was simulated by using a simplified trilinear σ–ε diagram parameters derived from the Barcelona test, as presented in Monte et al. (2016). The parameters used in the simulation for each fibre content (C_f) are gathered in Table 1.

Table 1: Parameters to define the constitutive equation of the tensioned FRC using BCN tests

C_f (kg/m³)	σ_1^* *(MPa)*	E_{cm} (MPa)	ε_1 *(‰)*	σ_2 *(MPa)*	ε_2 *(‰)*	σ_3 *(MPa)*	ε_3 *(‰)*
10	6.219	36292	0.171	1.799	0.271	0.255	25
20	5.983	36292	0.165	2.128	0.265	0.473	25
30	5.539	36292	0.153	2.011	0.253	0.452	25

3 Results and discussion

3.1 FRC characterization

The results presented in Table 2 show the average results and coefficient of variation (CV) of the compressive and BCN tests.

Table 2: Average results and CV (%) obtained in the compressive and Barcelona tests

C_f [kg/m³]	Compressive test f_{cm} [MPa]	Barcelona test $F_{p,cr}$ [kN]	$F_{p,0.02}$ [kN]	$F_{p,4.8}$ [kN]
10	49.4 (7%)	139.3 (2%)	87.9 (20%)	12.5 (23%)
20	50.5 (3%)	134.0 (11%)	103.9 (16%)	23.1 (18%)
30	47.7 (8%)	124.0 (9%)	95.5 (9%)	22.0 (21%)

This document is the intellectual property of the fib – International Federation for Structural Concrete. All rights reserved.
This PDF of fib Bulletin 95 is intended for use and/or distribution solely within fib National Member Groups.

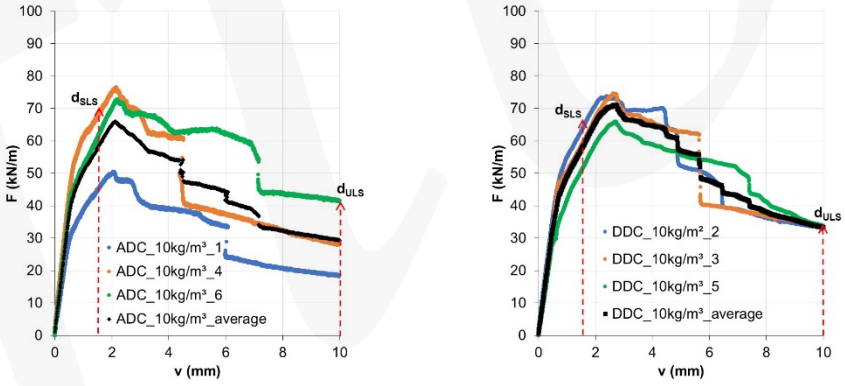
The fibre contents considered do not result in significant difference in the compressive strength of the FRC. This is confirmed in ANOVA test, at a level of significance of 0.05, which result a *p*-value equal to 0.701 (greater than 0.05).

The lowest CVs were obtained for the cracking loads ($F_{p,cr}$) determination in BCN tests (Table 2), these ranging between 2% and 11%. The cracking loads ($F_{p,cr}$) were not significantly influenced by the increase of C_f (*p*-value equal to 0,116 > 0.05). The residual loads present CVs between 9% and 23%. The highest CV are associated to higher crack openings ($F_{p,4.8}$), because the standard deviations do not decrease in the same proportion of the average values. Also, it can be noticed that the residual loads for the fibre content of 30 kg/m³ are lower than those for the 20 kg/m³. In fact, these results can be considered statistically equivalent, at a level of significance of 0.05 (*p*-value equal to 0.617 for $F_{p,0.02}$ and 0.988 for $F_{p,4.8}$).

The inductive method (Cavalaro et al., 2015) shows that most of the specimens present fibre content significantly higher than the design content. The average contents calculated were 15 kg/m³, 27 kg/m³ and 32 kg/m³, for the respectively design contents of 10 kg/m³, 20 kg/m³ and 30 kg/m³. The difference between the lower and intermediate fibre contents are much higher than the difference between the intermediate and superior, which could justify the tendency observed in the previous results (Table 2).

3.2 Three-edge bearing tests results

The TEBTs results are presented in terms of load (F) and diametric displacement ($\boldsymbol{v}$), considering the types of control (Actuator Displacement Control – ADC, Diametric Displacement Control – DDC and load control - LC). Fig. 2, Fig. 3 and Fig. 4 show the results for fibre content of 10, 20 and 30 kg/m³, respectively.



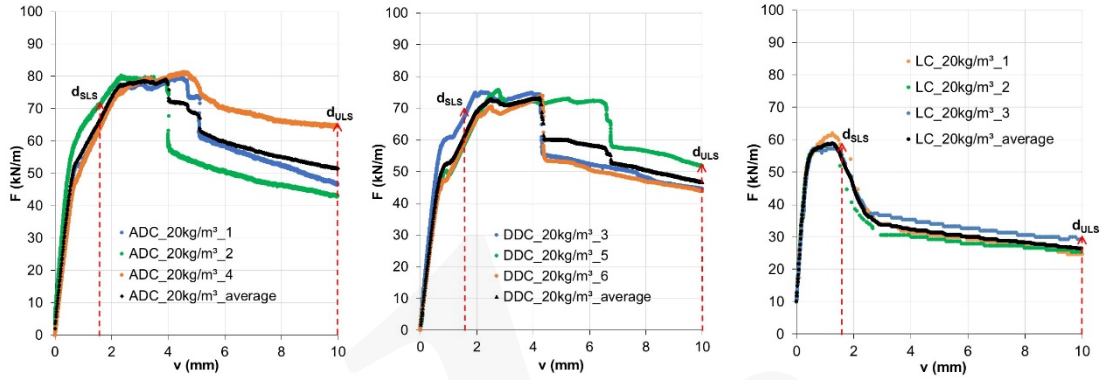
(a) (b)

Figure 2: F–v curves for the SFRCPs with 10 kg/m³: ADC (a); DDC (b)

In general, the TEBTs results presented low dispersion with the exception of the SFRCPs with 10 kg/m³ tested in ADC (Fig. 2a). For this specific group of tests, one of the pipes presents a significantly lower behaviour. This specimen was the unique which did not reach the design strength class (proof load – $F_c \geq 40$ kN/m and maximum load - $F_{max} \geq 60$ kN/m). Concerning the TEBT control system, the control provided by the actuator or pipe displacement can be considered equivalents. Even a statistical test, at a level of significance of 0.05, do not reject the equality of means (*p*-value equal to 0.144 > 0.05). On the other hand, tests performed with load control (LC) result significantly lower behaviour (Fig. 3c and Fig. 4c). Considering that the pipes are produced for the same resistant class, the requirements are achieved only with 35

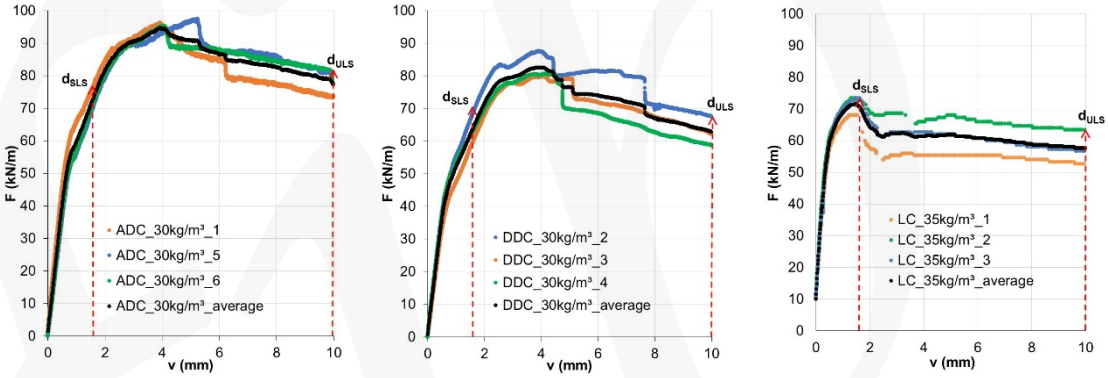
This document is the intellectual property of the fib – International Federation for Structural Concrete. All rights reserved.
This PDF of fib Bulletin 95 is intended for use and/or distribution solely within fib National Member Groups.

kg/m³ of fibres (Fig.4c). The closed loop system led to the pipes to achieve the strength requirements for the design class even for 10 kg/m³.



(a) (b) (c)

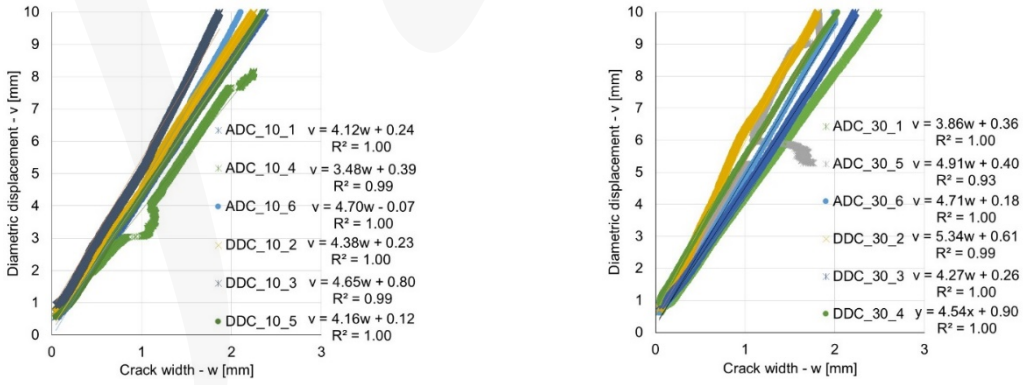
Figure 3: F–v curves for the SFRCPs with 20 kg/m³: ADC (a); DDC (b); LC (c)



(a) (b) (c)

Figure 4: F–v curves for the SFRCPs with 30-35 kg/m³: ADC (a); DDC (b); LC (c)

Fig. 5 presents the average experimental results in terms of crack width (w) and diametric displacement (v) for the SFRCPs 10 kg/m³ and 30 kg/m³.



(a) (b)

Figure 5: w–v curves for the SFRCPs: 10 kg/m³ (a); 30 kg/m³ (b)

The results of Fig. 5 indicate that the relation $w - v$ is linear; $v = aw + b$. The parameter a is the variation of v for a given variation in w ($\partial v/\partial w$), this representing the contribution of both

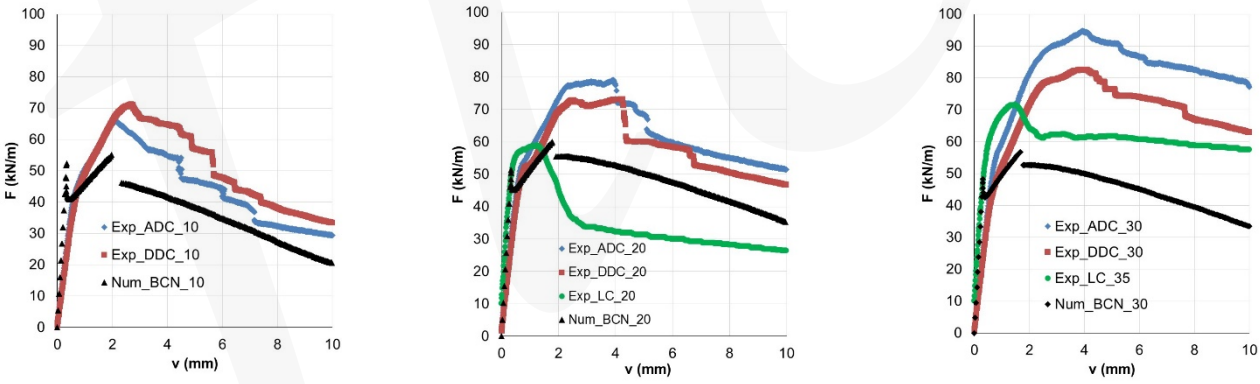
This document is the intellectual property of the fib – International Federation for Structural Concrete. All rights reserved.
This PDF of fib Bulletin 95 is intended for use and/or distribution solely within fib National Member Groups.

geometrical and sectional stiffness on the deformability of the system in terms of *v* as well as of *w*. The sectional stiffness is directly dependent on pipe thickness (*h*). The intercept b is the vertical displacement for the load F_{cr} prior cracking, v_{cr}. It can be remarked that the regression equations are similar for the different fibre content. Also, the equations are similar to the results presented in Monte *et al*. (2016), that present an equation $v = 6.63w + 1.61$ for FRPCs with 20 kg/m³ of steel fibres. The differences may be attributed to the instrument's accuracy used in this experimental program.

The relation ***w-v*** is useful to establish the level of crack opening during the post-cracking regime and the respective displacements. Based on this, it is possible to associate diametric displacements to the service limit state (d_{SLS}) and ultimate limit state (d_{ULS}) (see Fig. 2, Fig. 3 and Fig. 4), as proposed by Figueiredo *et al*. (2012), by taking into account the *fib* Model Code 2010 as a reference. Also, the authors proposed a relation between the values corresponding to d_{ULS} and d_{SLS}, and respective loads, in order to guarantee a minimum ductility. The relation proposed, based in historic results of TEBT performed with FRCPs, is $F_{ULS}=0.8 \cdot F_{SLS}$. This relation is reached for the fibre content of 22 kg/m³, considering a crack opening of 0.30 mm in SLS for the experimental results.

3.3 Numerical analysis

The force (*F*) – vertical displacement (*v*) experimental relationships for the FRCPs with 10, 20, 30 and 35 kg/m³ of steel fibres are compared with those assessed by using the MAP model, using the constitutive equation for simulating the tensile response of the FRC derived from the BCN (Table 1), are gathered in Fig. 6. Likewise, the cracking load (F_{cr}) and the loads associated to vertical displacements of 2, 6 and 10 mm are listed in Table 3.



(a) (b) (c)

Figure 6: F–v average experimental and numerical curves for the SFRCPs with: 10 kg/m³ (a); 20 kg/m³ (b); 30-35 kg/m³ (c)

This document is the intellectual property of the fib – International Federation for Structural Concrete. All rights reserved.
This PDF of fib Bulletin 95 is intended for use and/or distribution solely within fib National Member Groups.

Table 3: Comparison between experimental and numerical results for different load levels

	10 kg/m³			**20 kg/m³**			**30 kg/m³**		
	Exp [kN/m]	***MAP [kN/m]***	***ξ [%]***	***Exp [kN/m]***	***MAP [kN/m]***	***ξ [%]***	***Exp [kN/m]***	***MAP [kN/m]***	***ξ [%]***
F_{cr}	39.4	52.2	-33	47.5	50.5	-6	46.4	47.1	-1
F_{2mm}	65.3	52.3	20	71.3	56.4	21	76.5	52.7	31
F_{6mm}	45.4	38.8	14	59.1	47.6	19	80.4	45.2	44
F_{10mm}	31.4	27.0	14	49.1	35.3	28	70.8	33.4	53

From these results, on the one hand, it can be highlighted that the MAP tends to overestimate the cracking capacity of the pipe. This can be attributed to the magnitude considered for the flexural tensile strength of the concrete matrix ($f_{ct,fl}$), which magnitude might present variability up to 10-15% as well as to the geometric (diameter and thickness) tolerances of the pipe. On the other hand, it can be remarked that the model is capable to reproduce, from the safe side, the post-cracking tendency. Nonetheless, the numerical simulation for the pipe with 30 kg/m^3 should be reconsidered taking into account the differences obtained (which can lead to conservative designs). This lower performance can be directly attributed to the dispersion of the fibre amount measured in BCN specimens as mentioned above.

4 Concluding remarks

The results obtained in this experimental study clearly demonstrated that the use of a closed loop control system led to higher mechanical performance than the open system. These were already observed in historical evaluations of the flexural beam tests. On one hand, it is possible to state that the traditional open system regularly used to control the structural behaviour of the SFRCP is in the safety side, this underestimating the residual strength capacity of the components. The crack load was not influenced by the test set up as expected. On the other hand, these findings indicate that there is an interesting margin of optimization for fibre reinforcement design once the main contribution of fibres is related to the post-crack strength of the SFRCP.

It should be emphasized that this reinforcement optimization must be supported by adequate technological support, both in terms of quality control and in terms of modelling so that the reliability of the industrial production of these elements. The production of components in an industrial scale allows a control that could lead to a maximization of the mechanical performance (by reducing the scatter) and, as a result, to optimize the economic benefits.

The use of the model MAP in combination with the Barcelona test results allows reproducing, from the safe side, the post-cracking tendency. This approach can be seen as a strategy for designing fibre reinforced concrete pipes by avoiding the extensive and costly experimental programs based on trial and error (de la Fuente et al., 2012; de la Fuente et al., 2013).

This document is the intellectual property of the fib – International Federation for Structural Concrete. All rights reserved.
This PDF of fib Bulletin 95 is intended for use and/or distribution solely within fib National Member Groups.

5 Acknowledgements

The authors with to thank Fundação de Amparo a Pesquisa do Estado de São Paulo (FAPESP) for the economic support for this research (Projects Number 2013/03260-3, 2014/24410 and 2018/10065-6). The authors also thanks to Alírio Gimenez and all the crew of Fermix Indústria e Comércio Ltda for providing materials and fabrication of all pipes used in this study.

6 References

Abolmaali, A., Mikhaylova, A., Wilson, A. and Lundy, J., "Performance of Steel Fiber-Reinforced Concrete Pipes", Transportation Research Record: Journal of the Transportation Research Board, v. 2313, n. 1, 2012, pp. 168-177.

ASTM C497 (2018), "Standard Test Methods for Concrete Pipe, Manhole Sections or Tile." American Society for Testing and Materials, ASTM International, West Conshohocken, PA.

Banthia, N., Dubey, A., "Measurement of flexural toughness of fiber-reinforced concrete using a novel technique – Part 1: Assessment and Calibration", ACI Materials Journal, v. 96, n. 6, 1999, pp. 651-656.

Cavalaro, S., López, R., Torrents, J. and Aguado, A., "Improved assessment of fiber content and orientation with inductive method in SFRC", Materials and Structures, v. 48, n. 6, 2015, pp. 1859-1873.

de la Fuente A, Figueiredo A, Aguado A, Molins C, Chama Neto P J., "Experimentation and numerical simulation of steel fibre reinforced concrete pipes", Materiales de Construccion, v. 61, n. 302, 2011, pp. 239–56.

de la Fuente, A., Escariz, R. C., de Figueiredo, A. D., Molins, C. and Aguado A., "A new design method for steel fiber reinforced concrete pipes", Construction and buildings materials, v. 30, 2012, pp. 547-55.

de la Fuente, A., Escariz, R. C., de Figueiredo, A. D. and Aguado, A., "Design of macro – synthetic fiber reinforced concrete pipes", Construction and Building Materials, v. 43, 2013, pp. 523 – 532.

EN 1916 (2002). "Concrete pipes and fittings, unreinforced, steel fiber and reinforced"; 2002.

Fédération Internationale du Béton – FIB, "*fib* Model Code for Concrete Structures 2010", Switzerland, 2013. 402p.

Figueiredo A., "Evaluation of the test method for crushing strength of steel fiber reinforced concrete pipes", Proceedings of the 7th international RILEM symposium on fiber reinforced concrete (BEFIB 2008), Chennai, India, 2008.

Figueiredo, A. D, de la Fuente, A., Molins, C. and Aguado, A, "A new approach on crushing strength test for fiber reinforced concrete pipes" Proceedings of the 8th RILEM International Symposium on Fiber Reinforced Concrete, Guimarães, Portugal, 2012.

Gettu, R., Mobasher, B., Carmona, S., Jansen, D.C. "Testing of concrete under closed-loop control", Advanced Cement Based Materials, v. 3, n. 2, Mar. 1996, pp. 54-71.

Gopalaratnam, V. S., Gettu, R., "On the characterization of flexural toughness in fiber reinforced concretes", Cement and Concrete Composites, v. 17, n.3, 1995, pp. 239-254.

Gupta, R. and Banthia, N., "Effect of Open-Loop or Closed-Loop Deflection Control on Measured Toughness of FRC," Report No. SP248-6, ACI, Farmington Hills, Michigan, 2007, pp. 67–82.

This document is the intellectual property of the fib – International Federation for Structural Concrete. All rights reserved.
This PDF of fib Bulletin 95 is intended for use and/or distribution solely within fib National Member Groups.

Haktanir, T., Ari, K., Altun, F., Karahan, O., "A comparative experimental investigation of concrete, reinforced-concrete and steel-concrete pipes under three-edge-bearing test", Construction and Building Materials, v. 21, n. 8, 2007, pp. 1702–1708.

Monte, R., de La Fuente, A., Figueiredo, A., Aguado, A., "Barcelona test as an alternative method to control and design fiber-reinforced concrete pipes", ACI Structural Journal, v. 113, n. 6, 2016, pp. 1175-1184.

NBR 8890: Tubo de concreto de seção circular para águas pluviais e esgotos sanitários - requisitos e métodos de ensaio. Rio de Janeiro, 2018. 35p. (in Portuguese)

Park, Y., Abolmaali, A., Mohammadagha, M., Lee, S., "Structural performance of dry-cast rubberized concrete pipes with steel and synthetic fibers" Construction and Building Materials, v. 77, Feb. 2015, pp. 218–226.

Pujadas P, Blanco A, Cavalaro S, de la Fuente A, Aguado A., "New analytical model to generalize the Barcelona test using axial displacement. Journal of Civil Engineering Management, v. 19, n. 2, 2013, pp. 259–271.

UNE 83515 (2010), "Hormigones con fibras. Determinación de la resistencia a fisuración, tenacidad y resistencia residual a tracción. Método Barcelona", Asociación Española de Normalización y Certificación Madrid.

This document is the intellectual property of the fib – International Federation for Structural Concrete. All rights reserved.
This PDF of fib Bulletin 95 is intended for use and/or distribution solely within fib National Member Groups.
FRC2018: Fibre Reinforced Concrete: from Design to Structural Applications
Joint ACI-*fib*-RILEM International Workshop

Effect of synthetic fibers on the quasi-static and blast behaviour of reinforced concrete beams

Hassan Aoude[1], Yang Li[2], Roukaya Bastami[2] and Fawwaz Munir Ibrahim[3]

[1] : Associate Professor, University of Ottawa, Ottawa, Canada.

[2] : Graduate student, University of Ottawa, Ottawa, Canada.

[3] : Undergraduate student, University of Ottawa, Ottawa, Canada.

Abstract

This paper presents the results of a study examining the effect of synthetic fibers on the flexural and shear behaviour of beams tested under quasi-static and blast loading. In total, ten beams built with normal-strength concrete and synthetic fibers are studied, with five specimens tested under quasi-static four-point bending and a companion set of five beams tested under simulated blast loads using a high-capacity shock-tube. Test parameters include the effect of concrete type (plain vs. fiber-reinforced concrete), fiber type (two types of macro-synthetic fibers) and transverse reinforcement (in plain and fiber-reinforced concrete beams). Under slowly applied loads, the provision of synthetic fibers is shown to improve the residual shear capacity of beams built without stirrups, while the combined use of synthetic fibers and stirrups is found to improve flexural ductility. The effect of synthetic fibers on blast capacity is examined by comparing the mid-span displacements, failure modes and damage of beams tested under gradually increasing blast pressures. The results show that the use of synthetic fibers increases the blast capacity of beams built without transverse reinforcement, delaying shear failure. When combined with stirrups the use of synthetic fibers is shown to enhance damage tolerance and allow for better control of residual mid-span displacements at equivalent blasts.

Keywords

Blast, Shock-tube, FRC, SNFRC, Synthetic fibers, Shear, Flexure, Extreme loads.

This document is the intellectual property of the fib – International Federation for Structural Concrete. All rights reserved.
This PDF of fib Bulletin 95 is intended for use and/or distribution solely within fib National Member Groups.

1 Introduction

The addition of fibers to concrete results in several enhancements in its properties, including improved tensile resistance, toughness and ductility (Di Prisco et al. 2009). These improvements result from the ability of the randomly orientated fibers to arrest and redistribute cracking. Recently, there has been increased interest in the potential of using synthetic fiber reinforced concrete (SnFRC) in structural applications. Synthetic fibers can be varied in their composition (e.g. polyethene (PE), polypropylene (PP), polyvinyl alcohol (PVA), polyester (PES), nylon), geometry and physical characteristics (Zheng & Feldman, 1995). Macro-synthetic fibers, which are larger and coarser than traditional micro-synthetic fibers, can provide concrete with similar toughness and resistance to steel fibers and light gage steel reinforcement (Mahoney, 2005). In beams, researchers have shown that the use of macro-synthetic fibers can improve shear response and enhance ductility (Altoubat et al., 2009). The improved toughness and fragmentation resistance of SnFRC may also make it suitable to increase the damage tolerance of reinforced concrete members subjected to impact and blast loads (Coughlin et al., 2010; Richardson et al., 2016), however there is a need for further research to examine the potential benefits of using synthetic fibers in such extreme load applications.

This paper presents the results of a study examining the effects of macro-synthetic fibers on the flexural and shear behavior of beams subjected to blast loads. A total of ten reinforced concrete beams are studied, including five specimens which are tested under slowly applied four-point bending and a companion set of five beams tested under simulated blast pressures using a high-capacity shock-tube at the University of Ottawa. Test parameters include the effect of concrete type (plain vs. fiber-reinforced concrete), fiber type (two types of macro-synthetic fibers) and transverse reinforcement (in plain and fiber-reinforced concrete beams). The effect of synthetic fibers on blast capacity is examined by comparing the displacements, failure modes and damage of beams tested under gradually increasing blast pressures.

2 Experimental program

2.1 Specimen designs

Table 1 summarizes the properties of the ten reinforced concrete beams which were built and tested in this research. Five beams were tested under dynamic blast loading (D), with five companion specimens tested under quasi-static conditions (S). Among the five beam types, two were designated as control specimens with no fibers, with the remaining three beam types built with fiber-reinforced concrete (FRC) containing synthetic fibers. The control beams were cast with plain self-consolidating concrete (SCC), while FRC beams were cast with the same SCC mix and two types of macro-synthetic fibers, designated as S1 and S2, added at volume fractions (V_f) of 0.75% or 1%, respectively (6.75 and 9 kg/m^3). As shown in Figure 1, the beams had cross-sectional dimensions of 125 mm x 250 mm, a total length of 2440 mm and were simply supported over a span of 2232 mm. Longitudinal reinforcement consisted of 2-15M bars (A = 200 mm^2, d_b = 16 mm). For both the plain SCC and FRC beams, one set of specimens was detailed without transverse reinforcement to study shear response. The remaining specimens built with transverse reinforcement consisting of U-shaped stirrups made from 6.3 mm wire, spaced at 100 mm in the shear spans, to promote flexure failure. Two top 6.3 mm wires were also provided in the shear spans of all beams to facilitate construction. The specimen nomenclature reflects the test variables which include concrete type (plain SCC or FRC), fiber

This document is the intellectual property of the fib – International Federation for Structural Concrete. All rights reserved.
This PDF of fib Bulletin 95 is intended for use and/or distribution solely within fib National Member Groups.

type (S1 or S2), fiber content (0%, 0.75% or 1%) and shear reinforcement details ("100" for beams having stirrups spaced at 100 mm, and "0" for beams without stirrups).

Table 1: Beam test matrix

Series	Specimen Designation	Concrete Strength [MPa]	Fiber Type	Fiber content [%]	Stirrup spacing [mm]	Long. steel	Test type
Control	SCC-0%-0	48	-	-	-	2-15M	S/D
	SCC-0%-100	48	-	-	100	2-15M	S/D
FRC	FRC-0.75%(S1)-0	50	S1	0.75	-	2-15M	S/D
	FRC-0.75%(S1)-100	50	S1	0.75	100	2-15M	S/D
	FRC-1%(S2)-0	44	S2	1.0	-	2-15M	S/D

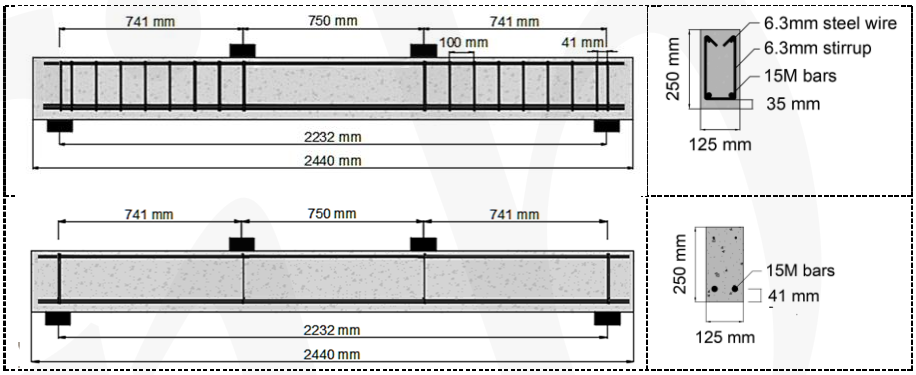


Figure 1: Dimensions and reinforcement for beams with & without shear reinforcement.

2.2 Materials

The SCC used in all specimens consisted of a pre-packaged mix with a specified strength of 40 MPa. The mix contained a maximum aggregate size of 10 mm with a sand-to-aggregate ratio of approximately 0.45 and a water-cement ratio of approximately 0.42. An air-entraining admixture, a super-plasticizer and a viscosity-modifying admixture (VMA) were incorporated into the blend in the form of dry powder. Two types of macro-synthetic fibers were considered in this study (see Figure 2f). The S1 fiber is a polypropylene/polyethylene blend macro-synthetic fiber which had a length of 50 mm, cross-section of 0.37 mm x 1.1 mm (aspect-ratio of 74), tensile strength of 625 MPa and partially fibrillate when mixed in concrete. The S2 fiber is a polypropylene/polyethylene blend macro-synthetic fiber which had a length of 50 mm, aspect ratio of 64, with tensile strength of 400 MPa, and were gray in color, with a crimped shape. Figure 2e shows typical slump flow values of the plain SCC mix and FRC mix with 0.75% S1 fibers; it is noted that the FRC mix cannot be classified as self-compacting (due to the reduced slump flow diameter), however the use of the base SCC mix allowed for good workability with only minor vibration required during placement. The average properties of the SCC and FRC in terms of compressive strength, obtained by testing 100 x 200 mm cylinders, are summarized in Table 1 (sample stress-strain curves are shown in Figure 2a). It is noted that the 1% S2 mix shows a reduction in compressive strength due to a loss in mix uniformity at this high fiber dosage. Sample flexural test results obtained from testing 100 x 100 x 400 mm prisms in accordance with the ASTM C1609 Standard are shown in Figure 2b-c. Typical stress-strain curves for the strength 15M longitudinal steel and 6.3 mm wire are shown in Figure 2d.

This document is the intellectual property of the fib – International Federation for Structural Concrete. All rights reserved.
This PDF of fib Bulletin 95 is intended for use and/or distribution solely within fib National Member Groups.

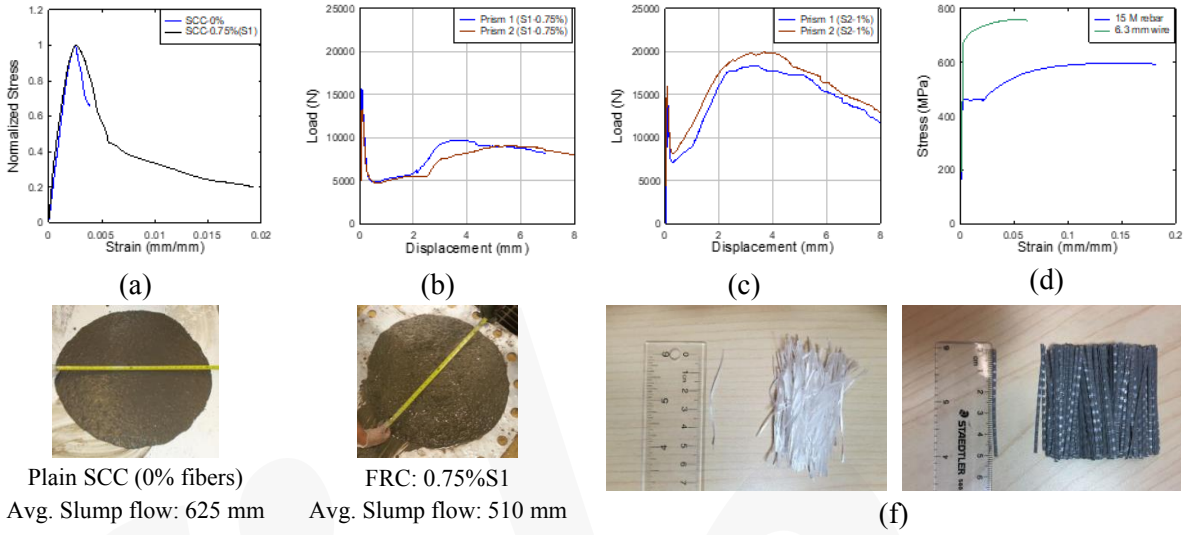


Figure 2: (a)Sample stress-strain curves in compression; (b) sample flexural prism test results (S1 fiber); (c) sample flexural prism test results (S2 fiber); (d) sample stress-strain curve for steel reinforcement in tension; (e) slump flow results (plain SCC and FRC containing 0.75% S1 fibers); (f) photos of fibers S1 and S2.

2.3 Test setup

The static series beams were tested under four-point bending using the setup shown in Figure 3d. The beams were simply supported over a span of 2232 mmm, with a constant moment region of 750 mm and two equal shear-spans of 741 mm. Loading was applied using a manually operated hydraulic jack with the load transferred to the specimens as two-point loads using a steel spreader beam. The load was recorded using two load-cells at the supports, with displacement at mid-span captured using a cable displacement transducer. Strains in the reinforcing bars were monitored using strain-gages which were applied to the tension steel at mid-span. Loading of the beams began under load-control until signs of shear failure or yielding were detected. Upon yielding or shear capacity, loading continued under displacement-control until failure (concrete crushing or shear failure).

Blast testing was conducted using the shock-tube facility at the University of Ottawa. As shown in Figure 3a, the shock-tube consists of four main components: (1) a variable length driver section, (2) a spool section, (3) an expansion section and (4) a rigid end test frame. The driver section generates the blast energy, while the firing of the shockwave is controlled using the spool section. The rigid end test frame has a 2m x 2m square opening where test specimens can be attached. A load transfer device (LTD) was used to collect the shockwave pressure at the shock-tube opening and redirect it onto the test specimens. The LTD resulted in the application of blast loading under four-point bending which closely matched the loading configuration used in static testing. Figure 3b shows a typical beam prior to testing along with the blast test setup. Complete displacement-time histories were recorded using two linear variable differential transducers (LVDT) placed at 1/2 (mid-height) and 1/3rd span of the beam. A high-speed camera was placed at the side of the beams during testing and recorded response at a frame rate of 500 frames per second. Testing of the beams was conducted under gradually increasing blast pressures until failure. The driver length was kept constant at 6 ft (1830 mm) for all tests, with the driver pressure (P_d) gradually increased from 20 psi (138 kPa) to 80 psi

This document is the intellectual property of the fib – International Federation for Structural Concrete. All rights reserved.
This PDF of fib Bulletin 95 is intended for use and/or distribution solely within fib National Member Groups.

(552 kPa). Blast 1 (P_d = 20 psi) was meant to test the specimens under elastic conditions, while Blast 2 (P_d = 40 psi) was meant to induce shear failure or bring the steel reinforcement in the beams close to yielding. Blasts 3 and 4 (P_d = 60 and 80 psi) were applied to cause damage and failure in those specimens which reached flexural capacity. It is noted that an intermediate blast corresponding to Blast 2B (P_d = 50 psi)) was also applied in the case of specimen FRC-0.75%(S1)-0. Examples of the resulting shockwaves for Blasts 1 to Blast 4 are shown in Figure 3c. Shockwave properties in terms of peak reflected pressure (P_r), positive phase duration (t_d) and reflected impulse (I_r), representing the area under the positive phase of the pressure-time history, are also summarized in Table 3.

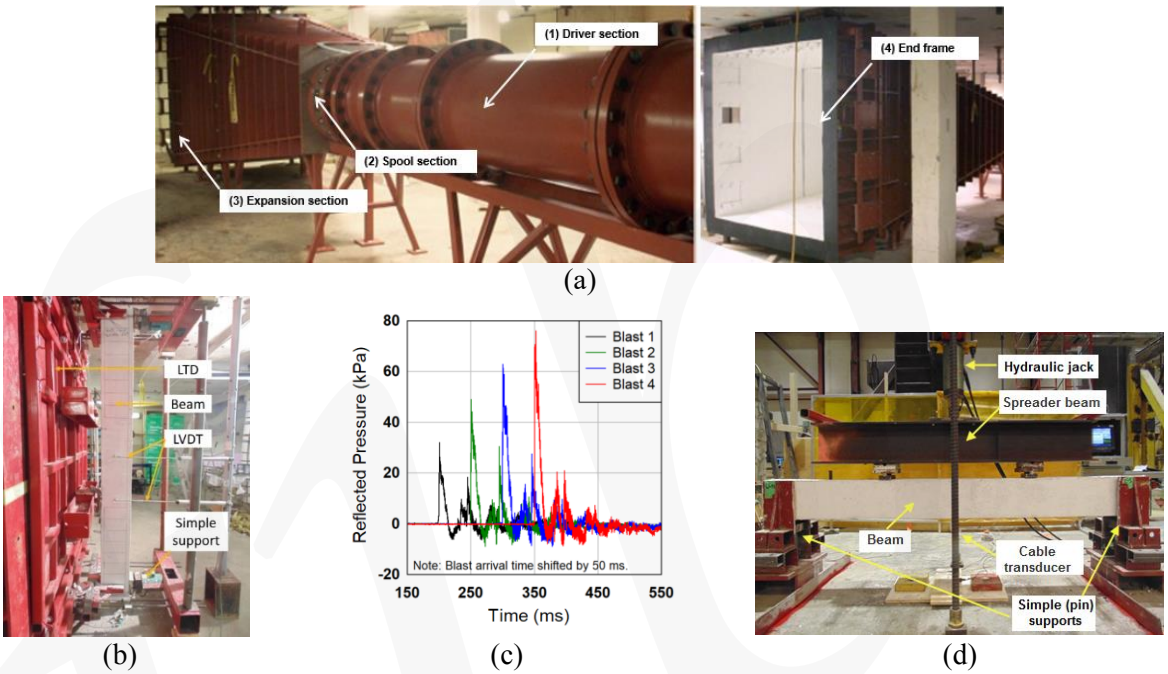


Figure 3: (a) Shock-tube, (b) blast setup, (c) sample shockwaves and (d) static setup

3 Results

3.1 Summary of results

The responses of the specimens which were tested under quasi-static loading are plotted in Figure 4. Table 2 summarizes key data extracted from the load-deflection curves, including yield load (P_y) and maximum load (P_{max}), yield displacement (Δ_y) and maximum displacement (Δ_{max}), beam stiffness after cracking, ductility (Δ_{max}/Δ_y) and toughness (area under the load-deflection curve until Δ_{max}). The maximum displacement is the point where the load drops to 85% P_{max}. Photos of the beams at the end of testing are shown in Figure 5. Table 3 summarizes the results for the beam specimens which were tested under blast loading, including the shockwaves properties for each test (P_r, I_r, t_d) as well as beam response in terms of maximum (D_{max}) and residual (D_{res}) mid-span displacements. A summary of post-blast photos showing failure modes is presented in Figure 6. The effects of synthetic fibers on shear and flexural response under static and blast loads are discussed in the sections that follow.

This document is the intellectual property of the fib – International Federation for Structural Concrete. All rights reserved.
This PDF of fib Bulletin 95 is intended for use and/or distribution solely within fib National Member Groups.

Table 2: Quasi-static test results

Beam ID	Load [kN]		Displacement [mm]			Stiffness [N/mm]	Ductility $\left(\frac{\Delta_{max}}{\Delta_y}\right)$	Toughness [kN·mm]
	Yield P_y	Max. P_{max}	Yield Δ_y	Max. Δ_{max}	End of test Δ_{end}			
SCC-0%-0	-	88.1	-	-	15.1	6870	-	758
SCC-0%-100	90.4	101.3	13.2	44.0	60.0	6873	3.33	4716
FRC-0.75%(S1)-0	-	85.7	-	18.1	36.4	6047	-	1529
FRC-1%(S2)-0	-	81.7	-	21.3	40.0	7429	-	2061
FRC-0.75%(S1)-100	91.3	99.0	12.3	44.4	70.0	7423	3.61	5683

* Δ_{max} = displacement at 85% drop in maximum load; Δ_{end} = displacement at end of testing.

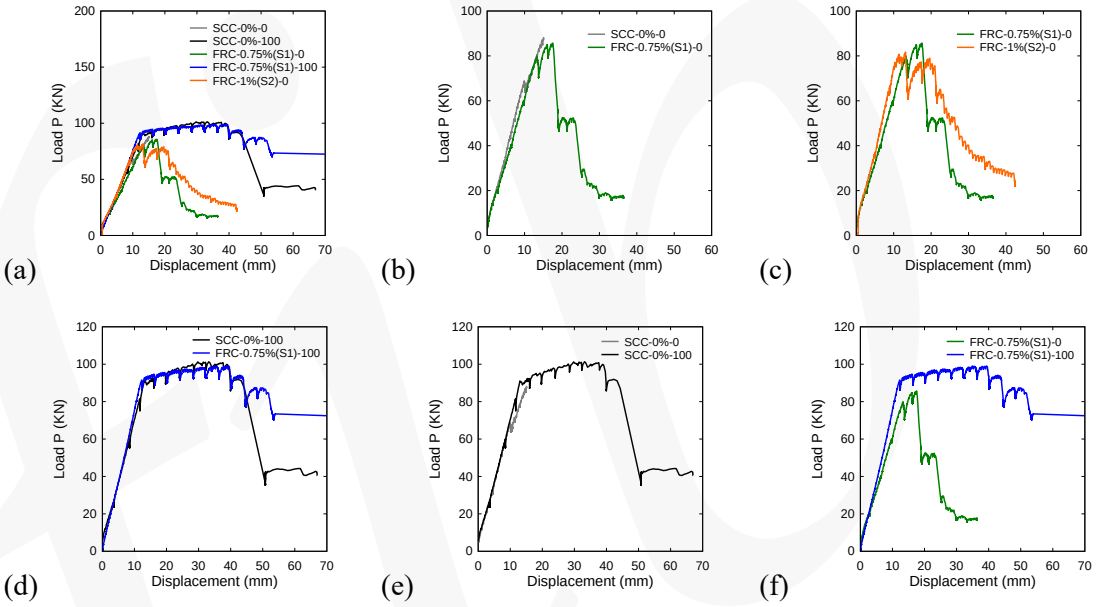


Figure 4: Static load-deflection curves: (a) all beams; (b) effect of fiber S1 on shear response; (c) effect of fiber type on shear response; (d) effect on fiber S1 on flexural response; (e) effect of stirrups in control beams;(f) effect of stirrups in FRC beams.

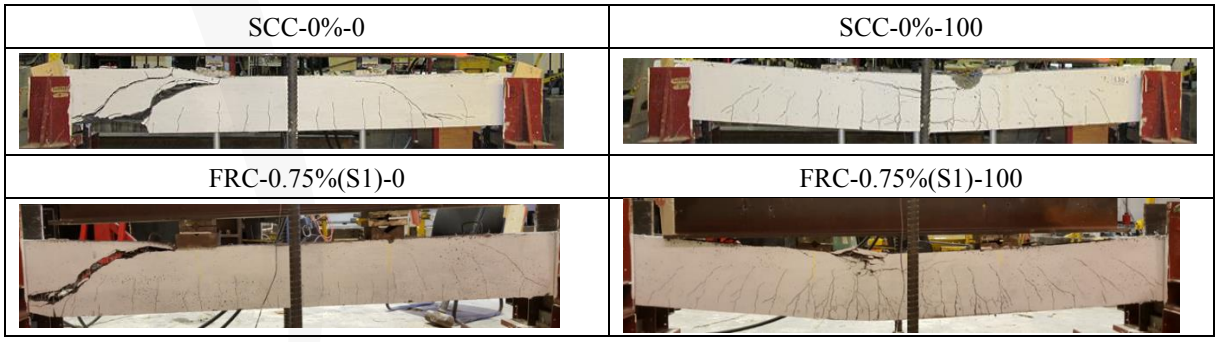


Figure 5: Photos of beams at end of quasi-static testing

This document is the intellectual property of the fib – International Federation for Structural Concrete. All rights reserved.
This PDF of fib Bulletin 95 is intended for use and/or distribution solely within fib National Member Groups.

Table 3: Shockwave properties and summary of blast test results

Series	Beam ID	Blast #	Shockwave Properties			Maximum Disp.	Residual Disp.	Failure mode
			P_r (kPa)	I_r (kPa·ms)	t_d (ms)	D_{max} (mm)	D_{res} (mm)	
Control Series	SCC-0%-0	1	29.6	196.8	13.3	11.7	1.1	Shear
		2	46.7	327.7	14.0	23.3	11.7	
	SCC-0%-100	1	30.7	185.6	12.1	11.5	0.8	Flexure
		2	49.3	328.6	13.3	23.3	3.5	
		3	65.2	458.9	14.1	41.7	19.5	
		4	71.8	544.2	15.1	84.2	55.2	
FRC Series	FRC-0.75%(S1)-0	1	30.7	179.6	11.7	10.8	1.9	Shear
		2	49.9	357.6	14.3	20.8	0.2	
		3	68.3	447.5	13.1	41.1	12.3	
	FRC-0.75%(S1)-100	1	32.2	235.8	14.6	11.7	0.0	Flexure
		2	49.2	323.9	13.2	23.1	4.7	
		3	63.1	449.2	14.2	37.0	9.7	
		4	76.1	512.8	13.5	81.0	36.6	
	FRC-1%(S2)-0	1	29.6	196.7	13.3	12.5	1.5	Shear
		2	47.2	350.0	14.8	21.7	10.5	
		3	63.2	470.8	14.9	54.9	37.0	

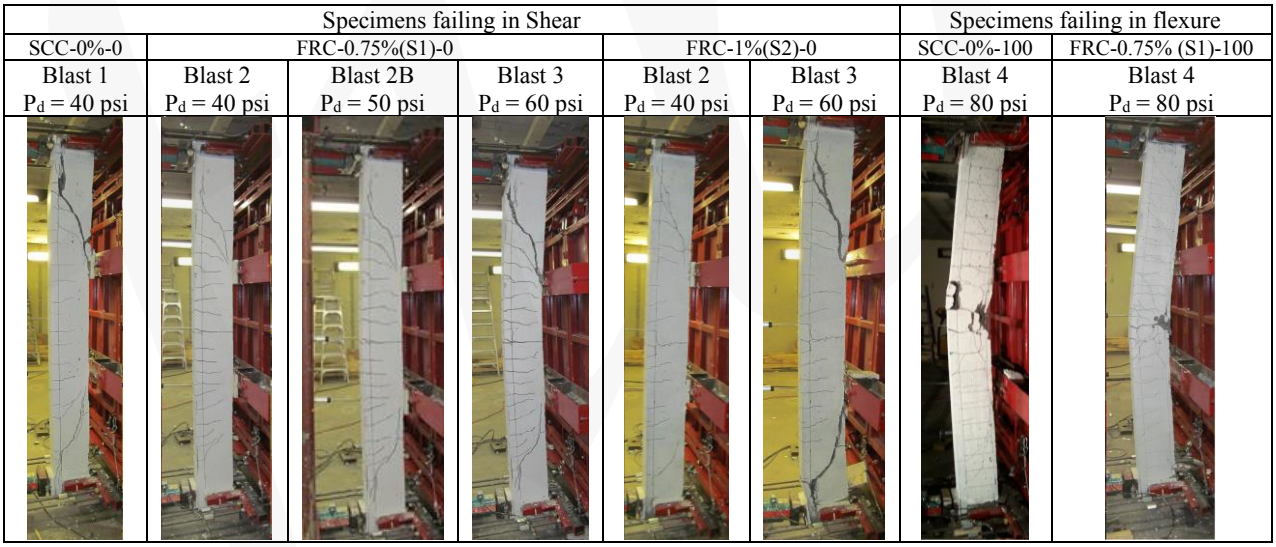


Figure 6: Progression of damage in beams tested under blast loading

3.2 Effect of synthetic fibers on shear response

Comparison between the behaviour of beams SCC-0%-0, FRC-0.75%(S1)-0, and FRC-1%(S2)-0 allows for an investigation into the effect of macro-synthetic fibers on shear resistance under static and dynamic blast loading conditions. All beams in this set were built without transverse reinforcement, with the first beam type built with plain SCC and the remaining two beams types built with FRC having 0.75% S1 and 1% S2 fibers, respectively. As seen in Figure 5 all three beams failed in shear under quasi-static loading. An examination of the results in Table 2 and Figure 4b shows that the use of synthetic fibers did not lead to an increase in shear capacity, however it improved ductility, allowing the FRC beams to carry load after peak, leading to a more gradual failure. In the control beam, the failure is brittle and occurs

This document is the intellectual property of the fib – International Federation for Structural Concrete. All rights reserved.
This PDF of fib Bulletin 95 is intended for use and/or distribution solely within fib National Member Groups.

suddenly after the formation of the first diagonal shear crack, which leads to beam collapse. In the case of the FRC beams, the failure is relatively more ductile as the fibers pullout across the critical shear crack (see sequence of failure in Figure 7). For example, the major shear crack in beam FRC-0.75%(S1)-0 was first observed at a mid-span displacement (Δ) of 16 mm, with the beam finally failing at Δ = 36 mm as the fibers gradually pulled-out at the critical shear crack. As a result, beams FRC-0.75%(S1)-0 and FRC-0.75%(S2)-0 show significantly larger toughness (area under the load-deflection curve) when compared to beam SCC-0%-0 (see Table 2). In terms of the effect of fiber type (see Figure 4c), both beams show similar response, with greater toughness recorded for the beam with S2 fibers, although this may be due to the use of 1% S2 vs. 0.75% S1 fibers; future tests should consider the same fiber dosage.

Under blast loading, the three companion beams failed in shear, but at different blast intensities (see Figure 6). The control beam (SCC-0%-0) failed at Blast 2 (Impulse, I_r = 330 kPa-ms), while beams reinforced with 0.75% of fiber S1 and 1% of fiber S2 survived this shot, and failed at Blast 3 (I_r = 450 and 470 kPa-ms, respectively). Examination of the displacement data shows that the three beams have similar maximum displacements at Blast 1, which is expected since the beams have similar stiffness. Due to the shear failure, the control beam shows a larger maximum displacement when compared to its FRC companions at Blast 2 (see Figure 8a). No significant difference is observed in terms of the effect of fiber type on blast performance. At blast 2 the two FRC beams show similar maximum displacements, although the beam with S1 fibers shows reduced residual displacement.

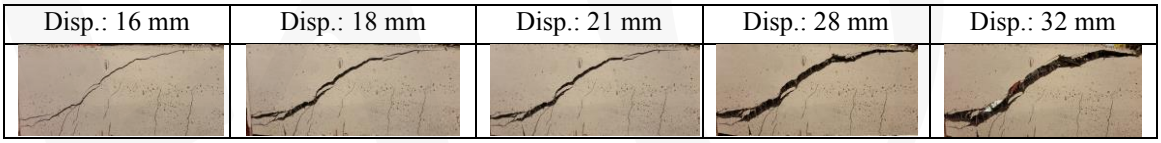


Figure 7: Sequence of shear failure in beam FRC-0.75%(S1)-0 with gradual fiber pullout

3.3 Effect of synthetic fibers on flexural response

The effect of synthetic fibers on flexural response under static and dynamic loading can be examined by comparing the behaviour of beams SCC-0%-100 and FRC-0.75%(S1)-100. Both beam types were reinforced with stirrups, with the first beam built with plain SCC and the second beam built with FRC and 0.75% of S1 fibers. The static load-deflection response of the beams is shown in Figure 4d where it can be seen that the use synthetic fibers does not lead to a significant effect on strength and stiffness. However, the use of fibers delays crushing of concrete in compression and therefore leads to an improvement in beam ductility (Δ_{max}/Δ_y = 3.6 vs. 3.3) and overall toughness (5683 vs. 4716 KN*mm). Crack widths are also better controlled in the FRC specimen, which also shows a more diffused cracking pattern, with a greater number of cracks in the mid-span region, when compared to the control specimen (see Figure 9). Crushing is also noticeably better controlled.

Under blast loading the beams show similar response, failing in flexure at Blast 4, however the provision of fibers leads to improved control of displacements and increased damage tolerance. The two beams have similar displacements at Blast 1 and 2 levels, which were intended to test the beams within the yield range. This result also corresponds to static test result, were the SCC and FRC beams were found to have similar flexural stiffness. At Blast 3, the use of synthetic fibers reduced maximum displacement by 11%, with a one-fold (100%) decrease in residual displacement, when compared to control beam SCC-0%-100 (see Figure

This document is the intellectual property of the fib – International Federation for Structural Concrete. All rights reserved.
This PDF of fib Bulletin 95 is intended for use and/or distribution solely within fib National Member Groups.

8b). At Blast 4, both beams failed with similar maximum displacement, however, the use of synthetic fibers significantly reduced residual displacement by 34% when compared to the control beam. The results from the blast series correspond to the observations made during static testing, where the use of fibers does not increase capacity but improves ductility. At failure, the control beam shows crushing in the compressive zone, with spalling of cover concrete in tension, leading to significant flying debris at failure. The use of fibers was found to better control crushing of concrete and eliminated spalling and secondary fragments, leading to improved damage tolerance (see Figure 9). Thus the use of fibers was effective in reducing secondary blast fragments which may pose a danger to building occupants.

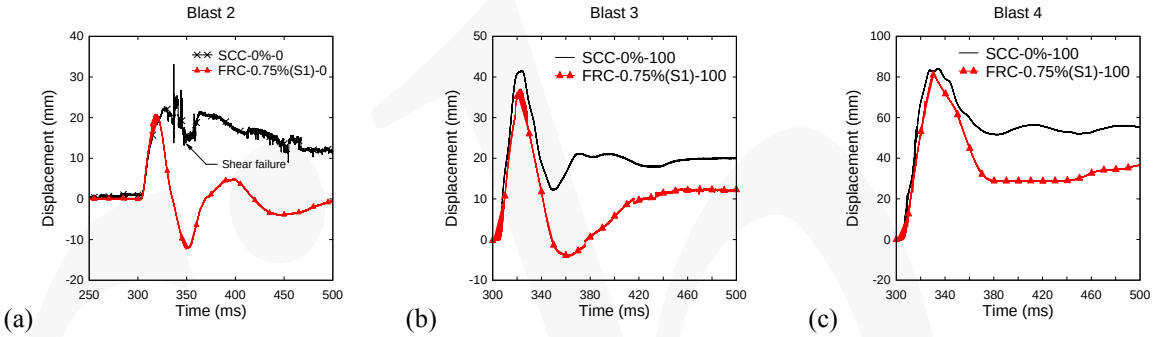


Figure 8: Comparison of displacement histories: control vs. FRC beams: (a) shear specimens at Blast 2, (b) flexural specimens at Blast 3 and (c) flexural specimens at Blast 4

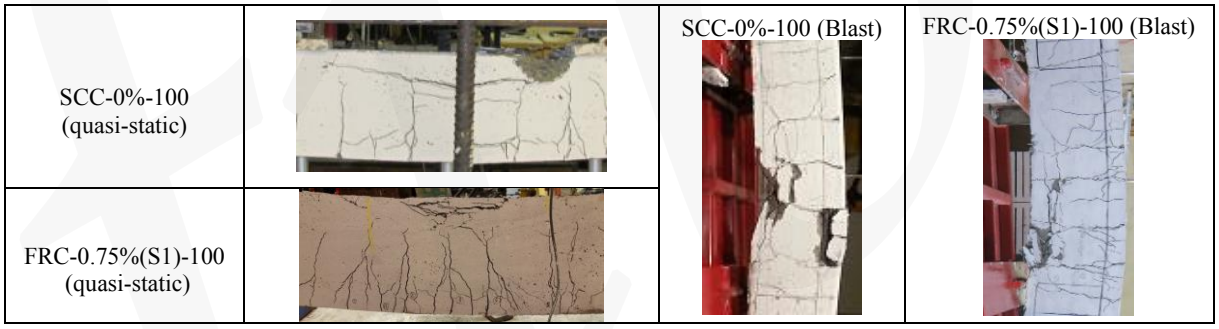


Figure 9: Damage in Control and FRC beams under static and blast loading

3.4 Effect of fibers on dynamic resistance

The use of load cells at the supports allowed for a measurement of the dynamic resistance of the beams during shock-tube testing. The static and dynamic load-deflection curves for beams SCC-0%-0 and FRC-0.75%(S1)-0 are presented in Figure 10a-b. Because the LTD has significant mass, the dynamic resistance was determined by considering the dynamic equilibrium of the entire beam-LTD system (support reactions, applied force and inertia forces) as outlined in Jacques and Saatcioglu (2020). As expected the beams show increased peak resistance under dynamic loading, with dynamic-to-static strength ratios of P_{max}^{D}/P_{max} = 1.50 and 1.80, respectively. Figure 10c compares the dynamic resistance curves of the two beams; it can be observed that both beams show similar stiffness, however larger peak resistance and toughness (area under dynamic curve) are recorded for beam FRC-0.75%(S1)-0, which further confirms the improved blast performance of the beam with 0.75%S1 fibers.

This document is the intellectual property of the fib – International Federation for Structural Concrete. All rights reserved.
This PDF of fib Bulletin 95 is intended for use and/or distribution solely within fib National Member Groups.

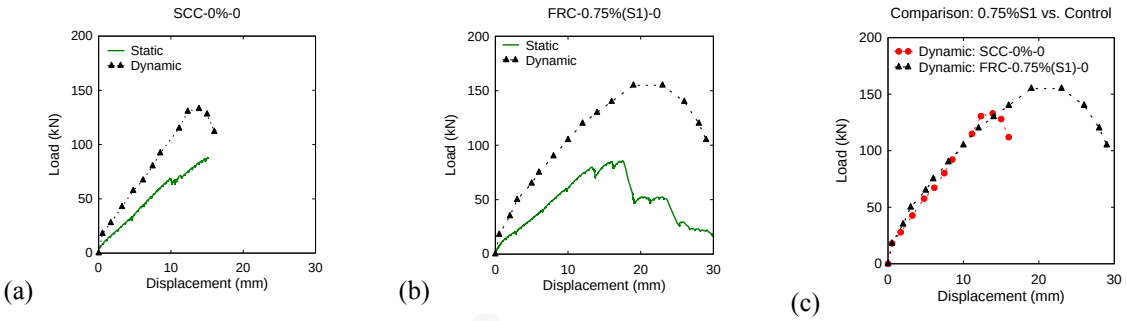


Figure 10: Dynamic resistances: (a) SCC-0%-0, (b) FRC-0.75%S1-0, (c) comparison

4 Conclusion

This paper examined the effect of macro-synthetic fibers on the shear and flexural behavior of ten reinforced concrete beams which were tested under quasi-static and blast loading. The following conclusions can be drawn from this study:

- The results indicate that while use of synthetic fibers improves shear behaviour (under both static and blast loading), it is not sufficient to replace transverse reinforcement in beams subjected to blast loads. The sudden shear failures in both the plain and FRC beams also indicates the importance of providing sufficient transverse reinforcement detailing in beams designed for blast effects;
- In beams detailed with sufficient shear reinforcement, the use of synthetic fibers was effective in improving ductility under static loads, and in controlling residual displacements and increasing damage tolerance under blast loads. The use of fibers was also effective in reducing secondary blast fragments which may pose a danger to building occupants.
- Based on this research, further studies examining the synergy between synthetic fibers and transverse reinforcement on the blast behaviour of beams is recommended.
- The beams in this study were tested under simulated blast loads using a shock-tube. Since the LTD has significant mass it can result in inertial effects which can affect dynamic response; this point should be considered when interpreting the test results.

5 References

Altoubat, S., Yazdanbakhsh, A., & Rieder, K.-A. (2009). *Shear behavior of macro-synthetic fiber-reinforced concrete beams without stirrups*, ACI Materials Journal, 106(4), 381-389.

Coughlin, A., Musselman, E., Schokker, A., & Linzell, D. (2010), *Behavior of portable fiber reinforced concrete vehicle barriers subject to blasts from contact charges*, International Journal of Impact Engineering, 37(5), 521-529.

Di Prisco, M., Plizzari, G., & Vandewalle, L. (2009), *Fibre reinforced concrete: New design perspectives*. Materials and Structures, 42(9), 1261-1281.

Mahoney, M. (2005). *Structural synthetic fibres for precast and slab-on-grade construction*. Construction Canada, 3(2005), 1-6.

Richardson, A., Coventry, K., Lamb, T., & Mackenzie, D. (2016), *The addition of synthetic fibres to concrete to improve impact/ballistic toughness*, Construction and Building Materials, 121, 612-621.

Zheng, Z., & Feldman, D. (1995), *Synthetic fibre-reinforced concrete*. Progress in Polymer Science, 20(2), 185-210

Jacques, E. & Saatcioglu, M. (2020). *High-Strain-Rate Response of Reinforced Concrete Lap-Spliced Beams*. Journal of Structural Engineering, 146(1), p.04019165.

This document is the intellectual property of the fib – International Federation for Structural Concrete. All rights reserved.
This PDF of fib Bulletin 95 is intended for use and/or distribution solely within fib National Member Groups.
FRC2018: Fibre Reinforced Concrete: from Design to Structural Applications
Joint ACI-*fib*-RILEM International Workshop

Strain-based fatigue failure criterion for steel-fiber reinforced concrete

E. Poveda[1], G. Ruiz[1], H. Cifuentes[2], R.C. Yu[1] and X.X. Zhang[1]

[1] : ETSI Caminos, C. y P., Universidad de Castilla-La Mancha, Ciudad Real, Spain.

[2] : ETS de Ingeniería, Universidad de Sevilla, Seville, Spain.

Abstract

This work proposes a new strain-based failure criterion for compression fatigue in steel-fiber reinforced concrete. It is based on the Spark and Menzies' relationship between the logarithm of the secondary strain rate per cycle and the specimen life expressed as the logarithm of the number of cycles until failure. This relationship permits calculating the critical strain at the failure of the specimen as the sum of two terms. The first one is the maximum strain in the first cycle due to the maximum compression stress. The second term is the increase of strain due to the remaining cycles until failure. Thus, failure occurs when the strain reaches a critical level during fatigue loading. On the contrary, the material continues resisting while its accumulated strain is lower than the critical one. This criterion is validated against a series of low-cycle fatigue tests in five types of concrete with different amounts of fiber that share the same concrete matrix. Besides, the experimental results show that the fibers delay the deformation and deterioration processes caused by fatigue. They also show that there is an optimum fiber content that maximizes fatigue life.

Keywords

Secondary strain rate, steel-fiber reinforced concrete, fibers, compression fatigue.

This document is the intellectual property of the fib – International Federation for Structural Concrete. All rights reserved.
This PDF of fib Bulletin 95 is intended for use and/or distribution solely within fib National Member Groups.

1 Introduction

Fiber-reinforced concrete (FRC) is a compound material in which fibers are oriented and distributed randomly in the concrete matrix. Its benefits in tensile tests are sufficiently proven since fibers control the growth and propagation of cracks by the stitching effect. The fiber content is a determining factor in the behavior of FRC. Nevertheless, insofar as compression, there is no consensus in the experimental bibliography on the benefits of adding fibers [1-3], especially in fatigue. Moreover, the existing bibliography is scarce and involves a limited variety of compositions [4,5] or a very reduced number of tests [6-7]. It is important to emphasize that fatigue in concrete increases the dispersion of the number of cycles that the specimen can resist [4,8-10] and that fibers further increase this dispersion [5,9]. For that reason, to obtain a statistical distribution of the resisted cycles it is necessary to resort to a considerable number of tests [11].

One of the most important features to identify fatigue damage is the cyclic creep curve that represents the evolution of the maximum strain versus the number of cycles until failure. Identification may be made of its three parts. The intermediate part or secondary branch is characterized by a linear increase of strain versus the number of cycles. Its slope is referred to as the secondary strain rate per cycle [8,9,12]. This parameter permits predicting fatigue life since there is a noticeable relationship between the logarithm of the secondary strain rate and the logarithm of the number of cycles until failure [5,8,12]. To our knowledge, this relationship has not been used to develop any strain-based failure criteria so far. The most used failure criterion is based on stress and is represented by curves plotting the stress levels, S, versus the number of cycles until failure, N. Recently, Blasón *et al.* [13] fitted the experimental cyclic creep curves to a Weibull tri-parametric distribution of minima. They use a double normalization of the maximum strain and the number of cycles until failure, which may lead to more precise criteria for strain failure when adjusting the entire test curve despite their greater complexity.

The rest of the article is structured in the following manner: Section 2 presents a new strain-based failure criterion for FRC in compression fatigue. Section 3 presents the validation of the criterion. Firstly, the characteristics of the concrete used are reported and subsequently, the criterion is validated against the experimental results. Finally, in section 4 we summarize the research and draw some relevant conclusions.

Failure criterion

In this section, a new strain-based fatigue failure criterion for FRC is presented. It derives from the Spark and Menzies' relationship [12] between the secondary strain rate per cycle in compression fatigue, $\partial\varepsilon/\partial n$, and the life expressed as the number of cycles resisted by a specimen, N, that is to say:

$$\log (\partial\varepsilon/\partial n) = m + s \log N \quad (1)$$

where m and s are constants. Recently it has been shown that this relationship is independent of the content of fibers [9], thereby being a characteristic feature of the base concrete. From Equation 1 we obtain:

$$\partial\varepsilon/\partial n = 10^{m} N^{s} \quad (2)$$

This document is the intellectual property of the fib – International Federation for Structural Concrete. All rights reserved.
This PDF of fib Bulletin 95 is intended for use and/or distribution solely within fib National Member Groups.

Multiplying Equation 2 by the number of cycles until failure we obtain:

$$\varepsilon_2 = N\,\partial\varepsilon/\partial n = 10^m\,N^{s+1} \tag{3}$$

in which ε_2 is the increase of the strain as a consequence of the cyclical load and the associated creep that cause the failure. Taking the decimal logarithms in Equation 3:

$$\log \varepsilon_2 = m + (s+1)\log N \tag{4}$$

From this equation and a term corresponding to the maximum strain in the first cycle, a new failure criterion based on strain may be formulated. The critical strain in fatigue is equal to an initial instantaneous strain, ε_1, due to the level of maximum stress plus the increase of the strain at failure, which may be estimated with Equation 3. Subsequently, the equation expressing the failure criterion is:

$$\varepsilon_c = \varepsilon_1 + \varepsilon_2 = \varepsilon_1 + 10^m\,N^{s+1} \tag{5}$$

where ε_c is the critical strain of fatigue failure. The failure of the material occurs when the strain reaches ε_c during the fatigue loading. Conversely, the material continues resisting if the accumulated strain is lower than the critical one, $\varepsilon \leq \varepsilon_c$.

Validation of the model

To study the influence of the fiber content on fatigue behavior [9], five types of self-compacting concrete were designed and manufactured. We maintained the same concrete matrix in all of them but varied the fiber content. Table 1 indicates the dosage of the concrete matrix. The steel fiber used is a HE 55/35 of ArcelorMittal. It has a length of 35 mm, an aspect ratio of 64 and has hooked-ends (see Fig. 1). The fiber content varies among the five concretes from 0 to 45 kg/m^3 in increments of 15 kg/m^3, thereby each concrete being identified by an H followed by the fiber content in kg/m^3. Per each dosage, eight cylinders of 100 mm in diameter and 200 mm in height (for characterization purposes) and six prisms of 100 × 100 × 420 mm^3 (to obtain 100 mm-edge cubic specimens) were cast.



Figure 1: Steel fiber used.

This document is the intellectual property of the fib – International Federation for Structural Concrete. All rights reserved.
This PDF of fib Bulletin 95 is intended for use and/or distribution solely within fib National Member Groups.

Table 1: Dosage of the concrete matrix

Components	Dosage (kg/m^3)
CEM II/B-L 32.5 N	360
Coarse aggregate	530
Siliceous sand	200
Limestone sand	975
MasterGlenium SKY 886	6.4
Water	222

Table 2 shows the mechanical properties of the concretes: compressive strength on cylinders, f_c, elastic modulus, E, Poisson coefficient, v, density, ρ, and compressive strength on cubes, f_{cu}. Each cell in the table shows the mean value of six tests and the corresponding standard deviation (in brackets). The compressive tests were carried out following the recommendations of the ASTM C39 [14] loaded at a stress rate of 0.3 MPa/s in 100 × 200 mm^2 (diameter × height) cylinders. Note that the elastic modulus is a little low due to the high presence of limestone aggregate in the matrix (42% in weight according to Table 1). However, E is within the typical range of normal concretes (14-42 GPa).

Table 2: Mechanical properties of the concretes used [9]
—mean values and standard deviation (in brackets)—

	H00	H15	H30	H45	H60
f_c (MPa)	31.6 (0.7)	32.5 (0.3)	30.7 (0.7)	32.1 (1.1)	30.3 (0.3)
E (GPa)	18.5 (1.2)	19.4 (0.6)	18.5 (0.5)	18.3 (0.2)	19.0 (0.5)
v	0.17 (0.01)	0.17 (0.00)	0.18 (0.01)	0.16 (0.01)	0.18 (0.01)
ρ	2310 (30)	2310 (10)	2280 (20)	2300 (20)	2280 (10)
f_{cu} (MPa)	33.4 (0.8)	35.1 (0.8)	32.6 (1.1)	30.7 (0.9)	30.1 (1.6)

Fatigue tests

The fatigue tests were conducted on 100 mm-edged cubes, loaded in compression at a constant amplitude. To determine the limits of the stress cycles, the reference cube compressive strength of each concrete, f_{cu} (see Table 2), was measured at a stress rate of 0.3 MPa/s using 6 cubes per type of concrete. The fatigue parameters were determined based on the failure predictions of the Model Code [15] for 1000 cycles. The maximum and the minimum stress level for the fatigue test were $\sigma_{max} = 0.8\, f_{cu}$ and $\sigma_{min} = 0.24\, f_{cu}$, and the frequency was 1/25 Hz.

This document is the intellectual property of the fib – International Federation for Structural Concrete. All rights reserved.
This PDF of fib Bulletin 95 is intended for use and/or distribution solely within fib National Member Groups.

Results and Discussion

Figure 2 shows the logarithm of the number of cycles that the specimens resisted in the fatigue tests for each type of concrete. Moreover, Fig. 2a gives the Weibull fitting (in solid lines) of the failure probability for each concrete and Fig. 2b plots the average value of the logarithm of resisted cycles versus the fiber dosage. As can be observed, the fatigue behavior of fiber reinforced concrete is better than that of plain concrete, although it presents a greater dispersion in results. Observe that the longest life is not obtained with the greatest quantity of fibers, but rather with an intermediate fiber content (45 kg/m^3), which may be considered optimal for the combination between this base concrete and this type of fiber. Intermediate fiber contents (30 kg/m^3 and 45 kg/m^3) lead to better fatigue results than higher contents. We think that this is so because high fiber contents distort the matrix and generate voids or pores within it.

Figure 3a represents one of the cyclic creep curves in fatigue obtained in the tests, that is to say, the evolution of the maximum deformation of each cycle, ε, against the number of cycles (expressed as n/N, where n is the current cycle and N is the total number of resisted cycles). In this type of curves, three well-differentiated phases are observed. The first phase consists of fast deformation growth. The second phase reflects a linear increase of the strain versus the number of cycles until, finally, an abrupt increase of the strain occurs followed by the final collapse of the specimen (third phase). Besides, this figure graphically represents the value of ε_2. Note that this value remains on the safe side since the strain in the third phase and therefore, that which produces the specimen collapse, is greater than ε_2 plus the initial strain.

From the second segment of the cyclic creep curves, we obtain the secondary strain rate per cycle. Figure 3b represents the logarithm of the secondary strain rate per cycle versus the logarithm of the number of cycles resisted. As can be observed, all these points adjust very well to a single straight line that responds to Equation 1 with a regression coefficient of 0.97. Note that this relationship is independent of the fiber content and thus it only depends on the concrete matrix [9].

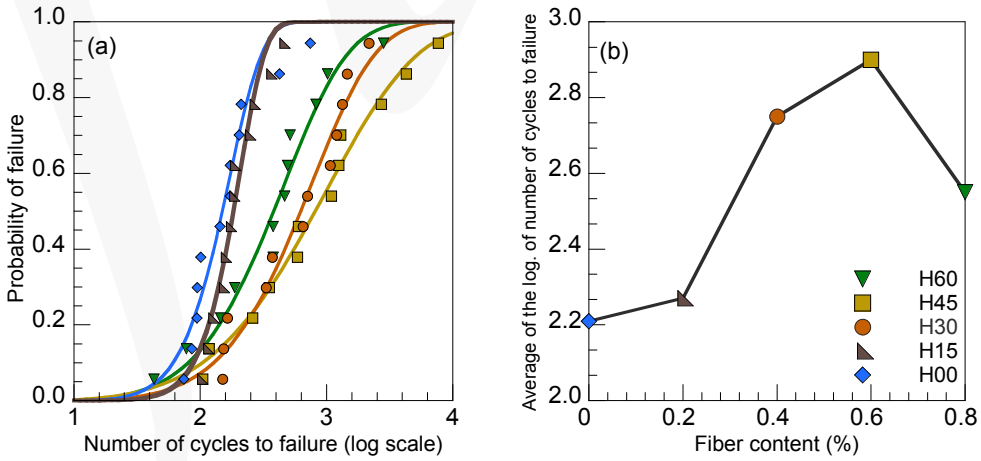


Figure 2: (a) Fatigue experimental results and Weibull fitting (in solid lines) and (b) average value of the logarithm of the number of cycles resisted in fatigue per batch

This document is the intellectual property of the fib – International Federation for Structural Concrete. All rights reserved.
This PDF of fib Bulletin 95 is intended for use and/or distribution solely within fib National Member Groups.

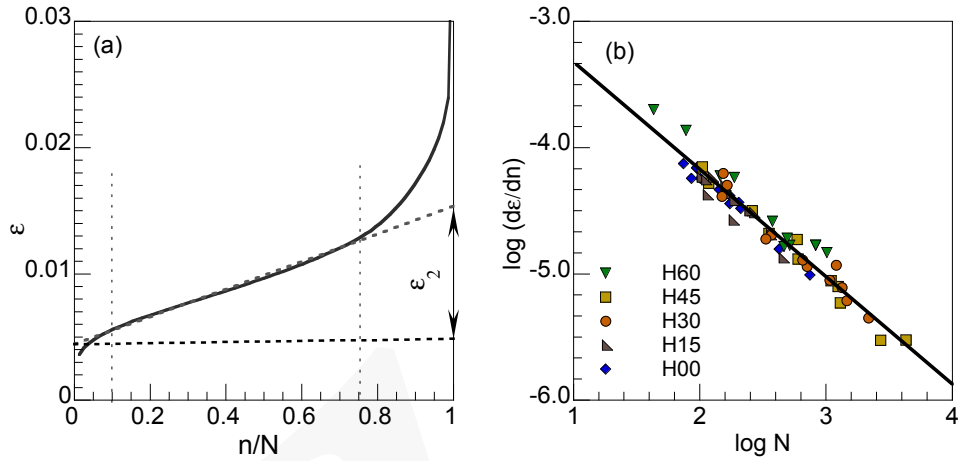


Figure 3: (a) Cyclic creep curve and (b) adjustment of regression in the experimental tests of the logarithm of the secondary strain rate with respect to the logarithm of the number of cycles

Extrapolating the failure criterion to $N = 1$ (which is a case similar to a monotonic test) we obtain that 10^m coincides approximately with the increase of the strain that would cause the failure of the specimen during the first cycle. This observation may be verified against our experimental results in the monotonic tests. Table 3 shows the maximum average strain during the first cycle of the tests for each type of concrete (ε_1, obtained as the mean strain at 0.87 f_{cu} of the six monotonic tests on cubes). On the other hand, it compares $\varepsilon_1 + 10^m$ with the average experimental strain corresponding to the reference strength, that is to say, ε_c corresponding to f_{cu}, that would commensurate with the critical strain ε_c in a fatigue test of only one cycle. As we can see, the values are very close and thus the fatigue criterion is valid for the asymptotic case of fatigue of only one cycle.

Figure 4 shows the strain-based fatigue failure criterion for these concretes according to Equation 5. It can be seen that the model errs on the safe side since the predicted ε_c is always smaller than the strain underwent by the specimens during the last cycles of the third stretch of the cyclic creep curve.

Table 3: Comparison between the critical strains provided by the model for N=1 and the experimental values for εc in the monotonic tests

	ε_1 [%]	$\varepsilon_1 + 10^m$ [%]	ε_c [%]
H00	0.38	0.71	0.71
H15	0.37	0.70	0.64
H30	0.33	0.66	0.62
H45	0.35	0.68	0.66
H60	0.39	0.72	0.77

This document is the intellectual property of the fib – International Federation for Structural Concrete. All rights reserved.
This PDF of fib Bulletin 95 is intended for use and/or distribution solely within fib National Member Groups.

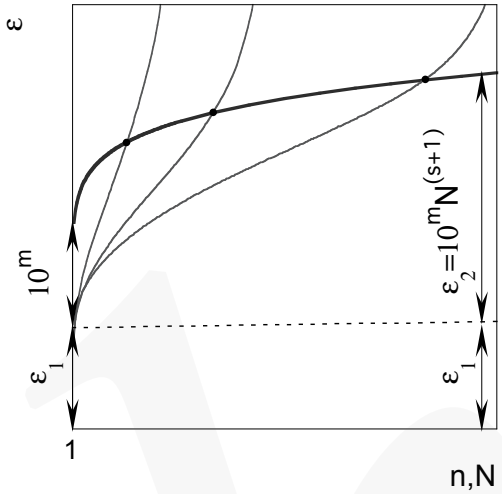


Figure 4: Failure criterion (bold line) compared with some experimental cyclic creep curves

Conclusions

This article proposes a new strain-based failure criterion for FRC in compression fatigue. To validate it, we have analyzed the ε-N curves of a series of FRCs made with the same base concrete and five fiber contents. From the Sparks and Menzies' relationship, we proposed a failure criterion that expresses the cyclic strain as a sum of two terms: the instantaneous strain due to the maximum stress in the first cycle, ε_1, plus the increase of strain due to the remaining cycles until failure, $\varepsilon_2 = 10^m N^{s+1}$. The failure does not occur until the strain in the test coincides with the critical strain $\varepsilon_c = \varepsilon_1 + \varepsilon_2$. This criterion shows that the failure occurs when the strain reaches a critical value that the matrix can no longer support (which involves mechanical strain and cyclic creep). On the other hand, this research shows that fibers, up to certain optimum fiber content, improve fatigue behavior.

This strain-based failure model can be used as an alternative to S-N models. It defines the critical strain at which the material fails as a function of the number of cycles. So, the fatigue life of any part of a structure can be estimated with the model, provided the actual strain cycles are measured or calculated.

Acknowledgements

The authors wish to thank the *Ministerio de Ciencia e Innovación*, Spain, for the financing received through the BIA2015-68678-C2-R and RTC-2017-6736-3 projects as well as Cementos Portland Valderribas S.A. and BASF, the providers of cement and super-plasticizer, respectively.

References

[1] ACI Committee 544 (1996), State-of-the-Art Report on Fiber Reinforced Concrete, ACI 544- 96 (reapproved 2002), American Concrete Institute, ACI Farmington Hills.

This document is the intellectual property of the fib – International Federation for Structural Concrete. All rights reserved.
This PDF of fib Bulletin 95 is intended for use and/or distribution solely within fib National Member Groups.

[2] S. Mindess, J.F. Young, and D. Darwin (2002). Concrete. Pearson Education, United States.

[3] A. Bentur and S. Mindess (2007). Fibre Reinforced Cementitious Composites. Taylor and Francis, London and New York.

[4] A. Medeiros, X.X. Zhang, G. Ruiz, R.C. Yu, and M.S.L. Velasco (2015). Effect of theloading frequency on the compressive fatigue behavior of plain and fiber reinforcedconcrete. International Journal of Fatigue, 70:342–350.

[5] P. B. Cachim, J.A. Figueiras, and P.A.A. Pereira (2002). Fatigue behavior of fiber-reinforced concrete in compression. Cement and Concrete Composites, 24(2):211–217.

[6] M. Grzybowski and C. Meyer (1993). Damage accumulation in concrete with and withoutfiber reinforcement. American Concrete Institute Journal, 90(6):594–604.

[7] T. Paskova and C. Meyer (1997). Low-cycle fatigue of plain and fiber reinforced concrete. American Concrete Institute Journal, 273–285.

[8] CEB (1988). Fatigue of concrete structures, State of the Art Report. Technical report, Bulletin d Information No. 188, Comité Euro-International du Béton, Case Postale, Lausanne.

[9] E. Poveda, G. Ruiz, H. Cifuentes, R. C Yu, and X.X Zhang (2017). Influence of the fiber content on the compressive low-cycle fatigue behavior of self-compacting SFRC. International Journal of Fatigue, 101:9–17.

[10] M. Tarifa, X. X. Zhang, G. Ruiz, and E. Poveda (2015). Full-scale fatigue tests of precast reinforced concrete slabs for railway tracks. Engineering Structures, 100:610–615.

[11] E. Castillo and A. Fernández-Canteli (2009). A unified statistical methodology for modeling fatigue damage. Springer Science.

[12] P.R. Sparks and J.B. Menzies (1973). The effect of rate of loading upon the static and fatigue strengths of plain concrete in compression. ACI, 25:83:73–80.

[13] S. Blasón, E. Poveda, G. Ruiz, H. Cifuentes, and A. Fernández-Canteli (2019). Twofold normalization of the cyclic creep curve of plain and steel-fiber reinforced concrete and its application to predict fatigue failure. International Journal of Fatigue, 120:215-217.

[14] ASTM C39/C39M (2015). Standard test method for compressive strength of cylindrical concrete specimens. ASTM International, West Conshohocken, PA.

[15] Model Code 2010, Final Draft (2012). *fib* Bulletin N. 65 and 66, EPFL Lausanne.

This document is the intellectual property of the fib – International Federation for Structural Concrete. All rights reserved.
This PDF of fib Bulletin 95 is intended for use and/or distribution solely within fib National Member Groups.
FRC2018: Fibre Reinforced Concrete: from Design to Structural Applications
Joint ACI-*fib*-RILEM International Workshop

Performance of Ductile FRCC under Cyclic Loads and Non-Linear FE Simulation

Georgiou Antroula[1], Pantazopoulou Stavroula[2]

[1] : University of Cyprus, Nicosia, Cyprus.

[2] : York University, Toronto, Canada.

Abstract

With the advent of strain hardening fiber reinforced cementitious composites (SHFRCC) the development of a new generation of structural systems that benefit from the inherent ductility of concrete in tension in order to reduce the amounts of transverse reinforcement (stirrups), shear strength, and tension-force development capacity to the main reinforcement is possible. In this study a number of tests are conducted to explore the behavior of SHFRCC materials under cyclic loads, simulating seismic effects. The experimental responses of two half-scale interior beam column connections subjected to reversed cyclic loading are compared; one of the connections was constructed with a cementitious matrix without fibers, and was detailed according with the Eurocode provisions for ductility class M (moderate, μ=3.5). The other connection was constructed with a SHFRCC mix; (2% by volume of PVA fibers was used to reinforce the matrix and the minimum amount of shear reinforcement allowed by Eurocode 2 for non-seismic detailing was used in the specimens). Several supporting experiments were also conducted to support analysis of the cyclic behavior (uniaxial tension, compression, splitting tests). The behavior of the members under reversed cyclic displacement is also simulated with advanced nonlinear Finite Element Analysis, with results that are correlated with the experimental observations. The SHFRCC specimen with minimum detailing showed improved performance and enormous ductility suggesting new possibilities to the seismic design of structures.

Keywords

Strain Hardening cementitious concrete; reversed cyclic loading; deformation capacity; ductility.

This document is the intellectual property of the fib – International Federation for Structural Concrete. All rights reserved.
This PDF of fib Bulletin 95 is intended for use and/or distribution solely within fib National Member Groups.

1 Introduction

Earthquake ground motion imposes reversed cyclic displacement demands on structures and where Capacity Design concepts are enforced, the "strong column-weak beam" requirement for frames is implemented in the form of plastic hinge formation in the beam-ends and at the base of ground-floor columns. Beam and column hinging regions must be detailed specifically in order to sustain excessive yielding in longitudinal reinforcement without shear failure (Eurocode 8-III, 2005). Whereas concrete tensile strength is neglected in estimating flexural strength, yet, spalling of the concrete cover in the compression zone is a usual failure that limits member resistance. Similarly, for shear design of beams that undergo reversed cyclic loading, the contribution of concrete to shear strength is usually neglected on account of diagonal shear cracking and stirrups are designed to carry all of the shear loading. This leads to excessive amounts of detailing and denser placement of shear reinforcement that complicates construction and casting.

In light of these practical limitations the use of a new type of composite material reinforced with short discontinuous fibers that exhibits strain hardening properties (SHFRCC) under tension and improved performance in compression is considered an ideal alternative. The improved performance in tension benefits the composite's behavior in shear as seen in the short span beams subjected to cyclic loading in previous studies (Kanta, Watanabe, & Li, 1998). Fischer & Li (2007) who studied the combined behavior of steel reinforcement in SHFRCC matrix have shown that strain hardening behavior of both components past yielding prevents localization of deformations leading to uniformly distributed yielding of the reinforcement over the length of the specimens they tested, increasing energy dissipation. The flexural behavior of beams with SHFRCC and FRP bars were experimentally investigated by Yuan and Pan (2013), that concluded that cracks diffuse to wider areas with many micro cracks in SHFRCC, leading to higher deformability, thereby reducing bond splitting. Additionally bar rupture at crack locations due to stress concentrations was avoided and the SHFRCC showed no delamination.

Limited experimental research concerning the reversed cyclic loading of steel reinforced SHFRCC members has been published to date [Lequesne, Parra-Montesinos, & Wight, (2016), Fischer & Li, (2003), Yuan, Pan, Dong, & Leung, (2014), Parra-Montesinos & Chompreda, (2006)] to support generalized conclusions; however, it is evident that – owing to its unique properties, SHFRCC can work effectively together with longitudinal steel reinforcement and improve the ductility of reinforced concrete structural members without the requirement of significant additional transverse reinforcement. The present paper investigates the behavior of SHFRCC-RC Structural members under cyclic loads, simulating seismic effects. To this end, the experimental responses of two half-scale interior beam column connections subjected to reversed cyclic loading are compared; one of the connections was constructed with a cementitious matrix without fibers, and was detailed according with the Eurocode provisions for ductility class M (moderate, μ=3.5). The other connection was constructed with a SHFRCC mix (2% by volume of PVA fibers was used to reinforce the matrix) and non-seismic detailing amounting to minimum code-specified transverse reinforcement;. Specimens were tested under flexure shear with no simultaneous axial load. The members' behavior under reversed loading was also simulated using Finite Element Analysis calibrating the material parameters through uniaxial tension, compression and splitting test results.

This document is the intellectual property of the fib – International Federation for Structural Concrete. All rights reserved.
This PDF of fib Bulletin 95 is intended for use and/or distribution solely within fib National Member Groups.

2 Experimental program

2.1 Specimen geometry and material properties

Specimen geometry is depicted in Fig. 1. Each specimen consisted of two cantilever flexural members with a shear span ratio of 3.5 connected with a stiff node which is used for loading by the actuator in both directions. The beams were supported on rollers both on their bottom and top faces. The entire system behaved like a beam under three point loading where each shear span was subjected to a shear force equal to half the machine load, and a linearly varying moment from zero at the supports to $M=(P/2)\cdot L_s$ at the connection with the rigid node, where L_s is the shear span length. Specimens were constructed of SCC with a high content of fly ash (FA) without coarse aggregate; one was made with SHFRCC mix with PVA fibers of 2% by volume, while in the other the cementitious matrix was the same as that of the SHFRCC but without the fibers (Control).

The Control Member was reinforced as per Eurocode 8:1, (2004) provisions for a DCM (i.e. q=3.5). The SHFRCC beam had the same longitudinal reinforcement but the minimum required transverse reinforcement for non-seismic construction was used - required to prevent buckling of the longitudinal bars in compression. The purpose of the tests was to investigate the beneficial action of the fibers on the shear/flexural capacities of members under reversed cyclic loading. Detailed analysis of the beams' detailing may be found elsewhere (Georgiou & Pantazopoulou, 2018).

2.2 Test setup and loading

The test was conducted on a 250 kN MTS hydraulic actuator, digitally controlled and attached on a self–reacting stiff steel frame (Fig. 1 (e)). The specimen assembly was supported on rollers at the edges (Fig. 1 (f)) in order to allow rotation at the supports while the central rigid node was attached to the load actuator. Thus the node was bound between an upper and a lower steel plate; threaded rods connected the two plates to the actuator. The setup did not allow horizontal translation of the rigid node, while it allows the beams to expand away from the node without the creation of spurious axial loads. The test specimen had a total length of 2.50 m, while the cross section of the beams was 200x200 mm. The shear span had a length of 700 mm, giving a shear span ratio a/h=3.5.

Table 1: Number of cycles and amplitude

No. of cycles	3	3	3	3	3	2	1	1	1
Amplitude Δ (mm)	2.25	6.00	9	13.5	18	22.5	27	31.5	36

Instrumentation comprising 13 LVDTs with various travel-lengths was used as shown in Fig. 1. A cyclic displacement history with full reversal of displacements was applied on the beam. The amplitudes of displacement and number of cycles are listed in Table 1. Twenty cycles were employed for the reversed loading, while loading was stopped at each peak in order to record the new cracks that were formed. When the test was stopped at each cycle the new cracks identified by close eye inspection were marked on the specimen and photos were taken as shown in Fig. 3. The test was performed under displacement control at a rate of 3 mm/min and was controlled by the actuator's movement. The chosen displacement level, that was used to determine the amplitude, was the deflection of the beams at yielding of the flexural reinforcement $\Delta_y=6.04mm$, estimated by sectional analysis.

This document is the intellectual property of the fib – International Federation for Structural Concrete. All rights reserved.
This PDF of fib Bulletin 95 is intended for use and/or distribution solely within fib National Member Groups.

2.3 Composite mix design

The cementitious matrix comprised 2% PVA fibers (SHFRCC mix) and mortar made of Portland Composite Cement CEM II 42.5 R. Silica sand used had a maximum grain size of 300 μm. A significant portion of the binding agent was Type F Fly ash (FA) with pozzolanic and physical properties that enhance the performance of concrete. Class F FA has been used in other studies as cement replacement at fractions ranging from 20-30% of the mass of cementitious material but in this research the amount of FA used was 120% by weight of the amount of cement. PVA fibers 12 mm long, 39 μm diameter were used. The nominal tensile strength was 1600 MPa, Young's Modulus was 40 GPa, the fibers' strain capacity was 6.5% and the density was 1300 kg/m^3. The longitudinal bars tensile yield strength was 500 MPa whereas stirrups were of mild steel (f_y=300 MPa) smooth bars. Detailed proportions of the two mixes are listed in Table 2.

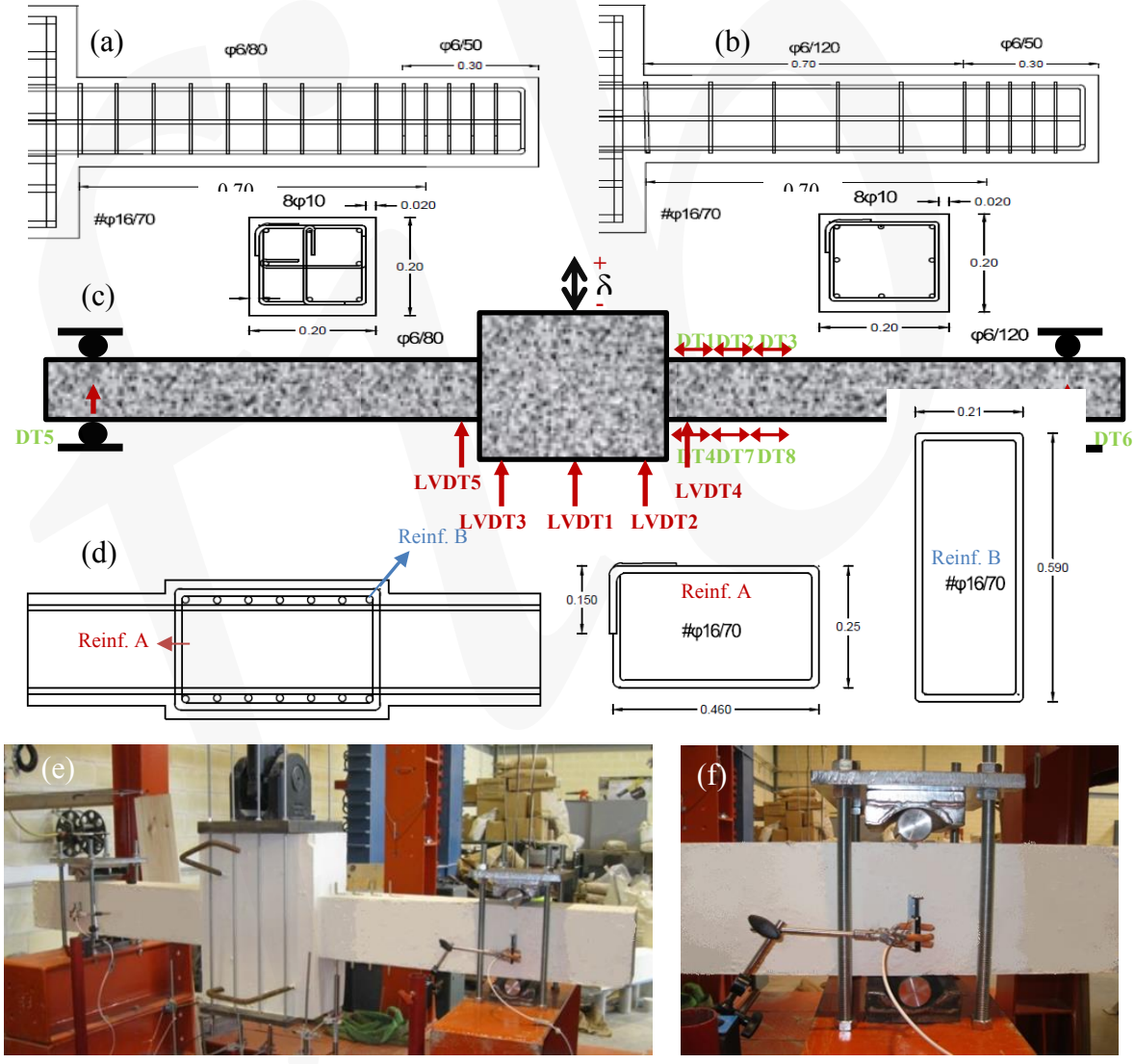


Figure 1: Stirrup detailing for (a) Member A: Control and (b) Member B: SHFRCC, (c) Test setup and measuring equipment, (d) top-view of rigid node dimensions and detailing, (e) Setup photo with LVDTs, (f) Support system.

This document is the intellectual property of the fib – International Federation for Structural Concrete. All rights reserved.
This PDF of fib Bulletin 95 is intended for use and/or distribution solely within fib National Member Groups.

Table 2: Mix proportions per weight

Mix	C	FA	S	W	SP	ρ_f (%V)
HVFA	1	1.2	0.80	0.60	0.012	2.0
SHFRCC	1	1.2	0.80	0.58	0.012	-

3 Experimental results

3.1 Material Properties under tension and compression

The uniaxial tensile, split cylinder and uniaxial compression tests required for determining the input parameters for the finite element modelling were carried out as per Georgiou and Pantazopoulou, (2016). The uniaxial coupons with a cross section of 25x50 mm are shown in Fig. 2a, as well as the average tensile stress-strain curves for the three SHCC specimens. The uniaxial tension tests were performed under displacement control, while the strain of the central 100 mm segment of constant dimensions were recorded with an LVDT as shown in Fig. 2a. The average of the three test results was fitted in a multilinear curve for better simulation of the behaviour of the material in the non-linear analysis. The most important behavioral parameter of SHFRCC is the tensile strength and strain capacity. During the formation of multiple cracks, the composite matrix-fiber system appears to strain-harden. Fibers bridging the cracks elongate but they also pull-out partially from the matrix at the crack locations. Beyond a limiting strain new cracks cease to form and crack localization occurs. Plain mix specimens (HVFA) were fractured incipiently during their extraction from the molds (they were very brittle) and therefore it was not possible to test them in tension.

Uniaxial compression tests were performed on cylinders, 100 mm in diameter by 200 mm in height (Fig. 2b), three for each mix design. Past work (Georgiou and Pantazopoulou, 2018) has shown that the extent of damage in concrete may be quantified by the lateral expansion of the cross section supporting the axial load; indeed, softening of the compressive strength is directly related to cracking parallel to the direction of loading and lateral expansion. Specimens with no fibers cracked and collapsed suddenly. Cracks were vertical, parallel to the load and extended deep inside the core of the specimen. After sudden collapse the specimens seemed unable to carry any remaining loads. In the case of the fiber reinforced composites multiple cracking developed all around the specimens. Cracking was visible close to 70% of the maximum load, with formation of multiple parallel cracks that increased in number up to the attainment of the peak load. Up till the end of the test no spalling of the specimen was observed. Figure 2 (b) plots the axial stress-axial strain (right) and axial stress-lateral strain (left) obtained from the compression tests of the SHFRCC materials and the results for the same matrix without fibers (mix HVFA). The results of three samples are depicted for each of the mixtures. An increase by 0.5% in the axial deformation of SHFRCC at peak load was reported; however, a stable descending branch marked the improved performance of the SHFRCC mixes. Note that lateral expansion is responsible for the steepness in the post peak branch in the compressive stress-strain response of concrete (Zanganeh and Pantazopoulou, 2001). In the case of SHFRCC, the behavior was improved and the post-peak decay was much milder as fibers were mobilized in the lateral direction bridging the cracks, transferring load and limiting lateral expansion of the cylinder under compression, as evidenced by the restricted growth of post-peak lateral strain as compared to the plain concrete specimens which undergo excessive, uncontrolled lateral expansion (Fig. 2b). The stress-strain curves suggest that past the peak load,

This document is the intellectual property of the fib – International Federation for Structural Concrete. All rights reserved.
This PDF of fib Bulletin 95 is intended for use and/or distribution solely within fib National Member Groups.

concrete with fibers behaves as if passively confined. The intensity of the effective confinement owing to the role of fibers is directly related to the materials' characteristic stress-strain behavior under splitting (Georgiou and Pantazopoulou, 2018). The contribution of the fibers in steel reinforced SHFRCC was demonstrated to greatly enhance the shear capacity of members in static loading as per previous research (Georgiou and Pantazopoulou, 2017), while the contribution in reversed cyclic loading ought to be investigated.

Additionally in Fig. 2c the test results from the split cylinder tests of the SHFRCC are presented along with photos of the samples showing the extensive cracking developed during the test. The graph shows the recorded deformation perpendicular (dx) and parallel (dy) to the cracking axis. The tests were performed using displacement controlled static loading.

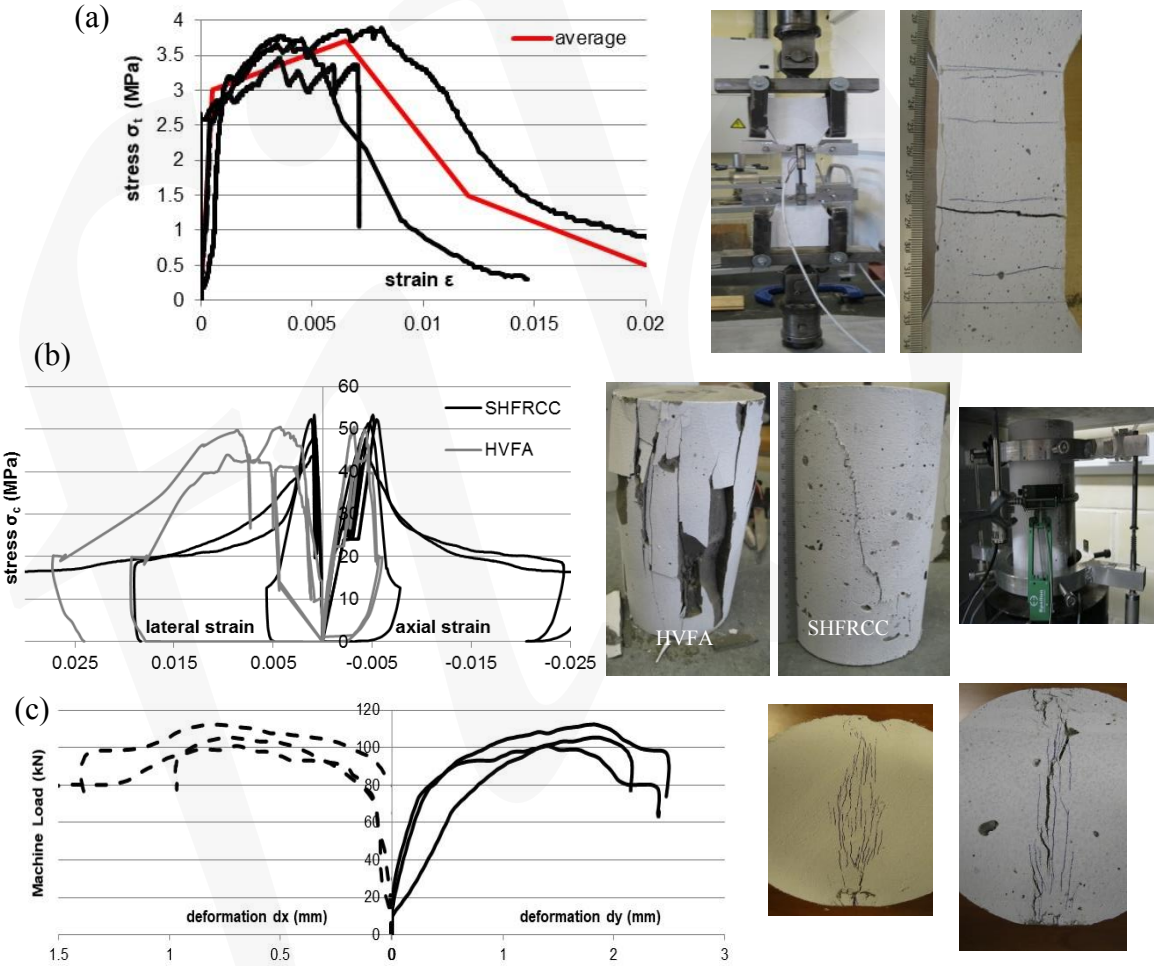


Figure 2: (a) tensile test, (b) compression test and (c) split cylinder test results

3.2 Members under reversed cyclic loading

Photos of the progressive failure of the Control and SHFRCC members are given in Fig. 3. The results indicate that the SHFRCC member -even though it only had Φ6/120 perimeter stirrups as compared to the Control member who had Φ6/80 stirrups (with 3 stirrup legs parallel to the loading per stirrup layer) - showed an improved behavior under reversed cyclic loading due to the presence of the fibers that contributed to the transfer of loads, the confinement of the regions under tension and compression, the increase of shear capacity of the member and the

This document is the intellectual property of the fib – International Federation for Structural Concrete. All rights reserved.
This PDF of fib Bulletin 95 is intended for use and/or distribution solely within fib National Member Groups.

sustained load capacity up to large level of deflections. Up to the point that the experiment with the SHFRCC was stopped the load-drift curve did not show any load drop leading to drift ductility in the order of μ_θ=6/1=6 (the test was terminated at that ductility without signs of strength degradation). In comparison, the Control beam which had been designed for DCM as per EC8-1 (2004), attained a drift ductility of μ_θ=4/1=4 with 20% loss of strength.

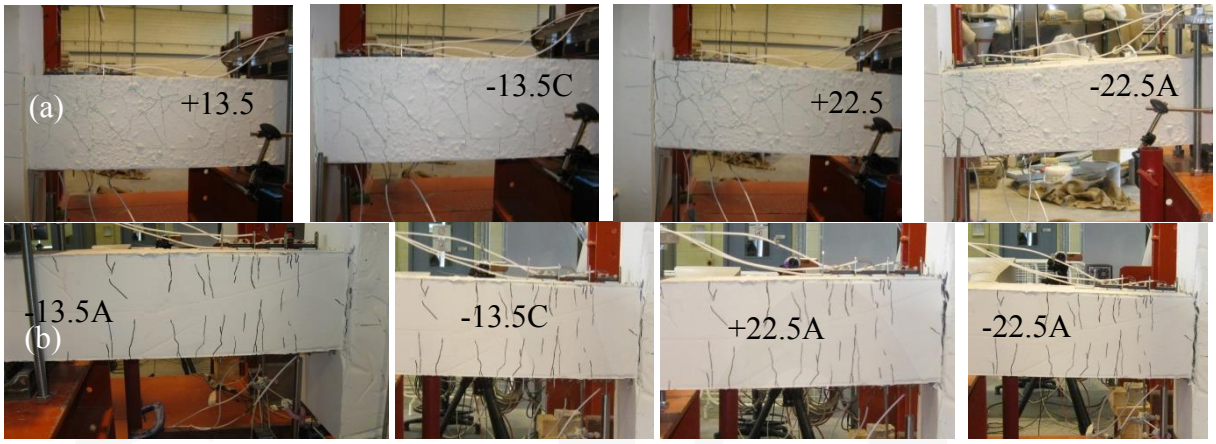


Figure 3: Crack pattern at various cycle levels for (a) Control and (b) SHFRCC

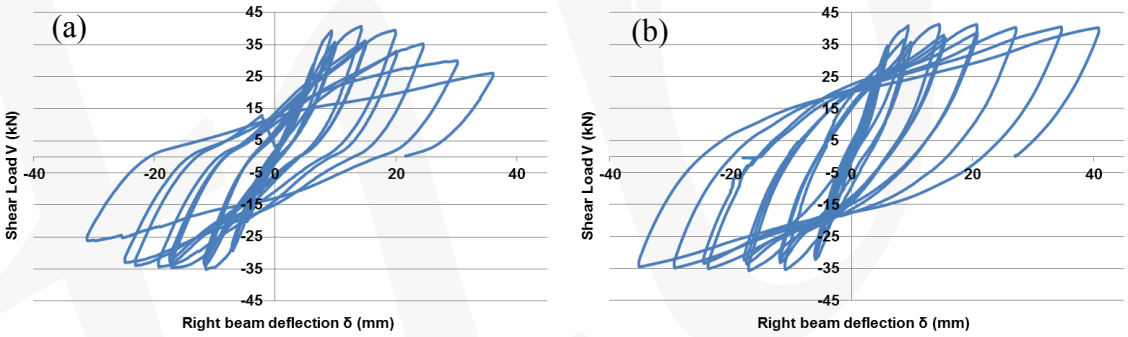


Figure 4: Shear Load-Right Beam Deflection for the (a) CONTROL and (b) SHFRCC

The Shear Load-Deflection diagrams from the two members are depicted in Fig. 4. The deflection recorded is based on the central LVDT1 that measures the deflection at the middle of the lower steel plate. Deflection is considered positive when the beam moves up and negative when moving down. When the Load, P, is positive in the diagrams of Fig. 4, the top cross section is under tension. Member shear *V=P/2*. To calculate the total deflection of the beams the average deflection at the supports (DT5+DT6)/2 is deducted from the total deflection of the central measuring LVDTs. The Control member shows yielding of the reinforcement at a deflection of 6.8 mm and a shear load of 34.7 kN. Past the yield point the specimen showed some mild hardening with a peak shear load of 40.7 kN at a central rigid node deflection of 12.8 mm. After the peak load softening of the curve initiated with a remaining shear load of 25 kN in the last cycle of 36 mm deflection. During the second and third cycle of each target deflection the shear load capacity decreased, while the loading path of the following higher target displacement coincided with the lower target of the last excursion. As deflection increased the residual deformations of the specimen also increased, while the energy absorption of the consequent cycles decreased. The shear load-deflection curve of the SHFRCC member shows yielding at a deflection of 7.6 mm and 39 kN shear load. Past the yielding the load carrying capacity remained constant throughout the remaining cycles at a shear load of 41 kN

This document is the intellectual property of the fib – International Federation for Structural Concrete. All rights reserved.
This PDF of fib Bulletin 95 is intended for use and/or distribution solely within fib National Member Groups.

even at a deflection level of 36 mm. The energy absorption capacity appeared to increase with each cycle and the members attained great ductility levels.

4 Finite element modeling

4.1 Material Properties

In Finite element analysis of reinforced concrete members the material properties that are used as input parameters define the relevance of the analysis results; mesh sensitivity and path dependence are common features of the analysis performance in these circumstances. In extending the existing modeling frameworks to the class of SHFRCC materials, there is still a lack of knowledge regarding many variables that are necessary input, such as fracture energy, tensile stress-strain in the softening range and the anticipated crack spacing. Empirical equations used to calibrate these variables for normal concrete cannot be directly transplanted in the SHFRCC materials on account of the fundamental differences in the constitutive behavior of the two material types. A calibrated model in the general purpose finite element code ABAQUS (2011) that implements the essentials of non-associated plasticity simulation is the so-called Concrete Damage Plasticity (CDP) model, (Lubliner, Oliver and Onate, (1989), Lee and Fenves, (1998)). An attractive aspect of the CDP model is the ability to model strain hardening of the behavior of a composite even under direct tension.

The essential parameters that are required to define the full response of the material in ABAQUS are β, m, f and γ. The parameters β and m describe the shape of the flow potential function and f and γ determine the shape of the yield function. In this model for the flow potential G, the Drucker-Prager hyperbolic function is determined by this form:

$$G(\bar{\sigma}) = \sqrt{(f_c - m \cdot f_t \cdot \tan\beta)^2 + \bar{q}^2} - \bar{p} \cdot \tan\beta - \sigma \tag{1}$$

Where f_t and f_c are the uniaxial tensile and compressive strengths of the material, β is the dilation angle measured in the p-q plane at high confining pressure and m is the eccentricity of the plastic potential surface. The elastic modulus is based on the concrete elasticity values in compression and is the same for tension and compression based on the material input parameters. Additionally, parameter μ is a viscosity parameter representing the relaxation time of the viscoplastic system (Karlsson and Sorensen, 2010). Cylinders and tensile coupons with the dimensions used in the experimental program were modeled in ABAQUS in order to calibrate the material laws of the two mix designs in tension and compression. The biaxial failure envelope by Kupfer, Hilsdorf and Rusch, (1969) for a concrete of 50 MPa compressive stress is used here identifying γ as 0.666 as well as the ratio of the biaxial to the uniaxial compressive strengths taken equal to 1.16.

FIB Model Code, (2010) in Chapter 5.1 provides calibrated equations for the determination of the mean value of the tensile strength of concrete, that may be estimated indirectly from the mean splitting strength $f_{ct,sp}$. The splitting strength $f_{ct,sp}$ is the mean value of the splitting test as determined from Eq. 2.

$$f_{ct,sp} = \frac{2 \cdot P}{\pi \cdot d \cdot l} \tag{2}$$

The formation of microcracks in finite element analyses of normal concrete is defined by introducing a crack opening law that was defined in this research by the stress-strain

This document is the intellectual property of the fib – International Federation for Structural Concrete. All rights reserved.
This PDF of fib Bulletin 95 is intended for use and/or distribution solely within fib National Member Groups.

relationship. In order to calibrate the material parameters to be used as input for the simulation of the large scale member, the experimental results from the uniaxial tension, split and compression were used as input parameters for simulating the uniaxial compression and split cylinder tests in ABAQUS. Parameters used for the elastic branch of the SHFRCC material are: density = 2000 kg/m^3, modulus of elasticity = 15.8 GPa and Poisson's ratio = 0.216. The dilation angle was determined by calibrating the uniaxial compression test to be 30°. The plastic true stress-strain laws of the material under tension and compression are listed in Table 3. True stress-plastic strain properties are derived from the experimental results by subtracting the elastic behavior of the materials from the point of yield onwards.

Table 3: Material law under tension and compression

Uniaxial compression (pairs of stress in MPa and strain values, multiplied by 1000)											
$\sigma_{pl,true}$	32.57	42.45	48.05	48.53	43.67	38.81	33.95	29.10	24.14	19.38	14.52
$\varepsilon_{pl,true}$	0.00	0.32	0.97	1.94	3.25	4.55	5.86	7.16	8.47	9.78	11.08
Uniaxial Tension (pairs of stress in MPa and strain values)											
$\sigma_{pl,true}$	5.09	7.00	5.09	0.50							
$\varepsilon_{pl,true}$	0.00	0.01	0.2	0.4							

4.2 Boundary conditions and loading

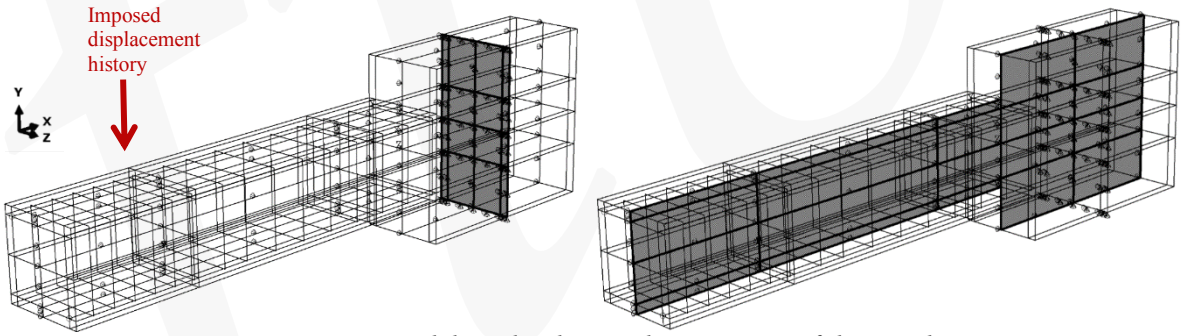


Figure 5: Modeling, loading and constraints of the members

The experiment was performed in ABAQUS simulating the members under consideration and the central rigid node. The mesh comprised hexahedral (brick) elements with a size of 30 mm, except from the critical region where the plastic hinge might occur (L_{crit}=h=200 mm), where the mesh size was 10 mm. The longitudinal reinforcement was modeled with truss elements (10 mm lengths). The mesh size is related to the fracture energy of an opening crack and therefore controls the softening branch of the tensile behavior of the composite accordingly. The steel reinforcement, both longitudinal and transverse, was implemented in the cementitious composite elements using perfect bond as boundary constraint. Two planes of symmetry were considered, one in the middle x-y plane and one in the middle y-z plane, at which planes, the displacement of all nodes in the z and x, y direction respectively were constrained as shown in Fig. 5. Load was applied as displacement (δ=40 mm) in the y direction, with a general static procedure, on the central node of the cross section at the roller support of the test.

This document is the intellectual property of the fib – International Federation for Structural Concrete. All rights reserved.
This PDF of fib Bulletin 95 is intended for use and/or distribution solely within fib National Member Groups.

4.3 Simulation results

The results from the monotonic push-off simulation are compared to the cyclic loading results from the experimental procedure in Fig. 6. Results are in good agreement both in relation to the Shear Load as well as the deflection of the member. On the same figure the axial stresses and strains corresponding to the yield point, maximum load and final step are also depicted.

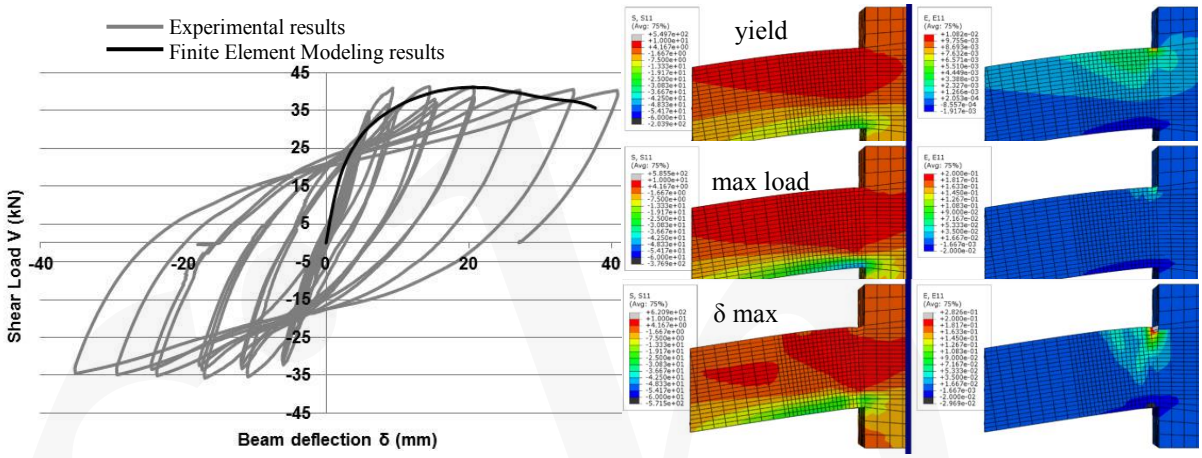


Figure 6: Simulation of the SHFRCC member under monotonic push-off analysis and comparison to the cyclic behavior, stresses and corresponding strains

5 Concluding remarks

The experimental results indicate that the SHFRCC specimen showed improved behavior under reversed cyclic loading due to the presence of the fibers that contributed to the transfer of loads, the confinement of the regions under tension and compression, the increase of shear capacity of the member and the sustained load capacity up to large levels of deflection (enhanced deformation capacity). After vigorous cyclic displacement reversals the test of the SHFRCC specimen was terminated, attaining the limit of stroke of the actuator. There was no evidence of strength loss in the load-resistance curve up to a ductility of six in terms of the relative drift ratio (μ_θ=6). By comparison, the Control specimen (reinforced as per EC8-I DCM) attained a drift ductility of μ_θ=4/1=4 at a strength loss of 20% of peak load. The experimental findings suggest the potential benefit from a shift of construction towards High Performance Structures. Additionally, the experimentally determined properties in uniaxial tension, split and compression of two mix designs, with and without fibers, were used to calibrate analytical models of the behavior of those composites. Results obtained from FE modeling analysis were compared with the experimental load-deflection curves. As tensile strength is a very important analysis parameter, procedures for its proper determination for the simulation of SHFRCC members must be incorporated into Modern Codes for these types of materials. Results obtained from direct tensile tests may underestimate the resistance and strain capacity of the composite when this is placed in a 3-D state of stress. Flaws and size effects (in terms of possible voids during compaction for the estimation of stress from the specimens' area, and the gauge length used in estimation of average strain from crack widths) may result in lower values than what may be supported in the presence of a more complex stress state and therefore the split cylinder results must be used for determining the materials' tensile parameter for simulation. More tests would be needed for checking repeatability, in order to generalize the findings; such further

This document is the intellectual property of the fib – International Federation for Structural Concrete. All rights reserved.
This PDF of fib Bulletin 95 is intended for use and/or distribution solely within fib National Member Groups.

testing would need to establish how the various parameters of the mix and the embedded reinforcement affect the behaviour.

6 References

Eurocode 8:3 (2005). Design of structures for earthquake resistance. CEN.

ABAQUS (2011). Abaqus/CAE, SIMULIA, p. 1–16.

Eurocode 8:1 (2004). Design of structures for earthquake resistance—Part 1: general rules, seismic actions and rules for buildings. CEN.

FIB Model Code. (2010). Model Code 2010. Federation Internationale du Beton (fib).

Fischer, G., & Li, V. C. (2003). Deformation Behavior of Fiber-Reinforced Polymer Reinforced ECC Flexural Members under Reversed Cyclic Loading Conditions. ACI Struc. Jour., 100(1), 25–35.

Fischer, G., & Li, V. C. (2007). Effect of fiber reinforcement on the response of structural members. Engineering Fracture Mechanics, 74(1–2), 258–272.

Georgiou, A., & Pantazopoulou, S. (2018). Performance of SHFRCC-RC concrete members under cyclic displacement reversals. In 16th Euro. Conf. on Earthq. Engin. Thessaloniki.

Georgiou, A. V., & Pantazopoulou, S. J. (2016). Effect of fiber length and surface characteristics on the mechanical properties of cementitious composites. Construction and Building Materials, 125, 1216-1228.

Georgiou, A. V., & Pantazopoulou, S. J. (2017). Behavior of Strain Hardening Cementitious Composites in Flexure/Shear. J. Mater. Civ. Eng. 10.1061/(ASCE)MT.1943-5533.0002041.

Georgiou, A. V., & Pantazopoulou, S. J. (2018). Experimental investigation on the confining effect of fibers in SHFRCC. Comp. Struc. 202, 29-37.

Kanta, T., Watanabe, S., & Li, V. C. (1998). Application of pseudo SHCC to shear resistant structural elements. In FRAMCOS-3 (pp. 1477–1490). Freiburg, Germany.

Kupfer, H., Hilsdorf, H., & Rusch, H. (1969). Behavior of Concrete Under Biaxial Stresses. Journal Proceedings, 66(8), 656–666.

Lee, J., & Fenves, G. L. (1998). Plastic-damage model for cyclic loading of concrete structures. Journal of Engineering Mechanics, 124(8), 892–900.

Lequesne, R., Parra-Montesinos, G., & Wight, J. (2016). Seismic Response of Fiber-Reinforced Concrete Coupled Walls. ACI Structural Journal, 113(3), 435–445.

Lubliner, J. J., Oliver, S., & Onate, E. (1989). A plastic-damage model for concrete. International Journal of Solids and Structures, 25(3), 229–326.

Parra-Montesinos, G., & Chompreda, P. (2006). Deformation capacity and shear strength of fiber reinforced cement composite flexural members subjected to displacement reversals. Journal of Structural Engineering, 133(3), 421–431.

Yuan, F., Pan, J., Dong, L., & Leung, C. K. Y. (2014). Mechanical Behaviors of Steel Reinforced ECC or ECC / Concrete Composite Beams under Reversed Cyclic Loading. J. Mat. in Civ. Eng., 26(8), 1–8. http://doi.org/10.1061/(ASCE)MT.1943-5533.0000935.

Yuan, F., & Pan, J. L. (2013). Experimental study on flexural behaviors of engineered cementitious composite beams reinforced with FRP bars. In 8th Intern. Conf. on fracture mechanics of concrete and concrete structures, FraMCoS-8 (pp. 390–401). Toledo, Spain.

Zanganeh, M., & Pantazopoulou, S. J. (2001). Triaxial tests of Fiber-reinforced concrete. Journal of Materials in Civil Engineering, 15(October), 340–348.

This document is the intellectual property of the fib – International Federation for Structural Concrete. All rights reserved.
This PDF of fib Bulletin 95 is intended for use and/or distribution solely within fib National Member Groups.
FRC2018: Fibre Reinforced Concrete: from Design to Structural Applications
Joint ACI-*fib*-RILEM International Workshop

Cyclic Damage to PVA Microfibre Embedded in Cementitious Matrix in Alternating Tension-Compression Regime

Majid Ranjbarian[1], Viktor Mechtcherine[1]

[1] : Technical University of Dresden, Dresden, Germany.

Abstract

The structures subject to dynamic loading demand more ductile materials to prevent catastrophic failure. The results of investigations on strain-hardening cement-based composites (SHCCs) distinguished this group of materials – due to their highly ductile behaviour – as a suitable alternative for structures with high resistance against seismic, impact and cyclic loadings. While mechanical properties of SHCC are determined mostly by bridging behaviour of dispersed fibres crossing cracks and properties of fibre-matrix interface, the dependency of these mechanisms on the loading regime is pronounced. Specifically, under cyclic loading, the number of cycles to failure decreases dramatically when SHCC is subject to alternating tension-compression regime. Degradation of fibres compressed between the crack faces and deterioration of their bridging capacity are responsible for such early failure and necessitate further investigations at the micro level. The article at hand presents the influence of loading history in cyclic tension-compression regime on the bridging capacity of the single PVA microfibre embedded in cementitious matrix. A novel double-sided single fibre pull-out setup is used for the experimental investigations. First the test setup, material composition and testing procedure are explained. Next, the results of double-sided pull-out specimens, tested under monotonic and cyclic tension-compression regimes, are discussed. It is shown that the deterioration of fibre bridging capacity can be assessed by applying cyclic loading in post-cracking stage, followed by pulling the fibre out of the matrix. Possibility of a change in pull-out behaviour of PVA microfibre from “fibre rupture” to “fibre pullout”, also a change of behaviour in post debonding regime from “hardening” to “softening” are also observed. Eventually, the results of microscopic analysis are presented and discussed, which show the specific phenomena responsible for changes in pull-out behaviour.

Keywords

SHCC, cement-based composites, PVA microfibre, fibre pull-out test, fatigue, cyclic tension-compression loading regime, cyclic damage

This document is the intellectual property of the fib – International Federation for Structural Concrete. All rights reserved.
This PDF of fib Bulletin 95 is intended for use and/or distribution solely within fib National Member Groups.

1 Introduction

The research on development of novel fibre-reinforced mineral-based composites with high ductility under tensile loading is the focus of many research projects, see e.g. (Mechtcherine & Curosu, 2017). Among them, strain hardening cement-based composites (SHCCs) with pronounced ductility achieved through multiple cracking is the subject of intensive research for more than two decades. One of the prominent envisaged applications are new structures and rehabilitation of existing structures subject to seismic loading and fatigue (Kesner & Billington, 2004). Yamamoto et al. applied SHCC as repair material on columns and performed cyclic loading tests. They reported positive influence of SHCC on seismic performance (Yamamoto, Yano, Kinoshita, Lim, & Shinya, 2018). The applicability of high performance fibre reinforced cementitious composite for seismic dampers was investigated by Fukuyama and Suwada, who reported high ductility of such structural elements (Fukuyama & Suwada, 2003). On material level, Jun and Mechtcherine investigated SHCC dumbbell-shaped specimen under cyclic purely tensile loading with various loading regimes; no pronounced effect of loading conditions on material performance was observed (Jun & Mechtcherine, 2010). However, Mueller and Mechtcherine showed that the number of cycles to failure in alternating tension-compression regime is much lower than the cyclic pure tension regime due to the compressive component (Müller & Mechtcherine, 2017). The early failure of SHCC was traced back to the severe damage of PVA microfibre through buckling and crashing between the crack faces in tension-compression regime. The authors suggested further investigations at the micro-level to identify and quantify the specific phenomena involved. Ranjbarian and Mechtcherine recently developed a novel setup, which enables further investigations on crack bridging behaviour of high performance microfibre at the meso- and micro-level (Ranjbarian & Mechtcherine, 2018). One of the advantages of this double-sided setup is the possibility of performing single and multiple fibre pull-out tests under cyclic tension-compression regime. Characterisation of the cyclic damage at the micro-level should help understanding the failure mechanisms and explain the SHCC behaviour on material and structural level. Furthermore, it should create a basis for purposeful material optimisation.

The article at hand presents the influence of loading history in tension-compression regime on the pull-out behaviour of PVA microfibre embedded in cementitious matrix. First, the experimental program and testing procedure are explained. A double-sided setup is used for the experiments, loading regimes of 200 and 2000 cycles in post-cracking stage are applied, immediately followed by pulling the fibre out of the matrix. The results are presented and compared with the pull-out behaviour of PVA microfibre tested in quasi-static monotonic regime. The results of microscopic analysis are eventually discussed, which shed light on the causes of different pull-out behaviour observed.

2 Experimental program

2.1 Specimen geometry and material properties

A new double-sided fibre pull-out setup (Ranjbarian & Mechtcherine, 2018) is used in this work for investigating the influence of cyclic pre-loading in tension-compression mode on microfibre bridging behaviour. As it is illustrated in Figure 1a, a PVA microfibre is embedded centrally in the matrix body and a pair of notches subdivide the length of specimen to a short

This document is the intellectual property of the fib – International Federation for Structural Concrete. All rights reserved.
This PDF of fib Bulletin 95 is intended for use and/or distribution solely within fib National Member Groups.

(l_s) and a long (l_f) embedded lengths, 2 mm and 6 mm, respectively. The width of the specimen (b) is 5 mm, reduced to 2 mm in the notch section (b_N), the thickness is 4 mm. Thus, the cross-section of the specimens is 4 mm × 5 mm, decreasing to 4 mm × 2 mm in the notch section.

Table 1 shows the mix composition of the SHCC matrix as it has been used also in other research projects at the TU Dresden, e.g. (Mueller and Mechtcherine 2017; Ranjbarian and Mechtcherine 2018). Mechanical properties of PVA microfibres Kuralon K-II REC 15 according to the producer, Kuraray (Japan) are available in Table 2.

Table 1: Composition of the matrix, in kg/m^3.

Cement CEM I 42.5 R-HS	**Fly ash**	**Water**	**Quartz sand**	**Superplasticizer**	**Viscosity agent**
505	621	338	536	10	4.8

Table 2: Physical and mechanical properties of PVA microfibres.

Fibre type	**Nominal diameter [µm]**	**Density [g/cm^3]**	**Tensile strength [MPa]**	**Young's modulus [GPa]**	**Strain capacity [-]**
Kuralon K-II REC 15	40	1.3	1600	40	0.06

After demoulding, the specimens were kept in a plastic bag in a sealed condition until a matrix age of 28 days.

2.2 Testing procedure

The end of the microfibre on top and bottom surfaces of the specimen is covered with candle wax to prevent any contact between fibre and glue. Then the specimen is glued between two aluminium blocks. A 1 kN capacity load cell is used for force measurement, while the displacement measurement is based on the movement of the machine's crosshead, see Figure 1a. To ensure the accuracy of the force values, the measurement errors were obtained by applying weights ranging from 1 g to 100 g, which showed that the small values measured by the force cell were absolutely reliable, while errors negligible.

The displacement-controlled loading regime consists of three different stages. First monotonic tensile load is applied with a displacement rate of 0.01 mm/s until the matrix breaks on the notches and the crack-opening displacement reaches 100 µm (U_o). Next, cyclic loading with a displacement rate of 1 mm/s and predetermined number of cycles follows to induce cyclic damage on the microfibre and fracture surface. The displacement-controlled upper (U_o) and lower reversal points (U_u) are respectively 100 µm and -10 µm, which corresponds approximately to 0.2 N tension force in fibre on the upper reversal point and 30 N compressive force on the lower reversal point. After reaching the predetermined number of cycles, the fibre is eventually pulled out with a displacement rate of 0.01 mm/s. The force-displacement curve progression during entire loading regime is schematically shown in Figure 1b.

This document is the intellectual property of the fib – International Federation for Structural Concrete. All rights reserved.
This PDF of fib Bulletin 95 is intended for use and/or distribution solely within fib National Member Groups.

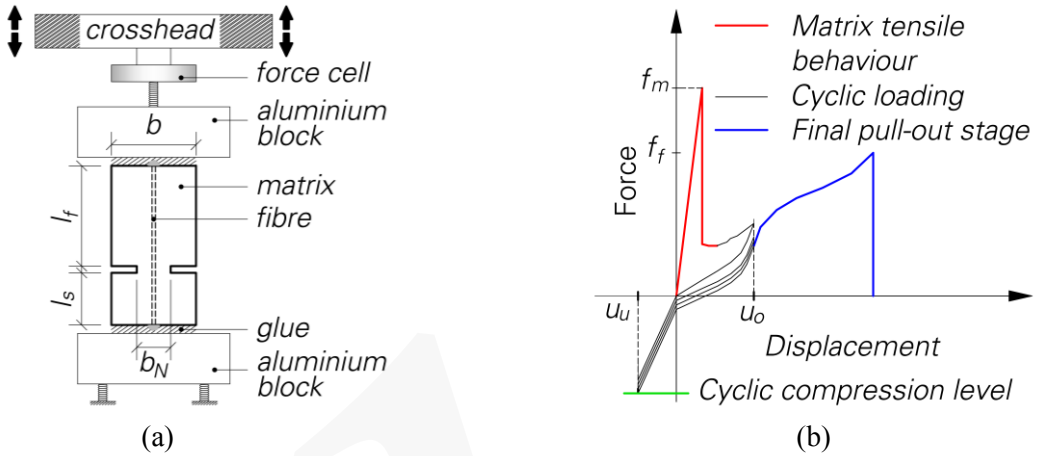


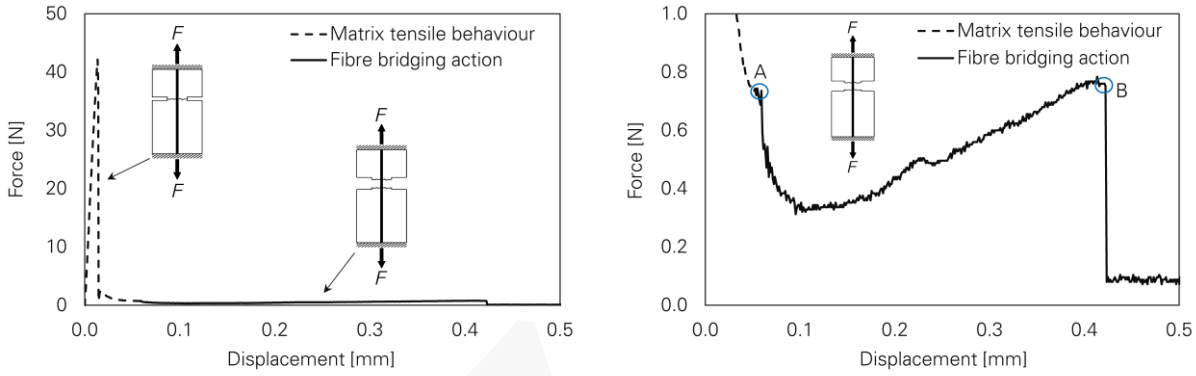
Figure 1: (a) Double-sided specimen geometry and setup configuration; (b) applied loading regime with Uu and Uo the lower and upper reversal points, respectively.

To show that pull-out behaviour of PVA microfibre can be influenced by cyclic pre-loading, first the results of a monotonically tested control specimen "M" will be presented. Then, the pull-out behaviour of two more specimens after exposure to 200 and 2000 loading cycles will be discussed. The latter specimens will be respectively called as "C200" and "C2000" in the next sections.

3 Results and discussion

Figure 2 illustrates the bridging behaviour of PVA microfibre embedded in cementitious matrix under quasi-static monotonic loading. It can be seen that increase in tensile force leads to failure of the matrix on the notch. The fracture process of the matrix for this specimen type was extensively discussed by the authors elsewhere (Ranjbarian & Mechtcherine, 2018). It is assumed that due to displacement at unstable matrix cracking, no unusual phenomenon occurred in the debonding and bridging processes. The post-cracking behaviour of the specimen including the softening behaviour of the matrix and fibre bridging action is shown in Figure 2b on a larger scale and important points are marked. The drop at "A" represents the failure of chemical bond between the matrix and fibre, while the drop at "B" is due to fibre rupture, see also (Katz & Li, 1996). More details about bridging behaviour of PVA microfibre embedded in cementitious matrix is provided elsewhere (Ranjbarian & Mechtcherine, 2018).

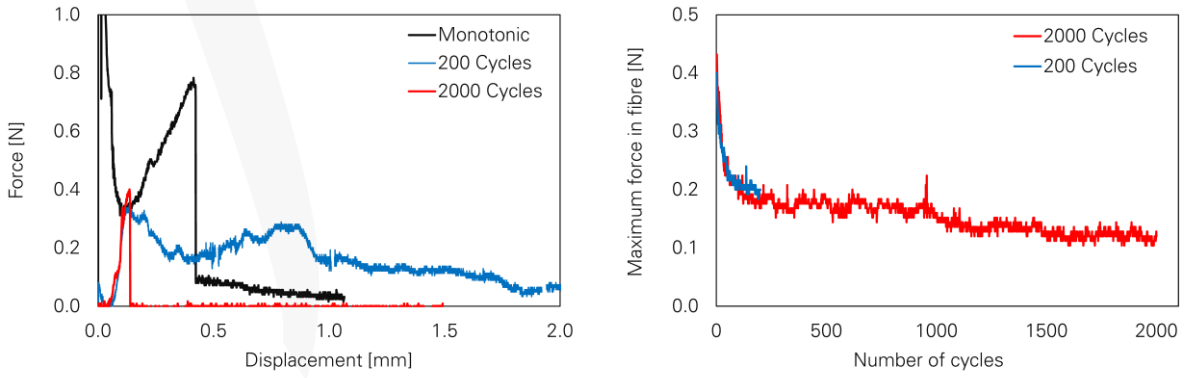
This document is the intellectual property of the fib – International Federation for Structural Concrete. All rights reserved.
This PDF of fib Bulletin 95 is intended for use and/or distribution solely within fib National Member Groups.



(a) (b)

Figure 2: Results of monotonically tested specimen: (a) the entire force-displacement curve, (b) fibre bridging part of the curve on a larger scale.

Figure 3a shows the force-displacement curves in the final pull-out stage of double-sided fibre pull-out tests under different loading regimes. It can be seen that cyclic pre-loading leads to different pull-out behaviour. For the case "C200", the fibre is in final pull-out stage completely pulled out from the matrix in "softening" regime. The frictional bond strength based on maximum pull-out force is 1.35 MPa. This is an unexpected pull-out behaviour for PVA microfibre embedded in cementitious matrix as chosen, as it usually tends to rupture in post debonding stage. In the specimen "C2000", the fibre eventually ruptured in the final pull-out stage. However, the rupture force and the corresponding displacement are in this case much lower than those of the control specimen. Another observation is the decrease in the maximum tensile force in fibre during cycling loading. As it is illustrated in Figure 3b, the decrease in the maximum tensile force in the fibre is specifically pronounced in the beginning of cyclic loading. With increasing number of cycles, the trend continues, but with a lower rate. The decrease in the tensile force results from the fact that the displacement-controlled upper reversal point is constant through the entire cyclic loading stage. This phenomenon can be traced back to the time-dependent nature of pull-out (Boshoff, Mechtcherine, & van Zijl, 2009a). Obviously, the relaxation in the fibre-matrix interface and/or the fibre itself is significant in the cyclic loading stage.



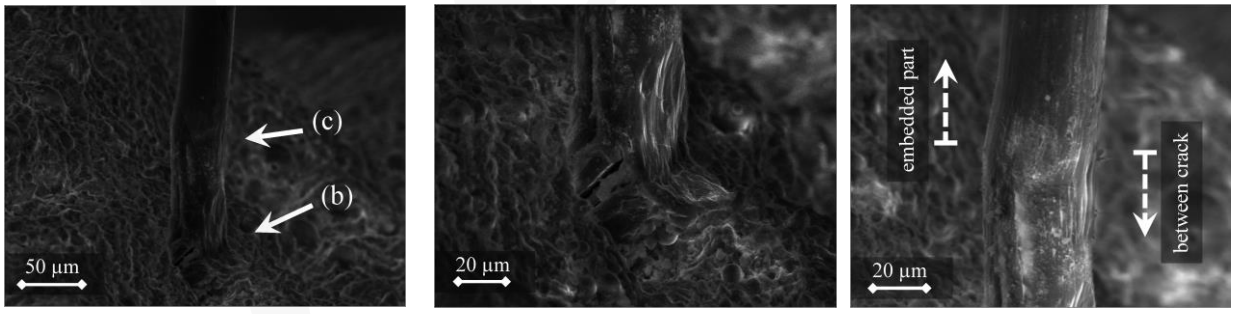
(a) (b)

Figure 3: a) Fibre bridging behaviour influenced by alternating tension-compression pre-loading, (b) maximum bridging force in the fibre in each cycle.

This document is the intellectual property of the fib – International Federation for Structural Concrete. All rights reserved.
This PDF of fib Bulletin 95 is intended for use and/or distribution solely within fib National Member Groups.

4 Specific phenomena

The specimens were microscopically analysed to find the reasons behind the different pull-out behaviours. Figure 4 shows the damage of a fibre for the case "C200". The fibre between the crack faces is severely damaged in cyclic tension-compression loading stage. Partial "delamination" and "peeling off" of the fibre as shown in Figure 4b seem to occur due to friction between the fibre and edges of the tunnel on the cracked section, while the beginning of defibrillation process can be seen on the border between the embedded part of the fibre and the part between the crack faces in Figure 4c. Since the fibre is completely pulled out, the access is provided to analyse microscopically the embedded part, where specific cyclic damage could be recognised, see Figure 5. It appears that the repeated fibre pull-out and push-in during cyclic loading regime causes superficial deteriorations of the embedded fibre, i.e. bidirectional scratching and abrasion. Such damage seems to occur during each cycle. Therefore, the damage develops differently and the expected "jamming effect" and "slip-hardening" (Boshoff, Mechtcherine, & van Zijl, 2009b; Katz & Li, 1996) as observed under monotonic loading does not take place; the fibre is rather pulled out in softening regime. Clearly, the overall bond between fibre and matrix is not strong enough to prevent complete fibre pull-out in this case, unlike the specimen tested under monotonic loading and the pull-out behaviour completely changes. Thus, another possible pull-out mechanism for embedded PVA microfibres in cementitious matrix can be recognized. The fibre can be completely pulled out from the matrix due to specific damage type on the embedded part of the fibre induced during cyclic tension-compression loading regime. The results presented in this paper is just part of the results obtained in an extensive testing program. The change in pull-out behaviour of PVA microfibre from "fibre rupture" to "fibre pull-out" caused by cyclic loading can occur with considerable probability. It is notable that for a group of specimens tested according to the case "C200", complete pull-out was observed in 5 cases out of 13. For the reference case "M", however, complete fibre pull-out was observed for none of 11 specimens tested.



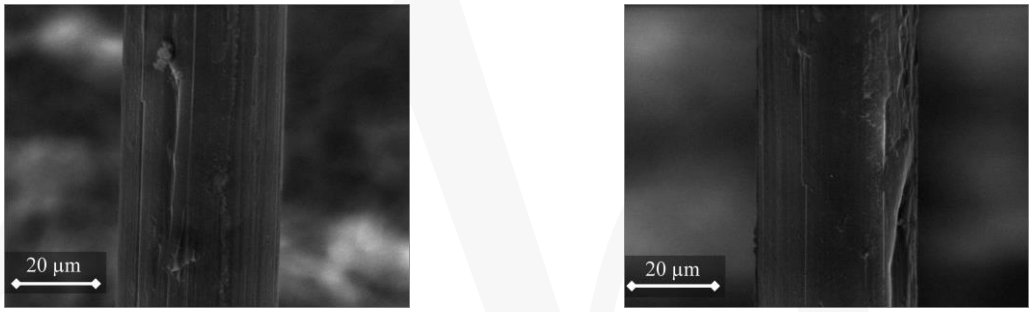
(a) (b) (c)

Figure 4: Damage due to cyclic loading on a completely pulled-out fibre ("C200"), (a) damage zone of the fibre between crack faces, (b) delamination and peeling off of the fibre, (c) beginning of defibrillation process.

The ruptured section of the fibre, for the case "C2000", is shown in Figure 6. Severe damage on the fibre part between the crack faces due to repeatedly opening and closing of the crack during cyclic tension-compression loading stage created a weak zone and the fibre

This document is the intellectual property of the fib – International Federation for Structural Concrete. All rights reserved.
This PDF of fib Bulletin 95 is intended for use and/or distribution solely within fib National Member Groups.

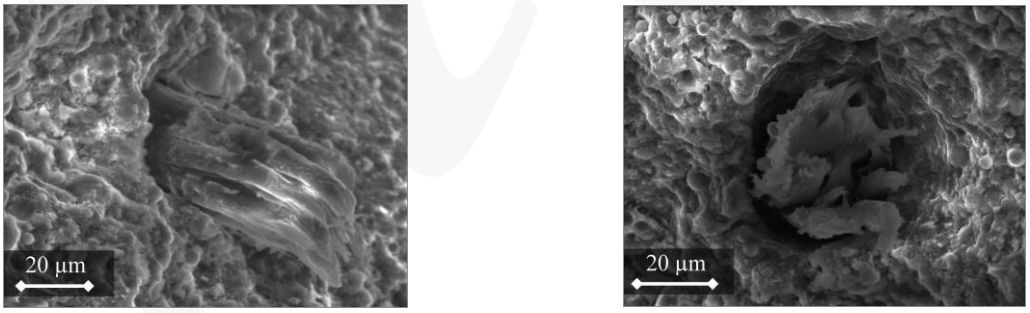
ruptured in the final pull-out stage on this location. The pull-out behaviour is in this case "fibre rupture", similar to control specimen, but the mechanism is totally different. Some involved phenomena could be buckling of the fibre under cyclic compression (Mueller & Mechtcherine, 2017) leading to defibrillation, also abrasion on the fibre surface in a bidirectional manner due to frictional forces between the fibre and edges of matrix tunnel close to the fracture surface. They cause flaws on the fibre surface in cyclic damage zone, which result in fibre degradation and can also be recognised by comparing the rupture force and displacement at rupture in Figure 3a.



(a) (b)

Figure 5: Damage due to cyclic loading as observed on a completely pulled-out fibre ("C200"), (a) and (b) damage zone belongs to the parts of the fibre in the "tunnel" (embedded).

Similar damage pattern can be seen when comparing Figure 6a and Figure 4c, however, with different damage severity, since damage development is a function of number of cycles (Müller & Mechtcherine, 2017) applied to these two specimens.



(a) (b)

Figure 6: Damage due to cyclic loading as observed on a ruptured fibre ("C2000"), (a) the damage zone belongs to the part of fibre between crack faces, (b) top view of the same fibre on the other side.

This document is the intellectual property of the fib – International Federation for Structural Concrete. All rights reserved.
This PDF of fib Bulletin 95 is intended for use and/or distribution solely within fib National Member Groups.

5 Concluding remarks

The following conclusions can be drawn on the basis of the results obtained:

1. A change in pull-out behaviour of PVA microfibre embedded in cementitious matrix from "fibre rupture" to "fibre pull-out", as well as from "hardening" to "softening" in post debonding stage is possible due to the damage induced under cyclic pre-loading in tension-compression mode. Therefore, the fibre-matrix interface parameters for such loading regime should be specifically determined.
2. The findings support the damage mechanisms suggested for SHCC under cyclic tension-compression regime by (Mueller & Mechtcherine, 2017). Local degradation of PVA microfibre compressed and buckled repeatedly between the crack faces due to cyclic compressive component is observed and its negative influence on crack bridging behaviour is shown.
3. The change in pull-out behaviour, also local degradation of the fibre can deteriorate the bridging capacity of the fibre and preventing multiple cracking on composite level, leading to lower ductility.
4. Failure localization due to fatigue can be distinguished from the failure localization under quasi-static monotonic loading for further investigations of SHCC characteristics on composite level. For assessment of fatigue behaviour of SHCC in tension-compression mode, loading history should be taken into account. The relevant parameters include cyclic compression level, number of cycles and probability of fibre pull-out instead of fibre rupture.
5. The mentioned phenomena are useful for future applications of SHCC for new construction and rehabilitation of existing structures which are expected to experience cyclic tension-compression loading.

6 Acknowledgements

This research project has been sponsored by the German Research Foundation (DFG) within the scope of Priority Programme 2020 "Cyclic deterioration of High-Performance Concrete in an experimental-virtual lab". The authors would like to express their gratitude for this financial support.

7 References

Boshoff, W. P., Mechtcherine, V., & van Zijl, G. P. A. G. (2009a). Characterising the time-dependant behaviour on the single fibre level of SHCC: Part 1: Mechanism of fibre pull-out creep. *Cement and Concrete Research*, *39*(9), 779–786. http://doi.org/10.1016/j.cemconres.2009.06.007

Boshoff, W. P., Mechtcherine, V., & van Zijl, G. P. A. G. (2009b). Characterising the time-dependant behaviour on the single fibre level of SHCC: Part 2: The rate effects on fibre pull-out tests. *Cement and Concrete Research*, *39*(9), 787–797. http://doi.org/10.1016/j.cemconres.2009.06.006

Fukuyama, H., & Suwada, H. (2003). Experimental Response of HPFRCC Dampers for Structural Control. *Journal of Advanced Concrete Technology*, *1*(3), 317–326. http://doi.org/10.3151/jact.1.317

Jun, P., & Mechtcherine, V. (2010). Behaviour of Strain-hardening Cement-based Composites

This document is the intellectual property of the fib – International Federation for Structural Concrete. All rights reserved.
This PDF of fib Bulletin 95 is intended for use and/or distribution solely within fib National Member Groups.

(SHCC) under monotonic and cyclic tensile loading. *Cement and Concrete Composites*, *32*(10), 810–818. http://doi.org/10.1016/j.cemconcomp.2010.08.004

Katz, A., & Li, V. C. (1996). A special technique for determining the bond strength of micro-fibres in cement matrix by pullout test. *Journal of Materials Science Letters*, *15*(20), 1821–1823. http://doi.org/10.1007/BF00275353

Kesner, K., & Billington, S. L. (2004). Tension, Compression and Cyclic Testing of Engineered Cementitious Composite Materials. Technical Report, Cornell University, School of Civil and Environmental Engineering, Ithaca, New York 14853.

Mechtcherine, V., & Curosu, I. (2017). Mineral-Bonded Composites for Enhanced Structural Impact Safety - A New Research Training Group GRK 2250 of the German Research Society. *Procedia Engineering*, *210*, 182–185. http://doi.org/10.1016/j.proeng.2017.11.064

Müller, S., & Mechtcherine, V. (2017). Fatigue behaviour of strain-hardening cement-based composites (SHCC). *Cement and Concrete Research*, *92*, 75–83. http://doi.org/10.1016/j.cemconres.2016.11.003

Ranjbarian, M., & Mechtcherine, V. (2018). A novel test setup for the characterization of bridging behaviour of single microfibres embedded in a mineral-based matrix. Cement and Concrete Composites, 92, 92–101. http://doi.org/10.1016/j.cemconcomp.2018.05.017

Yamamoto, S., Yano, Y., Kinoshita, K., Lim, S., & Shinya, K. (2018). Cyclic Loading Test on 0.2-Scale RC Column Models Repaired by Strain-Hardening Fiber-Reinforced Cement-Based Composites. In V. Mechtcherine, V. Slowik, & P. Kabele (Eds.), *Strain-Hardening Cement-Based Composites* (pp. 734–742). Dordrecht: Springer Netherlands.

This document is the intellectual property of the fib – International Federation for Structural Concrete. All rights reserved.
This PDF of fib Bulletin 95 is intended for use and/or distribution solely within fib National Member Groups.

5) SERVICE CONDITIONS AND DURABILITY

This document is the intellectual property of the fib – International Federation for Structural Concrete. All rights reserved.
This PDF of fib Bulletin 95 is intended for use and/or distribution solely within fib National Member Groups.
FRC2018: Fibre Reinforced Concrete: from Design to Structural Applications
Joint ACI-*fib*-RILEM International Workshop

Reduction of Flexural Crack Widths Using Synthetic Fibres in Reinforced Concrete

Erik Stefan Bernard[1]

[1] : Technologies in Structural Engineering Pty Ltd, Sydney, Australia.

Abstract

The use of steel fibres to reduce the width of flexural and tensile cracks in reinforced concrete members is now well recognised and aspects of this phenomenon have been incorporated into several codes internationally. Almost all the research work upon which this has been based has involved hooked-end steel fibres, with very little work undertaken using other types of fibre. However, the theories underlying how fibres assist in reducing crack widths are not specific to hooked-end steel fibres, so alternative types of fibre could work in a similar way to reduce crack widths in flexural and tensile members.

The current paper outlines work recently completed on the effect of several types of synthetic fibre on flexural crack widths in reinforced concrete members. The fibres have predominantly been manufactured using polypropylene, but other materials including aramide, nylon and PVA can also be used for this purpose and have been included in this investigation. Laboratory testing has demonstrated that synthetic fibres are fully capable of reducing flexural crack widths, but their efficacy is not consistent across all fibre types and designs. Testing appears to demonstrate that for a given dosage rate of fibre, the capacity of a FRC mix to limit flexural crack widths is related to the post-crack residual strength. However, some fibres can limit crack widths more effectively than is predicted by existing expressions for design width that are based primarily on post-crack residual strength. This suggests that post-crack toughness is not the only parameter contributing to crack width reduction in Reinforced Concrete members.

Keywords

Crack width, fibre reinforced concrete, post-crack performance, flexure, tension stiffening, conventional reinforcement

https://doi.org/10.35789/fib.BULL.0095.Ch34

This document is the intellectual property of the fib – International Federation for Structural Concrete. All rights reserved.
This PDF of fib Bulletin 95 is intended for use and/or distribution solely within fib National Member Groups.

1 Introduction

Flexural and tensile cracks can lead to corrosion of reinforcement in conventionally reinforced concrete (RC) members, so limits are normally placed on maximum in-service crack widths to reduce the probability of corrosion during the anticipated design life. Numerous investigations have been undertaken examining the possibility of using steel fibres to reduce crack widths in conventionally reinforced members and these have demonstrated that steel fibres are effective for this purpose (Vandewalle, 2000; Duport and Vanderwalle, 2003; Jansson et al, 2010; Deluce et al, 2014). Theories developed to explain the mechanism by which steel fibres reduce crack widths in reinforced concrete flexural members do not explicitly depend on the composition of the fibres but instead rely on the tensile stress generated by the fibres across cracks to reduce the spacing between cracks and thus crack widths (Abrishami and Mitchell, 1997; Bischoff, 2003). Since it is known that synthetic fibres are capable of generating substantial post-crack tensile stress, it is therefore possible that synthetic fibres may also be capable of reducing crack widths in reinforced concrete flexural members. This was demonstrated by Bernard (2016) for one type of embossed polypropylene macro-synthetic fibre, and Conforti et al (2018) for synthetic and glass fibres, but little work has otherwise addressed this issue.

The contribution of steel fibres to reduced flexural crack widths in RC flexural members has been recognized in guidelines such as Model Code 2010. Nearly all the research undertaken in relation to crack width reduction has used hooked-end steel fibres. While this prior work has established the concept that fibres can contribute to reduced flexural crack widths, the resulting expressions are specific to hooked-end steel fibres and are not necessarily applicable to other types of fibre. The current investigation was undertaken to examine whether alternative fibre types can also be used for this purpose.

In the present work, crack width estimates have been limited to the Serviceability Limit State at which the stress in the reinforcing bars is relatively moderate. This has nominally been taken to be 50 percent of the ultimate load capacity of a member. For ease of comparison, all the fibres examined in this investigation have been tested using an identical RC member configuration and the same nominal mix design for the concrete. While this has facilitated comparison of fibre performance, use of a single conventional reinforcement configuration has meant that identifying the full range of performance characteristics for each type of fibre in this application is not possible. In particular, many of the fibres may possibly perform better (or worse) using a different concrete mix design.

2 Experimental program

The experimental component of the investigation consisted of a series of trials in which 3600 mm long beams of 300×300 mm cross-section were cast using either plain concrete (as the control) or the same mixture reinforced with various types of fibre. The mix design for the concrete was the same for all the trials, and is listed in Table 1. The fibre types and mixture performance details are listed in Table 2. Conventional steel reinforcement comprising 3×16 mm deformed steel bars of 500 MPa nominal tensile strength and normal ductility (AS/NZS 4671) were placed with 30 mm clearance from the base. The specimens did not include any stirrups or compression steel as it was believed that inclusion of stirrups may influence the spacing between flexural cracks. Preliminary tests showed that shear failure did not occur for

This document is the intellectual property of the fib – International Federation for Structural Concrete. All rights reserved.
This PDF of fib Bulletin 95 is intended for use and/or distribution solely within fib National Member Groups.

this configuration. Four replicate RC beams were cast for each trial together with seven ASTM C1609/C1609M beams for post-crack performance assessment.

The fibres examined in the investigation included Dramix RC65/60 3D hooked-end steel fibres acting as a SFRC control (Table 2). Three macro-synthetic fibre types were included, BC48 as an embossed polypropylene (PP) fibre, MQ58 as an embossed polymer blend fibre, and Fibermesh 650 as a smooth tape PP fibre. Fibermesh 150 is a smooth circular micro-synthetic PP fibre. Of the remaining fibres, all were circular in cross-section and smooth except for the aramide fibre which had a rectangular cross-section and was partially twisted. Both the glass and basalt fibres were initially bundled but fragmented during mixing to produce dispersed micro fibres that were finely distributed throughout the mixture.

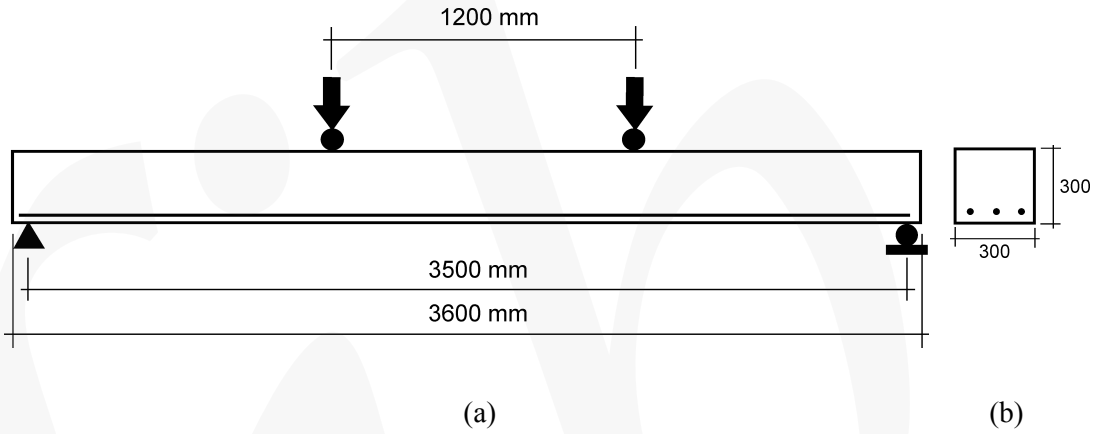


Figure 1: (a) Two-point lateral loading on each beam specimen, and (b) cross-section

The concrete used in the trials was produced in a commercial dry-batch plant with the 1.5 m^3 load required for each specimen set delivered to the laboratory in a truck-mounted agitator. Fibres were added to the batch at the lab, and about 500 mL/m^3 of PCE superplasticizer was required to maintain acceptable workability for each of the micro-synthetic FRC loads.

Table 1: Mix design for 32 MPa cast concrete mix used in all trials.

Ingredient	**Quantity (kg/m^3)**
10 mm CRG	1000
Coarse sand	460
Fine sand	250
GP cement	280
Fly ash	100
LR Water reducer	1330 mL/m^3
Target slump	150 mm

All of the beams were tested using essentially the same procedure. The beams were placed upon two roller supports on a span of 3500 mm and subjected to two equal point loads, each a distance of 1150 mm from the adjacent support (thus the central span was 1200 mm, Fig. 1). Load was applied using a 250 kN servo-controlled actuator operating in stroke-control. The initial central displacement of the beam was 3.0 mm loaded at a rate of 2 mm/min. The displacement was then stopped and the beam inspected for cracks. In some cases initial flexural cracks had occurred, in others there were no signs of flexural cracking. Load was then

This document is the intellectual property of the fib – International Federation for Structural Concrete. All rights reserved.
This PDF of fib Bulletin 95 is intended for use and/or distribution solely within fib National Member Groups.

increased in increments of 1.5 mm displacement applied at a rate of 2.0 mm/min followed by pauses to permit crack widths to be manually measured using a 100× optical field microscope. Each pause lasted approximately 5 minutes during which the stroke was held constant and crack widths were measured resulting in a series of steps in the record (Fig. 2a). This cycle of loading and holding the displacement continued for about 60-80 minutes until a total central displacement of about 25-30 mm had been sustained, by which time yielding of the tensile bars had occurred. Approximately 12-15 sets of crack width measurements, and corresponding loads, were recorded for each beam. The central deflection of the beam was measured relative to the supports using an LVDT placed under the centre of the beam.

Table 2: Test series and fibre characteristics for all the sets of specimens tested.

Set	Reinforcement	Type	Dosage (kg/m^3)	V_f (%)	UCS (MPa)	f_t (MPa)	$f_{0.75}$ (MPa)
1	Plain Concrete	-	-	-	44	6.14	0.00
2	RC65/60 3D	60 mm hook-end steel	20	0.25	48	7.44	2.87
3	BC48	48 mm embossed PP	4.5	0.50	43	6.68	2.47
4	MQ58	58 mm embossed poly	4	0.44	43	6.26	1.44
5	Aramide	1 × 30 mm twisted	4	0.30	45	5.89	2.49
6	Fibermesh 650S	60 mm tape PP	4.5	0.50	42	6.68	1.16
7	Fibermesh 150	∅32 µm micro-syn.	4	0.44	41	6.17	0.37
8	PA	∅135 µm 12 mm	4	0.42	47	6.31	0.36
9	Glass	∅30 µm 18 mm glass	4	0.16	42	6.23	0.00
10	Basalt	∅30 µm 20 mm basalt	4	0.12	46	5.79	0.00
11	PVA	∅26 µm 6 mm PVA	4	0.31	45	6.25	0.30

Crack widths were always measured on the side of the beam at a distance of 10 mm from the bottom face. This was necessary because the edges of the beams were quite rough which did not permit accurate estimation of crack widths. At about 50% of ultimate moment capacity (70 kN total load) the distance between each crack was measured using a steel rule on both sides of the beam. In most of the tests additional cracks arose as load increased, resulting in a steady decrease in the mean crack spacing. However, for the purposes of design, only those cracks that were present at the service load (presently taken to be 70 kN, or 40.2 kNm moment) are of interest to estimates of mean and maximum crack spacing. Only those cracks occurring in the region of uniform bending moment between the two load points were assessed in this investigation.

3 Test Results

Each series of four beams was tested at the same age of about 4 months, using the same testing procedure, leading to the generation of load-deflection curves of the type shown in Fig. 2a, ASTM C1609 beam results (eg. Fig. 2b), and records of mean crack width (Fig. 3). The plain concrete specimens were taken as controls against which mean crack spacing and widths for all the other sets were compared. The data show that almost all of the fibre configurations examined in this investigation caused the mean crack width to decrease, with the glass fibres proving the least effective and the PVA fibres the most effective. A substantial difference in mean crack spacing often occurred between nominally identical specimens (Fig. 4). This occurred because the number of flexural cracks in the central 1200 mm region of

This document is the intellectual property of the fib – International Federation for Structural Concrete. All rights reserved.
This PDF of fib Bulletin 95 is intended for use and/or distribution solely within fib National Member Groups.

uniform bending moment was not the same for all four beams within a set. It required a difference in crack count of only 1-2 to result in a substantially different mean crack spacing. This occurred, for example, for the BC48, MQ58, and PVA reinforced beam sets.

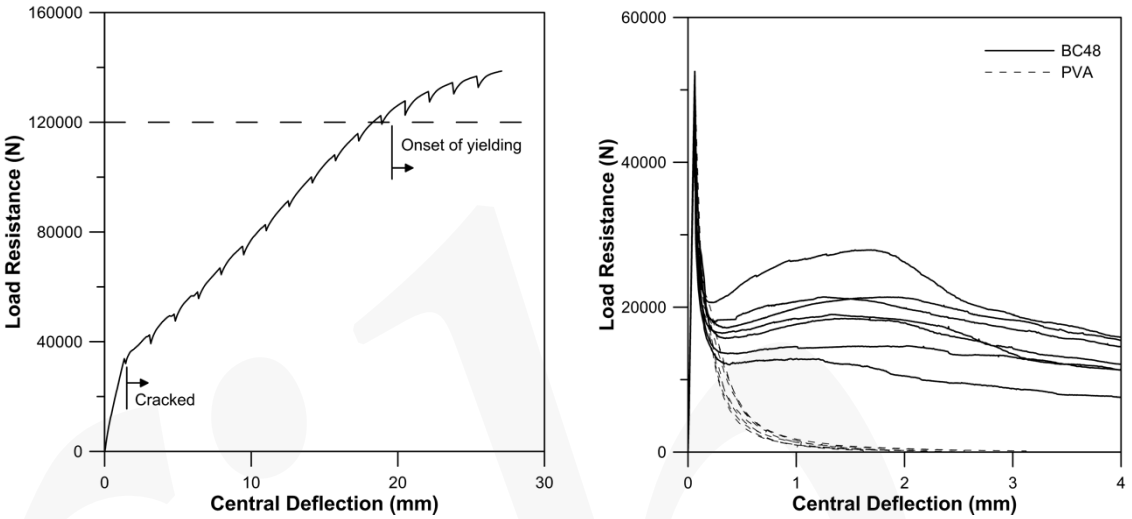


Figure 2: Example (a) load-deflection curve for beam with aramide fibres, (b) ASTM C1609 results.

The mean crack width results help to differentiate fibre types that show promise in reducing flexural crack widths from those that do not (Fig. 5). The Fibremesh 150 micro-synthetic fibres not only proved very difficult to consolidate at a dosage rate of 4 kg/m^3, but also proved ineffective for reducing crack widths. The PA (Nylon) fibres were less onerous in terms of mixability, but also proved ineffective for crack width reduction. The glass and basalt-based micro fibres were similarly unable to reduce crack widths compared to the plain concrete control. All the macro-synthetic fibres produced a similar reduction in crack width (with adjustment for dosage, given that the BC48 and FM650S were dosed at 4.5 kg/m^3 while the MQ58 and aramide fibres were dosed at 4 kg/m^3) and appeared comparable to the Dramix RC65/60 3D steel fibres at 20 kg/m^3 in terms of effectiveness at a moderate dosage rate.

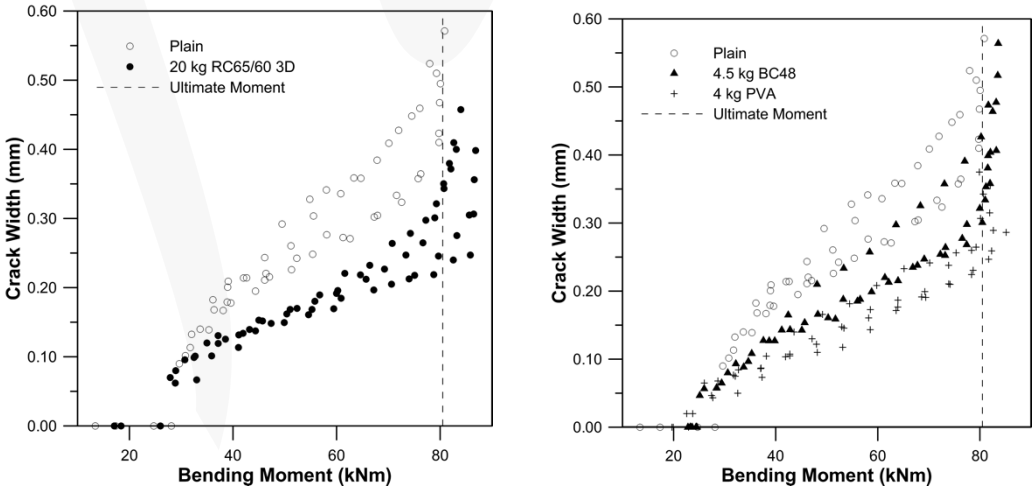


Figure 3: Crack width development for, (a) plain and RC65/60, and (b) BC48 and PVA.

This document is the intellectual property of the fib – International Federation for Structural Concrete. All rights reserved.
This PDF of fib Bulletin 95 is intended for use and/or distribution solely within fib National Member Groups.

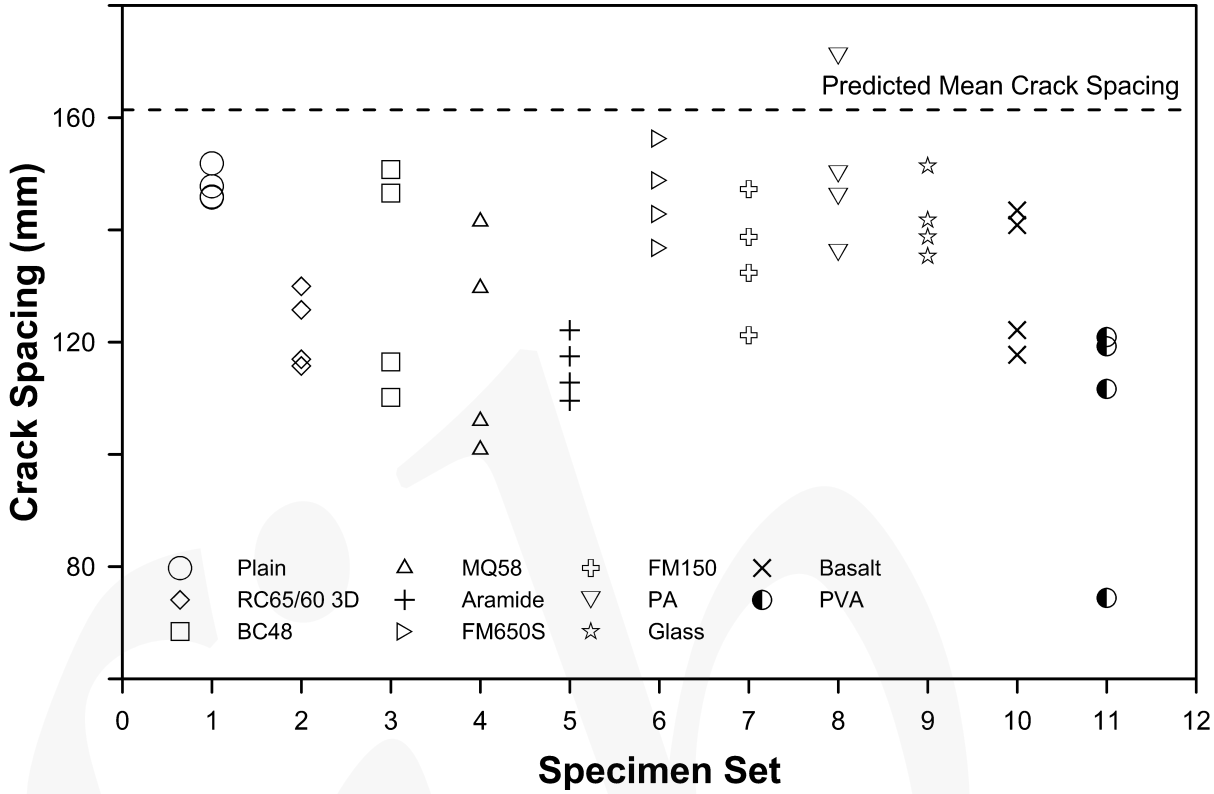


Figure 4: Mean crack spacing results for all beam specimen sets at 70 kN service load (50% of ultimate load), compared to predicted mean crack spacing for plain concrete.

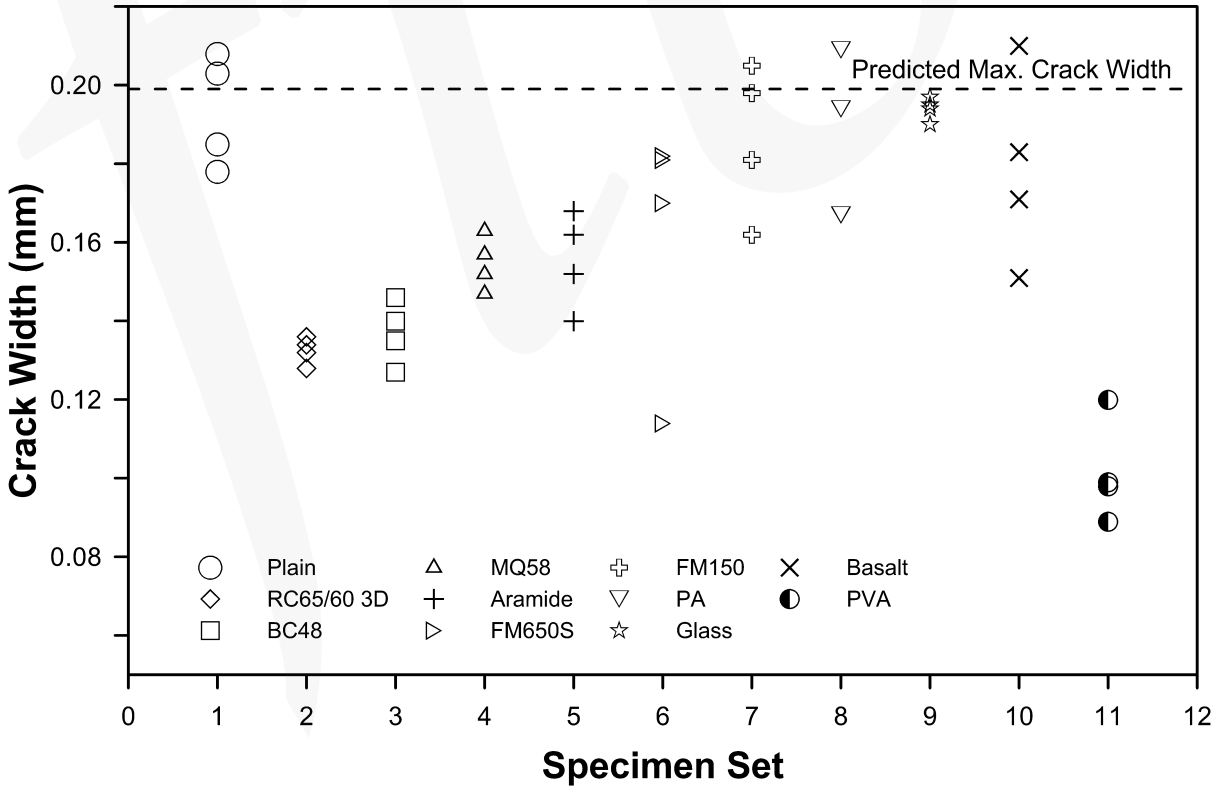


Figure 5: Mean crack width results for all beam specimen sets at 70 kN service load (50% of ultimate load), compared to predicted max crack width for plain concrete.

This document is the intellectual property of the fib – International Federation for Structural Concrete. All rights reserved.
This PDF of fib Bulletin 95 is intended for use and/or distribution solely within fib National Member Groups.

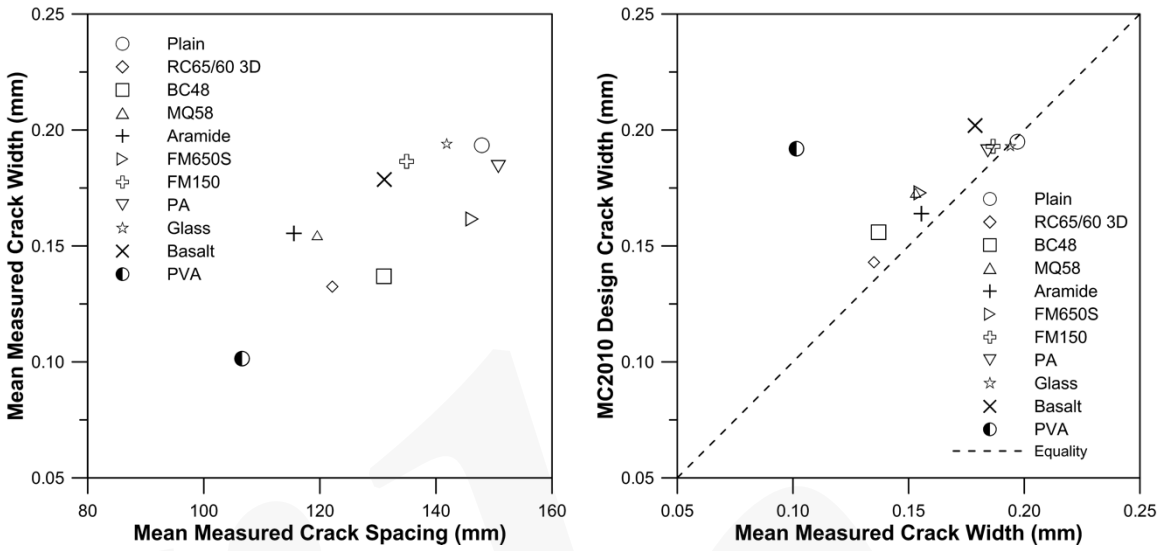


Figure 6: (a) Relationship between measured crack spacing and width for all beam specimen sets at 70 kN service load (50% of ultimate load), and (b) comparison of measured mean crack width at 70 kN load and predicted design crack width (based on ASTM C1609 beam results).

The stand-out performer in terms of both crack spacing and crack width reduction was the PVA micro-fibre. Although the spread in mean crack spacing results was high (Fig. 4), the mean crack width was reduced consistently across all four specimens and was equivalent to a 48% reduction in crack width compared to the plain concrete control for the addition of only 4 kg/m^3 of fibre (Fig. 5). Moreover, this dosage rate of fibre proved quite workable when 500 mL/m^3 of PCE superplasticizer was included.

4 Analysis

The mean measured crack width has been plotted against mean measured crack spacing at 50% of ultimate load in Fig. 6a to reveal a roughly linear relationship between the two parameters for the 11 specimen sets presently tested. The PVA fibre set resulted in measured crack width and spacing that were significantly lower than measured in any other set, but the relationship between these two parameters still appeared to conform to the same trend obtained for the other ten data sets.

The mean crack spacing was determined using the method described in Eurocode 2 (2004) and reproduced in AS3600. Based on the plain concrete section properties, the mean crack spacing was found to be 161.4 mm, which compares well with the measured mean crack spacing (Fig. 4). However, the predicted maximum crack spacing, normally taken as 70% larger than this, appears to be excessive at 230 mm. The predicted maximum crack width for the plain RC section based on Eurocode 2 was 0.199 mm, which compares well to the *mean* crack widths measured in the specimens (Fig. 5).

An attempt was made to compare the measured mean crack width for each set with predictions of design crack width based on the method described in Model Code 2010. However, the Model Code uses data on post-crack performance for FRC derived from

This document is the intellectual property of the fib – International Federation for Structural Concrete. All rights reserved.
This PDF of fib Bulletin 95 is intended for use and/or distribution solely within fib National Member Groups.

EN14651 beam tests, whereas ASTM C1609/C1609M beam tests were used in the current investigation. The predictions for w_d using Eq. 7.7-12 in the Model Code have therefore been made using estimates of f_{Ftsm} in Eq. 5.6-5 based on the residual strength at 0.75 mm central deflection in ASTM C1609/C1609M rather than f_{R1} from EN14651 (see Table 2 for beam test results). From the Model Code, Eq. 7.7-22 is reproduced as

$$w_d = \frac{1}{2}\frac{\phi_s}{\rho_{s.ef}}\frac{\left(f_{ctm} - f_{Ftsm}\right)}{\tau_{bm}}\frac{1}{E_s}\left(\sigma_s - \beta\sigma_{sr} + \eta_r\varepsilon_r E_s\right) \quad (1)$$

in which f_{Ftsm} has presently been taken as equal to 0.45 times the residual strength at 0.75 mm central deflection in ASTM C1609 beams; σ_s is the calculated stress in the steel based on a concrete section with (or without) fibres, σ_{sr} is the maximum stress in the steel (based on Eq. 7.6-6), and η_r is taken as zero (Table 7.6-2). The resulting predictions of w_d are slightly greater than the measured mean crack widths (see Fig. 6b) for all the mixes other than the PVA mix. The PVA mixture resulted in measured crack widths that were about half the predicted estimate, suggesting that PVA micro-fibres behave in a manner that is different from the other investigated fibres. It is interesting to note that the ASTM C1609 beams revealed load-deflection performance for the PVA fibre reinforced mixture that was far inferior to that evident for the steel and macro-synthetic FRC mixtures at 0.75 mm (Fig. 2b), yet the PVA mixture performed much better than any of the other mixtures. This could possibly have arisen because the PVA micro-fibre is very small and highly dispersed, which increased the likelihood that a fibre would intercept a micro-crack at the formation stage, thereby controlling growth. In contrast, the steel and macro-synthetic fibres were large and widely spaced, reducing the likelihood that they intersected a crack as it formed. Of the other data sets, the aramide fibre mixture appeared to result in crack widths that were somewhat larger than the trend evident in the majority of mixtures.

Note that almost all the FRC mixtures exhibited a higher residual strength in the range of 0.1-0.3 mm crack width than was evident at 0.75 mm central deflection (which corresponds to about 1.0 mm maximum crack width). It should be noted that the only parameters that varied between the 11 sets in the section analysis described in MC2010 were the compressive strength of the concrete (used to predict f_{ctm}) and the post-crack performance of the FRC (Table 2). The cracks were taken to lie in the stabilized cracking stage. The stress in the steel was taken to be that occurring for a plain or FRC concrete section with 3×16 mm bars.

If post-crack performance at a smaller crack width in the ASTM C1609 beams is used as the design parameter, then the predicted design crack width would have been larger for almost all the mixtures. This would have resulted in the trend line in Fig. 6b lying a little closer to equality for all the mixtures, and much closer for the PVA mix. This suggests that using a prediction method based on empirical data generated at 0.5-1.0 mm maximum crack width may not produce good estimates of in-service crack widths for FRC comprised of fibres that display rapid changes in performance in the immediate post-crack range.

5 Concluding remarks

A series of trials were undertaken in which large Reinforced Concrete beams were cast and tested using plain concrete and Fibre Reinforced Concrete to examine the effect of the addition of steel and synthetic fibres on flexural crack widths. The beams were loaded in four-point bending, and crack spacing and widths were measured for increasing applied moment.

This document is the intellectual property of the fib – International Federation for Structural Concrete. All rights reserved.
This PDF of fib Bulletin 95 is intended for use and/or distribution solely within fib National Member Groups.

The results demonstrated that fibres can reduce both the spacing and width of cracks when used in combination with conventional steel reinforcement.

Steel and macro-synthetic fibres made of polypropylene and aramide were found to substantially reduce flexural crack widths, and that the degree of crack width reduction was related to post-crack residual strength. The majority of micro-synthetic fibres, made from polypropylene, glass, and basalt, proved ineffective in reducing either crack spacing or width. However, PVA micro-fibres were found to be highly effective in reducing both crack spacing and width, and the efficacy of these fibres was much better than is suggested by the post-crack performance exhibited in standard beam tests. It is therefore apparent that some synthetic fibres are very effective for crack width control and deserve to be investigated in further detail for their potential use in reducing flexural crack widths in RC/FRC hybrid members.

6 Acknowledgements

The Author acknowledges the support provided by EPC Pty Ltd in funding this work, and Joshua Tolhurst and Keith Clarke in conducting the majority of the tests described in this paper.

7 References

Abrishami, H. H., and Mitchell, D., 1997. "Influence of Steel Fibres on Tension Stiffening," *ACI Structural Journal*, 94(6) pp769-776.

AS/NZS 4671: 2001 *Steel Reinforcing Materials*, Standards Australia, Sydney.

Australian Standard AS3600, 2014. *Concrete Structures*, Standards Australia, Sydney.

Australian Standard AS3600, 2014 *Concrete Structures*, Commentary, Standards Australia, Sydney

Bernard, E.S., 2016. "Investigation of Crack Width Control Using Barchip Macro-synthetic Fibres in Reinforced Concrete Beams", *World Tunneling Congress 2016*, San Francisco, April 22-28.

Bischoff, P. H., 2003. "Tension Stiffening and Cracking of Steel Fibre-Reinforced Concrete," *Journal of Materials in Civil Engineering*, ASCE, 15(2), pp. 174-182

Conforti, A., Zerbino, R., and Plizzari, G.A., 2018. "Influence of steel, glass and polymer fibers on the cracking behavior of reinforced concrete beams under flexure", Structural Concrete, 1-11. doi.org/10.1002/suco.201800079

Deluce, J.R., Lee, S-C., and Vecchio, F.J. 2014, "Crack Model for Steel Fibre-Reinforced Concrete Members Containing Conventional Reinforcement", *ACI Structural Journal*, 111(1) pp93-102.

Dupont, D., and Vandewalle, L., 2003, "Calculation of Crack Widths with the σ-ε Method," Test and Design Methods for Steel Fibre Reinforced Concrete: Background and Experiences, *Proceedings of the RILEM TC162-TDF Workshop*, RILEM Technical Committee 162-TDF, Bochum, Germany, pp119-144.

Eurocode 2, 2004. Design of Concrete Structures, British Standard BS EN 1992-1-1:2004, European Committee for Standardisation (CEN).

fib, 2012. *Model Code 2010*, Bulletin 65, Fèdération Internationale du Béton, Lausanne

This document is the intellectual property of the fib – International Federation for Structural Concrete. All rights reserved.
This PDF of fib Bulletin 95 is intended for use and/or distribution solely within fib National Member Groups.

Gilbert R.I. and Bernard, E.S., 2015. "Time-dependent Analysis of Macro-synthetic FRC Sections with Bar Reinforcement", *World Tunneling Congress 2015*, Dubrovnik, May 22-28.

Gilbert R.I., Mickleborough, N.C. and Ranzi, G., 2017. *Design of prestressed concrete to Eurocode 2*, Second Edition, CRC Press (Spon Press), Florida.

Jansson, A., Gylltoft, K., and Löfgren, I, 2010. "Flexural behaviour of members with a combination of steel fibres and conventional reinforcement", *Nordic Concrete Research*, (42) pp155–171.

Tiberti, G., Minelli, F., Plizzari, G.A., and Vecchio, F.J., 2014. "Influence of concrete strength on crack development in SFRC members", *Cement & Concrete Composites*, 45, pp176-185.

Vandewalle, L., 2000. "Cracking behaviour of concrete beams reinforced with a combination of ordinary reinforcement and steel fibres", *Materials and Structures*, 33, pp164-170.

This document is the intellectual property of the fib – International Federation for Structural Concrete. All rights reserved.
This PDF of fib Bulletin 95 is intended for use and/or distribution solely within fib National Member Groups.
FRC2018: Fibre Reinforced Concrete: from Design to Structural Applications
Joint ACI-*fib*-RILEM International Workshop

Influence of chloride-initiated corrosion on the surface aspect of steel fibre reinforced cementitious composites

Mylene M. Vieira[1], Sergio H. P. Cavalaro[2], Antonio Aguado[1]

[1] : Polytechnic University of Catalonia, Barcelona, Spain.

[2] : Loughborough University, Loughborough, United Kingdom.

Abstract

The corrosion of steel fibres at the surface of a cement composite affects the aesthetic of the structure. Few studies in the literature focus on establishing relationships between the fibre content and the surface corrosion of specimens when subjected to aggressive conditions. The objective of this study is to evaluate the correlation between the fibre content and the level of surface corrosion from a quantitative point of view. Two mixes of high performance cementitious composites with different steel fibre contents (90 and 190 kg/m^3) and the same water/cement ratio were designed. Prismatic specimens were cast and put through a cyclic process of wetting (48 hours submerged in salt water) and drying (48 hours at ambient temperature). Every 10 cycles, pictures were taken of the surface of each specimen and the area of corrosion was measured by means of an algorithm developed for the analysis. Results showed that the increase of fibre content is correlated with the increment of surface area of corrosion.

Keywords

Cement composite, Steel fibre, Corrosion, Aesthetic aspect.

https://doi.org/10.35789/fib.BULL.0095.Ch35

This document is the intellectual property of the fib – International Federation for Structural Concrete. All rights reserved.
This PDF of fib Bulletin 95 is intended for use and/or distribution solely within fib National Member Groups.

1 Introduction

High performance steel fibre reinforced cementitious composites (HPSFRCCs) are materials usually produced with high fibre contents. They are containing steel fibres in order to achieve ductile behaviour and, if possible, to eliminate the need of passive reinforcement [Resplendino, 2004]. The addition of steel fibres into the mix enhances crack control and its post-cracking mechanical behaviour. Due to the improved mechanical and physical characteristics, its use in infrastructures has led to numerous applications worldwide in the last five decades.

The use of ultra-high performance concrete (UHPC) in any infrastructure application requires to have adequate resistance to deterioration caused by the environment to which it is exposed [Russell and Graubeal, 2013]. In spite of HPSFRCCs dense matrix, the presence of porosity or cracks can allow the ingress of deleterious substances. Similar, to ordinary concrete structures, durability problems may appear in steel fibre reinforced concrete (SFRC) when subjected to corrosive environments [Jianhua, 2014]. The entry of chlorides in concrete is one of the essential causes for damage of concrete-structures through steel corrosion [Teichmann and Schmidt, 2004].

For SFRC, some of randomly and uniformly distributed fibres in the matrix actually are located at the surface of the element and are not protected from the surrounding environment by any concrete cover [ACI-544, 2010]. Therefore, when the steel fibres in cement composites are subjected to chloride attack a damaging effect may occur regarding the mechanical response or aesthetic aspect.

Some researchers evaluated the effects of chloride ingress in SFRCs on the mechanical response of the steel fibres [Mangat and Gurasami, 1987; Kosa and Naaman, 1990; Tran et al., 2015]. In general, studies in the literature focus mainly on corrosion arising in structures with cracks [Granju and Balouch, 2005; Raffie, 2012; Hashimoto et al., 2013].

Most of the studies regarding the aesthetic point of view investigated the chloride-initiated corrosion in SFRCs [Balouch et al., 2010; Serna and Arango, 2008; Mangat and Gurasami, 1988; Frazão et al., 2015]. In the case of HPSFRCCs with a high content of steel fibres the damaging effect caused by the formation of surface corrosion is significantly undesirable and not yet fully understood.

The objective of this paper is to evaluate the evolution of surface corrosion produced by chloride ingress in HPSFRCCs correlating the steel fibre content and the percentage of surface corroded area over cycles.

Firstly, the experimental programme consisted of subjecting specimens to an initial cyclic process of wetting (48 h submerged in distilled water) and drying (48 h at ambient temperature) for two complete cycles. Then, the durability test was carried out subjecting the samples to a cyclic process of wetting (48 h submerged in salt water) and drying (48 h at ambient temperature). Pictures were taken of the exposed surface of each specimen alter 5 cycles and then every 10 cycles. Finally, the corroded area was measured by processing the images with the use of algorithms developed for the analysis.

This document is the intellectual property of the fib – International Federation for Structural Concrete. All rights reserved.
This PDF of fib Bulletin 95 is intended for use and/or distribution solely within fib National Member Groups.

The conclusions derived from this study can provide data to predict the evolution related to aesthetic aspect for HPSFRCCs. Additionally, this work contributes results that can be used to set criteria for these materials under chloride attack.

2 Experimental program

2.1 Materials and composition

For the experimental program, two mixes of HPSFRCCs (F_90 and F_190) with fibre contents of 90 and 190 kg/m^3, respectively were used. The steel fibres used had characteristics (provided by the manufacturer) such as: a circular cross-section, straight ends, made of coll-draw wire, 13 mm of length (L), 0.20 mm of diameter (d) and 65 of aspect/ratio (L/d). The quantity of materials per m^3 of both three mix are described in Table 1.

Table 1: Cement composites mixes

Materials		**F_90**	**F_190**
Cement I 52.5R	kg/m³	800	800
Silica sand 0.3-0.4 mm	kg/m³	1131	1098
Water	kg/m³	129	129
Superplasticizer	l/m³	32	32
Nanosilica	l/m³	40	40
calcium carbonate powder	kg/m³	200	200
Steel fibre OL 13/0.20	kg/m³	90	190
W/C	-	0.23	0.23

2.2 Specimen preparation and durability test

For the tests, 10 prismatic specimens measuring 40 x 40 x 160 mm were cast for each mix. In order to produce the samples, dry materials (cement, silica sand and calcium carbonate) were weight automatically and placed in this order in a vertical axis mixer. The materials were mixed during one minute. Subsequently, the water, the nanosilica and the steel fibres were added manually and mixed during three or four minutes. Then, the mixes were dumped into a skip with straight outlet which poured the moulds automatically (see Figure 1a). After the filling, the excess of HPSFRCC was manually removed from the moulds. To avoid loss of water by evaporation a cure film was sprayed on all samples. The specimens were removed from the moulds 24 h after casting and stored at ambient temperature until the date of testing (see Figure 1b).

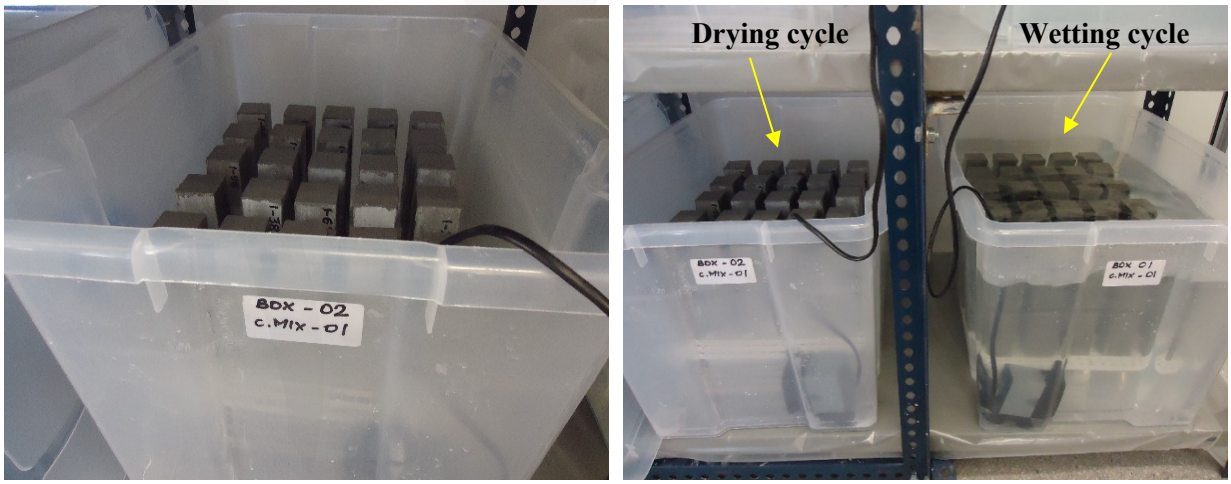
This document is the intellectual property of the fib – International Federation for Structural Concrete. All rights reserved.
This PDF of fib Bulletin 95 is intended for use and/or distribution solely within fib National Member Groups.



(a) (b)

Figure 1: Preparation of the specimens: pouring the moulds (a); specimens stored (b)

In order to allow the ingress of chlorides in only one direction, five faces of each specimen were waterproofed. A flexible water-based epoxy membrane was applied in two coating steps keeping an interval of 24 hours for re-coating. Afterwards, the specimens were stored for 7 days at ambient temperature until the fully cure of the epoxy membrane.
The durability test consisted of subjecting the samples to wetting (48 hours submerged in salt solution with 5% of NaCl) and drying (48 hours at ambient temperature). Before the cycles with salt water started, the samples were put through a cyclic process of wetting (48 hours submerged in distilled water) and drying (48 hours at ambient temperature) to ensure the same condition of the specimens in the beginning and during the cycle. After that, the sodium chloride was added to the distilled water to start the cycles of chloride attack.
During the cycles, the samples were organized in plastic boxes (see Figure 2a). A circulation pump was used during the wetting cycles to circulate the salt water. Manually, with the use of a suction pump, after two days of wetting cycles, the salt water was pumped from one box to another to start the drying cycles. Figure 2b shows the setup of the cycles.



(a) (b)

Figure 2: Wetting and drying cycles: samples in the box (a); durability test set-up (b)

This document is the intellectual property of the fib – International Federation for Structural Concrete. All rights reserved.
This PDF of fib Bulletin 95 is intended for use and/or distribution solely within fib National Member Groups.

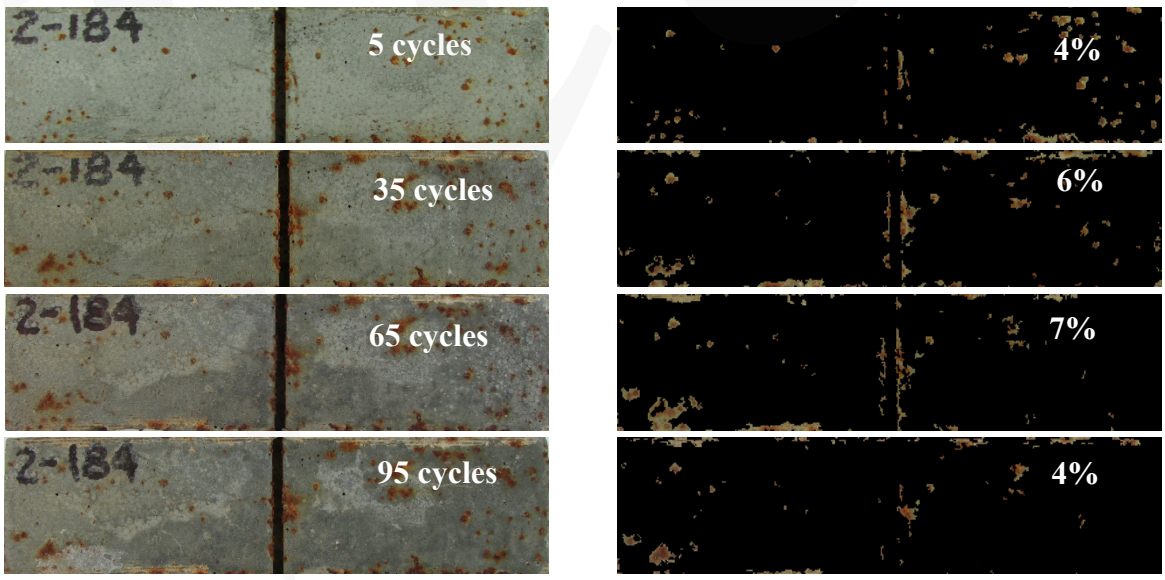
2.3 Analysis of the surface corrosion

For the analysis of surface corrosion, pictures of the same surface of each specimen were taken every 5 or 10 cycles. The method to determine the corroded surface area consisted of analysing the images with the aim to identify the evolution of the area which represented the corroded area. For that, an algorithm was developed and implemented in Matlab® using the HSV (Human Visual System) colour model.

The first step is to transform the image from RGB (Red, Green and Blue) to HVS and decompose it into three layers that represent the model: hue (H), saturation (S) and brightness value (V). For each of the layers the interest range is indicated by the histograms: for the hue, the pixels are separated with values from 0 (zero) to the threshold, for the saturation and brightness the pixels with values greater than the threshold are selected. In the sequence, the pixels that appear simultaneously in the range of interest of the three layers are selected. The identified pixels indicate areas with presence of surface corrosion. The relation between the identified pixels and the total quantity of pixels of the image (resolution) defines the percentage of area with presence of corrosion.

3 Results and analysis

The corroded surface area represents an average value of the same 10 specimens tested over cycles of each mix. For the analysis, the data of the measured corroded area were treated with the use of two statistic methods. At first the values of outliers were detected and then the 95% of confidence interval was calculated. Figures 3a and 3b show the pictures of the exposed surface of one specimen and the percentage of corroded area detected by the algorithm for the lowest fibre content studied (90 kg/m^3), respectively. The figures illustrate the evolution of the surface corrosion after 5, 35, 65 and 95 wetting and drying cycles.



(a) (b)

Figure 3: Surface corrosion for 90 kg/m^3 of fibres: samples (a); corrosion detected (b)

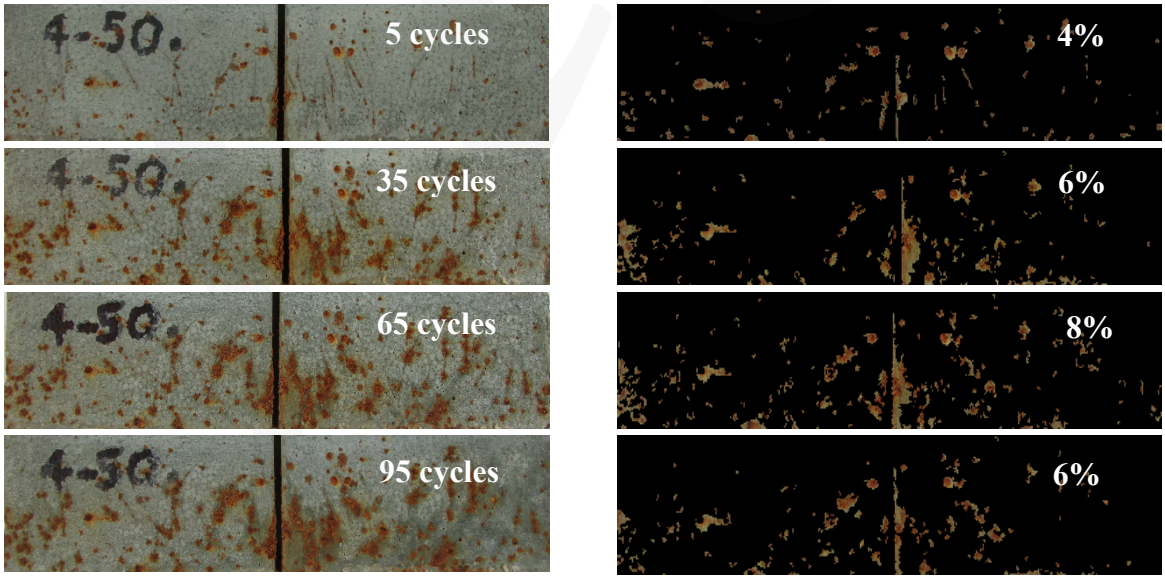
This document is the intellectual property of the fib – International Federation for Structural Concrete. All rights reserved.
This PDF of fib Bulletin 95 is intended for use and/or distribution solely within fib National Member Groups.

Figures 3a and 3b reveal the presence of surface corrosion for the lowest fibre content (90 kg/m^3). Already after 5 cycles, a level of corrosion was detected, increasing gradually until 65 cycles and after that (at 95 cycles) a decrease can be noticed. Such result may be a consequence of the accelerated process of corrosion for the salt solution cyclic condition to which the specimens were subjected. For HPSFRCCs the evolution of the percentage of corroded area throughout the cycles may be related to the amount of steel fibres covered by a thin layer very.

The process of corrosion is dependent on the rate with which the chlorides penetrate into the sample through the pores. Moreover, conditions as the quantity of iron, water and oxygen available to start the corrosion are needed. The duration of the wetting and drying also plays a key role in the beginning and development of the corrosive process. While during the wetting can enter water and chlorides, during the drying the oxygen penetrates into the pores. It should be remarked that during cycles of two days for each period (wetting and drying) water may remain the pores hereby reducing the entry of oxygen during the drying time.

In the case of HPSFRCCs, with a very dense matrix, the corrosion is more significant for the fibres very close to the surface. It indicates that the low porosity limits the corrosion to a very superficial layer of the specimens. Although, throughout the cycles, the chlorides still are entering into the pores deeper in the samples, the process of corrosion is slow due to the low availability of oxygen. Besides that, the products of iron oxidation generated deeper cannot reach the surface. The surface corrosion is limited by the mobilization of the products of corrosion from the pores close the surface carried by the flow of salt water outside during the drying.

The pictures of the exposed surface of one specimen and the percentage of corroded area detected by the algorithm for the highest fibre content studied (190 kg/m^3), are presented in Figures 4a and 4b, respectively. The presence of surface corrosion is studied at 5, 35, 65 and 95 wetting and drying cycles.



(a) (b)

Figure 4: Surface corrosion for 190 kg/m^3 of fibre samples (a); corrosion detected (b)

This document is the intellectual property of the fib – International Federation for Structural Concrete. All rights reserved.
This PDF of fib Bulletin 95 is intended for use and/or distribution solely within fib National Member Groups.

The results in Figures 4a and 4b show that a level of corrosion was observed already at 5 cycles of chloride attack for the samples with 190 kg/m^3 of fibre content. The corroded area increased until 65 cycles and then a decrease was observed at 95 cycles. Such behavior may indicate that under wetting and drying cycles with salt water the steel fibres localized close to the surface are prone to be corroded. Moreover, the evolution of the percentage of corroded area over cycles shows that the quantity of fibres available at a superficial layer of a specimen controls the surface corrosion.

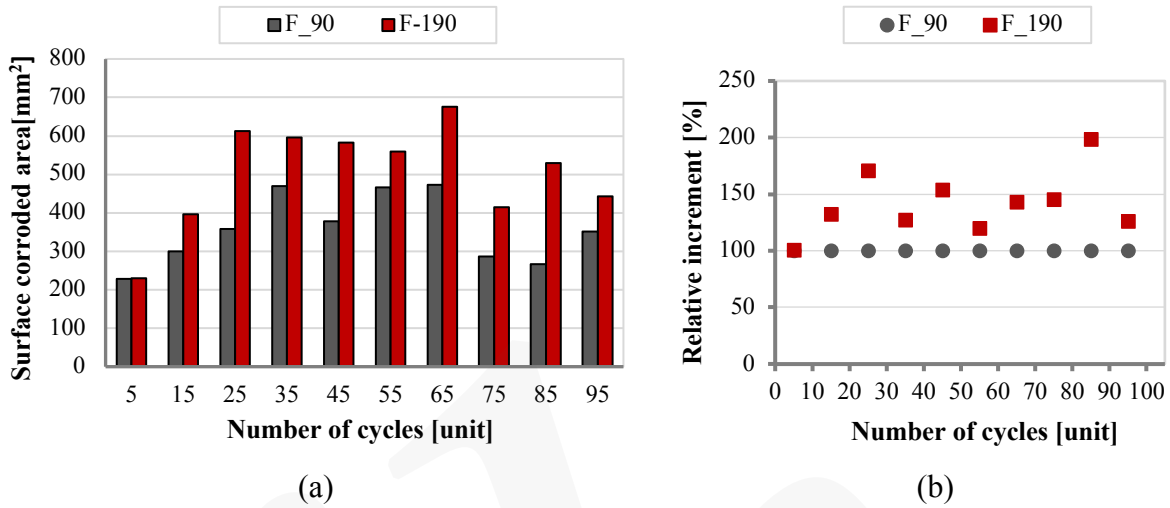
After 5 cycles the presence of corrosion detected in the samples may be the result of the amount of fibres in a surface layer reacting with the chlorides, water and oxygen present in the pores. Due to the high concentration of chlorides in the salt solution, the amount of free chlorides exceeds the critical value necessary to start the reactions in the pores and corrosion occurs very fast. In addition to that, the cycles favour the flow of salt water from the pores to the surface during the drying in order to attain equilibrium with the environment. Such movement mobilizes the products of corrosion through the pores and its deposition at surface.

Until 65 cycles the increment of corrosion may be the consequence of the great amount of fibres at the surface available to be corroded. In the case of micro steel fibres the expansion of products of corrosion generated is considered insufficient to produce micro-racks and spalling of the cementitious matrix. So, the formation of corrosion at surface may be controlled by the porosity and the water flow during the cycles. The increase of the quantity of fibres in cementitious composites might increase the porosity surrounding theses fibres which facilitates the mobilization of the iron oxides to the surface.

The decrease of corroded area at 95 cycles may be a result of the reduction of the quantity of steel fibres at surface. A level of leaching of the products of corrosion from the surface observed during all cycles may also contribute to the reduced corrosion detected. Besides that, the iron oxides generated deeper into the sample cannot be transported easily to the surface easily due to the low porosity. It should be remarked that the presence of products of corrosion in the pores can make the entry of salt solution and oxygen over cycles more difficult. So, a stabilization of the corroded area can be noticed as a consequence of all these mechanisms.

The influence of chloride corrosion on the surface aspect of HPSFRCCs is studied dependent on the steel fibre content. The graph of the surface corroded area at all cycles (5 to 95 cycles) is presented in Figure 5a. In addition to that, the relative increment of surface corrosion for the specimens with fibre contents of 190 kg/m^3 and 90 kg/m^3 of fibre (considered 100%) is illustrated in Figure 5b.

This document is the intellectual property of the fib – International Federation for Structural Concrete. All rights reserved.
This PDF of fib Bulletin 95 is intended for use and/or distribution solely within fib National Member Groups.



(a) (b)

Figure 5: Corrosion from 5 to 95 cycles: corroded area (a); relative increment (b)

The results in Figure 5a reveal that the increment of the surface corrosion is closely related to the increase of fibre content. The samples with 190 kg/m^3 of fibres presented higher values of corrosion when compared to the samples with 90 kg/m^3 of fibres at all cycles studied. Such behavior may be expected since the increment of fibre content in cementitious composites increases the presence of fibres close to the surface. The increase of the corroded area is not directly related to the increment of fibre content. However, more fibres produce a higher level of surface corrosion.

At 5 cycles, the samples with 90 and 190 kg/m^3 of fibres present very similar values of corroded area. This may be a result of the similar time to initiate the process of corrosion and the consequent mobilization of the iron oxides to the surface. From 5 to 65 cycles, the samples with a higher fibre content present a higher level of corrosion then the specimens with less fibres. The amount of fibres corroded and the porosity of the region close to the fibres allows the movement of the products of corrosion and its deposition at the surface. The scatter of the values may be a consequence of the process of fibre corrosion and leaching at surface which affects the measured area throughout the cycles.

From 65 to 95 cycles, a tendency of reduction of the surface corrosion was observed for both fibre contents. The results may indicate that the corrosion for the HPSFRCCs is limited to the layer very close to the surface. Although the ions of chlorides still are entering deeper into the samples over the cycles, the entry is slowed down by the mechanisms of diffusion. Moreover, the low level of porosity, of oxygen and of water reduces the level of fibres corrosion. As the process of corrosion and mobilization deeper in the sample occurs slowly and the wetting cycles favours the leaching, the surface corrosion is consequently reduced.

The relative increment of corroded area in Figure 5b shows that the increase of the fibre content caused an increment of corrosion alter all cycles. The higher the fibre content the higher the percentage of surface corrosion. It should be pointed ant that for both fibre content (90 and 190 kg/m^3) a damage at different levels regarding the aesthetic aspect was observed for the HPSFRCCs. Part of the steel fibres randomly distributed into the matrix may be localized in a layer very close to the surface and they are prone to be corroded in the chloride containing aggressive environment.

This document is the intellectual property of the fib – International Federation for Structural Concrete. All rights reserved.
This PDF of fib Bulletin 95 is intended for use and/or distribution solely within fib National Member Groups.

4 Conclusions

1. The results suggest that chloride corrosion produces a damage at different levels regarding the surface aspect for both steel fibre contents studied (90 and 190 kg/m^3). The presence of corrosion was observed at all cycles studied (5 to 95 cycles).
2. The increment of the fibre content increased the surface corrosion of the samples during cyclic wetting and drying. A higher fibre content in cementitious composites means more fibres close to the surface increasing the corroded area.
3. The analysis of the surface corrosion being indicated that for HPSFRCCs, the corrosion is limited to the fibres localized in a thin layer very close to the surface. High levels of porosity, the availability of iron, of salt solution and the presence of oxygen allow the corrosive reactions.
4. The corrosion presented, in general, an increment until 65 cycles for both fibre contents, and then a trend of stabilization occurs. Until 65 cycles, the corrosion is related to the oxidation of the fibres at the surface, and then, from 65 to 95 cycles, the process of corrosion occurs more slowly and potentially, deeper in the sample and a reduction of surface corrosion is observed.

5 Acknowledgements

The first author would like to thank CAPES (Coordenação de Aperfeiçoamento de Pessoal de Nível Superior - Processo Nº01.3117/2013-00).

6 References

ACI Committee 544 (2010), *Report on the Physical Properties and Durability of Fiber-Reinforced Concrete*, ACI 544.5R-10, American Concrete Institute, ACI Farmington Hills.

Balouch, S.U., Fouth, J.P., Granju, J.-L. (2010). "Surface corrosion of steel fibre reinforced concrete". Cement and Concrete Research, 40, 410-414.

Frazão C., Camões, A., Barros, J., Gonçalves, D. (2015). "Durability of steel fiber reinforced self-compacting concrete". Cement and Concrete Research, 40, 410-414.

Granju, J. L., Balouch, S. U. (2005). "Corrosion of steel fibre reinforced concrete from the cracks". Cement and Concrete Research, 35, 572-577.

Hashimoto, K., Toyoda, T., Yokota, H., Kono, K., Kawaguchi, T. (2013). "Tension-softening behavior and chloride ion diffusivity of cracked ultra-high strength fiber reinforced concrete". *Proc. RILEM –fib AFGC Int. Symp. on Ultra-High Performance Fibre-Reinforced Concrete*, Marseille, 257-264.

Jianhua, W. (2014). "The study of steel fiber reinforced concrete durability based on damage mechanisms". Research J. of Applied Sciences, Eng. and Tech., 7(3), 543-550.

Kosa, K., Naaman, A. E., (1990). "Corrosion of steel fibre reinforced concrete". ACI Structural Journal, 87, 27-37.

Mangat, P. S., Gurusamy, K. (1987). "Permissible crack widths in steel fibre reinforced marine concrete". Materials and Structures, 20, 338-347.

Mangat, P. S., Gurusamy, K. (1988). "Corrosion resistance of steel fibres in concrete under marine exposure". Cement and Concrete Research, 18, 44-54.

This document is the intellectual property of the fib – International Federation for Structural Concrete. All rights reserved.
This PDF of fib Bulletin 95 is intended for use and/or distribution solely within fib National Member Groups.

Rafiee, A. (2012). Computer modelling and investigation on the steel corrosion in cracked ultra- high performance concrete. Doctoral Thesis, Kassel University, Kassel.

Resplendino, J. (2004). "First recommendations for ultra-high-performance concretes and examples of applications". *Proc., Int. Symp. on Ultra High Performance Concrete,* Univ. Kassel, Germany, 79-90.

Russell H. G., Graybeal, B. A. (2013). "Ultra-High Performance Concrete: State-of-the-Art Report for the Bridge Community". FHWA-HRT-13-060, McLean, VA. 171p.

Serna, P., Arango, S. E. (2008) "Evolution of the flexural behaviour of precracked SFRC in marine environment. *Proc., Seventh Int. RILEM Symp.of Fibre-Reinforced Concrete: Design and Applications*, Chennai, 14, 595-605.

Teichmann, T., Schmidt, M. (2004) "Influence of the packing density of fine particles on structure, strength and durability of UHPC". *Proc., Int. Symp. on Ultra High Performance Concrete,* Univ. Kassel, Germany, 313-324.

Tran, N. T., Pyo, S., Kin, D. J. (2015). "Corrosion resistance of strain-hardening steel-fibre-reinforced cementitious composites". Cement and Concrete Composites, 63, 17-29.

This document is the intellectual property of the fib – International Federation for Structural Concrete. All rights reserved.
This PDF of fib Bulletin 95 is intended for use and/or distribution solely within fib National Member Groups.
FRC2018: Fibre Reinforced Concrete: from Design to Structural Applications
Joint ACI-*fib*-RILEM International Workshop

Serviceability Limit State Design of SFRC Members

Ali Amin[1], R. Ian Gilbert[2]

[1] : The University of Sydney, Sydney, Australia.

[2] : The University of New South Wales, Sydney, Australia.

Abstract

A significant body of research is available on the strength of steel fibre reinforced concrete (SFRC) members subjected to shear and flexure. The behaviour of SFRC under service loads has received less research attention. As the fibres are capable of transmitting tensile stress across a crack, the average tensile strain at a crack in a reinforced concrete member containing fibres is less than that in a similar member without fibres. As a result, the cracking and deformation characteristics of reinforced concrete structures can be significantly improved by adding fibres to the concrete mix. This paper first describes a physically rationale model of the tension stiffening behaviour of SFRC. With this behaviour quantified, expressions suitable for the design of SFRC members are derived for the control of instantaneous deflections and crack widths. Finally, a short example is provided.

Keywords

Steel fibre, concrete, serviceability, deflections, crack widths.

This document is the intellectual property of the fib – International Federation for Structural Concrete. All rights reserved.
This PDF of fib Bulletin 95 is intended for use and/or distribution solely within fib National Member Groups.

1 Introduction

In fibre reinforced concrete (FRC), the primary objective of the fibres is to bridge the cracks in concrete once they form and hence provide some post-cracking resistance in tension. Applications of the material are now common practice in the Australian infrastructure sector for industrial joint-less pavements, sprayed tunnel shotcrete linings, and some residential load bearing elements. A faster acceptance of the material has taken place in Europe and Asia with steel fibres used as the sole, primary reinforcement in some residential suspended slabs. Steel fibres have also been used to replace conventional bar reinforcement in carrying shear and bursting stresses in large span (~100 m) prestressed bridges.

Despite the increased awareness of the benefits of steel fibres by both practitioners and researchers, the use of SFRC in Australia has largely been limited to non-critical members, even though significant potential exists for full or partial replacement of costly, manually placed, steel bar reinforcement in a wide range of applications. SFRC systems have the potential to improve architectural freedom, allowing for non-orthogonal shapes and floor plans, which may otherwise be difficult with conventional reinforcing bar layouts and formwork systems.

The relatively slow take up of this material is possibly because standardized procedures for the design of SFRC have not been developed and, as a result, practicing engineers have little design guidance. In addition, some practitioners may be uncomfortable with the idea of relying on randomly placed fibres to provide post-cracking strength in bending or direct tension. Test methods that can correctly, and accurately, establish the constitutive behaviour of the material are required, particularly the post-cracking response in tension. Only when the material constitutive relationships for SFRC is determined with confidence can the material be reliably incorporated into structural elements. A catalyst in promoting this material to structural practitioners, however, is the establishment of physical mechanical models that can accurately explain and predict the material's response to a variety of load cases (gravity, fire, etc.). For SFRC, these models should be versatile enough to handle a range of inputs (fibre type, specimen geometry, loading conditions etc.) yet simple enough for routine use in structural design. An engineer should be able to give physical significance to the different parameters being calculated and understand why they are important. This has been addressed recently for SFRC in the publication of the *fib* Model Code 2010 and the Australian Bridge Code for Concrete Structures AS5100.5-2017.

This paper provides a description of tension stiffening pertaining to SFRC and how this can be included in the calculation of instantaneous deflections and for crack control under in-service conditions.

2 Tension stiffening and crack spacing in SFRC

While much research effort has been devoted to the understanding of the behaviour of structural members made of SFRC at the ultimate limit state, particularly in shear and flexure, significant benefits exist at service loads when steel fibres are incorporated into the concrete mix, specifically more finer closely spaced cracks and reduced deflections. Fibres not only transmit tensile stress across cracks, they also enhance the interaction and stress transfer from the reinforcing bar to the matrix by inhibiting the propagation of splitting cracks that occur as a result of localized stress points around the ribs of a deformed bar. The addition of fibres can

This document is the intellectual property of the fib – International Federation for Structural Concrete. All rights reserved.
This PDF of fib Bulletin 95 is intended for use and/or distribution solely within fib National Member Groups.

therefore improve the cracking and deformation characteristics of the composite. When both fibres and conventional reinforcing steels bridge a crack, the stress transmitted across the crack is shared between the reinforcing bar and the fibres. Consequently, the average strain, and hence stress, in the conventional steel bar under in-service conditions is lower than it would be without the fibres (provided the steel hasn't yielded and the fibres haven't completely pulled out), and this leads to finer and more closely spaced cracks.

Consider the instantaneous tensile load-displacement response of a plain concrete tension tie, square in cross section and reinforced with a single concentric reinforcing bar (see Figure 1). Neglecting any effects due to shrinkage, the response of the member prior to cracking is linear-elastic. The initial slope of the load-displacement relationship is directly proportional to the area of the transformed section. On first cracking, the stiffness of the tie drops significantly, however, with only one crack, much of the tie is uncracked. With an increase in applied load, more cracks develop along the length of the tie and the average stiffness of the member further decreases. If the concrete between the cracks carried no tensile stress, then the response would follow that of the bare bar. The difference between the actual behaviour of the tie shown in Figure 1 and that of the bare bar is referred to as '*tension stiffening*' and is attributed to the ability of concrete to carry tension between cracks as a result of the bond which is developed between the reinforcing steel and concrete matrix. Tension stiffening increases the member's rigidity/stiffness prior to the yielding of the steel bar and hence, has the capacity to affect the deformation and cracking characteristics of the member.

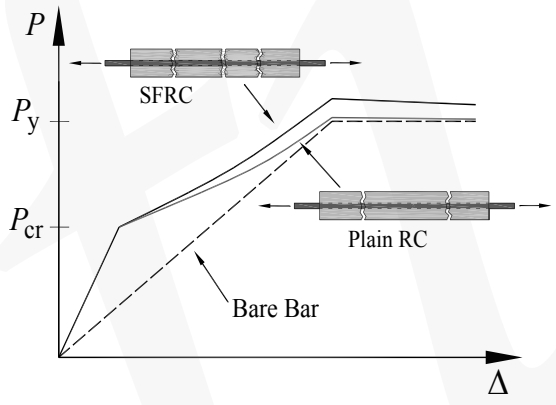


Figure 1: Tension stiffening in SFRC and plain concrete tension ties

The tension stiffening behaviour of SFRC is different to that of plain concrete. In plain concrete ties, the concrete carries no stress at the cracks, and can only carry tension between cracks. In SFRC tension ties, the fibres in the concrete matrix can carry tension across the crack and the fibre-concrete also carries tension between the cracks due to the bond between the steel fibres and the concrete and the reinforcing bar and the concrete. This leads to a greater resistance in tension, not just after cracking, but also after yielding of the reinforcing bar (as the fibres can still be effective at this stage).

Amin et al. (2016) developed a generalized tension stiffening model for SFRC tension ties based on the principles of the Tension Chord Model (TCM) of Marti et al. (1998). The TCM is a physically consistent tool often used to model the load-deformation behaviour of tensile regions in members with uniaxial stress states, such as in tension ties and the tensile zones in one-way beams and slabs. In their model, Amin et al. (2016) considered the stress along a given tension tie and assumed that the resistance provided by the three components of the tie (concrete bond, steel fibres and steel reinforcing bar) could be determined independently. This is shown in Figure 2, with the main difference to the original TCM being that at the crack, the fibres carry a stress equivalent to $\sigma_f(w)$. By the principle of compatibility, midway between cracks, the stress in the reinforcement is a minimum and the stress in the concrete is a maximum. If the maximum concrete stress between cracks reaches the tensile strength, f_{ct}, an additional crack occurs.

This document is the intellectual property of the fib – International Federation for Structural Concrete. All rights reserved.
This PDF of fib Bulletin 95 is intended for use and/or distribution solely within fib National Member Groups.

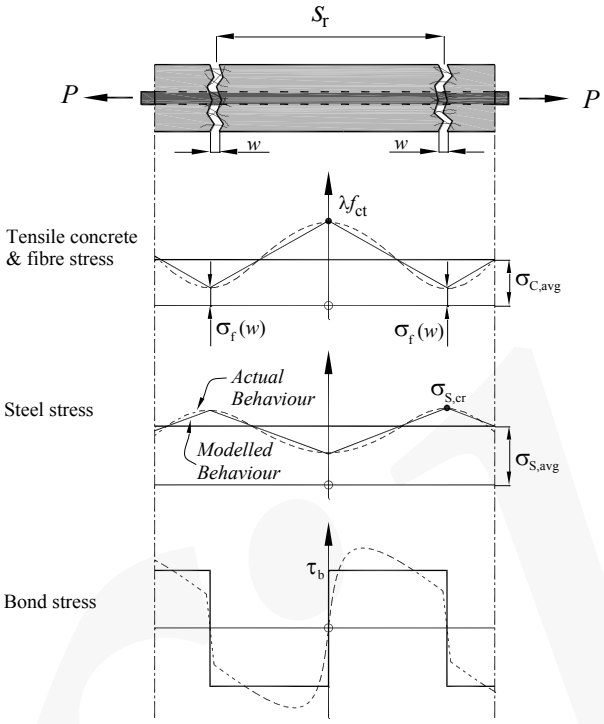


Figure 2: Tension chord model including effect of steel fibres and reinforcing bar

In developing an expression for the average tension stiffening along a SFRC tension tie, Amin et al. (2016) considered the stress distributions that occur at the two extreme scenarios of crack spacing. The element shown in Figure 3a, illustrates the maximum crack spacing (s_r) for a SFRC tension tie. This occurs when the section midway between two primary cracks is just at the point of cracking. It follows that the minimum crack spacing is $s_r/2$ when a primary crack occurs between two primary cracks s_r apart, as shown in Figure 3b, and the maximum force in the concrete between the cracks is limited to $(f_{ct}+\sigma_f(w))/2$. No further primary cracking can occur if the distance between the cracks is too small to develop sufficient force (through bond between the reinforcing steel and the surrounding concrete) to allow the stress within the concrete to reach its tensile strength, f_{ct}. This is the same rational as that adopted in the original TCM

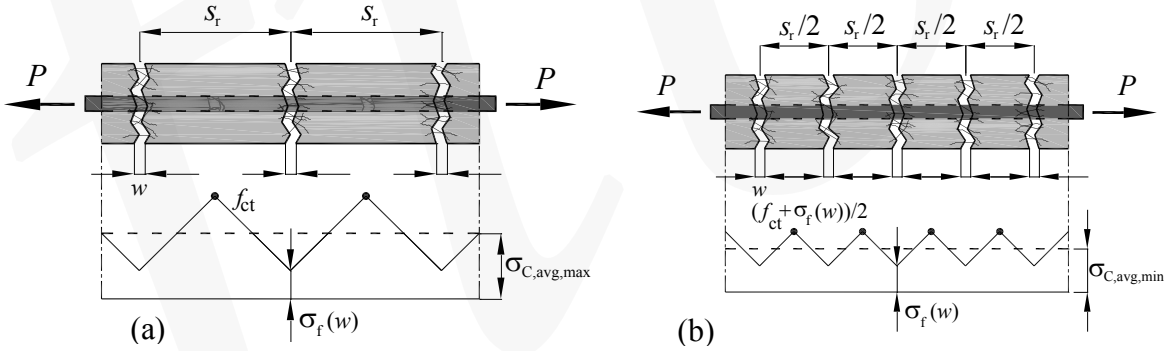


Figure 3: Tension chord model for SFRC: (a) Max crack spacing; (b) Min crack spacing

To appreciate the contribution of the fibres in a tension chord, consider the concrete stress distribution presented in Figure 4, in which two primary cracks exist at a crack spacing of s_r. The gradient of stress developed in the concrete between the crack and the location midway between the two primary cracks is assumed to be the same for SFRC and RC and is taken as a function of the bond stress between the reinforcing steel and cementitious matrix, the reinforcing ratio and the diameter of the bar. We note that we have assumed a constant steel to concrete bond law along the length of the chord (Marti et al. 1998). Noting that at the crack ($x = 0$, see Figure 4) the fibres transmit a tensile stress equivalent to $\sigma_f(w)$, the stress within the SFRC at any point x between the primary crack and at the location midway between the two primary cracks, $\sigma_c(x)$, may be taken as:

$$\sigma_c(x) = \sigma_f(w) + 4\tau_b\rho_{tc}x/d_b \quad \ldots 0 \le x \le s_r/2 \tag{1}$$

This document is the intellectual property of the fib – International Federation for Structural Concrete. All rights reserved.
This PDF of fib Bulletin 95 is intended for use and/or distribution solely within fib National Member Groups.

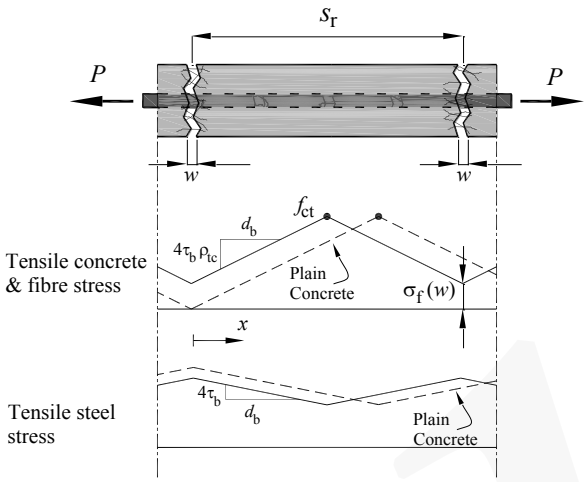


Figure 4: Crack spacing representation using TCM

where d_b is the diameter of the reinforcing bar, τ_b is a bond-stress parameter, usually taken as $\tau_b = 2f_{ct}$ for short term loading scenarios (Marti et al. 1998) and ρ_{tc} is the reinforcing ratio (A_{st}/A_{ct}). Similarly, the stress in the steel between two primary cracks depends on τ_b and d_b. At any point adjacent to the primary crack, the stress in the steel may be taken as:

$$\sigma_s(x) = \frac{T_s}{A_{st}} - \frac{4\tau_b x}{d_b} \quad \ldots 0 \le x \le s_r/2 \qquad (2)$$

where A_{st} is the cross-sectional area of steel, and T_s is the force in the steel reinforcing bar. Setting Equation 2 to f_{ct} at $x = s_r/2$ yields an expression for the maximum spacing, between two primary cracks:

$$s_{max} = \frac{\left(f_{ct} - \sigma_f(w)\right)d_b}{2\tau_b\rho_{tc}} \qquad (3)$$

By the TCM, the minimum crack spacing is half the maximum value, that is $s_{min} = s_{max}/2$. The median crack spacing is taken as λs_{max}, where $\lambda \in [0.5, 1]$. This is the same expression as derived by Pfyl (2003). Examining Figure 4 and Equation 3, it is clear that the inclusion of fibres, as a means of transmitting stress across a crack in concrete, reduces the crack spacing. This is a function of the maximum stress that can be carried after cracking and the initial crack width before the crack pattern has stabilized.

Now let us consider the average stress carried through a SFRC tension tie. For the maximum crack spacing scenario presented in Figure 3a, the average stress carried by the fibres and concrete is equivalent to:

$$\sigma_{C,avg,max} = 0.5 f_{ct}\left(1 + \sigma_f(w)/f_{ct}\right) \qquad (4)$$

where $\sigma_f(w)$ is the residual tensile stress carried by the SFRC at a crack opening displacement (COD), w. The average stress carried by the fibres and concrete along the tension chord for the minimum crack spacing scenario (Figure 3b) is equivalent to:

$$\sigma_{C,avg,min} = 0.25 f_{ct}\left(1 + 3\sigma_f(w)/f_{ct}\right) \qquad (5)$$

Amin et al. (2016) equated the median tension stiffening along the length of a given SFRC tension chord with many cracks by considering the average stress carried by the two scenarios above giving:

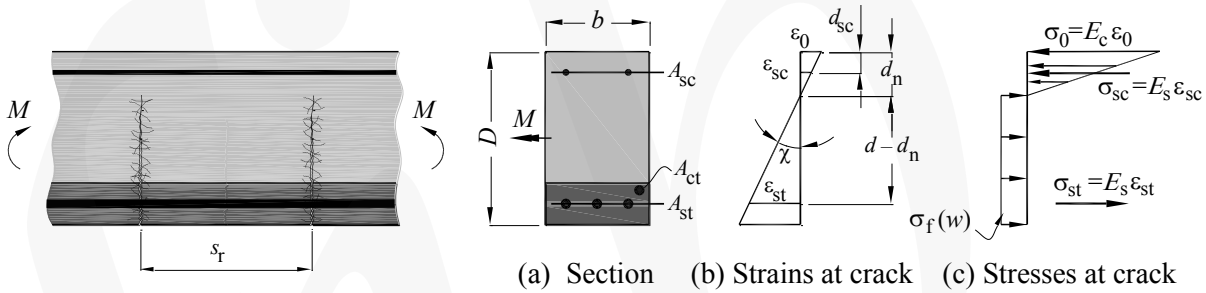
$$\sigma_{C,avg} = 0.125 f_{ct}\left(3 + 5\sigma_f(w)/f_{ct}\right) \qquad (6)$$

Amin (2015) extensively verified the TCM for many SFRC tension ties tested by a number of researchers (Deluce, 2011; Minelli et al 2015) and good correlation was shown against the experimental data when $\sigma_f(w)$ was taken as $f_{0.5}$ in Equations 3 and 6.

This document is the intellectual property of the fib – International Federation for Structural Concrete. All rights reserved.
This PDF of fib Bulletin 95 is intended for use and/or distribution solely within fib National Member Groups.

3 Simplified instantaneous deflection calculation

Consider a SFRC concrete beam of rectangular cross section after cracking. The beam can be idealized as a compression chord of depth d_n and width b and a cracked tension chord consisting of the tensile steel reinforcement A_{st} surrounded by an area of tensile concrete, A_{ct} (see Figure 5), with A_{ct} usually taken as one third of the area below the neutral axis. The short term, instantaneous deflection of a SFRC one-way member subjected to bending can be readily determined once the tension stiffening relationship of the element is established. Often, modelling the tension stiffening effect in deflection calculations for reinforced concrete members involves determining an average effective second moment of area (I_e) for a cracked member, where the effective second moment of area is empirically interpolated between the second moment of areas of the uncracked section (I_g) and the fully cracked section (I_{cr}). Deflections can then be determined by double integration of the curvatures $\chi = M/E_cI_e$ along the length of the member.



(a) Section (b) Strains at crack (c) Stresses at crack

Figure 5: Strains and stresses on a cracked SFRC rectangular section in flexure

Another method was developed by Kenel (2002) who extended the TCM and established moment-curvature relationships for different loading scenarios of reinforced concrete beams. Amin et al. (2017) adapted this model to include the beneficial effects of the fibres to the moment-curvature relationship of reinforced concrete through tension stiffening. The deflection at mid-span of a member cracked in bending may be taken as:

$$\delta = \delta_{cr} - \Delta\delta_1 \tag{7}$$

where δ_{cr} is the deflection of the member that would be obtained assuming the section is fully cracked over the entire length of the member and the term $\Delta\delta_1$ accounts for the tension stiffening effect of the cracked fibre reinforced concrete. Expressions for δ_{cr}, and $\Delta\delta_1$, are presented in Table 1 and their physical representation is illustrated in Figure 6. In Table 1, $I_g = bD^3/12$ and $M_{cr} = f_{ct}bD^2/6$ are suitable approximations for a rectangular section.

The term $\Delta\chi$ in Table 1 represents the tension stiffening component of curvature due to the cracked fibre-concrete. To account for the beneficial effects to tension stiffening of the fibres crossing the cracks in SFRC members, Amin et al. (2017) derived $\Delta\chi$ as:

$$\Delta\chi = [(0.75+ 1.25f_{0.5}/f_{ct})bf_{ct}]/(6A_{st}E_s) \tag{8}$$

To simplify the computational effort required in deriving an expression for I_{cr} for SFRC, a reasonable approximation for $I_{cr,SFRC}$ may be taken as 1.1 $I_{cr,RC}$, where $I_{cr,RC}$ is the 2nd moment of area for a non-fibre reinforced concrete section and can be evaluated from elastic analysis. For rectangular sections, $I_{cr,RC}$ is:

This document is the intellectual property of the fib – International Federation for Structural Concrete. All rights reserved.
This PDF of fib Bulletin 95 is intended for use and/or distribution solely within fib National Member Groups.

$$I_{cr,RC} = \frac{bd_{n,RC}^3}{3} + nA_{st}\left(d - d_{n,RC}\right)^2 + \left(n-1\right)A_{sc}\left(d_{n,RC} - d_{sc}\right)^2 \tag{9a}$$

$$d_{n,RC} = d\left(\sqrt{\left(n\rho + \left(n-1\right)\rho'\right)^2 + 2n\rho + \frac{2\left(n-1\right)d_{sc}\rho'}{d}} - n\rho - \left(n-1\right)\rho'\right) \tag{9b}$$

where $\rho = A_{st}/(bd)$, $\rho' = A_{sc}/(bd)$, n is the modular ratio E_s/E_c, and d is the effective depth of the section. Similarly, the depth to the neutral axis in a SFRC section may be approximated as $d_{n,SFRC} = 1.2\ d_{n,RC}$. Note that for lightly longitudinally reinforced members, the proposed simplifications may be overly conservative.

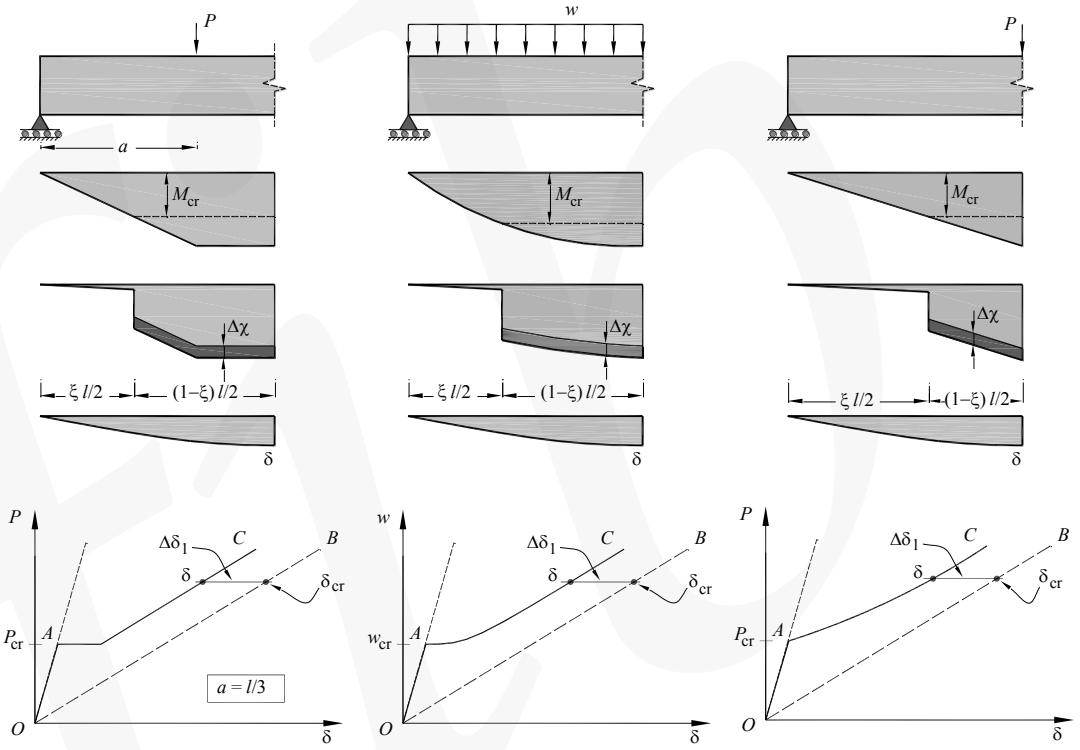


Figure 6: Beam notations, bending moments, curvatures and definitions of δ_{cr} and $\Delta\delta_1$

Table 1: Definitions of δ_{cr} and $\Delta\delta_1$ (see Kenel 2002, Amin et al. 2017)

	δ_{cr}	$\Delta\delta_1$	ξ
Four Point Bending	$\frac{Pl^2a}{24E_cI_{cr,SFRC}}\left(3-\frac{4a^2}{l^2}\right)$	$\Delta\chi\left(1-\xi^2\right)\frac{l^2}{8}$	$\frac{4M_{cr}}{Pl}$
Uniformly Distributed	$\frac{5wl^4}{384E_cI_{cr,SFRC}}$	$\Delta\chi\left(1-\xi^2\right)\frac{l^2}{8}$	$1-\sqrt{1-\frac{8M_{cr}}{wl^2}}$
Three Point Bending	$\frac{Pl^3}{48E_cI_{cr,SFRC}}$	$\Delta\chi\left(1-\xi^2\right)\frac{l^2}{8}$	$\frac{4M_{cr}}{Pl}$

This document is the intellectual property of the fib – International Federation for Structural Concrete. All rights reserved.
This PDF of fib Bulletin 95 is intended for use and/or distribution solely within fib National Member Groups.

4 Simplified instantaneous crack width calculation

For plain reinforced concrete tension ties, Gilbert (2008) determined an expression for the instantaneous crack width of a primary crack, w_i, in a reinforced concrete tension tie as being the difference between the elongation of the tensile steel between two primary cracks and the elongation of the concrete between the cracks. Following the notation introduced above, Gilbert's Equation for instantaneous cracks widths in plain reinforced concrete tension ties is written as:

$$w_i = \Delta_s - \Delta_c \tag{10a}$$

$$\Delta_s = \frac{2}{E_s}\int_0^{s_r/2}\left(\frac{T_s}{A_{st}} - \frac{4\tau_b x}{d_b}\right)dx = \frac{T_s s_r}{E_s A_{st}} - \frac{s_r^2 \tau_b}{E_s d_b} \tag{10b}$$

$$\Delta_c = \frac{2}{E_c}\int_0^{s_r/2}\left(\frac{4\tau_b \rho_{tc} x}{d_b}\right)dx = \frac{s_r^2 \tau_b \rho_{tc}}{E_c d_b} \tag{10c}$$

where T_s is the force in the longitudinal steel reinforcing bar (and equal to $T = M/z$ for members not containing fibres), E_s and E_c are the elastic moduli of the steel and concrete, respectively, and z is the internal lever arm between the tensile reinforcement and the resultant compressive force on the cracked section. To incorporate the stress carried by the fibres at the crack, Amin and Gilbert (2018) expressed Equation 10c as:

$$\Delta_c = \frac{2}{E_c}\int_0^{s_r/2}\left(\frac{4\tau_b \rho_{tc} x}{d_b} + \sigma_f(w)\right)dx = \frac{s_r^2 \tau_b \rho_{tc}}{E_c d_b} + \frac{s_r \sigma_f(w)}{E_c} \tag{11}$$

A close look at Equations 10a & 11 show that the crack width w_i is not an explicit equation of the independent variables since the stress carried by the fibres at a crack $\sigma_f(w)$ is itself a function of the crack width. Calculation of w_i therefore requires iteration. A detailed description of this process pertaining to SFRC beams can be found in Amin and Gilbert (2018). A conservative closed form solution to Equation 10 may be obtained by noting that Equation 11 approaches 0 as the applied moment increases to that which induces yielding to the longitudinal reinforcing steel. From an elastic analysis of a cracked cross-section subjected to a moment M_a greater than the instantaneous cracking moment M_{cr}, T_s may be approximated as:

$$T_s = \frac{nM_a\left(d - d_{n,SFRC}\right)}{I_{cr,SFRC}} A_{st} \tag{12}$$

where M_a is the applied moment on the section. Expanding Equation 10a we may express the instantaneous crack width for a SFRC beam as:

$$w_i = \frac{s_r}{E_s}\left[\frac{nM_a\left(d - d_{n,SFRC}\right)}{I_{cr,SFRC}} - \frac{s_r \tau_b}{d_b}\right] \tag{13}$$

Further research is required to accurately quantify any time-dependent changes of crack widths and deformations (i.e. due to the effects of compressive creep of the uncracked concrete in the compressive zone, tensile creep of concrete in the cracked part of the cross-section, bond creep between the reinforcement/fibres and the concrete, and shrinkage).

This document is the intellectual property of the fib – International Federation for Structural Concrete. All rights reserved.
This PDF of fib Bulletin 95 is intended for use and/or distribution solely within fib National Member Groups.

5 Example

5.1 Specimen geometry and material properties

Consider a uniformly loaded simply-supported SFRC beam of rectangular cross section, with width, b = 300 mm, overall depth, D = 500 mm and the span is 5 m. The beam is reinforced longitudinally with two 20 mm diameter bars at the top of the section (at a depth to the centre of the bars d_{sc} = 50 mm) and three 24 mm diameter bars at the bottom. The effective depth to the centroid of the bottom tensile bars d = 450 mm. The design strength of all reinforcing steels is 500 MPa. The beam is subjected to a short term factored loading equivalent to w_s = 35 kN/m resulting in an applied in service moment of 109.4 kNm. The beam is reinforced with 30 kg/m^3 (0.38%) Dramix® RC-65/35-BN cold drawn wire fibers. The characteristic compressive strength of the concrete is $f_c^{'}$ = 40 MPa, the characteristic uniaxial tensile strength is $f_{ct}^{'}$ = 3.05 MPa, the characteristic residual tension at a crack width of 0.5 mm is $f_{0.5}^{'}$ = 0.63 MPa and the elastic modulus (E_c) of the concrete is 33.5 GPa.

5.2 Instantaneous deflection

The depth to the neutral axis is first evaluated assuming no contribution provided by the fibres. In this case, the tensile and compressive reinforcement ratios are: $\rho = 1350/(300\times 450) = 0.0100$, $\rho' = 620/(300\times 450) = 0.0046$ and the modular ratio, $n = 200/33.5 = 5.97$. Substituting these values into Equation 9b and 9b gives $d_{n,RC} = 125.9$ mm and $I_{cr,RC} = 1063.9\times 10^6$ mm^4. Approximating the second moment of area for the SFRC beam as $1.1I_{cr,RC}$ gives $I_{cr,SFRC} = 1170.3\times 10^6$ mm^4. From Table 1:

$$\delta_{cr} = \frac{5wl^4}{384E_cI_{cr,SFRC}} = \frac{5\times 35\times 5000^4}{384\times 33500\times 1170\times 10^6} = 7.27 \text{ mm}$$

and the stiffening component provided by the cracked fibre reinforced concrete is

$$\Delta\delta_1 = \Delta\chi\left(1-\xi^2\right)l^2/8$$

where $\Delta\chi$ is given by Equation 8 and ξ is obtained from Table 1.

The cracking moment is evaluated as $M_{cr} = f_{ct}^{'}bD^2/6 = 3.05\times 300\times 500^2/6 = 38.13$ kNm. Solving yields $\Delta\delta_1 = 1.71$ mm and hence, the deflection of the beam under this applied load is equal to $\delta = \delta_{cr} - \Delta\delta_1 = 5.56$ mm.

5.3 Instantaneous crack width

The instantaneous crack width, w_i, of the section is a function of the crack spacing, s_r and the applied moment. The crack spacing is defined in Equation 3 and is a function of the effective reinforcing ratio ($\rho_{tc} = A_{st}/A_{ct}$) of the assumed tension tie, the bond strength between the fibre-concrete and reinforcing bar and $f_{0.5}^{'}$. Assuming $\tau_b = 2\ f_{ct}^{'}$ and A_{ct} is one third of the area below the neutral axis (and noting $d_{n,SFRC} \approx 1.2\ d_{n,RC}$) gives:

$$\rho_{tc} = \frac{1350}{1/3\times(500-1.2\times 125.9)\times 300} = 0.0387$$

This document is the intellectual property of the fib – International Federation for Structural Concrete. All rights reserved.
This PDF of fib Bulletin 95 is intended for use and/or distribution solely within fib National Member Groups.

and hence the crack spacing (Equation 3) and the instantaneous crack width (Equation 13) are:

$$s_r = \frac{(3.05-0.63)\times 24}{2\times 2\times 3.05\times 0.0387} = 123 \text{ mm} \quad \text{and}$$

$$w_i = \frac{123}{200000}\left[\frac{5.97\times 109.4\times 10^6 (450-1.2\times 125.9)}{1170\times 10^6} - \frac{123\times 2\times 3.05}{24}\right] = 0.08 \text{ mm}$$

Using the method above for the same member not containing any fibres (i.e. with $f'_{0.5} = 0$ MPa) results in $\delta = 6.72$ mm, $s_r = 155$ mm, $s_r = 0.12$ mm.

6 Concluding remarks

In this paper, rationale expressions suitable for design are presented to describe the in-service behaviour of SFRC beams. Following a description of the tension stiffening effect in SFRC members co-reinforced with conventional steel reinforcement a short design example is provided to highlight the benefits of utilising SFRC in reducing instantaneous deflections, crack widths and crack spacing.

7 References

Amin, A. 2015. Post cracking behavior of steel fiber reinforced concrete: from material to structure. *PhD Dissertation*. UNSW Australia.

Amin, A., and Gilbert, R.I. 2018. Instantaneous crack width calculation for steel fiber reinforced concrete flexural members. *ACI Structural Journal* 115(2): 535-544.

Amin, A., Foster, S.J., and Kaufmann, W. 2017. Instantaneous deflection calculation for steel fiber reinforced concrete one way members. *Engineering Structures* 131: 438-445.

Amin, A., Foster, S.J., and Muttoni, A. 2015. Derivation of the σ-w relationship for SFRC from prism bending tests. *Structural Concrete*, 16 (1): 93-105.

Amin, A., Foster, S.J., and Watts, M. 2016. Modelling the tension stiffening effect in steel fiber reinforced-reinforced concrete. *Magazine of Concrete Research* 68 (7): 339-352.

Deluce, J. 2011. Cracking behavior of steel fibre reinforced concrete containing conventional steel reinforcement. *MASc Dissertation*. The University of Toronto.

AS5100.5. 2017. Australian Standard, bridge design part 5: concrete. Standards Australia.

EN 14651. 2007. Test method for metallic fibre concrete- measuring the flexural tensile strength (LOP, residual). European Committee for Standardization: 17 pp.

fib Model Code 2010. 2013. *Model Code 2010*. Fédération Internationale du Béton: 402 pp.

Gilbert, R.I. 2008. Control of flexural cracking in reinforced concrete. *ACI Structural Journal* 105(3): 301-307.

Kenel, A. 2002. Biegetragverhalten und Mindestbewehrung von Stahlbetonbauteilen. *PhD Dissertation*, No.14874. Swiss Federal Institute of Technology, Switzerland. (in German).

Marti, P., Alvarez, M., Kaufmann, W., and Sigrist, V. 1998. Tension chord model for structural concrete. *Structural Engineering International* 8(4): 287-298.

Minelli, F and Plizzari, G. 2015. Derivation of a simplified stress-crack width law for Fiber Reinforced Concrete through a revised round panel test. *Cement and Concrete Composites*, 58: 95-104.

Pfyl, T. 2003. Tragverhalten von Stahlfaserbeton. *PhD Dissertation*, *IBK-Report* No.279. Swiss Federal Institute of Technology, Switzerland. (in German).

This document is the intellectual property of the fib – International Federation for Structural Concrete. All rights reserved.
This PDF of fib Bulletin 95 is intended for use and/or distribution solely within fib National Member Groups.
FRC2018: Fibre Reinforced Concrete: from Design to Structural Applications
Joint ACI-*fib*-RILEM International Workshop

The effect of fibres on corrosion of reinforced concrete

Carlos G. Berrocal[1,2], Karin Lundgren[1], Ingemar Löfgren[1,2]

[1] : Department of Architecture and Civil Engineering, Division of Structural Engineering, Chalmers University of Technology, Gothenburg, Sweden.

[2] : Thomas Concrete Group, Gothenburg, Sweden.

Abstract

In the present paper, long-term experiments involving natural corrosion of RC beams subjected to chloride solution cyclic exposure were carried out to investigate the effect of fibres on different aspects of the corrosion process as well as their contribution to the structural behaviour of RC elements damaged by corrosion. The long-term experiments were complemented with short-term accelerated corrosion experiments and mechanical tests to investigate the influence that low fibre contents may have on individual mechanisms that play an important role in the corrosion process of steel in concrete. These showed that fibres promote crack branching which results in a change of the internal crack pattern towards multiple thinner cracks, particularly near the reinforcement. This agrees with the long-term experiment results, which exhibited longer times to corrosion initiation for FRC beams with bending cracks and revealed a more distributed corrosion with more pits but less cross-sectional loss compared to bars in plain concrete. Fibres also proved beneficial in delaying corrosion-induced cracks and preventing cover spalling, which greatly enhanced the bond-behaviour of corroded bars. Furthermore, a positive effect of the fibres was also observed on the residual flexural capacity of corroded beams, which generally increased the load-carrying capacity and rotation capacity.

Keywords

Chloride-induced corrosion, durability, cracking, reinforcement bond, residual flexural capacity

This document is the intellectual property of the fib – International Federation for Structural Concrete. All rights reserved.
This PDF of fib Bulletin 95 is intended for use and/or distribution solely within fib National Member Groups.

1 Introduction

The mechanical and fracture properties of FRC have been extensively investigated for several decades. As a result, fibres are currently used in various applications such as industrial floors or slabs on grade to control shrinkage cracks as well as in tunnels as sprayed concrete or segmental linings. Moreover, the incorporation of design rules for FRC in recently released standards and codes, see e.g. (Model Code, 2010; Swedish Standards Institute, 2014), shows the increasing interest in using FRC in a broader range of structural applications. However, due to the casting-dependent distribution and orientation of the fibres throughout the concrete matrix, fibre reinforcement may, in many cases, be only used in combination with conventional reinforcement bars. Available research has shown that incorporating fibres into RC elements results in an improved mechanical performance with regards to increased load capacity and tension-stiffening as well as enhanced bond-behaviour. Nevertheless, one of the main advantages of FRC is the improved crack control mechanisms provided by crack-bridging fibres.

Cracks in RC elements are often regarded as preferential paths for the ingress of detrimental agents, such as CO_2 and chloride ions, that eventually result in the initiation of reinforcement corrosion. Moreover, numerous observations indicate that wider cracks shorten the time-to-corrosion initiation (Schiessl & Raupach, 1997; Tuutti, 1982), which has led current structural codes, see e.g. (ACI Committee 318, 2011; EN 1992-1-1 Eurocode 2, 2004), to prescribe strict crack width limitations as a way to mitigate the deterioration of RC structures due to corrosion of reinforcement. Consequently, combining fibres and conventional reinforcement to obtain narrower and more closely spaced cracks could be beneficial to delay the initiation of reinforcement corrosion, as shown in various investigations (Berrocal, Löfgren, Lundgren, & Tang, 2015; Sappakittipakorn & Banthia, 2012). Furthermore, several researchers have reported that steel fibres possess an enhanced corrosion resistance compared to traditional reinforcement bars (Dauberschmidt, 2006; Mangat & Gurusamy, 1988; Marcos-Meson et al., 2018). On the other hand, studies addressing the potential impact of fibres on the corrosion process of conventional reinforcement are very sparse (Grubb, Blunt, Ostertag, & Devine, 2007; Kim, Boyd, & Lee, 2010; Shaikh, Mihashi, & Kobayakawa, 2015) and have mainly focused on experimental results from uncracked specimens subjected to artificial corrosion through impressed current. Similarly, studies investigating the effect of fibres on the structural behaviour of RC elements with corroding reinforcement are even scarcer (Blunt, Jen, & Ostertag, 2015; Maalej, Ahmed, & Paramasivam, 2003), and have been mainly directed towards the study of cementitious composites with high fibre dosages exhibiting strain hardening behaviour.

To achieve a generalized deployment of FRC into a broader range of structures, including those susceptible to suffer corrosion damage, a sound understanding of how the fibres may influence the corrosion process of conventional rebars and the structural behaviour of corroded RC elements is required. The present paper summarizes the results from a PhD project aimed at investigating the effect of low fibres contents (<1% vol.) on different aspects of the corrosion process. These aspects include how the fibres, through a change of the internal crack morphology, may influence the ingress of detrimental agents into the concrete as well as the initiation and propagation phases of reinforcement corrosion. Moreover, the contribution of the fibres to the structural behaviour of RC elements damaged by corrosion has been also investigated through pullout and flexural tests.

This document is the intellectual property of the fib – International Federation for Structural Concrete. All rights reserved.
This PDF of fib Bulletin 95 is intended for use and/or distribution solely within fib National Member Groups.

2 Experimental programme

The experimental programme presented in this work is comprised of three different studies, the main study consisting of long-term experiments, referred to as experimental study A, and two short-term complementary experiments, referred to as experimental study B and C, respectively. Experimental study A was intended to encompass the different stages of the corrosion process while reproducing, as much as possible, realistic conditions. These conditions included the combination of naturally induced accelerated corrosion, flexural cracks formed under mechanical loading, varying crack widths and different loading conditions. The short-term experiments, on the other hand, were designed to isolate the effect of fibres on specific parameters relevant to the corrosion process, namely the effect on the internal crack morphology and the bond behaviour between concrete and corroding reinforcement. In the following, a brief description of each experimental study is provided.

2.1 Experimental study A: long-term corrosion experiments

A total of 54 beam specimens were cast. Six of these were kept uncracked and stored in potable water to be used as reference samples, while the remaining were subjected to different loading conditions and subsequently exposed to chlorides. The four conditions considered were:

(a) *Uncracked* specimens, which were never loaded.
(b) *Unloaded* specimens, which were loaded only once to induce cracking.
(c) *Cyclic* specimens, which were subjected to five load cycles to promote greater damage at the rebar-concrete interface.
(d) *Loaded* specimens, which were initially pre-cracked and subsequently reloaded with a sustained load to keep cracks open.

For all the beams subjected to loading, crack widths ranging from 0.1 to 0.4 mm were investigated. Moreover, four different series of specimens were cast:

(a) *Plain* series: without fibre reinforcement.
(b) *Steel* series: containing 0.5 % vol. of 35 mm end-hooked low-carbon steel fibres.
(c) *Hybrid* series: combining 0.35% vol. steel fibres and 0.15% 18 mm straight PVA fibres.
(d) *Synthetic* series: with 0.75% vol. 30 mm straight PVA fibres.

The specimens used in the experimental study were 1100 mm long beams with cross-sectional dimensions of 180×100 mm and reinforced with three Ø10 mm ribbed bars positioned with a clear concrete cover of 30 mm from the bottom and lateral sides. A self-compacting concrete mix with a water/cement ratio (*w/c)* of 0.47 was used for all the series in the experimental study. The reinforcement bars were of B500B steel grade and were used “as received” without applying any surface treatment prior to casting. Figure 1(a) shows the geometry of the beam specimens, including the reinforcement layout, and the different types of fibres used.

Experimental study A was subdivided into two phases. The first phase involved the pre-cracking and subsequent conditioning of the beams through cycles of partial immersion in 16.5% wt. NaCl solution beams to promote chloride-induced corrosion of the reinforcement. During the first phase, half-cell potential and corrosion rate measurements were performed periodically on two reinforcement bars from each beam, see Figure 1(b). The second phase

This document is the intellectual property of the fib – International Federation for Structural Concrete. All rights reserved.
This PDF of fib Bulletin 95 is intended for use and/or distribution solely within fib National Member Groups.

involved the assessment of the structural performance of the corroded RC beams and its correlation to the actual corrosion levels evaluated through weight loss measurements and 3D scanning technique. The setup used for the pre-cracking and structural assessment of the beams is illustrated in Figure 1(c) whereas an example of a 3D scanned pit and the corresponding sectional loss analysis are depicted in Figure 1(d). For further details on the experimental setup, the reader is referred to (Berrocal, 2017).

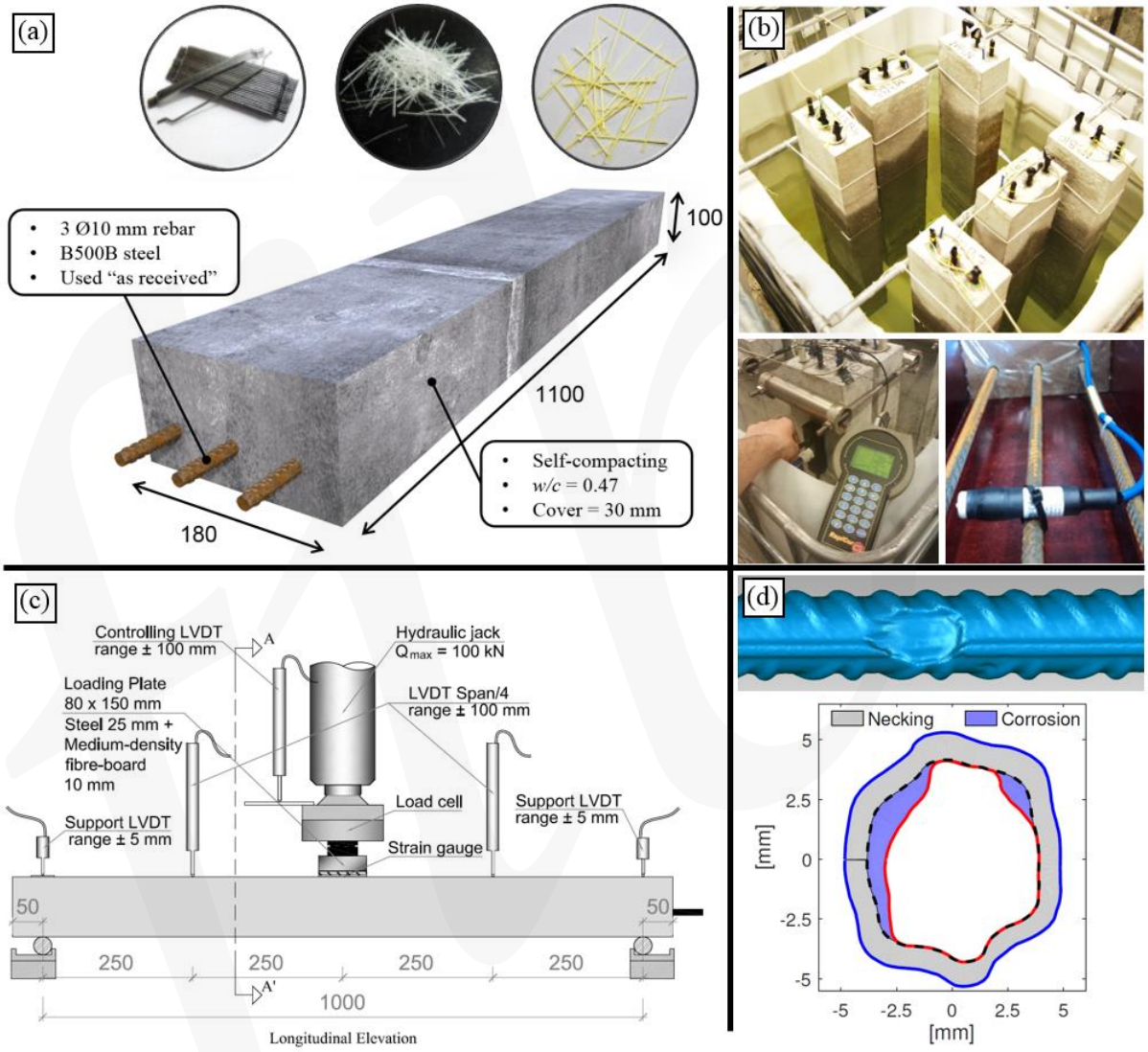


Figure 1: (a) Specimen geometry, reinforcement layout and fibre types. (b) Beams partially immersed in 16.5% wt. solution and the equipment used to monitor corrosion rate, RapiCor (left) and half-cell potential, ERE 20 (right). (c) Three-point bending setup used to pre-crack and assess the structural performance of the beams. (d) 3D scanned reinforcement bar displaying a corrosion pit and results of the sectional analysis to determine the local reduction of cross-section due to necking and due to corrosion. Measurements in mm.

2.2 Experimental study B: internal crack morphology

Three different concrete mixes were used to cast a total of twelve beams: plain concrete (PC) and steel fibre reinforced concrete (SFRC) as previously described, and a modified hybrid reinforced concrete (HyFRC) mix combining 35 mm long steel macro fibres at 0.5%

This document is the intellectual property of the fib – International Federation for Structural Concrete. All rights reserved.
This PDF of fib Bulletin 95 is intended for use and/or distribution solely within fib National Member Groups.

vol. and 8 mm long micro PVA fibres at 0.15% vol. The beam specimens had cross-sectional dimensions of 150×150 mm and a total length of 550 mm with a 10 mm deep notch at the centre of the bottom side to force cracking to occur at that location. In addition, every beam was reinforced with two ∅10 mm ribbed bars with a clear concrete cover of 50 mm from the notch tip.

Two surface crack widths, 0.5 and 1.0 mm, were investigated in the present study. The cracking procedure was carried with the notched side of the beams facing upwards to allow the injection of cracks with epoxy resin once the target crack width had been reached. The resin was mixed with fluorescent dye and was left to harden for 24 hours before unloading the beams. Subsequently, the beams were sawn to obtain two crack specimens out of each beam at the reinforcement sections which were later subjected to a vacuum impregnation followed by surface grinding to obtain samples suitable for microscopy. The relative position of the crack samples within the beam and the final result after the sample preparation are illustrated in Figure 2. Multiple images were taken along the path of the main and secondary cracks using a microscope outfitted with a CCD digital camera. Later, the images were processed with ImageJ and analysed with Matlab® to characterise the internal crack morphology. More information about the setup and image processing procedure can be found in (Berrocal, Löfgren, Lundgren, Görander, & Halldén, 2016).

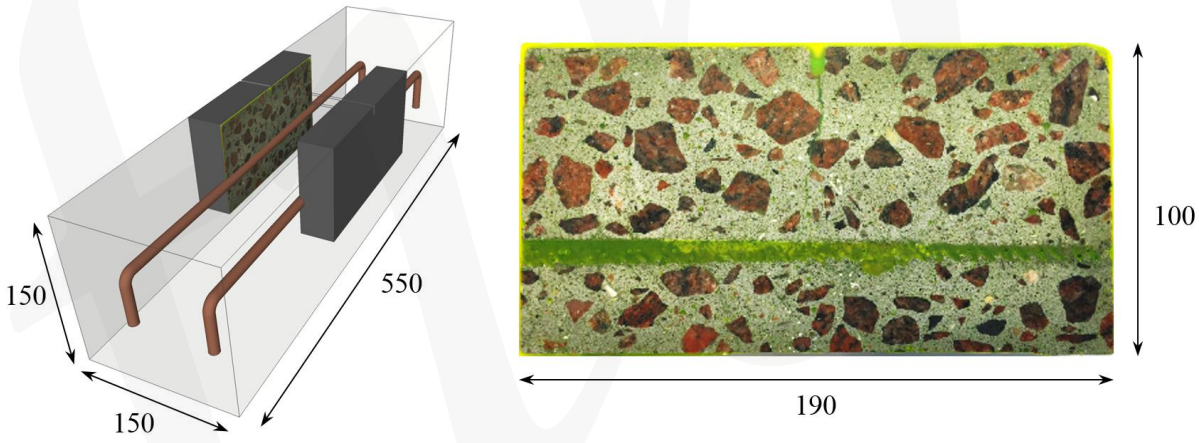


Figure 2: Schematic representation of the beam geometry and the position of the analysed sections and final sample results after vacuum impregnation and surface grinding. Measurements in mm.

2.3 Experimental study C: corrosion-induced cracking and bond behaviour

In this experimental study, 42 pull-out tests were performed on specimens divided into three groups: group I, uncorroded specimens used as reference samples; group II, specimens corroded up to the onset of corrosion-induced cracking; and group III, specimens corroded beyond the onset of splitting cracks. Furthermore, two different cover to bar diameter ratios, *c/Ø*, were investigated for the bond-behaviour and a third one was included for the crack initiation stage. The test specimens consisted of 100 mm high concrete cylinders with different diameters and a single Ø16 mm ribbed bar embedded along the cylinder axis with a bonded length of 70 mm. Two different mixes, namely plain concrete and steel fibre reinforced concrete, were used with the same mix proportions as in the experimental study A. However, sodium chloride was incorporated into the mix at 4% by weight of cement to immediately initiate corrosion of the steel bar.

This document is the intellectual property of the fib – International Federation for Structural Concrete. All rights reserved.
This PDF of fib Bulletin 95 is intended for use and/or distribution solely within fib National Member Groups.

The experimental procedure consisted of accelerated corrosion tests followed by pull-out tests, both of which are schematically represented in Figure 3(a) and Figure 3(b), respectively.

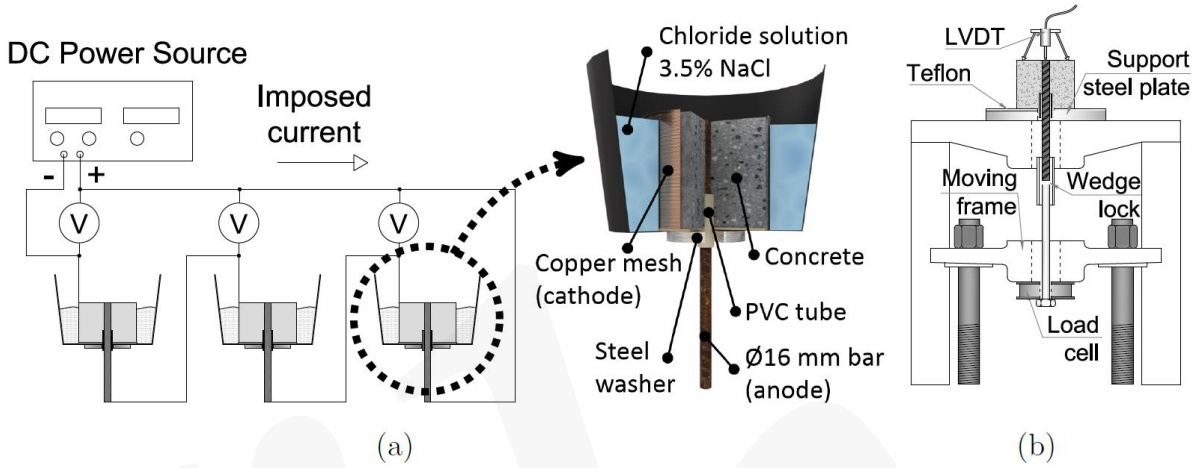


Figure 3: (a) Setup of accelerated corrosion tests and (b) setup of pull-out tests.

For the accelerated corrosion tests, an impressed current was applied to the specimens, connected in series, to achieve a constant current density of 100 μA/cm^2 within the bonded length of the rebar. Simultaneously, the electrical resistance was continuously monitored to identify the onset of cracking. The pull-out tests were carried out after the accelerated corrosion tests, during which the tensile load applied at the active end of the bar and the slip at the passive end were recorded. After the pull-out tests, the reinforcing bars were extracted from the cylinders and cleaned for gravimetric steel loss measurements to determine a uniform corrosion level. More details regarding the experimental procedure are available in (Berrocal, Fernandez, Lundgren, & Löfgren, 2017).

3 Results and discussion

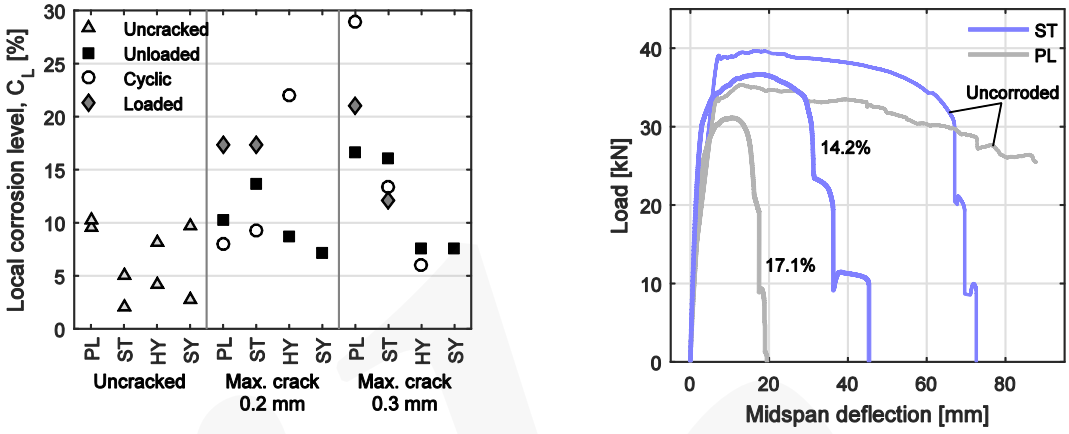
3.1 Experimental study A

The results from experimental study A showed that cracking was the main factor controlling the duration of the corrosion initiation phase. On average, the corrosion initiation time was decreased by one order of magnitude in specimens that had been loaded just once compared to uncracked specimens. A further decrease was observed in *loaded* specimens with open cracks. Regarding the local corrosion level at individual pits, which is presented in Figure 4(a), the difference between uncracked and cracked beams was less significant. On the other hand, no clear effect of the crack width could be observed either regarding the local corrosion level for the tested beams (note that flexural capacity tests and subsequent corrosion level measurements were only performed on beams with target crack widths of 0.2 and 0.3 mm). Nevertheless, open cracks did have an impact on the location of pits, thus all *loaded* beams exhibited localized pitting where the largest crack had formed.

Fibre reinforced mixes generally showed a slight improvement in terms of both corrosion initiation and local corrosion level compared to plain concrete. The *steel* series exhibited the most limited effect, followed by the *hybrid* series and the *synthetic* series, which displayed more consistent results. Additionally, fibres were found to promote a more distributed corrosion pattern in the reinforcement with numerous light corrosion spots compared to

This document is the intellectual property of the fib – International Federation for Structural Concrete. All rights reserved.
This PDF of fib Bulletin 95 is intended for use and/or distribution solely within fib National Member Groups.

corrosion in plain concrete which was characterized by fewer but more heavily corroded spots.



(a) (b)

Figure 4: (a) Local corrosion levels of the most critical pit in each beam specimens. (b) Load-deflection curves from flexural tests for two reference beams and two loaded beams with the greatest corrosion loss at the failure section (Corrosion levels displayed are the average of three rebars).

From the flexural capacity tests it was found that fibre reinforcement proved to be effective in preventing brittle failure of the beams during the flexural capacity tests while providing a more stable post peak behaviour. On the other hand, a change in failure from concrete crushing to steel rupture was observed in uncorroded specimens with steel fibres, see Figure 4(b). Regarding the residual capacity of corroded beams, it was observed that fibre reinforced series consistently showed a greater load capacity than *plain* series, although in relative terms, fibre reinforced and *plain* series displayed the same loss of load capacity with increasing local corrosion levels. The deformation capacity was found to decrease much more rapidly than load capacity given a certain cross-sectional loss due to corrosion, see Figure 4(b). Steel fibres did not significantly affect the deformation capacity of the beams although a small improvement was observed for the hybrid and synthetic series compared to plain concrete.

3.2 Experimental study B

From the experimental study B, the most apparent result regarding the effect of fibres on the internal crack pattern of RC elements was a qualitative change from a single wide crack in plain concrete specimens to a more complex system of multiple narrower cracks due to branching in fibre reinforced beams. A representative example of the crack pattern for each mix is presented in Figure 5(a). Quantitative information obtained from the image analysis procedure revealed that crack branching and tortuosity was accentuated by the addition of hybrid fibres compared to steel fibres only, whereas increasing the surface crack width had an impact on the crack branching but did not affect tortuosity.

A comparison of the crack width among the different mixes revealed that the accumulated crack width, i.e. the sum of individual crack widths at a certain distance from the surface, was not affected by the addition of fibre reinforcement. However, due to multiple crack branching, individual cracks were systematically narrower in fibre reinforced mixes. Based on Poiseuille's law, which correlates the water flow through a crack to the cube of the crack width, this effect could be beneficial to slow down the ingress of external agents through the cracks in concrete. On the other hand, it was observed that the maximum crack width, shown

This document is the intellectual property of the fib – International Federation for Structural Concrete. All rights reserved.
This PDF of fib Bulletin 95 is intended for use and/or distribution solely within fib National Member Groups.

in Figure 5(b) and 4(c) as the average over four samples, was also systematically reduced by the addition of fibres, a reduction that was more significant with increasing surface crack widths. This could have positive implications for the autogenous healing of cracks, which may heal due to precipitation of calcium carbonate crystals or continued hydration, among other causes, if the cracks are below a certain width, see (Edvardsen, 1999). Moreover, the effect of fibres was particularly noticeable near the reinforcement, hybrid fibres being most effective in reducing the crack width.

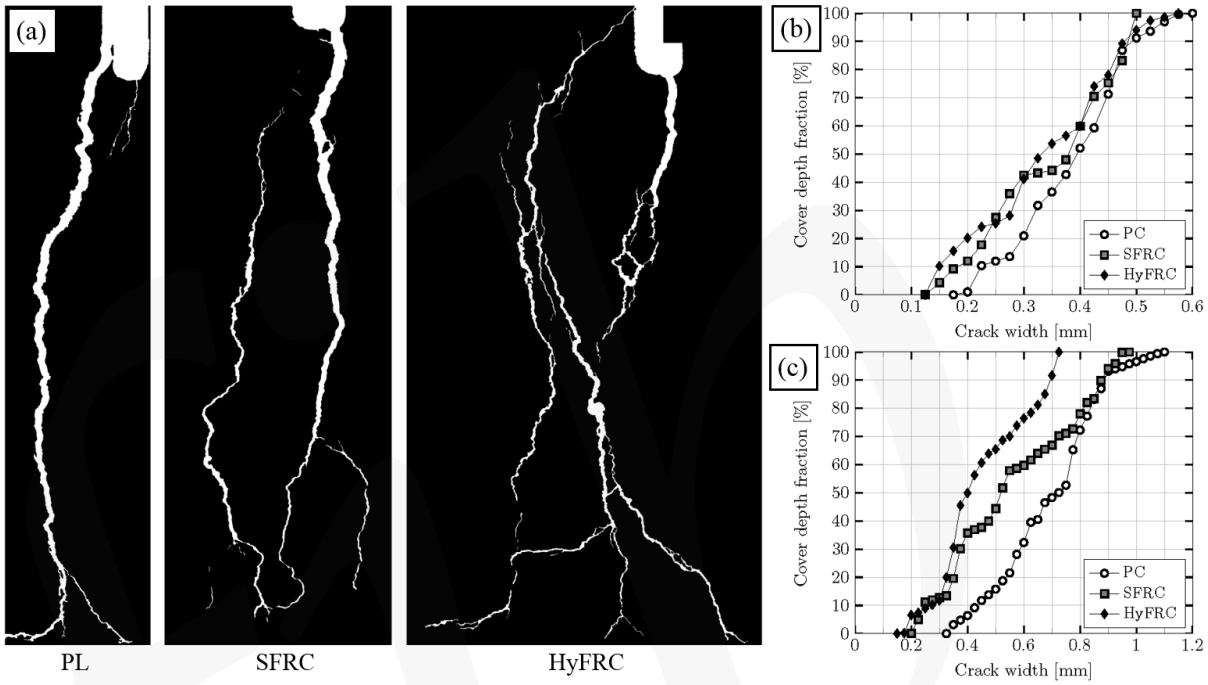
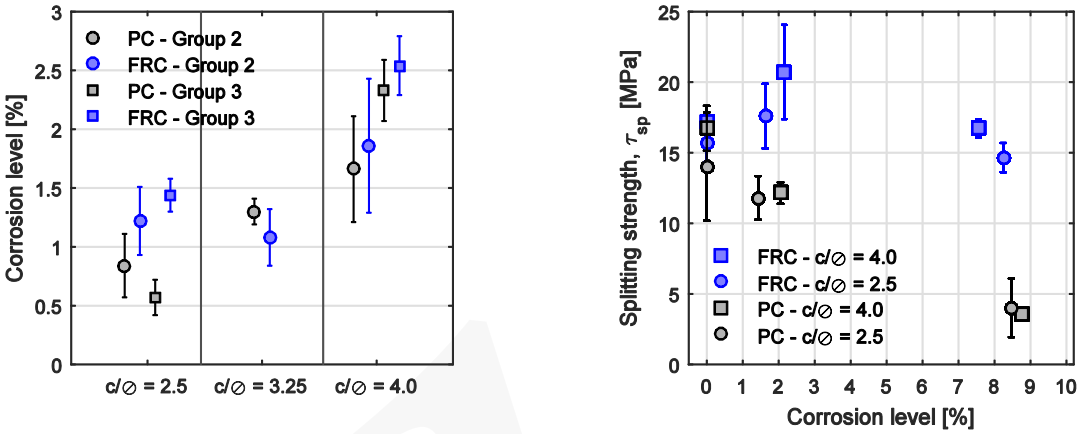


Figure 5: (a) Examples of the crack pattern observed for the different concrete mixes studied; (b) and (c) cumulative distribution curves showing the fraction of the cover with an average maximum crack width equal to the x coordinate, for 0.5 mm and 1.0 mm crack tip opening, respectively.

3.3 Experimental study C

During the accelerated corrosion tests, crack initiation was identified as the point in time when the electrical resistance started decreasing with no subsequent recovery. Thereafter, the corrosion level at crack initiation was determined based on the corrosion level measured at the end of the tests and assuming a linear relationship between time and corrosion level, according to Faraday's law. The corrosion level is defined in this study as the steel loss assumed concentrated and uniformly distributed along the bonded length of the bar. The relation between corrosion and crack initiation is presented in Figure 6(a). The results clearly show that, from the parameters investigated in this study, the $c/\varnothing$ played the most important role in delaying the initiation of corrosion-induced cracks, although its effect was more pronounced in PC specimens. Increasing the $c/\varnothing$ from 2.5 to 4.0, delayed crack initiation by a factor of 2 and 1.5 for PC and FRC specimens in Group II, respectively, whereas it delayed crack initiation by a factor of 4 and 1.75 for PC and FRC specimens in Group III, respectively. Adding fibre reinforcement had likewise a positive effect in delaying crack initiation, which was particularly noticeable in small $c/\varnothing$ test specimens. On the other hand, fibres had a lesser impact on crack initiation compared to the $c/\varnothing$, whereas specimens with fibres displayed a larger scatter than PC specimens.

This document is the intellectual property of the fib – International Federation for Structural Concrete. All rights reserved.
This PDF of fib Bulletin 95 is intended for use and/or distribution solely within fib National Member Groups.



(a) (b)

Figure 6: (a) Corrosion levels at crack initiation (markers indicate average values and error bars standard deviation). (b) Splitting strength determined experimentally as a function of the final corrosion level (markers indicate average values and error bars standard deviation).

The average splitting strength from all the pullout series is presented in Figure 6(b) as a function of the final corrosion level. As expected, fibres did not have a significant influence on the splitting strength in uncracked specimens, whereas a minor increase, attributable to the cover size, was observed. Upon corrosion-induced cracking, PC specimens suffered a moderate reduction of the splitting strength whereas it slightly increased for FRC, an effect that may be attributed to a higher normal stress at the interface due to corrosion. Finally, at higher corrosion levels the remaining splitting strength of PC specimens was only a small fraction of the initial one, with no apparent influence of the cover depth. Highly corroded FRC specimens, on the other hand, exhibited a nearly identical splitting strength as uncorroded ones. Moreover, the post-peak bond stresses of PC specimens rapidly dropped to nearly null values even in the absence of corrosion. Conversely, FRC displayed a residual bond stress of about 40% of the peak strength at 5 mm slips, regardless of the corrosion level.

4 Concluding remarks

The main conclusion from the current study is that FRC could be utilized to extend the service life RC structures exposed to chloride environments. Based on the results from the different experimental studies carried out, some of the mechanisms contributing to an extended service life are: (a) multiple cracking and arrested crack development leading to a slower ingress of depassivating substances, hence longer corrosion initiation periods, while contributing to a more distributed corrosion pattern with lower local corrosion and improved crack self-healing; (b) the increased passive confinement provided by FRC can delay the formation of corrosion-induced longitudinal cracks while crack-bridging fibres can supress cover spalling and maintain the integrity of the concrete-steel bond even at high corrosion levels; (c) fibres can increase the load and deformation capacity of concrete elements with corroding reinforcement while reducing the risk of brittle collapse, e.g. anchorage failure and shear failure, thereby mitigating the structural effects of corrosion damage.

References

ACI Committee 318. (2011). *318-11: Building Code Requirements for Structural Concrete and*

This document is the intellectual property of the fib – International Federation for Structural Concrete. All rights reserved.
This PDF of fib Bulletin 95 is intended for use and/or distribution solely within fib National Member Groups.

Commentary (p. 503). p. 503.

Berrocal, C. G. (2017). *Corrosion of Steel Bars in Fibre Reinforced Concrete: Corrosion mechanisms and structural performance*. PhD thesis - Chalmers University of Technology, Sweden.

Berrocal, C. G., Fernandez, I., Lundgren, K., & Löfgren, I. (2017). Corrosion-induced cracking and bond behaviour of corroded reinforcement bars in SFRC. *Composites Part B: Engineering*, *113*, 123–137. https://doi.org/10.1016/j.compositesb.2017.01.020

Berrocal, C. G., Löfgren, I., Lundgren, K., Görander, N., & Halldén, C. (2016). Characterisation of bending cracks in R/FRC using image analysis. *Cement and Concrete Research*, *90*, 104–116. https://doi.org/10.1016/j.cemconres.2016.09.016

Berrocal, C. G., Löfgren, I., Lundgren, K., & Tang, L. (2015). Corrosion initiation in cracked fibre reinforced concrete: Influence of crack width, fibre type and loading conditions. *Corrosion Science*, *98*, 128–139. https://doi.org/10.1016/j.corsci.2015.05.021

Blunt, J., Jen, G., & Ostertag, C. P. (2015). Enhancing corrosion resistance of reinforced concrete structures with hybrid fiber reinforced concrete. *Corrosion Science*, *92*, 182–191. https://doi.org/10.1016/j.corsci.2014.12.003

Dauberschmidt, C. (2006). Untersuchungen zu den Korrosionsmechanismen von Stahlfasern in chloridhaltigem Beton. Technischen Hochschule Aachen.

Edvardsen, C. (1999). Water Permeability and Autogenous Healing of Cracks in Concrete. *ACI Materials Journal*, *96*(4).

EN 1992-1-1 Eurocode 2. (2004). *EN 1992-1-1 Eurocode 2: Design of concrete structures - Part 1-1: General rules and rules for buildings*. Brussels, Belgium.

Grubb, J. A., Blunt, J., Ostertag, C. P., & Devine, T. M. (2007). Effect of steel microfibers on corrosion of steel reinforcing bars. *Cement and Concrete Research*, *37*(7), 1115–1126. https://doi.org/10.1016/j.cemconres.2007.04.012

Kim, B., Boyd, a. J., & Lee, J.-Y. (2010). Effect of transport properties of fiber types on steel reinforcement corrosion. *Journal of Composite Materials*, *45*(8), 949–959. https://doi.org/10.1177/0021998310380286

Maalej, M., Ahmed, S. F. U., & Paramasivam, P. (2003). Corrosion Durability and Structural Response of Functionally-Graded Concrete Beams. *Journal of Advanced Concrete Technology*, *1*(3), 307–316. https://doi.org/10.3151/jact.1.307

Mangat, P. S., & Gurusamy, K. (1988). Corrosion Resistance of Steel Fibres in Concrete under Marine Exposure. *Cement and Concrete Research*, *18*, 44–54.

Marcos-Meson, V., Michel, A., Solgaard, A., Fischer, G., Edvardsen, C., & Skovhus, T. L. (2018). Corrosion resistance of steel fibre reinforced concrete - A literature review. *Cement and Concrete Research*, *103*, 1–20. https://doi.org/10.1016/j.cemconres.2017.05.016

Model Code. (2010). fib Model Code for Concrete Structures. In *Structural Concrete* (Vol. 14). https://doi.org/10.1002/9783433604090

Sappakittipakorn, M., & Banthia, N. (2012). Corrosion of Rebar and Role of Fiber Reinforced Concrete. *Journal of Testing and Evaluation*, *40*(1). https://doi.org/10.1520/JTE103873

Schiessl, P., & Raupach, M. (1997). Laboratory Studies and Calculations on the Influence of Crack Width on Chloride-Induced Corrosion of Steel in Concrete. *ACI Materials Journal*, *94*(1), 56–61.

Shaikh, F. U. A., Mihashi, H., & Kobayakawa, A. (2015). Corrosion Durability of Reinforcing Steel in Cracked High-Performance Fiber-Reinforced Cementitious Composite Beams. *Journal of Materials in Civil Engineering*, *27*(8), 04014228. https://doi.org/10.1061/(ASCE)MT.1943-5533.0001191

Swedish Standards Institute. *SS 812310:2014. Fibre Concrete – Design of Fibre Concrete Structures*. , (2014).

Tuutti, K. (1982). Corrosion of steel in concrete. *CBI Report 4:82, The Swedish Cement and Cocnrete Institute.*, 468.

This document is the intellectual property of the fib – International Federation for Structural Concrete. All rights reserved.
This PDF of fib Bulletin 95 is intended for use and/or distribution solely within fib National Member Groups.
FRC2018: Fibre Reinforced Concrete: from Design to Structural Applications
Joint ACI-*fib*-RILEM International Workshop

Influence of the Post-Cracking Residual Strength Variability on the Partial Safety Factor

Albert de la Fuente[1], Sergio Henrique Cavalaro[2], Jesús Miguel Bairán[1]

[1] : Polytechnic University of Catalonia (UPC), Barcelona, Spain.

[2] : Loughborough University, Leicester, United Kingdom.

Abstract

The use of fibre reinforced concrete (FRC) in structural applications is increasing mainly due to improvements on the material technology and its acceptance in design codes (e.g., *fib* Model Code 2010). In that sense, the design of FRC is usually dealt with the same safety format established for reinforced concrete. In fib Model Code, for instance, the same magnitude of the partial safety factor for FRC compressive (f_c) and post-cracking flexural (f_R) strengths is assumed (1.50). It must be noticed that this assumption might be unrealistic, and on the unsafe side in terms of structural reliability, since f_R present higher intrinsic scatter (variability due to fibre orientation, distribution, dosage) than f_c. However, it has been experimentally and numerically confirmed, that this scatter decrease with the width of the cracked surface, so this assumption has lesser impact in structural elements with large cracked regions involved in the failure mechanism (e.g., slabs). The goal of this research is twofold: (1) to assess the influence of the width of the cracked region on the variability of f_R and (2) to calibrate partial safety factors for f_R based on the different target reliability indexes proposed in the fib Model Code 2010 for ultimate limit states and the variability obtained in the characterization tests.

Keywords

FRC; partial safety factor; post-cracking strength; structural reliability

This document is the intellectual property of the fib – International Federation for Structural Concrete. All rights reserved.
This PDF of fib Bulletin 95 is intended for use and/or distribution solely within fib National Member Groups.

1 Introduction

FRC presents a high scatter on the post-cracking behavior when tested in small-scale in the laboratory, but this scatter tends to reduce when the size of the element tested increases (di Prisco et al., 2016a, di Prisco et al., 2016b). In consequence, the design of FRC estimated from small-scale tests may not be representative of the real behavior of the material, and lead to a penalization of the design parameters.

To deal with this matter it is important to deep on the concept of the FRC scatter. In general terms, the sources of scatter involved in FRC can be divided in three groups (Cavalaro and Aguado 2015): (1) the production process (mixing, casting, vibrating and curing); (2) the testing process (setup and precision of the equipment) and (3) the intrinsic variability of the material (random distribution and orientation of fibers, mainly), which is part of the total variability. Whereas the scatter produced by production and testing processes are highly affected by the staff and machinery involved and can be considered constant independently of the scale of the specimen, the intrinsic scatter of the material depends on the distribution and orientation of the fibers, and this will always be present. Several studies indicate that there is a diminution of this type of scatter when the element size increases, in other reasons because the cracked surface also increases and so the number of fibers bringing the cracks.

In this regard, the partial safety factor to be used for assessing the design values of the post-cracking flexural residual concrete strength (f_R), γ_{fR}, highly depends on the variability of f_R. The magnitude proposed in the great majority of the codes for γ_{fR} is 1.50, particularly in the *fib* MC-2010; therefore, the same assumed for the compressive concrete strength (f_c). Nevertheless, the coefficient of variation (CV) associated to f_R use to range from 10 to 25% depending on the type of test, amount and type of fiber whilst the CV for f_c is below 10%. In consequence, assuming that the other sources of variability (ex., geometry and loads) remain unchanged, the reliability index (β) indirectly assumed when using γ_{fR} = 1.50 in ULS design can be lower than that required to control the failure probability values in acceptable ranges.

In view of this, the objective of this research contribution is two-fold: (1) quantify the effect of the cross-section dimensions on the intrinsic CV of f_{R3} and, (2) the effect of CV on the partial safety factor (γ_{fR}) to be used for assessing the design value of f_{R3}. Both objectives are oriented to assess the degree of structural reliability achieved with the safety factors currently used in the design of FRC precast tunnel segments.

2 Influence of the cross-section dimensions on the global CV_{fR3}

2.1 Assumptions and numerical procedure

The rigid-plastic constitutive model proposed in the *fib* MC-2010 has been considered to simulate the post-cracking behaviour in tension of FRC (Figure 1). This model is represented by a constant tensile stress block of intensity f_{Ftu} (ultimate residual strength) equal to $f_{R3}/3$; f_{R3} being the post-cracking flexural tensile strength for a crack mouth opening (CMOD) equal to 2.5 mm. This f_{R3} can be derived from a three-point bending test (3-PBT) performed on prismatic notched-beam of 150x150x550 mm according to EN 14651:2005.

For the parametric study, a representative range of widths and heights for precast tunnel segment ranging from 150 mm to 1,500 mm and 450 mm, respectively, were considered. The procedure consist in dividing the cracked area of the real-scale element (Figure 1) into smaller

This document is the intellectual property of the fib – International Federation for Structural Concrete. All rights reserved.
This PDF of fib Bulletin 95 is intended for use and/or distribution solely within fib National Member Groups.

cells of 150x150 mm^2, equal to the cracked area of the small-scale specimen of the 3-PBT. To each cell, a random value of f_{Ftu} is assigned following a normal distribution (log-normal distribution leads to similar results) with a mean value of 1.42 N/mm^2 (f_{R3m} = 4.26 N/mm^2) with CVs varying from 10% - 25 %, which is considered a sufficiently wide range to comprise the typical values of CV_{fR3} (Parmentier *et al*., 2008). Thus, each 150x150 mm^2 cell (i) has its own constitutive equation (constant block $f_{Ftu,i} = f_{R3k,i}/3$, f_{R3} following normal distribution). The f_{R3m} fixed corresponds to an experimental program that involved the testing of 30 FRC notched beams in the 3-PBT (Liao et al., 2016); however, contrarily to CV_{fR3}, f_{R3m} does not affect the variability of the ultimate bending moment (M_u) as long as it remains constant.

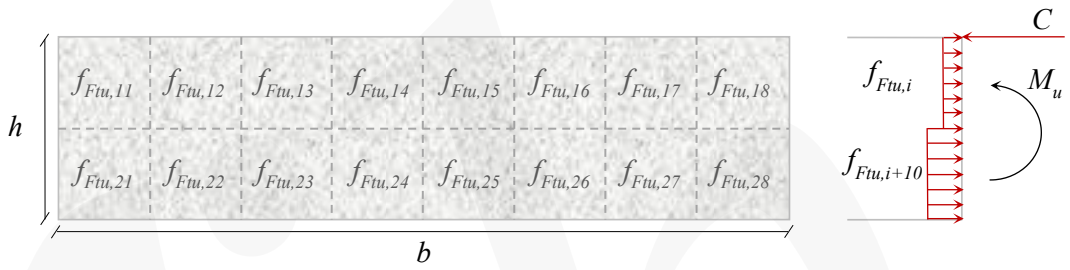


Figure 1: Stress distribution in ULS in a rectangular cross-section. Cells of 150x150 mm^2 with an f_{Ftu} established randomly considering a normal distribution for f_{R3}

The ultimate bending moment (M_u) for each section and distribution of f_{Ftu} is assessed by means of numerical integration and establishing the equilibrium and compatibility conditions (de la Fuente *et al*., 2012). To obtain statistically representative results, a convergence analysis is carried out resulting in a total of 300,000 simulations for each series considered, this allowing obtaining the statistical distribution of M_u for each of the series.

It can be proven that by considering the stress-diagram of Figure 1, the scatter of M_u coincides with that obtained for f_{Ftu} since the variables b and h are considered as deterministic. Hence, this procedure provides directly the intrinsic scatter of $f_{R3} = 3f_{Ftu} = 6M_u/bh^2$ for the respective sample size.

2.2 Results

Figure 2 depicts the relationship between the b and the intrinsic scatter CV_i of f_{R3} for each h and scatter of f_{R3} obtained in beam test on prisms with cross section 150x150 mm^2 (CV^{BT}).

An expected reduction of the intrinsic scatter with an increase of the size of the specimen can be noticed in Figure 2. The reason of this decrease when increasing b and/or h is related with the number of fibers crossing the cracked section. In this sense, the higher is the number of these the lower is the scatter since a mitigation of the variations on the probabilistic laws occur.

2.3 Simplified expression to estimate the intrinsic scatter

From the point of view of this study, the input variables considered of major influence in the CV_i of FRC are those related with the cracked area of the sample, i.e. b and h. Therefore, such expression will take into account both variables besides CV^{BT}. It is important to remark that the scatter due to other sources that are not intrinsic to the material (production and testing)

This document is the intellectual property of the fib – International Federation for Structural Concrete. All rights reserved.
This PDF of fib Bulletin 95 is intended for use and/or distribution solely within fib National Member Groups.

are not reflected in the numerical simulation. This scatter shall be considered apart once the intrinsic scatter of the real-scale sample is known.

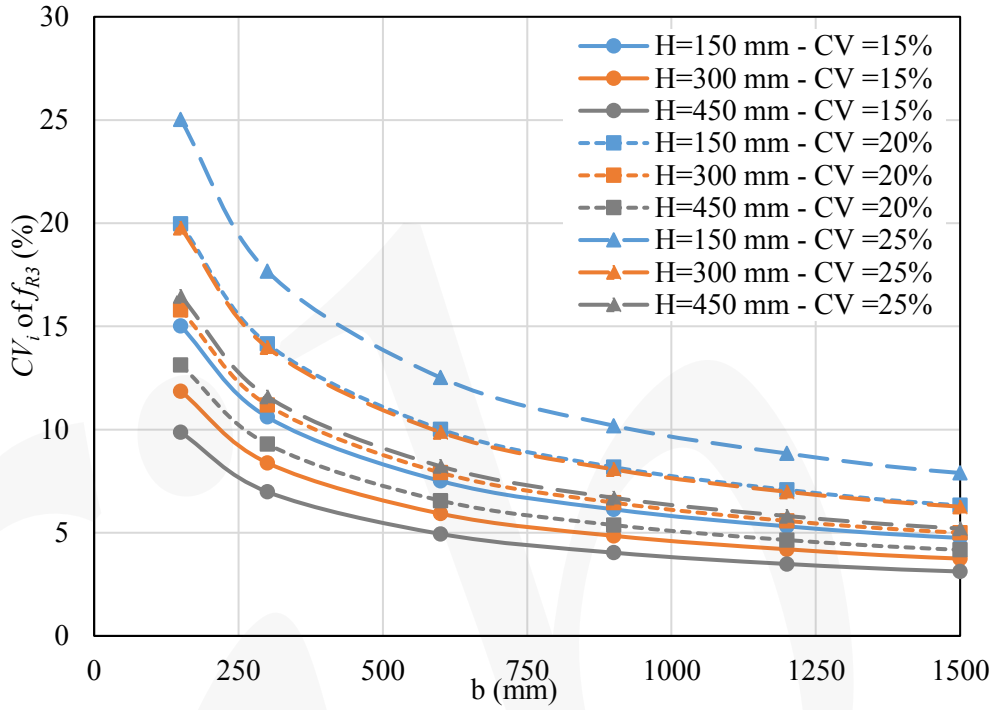


Figure 2: Intrinsic scatter of f_{R3} with CV_i^{BT} of: (a) 15%, (b) 20% and (c) 25%

The data of the parametric study is used to fit a function by resorting to multivariable regression. In the process, it is observed that the variables considered have different weights in the expression proposed. Consequently, powers to variables *h* and *b* are introduced as well as a constant k_1 into the Equation 1.

$$CV_i^{RS}=k_1 \cdot CV^{BT} \cdot h^{k_2} \cdot b^{k_3} \quad (1)$$

Table 1 presents the best-fit parameters of Equation 1. The superscripts RS and BT of equation 1 stand for *real-scale* and *bending test*, respectively, and the subscript *i* stands for intrinsic.

Prior to the calculation of the intrinsic scatter of f_{R3} on the real-scale specimen (CV_i^{RS}) with Equation 1, the scatter of f_{R3} obtained in the bending test (CV^{BT}) should be known.

Table 1: Parameters to estimate CV_i^{RS} of f_{R3}

Parameter	Values
k_1	79.02
k_2	-0.37
k_3	-0.50

In order to determine the total scatter of f_{R3} on the real-scale specimen, the scatter of f_{R3} due to production and testing processes needs to be taken into account. The global *CV* of f_{R3} can be expressed in terms of the different sources of scatter, grouped on in intrinsic scatter (CV_i)

This document is the intellectual property of the fib – International Federation for Structural Concrete. All rights reserved.
This PDF of fib Bulletin 95 is intended for use and/or distribution solely within fib National Member Groups.

and in other types (production and testing, CV_o), both for f_{R3}. If the total scatter approaches a normal distribution, the coefficient of variation of both sources will also do. From classic deductions for the sum of normal distributions, the total CV can be calculated through Equation 2.

$$CV^2=CV_i^2+CV_o^2 \tag{2}$$

Notice that Equation 2 is valid for f_{R3} obtained both from *small-scale* (3-PBTs) and *real-scale* specimens. In this regard, since it is not possible to obtain CV_i directly from the laboratory test, an assumption has to be done. According to (Cavalaro *et al*., 2015), the scatter of f_R due to properties intrinsic to the material is around 12%. The scatter due to other sources (CV_o) is the same regardless of the scale of the specimen since production and testing processes are assumed to follow the same procedure. With this, the calculation of the global CV_{fR3} of the real structure (CV^{RS}) can be dealt with Equation 3.

$$CV^{RS}=\sqrt{\left(CV_i^{RS}\right)^2+\left(CV^{BT}\right)^2-\left(CV_i^{BT}\right)^2} \tag{3}$$

In Equation 3, the first term is calculated with Equation 1, the second is obtained directly through the small-scale laboratory 3-PBTs and the third it is assumed to be around 12% as commented above. Figure 3 depicts the scatter of samples of different sizes calculated with Equation 3 and with CV^{BT} = 18.6%, equal to the average value obtained from the experimental program analyzed (Liao *et al*., 2016).

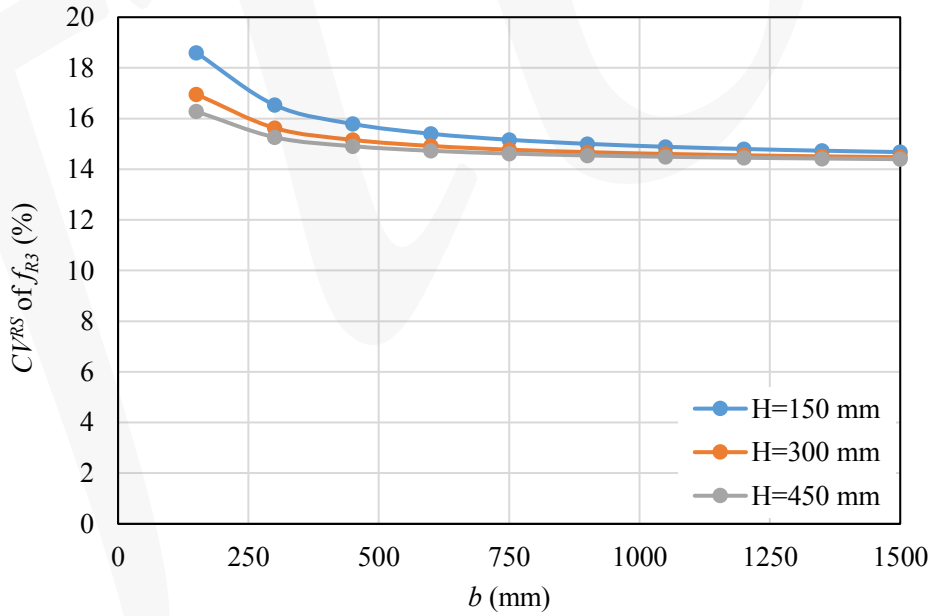


Figure 3: CV^{RS} of f_{R3} for different sizes of specimens

This document is the intellectual property of the fib – International Federation for Structural Concrete. All rights reserved.
This PDF of fib Bulletin 95 is intended for use and/or distribution solely within fib National Member Groups.

3 Influence CV_{fR3} on the partial safety factor for f_{R3} in ULS

3.1 Procedure and assumptions

In this paper, the authors have focused in those elements which requires only minimum reinforcement to guarantee ductile response in case of cracking. Probably, one of the structural elements in which FRC is often used are the precast concrete segmental tunnel linings for TBM constructed tunnels. In this regard, precast concrete segments are subjected mainly to compressive stresses during service, while cracking potential due to bending forces primarily occur during load transient conditions (e.g., demoulding, stacking, transport, placing). In order to calibrate the partial safety factor to be applied to f_R in the design of transient loading situations of segments subjected to bending, a reliability analysis was performed. The calculation of the reliability index (β) was carried out by using the FORM method (Melchers, 1999). This method requires the definition of the limit state function (g-function, Equation 4).

$$g(R,Q)=R-Q \tag{4}$$

The variables are grouped into resisting (R) variables and loads (Q). Each of these has its own representative probability density function. The failure occur when $g < 0$, $g = 0$ being the limit situation. In this research, since it is focused on precast fibre reinforced concrete tunnel segments susceptible to fail due to bending, the resistance is M_u (Equation 5). The load to be resisted is the cracking bending moment (M_{cr}, Equation 5), which leads to a tensile stress of magnitude equal to the tensile flexural strength of the concrete ($f_{ct,fl}$).

$$M_{cr}=\frac{bh^2}{6}f_{ct,fl} \tag{5}$$

In the vast majority of the cases, M_d are usually lower than M_{cr}; thus, the design criterion to derive the required value of f_{R3} consist in imposing $M_u \geq M_{cr}$ (Liao *et al.*, 2015a and Liao *et al.*, 2016). This criterion expressed in terms of moment (M) – curvature (χ) relationship of the most critical section (Figure 4) and also proposed in (Chiaia *et al.*, 2009a,b; Fantilli *et al.*, 2016a,b), allows guaranteeing the ductile behaviour of the segment in the event of cracking during any of these transient loading stages; that is, supracritical reinforcement.

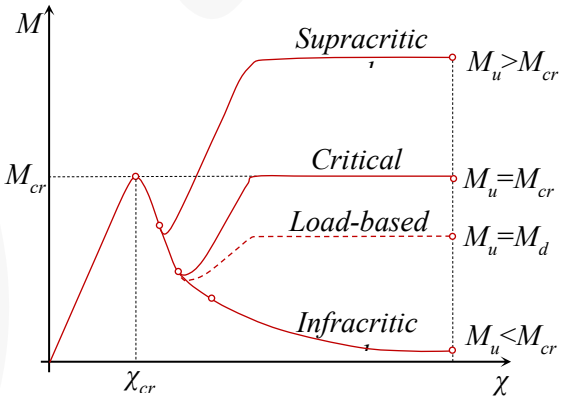


Figure 4: $M-\chi$ relationship of a cross-section with different reinforcement configurations

This document is the intellectual property of the fib – International Federation for Structural Concrete. All rights reserved.
This PDF of fib Bulletin 95 is intended for use and/or distribution solely within fib National Member Groups.

The *g*-function results in the Equation 6. If $g > 0$, f_{R3} is enough to lead to a supracritical failure while if $g = 0$, the failure is critical; both with associated ductility.

$$g(M_u,M_{cr})=\lambda \cdot f_{R3}-f_{ct,fl} \quad (6)$$

The bias factor (λ) is the ratio $M_{u,exp}/M_{u,est}$, where $M_{u,exp}$ is the M_u of the *real-scale* FRC segment obtained experimentally for a CMOD in the midspan section of 2.5 mm and $M_{u,est}$ is the M_u of the same segment estimated by means the stress pattern of Figure 1 (F_{ftu}, constant). The probability density function of λ has been derived from a set of 7 different full-scale bending tests experimental programs on FRC precast segments (27 elements in total) gathered into the literature.

In the reliability, analysis the probability of having Equation 6 less or equal than zero is computed with the random variables considered in Table 2.

Table 2: Random variables in reliability analysis

Variable	Description	Distribution	Mean [μ]	Deviation [σ]
λ	Model bias factor	Log-normal	1.04	0.33μ
$f_{ct,fl}$	Flexural tensile strength	Log-normal	According to concrete class	0.30μ
e	Geometry error	Normal	0.0	10 mm
f_{R3}	Post-cracking stress for CMOD=2.5mm	Log-normal	According to design	*

*Standard deviation of f_{R3} should be measured from statistical values obtained from the characterization.

By considering the procedure presented and assuming a ULS situation in which the design value of f_{R3} ($f_{R3d} = f_{R3k}/\gamma_{fR3k}$) and the average value of $f_{ct,fl}$ ($f_{ctm,fl} = f_{ctm} \cdot (1.6\text{-}h)$; $f_{ctm} = 0.30 \cdot f_{ck}^{2/3}$), a reliability index ($\beta$) for different values γ_{fR3k} can be computed. A representative set of design cases in which concrete class ranging from C25 to C60 and *h* between 200 mm and 400 mm were assumed.

3.2 Results and discussion

The limit state equation from which γ_{fR3k} can be assessed results in Equation 7 if $g = 0$.

$$\frac{f_{R3k}}{\gamma_{fR3k}}=f_{ctm} \cdot (1.6\text{-}h) \quad (7)$$

This partial safety factor γ_{fR3k}, as defined, is rather a global safety factor since the average value of f_{ct} is considered. In this regard, f_{ctm} is usually considered the representative value of f_{ct} in terms of cracking onset according most of the codes.

By following the FORM method and considering magnitudes of CV_{fR3} of 10, 15, 20 and 30%, the relationship $\beta - \gamma_{fR3k}$ depicted in Figure 5 is obtained. Values of CV_{fR3} between 10% - 15% could correspond to a FRC with a high homogeneity of the batch or a FRC characterized using the BCN test procedure UNE 83515:2010 whilst $CV_{fR3} > 15\%$ could correspond to a normal FRC tested under the notched-beam test EN 145651:2005 (Pujadas *et al*., 2013 and Pujadas *et al*., 2014).

Given the mean and deviation values of the variables gathered in Table 2, the Equation 8 provides an approximation for γ_{fR3k} as a function of the required β and the standard deviation observed in the 3-PBT for determining f_{R3}. Should the dimensions of the *full-scale* section of

This document is the intellectual property of the fib – International Federation for Structural Concrete. All rights reserved.
This PDF of fib Bulletin 95 is intended for use and/or distribution solely within fib National Member Groups.

the segment (b, h) want to be taken into account for determining the γ_{fR3k}, Equations 1-3 can be used for assessing the CV^{RS} of f_{R3} in the real-scale structure.

$$\gamma_{f_{R3k}}=0.80e^{0.56\beta\cdot CV_{f_{R3}}^{0.27}} \quad (8)$$

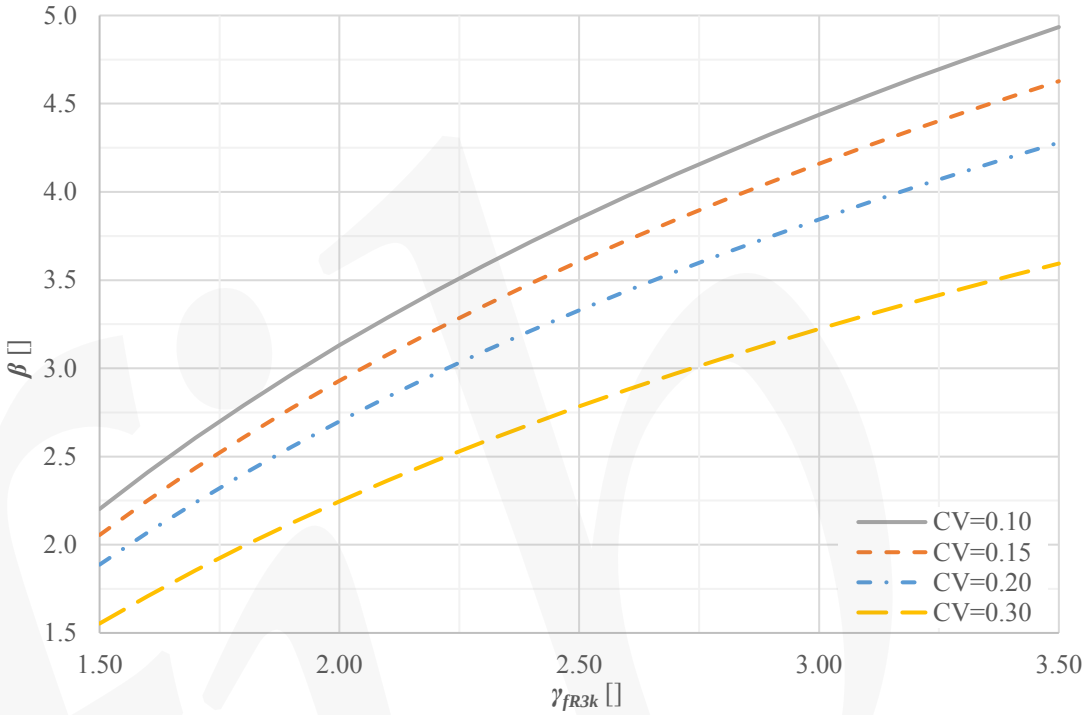


Figure 5: Relationship between β – γf_{R3k} for FRC tunnel segments subjected to flexure in ULS

As reference, a magnitude of β = 3.8 is commonly accepted for a ULS situation, which leads to a failure probability $p_f = 7.2\cdot10^{-5}$. Based on that, according to the assumptions and model developed herein, γ_{fR3k} varying from 2.51 (CV_{fR3} = 0.10) to 3.72 (CV_{fR3} = 0.30) should be considered in ULS for FRC tunnel segments during transient loading situations; contrarily, values of γ_{fR3k} = 1.50 (β = 1.7 if CV_{fR3} = 0.20) are currently proposed in the design codes. Therefore, the actual procedure leads to a reliability level rather associated to a SLS, for which values of β = 1.5 ($p_f = 6.7\cdot10^{-2}$) are established in the design codes.

However, it should be mentioned that using this γ_{fR3k} = 1.50 could be acceptable in transient loading situations since: (1) the segments are still not subjected to the final service conditions; hence, safety of other structures and both the functionality and serviceability of the tunnel is not compromised; (2) the likelihood of cracking is reduced (the ratio M_{cr}/M_d is normally higher than 1.50), therefore, fibres are not activated and consequently the intrinsic scatter would not be influencing the mechanical behaviour of the segment; (3) the consequences in case of a segment fails during transient situations can be controlled by using the suitable equipment and safety measures for the plant personnel, (4), if values of β = 3.8 are imposed, the amount of fibres required to reach the f_{R3k} resulting from considering γ_{fR3k} > 2.50 would increase dramatically and, as a consequence, the FRC solution for tunnel segments would not be longer attractive from both the technical and economic points view (whilst this solution has proven to be effective and safe).

This document is the intellectual property of the fib – International Federation for Structural Concrete. All rights reserved.
This PDF of fib Bulletin 95 is intended for use and/or distribution solely within fib National Member Groups.

4 Concluding remarks

The following concluding remarks can be highlighted:

1. The parametric and Monte-Carlo analyses carried out have permitted to derive an equation that allows estimating the CV of f_{R3} in the real structure (with the real dimensions of the cracked area) depending on the CV of f_{R3} obtained in the 3-PBT on notched-beam specimens. The equation allows confirming that f_{R3k} tend to f_{R3m} for elements with long cracks (ex., pile supported slabs and pavements).
2. The partial safety factor γ_{fR3k} = 1.50 that is usually used for ULS for transient loading situations leads to a reliability factor β close to 2.0 if CV_{fR3} ranges between 15% to 20%. This β is slightly higher than that accepted for SLS (β = 1.5) but not sufficient to reach the β = 3.8 commonly established for a ULS. In this sense, the designer should consider the relative cost of safety measures necessary to increase this reliability and the consequences of failure (see Table 3.3-3 of the *fib* Model Code 2010) to decide if this $\beta \approx 2.0$ can be accepted, or it should be increased by adopting measures (ex., reducing the tolerances of the lifting devices and/or of the supports position, increase the control of the FRC production).

5 Acknowledgements

The authors wish to express their gratitude to the Spanish Ministry of Economy, Industry and Competitiveness for the economic support in the scope of the project SAES (BIA2016-78742-C2-1-R).

6 References

Cavalaro, S.H.P., Aguado, A. (2015). Intrinsic scatter of FRC: an alternative philosophy to estimate characteristic values. *Mater. Struct*. 48, 3537–3555.

Chiaia, B., Fantilli, A.F., Vallini, P. (2009). Combining fibre-reinforced concrete with traditional reinforcement in tunnel linings. *Eng. Struct*. 31(7), 1600–1606.

Chiaia, B., Fantilli, A.P., Vallini, P. (2009). Evaluation of minimum reinforcement ratio in FRC members and application to tunnel linings. *Mater. Struct*. 42(3), 339–351.

de la Fuente A., Blanco A., Pujadas P., Aguado, A. (2012). Experiences in Barcelona with the use of fibres in segmental linings. *Tunn. Undergr. Space Technol*. 27(1), 60–71.

di Prisco, M., Martinelli, P., Parmentier, B. (2016). On the reliability of design approach for FRC structures according to Model Code 2010: the case of elevated slabs. *Struct. Conc*. 17(4), 588–602.

di Prisco, M., Martinelli, P., Dozio, D. (2016). The structural redistribution coefficient KRd: a numerical approach to its evaluation. *Struct. Conc*. 17(3), 390–407.

EN 14651:2005. Test method for metallic fibered concrete. Measuring the flexural tensile strength (limit of proportionality (LOP), residual).

Fantilli, A.P., Chiaia, B., Gorino, A. (2016). Volume fraction and ductility index of concrete beams. *Cem. Conc. Comp*. 65, 139–149.

Fantilli, A.P., Chiaia, B., Gorino, A. (2016). Unified approach for minimum reinforcement of concrete beams. ACI *Structural Journal* 113(5), 1107–1116.

fib Bulletins 65-66 (2010), Model Code 2010. fédération internationale du béton (fib), Lausanne (Switzerland).

This document is the intellectual property of the fib – International Federation for Structural Concrete. All rights reserved.
This PDF of fib Bulletin 95 is intended for use and/or distribution solely within fib National Member Groups.

Liao, L., de la Fuente, A., Cavalaro, S., Aguado, A. (2015a). Design of FRC tunnel segments considering the ductility requirements of the MC 2010. *Tunn. Undergr. Space Technol.* 47(3), 200–210.

Liao, L., de la Fuente, A., Cavalaro, S., Aguado, A., Carbonari, G. (2015b). Experimental and analytical study of concrete blocks subjected to concentrated loads with an application to TBM-constructed tunnels. *Tunn. Undergr. Space Technol.* 49(1), 295–306.

Liao, L., de la Fuente, A., Cavalaro, S.H.P., Aguado, A. (2016). Design procedure and experimental study on fibre reinforced concrete segmental rings for vertical shafts. *Mat. & Design* 92, 590–601.

Melchers, R.E. (1999). Structural Reliability Analysis and Prediction, Second Edition John Wiley & Sons, Chichester.

Parmentier, B., Vandewalle, L., Van Rickstal, F. (2008). Evaluation of the scatter of the postpeak behaviour of fibre reinforced concrete in bending: A step towards reliability. *Proceedings of the 7th RILEM International Symposium on Fiber Reinforced Concrete*: Design and Applications (BEFIB '08), 133–143.

Pujadas, P., Blanco, A., Cavalaro, S., de la Fuente, A., Aguado, A. (2013). New analytical model to generalize the Barcelona test using axial displacement. *J Civ Eng Manage*. 19(2), 259–271.

Pujadas P., Blanco A., Cavalaro S.H.P., de la Fuente A., Aguado A. (2014). Multidirectional double punch test to assess the post–cracking behaviour and fibre orientation of FRC. *Constr. Build. Mater*. 58, 214–224.

UNE 83515:2010. Fibre reinforced concrete. Determination of cracking strength, ductility and residual tensile strength. Barcelona test. Spanish Association for Standardization and Certification, AENOR. In English.

This document is the intellectual property of the fib – International Federation for Structural Concrete. All rights reserved.
This PDF of fib Bulletin 95 is intended for use and/or distribution solely within fib National Member Groups.
FRC2018: Fibre Reinforced Concrete: from Design to Structural Applications
Joint ACI-*fib*-RILEM International Workshop

Comparability of bond tests for repair and retrofit of concrete structures with Fiber Reinforced Concrete

Cristina Zanotti[1], Norbert Randl[2], Parisa Setayesh Gar[1], Bardia Kabiri Far[1], Martin Steiner[2]

[1] : University of British Columbia, Vancouver, Canada.

[2] : Carinthia University of Applied Sciences, Villach, Austria.

Abstract

Fiber Reinforced Concrete (FRC) is being increasingly applied in structural repair and retrofit of reinforced concrete structures. Not only fiber reinforcement improves the durability of reinforced concrete structures, but it also enhances compatibility of the repair material to the existing structure, further enhancing structural effectiveness and service life of the intervention. Furthermore, studies have shown that fiber reinforcement can significantly improve substrate-repair bond in both tension and shear. However, this benefit is not fully utilized in repair/retrofit design due to test uncertainties and lack of comprehensive data on correlations with other fundamental factors. In this study, the question of the appropriateness, reliability and sensitivity of current bond tests in case of FRC repairs is addressed. Several tension and shear bond tests on plain and fiber reinforced cement-based repairs are performed in parallel by two research teams at UBC (Canada) and CUAS (Austria), following a rigorous testing procedure to allow consistency among results from the two laboratories. The influence of repair strength and casting direction is also investigated. The effect of fiber reinforcement on bond is assessed while correlation, comparability, and sensitivity of different test set-ups and stress conditions are discussed.

Keywords

Bond test, Repair, Bond strength, Shear bond, Tensile bond, Adhesion, Friction, Fiber reinforced concrete, High strength concrete, Roughness

https://doi.org/10.35789/fib.BULL.0095.Ch39

This document is the intellectual property of the fib – International Federation for Structural Concrete. All rights reserved.
This PDF of fib Bulletin 95 is intended for use and/or distribution solely within fib National Member Groups.

1 Introduction

Bond between differently aged concretes is a key factor when repairing or retrofitting existing structures with new concrete layers. Parameters affecting bond and its durability as well as the appropriateness of techniques to evaluate bond in laboratory and in situ have been investigated. Still, development of durable, compatible cement-based repair materials that are effectively bound to the concrete substrate remains a pertinent topic of study. Major areas of investigation include: application of novel technologies to enhance bond and its durability, reliability of failure criteria and predictive models, reliability of laboratory and in situ bond tests, and non-destructive techniques for monitoring the quality of bond and interfaces. Bond strength depends on the stress condition by which failure takes place (tension, shear, or mixed) and the corresponding mechanisms activated at and nearby the interface. In general, cohesive bond is extremely important because, beyond being beneficial to resisting all modes of fracture, it is associated with the durability of the interface (resistance to damage, cracking, and ingress of contaminants). Cohesive bond is affected by interfacial adhesion and other micro-mechanical factors (e.g. localized fracturing, crack deviation, etc.). Unfortunately, adhesive and cohesive bonding are highly sensitive to many different parameters, e.g. composition of old and new concrete, interface roughness, cleanliness or moisture content of the old concrete surface.

Studies have shown that fibers may have a noticeable beneficial effect on the interfacial cohesive bond strength. Fibers have shown potential to enhance adhesion by improving the quality of the matrix at and near the interfacial transition zone and/or by resisting slip and detachment through additional mechanisms. These depend on fiber chemistry, size, geometry, quantity, stiffness, bonding, and the repair matrix, the quality of the concrete substrate, and the interface roughness (Banthia & Dubeau 1994, Lim & Li 1997, Wagner et al. 2013, Zanotti et al. 2014,2018). Nevertheless, these properties are not fully utilized due to uncertainties associated with assessment, modeling, and overall quantification of such beneficial effects. The procedures and setups for testing the adhesive bond in shear or tension have a significant impact on the resulting bond strength data (Zanotti & Randl 2019). This work represents the first steps of a research collaboration aimed at investigating the reliability of bond tests, especially in the case of fiber reinforced concrete repairs. In the project presented hereafter, a number of interface bond tests with different types of repair material were performed in parallel by two research teams at UBC (Canada) and CUAS (Austria). Different test set-ups in both tension and shear and bond strength of both normal strength and high strength concrete repairs with and without steel fiber reinforcement were compared.

2 Experimental program

2.1 Materials and specimen preparation

The mixture proportions of the concrete substrate and the four repair concretes adopted are shown in Table 1. The substrate is a normal strength concrete, while normal strength (NS) and high strength (HS) mortars were designed for the repair. These were applied without fiber reinforcement (NS-0% and HS-0%) and with a volume fraction V_f = 0.5% of 13 mm straight, uncoated steel fibers (NS-0.5% and HS-0.5%), with diameter of 0.16 mm (aspect ratio = 87, tensile strength = 3000 MPa, modulus of elasticity = 200 GPa). Concrete substrates were cast first, covered with plastic sheets soon after pouring, demolded 24 hours later, and cured in

This document is the intellectual property of the fib – International Federation for Structural Concrete. All rights reserved.
This PDF of fib Bulletin 95 is intended for use and/or distribution solely within fib National Member Groups.

standard conditions in a moist/temperature controlled room. After at least 14 days curing, substrates were sandblasted and cured again until they reached at least 28 days and the repair material was cast. Roughness was quantified and compared by Sand Patch Method (ASTM E965-15); a Mean Texture Depth MTD = 1.2-1.5 mm was obtained. Repair mortars were poured against substrates in optimum Saturated Surface Dry (SSD) condition (Morgan 1996) and eventually cured for 28 days as for the substrate.

Table 1: Mixture proportions [kg/m^3], fiber volume fraction, V_f, and materials' compressive & tensile strengths, fc & f_t

	CEM 1 42.5R	Silica fume	Fly ash type F	Sand	Crushed stone (2-11mm)	Superplasticizer	Water	V_f [%]	$f_c^{(1)}$ UBC [MPa]	$f_c^{(2)}$ CUAS [MPa]	$f_t^{(3)}$ UBC [MPa]	$f_t^{(4)}$ CUAS [MPa]
Substrate	450	-	-	1165	776	-	180	-	61	66	4.3	5.8
NS-0%	840	-	210	1680	-	-	420	-	60	46	3.8	4.7
NS-0.5%	840	-	210	1680	-	-	420	0.5	62	51	5.9	5.1
HS-0%	840	100	-	1295	-	11	210	-	104	90	7.4	5.2
HS-0.5%	840	100	-	1295	-	11	210	0.5	90	82	9.8	8.6

$^{(1)}$Measured on 100mmx200mm cylinders. $^{(2)}$Measured on 100mm cubes and converted as $f_c = f_{c,cube} * \alpha^{-1}$, where $\alpha = 1.2$ for NS concrete and $\alpha = 1.15$ for HS concrete. $^{(3),(4)}$Measured from splitting tension test on 75mmx150mm$^{(3)}$ & 100mmx200mm$^{(4)}$ cylinders (Eq. 1).

2.2 Testing program

A summary of the different bond tests performed is provided in Figure 1. Additionally, compressive strength tests on cylinders (100x200mm) and cubes (100mm) and indirect splitting cylinder (75x150mm & 100x200mm) tests were performed on substrate and repair materials. Splitting tensile strength (f_t) was determined as:

$$f_t = 2P/(\pi DL) \quad (1)$$

where P is the peak load, D = cylinder diameter, and L= cylinder length. Substrate-repair bond was tested in tension and shear. Among the most common tension tests lies the pull-off technique (Fig. 1c,d). However, the test is sensitive to various factors such as system misalignment, improper gluing of the loading disc, drilling-induced damage, core geometry, and related stress concentrations (Austin et al. 1995). Two different overlay thicknesses and coring depths were therefore considered. In addition, direct tension (Fig. 1a) and splitting (indirect) tension (Fig. 1b, Eq. 1) tests were performed, the former being considered to underestimate bond strength and the second typically providing a less conservative assessment (Momayez et al. 2005). Shear bond was tested under various combinations of shear and compressive stresses to evaluate different levels of activation of the shear slip resisting mechanisms. Modified Slant Shear Cylinders (MSSC) with various inclination of the bond plane between substrate and repair (Fig. 1e-g) were tested to apply different shear-normal stress ratios at the interface while loading the cylinder in compression. Based on the Mohr-Coulomb failure criteria, interfacial cohesion and friction coefficients were extrapolated from fitting of experimental data points (Austin at al. 1999, Zanotti et al. 2014):

This document is the intellectual property of the fib – International Federation for Structural Concrete. All rights reserved.
This PDF of fib Bulletin 95 is intended for use and/or distribution solely within fib National Member Groups.

$$\tau = \tfrac{1}{2}\sigma_o \sin(2\alpha) \quad (2)$$

$$\sigma_n = \sigma_o \sin^2(2\alpha) \quad (3)$$

$$\tau = c + \mu \cdot \sigma_n = c + \tan\phi \cdot \sigma_n \quad (4)$$

where τ = shear stress, σ_o = vertical stress, α = inclination of the bond plane, σ_n = normal stress (Fig. 1e), c = cohesion strength, μ·= friction coefficient, and ϕ = friction angle. In one lab, three slants were considered to apply different normal-shear stress ratios at the interface (with larger slant angles inducing greater levels of compression, Fig. 1e,f), while in the other lab, two slants but also a different cylinder size were used to evaluate possible size effects (Fig. 1g). Finally, the push-out test (Fig. 1h) was performed to assess direct shear bond strength (without compression, Randl et al. 2016).

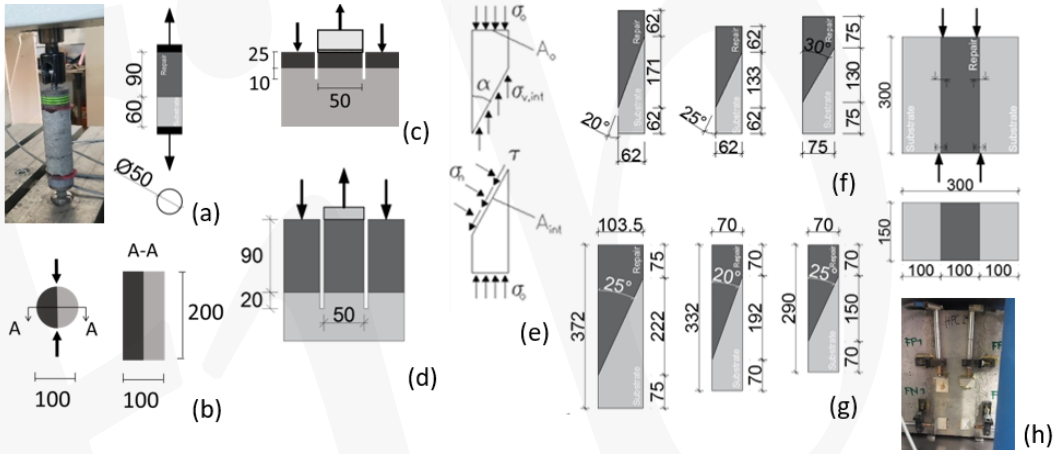


Figure 1: Bond tests performed (all dimensions in mm): (a) direct tension, (b) splitting tension, (c,d) pull-off, (e-g) slant shear, (h) push-out.

3 Results and discussion

3.1 Shear

Similar failure modes were observed during slant shear tests in the two labs. Normal strength repair concretes with and without fibers exhibited interfacial bond failure (Fig. 2a,d), while high strength concrete repairs failed in the majority of cases under compression before reaching interfacial bond strength, regardless the level of compressive stress applied (that is, for all the slant angles considered). Failure modes in slant shear tests highly depend on bond plane inclination, interfacial friction angle (see discussion of these parameters in Zanotti et al. 2014), and concrete strength ratios. Compressive failure initiated in the substrate and propagated through the full cylinders with vertical splitting cracks was observed in high strength (HS) concrete without fibers (H-S0%, Fig. 2b,f), while substrate failure was obtained in HS repairs with fibers (HS-0.5%, Fig. 2c,g). Cracks were visible in the HS-0.5% repairs but these were arrested by the steel fibers and nor the repair material neither the substrate-repair interface reached failure. In one instance only, HS repairs exhibited bond failure, namely: HS repairs without fibers, in the larger size slant shear cylinders (Fig. 2e). This result will be discussed in the next paragraphs together with bond strength values. Overall, material

This document is the intellectual property of the fib – International Federation for Structural Concrete. All rights reserved.
This PDF of fib Bulletin 95 is intended for use and/or distribution solely within fib National Member Groups.

failure in slant shear tests was more explosive at UBC (Fig. 2b,c), compared to CUAS (Fig. 2f,g). All specimens exhibited bond failure in push-out tests (direct shear, Fig. 5a).

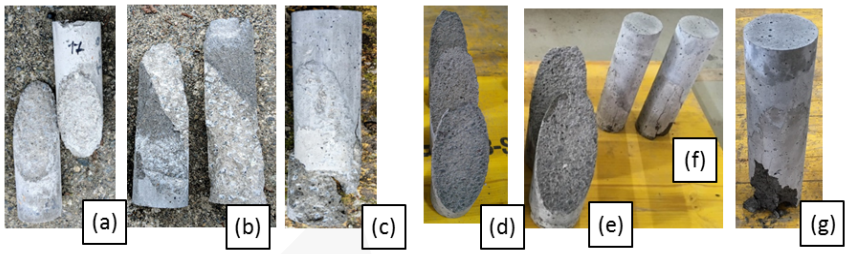


Figure 2: Slant shear test failure modes from UBC (a-c) and CUAS (d-g). (Zanotti & Randl 2019)

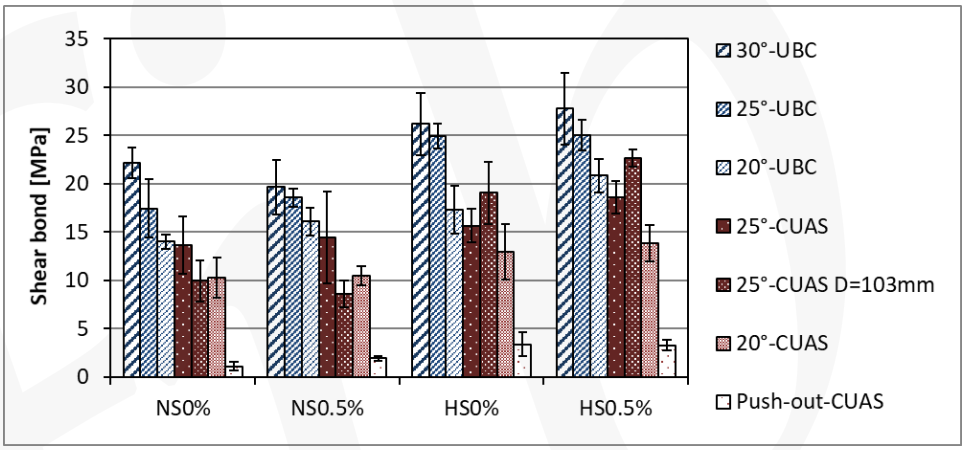


Figure 3: Bond stresses at failure for different repair materials, obtained from slant shear test with various slants (20°,25°,30°) and push-out test. (Zanotti & Randl 2019)

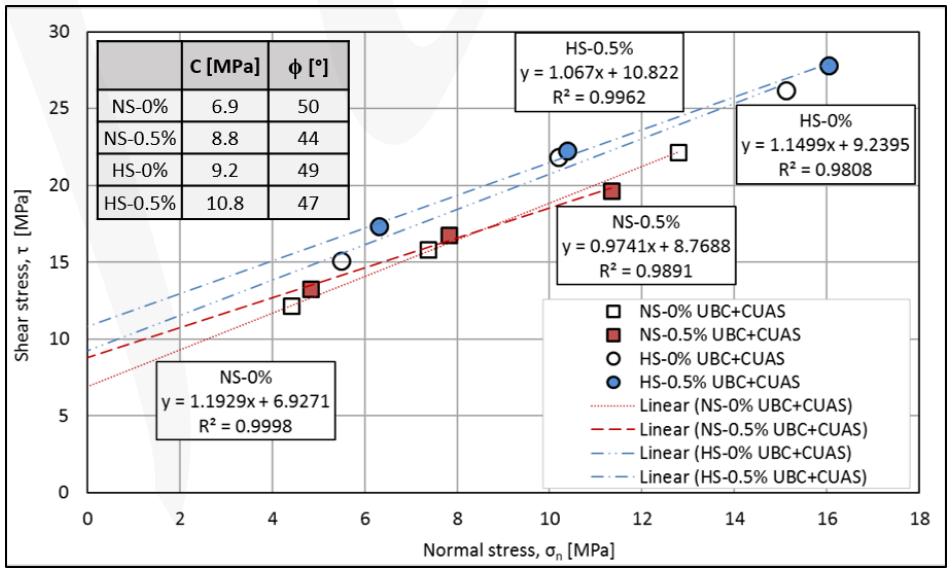


Figure 4: Average interfacial shear and normal stresses at failure from slant shear tests, and extrapolated values of cohesion, c, and friction angle, ϕ.

This document is the intellectual property of the fib – International Federation for Structural Concrete. All rights reserved.
This PDF of fib Bulletin 95 is intended for use and/or distribution solely within fib National Member Groups.

Shear bond stresses at failure obtained from various tests in the two labs are shown in Figure 3, while compressive and tensile strengths of materials are provided on the right-hand side of Table 1. As both labs had to make use of locally available aggregates and cement types, differences in the mechanical properties of the various concretes are to be expected. Even though chosen aggregate type and gradation as well as cement strength class were comparable, specific origin and shape of aggregates, cement composition as well as variations in mixing power/blades may affect microstructure and porosity (overall and locally) of the cement paste and the Interfacial Transition Zones (ITZs) between aggregate and cement paste and between fibers and cement paste, and, ultimately, chemical/physical bonding of the different phases and adhesive/cohesive micro-damage of the corresponding ITZs (Mindess et al. 2002). Bond test data (presented in the following paragraphs and sections) are even more sensitive to the aforementioned parameters and are therefore expected to be affected.

While the bond strength values obtained from all push-out tests and from slant tests on NS concrete are representative of bond strength, shear bond in most of the HS repairs tested is deemed to be higher than interfacial stresses at failure of slant specimens (reached by material compressive failure without achieving bond failure in most specimens). Quantitative comparisons regarding the effects of various parameters on bond can entail misleading conclusions in those instances. As expected, interfacial shear stresses at failure decrease for decreasing normal-shear stress ratios at the interface, because of a decrease in interfacial friction. The highest values are achieved with standard slant shear tests (largest slant, α=30°, and, thus, largest compression-shear ratio at the interface, Fig. 1e) and the lowest values are obtained with push-out tests (no intended compression at the interface). High strength repairs exhibit higher shear bond stresses than normal strength repairs. In agreement with previous results (Zanotti et al. 2018), the steel fibers' beneficial effect on shear bond is detected in the tests with lower compressive-shear stress ratios, where the cohesive component has a more significant impact on interfacial bonding (lower friction, Randl 2013).

For slant shear cylinders, size effect is observed in NS repairs (with and without fibers) with interfacial bond failure. By comparing the CUAS bond strength obtained with same slant (25°) and different diameters (70 mm vs 103 mm, Fig. 1g), one can note that the smaller the specimen size, the larger the bond strength values. Two main types of size effect are in place: (i) specimen size effect on the mechanical response of materials at and nearby the interface and (ii) effect of same roughness on shear bond of interfaces with different areas. Slant shear cylinders with same bond angles (either 25° or 20°) tested at UBC (D = 62 mm, Fig. 1f) exhibit higher bond strength than the ones tested at CUAS (D = 70 mm & 103 mm, Fig. 1g). These differences can be affected by the specimen size in the two labs, but also other factors should be considered. First of all, some variations in compressive and tensile strength of materials was detected (Table 1), which directly affect debonding mechanisms, beyond being an indicator of possible differences in the microstructure of the materials overall (due, for instance, to some differences in mixing procedures, grinding operations, etc.). Furthermore, the crack patterns observed from compressive failures of slant shear specimens with HS repairs (shown in Fig. 2b,c,e-g) and further discussed in the following paragraph) indicate that, in specimens with same slants but different diameters and proportions, different stress paths develop from the specimen edges and throughout the specimen height. Although these stress patterns cannot be visually observed in NS repair specimens, which failed at the interface, they still have an effect on the final stress distribution at and around the interface and, thus, on the bond strength values assessed (Austin et al. 1999). One could also attribute bond strength differences to variations of interfacial roughness. Although, based on

This document is the intellectual property of the fib – International Federation for Structural Concrete. All rights reserved.
This PDF of fib Bulletin 95 is intended for use and/or distribution solely within fib National Member Groups.

quantitative assessment (Section 2.1) and qualitative comparison, roughness was deemed consistent throughout the project, it is possible that local variations in the roughness profile may have affected the final strength.

Compared to the NS repairs discussed above, HS repairs exhibit different trends with respect to specimen size, with 103 mm CUAS specimens (25° slant) exhibiting higher bond stresses at failure than 70 mm CUAS specimens (with same 25° slant, Fig. 3). At a first glance, these results seem contradictory to size effect, but, once again, they can be explained by looking at failure modes and, in fact, they point out the importance of cylinder geometry in slant shear tests. As mentioned above, unlike NS repair specimens (all characterized by shear bond failure), HS repairs exhibited various failure modes, characterized by compressive failure of the substrate in the repairs with fibers (HS-0.5%, Fig. 2c,g) and compressive failure of the entire cylinder (both substrate and repair) in the case without fibers (Fig. 2b,f), except for HS-0% repair in 103 mm cylinder (Fig. 2e). Concerning the compression failure mode, the geometry of the cylinders has a major effect on the failure load: in the CUAS specimens, it is evident that the layer of the substrate directly at the load introduction represents the decisive zone, and this zone is subject to restraint resulting from friction between concrete and loading edge. This local confinement is more pronounced in the larger cylinders and results into a higher apparent compressive strength. Moreover, the distance between the loading edge and the start of the interface (75 mm) is smaller than the diameter (103 mm). In smaller cylinders, conversely, not only frictional forces are smaller, but also the distance between the loading edge and the start of the interface is equal to the diameter, so that possible confinement from the loading plate should dissipate before reaching interface and nearby materials.

Average values of shear and normal stresses at failure were calculated for each bond angle (i.e., for each interfacial shear-normal stress ratio) and plotted in Fig. 4 for the different repair materials. Data from 103 mm diameter cylinders, which exhibited a different response as per above discussion, were not considered. Shear-normal stress points were extrapolated to obtain shear bond coefficients based on the Mohr-Coulomb failure criterion (Eq. 4). A detailed description of this procedure and its statistical significance is available elsewhere (Zanotti et al. 2014, 2018). As expected, a linear fitting was acceptable ($R^2 = 0.981$-0.996). Concrete strength and fiber reinforcement mostly affect the cohesive component of bond. Cohesion varies from a minimum of 6.9 MPa for NS concrete without fiber to a maximum of 10.8 MPa for HS concrete with fibers. Addition of 13 mm steel fibers ($V_f = 0.5\%$) increases cohesion by 27%-23% for NS and HS, respectively, while switching from NS to HS concrete, cohesion is increased by 23%-33% with and without fibers, respectively. However, comparisons involving HS concrete are not conclusive due to the failure modes observed (mostly material rather than interfacial failure due to the higher bond, as shown in Fig.1b,c,f,g and previously discussed). Slight changes in friction can be regarded to as second order effects, mostly affected by the increase of the cohesive component of bond, which may locally reduce frictional effects due to changes in the failure plane (Zanotti et al. 2014, Randl 2013).

As expected, shear bond strength from push-out test is lower than that from slant shear test. This is mostly due to the intended application of compressive stresses at the interface in the slant shear test configurations adopted (Fig.1e), which, unlike the push-out test, are significantly affected by frictional and interlocking effects at the interface. Moreover, the interface is subject to minimal, secondary bending moment in the push-out test, due to unavoidable small eccentricities in loading and supports (Fig. 1h). This effect is probably the reason for rather low bond values that are typical with this set-up (Randl et al. 2016).

This document is the intellectual property of the fib – International Federation for Structural Concrete. All rights reserved.
This PDF of fib Bulletin 95 is intended for use and/or distribution solely within fib National Member Groups.

3.2 Tension

Tensile bond strengths obtained with various testing set-ups (Fig. 1a-d) are compared in Figure 6. Different failure modes were obtained in the pull-off tests. In the UBC pull-off test configuration (Fig. 1c), commonly used for overlay bond tests, most of the specimens failed in the substrate, and therefore tensile values are quite similar throughout the project because mostly affected by the tensile strength of the substrate. In summary, two failure modes were obtained with pull-off test at UBC, namely: (i) substrate failure (NS-0% & HS-0%, Fig. 5e) and (ii) mixed bond/substrate failure (NS-0.5% & HS-0.5%, Fig. 5f). Therefore, it appears that with steel fibers the failure moves closer to the interface. Shifting from substrate failures in plain repairs to mixed bond/substrate failure in repairs with $V_f = 0.5\%$, a slight decrease in the bond stresses at failure is recorded (NS-0% vs NS-0.5% and HS-0% vs HS-0.5%, Fig. 6).

This could be associated with localized stress concentrations emphasized (with this test set-up) by differences in matrix and fiber stiffness, with local changes in the matrix microstructure nearby the interface due, for instance, to bleeding effects, or even to interfacial damage during coring operations, which require higher mechanical action in the presence of steel fibers. Clearly, based on failure modes, these quantitative results provide only limited information on the bond (which is deemed to be somewhat higher than the bond stress reached at failure) and are strongly affected by non-uniform stress distributions through the specimen (substrate, repair, and interface, Austin et al. 1995).

Similar to what discussed for the slant shear test in Section 3.1, some of the effect of disturbed stress patterns can be mitigated by increasing the distance between loaded/restrained edges and the interface (Fig. 1d). With this set-up, the CUAS specimens resulted in higher pull-off tensile bond strength than the UBC specimens (Fig. 6). On the other hand, a longer coring operation might induce some additional damage in the specimen. This is highly dependent upon the quality of the coring system. Although HS-0.5% specimens experienced premature failure in the substrate, it must be noted that bond strength values obtained for the other species are quite high for pull-off tests, indicating that the damage should be limited in the end. The following failure modes were observed (Fig. 5b): (i) bond failure, substrate failure, or other premature failure (glue between core and load introduction) in NS-0%, (ii) bond failure in NS-0.5%, (iii) premature failure (during drilling) in HS-0%, and (iv) substrate failure in HS-0.5%. The premature failure observed with the HS-0% occurred at the interface during drilling and is attributed to some weakening of the bond due to unintended contamination of the interface of this single specimen when casting the overlay, even though it had been cleaned before, together with damage induced by drilling.

Direct tension tests (Fig. 1a) are very sensitive tests to perform and tend to provide lower bond values (Fig. 6). Nevertheless, bond failure (Fig. 5c) was observed in all the direct tension tests (other than the HS-0%, which failed during coring similarly to what observed for the pull-off test), and, consistently, bond strength increases for increasing concrete strength (NS-0% vs HS-0%) and increases with fibers (NS-0% vs NS-0.5%). Conversely, splitting tensile tests (Fig. 1c) tend to provide an overestimation of tensile strength due to confining stresses in the specimen. In case of concrete-concrete bond test, results are affected by the deviation of the failure plane (splitting crack, Fig. 5f) from the bond plane, which is influenced not only by stress patterns but also by the tortuosity/roughness of the bond plane and its alignment with the splitting load. Nevertheless, consistent trends are noted, with bond strength being higher in HS repairs compared to NS repairs and in repairs with fibers compared to the plain ones (both NS and HS).

This document is the intellectual property of the fib – International Federation for Structural Concrete. All rights reserved.
This PDF of fib Bulletin 95 is intended for use and/or distribution solely within fib National Member Groups.

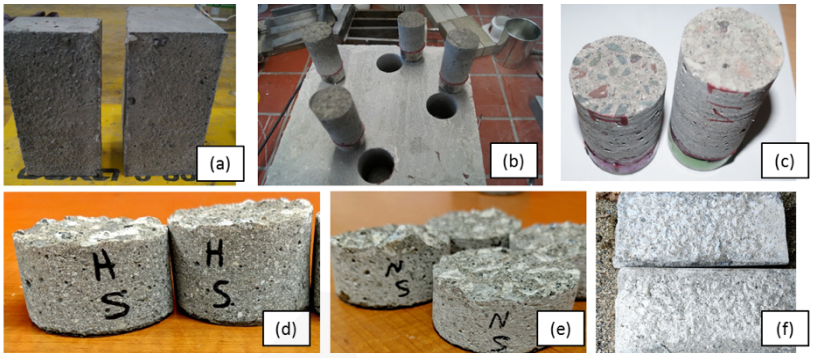


Figure 5: Bond failure from push-out test at CUAS (a) and failure modes from tensile bond tests at CUAS (b,c) and UBC (d-f). (Zanotti & Randl 2019)

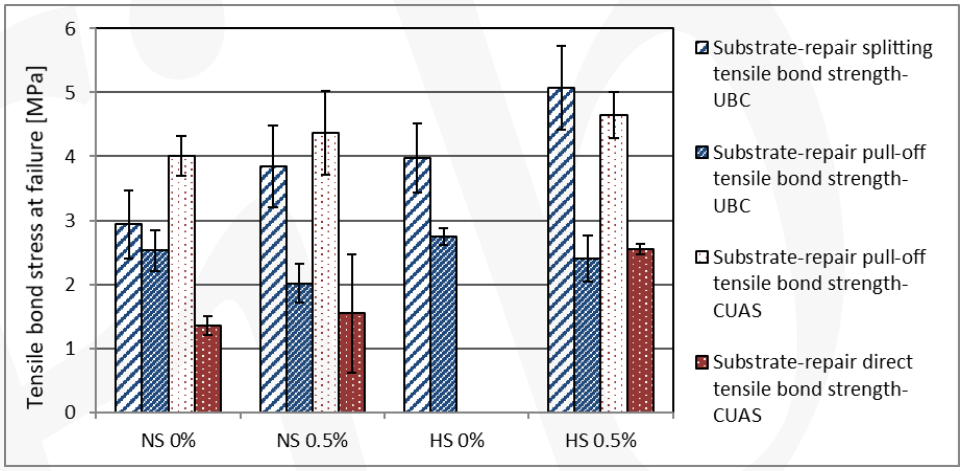


Figure 6: Tensile bond stresses at failure for different repair materials, obtained from various tensile bond tests (Fig. 1a-d). (Zanotti & Randl 2019)

4 Concluding remarks

An experimental study on substrate-repair bond was conducted in two independent labs in Canada and Austria, focussing on the effect of fibers, repair strength, and testing methods. The repairs (normal and high strength concretes) were poured against sandblasted substrates in SSD condition. The main conclusions can be summarized as follows:

- With the steel fibers used in this study, bond strength improvements were observed under shear stress with low or no compression applied;

- Bond strength improved for increasing repair strength as anticipated; only a lower bond limit was assessed for high strength repairs in slant shear tests due to premature substrate failure;

- Consistent trends were observed in the two labs overall. Test geometry significantly affected failure modes, stress paths, and resulting bond values. Pull-off and direct tension tests had larger scatter due to result sensitivity to local effects of direct tensile loading and drilling-induced damage. Shear bond strength from push-out test was lower than from slant test, even

This document is the intellectual property of the fib – International Federation for Structural Concrete. All rights reserved.
This PDF of fib Bulletin 95 is intended for use and/or distribution solely within fib National Member Groups.

when compared to extrapolated adhesion, mostly due to pronounced frictional/interlocking effects in the slant test, and slight bending due to small eccentricities in the push-out test.

- Therefore, a direct comparison of values from different tests (even when the same stress conditions are considered theoretically) is not recommended. In light of great uncertainty, a conservative approach is often recommended based on push-out and pull-off tests for shear and tension. However, these tests exhibit shortcomings and do not capture important factors. For instance, fiber orientation near the interface is unfavourable with the parallel casting direction of a push-out test, which is not representative of many common applications. Ongoing research efforts are aimed at developing more consolidated approaches, models, and conversion factors to navigate the variety of tests and parameters involved.

5 Acknowledgements

C. Zanotti would like to acknowledge the support of the National Science and Engineering Research Council of Canada, NSERC (grant number RGPIN-2016-03863).

6 References

ASTM E965-15 (2015), *Standard Test Method for Measuring Pavement Macrotexture Depth Using a Volumetric Technique*, West Conshohocken (PA), ASTM International.

Austin S, Robins P, Pan Y (1995), *Tensile bond testing of concrete repairs,* Materials and Structures, 28:249–259.

Austin S, Robins P, Pan Y (1999), *Shear bond testing of concrete repairs,* Cement and Concrete Research, 29(7):1067–1076.

Banthia N, Dubeau S (1994), *Carbon and steel microfiber-reinforced cement-based composites for thin repairs*. Journal of Materials Civil Engineering 6(1):88-99.

Lim YM, Li VC (1997), *Durable repair of aged infrastructures using trapping mechanism of Engineered Cementitious Composites*. Cement Concrete Comp 19:373-385.

Mindess S, Young JF, Darwin D (2002), *Concrete*, 2nd Ed., Prentice Hall.

Momayez A, Ehsani MR, Ramezanianpour AA, Rajaie H (2005), *Comparison of methods for evaluating bond strength between concrete substrate and repair materials*, Cement Concrete Research 35:748-757.

Morgan DR (1996), *Compatibility of concrete repair materials and systems*, Construction and Building Materials 10(1):57-67.

Randl N (2013), *Design recommendations for interface shear transfer in fib Model Code 2010*, Structural Concrete 14(3):230-241.

Randl N, Steiner M, Peyerl M (2016), *Sustainable strengthening of RC members with High Performance Concrete overlays*, IABMAS 2016:1308-1315.

Wagner C, Bretschneider N, Slowik V (2013), *Characterization of the interface between strain hardening cementitious repair layers and concrete subgrade*. FraMCoS-8 (SP).

Zanotti C, Banthia N, Plizzari G (2014), *A study of some factors affecting bond in cementitious fiber reinforced repairs*, Cement and Concrete Research, 63:117-126.

Zanotti C, Rostagno G, Tingley B (2018), *Further evidence of interfacial adhesive bond strength enhancement through fiber reinforcement in repairs*, Construction and Building Materials, 160:775-785.

Zanotti C, Randl N (2019), *Are concrete-concrete bond tests comparable?* Cement and Concrete Composites, 99:80-88.

This document is the intellectual property of the fib – International Federation for Structural Concrete. All rights reserved.
This PDF of fib Bulletin 95 is intended for use and/or distribution solely within fib National Member Groups.
FRC2018: Fibre Reinforced Concrete: from Design to Structural Applications
Joint ACI-*fib*-RILEM International Workshop

Characterization and Prediction of Microcracking in Reinforced UHPFRC Beams under Bending

Vicky Turgeon-Mallette[1], Luca Sorelli[1], David Conciatori[1], Julien Réthoré[2]

[1] : Université Laval, Quebec, Quebec, Canada.

[2] : Ecole Centrale de Nantes, Nantes, France.

Abstract

The capacity of Ultra-High Performance Fiber Reinforced Concrete (UHPFRC) to develop multiple micro-cracks instead and delay the localization of major cracks has great impact on the permeability and durability at serviceability state. In order to assess the durability of reinforced UHPFRC structures or rehabilitation layers, methods that accurately predict the microcrack width are necessary. This work aims at assessing the accuracy of some current analytical models to predict the crack width and growth of reinforced UHPFRC beam in bending by means of Digital Image Correlation (DIC) analysis of 4-point bending tests. DIC analysis was successfully employed to estimate the microcrack width and their spacing during loading. In particular, the following methods for predicting the growth of cracks of a reinforced FRC member are considered: (i) Eurocode 2; (ii) RILEM TC 162-TDF; (iii) the one proposed by Moffatt; (iv) the one proposed by Deluce. As expected Eurocode crack model overestimates the crack width as it does not consider the fiber contribution. RILEM and Moffatt models well predict the maximum crack width, but Deluce method is the most accurate to predict the mean crack width. The estimation of the crack spacing seems to the be critical factor which may require further improvement, especially for the crack spacing at serviceability states.

Keywords

Ultra-High Performance Fiber Reinforced Concrete (UHPFRC), Micro-cracks, Crack Width, Digital Image Correlation (DIC), Four Point Bending Test

This document is the intellectual property of the fib – International Federation for Structural Concrete. All rights reserved.
This PDF of fib Bulletin 95 is intended for use and/or distribution solely within fib National Member Groups.

1 Introduction

In North America and Europe, a greatest part of the concrete structures is approaching their design lifetime and need to be repaired and rebuilt. As a consequence, the cost of maintenance and reparation have considerably increased in the last years. Thanks to their crack resistance, Fiber Reinforced Concrete (FRC) is a promising repairing solution to increase structure lifetime and, thus, reducing these investments.

In this context, the use of Ultra-High Performance Fiber Reinforced Concrete (UHPFRC) has been proven to be a promising solution to strengthen existing structures by adding a strengthening and impermeable surface lawyer (1). In particular, cast-in-place UHPFRC layer with typical thickness of 25-50mm was applied to existing reinforced concrete (RC) elements. The impermeability of such layer UHPFRC layer play a major role in assuring post-reparation durability and reduce the maintenance expenses. For instance, for bridge deck slabs exposed to several environmental conditions, the allowable deformation in strain hardening UHPFRC is limited to 1.3‰ to guarantee water tightness (2). Thus, a reliable estimation of crack width is then critical for assessing the durability of FRC and UHPFRC structures in serviceability conditions. The tensile law of UHPFRC is characterized by high tensile strength (~8-20 MPa) and maximum strength deformation (>0.1-0.3%), which confers remarkable toughness (10-100 kJ/m^2) (3). In particular, the tensile law consists of an initial linear phase, followed by a strain hardening phase which is associated to multiple cracks formation, and finally a softening part with the formation of large localized cracks. Since at serviceability UHPFRC is in the strain hardening phase, the durability depends on the water permeability of UHPFRC with multiple cracks (4,5). Multiple microcracks with small widths can strongly reduce the water flow within a cracked concrete in serviceability conditions. From an experimental standpoint, the important effect of crack width on the water permeability has been widely investigated both for FRC (6) and UHPFRC (2). Moreover, the effect of the crack width is also important for the chloride diffusion (7).

Several crack models have been developed for predicting the crack spacing and crack widths of reinforced concrete and reinforced FRC. The Eurocode crack model (8), which was inspired by previous CEB-FIP crack model (9), allows predicting the crack spacing and crack opening for reinforced normal concrete. RILEM TC 162-TDF extended the Eurocode model for SFRC (10) by considering that a part of the tensile stress across the cracks is carried out by both the steel fibers and the steel rebar. Moffatt et al. (11) modified method of the Eurocode by considering the residual tensile stress due to the fiber bridging effect after first crack. Deluce et al. carried out experimental uniaxial tensile tests on FRC dog-bone sample to compare the mean crack spacing predicted by existing models with the one experimentally measured (12). Note that the mean spacing and width of microcracks were manually measured and few cracks were measured along the samples. Their results showed that experimental mean crack spacing was strongly overestimated by RILEM and Mofatt model. Then, Deluce et al. (13) extended the CEB-FIP crack model (9) providing a new relationship between the maximum crack width and average crack width which considers fiber volume and fiber aspect ratio (i.e., fiber length-to-diameter ratio). It is worth mentioning that all aforementioned methods have been developed and calibrated for Fiber Reinforced Concrete (FRC) materials that generally exhibit a softening response under uniaxial tension.

The scope of this preliminary work is to perform a preliminary study of the suitability of existing methods to predict the crack width of UHPFRC beams under bending. In particular,

This document is the intellectual property of the fib – International Federation for Structural Concrete. All rights reserved.
This PDF of fib Bulletin 95 is intended for use and/or distribution solely within fib National Member Groups.

Digital Image Correlation (DIC) technique were employed to accurately measure microcracks of UHPFRC beam under bending at different level of damage.

2 Experimental program

2.1 Material

The beams tested were made of Ductal® UHPFRC with 2% by volume of steel fibers and steel rebar (14). This UHPFRC exhibits tension hardening behavior in tension with multiple microcrack formation (15). The steel fibers have a length l_f of 14 mm and a diameter d_f of 0.185 mm. They have a Young modulus E_s of about 200 GPa and a yielding strength of 2860 MPa. The Young modulus and the mean compressive strength was characterized by compression tests on 3 cylinders of 112 mm (4.4 in) diameter according to ASTM C39 and C469. The considered UHPFRC was characterized by compression tests and 4 Point Bending Tests (4PBT). Compression strength f'_c and Young modulus E_c in compression were 198.2 ± 3.9 MPa and 58.2 ± 0.4 GPa, respectively. The flexural strength was about 29.8 ± 1.1 MPa.

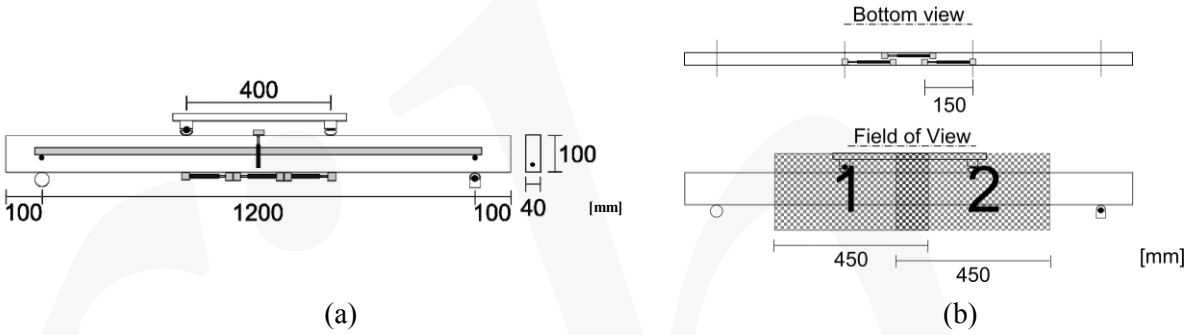
2.2 Flexural testing

Four-point bending tests (4PBT) were carried on un-notched UHPFRC beams with a span S of 1200 mm, a height h of 100 mm and a width b of 40 mm (Figure 1a). For experimental details see Duhamel-Labrecque (14). The mid-span deflection was measured by a LVDT, while the bottom surface was instrumented with 3 LVDTs in order to measure Crack Mouth Opening Displacement (CMOD) (Figure 1b). Figure 1 presents the test set-up and beam geometry. Only for one beam, a strain gauge was located in the middle of the rebar to measure its deformation. The forces were applied with a closed loop control system. A steel reinforcement with a diameter d_b of 8 mm is used. The steel bar cover was 15 mm.

For the identification of the tensile law, 3 different types of Inverse Analyses Models (IAM) were carried out, such as: (i) López analytical IAM (16). By developing an analytical relationship between the maximum deflection of a 4PBT and the curvature, Lopez and al. (16) developed an iterative inverse analysis. This method requires the force-deflection data obtained from an un-notched 4PBT without limitation on the dimension of the tested specimen. As drawback, this method predicts a linear stress-crack opening relationship in the post-cracking stage; (ii) López simplified IAM (17). Based on a statistical analysis, Lopez and al. (17) proposed a simplified inverse analysis which allows to directly identify the tensile law from 5 points identified on the experimental flexural curve stress vs. deflection of un-notched 4PBT. Notably, new Canadian code has adopted this approach to identify the tensile law of UHPFRC characterization (18). The main drawback of this inverse analysis is that the length-to-height ratio of the sample under 4PBT needs to be of 3 or 4.5. (iii) Dobrusky numerical IAM. Dobrusky and Chanvillard (19) developed a numerical inverse analysis method based on a modified force-based fiber-beam formulation where progressive loading is driven by a curvature of a nonlinear hinge. By a point-by-point procedure the numerical model allows identifying the tensile law of UHPFRC from a load-deflection curve of a UHPFRC beam under 4PBT. Full details of the model can be found (19). As for the identification of the tensile law, 3 UHPFRC beams without steel reinforcement with same section (40 mm x 100 mm) and reduced span of 400 mm were tested in 4PBT with a load span of 200 mm. Figure 2a compares the experimental force-deflection curves with the mean curve estimated by

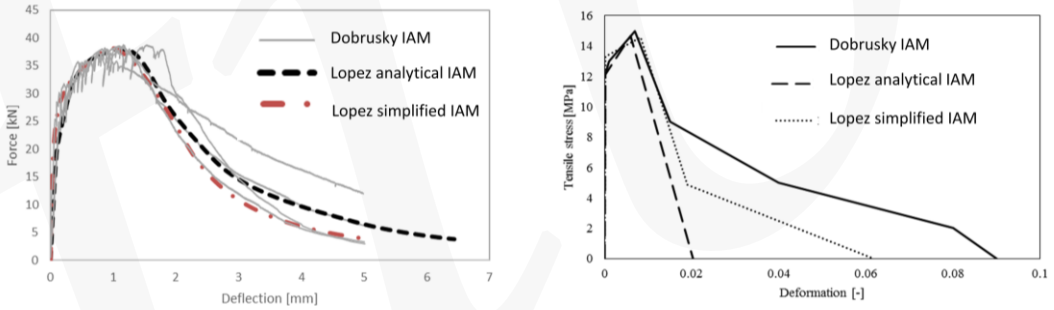
This document is the intellectual property of the fib – International Federation for Structural Concrete. All rights reserved.
This PDF of fib Bulletin 95 is intended for use and/or distribution solely within fib National Member Groups.

inverse analysis from Lopez analytical IAM and Dobrusky IAM. The load-deflection is fairly well predicted by the simulated curves. Figure 2a compares the tensile law identified with the 3 inverse analysis method (IAM) herein considered. As expected, the Lopez analytical IAM does now allow to identify the final part of the tensile law. In general, the 3 inverse IAM methods provide a similar tensile law. As average, the maximum tensile stress (f_{cr}) is estimated as 14.6 MPa. After the maximum stress, it is possible to convert the deformation in crack opening by multiplying for a characteristic length. As for the characteristic length proposed for bending test of FRC materials, we consider the L_{ch}=2/3 as proposed by French design recommendations (20). Full details of the inverse analysis can be found in (21).



(a) (b)

Figure 1: (a) Experimental test set-up and beam geometry for 4PBT; (b) bottom view and zones which were photographed by the 2 cameras for DIC analysis.



(a) (b)

Figure 2: (a) Comparison of the experimental load-deflection curves for unreinforced UHPFRC beam and the simulated curve with Dobrusky model; (b) Comparison of the tensile law identified by the 3 considered inverse analysis models.

2.3 Digital image correlation analysis and crack width calculation

The pictures of the beams are taken every 10 seconds throughout the bending tests with a total of 250-300 pictures (22). The moment vs. deflection curves of two tests are shown in Figure 3a. The crack width was also calculated according to the methods by DIC analysis by assessing the distance from 2 points aside of observed microcracks. Four different moment levels were considered as shown in Figure 3b, such as: cracking onset load (M_0), the maximum load applied (M_{max}) and two intermediary points in between M_0 and M_{max}.

This document is the intellectual property of the fib – International Federation for Structural Concrete. All rights reserved.
This PDF of fib Bulletin 95 is intended for use and/or distribution solely within fib National Member Groups.

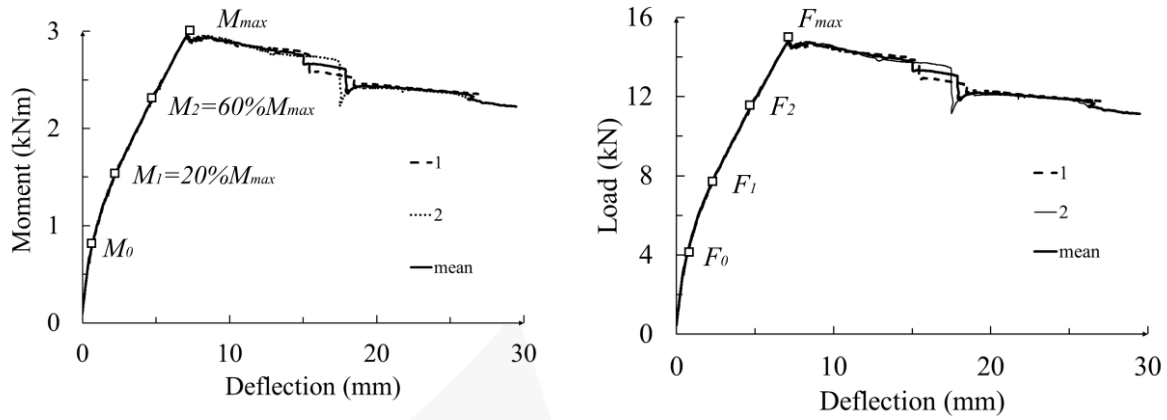


Figure 3: (a) Experimental moment-deflection curves considered in this work (with 4 points indicated); (b) Critical points of the force-deflection curve chosen points for crack width calculation.

As for plain concrete, the Eurocode estimates the maximum crack from the average crack spacing and the strain in steel rebar (ε_{s2}) as follows:

$$w_{\max}^{EC} = \beta s_m \zeta \varepsilon_{s2} \tag{1}$$

and

$$s_m = 50 + k_1 k_2 \frac{d_b}{4\rho_{ce}} \qquad \zeta = 1 - \beta_1 \beta_2 \left(\frac{M_{cr}}{M_a}\right)^2 \qquad M_{cr} = \frac{f_{tc}}{W} \tag{2a,2b, 2c}$$

where β = 1.3 for restrained cracking in sections with a minimum depth lesser than 300 mm or belowthe average crack spacing s_m (mm); k_1= 1.6 for plain bars; k_2=0.5 for pure bending; d_b is the bar diameter; ρ_{ce}=1.5% is the reinforcement ratio; ζ accounts for the tension stiffening; β_1= 0.5 for plain rebars; β_2=1 for short term loading; M_{cr} is the bending moment at first cracking (N·mm) which can be estimated from first cracking strength f_{tc} and elastic section modulus W, which is estimated to be 133'000 mm^3 with $f_{tc} = 0.6\sqrt{f_c'} = 8.4\,MPa$.

The RILEM TC 162-TDF method extended the previous formula to account for the fiber bridging by the following set of equations for maximum crack width calculation.

$$w_{\max}^{RILEM} = \beta s_m \varepsilon_{sm} \tag{3}$$

and

$$s_m = 50 + k_1 k_2 \frac{d_b}{4\rho_{ce}} \left(\frac{50}{l_f / d_f}\right) \qquad \varepsilon_{sm} = \frac{\sigma_s}{E_s}\left[1 - \beta_1 \beta_2 \left(\frac{\sigma_{sr}}{\sigma_s}\right)^2\right] \tag{4a,4b}$$

where ε_{sm}= mean strain in steel rebar; σ_s = stress in steel rebar in a cracked section (MPa); σ_{sr}= rebar stress at first cracking (MPa). Moffatt *et al.* (11) extended the presented formula for

This document is the intellectual property of the fib – International Federation for Structural Concrete. All rights reserved.
This PDF of fib Bulletin 95 is intended for use and/or distribution solely within fib National Member Groups.

predicting the maximum crack $w_{\max}^{Moffatt}$ by changing the mean crack spacing with the following equation

$$s_m = s_{m_0}\left(1-\frac{f_{res}}{f_{cr}}\right) \tag{5}$$

where f_{res}=is residual stress for a crack width of 0.5 mm; f_{cr} is the cracking strength. Note that this formula is conceived for an FRC strain softening material. Nevertheless, in the context of this preliminary study, we assumed f_{cr} as assumed equal to the tensile maximum strength of Figure 2b, and while f_{res} equal to about 8.5 MPa which corresponds to the post-peak stress at a deformation equal to the deformation at the maximum stress plus the equivalent deformation equal to 0.5mm/Lch=0.0075. The value of the characteristic length L_{ch} =2/3h=66.6mm as aforementioned.

Deluce (13) proposed a method to calculate maximum and average crack width as follows:

$$w_{avg}^{Deluce} = s_m \varepsilon_{t,avg} \tag{6}$$

$$w_{\max}^{Deluce} = \left(1.7+3.4\frac{V_f l_f}{d_f}\right) w_{avg}^{Deluce} \tag{7}$$

where $\varepsilon_{t,avg}$ is the average tensile strain of a member, the effective longitudinal bar spacing s_b, the reinforcement effectiveness parameter s_{mi} have been taken from CEB-FIB formulation (8) as follows:

$$s_m = 2\left(c_a+\frac{s_b}{10}\right)k_3+\frac{k_1 k_2}{s_{mi}} \qquad s_b = 0,5\sqrt{\frac{\pi d_b^2}{\rho_{ce}}} \le 15 d_b \tag{8a,8b}$$

$$s_{mi} = \frac{\rho_{ce}}{d_b}+k_f\frac{\alpha_f V_f}{d_f} \qquad k_3 = 1-\frac{\min(V_f;0,015)}{0,015}\left(1-\frac{1}{k_f}\right) \tag{9a,9b}$$

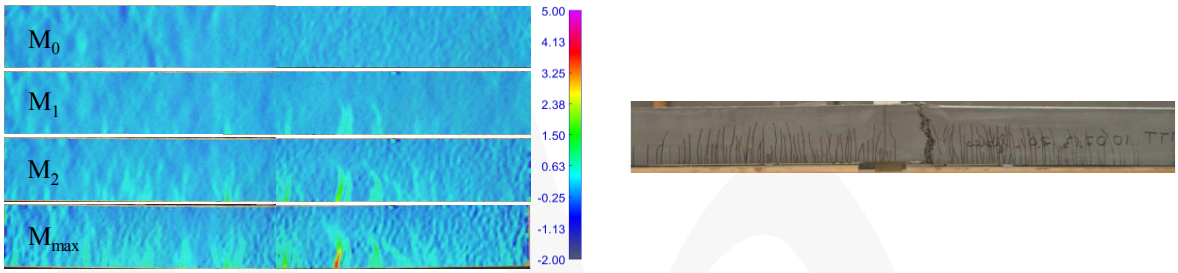
where $k_f = l_f/50d_f \ge 1$; $\varepsilon_{t,avg}$= average tensile strain; the fiber volume V_f≤0.15%; s_b=effective longitudinal bar spacing (mm); smi= steel fiber effectiveness parameter; k_1= 0.8 for plain bars; k_2=0.125 for pure bending; k_3= fiber content factor; k_f = factor for fiber effectiveness due to fiber ratio; fiber orientation factor α_f= 0.5 for random orientation;

3 Results and discussion

This section compares the crack width measured by DIC with the ones estimated by the considered methods at different moment levels. Figure 4a shows the deformation field measured by DIC analysis for the considered moment levels. The deformation field shows the strain concentration (i.e., microcracks). Visibly, the microcrack width and the microcrack spacing are not perfectly uniform along the beam even for a tension hardening UHPFRC with unnotched beam. Table 1 presents results of crack width calculation obtained from the methods previously explain and from DIC analysis. As for the crack models of Eurocode, RILEM and Moffatt it is possible to pass by maximum crack width to men crack width by

This document is the intellectual property of the fib – International Federation for Structural Concrete. All rights reserved.
This PDF of fib Bulletin 95 is intended for use and/or distribution solely within fib National Member Groups.

dividing with the parameter β. Deluce method provides a relationship Eq. (7) to pass from mean to maximum crack width. Maximum and average crack width for the two beams tested were estimated by DIC analysis. The coefficient of variation (COV) of the average crack width for all the observed cracks for the two tests repetition is also presented, but it meaning is limited due to small number of tests. A single micro-crack occurred at M_0, followed by the formation of multiple microcracks. Finally, a large crack localizes at M_{max}. The cracks spacing was also measured by visual inspection after testing (14).



(a) (b)

Figure 4: (a) DIC analysis results at 4 different load rates of 4PBT (14) (units are 103 microstrain); (b) example of microcracks visually observed by eye at the end of the test.

Table 1: Average results of crack width, in mm, obtain from different analytical methods and from DIC analysis.

	Predicted crack opening					Measured crack opening		
Moment level	w_{max}^{EC}	w_{max}^{RILEM}	$w_{max}^{Moffatt}$	w_{max}^{Deluce}	w_{ave}^{Deluce}	w_{max}^{DIC}	w_{ave}^{DIC}	COV
M_0	0.008	0.022	0.005	0.036	0.007	0.011	0.008	43%
M_1	0.091	0.061	0.054	0.100	0.018	0.055	0.015	108%
M_2	0.156	0.136	0.121	0.225	0.040	0.141	0.050	82%
M_{max}	0.290	0.251	0.2224	0.417	0.075	0.409	0.101	124%

The results summarized in Table 1 are also graphically presented in Figure 5a and 5b for maximum and average crack, respectively. Table 2 shows the percentage error between the actual crack width obtained with DIC analysis and that one estimated from analytical methods. As expected, Eurocode crack models overestimates the maximum crack width since it does not consider the fibre contribution. Moffatt model well predicts the maximum crack width for most moment level with exception for the moment M_0 where the crack widths are rather small (e.g., about 10 μm). RILEM method well predicts the maximum crack width for all moment levels. Deluce method seems to overestimate the maximum crack (Figure 5a), but is in well agreement with the average crack widths (Figure 5b). All the other crack models overestimate the average crack width (Figure 5b).

This document is the intellectual property of the fib – International Federation for Structural Concrete. All rights reserved.
This PDF of fib Bulletin 95 is intended for use and/or distribution solely within fib National Member Groups.

Table 2: Error percentage between experimental and predicted crack width.

Moment level	w_{max}^{EC}	w_{max}^{RILEM}	$w_{max}^{Moffatt}$	w_{max}^{Deluce}	w_{avg}^{Deluce}
M_0	- 67%	- 11%	- 80%	+ 47%	+ 22%
M_1	+ 64%	+ 9%	- 3%	+ 81%	+ 76%
M_2	+ 75%	+ 17%	+ 4%	+ 93%	+ 66%
M_{max}	+ 56%	+ 4%	- 7%	+ 72%	+ 55%

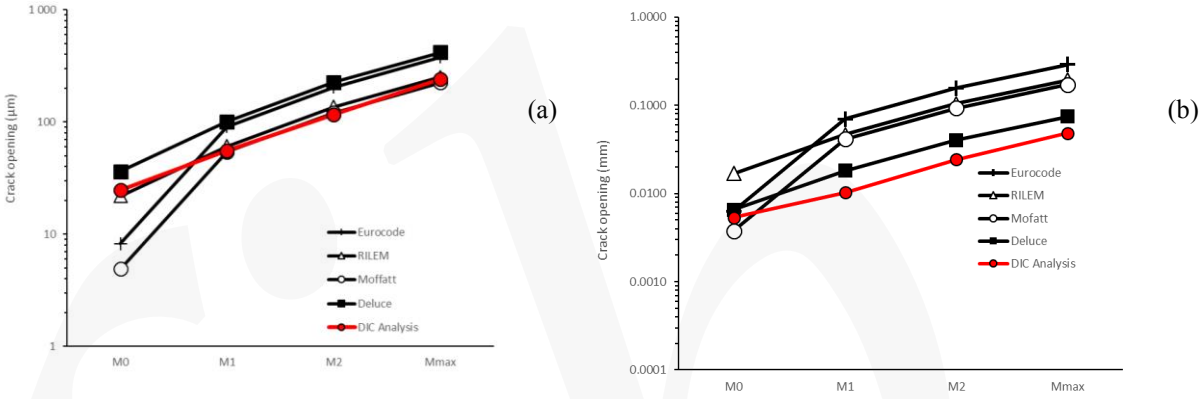


Figure 5: Comparison of the experimental and theoretical values for (a) maximum crack size and (b) average crack size.

This section aims at understanding the source of error of the considered methods. Figure 6 shows the strain distribution along the lateral surface of the beam that is known from DIC analysis at a chosen loading level. We consider herein a simple way to estimate the crack spacing. The number of relevant microcrack can be arbitrarily estimated by setting a strain threshold of 0.7%. The crack spacing can be estimated by dividing the length of the beam with the number of counted microcracks intercepting the strain threshold. Figure 6 shows the number of cracks counted at M_{max} for both beams tested.

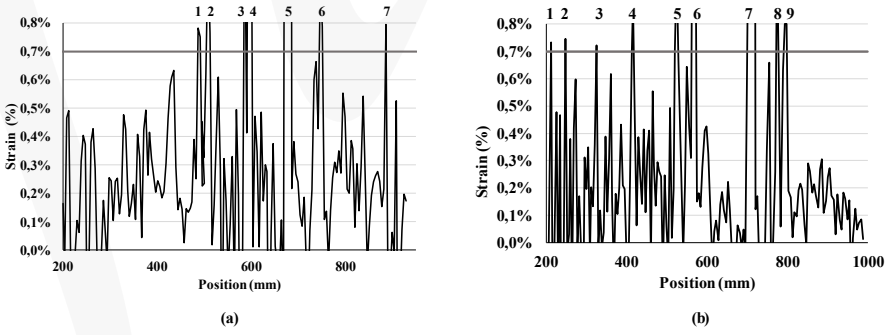


Figure 6: As for M_{max}, number of micro-cracks for a 0.7% strain for the first (a) and second (b) beam tested with DIC analysis.

Figure 7 shows the error on the estimation of the microcrack spacing at the different moment levels. At moment M_1, all the crack model overestimates the crack spacing as they all assume a constant crack spacing (Figure 7a). The crack spacing of all model well corresponds the observed one only for the maximum M_{max} (Figure 7b).

This document is the intellectual property of the fib – International Federation for Structural Concrete. All rights reserved.
This PDF of fib Bulletin 95 is intended for use and/or distribution solely within fib National Member Groups.

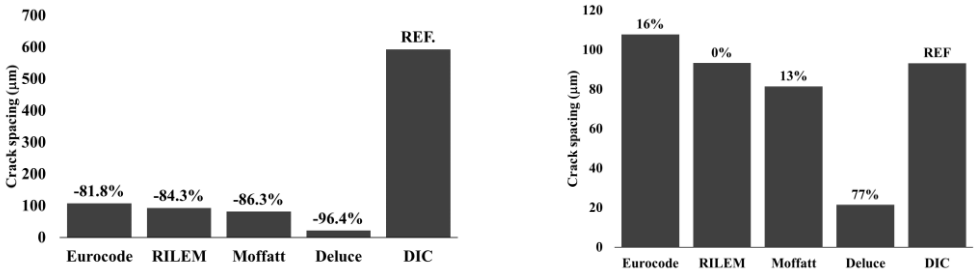


Figure 7: Comparison of the predicted and measured mean crack spacing at different moment levels: (a) M1; (b) Mmax.

4 Concluding remarks

Owing to the importance of microcrack width on UHPFRC durability, this preliminary work compares some existing analytical methods against experimental results by DIC analysis. Based on the present results, the following preliminary conclusions are drawn:

1. DIC allowed estimating the microcracks width during loading as well as their spacing for UHPFRC beam under bending. The strain profile was employed to estimate the effective number of microcrack as their distribution is far to be uniform;
2. Moffatt and RILEM method well predict the maximum crack widths at intermediate and maximum moments. At low load (M0) with crack opening of 20-50 μm, Moffett model underestimates the maximum crack width, while RILEM still provides a good prediction. Instead, Deluce model provides the best prediction of the mean crack width;
3. When crack spacing is considered, all crack models underestimate the crack spacing at low moment levels, but they are in good agreement with the measured values at the maximum moment M_{max}.

Further works should be carried out to statistically validate the crack models for UHPFRC to enhance the assumption of the constant crack spacing during loading.

5 Acknowledgements

We would like to acknowledge M. Youri Duhamel-Labrecque for the experimental results and Dr. Dominique Corvez of Lafarge Northern America the preparation of the samples.

6 References

1. Brühwiler E. UHPFRC technology to enhance the performance of existing concrete bridges. Struct Infrastruct Eng. 2020;16(1):94–105.
2. Charron J-P, Denarié E, Brühwiler E. Permeability of ultra high performance fiber reinforced concretes (UHPFRC) under high stresses. Mater Struct. 2007;40(3):269–77.
3. Chanvillard G, Rigaud S. Complete characterization of tensile properties of Ductal® UHPFRC according to the French recommendations. High Perform Fiber Reinf Cem Compos HPFRCC4 Rilem Proc PRO. 2003;30:21–34.
4. Wang W, Liu J, Agostini F, Davy CA, Skoczylas F, Corvez D. Durability of an ultra high performance fiber reinforced concrete (UHPFRC) under progressive aging. Cem Concr Res. 2014;55:1–13.

This document is the intellectual property of the fib – International Federation for Structural Concrete. All rights reserved.
This PDF of fib Bulletin 95 is intended for use and/or distribution solely within fib National Member Groups.

5. Fehling E, Schmidt M, Walraven J, Leutbecher T, Fröhlich S. Ultra-High Performance Concrete UHPC [Internet]. 2014. Available from: http://onlinelibrary.wiley.com/book/10.1002/9783433604076
6. Wang K, Jansen DC, Shah SP, Karr AF. Permeability study of cracked concrete. Cem Concr Res. 1997;27(3):381–93.
7. Şahmaran M. Effect of flexure induced transverse crack and self-healing on chloride diffusivity of reinforced mortar. J Mater Sci. 2007;42(22):9131–6.
8. Eurocode 2: Design of concrete structures - Part 1-1: General rules and rules for buildings. 2005;
9. Comité euro-international du béton. CEB-FIP model code for concrete structures. 1978.
10. RILEM TC 162-TDF. Final recommandation of RILEM TC 162-TDF: Test and design methods for steel fibre reinforced concrete sigma-epsilon-design method. Mater Struct. 2003;36(262):560–7.
11. Moffatt K. Analyse de dalles de pont avec armature réduite et béton de de fibres métalliques. Montréal, Qc: École Polytechnique de Montréal; 2001.
12. Deluce JR, Vecchio FJ. Cracking Behavior of Steel Fiber-Reinforced Concrete Members Containing Conventional Reinforcement. ACI Struct J. 2013;110(3).
13. Deluce JR, Lee S-C, Vecchio FJ. Crack model for steel fiber-reinforced concrete members containing conventional reinforcement. ACI Struct J. 2014;111(1):93.
14. Duhamel-Labrecque Y, Sorelli L, Réthoré J, Baby F, Toutlemonde F, Bernardi S. Identification of the Tensile Law of UHPFRC Materials from Bending Tests by Means of Digital Image Correlation. In Montpellier, France; 2017.
15. Guenet T, Baby F, Marchand P, Sorelli L, Toulemonde F, Bernardi S. Flexural Failure Modes Of Ribbed Triangular UHPFRC Plates: Experimental And Numerical Investigation. In: ", First International Symposium on UHPC. Des Moines, Iowa; 2016.
16. López JÁ, Serna P, Navarro-Gregori J, Camacho E. An inverse analysis method based on deflection to curvature transformation to determine the tensile properties of UHPFRC. Mater Struct. 2015 Nov;48(11):3703–18.
17. López JÁ, Serna P, Navarro-Gregori J, Coll H. A simplified five-point inverse analysis method to determine the tensile properties of UHPFRC from unnotched four-point bending tests. Compos Part B Eng. 2016 Apr;91:189–204.
18. CSA. S6-14 Code canadien sur le calcul des ponts routiers [Internet]. 2014. Available from: store.csagroup.org/
19. Dobrusky S, Chanvillard G. Inverse Analysis Tailored for UHPFRC. J Eng Mech. 2017 Sep;143(9):04017102.
20. AFNOR. BFUP : spécification, performance, production et conformité. [Internet]. 2016 juillet. Report No.: NF P 18-470. Available from: http://www.boutique.afnor.org/norme/nf-p18-470/betons-betons-fibres-a-ultra-hautes-performances-specification-performance-production-et-conformite-/article/866839/fa063353
21. Bouchard D, Sorelli, L., Conciatori D, Dobrusky S. Comparison of different methods of inverse analysis to assess the tensile law of UHPFRC from four points bending tests. In Desenzano, Italie; 2018.
22. Baril MA, Sorelli L, Réthoré J, Baby F, Toutlemonde F, Ferrara L, et al. Effect of casting flow defects on the crack propagation in UHPFRC thin slabs by means of stereovision Digital Image Correlation. Constr Build Mater. 2016;129:182–92.

This document is the intellectual property of the fib – International Federation for Structural Concrete. All rights reserved.
This PDF of fib Bulletin 95 is intended for use and/or distribution solely within fib National Member Groups.

Investigation of fiber effect on the geometrical property of crack and water permeability of cracked concrete

Yining Ding[1], Dong Li[1], Wei Zeng[1]

[1] : State Key Laboratory of Coastal and Offshore Engineering, Dalian University of Technology, Dalian 116024, China.

Abstract

The water permeability of the concrete with cracks has been studied in this paper. Cylindrical specimens with different fiber contents were pre-cracked, and specimens without any fiber reinforcement were also investigated as reference. The water permeability of the specimens with different crack width was measured by hydraulic permeability test. The measured data of the crack surface was collected by the self-developed data acquisition system, the total crack length and surface area of the samples were analyzed, the geometrical property of crack (tortuosity and roughness) was evaluated quantitatively. The results showed that the tortuosity and roughness of the cracked surface can be increased greatly by addition of the macro steel fiber. The coefficient of the water permeability of the specimens followed the Poiseuille law by considering of the influence of the crack geometrical property.

Keywords

Abstract: concrete; crack; water permeability; steel fiber; Poiseuille law

This document is the intellectual property of the fib – International Federation for Structural Concrete. All rights reserved.
This PDF of fib Bulletin 95 is intended for use and/or distribution solely within fib National Member Groups.

1 Introduction

Material transport properties, especially permeability, play an important role on its durability (Aldea et al. 1999a; Gérard et al. 1996; Park et al. 2012). Permeability controls the rate of penetration of moisture that may contain aggressive solutes. Traditionally, permeability of concrete is measured using un-cracked specimens (ASTM C 1202, 2012; ASTM C 1585, 2013; GB/T 50082, 2009), while in real structures, tensile cracks due to drying shrinkage and mechanical loading are almost unavoidable (Nilson et al. 2009). Although cracks themselves do not directly affect the durability of the concrete structures, the existence of cracks can significantly increase the penetration of moisture and salts into concrete. Some experiments have been conducted to evaluate the effects of the crack on permeability of concrete. Wang et al. (1997) measured the permeability of cracked concrete, and correlated the crack opening displacement (COD) with the permeability coefficient of the crack specimens. Shin et al. (2017) studied the influence of the crack type, water head and crack width on permeability of the concrete. Akhavan et al. (2012) studied the effect of crack geometry (effective crack width, crack tortuosity, and surface roughness) on water permeability of cracked mortar.

Fiber reinforced concrete (FRC) has great potential significance to construction (Ding et al. 2009). With the addition of fibers, the toughness of the concrete can be improved obviously. Rapoport et al. (2002) and Picadent et al. (2009) studied the influence of steel fiber reinforcement on concrete permeability, and the results showed that the addition of steel fibers demonstrated positive influence on permeability of cracked concrete. However, from the paper review, we found that there is still a lack of a systematic investigation of the fiber influence on crack geometry and permeability of concrete.

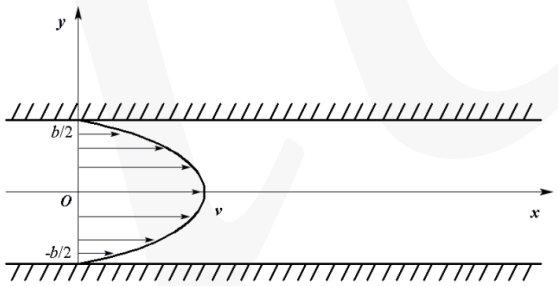


Figure 1: Parallel-plate model

The simplest model of flow through a rock fracture is the Poiseuille law (Bear, 1988; Zimmerman, 1996). Using the theory of laminar flow of incompressible Newtonian fluids inside a smooth parallel plate (Figure 1), the permeability coefficient of a crack k (m^2) can be identified as:

$$k = \frac{b^2}{12} \tag{1}$$

Where b is the crack width; Eq. (1) is strictly valid for a smooth, straight, and parallel plate crack. While real cracks in rock and concrete do not demonstrate such characteristics, the crack width often varies along the length of a crack; cracks are tortuous meaning their actual length is larger than their nominal length; and crack wall surfaces are rough (Akhavan et al. 2012; Akhavan, 2012; Rastiello, 2014). These features reduce the permeability of a crack.

This document is the intellectual property of the fib – International Federation for Structural Concrete. All rights reserved.
This PDF of fib Bulletin 95 is intended for use and/or distribution solely within fib National Member Groups.

$$k = \frac{\tau b_{\text{eff}}^2}{12\left(1+8.8R_{\text{r}}^{1.5}\right)} \tag{2}$$

Where τ is the crack tortuosity; R_{r} is the relative surface roughness, $R_{\text{r}}=R_{\text{a,g}}/(2*b_{\text{eff}})$; $R_{\text{a,g}}$ is the absolute surface roughness (see Eq.(6)); b_{eff} is the effective crack width.

Some researchers have introduced this model to calculate the theoretic flow of the cement (Akhavan et al. 2012; Akhavan, 2012). To account for the effect of crack geometry in permeability, in Eq. (2), the influence factors τ and R_{r} have been introduced. However, the investigation of fiber effects on the crack geometry (tortuosity and toughness) and permeability of concrete is still rare.

1.1 Material properties

In this program, the basic mixture proportion was shown in Table 1. The concrete was made with ordinary Portland cement (P•O 42.5R) and silica fume. The water to binder ratio was 0.43. The coarse aggregates were crushed gravel with a maximum size of 15 mm. and the fine aggregates (0-5mm) were river sand with fineness modulus of 2.56.

Table 1: Mix proportion

Cement (kg/m^3)	Silica fume (kg/m^3)	Water (kg/m^3)	Sand (kg/m^3)	Gravel (kg/m^3)	Super plasticizer (kg/m^3)
472.8	37.8	222.2	827.5	827.5	5.67

The widely used hooked-ended macro steel fibers have been added into the concrete samples. The parameters of the fiber are illustrated in Table 2.

Table 2: Properties of steel fiber

Types	Length (mm)	Diameter (mm)	Aspect ratio	Tensile strength (MPa)	Elastic modulus (GPa)
Steel fiber	35	0.55	65	1245	200

1.2 Test specimens

Cubic specimens (150×150×150mm) were cast to verify the compressive strength. Cylindrical specimens (100mm in diameter and 40mm height) slicing from a sample of (100mm in diameter and 300mm height) were adopted for the permeability test. All the specimens were de-molded after 24 h and cured in a curing room with 95% relative humidity at 20 ℃. In order to measure the crack information, each face of the cylindrical specimens was painted with white color before experiment (Rastiello et al. 2014).

1.3 Pre-cracking of samples using feedback controlled splitting test

The feedback controlled splitting test was performed in Figure 2 (Wang et al. 1997). First of all, two displacement transducers (LVDTs) were fixed on both sides of the specimen. Two pieces of plywood were placed between the loading plate and the specimen for the sake of preventing the fracture of specimens due to the local stress underneath the loading points (Aldea et al. 1999b). When the average displacement measured at both sides reached a

This document is the intellectual property of the fib – International Federation for Structural Concrete. All rights reserved.
This PDF of fib Bulletin 95 is intended for use and/or distribution solely within fib National Member Groups.

predetermined value, the test specimens were unloaded. The crack widths of approximately 50µm to 250µm at unloaded state have been selected for water permeability test.

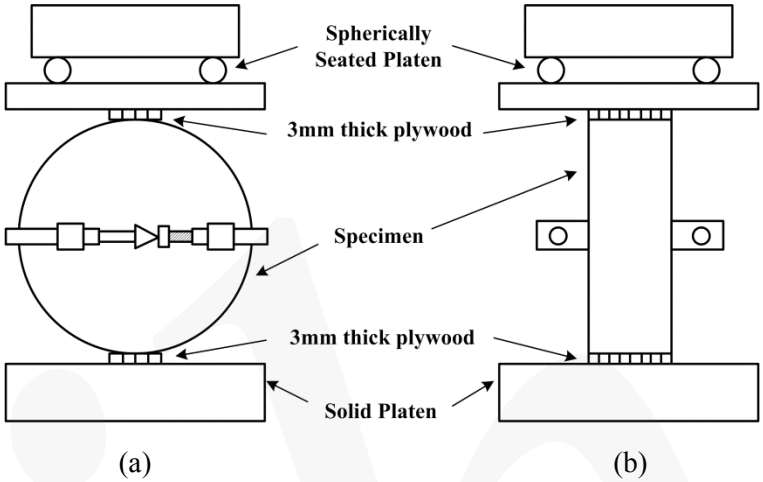


Figure 2: Schematics and test set-up of feedback controlled splitting test: (a) front face; (b) lateral face

1.4 Water permeability test

A self-designed device was introduced to the permeability test (see Figure 3). The device made with two steel vessels and a water pump. In order to avoid the water leakage at the contact surfaces, the O type rubbers were embedded in both steel vessels, and two silicon pad joints were also arranged between the vessel and the face of the sample. The epoxy was used at the lateral surfaces of the specimen, to avoid the risk of any water leakage from the specimen. During the test, the out flowed water was monitored,

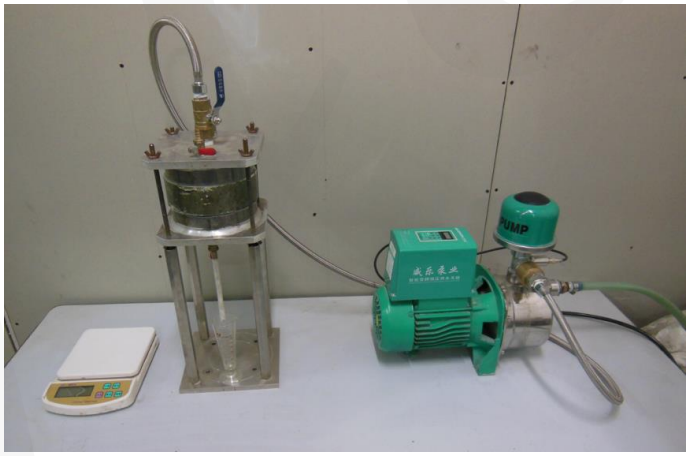


Figure 3: Hydraulic test

1.5 Effective crack width

The crack width was variable on the surface of the disk. The horizontal displacement measured by LVDTs was not a good representation of the actual crack profile. In order to build a prediction model for water permeability, the effective crack width should be considered (Akhavan et al. 2012). The method to calculate the effective crack width was given elsewhere (Ding et al. 2018).

This document is the intellectual property of the fib – International Federation for Structural Concrete. All rights reserved.
This PDF of fib Bulletin 95 is intended for use and/or distribution solely within fib National Member Groups.

1.6 Crack geometry

After the permeability test, a V-shaped mouth was made and the specimen was split into two pieces along the crack, and the fracture surfaces were analyzed to evaluate the crack tortuosity and surface roughness, the steel fibers of the fracture surface were cut with the needle-nosed pliers. A self-designed equipment was used for data acquisition (see Figure 4), the movement of the specimen is controlled according to a scan path. The interval of the y-axis is 0.5mm.

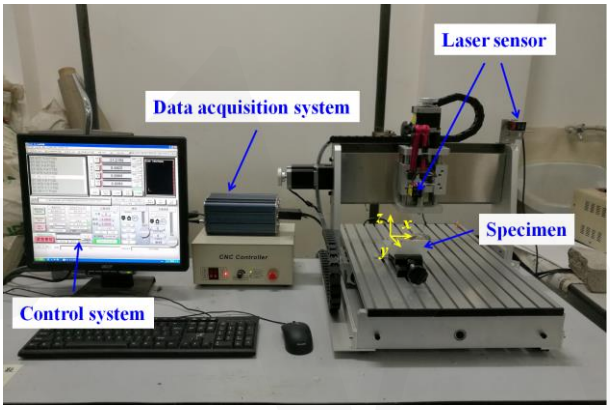


Figure 4: Data acquisition system

The crack tortuosity (τ) can be defined as follows (Akhavan, 2012):

$$\tau = \left(\frac{L_0}{L_t} \right)^2 \tag{3}$$

Where the L_t is the total crack length, L_0 is the projected crack length.

The method of calculating the projected crack length and the total crack length is demonstrated in Figure 5.

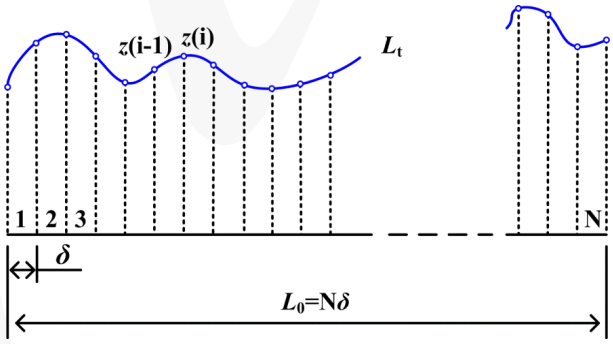


Figure 5: Explanation of the total crack length and the projected crack length

The total crack length L_t can be determined as follows:

$$L_t = \sum_{i=1}^{N} \sqrt{\left[z(i) - z(i\text{-}1) \right]^2 + \delta^2} \tag{4}$$

Where z(i), z(i-1) are the height corresponding to the point i and i-1, respectively; δ means the size of the element, N means the number of the element.

This document is the intellectual property of the fib – International Federation for Structural Concrete. All rights reserved.
This PDF of fib Bulletin 95 is intended for use and/or distribution solely within fib National Member Groups.

The absolute roughness is defined as follows (Akhavan et al. 2012):

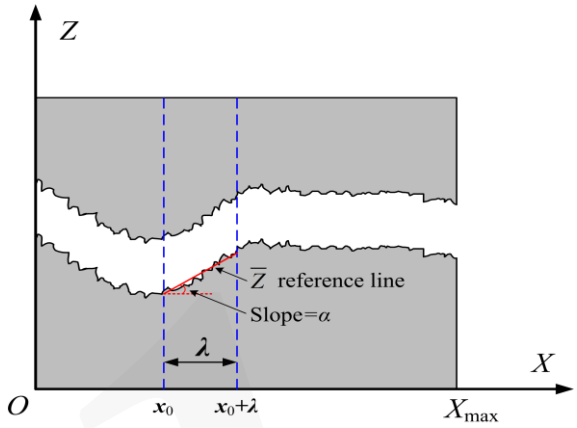


Figure 6: Absolute roughness

$$R_{a.l} = \frac{1}{\lambda}\sum\left(\left|\bar{z}(x) - z(x)\right|\cos\alpha\right) \tag{5}$$

$$R_{a.g} = \frac{1}{X_{max}\text{-}\lambda}\sum_{i=1}^{X_{max}-\lambda}\left(R_{a.l}\right)_i \tag{6}$$

Where $R_{a.l}$ is the local roughness over this segment; λ is the sample length; $R_{a.g}$ is the absolute roughness.

The crack roughness R_s can be defined as follows (Stroeven, 2000):

$$R_s = \frac{S_t}{S_0} \tag{7}$$

Where the S_t is the total surface area of the crack, S_0 is the projected area of the crack.

The total surface area S_t is determined by the projective covering method (Zhou and Xie, 2003), the schematic view of this method is shown in Figure 7.

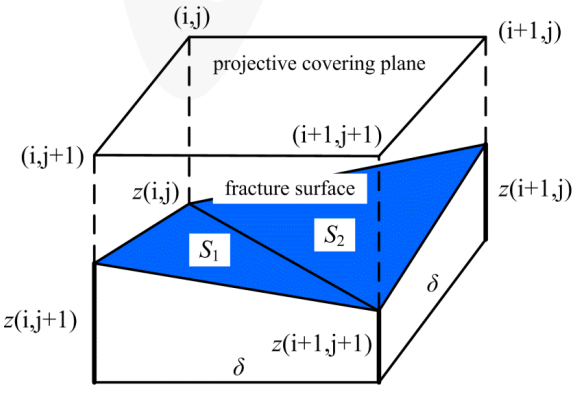


Figure 7: Projective covering method

In Figure 7, the z(i,j), z(i+1,j), z(i,j+1) and z(i+1, j+1) are the height corresponding to the (i,j), (i+1,j), (i,j+1) and (i+1,j+1), respectively.

The procedures for calculating of the crack geometry factors (τ, R_s, $R_{a,g}$) are carried out through MATLAB programming codes.

This document is the intellectual property of the fib – International Federation for Structural Concrete. All rights reserved.
This PDF of fib Bulletin 95 is intended for use and/or distribution solely within fib National Member Groups.

2 Results and discussion

2.1 Compressive strength

The mean compressive strength f_{cu} of the specimens at the age of 28 d are illustrated in Table 3. The addition of fibers aids in improving the toughness of concrete (Ding et al. 2009); however no clear influence on enhancing compressive strength was observed.

Table 3: Fiber content, the cubic compression strength of specimens

Matrix type	**Steel fiber (kg/m^3)**	**f_{cu} (MPa)**
NC	0	52.9
SF25	25	52.4
SF35	35	54.4
SF55	55	51.4

2.2 Crack tortuosity and roughness

For each type of the specimens, ten samples are studied. And the statistical analyses of the crack tortuosity factor τ and the surface roughness factor R_s are shown in Table 4.

Table 4: Comparison of the crack geometry

Types	**Crack tortuosity, τ**			**Surface roughness, R_s**		
	Average	**Standard deviation, σ**	**Coefficient of variation, CV(%)**	**Average**	**Standard deviation, σ**	**Coefficient of variation, CV(%)**
NC	0.8995	0.0249	2.8	1.1534	0.0596	5.2
SF25	0.8271	0.0214	2.6	1.2257	0.0285	2.3
SF35	0.8164	0.0543	6.6	1.2776	0.0662	5.2
SF55	0.7424	0.0724	9.7	1.5161	0.1632	10.8

From Table 4, it can be seen that:

- The standard deviation and the variation coefficient of τ and Rs are relatively small. It means that the τ and Rs can be introduced to verify the crack geometry.
- The value of τ decreases obviously with the increasing of fiber dosage. Compared to the NC specimen, the value of τ of the SF55 decreases by about 17%.
- The value of R_s increases with the increasing of fiber dosage. Compared to the NC specimen, the value of R_s of the SF55increases by about 31%.

2.3 Modified Poiseuille law

Figure 8 demonstrates the comparison of the test results and the predicted values based on Eq. (2).

This document is the intellectual property of the fib – International Federation for Structural Concrete. All rights reserved.
This PDF of fib Bulletin 95 is intended for use and/or distribution solely within fib National Member Groups.

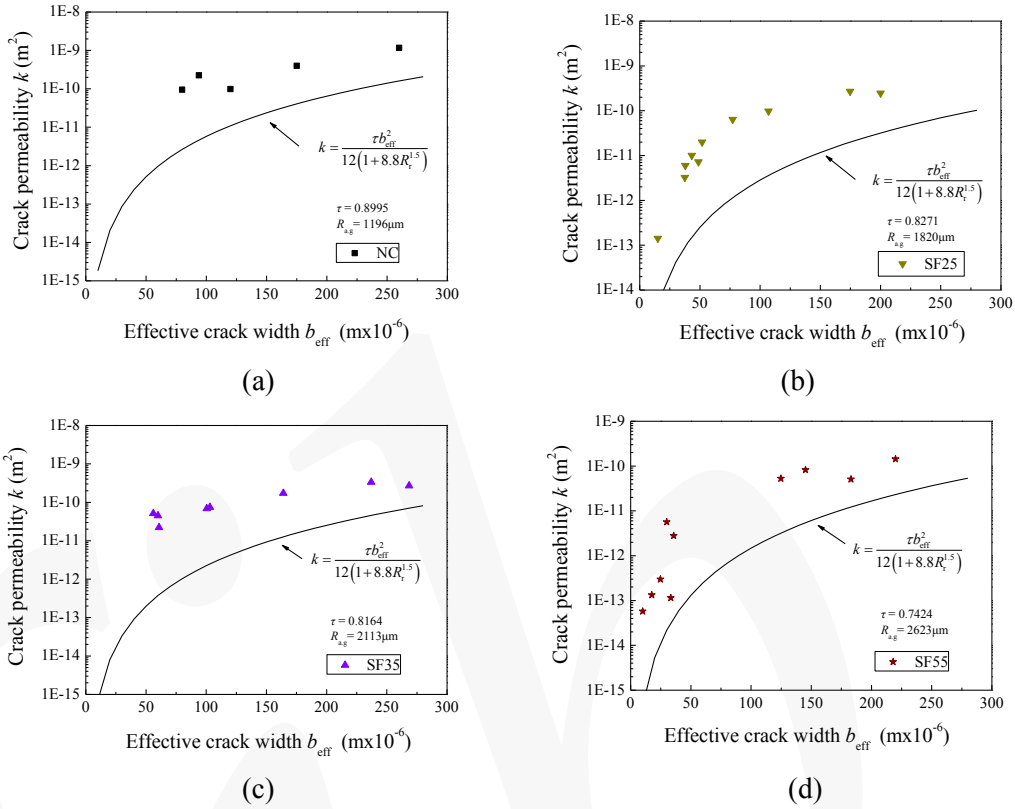
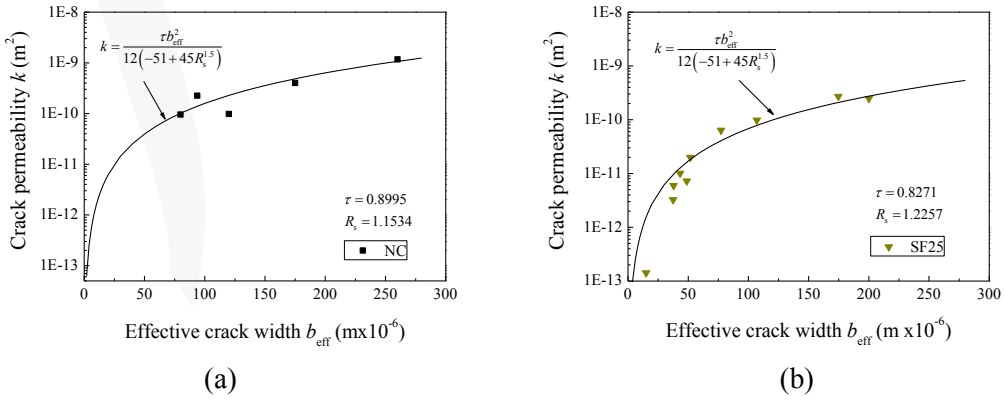


Figure 8: Comparison of the permeability coefficient between test value and predicted value suggested by Akhavan

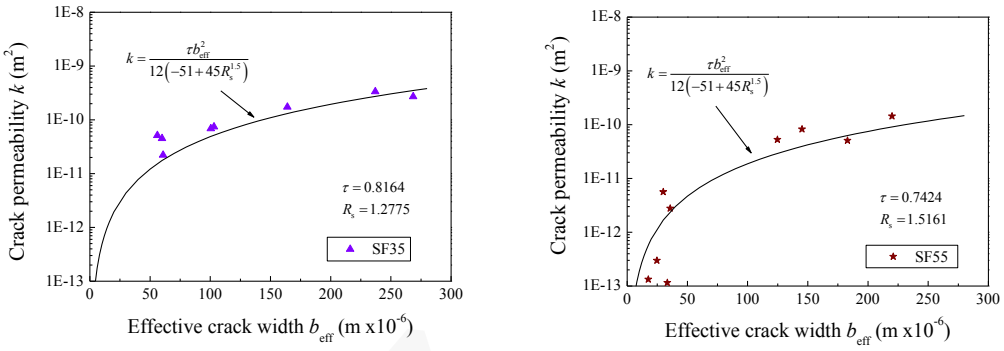
From Figure 8 and Table 5, it can be seen that when the sample length λ is 500μm, the values predicted by Eq. (2) is below the test values and show large deviations. The phenomenon is consistent with the results observed by Akhavan (Akhavan, 2012). Therefore, the surface roughness R_s is introduced to modify the Poiseuille law, see Eq. (8).

$$k = \frac{\tau b_{\text{eff}}^2}{12\left(-51+45R_s^{1.5}\right)} \tag{8}$$

Figure 9 shows the comparison of the test results and the values predicted by the Eq.(8). The correlation coefficient R^2 of all the specimens are illustrated in Table 6.



This document is the intellectual property of the fib – International Federation for Structural Concrete. All rights reserved.
This PDF of fib Bulletin 95 is intended for use and/or distribution solely within fib National Member Groups.



(c) (d)

Figure 9: Comparison of the permeability coefficient between test value and predicted value

Table 6: Results predicted by the recommended method

Types	τ	R_s	R^2
NC	0.8995	1.1534	0.974
SF25	0.8271	1.2257	0.962
SF35	0.8164	1.2776	0.917
SF55	0.7424	1.5161	0.837

From Figure 9 and Table 6, it can be seen that the values of the correlation coefficient R^2 of three group are larger than 0.900, the value of the correlation coefficient R^2 of only one group is below 0.900. The R^2 values of all the specimen is larger than 0.800. It means that the modified Poiseuille law can be used to predict the permeability of cracked concrete.

3 Conclusions

Based on the results of the investigation, the following conclusions can be drawn:

1. The crack tortuosity factor τ and surface roughness factor Rs can be adopted to evaluate the crack geometry.
2. The steel fibers can change the crack geometry (tortuosity and roughness) obviously.
3. The relative surface roughness Rr can be replaced by the surface roughness factor Rs to modify the Poiseuille law.
4. The modified Poiseuille law can be used to predicted the permeability of the cracked concrete.

4 Acknowledgements

The Authors would like to give their appreciation to the National Natural Science Foundation of China, Grants: 51578109.

This document is the intellectual property of the fib – International Federation for Structural Concrete. All rights reserved.
This PDF of fib Bulletin 95 is intended for use and/or distribution solely within fib National Member Groups.

5 References

Akhavan A, Shafaatian S M H, Rajabipour F (2012) *Quantifying the effects of crack width, tortuosity, and roughness on water permeability of cracked mortars*. Cement and Concrete Research, 42(2): 313-320.

Akhavan A (2012) *Characterizing saturated mass transport in fractured cementitious materials (Ph.D thesis)*. Pennsylvania Pennsylvania State University.

Aldea C M, Shah S P and Karr A (1999a) *Effect of cracking on water and chloride permeability of concrete*. Journal of Materials in Civil Engineering, 11(3): 181-187.

Aldea C M, Shah S P, Karr A (1999b) *Permeability of cracked concrete*. Materials and Structures, 1999, 32(5): 370-376.

ASTM C 1202 (2012) *Standard test method for electrical indication of concrete's ability to resist chloride ion penetration*. ASTM International.

ASTM C 1585 (2013) *Standard test method for measurement of rate of absorption of water by hydraulic-cement concretes*. ASTM International. 2013.

Bear J. *Dynamic of fluids in porous media*. New York: Dover Publications, 1988.

Ding, Y, Zhang Y and Thomas A (2009). *The investigation on strength and flexural toughness of fibre cocktail reinforced self-compacting high performance concrete*. Construction & Building Materials, 23(1), 448-452.

Ding Y, Li D and Zhang Y (2018) *Quantitative analysis of macro steel fiber influence on crack geometry and water permeability of concrete*. Composite Structures, 187: 325-335.

GB/T 50082 (2009) *Standard for test methods of long-term performance and durability of ordinary concrete*. China Architecture and Building Press.

Gérard B, Breysse D, Ammouche A, et al. *Cracking and permeability of concrete under tension*. Materials and Structures, 1996, 29(3): 141-151.

Nilson A, Darwin D, Dolan C (2009) *Design of concrete structures*. USA: McGraw-Hill.

Park S S, Kwon S J, Jung S H, et al. (2012) *Modeling of water permeability in early aged concrete with cracks based on micro pore structure*. Construction and Building Materials, 27(1): 597-604.

Picandet V, Khelidj A, Bellegou H. (2009) *Crack effects on gas and water permeability of concretes*. Cement and Concrete Research, 39(6): 537-547.

Rapoport J, Aldea C M, Shah S P, et al. (2002) *Permeability of cracked steel fiber-reinforced concrete*. Journal of Materials in Civil Engineering, 14(4): 355-358.

Shin, K J, Bae W, Choi S W, et al. (2017). *Parameters influencing water permeability coefficient of cracked concrete specimens*. Construction & Building Materials,151, 907-915.

Rastiello G, Boulay C, Pont S D, et al. *Real-time water permeability evolution of a localized crack in concrete under loading*. Cement and Concrete Research, 2014, 56(2): 20-28.

Stroeven P (2000) *A stereological approach to roughness of fracture surfaces and tortuosity of transport paths in concrete*. Cement and Concrete Composites, 22(5): 331-341.

Wang K, Jansen D C, Shah S P, et al. (1997) *Permeability study of cracked concrete*. Cement and Concrete Research, 27(3): 381-393.

Zhou H, Xie H (2003) *Direct estimation of the fractal dimensions of a fracture surface of rock*. Surface Review and Letters, 10(5): 751-762.

Zimmerman R W, Bodvarsson G S (1996) *Hydraulic conductivity of rock fractures*. Transport in Porous Media, 23(1): 1-30.

This document is the intellectual property of the fib – International Federation for Structural Concrete. All rights reserved.
This PDF of fib Bulletin 95 is intended for use and/or distribution solely within fib National Member Groups.
FRC2018: Fibre Reinforced Concrete: from Design to Structural Applications
Joint ACI-*fib*-RILEM International Workshop

Evaluation of Effective Moment of Inertia for Calculation of Short-Term Deflections of Steel Fiber Reinforced Concrete Flexural Members

Luis B. Fargier-Gabaldon[1], Mohamed Al-Tameemi[2], Gustavo J. Parra-Montesinos[3]

[1] : Visiting Professor, University of Wisconsin-Madison, USA

[2] : Research Assistant, University of Wisconsin-Madison, USA

[3] : C.K. Wang Professor of Structural Engineering, University of Wisconsin-Madison, USA

Abstract

The effect of discontinued, randomly distributed steel fibers on the effective moment of inertia (I_e) of lightly reinforced flexural members is evaluated through the testing of three pairs of specimens under four-point bending. The specimens consisted of a simply supported, 3660 mm long, 254 mm deep, and 610 mm wide one-way slab strip. All slab specimens contained minimum flexural reinforcement according to the ACI 318-14 Building Code. The first pair featured regular concrete (no fibers), while the second and third pairs included steel fibers in a volume fraction (V_f) of 0.26% and 0.38%, respectively. Beyond cracking, a substantial drop in the flexural stiffness was noticed in all specimens. The slabs with fibers, however, exhibited stiffer post-cracking response compared to their regular concrete counterparts. At yielding, a well-distributed cracking pattern was noticed in all test slabs, with maximum cracks widths of approximately 0.5 mm. It was found that the equation proposed by Bischoff (2005) to estimate the effective moment of inertia for concrete beams fits well the experimental data of the fiber-reinforced concrete slabs, given that the stiffening factor is set equal to one.

Keywords

Fiber Reinforced Concrete, Effective Moment of Inertia, Short-Term Deflections, Tension-Stiffening.

https://doi.org/10.35789/fib.BULL.0095.Ch42

This document is the intellectual property of the fib – International Federation for Structural Concrete. All rights reserved.
This PDF of fib Bulletin 95 is intended for use and/or distribution solely within fib National Member Groups.

1 Introduction

The shear behavior of Steel Fiber-Reinforced Concrete (SFRC) beams has been extensively investigated over the past three decades (see Parra-Montesinos 2006). The flexural stiffness of SFRC beams, however, has been little studied. In the following, a summary of experimental programs aimed at studying the flexural response of SFRC beams is provided.

Ashour and Wafa (1993) investigated the effect of fiber dosage (no fibers, or $V_f = 0.75$ and 1.0%) and shear span-to-depth ratio (a/d = 4 or 6) on the ultimate load, crack propagation, stiffness, and ductility of flexural members made with SFRC (concrete compressive strength of approximately 90 MPa), by testing eight beams under four-point bending with a distance between supports of either 2620 or 3680 mm. The steel fibers were 60 mm long ($L_f/D_f = 75$) with hooked-ends and a nominal tensile strength of 1100 MPa. Beams were 170 mm wide and 300 mm deep with a longitudinal reinforcement ratio of 1.2%. Shear reinforcement was provided only over the shear span through 8 mm bars (2 legs) spaced at 150 mm. All beams experienced significant flexural cracking over the constant moment span before a final failure due to concrete crushing in the compression zone occurred. It was found that the addition of fibers led to an increase in the shear strength, post-cracking flexural stiffness and ductility of the SFRC test specimens, when compared to the specimens with regular concrete (no fibers). It was also found that the equation for calculating effective moment of inertia given in the 318-89 ACI Building Code (same as in ACI 318-14) under-estimated the flexural stiffness of the SFRC test specimens, and that the fibers reduced the rate of transition from the gross moment of inertia to the fully cracked moment of inertia.

More recently, Kang et al. (2012) investigated the flexural-shear coupling behavior of regular concrete and SFRC beams through the testing of 12 specimens with steel fibers (hooked ends) in volume fractions of either 0.50 or 0.75%. Three regular concrete and six SFRC beams were designed to fail in flexure under four-point bending with a distance between support of 2730 mm (a/d =5.5 and a constant moment length of 1.90 d), while a shear failure was expected in one regular concrete and two SFRC beams (4270 mm long, a/d =2.5 or 2.80). Beams designed to fail in flexure were 125 mm wide and 250 mm deep, with a longitudinal reinforcement ratio of either 1.0% or 1.5%. These beams featured 50 mm long steel fibers ($L_f/D_f = 67$) with a tensile strength of 1100 MPa. Transverse reinforcement was provided only over the shear span through 10 mm bars (2 legs) spaced at 100 mm. Beams failing in flexure with fiber dosages of 0.50 and 0.75% by volume exhibited a displacement ductility up to 8, compared to a peak ductility of 6 obtained for nominally identical beams without fibers. The addition of fibers, however, had little effect on the flexural strength of the specimens.

Sahoo and Sharma (2014) investigated the effect of steel fiber content on the flexural behavior of SFRC beams with and without transverse reinforcement. Twelve beams were tested to failure; nine beams with SFRC and three with regular concrete (no fibers). Steel fibers were 60 mm long ($L_f/D_f = 75$) with a tensile strength of 1100 MPa. The beam cross section for all specimens was 150 mm wide by 300 mm deep and the distance between supports was 1800 mm. Main variables investigated were concrete compressive strength (ranging from 19 to 32 MPa), longitudinal reinforcement ratio (0.9 or 1.2%), shear span-to-depth ratio (a/d =3.5 or 2.3), and fiber content (no fibers or V_f ranging from 0.5 to 1.5% in increments of 0.25%). Eight of the beams were designed to fail in flexure under four-point bending with loads applied at third points (a/d =2.3), while the remaining four beams were designed to fail in shear under three-point bending (a/d =3.5). Four of the beams designed to fail in flexure had a longitudinal reinforcement ratio of 0.9% and featured 8 mm bars (2 legs) spaced at 150 mm as transverse

This document is the intellectual property of the fib – International Federation for Structural Concrete. All rights reserved.
This PDF of fib Bulletin 95 is intended for use and/or distribution solely within fib National Member Groups.

reinforcement. The remaining four beams designed to fail in flexure had a reinforcement ratio of 1.2% and transverse reinforcement spacing of 180 mm. It was found that the addition of steel fibers increased the ductility and shear strength of the test specimens when compared to the regular concrete specimens (no fibers), but had very little effect on the flexural strength. Beams failing in flexure with fiber dosages of 0.5 and 1.0% by volume exhibited a displacement ductility up to 6 and 9, respectively, compared to a peak ductility of 4 obtained for specimens without fibers. The final failure of the specimens was due to concrete crushing of the compression zone at mid-span. The behavior of fiber reinforced concrete elements in flexure was also investigated by Meda et al. (2012). Results from their experimental program indicate that fibers do not lead to a substantial increase in ultimate moment capacity while rotation capacity can decrease substantially due to localization of deformations.

2 Research significance

Despite the extensive experimental data available on the response of SFRC flexural elements with moderate to high ratios of longitudinal reinforcement, there is little or no information on the behavior of members with low reinforcement ratios, as those found in slabs, for which the design might be controlled by deflection limits. This research is aimed at generating information about the effective moment of inertia for calculating short-term deflections of these elements.

3 Experimental program

Three pairs of test specimens that represented a one-way slab strip were tested under four-point bending (a/d =5.6). The slab cross section and test setup are shown in Figure 1. All specimens featured minimum longitudinal reinforcement (Grade 420) in accordance with Section 7.6 of the ACI 318-14 Building Code (0.18%). The first pair of specimens was fabricated with regular concrete, while the second and third pairs featured steel fibers in volume fraction of 0.26% and 0.38%, respectively (Table 1). A local ready-mix concrete supplier provided the concrete and when used, fibers were added to the mixture at the concrete plant. The steel fibers were Dramix® 5D 65/60 BG (60 mm long and 0.90 mm in diameter, $L_f/D_f \approx 65$) with a multi hooked-end design and a nominal tensile strength of 2300 MPa. Strains at various locations in the longitudinal reinforcement were measured with strain gauges. The average strain field on one side of the slab was monitored through an infrared-based position tracking system (Optotrak Certus system by NDI Measurement Sciences).

Table 1: Summary of test specimens and material

Pair #	V_f(%)	Long. reinf. ratio	f'_c (MPa)	f_y (MPa)	f_{cr}* (MPa)	f_{pc}* (MPa)	f_{300}* (MPa)	f_{150}* (MPa)
1	0	0.0018	36	445	4.5	-	-	-
2	0.26	0.0018	43	532	4.4	3.1	3.0	2.3
3	0.38	0.0018	47	530	5.1	3.2	3.1	2.3

*** ASTM 1609 tests of 150 x 150 x 450 mm beams**

f_{cr}=first cracking stress

f_{pc}=maximum equivalent post-cracking stress

f_{300}=residual equivalent flexural stress at $L/300$ f_{150}=residual equivalent flexural stress at $L/150$
L=span length = 450 mm

This document is the intellectual property of the fib – International Federation for Structural Concrete. All rights reserved.
This PDF of fib Bulletin 95 is intended for use and/or distribution solely within fib National Member Groups.

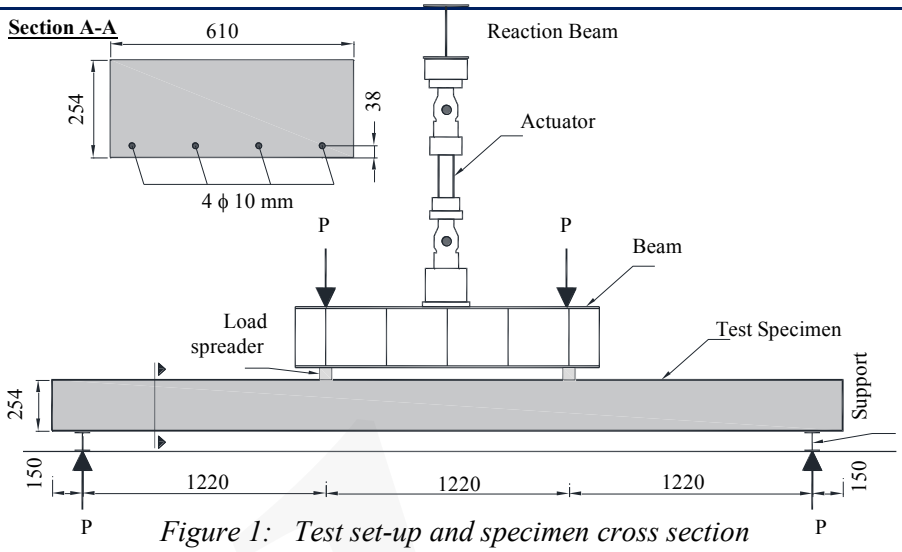


Figure 1: Test set-up and specimen cross section

4 Behavior of test specimens

The load versus mid-span deflection response of the test slabs is shown in Figure 2 (load P refers to half of the total applied load). The strains in the longitudinal reinforcement were monitored while the load was being increased to estimate the first cracking load. Immediately after cracking was noticed, all specimens were unloaded and reloaded again.

After initial cracking, the first slab made with regular concrete was unloaded and subjected to a mid-span displacement of approximately 4 mm (≈L/1000), and then unloaded and reloaded again. The second slab of Pair 1 was also unloaded/reloaded at approximately 6 mm (≈L/600) and 15 mm (≈L/240). The envelope of the load versus mid-span displacement response of the two specimens was almost identical (Figure 2a). For both specimens, cracking and yielding were first observed at bending moments of nearly 20 kN-m and 28 kN-m (including self-weight) at a mid-span displacement of approximately 1.0 mm (≈L/3600) and 10 mm (≈L/360), respectively. A well-distributed cracking pattern throughout the constant moment region was also observed in both specimens, characterized by flexural cracks with maximum widths of nearly 0.5 mm at first yielding, and a few hairline vertical cracks in the shear span region. The two specimens were ultimately loaded to a mid-span deflection of approximately 80 mm (≈L/50, Figure 3a). At this deflection level, the crack width ranged from 1.0 to 3.5 mm. The peak moment strength was of approximately 41.5 kN-m; that is, nearly 1.5 times the moment at first yielding.

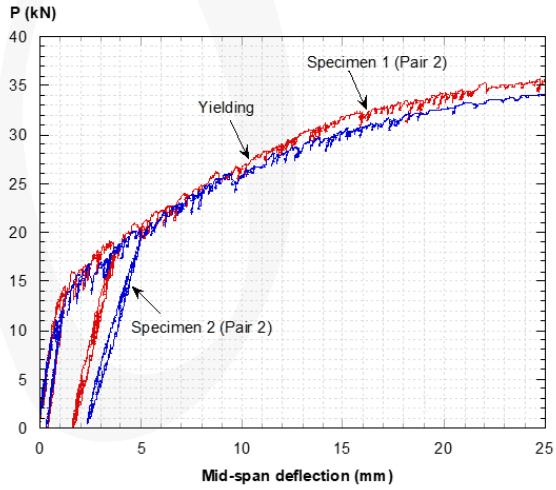
The second pair of specimens was reinforced with steel fibers in a volume fraction of 0.26%. Following unloading just after first cracking, this pair was subjected to a mid-span deflection of approximately 5 mm, then unloaded again followed by reloading to failure. The envelope of the load versus displacement response of these two specimens was almost identical (Figure 2b). Moments at cracking and yielding were approximately 22.5 kN-m and 38.5 kN-m, respectively, (that is, a nearly 10% and 40% increase compared to Pair 1), which, as in the slabs without fibers, corresponded to applied mid-span deflection of approximately 1.0 mm (≈L/3600) and 10 mm (≈L/360). At yielding, cracking was well distributed along the constant moment span with maximum crack widths of approximately 0.5 mm, as observed in the slabs without fibers. In both test slabs, however, at a mid-span deflection of approximately 6 mm, two of the cracks along the constant moment region started to grow at a faster rate than others. In the first SFRC test slab the width of these cracks reached 2.5 and 5.0 mm at a mid-span displacement of nearly 50 mm (≈L/70) (Figure 3b). As the test approached failure, a few more cracks formed in the

This document is the intellectual property of the fib – International Federation for Structural Concrete. All rights reserved.
This PDF of fib Bulletin 95 is intended for use and/or distribution solely within fib National Member Groups.

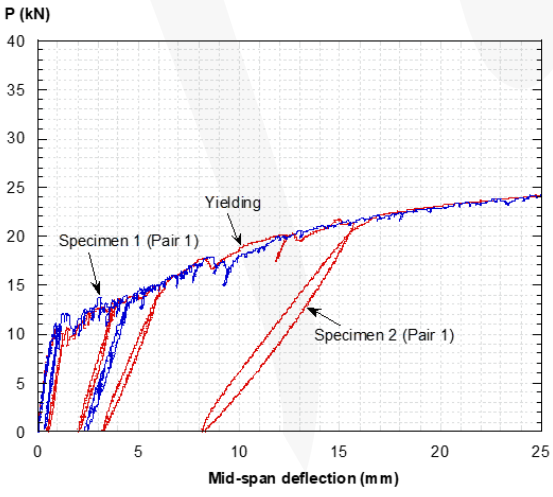
shear span region and the 5.0 mm wide crack grew up to 10 mm. A similar behavior was observed in the second SFRC test slab of this pair. The two specimens of this pair were loaded to peak bending moment of nearly 51.5 kN-m; that is, approximately 1.3 times the moment at first yielding. Fracture of the longitudinal reinforcement occurred at a mid-span deflection of approximately 75 mm (≈L/50) and 65 mm (≈L/60) for the first and second SFRC specimens of this pair, respectively.

The third pair of specimens was reinforced with steel fibers in a volume fraction of 0.38%. After unloading/reloading at first cracking (at a mid-span deflection of nearly 1.2 mm,≈L/2800), this pair was unloaded/reloaded at a mid-span deflection of approximately 3.6 mm (≈L/1000), 7.3 mm (≈L/500), 12 mm (≈L/300), 15 mm (≈L/240), and 20 mm (≈L/180). The flexural response of this pair was similar to that observed in the specimens with regular concrete (Pair 1, no fibers) and with fibers in a volume fraction of 0.26% (Pair 2). Yielding occurred at mid-span deflections of nearly 10 mm (≈L/360). However, the second SFRC test slab of this pair exhibited an increase in strength of approximately 14% when compared to its nominally identical counterpart. Moments at cracking were approximately 20 kN-m and 22.5 kN-m for the first and second SFRC test slab of this pair, respectively, while at yielding, bending moments were 34 and 38.5 kN-m.

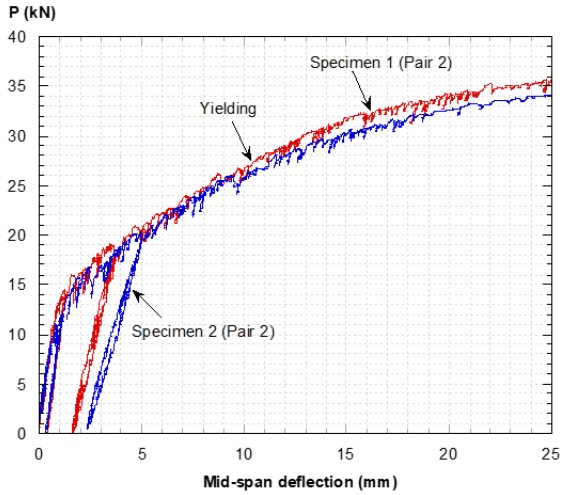
The moments at first cracking and yielding in the second specimen of this pair were approximately equal to those in the second pair. As in the other two pairs of specimens, maximum crack width at yielding was nearly 0.5 mm. In both SFRC test slabs of this third pair the width of three cracks was greater than 1.0 mm at a mid-span deflection of approximately 30 mm (≈L/120) and one of the cracks in the first test slab grew from 2.0 mm (at a mid-span deflection of approximately ≈ L/120) to 5.0 mm at a deflection of approximately 60 mm (L/60, Figure 3c).



(c) Pair 3, SFRC, V_f=0.38%



(a) Pair 1, regular concrete



(b) Pair 2, SFRC, V_f=0.26%

Figure 2: Load vs. displacement responses

This document is the intellectual property of the fib – International Federation for Structural Concrete. All rights reserved.
This PDF of fib Bulletin 95 is intended for use and/or distribution solely within fib National Member Groups.

The first and second specimens of this pair were loaded to peak bending moments of approximately 51.5 kN-m and 55 kN-m, respectively, (that is, nearly 1.5 times the moment at first yielding) prior to bar fracture occurred at a mid-span deflection of approximately 75 mm (≈L/50) and 80 mm (≈L/45) at the location of the widest cracks. Moments at cracking and yielding, deflection at cracking and failure modes are summarized in Table 2.



(a) Specimen 1 of Pair 1 (regular concrete), at nearly 80 mm (≈L/50) of deflection



(b) Specimen 1 of Pair 2 (SFRC, $V_f = 0.26\%$), main crack at mid-span at nearly 50 mm (≈L/70) of deflection



(c) Specimen 2 of Pair 3 (SFRC, $V_f = 0.38\%$), just prior to bar fracture

Figure 3: Cracking and deformations in tests specimens

Table 2: Summary moments and deflections at cracking and Failure modes

Pair	Specimen	$M_{cracking}$ (kN-m)	$M_{yielding}$ (kN-m)	Δ_{cr}	Failure mode
1	1 and 2	20.0	28.0	≅ L/3600	No failure[@]
2	1 and 2	22.5	38.5	≅ L/2800	Bar fracture
3	1	20.0	34.0	≅ L/3600	Bar fracture
3	2	22.5	38.5	≅ L/3600	Bar fracture

Δ_{cr}=midspan deflection at cracking

[@] Deflection capacity of the test-up was reached prior to failure

5 Effective Moment of Inertia

An effective moment of inertia (I_e) is typically used to compute short-term deflections. It is generally assumed to decrease from the gross (or transformed uncraked) moment of inertia (I_g) to the fully cracked moment of inertia (I_{cr}) as the applied loads are increased and the member approaches the first yielding point. This transition is attributed to the ability of concrete to carry tension forces in between cracks, which is commonly referred to as tension stiffening. The equation proposed by Branson (1965) is probably the most commonly used expression to estimate effective moment of inertia of concrete flexural members. It was originally adopted in the ACI 318-71 Building,

$$I_e = \left(\frac{M_{cr}}{M_a}\right)^m I_g + \left[1 - \left(\frac{M_{cr}}{M_a}\right)^m\right] I_{cr} \leq I_g \qquad (1)$$

This document is the intellectual property of the fib – International Federation for Structural Concrete. All rights reserved.
This PDF of fib Bulletin 95 is intended for use and/or distribution solely within fib National Member Groups.

where M_{cr} and M_a are the cracking moment and the applied service load moment, respectively. Note that as the M_{cr}/M_a ratio decreases from one towards nearly zero, the effective moment of inertia gradually changes from I_g to I_{cr}. In the ACI 318-14 Building Code m is set to 3, which is intended to account for the change in stiffness along the span of the member and for the tension stiffening effect under usual loading patters. Bischoff (2005) and Bischoff and Scanlon (2007) recognized that Branson's equation gives reasonable results for beams with reinforcement ratios ranging from 1% to 3%, but leads to an underestimation of the short-term deflections in flexural elements with reinforcement ratios lower than 1% (members in which $I_g/I_{cr} \gtrsim 3$). Bischoff (2005) proposed the use of Equation 2a as an alternative,

$$I_e = \frac{I_{cr}}{1 - \beta_c \left[1 - I_{cr}/I_g\right]\left(\frac{M_{cr}}{M_a}\right)} \leq I_g \tag{2a}$$

where the term β_c is the tension-stiffening factor. Bischoff (2005), and Bischoff and Scanlon (2007) recommended setting β_c equal to the ratio M_{cr}/M_a for reinforced concrete flexural members and members with fiber-reinforced polymer bars. Applying this recommendation, Equation 2a becomes,

$$I_e = \frac{I_{cr}}{1 - \left[1 - I_{cr}/I_g\right]\left(\frac{M_{cr}}{M_a}\right)^2} \leq I_g \tag{2b}$$

Equation 2b works well for the range of reinforcement ratios encountered in practice, including lightly reinforced members. Note that β_c decreases as the applied moment increases and thus, the magnitude of the effective moment of inertia decreases as the magnitude of the applied loads increases. In this investigation, Equation 2a was used to evaluate the effective moment of inertia of the lightly reinforced SFRC test specimens. When more experimental data become available, it is expected that Equation 2a can be expanded to account for the full range of reinforcement ratios encountered in practice.

The envelope of the load versus mid-span deflection response of the test specimens can be idealized as a trilinear relationship representing three stages of behavior; stage one up to cracking, stage two between cracking and first yield, and stage three after yielding of the longitudinal reinforcement. For convenience, the idealized response is presented in Figure 4 in terms of the M_a/M_{cr} ratio versus the corresponding normalized displacement ratio (Δ_a/Δ_{cr}). When normalized, the responses of the test slabs with fibers were nearly identical up to yielding. As can be observed, specimens with fibers exhibited an approximately 20% increase in the effective flexural stiffness (EI_e, where E is the Young's Modulus of concrete), when compared to slabs with regular concrete at the same M_a/M_{cr} ratio, while a 70% increase was observed in the post-cracking flexural rigidity (between cracking and yielding). These increments can be primarily attributed to the capacity of the steel fibers to transfer tension across cracks.

Figure 5a shows a comparison of the calculated mid-span deflection based on the effective moment of inertia obtained from Equation 2b and the idealized trilinear relationship for the regular concrete slabs. An almost perfect match can be observed up to first yielding. As reference, the calculated mid-span deflection based on the gross and fully cracked moments of inertia are shown as dashed lines.

Figures 5b and 5c show a comparison of the calculated mid-span deflection based on the effective moment of inertia obtained from Equation 2a with $\beta_c = 1$ and the idealized trilinear relationship for the SFRC test slabs (Pairs 2 and 3). The contribution of the steel fibers was ignored in the calculation of moment of inertia. After first cracking, an overestimation of the

This document is the intellectual property of the fib – International Federation for Structural Concrete. All rights reserved.
This PDF of fib Bulletin 95 is intended for use and/or distribution solely within fib National Member Groups.

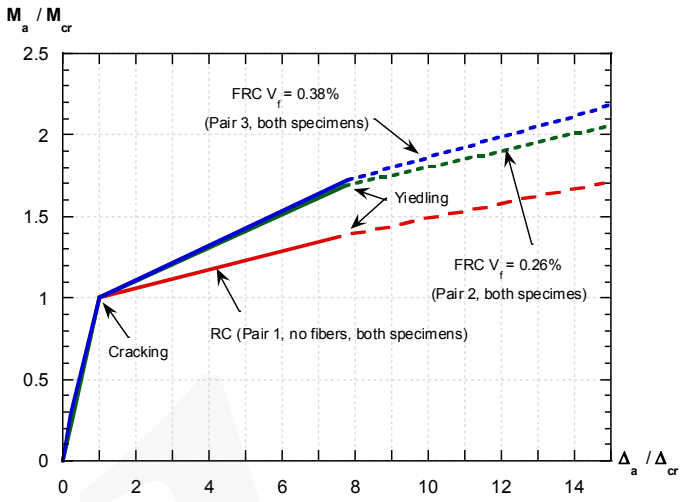
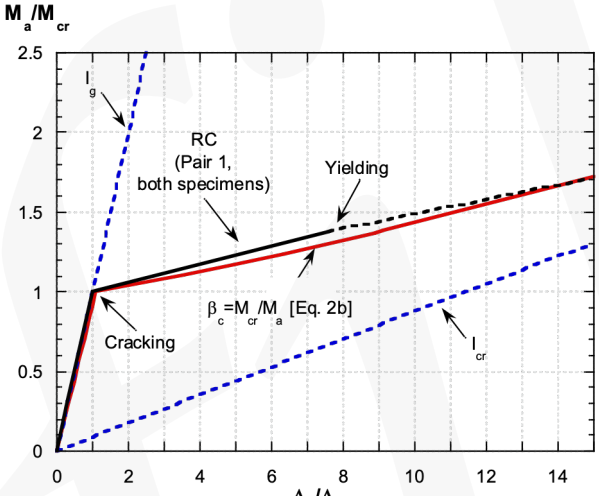
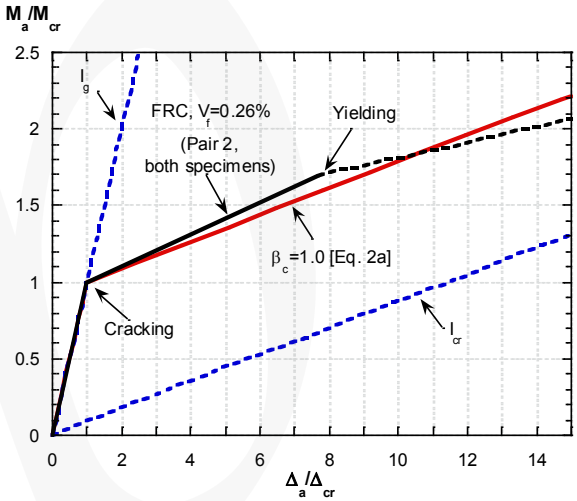


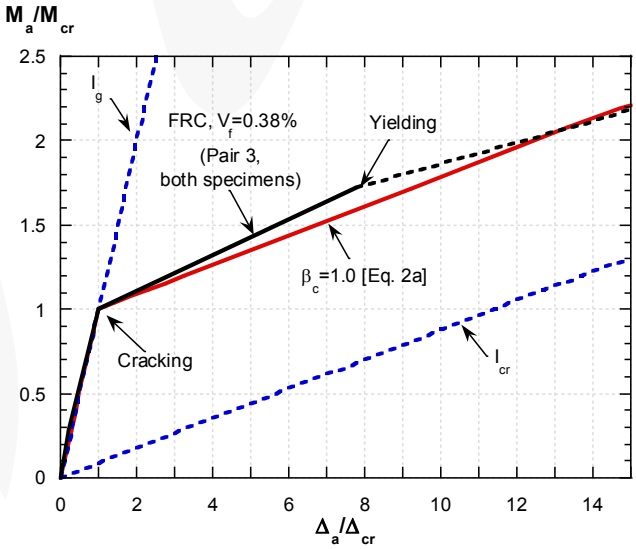
Figure 4: Idealized load vs. displacement envelope responses (normalized)



(a) Pair 1 (regular concrete, no fibers, both specimens)



(b) Pair 2 (SFRC, $V_f = 0.26\%$, both specimens)



(c) Pair 3 (SFRC, $V_f = 0.38\%$, both specimens)

Figure 5: Idealized load vs. displacement envelope responses (normalized) and comparison with Bischoff (2005) equation

This document is the intellectual property of the fib – International Federation for Structural Concrete. All rights reserved.
This PDF of fib Bulletin 95 is intended for use and/or distribution solely within fib National Member Groups.

deflection can be observed with a peak in the error of nearly 20% at yielding. In practice, M_a often ranges from 1/2 to 2/3 of the yield moment, and thus the error is smaller than that at yielding. Based on the information obtained from the test results and until more experimental data become available, the use of a constant stiffening factor $\beta_c = 1$ in Equation 2a is recommended to estimate short-term deflections of SFRC flexural members with Dramix® 5D 65/60 BG steel fibers in dosages ranging from 0.26 to 0.38% by volume.

6 Conclusions

Results from laboratory experiments suggest that slabs made of Steel Fiber Reinforced Concrete (SFRC) with hooked-end fibers in volume fractions between 0.26% and 0.38% exhibit a better short-term deflection control than nominally identical regular concrete slabs. The behavior of the test slabs with and without fibers was quite similar in terms of crack distribution and crack width up to yielding. The post-cracking and effective flexural rigidity (EI_e) of the slab specimens with fibers, however, increased by nearly 70 and 20%, respectively, when compared to their nominally identical counterparts made with regular concrete (no fibers). These increments can be primarily attributed to the ability of fibers to transfer tension across cracks. It was observed that the increase in fiber content from 0.26% to 0.38% did not have a significant effect on the post-cracking stiffness of the test specimens.

The use of the Equation 2a, proposed by Bischoff (2005), led to reasonable estimates of the effective moment of inertia for short-term deflection calculation of the tested SFRC specimens, given that the tension stiffening factor β_c is set to one, regardless of the magnitude of the applied moment.

7 Acknowledgements

The help of Jacob Zeuske and Sai Samanth in the preparation and testing of the slab specimens is greatly appreciated. The support of Bekaert in providing the funds for conducting this research is also appreciated. The conclusions expressed in this paper are those of the writers and do not necessarily reflect the views of the sponsor.

8 References

ACI Committee 318. “Building Code Requirements for Structural Concrete (ACI 318-14) and Commentary (ACI 318R-14),” American Concrete Institute, Farmington Hills, Michigan, 2014, 520 pp.

Parra-Montesinos, G. 2006. “Shear Strength of Beams with Deformed Steel Fibers,” Concrete International, V. 28, No. 11, pp. 57 -66.

Kang, T., Kim, W., Kwak, Y. and Hong, S. 2011. “Shear Testing of Steel Fiber-Reinforced Lightweight Concrete Beams without Web Reinforcement,” ACI Structural Journal, V. 108, No. 5, pp. 553-561.

Ashour, S. A. and Wafa, F. F. 1993. “Flexura Behavior of High-Strength Fiber-Reinforced Concrete Beams,” ACI Structural Journal, V. 90, No. 3, pp. 279-287.

Kang, T., Kim, W., Massone, L. and Galleguillos, T. 2012. “Shear-Flexure Coupling Behavior of Steel Fiber-Reinforced Concrete Beams,” ACI Structural Journal, V. 109, No. 4, pp. 435-444.

This document is the intellectual property of the fib – International Federation for Structural Concrete. All rights reserved.
This PDF of fib Bulletin 95 is intended for use and/or distribution solely within fib National Member Groups.

Sahoo, D. and Sharma, A. 2014. "Effect of Steel Fiber Content on Behavior of Concrete Beams with and without Stirrups," ACI Structural Journal, V. 111, No. 5, pp. 1157-1166.

Meda, A., Minelli, F., and Plizzari, G.A. (2012), "Flexural behaviour of RC beams in fibre reinforced concrete", Composites Part B: Engineering, Vol. 43, No 8, December 2012, ISSN 1359-8368, pp. 2930 -2937.

Branson, D. 1965. "Instantaneous and Time-Dependent Deflections of Simple and Continuous Reinforced Concrete Beams," APR Rep. No. 7, Part I, Alabama Highway Dept., Bureau of Public Roads.

ACI Committee 318. "Building Code Requirements for Reinforced Concrete and Commentary (ACI 318-89)," American Concrete Institute, Farmington Hills, Michigan, 1989, 353 pp.

ACI Committee 318. "Building Code Requirements for Reinforced Concrete (ACI 318-71)," American Concrete Institute, Farmington Hills, Michigan, 1971, 78 pp.

Bischoff, P. 2005. "Reevaluation of Deflection Prediction for Concrete Beams Reinforced with Steel and Fiber Reinforced Polymer Bars," Journal of Structural Engineering, ASCE, V. 131, No. 5, pp. 752-767.

Bischoff, P. and Scanlon, A. 2007. "Effective Moment of Inertia for Calculating Deflections of Concrete Members Containing Steel Reinforcement and FRP Reinforcement," ACI Structural Journal, V. 104, No. 1, pp. 68-75.

This document is the intellectual property of the fib – International Federation for Structural Concrete. All rights reserved.
This PDF of fib Bulletin 95 is intended for use and/or distribution solely within fib National Member Groups.

6) STRUCTURAL APPLICATIONS AND REHABILITATION

This document is the intellectual property of the fib – International Federation for Structural Concrete. All rights reserved.
This PDF of fib Bulletin 95 is intended for use and/or distribution solely within fib National Member Groups.
FRC2018: Fibre Reinforced Concrete: from Design to Structural Applications
Joint ACI-*fib*-RILEM International Workshop

Experimental Investigation of Hybrid Concrete Elements with Varying Fiber Reinforcement under Concentrated Load

Sven Plückelmann[1], Rolf Breitenbücher[1]

[1] : Ruhr University Bochum, Bochum, Germany.

Abstract

In special cases, concrete members are exposed to high locally concentrated loadings. Such concentrated loadings lead to a multi-dimensional stress state beneath the loaded area. Due to the load diffusion, large splitting tensile stresses are generated in the upper regions of the concrete member (i.e. St. Venant disturbance zone) and spread along directions perpendicular to the load. In order to resist these splitting tensile stresses, the state of the art is to reinforce concrete members with transverse steel reinforcement. An alternative approach is to add steel fibers to the concrete matrix. However, regarding economic concerns it may not appropriate to reinforce the entire concrete member with an adequate high amount of steel fibers, rather only those zones where high splitting stresses are expected.

The main objective of the presented experimental study was to investigate the load-bearing and fracture behavior of hybrid concrete elements with splitting fiber reinforcement under concentrated load. For this purpose, in a first step, hybrid specimens were produced containing both plain and fiber concretes. The reference specimens consisted exclusively of plain concrete, while the hybrid specimens were partially strengthened with various types of steel fibers only in the St. Venant disturbance zone, instead of a full range fiber reinforcement. The thickness of the reinforcement layer was varied in order to determine the optimal configuration of fiber reinforcement. Taking into account the influence of the casting direction on the fiber orientation and consequently on the bearing and fracture behavior, the hybrid specimens were cast either in standing or in lying molds by means of a “wet-on-wet” casting technique. These hybrid elements were then tested under concentrated load.

The test results showed that under concentric loads the maximum bearing capacity of the hybrid specimens increased progressively with growing thickness of the fiber reinforced concrete layer. In contrast to the plain concrete specimens, the fiber reinforcement led to a remarkable improvement in the post-cracking ductility. Compared to the fully reinforced specimens, the hybrid specimens that were only reinforced in the St. Venant disturbance zone exhibited - besides an almost identical bearing capacity - a similar local behavior in the post-cracking zone. Furthermore, a significant impact of the casting direction on the bearing as well as fracture behavior could be proved.

Keywords

Steel fiber reinforcement, hybrid reinforcement, splitting stresses, bearing behavior

This document is the intellectual property of the fib – International Federation for Structural Concrete. All rights reserved.
This PDF of fib Bulletin 95 is intended for use and/or distribution solely within fib National Member Groups.

1 Introduction

In mechanized tunneling, precast tunnel lining segments represent a typical example for concrete members that are exposed to high locally concentrated loadings (i.e. partial-area loading) transmitted onto a limited contact area, as they are subjected to high and concentrated jacking forces of the boring machine during the construction stage (Maidl et al., 2012). However, also in special cases of further structural applications, such as anchorages in post-tensioned concrete members, bearings over piers in bridge structures or stanchions over concrete footings, the situation of concentrated load introduction into concrete members frequently occurs.

The situation of concentrated load introduction leads to a load diffusion beneath the loaded area along with a multi-dimensional stress state (Iyengar, 1966, Leonhardt and Mönning, 1986). Zones of the concrete member directly beneath the loaded area are exposed to high compressive stresses (i.e. bearing stresses). However, due to the load diffusion large splitting tensile stresses are generated over some distance to the loaded area in the upper regions of the concrete member (i.e. St. Venant disturbance zone). The tensile splitting stresses spread along directions perpendicular to the load and tend to gradually diminish with increasing distance to the loaded area. Moreover, local tensile stresses (i.e. spalling stresses) are induced along the loaded edges of the concrete member. In particular due to the resulting splitting stresses, concrete damages in the form of chipping, spalling or cracking are the frequent consequence (Wichers, 2013).

In order to resist these splitting stresses and thus to prevent damages, the state of the art is to reinforce concrete members with transverse steel reinforcement. An alternative approach is to add steel fibers to the concrete matrix. However, regarding economic concerns it may not appropriate to reinforce the entire concrete member with an adequate high amount of steel fibers, rather only those zones where high splitting stresses are expected. Based upon this fact, a new design concept to manufacture hybrid concrete elements was developed.

Numerous theoretical as well as experimental investigations have been conducted in the past to study the behavior of plain or conventionally reinforced concrete elements under concentrated load (e.g. Ahmed et al., 1998 and Wichers and Empelmann, 2013). In the literature, also studies on the behavior of concrete elements with full range fiber reinforcement under concentrated already exist (e.g. Song and Breitenbücher, 2013 and Breitenbücher et al., 2014). Within these studies, various influencing parameters such as the dimensions and geometry of specimens, area ratio (i.e. ratio of total area to loaded area), eccentricities of load introduction, fiber type and content, concrete strength etc. have been investigated.

This paper focuses on the investigation of hybrid concrete elements with splitting fiber reinforcement under concentrated load. Instead of a full range reinforcement, the hybrid specimens were partially strengthened with various types of steel fibers only in the St. Venant disturbance zone. The aim was to determine the optimal configuration of fiber reinforcement, taking into account the thickness of the reinforcement layer as well as the influence of the casting direction on the fiber orientation. Special attention is attributed to the “wet-on-wet” casting technique for the production of the hybrid specimens. The experimental study presented here is based on the research of Song, 2017 and was conducted at the Ruhr University Bochum within the scope of the research project “SFB 837: Subproject B1: Optimized Structural Segments for Durable and Robust Tunnel Lining Systems”.

This document is the intellectual property of the fib – International Federation for Structural Concrete. All rights reserved.
This PDF of fib Bulletin 95 is intended for use and/or distribution solely within fib National Member Groups.

2 Experiments

2.1 Materials and specimens

All test specimens (prisms with dimensions of 15 × 15 × 30 cm³) were prepared using the base-mix design listed in Table 1. By adding steel fibers to this base-mix, two different steel fiber reinforced concretes (SFRCs) were produced. The characteristics of the end-hooked macro steel fibers (L: RC-80/60 BN) and straight micro fibers (S: FM 13/0.19) that were utilized are indicated in Table 2. One SFRC (L60) was produced with mono fiber reinforcement (60 kg/m³ of fiber type L) and the other SFRC (L60S60) with fiber-cocktail (60 kg/m³ of fiber type L and 60 kg/m³ of fiber type S). In order to maintain a sufficient workability, the SFRCs were modified by increasing the dosage of superplasticizer. The properties of fresh and hardened plain concrete (PC) and SFRCs were determined according to the relevant standards, as presented in Table 3.

Table 1: Base-mix design for the production of PC and SFRCs

Cement CEM I 52.5 R [kg/m³]	**Fly ash [kg/m³]**	**Aggregate [kg/m³]**	**Water [kg/m³]**	**w/c-ratio [-]**	**Superplasticizer [kg/m³]**
330	90	1850	148.5	0.45	1.3

Table 2: Characteristics of steel fibers

Fiber type	**Shape**	**Length [mm]**	**Diameter [mm]**	**Slenderness (l/d) [-]**	**Tensile strenght [kg/m³]**
RC 80/60 BN (L)	end-hooked	60	0.75	80	1225
FM 13/0.19 (S)	straight	13	0.19	68	2000

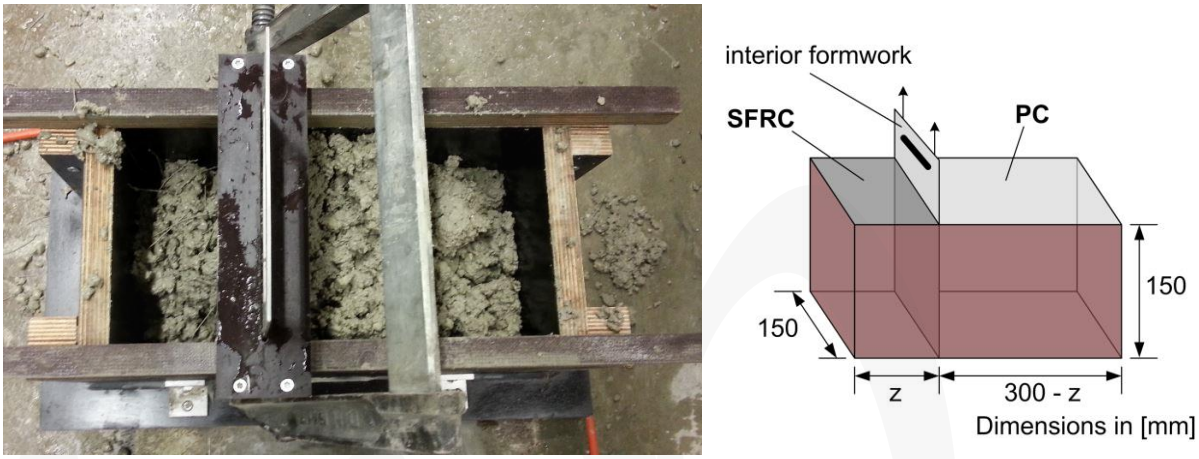
Table 3: Properties of fresh and hardened PC and SFRCs

Properties	**PC**	**L60**	**L60S60**
Flow consistency [cm] *(EN 12350-5)*	43	42	37
Bulk density [kg/dm³] *(EN 12350-6)*	1.36	2.44	2.47
Air void content [%] *(EN 12350-7)*	2.0	1.9	1.3
Compressive strength $f_{c,cube,28d}$ [MPa] *(EN 12390-3)*	84.5	87.0	88.0
Splitting tensile strength $f_{ct,28d}$ [MPa] *(EN 12390-6)*	4.0	6.7	7.5
Young's Modulus $E_{cm,28d}$ [GPa] *(EN 12390-13)*	36	37	37

For the concentrated loading tests hybrid concrete (HC) specimens containing both PC and SFRC were casted either in standing or lying molds. In the case of HC specimens casted in standing molds, PC was at first poured in the mold and compacted to a certain predefined layer thickness, followed by the placing of freshly mixed SFRC. The production of HC specimens casted in lying molds was characterized by the simultaneous placing of the two

This document is the intellectual property of the fib – International Federation for Structural Concrete. All rights reserved.
This PDF of fib Bulletin 95 is intended for use and/or distribution solely within fib National Member Groups.

different concretes in the mold. However, they were firstly separated by a steel plate served as a moveable interior formwork (Figure 1a). During the compacting this interior formwork was lifted up so that the concretes get in contact with each other in their fresh state ("wet-in-wet") without becoming mixed. Hence, a monolithic bonding between the two concretes could be achieved. The distance *z* of the steel plate (Figure 1b) is adjustable in order to enable the production of HC specimens with various layer thicknesses of fiber reinforcement.



(a) (b)

Figure 1: Photograph (a) and schematic description (b) of a special formwork used for the production of HC specimens.

2.2 Scope of experimental test program

As the incorporation of fiber reinforcement can alter the distribution of tensile splitting stresses and further the position of the maximum tensile splitting stresses (Song, 2017), the thickness z of the reinforcement layer was varied in order to determine the optimal configuration of fiber reinforcement. For comparison purpose, in addition to the HC specimens with reinforcement layer thicknesses of 50, 100 and 150 mm, also reference specimens only containing PC or SFRC were produced and tested under the same testing conditions. As illustrated in Figure 2a, the specimens were loaded either concentrically or eccentrically on their edge or corner at a constant area ratio of 9 (area ratio: ratio of total area A_c=150 × 150 mm² to loaded area A_{c0}=50 × 50 mm²). As reported by Breitenbücher et al. (2014), the casting direction has a significant impact on steel fiber orientation and thus consequently on the bearing and facture behavior of SFRC. Hence, the casting direction was varied in terms of using either standing or lying molds for the production of HC as well as fully reinforced specimens (cf. Chapter 2.1).

The experimental test program for specimens with fiber reinforcement type L60 is listed in Table 4, which is identical with that for specimens reinforced with L60S60 fiber-cocktail reinforcement. For each test series, three specimens were produced and tested.

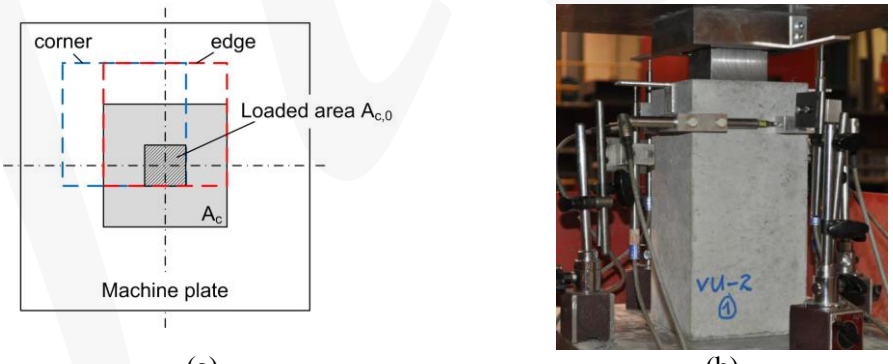
This document is the intellectual property of the fib – International Federation for Structural Concrete. All rights reserved.
This PDF of fib Bulletin 95 is intended for use and/or distribution solely within fib National Member Groups.

Table 4: Experimental test program for specimens with L60 fiber reinforcement

Type of fiber reinforcement	**Mold type**	**Load introduction**	**SFRC layer thickness z [mm]**	**Series index**
L60	s	m	50	L60_s_m_50
			100	L60_s_m_100
			150	L60_s_m_150
			300	L60_s_m_300
		e	100	L60_s_e_100
			300	L60_s_e_300
		c	100	L60_s_c_100
			300	L60_s_c_300
	l	m	50	L60_l_m_50
			100	L60_l_m_50
			150	L60_l_m_50
			300	L60_l_m_300
Mold type: s=standing, l=lying Load introduction: m=centric, e=edge, c=corner				

2.3 Test setup

The concentrated loading tests were performed using a servo-hydraulic testing machine with a maximum load capacity of 5 MN. The load was transmitted onto the upper surface of the specimens through a steel plate with a cross section of 50 × 50 mm². In the case of eccentric loading (edge and corner) the specimens were accordingly positioned on the bottom machine plate, as shown in Figure 2a. The load was applied with a constant loading rate of 0.5 mm/min. The horizontal and vertical displacements of the specimens were measured using LVDTs (Figure 2b).



(a) (b)

Figure 2: Positioning of the specimens for concentric and eccentric load introduction (a) and photograph of test setup for concentrated loading tests.

This document is the intellectual property of the fib – International Federation for Structural Concrete. All rights reserved.
This PDF of fib Bulletin 95 is intended for use and/or distribution solely within fib National Member Groups.

3 Results

3.1 Load bearing behavior

In Table 5 the mean values of ultimate local compressive stresses ($\sigma_{max}=F_{ult}/A_{c0}$) under concentric and eccentric loading are summarized. For comparison purpose, also the stress increases ($\Delta\sigma=\sigma_{max,i}/\sigma_{max,PC}$) of HC and fully reinforced specimens are indicated in relation to PC specimens. It can be seen that under concentric load the maximum bearing stress σ_{max} of HC specimens produced in standing molds increased progressively with growing thickness of the SFRC layer, in particular for HC specimens with fiber-cocktail reinforcement (L60S60). In this case, the incorporation of fiber reinforcement with a layer thickness of only 50 mm (i.e. 1/6 of the total specimen's height) led to an increase of 30.1 % compared to PC specimens. Interestingly, in comparison to fully reinforced specimens, all HC specimens produced in standing molds with a fiber reinforced layer thickness of 150 mm (i.e. 1/2 of the total specimen's height corresponding to the total height of the St. Venant disturbance for the cases investigated here) exhibited an almost identical bearing capacity (L60_s_m_150 vs. L60_s_m_300 and L60S60_s_m_150 vs. L60S60_s_m_300). This implies that in this case a full range reinforcement is not necessary and thus not very efficient.

Table 5: Results of concentric (a) and eccentric (b) loading tests

(a)

Series index	**σ_{max} [MPa]**	**$\Delta\sigma$ [MPa]**	**$\Delta\sigma$ [%]**
PC_m	152	-	-
L60_s_m_50	157	5	3.2
L60_s_m_100	194	42	28.1
L60_s_m_150	215	63	41.7
L60_s_m_300	214	62	41.4
L60_l_m_50	160	8	5.7
L60_l_m_100	165	13	8.9
L60_l_m_150	168	16	10.6
L60_l_m_300	173	21	14.0
L60S60_s_m_50	197	45	30.1
L60S60_s_m_100	247	95	62.8
L60S60_s_m_150	270	114	75.5
L60S60_s_m_300	266	118	77.8
L60S60_l_m_50	158	6	4.5
L60S60_l_m_100	181	29	19.4
L60S60_l_m_150	188	36	23.7
L60S60_l_m_300	201	49	32.5

(b)

Series index	**σ_{max} [MPa]**	**$\Delta\sigma$ [MPa]**	**$\Delta\sigma$ [%]**
PC_e	113	-	-
PC_c	83	-	-
L60_s_e_100	129	16	14.2
L60_s_e_300	141	28	24.8
L60_s_c_100	100	17	20.5
L60_s_c_300	110	27	32.5
L60S60_s_e_10	142	29	25.7
L60S60_s_e_30	161	48	42.5
L60S60_s_c_10	110	27	32.5
L60S60_s_c_30	100	27	32.5

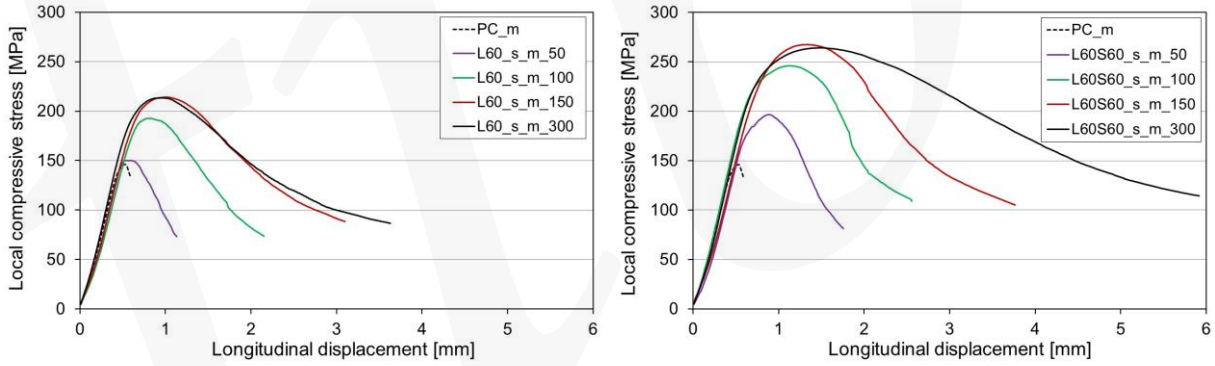
For HC specimens produced in lying molds, the increase in σ_{max} caused by the incorporation of fiber reinforcement was comparatively inconsiderable, especially for reinforcement layers thicker than 100 mm. As reported by Breitenbücher et al. (2014), this can be explained by the fact that in the case of specimens produced in lying molds, fibers are preferably orientated towards the loading direction. Consequently, compared to specimens produced in standing molds, a fewer number of fibers are aligned towards the directions of

This document is the intellectual property of the fib – International Federation for Structural Concrete. All rights reserved.
This PDF of fib Bulletin 95 is intended for use and/or distribution solely within fib National Member Groups.

splitting tensile stresses (perpendicular to the load direction). As a result, for specimens produced in lying molds, the crack-bridging capacity is significantly lower. However, this effect was not observed for mono fiber reinforcement with a layer thickness of only 50 mm. In this case, wall effects had a predominant impact on the orientation of the macro fibers.

Generally, the ultimate bearing capacity of concrete elements subjected to concentrated load tends significantly to diminish with increasing load eccentricity due to the reduction in the confinement effect of the surrounding concrete (Song, 2017). The results for HC specimens were absolutely consistent with this tendency. However, for HC specimens with a reinforcement layer thickness of 100 mm, the ultimate bearing capacity was up to 32.5 % higher than that of PC specimens (L60S60_s_c_100 vs. PC_c). Compared to fully reinforced specimens, the maximum reduction in the ultimate bearing capacity was only 11.8 %. Note that in the case of corner loading, the ultimate bearing capacity of HC specimens with a 100 m thick layer of fiber-cocktail reinforcement was similar to that of fully reinforced specimens (L60S60_s_c_100 vs. L60S60_s_c_300).

To analyze the influence of the investigated variables on the stress-displacement response, Figure 3-5 illustrate the stress-longitudinal displacement curves recorded for PC, HC and fully reinforced specimens. It can be seen that under the given testing conditions the structural stiffness in the pre-peak branch was nearly identical for all specimens, which is consistent with the fact that the young's modulus of PC and SFRCs (Table 3) were nearly identical, too.



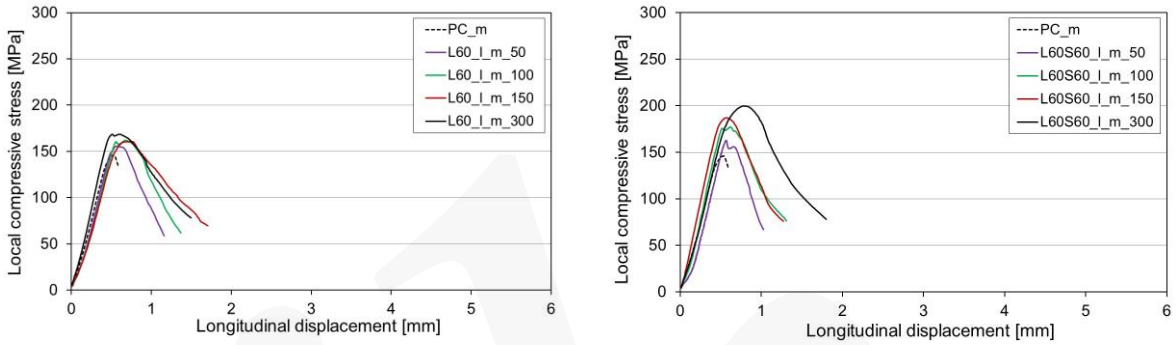
(a) (b)

Figure 3: Stress-displacement curves for specimens produced in standing molds under centric loading: L60 reinforcement (a) and L60S60 reinforcement (b)

For specimens produced in standing molds, the casting direction was identical to the loading direction. Based upon the explanations mentioned above, the resulting fiber orientation was not only beneficial with regard to the ultimate bearing capacity but also in terms of post-cracking behavior. Besides a significant increase in the bearing capacity also a remarkable improvement in the post-cracking ductility could be observed with increasing reinforcement layer thickness. Compared to the fully reinforced specimens, the HC specimens with a reinforcement thickness of 150 mm exhibited – apart from an almost identical bearing capacity - a similar stress-displacement behavior in the post-cracking zone (Figure 3a). However, in the case of fiber-cocktail reinforcement (L60S60), the HC specimens exhibited a quite more ductile behavior compared to HC specimens with mono fiber reinforcement (Figure 3b). This is mainly attributed to higher capability of stress redistribution of the

This document is the intellectual property of the fib – International Federation for Structural Concrete. All rights reserved.
This PDF of fib Bulletin 95 is intended for use and/or distribution solely within fib National Member Groups.

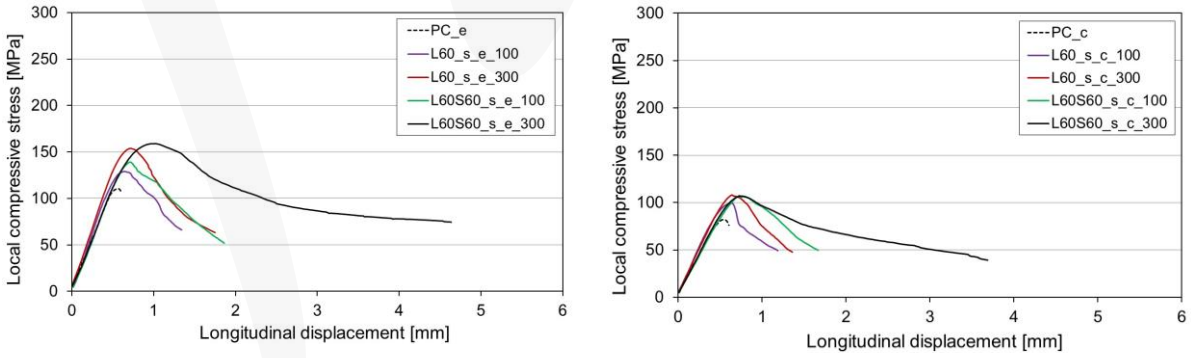
specimens due to the higher content of steel fibers. With progressing crack propagation and stress redistribution, also fibers in the lower section of the specimens were activated and thus the crack-bridging effect was further enhanced by the synergy of fiber-cocktail.



(a) (b)

Figure 4: Stress-displacement curves for specimens produced in lying molds under centric loading: L60 reinforcement (a) and L60S60 reinforcement (b)

HC specimens with L60 reinforcement produced in lying molds exhibited a certain improvement in the post-cracking ductility compared to PC specimens. However, this improvement was not very considerable (Figure 4a). For reinforcement layer thicknesses greater than 100 mm no noticeable difference in the post-cracking behavior could be observed. Although, for HC specimens with L60S60 reinforcement the improvements in terms of bearable concentrated loads as well post-cracking behavior were slightly higher compared to these of HC specimens with L60 reinforcement (Figure 4b). However, these improvements were not comparable to those of specimens produced in standing molds. Hence, it can be stated that the fiber orientation had a more dominant impact on the load bearing behavior than the type or thickness of fiber reinforcement.



(a) (b)

Figure 5: Stress-displacement curves for specimens under edge (a) and corner (b) loading

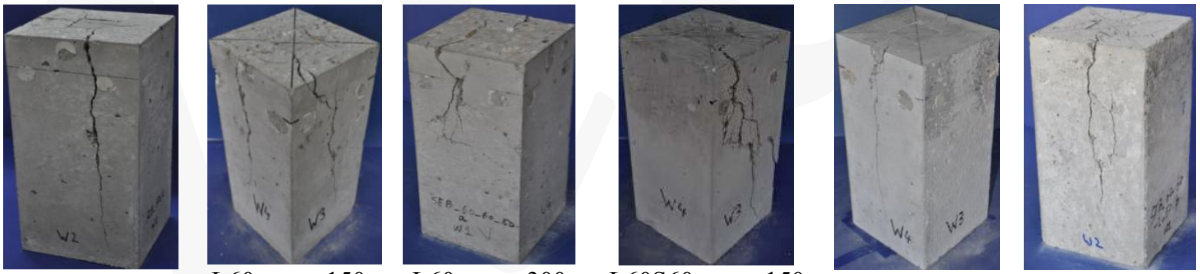
As shown in Figure 5, even in the case of eccentric (edge and corner) loading a more ductile post-cracking behavior was achieved by incorporating a steel fiber reinforced concrete layer with a thickness of only 100 mm. Compared to PC specimens, the best improvement

This document is the intellectual property of the fib – International Federation for Structural Concrete. All rights reserved.
This PDF of fib Bulletin 95 is intended for use and/or distribution solely within fib National Member Groups.

was observed in the case of fully reinforced specimens with L60S60 reinforcement. As explained above, this is related to the stress redistribution and the resulting activation of fibers in the lower section of the specimens in combination with the synergy effect of fiber-cocktail.

3.2 Fracture behavior and crack pattern

For all specimens, no visible cracking or spalling was observed until shortly before reaching the ultimate load. Soon afterwards, PC specimens showed an abrupt and brittle failure. Fully reinforced specimens as well as HC specimens, even with a reinforcement thickness of only 50 mm, showed a more or less ductile fracture behavior, in particular in terms of a gradual crack propagation. The characteristic fracture patterns of most tested specimens are shown in Figure 6 and Figure 7. In the case of concentric loading, HC specimens produced in standing molds (Figure 6b) featured a similar crack pattern as fully reinforced specimens (Figure 6c), which is characterized by a random multi-crack distribution on the testing surface and a longitudinal crack propagation on the lateral surfaces. However, in contrast to specimens with full range fiber reinforcement, for HC specimens the cracks on the lateral surfaces spread over half of their height. This characteristic crack pattern of HC specimens was more or less independent of reinforcement layer thickness and type of fiber reinforcement. However, for HC specimens with L60S60 reinforcement (Figure 6d), in addition to longitudinal cracks, transverse cracks were also observed on the lateral surfaces propagating along the borderline between PC and SFRC. For HC and fully reinforced specimens produced in lying molds (Figure 6e and 6f), the crack pattern under concentric load is almost identical to that of PC specimens (Figure 6a). It is characterized by two main cracks starting from the testing surface and propagating through the lateral surfaces.

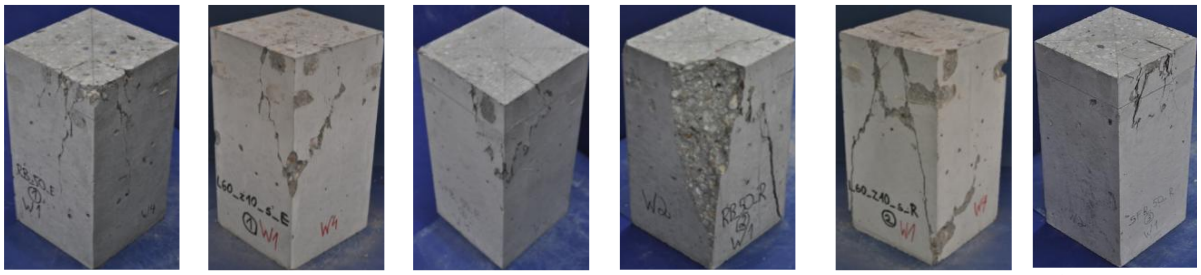


PC_m (a) | L60_s_m_150 (b) | L60_s_m_300 (c) | L60S60_s_m_150 (d) | L60_l_m_150 (e) | L60_l_m_300 (f)

Figure 6: Characteristic fracture patterns of tested specimens produced in standing molds (a-d) and produced in lying molds (e-f) under concentric loading

In the case of corner loading, HC specimens (Figure 7b) showed a nearly identical fracture pattern as that of fully reinforced specimens (Figure 7c). Even for PC specimens (Figure 7a) no major concrete spalling or chipping could be observed. In contrast, the failure of PC specimens under edge loading (Figure 7d) was characterized by the complete chipping of the specimen's corner adjacent to the loaded area. The HC specimens under edge loading (Figure 7e) did not showed such substantial damages. However, two main diagonal and continuous cracks were observed on the lateral surface in addition with minor concrete spalling close to the specimen bottom. For specimens with full range fiber reinforcement (Figure 7f) concrete damages were restricted only to local zones beneath the loaded area.

This document is the intellectual property of the fib – International Federation for Structural Concrete. All rights reserved.
This PDF of fib Bulletin 95 is intended for use and/or distribution solely within fib National Member Groups.



PC_c | L60_s_c_100 | L60_s_c_300 | PC_e | L60_s_e_100 | L60_s_e_300

(a) (b) (c) (d) (e) (f)

Figure 7: Characteristic fracture patterns of tested specimens produced in standing molds under eccentric loading

4 Acknowledgements

The Authors would like to give their appreciation to the German Science Foundation (DFG) for the financial support within the project "Optimized Structural Segments for Durable and Robust Tunnel Lining Systems" of the Collaborative Research Center SFB 837.

5 References

Ahmed, T., Burley, R., Rigden, S. (1998). *Bearing Capacity of Plain and Reinforced Concrete Loaded over a Limited Area.* ACI Structural Journal (Mai-Jun. 1998), pp. 330-342

Breitenbücher, R, Meschke, G., Song, F., Hofmann, M., Zhan, Y. (2014). *Experimental and numerical study on the load-bearing behavior of steel fiber reinforced concrete for precast tunnel lining segments under concentrated loads.* In: Proc. of the FRC 2014 Joint ACI-fib international Workshop, pp. 417-429

Empelmann, E., Wichers, M. (2009). Stabwerke und Teilflächenbelastung nach DIN 1045-1 und Eurocode 2 – Modelle und Anwendungen. Beton- und Stahlbetonbau 104 (2009), Issue 4. pp. 226-235

Iyengar, K. T. S. R. (1966). *A three-dimensional stress distribution problem in the anchorage zone of a post-tensioned concrete beam.* Magazine of Concrete Research, Vol. 18, issue 55, pp- 75-84

Leonhardt, F., Mönning, E. (1986). *Vorlesungen über Massivbau: Teil 2: Sonderfälle zur Bemessung im Stahlbetonbau.* 3rd Edition, Springer-Verlag

Maidl, B, Herrenknecht, M., Maidl, U., Whermeyer, G. (2012). *Mechanised Shield Tunneling.* 2nd Edition, Ernst & Sohn Verlag

Song, F. (2017). *Steel fiber reinforced concrete under concentrated load.* Doctoral thesis, Ruhr University Bochum. ISBN 978-3-410-65808-5

Song, F., Breitenbücher, R. (2013). *Study on the Load-bearing Behavior of Steel Fiber Reinforced Concrete (SFRC) under Localized Compression.* In: Proc. of the international Symposium on Tunneling and Underground Space Construction for Sustainable Development, pp. 336-339

Wichers, M. (2013). *Bemessung von bewehrten Betonbauteilen bei Teilflächenbelastung unter Berücksichtigung der Rissbildung.* Doctoral thesis, Technical University of Braunschweig.

This document is the intellectual property of the fib – International Federation for Structural Concrete. All rights reserved.
This PDF of fib Bulletin 95 is intended for use and/or distribution solely within fib National Member Groups.
FRC2018: Fibre Reinforced Concrete: from Design to Structural Applications
Joint ACI-*fib*-RILEM International Workshop

The behavior of concrete columns confined by UHP-FRCC jacketing

Alessandro P. Fantilli [1], Tomoya Nishiwaki [2], Valerio Lisi [1, 2], Monica Longo [1, 2]

[1] : Politecnico di Torino, DISEG – Department of Structural, Building and Geotechnical Engineering, Torino, Italy.

[2] : Tohoku University, LCEL – Life Cycle Engineering Laboratory, Sendai, Japan.

Abstract

Ultra-High Performance – Fiber Reinforced Cementitious Composites (UHP-FRCC) show excellent mechanical performances, and therefore can be effectively used to retrofit concrete structures. Similarly to the traditional Reinforced Concrete (RC) jacketing, also when a layer of UHP-FRCC is applied on an existing column a sort of confinement can be obtained. Accordingly, the purpose of this study is to investigate the performances of plain concrete cylinders, confined by UHP-FRCC and subjected to uniaxial compression. In some of the layers, high volume fly ash has also been used to replace part of the cement and reduce the environmental impact. As a result, the compressive strength of the concrete core can be enhanced by the presence of UHP-FRCC layer, but when partially using fly-ash, the confinement effect of the jacket reduced. To determine the best solution among the different proposed options, the eco-mechanical analysis was also carried out.

Keywords

Ultra-High Performance – Fiber Reinforced Cementitious Composites (UHP-FRCC), High Volume Fly Ash (HVFA), Confined concrete, Mechanical properties, Ecological properties.

This document is the intellectual property of the fib – International Federation for Structural Concrete. All rights reserved.
This PDF of fib Bulletin 95 is intended for use and/or distribution solely within fib National Member Groups.

1 Introduction

Fiber Reinforced Cementitious Composite (FRCC) has been introduced to increase the post-cracking tensile stress of concrete and, therefore, to enhance tensile and bending toughness (Mehta and Monteiro 2014). The acronym UHP-FRCC (Ultra- High Performance Fiber Reinforced Cementitious Composite) refers to a class of FRCC characterized by a strain-hardening behavior in tension, which occurs after the first cracking, and high compressive strength as well. According to the definition given by Wille et al. (2014), the UHP-FRCC composites can achieve a compressive strength higher than 150 MPa and, in the pre-softening stage in tension, the energy absorption capacity should be larger than 50 kJ/m^3. The ultra-high strength capacity can be obtained by using copious amount of cement and a low water/binder ratio. These two aspects lead to a highly dense microstructure, whose porosity is generally smaller than normal strength concrete (Herold and Muller 2014). For this reason, also excellent durability is guaranteed.

However, the sustainability of these cement-based mixtures, which mainly depends on the carbon footprint of cement production, is not always assured. As suggested by Habert and Roussel (2009), the UHP-FRCC mixtures should be tailored with the aim of assuring the ultra-high mechanical performances (i.e., by applying the performance strategy), but also maintaining the content of cement as low as possible (i.e., by applying the substitution strategy).

One of the most prominent applications of FRCCs is the retrofitting of existing structures, and in particular the jacketing of reinforced concrete columns and beams. Such structures are herein reproduced by placing a UHP-FRCC layer around a concrete cylinder. In addition, the above-mentioned substitution strategy has been implemented in the external layers by replacing part of the cement with fly ash, which is a by-product of the coal burning. The presence of fly ash can undoubtedly lead to a positive effect on the environmental impact, but it also reduces the strength of UHP-FRCC, especially at early age (Holman et al. 2013). For this reason, in the present paper, the performances of some concrete cores, confined by different UHP-FRCC jackets, are compared through the eco-mechanical analysis (Fantilli et al. 2013). In this way, it is possible to assess not only the confinement effect on the cores provided by the different UHP-FRCC mixtures, but also the ecological performances of the confining layer.

2 Experimental program

2.1 Specimen geometry

All the specimens, consisting of cylindrical concrete cores and UHP-FRCC jackets with different amounts of fly ash, were cast and tested in the Life Cycle Engineering Laboratory of Tohoku University – Sendai, Japan.

The cores (Fig. 1), with a radius R = 50 mm and a height L = 200 mm, were made with normal concrete (NC) and reinforced by a UHP-FRCC jacket, whose length L_j was lower than L. In this way, the jacket only confined the NC cores without offering a direct resisting contribution to compression. All the geometrical properties of the specimens are shown in Fig. 1 and Table 1.

This document is the intellectual property of the fib – International Federation for Structural Concrete. All rights reserved.
This PDF of fib Bulletin 95 is intended for use and/or distribution solely within fib National Member Groups.

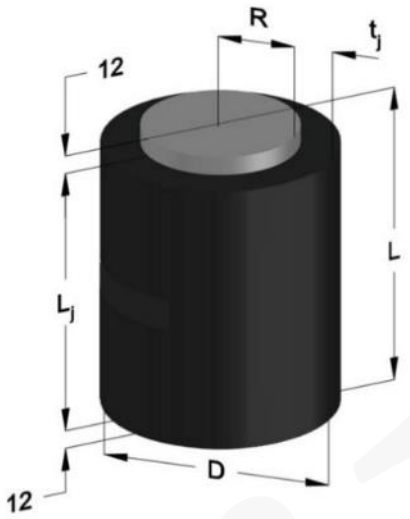


Figure 1: Specimens geometry.

Table 1: Geometrical properties of the specimens.

Core radius, R [mm]	Core length, L [m]	Jacket thickness, t_j [mm]	Jacket length, L_j [mm]	Total diameter, D [mm]
50	200	25	176	150

2.2 Materials properties

A single concrete mixture was used to cast the cores. It included High Early Strength Portland Cement (HESP Cement), water (W), fine aggregates (Sand) – with particles smaller than 5 mm, and coarse aggregate (Coarse) – with particles ranged between 5 mm and 20 mm. To improve the workability, also superplasticizer (SP) was added to the mixture. The mix proportion of the concrete cores is reported in Table 2.

Table 2: The concrete mixture used for the NC cores.

Specimen Designation	HESP Cement [kg/m^3]	Sand [kg/m^3]	Coarse [kg/m^3]	W [kg/m^3]	SP [kg/m^3]
CONCRETE CORES	300.3	836.0	900.3	171.7	1.7

Note: B: binder; HESP Cement: High Early Strength Cement; Sand: fine aggregate; Coarse: Coarse aggregate; W: water; SP: superplasticizer.

Conversely, three series of UHP-FRCC were tailored for the jacket layer shown in Fig. 1. (see Table 3 and Table 4). With respect to the absence of fly ash (FA0 series), in FA20 and FA70 series, the replacement rates of cement with fly ash were 20 and 70% by weight, respectively. The binder was composed of low heat Portland cement (LH Cement), silica fume (SF) and fly ash (FA). Also, silica sand (S) and wollastonite mineral fibers (Wo) were added to the mixture. In addition, superplasticizer (SP) and defoaming agent (DA) were diluted in the Water (W). All the series were fiber-reinforced with 1% in volume of steel micro-fibers (named OL, see Fig. 2a) and 1.5% of the volume of steel macro-fibers (named HDR, see Fig. 2b), whose properties are reported in Table 5.

This document is the intellectual property of the fib – International Federation for Structural Concrete. All rights reserved.
This PDF of fib Bulletin 95 is intended for use and/or distribution solely within fib National Member Groups.

Table 3: Mix proportions (wt.%) of the UHP-FRCC jackets

Series	Binder (B)			S / B (%)	Wo / B (%)	W / B (%)	SP / B (%)	D / B (%)	OL (vol.%)	HDR (vol.%)
	LHC / B (%)	FA / B (%)	SF / B (%)							
FA0	82	0	18	35	13	13.8	2.2	0.02	1.5	1.0
FA20	65.6	16.4								
FA70	24.6	57.4								

Note: B: binder; LH Cement: Low Heat Cement; FA: fly ash; SF: silica fume; S: aggregate; Wo: wollastonite; W: water; SP: Superplasticizer; D: defoaming agent; Ol: steel micro-fibers; HDR: steel macro-fibers.

Table 4: Mix proportions (kg/m3) of the UHP-FRCC jackets

Series	LHC	FA	SF	S	Wo	W	SP	D	OL	HDR
FA0	1218	-	267	520	193	215	33	0.30	118	79
FA20	939	235	258	501	186	205	37	0.29		
FA70	324	757	237	462	171	189	34	0.26		

Table 5: Propertied of the steel used to reinforce the UHP-FRCC layer

Fiber type	Density (kg/m^3)	Length (mm)	Diameter (mm)	Tensile strength (MPa)	Aspect ratio (-)
OL (Micro)	7850	6	0.16	2000	37.5
HDR (Macro)	7850	30	0.38	3000	78.9



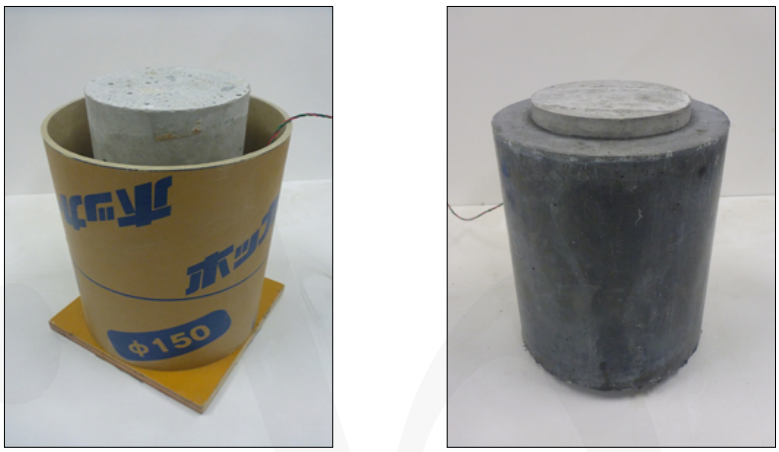
a) b)

Figure 2: Steel fibers added to the mixture: a) micro-fibers "OL"; b) macro-fibers "HDR".

This document is the intellectual property of the fib – International Federation for Structural Concrete. All rights reserved.
This PDF of fib Bulletin 95 is intended for use and/or distribution solely within fib National Member Groups.

2.3 Casting and curing procedures

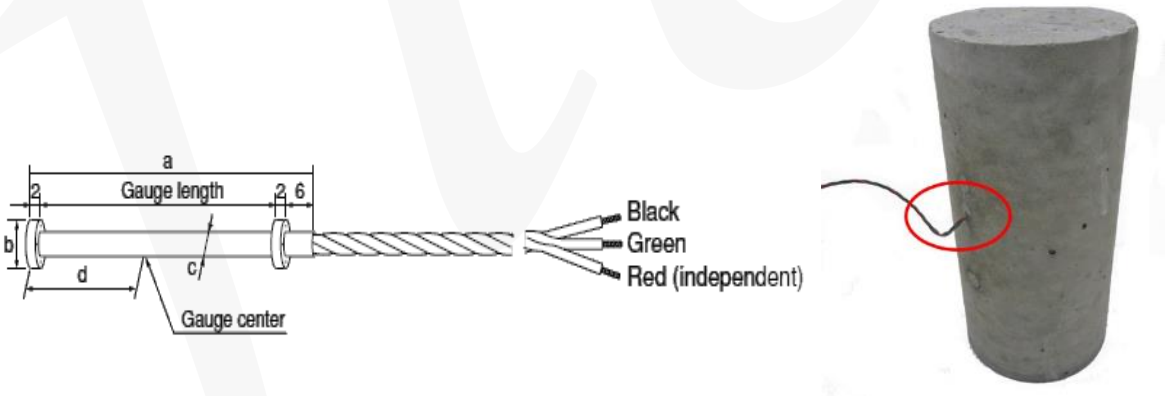
Paper cylindrical molds (150 mm in diameter and 178 mm in height) were used to cast the UHP-FRCC jackets around the concrete cores (Fig. 3).



a) b)

Figure 3: Jacket casting: a) lateral paper mound; b) final concrete cores confined by the jacket.

To measure the vertical strain, an embedded strain gauge was introduced within the concrete core (Fig. 4b). This type of strain gauge, consisting of a 3-wires system located in the center of the cores (Fig. 4a), allows the measurement of the vertical strains in normal concrete during the uniaxial compression test.



(a) (b)

Figure 4: Embedded strain gauges: a) 3-wire system; b) cylindrical core with the embedded strain gauge.

As illustrated in Fig. 5, the concrete cores were left 48 hours in the molds, at the temperature of 20 °C and 95% *RH*. After 11 days from the initial cast, the cores were confined by the UHP-FRCC jackets. Two days later, also the jacket's formworks were removed and all the specimens were subjected to steam curing at 90 °C in the following 48

This document is the intellectual property of the fib – International Federation for Structural Concrete. All rights reserved.
This PDF of fib Bulletin 95 is intended for use and/or distribution solely within fib National Member Groups.

hours. Finally, all the samples were stored in the same humidified environment (20 °C and 95% *RH*) until the test, performed 28 days after casting the NC cores.

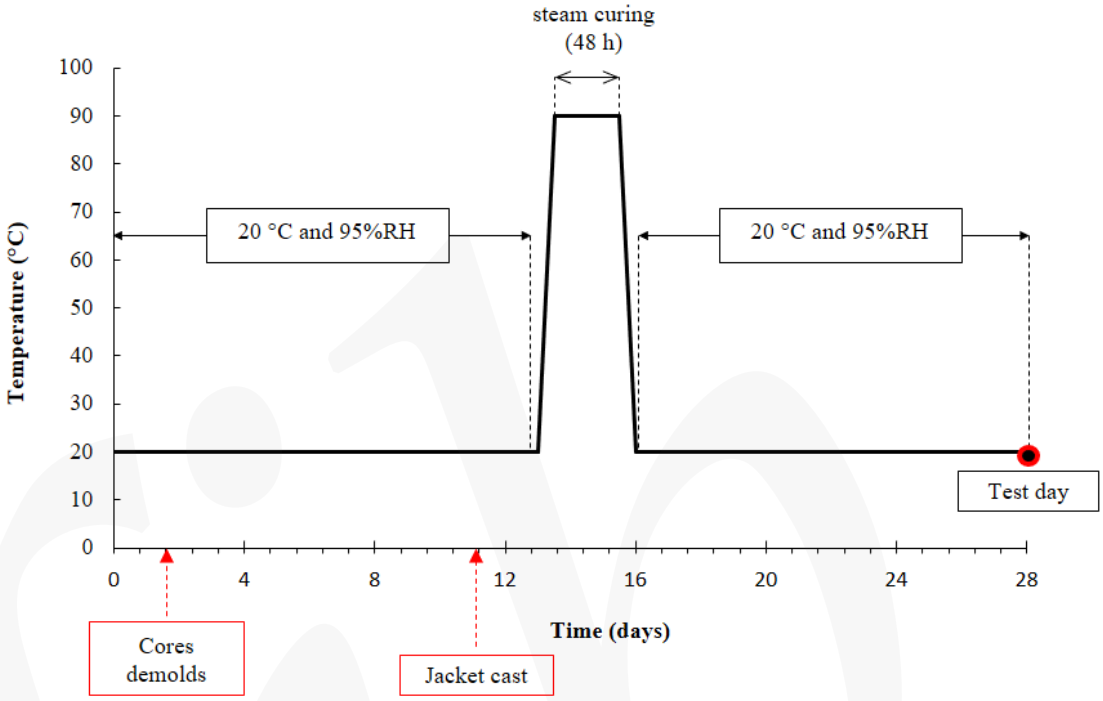


Figure 5: Curing procedure for the NC cores confined by UHP-FRCC jackets.

The following specimens were prepared and tested under uniaxial compression:

- 4 NC cores without any jacket (named NO JACKET)
- 3 NC cores with UHP-FRCC jacket made with only cement as binder (FA0 series)
- 3 NC cores with UHP-FRCC jacket made with FA20
- 3 NC cores with UHP-FRCC jacket made with FA70.

The tests were performed by controlling the displacement rate of the loading cell, whose stroke moved at a velocity of 0.3 mm per minute. Each test was stopped when the UHP-FRCC jacket was completely damaged, and all the measurements are reported and analyzed in the following sections.

3 Experimental results and discussion

3.1 Mechanical properties

As shown in Fig. 6, the mechanical performances of UHP-FRCC in tension decrese as the content of fly ashes increases. In the composite FA70, not only the tensile strength is the lowest, but also the residual stresses in the post cracking regime drastically reduce with respect to FA0.

Table 6 reports the average values of compressive strength, the Young's modulus of elasticity, and the Poisson's ratio measured the uniaxial compression tests. The Young's

This document is the intellectual property of the fib – International Federation for Structural Concrete. All rights reserved.
This PDF of fib Bulletin 95 is intended for use and/or distribution solely within fib National Member Groups.

Modulus and the Poisson's ratio were calculated at one-third of the maximum load, according to the Japanese standards (JIS A 1149). The average stress – strain curves are also plotted in Fig. 7.

All the specimens reinforced with the UHP-FRCC jackets showed a significant increment of the compressive strength, due to the confinement effect provided by the UHP-FRCC jacket. Although the Young's modulus of the NC cores does not vary significantly, a remarkable increment of ductility is clearly evident when the jacket is present.

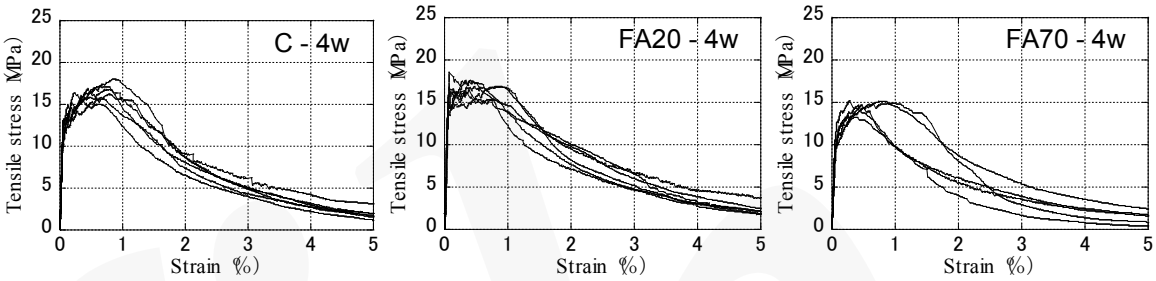


Figure 6: Stress-strain curves measured through uniaxial tensile tests.

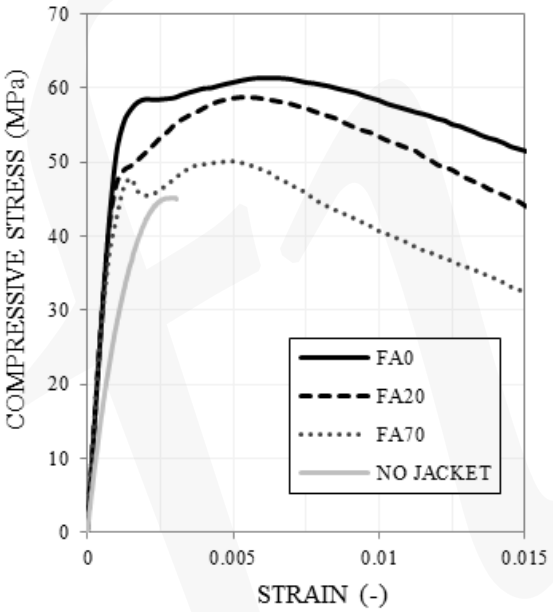


Figure 7: Stress-strain curves measured in the uniaxial compression tests.

Table 6: Mechanical properties of the specimens

Series	Max compressive stress, σ_{max} [MPa]	Young's modulus E_{cm} [GPa]	Poisson's Ratio ν [-]
NOJACKET	45.07	34.56	0.20
FA0	61.68	37.97	0.19
FA20	59.06	37.48	0.18
FA70	50.43	35.74	0.22

As illustrated in Fig. 8, with respect to the unconfined NC cores (i.e., NO JACKET), the strength of the specimens confined with FA0 jackets increases of about 40% (see Table 7). In all the other cases, the higher the amount of cement in the UHP-FRCC mixtures, the higher the confinement effect on the NC core. Specifically, the jackets made with FA20 and FA70 mixtures, improve the strength of the plain core of only 31% and 12%, respectively. Thus, replacing cement with fly ash leads to a reduced compressive strength of the NC cores, even if both the ductility and the environmental benefits remain.

This document is the intellectual property of the fib – International Federation for Structural Concrete. All rights reserved.
This PDF of fib Bulletin 95 is intended for use and/or distribution solely within fib National Member Groups.

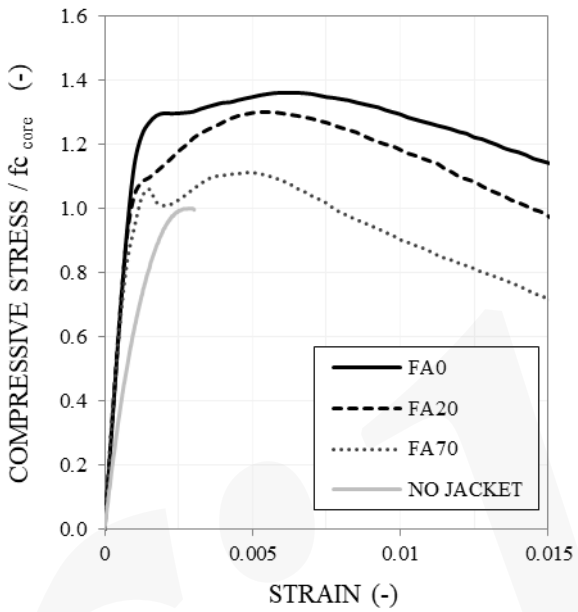


Figure 8: Stress-strain curves referred to $f_{c,\,core}$.

Table 7: Improvement due to jacketing

Series	Max stress / fc_{core} [-]	Compressive strength increase [%]
FA0	1.37	36.85
FA20	1.31	31.05
FA70	1.12	11.89

3.2 Eco-Mechanical analysis

As Fig. 9 shows, both the mechanical performances (Fig. 9a) and carbon footprint (Fig. 9b) of the NC cores jacketed by UHP-FRCC layers show similar trends (i.e., decrease with the content of fly ash).

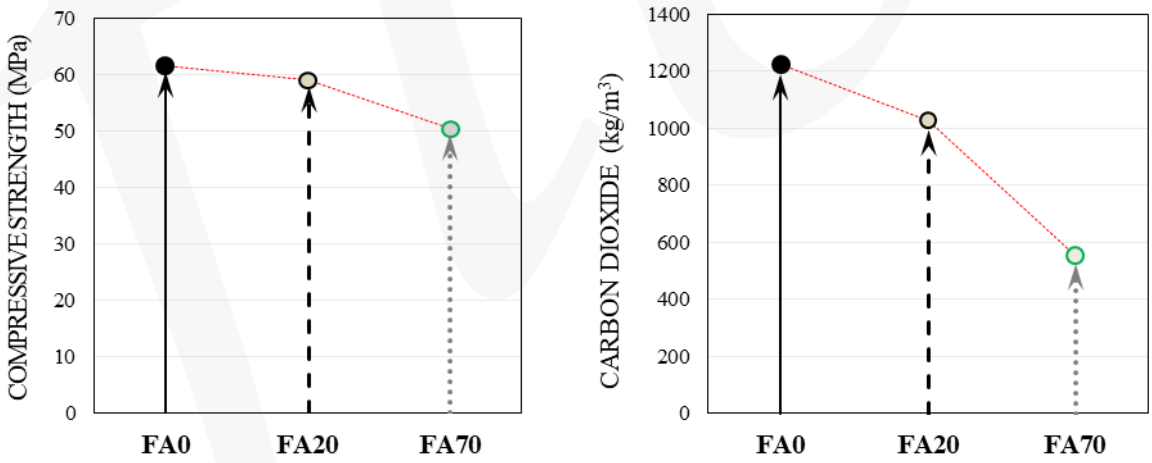


Figure 9: The performances of the UHP-FRCC mixtures: a) Compressive strength; b) Carbon footprint.

Thus, with the aim of tailoring more environmental friendly UHP-FRCCs, without compromising their mechanical performances, an eco-mechanical analysis is performed through the non-dimensional diagram shown in Fig. 10 (Fantilli and Chiaia 2013). On the horizontal axis of this chart, the Mechanical Index (*MI*) is reported and normalized with

This document is the intellectual property of the fib – International Federation for Structural Concrete. All rights reserved.
This PDF of fib Bulletin 95 is intended for use and/or distribution solely within fib National Member Groups.

respect to lower bound value of the desired mechanical properties (i.e., MI_{inf}). Similarly, the Ecological Index (*EI*) is reported on the vertical axis, and normalized with respect to the upper bound value of the ecological impact (i.e., EI_{sup}).

Four different zones can be defined within this non-dimensional diagram:

- Zone I: Low mechanical performances – Low ecological performances;
- Zone II: High mechanical performances – Low ecological performances;
- Zone III: High mechanical performances – High ecological performances;
- Zone IV: Low mechanical performances – High ecological performances.

Accordingly, the goal of the eco-mechanical analysis is to select the best solution among those falling within the third region (depicted in green), trying to avoid those located in the first zone (depicted in red).

In this study, the compressive strength was considered as *MI*. Whereas, to quantify the ecological performances, the mass of CO_2 released in atmosphere by the production of 1 m^3 of UHP-FRCC was assumed to be *EI*. Finally, the bounds MI_{inf} and EI_{sup} were considered as the mechanical response and the ecological impact, respectively, provided by FA0 mixture (i.e., MI_{FA0} and EI_{FA0}).

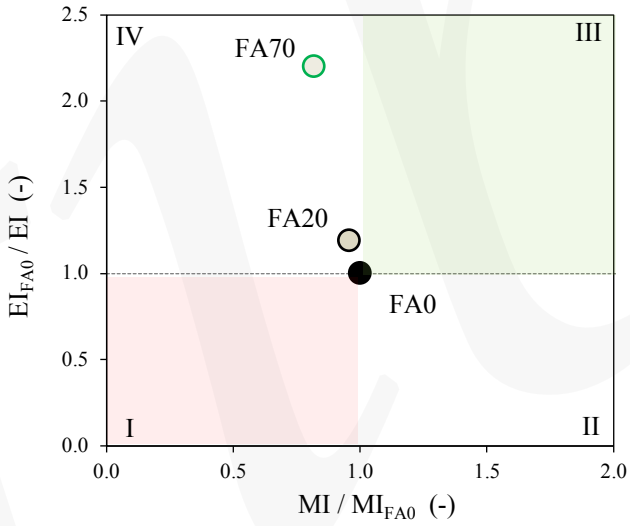


Figure 10: The eco-mechanical analysis performed for the NC cores confined by UHP-FRCC jackets

The results of the eco-mechanical analysis, illustrated in Fig. 10, confirm that the best solution is to reinforce the concrete cores with a UHP-FRCC layer without replacing the cement with fly ash (mixture FA0). However, this solution also offers the highest ecological impact. This is due to the fact that the lower the amount of cement in the UHP-FRCC mixtures, the lower the mechanical response of the NC cores under uniaxial compression. Even if the results offered by the mixture with 20% of cement replaced by fly ash are very close to those obtained without considering any substitution (i.e., MI/MI_{FA0} = 0.96, and EI_{FA0}/EI=1.19), FA20 falls into the Zone IV. Also, replacing 70% of cement with fly ash leads to a reduction of the confinement (MI/MI_{FA0} = 0.82) with a drastic improvement of ecological performance (EI_{FA0}/EI = 2.20).

To move the mixtures FA20 and FA70 from Zone IV to Zone III of Fig. 10, it is necessary to increase and optimize the jacket thickness t_j with respect to that used for FA0. Such increment will be the next step of this research project.

This document is the intellectual property of the fib – International Federation for Structural Concrete. All rights reserved.
This PDF of fib Bulletin 95 is intended for use and/or distribution solely within fib National Member Groups.

4 Concluding remarks

Based on the results of the experimental investigation previously described, the following conclusions are drawn:

1. The confinement effect provided by the UHP-FRCC jackets on NC cylinders increases the compressive strength and ductility, whereas Young's modulus does not vary significantly.
2. Although the confinement effect provided by the jacket reduces with the replacement rate of cement with fly ash, the ecological impact of UHP-FRCC drastically decreases with this substitution;
3. Using the eco-mechanical analysis, it is possible to assess both mechanical and ecological performances simultaneously, and therefore the best solution among the different proposed options can be selected.

Further research will be needed to apply the proposed jacketing method to the existing RC structures, e.g. avoid the steam curing and/or precast

5 Acknowledgments

This work was supported by JSPS KAKENHI Grant Number 26289186 and by the Italian Ministry of Education (PRIN 2015).

6 References

Fantilli, A.P., and Chiaia, B. (2013), *The work of fracture in the eco-mechanical performances of structural concrete*, Journal of Advanced Concrete Technology, V.11, pp.53-67.

Habert, G., and Roussel, N. (2009), *Study of two concrete mix-design strategies to reach carbon mitigation objectives*, Cement & Concrete Composites, V. 31, pp 397–402.

Herold, G., and Müller, H.S. (2014), *Measurement of porosity of Ultra High Strength Fibre Reinforced Concrete*, Proceedings of the International Symposium on Ultra High Performance Concrete, pp. 685-694.

Holman, K.R., Volz, J.S., and Myers, J.J. (2013), *Comparative Study on the Mechanical and Durability Behavior of High-Volume Fly Ash Concrete versus Conventional Concrete*, First international conference on concrete sustainability (ICCS 2013).

Mehta, P.K., and Monteiro, P.J.M. (2014), *Concrete – microstructure, properties, and materials*, New York, 4th Edition, McGraw-Hill.

Wille, K., El-Tawil, S., and Naaman, A.E. (2014), *Properties of strain hardening ultra high performance fiber reinforced concrete (UHP-FRC) under direct tensile loading*, Cement & Concrete Composites, V. 48, 2014, pp.53–66.

This document is the intellectual property of the fib – International Federation for Structural Concrete. All rights reserved.
This PDF of fib Bulletin 95 is intended for use and/or distribution solely within fib National Member Groups.
FRC2018: Fibre Reinforced Concrete: from Design to Structural Applications
Joint ACI-*fib*-RILEM International Workshop

A holistic calculation and design tool for structural SFRC members

Katharina Look[1], Peter Mark[1]

[1] : Institute of Concrete Structures, Ruhr University Bochum, Germany

Abstract

An open design tool is developed that uses spreadsheet analyses, optimisation methods and iterative analytical routines. Its idea is to offer a universal, intuitive instrument to economically design and optimise steel fibre reinforced concrete members with or without rebar. The tool comprises non-linear evaluations of sectional forces with the yield line theory, a cross sectional design in ultimate and serviceability limit states as well as backward oriented optimisations of reinforcements, cross sectional properties or fibre classes. It should be free of specific code regulations and thus just basis on the assumption of plane strains, an ideal bond and requires the definitions of uniaxial stress-strain laws, strain boundaries and fundamental design formulas. Boundary conditions, material parameters and sectional properties as well as results like strain or stress distributions, performance ratios and potentials of improvements are given in visualisations and commented figures. The non-linear equations of equilibrium are iteratively solved with reduced gradient methods. Doing so, recursive initial parameter settings of the strain plane are – amongst other regularisations – incorporated to achieve robust solutions.

Keywords

Design tool, spreadsheet analysis, SFRC, optimisation, yield line theory, cross section design

This document is the intellectual property of the fib – International Federation for Structural Concrete. All rights reserved.
This PDF of fib Bulletin 95 is intended for use and/or distribution solely within fib National Member Groups.

1 Introduction

Since international guidelines such as the ACI 544.4R-88 in the US, the forward-thinking Model Code 2010 or the German DAfStb-Guideline have been released, steel fibre reinforced concrete (SFRC) has not yet exploited its full potential regarding the opportunities it is designed and allowed for. Established fields of applications are still housing constructions and the design of industrial floors (Gödde et al. 2010-1). However, steel fibres bear potential to ramify cracks in concrete and transfer tensile stresses even after crack initiation. Therefore many advantages arise for both, the fresh and the hardened concrete (Heek et al., 2016). Several investigations validate an improved ductility of concrete in compression due to bridging of shear cracks originally induced by transversal stresses as well as fibre increased residual load bearing capacities in tension. Steel fibres improve the fire resistance and reduce the time-dependent phenomena creep and shrinkage (Heek et al., 2015). In case of cross sections subjected to shear, steel fibres increase the bearing capacity of the tensile strut by bridging the shear cracks. Moreover, an improved leak-tightness can be achieved, as cracks are visibly reduced. Evenly spread in the concrete matrix they also prevent concrete from spalling and thus help to minimize corrosion (Gödde et al., 2010-1). Nevertheless, steel fibres are not yet established in building practice comprehensively. To change this, the here presented design tool contributes, as more and more research projects focus on the use of SFRC in structural engineering (Smarslik et al., 2019), (Gaganelis et al., 2019), (Plückelmann et al., 2019), (Heek et al., 2018), (Landler et al., 2019), (Empelmann et al., 2020). For practically relevant cases and easy to adapt, it calculates internal forces of bedded slabs and rectangular cross sections subjected to bending and shear for structural design in the ultimate limit state and checks for limited crack-widths in serviceability conditions. Above all it offers a reversal kind of optimisation to deliver the best fibre class regarding given loads and is able to customise any design needs to individual boundary conditions.

2 Design of SFRC structures

2.1 Structural behaviour

Key factor regarding the post-cracking behaviour of SFRC is the fibre content. Distinction is made concerning supercritical and subcritical contents. The critical fibre content cannot exactly be quantified, as it is influenced by other factors such as the fibre orientation and distribution, the properties of the concrete mix, and the casting and production processes (Gödde et al., 2010-2). If supercritical fibre contents are used, the stress-strain curve of SFRC increases in the post-cracking region. Consequently, equilibrium can be fulfilled without rebar, and failure - even on a cross sectional level - would be ductile. For subcritical fibre contents, gains in the post-cracking region can only be realised in statically indeterminate systems and due to internal load redistributions. Thus, in case of statically determinate systems, which are typical for recent buildings, rebar is essential for subcritical fibre contents (Gödde et al., 2010-2). Due to the direct causality between load-bearing capacity and the benefits of steel fibres, a rethink must be made. The focus must be switched from cross sectional load-bearing to system load-bearing capacities.

2.2 Stress-strain relations

The structural behaviour of SFRC is influenced by a large number of different factors, such as fibre content, fibre type, concrete mixture, fibre orientation and distribution. Thus, it is not

This document is the intellectual property of the fib – International Federation for Structural Concrete. All rights reserved.
This PDF of fib Bulletin 95 is intended for use and/or distribution solely within fib National Member Groups.

possible to define universal material properties of SFRC. Classification of SFRC into fibre classes usually rests on four-point or notched three-point bending tests. Crack mouth opening displacements (CMOD) are recorded for $CMOD_1 = 0.5$ mm and $CMOD_3 = 2.5$ mm (*fib*, 2013) or at deflections of $\delta_{L1} = 0.5$ mm and $\delta_{L2} = 3.5$ mm (DAfStb-Guideline SFRC, 2013, Look et al., 2019). For these displacement states smeared stress-strain laws are derived for design. They uniformly base on two strain values, ε_1 and ε_2, at corresponding crack openings or deflections. At these strains, residual flexural tensile strengths are extracted into residual tensile strength f^{f}_{ct} values. These two quantities are fundamental to classify SFRC and used for designing in ULS ($f^{f}_{ct}(\varepsilon_2 = \varepsilon_u)$) and SLS ($f^{f}_{ct}(\varepsilon_1)$). Design guidelines usually assume idealized stress-strain diagrams for structural design. The courses according to DAfStb-Guideline are bi-linear (SDL1) or tri-linear (SDL2), respectively, incorporating the strength and strain values mentioned. For convenience, the default values of DAfStb-Guideline are assumed in the following, still allowing to change into variable other parameter settings.

3 Sectional forces according to the yield line theory

For the computation of sectional forces in slabs, several alternative methods are appropriate. Among these some account for linear-elastic, non-linear or plastic material behaviour. Steel fibres activate their true potential if concrete cracks. Thus, linear-elastic models are less suitable, because they are not able to capture the post-cracking gains of bearing capacities of SFRC introduced by redistribution effects. The calculation of sectional forces according to plastic approaches, such as the yield line theory, has proven itself suited in the past. Assuming rigid-plastic material behaviour, the areas of plasticisation, the cracks, are idealized in lines. Ignoring the elastic deformation of the system, these lines represent yield lines and form the joints which characterize the entire deformation of a slab (Schmitz, 2013). Besides, the developed design tool is currently restricted to bedded slabs only, but might be easily adapted for other slabs, too.

If a bedded slab is loaded with a single load at its centre, the positive moments grow at the bottom side first until the tensile strength is exceeded and cracks appear down there. Then the load-bearing capacity of plain RC is reached. If fibres are added to the concrete, the load can further be increased after cracking due to an internal redistribution of forces. This is limited, if negative moments induce cracking of the slab's top face. Now the bearing capacity of the SFRC is reached, since cracks on the top face are usually unwanted (Schmitz, 2013). Ready to use, explicit formulas to calculate sectional forces for bedded slabs and different load configurations were originally developed by Meyerhof (Meyerhof, 1962), (TR34, 2013) and are implemented here.

4 Cross sectional design

4.1 Bending and axial forces

Generally, the principle equilibrium of external and sectional forces is fundamental. To grant equilibrium, iterative numerical or analytical methods might serve (Gödde et al., 2015), (Gödde et al., 2010-2). Here, an optimisation approach is proposed with an objective function set-up for optimisations in spreadsheets. The formulation of the objective function, restrictions and the process of calculation are presented in the remainder.

This document is the intellectual property of the fib – International Federation for Structural Concrete. All rights reserved.
This PDF of fib Bulletin 95 is intended for use and/or distribution solely within fib National Member Groups.

4.1.1 Objective function

In general the aim of an optimisation is to minimize an objective function $f(\mathbf{x})$ which depends on a vector $\mathbf{x}$ of n optimisation variables x_i. The optimum must comply with all restriction by means of n_g equality constraints g_i, n_u inequality constraints u_i as well as the upper and lower limits of all optimisation variables x_i (Mark, 2003). Common restrictions for optimisation in case of a bending design in symmetric sections (uniaxial bending) are summarized in Table 1.

Table 1: Parameters of an optimisation and applications to bending design

	Mathematical formulation	*Formulation for bending design*
Aim	$f(\mathbf{x}) \longrightarrow \min.$	$A_{s,ges} = A_{s1} + A_{s2} \longrightarrow \min.$
Optimisation variables	$\mathbf{x} = (x_1,\dots, x_n)$ with $i = 1, \dots, n$	A_{s1},(A_{s2}), strain plane variables ε_{ct} and ε_c
Restrictions	$g_i = 0$ with $i = 1, \dots, n_g$ $u_i \le 0$ with $i = 1, \dots, n_u$	$M_{Ed} - M_{Rd} = 0$ with $M_{Rd} = \int_A \sigma z\, dA$ $N_{Ed} - N_{Rd} = 0$ with $N_{Rd} = \int_A \sigma\, dA$ $\xi - \xi_{lim} \le 0$ $A_{s2} - A_{s,set} = 0$
Limits of optimisation variables	$l_i \le x_i \le r_i$ with $i = 1, \dots, n$	$A_{s1} \ge 0$, $A_{s2} \ge 0$, $A_{s1} \le A_{s,max}$ 0 ‰ $\le \varepsilon_{ct} \le$ 25 ‰ and 0 ‰ $\ge \varepsilon_c \ge$ -3.5 ‰

4.1.2 Process of calculation

Fundamental for an accurate and fast solution is the proper choice of initial values. Well-guessed reinforcement amounts and initial strain states promote fast and stable results. The default reinforcement amount follows from suited rules of thumb for bending design as summarized in Table 2.

Table 2: Initial values for the calculation

Reinforcement	$A_{s1} = \frac{1}{f_{yd}}\left(\frac{M_{Ed}}{0.9(h-d_1)} + N_{Ed}\right)$ A_{s2} as pre-scribed by the user acc. to the fraction A_{s2}/A_{s1}
Strain distribution	*Iteration 1:* $\varepsilon_{ct} = \varepsilon_{ct,max}$; $\varepsilon_c = \varepsilon_{c,max}$ *& restart* *Iteration 2:* $\varepsilon_{ct} = \varepsilon_{ct,max}/2$; $\varepsilon_c = \varepsilon_{c,max}/2$ *& restart* *Iteration 3:* $\varepsilon_{ct} = \varepsilon_{ct,min}$; $\varepsilon_c = \varepsilon_{c,min}$ *& restart*
Accuracy	$\lvert M_{Ed} - M_{Rd}\rvert \le 0.01$ kNm $\lvert N_{Ed} - N_{Rd}\rvert \le 0.01$ kN

While the subscript *ct* denotes concrete's strains in the tensile fibre, *c* denotes the compressive strains in a cross section. Here, the initial maximum and minimum strains are chosen according to Table 3. Of course, a user might adjust these for his specific needs.

The two resistances M_{Rd} and N_{Rd} resulting from stress integrals can be solved for iteratively, numerically or analytically, just like the design itself. Actually, analytical integrations of

This document is the intellectual property of the fib – International Federation for Structural Concrete. All rights reserved.
This PDF of fib Bulletin 95 is intended for use and/or distribution solely within fib National Member Groups.

stresses with respect to the strains according to (DAfStb-Guideline SFRC, 2013) have been implemented.

Table 3: Initial strain values of the iteration steps

$\varepsilon_{ct,max}$	$\varepsilon_{c,max}$	$\varepsilon_{ct,min}$	$\varepsilon_{c,min}$
25.0 ‰	-3.5 ‰	0.1 ‰	-0.1 ‰

For optimisation an iterative solution employing generalized reduced gradients (GRG) is used. A solution is searched for an initial value in the direction of the negative gradient (steepest descent) until no numerical improvement can be achieved (Mark, 2003). For numerical stability, the solution space of strains is divided into three subdomains (iterations 1 to 3), which are sequentially explored to find the strain state that characterizes equilibrium. By default and without setting a tolerance limit manually, iteration would not end before an accuracy of 10^{-13} is gained. But, as this would exaggerate computational costs relative to the accuracies really needed, an absolute criterion is chosen that terminates iterations, if internal and external forces (N_{Rd} and N_{Ed}) do no longer deviate by 0.01 kN. This absolute and not relative criterion yields suitable results for practically used sections that go beyond about 0.01 m². Once the tolerance is met, the calculation is terminated and the results are accepted as output.

Since optimisations with GRG just find extrema but not necessarily global ones (Mark, 2003), the three subdomains span the total solution space and simultaneously vary the initial strains. Comparison of results by means of reinforcement amounts required in RC and SFRC member design is performed as a benchmark presented in Section 5.

4.2 Shear design

Both, the Model Code 2010 and the Eurocode 2, define explicit equations to cover the contributions of the various load-bearing mechanisms in shear design. Thus, for shear design an iterative approach is dispensable (Heek et al., 2017-2). For convenience, the equations implemented into the design tool are taken from the German version of Eurocode 2, DIN EN 1992-1-1/NAD and the DAfStb-Guideline, introducing an additive effect of shear bearing from fibre induced stresses proportional to the sectional area within the tensile shear strut.

4.3 Crack width limitation

As already the case for shear design, the limitation of crack-widths is explicitly defined in the codes, too. The derivation of the crack width w_k according to Equation (1) from DIN EN 1992-1-1/NAD incorporating additions of the DAfStb-Guideline bases on an axially pulled member and might serve as an example to quantify the benefits of steel fibres.

$$w_k = s_{r,max}(\varepsilon_{sm} - \varepsilon_{cm})(1 - \alpha_f)^2 \text{ with } \alpha_f = f_{ct}^f / f_{ctm} \quad (1)$$

The calculative crack width arises from a product of three factors. The maximum expected crack spacing in a member $s_{r,max}$ is multiplied by the difference of mean reinforcement and concrete strains $\varepsilon_{sm} - \varepsilon_{cm}$ and a third factor mapping the fibre effect α_f. This effect results to the ratio of the residual tensile strength of SFRC f_{ct}^f and the mean tensile strength of plain concrete f_{ctm}. Since the third factor is squared in Equation (1) fibres lead to an enormous decrease of rebar which makes SFRC an ideal building material for leak-tight structures or slabs under constraints.

This document is the intellectual property of the fib – International Federation for Structural Concrete. All rights reserved.
This PDF of fib Bulletin 95 is intended for use and/or distribution solely within fib National Member Groups.

5 Program

Microsoft Excel is the most popular spreadsheet software recently available and thus used to implement the optimisation routine. It already offers an in-build optimisation tool, the so called *Solver*, and possesses an on-board programming language, *Visual Basic for Applications (VBA)*. This language allows for scripting and saving source code separately and to call it on demand by functions working on the input data in the cells of the sheets.

5.1 Calculation of slabs

In order to cover the most typical fields of applications for SFRC, bedded slabs under usual pointwise load configurations are assumed. Figure 2 shows the input data sheet, referring to the example in Figure 1. Each input parameter is commented, what explains the input and makes the program user-friendly and intuitively operable.

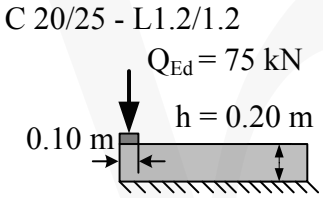


Figure 1: Example for the calculation of a bedded slab loaded at a corner

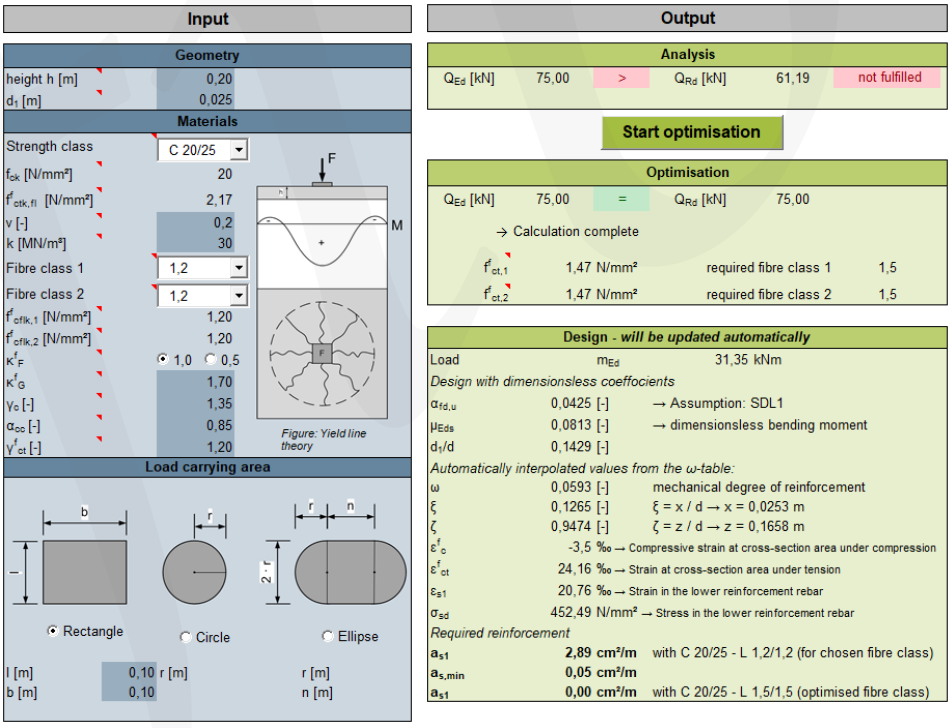


Figure 2: Input and output mask for slab calculation with loads and data according to the slab example

In order to make the program descriptive and easy to understand, most of the input parameters are queried by illustrations. If a cell does not have to be filled by the user, it is

This document is the intellectual property of the fib – International Federation for Structural Concrete. All rights reserved.
This PDF of fib Bulletin 95 is intended for use and/or distribution solely within fib National Member Groups.

automatically hidden. The computation starts by clicking the button "*Start calculation*". When a calculation is completed, the green output datasheet is updated (Figure 2). First, the program computes the resistance of a slab (*Analysis*). Regardless whether the analysis is fulfilled or not, the user can start the optimisation of fibre classes (*Optimisation*). By using optimisation tools the program now iteratively calculates the minimum required tensile strength of SFRC iteratively. Among others, the dimensionless bending moment (μ), the mechanical degree of reinforcement (ω), stresses (σ) and strains (ε) are given at the bottom of the spreadsheet (*Design*). Especially the required reinforcement ratios for the optimised and pre-given fibre class are shown.

5.2 Design of cross sections

Figure 3 shows a simply supported beam as an example for the design of cross sections by the tool. The program itself might be downloaded for free at: www.massivbau.rub.de.

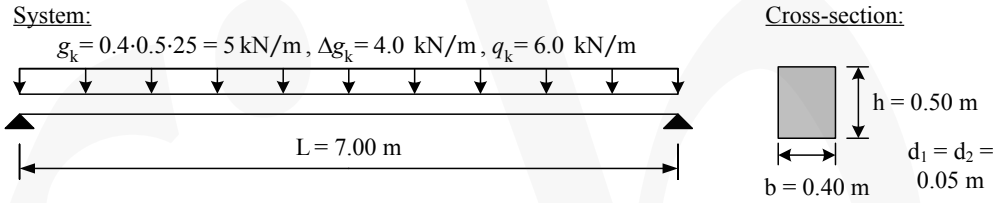


Figure 3: Example for cross sectional design

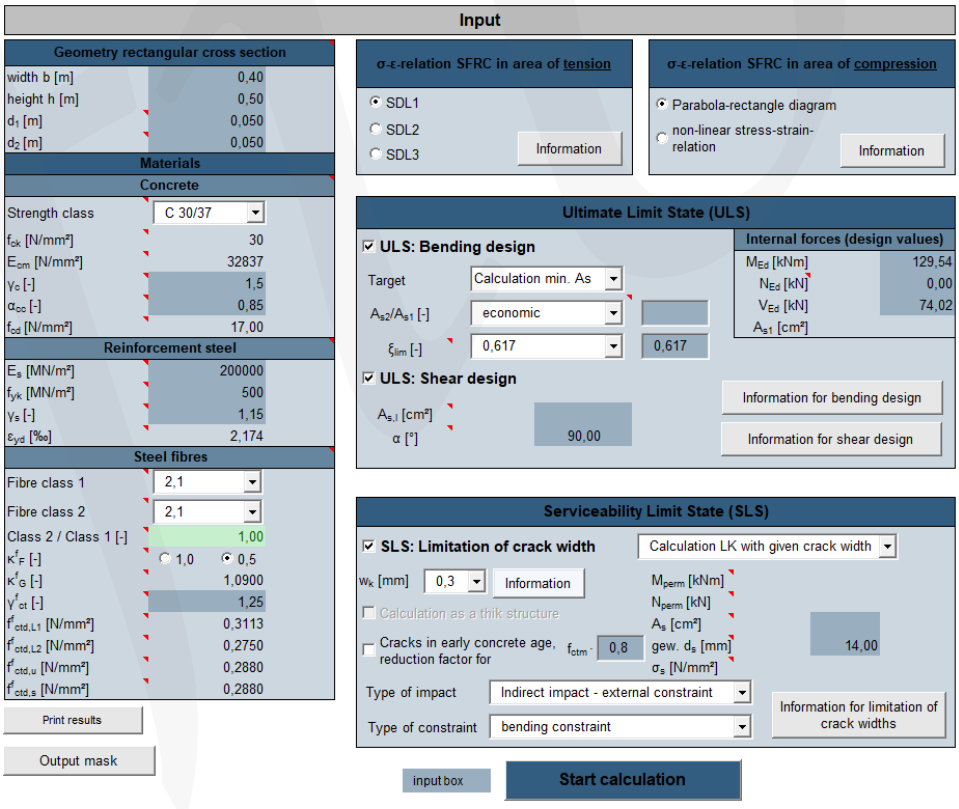


Figure 4: Input datasheet for the cross sectional design example

This document is the intellectual property of the fib – International Federation for Structural Concrete. All rights reserved.
This PDF of fib Bulletin 95 is intended for use and/or distribution solely within fib National Member Groups.

Figure 4 contains the associated input data for the design of rectangular cross sections: Geometry, material data and stress-strain-relations for tension and compression are chosen by the user. The same holds true for the restrictions concerning all three aims of design, bending, shear and crack limitation. Thus, the internal forces, the fraction of reinforcement in compression (A_{s2}/A_{s1}) or a limited height of the compressive zone must be pre-set.

Bending design - with steel fibres

F_{cd} [MN]	0,3247	a [m]	0,0246	Strain distribution [‰]	
F_{fd} [MN]	0,0506	z_f [m]	0,2802	**$-3{,}5 \le \varepsilon^f_c \le 0$**	**-3,377**
F_{s1d} [MN]	0,2741	z_{s1} [m]	0,4254	ε_{s2}	-0,539
F_{s2d} [MN]	0,0000	z_{s2} [m]	-0,0254	ε_{s1}	22,162
N^f_{Rd} [kN]	**0,00**	**M^f_{Rd} [kNm]**	**129,54**	**$0 \le \varepsilon^f_{ct} \le 25$**	**25,000**
σ_{s1d} [MN/m²]	453,82	σ_{s2d} [MN/m²]	-107,84	$\lvert M_{Ed,it}-M^f_{Rd}\rvert$	1847,134
A^f_{s1} [cm²]	6,04	A^f_{s2} [cm²]	0,00	$\lvert M_{Ed}-M^f_{Rd}\rvert$	0,000
		with steel fibres A^f_s [cm²] =	**6,04**	$\lvert N_{Ed}-N^f_{Rd}\rvert$	0,000
		$A^f_{s,min}$ [cm²]	1,47		
		decisive	6,04	Accuracy	0,010

Equilibrium?		ξ [-]	0,1322	κ^f_G [-]	1,0900
yes		$M_{Ed,it}$ [kNm]	1976,67	A_{s2} [cm²]	-

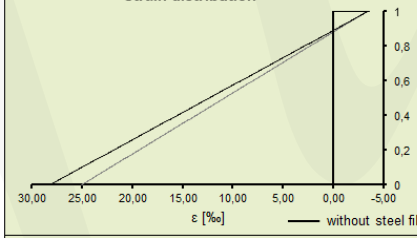
Figure 5: Internal calculations

Output

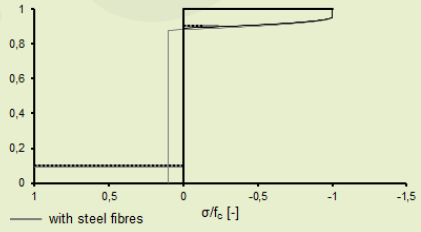
Results - Bending design

M_{Ed} / $M^f_{Ed,it}$	129,54 kNm	N_{Ed}	0 kN	$M_{Ed,it}$	kNm		with steel fibres	without steel fibres
	with steel fibres	without steel fibres				ε_c [‰]	-3,38	-3,49
x	0,0595 m	0,0551 m				ε_{s2} [‰]	-0,54	-0,33
z	0,4254 m	0,4271 m				ε_{s1} [‰]	22,16	25,00
erf. A_{s1}	6,04 cm²	6,64 cm²				ε_{ct} [‰]	25,00	28,17
erf. A_{s2}	0,00 cm²	0,00 cm²				Found equilibrium?	yes	yes
$A_{s,min}$	1,47 cm²	2,38 cm²				**without steel fibres erf. $A_{s,ges}$ [cm²] =**		**6,64**
						with steel fibres erf. $A^f_{s,ges}$ [cm²] =		**6,04**
strain level	**2-4**					**percentage of saved reinforcement**		**9,10%**

Strain distribution



Stress distribution



Notice for the stress distribution: For area of compression σ/f_{cd}; for area of tension σ/f_{ctm}

Results - Shear design

V_{Ed} [kN]	74,02	N_{Ed} [kN]	0,00
Pressure strut		fulfilled	
a_{sw} mathematically required?		no	
Tension strut			
cot(θ) [-]	3,000	$f^f_{ctR,u}$ [N/mm²]	0,4235
erf. a_{sw} [cm²/m]	0,00	erf. a^f_{sw} [cm²/m]	0,00
$a_{sw,min}$ [cm²/m]	3,71	$a^f_{sw,min}$ [cm²/m]	0,32
	decisive		decisive
without steel fibres erf. $a_{s,w}$ [cm²/m] =			**3,71**
with steel fibres erf. a^f_{sw} [cm²/m] =			**0,00**
percentage of saved reinforcement			**100,00%**

Results - Limitation of crack width

σ_s [N/mm²]	180,61		$f_{ct,eff}$ [N/mm²]	3,00
α_f [-]	0,1408			
w^f_k [mm]	0,09	<	$w_{k,gew.}$ [mm]	0,30
w_k [mm]	0,13	<	$w_{k,gew.}$ [mm]	0,30
$f^f_{cflk,i}$ [N/mm²]	2,10		required LK	-
$d^f_{s,lim}$ [mm]	-		$d_{s,gew.}$ [mm]	14
$d_{s,lim}$ [mm]	-		$d_{s,gew.}$ [mm]	14
$A^f_{s,min}$ [cm²]	-		$A_{s,min}$ [cm²]	-
percentage of saved reinforcement				-
percentage of minor crack widths				**26,18%**

Figure 6: Output mask for the results of the example

In Figure 5 a detail of the spreadsheet containing the parameters required for optimisation is displayed. It summarizes all resulting internal forces inter alia F_{fd} obtained from the analytically calculated bearing capacity of steel fibres that are updated in each iteration. If equilibrium is

This document is the intellectual property of the fib – International Federation for Structural Concrete. All rights reserved.
This PDF of fib Bulletin 95 is intended for use and/or distribution solely within fib National Member Groups.

finally fulfilled and the accuracy reached, the results are displayed on the output data sheet (Figure 6). For the example, one reads-off rebar savings of nearly 10 % in bending design, while shear design with fibres does not need reinforcement at all.

6 Conclusions and consequences for practical applications

1) Economic designs of SFRC members require specific non-linear evaluations of sectional forces like the yield line theory, iterative design tools to cover additive bearing abilities of fibres on the cross sectional level and optimisations of pre-set guesses of fibre class needs. The presented tools comprise all these three aspects.
2) On the one hand, classical forward-oriented cross sectional design can be realised by specifying the fibre class as an input. On the other hand, the required fibre class can be determined from a pre-scribed crack-width. Moreover, the fibre class for bedded slabs can be optimized and adapted to corresponding structural boundary conditions.
3) The tool is implemented into the most popular spreadsheet analysis tool recently available and is thus intuitively operated and due to commented figures and parameters user-friendly.
4) The implemented calculation runs stable and takes only a few seconds for computation. Simultaneously, results and output are calculated and displayed with a high accuracy.
5) Adaptations to other arbitrary standards are easily possible due to a general formulation of calculation tasks. The bending design is free of specific code regulations and thus just bases on the assumption of plane strains and processes arbitrary uniaxial stress-strain laws.

7 References

The Concrete Society (2013): *Technical report/Concrete Society. Vol. 34: Concrete industrial ground floors: A guide to design and construction*. 3rd ed.

DAfStb-Guideline (2013) *Steel Fibre Reinforced Concrete*. Deutscher Ausschuss für Stahlbeton (DAfStb).

DIN EN 1992-1-1 (2011) + NAD (2013) Eurocode 2: *Bemessung und Konstruktion von Stahlbeton- und Spannbetontragwerken, Teil 1-1: Allgemeine Bemessungsregeln und Regeln für den Hochbau*.

Empelmann, M.; Oettel, V.; Cramer, J. (2020): *Berechnung der Rissbreite von mit Stahlfasern und Betonstahl bewehrten Betonbauteilen*, Beton- und Stahlbetonbau 115(2), Ernst & Sohn, Berlin, Germany, pp. 136-145. (DOI 10.1002/best.201900065)

fib (2013): *fib* Model Code for concrete structures 2010, Federation internationale du beton (*fib*), Ernst & Sohn, Berlin, Germany.

Gaganelis, G.; Mark, P. (2019): *Downsizing weight while upsizing efficiency - An experimental approach to develop optimized ultra-light UHPC hybrid beams*, Structural Concrete 20(6), Ernst & Sohn, Berlin, Germany, pp. 1883-1895. (DOI 10.1002/suco.201900215)

Gödde, L.; Strack, M.; Mark, P. (2010-1): *M-N-Interaktionsdiagramme für stahlfaserverstärkte Stahlbetonquerschnitte - Anwendung am Beispiel von Tübbingen*, Beton- und Stahlbetonbau 105(5), Ernst & Sohn, Berlin, Germany, pp. 318-323. (DOI 10.1002/best.201000008)

This document is the intellectual property of the fib – International Federation for Structural Concrete. All rights reserved.
This PDF of fib Bulletin 95 is intended for use and/or distribution solely within fib National Member Groups.

Gödde, L.; Strack, M.; Mark, P. (2010-2): *Bauteile aus Stahlfaserbeton und stahlfaserverstärktem Stahlbeton – Hilfsmittel für Bemessung und Verformungsabschätzung nach DAfStb-Richtlinie „Stahlfaserbeton“*, Beton- und Stahlbetonbau 105(2), Ernst & Sohn, Berlin, Germany, pp. 78-91. (DOI 10.1002/best.200900067)

Gödde, L.; Mark, P. (2015): *Numerical simulation of the structural behaviour of SFRC slabs with or without rebar and prestressing*, Materials & Structures 48(6), pp. 1689-1701. (DOI 10.1617/s11527-014-0265-z)

Heek, P.; Tkocz, J.; Thiele, C.; Vitt, G.; Mark, P. (2015): *Fasern unter Feuer - Bemessungshilfen für stahlfaserverstärkte Stahlbetondeckenplatten im Brandfall*, Beton- und Stahlbetonbau 110(10), Ernst & Sohn, Berlin, Germany, pp. 656-671. (DOI 10.1002/best.201500046)

Heek, P.; Mark, P. (2016): *Zur Ermüdung von Beton und Stahlfaserbeton, Beton- und Stahlbetonbau* 111(4), Ernst & Sohn, Berlin, Germany, pp. 221-232. (DOI 10.1002/best.201500054)

Heek, P.; Ahrens, M. A.; Mark, P. (2017-1): *Incremental-iterative model for time-variant analysis of SFRC subjected to flexural fatigue*, Materials & Structures 50: 62. (DOI 10.1617/s11527-016-0928-z)

Heek, P.; Look, K.; Minelli, F.; Mark, P.; Plizzari, G. (2017-2): *Datenbank für querkraftbeanspruchte Stahlfaserbauteile – Bewertung der Bemessungsansätze nach DAfStb-Richtlinie und fib Model Code 2010*, Beton- und Stahlbetonbau 112(3), Ernst & Sohn, Berlin, Germany, pp. 144-154. (DOI 10.1002/best.201600075)

Heek, P.; Tkocz, J.; Mark, P. (2018): *A thermo-mechanical model for SFRC beams or slabs at elevated temperatures*, Materials & Structures 51:87. (DOI 10.1617/s11527-019-1340-2)

Landler, J.; Fischer, O. (2019): *Steigerung der Durchstanztragfähigkeit und Duktilität durch die Zugabe moderner Hochleistungsstahlfasern*, Beton- und Stahlbetonbau 114(9), Ernst & Sohn, Berlin, Germany, pp. 663-673. (DOI 10.1002/best.201900025)

Look, K.; Heek, P.; Mark, P. (2019): *Stahlfaserbetonbauteile praxisgerecht berechnen, bemessen und optimieren*, Beton- und Stahlbetonbau 114(5), Ernst & Sohn, Berlin, Germany, pp. 296-306. (DOI 10.1002/best.201800097)

Mark, P. (2003): *Optimierungsmethoden zur Biegebemessung von Stahlbetonquerschnitten*, Beton- und Stahlbetonbau 98(9), Ernst & Sohn, Berlin, Germany, pp. 511-519. (DOI 10.1002/best.200302240)

Meyerhof, G. G. (1962): *Load-carrying capacity of concrete pavements*, Journal of the Soil Mechanics and Foundations Division 88(3), pp. 89-116.

Plückelmann, S.; Breitenbücher, R.; Smarslik, M.; Mark, P. (2019): *Aufnehmbare Teilflächenspannung von hochfestem Stahlfaserbeton*, Beton- und Stahlbetonbau 114(9), Ernst & Sohn, Berlin, Germany, pp. 653-662. (DOI 10.1002/best.201900015)

Rilem Technical Committees: Rilem TC 162-TDF (2003): *Test and design methods for steel fibre-reinforced concrete, final recommendation: σ–ε design method*. Materials and Structures, Rilem, 36(8), pp. 560–567, (DOI 10.1007/BF02480834).

Schmitz, U. P. (2013): *Anwendung der Bruchlinientheorie*, Stahlbetonbau aktuell 2013, Bauwerk Beuth, pp. C.56–C.64.

Smarslik, M.; Mark, P. (2019): *Hybrid reinforcement design of longitudinal joints for segmental concrete linings*, Structural Concrete 20(6), Ernst & Sohn, Berlin, Germany, pp. 1926-1940. (DOI 10.1002/suco.201900081)

This document is the intellectual property of the fib – International Federation for Structural Concrete. All rights reserved.
This PDF of fib Bulletin 95 is intended for use and/or distribution solely within fib National Member Groups.
FRC2018: Fibre Reinforced Concrete: from Design to Structural Applications
Joint ACI-*fib*-RILEM International Workshop

FRCcalc - Software for design of fiber reinforced concrete elements according to MC2010 recommendations

Tiago Valente[1], Joaquim Barros[2] and Lúcio Lourenço[1]

[1] : CiviTest, Pesquisa de Novos Materiais para a Engenharia Civil, Lda., V. N. de Famalicão, Portugal.

[2] : University of Minho, Guimarães, Portugal.

Abstract

A new software, denominated *FRCcalc*, was developed for the analysis and design of fiber reinforced concrete (FRC) members based on the recommendations and design guidelines of MC2010. The software can be used to perform ultimate and serviceability limit state safety verifications of FRC structural members with and without conventional steel reinforcements, submitted to bending and shear. A main feature of the software is the possibility to run a comparative analysis of the structural performance between FRC and reinforced concrete (RC) cross sections.

Two examples of the analysis of FRC and RC cross sections using *FRCcalc* are presented. The first example explores the use of fiber reinforcement in members for increased structural performance and as a total or partial replacement of conventional steel reinforcement. In the second example, the accuracy of the software is assessed by comparing the flexural response of a FRC shallow beam predicted by *FRCcalc* with experimental and analytical results available in the literature.

Keywords

FRC design, MC2010, software, flexural, shear, crack width, crack spacing.

This document is the intellectual property of the fib – International Federation for Structural Concrete. All rights reserved.
This PDF of fib Bulletin 95 is intended for use and/or distribution solely within fib National Member Groups.

1 Introduction

The final version of *fib* Model Code 2010 (MC2010) [1], published in 2013, covers the design guidelines and recommendations for the design process of fiber reinforced concrete (FRC) structural members, namely how to determine the constitutive laws for FRC, and the methods for evaluation of the flexural and shear resistance of cross sections and crack control analysis.

The manual application of the design recommendations and guidelines can be too cumbersome in the design of complex structures, as the design of FRC members introduces concepts that can be new for some structural designers. As an example, a structural characteristic length of the FRC member is required for the definition of the constitutive laws of the FRC, which is dependent on the reinforcement distribution in the cross section and on the actions in the FRC member. In the design of a real FRC structure, this process can be very tedious, if performed manually.

A software capable of automating the safety verifications of FRC members according to the design recommendations of MC2010 can represent a very useful tool in the design process of structures, giving possibility of quickly compare several reinforcement solutions for technical and cost competitive assessment [2], [3].

2 Software for design of FRC members

Based on the MC2010 design recommendations and guidelines, a new software was developed to assist and automate the verifications of FRC members for serviceability (SLS) and ultimate limit state (ULS) conditions. The software, denominated *FRCcalc*, was developed to perform the analysis of rectangular cross sections with or without conventional passive steel reinforcements, submitted to axial, bending and shear forces.

A main feature of the software is the possibility to run a comparative analysis between FRC and reinforced concrete (RC) cross sections, which was implemented to assess the technical and economic attributes provided by the use of fiber reinforcement as a total or partial replacement of conventional reinforcement.

FRCcalc allows to perform the following analysis: (i) ultimate flexural capacity of FRC and RC members; (ii) evaluation of the moment *vs.* curvature relationship of FRC and RC members at ULS; (iii) ultimate shear capacity of FRC and RC members; (iv) evaluation of design crack width of FRC and RC members at SLS; (v) determination of moment *vs*. design crack width relationship of FRC and RC members at SLS; (vi) evaluation of stress limitation criteria of FRC and RC members at SLS.

In the analysis of the flexural response of FRC and RC cross sections it is assumed that the cross section remains plane after bending and the shear deformation can be ignored. The set of equilibrium and compatibility equations of a generic rectangular cross section, composed of FRC with longitudinal conventional reinforcements can be obtained in accordance to Figure 1.

FRCcalc allows to discretize two sets of top and bottom steel conventional reinforcements. Due to the presence of conventional steel reinforcements, the tensile zone of the cross section is divided in two parts, one with a height equal to the effective tensile depth, $h_{c,ef}$, and the other

This document is the intellectual property of the fib – International Federation for Structural Concrete. All rights reserved.
This PDF of fib Bulletin 95 is intended for use and/or distribution solely within fib National Member Groups.

corresponding to the depth $y - h_{c,ef}$, here y is the distance from the neutral axis to the most tensioned surface. A structural characteristic length, l_{cs}, must be determined for defining the post-cracking constitutive laws of each zone (due to different ultimate crack opening, w_u, which has a direct influence on the l_{cs}). If no conventional tensile reinforcement is applied, the division of the cross section is discarded, and an unique post-cracking stress-strain relationship for the FRC in the cross section is considered (l_{cs} is equal to the depth of the cross section).

Due to the dependence of the effective tensile height on the position of the neutral axis, during the analysis of the flexural response of a cross section of beams and slabs the value of $h_{c,ef}$ is not constant and is updated in each iteration of the analysis.

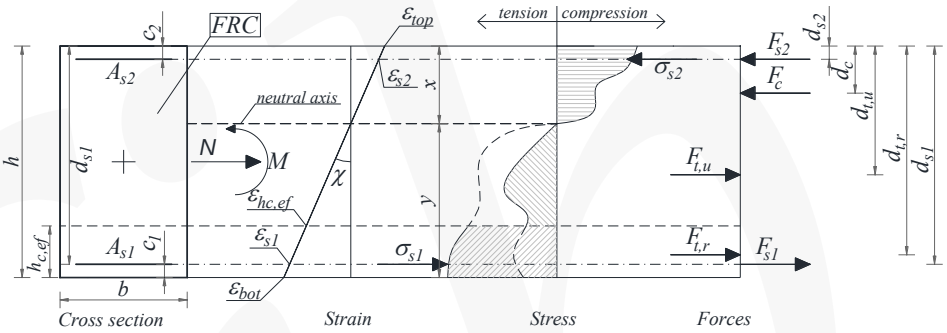


Figure 1: Generic rectangular FRC cross section for determination of moment-curvature relationship.

In order to simulate the behavior of FRC, plain concrete and conventional steel reinforcements in the cross section, the constitutive models available in MC2010 were implemented in *FRCcalc*.

For the compressive behavior of plain concrete and FRC, the bilinear compressive stress-strain law (Figure 7.2-10 of MC2010) is considered.

For the tensile behavior of steel reinforcements, the elastic-perfectly plastic model (Figure 7.2-15 of MC2010) is adopted.

To simulate the tensile behavior of FRC, it is assumed that the pre-peak stage has a similar response to plain concrete (Fig. 5.1-4 of MC2010). For the post-peak stage, the constitutive model to be adopted depends on the limit state verification. For ULS verification it is considered the linear model (Figure 5.6-7 of MC2010), adopting the structural characteristic length to convert the concept of crack opening in tensile strain. The complete stress-strain relationship for FRC in tension for ULS analysis is presented in Figure 2.

For the verification of the SLS conditions, one of the three stress-strain models presented in MC2010 (Figure 3) is applicable.

To estimate the ultimate shear capacity of FRC members both shear resistance models presented in MC2010 can be used in *FRCcalc*: the one where fiber reinforcement contribution is empirically considered by using the residual flexural strength (Equation 7.7-5 of MC2010); and the model based on the simplified modified compression field theory (SMCFT) (Equation 7.7-7 of MC2010).

This document is the intellectual property of the fib – International Federation for Structural Concrete. All rights reserved.
This PDF of fib Bulletin 95 is intended for use and/or distribution solely within fib National Member Groups.

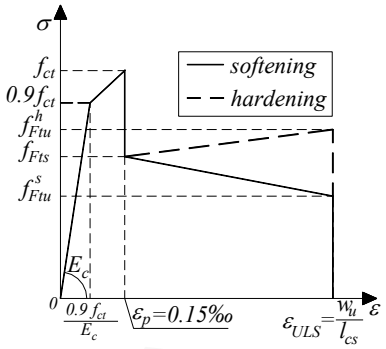


Figure 2: Tensile stress-strain diagram for ULS analysis of FRC.

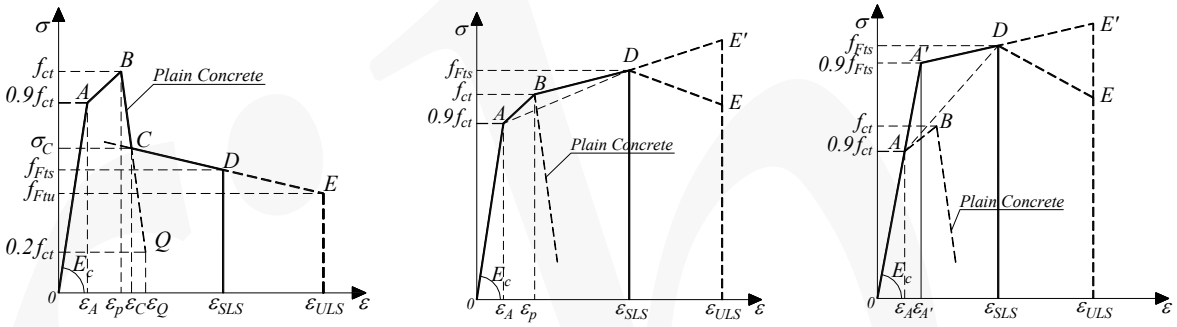


Figure 3: Tensile stress-strain diagrams for SLS analysis of FRC: (a) Case I; (b) Case II; (c) Case III.

The application of the SMCFT model resorts to the concept of the direct tensile strength of the FRC. Since MC2010 does not provide any guideline to estimate this property based on the toughness and strength classes of FRC, in *FRCcalc* is adopted the expression proposed by [4,5] to estimate the characteristic value of the post-cracking tensile stress of FRC, namely:

$$f_{Tk}(w) = k_G \min\left(0.4 f_{R2k} + 1.2\left(f_{R4k} - f_{R2k}\right)\xi(w),\ f_{ctk,\min}\right) \tag{1}$$

$$\xi(w) = \alpha w - 0.25 \tag{2}$$

The factor k_G in Equation (1) takes into account fiber alignment due to casting bias and wall-effect influence that occurs in the prism bending test. In Table 1 is presented the value of k_G considering the different prism bending test standards. The value of factor α in Equation (2) also depends on the prism bending test configuration and is presented in Table 1.

Table 1: Value of k_G and α depending on prism bending test standards [4].

Prism bending test standard	k_G	α
ASTM 1609 [6]	0.70	1/3
EN 14651 [7]	0.60	5/12
RILEM TC 162-TDF [8]	0.60	5/12
UNI 11039 [9]	0.60	43/84

For design situation where it is only prescribed the toughness and strength class of the FRC, it is possible to estimate the characteristic values of the residual flexural strength f_{R2k} and f_{R4k}, based on the following relationships [10], [11]:

This document is the intellectual property of the fib – International Federation for Structural Concrete. All rights reserved.
This PDF of fib Bulletin 95 is intended for use and/or distribution solely within fib National Member Groups.

$$f_{Rik} = k_1 \left(V_f \cdot \frac{l_f}{d_f} \right)^{k_2} \quad \dots \; i = 1,...,4 \tag{3}$$

where $k_1 = 7.5; 6.8; 6.0; 5.5$ and $k_2 = 0.80; 0.75; 0.70; 0.65$. Considering the value of f_{R1k} and f_{R3k} defined by the toughness class, it is possible to determine an average value for the factor $V_f l_f / d_f$, which is then considered to estimate f_{R2k} and f_{R4k} based on Eq. (3).

The SMCFT and the empirical models implemented in *FRCcal* were applied in an extended version of a shear tests database [12], and both exhibited satisfactory agreement with the shear tests results (average test to model prediction ratio was equal to 1.26 for both models, with a coefficient of variation equal to 20% for the SMCFT model and to 18% for the empirical model) [13].

The contribution to the shear resistance provided by the presence of conventional transverse steel reinforcement in a FRC cross section is only considered in the SMCFT model, and it is determined following the Level II approximation presented in §7.3.3.3 of MC2010. For RC cross sections, the shear resistance is determined in compliance with §7.3.3 of MC2010, namely the Level II approximation for members with transverse reinforcements.

The crack control assessment of FRC and RC members is determined according to §7.6.4 and §7.7.4.2 of MC2010.

Additionally, the *FRCcalc* also performs the stress limitation criteria at SLS by following the recommendations of §7.6.3 and §7.7.4.1 of MC2010.

FRCcalc was developed in Visual Basic for Application programming language and can be used in Microsoft Office Excel. The nonlinear system of equations for the analysis of the flexural and shear capacity of the cross section are iteratively solved resorting to the Microsoft Office Excel Solver algorithm [14].

The user interface window of the software is presented in Figure 4, where the geometry of the cross section and material properties data are inputted, as well as the type of analysis to be conducted (ULS and/or SLS).

The outputs of *FRCcalc* are presented in the form of a datasheet and graphs, namely: (i) structural characteristic length of the FRC cross section; (ii) maximum resisting bending moment of the FRC and RC cross sections; (iii) ultimate shear resistance of the FRC and RC cross sections; (iv) plot of the resisting moment *vs*. curvature of the FRC and RC cross sections; (v) design crack width and mean crack spacing of the FRC and RC cross sections; (vi) plot of the moment *vs.* design crack width of the FRC and RC cross sections; (vii) assessment of stress limitation at SLS for FRC and RC cross sections.

This document is the intellectual property of the fib – International Federation for Structural Concrete. All rights reserved.
This PDF of fib Bulletin 95 is intended for use and/or distribution solely within fib National Member Groups.

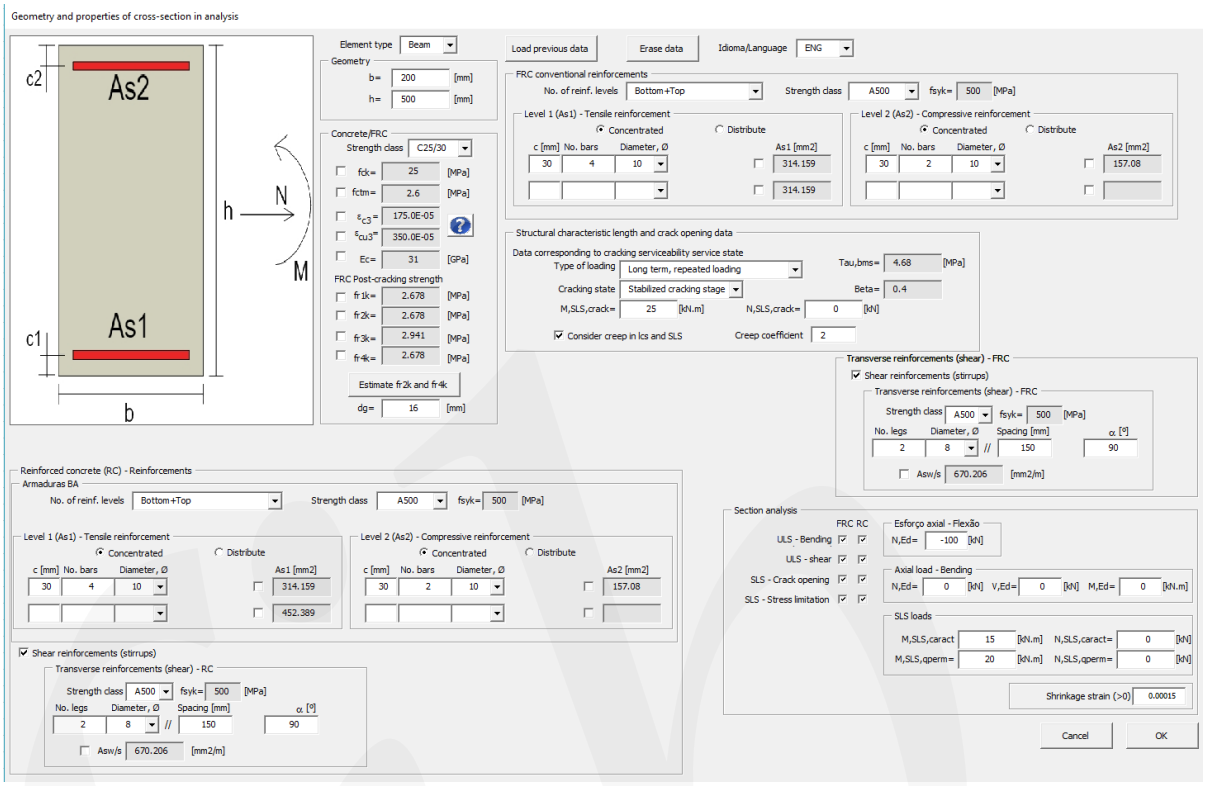
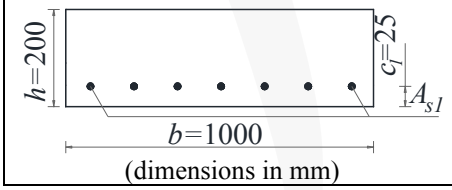


Figure 4: User interface window of the software.

3 Design examples

In the present section are presented two FRC structural members to be designed according to the MC2010 recommendations, by using the developed software, *FRCcalc*.

The first example corresponds to a slab submitted to bending and shear without axial force, where the possibility of partial replacement of conventional steel reinforcement by the addition of fibers to concrete is evaluated. The main properties of the cross section of the member are presented in Figure 5.



FRC:	**RC:**
C25/30 | 3b | ($f_{R1k} = 3.0MPa$ | $f_{R3k} = 2.1MPa$) | $d_g = 16mm$ | $\varphi_c = 0$ (creep factor) $A_{s1} = 251.327mm^2 (Ø8 / /200mm)$ A500NR Data for calculate l_{cs} : $M_{Ed,SLS,crack} = 18.0kN.m/m$	**RC:** C25/30 | $d_g = 16mm$ | $\varphi_c = 0$ | $A_{s1} = 392.699mm^2$ $(Ø10 / /200mm)$ A500NR

Figure 5: Example no. 1 data.

The moment *vs.* curvature relationships for the FRC and RC cross sections are presented in Figure 6a. The structural characteristic length of the FRC cross section presents the following

This document is the intellectual property of the fib – International Federation for Structural Concrete. All rights reserved.
This PDF of fib Bulletin 95 is intended for use and/or distribution solely within fib National Member Groups.

values: l_{cs}^{r} =134mm and l_{cs}^{u} =144mm, where l_{cs}^{r} and l_{cs}^{u} is the structural characteristic length in the effective tensile zone and in the remaining part of the cross section, respectively.

The design shear resistance of the FRC and RC members are, respectively, $V_{Rd}^{FRC} = 172.22kN$ and $V_{Rd}^{RC} = 121.54kN$, which represents a 42% increase of the shear strength of the cross section provided by the use of fiber reinforcement. The presented FRC shear resistance was determined according to the model based on the SMCFT theory, considering that $V_{Ed,ULS} = 35kN/m$, $M_{Ed,ULS} = 10kN.m/m$, and estimating that $f_{R2k} = 2.55MPa$ and $f_{R4k} = 2.35MPa$.

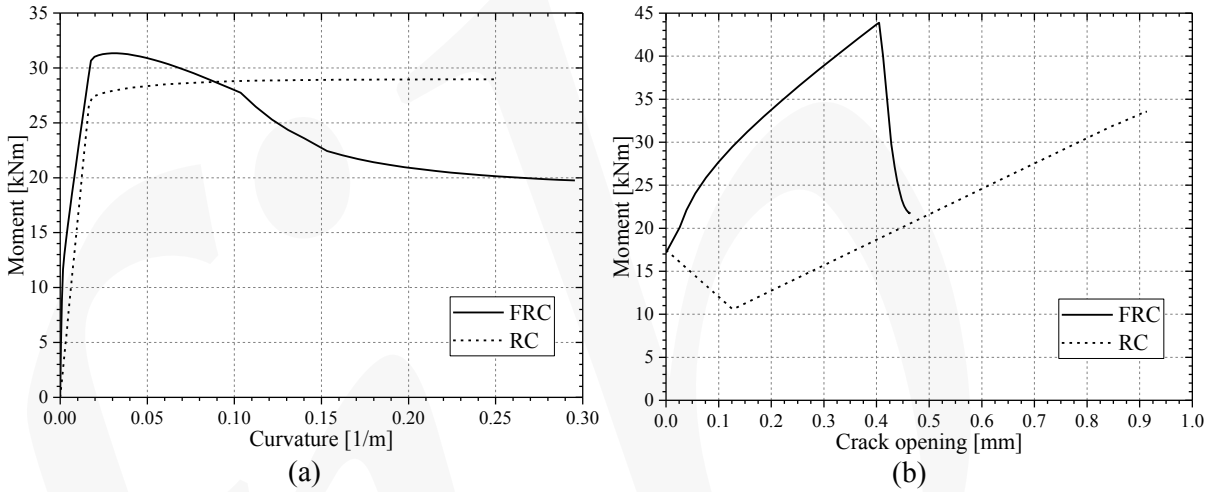


Figure 6: Results of example no.1 slab: (a) Bending moment vs. curvature relationship at ULS conditions; (b) Design crack width vs. resisting bending moment relationship at SLS conditions.

The relationship between the design crack width and the acting bending moment in the slab evaluated at SLS conditions is presented in Figure 6b. For the load combination corresponding to the cracking serviceability criteria ($M_{Ed,SLS,crack} = 18.0kN.m/m$), the FRC member presents a design crack width equal to w_d^{FRC} =0.02mm and a mean crack spacing of s_{rm}^{FRC} =91mm, while the RC member presents a design crack width value of w_d^{RC} =0.38mm and a mean crack spacing of s_{rm}^{RC} =323mm, corresponding to a 20x reduction of the design crack width provided by the use of fiber reinforcements. For a crack width corresponding to the minimum and maximum value of crack opening commonly adopted in the SLS verifications, the resisting bending moment of the FRC cross section is considerably higher than the RC cross section (2.3x higher for $w = 0.1mm$ and 2.4x for $w = 0.3mm$).

The stresses in the cross section for the verification of the MC2010 serviceability stress limitation criteria are presented in Table 2, considering that the acting bending moment for the quasi-permanent load combinations is $M_{Ed,SLS,qperm} = 15kN.m/m$ and for the characteristic load combination is $M_{Ed,SLS,char} = 28kN.m/m$. It can be seen that the use of fiber reinforcement provides a decrease of the stresses in the cross section when compared to the performance of a RC cross section, especially for the steel bars. For the RC cross section the stress limitation criteria defined in MC2010 is not verified for the tensile stress of the steel bars.

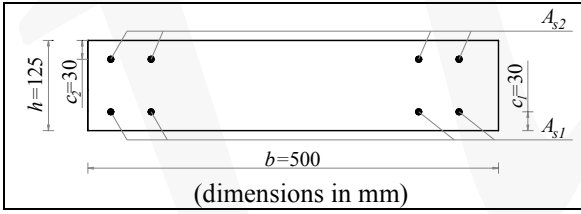
This document is the intellectual property of the fib – International Federation for Structural Concrete. All rights reserved.
This PDF of fib Bulletin 95 is intended for use and/or distribution solely within fib National Member Groups.

Table 2: Verification of stress limitation criteria for Example no.2 slab.

Concrete compressive stress			
Stress		Limit	Result
$\sigma_{c,FRC}^{SLS,char} = 6.83MPa$	$\leq$	$0.6 \cdot f_{ck}(t=28) = 15MPa$	Verified
$\sigma_{c,RC}^{SLS,char} = 8.92MPa$	$\leq$	$0.6 \cdot f_{ck}(t=28) = 15MPa$	Verified
$\sigma_{c,FRC}^{SLS,qperm} = 2.70MPa$	$\leq$	$0.4 \cdot f_{ck}(t=28) = 10MPa$	Verified
$\sigma_{c,RC}^{SLS,char} = 5.74MPa$	$\leq$	$0.4 \cdot f_{ck}(t=28) = 10MPa$	Verified
Steel tensile stress			
Stress		Limit	Result
$\sigma_{s,FRC}^{SLS,char} = 145.56MPa$	$\leq$	$0.8 \cdot f_{yk} = 400MPa$	Verified
$\sigma_{s,RC}^{SLS,char} = 439.87MPa$	$>$	$0.8 \cdot f_{yk} = 400MPa$	Not verified
FRC tensile stress			
Stress		Limit	Result
Not applicable: $f_{Ftsk} < f_{ctk}$			Verified

The second example corresponds to a polypropylene FRC shallow beam that was studied in [15], which was submitted to four point bending loading configuration in order to experimentally derive the flexural response of the member. In addition, the author also estimated the moment *vs.* curvature relationship of the FRC beam according to the MC2010 guidelines. The main properties of the cross section are presented in Figure 7.

In order to predict the flexural response of the beam, were conducted two analysis in *FRCcalc* considering two sets of values for the mechanical properties of the materials: a) characteristic values, with unitary values of the partial safety factors; b) design values with the partial safety factors of $\gamma_c = 1.50$, $\gamma_F = 1.50$ and $\gamma_s = 1.15$.



FRC:
C35/45 | FRC: $f_{R1k} = 2.14MPa$ | $f_{R3k} = 3.21MPa$
$A_{s1} = 113.10mm^2(4Ø6)$ | $f_{yk} = 550MPa$
$A_{s2} = 113.10mm^2(4Ø6)$ | $f_{yk} = 550MPa$

Figure 7: Cross section data of example no. 2.

The moment *vs.* curvature relationship of FRC beam obtained from *FRCcalc* and the results published by di Prisco *et al.* [15] are presented in Figure 8. It is possible to observe that the curve that considers characteristic values of the material properties, (charact. values), is very similar to the analytical response determined in [15]. In addition, it also presents a satisfactory approximation to the experimental results (the ratio between the predicted and the experimental ultimate bending resistance is equal to 87%). As it is expected, when design values of set of parameters are considered (design values), a reduction of the flexural capacity of the beam is obtained, and a ratio between the predicted and experimental ultimate bending resistance equal to 68% is obtained.

This document is the intellectual property of the fib – International Federation for Structural Concrete. All rights reserved.
This PDF of fib Bulletin 95 is intended for use and/or distribution solely within fib National Member Groups.

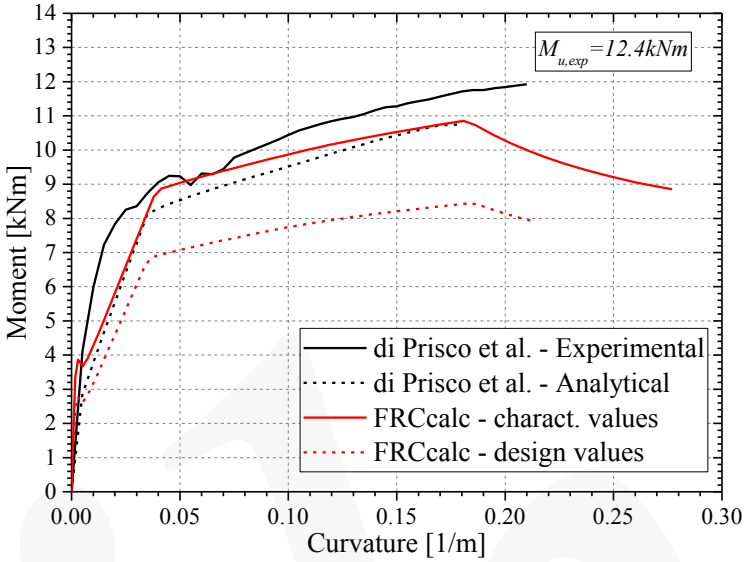


Figure 8: Comparison of the flexural response of FRC shallow beam between results of di Prisco et al.[15] and FRCcalc.

4 Conclusions

In the present work is presented a newly developed software for the design of the FRC cross sections according to MC2010 guidelines and recommendations. A brief description of the models and principles to estimate the flexural, shear and cracking response of FRC members are presented, including some design aspects not covered in MC2010 that were included in the software code. The main features of the software are described, including the ability to perform comparative analysis between FRC and RC cross sections.

Two examples regarding the use of FRC in structural elements are presented: in the first it was demonstrated the possibility of fiber reinforcement to partially replace conventional steel reinforcements. For this particular case, it was demonstrated that FRC member presented a higher ultimate bending and shear resistance and smaller crack spacing and crack width opening in comparison to the member without fiber reinforcement.

In the second example the accuracy of *FRCcalc* to predict the flexural response of FRC members was assessed. The moment *vs.* curvature relationship obtained by *FRCcalc* was very similar to the analytical curve published in the literature, moreover it also presented a good approximation to the experimental results.

Future developments of *FRCcalc* will address the consideration of the prestressed steel bars in the FRC/RC members and the implementation of calculation routines to perform economic studies on the use of fiber reinforcement as a replacement of conventional steel bars.

5 Acknowledgements

The first Author would like to acknowledge the grant SFRH/BDE/96381/2013 co-funded by CiviTest - Pesquisa de Novos Materiais para a Engenharia Civil, Lda. and by FCT - Portuguese Foundation for Science and Technology. The authors also acknowledge the support provided by the FCT project PTDC/ECM-EST/2635/2014.

This document is the intellectual property of the fib – International Federation for Structural Concrete. All rights reserved.
This PDF of fib Bulletin 95 is intended for use and/or distribution solely within fib National Member Groups.

6 References

[1] fib-federation internationale du beton, *fib Model Code for Concrete Structures 2010*. John Wiley & Sons, 2013.

[2] Ronald F. Zollo, "Fiber-reinforced concrete: an overview after 30 years of development," *Cem. Concr. Compos.*, vol. 19, no. 2, pp. 107–122, 1997, doi: 10.1016/S0958-9465(96)00046-7.

[3] A. M. Brandt, "Fibre reinforced cement-based (FRC) composites after over 40 years of development in building and civil engineering," *Compos. Struct.*, vol. 86, no. 1–3, pp. 3–9, Nov. 2008, doi: 10.1016/j.compstruct.2008.03.006.

[4] S. J. Foster, A. Agarwal, and A. Amin, "Design of steel fiber reinforced concrete beams for shear using inverse analysis for determination of residual tensile strength," *Struct. Concr.*, Sep. 2017, doi: 10.1002/suco.201700100.

[5] A. Amin, S. J. Foster, and A. Muttoni, "Derivation of the σ- *w* relationship for SFRC from prism bending tests," *Struct. Concr.*, vol. 16, no. 1, pp. 93–105, Mar. 2015, doi: 10.1002/suco.201400018.

[6] ASTM International, *Standard Test Method for Flexural Performance of Fiber-Reinforced Concrete (Using Beam With Third-Point Loading)*, vol. ASTM C1609. 2012.

[7] European Committee for Standardization, *Test method for metallic fibered concrete - Measuring the flexural tensile strength (limit of proportionality (LOP), residual)*, vol. EN 14651. 2005.

[8] RILEM TC 162-TDF, "Recommendations of RILEM TC 162-TDF: Test and design methods for steel fibre reinforced concrete: bending test," *Mater. Struct.*, vol. 35, no. 253, pp. 579–582, 2002, doi: 0.1617/13884.

[9] Italian Board for Standardization, *Steel Fiber Reinforced Concrete—Part I: Definitions, Classification Specification and Conformity—Part II: Test Method for Measuring First Crack Strength and Ductility Indexes*, vol. UNI 11039. 2003.

[10] Bernardo Nunes de Moraes Neto, "Punching behaviour of flat slabs of steel fibre reinforced concrete submitted to symmetric loading," PhD thesis, Universidade de Brasília, Brasília, Brasil, 2013.

[11] B. N. Moraes Neto, J. A. O. Barros, and G. S. S. A. Melo, "A model for the prediction of the punching resistance of steel fibre reinforced concrete slabs centrically loaded," *Constr. Build. Mater.*, vol. 46, pp. 211–223, Sep. 2013, doi: 10.1016/j.conbuildmat.2013.04.034.

[12] S. J. Foster and A. Argarwal, "Database for testing shear models for SFRC beams and one-way slabs without stirrups," School of Civil and Environmental Engineering, UNSW Sydney, Sydney, Australia, 2017.

[13] T. D. S. Valente, J. A. O. Barros, B. N. Moraes-Neto, and Y. H. Moussa, "Appraisal of MC2010 shear resistance approaches coupled with a residual flexural strength prediction model," *IOP Conf. Ser. Mater. Sci. Eng.*, vol. 596, p. 012004, Aug. 2019, doi: 10.1088/1757-899X/596/1/012004.

[14] *Microsoft Office Excel*. Microsoft.

[15] M. di Prisco, M. Colombo, and I. Colombo, "The role of the structural characteristic length in FRC structures," in *Proceedings of the 9th International Conference on Fracture Mechanics of Concrete and Concrete Structures*, 2016, doi: 10.21012/FC9.308.

This document is the intellectual property of the fib – International Federation for Structural Concrete. All rights reserved.
This PDF of fib Bulletin 95 is intended for use and/or distribution solely within fib National Member Groups.
FRC2018: Fibre Reinforced Concrete: from Design to Structural Applications
Joint ACI-*fib*-RILEM International Workshop

Retrofitting a full-scale two-story hollow clay block masonry building by Steel Fiber Reinforced Mortar coating

Sara S. Lucchini[1], Luca Facconi[2], Fausto Minelli[3], Giovanni A. Plizzari[4]

[1] : Ph.D., Post-doctoral fellow, Department DICATAM, University of Brescia, Italy.

[2] : Ph.D., Assistant Professor, Department DICATAM, University of Brescia, Italy.

[3] : Ph.D., Associate Professor, Department DICATAM, University of Brescia, Italy.

[4] : Professor, Department DICATAM, University of Brescia, Italy.

Abstract

The use of mortar coating reinforced only with randomly diffused steel fibers represents an effective technique for seismic retrofitting of masonry buildings. The present work aims at proving the effectiveness of that technique by testing a full-scale two-story hollow clay block masonry building subjected to a quasi-static cyclic lateral loading. The experimental program includes two tests involving the same building. The first test performed on the building without coating is carried out to pre-damage masonry in order to simulate the effects of a seismic action significant for ultimate conditions. The second test is performed to assess the behavior of the pre-damaged building after retrofitting. The paper presents the main properties and details of both the test building and the proposed retrofitting technique. As the test on the retrofitted specimen is still ongoing, only the main results concerning the unstrengthened building are reported and discussed.

To predict the response of the two experimental tests, 3D non-linear finite element simulations have been carried out and presented in the last section of the paper. The latter includes the comparison between the numerical prediction and the available experimental results.

Keywords

Steel Fiber Reinforced Mortar; Mortar coating; Retrofitting; Hollow block masonry; Cyclic test; Full-scale masonry test.

This document is the intellectual property of the fib – International Federation for Structural Concrete. All rights reserved.
This PDF of fib Bulletin 95 is intended for use and/or distribution solely within fib National Member Groups.

1 Introduction

The high vulnerability of existing masonry buildings to seismic actions have driven the research toward the development of ever new retrofitting techniques as well as the improvement of the traditional strengthening methods. Among the different techniques available (El Gawady et al., 2004; Papanicolaou et al., 2008; Lin et al., 2010), a possible retrofitting method consists in applying fiber reinforced mortar coating on the masonry surface in order to improve both the in-plane (Sevil et al., 2011; Facconi et al., 2018) and the out-of-plane resistance of the structure. The use of fibers randomly distributed in the mortar matrix allows reducing the construction time generally needed for placing conventional reinforcement. Moreover, a further advantage of steel fibers is represented by the possibility of reducing the coating thickness, since the minimum cover requirements for rebars are no longer necessary.

About tests on masonry retrofitted with reinforced coating, the experimental tests reported in the literature (Tomaževič et al., 2009; Gattesco et al., 2015; Dehghani et al., 2015, Facconi et al., 2016; Facconi et al., 2018) generally focus on small structural elements (i.e., walls, spandrels, etc.) tested under quasi static or dynamic conditions. Thus, new research studies should be carried out to better investigate the effect of coating on the global response of full-scale buildings. The present work aims at reducing such a lack of information by investigating the use of Steel Fiber Reinforced Mortar (SFRM) coating to retrofit masonry buildings. A full-scale Un-Reinforced Masonry (URM) building was tested under quasi-static lateral loading conditions. To highlight the structural performances of the proposed retrofitting technique, the structure was built with hollow (voids: 62%) block masonry having a low compressive strength. The experimental study was subdivided into two main stages: the first concerned the test performed to pre-damage the unstrengthened specimen; the second aimed at re-testing the pre-damaged building after the retrofitting work. The first part of the paper presents the main properties of the test specimen and discusses the experimental results provided by the test on the unstrengthened building. As the test on the retrofitted building is still ongoing, the related results will be described and discussed in future research reports. Based on the results of 3D non-linear finite element simulations, the second part of the manuscript shows the predicted response of the building without SFRM coating and with two different retrofit layouts as well as a comparison between the observed and the predicted behavior of the unstrengthened building.

2 Experimental program

2.1 Properties of the full-scale test building and description of the retrofitting technique

In order to assess the ability of the proposed technique to retrofit masonry buildings, a full-scale building was constructed in the laboratory of civil engineering of the University of Brescia. The structure was designed to represent the behavior of an existing building in which floors have a high in-plane stiffness and an effective connection with the bearing walls. Such an assumption aimed both at preventing any out-of-plane mechanism and at promoting a global-type response of the building when subjected to earthquake actions. As shown in Figure 2.1, the structure had a total length of 5750 mm (18.9 ft), a width of 4250 mm (13.9 ft) and a maximum height of 6700 mm (22.0 ft).

This document is the intellectual property of the fib – International Federation for Structural Concrete. All rights reserved.
This PDF of fib Bulletin 95 is intended for use and/or distribution solely within fib National Member Groups.

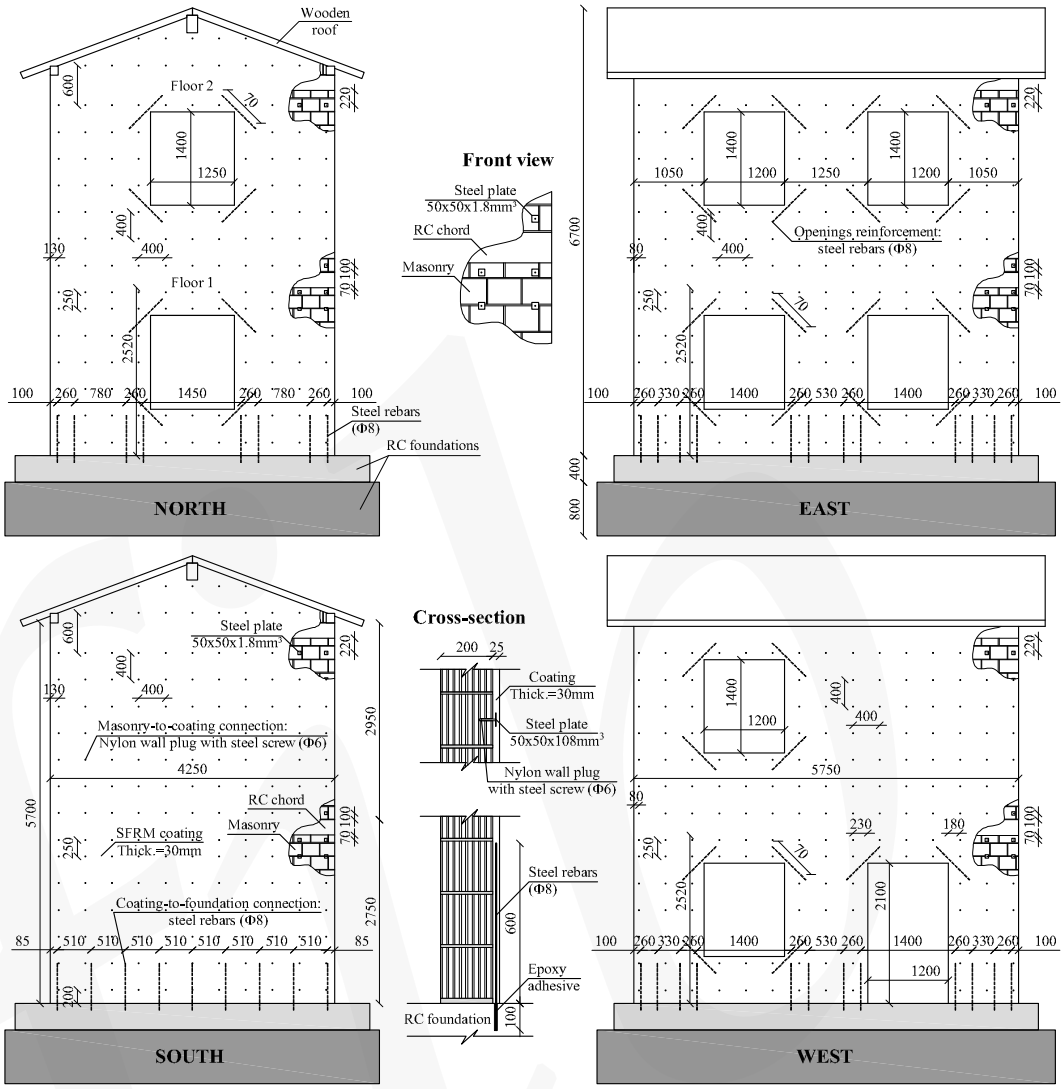


Figure 2.1: Geometry of the full-scale test building and main details of the retrofitting intervention. (dimensions in mm; 1 mm=0.04 in.)

The 200 mm (7.87 in.) thick walls were made of single wythe vertically perforated block masonry. Each floor consisted of 120 mm (4.72 in.) wide and 140 mm (5.51 in.) high wooden joists provided with a 20 mm (0.79 in.) thick wooden plank. A total of twenty 200 mm (7.87 in.) spaced steel dowels (diameter=16 mm [0.63 in.]; length = 130 mm [5.12 in.]) were inserted into pre-drilled holes to connect each joist to the 60 mm (2.36 in.) thick Reinforced Concrete (RC) slab laid on the plank. The 500 mm (19.69 in.) spaced joists were placed perpendicular to the longitudinal walls herein named as East and West façade. A schematic section view of the floors is depicted in Figure 2.2. The RC chords placed at the floor level allowed connecting the simply supported floor (i.e., the joist and the RC slab) with the four walls. The second wooden-concrete floor supported the pitched wooden roof. Finally, all the walls were laid on a strip RC foundation connected to the strong floor by Dywidag bars. After having performed the first test for pre-damaging the building (see section of Figure 2.1), a 30 mm (0.12 in.) thick SFRM coating was applied on the external surface of the four facades in order to improve both the in-plane and the out-of-plane resistance of the walls. As deeply

This document is the intellectual property of the fib – International Federation for Structural Concrete. All rights reserved.
This PDF of fib Bulletin 95 is intended for use and/or distribution solely within fib National Member Groups.

explained in Facconi et al. (2015), the retrofitting technique consists of different application phases that can summarized as follows: 1) a first thin layer of mortar (~5 mm [~0.20 in.] thick) not containing steel fibers is applied by a trowel on the water-wet surface of masonry; 2) a first layer of SFRM (~10 mm [~0.40 in.] thick) is then troweled on the wall surface; 3) coating-to-masonry connectors consisting of a nylon plug with steel screws are drilled into the masonry walls and provided with a 50x50x1.8 mm^3 (1.97x1.97x0.07 in^3) steel anchor plate placed within the coating thickness; 4) conventional reinforcing bars are placed vertically along the base perimeter of the walls to connect coating to the RC foundation. Each rebar has to be inserted into pre-drilled holes and then fixed by epoxy injection. Short straight rebars must be placed closed to the corners of opening to prevent localized cracks; 5) different layers of SFRM are successively troweled on the wall surface until the total required thickness is achieved; 6) once the coating application has been completed, water has to be sprayed on the wall surface at least for 2-3 days to mitigate potential shrinkage cracking.

2.2 Material properties

The single wythe walls of the building were made with hollow clay blocks having dimensions 250x200x190 mm^3 (9.84x7.87x7.48 in^3) and a high percentage of holes (62%) oriented normally to mortar bed joints. The compression tests performed on 32 clay units (16 parallel + 19 perpendicular) according to EN 772-1:2000 provided a mean compressive strength parallel and perpendicular to perforations equal to 12.7 MPa (1840 psi) (CV=13.5%) and 2.5 MPa (360 psi) (CV=10.1%), respectively. A ready-mix commercial cement-lime-send mortar was used to fill the 10 mm (0.39 in.) thick bed and head joints. Flexural and compressive tests performed on 30 40x40x160 mm^3 (1.58x1.58x6.30 in^3) mortar prisms according to EN 1015-11, provided a mean flexural strength of 3.4 MPa (490 psi) (CV=7.2%) and a mean compressive strength of 8.9 MPa (1290 psi) (CV=10.3%). To determine the compressive strength of masonry, whose density was 745 kg/m^3 (46.5 lb/ft^3), a series of uniaxial tests on masonry wallets were carried out according to EN 1052-1: 2001. Specimens with both vertical holes (i.e., perforations parallel to the loading direction) and horizontal holes (i.e., perforations perpendicular to the loading direction) were investigated. The wallets dimensions were 820x510x200 mm^3 (32.28x20.08x7.87 in^3) and 950x590x200 mm^3 (37.4x23.23x7.87 in^3), respectively. The former were characterized by a mean compressive strength of 2.9 MPa (420 psi) (CV=28.8%) and an elastic modulus of 8980 MPa (1300 ksi). The latter presented a mean compressive strength of about 0.6 MPa (90 psi) (CV=22.1%) and an elastic modulus of 1610 MPa (230 ksi). Note that the elastic moduli were calculated as the secant slope of the compressive stress-strain curve from the origin to 1/3 of the peak strength. Diagonal compression tests were also performed on 1200x1200x200 mm^3 (47.24x47.24x7.87 in^3) square panels according ASTM E 519-02: 2002. Those tests provided a mean diagonal tension (shear) strength of 0.26 MPa (40 psi) (CV=24.0%) and a corresponding shear strain of $0.28x10^{-3}$. A ready-mix cement-based commercial mortar was used for constructing the mortar coating applied on the building façades. Mortar was reinforced with 60 kg/m^3 (101 lb/yd^3 - 0.76% by volume) of high-strength double hooked-end steel fibers having a minimum tensile strength of 2800 MPa (400 ksi), a diameter of 0.4 mm (0.016 in.) and a length of 32 mm (1.26 in.) (fiber aspect ratio=80). The obtained SFRM has a density of about 2000 kg/m^3 (124.9 lb/ft^3). Tests performed on 40x40x160 mm^3 (1.58x1.58x6.30 in^3) SFRM prisms according to EN 1015-11 provided a mean flexural strength of 8.8 MPa (1280 psi) (CV=19.2%) and a mean compressive strength of 35.1 MPa (5090 psi) (CV=15.6%). Compressive tests performed on mortar cylinders according EN 12390-13: 2013 provided a mean elastic modulus of 20430 MPa (2960 ksi) (CV=8.4%). The

This document is the intellectual property of the fib – International Federation for Structural Concrete. All rights reserved.
This PDF of fib Bulletin 95 is intended for use and/or distribution solely within fib National Member Groups.

tensile fracture behavior of SFRM was investigated by three-point bending tests (3PBT) on 40(width)x150(height)x500(length) mm^3 (1.58x5.91x19.69 in^3) notched beams performed under CMOD (Crack Mouth Opening Displacement) control. According to EN 14651-5: 2005, the 3PBTs provided the limit of proportionality $f_{L,m}$ and the residual tensile strengths $f_{R1,m}$, $f_{R2,m}$, $f_{R3,m}$, $f_{R4,m}$, summarized in Table 2.1.

Table 2.1: SFRM tensile properties (1 MPa=145 psi)

	$f_{L,m}$	$f_{R1,m}$	$f_{R2,m}$	$f_{R3,m}$	$f_{R4,m}$
Mean [MPa]	3.76	5.8	6.87	6.68	6.09
CV [%]	18.9%	26.6%	26.8%	27.6%	28.2%

2.3 Test set-up and instrumentation

A schematic of the test set-up adopted to perform the cyclic tests is depicted in Figure 2.2.

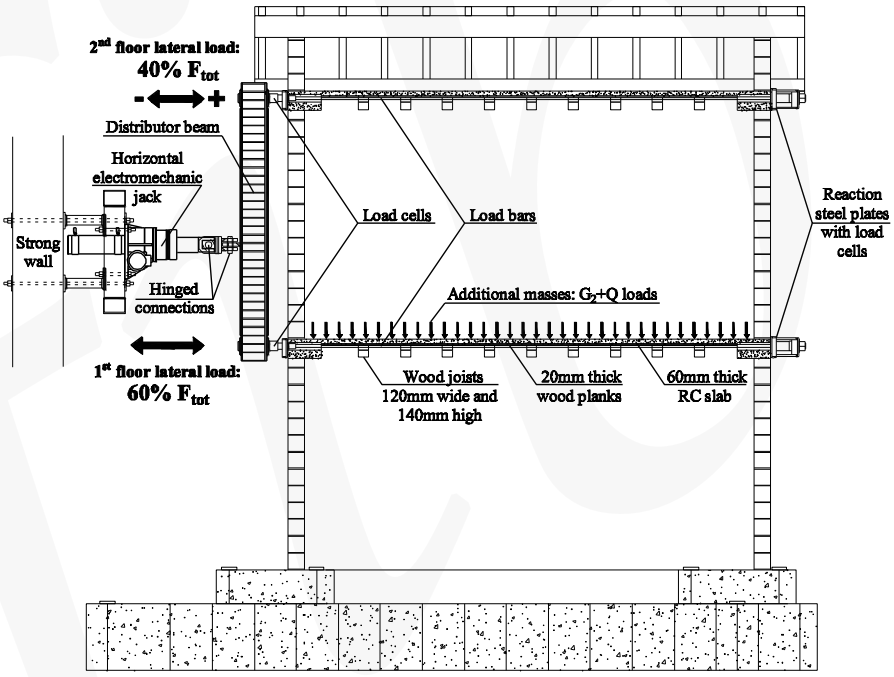


Figure 2.2: Schematic of test set-up (1 mm=0.04 in.)

A 1500 kN (337.2 kip) electromechanic jack fixed to a reaction wall was used to apply the lateral load to the structure. In order to ensure a load distribution proportional to the building masses, a steel distributor beam was designed so that the 60% of the total lateral load was applied to the first floor and the 40% to the second one. Each concentrated load was applied to the floors of the North or South façade by the RC chords running along the short sides of the building. A hinged connection was installed between the jack and the distributor beam to enable relative rotation in the vertical as well as in the horizontal plane. Concrete blocks were spread on the first floor to get a uniformly distributed overload $G_2+0.3\cdot Q$ of =2.6 kN/m^2 (54.3 psf), as required by the Eurocode for the seismic combination. A couple of load cells were connected to the distributor beam to measure the actual lateral loads acting at the two floor levels. A total of 28 potentiometric transducers (Figure 2.3) were installed on the East and

This document is the intellectual property of the fib – International Federation for Structural Concrete. All rights reserved.
This PDF of fib Bulletin 95 is intended for use and/or distribution solely within fib National Member Groups.

West façade of the building to monitor crack formation. Horizontal displacements were detected by the LVDTs placed in correspondence of the floors (i.e., instruments H1SW, H2SW, H1SE and H2SE) and of the slab foundation (i.e., instruments BSW, BNW, BSE, BNE). The quasi-static test was performed under displacement control, by progressively increasing the average top displacement of the building (i.e., average displacement detected by H2SW and H2SE) until the achievement of its maximum capacity.

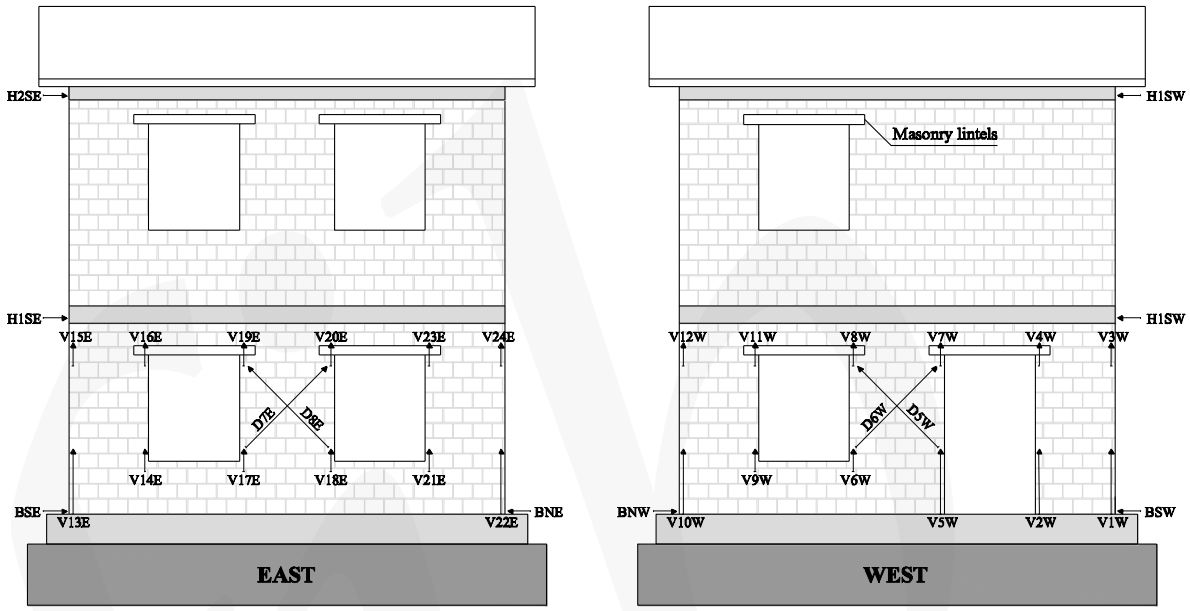


Figure 2.3: Instrumentation set-up

2.4 Results of the test on the not-retrofitted building

The lateral load (V)-displacement (δ) hysteretic curve obtained from the test on the unstrengthened building is plotted in Figure 2.4. Moreover, Table 2.2 reports the main test results related to both the positive (+) and the negative (-) loading direction. In more detail, the initial secant stiffness evaluated in the displacement range 0-0.6 mm (0-0.024 in.) (K^+_s, K^-_s), the lateral load at first cracking (V^+_{crack}, V^-_{crack}) and at peak (V^+_{peak}, V^-_{peak}), the lateral deflection at peak (δ^+_{peak}, δ_{-peak}) and the failure mode have been summarized.

The behavior of the unstrengthened building was governed by in-plane modes, particularly by shear failure of masonry piers. The first part of the response (Figure 2.4) was linear until rocking of the first-story piers occurred at a lateral load of about 120 kN (27 kip). Rocking mechanisms caused a progressive loss of stiffness that led to the attainment of the maximum capacity. The latter was achieved once diagonal cracks formed in the central pier located at the first story of the east wall. After the peak load attained in the positive loading direction, a reduction of the lateral capacity was observed because of the formation of new shear cracks in the slender piers located at the ground floor (Figure 2.5). As the damage observed at the maximum lateral displacement was quite severe, the test was temporarily interrupted to retrofit the specimen. The results of the cyclic test on the retrofitted test building will be presented and discussed in subsequent research reports.

This document is the intellectual property of the fib – International Federation for Structural Concrete. All rights reserved.
This PDF of fib Bulletin 95 is intended for use and/or distribution solely within fib National Member Groups.

Table 2.2: Comparison of the main experimental and numerical results (1 kN/mm=5.625 kip/in.; 1 kN=0.225 kip; 1 mm=0.04 in.)

Type	K^+_S [kN/mm]	K^-_S [kN/mm]	V^+_{crack} [kN]	V^-_{crack} [kN]	V^+_{peak} [kN]	V^-_{peak} [kN]	δ^+_{peak} [mm]	δ^-_{peak} [mm]
Experimental	125	132	120	128	180	179	2.4	3.4
Numerical	127	134	114	112	148	146	1.9	1.8

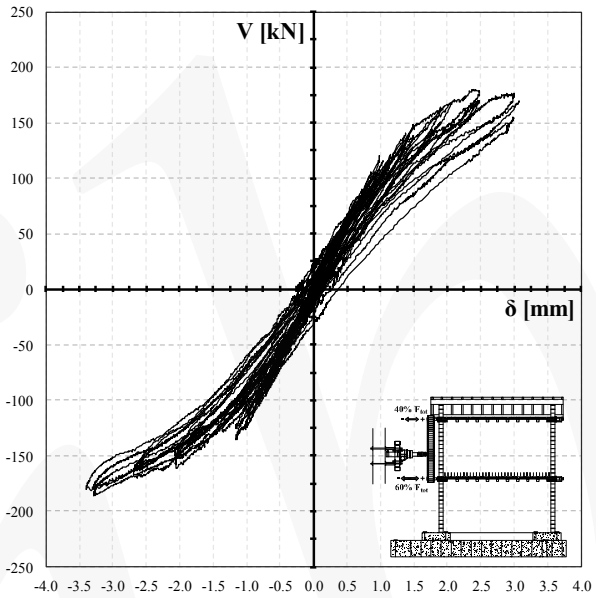


Figure 2.4: Base shear (V) - lateral displacement (δ) response of the unstrengthened building. (1 kN=0.225 kip; 1 mm=0.04 in.)



(a) (b)

Figure 2.5: Experimental crack pattern of East (a) and West (b) façade at ground floor (inner view)

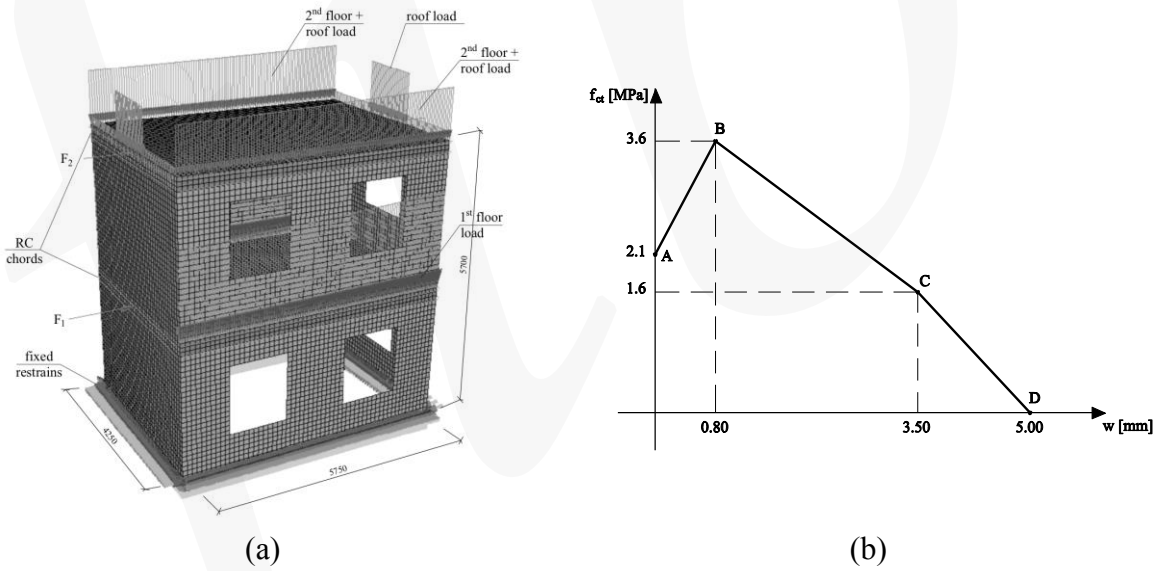
3 Numerical study

A series of Non-Linear Finite Element Analyses (NLFEAs) were carried out to predict the response of the full-scale building before and after retrofitting. The FE model (Figure 3.1a) was implemented in the commercial program DIANA 10.1. The model of the unstrengthened building consisted of 14418 eight-node quadrilateral isoparametric curved shell elements (CQ40S in DIANA code), having 2x2x7 Gaussian integration scheme and an average

This document is the intellectual property of the fib – International Federation for Structural Concrete. All rights reserved.
This PDF of fib Bulletin 95 is intended for use and/or distribution solely within fib National Member Groups.

dimension of 100 mm. To perform the analysis of the retrofitted structure, the regular curved shell elements were replaced with eight-node "layered" curved shell elements (CQ40L in DIANA code), whose "layered" geometry allowed to implement the masonry properties separately from those of coating. As no debonding of coating from masonry surface was generally observed in previous experimental tests (Facconi et al., 2018) carried out by the authors of the present work, the simulations were performed by assuming perfect bond at the mortar-to-coating interface. Reinforcement elements perfectly bonded to concrete/mortar were used to model rebars.

To simulate the fracture behavior of masonry and mortar coating, a smeared crack model based on the "total strain rotating" approach was adopted. The compressive behavior of masonry was represented by a parabolic law depending on the compressive strength f_c and the compressive fracture energy G_c. The Hordijk's model, including the tensile strength f_t and Mode-I fracture energy G^I_f, was chosen for representing the tensile stress-crack width behavior of masonry. The compressive and the tensile strength of the SFRM were represented by the Thorenfeldt model and the tensile stress-crack width law of Figure 3.1(b), respectively. Table 3.1 reports a summary of the mechanical parameters implemented in the model. A Von Mises yield criterion including strain-hardening was adopted for steel rebars connecting the SFRM coating to the building foundation. The yield and the ultimate tensile strength of reinforcing steel were assumed equal to 510 MPa (74.0 ksi) and 610 MPa (88.5 ksi), respectively.



(a) (b)

Figure 3.1: Numerical model: mesh of the full-scale building (a); trilinear curve of SFRM coating (b) (1 mm= 0.04 in.; 1 MPa=145 psi)

Table 3.1: Mechanical properties for building modelling (1 kg/m^3=0.062 lb/ft^3; 1 MPa=145 psi; 1 N/mm=5.625lbf/in.)

	γ [kg/m^3]	E [MPa]	f_c [MPa]	G_c [N/mm]	f_t [MPa]	G^I_f [N/mm]
Masonry	745	2100	3.015	3	0.1	0.01
SFRM	2040	20500	35	-	-	-

This document is the intellectual property of the fib – International Federation for Structural Concrete. All rights reserved.
This PDF of fib Bulletin 95 is intended for use and/or distribution solely within fib National Member Groups.

The simulations include one analysis on the unstrengthened building (MB) and two analyses on the building (MB-R and MB-R+SR) retrofitted with coating. Unlike MB-R, MB-R+SR was provided with steel reinforcing bars to connect coating to the RC foundation (see Figure 2.1). The main numerical results of the analyses are summarized and compared in Table 3.2. The total base shear-lateral deflection response of Figure 3.2(a) highlights the strength and stiffness improvement provided by the proposed technique. The steel rebars used to prevent rocking of the walls, allowed to effectively exploit the tensile toughness of SFRM. Therefore, the lateral capacity of MB-R+SR is approximately two times higher than the one obtained from the building without coating-to-foundation connections (MB-R).

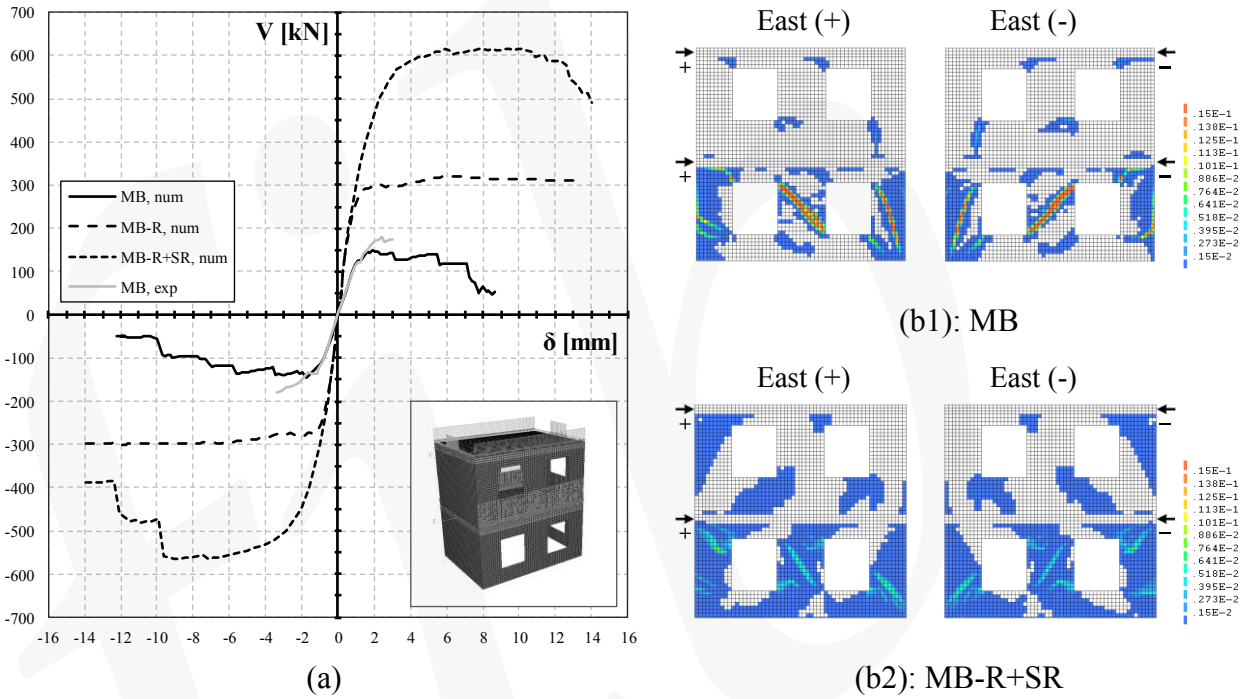


Figure 3.2: Base shear (V) - lateral displacement (δ) curves: comparison between numerical and experimental response (a); contours of principal tensile post-cracking strains of East façades (b1, b2). (1 kN=0.225 kip; 1 mm=0.04 in.)

Figure 3.2(b) shows the comparison between the failure patterns of the East façade before (b1) and after (b2) retrofitting with coating connected to the foundation. The tensile cracking strains are detected on the outer surface of the wall, in correspondence of a top floor displacement of 6 mm (0.24 in.), representative of the collapse of the unstrengthened building. The global response of both buildings was governed by flexural and diagonal shear failure mechanisms of piers placed at the ground floor. It is worth remarking that the cracks exhibited by MB-R+SR for a lateral displacement of 6 mm (0.24 in.) were less wide than those observed for the building MB. Figure 3.2(a) reports also the comparison between experimental and numerical lateral load-displacement curves related to the unstrengthened building. The numerical results are in good agreement with the experimental results in term of initial stiffness, whereas the maximum load is slightly underestimated (Table 3.2). The effectiveness of the numerical model in predicting the crack patterns is well highlighted by the comparison of the principal tensile strain contours of Figure 3.2(b1) with the actual damage pattern (Figure 2.5(a)) observed at the end of the experimental test. The comparison is limited to the ground floor of East façade, where damages were more significant. The

This document is the intellectual property of the fib – International Federation for Structural Concrete. All rights reserved.
This PDF of fib Bulletin 95 is intended for use and/or distribution solely within fib National Member Groups.

central pier showed a diagonal shear failure, while the external ones exhibited a rocking mechanism with cracks starting from the corners of the openings.

Table 3.2: Main results of the numerical study (1 kN/mm=5.625 kip/in.; 1 kN=0.225 kip)

	K^+_S [kN/mm]	ΔK^+_S [%]	K^-_S [kN/mm]	ΔK^+_S [%]	V^+_{peak} [kN]	ΔV^+_{peak} [%]	V^-_{peak} [kN]	ΔV^-_{peak} [%]
MB (experimental)	125	-	132	-	180	-	179	-
MB (numerical)	127	+2%(*)	134	+2%(*)	148	-18%(*)	146	-18%(*)
MB-R (numerical)	325	+156%(**)	336	+151%(**)	320	+116%(**)	300	+105%(**)
MB-R+SR (numerical)	334	+163%(**)	348	+160%(**)	616	+316%(**)	566	+288%(**)

(*) Relative comparison between experimental and numerical results: numerical compared to experimental.

(**) Relative comparison between numerical results: MB-R and MB-R+SR compared to MB.

4 Concluding remarks

The paper presented the main properties and details of a retrofitting technique for masonry buildings based on the application of a thin Steel Fiber Reinforced Mortar overlay on façades. The main experimental observations concerning the preliminary test on the unstrengthened building were presented. Moreover, the results of non-linear finite element analyses performed to predict the behavior of the retrofitted building were also reported. Based on the findings of the present research, the following main observations can be drawn:

1. The failure mechanism exhibited by the experimental test on the unstrengthened building was governed by diagonal shear and rocking of the first-story piers.
2. The failure mechanism of the unstrengthened building was properly predicted by the FE model. The numerical initial stiffness was in good agreement with the experimental one whereas the lateral resistance was slightly (-18%) underestimated.
3. The numerical study showed that the proposed technique was able to improve both the resistance (+110%) and the initial stiffness (+150%) of the structure (MB-R+SR) compared to the unstrengthened building (MB). Moreover, the coating-to-foundation connections used to prevent rocking mechanism of the masonry walls led to a lateral capacity about two times higher than that obtained for the building without steel connections (MB-R).

A more detailed description of the results of the present research, including the tests on the retrofitted building, will be reported in a future technical paper.

5 Acknowledgements

The research is part of the project “Sismacomf” supported by the University of Brescia. The partial support of Delta Phoenix S.r.l. is also gratefully acknowledged.

This document is the intellectual property of the fib – International Federation for Structural Concrete. All rights reserved.
This PDF of fib Bulletin 95 is intended for use and/or distribution solely within fib National Member Groups.

6 References

ASTM E519-02: 2002, *Standard Test Method for Diagonal Tension (Shear) in Masonry Assemblages*, ASTM International, West Conshohocken, PA.

Dehghani, A., Nateghi-Alahi, F., Fischer, G., "*Engineered cementitious composites for strengthening masonry infilled reinforced concrete frames*." Engineering Structures, 105, 197-208, 2015.

Diana 10.1. *Diana Finite Element Analysis* – User's Manual. TNO-Diana BV, Delft, The Netherlands, 2016

El Gawady, M., Lestuzzi, P., Badoux, M., "*A review of conventional seismic retrofitting techniques for URM*". Proc., 4th Int. Conf. on Advanced Composite Materials in Bridges and Structures, Calgary, Alta, Canada, 2004

EN 1052-1:2001 – *Methods of Test for Masonry. Determination of Compressive Strength*.

EN 14651-5: 2005, *Precast concrete products – test method for metallic fibre concrete – Measuring the flexural tensile strength*, European Standard.

EN 1015-11:2007: *Methods of test for mortar for masonry - Part 11: Determination of flexural and compressive strength of hardened mortar.*

EN 772-1:2011 - *Methods of tests for masonry units - Part 1: Determination of compressive strength.*

EN 12390-13: 2013. *Testing hardened concrete - Part 13: Determination of secant modulus of elasticity in compression.*

Eurocode (2006). *Basis of Structural Design*. EN 1990:2006.

Facconi, L., Conforti, A., Minelli, F., Plizzari, G., "*Improving shear strength of unreinforced masonry walls by nano-reinforced fibrous mortar coating*". Materials and Structures 48 (2015): 2557–2574. https://doi.org/10.1617/s11527-014-0337-0.

Facconi, L., Minelli, F., & Giuriani, E., "*Response of infilled RC frames retrofitted with a cementitious fiber-mesh reinforced coating in moderate seismicity areas*." Construction and Building Materials, 160, 574-587., 2018.

Facconi, L., Minelli, F., Lucchini, S., & Plizzari, G., "*Experimental study of solid and hollow clay brick masonry walls retrofitted by steel fiber-reinforced mortar coating*." Journal of Earthquake Engineering, 24(3), 381-402, 2020.

Facconi, L., & Minelli, F., "*Retrofitting RC infills by a glass fiber mesh reinforced overlay and steel dowels: experimental and numerical study*." Construction and Building Materials, 231, 117133, 2020.

Gattesco, N., Boem, I., Dudine, A., "*Diagonal compression tests on masonry walls strengthened with a GFRP mesh reinforced mortar coating*." Bulletin of Earthquake Engineering, 13(6), 1703-1726, 2015.

Lin, Y.W., Lawley, D., Wotherspoon, L., Ingham, J.M., "*Seismic retrofitting of an unreinforced masonry building using ECC shotcrete*". The New Zealand Concrete Industry Conference 2010, Wellington, New Zealand, 7-9 October, 2010

Papanicolaou, C.G., Triantafillou, T.C., Papathanasiou, M., Karlos, K., "*Textile reinforced mortar (TRM) versus FRP as strengthening material of URM walls: out-of-plane cyclic loading*" Materials and Structures (2008) 41:143–157

Tomaževič, M., Klemenc, I., Weiss, P., "*Seismic upgrading of old masonry buildings by seismic isolation and CFRP laminates: a shaking-table study of reduced scale models*". Bulletin of earthquake engineering, 7(1), 293-321, 2009.

This document is the intellectual property of the fib – International Federation for Structural Concrete. All rights reserved.
This PDF of fib Bulletin 95 is intended for use and/or distribution solely within fib National Member Groups.

7) HPFRC

This document is the intellectual property of the fib – International Federation for Structural Concrete. All rights reserved.
This PDF of fib Bulletin 95 is intended for use and/or distribution solely within fib National Member Groups.
FRC2018: Fibre Reinforced Concrete: from Design to Structural Applications
Joint ACI-*fib*-RILEM International Workshop

Structural behavior of prestressed Ultra-High Performance Fibre-Reinforced Concrete beams with and without openings: comparison between experimental results and finite element modelling techniques

Dario Redaelli[1], Joanna Yared Nseir[2]

[1] : University of Applied Sciences Western Switzerland, Fribourg, Switzerland.

[2] : Saint Joseph University, Beirut, Lebanon.

Abstract

This paper presents the results of a numerical study carried out by the authors to better understand the structural behavior of prestressed beams with web openings and to identify numerical modelling techniques that allow to adequately predict such behavior. Ultra-High Performance Fibre Reinforced Concrete (UHPC) beams are considered, with a focus on shear-controlled failure modes.

For all the beams considered in this study, prestressing is used to resist the main bending moment. However, no other reinforcement is added to the beams, in order to emphasize the structural contribution of the fibers and to focus on solutions that could be economically competitive for the precast industry.

The results of non-linear simulations performed with existing finite elements codes are compared and validated against experimental results of tests carried out at the University of Applied Sciences of Western Switzerland. The main assumptions of the numerical simulations are discussed, as well as the results and the limits of the analysis.

Keywords

Ultra-High Performance Concrete, Finite Elements, Prestressed Beams, Cellular Beams.

This document is the intellectual property of the fib – International Federation for Structural Concrete. All rights reserved.
This PDF of fib Bulletin 95 is intended for use and/or distribution solely within fib National Member Groups.

1 Introduction

Ultra-High Performances Fibre-Reinforced Concretes (UHPC) are characterized by impressive mechanical performances, durability, self-compacting capability and, thanks to the presence of the fibers, the possibility to transfer tensile forces without the need of secondary and constructive reinforcement that would be required in ordinary concrete members. Due to these properties, UHPC elements usually present small thicknesses, great lightness and complex geometries that result from static, architectural or functional optimization. The structural behavior of irregular elements of this kind often deviates from standard beam theory assumptions and its prediction requires the use of appropriate analytical or numerical modelling approaches.

In order to acquire a better understanding on the structural behavior of UHPC beams with irregular geometry, and to identify numerical modelling techniques that allow to predict such behavior, a test series of prestressed UHPC cellular beams was analyzed with nonlinear finite element models. This paper presents the preliminary results of numerical simulations carried out with two different approaches: the first approach adopts modelling assumptions that are as close as possible to the actual measured materials laws, while the second approach is based on strongly simplified equivalent elasto-plastic laws. The main assumptions of the numerical simulations are discussed, as well as the results and the limits of the two approaches.

2 Experimental results

The experimental campaign considered in this paper consists of five prestressed UHPC beams: a reference beam without openings and four beams with circular openings, whose diameter varies from 0.4 to 0.6 of the height of the beams. All the beams were tested in four-point bending in the laboratory of the School of Engineering and Architecture in Fribourg. Detailed information about the test series can be found in Moreillon et al. (2013).

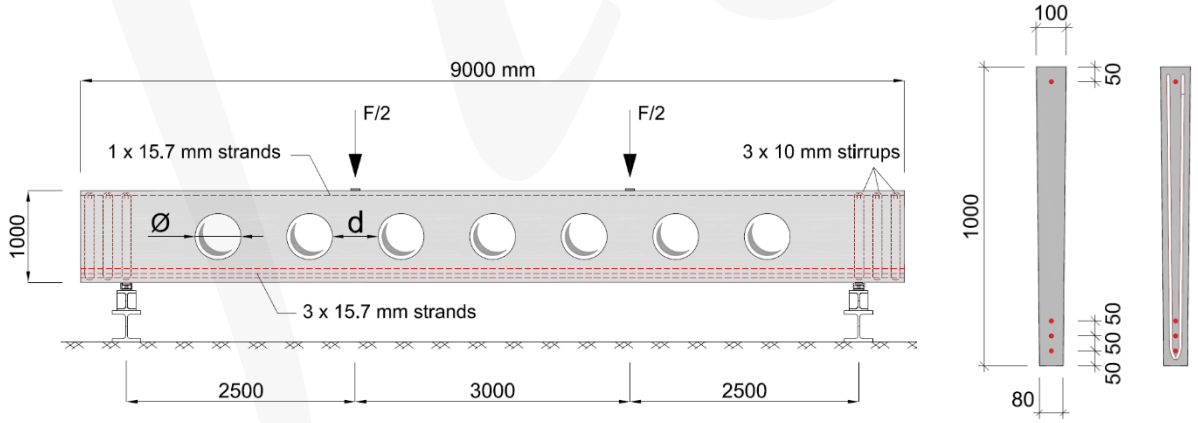


Figure 1: Test set-up and geometry of the beams, adapted from Moreillon et al. (2013)

Figure 1 shows the geometry and the test set-up of the beams, while Table 1 summarizes the properties of each beams and the most relevant test results. All the beams were reinforced with three Y1860S7 15.7 mm prestressing strands in the lower chord and one prestressing strand in the upper chord. The same initial prestressing force P_0 was applied to all the beams, except beam PU4, which was slightly more prestressed in order to evaluate the influence of P_0

This document is the intellectual property of the fib – International Federation for Structural Concrete. All rights reserved.
This PDF of fib Bulletin 95 is intended for use and/or distribution solely within fib National Member Groups.

on structural behavior. No other reinforcement was provided, except fibers and few stirrups in the anchorage areas of the strands (Fig. 1).

Table 1: Specimen designation and main properties, adapted from Moreillon et al. (2013)

	ϕ [mm] (see Fig. 1)	***d* [mm]** (see Fig. 1)	$f_{cm.cyl}$ **[N/mm²]**	E_{cm} **[N/mm²]**	P_0 **[kN]**	**Failure mode**	**Max load F_u [kN]**	**Deflection at F_u [mm]**
PU1	-	-	181	57000	4x125	Bending	587	62.3
PU2	400	600	168	57000	4x125	Bending	625	78.8
PU3	500	500	176	59000	4x125	Shear	519	59.0
PU4	500	500	178	58000	4x175	Shear	531	45.0
PU5	600	400	170	51000	4x125	Shear	418	44.7

Figure 2 schematically show the crack pattern observed after failure and the measured force-mid span deflection curves for all the beams. Beams PU1 and PU2 failed in bending, while beams PU3, PU4 and PU5 failed in shear with a distinctive "Vierendeel" frame effect.

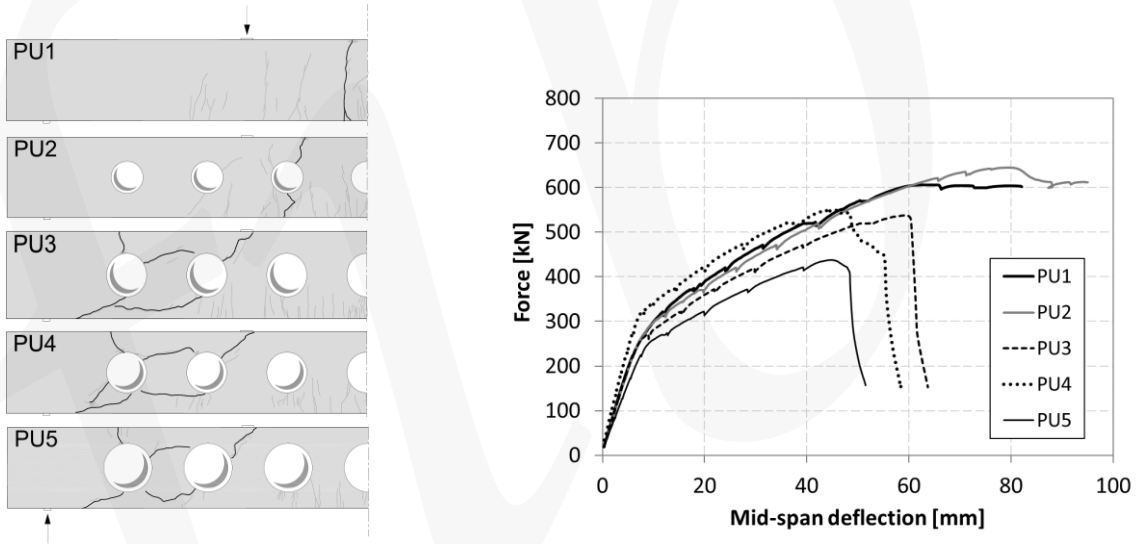


Figure 2: Crack patterns after failure (left) and measured force-mid span deflection curves of the beams considered in this study (right). Adapted from Moreillon et al. (2013)

Beam PU2 with 400 mm holes exhibited a higher bending strength than the reference beam without holes. Because of this unexpected behavior, which may have been induced by a particularly favorable orientation of the fibers in the lower chord of beam PU2, this beam is not considered in the following numerical analyses.

3 UHPC material properties for modelling

UHPC used for the beams is the BSI-Ceracem® from Eiffage, reinforced with 200 kg/m^3 (2.5% in vol.) high-strength steel straight fibers (length 20 mm, diameter 0.3 mm). The average compressive strength and elastic modulus measured on UHPC cylinders are given in Table 1. Jungwirth (2009) performed direct tensile tests on a comparable BSI-Ceracem® mix and observed a pseudo-plastic, multiple micro-cracking phase for a nearly constant stress

This document is the intellectual property of the fib – International Federation for Structural Concrete. All rights reserved.
This PDF of fib Bulletin 95 is intended for use and/or distribution solely within fib National Member Groups.

of about 9 N/mm^2, extending up to a deformation of approximatively 2.5 ‰ and followed by localization of the deformation in one softening crack.

Direct tensile tests were not realized in the experimental campaign considered herein (Moreillon et al., 2013). However, UHPC behavior in tension was indirectly measured with bending tests according to the French UHPC Interim Recommendations (2013). Tests were performed on 400x80x80 mm notched specimens (Fig. 3, right) sawn from a 80 mm thick prototype panel cast with the same procedure as the tested beams (Fig. 3, middle). Figure 3 shows the stress-crack opening curves obtained by inverse analysis (AFGC, 2013) for prisms sawn in the horizontal (H), diagonal (D) and vertical (V) direction. It is worth noting that, probably due to less favourable fibres orientations in the prototype panel than in direct tension specimens tested by Jungwirth (2009), no pseudo-plastic phase was detected for sawn prisms.

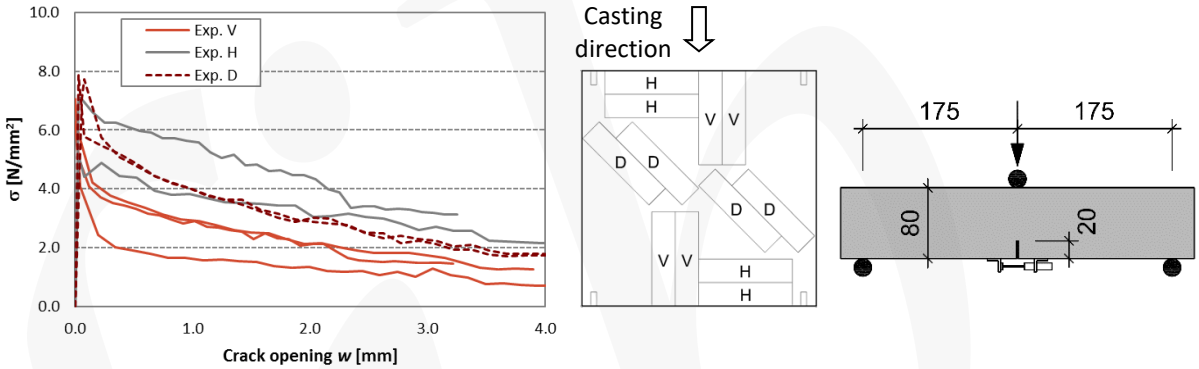
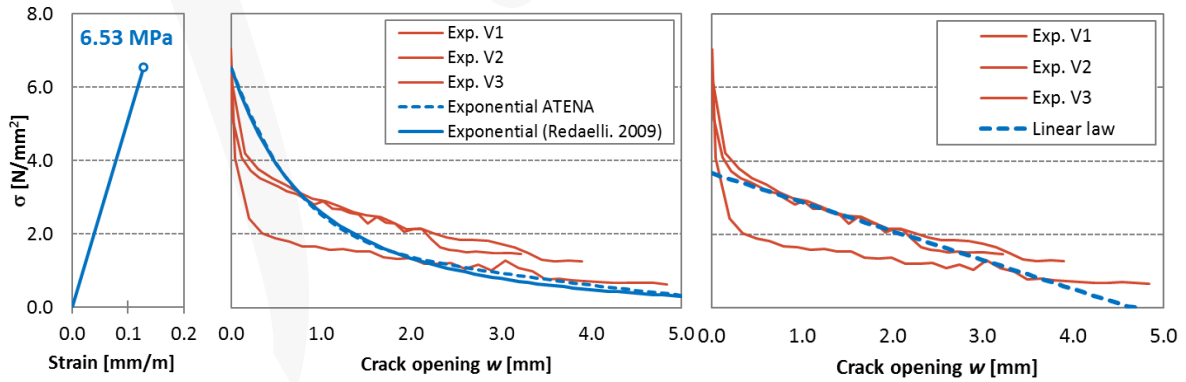


Figure 3: Stress-crack opening relations (left) obtained by inverse analysis from three-point bending tests (right) carried out on prisms sawn from a prototype panel (middle)

Collapse of beams PU3, PU4 and PU5 was promoted by nearly horizontal cracks associated with the "Vierendeel" effect (Fig. 2). Vertically sawn prisms can be considered as the most representative of tensile behavior in horizontal cracks: for modelling purposes, only these prisms are considered. Stress-crack opening curves adopted for modelling are given in Fig. 4: a linear elastic behavior is assumed up to the average value of matrix cracking strength measured on sawn prisms (6.53 MPa, Fig. 4-a). No multiple micro-cracking phase is assumed: according to Figure 3, softening behavior directly follows cracking of the matrix.



(a) (b1) (b2)

Figure 4: Constitutive curves used for modelling (blue lines) versus stress-crack opening curves obtained with inverse analysis on vertically sawn prisms. (a) pre-cracking model; (b1) post-cracking exponential models; (b2) post-cracking linear model.

This document is the intellectual property of the fib – International Federation for Structural Concrete. All rights reserved.
This PDF of fib Bulletin 95 is intended for use and/or distribution solely within fib National Member Groups.

For the softening branch, two alternative models are used. Figure 4-b1 presents an exponential model based on an equation which was shown to adequately represent the softening behavior of UHPC (Redaelli, 2009). The parameters of the equation are calibrated so that the integral of the model curve equals the average integral of experimental curves up to the value of the crack opening which is available for all the experimental curves (3.22 mm). Tensile stress rapidly decreases and completely vanishes when crack opening equals fibres half-length (w_u = 10 mm). As an alternative, Fig. 4-b2 presents a linear model obtained as an interpolation of the average experimental curve. According to this model, tensile stress drops at 3.66 N/mm^2 after cracking and vanishes when w_u = 4.64 mm. Both models have a very similar fracture energy G_F: 8.6 N/mm for the exponential model, 8.5 N/mm for the linear one.

Fig. 4-b1 also shows the exponential curve implemented in the finite element software ATENA and used for subsequent analyses. The analytical expression of this law (J. Cervenka et al, 2016) differs from the one suggested by Redaelli (2009). By assigning the same cracking stress and fracture energy, however, the two curves are practically superposed, despite the fact that Atena's model reaches a zero stress for a crack opening w_u = 6.96 mm.

4 Finite element modelling based on non-linear material laws

The first numerical study presented in this paper was performed with the finite element software Atena, from Cervenka Consulting (J. Cervenka et al., 2016). Several material laws as well as refined non-linear modelling capabilities are implemented in this software, allowing to simulate the structural response with material laws that closely fit the measured ones. Compressive strength and elastic modulus of UHPC are set according to Table 1, while a bilinear stress-strain law with hardening is used for reinforcement, with average material properties taken from Moreillon et al. (2013).

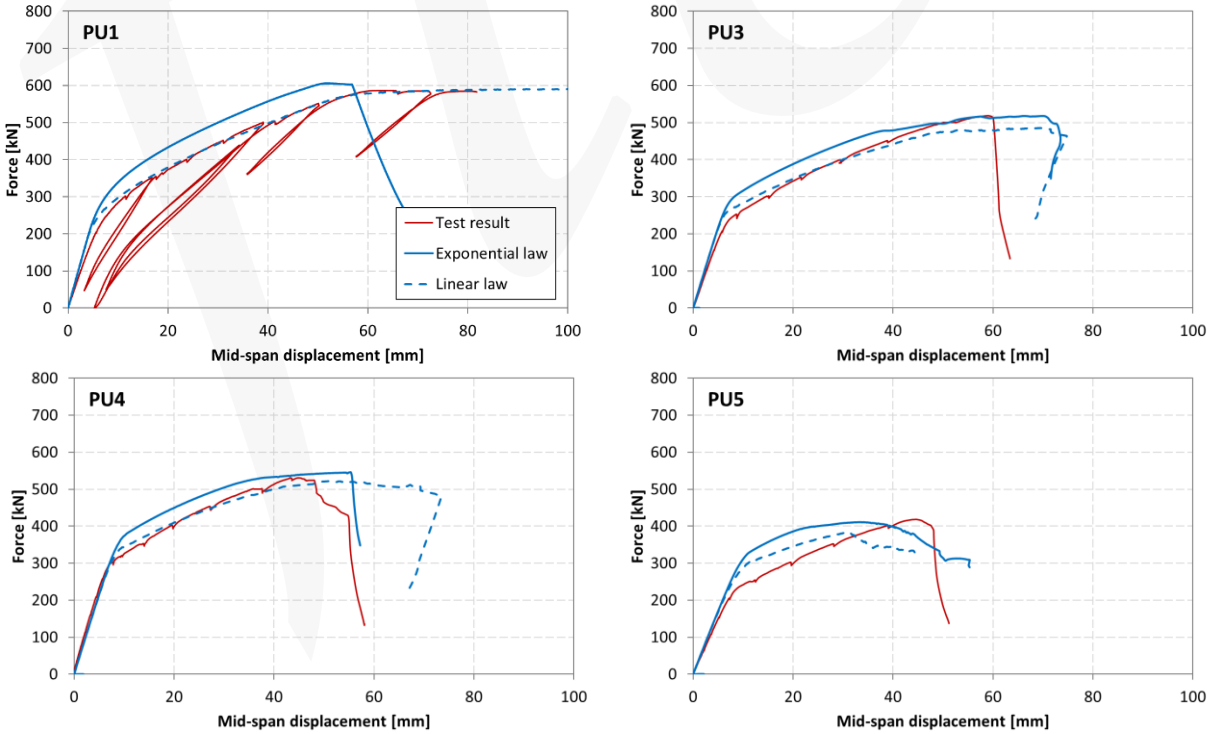
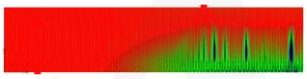
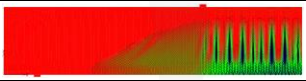
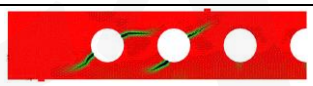
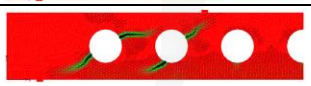
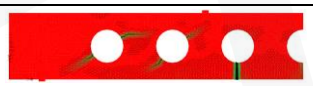
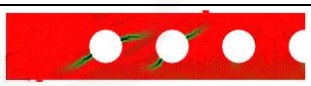
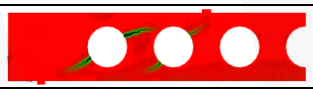
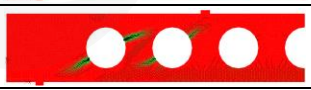


Figure 5: Comparison between test results and numerical results obtained with ATENA

This document is the intellectual property of the fib – International Federation for Structural Concrete. All rights reserved.
This PDF of fib Bulletin 95 is intended for use and/or distribution solely within fib National Member Groups.

Active prestressing is simulated as an external force applied over the introduction length at the ends of the beams. 10% prestressing losses are considered to account for UHPC creep and autogenous shrinkage. Cracking of concrete is modelled with a "smeared crack" approach that uses the stress-crack opening relations given in Figure 4 as input, in combination with the crack band theory, where the band width is defined as the projection of finite element dimensions in the direction of principal tension (J. Cervenka et al., 2016). Plane triangular isoparametric finite elements are used, with element size of 4 cm. Numerically stable results, closest to the experimental behavior, were obtained by using a "rotating crack model" approach, according to which no shear strain or stresses occur on crack planes (mode I fracture). The effect of transverse cracking on the compressive strength of concrete is considered in Atena through a function that progressively reduces compressive strength to a fraction c of the uniaxial value. The parameter c can be chosen by the user, while the shape of the function is fixed. Based on tests carried out by Fehling et al. (2011), $c = 0.7$ is chosen. This value has been successfully used by Ismali (2015) to model UHPC beams in torsion with Atena and by Baby (2013) to model UHPC beams in shear.

Table 2: Results of the non-linear finite element modelling carried out with ATENA.

	Exponential model			**Linear model**		
	Fail. mode	Crack pattern	F_{num}/F_{exp}	Fail. mode	Crack pattern	F_{num}/F_{exp}
PU1 (B)	B		1.03	B		1.00
PU3 (S)	S		1.00	S		0.93
PU4 (S)	B*		1.03	S		0.98
PU5 (S)	S		0.98	S		0.91
		Average	**1.01**		Average	**0.96**

B: bending failure. S: shear failure. B: bending failure in presence of significant shear cracking.*

Figure 5 compares the numerical force-mid span deflection curves to the experimental ones, while Table 2 summarized the results of the numerical modelling in terms of failure modes, crack patterns and ratio between numerical and experimental failure loads. The numerical results are in good agreement with the experimental ones in terms of shape of the curves, failure mode and ultimate load.

The exponential model for tensile softening of UHPC provides the best estimate of the ultimate load (see Table 2). However, it predicts an incorrect failure mode for beam PU4 and significantly overestimates the post-cracking stiffness of the beams. The linear model for tensile softening always leads to a correct prediction of the failure mode and to an accurate estimate of the post-cracking stiffness, tough being less precise on the failure load value. By comparing Fig. 2 (left) to figures given in Tab. 2, it can be observed that the numerically predicted crack pattern corresponds well to the experimentally observed one.

This document is the intellectual property of the fib – International Federation for Structural Concrete. All rights reserved.
This PDF of fib Bulletin 95 is intended for use and/or distribution solely within fib National Member Groups.

5 Finite element modelling based on elasto-plastic stress fields

The second numerical study presented in this paper is carried out with the open source finite element software j-Conc, developed at the Structural Concrete Laboratory of the Swiss Federal Institute of Technology in Lausanne. The theoretical bases of the model can be found in Fernández-Ruiz et al. (2007). Based on the theory of plasticity, the software was initially developed to predict the failure behavior of reinforced members made of ordinary concrete.

In this paper, preliminary analyses run with this software are presented with the main purpose to check its limits of applicability to UHPC structures.

Concrete in compression is modelled with an elastic-perfectly plastic law. To that, the so-called equivalent plastic strength $f_{c,pl}$ is used instead of the cylinder compressive strength $f_{c,cyl}$ (Muttoni et al., 1997). The equivalent plastic strength accounts for the reduced ductility of high strength concretes and for the detrimental effect of transverse tensile strain on compressive strength (factor η). In j-Conc, $f_{c,pl}$ is calculated with well-known equations fitted for ordinary concrete (Muttoni et al., 1997, Vecchio et Collins 1986, Fig. 6).

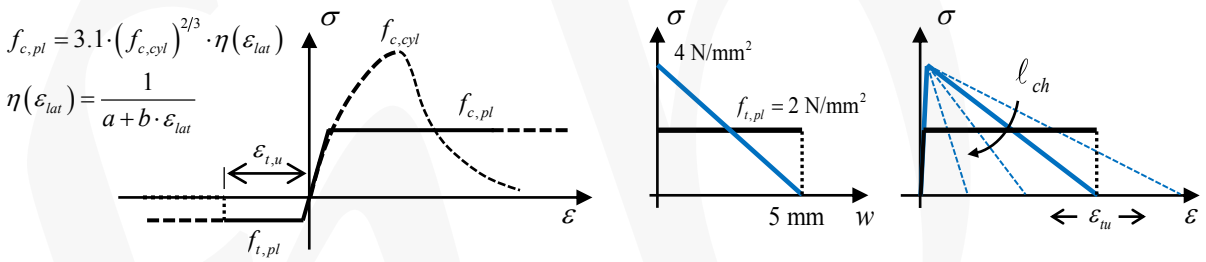


Figure 6: Left: elasto-plastic material modelling in j-Conc. Right: idealized stress-crack opening law used to study the influence of the characteristic length on the structural response of the beams (see Fig. 8)

An elasto-plastic law for concrete in tension can also be modeled in j-Conc, with unlimited ductility or with a limit ε_{tu} on strain capacity (Fig. 6). In this study, this elasto-plastic law in tension is used to model the post-cracking contribution provided by the fibers. The choice of the value to assign to the "equivalent tensile plastic strength", $f_{t,pl}$, is not trivial: it should allow to correctly reproduce the resultant of the tensile forces acting over the actual cracks. In this study, $f_{t,pl}$ is considered as a calibration parameter and its numerical value is varied while keeping an unlimited ductility (ε_{tu}=∞). The values of the average tensile stress (≈ G_F/w_u) associated with the exponential and linear stress-crack opening laws given in Fig. 4 correspond respectively to 0.86 N/mm^2 (w_u = 10 mm) and 1.83 N/mm^2 (w_u = 4.64 mm). The analysis of all the beams modelled with ATENA showed the maximal crack opening predicted at failure was always lower than w_u. Accordingly, the average value of the stress carried by fibers across cracks should be higher than the G_F/w_u values given above. Based on this, the parametric study was carried out with $f_{t,pl}$ values higher than 0.86 N/mm^2.

In compression, the models implemented in j-Conc for ordinary concrete are used without modification (Fig. 6, left). This is a very simplified hypothesis for UHPC, corresponding to the assumption that the presence of the fibers has no direct influence on the constitutive behavior of concrete in compression (post-pic ductility, η factor). As a consequence, fibers only contribute to crack control in tension, which indirectly provides a beneficial effect on η through the reduction of transverse tensile strains.

This document is the intellectual property of the fib – International Federation for Structural Concrete. All rights reserved.
This PDF of fib Bulletin 95 is intended for use and/or distribution solely within fib National Member Groups.

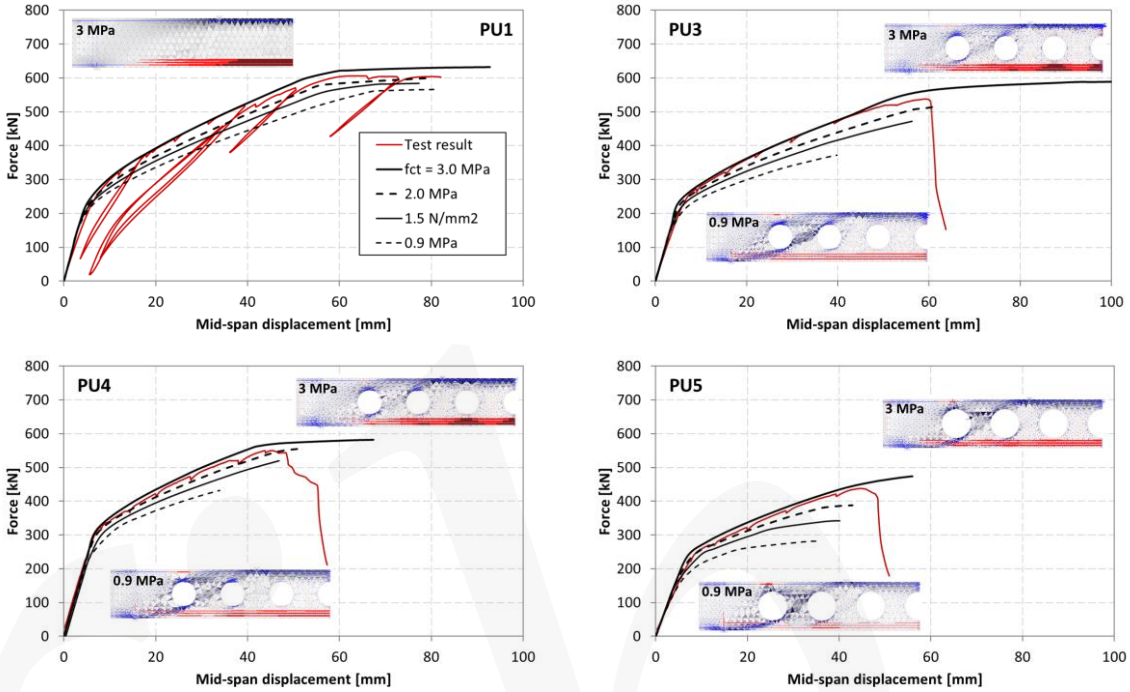


Figure 7: Comparison between test results and numerical results obtained with j-Conc

All models use constant strain triangular (CST) finite elements with a maximal size of 10 cm and automatic mesh refinement in the vicinity of geometric irregularities. Figure 7 presents the results of the parametric study, while Table 3 summarized the predicted failure modes and the ratios between numerical and experimental failure loads. Also shown in Fig. 7 are some representations of the state of stress determined by j-Conc at failure: strands are shown in dark red when they reach yielding, indicating a bending failure mode. Black concrete elements correspond to the situation $\sigma_c = f_{c,pl}$, which may be reached because of high compressive stresses (like in the upper chord of the beam) or because of high transversal tensile strains (via the η factor, mostly in the webs).

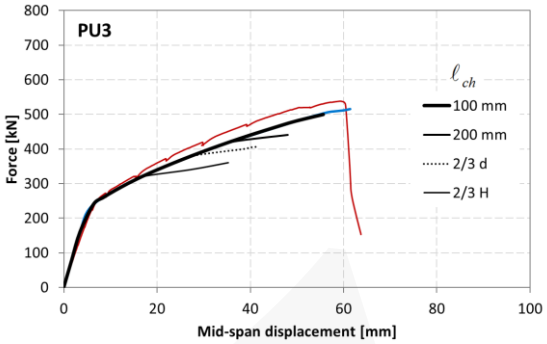
Table 3: Results of the non-linear finite element modelling carried out with j-Conc

	0.9 N/mm^2		1.5 N/mm^2		2.0 N/mm^2		3.0 N/mm^2	
	Mode	F_{num}/F_{exp}	Mode	F_{num}/F_{exp}	Mode	F_{num}/F_{exp}	Mode	F_{num}/F_{exp}
PU1 (B)	B	0.93	B	0.96	B	0.99	B	1.04
PU3 (S)	S	0.69	S	0.88	S	0.96	B	1.10
PU4 (S)	S	0.78	S	0.94	B	1.01	B	1.05
PU5 (S)	S	0.64	S	0.78	S	0.89	S	1.05
Average		**0.76**		**0.89**		**0.96**		**1.07**

Curves obtained with a perfectly plastic tensile strength of 2.0 N/mm^2 are in good agreement with the experimental ones, in terms of shape of the curves, failure mode and ultimate load, even though an incorrect failure mode is predicted for beam PU4 (bending instead of shear). The post cracking stiffness is somehow underestimated by the model, which

This document is the intellectual property of the fib – International Federation for Structural Concrete. All rights reserved.
This PDF of fib Bulletin 95 is intended for use and/or distribution solely within fib National Member Groups.

can be explained by the fact that the elastic-perfectly plastic law neglects the pre-cracking tensile strength of the matrix.



	l_{ch}	ε_{tu}
	[mm]	[-]
	100	0.05
	200	0.025
2/3 d	333	0.015
2/3 H	667	0.0075



Figure 8: Influence of the characteristic length value on the structural behavior

Results presented in Fig. 7 were obtained under the assumption of unlimited ductility in tension. The implications of this assumption shall be checked since, as a matter of fact, the actual contribution of fibers vanishes when crack opening reaches its ultimate value, w_u. This effect can be modeled in j-Conc by limiting the strain capacity to a given ε_{tu} value, which requires the definition of a characteristic length, l_{ch}. In the presence of a plastic constitutive model, however, it is questionable whether the characteristic length shall be related to finite element size or to a structural dimension. In bending, l_{ch} is usually related to the height h of a beam or to crack spacing, $2/3 \cdot h$ being a commonly accepted value. For beams considered in this study, local bending also occurs in the webs (frame effect), with a static height more related to d than to h (Fig. 8).

The influence of l_{ch} is studied by taking beam PU3 as a reference and varying l_{ch} from a value representative of finite element size (100 mm) to a value corresponding to $2/3 \cdot h = 667$ mm. A simplified stress-crack opening linear law is used (Fig. 6, right), with average stress of 2 MPa and ultimate crack opening of 5 mm. This idealized law is quite close to the actual law given in Fig. 4-b2. Thus, assuming $\varepsilon_{tu} \cong w_u/l_{ch}$, strain capacity ε_{tu} varies from 0.05 to 0.0075. The effect of this variation on the force-mid span displacement curve of beam PU3 is shown in Fig. 8, together with the reference curve obtained under the assumption of unlimited ductility (in blue). The influence of ε_{tu} on the structural response is very significant. Agreement between numerical and experimental results can only be achieved by assuming a low value of the characteristic length. The high ductility in tension that is required to achieve acceptable numerical results may be the counterpart of the very conservative assumptions that were made by neglecting the influence of the fibers on compressive behavior. Despite the relatively good agreement shown in Fig. 1, further theoretical analyses are required to justify the values of equivalent plastic strengths, characteristic length and tensile strain limit that shall be used to model UHPC with simplified plasticity-based approaches.

6 Conclusions

The experimental behavior of UHPC cellular beams was modelled with non-linear finite elements with the purpose to acquire a deeper understanding on the structural response of this type of elements and to determine the most adequate modelling assumptions and techniques.

This document is the intellectual property of the fib – International Federation for Structural Concrete. All rights reserved.
This PDF of fib Bulletin 95 is intended for use and/or distribution solely within fib National Member Groups.

In the first part of the paper, numerical simulations were carried out with non-linear material laws as close as possible to the measured ones. A very good agreement between numerical and experimental results was obtained by using tensile law derived from prisms sawn in a panel cast in the same way as the actual beams. Based on these results, numerical models of this type can be considered accurate enough to be used for further parametric analyses and structural optimization. From a more practical point of view, it is worth noting that, due to fiber orientation and distribution effects, the stress-crack opening laws derived from prisms sawn in the prototype panel were significantly weaker than the nominal laws expected based on small scale laboratory specimens tested in direct tension.

In the second part of the paper, numerical simulations were carried out with strongly simplified constitutive modelling assumptions: the tensile and compressive behavior of UHPC were modelled with elastic-perfectly plastic laws. The equivalent plastic strength in compression was determined with standard equations for ordinary concrete (the influence of the fibers in compression was neglected). The equivalent plastic strength in tension was considered as a calibration parameter. The preliminary results of this simplified modelling approach seem promising. However, they also showed that more profound research is needed to define the parameters of UHPC elasto-plastic laws (equivalent plastic strengths, characteristic length, strain limit in tension) on a theoretically sound basis.

In addition, the sensitivity of both modelling techniques to variation of numerical and mechanical parameters still has to be checked thoroughly.

7 References

L. Moreillon, J. Nseir, J. Tomás, R. Suter (2013), *Structural Behaviour of Cellular Beams in UHPFRC*, RILEM-*fib*-AFGC Int. Symposium on Ultra-High Performance Fibre-Reinforced Concrete UHPFRC 2013, October 1-3, 2013, Marseille, France

J. Jungwirth (2006), *Zum Tragverhalten von Zugbeanspruchten Bauteilen aus Ultra-Hochleistungs-Faserbeton*, Thèse EPFL n° 3429, 2006

AFGC (2013), *Ultra-High Performance Fibre-Reinforced Concretes – Interim Recommandations*, 2013

D. Redaelli, *Comportement et modélisation des éléments de structure en BFUHP avec armatures ordinaires*, Thèse EPFL n° 4298 (2009)

V. Červenka and J. Červenka (2016), *ATENA Program Documentation – Part 1 Theory*, 2016

M. Ismali (2015), *Behavior of UHPC Structural Members subjected to Pure Torsion*, Kassel university press, ISBN: 978-3-86219-952-5, 2015

F. Baby, P. Marchand, M. Atrach, F. Toutlemonde (2013), *Analysis of flexure-shear behavior of UHPFRC beams based on stress field approach*, Engineering Structures, Vol. 56, November 2013, Pages 194-206

M. Fernández-Ruiz, A. Muttoni (2007), *On Development of Suitable Stress Fields for Structural Concrete*, ACI Structural Journal, Vol 104(4), July 2007

A. Muttoni, J.Schwartz, B. Thürlimann (1997), *Design of Concrete Structures with Stress Fields, Birkhaüser*, Basel, Boston and Berlin, Switzerland, 1997

F.J. Vecchio, M.P. Collins (1986), *The Modified Compression-Field Theory for Reinforced Concrete Elements Subjected to Shear*, ACI JOURNAL, V. 83, No. 2, Mar.-Apr. 1986, pp. 219-231

This document is the intellectual property of the fib – International Federation for Structural Concrete. All rights reserved.
This PDF of fib Bulletin 95 is intended for use and/or distribution solely within fib National Member Groups.
FRC2018: Fibre Reinforced Concrete: from Design to Structural Applications
Joint ACI-*fib*-RILEM International Workshop

Use of a Probabilistic Explicit Cracking Model for Analysing the mechanical behaviour of an Ultra-High Performance Fibre Reinforced Concrete (UHPFRC) Beam Subjected to Shear Loading

Pierre Rossi[1], Dominic Daviau-Desnoyers[2], Jean-Louis Tailhan[1]

[1] : Université Paris-Est, IFSTTAR, MAT, F-75732, Paris, France

[2] : CIMA+, Montreal, Canada.

Abstract

The objective of this paper is to verify the validity of the probabilistic explicit cracking model developed for SFRC to simulate the behaviour of a reinforced UHPFRC beam subjected to a bending load leading to shear failure. The relevancy of the model is evaluated through the simulation of the mechanical behaviour of the beam. The parameters characterizing the tensile behaviour of the studied UHPFRC are determined from the 3-point bending tests performed on beams sawed from the reinforced UHPFRC beam.

The results suggest that the probabilistic explicit cracking model is relevant to analyze the mechanical behaviour of a reinforced UHPFRC beam and provide precise information about the cracking process of this type of material. The good agreement between the experimental result and the numerical simulations suggests that the studied UHPFRC behaves like usual FRC as the tensile strength and the mechanical effect of the fibres may be modelled by a perfectly brittle behaviour and a nonlinear softening behaviour

Keywords

Ultra-High Performance Fibre Reinforced Concrete; Numerical Model; Shear, Bending, Cracking

This document is the intellectual property of the fib – International Federation for Structural Concrete. All rights reserved.
This PDF of fib Bulletin 95 is intended for use and/or distribution solely within fib National Member Groups.

1 Introduction

New construction methods and technologies are in constant evolution in order to expand the lifespan of existing and new structures. As part of the new technologies, new advancements in concrete and cement-based products are gradually changing the design and construction worlds. Materials such as ultra-high performance fibre reinforced concrete (UHPFRC) are increasingly used in structural applications. One of the main reasons of its popularity is related to the existence of national and international recommendations for the design of UHPFRC structures.

These recommendations are efficient and conservative for designing simple statically determinate structures at ultimate limit state. However, they do not possess a sufficient physical base to propose relevant solutions for more complex structures such as statically indeterminate structures or more complex loadings as shear or punching situations. Moreover, the control of cracking in the serviceability limit state is one of the main interests of using UHPFRC. Crack control is very important for durability aspects and is certainly a major advantage of UHPFRC in comparison to structures using traditional reinforcement bars. Nowadays, existing design recommendations do not provide sufficient relevant information regarding cracking at the serviceability limit state (crack opening and spacing). In this way, the best approach for designing structures with respect to both safety and sustainable development is the use of finite element analysis.

The objective of this paper is to verify the validity of the probabilistic explicit cracking model developed for SFRC to simulate the behaviour of a reinforced UHPFRC beam subjected to a bending load leading to shear failure. This objective stems from the desire to validate the following hypothesis: UHPFRC having a compressive strength not exceeding 300 MPa and a percentage of fibres not exceeding 3%-volume have a cracking process and a mechanical behaviour in tension comparable to the ones observed in more classical SFRC (Rossi 2008).

The probabilistic explicit cracking model has been in constant development since the late 1980 (Rossi and Richer 1987, Rossi and Wu 1992, Tailhan, Dal Pont *et al.* 2010, Tailhan, Rossi *et al.* 2013, Rossi, Tailhan *et al.* 2014, Rossi, Daviau-Desnoyers *et al.* 2015, Tailhan, Rossi *et al.* 2015). Originally developed to analyze cracking of structures made of ordinary concrete, the model has been enhanced to simulate cracking in fibre reinforced concrete structures. An improvement of this probabilistic explicit cracking model to permit the analysis of steel fibre reinforced concretes (SFRC) cracking was proposed and validated for different type of SFRC with compressive strengths not exceeding 90 MPa. In the validation tests, beams were subjected to bending loads leading to shear or bending failure mechanisms.

2 Probabilistic Explicit Cracking Model of Steel Fibre Reinforced Concrete (SFRC)

The model is based on three main physical evidences that have been observed experimentally:

- Concrete is a heterogeneous material in which the heterogeneities can be modeled through a random spatial distribution of mechanical properties considered as dominant in the cracking process, namely the Young's modulus and the tensile strength (Rossi and Richer 1987).

This document is the intellectual property of the fib – International Federation for Structural Concrete. All rights reserved.
This PDF of fib Bulletin 95 is intended for use and/or distribution solely within fib National Member Groups.

- Scale effects of concrete cracking are taken into account by the fact that mechanical properties of the material such as the tensile strength depend on the size of the mesh elements chosen for the finite element analysis (Rossi and Richer 1987, Rossi, Wu *et al.* 1994). In contrast, the average post-cracking energy is considered independent of scale effects (observed experimentally, Rossi 2012).
- Cracking is explicitly treated through the random creation of kinematic discontinuities, which provides access to quantitative information on the cracking state (number of cracks, opening and spacing). Numerically speaking, these cracks are represented by interface elements.

The crack initiation criterion may be summarized as following: the interface element opens when the normal tensile stress at the centre of the interface element reaches a critical value. The critical value corresponds to the tensile strength of the material probabilized through a Weibull distribution function (Tailhan, Dal Pont *et al.* 2010). This critical value depends on the total volume of the two volumetric elements interfaced by the considered interface element. This means that the stress and the rigidity of the interface element briefly become equal to zero until the bridging effect of the fibres takes over. The criterion of crack creation is schematically presented in Figure 1.

Therefore, the creation of cracks in the cement matrix is represented by an elastic perfectly brittle behaviour, whereas the bridging effect of the fibres is described by the following modelling approach.

Normal and tangential stresses in the interface element linearly increase with normal and tangential displacements when a “broken” interface element re-opens to take into account the elastic effect of the fibres inside the crack. Physically speaking, the rigidity of the fibres (inside the cracks) is more important in tension than in shear. Thus, the interface element rigidity is considered different for normal and tangential displacements. In 2D, normal and tangential rigidities of the interface element are K_n’ and K_t’ respectively. The post-cracking elastic behaviour exists until it reaches a threshold value, ζ_0, related to the normal displacement (Figure 1). Once this limit value is reached, the mechanical behaviour of the interface element changes. The normal stress is considered as linearly decreasing with the normal displacement in order to take into account the damage of the bond between the concrete and the fibre, and fibre pullout. The decreasing evolution is obtained by a damage model.

Finally, the interface element is considered definitively broken when the normal displacement reaches a threshold value, ζ_c (Figure 1). This value corresponds to the state where the effect of fibres is considered negligible. It is determined from a uniaxial tensile test. At this point, its normal and tangential rigidities are set to zero.

The post-cracking energy dissipated by the bridging effect of the fibres is considered randomly distributed on the mesh elements. The random distribution is a log-normal distribution function with a mean value independent of the mesh elements size (scale effect independency, Rossi 2012) and a standard deviation that is due to the heterogeneity of the material increasing as the mesh elements size decreases. To model a given structural element, the distribution function is determined in the following manner:

- The mean value is directly obtained experimentally from a certain number of uniaxial tensile tests on notched specimens, more specifically from the load-crack opening experimental curves.
- The standard deviation, which depends on the mesh elements size, is determined by an inverse analysis approach that consists of simulating the uniaxial tests with different

This document is the intellectual property of the fib – International Federation for Structural Concrete. All rights reserved.
This PDF of fib Bulletin 95 is intended for use and/or distribution solely within fib National Member Groups.

element mesh sizes. As the mean value of the post-cracking energy is known from the experimental results, several numerical simulations are realized for each mesh size to determine the standard deviation that best fits the experimental results. The inverse analysis approach thus allows finding a relation between the standard deviation and the finite element mesh size.

The threshold parameters ζ_0 and ζ_c are determined by an inverse analysis approach to best fit the simplified triangular stress-displacement curve representing the post-cracking energy (Figure 1) to the experimental tensile softening curve.

Figure 1 presents the numerical mechanical behaviour adopted to represent the experimental post-cracking behaviour. Only the normal stress - normal displacement curve is considered in this figure.

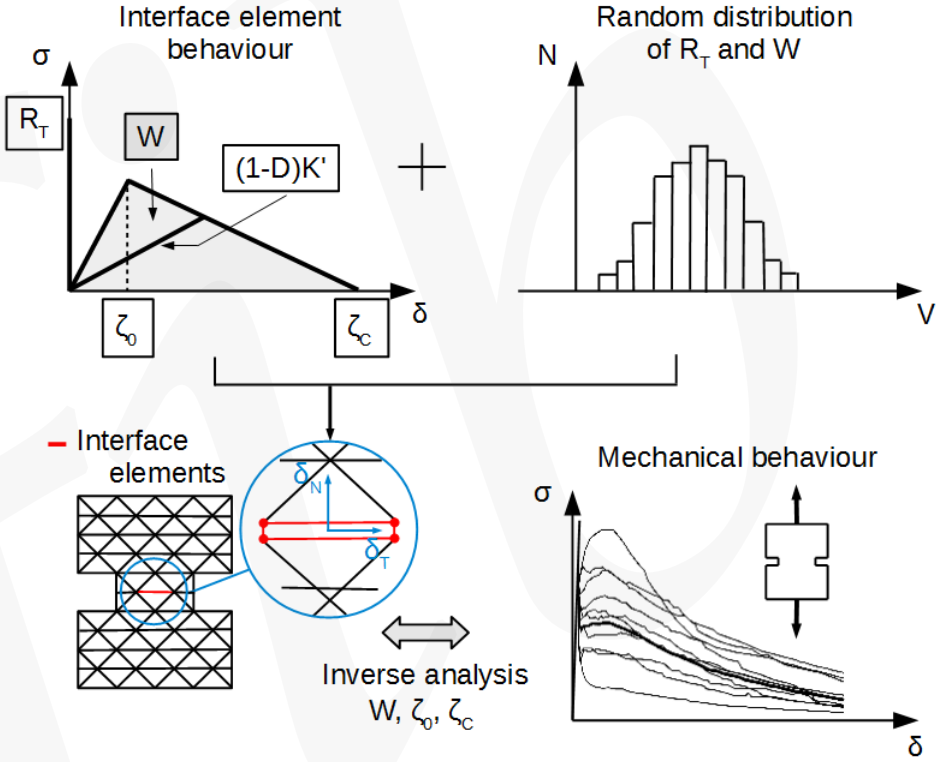


Figure 1: Principles of the explicit probabilistic cracking model of SFRC

3 Numerical Modelling of a reinforced UHPFRC beam submitted to shear loading

The probabilistic explicit cracking model developed for SFRC has been used to simulate the mechanical behaviour and cracking process of a longitudinally reinforced UHPFRC beam without transverse reinforcement bars. The beam was tested in an experimental campaign performed by Baby (2012) on the tensile behaviour of UHPFRC at the structural level.

3.1 Experimental Details

The beam, identified as BFUP-F-RC-NS in the experimental campaign, was designed to develop a shear failure mechanism. Therefore, its longitudinal reinforcement was designed to

This document is the intellectual property of the fib – International Federation for Structural Concrete. All rights reserved.
This PDF of fib Bulletin 95 is intended for use and/or distribution solely within fib National Member Groups.

avoid bending failure. The beam's cross section is presented in Figure 2. The reinforcement consisted of 5-HA20 and 1-HA25, the latter being placed in the middle of the bottom layer of rebars. Figure 3 shows the boundary conditions of the 4-point bending test, consisting of three roller supports and one pinned. The spans between the loading points and the supports were respectively 480 and 2000 mm.

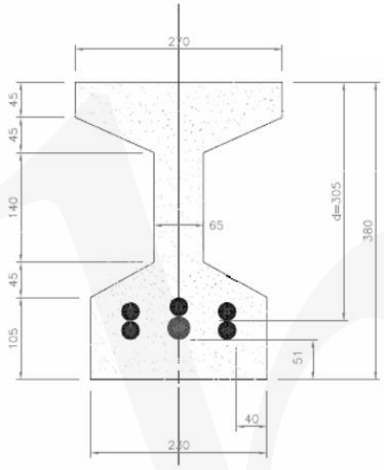


Figure 2: Cross section of the reinforced UHPFRC beam

The UHPFRC mix design used was a self-compacting concrete made of Portland cement, fine sand with a maximum aggregate size of 0.8 mm, silica fume, high-range water-reducing admixture, and straight steel fibres with a length of 13 mm and a diameter of 0.2 mm at 2.5 % by volume. The UHPFRC had a 28-day mean compressive strength of 212 MPa, a Young's modulus of 56 GPa and a Poisson's ratio of 0.185.

Small beams were tested under 3-point bending. These small beams were sawn at a 45° angle to the reinforced UHPFRC beam length after the test (in the non cracked zones). This choice was made to characterize the post cracking performance of the UHPFRC tacking into account a representative orientation of fibres in relation with shear cracks. The small beams were 280 mm long, 70 mm high and 60 mm wide, with a 2 mm wide and 8 mm deep notch sawn at mid-span from a single blade stroke. The support span was set to 210 mm. It should be noted that the small beams dimensions were not exactly identical as the beams were sawn from a larger beam. Therefore, the aforementioned dimensions represent the average dimensions of the small beams.

3.2 Characterization of the tensile behaviour of UHPFRC

Although some general parameters such as the 28-day compressive strength, Young's modulus and Poisson's ratio have been directly determined experimentally, the mechanical characteristics of the tensile behaviour of the studied UHPFRC must be determined by inverse analysis. The inverse analysis approach consists of simulating the 3-point bending tests performed on the small notched beams sawn from the reinforced UHPFRC beam to identify the average tensile strength (R_T) and its standard deviation ($\sigma(R_T)$), the average post-cracking energy (W) and its standard deviation ($\sigma(W)$), and the threshold parameters ζ_0 and ζ_c defining the simplified triangular representing the post-cracking energy.

Generally, the tensile strength and its scattering are determined using the analytical relations presented in Rossi and Wu (1992). These analytical functions correspond to the

This document is the intellectual property of the fib – International Federation for Structural Concrete. All rights reserved.
This PDF of fib Bulletin 95 is intended for use and/or distribution solely within fib National Member Groups.

distribution function of the tensile strength with regards to scale effects. Therefore, they mainly depend on the volume of the mesh elements and the maximum aggregate size. In fact, the maximum aggregate size characterizes the heterogeneity of the material, which is in turn at the origin of the scaling effect of the tensile strength of the rupture in tension. However, these analytical equations were obtained for concretes having compressive strengths between 30 and 130 MPa, in which the maximum aggregate size was much larger than the fibres. In contrast, the high volume of fibres combined with their dimensions (compared with the very small diameter of the aggregates used) make the fibres the main source of heterogeneity in the UHPFRC studied. They induce local stresses concentrations around them and facilitate the initiation of microcracks in the matrix and result in a reduction of the tensile strength. Therefore, the mean tensile strength and its scattering are determined by best fitting the linear elastic segment of the load-deflection curves obtained from the 3-point bending tests.

Figure 3 presents the finite element mesh used to model the 3-point bending tests to identify the mechanical characteristics of the tensile behaviour by inverse analysis. Ten two-dimensional simulations have been performed in plane stresses conditions.

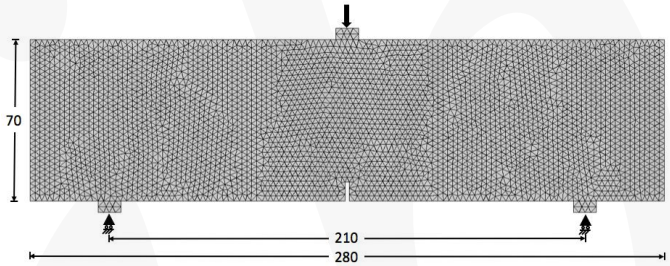


Figure 3: Finite element mesh of the notched beams tested in 3-point bending

Figure 4 presents the numerical *load-crack mouth opening displacement* curves obtained from the 3-point bending tests on the notched beams sawed at a 45° angle to the UHPFRC beam length in comparison to the experimental results. The results show a good agreement between the experimental results and the numerical simulations.

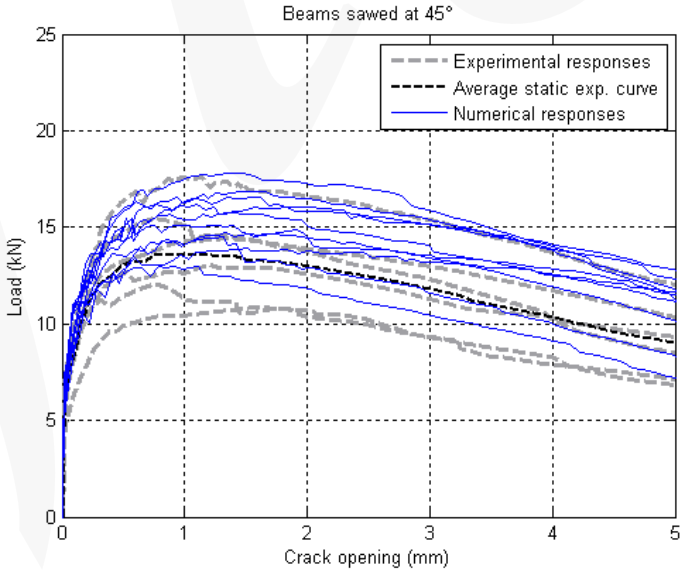


Figure 4: Experimental and numerical load-crack mouth opening displacement curves of the small beams

This document is the intellectual property of the fib – International Federation for Structural Concrete. All rights reserved.
This PDF of fib Bulletin 95 is intended for use and/or distribution solely within fib National Member Groups.

Figure 5 presents example of a crack patterns given by the numerical simulations of the 3-point bending tests of the beam sawed at 45°. The crack patterns were taken right after the initial loss of rigidity and before the peak load. Crack pattern shows the initiation of cracking at the top of the notch. The crack then propagates vertically until it reaches the compression zone, after which several cracks are created and propagate vertically as the initial crack's propagation is blocked.



Figure 5: Example of a cracking pattern of the beams sawed at 45°

The model parameters obtained through the inverse analysis approach are summarized in Table 1 . In addition, the parameters ζ_0 and ζ_c that best fitted the experimental results obtained from the 3-point bending tests are 0.035 mm and 5 mm. The good agreement between the experimental and numerical *load-crack mouth opening displacement* responses suggests that the numerical model originally developed for fibre reinforced concrete is relevant to model the bending behaviour of UHPFRC.

Table 1: Specimen designation and main properties

f_t [MPa]	$\sigma(f_t)$ [MPa]	W [MPa*mm]	σ(W) [MPa*mm]
8.43	1.31	60	72

3.3 Numerical Simulation of the Shear Behaviour of the Beam

Figure 6 presents the finite element mesh used for the reinforced UHPFRC beam simulations. Three two-dimensional simulations have been performed in plane stresses conditions.

To account the bulb-T section of the beam, a variable thickness (in the context of plane stresses simulations) has been considered on all its height. The reinforcement bars have been modelled with classical linear volume elements having a height corresponding to the rebar's diameter. Linear interface elements (similar to those used for simulating cracking of SFRC) have been used between all these volume elements to allow cracks to cross the rebars. Before cracking, the interface elements ensure the continuity of stresses and displacements by using a very high matrix of rigidity. After cracking, the rebar's effect on the cracks is considered as a linear elastic behaviour. This behaviour is modelled by setting the normal and tangential components of interface elements' stiffness to be much smaller than before cracking (Tailhan, Rossi *et al.* 2015). The values of these stiffness components are determined by best fitting the elastic rigidity of the beam. A realistic behaviour of the bond between concrete and rebars can be considered indirectly.

This document is the intellectual property of the fib – International Federation for Structural Concrete. All rights reserved.
This PDF of fib Bulletin 95 is intended for use and/or distribution solely within fib National Member Groups.

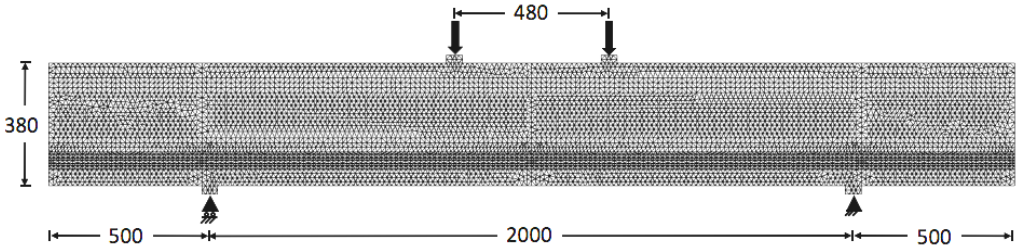


Figure 6: Finite element mesh of the reinforced UHPFRC beam

Figure 7 presents a comparison between the experimental load-deflection curve and the three numerical simulations. The results show a good coherence between the experimental result and the numerical simulations until a deflection of 5 mm, after which the numerical simulations underestimate the experimental behaviour. This may be explained by the numerical identification method for the tensile behaviour of the studied UHPFRC. As mentioned previously, the tensile behaviour of the studied UHPFRC was identified by an inverse analysis approach that consisted on simulating the 3-point bending tests performed on the notched beams sawed from the reinforced UHPFRC beam. Experimentally, it has been observed that multiple cracks initiate at the tip of the notch, therefore not representing the tensile behaviour of the material but rather a structural behaviour in which multiple cracks are sewed by a group of fibres. Therefore, this indirect approach generally underestimates the tensile behaviour of the material due to the stress concentrations occurring at the tip of the notch.

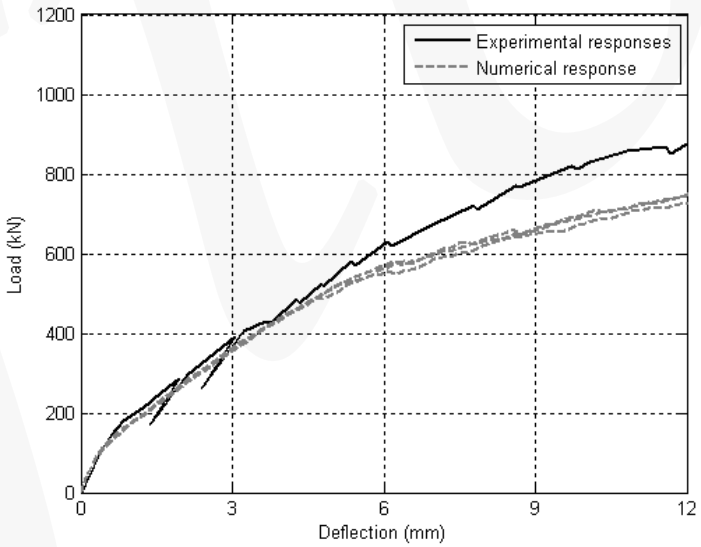


Figure 7: Experimental and numerical load-deflection curves of the reinforced UHPFRC beam submitted to shear loading

Figure 8 presents an example of cracking pattern obtained from the numerical simulations at a deflection of 5 mm. Only cracks larger than 100 µm are shown on the figure. The crack pattern shows that several bending cracks were created at the bottom fibre of the beam. Although bending cracks are first created, their propagation is rapidly blocked by the bending reinforcement. These cracks are mainly responsible for the initial loss of flexural rigidity observed at approximately 180 kN, after which the behaviour of the beam is controlled by its

This document is the intellectual property of the fib – International Federation for Structural Concrete. All rights reserved.
This PDF of fib Bulletin 95 is intended for use and/or distribution solely within fib National Member Groups.

shear behaviour. The crack pattern shows that three diagonal cracks with a maximum crack opening of 0.25 mm have formed. Their propagation is controlled by the bridging effect of the fibres as the beam has no stirrups.

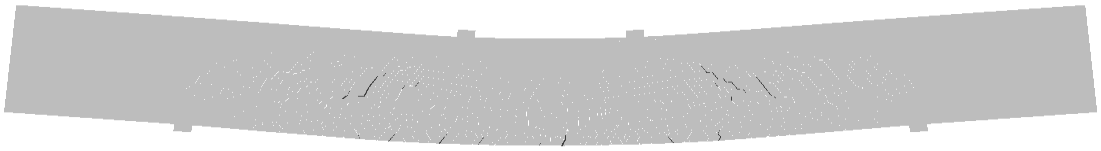


Figure 8: Example of cracking process of the reinforced beam loaded in shear

Figure 9 presents a comparison between the experimental load-deflection curve and the three numerical simulations with the same set of parameters but a 33% increase of the post-cracking energy distribution. The mean post-cracking energy and its standard distribution were respectively increase from 60 to 80 MPa*mm and from 72 to 96 MPa*mm. The results show that the shear behaviour is comparable to the experimental behaviour up to a deflection of 6 mm, after which the model underestimates the shear behaviour of the beam by less than 10%. This confirms that the 3-point bending tests underestimate the post-cracking energy of the tensile behaviour.

To summarize, the results show a good agreement between the experimental result and the numerical simulations both at the global and local scales. Therefore, the results suggest that the studied UHPFRC behaves like usual FRC as the tensile strength and the mechanical effect of the fibres may be modelled by a perfectly brittle behaviour and a nonlinear softening behaviour.

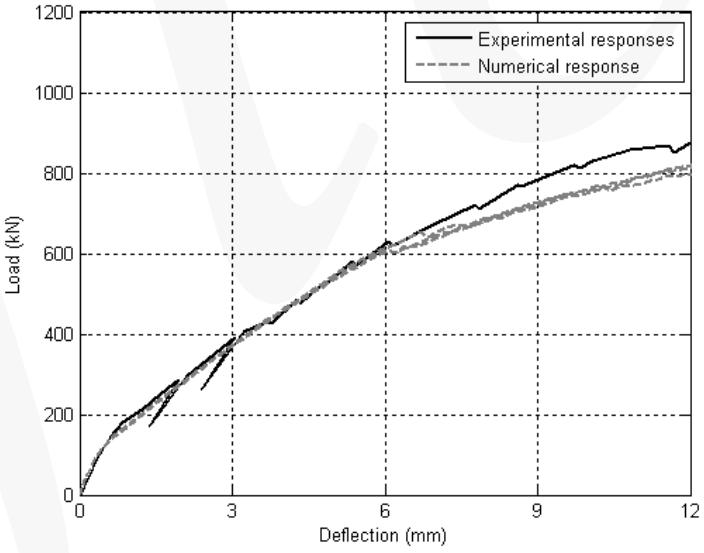


Figure 9: Experimental and numerical load-deflection curves of the reinforced UHPFRC beam submitted to shear loading with increased post-cracking energy

This document is the intellectual property of the fib – International Federation for Structural Concrete. All rights reserved.
This PDF of fib Bulletin 95 is intended for use and/or distribution solely within fib National Member Groups.

4 Conclusions

The objective of this paper is to verify the validity of the probabilistic explicit cracking model developed for SFRC to simulate the behaviour of a reinforced UHPFRC beam subjected to a bending load leading to shear failure. The relevancy of the model is evaluated through the simulation of the mechanical behaviour of the beam. The parameters characterizing the tensile behaviour are determined from the 3-point bending tests performed on beams sawed from the reinforced UHPFRC beam.

The main conclusion of this work can be summarized as follows.

- The probabilistic explicit cracking model is relevant to analyze the mechanical behaviour of a reinforced UHPFRC beam and provide precise information about the cracking process of this type of material.
- The good agreement between the experimental result and the numerical simulations suggests that the studied UHPFRC behaves like usual FRC as the tensile strength and the mechanical effect of the fibres may be modelled by a perfectly brittle behaviour and a nonlinear softening behaviour.

5 References

Baby, F. (2012). *Contribution à l'identification et la prise en compte du comportement en traction des BFUP à l'échelle de la structure. Structures et Matériaux*. Paris, France, Université *Paris-Est. Doctorate: 522 (in french)*.

Rossi, P. and S. Richer (1987). *Numerical Modelling of Concrete Cracking Based on a Stochastic Approach.* Materials and Structures **20**(119): 334-337.

Rossi, P. and X. Wu (1992). *Probabilistic model for material behaviour analysis and appraisement of concrete*. Magazine of Concrete Research **44**(161): 271-280.

Rossi, P., et al. (1994). *Scale effect on concrete in tension.* Materials and Structures **27**: 437-444.

Rossi, P. (2008). *Ultra-high performance fibre reinforced concretes (UHPFRCC): A summary of current knowledge*. Concrete International **30**(2): 31-34.

Rossi, P. (2012). *Experimental Study of Scaling Effect Related to Post-Cracking Behaviours of Metal Fibres Reinforced (MFRC).* European Journal of Environmental and Civil Engineering **16**(10): 1261-1268.

Rossi, P., et al. (2014). *Numerical modelling of cracking in Steel Fibre Reinforced Concretes (SFRC) structures.* Euro-C 2014 : Computational Modelling of Concrete Structures. H. M. Nenad Bicanic, Gunther Meschke, René de Borst. St. Anton am Arlberg, CRC Press. **2:** 463-471.

Rossi, P., et al. (2015). *Analysis of Cracking in Steel Fibre Reinforced Concrete (SFRC) Structures in Bending using Probabilistic Modelling.* Structural Concrete, Journal of the fib.

Tailhan, J.-L., et al. (2010). *From Local to Global Probabilistic Modeling of Concrete Cracking.* Annals of Solid and Structural Mechanics **1**: 103-115.

Tailhan, J.-L., et al. (2015). *Probabilistic numerical modelling of cracking in steel fibre reinforced concretes (SFRC) structures*. Cement and Concrete Composites **55**: 315-321.

Tailhan, J.-L., et al. (2013). *Multi Scale Probabilistic Approaches and Strategies for the Modelling of Concrete Cracking.* VIII International Conference on Fracture Mechanics of Concrete and Concrete Structures (FraMCoS-8). J. G. M. Van Mier, G. Ruiz, R. C. Andrade, Y. Zhang and X. X. Zhang, Portugal.

This document is the intellectual property of the fib – International Federation for Structural Concrete. All rights reserved.
This PDF of fib Bulletin 95 is intended for use and/or distribution solely within fib National Member Groups.
FRC2018: Fibre Reinforced Concrete: from Design to Structural Applications
Joint ACI-*fib*-RILEM International Workshop

UHPFRC Precast slabs and field-cast joints of the Isabey-Darnley pedestrian bridge

Jean-Philippe Charron [1], Clélia Desmettre [1], Étienne Cantin Bellemare [2]

[1] : Department of Civil, Geological and Mining Engineering, École Polytechnique Montréal, Montréal, Canada

[2] : Bridges and Tunnels Division - City of Montreal, Quebec, Canada

Abstract

A cast-in-place reinforced concrete footbridge built in 1967 suffering from extensive concrete spalling and rebar corrosion needed to be replaced. The use of a steel Pony-Warren truss combined with thin precast UHPFRC slabs linked by short UHPFRC field-cast joints was selected to build an innovative, durable and aesthetic footbridge minimizing impact on traffic during construction. Material rationalization allowed respective reductions of 64 % and 91 % of concrete and rebar volumes in the slab in comparison to a conventional reinforced concrete slab. The design process was completed with non-linear finite element calculations to obtain an adequate behaviour of the UHPFRC slabs and joints at service and ultimate limit states. A full-size proof specimen was then tested under positive bending moment and confirmed being adequate and fulfilling all the design specifications. Construction of the precast slab was successful and required less time than a conventional slab. The long-term performance provided by the UHPFRC slab will be followed up in the next decades.

Keywords

Ultra-High Performance Fiber Reinforced Concrete (UHPFRC); precast slabs; field-cast joints; pedestrian bridge; bending behavior.

This document is the intellectual property of the fib – International Federation for Structural Concrete. All rights reserved.
This PDF of fib Bulletin 95 is intended for use and/or distribution solely within fib National Member Groups.

1 Project overview

The Isabey-Darnley pedestrian bridge is located in Montreal (Quebec, Canada) over Highway 520 (average annual daily traffic of 30 000) close to the International Airport. This 61 m long footbridge built in 1967 suffered from extensive concrete spalling and rebar corrosion after 40 years of service (Figure 1a) and needed to be replaced. Among the replacement requirements, traffic delays and redirection below the structures had to be minimized and the new structure had to ensure an excellent durability under severe exposure conditions.

The replacement project objectives of the Bridges and Tunnels Division of the City of Montreal (owner of this bridge) were to design an innovative, durable and aesthetic footbridge minimizing impact on traffic during construction. In this context, the new structure designed by the City of Montreal had a 3-span steel Pony-Warren trusses (Figure 1b) supporting a thin deck made of ultra-high performance fiber reinforced concrete (UHPFRC) precast slabs linked by UHPFRC field-cast joints. This choice was based on the new developments made during a 10-years ongoing industrial research project leaded by Polytechnique Montreal on fiber reinforced concrete precast bridge components (Lachance et al., 2016; Verger-Leboeuf et al., 2017). The construction of the new footbridge was completed in December 2016.



(a) Old structure *(b) New structure*

Figure 1: Isabey-Darnley Pedestrian Bridge

2 Design of precast UHPFRC slabs and field-cast UHPFRC joints

2.1 Concept of the slab

The slab on the Isabey-Darnley pedestrian bridge consists in 11 precast UHPFRC thin elements : 9 interior elements of 5.7 m long and 2.25 m width, and 2 exterior elements of the same width but lengths of 5.9 and 2.1 m. The cross-section of precast slab elements is shown in Figure 2. It illustrates the limited reinforcement in positive and negative bending as well as for crack control requirements.

The precast UHPFRC slabs of 75-mm thick are linked by 125 mm wide UHPFRC field-cast joints (100 mm rebar splices for 10M rebar). The field-cast joints have the same cross-section of the precast slab elements. Their presence is two-folds, first establishes structural continuity from one slab element to the others, second provides a link with the supporting transverse steel beams, located under each joint and spaced at 1.9 m between the two steel Pony Warren trusses. The precast slab includes curbs on lateral extremities (Figure 2) which serve as a security cladding for pedestrians, favour water drainage and strengthen longitudinally the 75-mm thick slab.

This document is the intellectual property of the fib – International Federation for Structural Concrete. All rights reserved.
This PDF of fib Bulletin 95 is intended for use and/or distribution solely within fib National Member Groups.

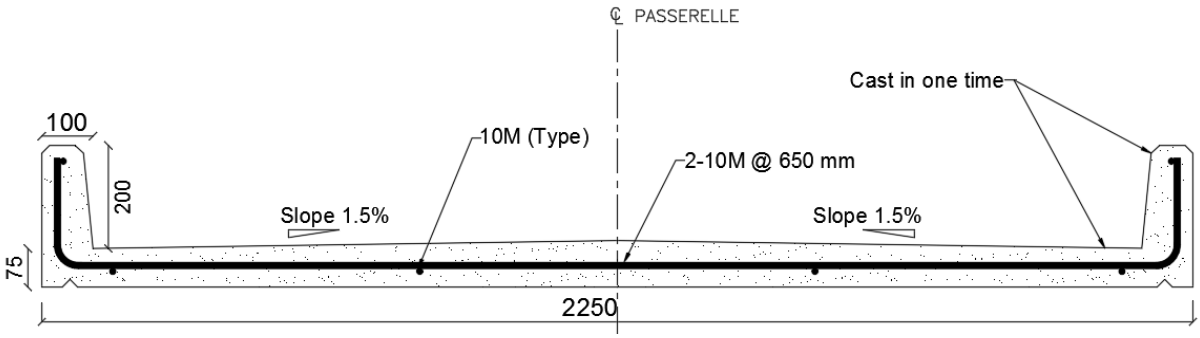


Figure 2: The 75mm-thick precast UHPFRC slab (dimensions are in millimeters)

2.2 Methodology

The design of the precast slabs and field-cast joints were made considering the Canadian Highway Bridge Design Code (CSA, 2006) for loads (dead, live, snow, ice, thermal gradient, handling and exceptional loads) and load combinations. Although the design of UHPFRC structures will be included in the 2019 edition of CSA-S6, the actual edition does not include these specifications. Thus recommendations of the French Association of Civil Engineering (AFGC) for UHPFRC structures (AFGC, 2013) were used in this pilot project for determining mechanical constitutive laws, durability requirements and quality control recommendations. Finite-element analysis with Atena 3D software (Cervenka, 2014) were performed to evaluate the structural behavior of the precast slabs and joints.

2.3 Material properties

UHPFRC technical specifications required for the project are listed in Table 1, they concerned composition, workability, mechanical properties as well as durability. The specifications about the tensile behavior (tensile strength, gain and peak strain) aimed to ensure the presence of an extended strain hardening behavior during which only microcracks develop in the material.

Table 1: Main specifications in the technical performance specifications for the contractor

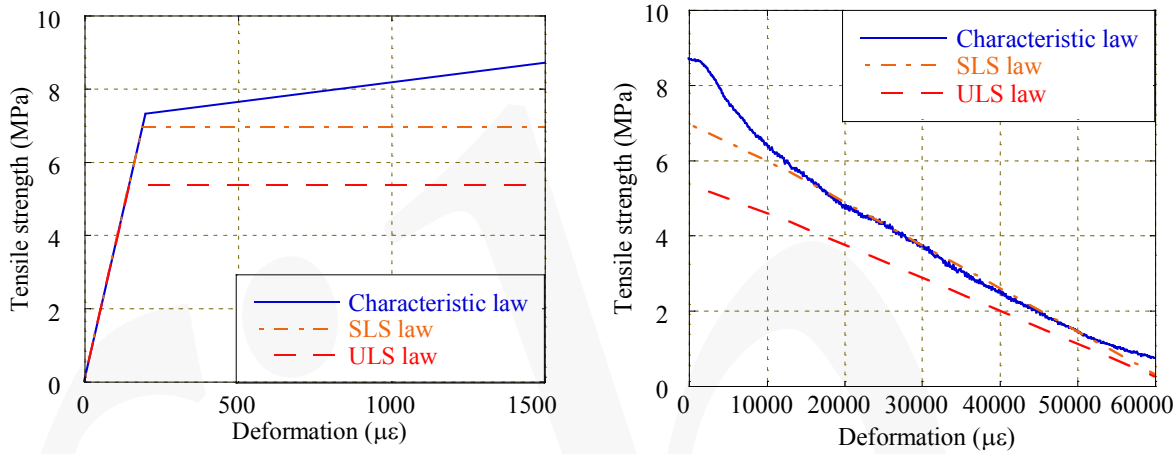
Composition		**Mechanical strength at 28 days**	
Cement type	GU, MH, HS *	Min. compressive strength (f_c)	100 MPa
Min. proportion of silica fume	8 %	Min. tensile strength (f_t)	10.5 MPa
Min. mass of binder	600 kg/m^3	Min. tensile gain (f_t /$f_{t\ elastic}$)	1.2
Max. water/binder ratio	0.25	Min. tensile strain at peak	1500 με
Max. diameter of aggregates	2.5 mm	**Durability**	
Min. quantity of steel fibers	312 kg/m^3	Chloride ion permeability	200 C
Workability		Max. loss at spalling	0.5 kg/m^2
Slump flow	700 ± 50 mm	Freeze-thaw resistance	95 %

* Standard Portland cement, moderate and high sulfate resistance Portland cements.

The tensile constitutive law considered for design was extracted from the mechanical behavior of six dogbone shape specimens of a UHPFRC reference mix that reaches the mechanical strength specified in Table 1. A characteristic tensile law was determined considering the standard deviation between the tensile mechanical behaviors of the six

This document is the intellectual property of the fib – International Federation for Structural Concrete. All rights reserved.
This PDF of fib Bulletin 95 is intended for use and/or distribution solely within fib National Member Groups.

specimens. Finally, as specified in the AFGC recommendations (AFGC, 2013), this characteristic tensile law was reduced by 20 % to consider the effect of the fiber orientation for serviceability limit state (SLS) verifications and by an additional security factor of 25 % for ultimate state (ULS) verifications. Figure 3 illustrates the characteristic law as well as the SLS and ULS design tensile laws obtained according to AFGC recommendations.



(a) Pre-peak behavior *(b) Post-peak behavior*

Figure 3: UHPFRC tensile behavior according to AFGC recommendations

2.4 Numerical simulations

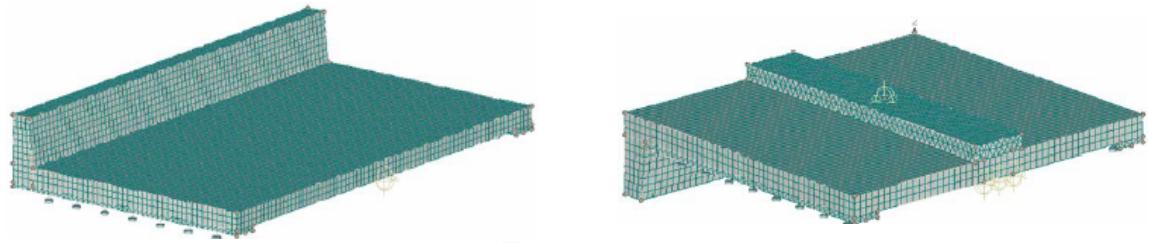
Numerical analyses were performed with the non-linear finite-elements (FE) software ATENA 3D (v.5.1.1) to evaluate the UHPFRC slabs and field-cast joints mechanical behavior (deflection and crack opening in service, rebar yielding and failure mode at ultimate). In these analyses, the slope of the slab road surface (1.5 %) was not considered. The precast slabs behavior was analyzed under positive and negative bending moment at SLS and ULS (span of 1.7 meters) as well as during the construction phases (maximum span of 5.5 m). Additional models were prepared to analyze the mechanical behavior of the field-cast joints in negative and positive bending moment (positive moment occurs with positive thermal gradient in the slab).

The concrete behavior was modeled by a fracture-plastic law. The plasticity model in compression is based on the Menetry-William failure surface which includes a hardening behaviour before reaching the compressive strength, followed by a softening behavior. The fracture model in tension is based on an orthotropic smeared crack model and on the crack band model. The SLS tensile law as well as the SLS compressive behavior of the reference mix were implemented in the models of the UHPFRC slabs and field-cast joints of the pedestrian bridge. Reinforcement was modeled with tensile truss elements having an elastic strength of 400 MPa.

The FE mesh and boundary conditions are illustrated in Figure 4 for the slab under positive bending moment as well as for the field-cast joint under negative bending moment. The displacement was restrained vertically at all supports and horizontally at one support. The models considered the transversal symmetry and only half of the section was thus modeled. Uniform surface loading was applied on road surface (not on the curbs) in the slab model, whereas uniform linear loading (representing the steel beam under the slab) was considered in the joint model. For the modeling of the joints, 2D interface materials with Mohr-Coulomb

This document is the intellectual property of the fib – International Federation for Structural Concrete. All rights reserved.
This PDF of fib Bulletin 95 is intended for use and/or distribution solely within fib National Member Groups.

criteria were introduced to reproduce the exposed aggregate interface between the precast slabs and the field-cast joint.



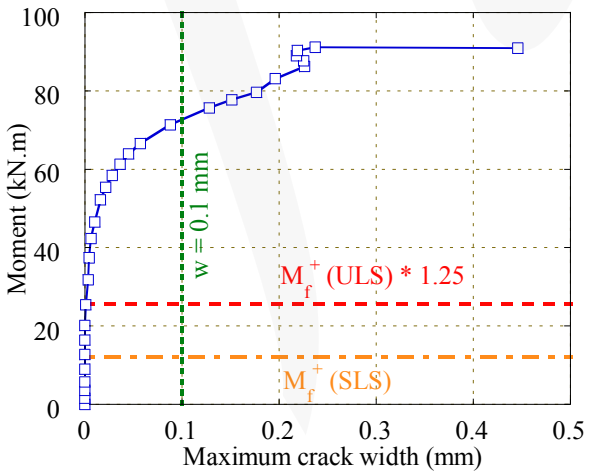
(a) Slab model under positive bending moment *(b) Joint model under negative bending moment*

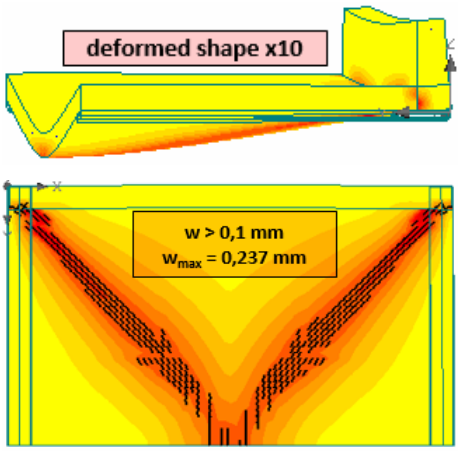
Figure 4: Finite element models

Figure 5 illustrates the longitudinal bending moment-crack width behavior of the slab under positive bending moment (critical condition), as well as the deformed shape and cracking pattern of the model. SLS and ULS strength requirements are shown. Because only the SLS constitutive law was implemented in the numerical model, the factored design moment, $M_f^+(ULS)$, was increased by the global material security factor of 25 % for an adequate comparison with the numerical result. Figure 6 illustrates the longitudinal bending moment-joint opening behavior of the field-cast joints under positive thermal gradient (critical condition), as well as the deformed shape and cracking pattern of the model.

Figure 5a and Figure 6a show that the designs selected for the slab and joint largely surpass the required SLS and ULS design moment and maximal crack width targeted at 0.1 mm at SLS to ensure an extended durability of the bridge deck. All others verification with models showed more capacity reserves at ULS and thinner crack widths at SLS.

The deformed shape and cracking pattern presented in Figure 5b illustrates the bidirectional behavior of the slab. This is due to the similar longitudinal and transversal spans (respectively 1700 and 2250 mm) of the slab over the steel frame, and also to the presence of the curbs that reinforce longitudinally the slab.

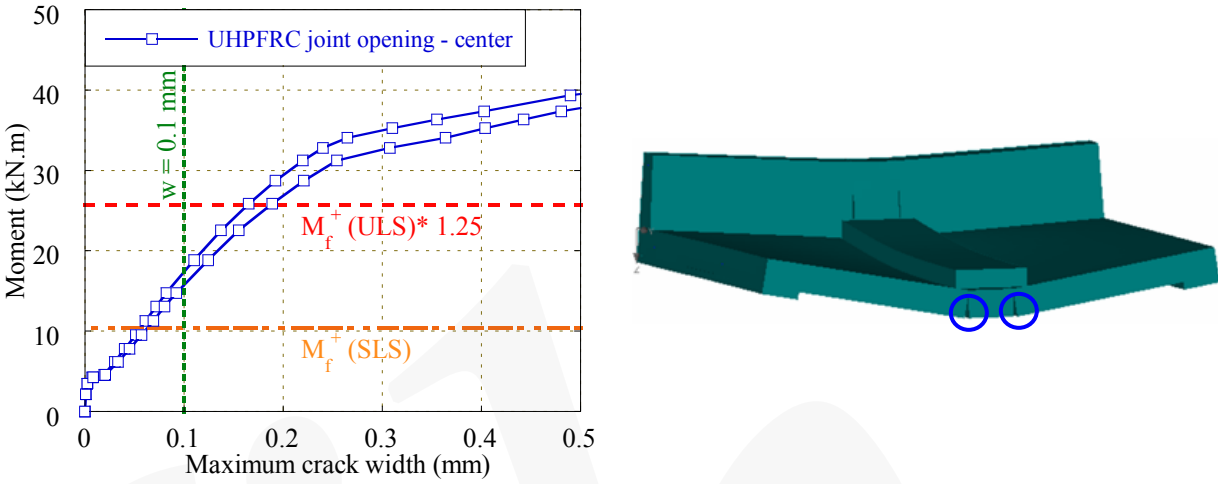




(a) Moment-maximum crack width behavior *(b) Cracking pattern at maximum load*

This document is the intellectual property of the fib – International Federation for Structural Concrete. All rights reserved.
This PDF of fib Bulletin 95 is intended for use and/or distribution solely within fib National Member Groups.

Figure 5: Numerical mechanical behavior of the slab under positive bending moment



(a) Moment-maximum crack width behavior *(b) Cracking pattern at maximum load*

Figure 6: Numerical mechanical behavior of the field-cast joints under positive bending moment

2.5 Design highlights

The exceptional durability of uncracked and cracked UHPFRC in comparison to conventional concrete (AFGC, 2013; Charron et al., 2008; Desmettre, 2011; Hubert et al., 2015; Jooss & Reinhardt, 2002) allowed utilization of a concrete cover of 25 mm according to AFGC recommendations. Moreover, the outstanding mechanical properties of UHPFRC permitted also material rationalization. Overall, the 75-mm thick UHPFRC slab led to a strong reduction of 64% in concrete volume and 91% in rebar volume in comparison to a conventional reinforced concrete slab. Furthermore, the improved bond of UHPFRC to rebar also allowed an important reduction of the bar lap splice (100 mm that represents 10 d_b, traditionally 40 d_b in reinforced concrete) in the joints connecting the slabs, and thus a reduction of the joint length (125 mm).

3 Laboratory test on a real size precast UHPFRC slab

3.1 Test setup and instrumentation

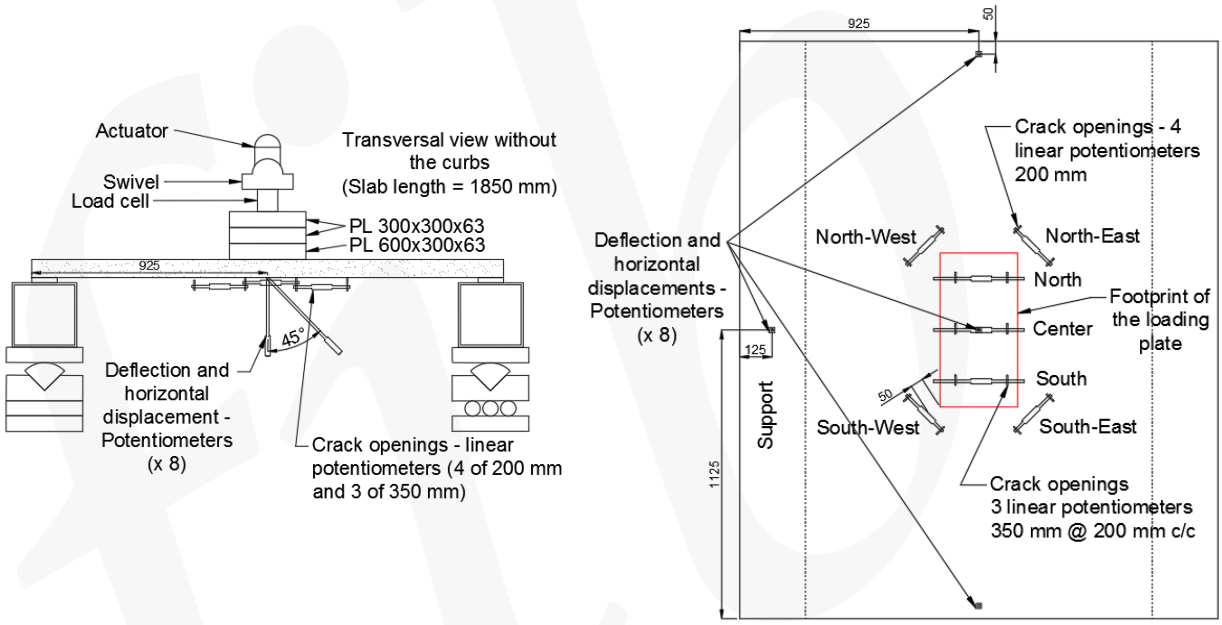
A proof specimen of the precast UHPFRC slabs having the cross-section illustrated in Figure 2 was tested under positive bending moment at Polytechnique Montreal Structural laboratory. The specimen represented one third of the total length of the precast slab, i.e. the length between two transverse beams of the steel frame of the pedestrian bridge.

The setup used to test the proof specimen is illustrated in Figure 7. The curbs of the slab are not shown in Figure 7b for simplification, but there were present at North and South slab extremities. The setup reproduced partly the real structure whose longitudinal spacing between two adjacent steel transverse I-beams is equal to 1900 mm center to center (c/c). Because the proof specimen had a length of 1850 mm, the longitudinal span for the test was equal to 1750 mm c/c of the supports. The transversal length of the proof specimen was 2250 mm as on the real structure. Steel HSS-beam (254x254x8.5 mm) were used to support the slab, having

This document is the intellectual property of the fib – International Federation for Structural Concrete. All rights reserved.
This PDF of fib Bulletin 95 is intended for use and/or distribution solely within fib National Member Groups.

similar flexural inertia and elastic modulus of the steel transverse I-beams of the structure. Therefore, the test on the proof specimen has reproduced the strengthening effect of the curbs on the slab mechanical behavior, but has not considered the effect of the slab continuity at supports.

Because it was not possible in laboratory to apply uniform loading surface as in the numerical models of the design phase, the load was applied at the center of the slab through three superimposed rectangular steel plates connected to a load cell and a 490-kN actuator. Deflections during the monotonic loading were measured with potentiometers at the center of the slab, below the curbs and below the HSS beams (Figure 7). The horizontal displacements were measured at the same locations. Seven additional linear potentiometers were installed at the slab bottom face (Figure 7b). Three of them recorded the crack widths in the longitudinal direction and four measured the crack widths formed at an angle of 45 degrees from the loading plate extremities.



(a) Elevation view, longitudinal direction *(b) View underneath the slab, longitudinal direction*

Figure 7: Laboratory test setup (dimensions are in millimeters)

3.2 Experimental results

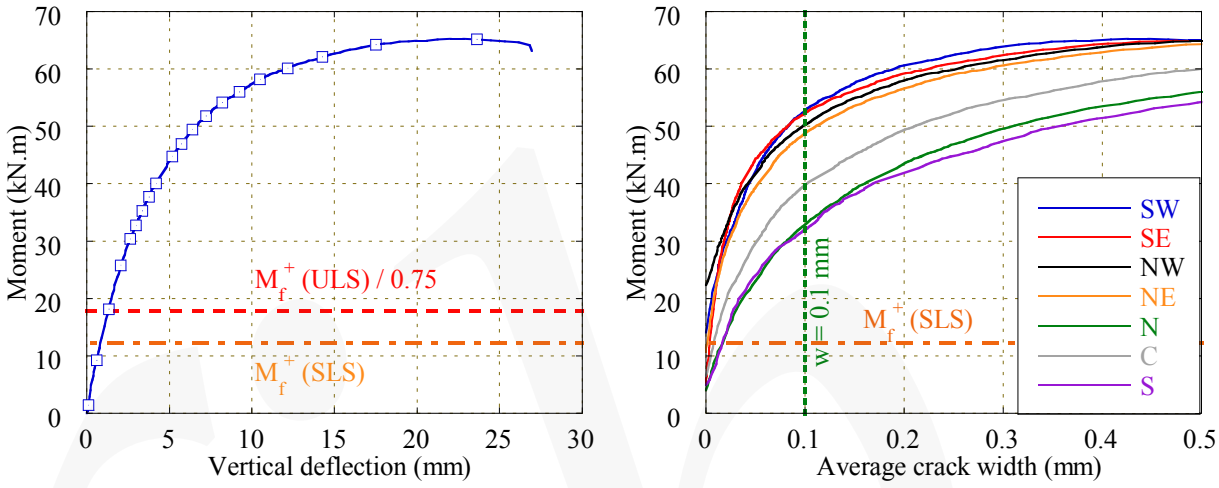
The moment-deflection behavior at the center of the slab is shown in Figure 8a with the SLS and ULS design moments of the structure. The moment-crack opening behavior is plotted in Figure 8b with the SLS design moment and the associated crack opening limit of 0.1 mm selected at the design process. The ULS design moment requirement and SLS crack opening limit were met easily.

The slab remained uncracked until a moment of 4 kN.m. Then cracks developed under the slab around the loading plate footprint before propagating at 45 degrees from the corners of the loading plate footprint up to the corners of the slab (Figure 9). This cracking pattern is explained by the bidirectional behavior of the slab. The total crack openings (Figure 8b) under the loading plate (South: S, Center: C and East: E) were wider than the total crack openings measured at 45

This document is the intellectual property of the fib – International Federation for Structural Concrete. All rights reserved.
This PDF of fib Bulletin 95 is intended for use and/or distribution solely within fib National Member Groups.

degrees at the corner of the loading plate (South-West: SW, North-West: NW, North-East: NE, South-East: SE), since the cracking was more diffuse at 45 degrees (Figure 9).

The mechanical behavior of the proof specimen of the slab was adequate and fulfilled all design specifications.



(a) moment-deflection response *(b) moment-crack opening response*

Figure 8: Slab behavior under monotonic loading



Figure 9: Cracking pattern underneath the slab at the end of the monotonic loading

4 Feed-back on the construction

The UHPFRC mix selected for the project was the UP-F4 material provided by King Packaging Materials. This UHPFRC had a water/binder ratio of 0.2 and a steel fiber content of 4 %-vol. Average compressive strength measured during the project was 124.9 MPa, tensile strength and tensile hardening were 12.0 MPa and 2730 µm/m respectively. All requirements stated in Table 1 for workability and durability were also achieved by the material.

This document is the intellectual property of the fib – International Federation for Structural Concrete. All rights reserved.
This PDF of fib Bulletin 95 is intended for use and/or distribution solely within fib National Member Groups.

The installation of the UHPFRC precast slabs of the Isabey-Darnley pedestrian bridge was completed in 2016 in two phases of 8 hours during the night (complete closing of the highway), while 3 periods of 8 hours during the night (partial closing of the highway) were required for the casting of the UHPFRC field cast joints under winter conditions. With the experience gained, only one period of 8 hours could have been required for the installation of the precast slabs and only 2 periods for the casting of the joints, noticeably limiting the impact on the road traffic.

As a comparison, the Barr pedestrian bridge was built in 2016 with a conventional cast-in-place reinforced concrete slab, it is located about 1 km from the Isabey Darnley pedestrian bridge over the same highway. The construction of the cast-in-place reinforced concrete slab lasted 19 days with 5 nights of traffic perturbation (complete closing of the highway). The utilization of UHPFRC precast slabs and field-cast joints allowed a significant reduction of on-site construction time, as well as a decrease of the traffic management and traffic perturbation around the bridge.

An economic study is ongoing to evaluate directs costs (materials, equipment, labors costs, etc.) and indirect costs (traffic management, construction time, maintenance and replacement costs, etc.) for the Isabey-Darnley pedestrian bridge lifespan. This study will provide a complete review of advantages and drawbacks provided by precast fiber reinforced concrete solution for the construction of concrete infrastructures.

The fabrication and installation of the slabs were carried out without any problems and the result was very satisfactory. This successful project gave interest to the City of Montreal in using UHPFRC in the future.

5 Conclusion

The Isabey-Darnley pedestrian bridge was a pilot application including precast UHPFRC slabs and field-cast UHPFRC joints. The project objectives were to design an innovative, durable and aesthetic footbridge minimizing impact on traffic during construction. These objectives were achieved. The main conclusions regarding the bridge slab are summarized below:

- The innovative design included precast UHPFRC slabs of 75 mm thick linked by 125 mm wide field-cast UHPFRC joints (100 mm rebar splices for 10M rebar). Material rationalization allowed respectively reduction of 64% and 91% of concrete and rebar volumes in comparison to a reinforced concrete slab.
- The design was completed with nonlinear finite element calculations. The mechanical behavior of the slab model under positive bending moment (critical condition), and field-cast joints model under positive thermal gradient (critical condition) have demonstrated that the selected design met easily the ULS design moment requirement and SLS crack opening limit.
- A full size precast UHPFRC slab was tested under positive bending moment. Test results confirmed that the mechanical behavior of the proof specimen was adequate and fulfilled all design specifications.
- The utilization of UHPFRC precast slabs and field-cast joints allowed a significant reduction of on-site construction time, as well as a decrease of the traffic management and traffic perturbation around the bridge.

This document is the intellectual property of the fib – International Federation for Structural Concrete. All rights reserved.
This PDF of fib Bulletin 95 is intended for use and/or distribution solely within fib National Member Groups.

6 Acknowledgements

This project was completed within the framework of an industrial research project funded by the Natural Sciences and Engineering Research Council of Canada, City of Montreal, PJCCI, Béton Brunet and Euclid. The Authors would like to give their appreciation to Ville de Montreal and Ville Mont-Royal for accepting this first pilot application of UHPFRC on one of their bridge infrastructures, and underline the contribution to this project of the general contractor, Entreprises Pera, the precast slab producer, Béton Genial, and the UHPFRC provider, King Material.

7 References

AFGC (2013). *Bétons fibrés à ultra-hautes performances - Recommandations* Association Française de Génie Civil, France.

Červenka, V.; Jendele, L.; and Červenka, J. (2014) *Atean Program Documentation*, Cervenka Consulting Ltd., Prague, Czech Republic, 290 pp.

Charron, J.-P., Denarié, E. and Brühwiler, E. (2008). *Transport properties of water and glycol in an Ultra High Performance Fiber Reinforced Concrete (UHPFRC) under high tensile deformation.* Cement and Concrete Research, 38, 689-698.

CSA (2006). *Canadian Highway Bridge Design Code - CAN/CSAS6-06*, Canadian Standards Association, Mississauga, Ontario, Canada

Desmettre, C. (2011). Contribution à l'étude de la perméabilité du béton armé sous sollicitations statiques et cycliques. Ph. D., École Polytechnique de Montréal, Montréal, Qc, Canada.

Hubert, M., Desmettre, C. and Charron, J.-P. (2015). *Influence of fiber content and reinforcement ratio on the water permeability of reinforced concrete.* Materials and Structures, 48(9), 2795-2807.

Jooss, M. and Reinhardt, H. W. (2002). *Permeability and diffusivity of concrete as function of temperature.* Cement and Concrete Research, 32, 1497-1504.

Lachance, F., Charron, J.-P. and Massicotte, B. (2016). *Development of precast bridge slabs in high-performance fiber-reinforced concrete and ultra-high-performance fiber-reinforced concrete.* ACI Structural Journal, 113(5), 929.

Verger-Leboeuf, S., Charron, J.-P. and Massicotte, B. (2017). *Design and Behavior of UHPFRC Field-Cast Transverse Connections between Precast Bridge Deck Elements.* Journal of Bridge Engineering, 22(7).

This document is the intellectual property of the fib – International Federation for Structural Concrete. All rights reserved.
This PDF of fib Bulletin 95 is intended for use and/or distribution solely within fib National Member Groups.
FRC2018: Fibre Reinforced Concrete: from Design to Structural Applications
Joint ACI-*fib*-RILEM International Workshop

Practical considerations on the application of the recent SIA 2052 guidelines on testing of Ultra-high-performance fiber-reinforced concrete

Roman Loser[1], Janis Justs[1], Pietro Lura[1,2]

[1] : Empa, Swiss Federal Laboratories for Materials Science and Technology, Dübendorf, Switzerland.

[2] : Institute for Building Materials (IfB), ETH Zurich, Switzerland.

Abstract

In this contribution, the experience of the application of the SIA 2052 guidelines for testing of Ultra-high-performance fiber-reinforced concrete (UHPFRC) at Empa is summarized. From the point of view of testing, UHPFRC is a challenging material that sets high requirements with regard to laboratory equipment, specimens' preparation and evaluation of results. The most important tests for UHPFRC classification, namely the evaluation of the uniaxial tensile behavior and of the flexural behavior, are discussed. In particular, a practical example illustrates to which extent probe preparation can influence the measurements of the material properties in tension.

Keywords

UHPFRC, tensile test, flexural test, strain-hardening, fiber orientation, reducing factor

This document is the intellectual property of the fib – International Federation for Structural Concrete. All rights reserved.
This PDF of fib Bulletin 95 is intended for use and/or distribution solely within fib National Member Groups.

1 Introduction

During the last few years, Ultra-high-performance fiber-reinforced concrete (UHPFRC) has progressed from the research lab and from niche applications to becoming a viable and in specific cases the preferred solution for increasingly large construction projects. The main characteristics of this material are high compressive strength, very dense matrix and strain-hardening, a behavior that can be obtained without any additional reinforcement. UHPFRC can be self-compacting and is therefore able to fill small gaps in formworks without any compaction or can be placed in layers of few centimeters. In new constructions, UHPFRC is therefore mainly used for very slender constructions, often in combination with complicated geometries. For example in MuCEM, Marseille (Figure 1), UHPFRC was used in structural elements such as tree-shaped columns, main floor beams, a footbridge as well as in architectural elements – the concrete skin façade and roof [1]. In the US, the Federal Highway Administration is increasingly using UHPFRC to connect precast concrete deck panels and other precast elements in their numerous infrastructure projects [2]. On the other hand, UHPFRC is receiving increased attention also in repair of conventional reinforced concrete structures. In these applications it is often applied as an additional layer, which acts in combination with the existing concrete and strengthens the structure [3, 4]. Moreover, due to its optimal combination of a very dense matrix and strain-hardening behavior, UHPFRC is able to bridge cracks in traditional concrete structures. It has therefore been additionally applied as sealing layer, e.g., in the case of bridge decks that are exposed to chloride penetration from deicing salts used in winter [5].

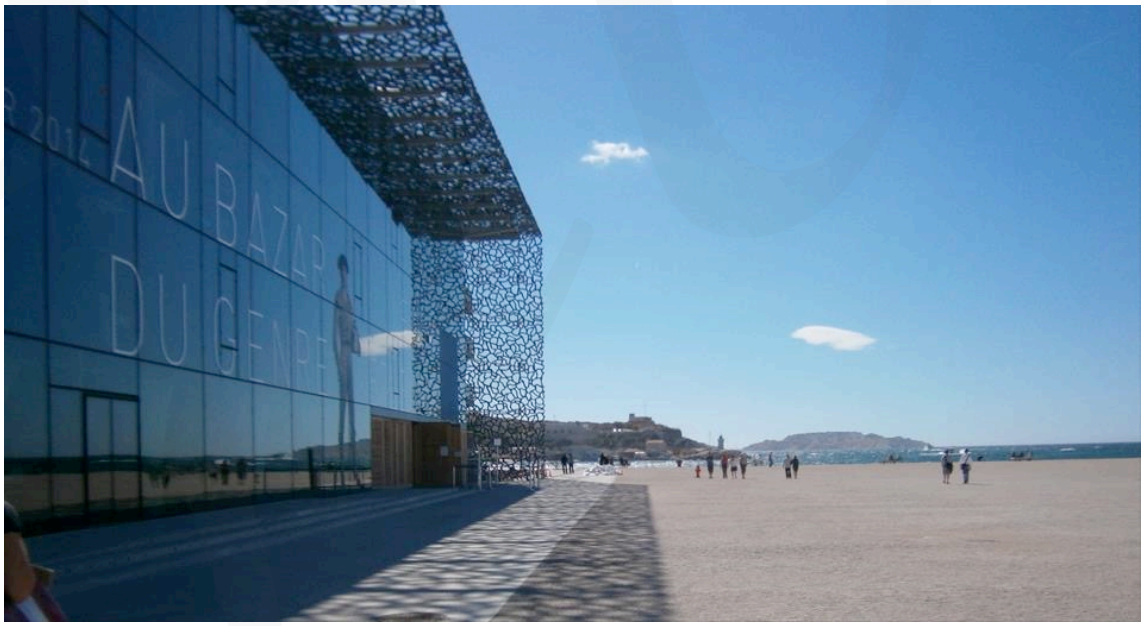


Figure 1: MuCEM, Marseille, details of the concrete skin façade and roof. Original file: Mucem.JPG by Zitronentarte 18.09.2013. The figure was cropped compared to the original. CC-BY-SA 4.0

Due to the recent increase in the use of UHPFRC, standards and guidelines were published recently (e.g., [6,7] for France) or they are in preparation in different countries (Canada, Japan, China, Germany, Austria, USA, etc.). In Switzerland, the guidelines *SIA MB 2052:*

This document is the intellectual property of the fib – International Federation for Structural Concrete. All rights reserved.
This PDF of fib Bulletin 95 is intended for use and/or distribution solely within fib National Member Groups.

Ultra-high performance fiber reinforced concrete (UHPFRC) - Materials, design and execution was published in 2016. In the meantime, the first practical experience with the application of these guidelines has been gathered at Empa. From the point of view of testing, UHPFRC can be described as a challenging material that sets very high requirements with regard to laboratory equipment, specimens' preparation and evaluation of result. In this contribution, the guidelines currently employed in Switzerland will be presented and the most important tests for UHPFRC classification, namely the evaluation of the direct tensile and flexural behavior, will be discussed.

2 The guidelines SIA MB 2052

2.1 General content

In a short document of only 30 pages, SIA MB 2052 gives very concise guidelines divided into the following chapters:

- Field of application;
- Fundamentals on construction technique, dimensioning, durability and quality control;
- Materials: composition, properties of UHPFRC and reinforced UHPFRC;
- Dimensioning;
- Structural design;
- Execution.

In the appendix to the guidelines, additional remarks about quality control and testing of UHPFRC are presented. Moreover, two different tests for the evaluation of the material properties in tension are defined in the appendix: 1) uniaxial tensile tests on bone-shaped specimens and 2) bending strength tests on strip-shaped slab beams. As these two tests deliver the main materials properties for classification of UHPFRC, this paper will focus mainly on these tests.

2.2 Classes of UHPFRC

According to SIA MB 2052, UHPFRC is divided into three different classes (Table 1). The classes are defined by the following material properties:

f_{Utek}: characteristic value of elastic limit tensile strength;

f_{Utuk}: characteristic value of tensile strength;

ε_{Utu}: strain-hardening (strain at tensile strength);

f_{Uck}: characteristic value of compressive strength.

The compressive strength is obtained from compression tests on either cubes (100 mm), cylinders (∅70 mm, h 140 mm) or broken half-prisms with section 40 × 40 mm^2. The conversion factor cubes/cylinders is 1.4. No strength classes are defined, but only a minimum value for the strength that needs to be met is specified. With 120 MPa for the cube compressive strength, it is the same for all classes defined above.

This document is the intellectual property of the fib – International Federation for Structural Concrete. All rights reserved.
This PDF of fib Bulletin 95 is intended for use and/or distribution solely within fib National Member Groups.

f_{Utek}, f_{Utuk} and ε_{Utu} are derived from direct tensile tests and bending tensile tests defined in the appendix of the guidelines. These measurements have to be performed by manufacturers at defined intervals as a quality-control assessment. The average of a series of 6 specimens is used as the characteristic value to assign the tested UHPFRC to one of the three classes shown in Table 1.

Table 1: Classes of UHPFRC according to SIA MB 2052

Class		**UO**	**UA**	**UB**
		No strain-hardening	strain-hardening	
f_{Utek}	MPa	≥ 7.0	≥ 7.0	≥ 10.0
f_{Utuk} / f_{Utek}	-	> 0.7	> 1.10	> 1.20
ε_{Utu}	‰	-	> 1.5	> 2.0
f_{Uck}	MPa	≥ 120	≥ 120	≥ 120

2.3 Testing of UHPFRC in tension

Direct tensile test

Direct tensile tests are performed on bone-shaped specimens as shown in Figure 2, which are produced in moulds of the required geometry. A testing series consists of six specimens. Strain is measured on all four sides of the specimens. Standard strain is based on $l_{mes,1}$ according to Figure 2, while $l_{mes,2}$ is used in case the localized crack is occurring outside the interval $l_{mes,1}$. The outcome of the test is a stress-strain curve where the values f_{Ute}, f_{Utu} and ε_{Utu} can be directly extracted from the exemplary graph shown in Figure 3.

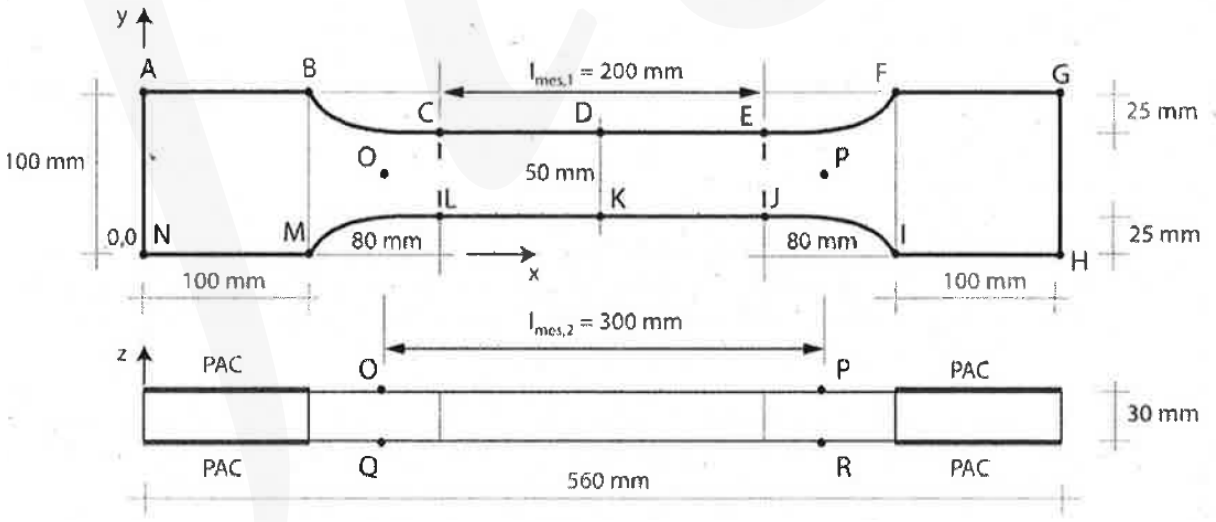


Figure 2: Geometry of bone-shaped specimens for direct tensile test according to SIA MB 2052

This document is the intellectual property of the fib – International Federation for Structural Concrete. All rights reserved.
This PDF of fib Bulletin 95 is intended for use and/or distribution solely within fib National Member Groups.

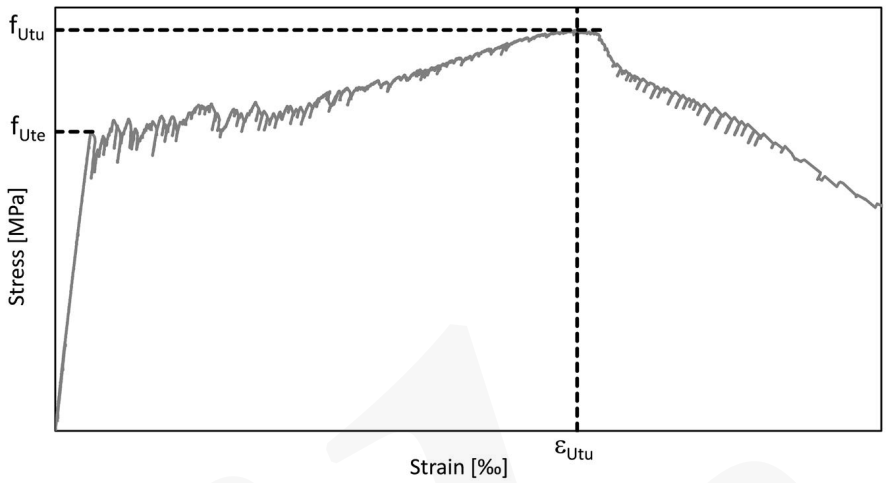


Figure 3: Definition of f_{Ute}, f_{Utu} and ε_{Utu} in a stress-strain curve derived from a direct tensile test

Bending tensile test

Bending tensile tests are performed on strip-shaped slab beams with dimensions of 500 × 100 × 30 mm^3, which are produced in moulds of the required geometry. Also in this case, a testing series consists of six specimens. The measurement consists of a four point bending test according to Figure 4, where the deflection is measured in the middle of the span. The test is delivering a force-deflection curve where the values f_{Ute}, f_{Utu} and ε_{Utu} are derived indirectly by a simplified inverse analysis of the curve.

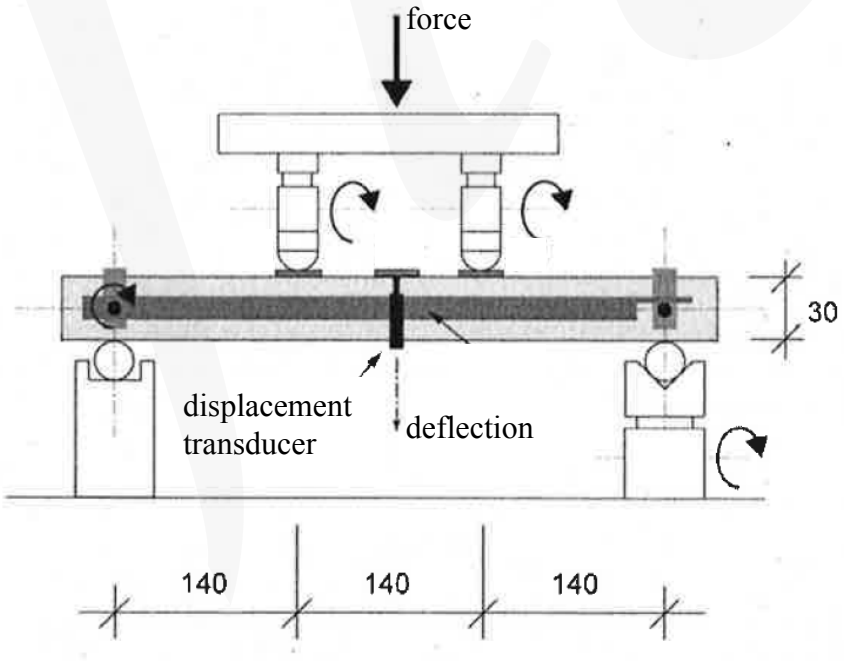


Figure 4: Test setup for bending tensile test according to SIA MB 2052

This document is the intellectual property of the fib – International Federation for Structural Concrete. All rights reserved.
This PDF of fib Bulletin 95 is intended for use and/or distribution solely within fib National Member Groups.

3 Influence of fiber orientation on test results

The results of the direct tensile test and the bending tensile test are crucial for the classification of a UHPFRC. Therefore, the results have to represent the material behavior and they have to be reproducible. However, as the stress in the tensile tests is oriented in one direction, the fiber orientation has a large impact on both the tensile strength f_{Utu} and the strain-hardening ε_{Utu}. The highest and most reproducible values with the lowest scatter are obtained when all fibers are perfectly oriented in the direction of the tensile stress induced by the test setup. As soon as there are some small local inhomogeneities, mainly resulting from local differences in fiber distribution, considerably lower values are consistently found. In addition, the scatter in tensile strength f_{Utu} and strain-hardening ε_{Utu} between nominally identical specimens increases substantially in these conditions. Finally, the results of direct tensile tests and bending tensile tests can differ considerably, which makes the classification of the UHPFRC difficult, as the classification depends on both measurements. In the production of the test specimens, 1) a homogeneous distribution of the fibers in the starting mix, 2) the flowability of the fresh UHPFRC and 3) the manner of formwork filling have all been shown to play a decisive role for the final properties of the material.

The experience gathered at Empa after developing and testing several UHPFRC recipes shows that the manner of formwork filling is the critical parameter. An example from practice is illustrated in Figure 5, which shows results of direct tensile tests according to the SIA 2052 guidelines. The black curves (A) correspond to the first trial, in which the specimens were produced in the manufacturer's laboratory and brought to the testing lab. In the experimental results, a large scatter after having reached the elastic limit strength is apparent, while the curves do not show any clear strain-hardening behavior for all specimens. The tested UHPFRC fulfilled the requirements for UO (see Table 1) only but not for UA, which was the classification the manufacturer was aiming for. Based on these results, the composition of the mixtures was optimized in different steps, resulting in the green curves (B). There was still a considerable scatter in the results, with some specimens showing a distinct strain-hardening behavior and others without any strain-hardening, even if the manufacturer paid special attention when filling the formworks. The class UA was still not reached due to the limited strain-hardening on average. Having a closer look at the fracture cross-section of the final localized crack, a considerable difference in fiber orientation was observed (Figure 6). In particular, in specimens without any strain-hardening, no clear alignment of the fibers in the direction of the load was observed, while the alignment was very clear in specimens with distinct strain-hardening.

The SIA MB 2052 guideline states that the scatter between the 6 curves of a test series needs to be evaluated. However, it contains no precise instructions as to how this evaluation needs to be made and what the exclusion criteria are supposed to be. With a small cross-section of 30 × 50 mm^2 and a specimen length of about 300 mm in the tensile test, there is a high probability that at least one large local inhomogeneity is present in the specimen. This inhomogeneity usually comes from small vortices during casting, in which locally the fibers align perpendicularly to the tensile test direction. Once such inhomogeneity is present, the local crack will open at that location. Depending on how many fibers are not aligned at this point in the tensile direction, the global strain-hardening measured on the specimen is reduced and in extreme cases, no strain-hardening at all is measured. It can thus be concluded that the large scatter and the lack of strain-hardening behavior of most test specimens in series (B) of Figure 5 are caused by random local inhomogeneities, which arise due to the production

This document is the intellectual property of the fib – International Federation for Structural Concrete. All rights reserved.
This PDF of fib Bulletin 95 is intended for use and/or distribution solely within fib National Member Groups.

process of the tested specimens. Thus, it can be concluded that these results do not reflect the general material behavior, but mainly the quality of the test specimen production. This can obviously not be the goal of the material classification of an UHPFRC. An assessment of the scatter as required by the guidelines is therefore operator-dependent and to a certain extent subjective, since the influence of the test specimen production on the fiber orientation from the test results is not always obvious. This is especially true if the test specimens were not produced by the laboratory in which they are tested and no precise information about the manufacturing process is available (this is unfortunately often the case in practical applications).

In the present case, it can be concluded that the optimization of the formulation was carried out by the manufacturer based on results that were decisively influenced by random local inhomogeneities originating from the test specimen production. In addition, the reproducibility of the results is clearly limited, which additionally adversely affects material development.

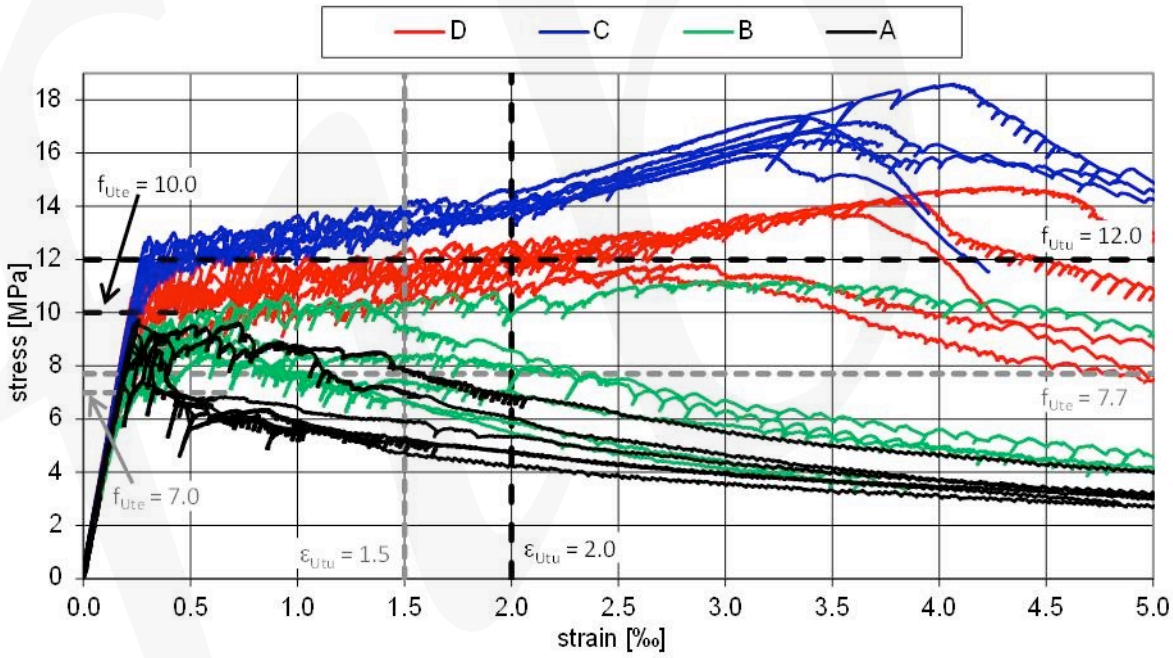


Figure 5: Example curves from direct tensile tests according to the SIA 2052 guidelines for the development of a UHPFRC mixture. Series of 6 specimens for every trial. Including limit values for class UA (dashed gray) and UB (dashed black)

This document is the intellectual property of the fib – International Federation for Structural Concrete. All rights reserved.
This PDF of fib Bulletin 95 is intended for use and/or distribution solely within fib National Member Groups.

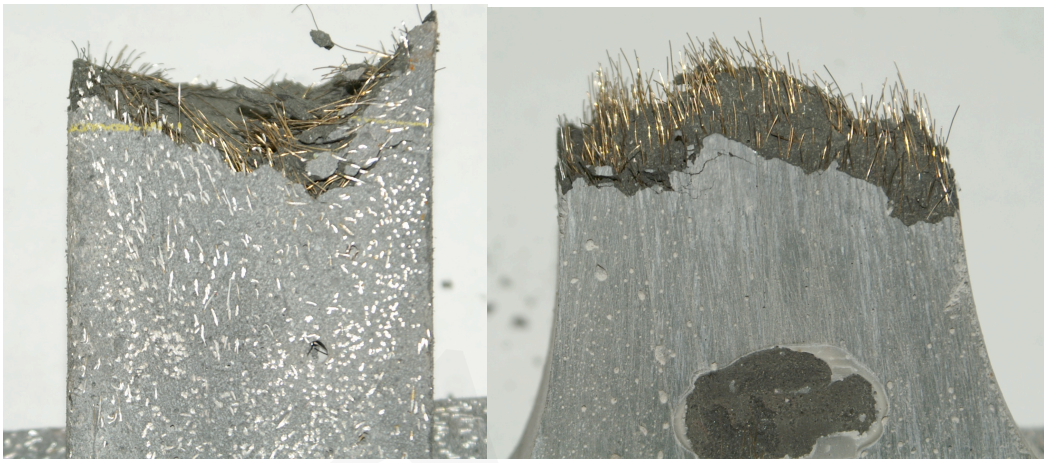


Figure 6: Fiber orientation in the fractured cross-section of the final localized crack, shown for two specimens of the same testing series. Specimen without any strain-hardening (left) and with distinct strain-hardening (right)

To investigate further the above-discussed influence of specimen manufacturing on the material properties, a UHPFRC with identical mixture composition as for Series (B) was mixed again at the Concrete and Construction Chemistry Laboratory at Empa. The formwork was filled in several layers with a long half pipe, allowing the UHPFRC to flow very homogenously into the formwork from one side to another. The filling in several layers should reduce the probability to have local inhomogeneities covering the whole cross-section. The resulting stress-strain curves (blue curves (C) in Figure 5) are completely different from the curves (B), with much higher values for f_{Ute}, f_{Utu} and ε_{Utu} and with very small scatter. Indeed, the results of series (C) fulfill the requirements for the highest class UB shown in Table 1. Based on these results, it can be assumed that the average of the six curves represents the materials properties in case of fiber orientation in the direction of the tensile stress. These results have a very good reproducibility within one series, which makes it possible to optimize the mixture in regard to the mechanical properties. As a last step, the UHPFRC was produced again with the identical mixture composition but at the construction site, with disadvantageous production conditions compared to laboratory conditions. However, the manner of specimen production was identical to the one employed for series (C). The obtained values (red curves (D) in Figure 5) were somewhat lower and with a larger scatter compared to lab conditions (C). However, the scatter in the red curves (D), representing the material properties of the UHPFRC produced under construction site conditions is very limited up to quite large strains and increases only thereafter. In any case, the values are much higher and more homogeneous compared to series (B), which emphasizes the importance of the manner of formwork filling. However, even in case of perfect formwork filling it can be concluded that a certain safety margin must be provided to fulfill the requirements for a certain class, even in cases where the specimens are produced under construction site conditions.

The experience with different test series in which both direct tensile tests and bending tensile tests were conducted shows that the influence of the formwork filling on the fiber orientation also applies to the four point bending test. However, the stress distribution in the specimen is different and therefore the influence of a certain local inhomogeneity is not the same in case of both testing procedures. Therefore, the comparability of the test results

This document is the intellectual property of the fib – International Federation for Structural Concrete. All rights reserved.
This PDF of fib Bulletin 95 is intended for use and/or distribution solely within fib National Member Groups.

between the two procedures is not optimal in case of the presence of local inhomogeneities and an assessment of the results in regard to optimization of a mix is additionally hindered.

4 Transferability of test results to structures

As shown in Section 3, only a defined fiber orientation results in reproducible curves in case of uniaxial tensile stresses and consequently in an upper limit of the mechanical properties. However, these results can only be directly transferred to structures for the case of slender members loaded in tension. In the case of slabs, the fiber orientation is at least two dimensional, invariably resulting in lower mechanical properties. On the other hand, the influence of local inhomogeneities in fiber distribution is less pronounced in such cases compared to the direct tensile tests.

In the SIA MB 2052 guidelines, two reducing factors that take into account the fiber orientation are defined. η_k is the fiber orientation factor, which is 0.90 in case of global load-bearing (redistribution of stresses is possible) and 0.75 in case of local load-bearing (no stress redistribution is possible). η_{hU} takes into account the influence of the thickness of the component and is going from 1.0 for thicknesses up to 50 mm down to 0.8 for thicknesses up to 100 mm.

Comparing these factors with the results in Figure 5, a preliminary conclusion is that they do not appear to be conservative for the case of the specific UHPFRC examined here. However, the characteristic values of f_{Utek} and f_{Utuk} are additionally divided by a resistance factor of $\gamma_U = 1.50$.

Since the manner of placing UHPFRC has a tremendous influence on the fiber orientation and therefore on the mechanical properties, the guidelines give additional restrictions for load-bearing UHPFRC. In cases where the share of UHPFRC in the total load-bearing capacity is higher than 30%, prototypes of the components have to be produced and the mechanical properties have to be determined on specimens obtained by cutting the prototypes and then assessed according to [8].

5 Concluding remarks

The strain-hardening behavior of a UHPFRC is the characteristic feature of this material. The possibility of testing this material behavior in a reproducible manner with simple tensile tests is not only decisive for the classification of a UHPFRC recipe, but also for material development and quality control performed by the manufacturers.

As has been shown in this contribution, the production of test specimens with fibers oriented as homogeneously as possible in the tensile direction is the decisive factor for reproducible results, which requires the corresponding know-how of the workers involved. This inevitably results in an upper limit of mechanical properties that is obtained for UHPFRC produced in a specialized testing laboratory. UHPFRC produced under construction site conditions and test specimens of the same formulation produced locally may show reduced mechanical performance despite the fact that utmost care was taken to prepare the specimens. This is in particular true for the strain hardening behavior.

It has been shown that the mechanical properties, in particular the strain-hardening behavior, are strongly influenced by the local fiber orientation. The transferability of the test results to a

This document is the intellectual property of the fib – International Federation for Structural Concrete. All rights reserved.
This PDF of fib Bulletin 95 is intended for use and/or distribution solely within fib National Member Groups.

specific application on the construction site must therefore be critically examined. For this reason, it is essential to carry out tests on prototypes of the actual concrete component when the share of UHPFRC in the total load-bearing capacity is relatively high, as is also required by the SIA 2052 guideline. For on-site testing, the required tests defined in the guideline should be revised so that an appropriate information on quality is available for any type of workability.

6 References

[1] R. Ricciotti, J. Portelatine, F. Nicolas, (2011). *Museum of European and Mediterranean Civilizations (MuCEM): High UHPFRC Content Structure Design.* Designing and Building with UHPFRC (eds F. Toutlemonde and J. Resplendino), John Wiley & Sons, Inc., Hoboken, NJ USA. doi: 10.1002/9781118557839.ch33

[2] B. Graybeal, (2014). *Design and Construction of Field-Cast UHPC Connections.* FWHA publication No: FHWA-HRT-14-084,.

[3] E. Brühwiler, E. Denarié, (2013). *Rehabilitation and Strenghtening of Concrete Structures Using Ultra-High Performance Fibre Reinforced Concrete*. Structural Engineering International. 23(4):450-7.

[4] K. Wassmann, E. Brühwiler, P. Lunk, (2016). *Strengthening of RC slabs using UHPFRC – Concept and applicatios*. 4th International Symposium on UHPC and High Performance Construction Materials, Kassel, 9.-11.03.2016.

[5] E. Brühwiler et al., (2015). *Strengthening the Chillon viaducts deck slabs with reinforced UHPFRC*. IABSE Conference – Structural Engineering: Providing Solutions to Global Challenges, September 23-25 2015, Geneva, Switzerland

[6] NF P 18-470 (2016). *Béton fibrés à ultra-hautes performances – Spécifications, performance, production et conformité*, AFNOR, Paris.

[7] NF P 18-710 (2016). *Calcul des structures en béton – Régles spécifiques pour les bétons fibrés à ultra-hautes performance (BFUP)*, AFNOR, Paris.

[8] Recommondation AFGC (2013). *Ultra High Performance Fibre-Reinforced Concretes.*

This document is the intellectual property of the fib – International Federation for Structural Concrete. All rights reserved.
This PDF of fib Bulletin 95 is intended for use and/or distribution solely within fib National Member Groups.
FRC2018: Fibre Reinforced Concrete: from Design to Structural Applications
Joint ACI-*fib*-RILEM International Workshop

Effect of Fibers on the Flexural Behaviour of Beams Built with High-Strength Concrete and High-Strength Reinforcement

Roukaya Bastami[1], Yang Li[1], Omar Algassem[1], Hassan Aoude[2]

[1] : Graduate student, University of Ottawa, Ottawa, Canada.

[2] : Associate Professor, University of Ottawa, Ottawa, Canada.

Abstract

Recently there has been increased interest in the use of high-strength concrete (HSC) and high-strength reinforcement (HSR) in structures. The high-performance properties of these materials can allow for more efficient structural designs and reduced reinforcement congestion which can improve constructability. On the other hand, both HSC and HSR show reduced strain capacity when compared to more conventional materials, which can raise concerns about the ductility of structures built with these materials. The provision of steel fibers is one solution to reduce the brittleness of high-strength concrete. Similarly, the use of fiber-reinforced HSC may be better suited for structures built with high-strength reinforcement due to the increased strain-capacity of fiber-reinforced concrete in compression. This paper presents the results of a study examining the effect of steel fibers on the flexural behaviour of beams built with high-strength concrete and high-strength reinforcement. As part of the study, a total of six high-strength concrete beams, built with and without fibers, and reinforced with normal-strength (Grade 400 MPa) and high-strength (Grade 690 MPa) bars are tested under four-point bending. Test parameters include the effect of concrete type (plain HSC vs. fiber-reinforced HSC), reinforcement type (normal-strength vs. high-strength bars) behaviour. As expected, the use of fibers improved the overall load-deformation response of HSC beams built with normal-strength reinforcement. The improved toughness of fiber-reinforced HSC is also shown to be better suited for beams built with high-strength reinforcement when compared to plain HSC, resulting in improved ductility.

Keywords

High-strength concrete, High-strength reinforcement, Fibers, Steel fibers, Beams, Flexure

This document is the intellectual property of the fib – International Federation for Structural Concrete. All rights reserved.
This PDF of fib Bulletin 95 is intended for use and/or distribution solely within fib National Member Groups.

1 Introduction

The provision of fibers in concrete improves many of its properties, including enhanced tensile resistance, post-cracking capacity and flexural toughness (Di Prisco et al. 2009). Similarly, the confining ability of fibers improves the strain capacity and ductility of concrete in compression (Campione et al. 2010). In beams, the improved diagonal tension capacity of fiber-reinforced concrete (FRC) allows for increased shear resistance, while its improved compressive and tensile properties allow for enhanced flexural ductility (Meda et al. 2005, 2012).

Recently there has been increased interest in the use of high-strength concrete (HSC) and high-strength reinforcement (HSR) in structures. HSC may be defined as concrete which has a compressive strength greater than 55 MPa (ACI, 2016), while high-strength steel reinforcement may be defined as steel reinforcement having yield strengths exceeding 500 MPa (ATC, 2014). The high-performance properties of these materials can allow for more efficient structural designs and reduced reinforcement congestion which can improve constructability. On the other hand, both HSC and HSR show reduced strain capacity when compared to conventional concrete and steel, which can raise concerns about the ductility of structures built with these materials (Mast et al., 2008). The provision of fibers is one solution to reduce the brittleness of high-strength concrete. Similarly, the use of fiber-reinforced HSC may be better suited for structures built with high-strength reinforcement due to the increased toughness and strain-capacity of fiber-reinforced concrete in compression.

This paper presents the results of a study examining the effect of steel fibers on the flexural behaviour of beams built with high-strength concrete and high-strength reinforcement. As part of the study, a total of eight high-strength concrete beams, built with and without fibers, and reinforced with two different ratios of normal-strength (Grade 400 MPa) and high-strength (Grade 690 MPa) bars are tested under four-point bending. Test parameters include the effect of concrete type (plain HSC vs. fiber-reinforced HSC), reinforcement type (normal-strength vs. high-strength bars).

2 Experimental program

2.1 Specimen geometry and material properties

A total of eight (8) beam specimens were tested as part of this investigation. Concrete in the beams consisted of plain high-strength concrete (HSC) or high-strength fiber reinforced concrete (HSFRC) containing steel fibers. The specimens are subdivided in four series. Series 1 beams were built with plain HSC, stirrups and conventional (Grade 400 MPa) American Size No.4 (A_b = 129 mm^2) or Canadian size 15M (A_b = 200 mm^2) reinforcing bars, resulting in tension steel ratios of ρ = 1% and 1.6%. Series 1F included 2 companion beams built with HSFRC and No.4/15M normal-strength bars, but without stirrups. Series 2 beams were built with stirrups and American Size No.4 or No. 5 high-strength (Grade 690 MPa) ASTM A1035 bars, while Series 2F included 2 companion beams built HSFRC, stirrups and No.4/No.5 high-strength reinforcement.

As shown in Figure 1, the beams had dimensions of 125 mm x 250 mm x 2440 mm, and were tested over a simply-supported span of 2232 mm. The HSFRC beams in Series 1F were reinforced without transverse reinforcement, since it was expected the fibers would be sufficient

This document is the intellectual property of the fib – International Federation for Structural Concrete. All rights reserved.
This PDF of fib Bulletin 95 is intended for use and/or distribution solely within fib National Member Groups.

to prevent shear failure. The remaining beams in Series 1, 2 and 2F were reinforced with U-shaped stirrups made from 6.3 mm steel wire, spaced at 100 mm in the shear spans to promote flexure failure. It was decided to include stirrups in Series 2F due to the increased shear demands imposed by the high-strength reinforcement. To facilitate construction, 2 - 6.3 mm bars were also provided at the top of the beam sections (in the shear spans only). It in noted that all beams in this study failed in flexure, and the constant moment region for all specimens was identical and did not contain stirrups.

Table 1 and Figure 1 show a summary of the beam designs in each series and provides information on concrete type, fiber content (0% or 1%), fiber type (ZP fibers), longitudinal steel bar size (No.4, 15M or No.5 bars) and longitudinal reinforcement type (normal-strength vs. high-strength, where "HS" refers to the use of high-strength bars).

Table 1: Specimen designation and main properties

Series	Beam I.D.	Concrete		Fibers			Longitudinal Reinforcement			Stirrups provided?
		Mix	f'_c (MPa)	Type	Length (mm)	V_f (%)	Type	Grade (MPa)	Amount & Size	
Series 1	HSC-0%-No.4	HSC	108	-	-	-	NS	400	2-No.4	Yes
	HSC-0%-15M	HSC	107	-	-	-	NS	400	2-15M	Yes
Series 1F	HSC-1%ZP-No.4	HSFRC	108	Steel ZP	30	1.0	NS	400	2-No.4	No
	HSC-1%ZP-15M	HSFRC	106	Steel ZP	30	1.0	NS	400	2-15M	No
Series 2	HSC-0%-No.4(HS)	HSC	96	-	-	-	HS	690	2-No.5	Yes
	HSC-0%-No.5(HS)	HSC	95	-	-	-	HS	690	2-No.5	Yes
Series 2F	HSC-1%ZP-No.4(HS)	HSFRC	104	Steel ZP	30	1.0	HS	690	2-No.4	Yes
	HSC-1%ZP-No.5(HS)	HSFRC	104	Steel ZP	30	1.0	HS	690	2-No.5	Yes

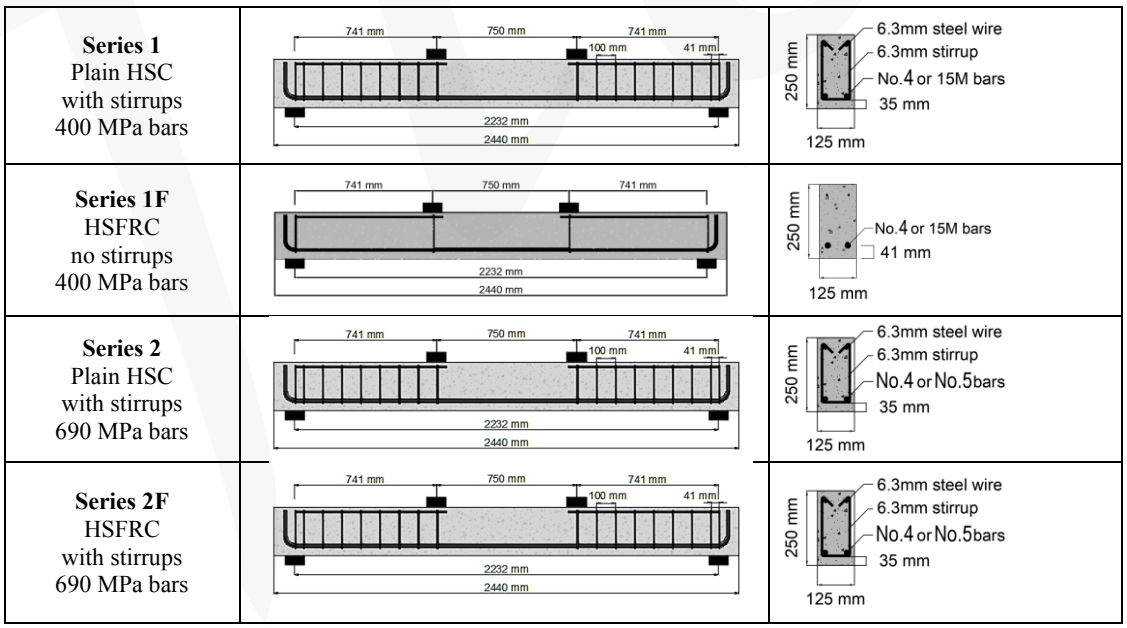


Figure 1: Beam dimensions and reinforcing details (specimens in Series 1,1F, 2 and 2F)

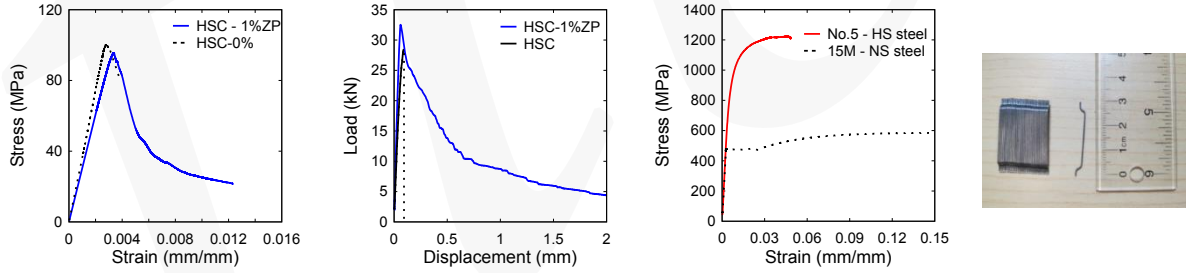
This document is the intellectual property of the fib – International Federation for Structural Concrete. All rights reserved.
This PDF of fib Bulletin 95 is intended for use and/or distribution solely within fib National Member Groups.

2.2 Material parameters

The high-strength concrete mix in this study contained Portland cement, slag, silica fume, two sizes of coarse aggregate (13 mm and 20 mm), sand and liquid admixtures (a super-plasticizer and a set retarder) and had a target strength of 100 MPa (see Table 2). HSFRC containing steel fibers was constructed with the same HSC base mix, with fibers added at a volumetric fiber content of 1% (78 kg/m^3). The hooked-end ZP steel fibers had a length of 30 mm, diameter of 0.55 mm and tensile strength of 1350 MPa. The compressive strengths of the concrete in each beam, obtained by testing 100 mm x 200 mm cylinders, are reported in Table 1. Figure 2a shows sample stress-strain curves for the two concrete types, where it can be seen that the use of steel fibers improves the compressive toughness of the HSC concrete. Flexural strength and toughness were assessed by testing 100 x 100 x 400 mm prisms in accordance with the ASTM C1609 standard (sample load-deflection curves are shown in Figure 2b) and average toughness and residual stress results are reported in Table 2. Sample stress-strain curves for the normal-strength and high-strength bars in tension are shown in Figure 2c.

Table 2: Concrete mixes properties and ASTM C1609 test results

Concrete	Mix constituents (kg/m^3)								ASTM C1609 results			
	Cement	Slag	Silica Fume	Sand	Fine Aggregate (13 mm)	Coarse Aggregate (19 mm)	Water	Fiber content	Peak stress (MPa)	Toughness T_{150} (J)	Residual stress at L/600 (MPa)	Residual stress at L/150 (MPa)
HSC	373	164	48	734	560	560	157	-	8.53	-	-	-
HSFRC	373	164	48	734	560	560	157	78	9.76	21.7	4.17	1.44



a) Concrete in compression (stress-strain)

b) Concrete in flexure (load-deflection)

c) Longitudinal steel in tension (stress-strain)

d) Steel fibres

Figure 2: Material test results and fibers

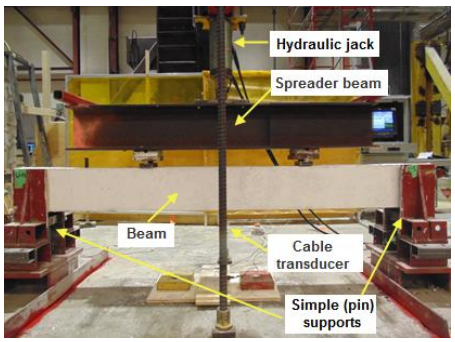


Figure 3: Beam setup for static four-point bending tests

This document is the intellectual property of the fib – International Federation for Structural Concrete. All rights reserved.
This PDF of fib Bulletin 95 is intended for use and/or distribution solely within fib National Member Groups.

2.3 Test setup

The setup shown in **Figure 3** was used to test all beams under quasi-static four-point bending. The beams were simply supported over a span of 2232 mm, with a constant moment region of 750 mm and two equal shear-spans of 741 mm. A manually operated hydraulic jack was used to apply the loading which was then transferred to the specimens as two point loads using a steel spreader beam. Load was recorded using a load-cell placed below the hydraulic jack, with displacement at mid-span captured using a cable displacement transducer. Strains in the reinforcing bars were monitored using strain-gages which were applied on the tension steel at mid-span. Loading of the beams began under load-control until signs of yielding were detected. Upon yielding, loading continued under displacement-control until failure of the specimens (concrete crushing or 15% drop in load after peak).

3 Experimental results

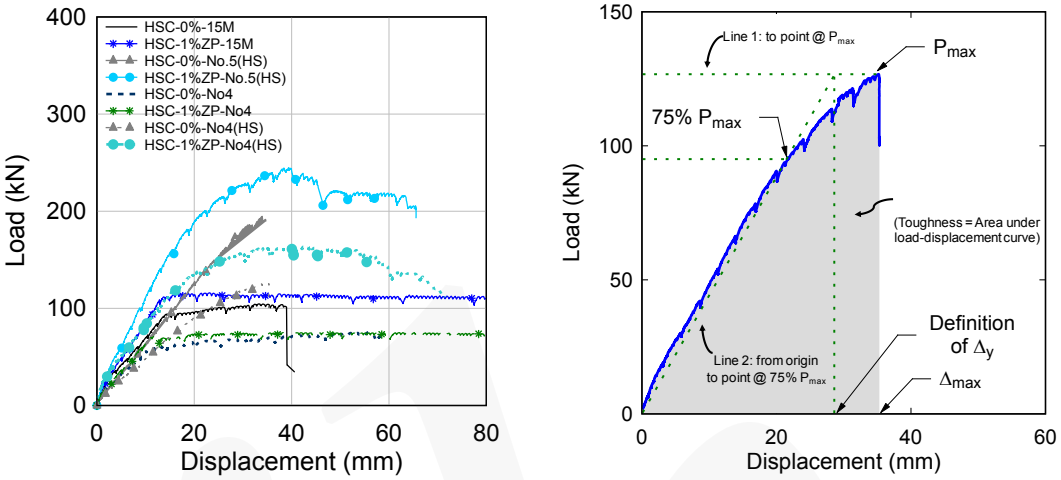
3.1 Summary of results

The load-deflection response of the Series 1/1F and 2/2F specimens are plotted in Figure 4a. Photographs of the beams at the end of testing, are shown in Figure 5. Table 3 summarizes key data extracted from the load-deflection curves, including yield load (P_y) and maximum load (P_{max}), yield displacement (Δ_y) and maximum (failure) displacement (Δ_{max}), beam stiffness after cracking, ductility (Δ_{max}/Δ_y) and toughness (A_u), taken as the area under the load-deflection curve until Δ_{max}, as well as failure mode. The failure of all beams was in flexure in the constant moment region. The beams with high-strength reinforcement do not show well-defined yield points due to the nature of the steel stress-strain relationship; therefore, yielding was estimated using the method shown in Figure 4b, where the yield displacement is found from an equivalent elasto-plastic system with reduced secant stiffness at 0.75 of the ultimate load P_{max} (Park, 1989). Displacement Δ_{max}, corresponded to the displacement at 15% reduction in peak resistance or sudden loss in load-carrying capacity, while it was taken until the end of testing for those fiber-reinforced concrete specimens that did not show a significant drop in capacity.

Table 3: Experimental results extracted from load-deflection curves

Beam I.D.	Load		Displacement		Stiffness (kN/m)	Ductility Δ_{max}/Δ_y	Toughness A_u (J)	Failure mode
	Yield P_y (kN)	Max. P_{max} (kN)	Yield Δ_y (mm)	Failure Δ_{max} (mm)				
HSC-0%-No.4	58.1	75.5	10.9	58.6	5.3	5.4	3180	Flexure (concrete crushing)
HSC-0%-15M	94.5	104.6	14.9	40.7	5.6	2.7	3272	Flexure (concrete crushing)
HSC-1%ZP-No.4	70.0	75.1	12.8	82.2	5.5	6.4	5621	Flexure (fiber pullout)
HSC-1%ZP-15M	111.6	115.9	14.5	124.0	7.7	8.6	12888	Flexure (fiber pullout)
HSC-0%-No.4(HS)	118.4	126.7	29.2	35.2	4.1	1.2	2655	Flexure (concrete crushing)
HSC-0%-No.5(HS)	185.4	194.7	31.4	34.0	5.9	1.1	4100	Flexure (concrete crushing)
HSC-1%ZP-No.4(HS)	139.1	163.7	22.9	71.4	6.1	3.1	9303	Flexure (bar rupture)
HSC-1%ZP-No.5(HS)	214.8	244.6	26.0	65.5	8.3	2.5	12264	Flexure (fiber pullout)

This document is the intellectual property of the fib – International Federation for Structural Concrete. All rights reserved.
This PDF of fib Bulletin 95 is intended for use and/or distribution solely within fib National Member Groups.



(a) (b)

Figure 4: (a) Load-deflection curves and (b) method for determining Δ_y in HS specimens

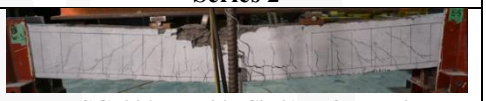
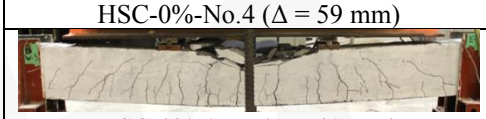
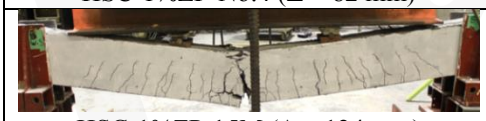
Series 1	Series 2
 HSC-0%-No.4 (Δ = 59 mm)	 HSC-0%-No.4(HS) (Δ = 35 mm)
 HSC-0%-15M (Δ = 41 mm)	 HSC-0%-No.5(HS) (Δ = 34 mm)
Series 1F	**Series 2F (No.5-HS)**
 HSC-1%ZP-No.4 (Δ = 82 mm)	 HSC-1%ZP- No.4(HS) (Δ = 71 mm)
 HSC-1%ZP-15M (Δ = 124 mm)	 HSC-1%ZP- No.5(HS) (Δ = 60 mm)

Figure 5: Series 1, 2 and 1F, 2F beams photos at end of testing

3.2 Effect of fibers in beams with Normal-strength (400 MPa) bars

The effect of fibers on the flexural response of the high-strength concrete beams designed with normal-strength bars can be examined by comparing the responses of beam HSC-0%-15M and HSC-0%-No.4 constructed with plain HSC, and companion beams HSC-1%ZP-15M and HSC-1%ZP-No.4 which were built with 1% of steel fibers. All beams in this comparison were reinforced with normal-strength (Grade 400 MPa) consisting of either No.4 or 15M bars. The HSFRC beams in this comparison were built without transverse reinforcement, whereas the control plain HSC beams contained stirrups spaced at 100 mm in the shear spans.

This document is the intellectual property of the fib – International Federation for Structural Concrete. All rights reserved.
This PDF of fib Bulletin 95 is intended for use and/or distribution solely within fib National Member Groups.

Figure 6a compares the response of the specimens with 15M bars where it can be seen that the use of 1% steel fibers substitutes for stirrups and improves flexural response by increasing strength, stiffness and ductility. Beam HSC-1%ZP-15M shows increases of 11% and 21% in strength and stiffness when compared to the plain HSC companion. More impressive is the increase in ductility where the steel fiber-reinforced concrete beam continues to carry load without a noticeable drop in capacity until the end of testing (deflection of 124 mm). As a result, the ductility ratio increased by 213% when comparing HSC-1%ZP-15M and HSC-0%-15M (Δ_{max}/Δ_y = 8.55 vs. 2.73). Similarly, the fiber-reinforced specimen shows superior toughness (A_u), with a 294% improvement in energy-absorption capacity when compared to the plain HSC beam. The enhanced ductility can be related to the ability of fibers to delay crushing of concrete in the beam compression zone as well as the ability of HSFRC to carry tensile stresses after cracking (see Figure 5). An improvement in stiffness and ductility is also observed when comparing the responses of the plain HSC and HSFRC specimens with No.4 bars in Figure 6b, although both beams show similar ultimate strength. Crushing is also well controlled in beam HSC-1%ZP-No.4, with failure occurring in flexure and damage limited to fiber pullout.

3.3 Effect of fibers in beams with High-strength (690 MPa) bars

This comparison examines the effect of fibers on the response of HSC beams detailed with high-strength (Grade 690 MPa) reinforcement. Included are beams HSC-0-No.4(HS) & HSC-0-No.5HS which were built plain HSC and No.4 & No.5 bars respectively, and companion beams HSC-1%ZP-No.4(HS) & HSC-1%ZP-No.5(HS) which were built with HSFRC containing 1% steel fibers. All beams in this comparison contained stirrups in the shear spans.

The comparison of the load-deflection responses of the beams with No.5 and No.4 high-strength bars are shown in Figure 6c and 6d, where it can be seen that the use of steel fibers significantly improves the structural response of the beams with high-strength bars. For example, the increases in strength and stiffness are recorded to be 26% and 40% when comparing the steel fiber-reinforced and plain HSC beams with No.5 bars. While all beams show rounding of the load-deflection curve due to the nature of the high-strength steel, the plain HSC beam fails suddenly by crushing of concrete due to the high strain demands imposed by the high-strength bars on the HSC compression zone. In contrast, a clear post-peak response is developed in both steel fiber-reinforced specimens, which show significant enhancements in maximum displacement, ductility and overall toughness of 93%, 131% and 200% in the No.5 set, and improvements of 103%, 158% & 250% in the No.4 set. The enhanced behaviour results from the high compressive toughness of steel HSFRC which allows for gradual failure of concrete in the compression zone, and the development of sustained post-peak response. The beam responses are further enhanced by the ability of steel fibers to redistribute cracking and improve the tensile capacity of HSC. The comparisons clearly demonstrate that the high toughness properties of HSFRC are better suited for high-strength reinforcement when compared to plain high-strength concrete.

It is important to note that while both HSFRC beams fail in flexure with high deformation capacity, the beam with No.4 high-strength bars (ρ = 1%) eventually fails by bar rupture at one localized crack at mid-span (Figure 5). Conversely, the beam with No.5 bars (ρ = 1.6%) fails due to excessive crack opening and fiber pullout. The result can be explained by the lower tension steel ratio in beam HSC-1%ZP-No.4(HS), the effects of fibers on crack localization and the reduced strain capacity of the high-strength ASTM A1035 reinforcement in tension.

This document is the intellectual property of the fib – International Federation for Structural Concrete. All rights reserved.
This PDF of fib Bulletin 95 is intended for use and/or distribution solely within fib National Member Groups.

3.4 Effect of steel reinforcement type in plain HSC beams

Comparisons of the performances of beams HSC-0%-No.4 vs. HSC-0%-No.4(HS) and HSC-0%-15M vs. HSC-0%-No.5(HS) allow for an examination of the effect of high-strength reinforcement in the plain high-strength concrete beams. As shown in Figure 6e, the beam reinforced with No.5 high-strength bars shows an 86% increase load-carrying capacity when compared to the companion with 15M normal-strength bars, with a 25% increase in energy-absorption capacity (A_u = 4100 vs. 3272 KN-mm). The increased beam capacity can be explained by the ratio between the actual yield strengths of the two bars types (f_y $929\ vs. 471\ MPa$). As seen in Figure 4a, a similar increase in ultimate load is observed when comparing the two HSC beams in the No.4 set. The shape of the load-deflection curves was also affected by the steel type; the beams with normal-strength bars had a clear yield plateau with large plastic deformations before failure. In contrast, the use of high-strength bars results in more brittle behaviour, with lower failure displacements and ductility when compared to the companion beams with normal-strength bars. For example, the ductility ratio goes from Δ_{max}/Δ_y = 2.7 to 1.1 when comparing beams HSC-0%-15M and HSC-0%-No.5HS. Failure in the beams with high-strength bars is sudden and occurs due to explosive failure of the plain high-strength concrete in the compression zone (see Figure 5).

3.5 Effect of steel reinforcement type in HSFRC beams

This comparison examines the effect of reinforcement type in the HSFRC beams. Figure 6f compares the response of beams HSC-1%ZP-15M vs. HSC-1%ZP-No.5(HS) which were built with steel fibers and 15M/No.5 normal-strength/high-strength bars, respectively. It is noted that stirrups were not provided in the beams with normal-strength steel, however failure of all beams occurred in flexure in the central constant moment region which did not contain stirrups.

The comparison in the 15M/No.5 set shows that the use of high-strength bars significantly increased the load-carrying capacity of the steel fiber-reinforced HSFRC beam, with a 111% increase in P_{max} when compared to the companion with Grade 400 MPa reinforcement. It is interesting to note that the effect of high-strength bars in increasing strength is more significant in the HSFRC set when compared to the plain HSC set (increase of 111% vs. 86% in P_{max}). Stiffness of the companion fiber-reinforced concrete beams isn't noticeably affected by the steel type as both steels have similar elastic modulus. As expected, the use of high-strength bars leads to a reduction in HSFRC beam ductility (Δ_{max}/Δ_y = 2.5 vs. 8.6 for the beams with 690 and 400 MPa bars, respectively). Despite the relative reduction in ductility ratio, beam HSC-1%ZP-No.5(HS) shows a clear post-peak response, with large displacements recorded before failure (Δ_{max} = 66 mm, ~ L/34). This beam also shows similar energy absorption capacity (toughness) when compared to the companion HSFRC beam with normal-strength bars (see Table 2). The comparison demonstrates that the high toughness properties of HSFRC in compression and tension are well suited for beams detailed with high-strength reinforcement resulting in a synergy effect which allows for high flexural strength.

Similar results are observed when comparing the load-deflection responses of the beams with No.4 bars (refer to Figure 4a), however as shown in Figure 5, the failure mode transitions from fiber pullout in HSC-1%ZP-No.4, to bar rupture in beam HSC-1%ZP-No.4(HS) as high-strength reinforcement is introduced. As noted before this can be explained by the coupled effects of fibers on crack localization, and the reduced tension strain capacity of the high-

This document is the intellectual property of the fib – International Federation for Structural Concrete. All rights reserved.
This PDF of fib Bulletin 95 is intended for use and/or distribution solely within fib National Member Groups.

strength steel. As such, this failure mode should be considered when designing HSFRC beams with high-strength ASTM A1035 reinforcement, especially as the tension steel ratio is reduced.

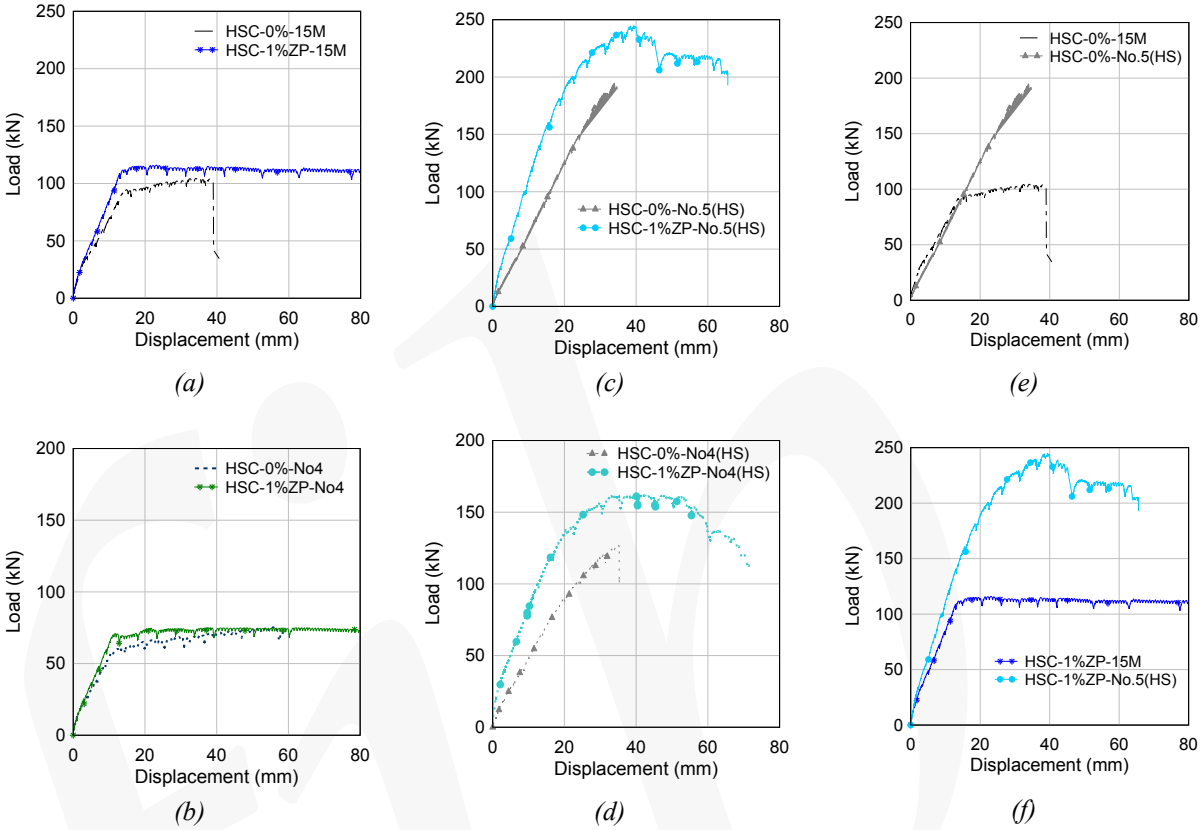


Figure 6: Effect of parameters on beam test results: (a) effect of fibres in beams with 400 MPa steel and 15M bars; (b)effect of fibres in beams with 400 MPa steel and No.4 bars, (c) effect of fibres in beams with 690 MPa steel and No.5 bars; (d) effect of fibres in beams with 690 MPa steel and No.4 bars; (e) effect of steel type in plain HSC beams; (f) effect of steel type in HSFRC beams.

4 Concluding remarks

This paper presented an experimental study examining the effect of fibers on the flexural response of high-strength concrete beams built with normal-strength and high-strength reinforcement. The following conclusions can be drawn from this study:

1. The results show that the use of fibers in high-strength concrete beams detailed with conventional reinforcement leads to improvements in load-deflection response. In this study the use of 1% hooked-end steel fibers was sufficient to replace transverse reinforcement and resulted in significant enhancement in beam ductility;
2. Comparison between the response of the beams with normal-strength and high-strength reinforcement shows that the two steel types result in distinct flexural behaviour in HSC and HSFRC beams. In HSC beams the use of high-strength bars results in an increase in load-carrying capacity at the expense of reduced ductility due to sudden failure of high-strength concrete in the beam compression zone. The use of steel fiber reinforced

This document is the intellectual property of the fib – International Federation for Structural Concrete. All rights reserved.
This PDF of fib Bulletin 95 is intended for use and/or distribution solely within fib National Member Groups.

concrete, with its increased toughness was better able to balance the high-strain demands imposed by the high-strength reinforcement allowing for a more ductile flexural response.

3. The possibility of tension bar rupture should be considered in the design of HSFRC beams containing ASTM A1035 reinforcement due to the coupled effects of fibers on crack localization and the reduced tension strain capacity of this high-strength reinforcement.

Finally, it is acknowledged that the beams in Series 1F of this study were designed without stirrups, while the remaining specimens in Series 1, 2 and 2F had minimum stirrups in their shear spans. To allow for more clear one-to-one comparisons it is recommended that future tests include specimens with identical reinforcing cages.

5 Acknowledgements

The Authors would like to thank MMFX Technologies Corporation and Bekaert for donations of high-strength steel and fiber materials used in this study.

6 References

ACI Committee. (2016). *ACI Concrete Terminology*, ACI CT-13, American Concrete Institute, Farmington Hills, Michigan, 78 p.

ATC (2014), *Roadmap for the use of high-strength reinforcement in reinforced concrete design*, Applied Technology Council Report ATC -115, Redwood City, California, 197p.

Campione, G., Fossetti, M. & Papia, M. (2010), *Behavior of fiber-reinforced concrete columns under axially and eccentrically compressive loads*. ACI Structural Journal, 107 (3), 272-281.

Di Prisco, M., Plizzari, G., & Vandewalle, L. (2009). *Fibre reinforced concrete: New design perspectives*. Materials and Structures, 42(9), 1261-1281.

Mast, R. F., Dawood, M., Rizkalla, S. H., & Zia, P. (2008), *Flexural strength design of concrete beams reinforced with high-strength steel bars*. ACI Structural Journal, 105(5), 570-577.

Meda, A., Minelli, F., Plizzari, G.A. & Riva P. (2005), *Shear behaviour of steel fibre reinforced concrete beams*. Materials and Structures, 38 (3), 343-351.

Meda, A., Minelli, F., & Plizzari, G. A. (2012). *Flexural behaviour of RC beams in fibre reinforced concrete*. Composites Part B: Engineering, 43(8), 2930-2937.

Park R. (1989), *Evaluation of ductility of structures and structural assemblages from laboratory testing*, Bulletin of the New Zealand national society for earthquake engineering, 22(3), 155-166.

This document is the intellectual property of the fib – International Federation for Structural Concrete. All rights reserved.
This PDF of fib Bulletin 95 is intended for use and/or distribution solely within fib National Member Groups.
FRC2018: Fibre Reinforced Concrete: from Design to Structural Applications
Joint ACI-*fib*-RILEM International Workshop

Fibre effect on shear behaviour of UHPC beams

Norbert Randl[1], Tamás Mészöly[1]

[1] : Carinthia University of Applied Sciences, Austria.

Abstract

The load bearing behaviour of fibre reinforced UHPC members in shear has not yet been investigated sufficiently. Therefore, an experimental campaign was conducted, investigating the behaviour of I-shaped beams made of Ultra-High Performance Concrete (UHPC) subjected to shear loading. The height of the beams was 350 mm, and the single span length 3.00 m. The main parameters were the fibre content (up to 2% by volume) and the degree of stirrup reinforcement (no stirrups or diameter 10 mm bars, spacing 125 to 300 mm).

A total of 20 tests were performed, all of them ending up in typical shear failure: pronounced shear cracks formed along the web between support and load introduction at a level of 60-70% of the ultimate load. The cracking process was monitored by a digital image correlation (DIC) measurement system.

A decisive effect of the fibres was observed: the addition of 1% to 2% fibres by volume led to a more distributed crack pattern as well as a significant increase of the ultimate load. The enhancement of the shear load capacity was not proportional to the fibre content, but corresponded quite well with the UHPFRC's residual tensile strength in the post-cracking stage. The interaction with varying degrees of stirrup reinforcement was assessed as well.

Keywords

UHPC, UHPFRC, fibre reinforcement, stirrups, shear load

This document is the intellectual property of the fib – International Federation for Structural Concrete. All rights reserved.
This PDF of fib Bulletin 95 is intended for use and/or distribution solely within fib National Member Groups.

1 Introduction

The behaviour of UHPC ("UHPFRC" with fibres) beams subject to shear loading is still in the focus of ongoing research programs. The difficulty is that on one side shear behaviour itself is a complex phenomenon, while on the other side UHPC is a rather new material that still needs to be fully explored. Above that, it is known that fibres have a significant impact on a concrete beam's shear load bearing capacity in general.

Therefore, it is not surprising that there is only few literature available on this topic. Voo et al. (2010) tested the shear resistance of fibre reinforced and prestressed UHPC beams with varying steel fibre content. Bertram (2012) investigated prestressed UHPC beams and developed a model based on the addition of the various contributing effects, taking into account the inclination of the upper and lower chords and their own stiffness in shear. The kind of additive approach is in principle similar to existing models for predicting the shear load bearing capacity of steel fibre-reinforced members made of normal strength concrete. Baby et al. (2014) conducted an experimental campaign with 11 I-shaped UHPC beams, thereby varying the fibre type and content, the amount of shear reinforcement, the concrete mixes, the presence of prestressing and the application of heat treatment. The results were used to evaluate current shear design models at serviceability limit state and also at ultimate limit state. Thiemicke and Fehling (2016) carried out tests on the shear behaviour of fibre-reinforced I-shaped UHPC beams with a maximum fibre content of 1 vol.-%.

The present experimental study provides additional test results to the rather limited available data basis for UHPC in shear and investigates systematically the effect of fibres, stirrups and their interaction on the shear behaviour. Finally, the current shear design equation of the widely acknowledged French recommendations for UHPFRC (AFGC (2013)), which is based on an additive approach of the contributing strengths, is evaluated on the basis of the test results.

2 Experimental program

2.1 Specimen geometry and material properties

A number of 20 beams made of UHPC were subjected to monotonic shear loading until failure. The test setup was a three-point bending configuration with the exception of the first two beams (B1 and B2) where a four-point setup was chosen. B1 and B2 beams were part of an earlier testing series, where mainly flexural tests were performed, and the effect of the different amount of longitudinal reinforcement and fibres on the failure mode and on the ultimate load were investigated. In order to ensure the intended shear failure mode, an I-shaped cross section was designed. The single span of the 3.50 m long beams was 3.00 m and the height of the I-shaped cross section was 350 mm, the thickness of the web 58 mm and the width of the flanges 200 mm. The shear-span-to-depth ratio a/d was larger than 3 (3.5 for the three-point and 3.2 for the four-point bending configuration, respectively) in all tests in order to prevent possible direct load transfer to the support closest to the load introduction. The estimated flexural failure load was over a vertical load of 1400 kN for the four-point setup and around 1000 kN for the three-point setup. Table 1 summarizes the different tested configurations. Steel fibre content was varied from 0 vol.-% to 2 vol.-%. Some of the beams were provided with stirrups ø10 (Fig. 1) with spacings listed in Table 1.

This document is the intellectual property of the fib – International Federation for Structural Concrete. All rights reserved.
This PDF of fib Bulletin 95 is intended for use and/or distribution solely within fib National Member Groups.

The maximum aggregate size used for the UHPC was 0.4 mm, the mixture itself had been developed previously (Randl et al. 2014) and consists of the following ingredients: Portland cement type CEM I 42.5 R HS, silica fume, quartz powder, quartz sand, superplasticizer and water. The water-to-binder ratio, taking into account a 70% water content in the superplasticizer, was 0.21. The used fibres were straight and smooth steel wire fibres with a nominal tensile strength of 2000 MPa, a nominal diameter $ø_f$ = 0.2 mm and a nominal length l_f of 15 mm, resulting in an aspect ratio ($l_f/ø_f$) equal to 75.

Table 1: Overview of tested beam configurations

Fibre content [vol.-%]	**Stirrups**			
	No stirrups	Ø10/125mm	Ø10/200 mm	Ø10/300 mm
0	B21, B23, B27	B22, B35	B16	B18
1	B20, B24, B29	–	B36	B28
2	B19, B25, B30	B1, B2	B15, B26	B17

The average value of the compressive strength measured on cubes with a side length of 100 mm was around 166 MPa 28 days after casting and 171 MPa on the day of testing. The cubes for the 28 days compressive strength were stored and tested according to ÖNORM EN 12390-2 (2009). The cubes reflecting the compressive strength on the day of testing were stored under laboratory conditions.

The longitudinal reinforcement at the bottom side of the beam specimens was a high grade steel S900/1100 with a nominal yield strength $R_{p0.2}$ of 900 MPa. A total of 7 reinforcing bars ø20 were provided, resulting in a longitudinal reinforcement ratio of 5.1%. For the stirrups ø10 a traditional reinforcing steel B 550B was used (Fig. 1).

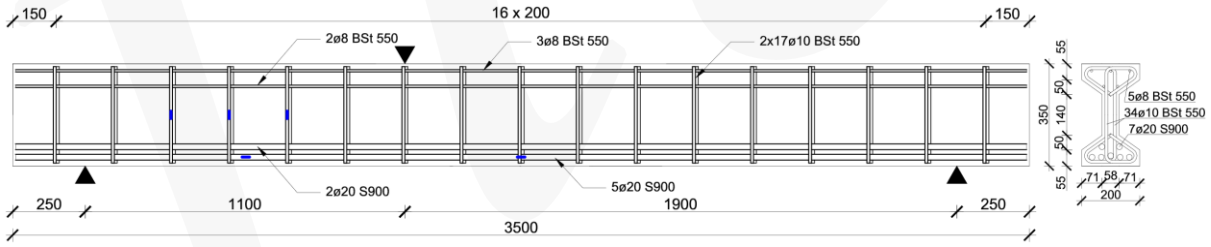


Figure 1: Outline of the three-point test setup (front view and section view)

3 Test results

All tests resulted in a typical shear failure. Pronounced shear cracks developed first in the web between support and load introduction and propagated finally into the compression flange (Fig. 2). Representative load – displacement curves are shown in Fig. 3. In general the addition of fibres led to significantly higher load capacities. Moreover especially with a fibre content of 2 vol.-% the beams behaved stiffer than the beams without or with less fibres. In general fibre-reinforced beams showed a very fine crack distribution and only at higher load levels two or three larger cracks localized. At the very end these cracks started to open excessively until final failure of the beam.

This document is the intellectual property of the fib – International Federation for Structural Concrete. All rights reserved.
This PDF of fib Bulletin 95 is intended for use and/or distribution solely within fib National Member Groups.

During the whole testing procedure the strains in the stirrups were recorded via strain gauges glued to the vertical legs of usually three stirrups at the expected crossing of the diagonal strut and the stirrups. Nearly all stirrups with applied strain gauges reached the steel yield strain; depending on the amount of stirrups usually at a load level of about 60% to 80% of the ultimate load. In general, all beams reinforced with fibres and/or stirrups exhibited a less brittle behaviour than the UHPC beams without fibres.

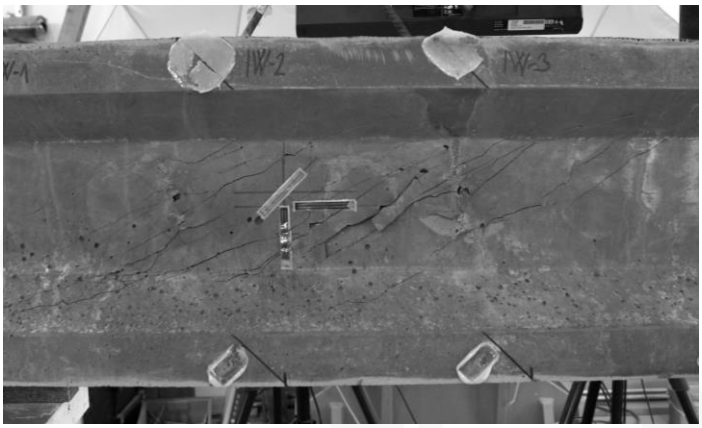


Figure 2: Typical shear failure pattern of tested UHPC beam (front view of beam B18)

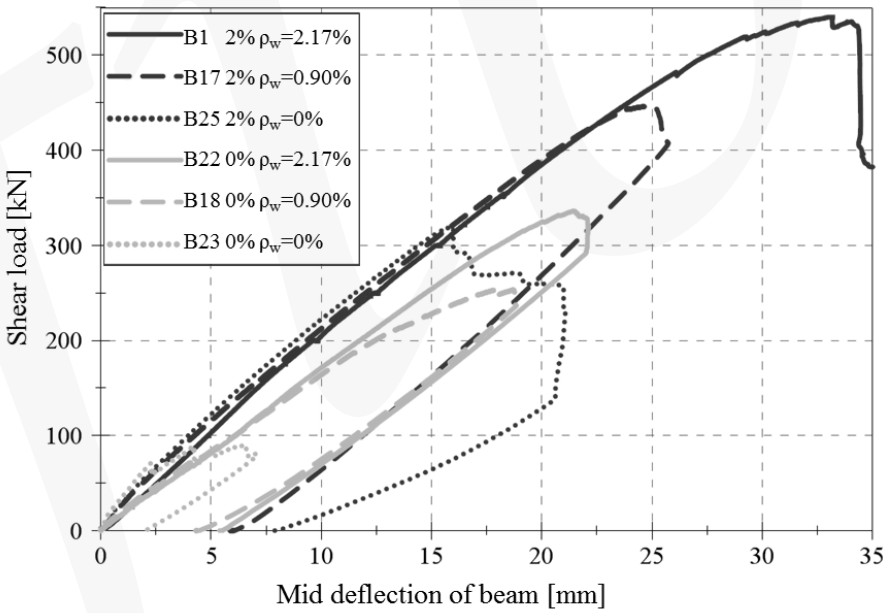


Figure 3: Representative load-displacement curves of the tested configurations

A digital image correlation system was used to record the crack formation at each load stage. Fig. 4 shows the crack patterns of a heavily stirrup reinforced beam without fibres (left hand side) in comparison to a fibre reinforced beam (2 vol.-%) without stirrups on the right hand side, derived from the calculated major principal strains of the DIC system measurements. Fig. 4 clearly shows the formation of very fine hairline cracks due to the fibre effect and the localization of two main cracks. In contrast, stirrups allowed for the formation

This document is the intellectual property of the fib – International Federation for Structural Concrete. All rights reserved.
This PDF of fib Bulletin 95 is intended for use and/or distribution solely within fib National Member Groups.

of a pronounced truss model. So in fact the crack pattern of both configurations diverges significantly. However, in the considered case it is interesting to observe that nevertheless both beams reached a similar ultimate load. At ultimate load, in case of the beams with stirrups and without fibres, the largest shear crack width was between 0.5 mm and 0.7 mm. In the case of beams with fibres and without stirrups at the ultimate load level two or three very large cracks localized and opened more than 1.0 mm in the web. Beside the two or three very large inclined shear cracks, the opening of the other cracks in the web remained below 0.1–0.2 mm. More details about the crack evaluation can be found in Mészöly and Randl (2018).

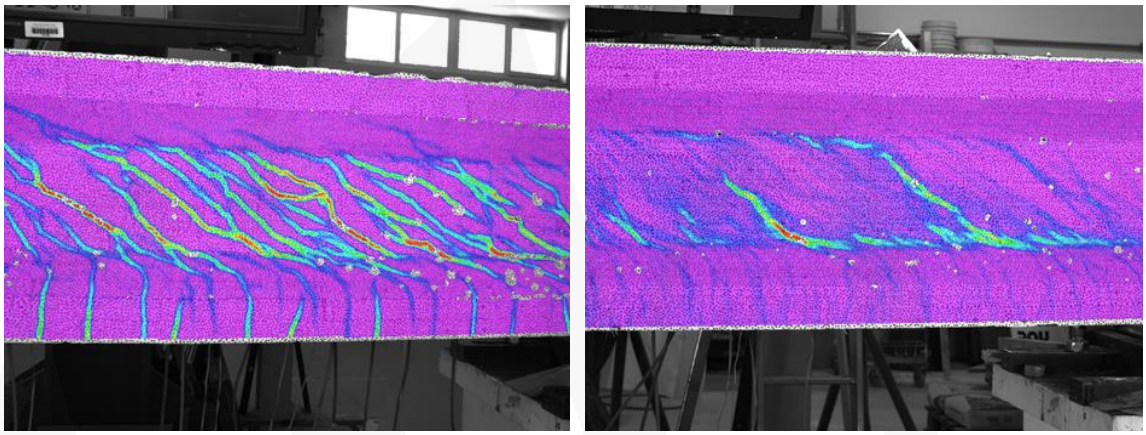


Figure 4: Crack pattern for beams B22 (left) and B30 (right) at a load level of 500 kN

Test results are listed in the following Table 2, arranged in a way that fibre content and related number of stirrups increase from top to bottom. The amount of stirrups is reflected in the reinforcement degree ρ_w [%].

Table 2: Summary of recorded maximum loads at each test

Beam No.	f_{cm} (MPa)	fibres (vol.-%)	stirrups (ρ_w [%])	$F_{u,test}$ (kN)	$V_{u,test}$ (kN)	$V_{u,calc}$ (kN)	$V_{u,test}/V_{u,calc}$ (-)
B21	160.8	**0**	0	130	83	49	1.69
B23	169.6	**0**	0	98	62	53	1.19
B27	166.6	**0**	0	79	50	53	0.95
B18	174.9	**0**	0.90	400	253	199	1.27
B16	168.2	**0**	1.35	474	300	274	1.10
B22	154.3	**0**	2.17	532	337	394	0.86
B35	172.9	**0**	2.17	583	369	391	0.94
B20	161.9	**1**	0	419	266	208	1.28
B24	174.8	**1**	0	314	199	187	1.06
B29	186.5	**1**	0	487	308	199	1.55
B28	165.6	**1**	0.90	628	398	340	1.17
B36	169.8	**1**	1.35	703	445	396	1.12

This document is the intellectual property of the fib – International Federation for Structural Concrete. All rights reserved.
This PDF of fib Bulletin 95 is intended for use and/or distribution solely within fib National Member Groups.

B19	160.4	**2**	0	397	251	238	1.06
B25	188.4	**2**	0	504	319	227	1.41
B30	177.5	**2**	0	564	357	219	1.64
B17	170.4	**2**	0.90	704	446	391	1.14
B15	169.7	**2**	1.35	700	443	422	1.05
B26	162.8	**2**	1.35	814	516	495	1.04
B1	185.2	**2**	2.17	1080	540	537	1.01
B2	184.2	**2**	2.17	1155	578	537	1.14

A significant contribution of the fibres to the overall shear loading capacity can be clearly identified: without stirrups, 1 vol% of fibres leads to a nearly four times higher capacity than without fibres (+193 kN shear load increase) and 2 vol% of fibres results in an increasing factor of around 4.7 (+245 kN shear load enhancement). In general the load gain in shear due to the fibres was not proportional to the fibre content. This tendency fits to observations made by Thiemicke and Fehling (2016). For the considered beam geometry and setup, the load gain with 2 vol% of fibres is similar to the effect achieved alternatively by the arrangement of stirrups ø 10 mm at a distance of 200 mm, however associated with larger deflections.

Together with stirrups, the effect of the fibres was somewhat smaller than without stirrups but still significant: independent from the stirrup amount, an average increase of shear strength of around +200 kN was recorded when changing from 0 vol.-% to 2 vol.-% of fibres. Concerning on the other hand the effect of the stirrups, it can be noted that the increase of shear resistance due to stirrups was larger for beams without fibres and less expressed for beams with fibres. The difference in shear resistance is attributed to an observed change of the inclination of the cracks. However, some effect of the stirrups on the fibre orientation together with the casting procedure cannot be excluded.

Finally all beam test results were evaluated on the basis of the provisions given in AFGC (2013). In the calculation, instead of design and characteristic values, the mean values of the material properties and the real dimensions were applied. AFGC (2013) recommends an additive approach for the prediction of the design shear resistance:

$$V_{Rd} = V_{Rd,c} + V_{Rd,s} + V_{Rd,f} \quad (1)$$

where $V_{Rd,c}$ is the concrete term, $V_{Rd,s}$ the contribution of shear reinforcement and $V_{Rd,f}$ the shear resistance provided by the fibres as follows:

$$V_{Rd,f} = (A_{fv} \cdot \sigma_{Rd,f})/\tan\theta \qquad \text{where} \quad A_{fv} = b_w \cdot z \quad (2)$$

The value for the inner lever arm "z" was between 270-279 mm, depending on the real (measured) geometry and loading conditions. The calculation approach as per AFGC requires the assumption of the inclination θ of the compression struts to the beam axis. The angle was derived from the tests as an average value in each shear region, and varied only slightly between 28° and 34°. The residual tensile strength ($\sigma_{R,f}$) required for the derivation of the fibre contribution was determined on the basis of flexural tests on prisms 150×150×700 mm (Randl and Mészöly (2015)). The $\sigma_{R,f}$ values were back-calculated from the tensile stress vs. crack width curves (Fig. 5) based on the calculation approach presented in (AFGC (2013)) for an ultimate crack width value of 0.5 mm as observed in the beam tests just before failure,

This document is the intellectual property of the fib – International Federation for Structural Concrete. All rights reserved.
This PDF of fib Bulletin 95 is intended for use and/or distribution solely within fib National Member Groups.

resulting in a residual tensile strength value of 5.0 MPa for beams with 1 vol.-% and 6.3 MPa for beams with 2 vol.-% of fibres.

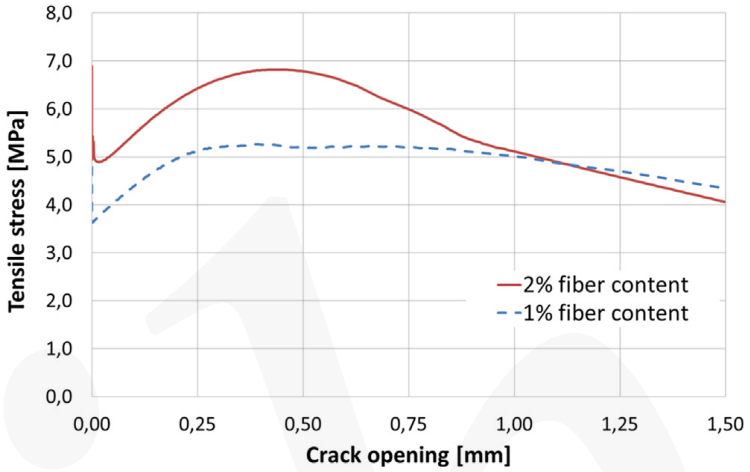


Figure 5: Tensile stress vs. crack opening curves (from Randl and Mészöly (2015))

As a conclusion it can be stated that the AFGC approach predicts the test results quite well, however being about 15 to 20% on the conservative side. The mean ratio of tested versus calculated shear strength (single values are listed in Table 2) is 1.18 and the coefficient of variation 0.19. As can be seen, the approach as per AFGC 2013 in the present study slightly underestimates the contribution of the fibres especially without stirrup reinforcement and in turn overestimates the contribution of the stirrups. This can also be deduced from Fig. 6 where the ratio $V_{u,test}/V_{u,calc}$ is displayed over the fibre content: obviously the overall dependency on the fibre content is met quite well by considering the residual tensile strength of the fibre reinforced UHPC, even though the degree of stirrup reinforcement ρ_w varies significantly.

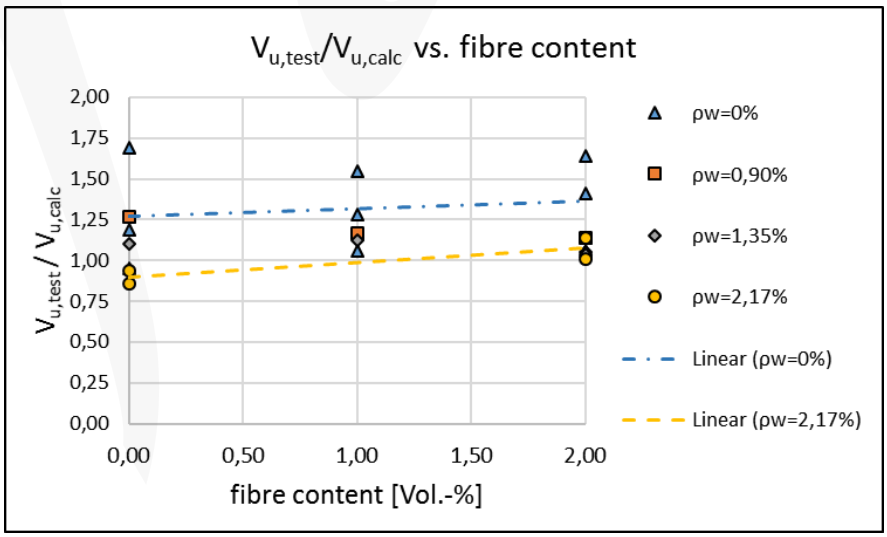


Figure 6: Relationship between $V_{u,test}$ / $V_{u,calc}$ (calculated as per AFGC-approach) and fibre content

This document is the intellectual property of the fib – International Federation for Structural Concrete. All rights reserved.
This PDF of fib Bulletin 95 is intended for use and/or distribution solely within fib National Member Groups.

4 Concluding remarks

The experimental study presented in here reveals the significant effect of steel fibres for the load bearing capacity of UHP(FR)C beams in shear. In order to account for possible interaction effects, in several tests varying amounts of stirrups had been provided, too. A systematic variation of the different parameters allows for an identification of the single mechanisms and contributions of fibre reinforcement as well as stirrups, also when combined and interacting with each other. The main observations of the present test campaign can be summarized as follows:

1. With the addition of steel fibres, the shear load capacity of UHPC beams can be enhanced significantly, comparable to the load gain with certain amounts of stirrup reinforcement.
2. The effect of the steel fibres on the beam's shear resistance is quite proportional to the UHPFRC's residual tensile capacity in the post-cracking stage as derived from small bending prisms: increasing the fibre content from 1 to 2 vol.-% increased the shear capacity by 20%, while the residual strength increased by 25%.
3. The effect of additional stirrups does not seem to be strongly affected by the presence of fibres: changing the stirrup distance from 300 mm to 125 mm led to a shear load gain of +100 kN without, and +113 kN with 2 vol.-% of fibres. When stirrups were provided, the contribution of additional fibres in turn reduces somewhat, which can be attributed to disturbances on the orientation of fibres in the vicinity of the stirrups: changing the fibre amount from 1 to 2 vol.-% led to a shear load gain of +52 kN without stirrups, and +34 kN with stirrups at a distance of 200 mm.
4. The steel fibres have a pronounced beneficial effect on the crack distribution.
5. At same ultimate load level, the crack pattern at failure differs significantly depending on whether the reinforcement consists of either fibre or stirrup reinforcement.
6. The French recommendation for UHPFRC (AFGC (2013)) allows for an adequate prediction of the shear resistance about 15% to 20% on the conservative side, however somewhat underestimating the effect of the fibres and overestimating the effect of shear reinforcement.

5 Acknowledgements

Most of the tests had been performed in the frame of the HiPerComp project (grant number 826881) funded by the Austrian Research Promotion Agency (FFG), which is gratefully acknowledged by the authors.

6 References

AFGC (Association Francaise de Genie Civil) (2013), *Ultra High Performance Fibre-Reinforced Concretes – Recommendation*, Revised ed.

Baby F, Marchand P, Toutlemonde F. (2014), *Shear behavior of ultrahigh performance fiber-reinforced concrete beams. I: Experimental investigation.* ASCE Journal of Structural Engineering 2014; 140(5). https://doi.org/10.1061/(ASCE)ST.1943-541X.0000907

This document is the intellectual property of the fib – International Federation for Structural Concrete. All rights reserved.
This PDF of fib Bulletin 95 is intended for use and/or distribution solely within fib National Member Groups.

Baby F, Marchand P, Toutlemonde F. (2014), *Shear behavior of ultrahigh performance fiber-reinforced concrete beams. II: Analysis and Design Provisions*, ASCE Journal of Structural Engineering 2014; 140(5). https://doi.org/10.1061/(ASCE)ST.1943-541X.0000908

Bertram, G. (2012), *Zum Verbund- und Querkrafttragverhalten von Spannbetonträgern aus Ultra-hochfestem Beton*, Doctoral Thesis, RWTH Aachen (in German)

Mészöly, T., Randl, N. (2018), *Shear behavior of fiber-reinforced ultra-high performance concrete beams,* Engineering Structures, 168, 2018, pp. 119–127. DOI: https://doi.org/10.1016/j.engstruct.2018.04.075

ÖNORM EN 12390-2 (2009), *Testing hardened concrete — Part 2: Making and curing specimens for strength tests*, Austrian Standards Institute

Randl, N., Mészöly, T. (2015), *Load Bearing Behaviour of UHPFRC Beams Reinforced with High Grade Steel*, Key Engineering Materials, 629-630, 2015, pp 551–559, DOI: https://doi.org/10.4028/www.scientific.net/KEM.629-630.551

Randl, N., Steiner, T. et al. (2014), *Development of UHPC mixtures from an ecological point of view*, Construction and Building Materials, 67 Part C, pp 373–378, DOI: https://doi.org/10.1016/j.conbuildmat.2013.12.102.

Thiemicke, J., Fehling, E. (2016), *Proposed Model to predict the Shear Bearing Capacity of UHPC-Beams with combined Reinforcement*, Proceedings of HiPerMat 2016 – 4th International Symposium on Ultra-High Performance Concrete and High Performance Construction Materials, Kassel University Press; Kassel

Voo, Y.L., Poon, W.K., Foster, S. (2010), *Shear Strength of Steel Fiber-Reinforced Ultrahigh-Performance Concrete Beams without Stirrups*, Journal of Structural Engineering 136(11), DOI: https://doi.org/10.1061/(ASCE)ST.1943-541X.0000234

This document is the intellectual property of the fib – International Federation for Structural Concrete. All rights reserved.
This PDF of fib Bulletin 95 is intended for use and/or distribution solely within fib National Member Groups.

The *fib* (International Federation for Structural Concrete - Fédération internationale du béton) is grateful for the invaluable support of the following national member groups and sponsoring members, which contributes to the publication of *fib* technical bulletins, the *Structural Concrete* journal and *fib*-news.

National member groups

UNNOBA - Universidad Nacional del Nor Oeste de la Provincia de Buenos Aires, Argentina
CIA - Concrete Institute of Australia
ÖBV - Österreichische Bautechnik Vereinigung, Austria
GBB-BBG - Groupement Belge du Béton, Belgium
ABCIC - Associação Brasileira da Construção Industrializada de Concreto, Brazil
ABECE - Associação Brasileira de Engenharia e Consultoria Estrutural, Brazil
IBRACON - Instituto Brasileiro do Concreto, Brazil
CPCI (Canadian Precast Prestressed Concrete Institute)
Université Laval, Canada
CCES - China Civil Engineering Society
Cyprus University of Technology
Cyprus Association of Civil Engineers
Česká Betonářská Společnost, Czech Republic
DBF - Dansk Betonforening, Denmark
SB - Suomen Betoniyhdistys, Finland
AFGC - Association Française de Génie Civil, France
DAfStb - Deutscher Ausschuss für Stahlbeton, Germany
Technical Chamber of Greece
University of Patras, Department of Civil Engineering, Greece
Hungarian Group of the *fib*
The Institution of Engineers, India
fib-Indonesia
University of Amirkabir, Iran
IACIE - Israeli Association of Construction and Infrastructure Engineers
AICAP - Associazione Italiana Calcestruzzo, Armato e Precompresso, Italy
CTE - Collegio dei tecnici della industrializzazione edilizia, Italy
ITC - CNR, Istituto per le Tecnologie della Costruzione, Italy
ReLUIS, Italy
JCI - Japan Concrete Institute
JPCI - Japan Prestressed Concrete Institute
Administration des Ponts et Chaussées, Luxembourg
fib Netherlands
NZCS - New Zealand Concrete Society
NB - Norsk Betongforening / Norwegian Concrete Association
Polish Academy of Sciences, Committee for Civil Engineering, Poland
GPBE - Grupo Português de Betão Estrutural, Portugal
Polytechnic University of Timisoara, Romania
Technical University of Civil Engineering, Romania
University of Transylvania Brasov, Faculty of Civil Engineering, Romania
Association for Structural Concrete, Russia
SNK *fib*, Slovakia
Slovenian Society of Structural Engineers, Slovenia

This document is the intellectual property of the fib – International Federation for Structural Concrete. All rights reserved.
This PDF of fib Bulletin 95 is intended for use and/or distribution solely within fib National Member Groups.

The Concrete Institute, South Africa
KCI - Korean Concrete Institute, South Korea
ACHE - Asociación Cientifico-Técnica del Hormigon Estructural, Spain
SB - Svenska Betongföreningen, Sweden
Délégation nationale suisse de la *fib*, Switzerland
TCA - Thailand Concrete Association
ITU - Istanbul Technical University, Turkey
NIISK - Research Institute of Building Constructions, Ukraine
Society of Engineers, United Arab Emirates
fib UK, United Kingdom
ASBI - American Segmental Bridge Institute, United States of America
PCI - Precast/Prestressed Concrete Institute, United States of America
PTI - Post-Tensioning Institute, United States of America

Sponsoring members

Strong Force-MGC W.L.L., Bahrain
Liuzhou OVM Machinery Company, China
Shenzhen University, China
Peikko Group Corp., Finland
Consolis, France
ECS - European Engineered Construction Systems Association, Germany
FBF - Betondienst, Germany
ISB - Institut für Stahlbetonbewehrung, Germany
MKT - Metall-Kunststoff-Technik, Germany
Progress Group GmbH, Germany
Larsen & Toubro Ltd, ECC Division, India
FUJI P. S. Corporation, Japan
IHI Construction Service Company, Japan
Oriental Shiraishi Corporation, Japan
P. S. Mitsubishi Construction Company, Japan
SE Corporation, Japan
Sumitomo Mitsui Construction Company, Civil Engineering Division, Japan
Cimenterie Nationale S.A.L., Lebanon
Hilti, Liechtenstein
BBR VT International, Switzerland
Sika Schweiz, Switzerland
VSL International, Switzerland
PBL Group, Thailand
CEG – The Consulting Engineers Group, United States of America

This document is the intellectual property of the fib – International Federation for Structural Concrete. All rights reserved.
This PDF of fib Bulletin 95 is intended for use and/or distribution solely within fib National Member Groups.

fib Bulletins published since 1998

1 *Structural Concrete – Textbook on Behaviour, Design and Performance*; Vol. 1: *Introduction, Design Process, Materials*
Manual - textbook (244 pages, ISBN 978-2-88394-041-3, July 1999)

2 *Structural Concrete – Textbook on Behaviour, Design and Performance*; Vol. 2: *Basis of Design*
Manual - textbook (324 pages, ISBN 978-2-88394-042-0, July 1999)

3 *Structural Concrete – Textbook on Behaviour, Design and Performance*; Vol. 3: *Durability, Design for Fire Resistance; Member Design, Maintenance; Assessment and Repair, Practical aspects*
Manual - textbook (292 pages, ISBN 978-2-88394-043-7, December 1999)

4 *Lightweight aggregate concrete: Extracts from codes and standards*
State-of-the-art report (46 pages, ISBN 978-2-88394-044-4, August 1999)

5 *Protective systems against hazards: Nature and extent of the problem*
Technical report (64 pages, ISBN 978-2-88394-045-1, October 1999)

6 *Special design considerations for precast prestressed hollow core floors*
Guide to good practice (180 pages, ISBN 978-2-88394-046-8, January 2000)

7 *Corrugated plastic ducts for internal bonded post-tensioning*
Technical report (50 pages, ISBN 978-2-88394-047-5, January 2000)

8 *Lightweight aggregate concrete*: Part 1 (guide) – *Recommended extensions to Model Code 90*; Part 2 (technical report) – *Identification of research needs*; Part 3 (state-of-art report) – *Application of lightweight aggregate concrete* (118 pages, ISBN 978-2-88394-048-2, May 2000)

9 *Guidance for good bridge design*: Part 1 – Introduction, Part 2 – *Design and construction aspects*
Guide to good practice (190 pages, ISBN 978-2-88394-049-9, July 2000)

10 *Bond of reinforcement in concrete*
State-of-art report (434 pages, ISBN 978-2-88394-050-5, August 2000)

11 *Factory applied corrosion protection of prestressing steel*
State-of-art report (20 pages, ISBN 978-2-88394-051-2, January 2001)

12 *Punching of structural concrete slabs*
Technical report (314 pages, ISBN 978-2-88394-052-9, August 2001)

13 *Nuclear containments*
State-of-art report (130 pages, 1 CD, ISBN 978-2-88394-053-6, September 2001)

14 *Externally bonded FRP reinforcement for RC structures*
Technical report (138 pages, ISBN 978-2-88394-054-3, October 2001)

15 *Durability of post-tensioning tendons*
Technical report (284 pages, ISBN 978-2-88394-055-0, November 2001)

16 *Design Examples for the 1996 FIP recommendations Practical design of structural concrete*
Technical report (198 pages, ISBN 978-2-88394-056-7, January 2002)

17 *Management, maintenance and strengthening of concrete structures*
Technical report (180 pages, ISBN 978-2-88394-057-4, April 2002)

18 *Recycling of offshore concrete structures*
State-of-art report (33 pages, ISBN 978-2-88394-058-1, April 2002)

19 *Precast concrete in mixed construction*
State-of-art report (68 pages, ISBN 978-2-88394-059-8, April 2002)

This document is the intellectual property of the fib – International Federation for Structural Concrete. All rights reserved.
This PDF of fib Bulletin 95 is intended for use and/or distribution solely within fib National Member Groups.

20 *Grouting of tendons in prestressed concrete*
Guide to good practice (52 pages, ISBN 978-2-88394-060-4, July 2002)

21 *Environmental issues in prefabrication*
State-of-art report (56 pages, ISBN 978-2-88394-061-1, March 2003)

22 *Monitoring and safety evaluation of existing concrete structures*
State-of-art report (304 pages, ISBN 978-2-88394-062-8, May 2003)

23 *Environmental effects of concrete*
State-of-art report (68 pages, ISBN 978-2-88394-063-5, June 2003)

24 *Seismic assessment and retrofit of reinforced concrete buildings*
State-of-art report (312 pages, ISBN 978-2-88394-064-2, August 2003)

25 *Displacement-based seismic design of reinforced concrete buildings*
State-of-art report (196 pages, ISBN 978-2-88394-065-9, August 2003)

26 *Influence of material and processing on stress corrosion cracking of prestressing steel – case studies*
Technical report (44 pages, ISBN 978-2-88394-066-6, October 2003)

27 *Seismic design of precast concrete building structures*
State-of-art report (262 pages, ISBN 978-2-88394-067-3, October 2003)

28 *Environmental design*
State-of-art report (86 pages, ISBN 978-2-88394-068-0, February 2004)

29 *Precast concrete bridges*
State-of-art report (83 pages, ISBN 978-2-88394-069-7, November 2004)

30 *Acceptance of stay cable systems using prestressing steels*
Recommendation (80 pages, ISBN 978-2-88394-070-3, January 2005)

31 *Post-tensioning in buildings*
Technical report (116 pages, ISBN 978-2-88394-071-0, February 2005)

32 *Guidelines for the design of footbridges*
Guide to good practice (160 pages, ISBN 978-2-88394-072-7, November 2005)

33 *Durability of post-tensioning tendons*
Recommendation (74 pages, ISBN 978-2-88394-073-4, December 2005)

34 *Model Code for Service Life Design*
Model Code (116 pages, ISBN 978-2-88394-074-1, February 2006)

35 *Retrofitting of concrete structures by externally bonded FRPs*
Technical Report (224 pages, ISBN 978-2-88394-075-8, April 2006)

36 *2006 fib Awards for Outstanding Concrete Structures*
Bulletin (40 pages, ISBN 978-2-88394-076-5, May 2006)

37 *Precast concrete railway track systems*
State-of-art report (38 pages, ISBN 978-2-88394-077-2, September 2006)

38 *Fire design of concrete structures – materials, structures and modelling*
State-of-art report (106 pages, ISBN 978-2-88394-078-9, April 2007)

39 *Seismic bridge design and retrofit – structural solutions*
State-of-art report (300 pages, ISBN 978-2-88394-079-6, May 2007)

40 *FRP reinforcement in RC structures*
Technical report (160 pages, ISBN 978-2-88394-080-2, September 2007)

41 *Treatment of imperfections in precast structural elements*
State-of-art report (74 pages, ISBN 978-2-88394-081-9, November 2007)

42 *Constitutive modelling of high strength / high performance concrete*
State-of-art report (130 pages, ISBN 978-2-88394-082-6, January 2008)

This document is the intellectual property of the fib – International Federation for Structural Concrete. All rights reserved.
This PDF of fib Bulletin 95 is intended for use and/or distribution solely within fib National Member Groups.

43 *Structural connections for precast concrete buildings*
Guide to good practice (370 pages, ISBN 978-2-88394-083-3, February 2008)

44 *Concrete structure management: Guide to ownership and good practice*
Guide to good practice (208 pages, ISBN 978-2-88394-084-0, February 2008)

45 *Practitioners' guide to finite element modelling of reinforced concrete structures*
State-of-art report (344 pages, ISBN 978-2-88394-085-7, June 2008)

46 *Fire design of concrete structures —structural behaviour and assessment*
State-of-art report (214 pages, ISBN 978-2-88394-086-4, July 2008)

47 *Environmental design of concrete structures – general principles*
Technical report (48 pages, ISBN 978-2-88394-087-1, August 2008)

48 *Formwork and falsework for heavy construction*
Guide to good practice (96 pages, ISBN 978-2-88394-088-8, January 2009)

49 *Corrosion protection for reinforcing steels*
Technical report (122 pages, ISBN 978-2-88394-089-5, February 2009)

50 *Concrete structures for oil and gas fields in hostile marine environments*
State-of-art report (36 pages, IBSN 978-2-88394-090-1, October 2009)

51 *Structural Concrete – Textbook on behaviour, design and performance*, Vol. 1
Manual – textbook (304 pages, ISBN 978-2-88394-091-8, November 2009)

52 *Structural Concrete – Textbook on behaviour, design and performance*, Vol. 2
Manual – textbook (350 pages, ISBN 978-2-88394-092-5, January 2010)

53 *Structural Concrete – Textbook on behaviour, design and performance*, Vol. 3
Manual – textbook (390 pages, ISBN 978-2-88394-093-2, December 2009)

54 *Structural Concrete – Textbook on behaviour, design and performance*, Vol. 4
Manual – textbook (196 pages, ISBN 978-2-88394-094-9, October 2010)

55 *fib Model Code 2010, First complete draft* – Volume 1
Draft Model Code (318 pages, ISBN 978-2-88394-095-6, March 2010)

56 *fib Model Code 2010, First complete draft* – Volume 2
Draft Model Code (312 pages, ISBN 978-2-88394-096-3, April 2010)

57 *Shear and punching shear in RC and FRC elements - Workshop proceedings*
Technical report (268 pages, ISBN 978-2-88394-097-0, October 2010)

58 *Design of anchorages in concrete*
Guide to good practice (282 pages, ISBN 978-2-88394-098-7, July 2011)

59 *Condition control and assessment of reinforced concrete structures exposed to corrosive environments (carbonation/chlorides)*
State-of-art report (80 pages, ISBN 978-2-88394-099-4, May 2011)

60 *Prefabrication for affordable housing*
State-of-art report (130 pages, ISBN 978-2-88394-100-7, August 2011)

61 *Design examples for strut-and-tie models*
Technical report (220 pages, ISBN 978-2-88394-101-4, September 2011)

62 *Structural Concrete – Textbook on behaviour, design and performance*, Vol. 5
Manual – textbook (476 pages, ISBN 978-2-88394-102-1, January 2012)

63 *Design of precast concrete structures against accidental actions*
Guide to good practice (78 pages, ISBN 978-2-88394-103-8, January 2012)

64 *Effect of zinc on prestressing steel*
Technical report (22 pages, ISBN 978-2-88394-104-5, February 2012)

65 *fib Model Code 2010*, Final draft – Volume 1
Model Code (350 pages, ISBN 978-2-88394-105-2, March 2012)

This document is the intellectual property of the fib – International Federation for Structural Concrete. All rights reserved.
This PDF of fib Bulletin 95 is intended for use and/or distribution solely within fib National Member Groups.

66 *fib Model Code 2010*, Final draft – Volume 2
Model Code (370 pages, ISBN 978-2-88394-106-9, April 2012)

67 *Guidelines for green concrete structures*
Guide to good practice (56 pages, ISBN 978-2-88394-107-6, May 2012)

68 *Probabilistic performance-based seismic design*
Technical report (118 pages, ISBN 978-2-88394-108-3, July 2012)

69 *Critical comparison of major seismic codes for buildings*
Technical report (216 pages, ISBN 978-2-88394-109-0, August 2013)

70 *Code-type models for structural behaviour of concrete*
State-of-art report (196 pages, ISBN 978-2-88394-110-6, November 2013)

71 *Integrated life cycle assessment of concrete structures*
State-of-art report (62 pages, ISBN 978-2-88394-111-3, December 2013)

72 *Bond and anchorage of embedded reinforcement: Background to the fib Model Code for Concrete Structures 2010*
Technical report (170 pages, ISBN 978-2-88394-112-0, May 2014)

73 *Tall buildings: Structural design of concrete buildings up to 300m tall*
State-of-the-art report (158) pages, ISBN 978-2-88394-113-7, August 2014)

74 *Planning and design handbook on precast building structures*
Manual – textbook (313 pages, ISBN 978-2-88394-114-4, September 2014)

75 *Polymer-duct systems for internal bonded post-tensioning*
Recommendation (172 pages, ISBN 978-2-88394-115-1, December 2014)

76 *Benchmarking of deemed-to-satisfy provisions in standards: Durability of Reinforced Concrete Structures Exposed to Chlorides*
State-of-the-art-report (191 pages, ISBN 978-2-88394-116-8, May 2015)

77 *Corrugated-steel-web bridges*
State-of-the-art-report (110 pages, ISBN 978-2-88394-117-5, December 2015)

78 *Precast-concrete buildings in seismic areas*
State-of-the-art-report (273 pages, ISBN 978-2-88394-118-2, March 2016)

79 *Fibre-reinforced concrete - From design to structural applications*
ACI-*fib* workshop proceedings (480 pages, ISBN 978-2-88394-119-9, May 2016)

80 *Partial factor methods for existing concrete structures*
Recommendation (129 pages, ISBN 978-2-88394-120-5, December 2016)

81 *Punching of structural concrete slabs: Honoring Neil M. Hawkins*
ACI SP-315, ACI-*fib* symposium proceedings (378 pages, ISBN 978-2-88394-121-2, April 2017)

82 *Precast segmental bridges*
Guide to good practice (183 pages, ISBN 978-2-88394-122-9, August 2017)

83 *Precast Tunnel Segments in Fibre-Reinforced Concrete*
State-of-the-art report (162 pages, ISBN 978-2-88394-123-6, November 2017)

84 *Precast insulated sandwich panels*
State-of-the-art report (129 pages, ISBN 978-2-88394-124-3, December 2017)

85 *Towards a rational understanding of shear in beams and slabs*
Technical Report (338 pages, ISBN 978-2-88394-125-0, May 2018)

86 *Safety and performance concepts*
Guide to good practice (357 pages, ISBN 978-2-88394-126-7, August 2018)

87 *2018 fib Awards for Outstanding Concrete Structures*
Bulletin (39 pages, ISBN 978-2-88394-127-4, October 2018)

This document is the intellectual property of the fib – International Federation for Structural Concrete. All rights reserved.
This PDF of fib Bulletin 95 is intended for use and/or distribution solely within fib National Member Groups.

88 *Sustainability of precast structures*
State-of-the-art report (153 pages, ISBN 978-2-88394-128-1, December 2018)

89 *Acceptance of cable systems using prestressing steels*
Recommendation (153 pages, ISBN 978-2-88394-129-8, March 2019)

90 *Externally applied FRP reinforcement for concrete structures*
Technical report (229 pages, ISBN 978-2-88394-131-1, July 2019)

91 *Floating concrete structures*
State-of-the-art report (99 pages, ISBN 978-2-88394-133-5, August 2019)

92 *Serviceability Limit State of Concrete Structures*
Technical report (209 pages, ISBN 978-2-88394-135-9, September 2019)

93 *Brith Certificate and Through-Life Management Documentation*
Technical report (96 pages, ISBN 978-2-88394-137-3, June 2020)

94 *Precast concrete bridge continuity over piers*
Technical report (50 pages, ISBN 978-2-88394-139-7, July 2020)

Abstracts for *fib* Bulletins and lists of available CEB Bulletins and FIP Reports are available on the *fib* website at www.fib-international.org/publications.

This document is the intellectual property of the fib – International Federation for Structural Concrete. All rights reserved.
This PDF of fib Bulletin 95 is intended for use and/or distribution solely within fib National Member Groups.

Fibre Reinforced Concrete: From Design to Structural Applications

Proceedings of the ACI-*fib*-RILEM International Workshop - FRC2018

Contents

1 Mechanical Characterization
2 Shear
3 Bridges/Elevated Slabs/Precast Elements/Tunnel Linings
4 Seismic and Special Loading Conditions
5 Service Conditions and Durability
6 Structural Applications and Rehabilitation
7 HPFRC

ISBN 978-2-88394-142-7

International Federation for Structural Concrete
Fédération internationale du béton
www.fib-international.org

ISSN: 1562-3610